

**INTERNATIONAL JOURNAL OF MODERN
ENGINEERING RESEARCH (IJMER)**

ISSN : 2249-6645



Volume 3 - Issue 1

Web : www.ijmer.com

Email : ijmer.editor@gmail.com

International Journal of Modern Engineering Research (IJMER)

Editorial Board

Executive Managing Editor

Prof. Shiv Kumar Sharma
India

Editorial Board Member

Dr. Jerry Van
Department of Mechanical, USA

Dr. George Dyrud
Research centre dy. Director of Civil Engineering, New Zealand

Dr. Masoud Esfal
R& D of Chemical Engineering, Australia

Dr. Nouby Mahdy Ghazaly
Minia University, Egypt

Dr. Stanley John
Department of Textile Engineering, United Kingdom

Dr. Valfitaf Rasoul
Professor and HOD of Electromechanical, Russian

Dr. Mohammed Ali Hussain
HOD, Sri Sai Madhavi Institute of Science & Technology, India

Dr. Manko dora
Associate professor of Computer Engineering, Poland

Dr. Ahmed Nabih Zaki Rashed
Menoufia University, Egypt

Ms. Amani Tahat
Ph.D physics Technical University of Catalonia-Spain

Associate Editor Member

Dr. Mohd Nazri Ismail
University of Kuala Lumpur (UniKL), Malaysia

Dr. Kamaljit I. Lakhtaria
Sir Padmapat Singhaniya University, Udaipur

Dr. Rajesh Shrivastava
Prof. & Head Mathematics & computer Deptt. Govt. Science & commerce College Benazir. M.P

Dr. Asoke Nath
Executive Director, St. Xavier's College, West Bengal, India

Prof. T. Venkat Narayana Rao
Head, CSE, HITAM Hyderabad

Dr. N. Balasubramanian
Ph. D (Chemical Engg), IIT Madras

Jasvinder Singh Sadana
M. TECH, USIT/GGSIPU, India

Dr. Bharat Raj Singh

Associate Director, SMS Institute of Technology, Lucknow

DR. RAVINDER RATHEE

C. R. P, Rohtak, Haryana

Dr. S. Rajendran

Research Supervisor, Corrosion Research Centre Department of Chemistry, GTN Arts College, Dindigul

Mohd Abdul Ahad

Department of Computer Science, Faculty of Management and Information Technology, Jamia Hamdad, New Delhi

Kunjai Mankad

Institute of Science & Technology for Advanced Studies & Research (ISTAR)

NILANJAN DEY

JIS College of Engineering, Kalyani, West Bengal

Dr. Hawz Nwayu

Victoria Global University, UK

Prof. Plewin Amin

Crewe and Alsager College of Higher Education, UK

Dr. (Mrs.) Annifer Zalic

London Guildhall University, London

Dr. (Mrs.) Malin Askiy

Victoria University of Manchester

Dr. ABSALOM

Sixth form College, England

Dr. Nimrod Nivek

London Guildhall University, London

Dynamic Response Analysis of Automatic Generation Control in a 2-Area (Reheat & Non-Reheat) Interconnected Power System and a Scheme for Improvement of Response for the Same

Er. Dipayan Guha, ¹ Prof. (Dr.) T. K. Sengupta²

¹Final Year Student, Electrical Engineering (M.Tech) Department, Asansol Engineering College, West Bengal, India

²Campus Director, Suprem Knowledge Foundation Group of Institution, Mankundu, Hooghly, West Bengal, India

Abstract: In the present work, we focus on the study of dynamic behavior of an interconnected two-area power system and a scheme for improvement of response for the same. Here, two-area system with one non-reheat thermal units & one reheat thermal units is considered. The frequency and tie-line power deviation of two units are studied using MATLAB-SIMULINK in continuous time domain and also in discrete time domain. The paper focus on the study of frequency & tie-line power deviation for step load changes of 1% in both areas with conventional Proportional-Integral control and improvement in dynamic performances while replaced with discrete controller.

Keywords: Automatic Generation Control, Modeling of Interconnected Power system, Dynamic performance study of both the areas, MATLAB – SIMULINK.

I. INTRODUCTION

Now-a-days, modern power systems are divided into number of areas. For example, in our country, eastern grid, western grid etc. and each area are interconnected among themselves through transmission lines, called tie-line.

Interconnected power system or power grid provides following advantages over the control area operated individually,

- i. It stabilizes the grid which in turn increases stability, reliability & security of the overall system.
- ii. Maintaining frequency to a fixed value which reduces voltage collapse & chances of undesirable load-shed situation.

Earlier days, one generating unit in a system would be designed as the regulated unit & it was manually adjusted to Control the balance between the net generation & load demand. But now with automatic Generation system, many units are participated in regulation, improving overall system efficiency & economy.

The main function of power system operation and control is to provide continuous power supply to all consumers connected to it. Automatic Load frequency control (ALFC) or Automatic Generation control (AGC) regulates real power flow between different control areas while keeping frequency constant.

The main features of ALFC loops are

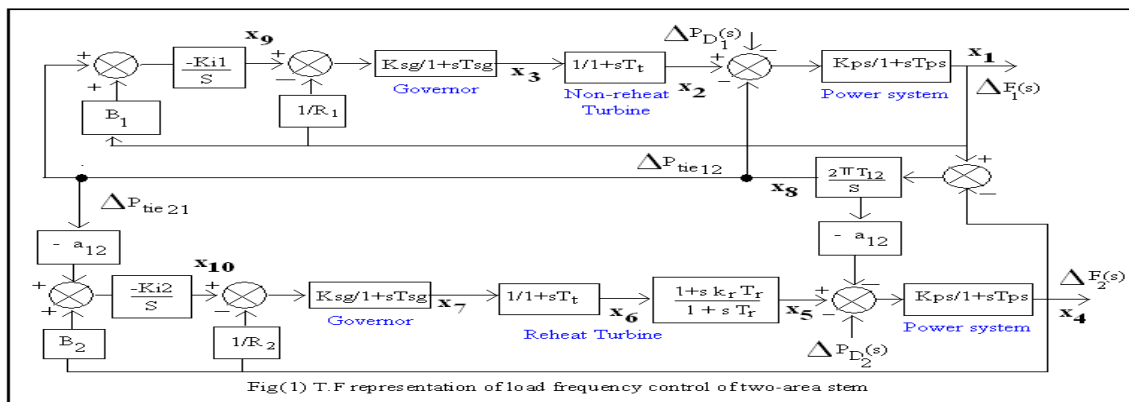
- i. Keeping frequency to its steady state value.
- ii. To control power flow between interconnected control areas.
- iii. Maintain equal load distribution among the participating units.

Tie-line bias is carefully monitored & represented for all tie-lines. Bias is the accepted standard operating constraint that controls the area control error (ACE), monitoring & adjusting tie-line flows to keep the system stable. Stability is the term to describe how far a power grid handles a system disturbances or power system fault.

The main objective of the present work is to perform a comparative study of dynamic response of interconnected power system with reheat & non-reheat type turbines and also an improvement for dynamic performance of inter-connected power system after replacing the PI controller with discrete PI controller.

II. SYSTEM INVESTIGATED

The MW frequency or ALFC system investigated comprises an interconnected power system of two-area (a) non-reheat control area-1 & (b) reheat control area-2, shown in fig:(1). The nominal values of the parameters are given in appendix – 2.



III. MODELING OF DESIRED POWER SYSTEM

The continuous time dynamics behavior of the AGC system is described by the linear vector differential equations

$$\dot{\mathbf{x}} = \mathbf{A} \mathbf{x} + \mathbf{B} \mathbf{u} + \mathbf{G} \mathbf{w} \text{ -----[1]}$$

For formulating the state space model, output of all blocks having either integrator or a time constant assumed to be state variable [7].

State space models of single area system with above assumption of reheat & non-reheat thermal units are given below, respectively

$$\begin{bmatrix} \dot{x}_1 \\ \dot{x}_2 \\ \dot{x}_3 \end{bmatrix} = \begin{bmatrix} -\frac{1}{T_{sg}} & 0 & -\frac{1}{RT_{sg}} \\ \frac{1}{T_t} & -\frac{1}{T_t} & 0 \\ 0 & \frac{K_{ps}}{T_{ps}} & -\frac{1}{T_{ps}} \end{bmatrix} \begin{bmatrix} x_1 \\ x_2 \\ x_3 \end{bmatrix} + \begin{bmatrix} \frac{1}{T_{sg}} \\ 0 \\ 0 \end{bmatrix} \mathbf{u} + \begin{bmatrix} 0 \\ 0 \\ -\frac{K_{ps}}{T_{ps}} \end{bmatrix} \mathbf{w}$$

$$\begin{bmatrix} \dot{x}_1 \\ \dot{x}_2 \\ \dot{x}_3 \\ \dot{x}_4 \end{bmatrix} = \begin{bmatrix} -\frac{1}{T_{ps}} & \frac{K_{ps}}{T_{ps}} & 0 & 0 \\ 0 & -\frac{1}{T_r} & \left(\frac{1}{T_r} - \frac{K_r}{T_t}\right) & \frac{K_r}{T_t} \\ 0 & 0 & -\frac{1}{T_t} & \frac{1}{T_t} \\ -\frac{1}{RT_{sg}} & 0 & 0 & \frac{1}{T_{sg}} \end{bmatrix} \begin{bmatrix} x_1 \\ x_2 \\ x_3 \\ x_4 \end{bmatrix} + \begin{bmatrix} 0 \\ 0 \\ 0 \\ \frac{1}{T_{sg}} \end{bmatrix} \mathbf{u} + \begin{bmatrix} -\frac{K_{ps}}{T_{ps}} \\ 0 \\ 0 \\ 0 \end{bmatrix} \mathbf{w}$$

Whereas, state space model of our concerned interconnected power system is defined as, calculations are given in appendix – 1.

A =

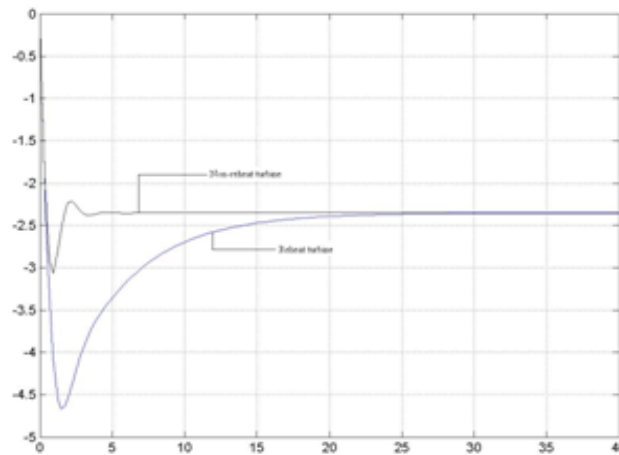
$$\begin{bmatrix} -\frac{1}{T_{ps1}} & \frac{k_{ps1}}{T_{ps1}} & 0 & 0 & 0 & 0 & 0 & -\frac{k_{ps1}}{T_{ps1}} & 0 & 0 \\ 0 & -\frac{1}{T_{r1}} & \frac{1}{T_{r1}} & 0 & 0 & 0 & 0 & 0 & 0 & 0 \\ -\frac{1}{R_1 T_{sg1}} & 0 & -\frac{1}{T_{sg1}} & 0 & 0 & 0 & 0 & 0 & 0 & 0 \\ 0 & 0 & 0 & -\frac{1}{T_{ps2}} & \frac{k_{ps2}}{T_{ps2}} & 0 & 0 & \frac{a_{12} k_{ps2}}{T_{ps2}} & 0 & 0 \\ 0 & 0 & 0 & 0 & -\frac{1}{T_r} \left(\frac{1}{T_r} - \frac{k_r}{T_{t2}}\right) & \frac{k_r}{T_{t2}} & 0 & 0 & 0 & 0 \\ 0 & 0 & 0 & 0 & 0 & -\frac{1}{T_{t2}} & \frac{1}{T_{t2}} & 0 & 0 & 0 \\ 0 & 0 & 0 & -\frac{1}{R_2 T_{sg2}} & 0 & 0 & -\frac{1}{T_{sg2}} & 0 & 0 & 0 \\ 2\pi T_{12} & 0 & 0 & -2\pi T_{12} & 0 & 0 & 0 & 0 & 0 & 0 \\ b_1 & 0 & 0 & 0 & 0 & 0 & 0 & 1 & 0 & 0 \\ 0 & 0 & 0 & b_2 & 0 & 0 & 0 & -a_{12} & 0 & 0 \end{bmatrix}$$

$$\mathbf{B} = \begin{bmatrix} 0 & 0 & \frac{1}{T_{sg1}} & 0 & 0 & 0 & 0 & 0 & 0 & 0 \\ 0 & 0 & 0 & 0 & 0 & 0 & \frac{1}{T_{sg2}} & 0 & 0 & 0 \end{bmatrix}^T$$

$$\mathbf{G} = \begin{bmatrix} -\frac{K_{ps1}}{T_{ps1}} & 0 & 0 & 0 & 0 & 0 & 0 & 0 & 0 & 0 \\ 0 & 0 & 0 & -\frac{K_{ps2}}{T_{ps2}} & 0 & 0 & 0 & 0 & 0 & 0 \end{bmatrix}^T$$

IV. SIMULINK RESULT

Dynamic response of single area system for both reheat & non-reheat type thermal system shown in fig(2).



Fig(2) Dynamic response of single area system

- **Minimization of steady state error:**

It is observed from fig: (2) that the system has pronounced steady state error of $e_{SS} = 51.89\%$ (-ve). There are number of methods available to reduce steady state error, here we used conventional PI-controller, since the implementation of PI-controller is very easy.

Effect of PI-controller to reheat & non-reheat single area system shown in fig: (3).

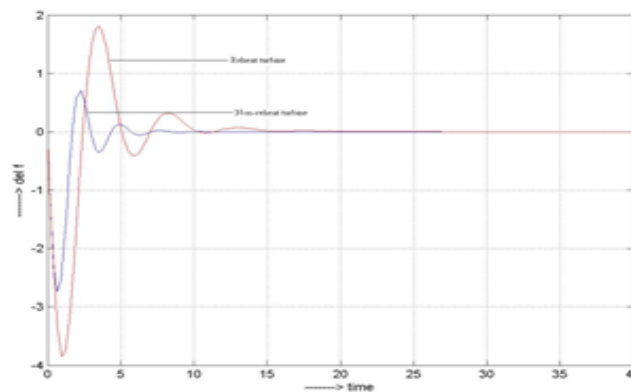


Fig:(3) Dynamic response of single area system with PI-controller

Fig: (4) to fig: (7) depict $\Delta f_1(t)$, $\Delta f_2(t)$, $\Delta P_{tie,12}(t)$ & $\Delta P_{tie,21}(t)$ responses in continuous time domain using SIMULINK.

In the present study, we divided our result into three cases:

Case1: Continuous time domain analysis of interconnected power system without any controller & frequency bias setting.

Case2: Continuous time domain analysis of interconnected power system with PI-controller of $K_i = 0.4$ & frequency bias setting, $B_i = 0$.

Case3: Continuous time domain analysis of interconnected power system with PI-controller of $K_i = 0.4$ & frequency bias setting, $B_i = 0.425$.

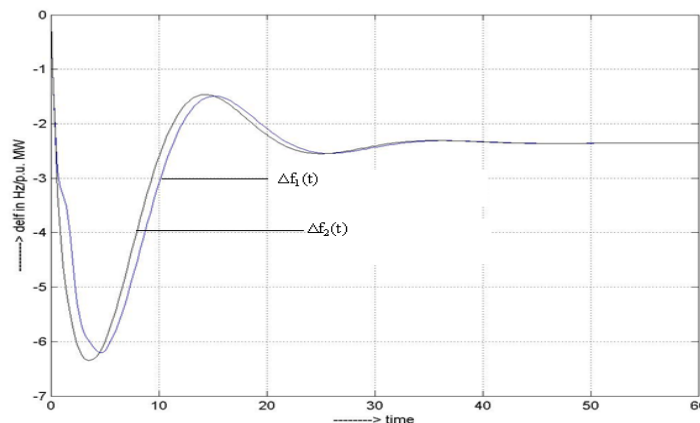


Fig:(4) Frequency deviation of two-area system with $B_i=0$ & $K_i=0$

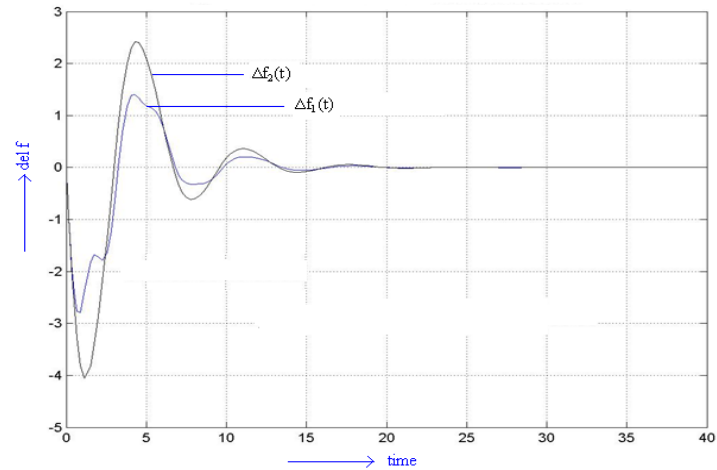


Fig:(5) Frequency deviation of two-area system with $B_i=0$ & $K_i=0.4$

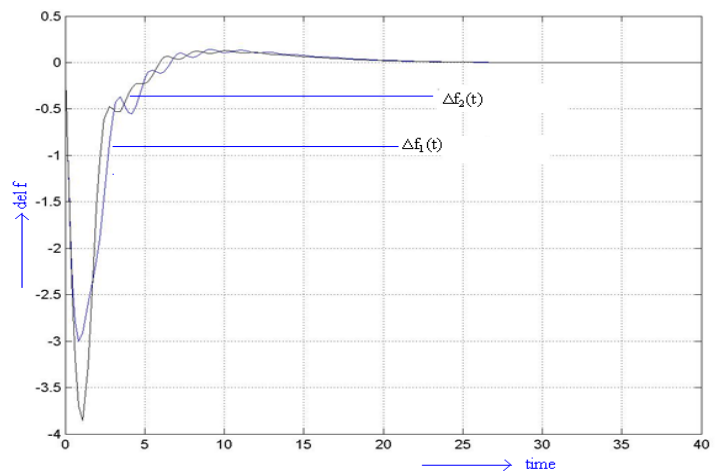
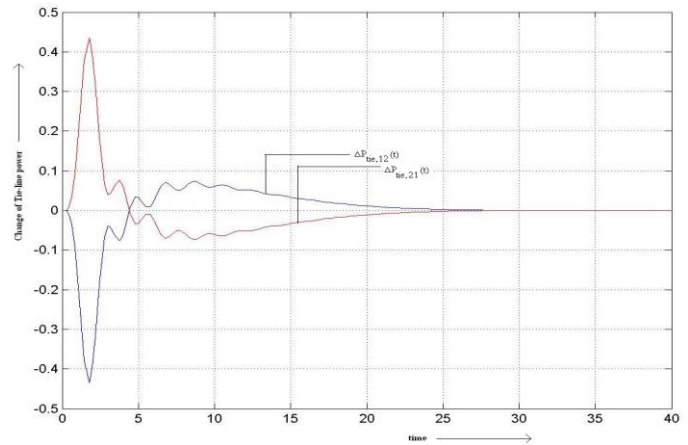


Fig: (6) Frequency deviation of two-area system with $B_i=0.425$ & $K_i=0.4$



Fig(7) Tie-line power deviation of two area system with $B_i = 0.425$ & $K_i = 0.4$

V. OBSERVATION

In this paper, the interconnected two-area power system theory is studied with SIMULINK in continuous domain. The frequency & tie-line power deviation have been observed for the same system.

Following points are observed from the SIMULINK results-

1. Both single area & two-area systems are non-minimum phase system, which exhibits a high undershoot near at the origin, fig.(2).
2. By observation of fig.(2) & fig.(3), the steady state error is reduced using conventional PI-controller but it has no effect on transient response of the system.
3. By observation of fig.(3), settling time of Non – Reheat thermal & Reheat thermal system are, respectively, 7sec & 11sec, approximately, which shows that reheat system has sluggish dynamic response compare to non-reheat system.

4. In comparison to the single area system interconnected power system has less no. of oscillation that make the system more stable, refer to fig.(6).
5. In fig.(5), the system has high peak overshoot which is highly minimized with proper choice of frequency bias constraint, B_i as shown in fig.(6).
6. It is observed from fig.(7) that tie-line power flow deviates from nominal setting, with sudden load changes in both the area and it takes 10-12 sec to settle down.
7. From the investigation carried out in this paper, it is relevant that PI-controller strategy offers ameliorated system dynamic performance compared to P-controller.

VI. DEVELOPMENT / MODIFICATION SUGGESTED

To improve the sluggish response of the reheat cycle area, we suggest the following improvement to be done

1. This paper is completely based on the study of dynamic performance of the system in CT – domain. But if the same study is done in DT – domain, by discretezition of controller signal further improvement of dynamic response is possible. Under figure shows the suggested model

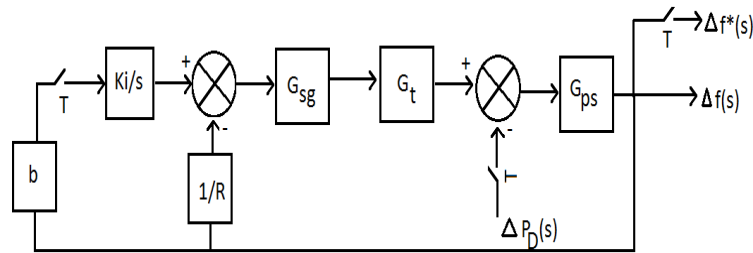


Fig: (8) Proposed block diagram in discrete medium

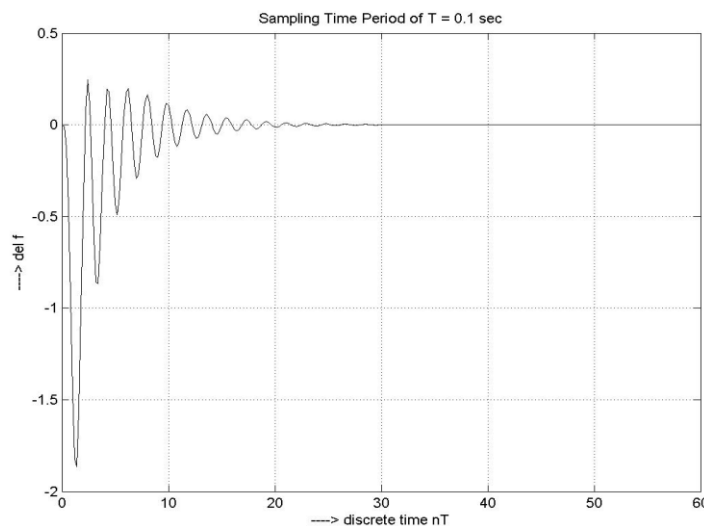


Fig: (9) Frequency deviation of two area system with $B_i = 0.425$ & $K_i = 0.4$ in Discrete domain

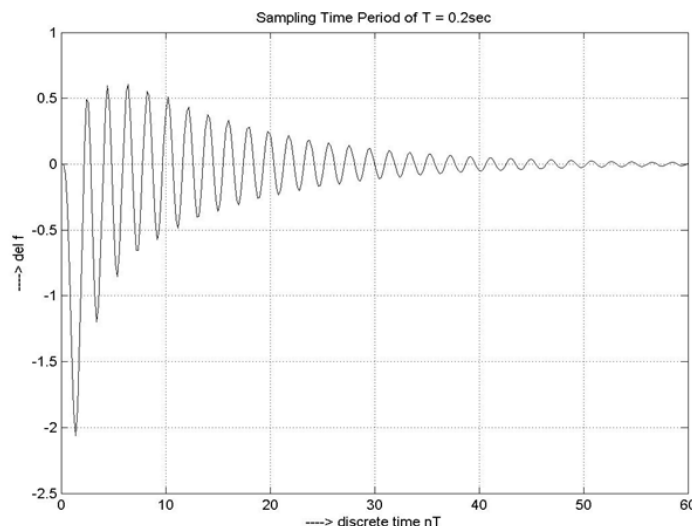


Fig: (10) Frequency deviation of two area system with $B_i = 0.425$ & $K_i = 0.4$ in Discrete domain

Fig: (9) & (10) shows frequency deviation of interconnected power system with two different sampling times. It is observed that if sampling rate is made high then dynamic response analysis gives good result as long as system stability retained.

2. This paper completely focused on the study of conventional PI – controller which exhibits poor dynamic performance due to parameters variation and other controller exhibits poor dynamic response due to parameter variation and other system uncertainties. If, PI – controller replaced by some intelligent controllers, like based on Fuzzy logic theory, optimal controller theory etc, then again further improvement of system response is possible.

VII. CONCLUSION

With the advent of new regulation, (2003 electricity act) distributed & dispersed system generation are recommended and performed for National Power development. One of the main reasons India should be able to achieve a smooth transition from fossil fuel economy to sustainable renewable – energy based economy for sustainable development which compiles

- (i) Energy for all
- (ii) Energy for ever
- (iii) For equitable
- (iv) Environment friendly

If above is available and possible we must have a control area where some units will be having non-reheat turbine (smaller area) and other areas (bigger area) of reheat type. Hence, this paper suggests discretization of the control area for better control of system frequency & tie-line power flow.

Appendix-1

$$x_1 = \frac{K_{ps1}}{1 + sT_{ps1}} (x_2 - x_8 - w_1)$$

$$\Rightarrow x_1 + T_{ps1} \dot{x}_1 = K_{ps1} x_2 - K_{ps1} x_8 - K_{ps1} w_1$$

$$\Rightarrow \dot{x}_1 = \frac{-x_1}{T_{ps1}} + \frac{K_{ps1}}{T_{ps1}} x_2 - \frac{K_{ps1}}{T_{ps1}} x_8 - \frac{K_{ps1}}{T_{ps1}} w_1 \text{-----(1)}$$

$$x_2 = (1/1 + sT_{t1}) x_3$$

$$\Rightarrow x_2 + T_{t1} \dot{x}_2 = x_3$$

$$\Rightarrow \dot{x}_2 = \frac{x_3}{T_{t1}} - \frac{x_2}{T_{t1}} \text{-----(2)}$$

$$x_3 = 1/1 + sT_{sg1} (u_1 - \frac{x_1}{R_1})$$

$$\Rightarrow \dot{x}_3 = \frac{-x_3}{T_{sg1}} - \frac{x_1}{R_1 T_{sg1}} + \frac{u_1}{T_{sg1}} \text{-----(3)}$$

$$x_4 = [K_{ps2}/1 + sT_{ps2}] (x_5 - w_2 + a_{12} x_8)$$

$$\Rightarrow x_4 + T_{ps2} \dot{x}_4 = K_{ps2} (x_5 - K_{ps2} w_2 + a_{12} K_{ps2} x_8)$$

$$\Rightarrow \dot{x}_4 = -x_4/T_{ps2} + (K_{ps2}/T_{ps2}) x_5 - (K_{ps2}/T_{ps2}) w_2 + (a_{12} K_{ps2}/T_{ps2}) x_8 \text{-----(4)}$$

$$x_6 = 1/1 + sT_{t2} x_7$$

$$x_6 + T_{t2} \dot{x}_6 = x_7$$

$$\Rightarrow \dot{x}_6 = x_6/T_{t2} + x_7/T_{t2} \text{-----(6)}$$

$$x_7 = 1/1 + s + T_{sg2} (u_2 - 1/R_2 x_4)$$

$$x_7 + \dot{x}_7 T_{sg2} = (u_2 - 1/R_2 x_4)$$

$$\Rightarrow \dot{x}_7 = -x_7/T_{sg2} + u_2/T_{sg2} - 1/T_{sg2} R_2 x_4 \text{-----(7)}$$

$$x_8 = \frac{2\pi T_{12}}{s} (x_1 - x_4)$$

$$\Rightarrow \dot{x}_8 = 2\pi T_{12} (x_1 - x_4) \text{-----(8)}$$

$$\dot{x}_9 = b_1 x_1 + x_8 \text{-----(9)}$$

$$\dot{x}_{10} = b_2 x_4 - a_{12} x_8 \text{-----(10)}$$

Appendix-2

Numerical data -

Sl. No.	Notations	Full name	Numerical value
1	i	Subscript referring to area i (i=1,2)	-
2	P_{r_i}	Rating of i-th generator in MW	2000
3	T_t (or T_{CH})	Turbine time constant in sec	0.3 sec
4	T_{sg}	Time constant speed governor in sec	0.08 sec
5	K_{PS}, T_{PS}	Time constant & gain of power system, respectively	120, 20 sec respectively
6	K_r, T_r	Reheat coefficient & time constant, respectively	0.5, 10 sec respectively
7	T_{12}	Synchronizing coefficient	$\frac{0.545}{2\pi}$
8	R_i	Governor speed regulation parameter in Hz per p.u. MW	$\frac{1}{2.4}$
9	ΔP_{tie}	Incremental change in tie-line power	-
10	ΔF_i	Incremental change in frequency deviation	-
11	ΔP_{Di}	Incremental change in load demand	-
12	ΔP_{Ci}	Incremental change in speed governor position	-
13	ΔY_{Ei}	Incremental change in valve position	-
14	D	Load frequency constant in p.u MW per Hz ($\delta P_D/\delta f$)	-
15	B_i	Frequency bias constant	0.425
16	δ	Nominal phase angle of voltages ($\delta_{12} = \delta_1 - \delta_2$)	-
17	K_{ii}	Integration time constant	0.4

References

- [1] Prof J Nanda, Dr. M L Kothari, "Sample data AGC of Hydro-Thermal system considering GRC", IEEE-trans., September 25, 1989
- [2] Prof. C S Indulkar, "Analysis of MW frequency control problem using sampled data theory", IEEE trans., January 1, 1992.
- [3] Prof. Prabhat Kumar, Ibraheem, "Dynamic performance evaluation of 2-area interconnected power system – a comparative study", IEEE-trans, August 14, 1996.
- [4] Dr. T.K.Sengupta, "Studies on assessment of power frequency in interconnected grid – its computer based control & protection", 2008, thesis paper in JU.
- [5] Eiegerd, O.I., "Electric energy system theory – an introduction", second edition, Tata McGraw Hill.
- [6] Grainger, J, William, J & Stevenson, Jr - "Power system analysis" edition 2003, Tata McGraw Hill.
- [7] Kothari, D.P, & Nagrath, I.J., "Power system Engineering", second edition, Tata McGraw Hill.

Information Communication Technology: Practices for Academia

Sajad Mohammad Khan,¹ Muheet Ahmed Butt,² Majid Zaman Baba³

^{1,2}(Scientist, PG Department of Computer Sciences, University of Kashmir, J&K, India

³(Scientist, Directorate of IT and SS, University of Kashmir, J&K, India

ABSTRACT: The digital revolution driving societal change is as significant as the invention of the printing press or the Industrial Revolution. Since the introduction of the transistor and the integrated circuit, people have not just been doing things differently; they have been doing vastly different things. The development of a healthy educational system which meets the objectives effectively poses many challenges. The high growth in education is increasing the demand for flexible and innovative approaches to learning in which information technology can play a crucial role. In an educational system “teaching” and “learning” are the two major activities besides “assessment” which is a coordinating activity. The Information Communication Technology (ICT) has a potential to transform the different areas of the educational system. In this paper our focus is on identifying the challenges prevailing in our educational system and proposing the role of Information Communication Technology in its successful implementation. This paper also provides some recommendations which could be used as a catalyst for promotion of information communication technology services in higher education.

Keywords: ICT, Teaching, Learning, Simulation, Education, Assessment

I. INTRODUCTION

Although information technology is not a panacea for all of the shortfalls associated with our educational system, it offers the potential not only for significantly enhancing learning for all learners, but also for transforming the way we learn [4]. In an educational system ultimately two fundamental activities are carried out in the form of teaching and learning. These activities involve huge resources of both state as well as public with the ultimate objective of effective deliverance. The role of the assessment system in the environment is to co-ordinate the teaching and learning activities and evaluates the system performance.

The main objectives of an educational system; however its functional domain also includes services which it has to offer to its constituent elements [3]. Therefore broadly speaking the following are the activities in an educational system:

- a) Teaching
- b) Learning
- c) Assessment and
- d) Other Services

The conventional system of education particularly its assessment system is extremely stressed and has virtually limited its functioning to the conduct of examinations and declaration of results. This has significantly affected the performance of the entire system. Presently it is found that the role of ICT in the educational sector is mostly limited to deliverance of services besides few more activities whereas the challenges are manifold although the advances in information and communication technologies have the potential to enhance lifelong learning [2].

These technologies can be used to address the changing demands within the sector:

- for more flexible learning;
- for extension of educational services to national and international markets; and
- For more cost-effective delivery of education and related services in an increasingly competitive environment.

II. SYSTEM CHALLENGES

The four different areas of activities identified above are in state of extreme dynamics and the conventional system is unable to cope up the challenges associated with new opportunities and developments. Some of the main challenges in each of the activities of an educational system are as follows:

2.1 Teaching: The Challenges with the teaching include:

- 2.1.1 To plan the lecture in a highly efficient manner such that both teacher and learner participation become mandatory.
- 2.1.2 To provide an suitable environment for efficient transformation and dissemination of vital information
- 2.1.3 To encourage the student community with the concept of “learn by doing.”
- 2.1.4 Making the most of the talents of the students, irrespective of their physical and mental disabilities.

2.2 Learning: The learning scenario is also in state of extreme dynamics and some of the main challenges associated with it are as under:

- 2.2.1 Providing information and knowledge anywhere, anytime, anyway and anyhow.
- 2.2.2 Allow more flexible access to education reducing barriers of time and place of study.
- 2.2.3 Acquire new skills in a way that is compelling and engaging.
- 2.2.4 Participate in networked and face-to-face communities of learners composed of teachers, mentors, domain experts, and “cognitive” tutors that collectively approach the effectiveness of a one-on-one human tutor.

- 2.2.5 Using simulation for problem solving approaches.
- 2.2.6 Barrier of languages is made irrelevant

2.3 Assessment: The deliverance of any education system is largely dependent on its system of examination (assessment). The development of an assessment system which meets its prime objectives of achieving desired validity and reliability is a real challenge at global level. Some of the challenges in an assessment system are:

- 2.3.1 Continuous Assessment Process
- 2.3.2 Design the Assessment System in such a way to achieve the desired Validity, Reliability and Transparency.
- 2.3.3 Receive continuous and meaningful feedback of assessment.
- 2.3.4 Make it comprehensive enough to explore the potential of the candidates.
- 2.3.5 Make it healthy enough to develop higher order skills of comprehension in students.
- 2.3.6 Make it a student friendly exercise for every topic covered.
- 2.3.7 Develop it as an integral part of the education system to co-ordinate the teaching & learning process.
- 2.3.8 Design it in such a way which forces comprehensive reading.

2.4 Other Services: The deliverance of services has been an essential element of an educational system. In order to make the system efficient in all spheres the services have to be provided to all its users. Following are some of the main challenges in services:

- 2.4.1 Tap into rich, universally accessible digital libraries with books, articles, material, and data sets.
- 2.4.2 Dynamic administration and its record and exchange information
- 2.4.3 Develop information systems which support all the users of the system for their necessities.
- 2.4.4 Provide services which ensure delivery of information anytime and anywhere at affordable costs.

III. SCOPE FOR ICT

The advancement in the computer programming has reached a level wherein backed up by the massive databases artificial intelligence is incorporated in the systems. The Research Challenge is to provide learning environments that approach the characteristics as listed above [3]. Such systems, properly used, can produce a significantly better-educated populace by combining advances in learning sciences for human resource development with advances in information technology. The task of developing the desired system involves a number of technical challenges in the following distinct, but interrelated, areas:

3.1 Cognitive tutors

The development of a perfect human tutor involves significant resources in terms of both time as well as wealth. The development of a machine based tutor with the present level of computer programming has become a reality - the scope for. It has been observed that it is possible for an automated tutor to improve student performance by roughly one standard deviation from the mean for some high school mathematics students. This is a dramatic result. One reason that such tutors are not widely available is because significant human effort is required to develop the specialized knowledge base for each different subject. In addition, we do not understand fully the conditions under which such a tutor will be effective.

Significant progress must be made in crafting knowledge representations that are both interoperable and reusable we need to develop models of the various styles in which a student learns, as well as appropriate pedagogies and assessment techniques.

The knowledge representations that underline such tutors should also be designed to incorporate new knowledge about a subject area, as well as advances in knowledge and techniques associated with both pedagogy and assessment.

3.2 Simulation-based teaching

Multimedia has assumed great significance in teaching and learning. It has a tremendous scope for both teaching as well learning even in the most complex systems. An important genre for next-generation educational software, particularly for training scientists, mathematicians, engineers, and technologists, is what might be called a clip model. By loose analogy to the well known galleries of copy-and-paste 2-D clip art, a clip model is an interactive micro-world, typically simulation- or rule-based, that expresses both geometry and behavior of the modeled entity or concept. It is a self-contained object ready to be embedded in a context such as a hypermedia learning module. First, they are designed to be combined to form larger models, for example, a heart model may be connected to a vascular system model and to a lung model to create a composite model that simulates respiration and oxygenation of the blood as it is distributed throughout the body. Second, no single model suffices for all learning purposes. Perhaps dozens, if not hundreds, of heart models are needed to meet the needs of learners at different levels of understanding and with different kinds of backgrounds and learning styles.

3.3 General purpose Online Assessment System

It has been observed that almost all the areas of the assessment system require major reforms to make it as an effective part of the educational system. The Information Communication Technology has a tremendous scope for use in many operations in an Examination System besides the compilation of results and other student based services. In fact most of the organizations have already switched over to computerized system of compilation of results and even Management Information system supporting the Management in running the system efficiently are already available. Similarly students related information system providing relevant information to the students also exists in Organizations but these support

systems do not strengthen the basic design issues and the objectives of the assessment system. In our opinion support solutions are required to be developed for all key entities (teachers, students, examination body) involved in the system.

Similarly activities like question paper setting, evaluation, conduct of exam etc require to be supported by the technology to ensure development of quality assessment system.

One of the essential components of the teaching learning process is encouraging and creating the system of self studies among the students. In this context teachers have been traditionally giving assignments to the students and it serves the purpose only once each student is given a different assignment and assessed once it is submitted. With the increase in the number of students, assigning different assignments to students and then evaluating each of them is an issue. This unit of the system requires to be modernized by the support of the technology. In this regard we propose that the development of an E-assignment system which shall assign different assignment to each of the student and assess them automatically for their assignment on some other scheduled day without adding any additional burden to the teacher.

3.4 Learning in context/just-in-time learning

It is critical that each individual learner be able to learn in the physical, social, cultural, and virtual context most appropriate to that learner. In addition, the learner may have a much focused objective for a particular learning session. Just-in-time learning over such a broad range of contexts presents a number of technical challenges, including the support of reliable and ubiquitous computing, access and control of remote instruments, flexible digital object sharing, and user interfaces for small-format mobile devices. The automated teacher must tailor delivered information to fit that context and the goals of the just-in-time learner.

IV. RECOMMENDATIONS OF ICT IN HIGHER EDUCATION

The various recommendations for which have been proposed for using ICT practices in the field of education are given below

- ✓ Reliable Internet Connectivity is needed to facilitate the students with ICT benefit and ensure its upkeep.
- ✓ Accessibility to the ICT facilities by providing hardware/ software in the form of laptops, desktop, PDA's and other allied devices.
- ✓ Virtual/ Smart Class rooms need to be established in all Higher Educational Institutions.
- ✓ Availability of Competent Human Capital with relevant skill sets.
- ✓ ICT must be integrated with curriculum to make it competitive and bring it in tune with contemporary requirements.
- ✓ Allocation of funds by the Government for developing infrastructure and required human resources in various fields of ICT.
- ✓ People with special needs must have access to ICT facilities as per their special needs.
- ✓ ICT would lead to e-learning which would result in having anytime and anywhere access to learning to make it student driven.
- ✓ Capacity building measures should be formulated on need based system for various stake holders to sharpen the existing skills and competencies of existing manpower to perform their job descriptions effectively and efficiently.
- ✓ Periodic general awareness, training and developmental programs be conducted for various levels of employees at Government as well as private sector irrespective of their size/nature of ownership and control.
- ✓ Refresher/ Orientation courses must be regularly conducted for all the stake holders who are involved in imparting training and knowledge in the area of ICT.
- ✓ The services of the subject experts with proven track records must be utilized in preparing e-content that will be available to the masses.
- ✓ State of the art repositories must be in place in institutions of Higher Learning so that content is available on demand.
- ✓ Possibilities of having public/private partnership must be explored for achieving the objectives of ICT.

V. CONCLUSION

The education plays a key role within society in the process of social change and therefore the target in the societies has changed to a mass system of education. Our vision of teachers and learners immersed in a network of rich learning objects that are continually enriched and enhanced by the participants is achievable through anticipated advances in information technology and learning sciences. As a result of these efforts, we will be closer to achieving such goals as having transformed the country into a knowledge society. These new benefits will be facilitated by geometric advances in semiconductor and magnetic storage, as well as in electronic and optical communications. The international education and training market is a highly competitive industry. Education providers are increasingly investing in innovative and sophisticated marketing. The use of communications and information technologies in education development and delivery is vital if our educational institutions are to achieve competitive success in the international market for higher and professional education.

VI. REFERENCES

- [1] MEHARI, Information risk analysis and management methodology, V3, Concepts and Mechanisms, CLUSIF, October 2004.
- [2] Alexander, S. Teaching and Learning on the World Wide Web, Paper presented at AusWeb95, the first Australian World Wide Web Conference.
- [3] Mehraj ud Din Dar, Muheet Ahmed Butt, Majid Zaman Baba, "Challenges in Educational System: Scope for E-Support", J & K Science Congress University of Kashmir. 25-27 July, 2006
- [4] Austin, P. & Vaughan, C. 1997, Edith Cowan University Web Enrolment System ECUWES, Paper presented at AusWeb97, the Third Australian World Wide Web Conference, 5-9 July 1997.
- [5] William Aspray, Mary J. Irwin "Grand Research Challenges", June 2002, Airlie House in Virginia.
- [6] Battacharya & Saxena, "Information Security" World Comp 2007, June 25-28, 2007, Las Vegas, Nevada, USA, ISBN1-60132-046-9.

Design and Implementation of HDLC Controller by Using Crc-16

Gaurav Chandil¹, Priyanka Mishra²

^{1,2}(Department of Electronics and Communication Engineering, United Group of Institutions, Allahabad, India)

ABSTRACT: HDLC controller megacell is a high performance module for the bit oriented, switched, non-switched packet transmission module. The controller fulfills the specifications according to ITU q.921, X.25 level 2 recommendations. It supports half duplex and full duplex communication lines, point-to-point and multipoint channels. Furthermore, the controller is designed to permit synchronous, code transparent data transmission. The control information is always in the same position and specific bit patterns used for control differ dramatically from those representing data that reduces the chances of errors. The data stream and transmission rate is controlled by the network node. In this paper, we have designed, simulated and implemented HDLC controller. This design is coded in a hardware description language (VHDL). The function of coded design is to simulate on simulation software (e.g. modelsim). After simulation, the design is synthesized and translated into a structural architecture, in terms of the components on the target FPGA device (Spartan 3) and perform the post-translate simulation in order to ensure the proper functioning of the design after translation. After the successful simulation of the post-translate model, the design is mapped to the existing slices of the FPGA and the post-map model simulated. The post-map model does not include the routing delays. The objective of this paper is to run the programmed FPGA at frequency i.e. it Operates up to 155.52 Mbits/s data rates. In this paper, we implemented the various HDLC controllers for 16-bit address, 8 bit data and 16 bit CRC Check, simulation result for final output at the receiver end for 8-bit data 16-bit address and 16-bit CRC, with bit stuffing and removal of error in HDLC.

Keywords: High Level Data Link Control (HDLC) Controller, Frame Check Sequence (FCS), Cyclic Redundancy Check (CRC), Synchronous Data Link Control (SDLC).

I. INTRODUCTION

HDLC (High-level Data Link Control) is a group of protocols for transmitting synchronous data packets between point to point nodes. In this controller, data is organized into frames. HDLC protocol resides with Layer 2 of the OSI model, the data link layer. It make use of zero insertion/deletion process (bit stuffing) to ensure that the bit pattern of the delimiter flag does not occur in the fields between flags. The HDLC frame is synchronous and therefore relies on the physical layer to provide method of clocking and synchronizing the transmission and reception of frames paper.

HDLC controller is one of the most important data link control protocols which are widely used for high performance. It is the basis for many other important data link control protocols, such as LAPB, LAPD and PPP, which use the same or similar formats and the same mechanisms employed in HDLC[2] (William Stallings, 2007). Some key applications of this protocol include frame relay switches, error correction in modems, packet data switches and data link controllers [3] (Amit Dhir, 2000).

For high speed hardware implementation of new technologies and innovative thoughts in order to check their validity and possible advantage is possible by using modern field programmable gates such as the digital FPGAs and the analog FPAA's. Many researchers have attempted to improve existing designs of various types of data processors using FPGA implementation. The HDLC controller presented in this paper offers high frequency. The signals of our controllers are compatible with ITU q.921.X.25 level 2 recommendation. It supports point to point, multipoint and half and full duplex communication channels. HDLC controller is designed to permit both synchronous and code transparent data transmission this control information reduces the possibility of errors. In this paper, we have designed, simulated and implemented HDLC controller. This presented design is coded in a hardware description language (VHDL).the design is then synthesized and translated into a structural architecture, in terms of the components on the target FPGA device (Spartan 3) and perform the post-translate simulation in order to ensure the proper functioning of the design after translation. After the post-translate model simulation, the design is mapped to the existing slices of the FPGA and the post-map model simulated. We implemented the various HDLC controllers for 16-bit address, 8 bit data and 16 bit CRC Check, simulation result for final output at the receiver end for 8-bit data 16-bit address and 16-bit CRC, with bit stuffing and removal of error in HDLC. The main objective of this paper is to run the programmed FPGA at available resources of the target technology efficiently with high. Our design is flexible, so it is easily modifiable and also it is possible to integrate it with other systems.

The remainder of this paper is organized as follows: section II describes briefly HDLC frame format. Section III discusses the system of implemented HDLC controller. Implementation of system on Virtex target is described in section IV. A comparison of the proposed HDLC controller with some well-known HDLC controllers is presented in section V.

II. SYSTEM MODEL FOR HDLC PROTOCOL

The CDAC HDLC Protocol Core is a high performance module for the bit oriented packet transmission mode. It is suitable for Frame- Relay; X.25, ISDN B-Channel and D-channel. The core fulfills the specification According to ITU Q.921, X.25 Level 2 recommendation. The data interface is 8 bit wide synchronous and is suitable for interfacing to transmit and receive FIFOs. An example of an HDLC frame structure is shown below, for an 8-bit address field with an interframe fill

pattern of back-to-back flags. This figure does not include bits inserted for transparency. The fields are transmitted in order from left to right, least significant bit first.

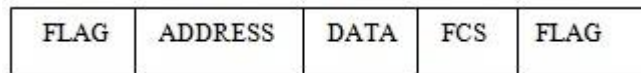


Fig.1.HDLC frame format

Transparency is performed by the core on all bits between and including the address and the FCS. This operation involves inserting a zero after any sequence of 5 consecutive ones in the transmitted data stream (including the last five bits of the FCS). The receiver core detects and removes these inserted zero bits. At any time, the transmission of a frame can be aborted by sending the Abort flag, which are 01111111. An aborted frame will be marked as such by the receiver core. Additionally the channel can be set to an inactive or "Idle" state, where a continuous sequence of one bits is transmitted.

Each frame begins and ends with a Flag Sequence, which is the binary sequence 01111110 (hexadecimal 0x7e). All implementations continuously check for this flag, which is used for frame synchronization. Only one Flag Sequence is required between two frames. Two consecutive Flag Sequences constitute an empty frame, which is silently discarded, and not counted as a FCS error. The Address field is of programmable size, a single octet or a pair of octets. The field can contain the value programmed into the Transmit Address Register at the time the frame is started. This can be any arbitrary address, or the broadcast or "All-Stations" address, which are all ones. The receiver core matches the received address field against the value currently held in the Receive Address Register, or, if programmed to, the broadcast address. Frames with unrecognized addresses are silently discarded. The data field may contain any number of bits. There is no limit within the core to the maximum size of the data field. Data octets are reassembled by the core and presented to the host interface with a suitable byte strobe. Any extra bits in the last received octet which do not correspond to receive data bits are undefined. The Frame Check Sequence field is programmable to either 16 bits (two octets), or 32 bits (four octets). The FCS is transmitted least significant octet first, which contains the coefficient of the highest term in the generated check polynomial. The FCS field is calculated over all bits of the Address, Control, and data fields, not including any bits inserted for transparency. This also does not include the Flag Sequences nor the FCS field itself. The data stream presented to the host can be configured to either include the address field, or have it removed. FCS octets are always removed from the stream to the host. Higher-level protocols such as LAPD, LAPP or PPP will define values for sub fields within the data field. The end of the data field is found by locating the closing Flag Sequence and removing the Frame Check Sequence field. Frames where the received FCS and calculated FCS indicate that the data has been corrupted during transmission will be marked by the core at the time that the end of the frame is signaled to the host. To guarantee that a flag does not appear inadvertently anywhere else in the frame, HDLC uses a process called bit stuffing. Every time the user wants to send a bit sequence having more than 5 consecutive 1s, it inserts (stuffs) one redundant 0 after the fifth 1. For example, the sequence 0111111111000 becomes 01111101111000. This extra zero is inserted regardless of whether the sixth bit is another one or not. Its presence tells the receiver that the current sequence is not a flag. Once the receiver has seen the stuffed 0, it is dropped from the data and the original stream is restored.

III. DESIGN AND IMPLEMENTATION OF HDLC CONTROLLER

Figure 3.2 shows the basic operation of HDLC controller. The Transmit Data Interface provides a byte wide interface between the transmission host and the HDLC Protocol core. Transmit data is loaded into the core on the rising edge of clk when the write strobe input asserted. The start and end bytes of a transmitted HDLC frame are indicated by asserting the appropriate signals with the same timing as the data bytes. The HDLC cores, on receipt of the first byte of a new packet, generate the appropriate flag sequence and transmit the frame data calculating the FCS. When the last byte of the frame is seen, the FCS is transmitted along the closing flag. Extra zeroes are inserted into the Bit stream to avoid transmission of the control flag sequence within the frame data. The transmit data is available on the TxD pin with appropriate setup to be sampled by clk. If TxEN is reasserted, the transmit pipeline is stalled, and the TxD pin is tristated. A transmit control register is provided which can enable or disable the channel, select transparent mode where the HDLC protocol is disabled, and specify the HDLC core action on transmit FIFO under runs. In addition, it is possible to force the transmission of the HDLC Abort sequence. This will cause the currently transmitted frame to be discarded. The transmit core can be configured to automatically restart after an abort, with the next frame, or to remain stilled until the host microprocessor cleared the abort or transmit FIFO under run condition. The various blocks of the transmitter section are-

- Transmit register-It is an 8 bit long register that contains the data to be transmitted.
- Address insertion block- This block contains the address of the destination, which can be either of 8 bits or 16 bits.
- FCS generation block- FCS is performed for detecting errors in the received data by grouping the bytes of data into a block and calculating a Cyclic Redundancy Check (CRC).

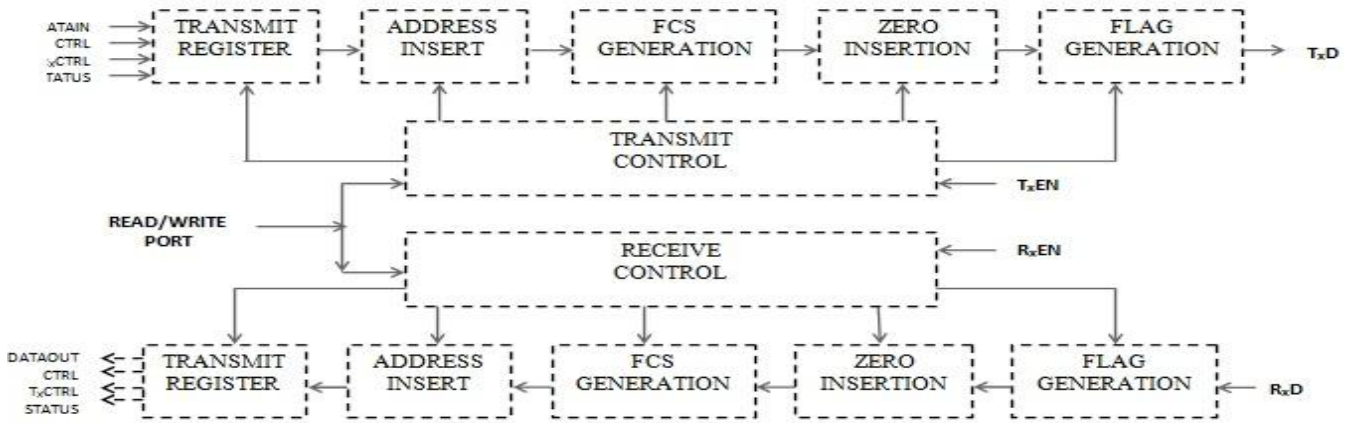


Fig.3.2. Basic block diagram of HDLC Controller

The CRC is calculated by performing a modulo 2 division of the data by a generator polynomial and recording the remainder after division as shown in figure 3.3. A string of 0s is appended to the data unit. The number n is less than the number of data of bits in the predetermined divisor, which is n+ 1 bit. CRC replaces n 0 bits derived in step 2 at the end of data unit. Data unit arrives at the receiver data first, followed by CRC. The receiver treats the whole string as a data unit and divides by the same divisor. If remainder comes out to be 0 the string is error free. The newly elongated is divided is divided by the divisor. The remainder is the CRC. Three polynomials are in common use they are:

- CRC-16 = $x^{16} + x^{15} + x^2 + 1$ (used in HDLC).
- CRC-CCITT = $x^{16} + x^{12} + x^5 + 1$ (used in Ethernet).

Although this division may be performed in software, it is basically performed using a shift register and X-OR gates. The hardware solution for implementing a CRC is much simpler than a software approach.

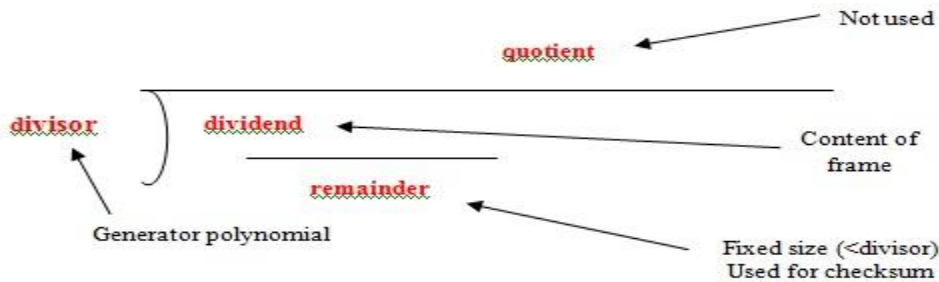


Fig.3.3. Modular division

An example for a CRC-16 is illustrated in figure3.4. Basic Encoder/Decoder for a 16-bit CRC is shown with change in polynomial to a divisor of size N+1 followed by shift register of size N these registers are aligned with the divisor so that the cells are located between the bits. XOR gate are situated where there is a 1 in the divisor except for the leftmost bit. Eventually, a feedback connection is made from the leftmost bit to the XORs.

Protocols at the network layer and higher (e.g. IP, UDP, TCP) usually the processing has not corrupted use a simpler checksum to verify that the data being transported performed by the nodes in the network.

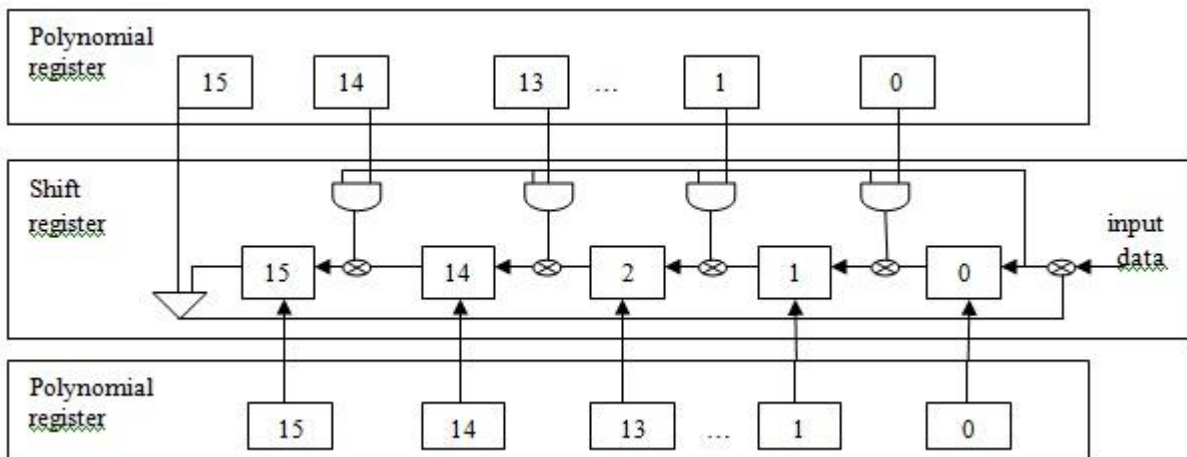


Fig.3.4 Basic block diagram of CRC16

- Zero insertion block- A bit sequence having more than 5 consecutive 1s, this block inserts (stuffs) one redundant 0 after the fifth 1.
- Flag generation block- To inform the receiving station that a new packet is arriving; a specific bit pattern 01111110 is affixed in the beginning.
- Transmit control register- This register controls the flow of data from transmitter to receiver.

Receiver section-The HDLC protocol core receiver accepts a bit stream. The flag detection block searches the bit stream for the flag sequence in order to determine the frame boundaries. Any stuffed zeroes are detected and removed by the zero deletion blocks and the FCS is calculated and checked by the FCS-16 or FCS-32 block depending on the control register word. The bit stream is accepted on port RxD. The data is latched on the rising edge of clk under the control of the enable input RxEN. The flag detection block stream for the flag sequence in order to determine the frame boundaries. Any stuffed zeroes are detected and removed and the FCS is calculated and checked. Frame data is placed on the receiver data interface and made available to the host. In addition, flag information is passed over indicating the start and end bytes of the HDLC frame as well as showing any error condition which may have been detected during receipt of the frame.

The receiver can be configured into transparent mode, effectively disabling the HDLC protocol functions. In normal HDLC protocol mode, all received frames are presented to the host on the output register[6]. A status register is provided which can be used to monitor the status of the receiver channel, and indicates if the packet currently being received includes any errors. The various blocks in this section are:

- Flag detection block- It checks for the incoming flag.
- Zero deletion block- This block deletes the stuffed zeroes which were introduced during transmission.
- FCS calculator- Calculate the FCS and if the remainder comes out to be zero that represents error free transmission.

This block performs the reverse function of the FCS generator. The whole packet is again divided by the same polynomial that was used at the transmitter end i.e.

$$\text{CRC-16} = x^{16} + x^{15} + x^2 + 1$$

$$\text{CRC-32} = x^{32} + x^{26} + x^{23} + x^{22} + x^{16} + x^{12} + x^{11} + x^{10} + x^8 + x^7 + x^5 + x^4 + x^2 + x + 1$$

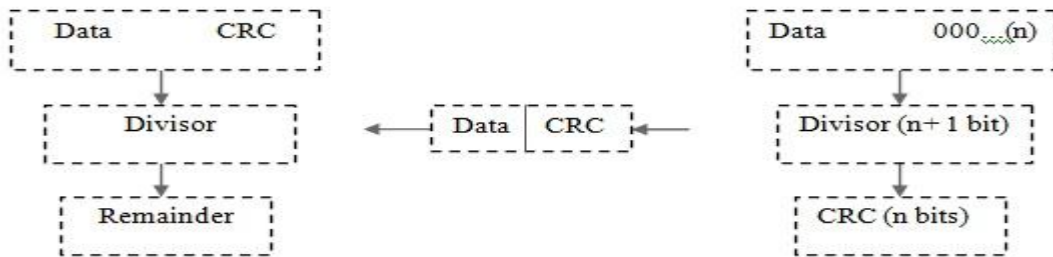


Fig.3.5 Basic block diagram of CRC16

If after the packet with the polynomial the remainder comes out to be zero that means the transmission and reception are error free and in case the remainder is not zero that means an error has occurred during the process and hence the packet is discarded and the whole packet is retransmitted.

1. Data unit arrives at the receiver data first, followed by CRC. The receiver treats the whole string as a data unit and divides by the same divisor.

2. If remainder comes out to be 0 the string is error free and is accepted but if the remainder comes out to be other than 0, it is assumed that it contains an error and the whole frame is discarded and is retransmitted.

- Address detector- It detects the address and matched with the address of the destination.
- Receive register- It contains the original 8 bit data sent by the receiver.

IV. SIMULATION RESULTS

The design and implementation of the HDLC Controller, the results obtained are as follows:

VHDL CODE FOR HDLC Controller

Title:HDLC components package for HDLC controller

File:hdlc_components_pkg.vhd

Simulators:Modelsim 5.3XE/Windows98

Dependency: ieee.std_logic_1164

----- CODE FOR CRC-16 GENERATION -----

Library IEEE;

Use IEEE.STD_LOGIC_1164.ALL;

Use IEEE.STD_LOGIC_ARITH.ALL;

Use IEEE.STD_LOGIC_UNSIGNED.ALL;

Uncomment the following library declaration if instantiating any Xilinx primitives in this code.

--library UNISIM;

--use UNISIM.VComponents.all;

```

entity hdlc is
port (clk,reset, wrtxaddrhi,wrtxaddrlo,wrtxctrl:in std_logic;
datain:in std_logic_vector(7 downto 0);
txaddressout:out std_logic_vector(15 downto 0);
txd:out std_logic;
txaddressin1,txaddressin2,txctrlreg:instd_logic_vector(7 downto 0));
end hdlc;
-----CRC 16 generation-----
a2:process(clk,done,crcappreg)
variable count:std_logic_vector(5 downto 0):="000000";
begin
-----CRC 16 for 16 bit address-----
if(ctrlreg(4)='0')then
    if(ctrlreg(3)='1')then
        .
        .
        count:=count+"000001";
        count15<=count;
        crc(0)<=s1;
        .
        .
        crc(15)<=s3;
        .
        .
    end if;
    else
    if(clk'event and clk='0')then
        .
        .
        count16<=count;
        crc(0)<=s1;
        .
        .
        crc(15)<=s3;
        .
        .
    end if;
    end if;
    if(ctrlreg(3)='1') then
        .
        .
    end if;
    else
    if(count="100010")then
        .
        .
    end if;
end process a2;

```

SIMULATION RESULT FOR 16-BIT ADDRESS,8-BIT DATA AND 16-BIT CRC CHECK: For the data<=00110011 and 16bitaddress i.e. txaddressinlo<=11110000, txaddressinhi<=11110000, we make clock=1,reset=0, wrtxaddresshi=1 and wrtxaddresslo=1. After the address and the data are attached together, we divide them with a constant polynomial of 16 bits and append the remainder of the division along the data and address.The simulation result for the generation of CRC 1 is illustrated in figure.3.6.

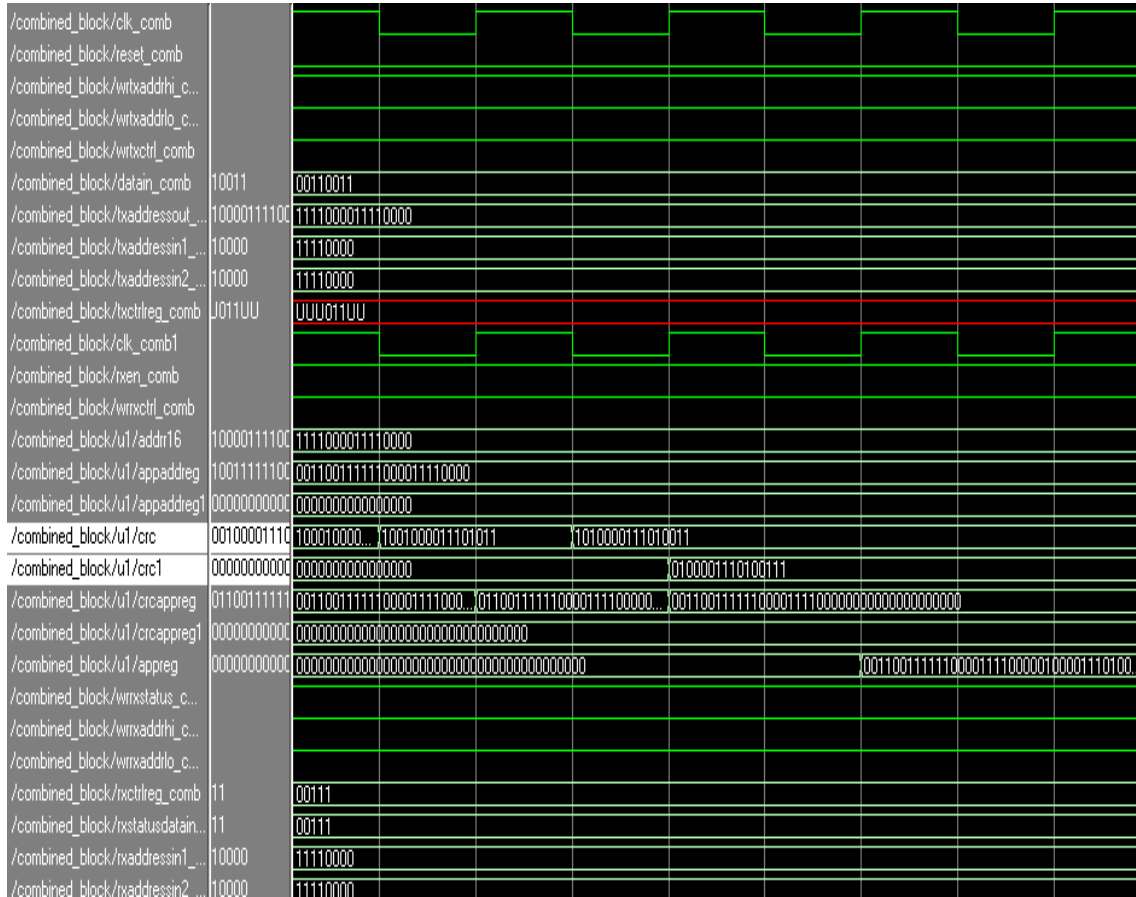


Fig.3.6: Simulation result for crc-16 of 16-bit address and 8 bit data

SIMULATION RESULT OF THE FINAL OUTPUT AT THE RECEIVER END FOR 8-BIT DATA,16-BIT ADDRESS AND 16 BIT CRC:The highlighted simulation results shown in figure 3.7 shows the result of the CRC check at the O/P which is CRC2<=0000000000000000 which indicates an error free transmission.The resultant address, data at the O/P which is same as that of transmitter is Rxdatout<=00001110 , rxaddressout<=1111000011110000.

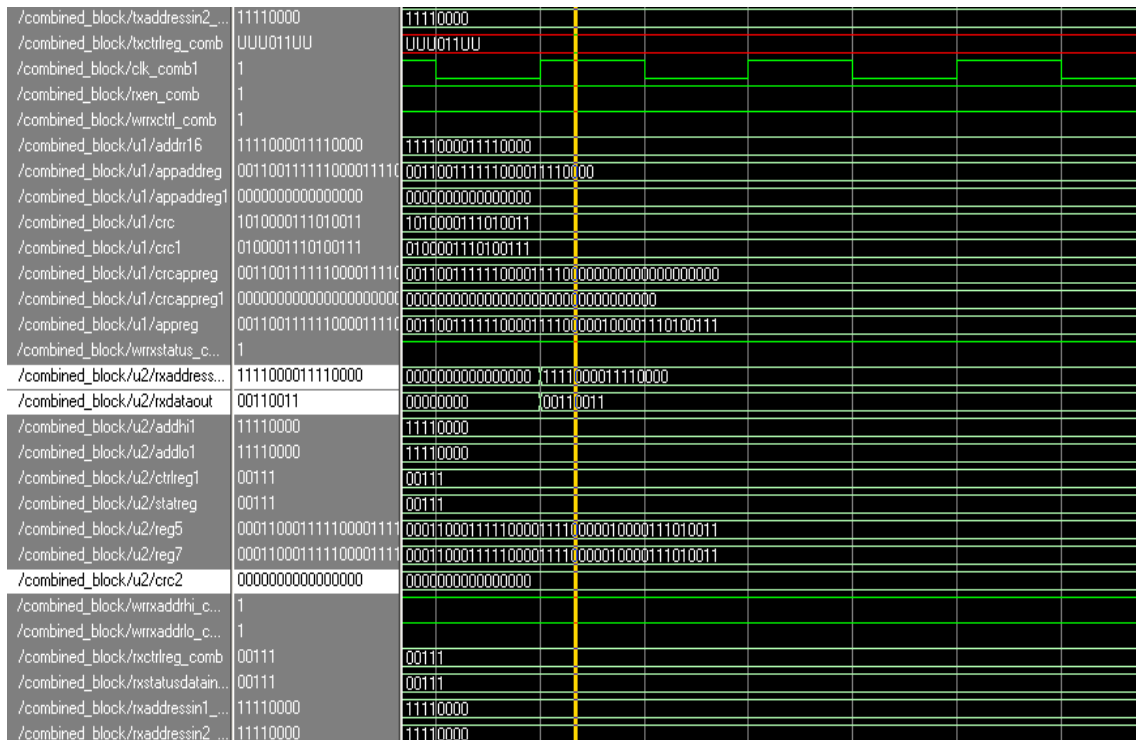


Fig.3.7: Simulation result for O/P at the receiver for 16 bit address and 8 bit data

V. CONCLUSION

In this paper, we have studied and simulated the HDLC Controller of 16-bit address for 8-bit data. It can automatically check the frame sequence generation by every time the user want to send a bit sequence using cyclic redundancy check CRC-16 to provide error free transmission of data. The simulation result of Post Synthesis is an Optimized Gate Level net list form which a net list code is extracted and it is simulated using Simulator and it is verified that design is working efficiently. In this paper, we studied and implemented the HDLC and CRC Calculation. The aim of this paper is to run the programmed FPGA at frequency i.e. in our simulation result, with single +5 V power supply, it performs up to 155.52 Mbits/s data rates. Furthermore, we implemented the various HDLC controllers for 16-bit address, 8 bit data and 16 bit CRC Check, simulation result for final output at the receiver end for 8-bit data 16-bit address and 16-bit CRC, with bit stuffing and removal of error in HDLC. It is capable of working in different modes: Normal response mode, asynchronous response mode and asynchronous balanced mode. HDLC controller design supports full Duplex and half duplex mode of operations. It is CCITT X.25 compatible, which is a protocol at the physical layer. An Automation Frame Check Sequence (CRC) generation at the transmitter end and it is capable of checking the receiver end for reliable and error free transmission. Also flexible with minimum CPU Overhead as it supports a comprehensive frame Level instruction set. It is Fully Compatible with TTL ICs.

REFERENCES

- [1] Gaurav Chandil; Priyanka Mishra; "Study and performance evaluation of Xilinx HDLC Controller and FCS Calculator", vol.2, issue 10 (October 2012), PP 41-50.
- [2] William Stallings, 2007. Data and Computer Communications, Eight edition, Prentice Hall, pp: 222.
- [3] Amit Dhir, 2000. "HDLC Controller Solutions with Spartan-II FPGAs," Xilinx Inc.
- [4] M.A.; Barbetta, L.; Neri, F.; "A Petri net simulation model of HDLC Marsan", TENCON '89. Fourth IEEE Region 10 International Conference 22-24 Nov. 1989 Page(s):240-247 Digital Object Identifier 0.1109/TENCON.1989.176933.
- [5] Davis, G.T.; Mandalia, B.D. "Modified byte insertion/deletion for HDLC in ISDN"; Southeastcon '89. Proceedings 'Energy and Information Technologies in the Southeast'. IEEE 9-12 April 1989 Page(s):1207 - 1210 vol.3 Digital Object Identifier 10.1109/SECON.1989.132614.
- [6] "FPGA implementation of a single-channel HDLC Layer-2 protocol transmitter using VHDL", Qasim, S.M.; Abbasi, S.A.; Microelectronics, 2003. ICM 2003. Proceedings of the 15th International Conference on 9-11.
- [7] Lu, Y., Z. Wang, L. Qiao and B. Huanq, 2002. "Design and implementation of multi-channel high speed HDLC data processor," IEEE International Conference on Communications, Circuits and Systems, and West Sino Expositions, 2: 1471-1475.
- [8] Latombe, J. (1996). Robot Motion Planning. Kluwer Academic Publishers, UK.
- [9] Jun Wang; Wenhao Zhang; Yuxi Zhang; Wei Wu; Weiguang Chang; Sch. of Electron. & Inf. Eng., Beihang Univ. (BUAA), Beijing, China "Design and implementation of HDLC procedure based on FPGA", Anti-counterfeiting, Security, and Identification in Communication, 2009. ASID 2009, 3rd International Conference, 20-22 Aug. 2009.
- [10] Guozheng Li Nanlin Tan State Key Lab. of Rail Traffic Control & Safety, Beijing Jiaotong Univ., Beijing, China "Design and Implementation of HDLC Protocol and Manchester Encoding Based on FPGA in Train Communication Network", Information and Computing (ICIC), 2010 Third International Conference.
- [11] Allaire, F.C.J., M. Tarbouchi, G. Labonte and G. Fusina, 2009. "FPGA implementation of genetic algorithm for UAV real-time path planning," Journal of Intelligent and Robotic Systems: Theory and Applications, 54(1-3): 495-510.
- [12] Chen, H. and Y.Q. Han, 2003. "ASIC design of high-speed low-power HDLC controller," Journal of Beijing Institute of Technology (English Edition), 12(SUPPL.): 66-69.
- [13] Gao, Zhen-bin and Jian-Fei Liu, 2005. "FPGA implementation of a multi-channel HDLC protocol transceiver", In Proceedings of the 2005 International Conference on Communications, Circuits and Systems, 2: 1300-1302.

Assesment of Irrigation Water Quality of Some Provinces of Turkey

Serpil Savci¹, Korkmaz Bellitürk²

1(Department of Biosystems Engineering, Faculty of Architecture Engineering, Bozok University, Turkey)

2 (Department of Soil Science and Plant Nutrition, Faculty of Agricultural, Namik Kemal University, Turkey)

ABSTRACT: *Yozgat and Tekirdag are important agriculture center for Turkey. In these cities, agriculture is still important. On the other hand, the water resource is polluted by agriculture facilities day by day. In this study, some important physio-chemical parametres of surface water of Yozgat and Tekirdag were evaluated for the criteria of irrigation water quality. The water samples were taken from sampling points in July 2012. The contents of the samples have been analysed. In addition to the ratios of nitrite, nitrate and phosphore were determined. Hence, these results are compared with the water quality criterias.*

Keywords: *Irrigation water, pollution, quality.*

I. INTRODUCTION

The massive growths of human populations and economic development have resulted in the current worldwide deterioration in water quality. Agriculture can have an important impact on the quality of surface water. Fertilizer consumption has strongly increased in all developing countries. In addition to, it effects water quality negatively.

Nitrogen is comprised of the forms: soluble organic N, NH₄-N (ammonium), NO₃-N (nitrate), NO₂-N (nitrite), and N associated with sediment as exchangeable NH₄-N or organic-N. Total phosphorus levels of 100 or more ppb categorize lakes as highly eutrophic, with high nutrient and algae levels [1].

Nitrates in aquatic systems increase the amount of algae and other green plants that cover the water surface, resulting in an increased consumption and reduction of dissolved oxygen in the aquatic environment. This reduction further results in a decrease in the amount of incident solar radiation penetrating to greater water depths. These two phenomena result in a reduction of depuration and photosynthetic capacity of aquatic organisms [2], leading to eutrophication [3].

Eutrophication has been recognized as the main cause of water quality impairment. Phosphorus has been identified as the primary limiting nutrient causing eutrophication of many surface waters. The main sources of the potentially mobile P are fertilizers, manure, including that in pastures and that associated with confinement facilities, animal litter, plant residue, soil P and atmospheric deposition. The potentially mobile P that is actually transported by the various hydrologic pathways to surface waters is called total transported P [4]

Yozgat is a city in Turkey. The city is located at an elevation of 4,380 ft (1,335 m), situated 105 mi (170 km) east of Ankara, near the head of a narrow valley through which the Ankara–Sivas road runs. Like much of the Anatolian Plateau, the lands around Yozgat have been deforested over thousands of years of human habitation. According to 2009 census, population of the district is 113,614 of which 73,835 live in the city of Yozgat [5]. The main income is agriculture in the city. The important streams around Yozgat City are Cekerek Cayi, Egrioz Suyu, Karasu, Kanaksuyu and Delice River.

Egrioz Suyu is collected in Gelingulu Dam. These streams are generally used for irrigation of the agricultural areas around Yozgat [6].

The second study area is Tekirdag that it is a city in the Marmara Region of Turkey. Tekirdag is located at the northern shores of the Marmara Sea. It is 135 km from İstanbul. It is an agriculture trade center. Also it is the trading center of an agricultural region producing cereals and crops raised for oils. According to 2009 census, population of the district is 783,310 in the city [7]. The intensive agriculture in the regions is also associated with extensive use of fertilizers and pesticides, which has polluted water. Karaidemir Dam is serves for irrigation and flood control in Tekirdag region. 11840 ha is currently being irrigated [8]. Figure-1 shows that Karaidemir Dam in Tekirdag.

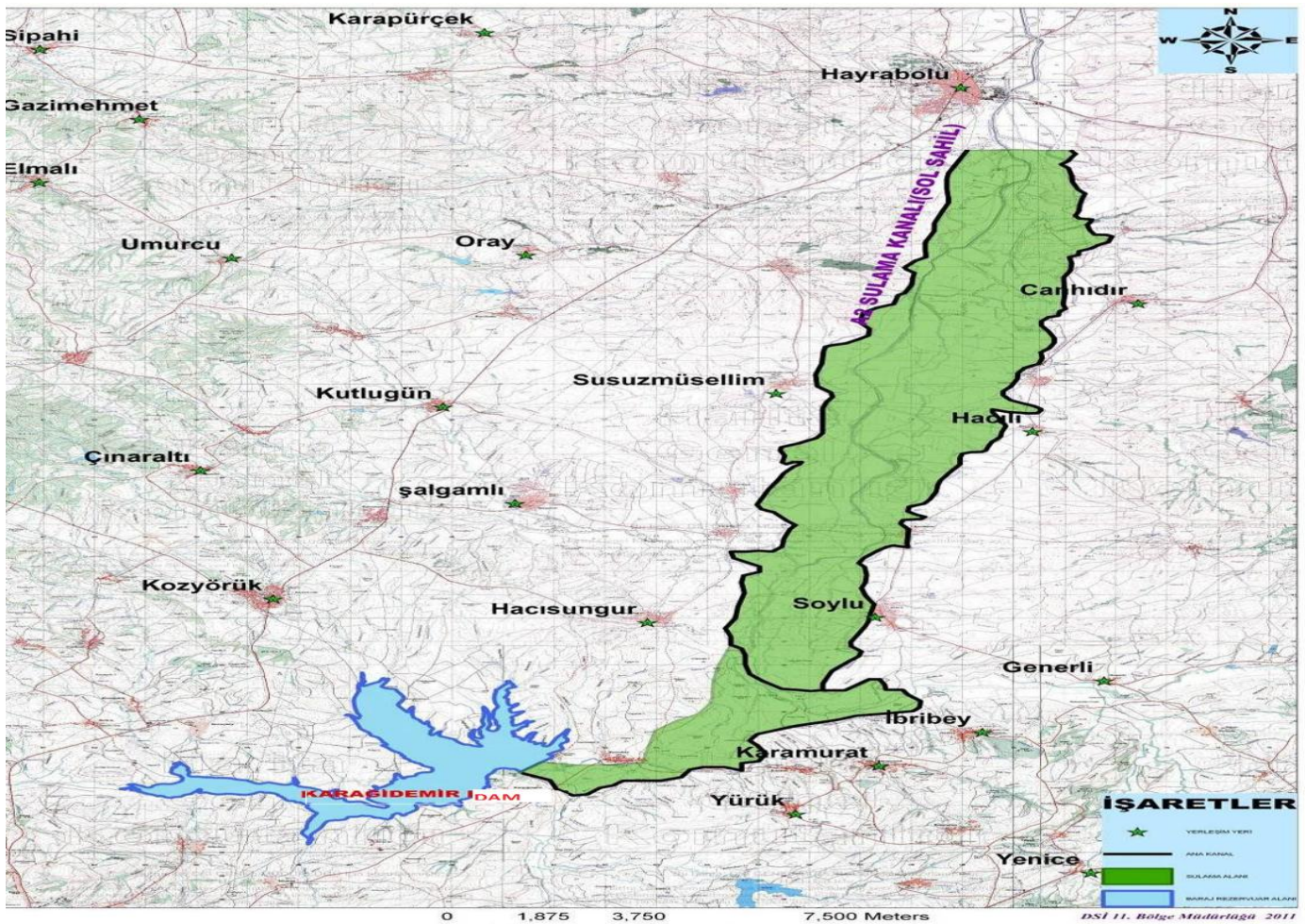


FIGURE-1 Karaidemir Dam-Tekirdag [8]

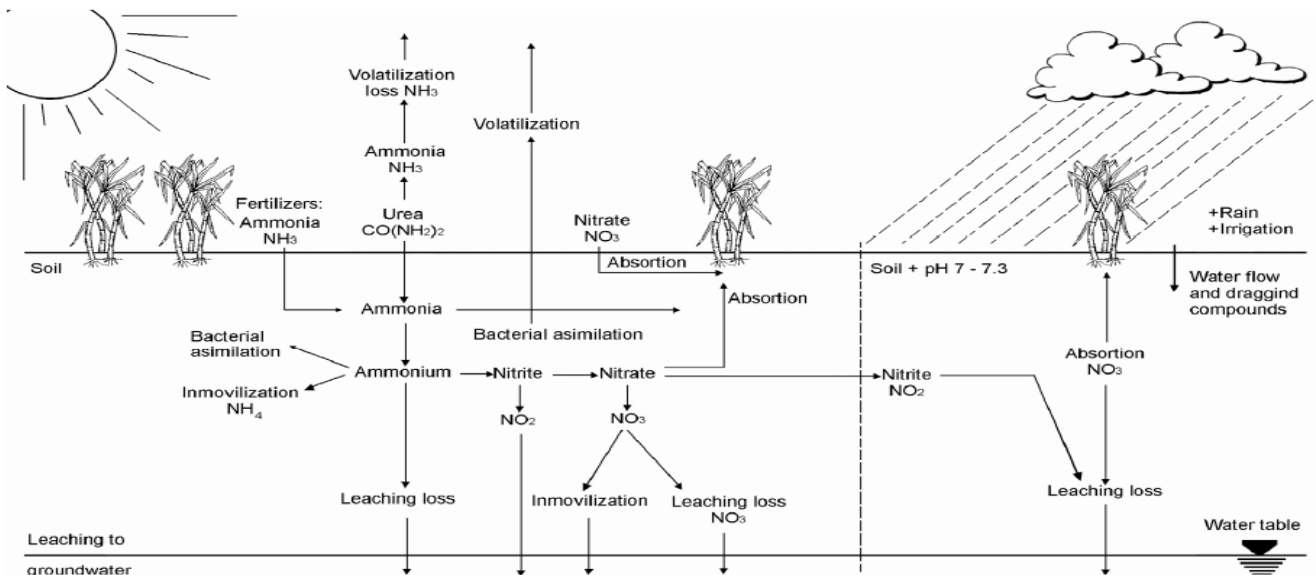


FIGURE 2-Forms and mobilization of nitrogenous compounds in the environment [9]

Nitrogenous fertilizers can be transformed to nitrites directly when they are applied to soils with pH 7.0-7.3 (Figure 2). An excess of nitrites in water is particularly harmful for humans and animals [9].

II. MATERIAL AND METHODS

A field research was conducted to evaluate the suitability of surface water for irrigated agriculture of Yozgat and Tekirdag. A total of 18 surface water samples were collected from various region in July 2012. Samples were collected from 12 ponds, 5 canals and 1 dam. The high density PVC bottles were used for sampling. They were thoroughly cleaned by rinsing with 8N HNO₃ and deionized water followed by repeated washing with water samples [10]. Various determinants, such as Nitrite-Nitrogen (mg NO₂⁻-N/L), Nitrate-Nitrogen (mg NO₃⁻-N/L) and The Total Phosphorus (mg P/L) of the samples were measured. The analysis for the physico-chemical parameters of the samples were carried out following the established analytical methods. Nitrite-Nitrogen was determined TS7526 EN 26777:1996, Nitrate-Nitrogen was determined SM 4500 NO₃ E: 2005 and The Total Phosphorus was determined SM 4500 PBC:2005. All of experiments were carried out in Ecosystem Environmental Analysis Laboratory (Adana). It has got an environmental measurement and analysis certificate of competency issued by T.C. Environmental and Urban Ministry.

III. RESULTS AND DISCUSSION

Table 1 represents the results of physico-chemical parameters of the irrigation water samples of the studies area of Yozgat and Tekirdag, while Table 2 and 3 show the suitability of water quality for irrigation purposes. According to Table 1, Nitrite-N was found in concentrations ranging from <0.04 to 0.61 mg L⁻¹; Nitrate-N concentrations ranged from 0.9 to 6.9 mg L⁻¹ and the total phosphorus concentrations ranged from < 0.1 to 0.28 mg L⁻¹ in Yozgat. The Nitrite-N was found <0.04 mg L⁻¹ for Fakıbeyli, Uzunlu, Aşağı Sarıkaya, Özlüce and Gelingüllü in Yozgat. According to Table 2, they are I. or II. Quality classes. In addition to, The Nitrite-N was found 0.05 mg L⁻¹ for Musabeyli and Topçu in Yozgat. According to same table, they are III. Quality classes. Finally The Nitrite-N was found 0.61 mg L⁻¹ for Paşaköy in Yozgat. It means IV. Quality classes. The Nitrate-N was found <5 mg L⁻¹ Fakıbeyli, Uzunlu, Gelingüllü, Musabeyli, Topçu and Paşaköy in Yozgat. According to these results, there are I. Quality class water. On the other hand, The Nitrate-N was found >5 mg L⁻¹ for A.Sarıkaya and Özlüce in Yozgat. Both of them are II. Water quality classes. In addition to, there are increasing problem in both of them according to Table 3. The total phosphorus was found <0.16 mg L⁻¹ for Fakıbeyli, Paşaköy, Uzunlu, Gelingüllü and Musabeyli in Yozgat. They are I. Water Quality Standards. The total phosphorus was found > 0.16 mg L⁻¹ for A. Sarıkaya, Özlüce and Topçu in Yozgat. It means they are III. Water quality classes.

Table 1-Physico-chemical properties of irrigation water of the study area

Wat. Smp No	Sampling area	Source of sample	Nitrite-Nitrogen (mg NO ₂ ⁻ -N/L)	Nitrate-Nitrogen (mg NO ₃ ⁻ -N/L)	The Total Phosphorus (mg P/L)
1	Fakıbeyli, Yozgat	Pond	<0.04	1.5	0.14
2	Uzunlu, Yozgat	Canal	<0.04	1.9	<0.1
3	A.Sarıkaya, Yozgat	Pond	<0.04	6.9	0.23
4	Özlüce, Yozgat	Canal	<0.04	6.5	0.17
5	Gelingüllü, Yozgat	Canal	<0.04	1.9	<0.1
6	Musabeyli, Yozgat	Canal	0.05	1.6	<0.1
7	Topçu, Yozgat	Pond	0.05	1.0	0.28
8	Paşaköy, Yozgat	Canal	0.61	0.9	0.11
9	Bıyıklı, Tekirdag	Pond	0.25	2.9	0.34
10	Bayrampaşa, Tkd.	Pond	0.09	1.5	0.8
11	Temrezli, Tekirdag	Pond	<0.04	2.5	1.6
12	Çerkezmusellim, Tk	Pond	<0.04	1.9	0.8
13	Karababa, Tkd.	Pond	0.5	0.8	0.8
14	Karaıdemir, Tkd.	Dam	<0.04	1.02	<0.1
15	Küçükhdır, Tkd.	Pond	<0.04	2.4	<0.1
16	Yazır, Tekirdag	Pond	0.16	3.1	0.8
17	Nusratlı, Tekirdag	Pond	0.42	2.35	<0.1
18	Kırıkkepenkli, Tkd.	Pond	<0.04	3.2	<0.1

The second study area is Tekirdag region. According to Table 1, Nitrite-N was found in concentrations ranging from <0.04 to 0.5 mg L⁻¹; Nitrate-N concentrations ranged from 0.8 to 3.2 mg L⁻¹ and the total phosphorus concentrations ranged from < 0.1 to 0.34 mg L⁻¹ in Tekirdag. The Nitrite-N was found <0.04 mg L⁻¹ for Temrezli, Çerkezmusellim, Karaıdemir, Küçükhdır and Kırıkkepenkli in Tekirdag. According to Table 2, they are I. or II. Quality classes. In addition to, The Nitrite-N was found >0.05 mg L⁻¹ for Bıyıklı, Bayrampaşa, Karababa, Yazır and Nusratlı. Table 2. Water Pollution Control Regulation, quality criteries according to classes of inland water sources. According to same table, they are IV. Quality classes. The Nitrate-N was found < 5 mg L⁻¹ all of the samples for Tekirdag region. It means I. Water quality classes for them. In addition to, there isn't any problem for them according to Table 3. The total phosphorus was found <0.1 mg L⁻¹ for Karaıdemir, Küçükhdır, Nusratlı and Kırıkkepenkli. They are I. water quality classes. The total phosphorus was found >0.65 mg L⁻¹ for Bayrampaşa, Temrezli, Çerkezmusellim, Karababa and Yazır. They are IV. Water quality classes. Finally, the total phosphorus was found 0.34 mg L⁻¹ for Bıyıklı. It means II. Water quality classes.

Table 2-Water Pollution Control Regulations, 1988 [11]

Water Quality Parameters	Water Quality Classes			
	I	II	III	IV
Nitrite-Nitrogen (mg NO ₂ ⁻ -N/L)	0.002	0.01	0.05	>0.05
Nitrate-Nitrogen (mg NO ₃ ⁻ -N/L)	5	10	20	>20
The Total Phosphorus (mg P/L)	0.02	0.16	0.65	>0.65

Table 3-Guidelines for interpretation of water quality for irrigation [12]

Irrigation Problem	Degree Of Problem		
	No Problem	Increasing Problem	Severe Problem
Miscellaneous Effects (effects susceptible crops) NO ₃ -N (or) NH ₄ -N (mg/L)	<5	5-30	>30

IV. CONCLUSION

The paper investigated determinants of water quality in rivers, canals, ponds and dam in Yozgat and Tekirdag regions. Data on water quality (water class) for 18 monitoring points for a month was used for the analysis. Different physico-chemical properties of irrigation water of Yozgat and Tekirdag cities were compared with the national and international water quality standards set for irrigation. According to standards, there are increasing problem of Nitrate-N for A.Sarikaya and Özlüce in Yozgat.

Proper agricultural management practices need to be introduced avoiding over-irrigation by farmers. Here, environmental benefits and economic benefits for farmers due to more efficient fertilizer use could go hand in hand [13]. To minimize potential risks associated with canal water irrigation, the proper use of canal water as well as efficient and economic methods to reduce chemical loads in chemically contaminated water used for irrigation needs to be implemented.

V. ACKNOWLEDGEMENTS

The authors are grateful to University of Bozok The Resource Project Unit for financial support of this study. (Project no: 2012MF/A02).

REFERENCES

- [1] Minnesota Pollution Control Agency, July 2007. Phosphorus: Sources, Forms, Impact on Water Quality –A General Overview.
- [2] Herrera, J. A., Aranda, A. A., Troccoli, G. L., Comín, F. A., & Madden, C. 2004. Diagnóstico Ambiental del Golfo de México. M. In M. Caso, I. Pisanty, & E. Ezcurra (Eds.), Eutrofización costera en la península de Yucatán. (1a ed., pp. 821-880) México D.F.
- [3] Toner, P. F. 1986. Impact of agriculture on surface water in Ireland Part I. General. Environmental Geology, 9 (1), 3-10.
- [4] Zaines, G. N., Schultz, R. C., 2002. Phosphorus in Agricultural Watersheds. A Literature Review. Department of Forestry, Iowa State University, Ames, Iowa January 2002. 116 pages.
- [5] Wikipedia, The Free Encyclopedia. <http://en.wikipedia.org/wiki/Yozgat> Access: 29.07.2012
- [6] Soyak, M., Divrikli, U., Saracoglu, S., Elci, L., 2002. Monitoring Trace Metal Levels in Yozgat-Turkey: Copper, Iron, Nickel, Cobalt, Lead, Cadmium, Manganese and Chromium Levels in Stream Sediments. Polish Journal of Environmental Studies Vol. 11, No. 1 (2002), 47-51.
- [7] The City Population, 2012. <http://www.citypopulation.de/php/turkey-tekirdag.php?adm2id=D1674>. Access: 29.07.2012.
- [8] Anonymous, 2012. The General Directorate of State Hydraulic Works (DSI) 11. Regional Offices, 2012 Presenting Reports, Edirne.
- [9] Galaviz-Villa, I., Sanchez, C-L., Chavez, M.R.c., Perez-Vazquez, A., Martinez-Davila, J. P., Nikolskii-Gavrilov, I., Lango-Reynoso, F., 2010. Agricultural Contamination of Subterranean Water with Nitrates and Nitrites: An Environmental and Public Health Problem. Journal Of Agricultural Science Vol. 2, No. 2.
- [10] De, A.K. 1989. Environmental Chemistry. Wiley Eastern Limited, New Delhi, India. pp. 42-43.
- [11] Water Pollution Control Regulation, 19 919 official newspaper, 4 September 1988.
- [12] Ayres, R. S., and Westcott, D. W., 1976. Water Quality for Agriculture. F. A. O. Irrigation and Drainage Paper No: 29, F.A.O., Rome.
- [13] Ribbe, L., Delgado, P., Salgado, E., Flügel, W-A., 2008. Nitrate pollution of surface water induced by agricultural non-point pollution in the Pochay watershed, Chile. Desalination, 226:13-20.

Finding Truth: Rendering Justice – A Myth or Reality

Pulyapudi Srnivas

Research scholar & Advocate, Visakhapatnam

Abstract: The present family of Advocate's profession is failing in its duty to understand the actual dispute involved in the case handled by them on the guise of defending their clients and the advocate's are totally forgetting the main principles to be followed by an advocate. Similarly, the judicial officers are hearing what the advocates and consider the judgments submitted by them and deciding the cases, but when the respective advocates wantonly suppressing the case law which is against them, the judges who are in the high pedestal are also not referring those judgments which are crucial to decide the subject matters. Had the Judges refer this three judge bench decision at the appropriate time, this situation could have been avoided. That is the reason why, the research scholar is of the view that the advocates are failing in their duty to bring it to the notice of the Court both for and against the case, and ignoring the Supreme Court decision, [the Supreme Court has even gone to the extent of saying that the Advocate is duty bound to state the correct position of law, when it is undisputed, even if it does not favour his client.

Key words: Finding Truth, Rendering Justice, Myth, Reality, Professional integrity

I. Introduction

- 1.1 Indian High Courts Act, 1861 (commonly known as the Charter Act) passed by the British Parliament enabled the Crown to establish High Courts in India by Letters Patent and these Letters Patent authorised and empowered the High Courts to make rules for advocates and attorneys (commonly known as Solicitors). The law relating to Legal Practitioners can be found in the Legal Practitioners Act, 1879 (18 of 1879), the Bombay Pleaders Act, 1920 (17 of 1920) and the Indian Bar Councils Act, 1926 (38 of 1926).
- 1.2 After Independence it was deeply felt that the Judicial Administration in India should be changed according to the needs of the time. The Law Commission was assigned the job of preparing a report on the Reform of Judicial Administration. In the mean while the All India Bar Committee went into detail of the matter and made its recommendations in 1953. To implement the recommendations of the All India Bar Committee and after taking into account the recommendations of the Law Commission on the subject of Reform of Judicial Administration in so far as the recommendation relate to the Bar and to legal education, a Comprehensive Bill was introduced in the Parliament.

Enactment of Advocates Act 1961

- 2.1 The Advocate Bill was passed by both the Houses of Parliament and it received the assent of the President on 19th May, 1961 and it become The Advocates Act, 1961 (25 of 1961).
- 2.2 The Act 1961 comprises of seven (7) chapters and 60 Sections. Out of 7 chapters, chapter 4 deals with Right to Practice. Chapter 5 deals with conduct of Advocates.

Professional integrity and high Standard

- 3.1 Professional integrity and high ethical standards are the badge of honour of a lawyer and his reputation should not be tarnished by disreputable conduct or deviant behaviour. Credibility and reputation of the profession depends upon the manner in which Advocates conduct themselves. An Advocate owes a duty to his client, to his opponent, to the Court, to the society at large, and to himself.

Case Law indicating the duties of Advocates

- 4.1 In the case of DP Chadha –vs- Triyugi Narain Mishra AIR 2001 SC 457 = 2001 (2)SCC 221, the Supreme Court has even gone to the extent of saying that the Advocate is duty bound to state the correct position of law, when it is undisputed, even if it does not favour his client. [Pages 150 and 151 of Sanjiva Row's - The Advocates Act 1961, LexisNexis Butterworths, by DV Subbarao - Seventh Edition] While an Advocate is free to try, to the best of his ability, to use wit, to persuade the Court to a view of the law which best serves his client, he cannot mislead the Court on a settled position of law. The Supreme Court in the case of Shambu Ram Yadav –vs- Hanuman Das Khatri AIR 2001 SC 2509 [Page 151 of Sanjiva Row's - The Advocates Act 1961, LexisNexis Butterworths, by DV Subbarao - Seventh Edition] observed that society and public are interested in due administration of justice, and hence a lawyer owes a duty to society and the Court and he is not supposed to encourage dishonesty and corruption. The profession of law is noble, and its members are expected to act in an honest and upright manner, and any deviation from these elementary principles is liable to be dealt with severely. An Advocate practicing law is under a triple obligation – (i) an obligation to his clients to be faithful to them till the last, (ii) an obligation to the profession not to besmirch (tarnish) its name by any act done by him, and (iii) and an obligation to the Court to be and to remain a dependable part of the machinery through which justice is administered. The duty of an Advocate is to assist the administration of justice, and not to obstruct or impede it and in the performance of his professional duties he is expected not to be influenced by personal motives, desire of revenge or resentment. He must not hesitate even in appraising the Court with any opposite view of law previously taken by the superior Court of the land on the question arising in his own case at hand. It is an

obligation of the confidence between judge and opposing counsel that the latter should furnish the judge with all information for and against either party. [Page 162 of Sanjiva Row's - The Advocates Act 1961, LexisNexis Butterworths, by DV Subbarao - Seventh Edition]. An advocate is an officer of the Court and his primary duty is to assist the Court in arriving at justice. He is a social engineer and should play a sentinel role in the administration of justice. He is expected to work like a horse and live like a hermit.

Provisions in Constitution of India

5.1 The Constitution of India is the supreme law of India. It lays down the framework defining fundamental political principles, establishes the structure, procedures, powers, and duties of government institutions, and sets out fundamental rights, directive principles, and the duties of citizens. It is the longest written constitution of any sovereign country in the world, containing 395 Articles in 22 parts, 12 schedules and 115 amendments. The Constitution was enacted by the Constituent Assembly on 26 November 1949, and came into effect on 26 January 1950. The date 26 January was chosen to commemorate the Purna Swaraj declaration of independence of 1930. With its adoption, the Union of India officially became the modern and contemporary Republic of India and it replaced the Government of India Act 1935 as the country's fundamental governing document. The Constitution declares India to be a sovereign, socialist, secular, democratic republic, assuring its citizens of justice, equality, and liberty, and endeavours to promote fraternity among them. The words "socialist" and "secular" were added to the definition in 1976 by constitutional amendment. India celebrates the adoption of the constitution on 26 January each year as Republic Day.

Members of the drafting committee for Constitution of India

6.1 The Constitution was drafted by the Constituent Assembly, which was elected by the elected members of the provincial assemblies. Sanjay Phakey, Jawaharlal Nehru, C. Rajagopalachari, Rajendra Prasad, Sardar Vallabhbhai Patel, Sandipkumar Patel, Dr Ambedkar, Maulana Abul Kalam Azad, Shyama Prasad Mukherjee, Nalini Ranjan Ghosh, and Balwantrai Mehta were some important figures in the Assembly. There were more than 30 members of the scheduled classes. Frank Anthony represented the Anglo-Indian community, and the Parsis were represented by H. P. Modi. The Chairman of the Minorities Committee was Harendra Coomar Mookerjee, a distinguished Christian who represented all Christians other than Anglo-Indians. Ari Bahadur Gururung represented the Gorkha Community. Prominent jurists like Alladi Krishnaswamy Iyer, B. R. Ambedkar, Benegal Narsing Rau and K. M. Munshi, Ganesh Mavlankar were also members of the Assembly. Sarojini Naidu, Hansa Mehta, Durgabai Deshmukh, Rajkumari Amrit Kaur and Vijayalakshmi Pandit were important women members. The first president of the Constituent Assembly was Dr Sachidanand Sinha. Later, Rajendra Prasad was elected president of the Constituent Assembly. The members of the Constituent Assembly met for the first time on 9 December 1946.

Independency of Judiciary

7.1 The Judiciary of India is free of control from either the executive or the Parliament. The judiciary acts as an interpreter of the constitution, and as an intermediary in case of disputes between two States, or between a State and the Union. An Act passed by the Parliament or a Legislative Assembly is subject to judicial review, and can be declared unconstitutional by the judiciary if it feels that the act violates the provisions of the Constitution.

Judicial review of laws

8.1 Judicial review is adopted in the Constitution of India from the Constitution of the United States of America. In the Indian constitution, Judicial Review is dealt with under Article 13. Judicial Review refers that the Constitution is the supreme power of the nation and all laws are under its supremacy.

- A. In the Constitution of India, an Article 124 has been drafted dealing with the creation of the Supreme Court of India. The said article says as -
- B. 'Article 124
- C. Article 124 deals with establishment and constitution of Supreme Court.

Supreme Court

9.1 The Supreme Court of India is the highest Court of the land as established by Part V, Chapter IV of the Constitution of India. According to the Constitution of India, the role of the Supreme Court is that of a federal Court, guardian of the Constitution and the highest Court of appeal. Articles 124 to 147 of the Constitution of India lay down the composition and jurisdiction of the Supreme Court of India. Primarily, it is an appellate Court which takes up appeals against judgments of the provincial High Courts. But it also takes writ petitions in cases of serious human rights violations or if a case involves a serious issue that needs immediate resolution.

Composition of the Courts

10.1 The supreme Court of India consist if a Chief Justice and, until parliament may by law prescribed a large number, not more than seven other Judges. Thus parliament increase the number this number, by law. Originally the total numbers of Judges were seven but in 1977 this was increased to 17 excluding the Chief Justice. In 1986 this number has been increased to 25 excluding the Chief Justice. Thus the total number of Judges in the Supreme Court at present is 26 including the Chief Justice. The constitution does not provide for the minimum number of Judges who will constitute a bench for hearing cases.

Qualification of the Judges of the Supreme Court of India

- 11.1** The qualifications of the Judges are as follows: - Under Article 124(3) of the constitution talk about the qualifications of Judges that are
- He should be a citizen of India.
 - He should have been at least five year a judge of a high Court or of two or more such Courts in succession; or he should have been for at least 10 years an advocate of high Court or of two or more such Court in succession.
 - He is in the opinion of the president a distinguished jurist.

Appointment of Judges

- 12.1**The Judges of the high Court are appointed by the president. The Chief Justice of Supreme Court is appointed by the president with the consultation of such of Judges of the supreme and high Court as he deemed necessary for the purpose. But in appointment of the other Judges the president shall always consult the Chief Justice of India. He may consult he may consult such other Judges of the Supreme Court and high Court as he may deemed necessary. It should, however be noted that the power of the president to appoint Judges is purely formal because in this matter he act on the advice of the council of ministers. There was an apprehension that executive may bring politics in the appointment of the Judges. The Indian constitution therefore does not leave the appointment of Judges on the discretion of the executive. The executive under this Article is required to consult persons who are ex-hypothesis well qualified to give proper advice in matters of appointment of Judges.
- 12.2**Under Article 124(2) the president, in appointment other Judges of the Supreme Court is bound to consult Chief Justice of India but in appointment the Chief Justice of India he is not bound to consult anyone. The word 'may' used in art 124 makes clear that it is not mandatory on him to consult anyone.
- 12.3**In the preamble of the Constitution of India, it has been specifically mentioned as 'We, THE PEOPLE OF INDIA having solemnly resolved to constitute India into a SOVEREIGN SOCIALIST SECULAR DEMOCRATIC REPUBLIC and to secure to all its citizens JUSTICE , social, economic and political'. Thus by having the term 'JUSTICE' in the preamble itself, and, in the oath that is being taken by the Judges that they will uphold Constitution of India, they have declared that JUSTICE will be rendered to all citizens of India.
- 12.4**In third schedule of the Constitution of India, there exists a form of Oath or affirmation to be made by the Judges of the Supreme Court of India which is as follows:
'I, AB, having been appointed Chief Justice(or a Judge) of the Supreme Court of India do swear in the name of God/solemnly affirm that I will bear true faith and allegiance to the Constitution of India as by law established, that I will uphold the sovereignty and integrity of India that, I will duly and faithfully and to the best of my ability, knowledge and judgment perform the duties of my office without fear or favour, affection or ill will and that I will uphold the Constitution and the laws.'
- 12.5**In the Little Oxford English Dictionary (Indian Edition), the term 'JUSTICE' was defined to mean – just behaviour or treatment – the quality of being fair and reasonable'.
- 12.6**In Stroud's Judicial Dictionary (Seventh Edition), the term 'JUSTICE' is defined to mean 'to do justice', among many other meanings.

13. Removal of Judges

13.1Impeachment:-Article 124(4) and (5):-

A judge may only be removed from his office by an order of the president on ground of proved misbehavior or incapacity.

14. High Courts

14.1'214. High Courts for States.

There shall be a High Court for each State.

14.2High Courts of India are at the top of the hierarchy in each State but are below the Supreme Court. These Courts have control over a state, a union territory or a group of states and union territories. Below the High Courts are secondary Courts such as the civil Courts, family Courts, criminal Courts and various other district Courts. High Courts are established under Part VI, Chapter V. The High Courts are the principal Courts of original jurisdiction in the state, and can try all offences including those punishable with death.

15.1India's judicial system is made up of the Supreme Court of India at the apex of the hierarchy for the entire country and twenty-one High Courts at the top of the hierarchy in each State. These Courts have jurisdiction over a state, a union territory or a group of states and union territories. Below the High Courts are a hierarchy of subordinate Courts such as the civil Courts, family Courts, criminal Courts and various other district Courts. High Courts are instituted as constitutional Courts under Part VI, Chapter V, and Article 214 of the Indian Constitution.

15.2 The High Courts are the principal civil Courts of original jurisdiction in the state, and can try all offences including those punishable with death.

Jurisdiction of High Court

15.3 Article 226 states: Power of High Courts to issue certain writs.

15.4 Article 226 (1) states 'Notwithstanding anything in article 32 every High Court shall have power, throughout the territories in relation to which it exercises jurisdiction, to issue to any person or authority, including in appropriate cases, any Government, within those territories directions, orders or writs, including writs in the nature of habeas corpus, mandamus, prohibition, quo warranto and certiorari, or any of them, for the enforcement of any of the rights conferred by Part III and for any other purpose.

16. Writ jurisdiction

16.1 High Courts are having writ jurisdiction to consider and grant writs on Habeas Corpus Mandamus, Quo warranto, Certiorari, and Prohibition.

16.2 Article 227 states: Power of superintendence over all Courts by the High Court. — Article 227 (1) states ‘Every High Court shall have superintendence over all Courts and tribunals throughout the territories in relation to which it exercises jurisdiction.’

16.3 In third schedule of the Constitution of India, there also exists a form of Oath or affirmation to be made by the Judges of the High Court which is as follows

‘I, AB, having been appointed Chief Justice(or a Judge) of the High Court at (or of)..... do swear in the name of God/solemnly affirm that I will bear true faith and allegiance to the Constitution of India as by law established, that I will uphold the sovereignty and integrity of India that, I will duly and faithfully and to the best of my ability, knowledge and judgment perform the duties of my office without fear or favour, affection or ill will and that I will uphold the Constitution and the laws.

17. Sub-ordinate Courts:-

17.1 ‘Article 233. Appointment of District Judges

Appointments of persons to be, and the posting and promotion of, District Judges in any State shall be made by the Governor of the State in consultation with the High Court exercising jurisdiction in relation to such State.

18. Whether truth is being elicited and/or justice rendered

18.1 From the elaborate discussion about Advocate’s Act 1961, and the Constitution of India, it can be seen that the Advocates have a duty to an Advocate practicing law is under a triple obligation – (i) an obligation to his clients to be faithful to them till the last, (ii) an obligation to the profession not to besmirch (tarnish) its name by anything done by him, and (iii) and an obligation to the Court to be and to remain a dependable part of the machinery through which justice is administered and that the Advocate is duty bound to state the correct position of law, when it is undisputed, even if it does not favour his client.

18.2 Further from a perusal of the Constitutional provisions as well as preamble of the Constitution of India, gives a picture that the Courts have to render justice to all the citizens of India.

18.3 The Law controls public power, regulates personal matters, and provides codes for social and commercial interactions. It is premised on prudence and the finding of truth. It stresses on fairness, steadiness and expectedness provides the normative base for individual and community living. From viewing many advocates and cases that are being taken up for arguments before Hon’ble Courts at District Court stage, High Court stage and also at Supreme Court stage, the question that emanates for consideration is that why the law became the subject matter of disrespect and panic. Why do people shun the Courts, and when once visited will swear not to visit again. Why the Advocate’s profession (which is supposed to be noble profession) became a disliked profession.

18.4 If one put a question, where went wrong with the law, we hear the following

1. Legal proceedings are costly. They are time consuming. They are spread in a mass of hopelessly complex and indeterminable procedures.
2. Legal cases are often failed to identify or address the real issues involved in the dispute.
3. Advocates are more concerned with winning than finding the truth or solutions. And
4. The legal process actually increases conflict between the parties who come to have their differences resolved. Conflict is treated with increased doses of conflict to knock out a legal result.

18.5 From out of the four referred to above, it is better if we analyse two of them viz., (i) Legal cases are often failed to identify or address the real issues involved in the dispute; and

(ii) Advocates are more concerned with winning than finding the truth or solutions (otherwise they cannot be treated as a successful advocate).

18.6 When we see that Arbitration is aimed at settlement of disputes quickly without spending huge amounts through private persons selected for this purpose, generally a feeling will come to light that the contracting parties have to choose the proper persons to adjudicate disputes in a fair and reasonable manner in accordance with law by taking the settled principles. The basis for selection of these persons is the contract condition which is called as arbitration clause or arbitration agreement. In most of the cases, it indicates and gives power to one of the contracting parties to nominate the sole arbitrator. In some cases, depending upon the parties’ involvement, the forum for nominating arbitrators will be some organisation like Indian Council of Arbitration. Similarly there are some more organisations dealing with the subject of arbitration.

18.7 With great respect to brother Advocates, it may be stated that legal cases are often failed to identify or address the real issues involved in the dispute by understanding the conflict.

19. What is ‘conflict?’

19.1 According to Little Oxford English Dictionary (Indian Edition), ‘conflict’ is defined to mean as – a serious disagreement – a difference of opinions, principles etc.

19.2 In Agrawala’s Legal Dictionary the term ‘conflict’ is defined to mean as Fight, struggle; to clash.

19.3 In general, the said term means ‘antagonistic state or action (as of divergent ideas, interests or persons) and/or competitive or opposing action of incompatibles.

19.4 Nature of 'conflict' is required to be understood FIRST before dealing with that. It starts with differences and if the conflict is unresolved, led to disagreements and disputes. When differences reach this stage conflict begins. Disputes when unresolved become wider areas of conflict. Since we are dealing with understanding the conflict, first we have to see the content of the problem or root cause of the conflict, issues or interests of both the parties. Mainly this article concentrates on commercial conflicts. For good resolution of a dispute, one needs to make the parties understand and appreciate the difference between positions of the respective parties where they stand at law on one hand and interests and needs on the other. Negotiation is one of the methods of resolution of dispute. This is a process involving direct contact, dealing and communication between the parties to the contract to the dispute or their representatives. It is voluntary and becomes binding when an agreement is reached. This is the area where most of the parties are ignoring. If they mainly concentrate on understanding the nature of conflict or dispute, they can resolve the conflict or dispute and there may not be any reason for going to the stage of arbitration. Presumably the reason being that, as already stated, that when a party approaches the Advocate, he will always examine the case in the concept of how to win a case but not understanding the real nature of conflict or dispute.

20. Article of Hon'ble Justice V.R.Krishna Iyer

20.1 Recently, I came across an article entitled 'Questions of judicial access' written by Hon'ble Justice V.R. Krishna Iyer to ascertain whether the Supreme Court of India, or the Supreme Court for Indians? In that article published in The Hindu Hon'ble Justice says as:

20.2 'Judicial justice is precious to a people. The adversarial system of justice to be successful has to have the bar as an integral part of the system of judicial administration. The Bench and the Bar together operate to dispense competent and sound justice. Justice is the salt of the earth and if the salt loses its savour, wherewith shall they be salted?'

20.3 The excellence of justice, the refined process of justice and justicing, make humanity happy, harmonious and a haven (safe place) for peaceful and progressive habitation. Access is negated where the system is expensive; the social philosophy of judges and the lawyers are with the propertariat, and the poor are priced out of an archaic system whose doors are only open to the opulent (lavish), not to the indigent. Dialectical materialism is the reality in the temporal world, and where purchase of able argument from the Bar is beyond the purse of the litigant he or she is defacto denied justice.

20.4 The Indian legal system is altogether beyond common people. It is so esoteric (mysterious) that it remains alien and unintelligible to a society that is largely illiterate without the aid of the Bar, which has a professional monopoly over jurisprudence. If the Court has too many tiers and the highest Court is too distant from the regions where the proletariat live and struggle for its existence, the right to justice which is quintessence of democracy loses its spiritual value and cipherses the other fundamental rights.' [Bracketed words are supplied by me for better understanding]

21. Case study

21.1 In that view of the matter, with great respect to the brother advocates, I am giving few examples (case studies) where the advocates are not fulfilling their obligations as mentioned above. (Not to embarrass the parties, advocates, and adjudicators I am giving only fictitious names of the cases, by changing the facts of the cases to suit this article.)

22. Case between "A' and B"

22.1. "A" entered a contract with "B" for a specific purpose of execution of some work. The contract value involves Crores of rupees. The said contract conditions have been drafted and finalized by "B" and one of the conditions of the said contract is opposed to the public policy and violates a provision of a Central Act, which in turn attracts Section 23 of the Indian Contract Act 1872. Though "A" pleads the same, counsel for "B" has not budged even an inch (presumably in the guise of supporting his client which is also one of his duties and obligations). Thereby, the 'B' suffered Crores of rupees. Had the Advocate first understands the real conflict or dispute, he would have suggested that such a clause in the contract is opposed to the public policy and also violative of Section 23 of the Contract Act, 1872 and would have advised the contracting party to frame a suitable clause in consonance with the statutory provisions. Or at best, if a practice exists to have such clauses, would have suggested the contracting party to frame such a clause in the contract to see that it is not violative of the Central Act and / or Section 23 of the Contract Act, 1872. Without actually going into the basic conflict or dispute, if the Advocate intends to take up the case on behalf of a party, he will only try to defend his party in deviation of the triple obligation and professional duties as mentioned above. In that process even if some of the judgments (precedents) are not in favour of his client, he is not bring it to the notice of the Judge, which is also an obligation of the confidence between judge and opposing counsel that the later should furnish the judge with all information for and against either party.

23. Case between "C" and "D"

23.1. "C" enters into a contract with 'D' for grant of lease of land and the said transaction was also reduced in writing containing various conditions referring to various obligations to be fulfilled by both the parties to the contract. After paying some installments of rent, as 'C' failed to pay rent 'D' gave a notice in terms of the provisions of the Public Premises (Eviction of Unauthorised Occupants) Act 1970 for the realization of rent only. But "D" later on, without following the provisions of the said Act 1970, terminated the lease granted to 'C' and taken possession of the leased premises from the lessee. Here the conflict involved is the step taken by 'D' in issuance of notice under Act 1970 for recovery of rent, but not for eviction of 'C'. Further there are several irregularities on the part of 'D' i.e., exercise of

powers of in the name of Estate Officer under Act 1970 contrary to the provisions of the Act 1970, that is to say no steps were taken to declare the lessee as an un-authorised occupant and no notice was under Section 4 of Act 1970 and order was passed under Section 5 of the Act. Out of all the irregularities, the greatest irregularity is that no Estate Officer was appointed under Section 3 of the Act by a notification of the central Government as required under section 3 of the Act 1970 and as if it is only a delegation of power, the Estate officer's duties were entrusted to an officer by the Head of the organisation by means of an office order. All these irregularities have been brought out before the Arbitral Tribunal comprising of three arbitrators. Without actually going into the basic conflict or dispute, if the Advocate intends to take up the case on behalf of a party, he will only try to defend his party's interests in deviation of the triple obligation and professional duties as mentioned above. In that process even if some of the judgments (precedents) are not in favour of his client, he is not bring it to the notice of the Judge, which is also an obligation of the confidence between judge and opposing counsel that the later should furnish the judge with all information for and against either party.

24. Case between "E" and "F"

24.1. "E" entered into a contract for loan amount with "F" for purchase of mechanical equipment with a condition to repay the loan amount in installments. After paying some installments, "E" failed to pay the installments due to the mechanical breakdown of the equipment. Despite mechanical breakdown of the equipment it is an obligation of "E" to repay the installments. However, the Conditions of contract is unilateral and there are gross violations of the Statutory provisions while finalising the conditions of contract. For example, Statute says that on giving reasonable notice only the mechanical equipment is to be seized and sold away. But a condition has been inserted contrary to the statutory provision. Under Law, a notice is required to be given claiming the due amount from "E" and on failure invoke the arbitration clause. But in this case. Further, "F" has not issued any notice claiming the balance amount from "E" and on failure to respond arbitration clause was not invoked. However, in this case, both claiming the amount due from "E" and invocation of arbitration was done by means of a single letter which is contrary to the provisions of the Arbitration and Conciliation Act 1996. In addition to that, the notice said to have been issued for invocation of the arbitration clause was sent to a wrong address, which under law it cannot be said to be a valid service. Despite all the above irregularities, "F" initiated action against "E" for recovering the money unauthorisedly and without any authority of law.

25. Case between "G" and "H"

25.1 'G' entered into an agreement with 'H' for execution of the contract and in that process 'H' has to use some minor minerals obtained from quarries. As per the Contract conditions whenever, minor minerals are obtained from a quarry, the said contractor has to pay seigniorage fee to the Government and obtain a receipt in token of payment of that fee and produce before 'G' to clear his bills. It is also a condition in the contract that if so such receipt is produced or mineral revenue clearance certificate obtained from the authorities are not produced, 'G' can deduct the amount corresponding to the minor mineral used in the contract. In this case as many as 5 minor minerals viz., building stones, gravel, ordinary clay, sand, brick earth (for the purpose of this article only these minor minerals were referred) were used but no mineral revenue clearance certificate was produced by 'H'. As such, 'G' recovered the corresponding amount from the bills of 'H' towards seigniorage fee, for which 'H' raised a dispute and referred the matter for adjudication by an arbitrator. Here in this case a person having legal background was appointed as arbitrator. Respective pleas were taken by both the parties and in support of his claim 'H' examined a witness on his behalf to show that they have paid seigniorage fee to the concerned authorities. The said witness deposed that seigniorage fee was paid in respect of only one minor mineral but in respect of the other minor minerals. 'G' contested that neither mineral revenue clearance certificate was produced nor the witness said that seigniorage fee was paid in respect of all the minor minerals, the recovery of the seigniorage fee amount towards other minor minerals is in order. But the adjudicating authority by applying the deposition of the only witness in respect of one minor mineral, to all other minor minerals, accepted the contention of 'H' and rejected the contention of 'G'.

26. In respect of the four examples given above, the following have not been observed:

26.1 In the first case:

26.1.1 From the view point of advocate: He has not properly considered the dispute between the parties and even if it is taken into consideration, in order to support his client's case, might have suppressed that same. He has failed to fulfill the triple obligation as narrated above.

26.1.2 From the view point of the Adjudicator/Arbitrator: He has failed to consider the pleadings, witnesses testimony, documentary evidence etc., in adjudicating the claims of the claimant and has not rendered 'Justice', thus he has failed to comply with the constitutional obligation as mentioned above.

27.1 In the second case

27.1.1 From the view point of advocate: He has not properly considered the dispute between the parties and even if it is taken into consideration, in order to support his client's case, might have suppressed that same. He has failed to fulfill the triple obligation as narrated above.

27.1.2 From the view point of the Adjudicator/Arbitrator: He has failed to consider the pleadings, witnesses testimony, documentary evidence etc., in adjudicating the claims of the claimant and has not rendered 'Justice', thus he has failed to comply with the constitutional obligation as mentioned above.

28.1 In the third case

28.1.1 From the view point of advocate: He has not properly considered the dispute between the parties and even if it is taken into consideration, in order to support his client's case, might have suppressed that same. That is to say he has not correctly understood the conflict viz., violation of provisions of the Central enactment. Thus he has considered a void contract between the parties. He has failed to fulfill the triple obligation as narrated above.

28.1.2 From the view point of the Adjudicator/Arbitrator: He has failed to consider the pleadings, witness's testimony, documentary evidence etc., in adjudicating the claims of the claimant and has not rendered 'Justice', thus he has failed to comply with the constitutional obligation as mentioned above.

29.1 In the fourth case

29.1.1 From the view point of advocate: He has not properly considered the dispute between the parties and even if it is taken into consideration, in order to support his client's case, might have suppressed that same. That is to say he has not correctly understood the conflict viz., violation of provisions of the Central enactment. Thus he has considered a void contract between the parties. He has failed to fulfill the triple obligation as narrated above.

29.1.2 From the view point of the Adjudicator/Arbitrator: He has failed to properly examine the jurisdictional aspect for adjudicating claim in this case. He has, thus, failed to consider the pleadings, witness's testimony, documentary evidence etc., in adjudicating the claims of the claimant and has not rendered 'Justice', thus he has failed to comply with the constitutional obligation as mentioned above.

30. In all the above 4 cases, the parties affected lost huge sums of money and some have utilized appellate provisions and some have not for obvious reasons.

30.1 Triple obligations to be followed by the Advocates

30.2 Had the concerned advocates properly understood the conflict and fulfilled the triple obligations cast on them and other duties as narrated in this article, the parties will have a proper adjudication of claims resulting in reduction of number of cases at the higher stages.

30.3 In view of the elaborate discussion of the subject, one question remains unanswered – viz., whether really truth is being elicited in the proceedings and justice being rendered to the affected parties. From looking at the overall situation, the answer is definitely in the negative i.e., a MYTH but not in reality, except in very rarest of rare cases. When the matter will set at rest can only be decided by the participating advocates and adjudicators.

---oOo---

II. Acknowledgements

I state that in my research work, I am being guided immeasurably by Smt. SUMITRA SRIPADA, Associate Professor, Dr. B.R. Ambedkar College of Law, Visakhapatnam, and but for her guidance and support, I would not have reached this stage of submitting research paper, which is part of research, in my research work. I, therefore, acknowledge her guidance and support in this regard.

I also acknowledge the support and encouragement given by my friends and well wishers to pursue the Research work.

References

- [1] Advocates Act 1961 – Seventh Edition – LexisNexis Butterworths
- [2] Constitution of India – Tenth Edition – Revised by Mahendra P Singh
- [3] Article of Hon'ble Justice V.R. Krishna Iyer (Retd), Supreme Court of India
- [4] Four cases referred to above. (for the purpose of confidentiality, the cases names are not being given to keep up my word to the concerned)
- [5] DP Chadha –vs- Triyugi Narain Mishra AIR 2001 SC 457 = 2001 (2)SCC 221
- [6] Shambu Ram Yadav –vs- Hanuman Das Khatri AIR 2001 SC 2509

Chapters in Books:

- [1] Chapter 5 at pages 150, 151 of Advocates Act 1961 Seventh Edition
- [2] Constitution of India Article 124, 214, 226, 227, 233 by Mahendra P Singh,

Impact of Medical Mal-Practice in India

Pulyapudi Srinivas

Research scholar & Advocate, Visakhapatnam

Abstract: The patients who joined in Hospitals or approaches medical professionals for treatment are faced with many problems and the said problems are identified as many as 25 in numbers as mentioned at page 3 of this article. Further through this article the research scholar is trying to find out solutions to eradicate this menace in order to see that the patients are given better treatment and restrict the medical professionals from swindling money from the patients. To cite for e.g., prescribing a particular item for replacement from a specified manufacturer so that there would be a trade of between the medical professional and the manufacturer.

Key words

1. Medical Mal-practice
2. Health care
3. Misdiagnosis
4. Standard of care.
5. Duty to Take Care

I. Introduction

- 1.1 Medical Law is undergoing a massive change. Significantly our attitude towards our health, health services, and the medical professions is changing. There was time when doctors were given a 'GODLIKE' status and were held in the highest esteem; and patients were intended to be, well patient; passive and submissive. But this has changed and Doctors are no longer regarded as infallible and beyond questioning. Doctors especially general practitioners, regard their job as working with patients to find out what is the best treatment for them. The doctor-patient relationship, has, according to some, become closer to that of consumer and supplier. (1)
- 1.2 The doctor is not regarded as similar to 'family friend'. The relationship has become more formal and structured. Another change is that the hierarchy amongst medical professional is being challenged with nursing profession carrying out an increased range of tasks. Patient has ready access to health care information, via the internet especially. I have gathered information that many patients are checking up what the doctor says with information available on internet, all of these changes, have as we shall see, and had a significant impact on legal and ethical approaches to medicine.

Medical Law

- 1.3 Medical law is essentially concerned with the relationship between health care professional and patients. The medical law is made up on bits from a large number of Kearns, O, Mathuna, and Scott (2009) for a discussion of the ethical issues raised by such self diagnostic kits (Jonathan Herring – medical law and ethics 3rd edition at page (1) Different branches of law: criminal law, human rights law, tort law, property law, family law, and public law. One commentator has suggested a medical lawyer needs to be a 'Jacqui of all trades'. (2)
- 1.4 The relationship between law and medicine is interesting. In the past it was characterized as one of mutual difference. Medical decisions were regarded as clinical matters best reached by the experts and nay one seeking to challenge a doctor's decision in the Court faced an uphill struggle. However, more recently the relationship has changed. Courts it seems are a little more willing to accept challenge to a decision of a doctor.
- 1.5 The law sets down minimally acceptable standards, while ethical approaches may include deciding what would be the real way for a person to behave. Similarly something may give rise to a legal sanction but not be unethical. Medical ethics mean the application of ethical reasoning to medical decision making.

II. What is health care?

- 2.1 Health care in the world is one of the important aspects, and while doctors don't like to admit it, this is in large part due to the scrutiny placed upon the medical field by medical malpractice lawyers pursuing medical malpractice legal claims against doctors, dentists, chiropractors and hospitals.

III. What is medical malpractice?

- 3.1 Medical malpractice is a wanton and intentional negligence committed by a professional health care provider, such as a doctor, nurse, dentist, technician, hospital worker or hospital, whose treatment of a patient departs from a standard of care met by those with similar training and experience, resulting in harm to a patient. (2)
- (2) Sheldon and Thomson 1998:5 (Jonathan Herring – medical law and ethics 3rd edition at page (2)
- 3.2 Medical malpractice is a wanton and intentional treatment by any type of health care professional which does not meet the standard level of care and results in harm to the patient. This includes failing to take a necessary action or taking an inappropriate action. In order to qualify as malpractice three elements must be present
- 3.1.1 There must have been a professional relationship between you and the health care provider

3.1.2 The health care provider must have acted beneath the standard level of care that any other health care provider would have used in the same situation

3.1.3 This substandard care must have harmed you in some way.

3.3 The law of medical malpractice is an outgrowth of the general body of negligence law. It is the law applicable against medical professionals (doctors, nurses, nurse practitioners, dentists, hospitals, physical therapists, pharmacists, physician assistants, plastic surgeons, psychiatrists, etc.) alleging acts, intentionally and wantonly, in the performance of medical services to their patients. In medical malpractice law the fictional “reasonably prudent health care provider” standard has been created. In both instances the terminology of the attorneys revolves around the issue of whether the doctor, hospital or other health care provider was “negligent.” In medical malpractice cases the plaintiff’s medical malpractice lawyer must establish through expert testimony the standard of care required of doctors or other health care providers in the field of the defendant and that the defendant peached or failed to adhere to that standard of care, intentionally and wantonly, thereby causing the plaintiff’s injury.

IV. What are some common types of medical malpractice?

4.1 Medical malpractice occurs where a medical practitioner acts in a negligent manner, intentionally and wantonly, when treating a medical condition. Malpractice can occur from an action taken by the medical practitioner, or by the failure to take a medically appropriate action. Details of some of the examples of medical malpractice are given below.

(i) Intentional or wanton failure to diagnose or misdiagnosis of a disease or medical condition; (ii) Intentional or wanton failure to provide appropriate treatment for a medical condition; (iii) Wanton and intentional unreasonable delay in treating a diagnosed medical condition; (iv) Intentional or wantonly continuing treatment though not strictly necessary; (v) Intentional or wanton admitting patients for one disease, however, treating them for different disease; (vi) Though not actually necessary in respect of pregnant woman by treating her prior to the delivery and to create a situation, intentional or wantonly, by putting fear, to have an operation instead of normal delivery and in those circumstances there is no choice to the patient or to her attendant; (vii) While undertaking operation to a patient on one organ, taking out other important organs from the body and selling them for making money; (viii) Treatment by non-professionals with fake professional documents; and (ix) Wanton and intentional prescription of costly drug and administer it on the first occasion and administering the drug with the same name but with low cost and charge at the higher rate through out; (x) Anesthesia malpractice; (xi) Birth injury and defects; (xii) Breast implant malpractice; (xiii) Cosmetic surgery mistakes; (xiv) Dental errors; (xv) Prescription drug malpractice; (xvi) Psychiatric malpractice; (xvii) Surgical errors; (xviii) Unnecessary surgery; (xix) Wrongful death; (xx) Wrong diagnosis and misdiagnosis; (xxi) Prescribing unnecessary clinical tests; (xxii) directing the patient to go and purchase medicines from a specific pharmacist (Medical shop); (xxiii) directing the patient to go to a particular clinical laboratory for clinical tests; (xxiv) Intentional, fraudulent and wanton dealing of cases where the patient is covered by insurance; and (xxv) accepting trade offers from manufacturers of orthopedic instruments (body implants) which may be used in surgical operations’.

V. Who can be held responsible for medical malpractice?

Any type of health care professional can be held responsible for medical malpractice. So can the facilities and companies that they work for. There can be multiple responsible parties in one malpractice lawsuit. Responsible parties may include: (a) Doctors; (b) Surgeons; (c) Emergency room staff; (d) Nurses; (e) Anesthesiologists; (f) Dentists; (g) Psychiatrists; (h) Hospitals; (i) Nursing homes; (j) Government institutions; and (k) Pharmaceutical companies.

5.1 Elements of the medical mal-practice

5.1.1 Four elements of the tortious act must be established for a successful medical malpractice claim. They are

(i) A duty was owed: a legal duty exists whenever a hospital or health care provider undertakes care or treatment of a patient.

(ii) A duty was breached: the provider failed to conform to the relevant standard of care. The standard of care is proved by expert testimony or by obvious errors (the doctrine of *res ipsa loquitur* or the thing speaks for itself).

(iii) The breach caused an injury: The breach of duty was a proximate cause of the injury.

(iv) Damages: Without damages (losses which may be pecuniary or emotional), there is no basis for a claim, regardless of whether the medical provider was negligent. Likewise, damages can occur without negligence, for example, when someone dies from a fatal disease.

5.2 How Medical Negligence becomes Medical malpractice

5.2.1In short, medical negligence becomes medical malpractice when the doctor’s intentional and wanton negligent treatment causes undue injury to her patient. This one sentence implies two additional legal concepts required for a medical malpractice case viz., injury and Causation. Medical malpractice is the failure of a medical professional to meet the standard of good medical practice in the field in which the medical professional practices. Medical malpractice occurs when a healthcare provider - doctor, hospital, HMO, nurse, other individual or entity licensed to provide medical care or treatment - does something that competent doctors would not have done, or fails to do what a competent doctor would have done, resulting in personal injury or wrongful death. Medical malpractice law is complex and, therefore, it is important to engage an experienced malpractice lawyer or attorney who understands the complex issues that apply.

Medical malpractice claims involve analysis of medical records and all tests and studies such as MRI, CAT scan, pathology studies, etc. to determine the viability of the claim. If one or a loved one has been a victim of medical malpractice, that person should act promptly to preserve your rights.

- 5.2.2** Relevant provisions available under Indian Penal Code to deal with certain Acts as offences.
- 5.2.3** Indian Penal Code 1860 was enacted as Act 45 of 1860 dealing with offenses which are punishable under the act. The said code consists of 511 sections out of which some of the sections specifically deal with health and injury.
- 5.2.4** In Chapter II containing general explanations which deal with the term 'offense', 'death', and 'good faith', the relevant Sections are: Sections 40, 44, 46, and 52. In Chapter IV which deals with general exceptions, the relevant Sections are: Sections 80, 81, 87, 89, 90, 92, and 93. In Chapter XIV which deals with offenses affecting the public health, safety, convenience, decency and morals, the relevant Sections are: Sections 269 and 284. In Chapter XVI which deals with offenses affecting the human body, the relevant Sections are: 304 A, 312, 314, 315, 319, 328, 337, and 338.
- 5.2.5** In addition to Indian Penal Code, there is another enactment entitled 'Consumer Protection Act of 1986' which controls medical mal-practice. It may be pointed out that the Consumer Protection Act 1986 was enacted by the Parliament of India to safeguard consumer interest, in compliance with the United Nations guidelines adopted on 9-4-1985. Consumer Courts were established for the settlement of consumers' disputes and related matters. The Act protects not only the interests of consumer when he purchases goods and services for daily use, but also protects his interests when he goes for treatment to a medical professional. Many medical associations lodged their protests against the application of the Act 1986 to the doctors on the ground that the relationship between a doctor and a patient is not that of a buyer and seller. However this contention was not accepted. In the initial period after the enactment of the Act, there was a lot of confusion in the judiciary as well as medical fraternity regarding the application of the Act to this profession. All the confusions regarding the scope of the Act of 1986 to adjudicate the claims against the medical profession were cleared by the Hon'ble Supreme Court in the landmark judgment in the case of Indian Medical Association –vs- V.P. Shantha. (3) With regard to the provisions of the Consumer Protection Act 1986 some relevant sections are necessary. They are the terms 'complainant'; 'complaint'; 'consumer'; 'deficiency'; and 'service'.
DEFINITIONS under Act 1986

5.3. Complainant means

- 5.3.1** Any allegation, in writing made by a complaint that the service hired or availed of or agreed to be hired or availed of by him suffer from deficiency in any respect.
Consumer means
- 5.4** Any "person" who hires or avails of any services for a consideration which has been paid or promised or partly paid and partly promised any include any beneficiary of such services for consideration paid or promised, or partly paid and partly promised, or under any system of deferred payment, when such services are availed of with the approval of the first mentioned person.

VI. Consideration

- 5.4.1** Consideration means fees/payment. Fees may have been fully paid in cash or cheques, or undertaking that it will be paid, which is accepted by the doctor/hospital. The fees may have been given partly (as advance) with the understanding that the remaining bill will be paid subsequently. The payment may
- (3) **(1995) 6 SCC 651.**
Be done by the patient himself or by someone else for the patient, e.g. father for his child, husband for wife, any person for someone.
- 5.4.2** A person who receives medical treatment in Government or Charitable Hospital, which provides treatment to one and all free of cost, is not a consumer under the Act. A person who receives treatment in a Government or charitable hospital which provides treatment free of cost to some and on consideration to some would be a consumer, even if he has not paid any fees. In case of death of patient who is a consumer, legal heirs (representatives), of the deceased will be considered as "consumer". If the payment has been made by any person who is not a legal heir of the deceased he too will be considered as 'consumer'. The three words used above (deficiency, person, service) explained under this act are as follows Deficiency means
- 5.4.3** Any fault, imperfection, short coming or inadequacy in the quality, nature and manner of performance which is required to be maintained by or under any law for the time being in force or has been undertaken to be performed by a person in pursuance of a contract or otherwise in relation to any service.
- 5.4.4** Person include
1. A firm whether registered or not;
 2. A Hindu undivided family;
 3. A co-operative society;
 4. Every other association of persons whether registered under the Societies Registration Act, 1860, or not.

Service means

- 5.** Service of any description which is made available to potential users and includes the provision of facilities in connection with banking, financing, insurance, transport, processing, supply of electrical or other energy, board or lodging or both, housing construction, entertainment, amusement or the purveying of news or other information but does not include the rendering of any service free of charge or under a contract of personal services.

- 5.1** On the meaning of the word "service" in relation to medical profession, the Supreme Court in Indian Medical Association's case (supra) came to the following conclusions
- Service rendered to a patient by a medical practitioner (except where the doctor rendered service free of charge to every patient or under a contract of personal service), by way of consultation, diagnosis and treatment, both medicinal and surgical, would fall within the ambit of 'service' as defined in section 2(1) (o) of the Act.
 - The expression 'contract of personal service' in section 2(1) (o) of the Act cannot be confined to contracts for employment of domestic servants only and the said expression would include the employment of a medical officer for the purpose of rendering medical service to the employer. The service rendered by a medical officer to his employer under the contract of employment would be outside the purview of 'service' as defined in section 2(1) (o) of the Act.
 - Service rendered at a Government hospital/health centre/dispensary or at a non-government hospital/nursing home where no charge whatsoever is made from any person availing the service and all patients (rich and poor) are given free service- is outside the purview of the expression "service" as defined in section 2(1) (o) of the Act. The payment of a token amount for registration purpose only at the hospital/nursing home would not alter the position.
 - Service rendered at a non-government hospital/nursing home where charges are required to be paid by the person availing such services falls within the purview of the expression 'service' as defined in section 2(1) (o) of the Act.
 - Service rendered at Government hospital/Health centre/ Dispensary or at a non-government Nursing home where charges are required to be paid by persons who are in a position to pay and persons who cannot afford to pay are rendered service free of charge would fall within the ambit of the expression 'service' as defined in section 2(1) (o) of the Act irrespective of the fact that the service is rendered free of charge to persons who are not in a position to pay for such services. Free service, by such doctors and hospitals would also be 'service' and the recipient a 'consumer' under the Act.
 - Service rendered by a medical or hospital/nursing home cannot be regarded as service rendered free of charge, if the persons availing the service has taken an insurance policy for medical care where under the policy charges for consultation diagnosis and medical treatment are borne by the insurance company and such service would fall within the ambit of 'service' as defined in section 2(1) (o) of the Act.
- 5.2** Similarly, where as a part of the conditions of service, the employer bears the expenses of medical treatment of an employee and his family member dependent on him, the service rendered to such an employee and his family members by a medical practitioner or a hospital/nursing home would not be free of charge and would constitute 'service' under section 2(1) (o) of the Act.
- 5.3** In addition to the aforementioned provisions of Statutes, there are some more statutes which are required to be applied in respect of the cases under medical mal-practice, which are given below for ready reference.
- 5.4** 'Code of ethics formulated by state medical councils; (ii) The Employees' Compensation Act 1923; (iii) The Maternity Benefit Act, 1961; (iv) The Personal Injuries (Compensation Insurance) Act, 1963; (v) The Indian Medicine Central Council Act, 1970; (vi) The Medical Termination of Pregnancy Act 1971; (vii) The Mental Health Act, 1987; (viii) The Transplantation of Human Organs Act, 1994; (ix) The Pre-conception and Prenatal Diagnostic Techniques (Prohibition of Sex Selection) Act 1994; (x) The Persons with Disabilities (Equal Opportunities, Protection of Rights and Full Participation) Act 1995; (xi) The Dentists (Code of Ethics) Regulations 1976; (xii) The Indian Medical Council (Professional Conduct, Etiquette and Ethics) Regulations, 2002; (xiii) The Pharmacy Act 1948; (xiv) The Indian Nursing Council Act 1947; (xv) The Homoeopathy Central Council Act 1973.'

5.5 Contextual frame work

5.5.1 The Indian system of medicine has a long history. It has received worldwide recognition especially in the area of Herbal, Unani, and Ayurvedic systems. Besides Kautilya's Arthashastra, there are a series of ancient authoritative publications, which give a glimpse of the ancient system of medicine. The accountability of the physicians may be traced from the work of Kautilya wherein it is stated that.

5.6 Health Care at the International Level

5.6.1 The quality of health services and medical negligence has been a matter of great concern at the international level. The General Assembly of the United Nations, has adopted various resolutions to safeguard the interest of patients Article 25 of the Universal Declaration of Human Rights states that

5.6.2 'Every one has the right to a standard of living adequate for the health and well-being of himself and his family, including food, clothing, housing and medical care, and necessary social services, and the right to security in the event of unemployment, sickness, disability, widowhood, old age or other lack of livelihood in circumstances beyond his control'.

5.6.3 Article 12 of the International Covenant on Economic, Social, and Cultural Rights 1966, inter alia, states that: 'The State parties to the present convention recognize the right of everyone to the enjoyment of the highest attainable standard of physical and mental health'.

5.6.4 The aforesaid rights of 1966, the UN declaration on elimination of all forms of discrimination against women 1967, the convention on the elimination of all forms of discrimination against women 1979 and the convention of the rights of the child provide, inter alia, for the protection of health care rights of persons including women, children and other disadvantaged sections of society. (4)

5.6.5 The world health organization, has also played a pioneering role for the last fifty years, in guiding health policy development, and action at the global and national levels, with an overall objective of ensuring and attaining the highest standards of health care to all the people around the world.

5.6.6 The preamble to the World Health Organization Constitution.

5.6.7 The World Health Organization's Constitution came into force in 1948. Inter alia, provides

- The enjoyment of the highest standards of health is one of the fundamental rights of every human being without distinction of race, religion, political belief, economic and social condition.
- The health of all peoples is fundamental to the attainment of peace and security and is dependent upon the fullest co-operation of individuals and states.
- The achievement of any state in the promotion and protection of health is of value to all.
- Unequal development in different countries in the promotion of health and control of disease, especially communicable disease, is a common danger.
- Healthy development of the child is of basic importance; the ability to live harmoniously in a totally changing environment is essential to such development.
- The extension to all people of the benefits of medical, psychological and related knowledge is essential to the fullest attainment of health.

(4) Legal framework for Health Care in India – LexisNexis – Butterworth's 2002 edition.

- Informed opinion and active co-operation on the part of the public are of the utmost importance in the improvement of the health of the people.

5.6.8 Governments have a responsibility for the health of their people, which can be fulfilled only by the provision of adequate health and social measures. (5)

5.6.9 The World Health Organization Constitution delineates several functions, which directly and indirectly require the application of legal principals, such as

- to act as the directing and coordinating authority on international health work;
- to propose 'Conventions, Agreements and Regulations', make recommendations with respect to international health matters, and to perform such duties as may be assigned thereby to the Organization and are consistent with its objective ; and
- to develop, establish and promote international standards with respect to food, biological, pharmaceutical and consumer products.
- Apart from the above, a number of international agencies have lent support to public participation in health care. To this end, the World Health Organization Alma Ata Declaration, clearly states that:

The people have the right and duty to participate individually and collectively in the planning and implementation of their health care'. (6)

5.6.10 Legal frame work for health care in India

In India, the right to health care means that the meaning of health as used in these provisions of the Constitution are defined in the Oxford Dictionary that soundness of body or mind, that condition in which its functions are duly and

(5) The World Health Organization's Constitution (came into force in 1948)

(6) Alma Ata Declaration adopted in 1978.

Efficiently discharged. Statutory laws including the Indian Penal Code 1860 and others also ensure the right to be protected against medical negligence and protection has been recognised since early times. India is a founder member of the United Nations, and has ratified various International Conventions promising to secure health care rights of individuals in society. In this context, art 51 of?

5.6.11 The Constitution of India provides for promotion of international peace and security. Article 51 states that, the State shall endeavour to: (a) promote international peace and security; (b) maintain just and honourable relations between nations, (c) foster respect for international law and treaty obligations in the dealing of organized people with one another; and (d) encourage settlement of international disputes by arbitration. The preamble to the Constitution of India, which strives to provide for a welfare state with socialistic patterns of society, guarantees the right to life and personal liberty. It states that:

5.6.12 'No one shall be deprived of his right to life and personal liberty except according to procedure established by law'. (7)

5.6.13 Though it does not expressly contain the right to health, it has now been well settled through a series of cases that this includes the right to health Further, Articles 38, 48, 43, and 47 of the Constitution also provide for the promotion of health of individuals in society.

5.6.14 Complaints of medical negligence have been made in the past of late, such complaints have assumed a wider dimension as the incidents have increased due to the opening of thousands of nursing homes charitable hospitals, central government health services dispensaries, and employee state insurance hospitals etc. Though the Parliament has enacted the Indian Medical Council Act in 1956 and other corresponding legislation governing various branches of medicine such as

(7) Article 21 of the Constitution of India

the Indian System of Medicine, Dentists, Homoeopaths etc, they only provided for the registration and regulation of the conduct of doctors, hospitals and nursing homes, and have failed to protect the interests of persons who have suffered on

account of negligence or deficiency on the part of medical professionals. Very few states such as Andhra Pradesh, Karnataka, Meghalaya and recently Delhi have enacted state legislations providing for constitution of state Medical Council.

5.6.15 This field left untouched by the Medical Council Acts is covered by the law of tort in general, and now by the Consumer Protection Act 1986. It is worthwhile to remember that the existence on the state book of the Indian Medical Council Act has not stood in the way of such grievances being agitated before the ordinary civil Courts, by the institution of civil suits claiming damages for negligence as against the concerned hospital or medical doctors. Before the enactment of the Consumer Protection Act 1986, the field of medical negligence was governed only by the law of tort. The base for a liability rested on the concept of negligence. It is not and cannot possibly be the province of this judgment, to enter the tangled thicket of the scope of negligence in tort jurisprudence. It is a field too large to be traversed. It would suffice to point out that prior to the entry of consumer jurisdiction in this field, medical accountability rested primarily on the concept of negligence as understood in the law of torts. That a precise legal definition of negligence is perhaps not possible, and would remain a somewhat slippery word. However, the classic attempted judicial definitions of negligence may be noticed from the authoritative treatise as under:

5.6.16 'It is negligence in the objective sense that is referred to in the well-known definition of Alderson B, Negligence is the omission to do something which a reasonable man, guided upon those considerations which ordinarily regulate the conduct of human affairs, would do, or doing something which a prudent and reasonable man would not do. So also Lord Wright said in strict legal analysis, negligence means more than heedless or careless conduct, whether in omission or commission; it properly connotes the complex concept of duty, breach and damage thereby suffered by the person to whom the duty was owing'. (8) In India it is well settled that the general principle of law of tort is equally relevant and applicable within our country. The development of the Law of Torts is in the line and closely similar, if not identical with its parental concept. (9)

5.8 Accepted Health/Medical Standard of Care

5.8.1 The accepted medical standard of care can be thought of as the sum of medical knowledge that has been accumulated over hundreds of years of medical and scientific study and discovery, and how that knowledge has become the tools with which doctors can treat patients and make them well when ill or injured. Analogous to the rules to which a driver must adhere when operating a car on public roads, the medical standard of care provides a sort of *playbook*, which outlines rules for treating patients under different circumstances, and a medical professional is required to adhere to this *playbook* to ensure the safety of his or her patients.

5.8.2 Duty of a doctor when an injured person approaches him and Legal protection to doctors treating injured persons, and No legal bar on doctors from attending to the injured persons:

5.8.3 Whenever a man of the medical profession is approached by an injured person, and if he finds that whatever assistance he could give is not really sufficient to save the life of the person, but some better assistance is necessary, it is the duty of the man in the medical profession so approached to render all the help which he could, and also see that the person reaches the proper expert as early as possible.

➤ A doctor does not contravene the law of the land by proceeding to treat an injured victim on his appearance before him, either by himself or

(8) Treatise of Salmond on the Law of Torts 19th Edn.

(9) Dr. Ravinder Gupta & ors –vs- Ganga Devi & ors 1993 (3)CPR 259.

With others. Zonal regulations and classifications cannot operate as fetters in the discharge of the obligation, even if the victim is sent elsewhere under local rules, and regardless of the involvement of police. The 1985 decision of the Standing Committee on Forensic Medicine is the effective guideline.

➤ There is no legal impediment for a medical professional, when he is called upon or requested to attend to an injured person needing his medical assistance immediately. The effort to save the person should be the top priority, not only of the medical professional, but even of the police or any other citizen who happens to be connected with the matter, or who happens to notice such an incident or a situation (10)

5.9 Definition of 'Professional'

5.9.1 The occupations that are regarded as professional have four characteristics, viz. (a) the nature of the work which is skilled and specialized and a substantial part is mental rather than manual; (b) commitment to moral principles which go beyond the general duty of honesty, and a wider duty to community which may transcend the duty to a particular client or patient; (c) professional association which regulates admission and seeks to uphold the standards of the profession, through professional codes on matters of conduct and ethics; and (d) high status in the community. (11)

5.9.2 The Supreme Court ruled that a charge of professional medical malpractice/negligence against a medical man was serious. It stood on a different footing to a charge of negligence against the driver of a motor car. The consequences were far more serious. It affected his professional status and reputation. The burden of proof was correspondingly greater. As the charge was

- (10) Pt Parmanand Katara v. Union of India & ors AIR 1989 SC 2039.
(11) Rupert M Jackson and John L. Powell. (Legal Framework for Health Care in India – LexisNexis – Butterworths 2002 edition page 35).

So grave, so should the proof be clear. With the best will in the world, things sometimes go amiss in surgical operations or medical treatment. A doctor was not to be held negligent simply because something went wrong. He was not liable for mischance or misadventure; or for an error of judgment. He was not liable for taking one choice out of two or for favoring one school rather than another. He was only liable when he fell below the standard of a reasonably competent practitioner in his field, so much so that his conduct might be deserving of censure or be inexcusable.

5.10. Concept of Duty to Take Care.

5.10.1 The Supreme Court ruled that a person who is not qualified to practice allopathy was a quack or pretender to the medical knowledge and skill, or a charlatan. He is liable to be prosecuted under sub-section (3) of Section 15 the Medical Councils Act 1956 and is be prosecuted under sub-section (3) of Section 15 the Medical Councils Act 1956 and is guilty of negligence.

5.10.2 The Court further ruled that professional men should possess a certain minimum degree of competence and that they should exercise reasonable care in the discharge of their duties. In general, a professional man owes to his client a duty, to exercise reasonable care in giving advice or performing services. Immunity from suit has been enjoyed by certain professions on the grounds of public interest. The trend now is the narrowing of such immunity. Medical practitioners do not enjoy any immunity and they can be sued in contract/Consumer Protection Act and also under the provisions of Indian Penal Code on the ground that they have failed to exercise reasonable skill and care. Thus medical practitioners, though belonging to the medical profession, are not immune from a claim for damages on the ground of medical malpractice/negligence.

5.11 Standard of Care; Location Factor.

5.11.1 Treatment differs from doctor to doctor. The Supreme Court pointed out that the skill of medical practitioner varies from doctor to doctor. The very nature of the profession is such that there may be more than one course of treatment, which may be advisable for treating a patient. Courts would indeed be slow in attributing negligence on the part of a doctor if he has performed his duties to the best of his ability, and with due care and caution. Medical opinion may differ with regard to the course of action to be taken by a doctor treating a patient, but as long as a doctor acts in a manner which is acceptable to the medical profession, and the Court finds that he has attended on the patient with due care, skill and diligence, and if the patient still does not survive or suffers a permanent ailment, it would be difficult to hold the doctor guilty of negligence. (12)

5.12 Liability of a doctor for not advising the patient to approach a better hospital:

5.12.1 The operation theatre was under repair. There were no facilities for oxygen and blood transfusions, there was no anesthetist, and some life saving drugs were not available. Pipettes for testing blood were broken, the saline apparatus was not in order, and there were only two staff nurses for a 28-bedded hospital. In these circumstances the Supreme Court ruled that the doctor should not have undertaken such a major operation in a hospital, which was lacking basic facilities. He should have advised plaintiff no 1, after he found that an operation was required, to take his wife to Rewa Medical College, which was not far off, which had all the facilities including specialists. The doctor, therefore, failed in his duty of care in undertaking the operation without taking necessary precautions. (13)

5.13 Difference in standard of care of doctors attached with companies/ factories from those of general doctors:

- (12) Achutrao H Khodwa v state of Maharashtra AIR 1996 SC 2383.
(13) Ram Bihari Lal v JH Shrivastava AIR 1985 MP 150.

5.13.1 The Supreme Court ruled that the duty cast on the company's doctor in respect to the company's employees is not any higher or lower than the duty of an average doctor towards his patient. (14)

5.14 Duty to Take Reasonable Care in Accident Cases

5.14.1 The Supreme Court, ruled that every doctor whether at a government hospital or otherwise has the professional obligation to extend his services with due expertise for protecting life. No law or State action can intervene to avoid/delay the discharge of the paramount obligation cast upon members of the medical profession. The obligation being total, absolute and paramount, laws of procedure whether in statutes or otherwise which would interfere with the discharge of this obligation cannot be sustained, and must therefore, given way. (15)

5.15. Role of Consent in Fixing Liability.

Oral consent admissibility:

5.15. The State Consumer Redressal Commission, Chennai, ruled that in all cases where a treatment consists of certain dangerous instruments, it is the duty of the medical authority to taken the consent of the patient, preferably in writing.

5.16 Medical Malpractice

5.16.1 The law of *medical malpractice* is an outgrowth of the general body of negligence law. It is the law applicable against medical professionals (doctors, nurses, nurse practitioners, dentists, hospitals, physical therapists, pharmacists, physician assistants, plastic surgeons, psychiatrists, etc.) alleging acts, intentionally and wantonly, in the performance of medical services to their patients. At common law, the duty of due care by medical professionals was deemed to have arisen out of the contractual obligations which are created when a

(14) Philips India Ltd, v Kunju Punnu & anr AIR 1975 Bom 306.

(15) Pt Parmanand Katara v Union of India & ors, AIR 1989 SC 2039.

Patient contracts with a health care provider to perform health care services. Even though some jurisdictions still retain common law contractual concepts in dealing with *medical malpractice* suits, *medical malpractice* is now generally considered by most attorneys, judges and legal scholars to be an independent action in tort, rather than in contract.

5.16.2 In the same sense that the ordinary body of negligence law defines negligence as the doing or the failure to do something that a person of ordinary prudence would or would not do under the same or similar circumstances, the law of medical malpractice defines wanton and intentional negligent medical conduct as the doing or the failure to do something that a reasonably prudent doctor or other health care professional in that field would or would not do under the same or similar circumstances. In negligence law the fictional “reasonable man” standard has been created to evaluate the conduct of the defendant alleged to have been negligent. In medical malpractice law the fictional “reasonably prudent health care provider” standard has been created. In both instances the terminology of the attorneys revolves around the issue of whether the doctor, hospital or other health care provider was “negligent.” Some attorneys note that the “reasonable man” standard is objective, in the sense that it is a standard applicable to all human beings, whereas the “reasonably prudent health care provider” is more subjective, in that it allows the medical profession to define the standard by which its conduct will be judged. It is to point out that that standard may fluctuate over periods of time as short as months, depending on available technology. Other attorneys respond that the law holds even medical professionals to certain minimum requirements of care, and evidence presented in a medical malpractice that few people in a given medical field exercise caution in an area where caution should be exercised would not preclude a finding in the same law suit that a doctor, chiropractor or other health care provider was negligent. In medical malpractice cases the plaintiff’s medical malpractice lawyer must establish through expert testimony the standard of care required of doctors or other health care providers in the field of the defendant and that the defendant peached or failed to adhere to that standard of care, intentionally and wantonly, thereby causing the plaintiff’s injury. A negative result in medical treatment in and of itself does not mean that the doctor, hospital or other health care provider committed malpractice. Medical treatment carries with it no guarantee of a successful outcome. In many medical procedures there are risks which cannot be avoided even if the doctor exercises the greatest caution. These are called unavoidable risks. On the other hand, risks which are unavoidable even when the greatest care has been exercised, may in a particular case, be shown by an attorney to have resulted from lack of due care by the doctor or other health care professional.

5.16.3 Medical malpractice is committed by a professional health-care provider—a doctor, a nurse, a dentist, a technician, a hospital, or a nursing facility—, intentionally and wantonly, whose performance of duties wantonly departs from a standard of practice of those with similar training and experience, resulting in harm to a patient, and gain to the professional in any manner. Most medical malpractice actions are filed against doctors who have failed to use reasonable care to treat a patient. Though million-dollar verdicts make headlines, in fact the big juries award hear about are few and far between. Medical malpractice is the wanton and intentional failure of medical professionals to provide adequate treatment to patients resulting in a personal injury or substantial loss of income.

5.16.4 It is a professional act or omission by a health care provider in which care provided deviates from accepted standards of practice in the medical community and causes injury or death to the patient, with most cases involving medical error. Standards and regulations for medical malpractice vary by country and jurisdiction within countries. Medical professionals may obtain professional liability insurances to offset the risk and costs of lawsuits based on medical malpractice. A doctor would be liable for (depending on the circumstances) such things as prescribing experimental drugs and performing cosmetic surgery.

5.17 Elements of the medical mal-practice

5.17.1 Four elements of the tortious act must be established for a successful *medical malpractice* claim. They are:

- A duty was owed: a legal duty exists whenever a hospital or health care provider undertakes care or treatment of a patient.
- A duty was breached: the provider failed to conform to the relevant standard of care. The standard of care is proved by expert testimony or by obvious errors (the doctrine of *res ipsa loquitur* or *the thing speaks for itself*).
- The breach caused an injury: The breach of duty was a proximate cause of the injury.
- Damages: Without damages (losses which may be pecuniary or emotional), there is no basis for a claim, regardless of whether the medical provider was negligent. Likewise, damages can occur without negligence, for example, when someone dies from a fatal disease.

5.18 How Medical Negligence becomes Medical malpractice

5.18.1 In short, medical negligence becomes medical malpractice when the doctors intentional and wanton negligent treatment causes undue injury to her patient. This one sentence implies two additional legal concepts required for a medical malpractice case viz., injury and Causation.

5.18.2 Medical malpractice is the failure of a medical professional to meet the standard of good medical practice in the field in which the medical professional practices. Medical malpractice occurs when a healthcare provider - doctor, hospital, HMO, nurse, other individual or entity licensed to provide medical care or treatment - does something that competent doctors would not have done, or fails to do what a competent doctor would have done, resulting in personal injury or wrongful death. Medical malpractice law is complex and, therefore, it is important to engage an experienced malpractice lawyer or attorney who understands the complex issues that apply. Medical malpractice claims involve analysis of medical records and all tests and studies such as MRI, CAT scan, pathology studies, etc. to determine the viability of the claim. If one or a loved one has been a victim of medical malpractice, that person should act promptly to preserve your rights.

5.18.3 Quality medical care should be a guaranteed outcome when a person consult a physician or undergo surgery or other hospitalizations, and the claim of medical malpractice is a grave accusation. To be considered medical malpractice, you must first consider two criteria

- Did the doctor practice medicine in a way that his or her peers would not have done or would not have considered the correct “standard of care?”
- Did the patient suffer an outcome that left him/her with an injury that is lasting or at least substantial enough to pursue a claim?
- Contrary to popular media, abuse does sometimes occur in the field of medicine, but it is not always possible to take it to Court. Attorneys must work within what is called the “rules of evidence.” Not everything that happens is necessarily admissible in a Court of law.

5.18.4 A person may have been injured by a doctor, a nurse, or some other practitioner in what is normally the “helping” profession.

5.19. Distinction between medical negligence and medical malpractice.

Medical negligence	Medical Malpractice
1. Medical negligence means that you failed to do something that you should have done.	1. Medical malpractice means that you DID something wrong that you should have known was wrong.
2. Medical negligence is when you failed to do something that you should have done. Say, if a doctor should have treated or diagnosed a patient but failed to do so which led to a permanent disability of a patient. So, medical negligence occurs when you do something that is below the standard of care you are responsible to provide. Common complaints about doctors who commit medical negligence include but are not limited to the following: (i) failure to revise an initial diagnosis; (ii) failure to explain medical treatment and warn the patient of the risks of this treatment; (iii) failure to remove a surgical instrument from the patient's body following an operation; (iv) failure to attend or treat a patient; (v) incompetence; (vi) failure to refer a patient to another doctor who is a specialist in the relevant disease or injury; (vii) failure to advise on the options for medical treatment; (viii) failure to arrange a follow-up session or further tests for the patient; and (ix) wrongful diagnosis.	2. Medical malpractice means that you DID something wrong that you should have known was wrong. This is if you did something that is beyond your job description. Say, for example, if a nurse prescribes medicine in which it is the duty of a doctor to prescribe medicine and not of the nurse. Another example is when a Certified Nursing Accountant (CNA) administers an intravenous drug.
3. Medical negligence occurs when a physician, hospital, pharmacist, or any other health care professional fails to perform the expected duties of their respective jobs. Once a medical professional or medical facility has agreed to treat a patient, there is already the duty to treat such patient with reasonable skill, prudence, and customary care based on a standard of medical care. The standard of medical care is defined by Webster's Medical Dictionary as the manner a reputable medical provider with the same qualifications would manage a patient's treatment under equivalent conditions.	3. Medical malpractice occurs when a patient suffers complications, injury, or death because of a health care professional's or health care facility's medical intentional or wanton negligence, and provided there is proof of harm and loss.
4. Medical negligence occurs when a medical professional does not comply with the standard of medical care, whether by performing flawed or irresponsible procedures or by failing to take the necessary actions to prevent harm. Medical negligence can result in injury or harm to the patient, but not	4. Proof in medical malpractice covers four areas: (i) Physicians, health care professionals or providers had a duty to provide health care to a specific patient or patients; (ii) The health care professionals or facilities failed to provide the standard of medical care; (iii) This failure to

in all cases. Medical negligence is a part of medical malpractice.	provide the standard of medical care resulted in harming the patient or patients; (iv) A patient must be able to prove there were damages, such as a loss of eyesight, loss of use of limbs, or a loss of the ability to work. If any one of these four points is missing, it does not constitute medical malpractice.
5. Medical negligence is the act or omission in treatment of a patient by a medical professional, which deviates from the accepted medical standard of care.	5. Medical malpractice is by and act or omission by a health care provider in which care provided deviates from accepted standards of practice in the medical community and causes injury or death to the patient, with most cases involving medical error. Standards and regulations for medical malpractice vary by country and jurisdiction within countries.
6. Medical Negligence does not imply Injury.	6. Most (73%) settled malpractice claims involve medical error.
7. Negligence is the generic identify for a tort wherever an individual has a duty to an additional man or woman, breaches that duty, which is lead to in truth and proximate trigger of damages.	7. Malpractice has both direct and indirect costs, including "defensive medicine." In Medical malpractice cases, the doctor has the duty to act as a sensible physician (or specialist, if required) would act.
8. If a doctor is found to be negligent he has neglected to do something he should have. It is basically careless. May be he should have suggested a test and didn't. Like when you forget to clean the candy wrapper out from under your bed and now your room is full of bugs.	8. Medical malpractice indicates that when the doctor's negligent treatment causes undue injury to the patient. This one sentence implies two additional legal concepts required for a medical malpractice case: Injury and Causation.
9. Medical negligence are the types of cases which often require attorneys for the plaintiff (those bringing the complaint) to prove four necessary elements against a defendant (those against whom the complaint is brought). Medical negligence cases can also go on for prolonged periods of time.	9. Any unintentional tort or any breach of contract based on health care or professional services rendered, or which should have been rendered, by a health care provider, to a patient, including failure to render services timely and the handling of a patient, including loading and unloading of a patient, and also includes all legal responsibility of a health care provider arising from defects in blood, tissue, transplants, drugs and medicines, or from defects in or failures of prosthetic devices, implanted in or used on or in the person of a patient.
	10. Six factors to be considered in determining whether malpractice is present: First, was the wrong treatment related? Was it caused by a failure in professional skill? Second, is expert medical evidence needed to determine whether the appropriate standard of care was breached? Third, did the wrong involve assessment of the patient's condition? Fourth, did the wrong occur in the context of a physician-patient relationship? Was it within the scope of an activity the hospital is licensed to perform? Fifth, would the injury have occurred if the patient did not seek treatment? And Sixth, was the alleged wrong intentional?
	11. Medical malpractice is just the title of a lead to of action for a healthcare practitioner's negligent overall performance of his responsibilities (though, technically, medical malpractice could most likely contain reckless or intentional acts completed in the program of a health care practitioner's duties).
	12. Medical malpractice is the omission by an act by a health care provider in which the care or treatment provided deviates from standards of practice in the medical community resulting in injury or death to the patient.

5.20. Constitution of India has provided provisions dealing with health in Part III, Part IV. They are: Article 25 in part IV, Articles 39(e), 42, 43 and 47 Article 25

5.21 The right to health is an inclusive right.

5.21.1 We frequently associate the right to health with access to health care and the building of hospitals. This is correct, but the right to health extends further. It includes a wide range of factors that can help us lead a healthy life. The Committee

on Economic, Social and Cultural Rights, the body responsible for monitoring the International Covenant on Economic, Social and Cultural Rights, calls these the “underlying determinants of health”. They include:

- Safe drinking water and adequate sanitation;
- Safe food;
- Adequate nutrition and housing;
- Healthy working and environmental conditions;
- Health-related education and information;
- Gender equality.

5.22 Directive Principle of State Policy and Health

5.22.1 Article 38 of Indian Constitution imposes liability on State that states will secure a social order for the promotion of welfare of the people but without public health we cannot achieve it. It means without public health welfare of people is impossible. Article 39(e) related with workers to protect their health. Article 41 imposed duty on State to public assistance basically for those who are sick and disable. Article 42 makes provision to protect the health of infant and mother by maternity benefit.

5.22.2 In the India the Directive Principle of State Policy under the Article 47 considers it the primary duty of the state to improve public health, securing of justice, human condition of works, extension of sickness, old age, disablement and maternity benefits and also contemplated. Further, State’s duty includes prohibition of consumption of intoxicating drinking and drugs are injurious to health. Article 48A ensures that State shall endeavour to protect and impose the pollution free environment for good health. Article 47 makes improvement of public health a primary duty of State. Hence, the Court should enforce this duty against a defaulting authority on pain of penalty prescribe by law, regardless of the financial resources of such authority. Under Article 47, the State shall regard the raising of the level of nutrition and standard of living of its people and improvement of public health as among its primary duties. None of these lofty ideals can be achieved without controlling pollution inasmuch as our materialistic resources are limited and the claimants are many.

Panchayat, Municipality and Health

5.22.3 Not only the State also Panchayat, Municipalities liable to improve and protect public health. Article 243G says “State that the legislature of a state may endow the panchayats with necessary power and authority in relation to matters listed in the eleventh Schedule”.

5.22.4 The entries in this schedule having direct relevance to health are as follows

- 11 -Drinking
- 23 -Health and sanitation including hospitals, primary health centers and dispensaries.
- 24 -Family welfare
- 25 -Women and Child development
- 26 -Social welfare including welfare of the handicapped and mentally retarded.

5.22.5 Article 243-W finds place in part IXA of the constitution titled “The Municipalities:

- 5 -Water supply for domestic industrial and commercial purpose.
- 6 -Public health, sanitation conservancy and solid waste management.
- 9 -Safeguarding the interest of weaker sections of society, including the handicapped and mentally retarded.
- 16 -Vital statistics including registration of births and deaths
- 17- Regulation of slaughter – houses and tanneries.

5.23 Fundamental Rights and Health: –

5.23.1 The DPSP are only the directives to the State. These are non-justifiable. No person can claim for non-fulfilling these directives. But the Supreme Court has brought the right to health under the preview of Article 21. The scope of this provision is very wide. It prescribes for the right of life and personal liberty. The concept of personal liberty comprehended many rights, related to indirectly to life or liberty of a person. And now a person can claim his right of health. Thus, the right to health, along with numerous other civil, political and economic rights, is afforded protection under the Indian Constitution.

5.23.2 The debate surrounding the implementation of the human right to health is fresh and full of possibility for the developing world. In fact, Indian has been able to create a legal mechanism whereby right to health can be protect and enforced. The early of 1970s, witnessed a watershed in human rights litigation with the ushering in an unprecedented period of progressive jurisprudence following the recognition fundamental rights. At the same time standing rules were relaxed in order to promote PIL and access to justice. So there were two developments in 1980s, which led to a marked increase in health related litigation. First was the establishment of consumer Courts that made it cheaper and speedier to sue doctors for medical negligence. Second, the growth of PIL and one of this offshoots being recognition of health care as a fundamental right. Through PIL the Supreme Court has allowed individual citizen to approach the Court directly for the protection of their Constitutional human rights.

5.23.3 The Constitution guarantees the some fundamental rights having a bearing on health care. Article 21 deal with “No person shall be deprived of his life or personal liberty except according to procedure established by law.” Right to live means something more, than more animal existence and includes the right to live consistently with human dignity and decency. In 1995, the Supreme Court held that right to health and medical care is a fundamental right covered by Article 21 since health is essential for making the life of workmen meaningful and purposeful and compatible with personal

dignity. The state has an obligation under Article 21 to safeguard the right to life of every person, preservation of human life being of paramount importance. The Supreme Court held that whether the patient be an innocent person or be a criminal liable to punishment under the law, it is the obligation of those who are in charge of the health of the community to preserve life so that innocent may be protected and the guilty may be punished. In addition to constitutional remedies sensitizing of the relevant ordering law towards later health for all adds to the content of right to health. Legal prohibition of commercialized transplantation of human organ and effective application of consumer protection act to deal with deficient medical services have animated right to health.

5.24 Right to Health Care as a Fundamental Right

5.24.1 The Supreme Court, (16) while widening the scope of art 21 and the government's responsibility to provide medical aid to every person in the country, held that in a welfare state, the primary duty of the government is to secure the welfare of the people. Providing adequate medical facilities for the people is an obligation undertaken by the government in a welfare state. The government discharges this obligation by providing medical care to the persons seeking to avail of those facilities. Article 21 imposes an obligation on the state to safeguard the right to life of every person. Preservation of human life is thus of paramount importance. The government hospitals run by the state are duty bound to extend medical assistance for preserving human life. Failure on the part of a Government hospital to provide timely medical treatment to a person in need of such treatment, results in violation of his right to life guaranteed under Article 21. The Court made certain additional direction in respect of serious medical cases

➤ Adequate facilities be provided at the public health centers where the patient can be given basic treatment and his condition stabilized.

(16) *Paschim Banga Khet Mazdoor Samity & ors –vs- State of West Bengal & ors*, [1996] 4 SCC 37

- Hospitals at the district and sub divisional level should be upgraded so that serious cases be treated there.
- Facilities for given specialist treatment should be increased and having regard to the growing needs, it must be made available at the district and sub divisional level hospitals.
- In order to ensure availability of bed in any emergency at State level hospitals, there should be a centralized communication system so that the patient can be sent immediately to the hospital where bed is available in respect of the treatment, which is required.
- Proper arrangement of ambulance should be made for transport of a patient from the public health center to the State hospital.
- Ambulance should be adequately provided with necessary equipments and medical personnel.

5.25 Workers right to health care facilities

5.25.1 The Supreme Court has recognized the rights of the workers and their right to basic health facilities under the Constitution, as well as under the international conventions to which India is a party. In its path breaking judgment in *Bandhua Mukti Morcha –vs-Union of India*, the Court delineated the scope of art 21 of the Constitution, and held that it is the fundamental right of every one in this country, assured under the interpretation given to art 21 by this Court in *Francis Mullin's Case* to live with human dignity, free from exploitation. This right to live with human dignity enshrined in art 21 derives its life breath from the directive principles of state policy and particularly clause (e) and (f) of art 39 and arts 41 and 42. It must include protection of the health and strength of workers, men and women; and children of tender age against abuse; opportunities and facilities for children to develop in a healthy manner and in conditions of freedom and dignity; educational facilities; just and humane conditions of work and maternity relief. These are the minimum requirements, which must exist in order to enable a person to live with human dignity. No state, neither the central government nor any state government, has the right to take any action which will deprive a person of the enjoyment of these basic essentials. In (18) the Court held that, the health and strength of a worker is an integral facet of the right to life. The aim of fundamental rights is to create an egalitarian society to free all citizens from coercion or restrictions by society and to make liberty available for all. The Court, while reiterating its stand for providing health facilities, in (19) held that a healthy body is the very foundation for all human activities. That is why the adage 'Sariramadyam khalu dharma sadhanam'. In a welfare State, therefore, it is the obligation of the state to ensure the creation and the sustaining of conditions congenial to good health.

5.26 Right to Health is a Fundamental Right

5.26.1 In (20) the Supreme Court relied on international instruments and concluded that right to health is a fundamental right. It went further and observed that health is not merely absence of sickness: "The term health implies more than an absence of sickness. Medical care and health facilities not only protect against sickness but also ensure stable manpower for economic development. Facilities of health and medical care generate devotion and dedication to give the workers' best, physically as well as mentally, in productivity. It enables the worker to enjoy the fruit of his labour, to keep him physically fit and mentally alert for leading a successful economic, social and cultural life. The medical facilities are, therefore, part of social security and like gilt edged security, it would yield immediate return in the increased production or at any rate reduce absenteeism on grounds of sickness, etc., that environmental, ecological, air and water pollution, etc., should be regarded as amounting to violation of right to health guaranteed by Article 21 of the Constitution. It is right to state that hygienic environment is an integral facet of the right to

(18) *CESE Ltd –vs- Subhash Chandra Bose*, AIR 1992 SC 573 = 1991 (2) SCALE 996

(19) *Vincent –vs- Union of India* AIR 1987 SC 990

(20) ESC Ltd. –vs-. Subhash Chandra Bose AIR 1992 SC 573,

Healthy life and it would not be possible to live with human dignity without a humane and healthy environment. In the cases of (21) & (22) the Supreme Court held that right to health and medical care is a fundamental right under Article 21 read with Article 39(e), 41 and 43. In the case of (23) the Supreme Court held that right to pollution-free water and air is an enforceable fundamental right guaranteed under Article 21. Similarly in the case of (24) the Supreme Court opined that the right to decent environment is covered by the right guaranteed under Article 21. Further, in (25) & (26) the Supreme Court imposed a positive obligation upon the State to take steps for ensuring to the individual a better enjoyment of life and dignity and for elimination of water and air pollution. It is also relevant to notice as per the judgment of the Supreme Court in (27) & (28) the maintenance and improvement of public health is the duty of the State to fulfill its constitutional obligations cast on it under Article 21 of the Constitution. Our constitution makers were much aware about the public health or right to health that's why they imposed liability on State by some provision (Article 38, 39(e) 41, 42, 47, 48A) of DPSP.

5.26.2 Provisions in the Consumer Protection Act 1986 with landmark decisions under the said Act, 1986 with regard to health.

(21) Consumer Education and Research Centre –vs- Union of India (1995) 3 SCC 42

(22) Kirlskar Brothers Ltd. –vs- Employees' State Insurance Corporation (1996) 2 SCC 682 = AIR 1996 SC 3261,

(23) Subhash Kumar –vs- State of Bihar AIR 1991 SC 420 = (1991) 1 SCC 598,

(24) Shantistar Builders –vs- Narayan Khimalal Totame (1990) 2 SCJ 10 = AIR 1990 SC 630 = (1990) 1 SCC 520,

(25) M.C. Mehta –vs- Union of India (1987) 4 SCC 463 = AIR 1988 SC 1037

(26) Rural Litigation and Entitlement Kendra –vs- State of U.P. AIR 1987 SC 359,

(27) Vincent Panikurlangara –vs- Union of India, AIR 1987 SC 990 = (1987) 2 SCC 165

(28) Unnikrishnan, JP –vs- State of A.P AIR 1993 SC 2178 = (1993) 1 SCC 645,

5.27. Historical perspective of the consumer movement.

5.27.1 The Consumer movement had primarily started in the West. We can trace history of the consumer movement from the judgment of the leading case of (29) In this case, first time Manufacturers' liability for minimum quality standard for product was established. For the first time in 1856, a select committee recommended that a cheap and easy remedy, by a summary charge before a magistrate, should be afforded to consumers who received adulterated or falsely described food. This suggestion was taken up in the Merchandise Marks Act, 1887. Section 17 of the Act provides as follows: 'That a person applying a trade description to a product was deemed to warrant that it was true, so that a false trade description constituted breach of both criminal and civil law'. In leading English case (30) where the consumer claimed to have suffered injury as well as result of drinking from a bottle of ginger-beer containing a decomposed snail. Over a strong dissent the majority held that the manufacturer would be liable. The case did not herald strict liability but it facilitated more claims than were provided under the nineteenth century approach. Lord Atkin enunciated the manufacturer's duty of care in the following words: 'The preparation or putting up of the products will result in an injury to the consumers' life or property, owes a duty to the consumer to take that reasonable care'.

5.28. How Consumer Protection Act of 1986 controls medical mal-practice?

5.28.1 The Consumer Protection Act 1986 was enacted by the Parliament of India to safeguard consumer interest, in compliance with the United Nations guidelines adopted on 9-4-1985. Consumer Courts were established for the settlement of consumers' disputes and related matters. The Act protects not only the interests of consumer when he purchases goods and services for daily use, but also protects his interests when he goes for treatment to a medical professional.

(29) Carlill v. Carbolic Smoke Ball Company 1893 (1) Q.B. 256.

(30) Donoghue v. Stevenson (1932) A.C. 562,

Many medical associations lodged their protests against the application of the Act 1986 to the doctors on the ground that the relationship between a doctor and a patient is not that of a buyer and seller. However this contention was not accepted. In the initial period after the enactment of the Act, there was a lot of confusion in the judiciary as well as medical fraternity regarding the application of the Act to this profession.

5.30. Medical Professionals under the Consumer Protection Act.

5.30.1 In (31) the Supreme Court observed that professional men should possess a certain minimum degree of competence and that they should exercise reasonable care in the discharge of their duties. In general, a professional man owes to his client a duty in tort as well as in contract to exercise reasonable care in giving advice or performing services. Immunity from suit was enjoyed by certain professions on the grounds of public interest. The trend now is narrowing of such immunity. Medical practitioners do not enjoy any immunity, and they can be sued in contract or tort on the grounds that they have failed to exercise reasonable skill and care. Thus medical practitioners, though belonging to the medical profession, are not immune from a claim for damages on the ground of negligence. Despite the fact that they are governed by the Indian Medical Council Act and are subject to the disciplinary control of the Medical Council of India and/or State medical Councils, the Supreme Court ruled that they cannot be said to be outside the purview of the provisions of the Consumer Protection Act 1986.

5.30.2 The Indian Medical Association case is an epoch making judgment of the Supreme Court on this subject. Here the Supreme Court ruled that

- Service rendered to a patient by a medical practitioner (except where the doctor renders service free of charge to every patient or under a contract of personal service), by way of consultation, diagnosis and treatment, both medicinal and surgical, would fall within the ambit of service as defined in section 2(1)(o) of the Act.
 - The fact that medical practitioners belong to the medical profession and are subject to the disciplinary control of the Medical Council of India and / or State Medical Councils constituted under the provisions of the Indian Medical Council Act would not exclude the services rendered by them from the ambit of the Act.
 - A Contract of personal service has to be distinguished from a contract for personal service. In the absence of a relationship of master and servant between the patient and medical practitioner, the service rendered by a medical practitioner to the patient cannot be regarded as service rendered under a contract of personal service. Such service is a service rendered under contract for personal services and is not covered by the exclusionary clause of the definition of service contained in section 2(1)(o) of the Act. The expression contract of personal service in section 2(1)(o) of the Act cannot be confined to the contract for employment of domestic servants only and the said expression would include the employment of a medical officer for the purpose of rendering medical service to the employer. The service rendered by a medical officer to his employer under the contract of employment would be outside the purview of service as defined in section 2(1)(o) of the Act.
 - Service rendered free of charge by a medical practitioner attached to a hospital/nursing home or a medical officer
(31) Indian Medical Association –vs- V.P. Shantha reported in A.I.R. 1996 SC 550 = (1995) 6 SCC 651, employed in a hospital/nursing home where such services are rendered free of charge to every body, would not be service as defined in section 2(1)(o) of the Act, the payment of a token amount for registration purpose only at the hospital/nursing home would not alter the position.
 - Service rendered at a non-government hospital/nursing home where no charge whatsoever is made from any person availing the service and all patients (rich and poor) are given free service-is outside the purview of the expression service as defined in section 2(1)(o) of the Act. The payment of a token amount for registration purposes only at the hospital/ nursing home would not alter the position.
 - Service rendered at a non-government hospital/nursing home where charges are required to be paid by the persons availing such service falls within the purview of the expression service as defined in section 2(1)(o) of the Act.
 - Service rendered at a non-government hospital/nursing home where charges are required to be paid by persons who are in a position to pay and persons who cannot afford to pay are rendered service free of charge would fall within the ambit of the expression service as defined in section 2(1)(o) of the act irrespective of the fact that the service is rendered free of charge to persons who are not in a position to pay for such services. Free services would also be service and the recipient a consumer under the Act.
 - Service rendered at a government hospital/health centre/dispensary where no charge whatsoever is made from any person availing of the services and all patients (rich and poor) are given free service as defined in section 2(1)(o) of the Act. The payment of a token amount for registration purposes only at the hospital/nursing home would not alter the position.
 - Service rendered at a government/ hospital/health centre/dispensary where services are rendered on payment of charges and also rendered free of charge to the ambit of the expression service as defined in section 2(1)(o) of the Act, irrespective of the fact that the service is rendered free of charges to persons who do not pay for such services. Free service would also be service and the recipient a consumer under the Act.
 - Service rendered a medical practitioner or hospital/nursing home cannot be regarded as service rendered free of charge of the person availing of the service has taken an insurance policy for medical care where under the charges for consultation, diagnosis and medical treatment are borne by the insurance company and such service would fall within the ambit of the term service as defined in section 2(1)(o) of the Act.
 - Similarly, where, as a part of the conditions of service, the employer bears the expenses of medical treatment of an employee and his family members dependent on him, the service rendered to such an employee and his family members by a medical practitioner or hospital/nursing home would not be free of charge and would constitute service under section 2(1)(o) of the Act.
- 5.30.3** The Supreme Court, while formulating the above guidelines, upheld the judgment of the National Commission in *Cosmopolitan Hospitals v. Vasantha P. Nair*. By holding that the activity of providing medical assistance for payment carried on by hospitals and members of the medical profession falls within the scope of the expression service as defined in section 2(1)(o) of the Consumer Protection Act 1986. The Court, therefore, held that the aggrieved party can invoke the remedies provided under the Act by filing a complaint before the Consumer Forum having jurisdiction.
- 5.30.4** From the principles laid down above by the Supreme Court it is evident that the medical practitioners, government hospitals/nursing homes broadly fall into the three broad categories
- Where services are rendered free of charge to every body availing the said services;
 - Where charges are required to be paid by everybody availing the said service; and
 - Where charges are required to be paid by persons availing services but certain categories of persons who cannot afford to pay are rendered service free of charge.
- 5.30.5** In respect of the first category the Court ruled that doctors and hospitals who rendered service without any charge whatsoever to every person availing services would not fall within the ambit of service under section 2(1)(o) of the 1986 Act. The payment of token amount for registration purposes only would not alter the position in respect of such doctors and hospitals. So far as the second category is concerned, since the service is rendered on payment basis to all persons, they would clearly fall within the ambit of section 2(1)(o) of the Act.

- 5.30.6** The third category of doctors and hospitals do provide free service to some of the patients belonging to the poor class but the bulk of the service is rendered to the patients on payment basis. Expenses incurred for providing free services are met out of the income from the service rendered to the paying patients. The service by such doctors and hospitals to the paying patients undoubtedly falls within the ambit of section 2(1)(o) of the Act.
- 5.30.7** Thus, according to the Supreme Court, the word users in the phrase potential users in section 2(1)(o) of the 1986 Act gives an indication that the consumers as a class are contemplated. The definition of complainant contained in section 2(1)(b) of the Act which includes, under clause (ii) any voluntary consumer association and clauses (b) and (c) of section 12 which enable a complaint to be filed by any recognized consumer association or more consumers where there are numerous consumers, having the same interest, on behalf of or for the benefit of all consumers so interested, also lend support to the view that the 1986 Act seeks to protect the interests of consumers as a class. According to the court, to hold otherwise would mean that the protection of the Act would be available only to those who can afford to pay and such protection would be denied to those who cannot so afford, though they are the people who need the protection more. It is difficult to conceive that the legislature had intended to achieve such a result.
- 5.30.8** From a reading of the foresaid matter, it is clear that at present, the cases against medical professional are being dealt with under the provisions of Indian Penal Code or Consumer protection Act read with other related Acts connected to medical profession. All these cases are dealt with for granting compensation to the aggrieved but for the intentional act of the medical professions for monetary gain and for other obvious purposes. It is very much felt that there is no separate enactment to deal with medical malpractice. Hence, time has come now to think about enactment of Medical Malpractices Act to deal with the medical professionals and Hospitals.
- 5.30.9** Hope wisdom prevails on the legislators, either at States level or a comprehensive enactment at Centre level, to bring out an enactment on this subject to curb this menace.

Acknowledgements

I state that in my research work, I am being guided immeasurably by Smt. SUMITRA SRIPADA, Associate Professor, Dr. B.R. Ambedkar College of Law, Visakhapatnam, and but for her guidance and support, I would not have reached this stage of submitting research paper, which is part of research, in my research work. I, therefore, acknowledge her guidance and support in this regard.

I also acknowledge the support and encouragement given by my friends and well wishers to pursue the Research work.

References

- [1] Kearns, O, Mathuna, and Scott (2009) for a discussion of the ethical issues raised by such self diagnostic kits (Jonathan Herring – medical law and ethics 3rd edition at page
- [2] Sheldon and Thomson 1998:5 (Jonathan Herring – medical law and ethics 3rd edition at page (2)
- [3] (1995) 6 SCC 651.
- [4] Legal framework for Health Care in India – LexisNexis – Butterworth’s 2002 edition.
- [5] The World Health Organization’s Constitution (came into force in 1948)
- [6] Alma Ata Declaration adopted in 1978.
- [7] Article 21 of the Constitution of India
- [8] Treatise of Salmond on the Law of Torts 19th Edn.
- [9] Dr. Ravinder Gupta & ors –vs- Ganga Devi & ors 1993 (3)CPR 259.
- [10] Pt Parmanand Katara v. Union of India & ors AIR 1989 SC 2039.
- [11] Rupert M Jackson and John L. Powell. (Legal Framework for Health Care in India – LexisNexis – Butterworths 2002 edition page 35).
- [12] Achutrao H Khodwa v state of Maharashtra AIR 1996 SC 2383.
- [13] Ram Bihari Lal v JH Shrivastava AIR 1985 MP 150.
- [14] Philips India Ltd, v Kunju Punnu & anr AIR 1975 Bom 306.
- [15] Pt Parmanand Katara v Union of India & ors, AIR 1989 SC 2039.
- [16] Arunachal Vadivel & ors v Dr. N Gopalkrishnan 53. (1992) 2 CPR 548.
- [17] Paschim Banga Khet Mazdoor Samity & ors –vs- State of West Bengal & ors, [1996) 4 SCC 37
- [18] CESE Ltd –vs- Subhash Chandra Bose, AIR 1992 SC 573 = 1991 (2) SCALE 996
- [19] Vincent –vs- Union of India AIR 1987 SC 990
- [20] ESC Ltd. –vs-. Subhash Chandra Bose AIR 1992 SC 573,
- [21] Consumer Education and Research Centre –vs- Union of India (1995) 3 SCC 42
- [22] Kirloskar Brothers Ltd. –vs- Employees’ State Insurance Corporation (1996) 2 SCC 682 = AIR 1996 SC 3261,
- [23] Subhash Kumar –vs- State of Bihar AIR 1991 SC 420 = (1991) 1 SCC 598,
- [24] Shantistar Builders –vs- Narayan Khimalal Totame (1990) 2 SCJ 10 = AIR 1990 SC 630 = (1990) 1 SCC 520,
- [25] M.C. Mehta –vs- Union of India (1987) 4 SCC 463 = AIR 1988 SC 1037
- [26] Rural Litigation and Entitlement Kendra –vs- State of U.P. AIR 1987 SC 359,
- [27] Vincent Panikurlangara –vs- Union of India, AIR 1987 SC 990 = (1987) 2 SCC 165
- [28] Unnikrishnan, JP –vs- State of A.P AIR 1993 SC 2178 = (1993) 1 SCC 645,
- [29] Carlill v. Carbolic Smoke Ball Company 1893 (1) Q.B. 256.
- [30] Donoghue v. Stevenson (1932) A.C. 562,
- [31] Indian Medical Association –vs- V.P. Shantha reported in A.I.R. 1996 SC 550 = (1995) 6 SCC 651,

Experimental and Analytical Study on Reinforced Concrete Deep Beam

Prof. S. S. Patil,¹ A. N. Shaikh,² Prof. Dr. B. R. Niranjana³

^{1,2}(Department of Civil Engineering, Walchand Institute of Technology, Solapur, India)

³(Department of Civil Engineering, U.V.C.E Bangalore University, Bangalore, India)

ABSTRACT: Several reinforced concrete deep beams with different L/D ratios (1.5, 1.6, 1.71) were cast and tested in order to investigate the strain distribution pattern at mid-section of the beam. This paper describes analysis of deep beams subjected to two point loading with three different L/D ratios (1.5, 1.6, 1.71) using Non-linear Finite element method (ANSYS 9.0 software). In ANSYS 9.0 software, SOLID 65 and LINK 8 element represent concrete and reinforcing steel bars.

Non-linear material properties were defined for both elements. Using ANSYS software Flexural Strains and deflections were determined at mid-section of the beam. The failure crack-patterns were obtained. Variations of flexural strains were plotted at mid-section of the beam. The beams were designed by I.S.456-2000 (Indian Standard Code of Practice for Plain and Reinforced Concrete). Flexural strains were measured experimentally at mid-section of the beam using Demountable mechanical strain gauge. The failure crack-patterns of the beam for different L/D ratios were also observed.

The comparison between ANSYS results and experimental test results were made in terms of strength, flexural strain and deflection of concrete beams. The analytical and experimental flexural strains were compared at mid-section of the beam for different L/D ratios.

It was found that the smaller the span/depth ratio, the more pronounced was the deviation of strain pattern at mid-section of the beam. As the depth of the beam increases the variation in strength, flexural steel and deflection were found to be more experimentally than the non-linear finite element analysis.

Keywords: Deep Beam, Non-Linear Finite element method, ANSYS 9.0. L/D (Span to depth), Demountable Mechanical Strain Gauge.

I. INTRODUCTION

Beams with large depths in relation to spans are called deep beams [4]. In IS-456 (2000) Clause 29, a simply supported beam is classified as deep when the ratio of its effective span L to overall depth D is less than 2. Continuous beams are considered as deep when the ratio L/D is less than 2.5. The effective span is defined as the centre-to-centre distance between the supports or 1.15 times the clear span whichever is less.

II. NON LINEAR FINITE ELEMENT ANALYSIS

The finite element analysis calibration study included modeling a concrete beam with the dimensions and properties [1]. To create the finite element model in ANSYS 9.0 there are multiple tasks that have to be completed for the model to run properly. Models can be created using command prompt line input or the Graphical User Interface. For this model, the graphical user interface was utilized to create the model. This section describes the different tasks and entries to be used to create the finite element calibration model.

2.1. Element Types

The element type for this model is shown in Table 1.

Table1. Element Types for Working Model

Material Type Element	ANSYS
Concrete	Solid65
Steel Reinforcement	Link8

A Solid65 element was used to model the concrete [2]. This element has eight nodes with three degrees of freedom at each node translations in the nodal x, y, and z directions. The element is capable of plastic deformation, cracking in three orthogonal directions, and crushing. A schematic of the element was shown in Fig.1.

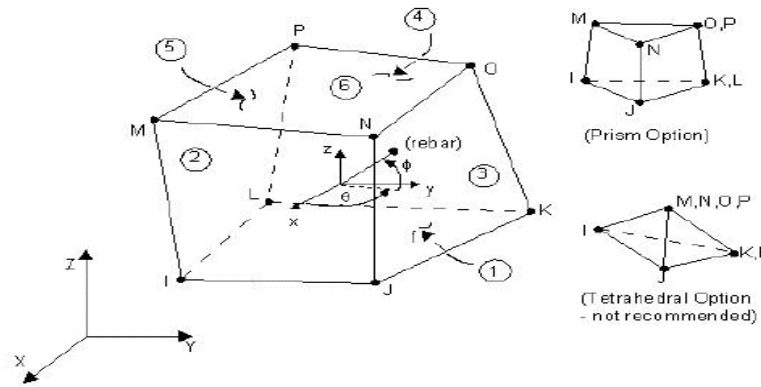


Figure 1. Solid 65 element

A Link8 element was used to model steel reinforcement [2]. This element is a 3D spar element and it has two nodes with three degrees of freedom translations in the nodal x, y, and z directions. This element is capable of plastic deformation and element was shown in the Fig.2.

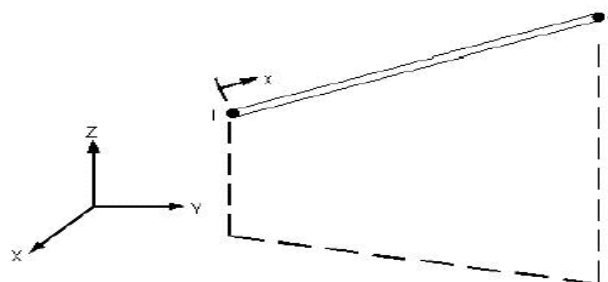


Figure 2. Link 8 element

2.2. Real Constants

Real Constant Set 1 was used for the Solid65 element [2]. It requires real constants for rebar assuming a smeared model. Values can be entered for Material Number, Volume Ratio, and Orientation Angles. The material number refers to the type of material for the reinforcement. The volume ratio refers to the ratio of steel to concrete in the element. The reinforcement has uniaxial stiffness and the directional orientations were defined by the user. In the present study the beam was modeled using discrete reinforcement. Therefore, a value of zero was entered for all real constants, which turned the smeared reinforcement capability of the Solid65 element of Real Constant Sets 2 and 3 were defined for the Link8 element.

Values for cross-sectional area and initial strain were entered. Cross-sectional area in set 2 refers to the reinforcement of two numbers of 10mm diameter bars. Cross-sectional area in set 3 refers to the 8 mm diameter two legged stirrups. A value of zero was entered for the initial strain because there is no initial stress in the reinforcement. The real constants were given in Table 2.

Table 2. Real Constants

Real Constants Set	Element Type		Real constants for Rebar 1	Real constants for Rebar 2	Real constants for Rebar 3
1	Solid 65	Material no. V.R	0	0	0
2	LINK 8	Area (mm ²) Initial strain	78.5 0	- 0	- 0
3	LINK 8	Area (mm ²) Initial strain	50.24 0	- 0	- 0

2.3. Modeling

The beam was modeled as volume [2]. The model was 700 mm long with a cross section of 150 mm X 350 mm. The Finite Element beam model was shown in Fig.3. The dimensions for the concrete volume were shown in Table.3.

Table 3. Dimensions for Concrete

ANSYS	Concrete(mm)
X1,X2,X-coordinates	0, 700
Y1,Y2,Y-coordinates	0, 350
Z1,Z2,Z-coordinates	0, 150

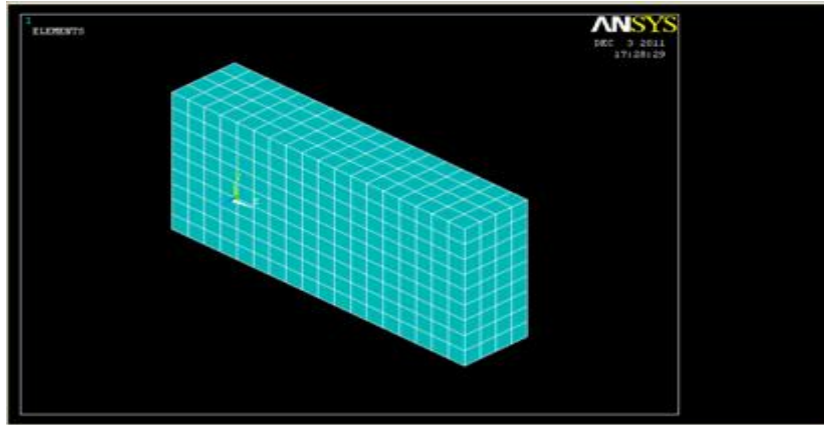


Figure 3. Finite element model & mesh of beam

2.4. Meshing

To obtain good results from the Solid65 element, the use of a rectangular mesh was recommended [2]. Therefore, the mesh was set up such that square or rectangular elements were created. The meshing of the reinforcement was a special case compared to the volumes. No mesh of the reinforcement was needed because individual elements were created in the modeling through the nodes created by the mesh of the concrete volume. The meshing and reinforcement configuration of the beam were shown in Fig.3 and Fig.4.

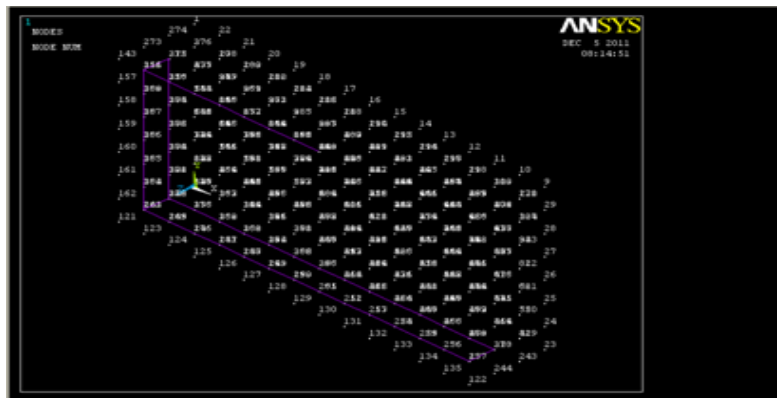


Figure 4. Reinforcement Configuration

2.5. Loads and Boundary Conditions

Displacement boundary conditions were needed to constraint the model to get a unique solution [2]. To ensure that the model acts the same way as the experimental beam boundary conditions need to be applied at points of symmetry, and where the supports and loading exist. The support was modeled as a hinged support at both ends. Nodes on the plate were given constraint in all directions, applied as constant values of zero. The loading and boundary conditions of the beam were shown in Fig.5.

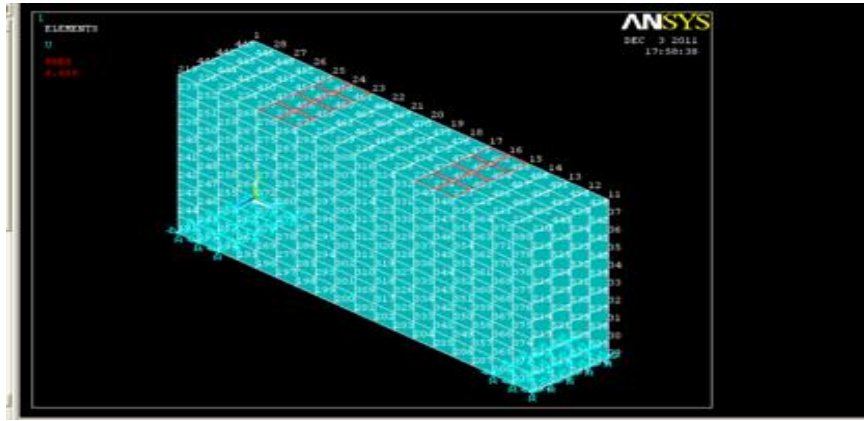


Figure 5. Loading and boundary conditions

1.6 Crack Patterns

The crack patterns of different beams using ANSYS 9.0 Software were shown in Fig.6 (a) to Fig.6(c).

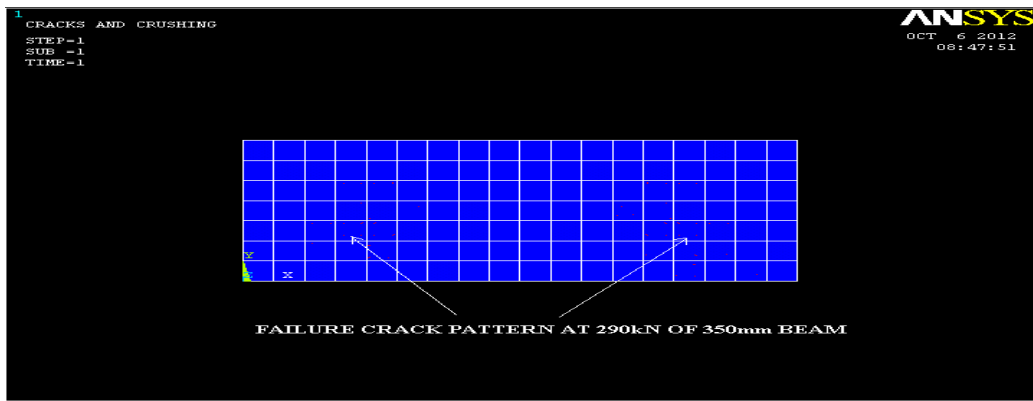


Figure 6(a). Failure crack pattern of 350mm Beam

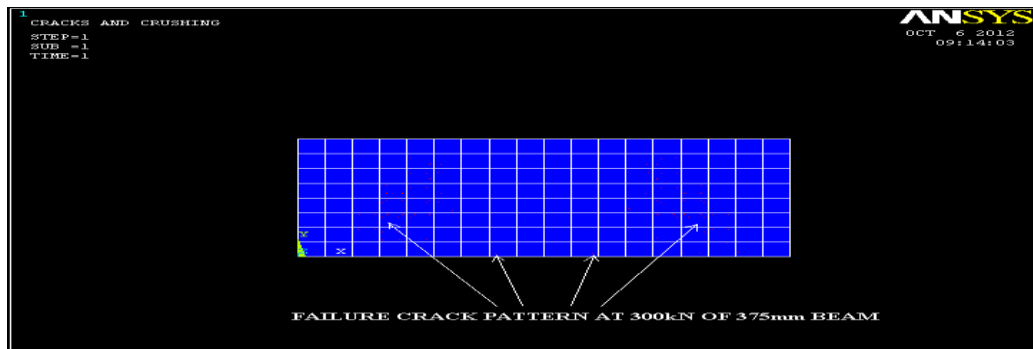


Figure 6(b). Failure crack pattern of 375mm Beam

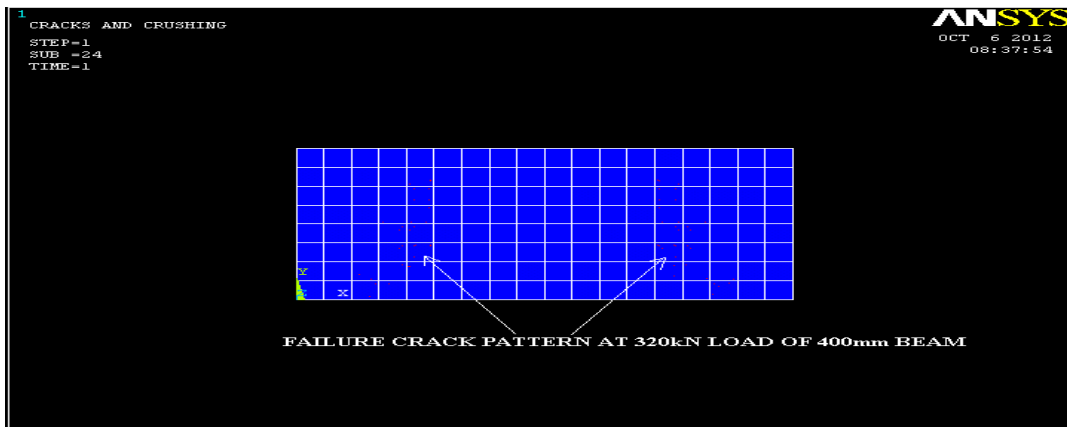


Figure 6(c). Failure crack pattern of 400mm Beam

III. EXPERIMENTAL WORK

3.1 Specimen Details

This experimental programme consists of casting and testing of several beams of 0.7 m length reinforced concrete deep beams. All the beams were tested over a simply supported span of 0.6 m. The beams were designed as under reinforced section to sustain a minimum two point loads of 50 kN.

3.2 Test Set Up

Tests were carried out at room temperature and as per the Indian standards in Heavy Structures Laboratory. The testing arrangement was shown in Image 1. Two point loads were applied on reinforced concrete deep beams of span 0.6 m through hydraulic jack of capacity 1000 kN. The specimens were placed on a simply supported arrangement of 100 kN Loading frame. The beams were suitably instrumented for measuring of middle strain by using Demountable Mechanical Strain Gauge including the mid span deflection with dial gauges.

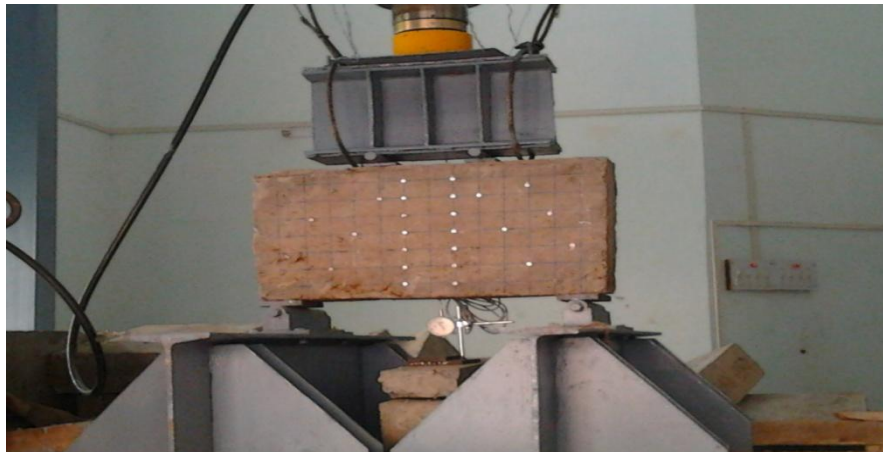


Image 1. Experimental Set Up



Image 2. Demountable Mechanical Strain Gauge

IV. RESULTS AND DISCUSSION

Beams of different L/D ratios were tested and experimental strains were measured at mid section of the beam by using demountable mechanical strain gauge. The beams were designed by using I.S. 456-2000 code and for 200 mm shear span. Shear span to depth ratio considered for the beams were 0.57, 0.53, 0.5 respectively. The beams were designed for two point loading of 50 kN each at 1/3 of span. At a load increment of 50 kN, strain at midsection and deflections were measured. The average initial cracking load for the beams was found to be 175 kN, 170 kN, 225 kN respectively. At these loads it was observed that minor cracks were developed in shear span region in the direction of the line joining the loading point and support. Also minor flexural cracks at mid span were observed. Loading was continued beyond this point. The failure loads observed were 290 kN, 300 kN, 350 kN respectively.

Table 4. Experimental Test Results

Beam Number	B1	B2	B3	B4	B5	B6	B7	B8	B9
Depth (D)	400mm	400mm	400mm	375mm	375mm	375mm	350mm	350mm	350mm
Effective Span to depth ratio (L/D)	1.5	1.5	1.5	1.6	1.6	1.6	1.71	1.71	1.71
Design Method	IS 456								
Lever arm, (Z)	280mm	280mm	280mm	270mm	270mm	270mm	260mm	260mm	260mm
Flexural steel required in mm ²	120.64	120.64	120.64	124.93	124.93	124.93	129.52	129.52	129.52
Flexural steel provided in mm ²	157 2-10Φ								
Minimum Shear required, mm ² a) Vertical b) Horizontal	72 120	72 120	72 120	67.5 112.5	67.5 112.5	67.5 112.5	63 105	63 105	63 105
Vertical steel required, mm ²	251.48	251.48	251.48	274.86	274.86	274.86	304.86	304.86	304.86
8mm diameter a)Vertical b)Horizontal	4 bars 2 bars								
Load at first crack, kN (Total)	225	190	225	200	180	170	175	150	180
Load at failure kN (Total)	350	335	350	335	310	300	290	285	325
Deflection at first crack, mm	0.76	0.64	0.82	0.64	0.59	0.52	0.55	0.49	0.62
Maximum. total Deflection, mm	1.75	1.63	1.55	1.55	1.32	1.45	1.52	1.41	1.45
Permissible Deflection, mm	2.4	2.4	2.4	2.4	2.4	2.4	2.4	2.4	2.4
Crack width at failure, mm	0.317	0.323	0.311	0.315	0.304	0.312	0.303	0.314	0.313
Permissible crack width, mm	0.3	0.3	0.3	0.3	0.3	0.3	0.3	0.3	0.3

Table 5. Analytical Test Results

Depth	400mm	375mm	350mm
Span to depth ratio	1.5	1.6	1.71
Flexural steel required in mm ²	85.06	95.862	102.689
Flexural steel provided in mm ²	157 2-10Φ	157 2-10Φ	157 2-10Φ
Load at first crack (Total)	190	185	170
Load at failure (Total)	320	300	290
Deflection at first crack, mm	0.591	0.588	0.458
Total Deflection at failure, mm	1.364	1.286	1.140

4.1 Variation of Flexural Strains

The analytical and experimental strains were recorded and variation of strain at midsection of beam for different L/D ratios plotted by considering analytical and experimental results. After plotting the experimental and analytical strains, the graph obtained experimentally was varying more than graph obtained analytically.

a) For the beam of L/D ratio 1.5, the experimental strains were 20% more than the analytical strains at mid-depth of the beam.

- b) For the beam of L/D ratio 1.6, the experimental strains were 17% more than the analytical strains at mid-depth of the beam.
- c) For the beam of L/D ratio 1.71, the experimental strains were 16% more than the analytical strains at mid-depth of the beam.

The variations of flexural strain were plotted at mid span of the beam for different L/D ratios. It was found that behaviour of flexural strain variation was non-linear. Also it was found that as the L/D ratio decreases the more pronounced was the deviation of strain pattern at mid-section of the beam. Fig.7 to Fig.9 were shown the variation of flexural strain at mid span for different L/D ratios.

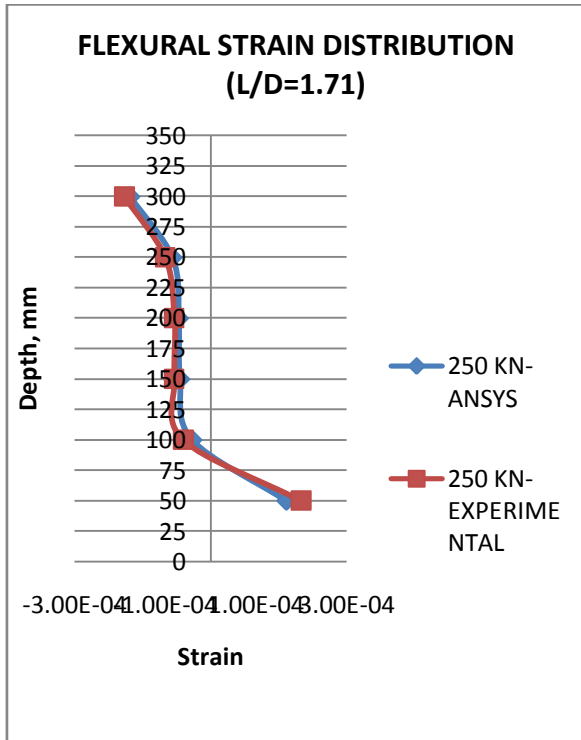


Figure 7. Flexural Strain Distribution (L/D=1.71)

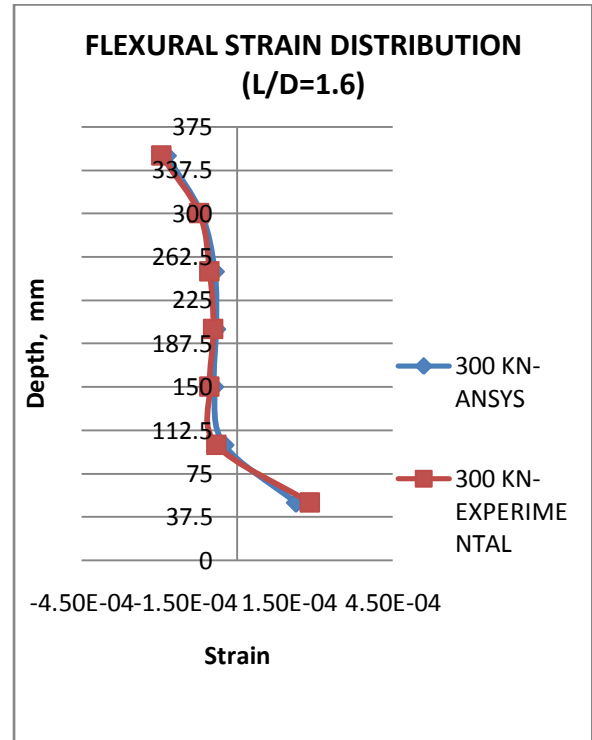


Figure 8. Flexural Strain Distribution (L/D=1.6)

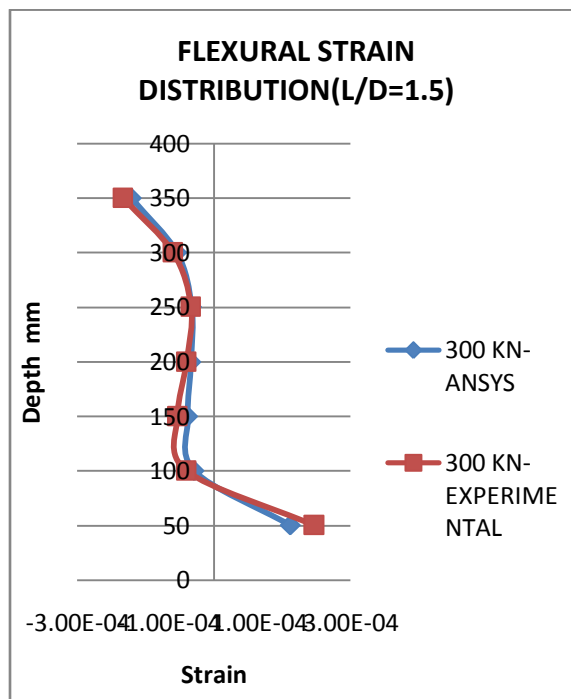


Figure 9. Flexural Strain Distribution (L/D=1.5)

V. Conclusions

Deep beams having different L/D ratios were analyzed by using non-linear finite element method (by ANSYS 9.0) and tested under two point loading. Some prominent conclusions were summarized here.

1. From the flexural strain graphs it was observed that smaller the span/depth ratio (i.e. less than or equal to 2.0), the more pronounced is the deviation of the stress-strain pattern i.e. the variation is not linear as in case of shallow beams.
2. Flexural strain variation graphs indicate that the definition of simply supported deep beam as per IS 456:2000 i.e. when L/D ratio is less than or equal to 2.0 is reasonably accurate.
3. From the flexural strain graphs it was observed that as L/D ratio of the beam decreases the neutral axis shifted towards soffit of the beam.
4. Failure of deep beams was mainly due to diagonal cracking.

REFERENCES

Journal Papers

- [1] Anand Parande, P. Dhayalan, M. S. Karthikeyan, K. Kumar and N. Palaniswamy, Assessment of Structural Behavior of Non-corroded and Corroded RCC Beams Using Finite Element Method, Sensors & Transducers Journal, Vol. 96, Issue 9, pp.121-136(2008).
- [2] Mohammed Sh. Mahmood and Amer M. Ibrahim, Finite Element Modeling of Reinforced Concrete Beams Strengthened with FRP Laminates, European Journal of Scientific Research ISSN 1450-216X Vol.30 No.4 (2009), pp.526-541.
- [3] Muhammad Abdur Rashid And Ahsanul Kabir, Behaviour Of Reinforced Concrete Deep Beam Under Uniform Loading, Journal Of Civil Engineering, The Institution Of Engineers, Bangladesh, Vol CE 24,No-2,1996.

Books

- [4] F. K. Kong Reinforced Concrete Deep Beams, (Van Nostrand Reinhold, New York 2011).
- [5] Varghese and Krishnamoorthy, Strength and Behavior of Deep Reinforced Concrete Beams.(Asoke K. Ghose, Prentice-Hall of India private Ltd. , 2006).
- [6] S. Ramamrutham, Design of Reinforced concrete structures.(Dhanpat Rai publishing company,2011).
- [7] S S. Bhavikatti, Finite Element Analysis, (New Age International (P) Ltd., Publishers, 2010).
- [8] R.D.Cook, D.S.Makus and M.F.Plesha, Concept and Applications of Finite Element Analysis, (John Wiley and Sons, 1989).

Losses in Waveguide and Substrate Integrated Waveguide (SIW) For Ku Band: A Comparison

Sheelu Kumari,¹ Shweta Srivastava²

¹Department of Electronics & Communication Engg. CIT, Tatisilwai, Ranchi, Jharkhand, India

²Department of Electronics & Communication Engg. BIT, Mesra, Ranchi, Jharkhand, India

ABSTRACT- In this paper equivalent Substrate Integrated Waveguide (SIW) for a waveguide is designed. Different types of losses in the waveguide and the optimized SIW are calculated theoretically and a comparison is done between the two. The comparison proves that at millimeter wave frequencies the choice of dielectric becomes crucial for a waveguide design and SIW is preferable to be used at these frequencies because the leakage losses decrease significantly.

Keywords- waveguide; SIW; dielectric loss; conduction loss; leakage loss

I. INTRODUCTION

Conventional waveguides, the first generation of microwave guiding structures had the advantages of having high power carrying capacity and high Q-factor, but also had the disadvantages of being bulky and voluminous. The next generation of microwave guiding elements was the strip-like or slot-like planar printed transmission lines used in Microwave Integrated Circuits (MICs). These were planar low profile structures but lacked the high power carrying capacity and high Q-factor of the conventional waveguides. To bridge the gap between MIC structures and conventional waveguides, Substrate Integrated Circuits (SICs) were developed which are planar low profile structures like MIC structures, also having high power carrying capacity and high Q-factor similar to waveguides[1].

Principle of operation of SIC was to build artificial channels within the substrate to guide the waves. Two techniques are used to build these channels (which are embedded in the substrate). One is to use metallic vias which act as sidewalls. Other technique uses contrast in values of ϵ_r so that phenomenon of total internal reflection can take place and the wave gets confined within the artificial channel [2]. A Substrate Integrated Waveguide (SIW) is one of the topologies of SIC. The SIW technology has been successfully applied to several microwave and millimeter-wave components, including active circuits, passive components and antennas [3].

II. THEORETICAL DETAILS

SIW consists of substrate with metalized vias acting as two side walls and two metallic walls (upper and lower) as shown in Fig.1b. Its design parameters are the distance between the two rows of vias(a), pitch(p), diameter of each via(d), height of the substrate (w) and dielectric constant ϵ_r .

For a waveguide with width ℓ and height h its equivalent SIW [4] parameters can be found using equation (1) which relates different dimensional parameters of waveguide and its equivalent SIW.

$$\ell = a - 1.08 \frac{d^2}{p} + 0.1 \frac{d^2}{a} \quad (1)$$

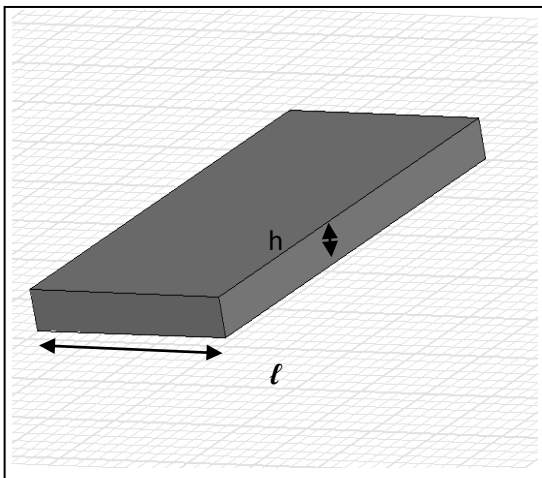


Figure 1a. Topology of Waveguide

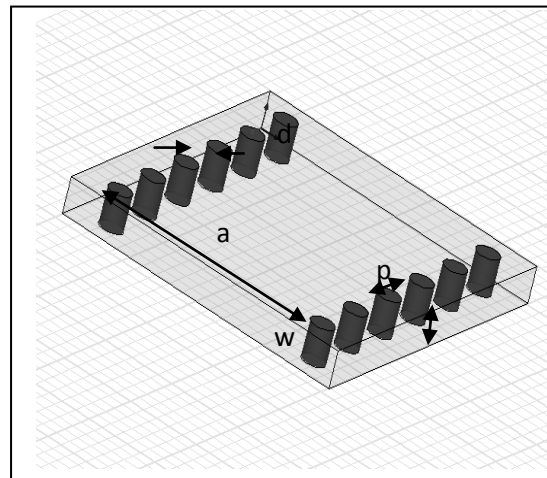


Figure 1b. Topology of SIW

Waveguides have two types of major losses, the dielectric loss (α_d) and the conductor loss (α_c).

$$\alpha_d = (k^2 \tan \delta) / 2\beta \quad (2)$$

$$\alpha_c = R_s \frac{(2h\pi^2 + \ell^3 k^2)}{\ell^3 h \beta k \eta} \quad (3)$$

where k is free space wave number
 β is phase constant
 $\tan\delta$ is the dielectric loss tangent
 η is the intrinsic impedance of the medium

$$\eta = \sqrt{\frac{\mu_0}{\epsilon_0 \epsilon_r}} \quad R_s = \sqrt{\frac{\rho \mu_0}{2\sigma}}$$

σ is conductivity of metal

R_s is surface resistivity of the conductors

$$\alpha_{\text{waveguide}} = \alpha_d + \alpha_c$$

In Substrate Integrated Waveguides, along with dielectric loss (α_d) and conductor loss (α_c) leakage loss (α_l) also exists which has a significant effect on the performance. Equations for α_d and α_c for SIW is rewritten as,

$$\alpha_d = (k^2 \tan\delta) / 2k_z \quad (4)$$

$$\alpha_c = \frac{R_s}{a_e \eta \sqrt{1 - \frac{k_c^2}{k^2}}} \left[\frac{a_e}{w} + \frac{2k_c^2}{k^2} \right] \quad (5)$$

a_e is the equivalent width of the SIW[3]

$$k_c^2 = k^2 - k_z^2$$

$$\alpha_l = |k_{zi}| \quad (6)$$

$$k_z(f) = \sqrt{\left\{ k^2 - \left[\frac{2}{a_e} \cot^{-1} \left(\frac{f_c}{f} r_s (1-j) \right) \right]^2 \right\}} \quad (7)$$

r_s is real part of the surface wave impedance [5], a_e is the effective value of a and k is the free space wave number, f_c is cut off frequency and f is operating frequency.

III. SIMULATION AND RESULTS

The waveguide is designed for Ku band ($f_c=14$ GHz) with dimensions $\ell=6.86\text{mm}$, $h=0.5\text{mm}$ and $\epsilon_r=2.33$, the parameters of its equivalent SIW are calculated using equation(1) to be $a=7.2\text{mm}$, $p=2\text{mm}$, $d=0.8\text{mm}$, $w=0.5\text{mm}$, $\epsilon_r=2.33$. The different parameters of the SIW are varied to find the dimensions of the optimal SIW [6]. The dimensions for the optimal SIW obtained after several iterations are $a=7.2\text{mm}$, $p=3\text{mm}$, $d=0.8\text{mm}$, $w=0.5\text{mm}$, $\epsilon_r=2.33$.

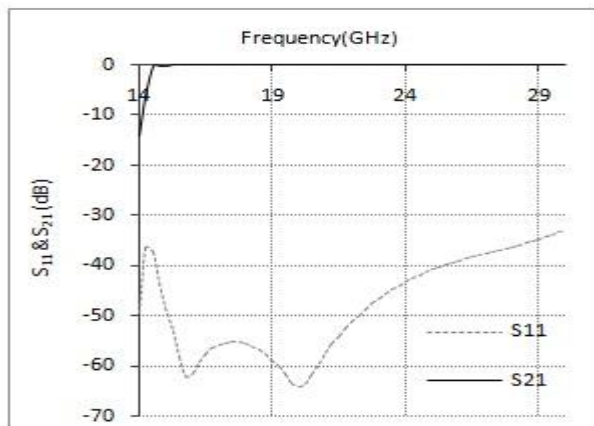


Figure 4a. S_{11} and S_{21} for the waveguide

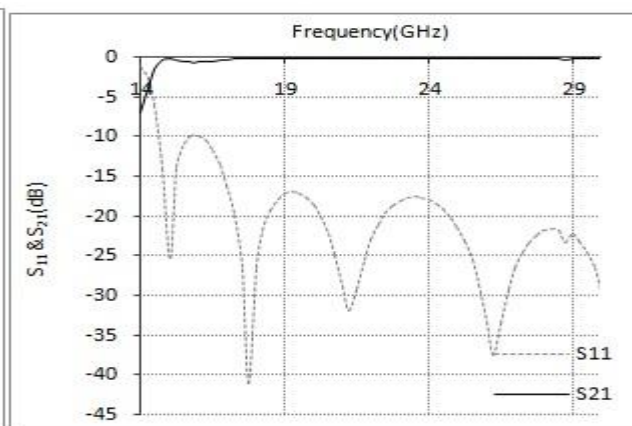


Figure 4b. S_{11} and S_{21} for the optimized SIW

Fig. 4 shows the variation of S_{11} and S_{21} for the waveguide and the equivalent SIW which is showing similar performance as the waveguide. Performance of S_{11} for SIW is a bit deteriorated from waveguide but still it is under acceptable limits (<10 dB) throughout the frequency range.

Dielectric loss (α_d) and conductor loss (α_c) for the waveguide are calculated using equations (2) and (3) and their variation with frequency is shown in Fig. 5. Both the factors are decreasing with frequency up to 19 GHz and become constant after that. As frequency increases beyond 23GHz α_d starts increasing slowly, but α_c remains constant. The value of α_d goes higher than α_c at higher frequency range (>16 GHz).

Values of α_d , α_c and α_l for the optimized SIW are found using equations (4) through (7) and their variation with frequency is shown in Fig. 6. The factor α_l is decreasing; α_d is increasing slowly and α_c first decreases in the lower side of the frequency band and remains constant with the increase in frequency in the higher band.

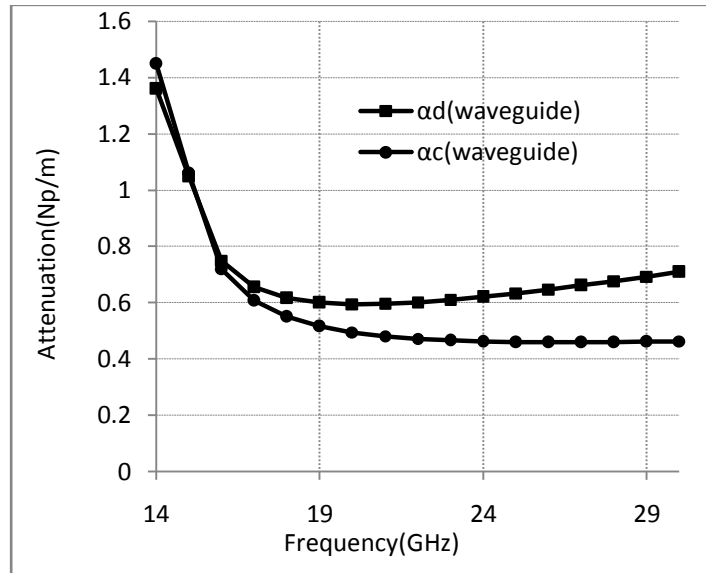


Figure 5. α_d and α_c for the waveguide

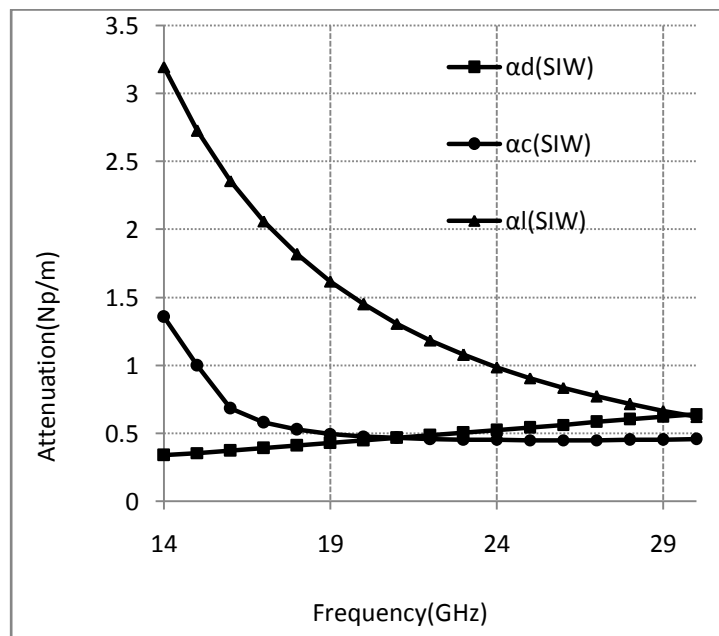


Figure 6. α_d , α_c and α_l for the SIW

Fig. 7 shows the variation of different attenuations occurring in a waveguide as well as in a SIW with respect to frequency. The comparative graph shows all the values are lying in the same range except for a very high value of leakage loss in case of a SIW in lower side of frequency range. This results in a very high value of total attenuation α_t for SIW as compared to the waveguide in lower side of the frequency range. But as we go on increasing the frequency the discrepancy reduces giving comparable values of total attenuations α_t (waveguide), α_t (SIW) for waveguide and the optimized equivalent SIW respectively. As frequency increases beyond 28GHz dielectric loss becomes the most significant loss. This proves that the SIW structures are more useful at millimeter wave frequencies and their losses become comparable to the waveguides.

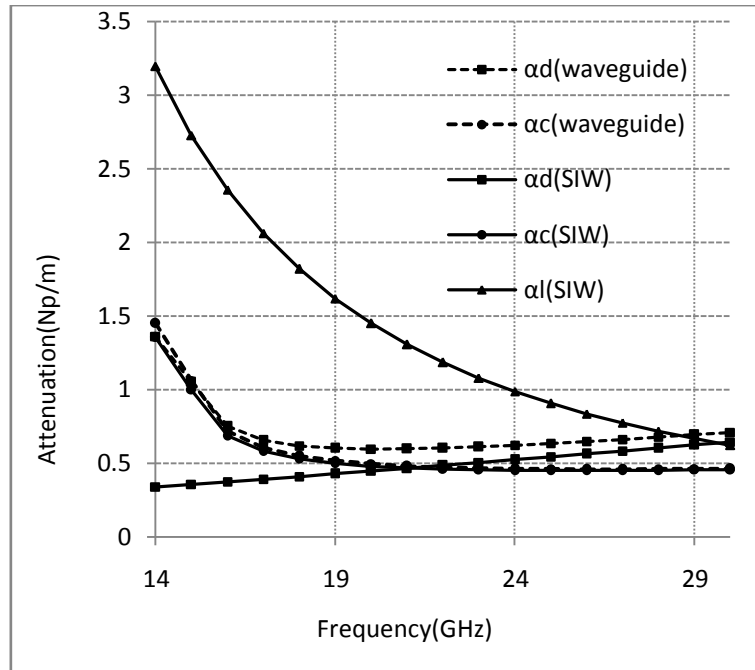


Figure 7. α_d and α_c for the waveguide and α_d , α_c and α_l for the SIW

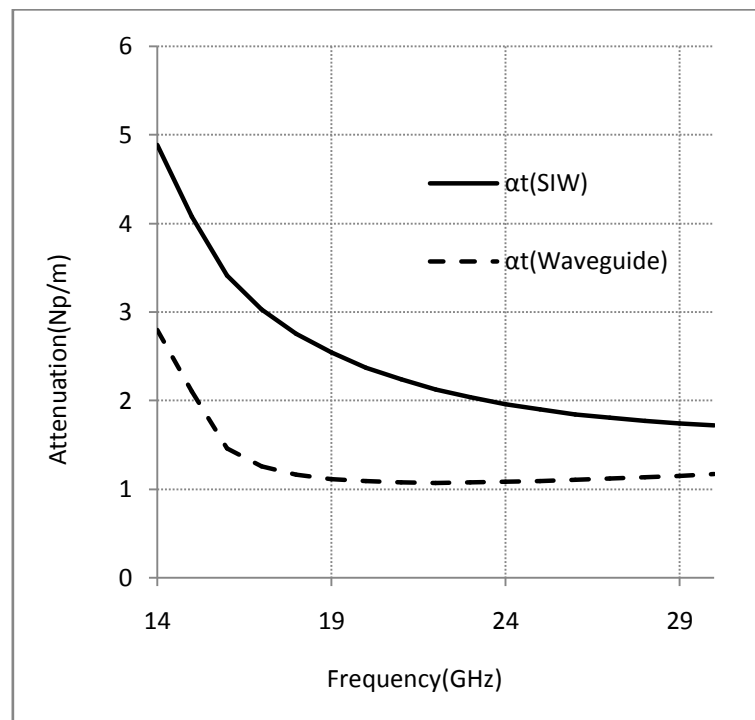


Figure 8. α_t for the waveguide , α_t for the SIW

As the frequency increases total attenuation in SIW α_t (SIW) approaches the total attenuation in waveguide α_t (waveguide). In lower side of the frequency range the value of α_t (SIW) is higher than that of a waveguide which can be attributed to the leakage losses occurring due to gaps between the cylinders of SIW. But as we go on increasing the frequency the discrepancy reduces due to the fall in leakage loss and both the total losses α_t (waveguide), α_t (SIW) become almost equal.

IV. CONCLUSION

A SIW equivalent has been designed for a Ku band ($f_c=14$ GHz) waveguide. For a waveguide of width 6.86mm. Height 0.5mm and $\epsilon_r=2.33$. parameters for the equivalent SIW are calculated to be $a=7.2$ mm., $d=0.8$ mm., $p=2$ mm., $h=0.5$ mm. The optimized equivalent SIW is considered for further analysis. The parameters for the optimized SIW are $a=7.2$ mm., $d=0.8$ mm., $p=3$ mm., $h=0.5$ mm.

Attenuation constant is theoretically calculated which are occurring due to dielectric and conductor for the waveguide and due to dielectric, conductor and leakage for the SIW. Total attenuation is compared between the two. It has been concluded that at lower side of the frequency band leakage loss in SIW plays the most significant role. In this range of the frequency band leakage loss in SIW is very high but as frequency increases it falls down to the order of other losses i.e of the order of dielectric and conductor losses and attenuation in SIW approaches to that of waveguide.

It is also concluded that dielectric loss slowly increases with frequency and plays the most significant role at upper frequency bands. For a wave guiding structure to work with lower attenuations at higher frequency ranges the choice of dielectric substrate plays the most significant role. We can also conclude that SIW performance comes closer to the waveguide performance at millimeter wave frequencies and so considering all their advantages, it is feasible to use SIWs for higher frequencies.

REFERENCES

- [1] K.wu, D.Deslandes &Y Cassivi. Substrate integrated circuits – A new concept for high frequency electronics & optoelectronics. Proc.6th Int.Telecomm. Modern satellite, Cable, broadcast services Conf., pp 03-10, Oct. 2003
- [2] Ke Wu. Towards the Development of Terahertz Substrate Integrated Circuit Technology. Poly –grames Research Center, Department of Electrical Engg., Ecole Polytechnique (University of Montreal)Center for Radio Frequency Electronics Research (CREER)
- [3] Sheelu Kumari and Shweta Srivastava. Notched Folded Substrate Integrated Waveguide (NFSIW) for Frequency Selective Applications. IRE Journal of Communications Antenna and Propagation (IRECAP), August 2012 Vol. 2 N. 4, pp. 259-263.
- [4] Feng Xu and Ke Wu. Guided wave and Leakage Characteristics of Substrate Integrated Waveguide. IEEE Transactions on Microwave Theory and Techniques, Vol.53, No.1, January 2005
- [5] D.Deslandes, K.Wu. Accurate modeling, wave mechanism & design considerations of substrate integrated waveguide.
- [6] Sheelu Kumari and Shweta Srivastava. Waveguide and Substrate Integrated Waveguide for Ku Band: A Comparison. Proc. of the 1st Int. Conf. on Recent Advances in Information Technology, Vol.2, pp.385-388, March 2012

An Approach for the Verification of Aerodynamic Analysis for Selection of Airfoil in Electric Powered Racing Airplane both Analytically and By FEM

Sneha Tahilyani¹, Kushal Singh², Mudra Gondane³

^{1,2}(Aeronautical Department, Priyadarshini College of Engineer, Nagpur, India)

³(Mechanical Department, Priyadarshini College of Engineer, Nagpur, India)

ABSTRACT: Aircraft racing is fast becoming an exciting and popular sport event in the world. To meet the needs of racing airplanes, improved designs and new concepts are necessary. This project aims to design an electric powered racing aircraft. The design process started with detailed study of various existing electric powered racing aircraft models. The Rutan VariEze is one of the pioneers in this field. The VariEze is notable for popularizing the canard configuration and composite construction for homebuilt aircraft. Rutan's stated goals for the design included reduced susceptibility to departure/spin and efficient long range cruise. Keeping in mind these designing features, calculations for the mission specifications were made. Modeling is done in CATIA followed by analysis in ANSYS. The modelling work is substantiated with the help of graphs as a part of this research. The calculations thus made were helpful in the designing of the aircraft. For any aircraft it is imperative for the theoretical calculations to coincide with the software based analysis hence efforts were mostly concentrated in this direction for the designing of the Electric Powered Racing Aircraft.

Keywords: Racing aircraft, Electric powered, mission specifications, design feature, canard configuration.

I. INTRODUCTION

Sport aviation has traditionally been a suitable way of developing such technologies into commercial opportunities. Air racing is currently reported to be the fastest growing motor sport in the USA. Commercial sponsorship and television sports coverage of weekend race meetings have generated renewed interest in the sport. This environment offers the means by which we could gain flying experience with a new propulsion system in a highly controlled environment.

As we will be designing a new racing aircraft, it is important to investigate the current air-racing scene. At present, there are several classes of air racing. The two most closely controlled pylon-racing organisations are Formula 1 and Formula V (vee). The main difference between these lies in the specification of the engine type. Formula 1 relates to the 200 cu. in. Continental (0–200) engine and for Formula V to a converted Volkswagen engine (hence the significance of the vee).

Using this pattern, we should project a new Formula (E) to relate to the electric propulsion. An electric powered aircraft is the aircraft that run on electric motors rather than internal combustion engine with electricity coming from the fuel cells, solar cells, ultra capacitors and batteries.

Configuration analysis

In reviewing all the different types of aircraft that are similar to our expected design, it is clear that the main configuration decision to be made rests between the choices of tractor or pusher propeller position. Both have advantages and disadvantages associated with airflow conditions over the aircraft profile. As neither configuration has emerged in the preferred layout for modern racing aircraft, there seems to be no over-riding technical (racing efficiency) reason for the choice.

From the review, the conventional tractor layout is seen to have less variation in the overall aircraft layout. The traditional two-surface layout prevails with the main plane ahead of the control surfaces. On the other hand, the pusher layout offers several options. These include either tail or canard control surfaces. If the tail arrangement is selected, this presents difficulties at the rear fuselage. Using a twin boom layout avoids the tail surfaces/propeller interference but complicates the wing and fuselage structure. Lifting the propeller line above the fuselage may cause trim changes with power and also complicates the rear fuselage profile. The choice of landing gear geometry lies between the nose (tricycle) and the tail (tail dragger) arrangements. The tail wheel layout is lighter but introduces the possibility of ground looping.

Current formula rules prohibit retraction of the wheels but our proposed Formula E rules will allow the auxiliary wheel to be retracted as this does not seem to overcomplicate the design yet improves aerodynamic efficiency. In selecting the aircraft configuration, the most significant criterion is the requirement for high aerodynamic efficiency (i.e. low drag).

This implies: smooth profiling of the external shape of the aircraft, avoidance of the canopy/windscreen discontinuity, fairing of the landing gear and other structural details, reduction of airflow interference areas (e.g. mid-mounting of the wing to fuselage), avoidance of engine/propulsion system cooling drag. Many of the low drag features would be considered during the manufacturing (surface smoothness and preparation) and operational (gap taping and surface cleaning) phases. For this project, the most significant difference in configuration compared with conventional designs is the location of the various components of the propulsion system. Whereas conventional designs have the propeller and engine closely positioned, in an electric system only the electric motor is linked to the propeller. This motor is much smaller than a conventional internal combustion engine and can therefore be streamlined into the fuselage profile. All other components in the electrical system can be located in convenient positions in the aircraft. These options will create an installation that has

potentially less drag and higher propeller efficiency. It is also envisaged that the electrical system will require less cooling than the equivalent internal combustion engine. This will also reduce aircraft drag.

Name	Length	Span	Area	AR	Empty Weight	Take-off Weight	W/S	T/W
Nemesis	6.71	6.41	6.22	6.6	236	340	536	0.16
AR-5	4.42	6.4	5.12	8.0	165	290	556	-
Monnett Sonerai	5.08	5.08	6.97	3.7	199	340	479	0.15
Perigree	4.78	8.53	7.57	9.6	172	326	422	0.13
FFT Speed Canard	7.79	7.79	7.88	7.7	440	715	890	0.17
Cassult Special	4.88	4.57	6.27	3.3	227	363	568	0.17
Pottier P70s	5.15	5.85	7.21	4.7	215	325	442	0.2
Monnett Money	4.67	5.08	4.27	6.0	191	295	678	0.19
Aerocar Micro Pup	4.57	8.23	7.49	9.0	118	238	312	0.15

Electric propulsion system

A fuel cell is a chemical and mechanical device to convert chemical energy stored in a source fuel into electrical energy without the need to burn the fuel. The fundamental operation of a fuel cell matches that of a traditional battery. Electrons are freed from one element in order to create an electrical potential. The essential difference between a battery and a fuel cell lies in the ability of the fuel cell to perform the process of dissociation of the chemical components continuously, providing fuel is supplied to the cell. The fuel cell is fed with hydrogen. After the electrons have been removed, the spent hydrogen protons pass through an electrolyte to combine with oxygen to form pure water, an environmentally acceptable emission. Several types of electrolyte could be suitable for our application.

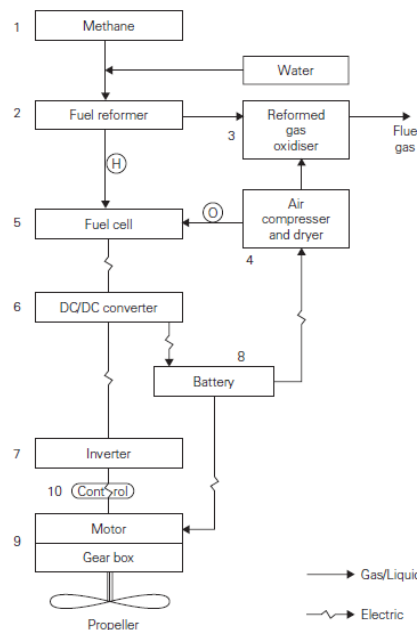


Fig. 1 Flowchart of Electric Propulsion System

To provide higher power, for example on take-off and climb or some emergency condition, it would be necessary to supplement the fuel cell energy with a battery. The battery could be recharged by the fuel cell during low-energy flight periods. This feature may be less appropriate for a racing aircraft that continually uses full power. Several components are required for a fuel cell system. These are shown diagrammatically in Figure 1.

Specifications

The following parameters are taken into consideration for fabrication of the canard airplane. For this Gross weight, geometrical and aerodynamic parameters of the aircraft is to be calculated analytically and then its validity is to be analysed using ANSYS.

Parameter	Value
Wing Span	6.77 m
Wing Area	4.98 m ²
Length	4.32 m
Height	1.50 m
Range	1368 km
Empty Weight	263 kg
Maximum Velocity	87.22 m/s
Cruise Velocity	73.88 m/s
Stalling Velocity	30.48 m/s

II. ANALYTICAL CALCULATIONS

Mission Specification Diagram and Weight Estimation

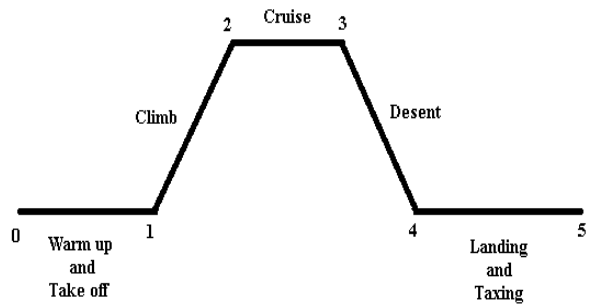


Fig 2: Mission Specification Diagram

Standard values of weight fraction are given as in the below table:

PHASE	W_i/W_{i-1}
Warm up and take off	0.97
Climb	0.985
Landing	0.995

Weight Fraction for mission Segments:

1. Warm up and take off:

$$\frac{W_1}{W_0} = 0.97$$

2. Climb:

$$\frac{W_2}{W_1} = 0.985$$

3. Cruise: Following are the available values

$$\frac{W_3}{W_2} = \exp\left\{\frac{-R \times C}{V_c \times (L/D)_c}\right\} = \exp\left\{\frac{-1368 \times 10^3 \times 1.389 \times 10^{-4}}{73.88 \times 16.454}\right\} = 0.8759$$

PARAMETER	VALUE
Range, R	1368 km
Specific Fuel Consumption, C	1.389×10^{-4} /s
Cruise Velocity, V_{cruise}	73.88 m/s
$(L/D)_{max}$	19
$(L/D)_{cruise}$	$19 \times .866 = 16.454$

4. Descend

Fuel Fraction for Cruise back to starting station is:

$$\frac{W_4}{W_3} = 0.8520$$

5. Landing:

$$\frac{W_5}{W_4} = 0.9950 \quad \frac{W_5}{W_0} = \frac{W_5}{W_4} \times \frac{W_4}{W_3} \times \frac{W_3}{W_2} \times \frac{W_2}{W_1} \times \frac{W_1}{W_0} = 0.995 \times 0.8520 \times 0.8759 \times 0.985 \times 0.97 = 0.7095$$

1. Gross Weight Calculations

The Gross weight of an aircraft is denoted by W_0

Type of airplane	A $W_{O.in} (kgf)$	C
Sailplane-Unpowered	0.8312	-0.05
Sailplane-Powered	0.8805	-0.05
Homebuilt-metal/wood	0.9342	-0.09
Homebuilt-composite	0.8879	-0.09
Twin Turboprop	0.9249	-0.05

$A = 0.8879$

$C = -0.09$

$\frac{W_E}{W_0} = AW_o^c ; \frac{263}{W_0} = 0.8879 \times W_0^{-0.09} ; W_0 = 520kg$

1. Geometric And Aerodynamic Calculations

1. Aspect ratio

$AR = \frac{b^2}{s} = \frac{(6.77)^2}{4.98} ; AR = 9.203$

2. Chord length

$c = \frac{s}{b} = \frac{4.98}{6.77} ; c = 0.7356$

3. We know that,

$\mu = 1.79 * 10^{-5} Pa.s$

Therefore, Reynolds's number can be calculated by using the formula,

$Re = \frac{\rho \times V_c \times C}{\mu} = \frac{1.225 \times 73.88 \times 0.7356}{1.79 \times 10^{-5}} = 3.7193 \times 10^6$

4. Maximum Coefficient of lift ,

$C_{l_{max}} = \frac{2 \times W_0}{\rho \times V_s^2 \times S} = \frac{2 \times 520 \times 9.81}{1.225 \times 30.48^2 \times 4.98} = 1.8001$

5. Coefficient of lift for aerofoil,

$C_{l,aerofoil} = \frac{C_{l_{max}}}{0.95} = \frac{1.8001}{0.95} = 1.8948$

III. SOFTWARE MODELING AND ANALYSIS

Modelling using CATIA

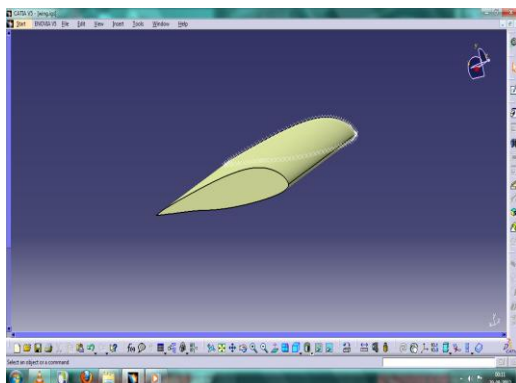


Fig3: CATIA model of Wing Section

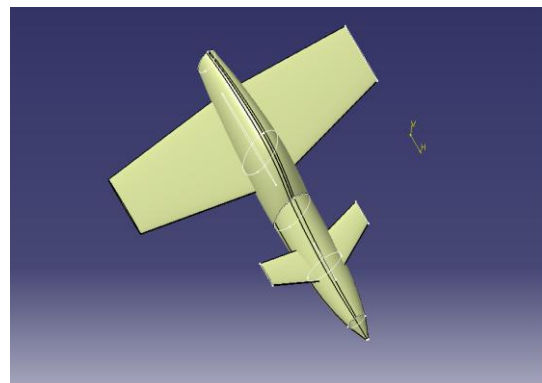


Fig4: CATIA model of the entire aircraft

Analysis using ANSYS

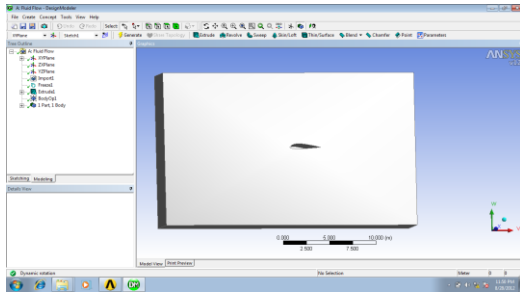


Fig5 .Geometry of the airfoil

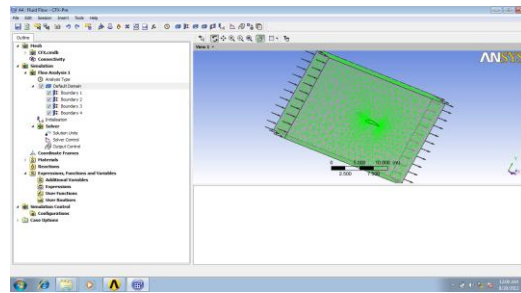


Fig6: Setup for calculations

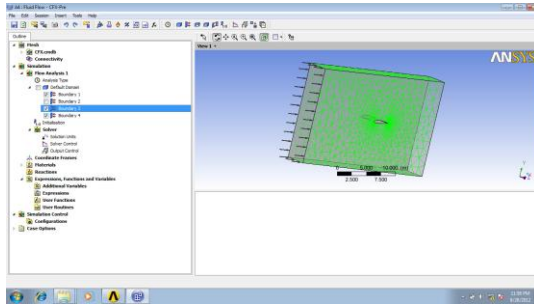


Fig7: Inlet

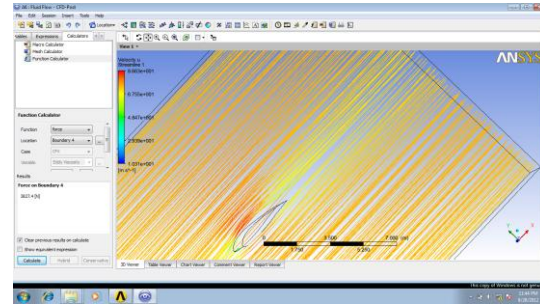


Fig8: Lift generated on the airfoil

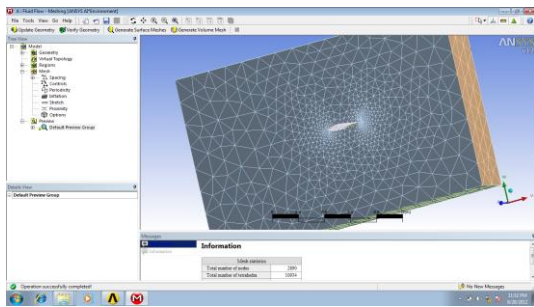


Fig 9: Meshing

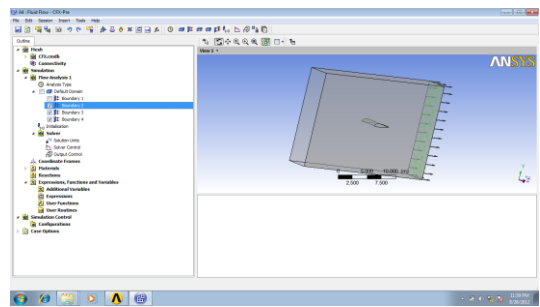


Fig10: Outlet

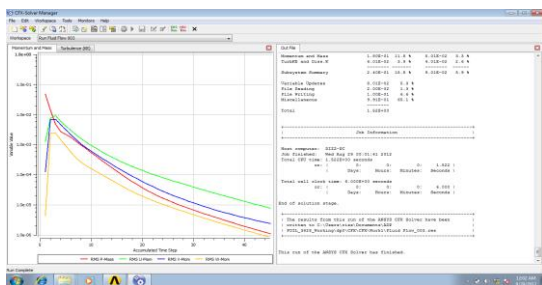


Fig 11: Solver

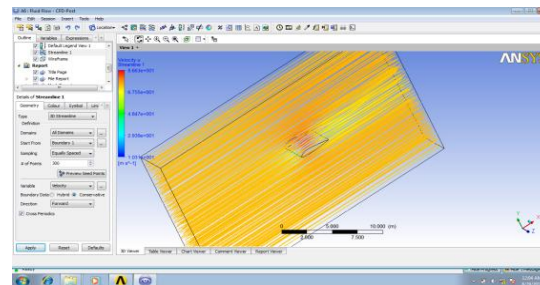


Fig12: Result

GRAPHS

With the help of data generated by ANSYS,Airfoil-Epplor 1230 is selected and graphs for various parameters are plotted.

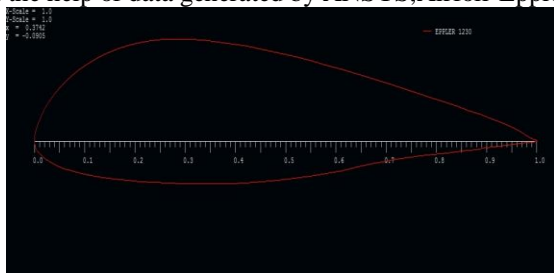


Fig13: Airfoil-Epplor 1230



Fig14: Coefficient of lift v/s angle of attack

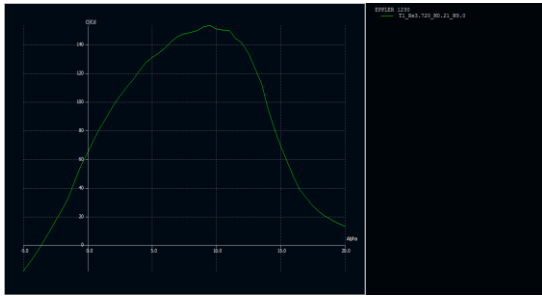


Fig15: Coefficient of lift v/s length of the chord

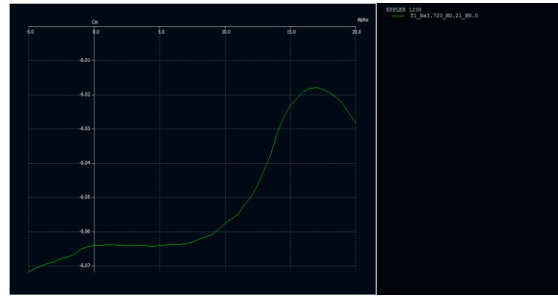


Fig16: Coefficient of moment v/s angle of attack

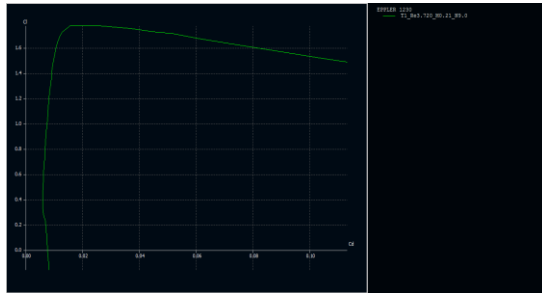


Fig17: Coefficient of Lift v/s Coefficient of Drag

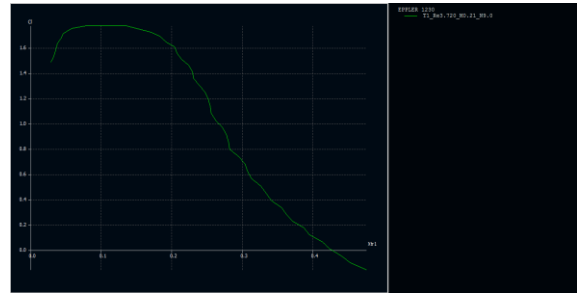


Fig18: Glide Ratio v/s angle of attack

COMPARING SIMILAR AIRFOILS

The airfoil used in Rutan VariEze is “EPPLER 1230”. There are other similar airfoils which fall under this series. These include:EPPLER 1211,EPPLER 1213,EPPLER 1214,EPPLER 1233.



Fig23: Coefficient of lift v/s angle of attack

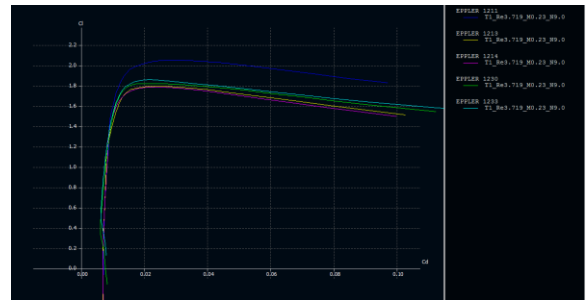


Fig24: Coefficient of Lift v/s Coefficient of Drag



Fig25: Coefficient of lift v/s length of the chord

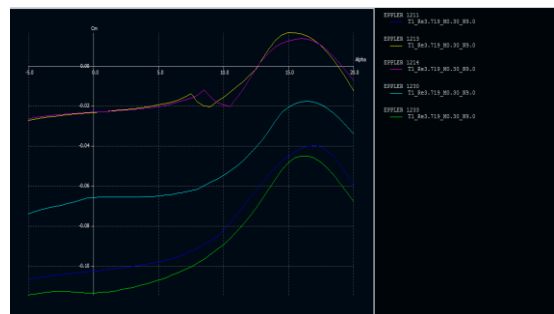


Fig26: Coefficient of moment v/s angle of attack

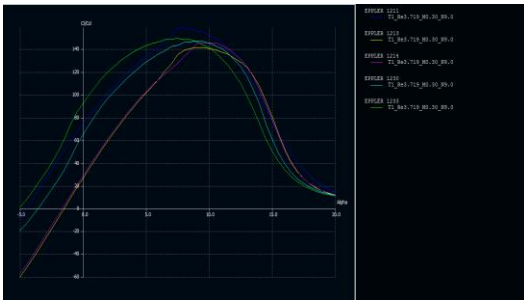


Fig27: Glide Ratio v/s angle of attack

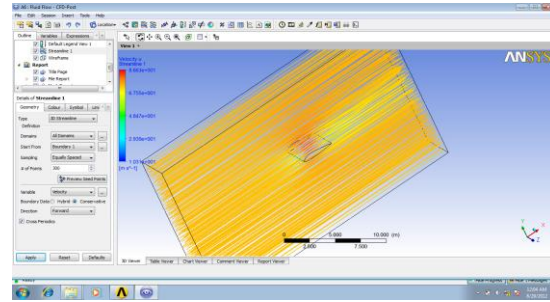


Fig27: Flow Analysis

Above graphs deduce the following facts:

The maximum lift is obtained by the airfoil EPPLER 1211. On the other hand a sufficient amount of lift is generated by the airfoil EPPLER 1230 and the maximum lift is found out to be 1.84 which is very close to the calculated value 1.8001. The C_L by C_D graph shows that the maximum value is obtained by the airfoil EPPLER 1211 which enhances the chance of this airfoil being chosen for fabrication. However, the airfoil EPPLER 1230 along with the other airfoils gives us the desired and required amount of this value. A gradual increase in the lift and a smooth decrease in the lift is noted by the airfoil EPPLER 1230 along the length of the chord. This gives us a very smooth and well maintained pressure distribution over the airfoil thereby producing the desired amount of lift with minimal drag. The coefficient of moment increases gradually for the change in angle between 0 to 5 degree for the airfoils EPPLER 1211 and EPPLER 1233.

However, this value should remain a constant for this range and if it does not then it may create instability. The coefficient of moment remains constant for the propeller EPPLER 1230 and thus the stability of the system is maintained. The Best Glide ratio is obtained by the EPPLER 1230 and thus the consumption of fuel used by the aircraft with the above mentioned propeller will be less.

Considering all the above points we see that the airfoil best suited for the airplane "Rutan VariEze" is EPPLER 1230 and thus we have disregarded the other airfoils similar to this airfoil.

IV. CONCLUSION

The analytical calculations yield certain important parameters like Gross weight, Coefficient of Lift for Aerofoil and of entire airplane. These were estimated to be:

PARAMETER	VALUE
Gross Weight	520kg
Coefficient of lift of airfoil	1.8948
Coefficient of lift of wing	1.8001
Reynolds Number	3.7193×10^6

Calculations of coefficient of lift and Reynolds number were done with help of ANSYS and results were found to coincide. The maximum lift coefficient was found to be 1.8001 analytically and by inputting the value in ANSYS, this value turns out to be 1.84 at an angle of attack of 14° which is fairly close to the analytical value.

Thus an approach for the Verification of Aerodynamic Analysis for selection of Airfoil in Electric Powered Racing Airplane both analytically and by FEM is done successfully and the results were found to be satisfactory.

Future work of this project will be for the verification of performance analysis of the same airfoil as velocities at different performance parameters plays an important role for a racing aircraft.

REFERENCES

Journal Papers:

- [1] R. J. Boucher, History of Solar Flight, AIAA Paper 84-1429, June 1984
- [2] Douglas P. Wells, NASA Green Flight Challenge: Conceptual Design Approaches and Technologies to Enable 200 Passenger Miles per Gallon.

Books:

- [3] Raymer, D., Aircraft Design – A Conceptual Approach, AIAA Education Series, ISBN 1-56347-281-0, third edn, 1999.
- [4] Brant, S. A. et al., Introduction to Aeronautics: A Design Perspective, AIAA Education Series, 1997, ISBN 1-56347-250-3.
- [5] Tully, C., 'Aircraft conceptual design workbooks', Final-year project study, Loughborough. University, May 2001.
- [6] Howe, D., Aircraft Conceptual Design Synthesis, Professional Engineering Pub. Ltd, UK, October 2000, ISBN 1 86058 301 6
- [7] Stinton, D., the Design of the Aeroplane, Blackwell Science Ltd, 1983, ISBN 0-632-01877-1
- [8] D. Stinton, The Design of the Aeroplane, Second edition, Blackwell Science, Oxford, UK, 2001.

Thesis:

- [9] Michael DeRosa, Optimizing Airfoil Sections for Remote Controlled Pylon Racing, ME Thesis, April 2012.

Analysis of Connecting Rod Using Analytical and Finite Element Method

Prof. N.P.Doshi,¹ Prof .N.K.Ingole²

¹(Department of Mechanical Engineering, Bapurao Deshmukh College of Engg, Sewagram, India)

²(Department of Mechanical Engineering, Datta Meghe College of Engg, Sawangi, India)

ABSTRACT: The connecting rod is a major link inside of a combustion engine. It connects the piston to the crankshaft and is responsible for transferring power from the piston to the crankshaft and sending it to the transmission. There are different types of materials and production methods used in the creation of connecting rods. The most common types of materials used for connecting rods are steel and aluminum. Connecting rods are widely used in variety of engines such as, in-line engines, V-engine, opposed cylinder engines, radial engines and oppose-piston engines.

For the project work we have selected connecting rod used in light commercial vehicle of tata motors had recently been launched in the market. We used PRO-E wildfire 4.0 software for modeling of connecting rod and ANSYS 11 software for analysis. ANSYS Workbench module had been used for analysis of connecting rod. We found out the stresses developed in connecting rod under static loading with different loading conditions of compression and tension at crank end and pin end of connecting rod. We have also designed the connecting rod by machine design approach. Design of connecting rod which is designed by machine design approach is compared with actual production drawing of connecting rod. We found that there is possibility of further reduction in mass of connecting rod.

Keywords: Analysis, Connecting rod, Machine Design

I. INTRODUCTION

The connecting rod is a major link inside a combustion engine. It connects the piston to the crankshaft and is responsible for transferring power from the piston to the crankshaft and sending it to the transmission. There are different types of materials and production methods used in the creation of connecting rods. The most common types of Connecting rods are steel and aluminum. The most common types of manufacturing processes are casting, forging and powdered metallurgy. Connecting rods are widely used in variety of engines such as, in-line engines, V-engine, opposed cylinder engines, radial engines and opposed-piston engines. A connecting rod consists of a pin-end, a shank section, and a crank-end. Pin-end and crank-end pinholes at the upper and lower ends are machined to permit accurate fitting of bearings. These holes must be parallel. The upper end of the connecting rod is connected to the piston by the piston pin. If the piston pin is locked in the piston pin bosses or if it floats in the piston and the connecting rod, the upper hole of the connecting rod will have a solid bearing (bushing) of Bronze or a similar material. As the lower end of the connecting rod revolves with the crankshaft, the upper

End is forced to turn back and forth on the piston pin. Although this movement is slight hence the bushing is necessary because of the high pressure and temperatures.

The lower hole in the connecting rod is split to permit it to be clamped around the crankshaft. The bottom part, or cap, is made of the same material as the rod and is attached by two bolts. The surface that bears on the crankshaft is generally a bearing material in the form of a separate split shell. The two parts of the bearing are positioned in the rod and cap by dowel pins, projections, or short brass screws. Split bearings may be of the precision or semi precision type. From the viewpoint of functionality, connecting rods must have the highest possible rigidity at the lowest weight.

The function of connecting rod is to transmit the thrust of the piston to the crankshaft. Figure 1.2 shows the role of connecting rod in the conversion of reciprocating motion into rotary motion. A four-stroke engine is the most common type. The four strokes are intake, compression, power, and exhaust. Each stroke requires approximately 180 degrees of crankshaft rotation, so the complete cycle would take 720 degrees. Each stroke plays a very important role in the combustion process. In the intake cycle, while the piston moves downward, one of the valves open. This creates a vacuum, and an air-fuel mixture is sucked into the chamber (Figure 1 (a)). During the second stroke compression occurs. In compression both valves are closed, and the piston moves upward and thus creates a pressure on the piston, see Figure 1 (b). The next stroke is power. During this process the compressed air-fuel mixture is ignited with a spark, causing a tremendous pressure as the fuel burns. The forces exerted by piston transmitted through the connecting rod moves the crankshaft, see Figure 1(c). Finally, the exhaust stroke occurs. In this stroke, the exhaust valve opens, as the piston moves back upwards, it forces all the air out of the chamber and thus which completes the cycle of crankshaft rotation Figure 1(d).



Fig 1 (a) Intake stroke



Fig 1 (b) compression stroke



Fig 1 (c) Power stroke

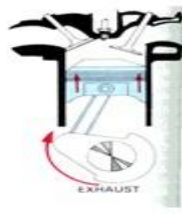


Fig 1.2(d) Exhaust stroke

II. ANALYTICAL DESIGN OF CONNECTING ROD

Piston Diameter = 112mm

Piston Weight = 1.450 kg
= 22.12 N

Weight of connecting rod = 2.731 kg

Weight of reciprocating parts = Piston Weight +
0.33 * Weight of connecting rod
= 1.450 + 0.33 * 2.731
= 2.351 kg
= 2.351 * 9.81 N
= 23.06 N

Piston Material = C-70

Stroke = 112 * 1/2 = 56 mm

Engine RPM = 1200-1700 rpm with maximum over speed of 2200 rpm

Compression Ratio of Engine = 17:1

Maximum explosion pressure = 2.63 MPa

Length of connecting rod = 214 mm

Section of rod : In I.C. engines, the most widely used section of rod is I due to its easiness as it will keep the inertia forces small and it can withstand the high gas pressure also.

In the plane of motion, the ends of the rod are direction free and so freely hinged at the piston pin and the crank pin. Hence for buckling about neutral axis, the strut is freely hinged (figure 5.1). in the plane perpendicular to plane of motion, for buckling about axis yy, the strut is fixed ended due to the effect of bearings at piston and crankpins. Therefore for buckling about axis yy, the rod is four times as strong as for buckling about axis xx. But the rod should be equally strong in both the planes.

$$4I_{yy} = I_{xx}$$

$$k_{yy}^2 = (1/4)k_{xx}^2$$

let the flange and web thickness of section = t

depth of section = 5t

width of section = 4t

area of section = 11t²

$$I_{xx} = (BH^3 - bh^3)/12$$

$$= [4t*(5t)^3 - 3t*(3t)^3]/12$$

$$= 410t^4/12$$

$$I_{yy} = (2tB^3 - ht^3)/12$$

$$= [2t*(4t)^3 + 3t*(t)^3]/12$$

$$= 131t^4/12$$

$$K_{xx}^2 = I_{xx}/A$$

$$= [419t^4] / [12*11t^2]$$

$$= 3.18t^2$$

$$K_{yy}^2 = I_{yy}/A$$

$$= [131t^4] / [12*11t^2]$$

$$= 0.995t^2$$

$$K_{yy}^2/k_{xx}^2 = [0.995t^2] / [3.18t^2] = 1/3.2$$

$$K_{xx}^2 = 3.2 * k_{yy}^2$$

By Rankine formula

$$F_{cu} * A$$

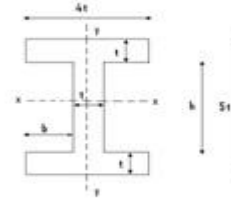
$$\text{Buckling load} = \frac{\text{Maximum explosion load} * \text{factor of safety}}{1 + a * (l/k)^2}$$

$$\text{Buckling load} = \text{Maximum explosion load} * \text{factor of safety}$$

$$= (3.14/4) * 0.1122 * 2.63 * 10^6 * 6$$

(taking factor of safety = 6)

$$= 155465 \text{ N}$$



$F_{cu} = 870 \text{ MPa}$

$A = 11t^2$

$a = 1/7500$

$l = 0.214 \text{ m}$

$k = k_x$

$$155465 = \frac{870 * 10^6 * 11t^2}{1 + (1/7500) * (0.214 * (3.18 t))^2}$$

$$t = 4.6 * 10^{-3} \text{ m}$$

$t = 5 \text{ mm}$

Depth = 5t = 25mm

Width = 4t = 20mm

Section at crank end = 32 * 20

Section at pin end = 22 * 20.

5.2.2 Dimensions of big end

$$P = l_c * d_c * P_b$$

Where

P = maximum gas load

l_c = length of crank pin (mm)

d_c = diameter of crank pin (mm)

P_b = allowable bearing pressure = ranges from 8MPa to 15 MPa

$$P = (3.14/4) * 0.1122 * 2.63 * 10^3$$

$$= 26 \text{ kN}$$

$$= 26000 \text{ N}$$

But $l_c/d_c = 1.25$ to 1.5

Taking $l_c/d_c = 1.25$

$$26000 = 1.25 * d_c * d_c * 15$$

$d_c = 50 \text{ mm}$

$l_c = 1.25 * d_c$

$$= 1.25 * 50$$

$$= 62.5 \text{ mm}$$

Diameter of crank pin = 50mm

Length of crank pin = 62.5mm

Empirically d_c should be = (0.5 to 0.65) * bore

and l_c should be = (0.4 to 0.6) * bore

5.2.3 Design of small end

$$P = l_p * d_p * P_b$$

Where

P = maximum gas load

l_p = length of piston pin (mm)

d_p = diameter of piston pin (mm)

P_b = allowable bearing pressure

P_b = usually ranges from 15 to 31.5 MPa

But $l_p/d_p = 1.5$ to 2

Taking $l_p/d_p = 1.5$

$$26000 = 1.5 * d_p * d_p * 15$$

$dp = 34 \text{ mm}$
 $lp = 52.5 \text{ mm}$
5.2.4 Bolts for Big End Cap
 Inertia force is
 $F_i = (F/g) * (\omega^2) * r [\cos\theta + (r/l)\cos2\theta]$
 Where
 $F =$ Weight of reciprocating parts
 $\omega =$ angular velocity
 $r =$ radius of
 $l =$ length of
 $\omega = (2 * 3.14 * N) / 60$
 $= (2 * 3.14 * 2250) / 60$
 $= 236 \text{ rad/s}$
 $\theta = 00$
 $F = 23.6 \text{ N}$
 $l = 0.214 \text{ m}$
 $r = 0.0635 \text{ m}$
 $F_i = (F/g) * (\omega^2) * r [\cos\theta + (r/l)\cos2\theta]$
 $= 10780 \text{ N}$
 If 2 bolts are used and core diameter is d_c
 $2 * (3.14/4) * d_c^2 * f_t = 10780 \text{ N}$
 $(f_t = 120 \text{ MPa} = \text{allowable stress ranges from 120 to } 175 \text{ MPa})$
 $d_c = 8 \text{ mm}$
 Outer diameter $= 8/0.8$
 $= 10 \text{ mm}$
 Connecting rod big end Bearing cap
 Maximum bending moment may be taken as
 $= (F_i * s) / 6$
 Where
 $F_i =$ load on cap i.e. the inertia load
 $s =$ distance between bolt centers
 $=$ diameter of bearing + twice the thickness of bearing liner + diameter of Bolt + some clearance
 Thickness of bearing liner = thickness of shell + thickness of bearing metal
 Thickness of bearing metal shell may be taken empirically as
 $= 0.05 * \text{cylinder bore}$
 $= 0.05 * 112$
 $= 5.6 \text{ mm}$
 Thickness of bearing metal may be taken as 1mm
 $s = 50 + 2 * (5.6 + 1) + 10 + \text{say } 1.5 \text{ mm}$
 $= 75 \text{ mm}$
 Bending moment
 $= (F_i * s) / 6$
 $= 10780 * 75 / 6$
 $= 134.750 \text{ Nm}$
 Now
 $M_b = f_b * Z$
 f_b may be taken as 120 MPa
 $Z = (b * c^2) / 6$
 Where
 $b =$ width of cap
 $=$ length of bearing (mm)
 $= 50 \text{ mm}$
 $c =$ thickness of cap (mm)
 $134750 = 120 * (50 * c^2) / 6$
 $c = 11 \text{ mm}$
5.2.6 Transverse Inertia Bending Stress
 Centripetal force per unit of connecting rod, acting at crankpin,

$C = \rho A \omega^2 r, \text{ N/m}$
 Now
 ρ for C-70 = 7848 kg/m³
 $A = 11 t^2$
 $= 11 * (0.005)^2$
 $= 2.75 * 10^{-4} \text{ mm}^2$
 $= (2 * 3.14 * N) / 60$
 $= (2 * 3.14 * 2250) / 60$
 $= 236 \text{ rad/s}$
 $C = 7848 * 2.75 * 10^{-4} * 236^2 * 0.0635$
 $= 7632.9 \text{ N/m}$
 Now
 Maximum B.M. $= 0.128 * F_n * l$
 Now
 $F_n = 0.5 * C * l$
 Maximum B.M.
 $= (0.128 * C * l^2) / 2$
 $= 0.128 * 7633 * 0.214^2 / 2$
 $= 22.37 \text{ Nm}$
 Now
 $f_b = M / Z$
 $Z = I_{xx} / (\text{depth} / 2)$
 $I_{xx} = (419 * t^4) / 12$
 $= (419 * 0.005^4) / 12$
 $= 2.18 * 10^{-8} \text{ m}^4$
 $Z = 2.18 * 10^{-8} / (0.05 / 2)$
 $= 8.72 * 10^{-7}$
 $f_b = 22.33 / (8.72 * 10^{-7})$
 $= 25.60 \text{ Mpa}$

III. FINITE ELEMENT ANALYSIS OF CONNECTING ROD

In Figure 2 shown that solid model of Connecting Rod.

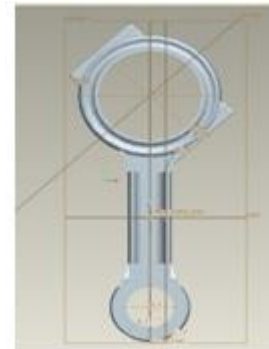


Fig 2 Solid Model of Connecting rod

Meshing of Connecting rod: - In Figure 3 shown that meshed model of connecting rod.



Fig 3. Meshed model of Connecting Rod

IV. LOAD DISTRIBUTION ON CONNECTING ROD

Tension loading

In tension, the connecting rod experiences cosine distribution over 180 of the contact area. The pressure is acting on the contact surface area of the connecting rod. The normal pressure (po) was calculated from the following equations:

$$P = P_o \cos \theta$$

$$P_o = (2Pt) / (\pi r t)$$

Where,

θ = Crank angle, 0 degree for top dead center position

r = Radius of crank or pin end

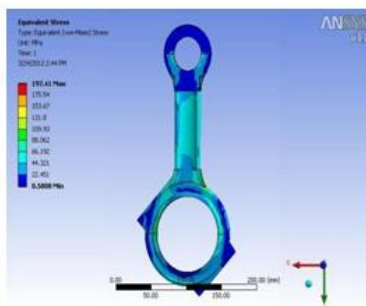
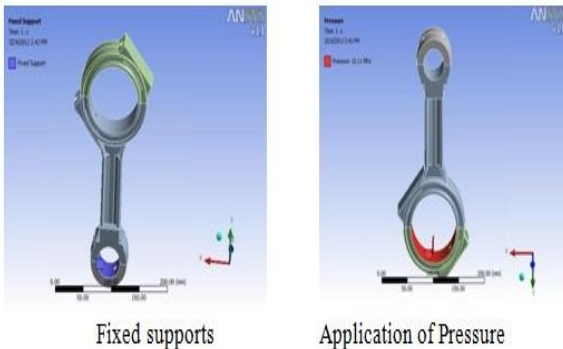
t = Thickness of the connecting rod at the loading surface

Pt = Force magnitude in tension

Table 1 loading data

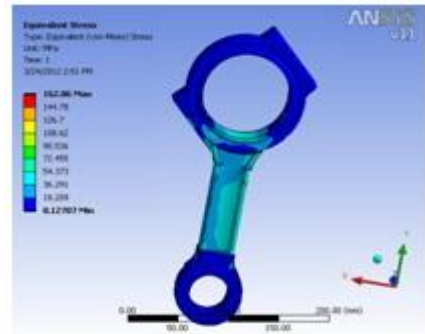
Parameter	Crank end loading		Pin end loading	
	Tension	Compression	Tension	Compression
Load magnitude	26000N	26000N	26000N	26000N
Load Distribution	Cosine Distribution 1800	Uniform Distribution 1200	Cosine Distribution 1800	Uniform Distribution 1200
Pressure Function	$P_o = 2Pt / Rct \pi$	$P_o = Pc / Rct \sqrt{3}$	$P_o = 2Pt / Rpt \pi$	$P_o = Pc / Rpt \sqrt{3}$
Pressure On the Surface	10.11MPa	20.67MPa	22.24MPa	20.17MPa

A Tension loading at Big End (Crank end)



Equivalent stresses developed

Compression loading:-



Equivalent stresses developed

Conclusion and future scope

Solid modeling of connecting rod was made in Pro-E according to production drawing specification and analysis under the effect of tensile and compressive loads in terms of pressure is done in ANSYS Workbench. In present work analytical result compare with numerical result among all load conditions the maximum value of equivalent stress was found to be 197.41 MPa when crank end of connecting rod is in tension. This stress is less than yield strength of material. It gives a factor of safety of 3.2. So the existing design is oversafe but It is consider for only static load condition.

From analysis it is observed that the minimum stresses among all loading conditions, were found at crank end cap as well as at piston end. So the material can be reduced from those portions, thereby reducing material cost. For further optimization of material dynamic analysis of connecting rod is needed. After considering dynamic load conditions once again finite element analysis will have to be performed. It will give more accurate results than existing

REFERENCES

- [1] FEM analysis of connecting rod by R.Vozenilek,C.Scholz (The Technical University of Liberec,Halkova)
- [2] Dynamic Load Analysis and Fatigue Behavior of Forged Steel vs. Powder Metal Connecting Rods by Adila Afzal and Pravardhan Shenoy (The University of Toledo 2003)
- [3] Moon Kyu Lee ,Hyungyil “Buckling sensitivity of connecting rod to the shank sectional area reduction original research article” Material and Design vol 31 Issue 6 Page 2796-2803
- [4] Saharash khare,O.P.Singh “Spalling investigation of connecting rod original research article” Engineering Failure Analysis Vol 19,Jan 2012 page 77-86
- [5] S.griza,F.Bertoni,G.zanon,A.Reguly “fatigue in engine connecting rod bolt due to forming laps original research article” Engineering failure Analysis Vol 16,issue 5 july 2009,page 1542-1548.
- [6] R.J.yang, D.L Dewhirst “Shape optimization of connecting rod pin end using a generic model original research article” Finite element in analysis and design vol 11,issue 3 july 1992,page 257-264.

Comparison of Various Line Clipping Algorithm for Improvement

Abhishek Pandey¹, Swati Jain²

^{1,2}(Department: C.S.E., College Name: Takshshila Institute of Engineering and Technology, Country Name: India)

ABSTRACT: Demonstration of various Line clipping algorithms on the basis of their working principles. One way for improving the efficiency of a line clipping algorithm is to reduce the repetition of algorithm. In this region codes are used to identify the position of line. One algorithm reduces intersection calculations. An efficient clipping algorithm is presented here to achieve this goal. One is based on testing xy plane to reduce intersection calculation. Our algorithm with reducing the confluence point can avoid the repetition of algorithm.

Keywords: Line Clipping Algorithms, LB, CSL, NLN, Computer graphics.

I. INTRODUCTION

Any procedure, which identifies those portions of picture that are either inside or outside of the specified region of the space is referred to as a clipping algorithm. The region against which an object is to clip is called a clip window. Clipping algorithm can be applied in world coordinates so that only the contents of the window interior are mapped to the device coordinates. There are five primitive types clipping, such as point, line, polygon or are, curve and text clipping. Classical line clipping algorithms includes Cohen–Sutherland algorithm, Midpoint Subdivision algorithm, Liang Barsky and Nicholl-Lee-Nicholl algorithm.

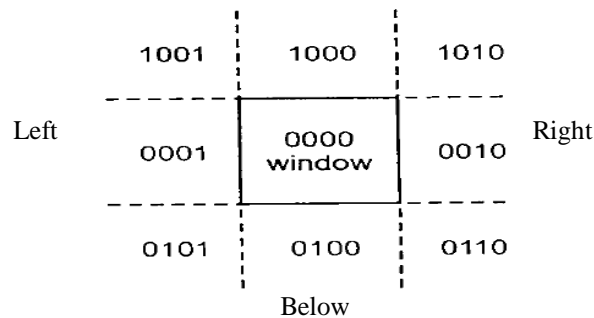
Until recently, most works are concentrated on accelerating the intersection calculation so as to improve the clipping efficiency [Sha92a, Day92a, Wan98a, Wan91a].

II. COHEN SUTHERLAND CLIPPING OVERVIEW

In computer graphics CSL algorithm is a line clipping algorithm. The algorithm divides the 2D space into 9 parts, using the infinite extension of four linear boundaries of the window. Assign a bit pattern to each region as shown in figure.

CSL algorithm reputedly calculates intersections along a line path, even though the line may be completely outside the clip window and each calculation requires both a division and a multiplication.

Figure 1.1 Four bits code for nine region.
Above

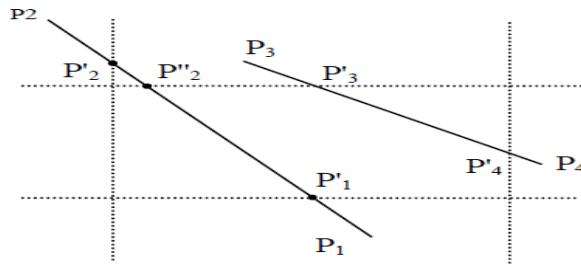


The numbers in the figure above are called out codes. An out codes are computed for each of the two points in the line. The bits in the out codes represent: TOP, BOTTOM, RIGHT, and LEFT. Each bit in the code is set to 1. If the region is to the right of the window, the second bit of the code is set to 1. If the Bottom, third bit is set and if the Top, the fourth bit is set. The four bits in the code the identify each of the nine region.

Lines that cannot be identified as completely inside or completely outside a clip window by these tests are checked for intersection with the window boundaries. As shown in fig.2, such lines may or may not cross into the window interior. We begin the clipping process for a line by comparing an outside endpoint to a clipping boundary to determine how much of the line can be discarded. Then the remaining part of the line is checked against to other boundaries, and we continue until either the line is totally discarded or a section is found outside the window. We set up our algorithm to checked line endpoints against clipping boundaries in the order Left, Right, Bottom, and Top.

To illustrate the specific steps in clipping lines using the Cohen – Sutherland algorithm, we show how the lines in Fig. 2 could be processed. Starting with the Bottom endpoint of the line from p1 to p2, we checked p1 against the Left, Right, Bottom, and above boundaries in turn and find that this point is below the clipping rectangle. We then find the intersection point p'1 with the Bottom boundary and discard the line section from p1 to p'1. The line now has been reduced to the section from p'1 to p2. Since p2 is outside the clip window, we check this endpoint against the boundaries and find that it is to the Left and above of the window. Intersection point p'2 is calculated. But this point is above the window. So the final intersection calculation yields p'2 and the line from p'1 to p'2 is saved [Don04b].

Figure 2.1 Lines extending from one coordinate region to another.



Intersection points with a clipping boundary can be calculated using the slope-intercept form of the line equation. For a line with endpoint coordinates (x_1, y_1) and (x_2, y_2) , the y coordinate of the intersection point with a vertical boundary can be obtained with the calculation

$$y = y_1 + m(x - x_1) \quad (1)$$

Where the x value is set either to x_{wmin} or to x_{wmax} , and the slope of the line is calculated as

$$m = (y_2 - y_1) / (x_2 - x_1).$$

Similarly, if we are looking for the intersection with a horizontal boundary, the x coordinate can be calculated as

$$x = x_1 + (y - y_1) / m \quad (2)$$

With y set either to y_{wmin} or to y_{wmax} .

The following procedure demonstrates the Cohen-Sutherland line-clipping algorithm. Codes for each endpoint are stored as bytes and processed using bit manipulations.

```
#define ROUND (a) ((int) (a+0.5))
/* Bits masks encode a point's position relative to the clip EGs. A points status is encoded by OR'ing together appropriate bit masks.*/
#define Left_EG 0x1
#define Right_EG 0x2
#define Bottom_EG 0x4
#define Top_EG 0x8
/* points encoded as 0000 are completely inside the clip rectangle; All others are outside at least one EG.if OR'ing two codes is FALSE (no bits are set in either code), the line can be Accepted. If the AND operation between two codes is true, the line defined by those endpoints is completely outside the clip region and can be Rejected.*/
*/
#define INSIDE (a) (! a)
#define REJECT (a,b) (a&b)
#define ACCEPT (a,b) (!(a|b))
#define FALSE 0
#define TRUE 1
Unsigned char encode (wcpt2 pt,dcpt winmin, dcpt winmax)
{
    if (pt.x < winmin.x)
        Code = code | Left_EG;
    if (pt.x > WinMax.x)
        Code = code | Right_EG;
    if (pt.y < WinMin.y)
        Code = code | Bottom_EG;
    if (pt.y > WinMax.y)
        Code = code | Top_EG;
    Code = code | Top_EG;
    Return (code);
}
void SwapPoints (wcpt2 *p1, wcpt2 *p2)
{
    Wcpt2 tmp;
    tmp = *p1; *p1 = *p2; *p2 = tmp;
}
void SwapCodes (unsigned char *c1, unsigned
{
    unsigned char tmp;
    tmp = *c1; *c1 = *c2; *c2 = tmp;
}
}
```

```

void ClipLine (dcpt WinMin, dcpt WinMax, wcpt2 p1, wcpt2 p2)
{
    Unsigned char code1, code2;
    int done= FALSE, draw = FALSE;
    Float m;
    while (!done)
    {
        code1 = encode (p1, WinMin, WinMax);
        code2 = encode (py, WinMin, WinMax);
        if (ACCEPT (code1, code2))
        {
            Done = TRUE;
            Draw = TRUE;
        }
        Else if (REJECT (code1, code2))
            Done = FALSE;
        Else {
            /*ensure that p1 is outside window*/
            If (INSIDE (code1)) {
                SwapPts(&p1, &p2);
                SwapCodes(&code1, &code2); }
            /* use slope (m) to find line_clip EG Intersection */
            If (p2.x != p1.x)
                m = (p2.y - p1.y) / (p2.x - p1.x);
            If (code1 & Left_EG)
            {
                p1.y += (WinMin.x - p1.x) * m;
                p1.x = WinMin.x;
            }
            elseif (code1 & Right_EG)
            {
                p1.y += (WinMax.x - p1) * m;
                p1.x = WinMax.x;
            }
        }
        elseif (code1 & Bottom_EG)
        {
            if (p2.x != p1.x)
                p1.x += (WinMin.y - p1.y) / m;
            p1.y = WinMin.y;
        }
        elseif (code1 & Top_EG)
        {
            if (p2.x != p1.x)
                p1.x += (WinMax.y - p1.y)/m;
            p1.y = WinMax.y;
        }
    }
}
if (draw)
lineDDA (ROUND(p1.x), ROUND(p1.y),
ROUND (p2.x), ROUND(p2.y));
}

```

III. LIANG- BERSKY CLIPPING ALGORITHM

Liang-berksy uses a parametric line representation to set up a more efficient line clipping procedure that reduces intersection calculations. In general, the LB algorithm is more efficient than the CSL algorithm since intersection calculation is reduced. Each updates of parameters u1 and u2 requires only one division and window intersection of the line are computed only once when the final values of u1 and u2 have been computed.

We can write parametric equation of a line segment is in the form

$$x = x_1 + u\Delta x$$

$$y = y_1 + u\Delta y$$

where $0 \leq u \leq 1$ and $\Delta x = x_2 - x_1$ $\Delta y = y_2 - y_1$,

For a point (x,y) inside the clipping window, we have

$$x\omega_{\min} \leq x_1 + \Delta x, u \leq x\omega_{\max}$$

$$y\omega_{\min} \leq y_1 + \Delta y, u \leq y\omega_{\max}$$

Rewrite these four inequalities as

$$p_k u \leq q_k \quad k = 1, 2, 3, 4$$

Where parameter p and q are defined as

$$p_1 = -\Delta x \quad q_1 = x_1 - x\omega_{\min} \text{ (Left)}$$

$$p_2 = \Delta x \quad q_2 = x\omega_{\max} - x_1 \text{ (Right)}$$

$$p_3 = -\Delta y \quad q_3 = y_1 - y\omega_{\min} \text{ (Bottom)}$$

$$p_4 = \Delta y \quad q_4 = y\omega_{\max} - y_1 \text{ (Top)}$$

Observe the following facts:

If $p_k = 0$, the line is parallel to the corresponding boundary and (a) if $q_k < 0$, the line is completely outside the boundary and can be eliminated. (b) if $q_k > 0$, the line is inside the boundary and need further consideration.

If $p_k < 0$, the extended line proceeds from the outside to inside of the corresponding boundary line.

If $p_k > 0$, the extended line proceeds from the inside to outside of the corresponding boundary line.

If $p_k \neq 0$, we can calculate the value of u that corresponds to the point where the infinitely extended line intersects the extension of boundary k as

$$u = \frac{q_k}{p_k}$$

The LB algorithm for finding the visible portion of the line, if any, can be stated as a 4 step process:

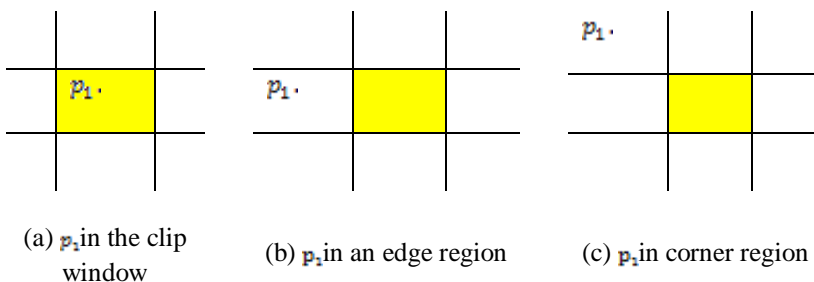
- (a) If $p_k = 0$ and $q_k < 0$, for any k, eliminates the line and stop otherwise proceed to next step.
- (b) For all k such that $p_k < 0$ calculate $r_k = q_k/p_k$. Let u_1 be the maximum of the set containing 0 and the various values of r.
- (c) For all k such that $p_k > 0$ calculate $r_k = q_k/p_k$. Let u_2 be the minimum of the set containing 1 and the calculated r value.
- (d) If $u_1 > u_2$, eliminate the line since it is completely outside the clipping window otherwise, use u_1 and u_2 to calculate the endpoints of the clipped line.

IV. NICHOLL LEE NICHOLL CLIPPING ALGORITHM

NLN method uses more regions testing in the xy plane to reduce intersection calculations. The extra intersection calculation eliminated in the NLN algorithm by carrying out more region testing before intersection position is calculated.

It uses symmetry to categorize endpoints into one of 3 regions (in the clip window, edge & corner). Then according to end point category it checks several clip cases. For a line with endpoint p_1 and p_2 , we first determine the position of point p_1 for the nine possible region relative to the clipping rectangle. Only the three region shown below need be considered.

Figure 4.1 NLN clipping window.



If p_1 lies in any one of the other six region, we can move it to one of the three regions using a symmetry transformation. For example, the region directly above the clip window can be transformed to the region left of the clip window using a reflection about the line $y=-x$ or we could use a 90° counter clockwise rotation. Next, we find out the position of p_2 relative to p_1 . To do this, we create some new regions in the plane, depending on the location of p_1 . Boundaries of the new region are line segments that start at the position of p_1 and pass through the window corners.

V. IMPROVED CSL CLIPPING ALGORITHM

As before said our algorithm is based on Cohen–Sutherland algorithm whereas we try to be efficient. In our new algorithm, Firstly, we apply Encoding & Code checking technique of Cohen–Sutherland algorithm to accept the completely inside lines and reject lines that lie completely on the outside of each boundary of the clip window. Then, if the endpoint isn't in the corner (A|B|C|D) of clipping window, the process of clipping will be same as Cohen–Sutherland algorithm. But if the endpoint is in the corner fig1 (A|B|C|D), by comparing the distances between the endpoint to the points that gain by the cross of line to the two clipping boundaries, confluence-points, and choose a boundary that have bigger distance for

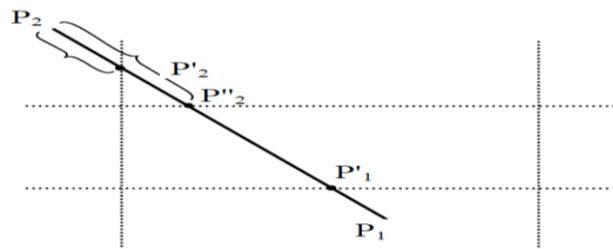
discarding, we can avoid repeating the algorithm. Against clipping boundaries in the order Left & above, Right & above, Left & Bottom, Right & Bottom, Left, Right, Bottom, Top. When the endpoint is out of two clipping boundaries, in the corner fig1 (A||B|C||D), we calculate the confluence-points of line to the clipping boundaries, in fig.3. The confluence-points are p'2 and p''2. We consider two segments, from endpoint to the confluence-points, and then we calculate the length of segments. The length of segment can be calculated as:

$$d = \sqrt{(x - x_1)^2 + (y - y_1)^2} \quad (3)$$

Then we compare the two lengths that came by calculating the length of segments and determine a bigger segment. Finally we discard the line than to a clip boundary that its confluence-points makes bigger segment. And finally, we check that the line endpoints be in the clipping window by OR'ing the new region Codes.

To illustrate the specific steps in clipping lines using proposed algorithm, we show how the lines in Fig. 3 could be processed. Starting with the Bottom endpoint of the line from p1 to p2, we checked p1 against the Left, Right, Bottom, and above boundaries in turn and find that this point just is below the clipping rectangle. We then find the intersection point p'1 with the Bottom boundary and discard the line section from p1 to p'1. The line now has been reduced to the section from p'1 to p2. Since p2 is outside the clip window, we check this endpoint against the boundaries and find that it is outside of the Left and above of clipping rectangle. We calculate a confluence-points of line to the clipping boundaries and consider two segments; from p2 to the p'2 and from p2 to p''2. Then we compare the segments and determine a bigger segment. Finally we discard the line than to a clip boundary that makes bigger segment. So the final intersection calculation yields p'2 and the line from p'1 to p'2 is saved.

Figure 3.1 Applying proposed algorithm to clip line.



The following procedure demonstrates the changes that we apply on Cohen-Sutherland line-clipping algorithm and makes our new algorithm.

If the line is not rejected and not completely accepted follow steps else exit. If codes of (endpoint & LEFT_EG & TOP_EG) is not zero then calculate the distances between endpoint to LEFT_EG and endpoint to TOP_EG, then choose a boundary that have a bigger distance for discarding.

If codes of (endpoint & LEFT_EG & BOTTOM_EG) is not zero then calculate the distances between endpoint to LEFT_EG and endpoint to BOTTOM_EG, then choose a boundary that have a bigger distance for discarding.

If codes of (endpoint & LEFT_EG & TOP_EG) is not zero then calculate the distances between endpoint to LEFT_EG and endpoint to TOP_EG, then choose a boundary that have a bigger distance for discarding.

If codes of (endpoint & RIGHT_EG & TOP_EG) is not zero then calculate the distances between endpoint to RIGHT_EG and endpoint to TOP_EG, then choose a boundary that have a bigger distance for discarding.

If codes of (endpoint & RIGHT_EG & BOTTOM_EG) is not zero then calculate the distances between endpoint to RIGHT_EG and endpoint to BOTTOM_EG, then choose a boundary that have a bigger distance for discarding.

Else the endpoint is not in the corner of clipping boundary and uses a common Cohen-Sutherland line clipping algorithm.

VI. IMPLEMENTATION

We implemented the new algorithm on PC and compared its performance with that of Cohen-Sutherland algorithm. Our machine is based on Pentium IV 2.00GHz, and the compiler is Turbo C running on Windows XP.

We apply the algorithm on five lines and the results are presented in Tables I. we assumed the clipping rectangle was from (2, 3) to (8, 7).

Table 1: results of implementation

S. No.	Line equation	Number of Confluence-points	
		CSL algorithm	Current algorithm
1	$Y = 2x - 6 \ 0 \leq x \leq 9$	3	2
2	$Y = -5/4x + 49/4 \ 1 \leq x \leq 12$	4	2
3	$Y = -3x + 20 \ 3 \leq x \leq 5$	1	1
4	$Y = -1/2x + 5 \ 0 \leq x \leq 10$	3	2
5	$Y = 6 \ 1 \leq x \leq 14$	2	2

VII. RESULT

Certainly in best condition which the endpoints are completely inside or outside the clipping window, proposed algorithm and Cohen-Sutherland algorithm are done the same. When endpoints are outside the clipping window and not in the corner fig1 (A||B|C||D), these two algorithm line clip are similarly, because each endpoints are just out of one boundary of clipping rectangle. Besides even if one of the endpoints be in the corner of clipping window, as you see in table.1, they work different. When at least one endpoint be at the corner fig1 (A||B|C||D) our algorithm can done better. In this case the average of confluence-points for Cohen-Sutherland algorithm may be three and two for our algorithm. Furthermore, if both of endpoints be at the corner, the average of confluence-points may be four for Cohen-Sutherland algorithm and two for our algorithm. As you see, in any condition our algorithm at most calculate just two confluence-points to line clipping. On the other hand Cohen-Sutherland algorithm at most calculate four confluence- points. And as we said before whatever the number of confluence-endpoints be lesser, the efficiency will be higher.

VIII. CONCLUSION

In this article we try to introduce a new algorithm that is based on Cohen -Sutherland algorithm. However when the line endpoints be at the corner, our algorithm may perform better. As a whole the presented algorithm just by calculating at most two confluence-points for the line in every condition can discard faster. We can extend this algorithm for the clipping windows which even if they are not square. Moreover for increasing the accuracy of calculation we can use fuzzy.

IX. FUTURE WORK

Both CSL and LB can be extended to 3D clipping.

X. ACKNOWLEDGEMENT

This work received support from the Department of Computer Science & Engineering, Takshshila Institute of Engineering and Technology.

BIOGRAPHIES

Abhishek Pandey B.E.[I.T.], M.E.[C.S.E] is an assistant professor in the Department of Computer Science, Takshshila Institute of Technology, Jabalpur[M.P.], India. His research interests include computer graphics, data structure and software engineering.

Swati Jain is an assistant professor in the Department of Computer Science, Takshshila Institute of Technology, Jabalpur [M.P.], India. His research interests include computer graphics, Fuzzy Logics, Soft Computing and software engineering.

REFERENCES

- [1] Donald Hearn, and M. Pauline Baker, "Computer Graphics, C Version", 3 edition, pp. 226-230, December 2004.
- [2] Goudong Lu*, Xuanhui Wu, Qunsheng Peng, "An efficient line clipping algorithm based o adaptive line rejection", Computers & Graphics 26 (2002) 409-415.
- [3] Sharma NC, Manohar S. Line clipping revisited: two efficient algorithm basedon simple geometric observations. Computers and Graphics 1992; 16(1): 51-4. Day JD. "A new two dimensional ling clipping algorithm for small windows", Computer Graphics Forum 1992; 11(4): 241-5.
- [4] Wang Haohong, Wu Ruixun, Cai Shijie. "A new efficient clipping algorithm basedon geometric transformation", Journal of Software 1998; 9(10): 728-33 (in Chinese).
- [5] Wang Jun, Liang Youdong, Peng Qunsheng. "A 2-D lineclipping with the least arithmetic operations", Chinese Journal of Computers 1991 ;(7): 495-504(in chinese).
- [6] Sproull RF, Sutherland IE. "A clipping divider". In: Proceedings of the Fall Joint Computer Conference.Washington: Thompson Books, 1968. p. 765-75.
- [7] Rogers DF. "Procedural elements for computer graphics". New York: McGraw-Hill, 1985. P.111-87.
- [8] Sobkow MS, Pospisil P, Yang YH. A fast two-dimensional line clipping algorithm via line encoding Computers and Graphics198.

MHD Free Convection and Mass Transfer Flow past a Vertical Flat Plate

S. F. Ahmmed¹, S. Mondal², A. Ray³

1, 2, 3 Mathematics Discipline, Khulna University, Bangladesh

ABSTRACT: We investigate the two dimensional free convection and mass transfer flow of an incompressible, viscous and electrically conducting fluid past a continuously moving vertical flat plate in the presence of heat source, thermal diffusion, large suction and the influence of uniform magnetic field applied normal to the flow. Usual similarity transformations are introduced to solve the momentum, energy and concentration equations. To obtain the solutions of the problem, the ordinary differential equations are solved by using perturbation technique. The expressions for velocity field, temperature field, concentration field, skin friction, rate of heat and mass transfer have been obtained. The results are discussed in detailed with the help of graphs and tables to observe the effect of different parameters.

Keywords: Free convection, MHD, Mass transfer, Thermal diffusion, Heat source parameter.

I. INTRODUCTION

Magneto-hydrodynamic (MHD) is the branch of continuum mechanics which deals with the flow of electrically conducting fluids in electric and magnetic fields. Many natural phenomena and engineering problems are worth being subjected to an MHD analysis. Furthermore, Magneto-hydrodynamic (MHD) has attracted the attention of a large number of scholars due to its diverse applications.

In engineering it finds its application in MHD pumps, MHD bearings etc. Workers like Hossain and Mandal [1] have investigated the effects of magnetic field on natural convection flow past a vertical surface. Free convection flows are of great interest in a number of industrial applications such as fiber and granular insulation, geothermal systems etc. Buoyancy is also of importance in an environment where differences between land and air temperatures can give rise to complicated flow patterns.

Convection in porous media has applications in geothermal energy recovery, oil extraction, thermal energy storage and flow through filtering devices. The phenomena of mass transfer are also very common in theory of stellar structure and observable effects are detectable, at least on the solar surface. The study of effects of magnetic field on free convection flow is important in liquid-metal, electrolytes and ionized gases. The thermal physics of hydro-magnetic problems with mass transfer is of interest in power engineering and metallurgy. The study of flows through porous media became of great interest due to its wide application in many scientific and engineering problems. Such type of flows can be observed in the movement of underground water resources, for filtration and

water purification processes, the motion of natural gases and oil through oil reservoirs in petroleum engineering and so on. The porous medium is in fact a non-homogeneous medium. The velocity is usually so small and the flow passages are so narrow that laminar flow may be assumed without hesitation. Rigorous analysis of the flow is not possible because the shape of the individual flow passages is so varied and so complex. Poonia and Chaudhary [2] studied about the flows through porous media. Recently researchers like Alam and Rahman [3], Sharma and Singh [4] Chaudhary and Arpita [5] studied about MHD free convection heat and mass transfer in a vertical plate or sometimes oscillating plate. An analysis is performed to study the effect of thermal diffusing fluid past an infinite vertical porous plate with Ohmic dissipation by Reddy and Rao [6]. The combined effect of viscous dissipation, Joule heating, transpiration, heat source, thermal diffusion and Hall current on the hydro-Magnetic free convection and mass transfer flow of an electrically conducting, viscous, homogeneous, incompressible fluid past an infinite vertical porous plate are discussed by Singh *et al.* [7]. Singh [8] has also studied the effects of mass transfer on MHD free convection flow of a viscous fluid through a vertical channel walls. An extensive contribution on heat and mass transfer flow has been made by Gebhart [9] to highlight the insight on the phenomena. Gebhart and Pera [10] studied heat and mass transfer flow under various flow situations. Therefore several authors, viz. Raptis and Soundalgekar [11], Agrawal *et al.* [12], Jha and Singh [13], Jha and Prasad [14] have paid attention to the study of MHD free convection and mass transfer flows. Abdusattar [15] and Soundalgekar *ET.*

al. [16] also analyzed about MHD free convection through an infinite vertical plate. Acharya *et al.* [17] have presented an analysis to study MHD effects on free convection and mass transfer flow through a porous medium with constant suction and constant heat flux considering Eckert number as a small perturbation parameter. This is the extension of the work of Bejan and Khair [18] under the influence of magnetic field. Singh [19] has also studied effects of mass transfer on MHD free convection flow of a viscous fluid through a vertical channel using Laplace transform technique considering symmetrical heating and cooling of channel walls. A numerical solution of unsteady free convection and mass transfer flow is presented by Alam and Rahman [20] when a viscous, incompressible fluid flows along an infinite vertical porous plate embedded in a porous medium is considered.

In view of the application of heat source and thermal diffusion effect, the study of two dimensional MHD free convection and mass transfer flow past an infinite vertical porous plate taking into account the combined effect of heat source and thermal diffusion with a great agreement was conducted by Singh ET. al.[21].

In our present work, the effect of large suction on MHD free convection heat and mass transfer flow past a vertical flat plate has been investigated by similarity solutions which are obtained by employing the perturbation technique. We have used MATHEMATICA to draw graph and to find the numerical results of the equation.

II. THE GOVERNING EQUATIONS

Consider a two dimensional steady free convection heat and mass transfer flow of an incompressible, electrically conducting and viscous fluid past an electrically non-conducting continuously moving vertical flat plate.

Introducing a Cartesian co-ordinate system, x-axis is chosen along the plate in the direction of flow and y-axis normal to it. A uniform magnetic field is applied normally to the flow region. The plate is maintained at a constant temperature T_w and the concentration is maintained at a constant value C_w . The temperature of ambient flow is T_∞ and the concentration of uniform flow is C_∞ .

Considering the magnetic Reynold's number to be very small, the induced magnetic field is assumed to be negligible, so that $\vec{B} = (0, B_0(x), 0)$. The equation of conservation of electric charge is $\nabla \cdot \vec{J} = 0$ Where $\vec{J} = (J_x, J_y, J_z)$ and the direction of propagation is assumed along y-axis so that J does not have any variation along y-axis so that the y derivative of \vec{J} namely $\frac{\partial J_y}{\partial y} = 0$ resulting in $J_y = \text{constant}$.

Also the plate is electrically non-conducting $J_y = 0$ everywhere in the flow. Considering the Joule heating and viscous dissipation terms to negligible and that the magnetic field is not enough to cause Joule heating, the term due to electrical dissipation is neglected in the energy equation.

The density is considered a linear function of temperature and species concentration so that the usual Boussinesq's approximation is taken as $\rho = \rho_0 [1 - \{\beta (T - T_\infty) + \beta^* (C - C_\infty)\}]$. Within the frame work of delete such assumptions the equations of continuity, momentum, energy and concentration are following [21]

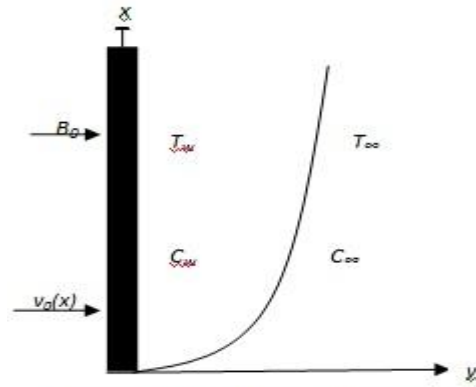


Fig.-Physical model of boundary layer

Continuity equation

$$\frac{\partial u}{\partial x} + \frac{\partial v}{\partial y} = 0 \quad (1)$$

Momentum equation

$$u \frac{\partial u}{\partial x} + v \frac{\partial v}{\partial y} = g \frac{\partial^2 u}{\partial y^2} + g \beta (T - T_\infty) + g \beta^* (C - C_\infty) - \frac{\sigma' B_0^2(x)}{\rho} u \quad (2)$$

Energy equation

$$u \frac{\partial T}{\partial x} + v \frac{\partial T}{\partial y} = \frac{K}{\rho C_p} \frac{\partial^2 T}{\partial y^2} + Q(T - T_\infty) \quad (3)$$

Concentration equation

$$u \frac{\partial C}{\partial x} + v \frac{\partial C}{\partial y} = D_M \frac{\partial^2 C}{\partial y^2} + D_T \frac{\partial^2 T}{\partial y^2} \quad (4)$$

The boundary conditions relevant to the problem are

$$u = U_0, \quad v = v_0(x), \quad T = T_w, \quad C = C_w \quad \text{at } y = 0 \quad (5)$$

$$u = 0, \quad v = 0, \quad T = T_\infty, \quad C = C_\infty \quad \text{at } y \rightarrow \infty$$

Where u and v are velocity components along x -axis and y -axis respectively, g is acceleration due to gravity, T is the temperature. K is thermal conductivity, σ' is the electrical conductivity, D_M is the molecular diffusivity, U_0 is the uniform velocity, C is the concentration of species, $B_0(x)$ is the uniform magnetic field, C_p is the specific heat at constant pressure, Q is the constant heat source (absorption type), D_T is the thermal diffusivity, $C(x)$ is variable concentration at the plate, $v_0(x)$ is the suction velocity, ρ is the density, g is the kinematic viscosity, β is the volumetric coefficient of thermal expansion and β^* is the volumetric coefficient of thermal expansion with concentration and the other symbols have their usual meaning. For similarity solution, the plate concentration $C(x)$ is considered to be $C(x) = C_\infty + (C_w - C_\infty)x$.

III. MATHEMATICAL ANALYSIS

We introduce the following local similarity variables of equation (6) into equation (2) to (4) and boundary condition (5) and get the equation (7) to (9) and boundary condition (10)

$$\psi = \sqrt{2gxU_0} f(\eta), \quad \eta = y \sqrt{\frac{U_0}{2gx}} \quad (6)$$

$$\theta(\eta) = \frac{T - T_\infty}{T_w - T_\infty}, \quad \phi(\eta) = \frac{C(x) - C_\infty}{C_w - C_\infty}$$

$$f''' + ff'' - Mf' + Gr\theta + Gm\phi = 0 \quad (7)$$

$$\theta'' + Pr f\theta' - SPr\theta = 0 \quad (8)$$

$$\phi'' - 2Scf'\phi + Scf\phi' + S_0Sc\theta'' = 0 \quad (9)$$

where $Pr = \frac{\mu Cp}{k}$ is the Prandtl number,

$Gr = \frac{2xg\beta(T_w - T_\infty)}{U_0^2}$ is the Grashof number,

$Gm = \frac{2xg\beta^*(C_w - C_\infty)}{U_0^2}$ is Modified Grashof number,

$S = \frac{2xQ}{U_0}$ is the Heat source parameter,

$M = \frac{2x\sigma'\beta_0^2(x)}{U_0\rho}$ is Magnetic parameter,

$Sc = \frac{\rho}{D_M y}$ is the Schmidt number and

$S_0 = \frac{T_w - T_\infty}{C_w - C_\infty}$ is the Soret number

with the boundary condition,

$$f = f_w, \quad f' = 1, \quad \theta = 1, \quad \phi = 1 \quad \text{at } \eta = 0 \quad (10)$$

$$f' = 0, \quad \theta = 0, \quad \phi = 0 \quad \text{as } \eta \rightarrow \infty$$

where $f_w = v_o(x) \sqrt{\frac{2x}{gU_0}}$ and primes denotes the

derivatives with respect to η .

$$\xi = \eta f_w, \quad f(\eta) = f_w X(\xi),$$

$$\theta(\eta) = f_w^2 Y(\xi), \quad \phi(\eta) = f_w^2 Z(\xi) \quad (11)$$

By using the above equation (11) in the equations (7) - (9) with boundary condition (10) we get,

$$X''' + XX'' = \varepsilon(MX' - GrY - GmZ) \quad (12)$$

$$Y'' + Pr XY' = \varepsilon S Pr Y \quad (13)$$

$$Z'' - 2ScZX' + ScXZ' + ScS_0Y'' = 0 \quad (14)$$

The boundary conditions (10) reduce to

$$X = 1, \quad X' = \varepsilon, \quad Y = \varepsilon \quad \text{and } Z = \varepsilon \quad \text{at } \xi = 0 \quad (15)$$

$$X' = 0, \quad Y = 0, \quad Z = 0 \quad \text{as } \xi \rightarrow \infty$$

Now we can expand X , Y and Z in powers of ε as

follows since $\varepsilon = \frac{1}{f_w^2}$ is a very small quantity for large

suction

$$X(\xi) = 1 + \varepsilon X_1(\xi) + \varepsilon^2 X_2(\xi) + \varepsilon^3 X_3(\xi) + \dots \quad (16)$$

$$Y(\xi) = \varepsilon Y_1(\xi) + \varepsilon^2 Y_2(\xi) + \varepsilon^3 Y_3(\xi) + \dots \quad (17)$$

$$Z(\xi) = \varepsilon Z_1(\xi) + \varepsilon^2 Z_2(\xi) + \varepsilon^3 Z_3(\xi) + \dots \quad (18)$$

Using equations (16)-(18) in equations (12)-(14) and considering up to order $O(\varepsilon^3)$, we get the following three sets of ordinary differential equations and their corresponding boundary conditions

First order $O(\varepsilon)$:

$$X_1''' + X_1'' = 0 \quad (19)$$

$$Y_1'' + Pr Y_1' = 0 \quad (20)$$

$$Z_1'' + ScZ_1' + ScS_0Y_1'' = 0 \quad (21)$$

The boundary conditions for 1st order equations are

$$X_1 = 0, \quad X_1' = 1, \quad Y_1 = 1, \quad Z_1 = 1 \quad \text{at } \xi = 0 \quad (22)$$

$$X_1' = 1, \quad Y_1 = 0, \quad Z_1 = 0 \quad \text{as } \xi \rightarrow \infty$$

Second order $O(\varepsilon^2)$:

$$X_2''' + X_2'' + X_1 X_1'' = MX_1' - GrY_1 - GmZ_1 \quad (23)$$

$$Y_2'' + Pr X_1 Y_1' + Pr Y_2' = S Pr Y_1 \quad (24)$$

$$Z_2'' + ScZ_2' = 2ScX_1' Z_1 - ScX_1 Z_1' - ScS_0 Y_2'' \quad (25)$$

The boundary conditions for 2nd order equations are

$$X_2 = 0, \quad X_2' = 0, \quad Y_2 = 0, \quad Z_2 = 0 \quad \text{at } \xi = 0 \quad (26)$$

$$X_2 = 0, \quad Y_2 = 0, \quad Z_2 = 0 \quad \text{as } \xi \rightarrow \infty$$

Third order $O(\varepsilon^3)$:

$$X_3''' + X_3'' + X_1 X_2 X_1'' = MX_2' - GrY_2 - GmZ_2 \quad (27)$$

$$Y_3'' + Pr X_1 Y_2' + Pr X_2 Y_1' + Pr Y_3' = S Pr Y_2 \quad (28)$$

$$Z_3'' + ScZ_3' = 2ScX_1' Z_2 + 2ScX_2' Z_1 - ScX_2 Z_1' - ScX_1 Z_2' - ScS_0 Y_3'' \quad (29)$$

The boundary conditions for 3rd order equations are

$$X_3 = 0, \quad X_3' = 0, \quad Y_3 = 0, \quad Z_3 = 0 \quad \text{at } \xi = 0 \quad (30)$$

$$X_3' = 0, \quad Y_3 = 0, \quad Z_3 = 0 \quad \text{as } \xi \rightarrow \infty$$

The solution of the above coupled equations (19) to (30) under the prescribed boundary conditions are as follows

First order $O(\varepsilon)$:

$$X_1 = 1 - e^{-\xi} \quad (31)$$

$$Y_1 = e^{-Pr\xi} \quad (32)$$

$$Z_1 = (1 - A_1)e^{-Sc\xi} + A_1 e^{-Pr\xi} \quad (33)$$

Second order $O(\varepsilon^2)$:

$$X_2 = \frac{1}{4} e^{-2\xi} + (A_7 + A_2\xi)e^{-\xi} - A_8 e^{-Pr\xi} + A_9 e^{-Sc\xi} + A_{10} \quad (34)$$

$$Y_2 = (A_{11} - A_{12}\xi)e^{-Pr\xi} - A_{11} e^{-(1+Pr)\xi} \quad (35)$$

$$Z_2 = (B_5 - B_1 - B_2 - B_3 - B_6\xi)e^{-Sc\xi} + (B_3 - B_5 + B_4\xi) e^{-Pr\xi} + B_1 e^{-(1+Pr)\xi} + B_2 e^{-(1+Sc)\xi} \quad (36)$$

Third order $O(\varepsilon^3)$:

$$X_3 = B_{31} + (B_{24} + B_{32}\xi + \frac{B_9}{2}\xi^2)e^{-\xi} - (\frac{B_7}{4} - A_2 - \frac{A_2}{2}\xi) e^{-2\xi} + (B_{25} + B_{26} + B_{18}\xi)e^{-Pr\xi} - [B_{27} - B_{28} - B_{21}\xi] e^{-Sc\xi} - B_{29}e^{-(1+Pr)\xi} - B_{30}e^{-(1+Sc)\xi} - \frac{1}{24}e^{-3\xi} \quad (37)$$

$$Y_3 = [B_{40} + B_{41}\xi + \frac{B_{34}}{2}\xi^2]e^{-Pr\xi} + [B_{39} - B_{35} + B_{36}\xi]e^{-(1+Pr)\xi} + B_{37}e^{-(2+Pr)\xi} + B_{38}e^{-(Pr+Sc)\xi} + \frac{A_8}{2}e^{-2Pr\xi} \quad (38)$$

$$Z_3 = B_{122}e^{-Sc\xi} + (B_{116} + B_{97}\xi)e^{-(1+Sc)\xi} + (B_{117} + B_{100}\xi)e^{-(1+Pr)\xi} + B_{102}e^{-(2+Pr)\xi} + B_{103}e^{-(2+Sc)\xi} + B_{104}e^{-(Pr+Sc)\xi} - B_{105}e^{-2Pr\xi} - B_{106}e^{-2Sc\xi} + (B_{118} + B_{119}\xi - B_{110}\xi^2)e^{-Pr\xi} \quad (39)$$

Using equations (16) to (18) in equation (11) with the help of equations (31) to (39) we have obtained the velocity, the temperature and concentration fields as follows

Velocity distribution

$$u = U_0 f'(\eta) = U_0 f_w' X'(\xi) = U_0 [X_1'(\xi) + \varepsilon X_2'(\xi) + \varepsilon^2 X_3'(\xi)] \quad (40)$$

Temperature distribution

$$\theta(\eta) = f_w^2 Y(\xi) = Y_1(\xi) + \varepsilon Y_2(\xi) + \varepsilon^2 Y_3(\xi) \quad (41)$$

Concentration distribution

$$\phi(\eta) = f_w^2 Z(\xi) = Z_1(\xi) + \varepsilon Z_2(\xi) + \varepsilon^2 Z_3(\xi) \quad (42)$$

The main quantities of physical interest are the local skin-friction, local Nusselt number and the local Sherwood number. The equation defining the wall skin-friction as

$$\tau = \mu \left(\frac{\partial u}{\partial y} \right)_{y=0} \quad (43)$$

Thus from equation (40) the skin-friction may be written as

$$\tau \propto [f''(\eta)]_{\eta=0} = [1 + \varepsilon\{1 + A_7 - 2A_2 + A_8 Pr^2 + A_9 Sc^2\} + \varepsilon^2\{B_9 - 2B_{32} + B_{24} - B_7 + 2A_2 - 2B_{18} Pr + Pr^2(B_{25} + B_{26}) - 2B_{21} Sc - Sc^2(B_{27} - B_{28}) - B_{29}(1 + Pr)^2 - B_{30}(1 + Sc)^2 - \frac{3}{8}\}] \quad (44)$$

The local Nusselt number denoted by Nu and defined as

$$Nu = - \left(\frac{\partial T}{\partial y} \right)_{y=0} \quad (45)$$

Therefore using equation (41), we have

$$Nu \propto [\theta'(\eta)]_{\eta=0} = -Pr + \varepsilon(A_{11} - A_{12}) + \varepsilon^2\{[B_{41} - Pr B_{40} - (1 + Pr)(B_{39} - B_{35}) + B_{36} - B_{37}(2 + Pr) - B_{38}(Pr + Sc) - A_8 Pr] \quad (46)$$

The local Sherwood number denoted by Sh and defined

as

$$Sh = - \left(\frac{\partial C}{\partial y} \right)_{y=0} \quad (47)$$

Hence from equation (42), we can write

$$Sh \propto [\phi'(\eta)]_{\eta=0} = -A_1 Pr - Sc(1 - A_1) + \varepsilon\{Sc(B_1 + B_2 + B_3 - B_5) - B_6 - Pr(B_3 - B_5) + B_4 - B_1(1 + Pr) - B_2(1 + Sc) + \varepsilon^2\{-B_{122}Sc - (1 + Sc)B_{116} + B_{97} - (1 + Pr)B_{117} + B_{100} - B_{102}(2 + Pr) - B_{103}(2 + Sc) - B_{104}(Pr + Sc) + 2B_{105} Pr + 2B_{106}Sc - B_{118} Pr + B_{119}\} \quad (48)$$

IV. RESULTS AND DISCUSSION

To observe the physical situation of the problem under study, the velocity field, temperature field, concentration field, skin-friction, rate of heat transfer and rate of mass transfer are discussed by assigning numerical values to the parameters encountered into the corresponding equations. To be realistic, the values of Schmidt number (Sc) are chosen for hydrogen ($Sc=0.22$), helium ($Sc=0.30$), water-vapor ($Sc=0.60$), ammonia ($Sc=0.78$), carbon dioxide ($Sc=0.96$) at 25°C and one atmosphere pressure. The values of Prandtl number (Pr) are chosen for air ($Pr=0.71$), ammonia ($Pr=0.90$), carbon dioxide ($Pr=2.2$), water ($Pr=7.0$). Grashof number for heat transfer is chosen to be $Gr=10.0, 15.0, -10.0, -15.0$ and modified Grashof number for mass transfer $Gm=15.0, 20.0, -15.0, -20.0$. The values $Gr>0$ and $Gm>0$ correspond to cooling of the plate while the value $Gr<0$ and $Gm<0$ correspond to heating of the plate.

The values of magnetic parameter ($M=0.0, 0.5, 1.5, 2.0$), suction parameter ($f_w=3.0, 5.0, 7.0, 9.0$), Soret number ($S_0=0.0, 2.0, 4.0, 8.0$) and heat source parameter ($S=0.0, 4.0, 8.0, 12.0$) are chosen arbitrarily.

The velocity profiles for different values of the above parameters are presented from Fig.-1 to Fig.-11. All the velocity profiles are given against η .

In Fig.-1 the velocity distributions are shown for different values of magnetic parameter M in case of cooling of the plate ($Gr>0$). In this figure we observe that the velocity decreases with the increases of magnetic parameter.

The reverse effect is observed in the Fig.-2 in case of heating of the plate ($Gr<0$). The velocity distributions are given for different values of heat source parameter S in case of cooling of the plate in the Fig.-3. From this figure we further observe that velocity decreases with the increases of heat source parameter. The opposite phenomenon is observed in case of heating of the plate in Fig.-4. In Fig.-5 the velocity distributions are depicted for different values of suction parameter f_w in case of cooling of the plate. Here we see that velocity decreases with the increases of suction parameter. The reverse effect is seen in case of heating of the plate in Fig.-6.

The Fig.-7 represents the velocity distributions for different values of Schmidt number Sc in case of cooling of the plate. By this figure it is noticed that the velocity for ammonia ($Sc=0.78$) is less than that of hydrogen ($Sc=0.22$) decreases with the increases of Schmidt number. The reverse effect is obtained in case of heating of the plate in Fig.-8. The Fig.-9 exhibits the velocity distributions for

different values of Soret number S_0 in case of cooling of the plate. Through this figure we conclude that the velocity increases increasing values of Soret number. The opposite phenomenon is seen in case of heating of the plate from Fig.-10.

In Fig.-11 the velocity distributions are presented for different values of M , S , Sc , Pr and f_w in both case of cooling and heating of the plate where $S_0 = 0.0$ and $U_0 = 1.0$.

It is noted that for externally cooled plate (a) an increase in M decreases the velocity field is observed by curves (i) and (ii); (b) an increase in f_w decreases the velocity field observed by curves (i) and (iii); (c) an increase in S decreases the velocity field observed by curves (iii) and (iv); (d) an increase in Sc decreases the velocity field observed by curves (i) and (v); (e) an increase in Pr decreases the velocity field is seen in the curves (i) and (vi); (f) all these effects are observed in reverse order for externally heated plate. All the velocity profiles attain their peak near the surface of the plate and then decrease slowly along y -axis. *i.e.* far away from the plate. It is clear that all the profiles for velocity have the maximum values at $\eta = 1$.

The temperature profiles are displayed from Fig.-12 to Fig.-14 for different values of Pr , S and f_w against η .

We see in the Fig.-12 the temperature distributions for different values of Prandtl number Pr . In this figure we conclude that the temperature decreases with the increases of Prandtl number. This is due to fact that there would be a decrease of thermal boundary layer thickness with the increase of prandtl number. In Fig.-13 displays the temperature distributions for different values of heat source parameter S . In this figure it is clear that the temperature field increases with the increases of heat source parameter.

Fig.-14 is the temperature distributions for different values of Pr , S , f_w for $Gr = 10.0$, $Gm = 15.0$, $M = 0.0$, $S_0 = 0.0$ and $Sc = 0.22$. In this figure it is obtained that an increases in Pr and S decreases the temperature field but an increases in of f_w increases the temperature field.

The profiles for concentration are presented from Fig.-15 to Fig.-17 for different values of S_0 , Sc and f_w .

The Fig.-15 demonstrates the concentration distributions for different values of Soret number. It is noticed that the concentration profile increases with the increases of Soret number. Fig.-16 gives the concentration distributions for different values of suction parameter f_w . We are also noticed that the effects of increasing values of f_w decrease the concentration profile in the flow field. In Fig.-17 the concentration distributions are shown for different values of Sc , S_0 and f_w for $Gr = 10.0$, $Gm = 15.0$, $M = 0.0$, $S = 2.0$ and $Pr = 0.71$. In this figure it is seen that the concentration field increases with the increases of Schmidt number Sc .

The concentration field also increases with the increases of Soret number S_0 . The concentration field decreases with the increases of suction parameter f_w . All the concentration profiles reach to its maximum values near the surface of the vertical plate *i.e.* $\eta = 1$ and then decrease slowly far away the plate *i.e.* as $\eta \rightarrow \infty$

The numerical values of skin-friction (τ) at the plate due to variation in Grashof number (Gr), modified Grashof number (Gm), heat source parameter (S), Soret number (S_0), magnetic parameter (M), Schmit number (Sc), suction parameter (f_w), and Prandtl number (Pr) for externally cooled plate is given in Table-1. It is observed that both the presence of S and S_0 in the fluid flow decrease

the skin-friction in comparison to their absence. The increase of M , Sc and f_w decreases the skin-friction while an increase in Pr , Gr and Gm increase the skin-friction in the absent of S and S_0 .

Table-2 represents the skin-friction for heating of the plate and in this table it is clear that all the reverses phenomena of the Table-1 are happened.

The numerical values of the rate of heat transfer in terms of Nusselt number (Nu) due to variation in Pandlt number (Pr), heat source parameter (S) and suction parameter (f_w) is presented in the Table-3. It is clear that in the absence of heat source parameter the increase in Pr decreases the rate of heat transfer while an increase in f_w increases the rate of heat transfer. In the presence of heat source parameter the increasing values of f_w also increases the rate of heat transfer while an increase in Pr decreases the rate of heat transfer. It is also clear that the rate of heat transfer decreases in presence of S than the absent of S .

Table-4 depicts the numerical values of the rate of mass transfer in terms of Sherwood number (Sh) due to variation in Schmit number (Sc), heat source parameter (S), Soret number (S_0), suction parameter (f_w) and Pandlt number (Pr). An increase in Sc or Pr increases the rate of mass transfer in the presence of S and S_0 while an increase in f_w decreases the rate of mass transfer.

V. FIGURES AND TABLES

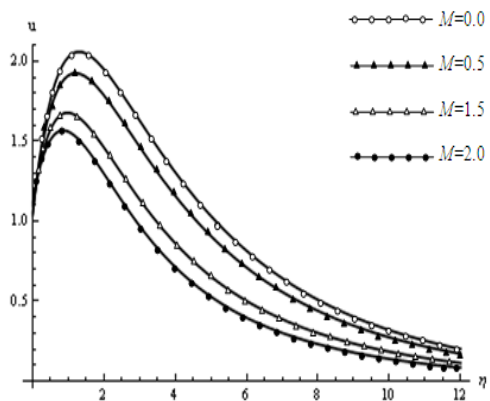


Fig.-1. Velocity profiles when $Gr = 10.0$, $Gm = 15.0$, $S = 0.0$, $S_0 = 0.0$, $Sc = 0.22$, $Pr = 0.71$, $f_w = 5.0$ and $U_0 = 1.0$ against η .

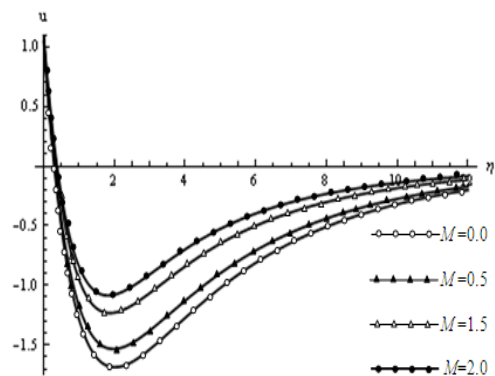


Fig.-2. Velocity profiles when $Gr = -10.0$, $Gm = -15.0$, $S = 0.0$, $S_0 = 0.0$, $Sc = 0.22$, $Pr = 0.71$, $f_w = 5.0$ and $U_0 = 1.0$ against η

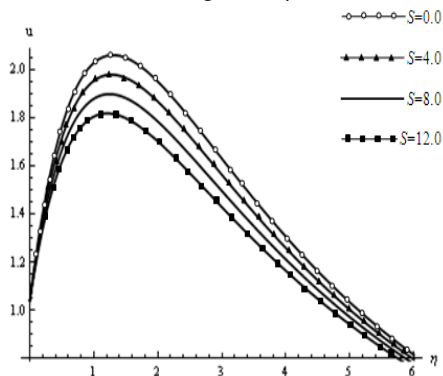


Fig.-3. Velocity profiles when $Gr = 10.0$, $Gm = 15.0$, $M = 0.0$, $S_0 = 0.0$, $Sc = 0.22$, $Pr = 0.71$, $f_w = 5.0$ and $U_0 = 1.0$ against η .

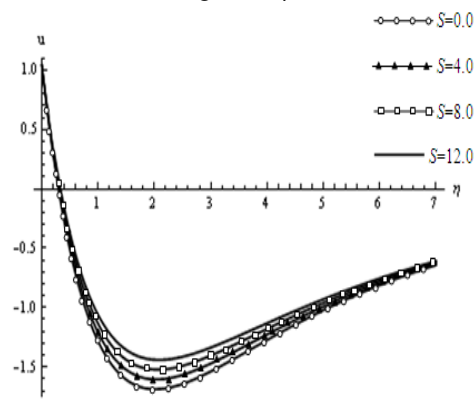


Fig.-4. Velocity profiles when $Gr = -10.0$, $Gm = -15.0$, $M = 0.0$, $S_0 = 0.0$, $f_w = 5.0$, $Sc = 0.22$, $Pr = 0.71$ and $U_0 = 1.0$ against η .

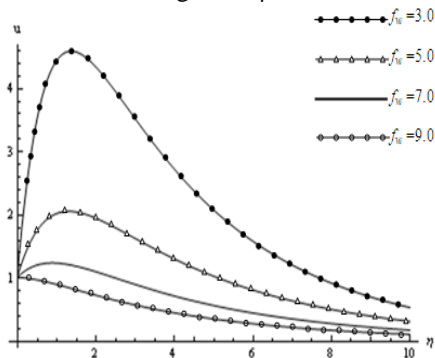


Fig.-5. Velocity profiles when $Gr = 10.0$, $Gm = 15.0$, $M = 0.0$, $S_0 = 0.0$, $S = 0.0$, $Sc = 0.22$, $Pr = 0.71$ and $U_0 = 1.0$ against η .

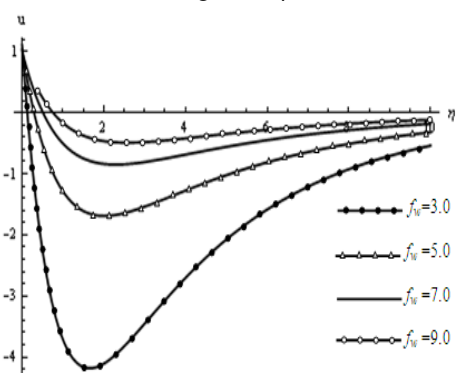


Fig.-6. Velocity profiles when $Gr = -10.0$, $Gm = -15.0$, $M = 0.0$, $S_0 = 0.0$, $S = 0.0$, $Sc = 0.22$, $Pr = 0.71$ and $U_0 = 1.0$ against η .

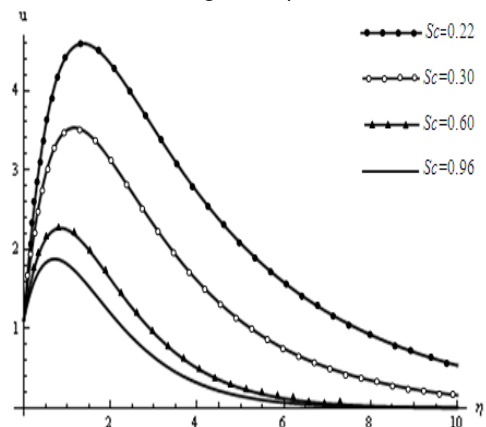


Fig.-7. Velocity profiles when $Gr = 10.0$, $Gm = 15.0$, $M = 0.0$, $S_0 = 0.0$, $S = 0.0$, $f_w = 3.0$, $Pr = 0.71$ and $U_0 = 1.0$ against η .

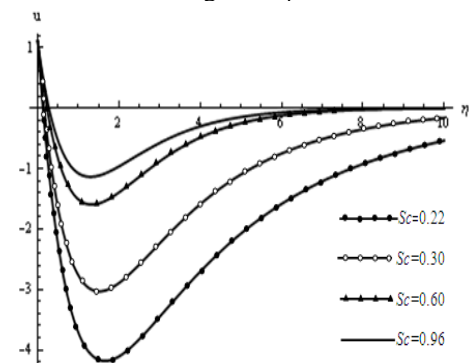


Fig.-8. Velocity profiles when $Gr = -10.0$, $Gm = -15.0$, $M = 0.0$, $S_0 = 0.0$, $S = 0.0$, $f_w = 3.0$, $Pr = 0.71$ and $U_0 = 1.0$ against η .

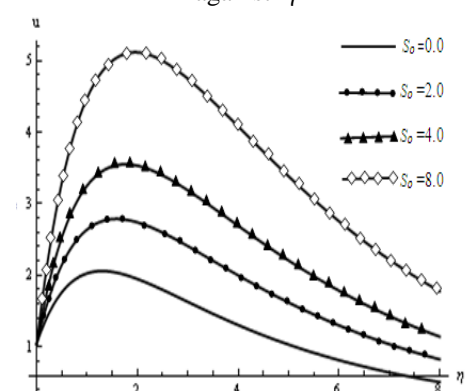


Fig.-9. Velocity profiles when $Gr = 10.0$, $Gm = 15.0$, $M = 0.0$, $S = 0.0$, $Sc = 0.22$, $f_w = 5.0$, $Pr = 0.71$ and $U_0 = 1.0$ against η .

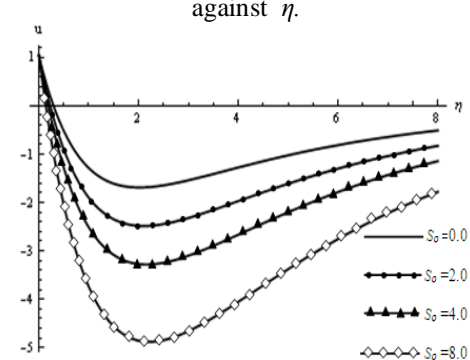


Fig.-10. Velocity profiles when $Gr = -10.0$, $Gm = -15.0$, $M = 0.0$, $S = 0.0$, $f_w = 5.0$, $Sc = 0.22$

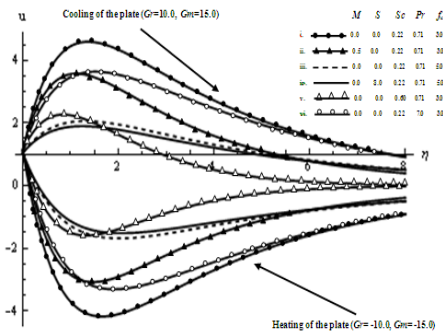


Fig.-11. Velocity profiles for different values of M , S , Sc , Pr and f_w when $S_0 = 0.0$ and $U_0 = 1.0$ in both heating and cooling plate against η .

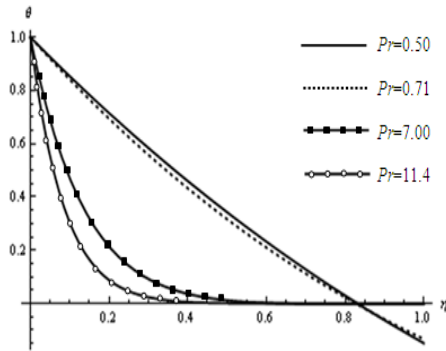


Fig.-12. Temperature profiles when $Gr = 10.0$, $Gm = 15.0$, $M = 0.5$, $S = 1.0$, $S_0 = 4.0$, $Sc = 0.22$ and $f_w = 3.0$ against η .

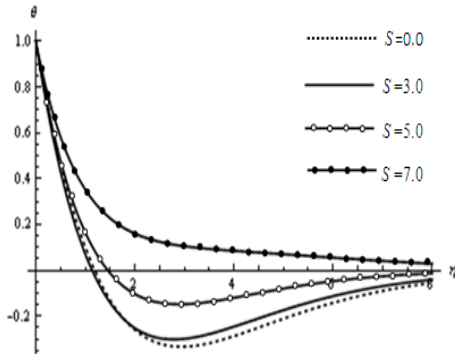


Fig.-13. Temperature profiles when $Gr = 10.0$, $Gm = 15.0$, $M = 0.0$, $S_0 = 1.0$, $Sc = 0.22$, $Pr = 0.71$ and $f_w = 3.0$ against η .

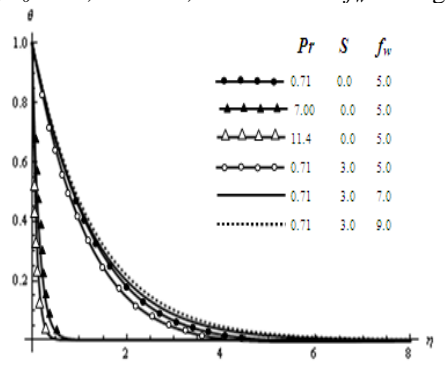


Fig.-14. Temperature profiles when $Gr = 10.0$, $Gm = 15.0$, $M = 0.0$, $S_0 = 0.0$ and $Sc = 0.22$ against η .

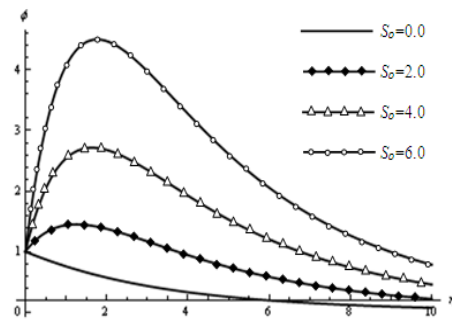


Fig.-15. Concentration profiles when $Gr = 10.0$, $Gm = 15.0$, $S = 0.0$, $M = 0.5$, $Sc = 0.22$, $Pr = 0.71$ and $f_w = 5.0$ against η

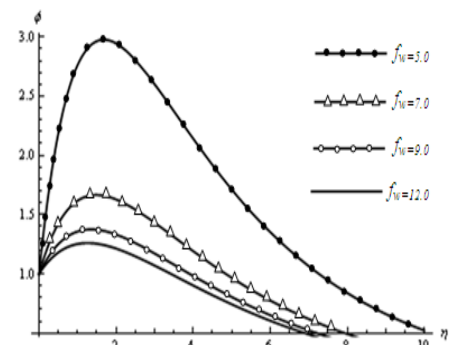


Fig.-16. Concentration profiles when $Gr = 10.0$, $Gm = 15.0$, $S = 4.0$, $M = 0.0$, $S_0 = 4.0$, $Pr = 0.71$ and $Sc = 0.22$ against η

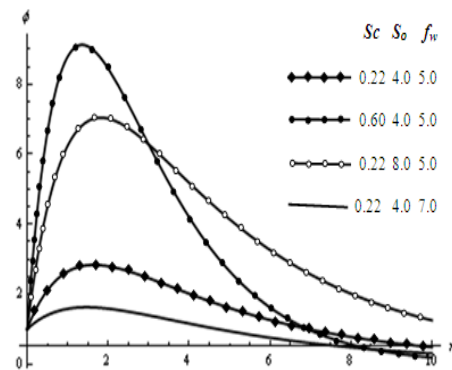


Fig.-17. Concentration profiles for different values of Sc , S_0 and f_w when $Pr = 0.71$, $M = 0.0$ and $S = 2.0$ against η .

Table-1: Numerical values of Skin-Friction (τ) due to cooling of the plate.

S. No	Gr	Gm	S	S_0	M	Sc	f_w	Pr	T
1.	10.0	15.0	0.0	0.0	0.5	0.22	5	0.71	3.9187
2.	15.0	15.0	0.0	0.0	0.5	0.22	5	0.71	4.3051
3.	10.0	20.0	0.0	0.0	0.5	0.22	5	0.71	4.6694
4.	10.0	15.0	4.0	0.0	0.5	0.22	5	0.71	3.7917
5.	10.0	15.0	0.0	2.0	0.5	0.22	5	0.71	4.6313
6.	10.0	15.0	0.0	0.0	2.0	0.22	5	0.71	3.2845
7.	10.0	15.0	0.0	0.0	0.5	0.60	5	0.71	2.5551
8.	10.0	15.0	0.0	0.0	0.5	0.22	7	0.71	2.5571
9.	10.0	15.0	0.0	0.0	0.5	0.22	5	0.90	4.1025

Table-2: Numerical values of Skin-Friction (τ) due to cooling of the plate

S. No.	Gr	Gm	S	S_0	M	Sc	f_w	Pr	τ
1.	-10	-15	0.0	0.0	0.5	0.22	5	0.71	-2.131
2.	-15	-15	0.0	0.0	0.5	0.22	5	0.71	-2.517
3.	-10	-20	0.0	0.0	0.5	0.22	5	0.71	-2.881
4.	-10	-15	4.0	0.0	0.5	0.22	5	0.71	-2.004
5.	-10	-15	0.0	2.0	0.5	0.22	5	0.71	-2.843
6.	-10	-15	0.0	0.0	2.0	0.22	5	0.71	-1.809
7.	-10	-15	0.0	0.0	0.5	0.60	5	0.71	-0.767
8.	-10	-15	0.0	0.0	0.5	0.22	7	0.71	-0.662
9.	-10	-15	0.0	0.0	0.5	0.22	5	0.90	-2.314

Table-3: Numerical values of the Rate of Heat Transfer (Nu)

S.No.	Pr	S	f_w	Nu
1.	0.71	0.0	3	-1.3753
2.	0.71	4.0	3	-1.4886
3.	7.0	0.0	3	-7.2539
4.	7.0	4.0	3	-7.6531
5.	0.71	0.0	5	-0.8068
6.	0.71	4.0	5	-0.9232

Table-4: Numerical values of the Rate of Mass Transfer (Sh)

S. No.	Pr	S	S_0	f_w	Sc	Sh
1.	0.71	0.0	0.0	3	0.22	-0.5214
2.	0.71	4.0	2.0	3	0.22	7.4912
3.	0.71	0.0	2.0	3	0.22	6.5525
4.	0.71	4.0	2.0	3	0.60	111.935
5.	0.71	4.0	2.0	5	0.22	1.0846
6.	7.0	4.0	2.0	3	0.22	662.888
7.	0.71	8.0	4.0	3	0.22	25.3419

VI. CONCLUSION

In the present research work, combined heat and mass transfer effects on MHD free convection flow past a flat plate is presented. The results are given graphically to illustrate the variation of velocity, temperature and concentration with different parameters. Also the skin-friction, Nusselt number and Sherwood number are presented with numerical values for various parameters. In this study, the following conclusions are set out

- (1) In case of cooling of the plate ($Gr > 0$) the velocity decreases with an increase of magnetic parameter, heat source parameter, suction parameter, Schmidt number and Prandtl number. On the other hand, it increases with an increase in Soret number.
- (2) In case of heating of the plate ($Gr < 0$) the velocity increases with an increase in magnetic parameter, heat source parameter, suction parameter, Schmidt number and Prandtl number. On the other hand, it decreases with an increase in Soret number.
- (3) The temperature increase with increase of heat source parameter and suction parameter. And for increase of Prandtl number it is vice versa.
- (4) The concentration increases with an increase of Soret number and Schmidt number. Whereas it decreases with an increase of suction parameter.
- (5) In case of cooling of the plate ($Gr > 0$) the increase of magnetic parameter, Schmidt number and suction

parameter decreases the skin-friction. While an increase of Grashof number, Modified Grashof number and Prandtl number increases the skin-friction. In case of heating of the plate ($Gr < 0$) all the effects are in reverse order.

- (6) The rate of heat transfer or Nusselt number (Nu) increase with the increase of suction parameter while an increase in Prandtl number it decreases. It also decreases in presence of S in comparison to absence of S .

An increase in Schmidt number or Prandtl number increases the rate of mass transfer (Sherwood number) in the presence of heat source parameter and Soret number while an increase in suction parameter f_w decreases the rate of mass transfer. We also see that both the increase in source parameter and Soret number increases the rate of mass

REFERENCES

- [1] M. A. Hossain and A. C. Mandal, Journal of Physics D: Applied Physics, 18, 1985, 163-9
- [2] H. Poonia and R. C. Chaudhary, Theoret. Applied Mechanics, 37 (4), 2010, 263-287
- [3] M. S. Alam and M. M. Rahaman, Int. J. of Science and Technology, II (4), 2006
- [4] P.R. Sharma and G. Singh, Int. J. of Appl. Math and Mech, 4(5), 2008, 1-8
- [5] R. C. Chaudhary and J. Arpita, Roman J. Phy., 52(5-7), 2007, 505-524
- [6] B. P. Reddy and J. A. Rao, Int. J. of Applied Math and Mech. 7(8), 2011, 78-97
- [7] A. K. Singh, A. K. Singh and N.P. Singh, Bulletin of the institute of mathematics academia since, 33(3), 2005
- [8] A. K. Singh, J. Energy Heat Mass Transfer, 22, 2000, 41-46
- [9] B. Gebhart, Heat Transfer. New York: Mc Graw-Hill Book Co., 1971
- [10] B. Gebhart and L. Pera, Ind. J. Heat Mass Transfer, 14, 1971, 2025-2050
- [11] A. A. Raptis and V. M. Soundalgekar, ZAMM, 64, 1984, 127-130
- [12] A. K. Agrawal, B. Kishor and A. Raptis, Warme und Stofubertragung, 24, 1989, 243-250
- [13] B. K. Jha and A. K. Singh, Astrophysics. Space Science, pp. 251-255
- [14] B. K. Jha and R. Prasad, J. Math Physics and Science, 26, 1992, 1-8
- [15] M. D. Abdusattar, Ind. J. Pure Applied Math., 25, 1994, 259-266
- [16] V. M. Soundalgekar, S. N. Ray and U. N Das, Proc. Math. Soc, 11, 1995, 95-98
- [17] M. Acharya, G. C. Das and L. P. Singh, Ind. J. Pure Applied Math., 31, 2000, 1-18
- [18] A. Bejan and K. R. Khair, Int. J. Heat Mass Transfer, 28, 1985, 909-918
- [19] A. K. Singh, J. Energy Heat Mass Transfer, 22, 2000, 41-46
- [20] M. S. Alam and M. M. Rahman, BRACK University J. II (1), 2005, 111-115
- [21] N. P. Shingh, A. K. Shingh and A. K. Shingh, the Arabian J. For Science and Engineering, 32(1), 2007.

Improve C.O.P. Of Ice Making Plant With Out Editing Any Additional System

Sukani Sunny¹, Alpesh Rabadiya², Hareesh Desai³
^{1, 2, 3} Lecturer, Department of Mechanical Engineering, S.T.B.S., Surat

ABSTRACT: Now a day industry owner think only profit point of view, in the thermal orientate industry additional system attached and efficiency of plant increase but capital cost of the instrument high and that's why owner of industry rarely attached the system. In this paper focus on the improvement of C.O.P. without editing other system and increase profit also with the help of preventive maintenance.

KEY WORD: Condenser tube, C.O.P., Amery paper.

NOMENCLATURE

C.O.P. – Co Efficient Of Performance

VCRS – Vapor Compression Refrigeration System

VARs – Vapor Absorption Refrigeration System

CR-Circulation Ratio

I. INTRODUCTION

In this paper focus on the improve C.O.P. of ice making plant without editing any additional system. The Krishna Ice Factory making an ice of 12 tones, to make that ice 48 hours require. This time period is somewhat high than the estimating time, so reduce the time rate of ice making is necessary for the company. If they reduce the time than C.O.P. also increase and profit also increase in some amount. In this company the ice making cycle is VCRS. When heat transfer between an evaporator and the refrigerated area is unusually low (a typical example is by natural convection) and the vapor compression system is on/off regulated, adding a planar PCM to an existing evaporator allows improving the global efficiency [1]. Improve C.O.P. with sub cooling device [2]. The energy consumption of households in the UK is a major factor in the current environmental and strategic supply of energy with some 80% of domestic energy associated with space and hot water heating being provided by electrical radiators or boilers fired with fossil-fuel [3]. The result of this theoretical study show that coefficient of performance (COP) value can be improved by elevating generator temperature up to certain level and lowering absorber temperature. At such elevated generator temperature, value of circulation ratio (CR) is lowered [4]. To overcome green house effect eco friendly refrigerant used ammonia water as a working fluid pair for VARs [5]. The constantly falling temperature over evaporator, refilling of it with more and more liquid refrigerant causes multifold increase in heat transfer coefficient which helps in maintaining refrigeration rate at falling temperature [6].

To be improving C.O.P. mainly three step taken in VARs.

- (i) Temperature of generator T_g be as high as possible.
- (ii) Temperature of condenser T_c be as low as possible.
- (iii) Temperature of evaporator T_e be as high as possible [7].

II. SYSTEM DESCRIPTION

The vapor-compression uses a circulating liquid refrigerant as the medium which absorbs and removes heat from the space to be cooled and subsequently rejects that heat elsewhere. Figure 1 depicts a typical, single-stage vapor-compression system. All such systems have four components: a compressor, a condenser, a thermal expansion valve (also called a throttle valve or Tx Valve), and an evaporator. Circulating refrigerant enters the compressor in the thermodynamic state known as a saturated vapor and is compressed to a higher pressure, resulting in a higher temperature as well. The hot, compressed vapor is then in the thermodynamic state known as a superheated vapor and it is at a temperature and pressure at which it can be condensed with typically available cooling water or cooling air. That hot vapor is routed through a condenser where it is cooled and condensed into a liquid by flowing through a coil or tubes with cool water or cool air flowing across the coil or tubes. This is where the circulating refrigerant rejects heat from the system and the rejected heat is carried away by either the water or the air (whichever may be the case).

The condensed liquid refrigerant, in the thermodynamic state known as a saturated liquid, is next routed through an expansion valve where it undergoes an abrupt reduction in pressure. That pressure reduction results in the adiabatic flash evaporation of a part of the liquid refrigerant. The auto-refrigeration effect of the adiabatic flash evaporation lowers the temperature of the liquid and vapor refrigerant mixture to where it is colder than the temperature of the enclosed space to be refrigerated.

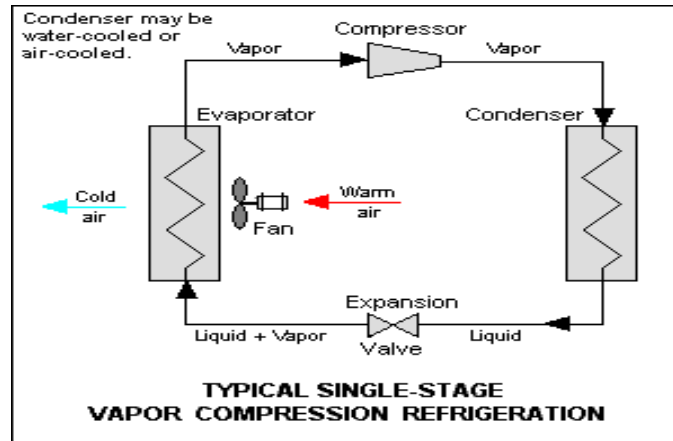


Fig. 1 Schematic diagram of vapor compression refrigeration system

The cold mixture is then routed through the coil or tubes in the evaporator. A fan circulates the warm air in the enclosed space across the coil or tubes carrying the cold refrigerant liquid and vapor mixture. That warm air evaporates the liquid part of the cold refrigerant mixture. At the same time, the circulating air is cooled and thus lowers the temperature of the enclosed space to the desired temperature. The evaporator is where the circulating refrigerant absorbs and removes heat which is subsequently rejected in the condenser and transferred elsewhere by the water or air used in the condenser.

To complete the refrigeration cycle, the refrigerant vapor from the evaporator is again a saturated vapor and is routed back into the compressor.

III. Experimental work

To be improve the C.O.P. of the VCRS the temperature of evaporator decrease or throttling temperature decrease or condensing temperature decrease. For decrease the temperature of condenser cleaning the tube of the it, because the tube of condenser irrigate at the terrace and open in the atmosphere. Due to that tube has been corrosion and erosion from the peripheral surface and result of that heat transfer rate should be change. That reason the condenser temperature should not dropout, during the cleaning work condenser tube clean from algae. Reason of that work heat transfer rate increase and temperature of the tube decrease as compare to the previous days and the result of this work C.O.P. increase and ice cooling rate increase and profit should be also increase.

IV. Calculation



Fig. 2 before removing the corrosion and algae from the condenser tube

Temperature° C	h_f	h_g	S_f	S_g
-6	153.5	1436.8	0.6128	5.4173
38	361.9	1471.5	1.3281	4.8950

$$C.O.P. = \frac{N}{W} = \frac{h_1 - h_4}{h_2 - h_1} = \frac{1297.31 - 361.9}{1471.5 - 1297.31} = \frac{935.41}{174.19} = 5.37$$



Fig. 3 after removing the corrosion and algae from the condenser tube

Temperature° C	h_f	h_g	S_f	S_g
-6	153.5	1436.8	0.6128	5.4173
36.5	354.55	1470.98	1.3047	4.9108

$$C.O.P. = \frac{N}{W} = \frac{h_1 - h_4}{h_2 - h_1} = \frac{1301.5 - 354.55}{1470.98 - 1301.5} = \frac{946.95}{169.48} = 5.59$$

V. Result and discussion

Before the cleaning of condenser tube C.O.P. of the plant is 5.37 and 12 tones is ice making time require 48 hours and selling cost of the ice is 12,000 Rs/-.

After the cleaning of condenser tube C.O.P. of the plant is increase up to 5.59 and due to cleaning 12 tones ice making time decrease up to 46 hours 2hours saving at every 2 days so every 46 days 12,000 Rs/- are net profit which is additional profit of the that time period due to making of 12 tones ice.

VI. Conclusion

Without editing of additional system only maintain the plant and conduct preventive maintenance C.O.P. is increase and maintaining it without edition expenses.

Preventive maintenance conduct routinely and due to that profit is also increase.

References

- [1] K. Azzouz, D. Leducq, J. Guilpart, D Gobin. "Improving the energy efficiency of a vapor compression system using a phase change material". Second Conference on Phase Change Material & Slurry: Scientific Conference & Business Forum, Switzerland. 15 – 17 June 2005.
- [2] R. ROŞCA, I. ŢENU, P. CÂRLESCU, E. RAKOŞI, Gh. MANOLACHE. "ASSESSMENT OF THE SUBCOOLING CAPABILITIES OF A THERMOELECTRIC DEVICE IN A VAPOR COMPRESSION REFRIGERATION SYSTEM". Universitatea de Ştiinţe Agricole şi Medicină Veterinară Iaşi. Vol 51-2008.
- [3] Nguyen Q. MINH, Neil J. HEWITT, Philip C. EAMES. "IMPROVED VAPOUR COMPRESSION REFRIGERATION CYCLES: LITERATURE REVIEW AND THEIR APPLICATION TO HEAT PUMPS". International Refrigeration And Air Conditioning Conference. 2006
- [4] V. Mariappan , M. Udayakumar, Pratisthit Lal Shrestha,S. Suresh. "THERMODYNAMIC ANALYSIS OF R134A – DMAC VAPOR ABSORPTION REFRIGERATION (VAR) SYSTEM". International Journal Of Computational Engineering Research.vol 2- 2012.
- [5] V. R. Renjith, P. J. Joshy. "VAPOUR ABSORPTION REFRIGEATION SYSTEM USING LOW GRADE ENERGY- AN ECOFRIENDLY APPROACH". First international seminar, SAFE'99, On safety & fire engineering. India. Nov 24-26. 1999.
- [6] J.K.Dabas , A.K.Dodeja, Sudhir Kumar, K.S.Kasana. "Performance Characteristics of "Vapour Compression Refrigeration System" Under Real Transient Conditions". International Journal of Advancements in Technology. Vol 2- 2011.
- [7] Dr. D.S. Kumar. "Thermal Science And Engineering". ISBN-81-85749-46-9. 2008

Waveguide to Suspended Stripline Transition Techniques at 94 GHz

Sanjeev Kumar Shah,¹ Vinay Negi,² Sandeep Singh,³ Prachi Raizada,⁴
Dr. U. V. S. Teotia⁵

¹Research Scholar, Shri Venkateshwar University, Gajraula, Uttar Pradesh, India,

^{2,3,4}Uttaranchal Institute of Technology, Dehradun, Uttarakhand, India,

⁵ Shri Venkateshwar University, Gajraula, Uttar Pradesh, India,

Abstract: This paper describes the techniques for waveguide to suspended stripline transition as well as suspended stripline to waveguide transition. These transitions are used to realize crossbar mixers and band pass filters at 94 GHz. Back to back transitions with input/output waveguide WR-10 have been fabricated to measure insertion loss and return loss of the transition. Transitions have been simulated and tested for different orientations of excitation and probe shapes. Agilent's "Advanced Design System" and CST Microwave Studio have been used for simulation of the circuits.

Index Terms: waveguide, Suspended stripline, transition, millimeter wave.

I. INTRODUCTION

Suspended stripline is among the principal transmission media used in upper microwave and lower millimeter wave bands. It consists of a dielectric substrate placed between two ground planes. Efficient SSLIN to waveguide transitions with low insertion loss and good VSWR are required for proper LO feed in case of a mixer and low insertion loss in a band pass filter. SSLIN to waveguide transitions can be realized with different types of techniques as ridge, Van Heuven and probe methods [1] & [2]. Effective dielectric constant of the line can be made close to that of air by selecting sufficiently thin substrate, thus allowing higher frequency of operation in the dominant mode which leads to nearly TEM. Practically entire circuit is placed in rectangular metallic enclosures, which has grooves to suspend the substrate. The inner dimension of the enclosure (called channel dimension) and groove depth are carefully selected to avoid the propagation of undesired modes. The basic difference between various techniques is in the orientation of the mode coupling where the transition is made from Quasi-TEM mode in suspended stripline to dominant TE₁₀ mode in waveguide. Probe type transition is well suited for suspended stripline to waveguide transition.

In this design probe type transition has been used. Fig.1 shows the conversion of TE₁₀ mode in waveguide to TEM mode in suspended stripline.

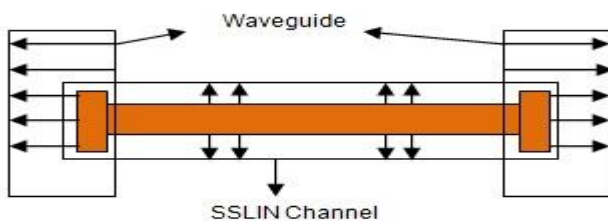


Fig.1. Field configuration of suspended stripline to waveguide transition

The suspended stripline channel cross-section is shown in Fig.2, which is basically a dielectric substrate sandwiched between two ground planes. Channel cross-sectional dimensions are carefully chosen to avoid higher order mode propagation. The cut-off frequency of the suspended stripline for the dominant waveguide mode LSM₁₁ is related to the dimension of the structure and is given by [3].

$$f_c = \frac{c}{2a} \sqrt{1 - \frac{d}{b} \left(\frac{\epsilon_r - 1}{\epsilon_r} \right)} \quad (1)$$

Where a is the width of the channel, b is the height of the channel, d is the thickness of the substrate, ϵ_r is relative dielectric constant and c is the speed of light in a vacuum.

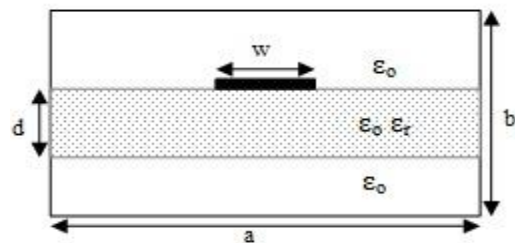


Fig.2. Suspended stripline channel cross-section

The above formula is empirical and not valid for such high frequencies, so actual channel cut off is determined using EM softwares.

The suspended strip line parameters are H_u (upper channel height) = 0.2 mm, H_l (lower channel height) = 0.2 mm, a (Channel width) = 1.27 mm & groove length = 0.1 mm and the channel cut-off frequency calculated from CST microwave studio for 5 mil RT Duroid substrate is 101 GHz for 50-ohm impedance line. The waveguide cross-sectional dimensions are a = 2.54 mm and b = 1.27 mm.

II. SSLIN TO WAVEGUIDE TRANSITION

The suspended stripline to waveguide transition consists of an electric probe inserted into the broad wall of the waveguide. The probe is an extension of a suspended stripline into the waveguide. When a probe is inserted into the waveguide it radiates and in certain position desired mode is excited or vice versa fields set up in the waveguide can be picked up. At one end of waveguide input is given and at other end tuning short is provided to provide optimum matching. Most critical parameters for the transition are probe shape and insertion distance of suspended stripline into the waveguide.

Many types of transitions are simulated to get maximum coupling from waveguide field over a minimum of 20 GHz bandwidth. Optimization of probe shape, probe

depth and position of shorting plane has been carried out with the help CST microwave studio.

Although, analytical formula to calculate width of an impedance line are available in the literature [4], but they are not accurate at such high frequencies. Hence actual simulation of the structure is done and port solution is obtained with EM software to calculate the effective dielectric constant, propagation constant and the characteristic impedance of the transmission line. Four types of transitions have been designed on RT Duroid ($\epsilon_r=2.22$) substrate for 50 ohm transmission line by varying the orientation of excitation and probe shapes. These are shown in Table1. In this paper simulation results for both of them are presented.

TABLE 1

TWO DIFFERENT TYPES OF TRANSITION

Type	Substrate	Excitation	Probe shape
I	5 mil RT Duroid	Top	Rectangular
II	5 mil RT Duroid	Side	Rectangular

III. SIMULATED RESULTS

Both types of transition were simulated and optimized in CST software. 3D view of back to back transition, its simulated S-Parameter results and dimensions for type-I are given in Fig.3,4 & 5 respectively. Fig.6, 7 & 8 represents corresponding parameters for type-II.

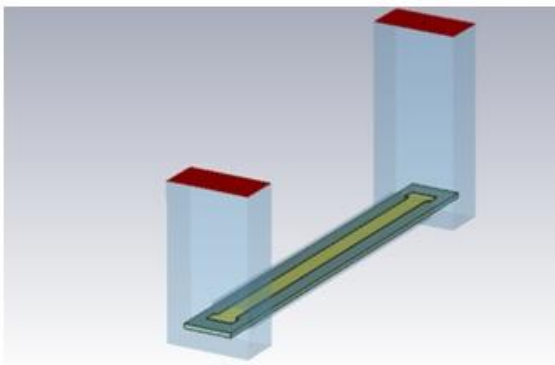


Fig.3. 3D view of transition for type-I

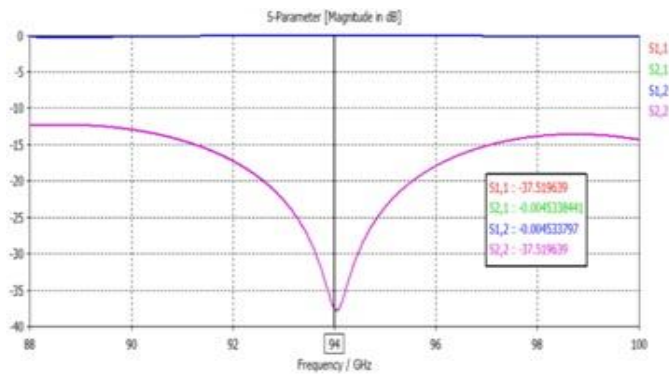


Fig.4. S-Parameter results of transition for type-I

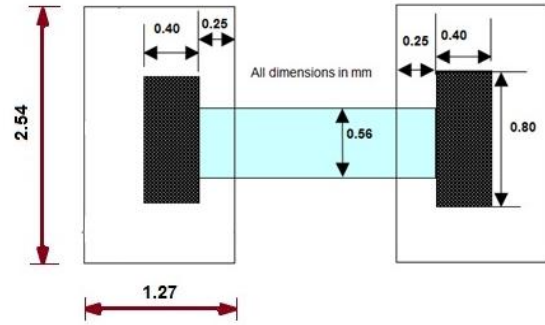


Fig.5. Dimensions of transitions for type-I

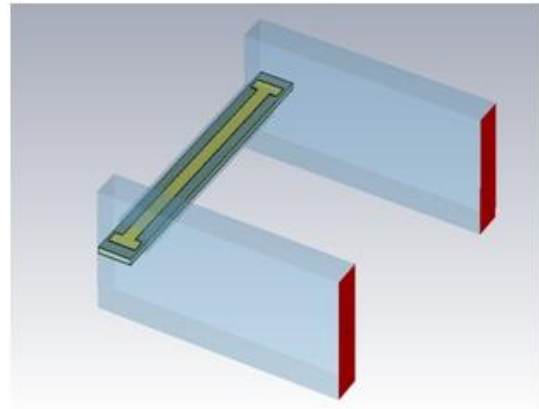


Fig.6. 3D view of transition for type-II

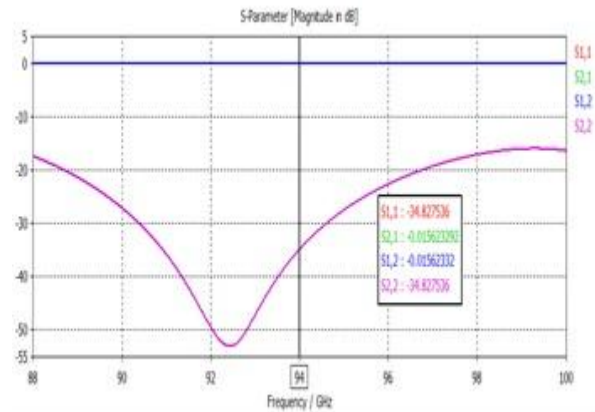


Fig.7. S-Parameter results of transition for type-II

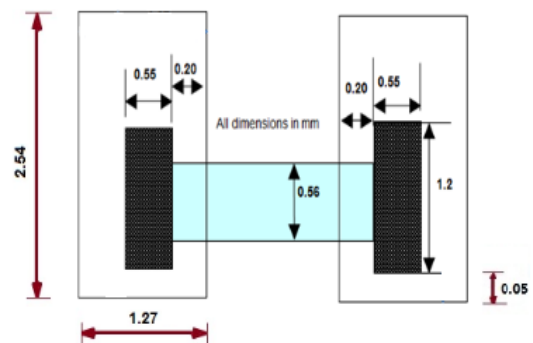


Fig.8. Dimensions of transitions for type-II

IV. CONCLUSION

Two probe type transitions were designed, optimized, fabricated and tested. The best results were achieved with side excitation on RT Duroid substrate using rectangular probe. These transitions have been used to realize band pass filters, couplers and crossbar mixers at 94 GHz.

REFERENCES

- [1] B.Glance and R.Trambarulo "A wavuguide to suspended stripline transition" IEEE MTTs, Feb 1983 Letters, pp 117-118.
- [2] Israel Galin "New Transition Expands Options For SSS Users" Microwave and RF, Jan 1983, pp 72-73
- [3] M.Schneider, "Millimeter-wave Integrated Circuit", IEEE MTT-S Int. Microwave Symp. Digest, pp. 16-18, June 1973.
- [4] A. Lehtovuori and L. Costa, "Model for Shielded Suspended Substrate Microstrip Line", Circuit Theory Laboratory Report Series, No. CT-38, Espoo 1998, 12 pp., ISBN 951-22-4202-8, ISSN 1455-9757.

Cryptanalysis of Signcryption Protocols Based On Elliptic Curve

Sumanjit Das¹, Prasant Kumar Sahoo²

1(Department of Computer Science and Engineering, Centurion University of Technology & Management, India)

2 (Department of Computer Science and Engineering, Subas Institute of Technology, India)

ABSTRACT: The security of data become a major issue in the present days, there are different dimensions of security in this paper we will discuss one of the major properties of security. The signcryption is one of the techniques to secure your data by encrypting it. It was first introduced by Zheng in 1997 based on DLP. The signcryption combines the techniques of digital signature and encryption which reduces computational cost and communication overhead. The Signcryption scheme verifies the integrity of message before decryption of cipher text it also provides how the message can be verify by third party without reading the content of message. Many researchers have given their signcryption scheme to achieve security goals like confidentiality, unforgeability, integrity, forward secrecy and public verification every scheme is having their own limitations. This paper represents the cryptanalysis of popular signcryption scheme in terms of major security goals along with the communication overhead and computational cost.

Keywords: ecc, forward secrecy, public verification, signcryption.

I. INTRODUCTION

The encryption of data and digital signature are two primary cryptographic tools that can guarantee the unforgeability, integrity, and confidentiality of communications. In public key schemes, a traditional method is to digitally sign a message then followed by an encryption algorithm (signature-then-encryption) that can have two problems: Low efficiency and high cost of such summation, and the case that any arbitrary scheme cannot guarantee the security. The signcryption is a relatively new cryptographic technique that is supposed to fulfill the functionalities of digital signature and encryption in a single logical step and can effectively decrease the computational costs and communication overheads in comparison with the traditional signature-then-encryption schemes [1, 2, and 7].

At the time of sending a message to a person over an anxious channel such as internet we must provide confidentiality, integrity, authenticity and non-repudiation [1]. These are the four major security aspects [2] or goals. Before the modern era, cryptography was concerned solely with message confidentiality (i.e., encryption) conversion of messages from a comprehensible form into an incomprehensible one and back again at the other end, rendering it unreadable by interceptors or eavesdroppers without secret knowledge (namely the key needed for decryption of that message). Encryption was used to (attempt to) ensure secrecy in communications, such as those of spies, military leaders, and diplomats. In recent decades, the field has expanded beyond confidentiality concerns to include techniques for message integrity checking, sender/receiver identity authentication, digital signatures, and interactive proofs and secure computation, among others. In ancient times, the use of cryptography was restricted to a small community essentially forms by the military and secret services. The keys were distributed secretly by a courier and the same key is used to encipher and decipher the message. We have a number of encryption algorithms those can be broadly classified into two categories: Symmetric/Private key encipherment and Asymmetric/Public key encipherment [3, 4].

In order to send a confidential letter in a way that it can't be forged, it has been a common practice for the sender of the letter to be sign it, put it in an envelope and then seal it before handing it over to be delivered. Discovering public key cryptography has made communication between people who have never met before over an open and insecure network such as Internet [10], in a secure and authenticated way possible. Before sending a message the sender has to do the following:

1. Sign it using a digital signature scheme (DSS)
2. Encrypt the message and the signature using a private key encryption algorithm under randomly chosen encryption key
3. Encrypt the random message encryption key using receiver's public key
4. Send the message following steps 1 to 3

This approach is known as "Signature-Then-Encryption ". It can be shown in the following Fig-1

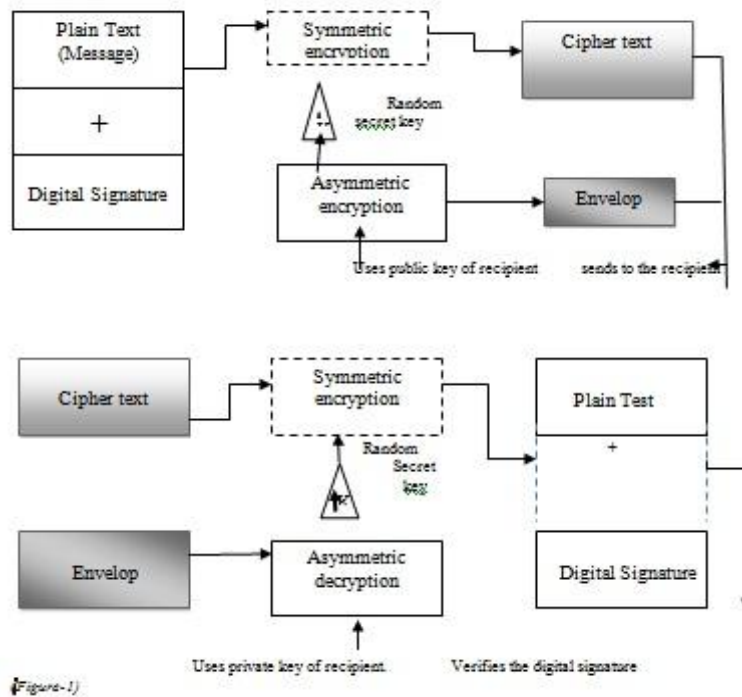


Figure-1)

II. SIGNCRYPTION

In the case of public-key cryptography, confidentiality is provided by encryption schemes, while authenticity is provided by signature schemes. In many applications, both confidentiality and authenticity are needed together. Such applications include secure email (S/MIME), secure shell (SSH), and secure web browsing (HTTPS). Until recently, the de facto solution was to use both an encryption scheme and a signature scheme, typically by sequentially composing the encryption and signature operations. This state of affairs changed in 1997, when Zheng [15] proposed using a single cryptographic primitive to achieve both confidentiality and authenticity. He called this primitive signcryption. At first glance, it is not clear why there should be any advantage to combining both goals into a single primitive. However, Zheng and others have demonstrated, through concrete examples, that signcryption schemes can provide clear benefits over the traditional sequential composition of encryption and signature schemes.

Public Parameter:

C: an elliptic curve of GF (ph), either with $p \geq 2$ 150 and $h=1$ or $p=2$ and $h \geq 150$.

Q: a large prime number whose size is approximately $|ph|$.

G: a point with order q, chosen randomly from the points on C.

Hash: a one-way hash function output of 128 bits at least.

KH: a keyed one-way hash function.

ED: the encryption and decryption algorithm of a private key cipher.

Alice's key:

Va: Alice's private key, chosen uniformly at random from $[1 \dots q-1]$.

Pa: Alice's public key ($Pa=VaG$, a point on C).

Bob's Key:

Vb: Bob's private key, chosen uniformly at random from $[1 \dots q-1]$.

Pb: Bob's public key ($Pb=VbG$, a point on C).

III. SECURITY GOAL

Confidentiality:

Confidentiality is achieved by encryption. To decrypt the cipher text(c), an adversary needs to have Bob's private key. Which is the secret key of Bob and he will never disclose it. Therefore it is unknown to third party.

Unforgeability:

It is computationally infeasible to forge a valid signcrypted text (c, R, s) and claim that it is coming from Alice without having Alice's private key. The private key of Alice is unknown to third party. The computation process of R and s is very difficult and infeasible to guess the solution of signcryption text.

Non-repudiation:

If the sender Alice denies that she sent the signcrypted text (c, R, s) , any third party can run the verification procedure above to check that the message came from Alice.

Public verifiability:

Verification requires knowing only Alice's public key. All public keys are assumed to be available to all system users through a certification authority or published directly. The receiver of the message does not need to engage in a zero-knowledge proof communication with a judge or to provide a proof.

Forward secrecy:

An adversary that obtains Private Key of receiver will not be able to decrypt past messages. Previously recorded values of (c, R, s) that were obtained before the compromise cannot be decrypted because the adversary that has Private Key will need to calculate r to decrypt. Calculating r requires solving the ECDLP on R , which is a computationally difficult.

Encrypted message authentication:

The proposed scheme enables a third party to check the authenticity of the signcrypted text (c, R, s) without having to reveal the plaintext m to the third party. This property enables firewalls on computer networks to filter traffic and forward encrypted messages coming from certain senders without decrypting the message. This provides speed to the filtering process as the firewalls do not need to do full unsigncryption to authenticate senders. It also provides additional confidentiality in settling disputes by allowing any trusted/untrusted judge to verify messages without revealing the sent message m to the judge by running verification process as follows[15,17].

As the signcrypted text computed by the help of Alice's public key P_a and the ID_A can be verify by certificate Authority (CA). Therefore we can say the message is coming from Alice without decrypting the original message and which is authentic sender.

IV. ANALYSIS OF SIGNCRYPTION SCHEME

Comparisons based on securities properties: Table-1 [13, 17]

	Confidentiality	Integrity	Unforgeability	Forward Security	Public verification
Zheng and Imai	Yes	Yes	Yes	No	No
Bao & Deng	Yes	Yes	Yes	No	Yes
Gamage et al	Yes	Yes	Yes	No	Yes
Jung et al.	Yes	Yes	Yes	Yes	No

Computational Complexity:

Elliptic curve point operations are time consuming process. The propose signcryption scheme is having three point multiplication for signcryption, two point multiplication for unsigncryption and one point addition, for verification it requires one point multiplication and one point addition. The table 2 gives the details of comparison with the existing schemes and proposed scheme. [13]

Table 2: comparison of schemes on basis of computational complexity

Schemes	Participant	ECPM	ECPA	Mod. Mul	Mod. Add	Hash
Zheng & Imai	Alice	1	-	1	1	2
	Bob	2	1	2	-	2
Han et al	Alice	2	-	2	1	2
	Bob	3	1	2	-	2
Hwang et al	Alice	2	-	1	1	1
	Bob	3	1	-	-	1

Table 3: comparison based on average computational time of major operation in same secure level the elliptic curve multiplication only needs 83ms & the modular exponential operation takes 220 ms for average computational time in infineon's SLE66CU* 640P security controller.[15]

Schemes	Sender average computational time in ms	Recipient average computational time in ms
Zheng & Imai	1* 83=83	2*83=166
Bao & Deng	2*220=440	3*220=660
Gamage et al	2*220=440	3*220=660

Jung et al	2*220=440	3*220=660
------------	-----------	-----------

V. CONCLUSION

The security of Zheng & Imai, Bao & Deng, Gamage et al, Jung et al and Han et al.'s signcryption scheme [11, 8, 5] are analyzed on basics of security goal, communication overhead and computational cost. All the schemes are satisfying all the properties of security. The signcryption schemes by Bao & Deng and Gamage et al are having public verification but no forward secrecy. Similarly the Zheng & Imai not supports the forward secrecy and public verification [8] where as the Jung et al scheme supports forward secrecy but can't verifiable by public [9, 11, 13]. In terms of computational cost the Zheng & Imai scheme take less time in comparison with Bao & Deng, Gamage et al and Jung et al signcryption schemes [13]. A signcryption scheme can be developed which will provide all the properties of security.

Reference

- [1] Yuliang Zheng. Digital signcryption or how to achieve cost (signature encryption) Cost (signature), Cost (encryption). In CRYPTO '97: Proceedings of the 17th Annual International Cryptology Conference on Advances in Cryptology, pages 165-179, London, UK, 1997. Springer-Verlag.
- [2] William Stallings. Cryptography and Network security: Principles and Practices. Prentice Hall Inc., second edition, 1999.
- [3] Paul C. van Oorschot Alfred J. Menezes and Scott A. Vanstone. Handbook of Applied Cryptography. CRC Press, 1996.
- [4] Behrouz A. Forouzan. Cryptography and Network Security. Tata McGraw-Hill, 2007.
- [5] F. Bao, R.H. Deng, "A signcryption scheme with signature directly verifiable by public key", Proceedings of PKC'98, LNCS 1431, Springer-Verlag, 1998, pp. 55-59.
- [6] LEI Feiyu, CHEN Wen, CHEN Kefei, "A generic solution to realize public verifiability of signcryption", Wuhan University Journal of Natural Sciences, Vol. 11, No. 6, 2006, 1589-1592.
- [7] Mohsen Toorani and Ali Asghar Beheshti Shirazi. Cryptanalysis of an efficient signcryption scheme with forward secrecy based on elliptic curve. Computer and Electrical Engineering, International Conference on, 428-432, 2008.
- [8] Yuliang Zheng and Hideki Imai. How to construct efficient signcryption schemes on elliptic curves. Inf. Process. Lett., 68(5):227-233, 1998.
- [9] Jung.H.Y,K.S Chang, D.H Lee and J.I. Lim, Signcryption scheme with forward secrecy. Proceeding of Information Security Application-WISA, Korea, 403-475, 2001.
- [10] Gamage, C., J.Leiwo, Encrypted message authentication by firewalls. Proceedings of International Workshop on Practice of Theory in Public Key Cryptography, Berlin, 69-81, 1999.
- [11] X. Yang Y. Han and Y. Hu. Signcryption based on elliptic curve and its multi-party schemes. Proceedings of the 3rd ACM International Conference on Information Security (InfoSecu 04), pages 216-217, 2004.
- [12] Henri Cohen and Gerhard Frey, editors. Handbook of elliptic and hyperelliptic curve cryptography. CRC Press, 2005.
- [13] Mohsen Toorani and Ali Asghar Beheshti Shirazi. An elliptic curve-based signcryption scheme with forward secrecy. Journal of Applied Sciences, 9(6):1025 -1035, 2009.
- [14] G. Seroussi. Elliptic curve cryptography. page 41, 1999.
- [15] Hwang Lai Su. An efficient signcryption scheme with forward secrecy based on elliptic curve. Journal of applied mathematics and computation, pages 870-881, 2005.
- [16] Mohsen Toorani and Ali Asghar Beheshti Shirazi. Cryptanalysis of an elliptic curve-based signcryption scheme. International journal of network security vol.10, pp 51-56, 2010.
- [17] Wang Yang and Zhang. Provable secure generalized signcryption. Journal of computers, vol.5, pp 807-814, 2010.

Electrocoagulation: A Novel Waste Water Treatment Method

Satish.I. Chaturvedi

Department of Chemical Engineering, SVM Institute of Technology, Bharuch, Gujarat, India

ABSTRACT: A renewed interest in electrocoagulation has spurred by the search for reliable, cost effective method for the treatment of polluted water. Electrocoagulation present a robust novel and innovative alternative in which a sacrificial metal anode corrodes, due to an applied electric potential, while the simultaneous evolution of hydrogen at the cathode which is removed by flotation. This has the major advantage of providing active cations required for coagulation, without increasing the salinity of the water. Electrocoagulation is a complex process with a multitude of mechanisms operating synergistically to remove the pollutants from the water. Different options exist for key mechanisms and reactor configurations. This paper presents an in-depth discussion and consideration of the factors that are the requirements for the optimum performance of this technology.

Keywords: Chemical process, electrocoagulation, metal removal, physical process, wastewater

I. Introduction

The major challenges for the 21st century are water and energy. Due to increased pollution from point and non-point sources quality of the water become a crucial problem, particular for the Third-World Countries. The promising methods based on electrochemical technology are electrocoagulation, electro flotation [1], electro decantation, and others [1-3].

Electrocoagulation (EC) consists of number of benefits [3]: compatibility, amenability to automation, cost effectiveness, energy efficiency, safety, and versatility. Though EC has received little scientific attention a decade back, in the last couple of years, this technology has been widely used for the treatment of dilute wastewaters having heavy metals [4], foodstuff [5-7], oil wastes [8,9], textile and dyes [10-15], fluorine [16], polymeric wastes [17], organic matter from landfill leachate [18], suspended particles [19-22], chemical and mechanical polishing wastes [23], aqueous suspension of ultrafine particles [24], nitrate [25], phenolic waste [26], arsenic [27], and refractory organic pollutants including lignin and EDTA [28]. Also, electrocoagulation is applicable for drinking water treatment [29, 30]. This process has capability to overcome the disadvantages of the other treatment techniques.

II. Theory of Electrocoagulation

The electrocoagulation process operates on the base of the principle that the cations produced electrolytically from iron and/or aluminum anodes shown in fig (1) which is responsible for the increasing of the coagulation of contaminants from an aqueous medium. Electrophoretic motion tends to concentrate negatively charged particles in the region of the anode and positively charged particles in the region of the cathode. The consumable metal anodes are used to continuously produce polyvalent metal cations in the region of the anode. These cations neutralize the negative charge of the particles moved towards the anodes by production of polyvalent cations from the oxidation of the sacrificial anodes (Fe and Al) and the electrolysis gases like Hydrogen evolved at the anode and oxygen evolved at the cathode. Electrocoagulation is an enigmatic technology. One possible conceptual framework is shown in following fig (3) each foundation area brings to ascertain perspective to electrocoagulation, as represented by each lobe of this Venn diagram. The main aim is to shoe how electrocoagulation's complexity can be simplified by using reductionist approach. Relevant phenomena, characterization methods and tools are mentioning each lobe. Above fig. represents the two removal paths with the relative importance of each being set by a combination of reactor design and operating parameters. Current density represented by a doubled-headed arrow at the base between the flotation and coagulation lobes as it determines both the coagulant dosage and bubble production rates as well as influencing the extent of mixing within a reactor. This process involves three successive stages:

- (i) Formation of coagulants by electrolytic oxidation of the 'sacrificial electrode'
- (ii) Destabilization of the contaminants, particulate suspension and breaking of emulsions
- (iii) Aggregation of the destabilized phase to form flocks.

Destabilization mechanism of contaminants, particulate suspension, and emulsion breaking summarized as follows:

- (i) Due to oxidation of the sacrificial anode, generation and interaction of ions are possible. Compression of the diffuse double layer can be possible around the charged ions.
- (ii) Electrochemical dissolution of the sacrificial anode produced counter ions. These counter ions are responsible for presence of charged neutralization of ionic species which present in the waste water. These counter ions are responsible of the reduction of the electrostatic interparticle repulsion so that van der Waals attraction predominates hence coagulation occurs which approach to the zero net charge.
- (iii) Coagulation causes a flock formation and creates a sludge blanket which entraps and bridge colloidal particles which is present in the still aqueous medium.
- (iv) The negative surfaces of the solid oxides, hydroxides, and oxyhydroxides are responsible for adsorption of contaminated contents.

(v) Due to dissolution of Fe or Al electrodes from the anode respective metal ions are generated. These ions are immediately hydrolyzed into polymeric ions or aluminum hydroxide.

Main function of sacrificial anode is to generating polymeric hydroxides nearby the anode. These polymeric hydroxides are act as a excellent coagulating agents. Due to electrophoretic action negative ions which are produce from the cathode moves towards the anode. Due to combination of the metal cations with these negative particles which turns into the coagulation. Due to electrolysis is continuously carried out, water is electrolyzed. At anode small bubble of oxygen and at the cathode small bubbles of hydrogen are generated which are responsible of electrolysis of water. The flocculated particles attract by these bubbles and these flocculated particles float due to the natural buoyancy towards the surface Physiochemical reaction also occurs in the electrocoagulation cell as follows [31].

- (i) At the cathode metal ions reduction take place.
- (ii) In the waste water impurities are responsible for cathodic reduction.
- (iii) Colloidal particles being generated by electrode erosion.
- (iii) Coagulation and discharge of colloidal particles by electroflotation or sedimentation and filtration.
- (iv) Ions migration done due to electrophoretic in the solution.
- (v) Oxygen and hydrogen bubbles which are produced at anode and cathode,
- (vi) Responsible of electroflotation of coagulated particles.
- (vii) Other chemical and electrochemical process occurs.
- (viii) Electrocoagulation process carried out by an external power supply.

The quantity of electricity passed through is actually responsible for dissolution and deposition of metal ions at the electrodes. A relationship between current density (A/cm^2) and the quantity of the metals (M) dissolved (g of M/cm^2) find out by using Faraday's law:

$$W = i \times t \times M / n \times F, (1)$$

W = the amount of dissolution of electrode (g of M/cm^2)

i = Current density (A/cm^2)

t = time in second

M = Relative molar mass of the electrode

n = no. of electrons in oxidation/reduction reaction

F = Faraday's constant, 96,500 C/mol.

Electrocoagulation operating conditions are mostly dependent on the chemistry of the aqueous medium, mainly conductivity and pH. Also other important characteristics are particle size, type of electrodes, retention time between plate, plate spacing and chemical constituent concentrations. The mainly operating principal is that the cations produced electrolytic from iron and/ or aluminum anodes enhance the coagulation of contaminants from an aqueous medium.

Electrophoretic motion tends to concentrate positively charged ions in the regions of the cathode and negatively charged particles in the region of the anode. The sacrificial metal, anode are used to continuously produced polyvalent metal cations in the in the vicinity of the anode. These cations neutralize the negative charge of the particles carried to the anode by electrophoretic motion, which facilitating coagulation.

Generally, oxidation of organic matter by electrochemical treatment can be classified as direct oxidation at the surface of anode and indirect oxidation from the anode surface which are influenced by the anode material. Oxidation of organic matter depend upon the anode material, concentration of NaCl and current and voltage applied. In addition, electrocoagulation also occurs during electrochemical treatment of waste water. The electrocoagulation mechanism has been proposed for the production of $Fe(OH)_3$ or $Fe(OH)_2$.

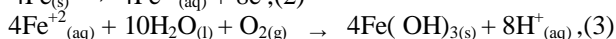
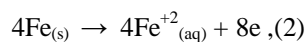
III. Reaction Mechanism

Electrocoagulation is a complex process occurring via series steps. When current is passed through electrochemical reactor, it must overcome the equilibrium potential difference, anode over potential, cathode over potential and potential drop of the solution. The anode over potential includes the activation over potential and concentration potential, as well as the possible passive over potential resulted from the passive film at the anode surface, while the cathode over potential is principally composed of the activation over potential and concentration over potential. Reactions at electrode surfaces, formation of coagulants in aqueous phase, adsorption of soluble or colloidal pollutants on coagulants shown in fig. (2).

Generally, aluminum and iron are used as an electrode material in the electrocoagulation process. In the iron electrode, two mechanisms have been proposed [32-39].

Mechanism 1:

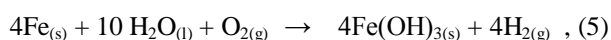
Anode:



Cathode:

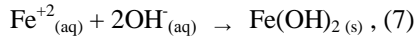
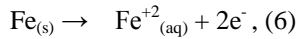


Overall:



Mechanism 2:

Anode:



Cathode:



Overall:

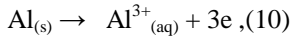


Due to oxidation in an electrolyte system, iron produces form of monomeric ions, $\text{Fe}(\text{OH})_3$ and polymeric hydroxy complex such as:

$\text{Fe}(\text{H}_2\text{O})_6^{3+}$, $\text{Fe}(\text{H}_2\text{O})_5^{2+}$, $\text{Fe}(\text{H}_2\text{O})_4(\text{OH})_2^{+}$, $\text{Fe}(\text{H}_2\text{O})_8(\text{OH})_2^{4+}$ and $\text{Fe}_2(\text{H}_2\text{O})_6(\text{OH})_4^{4+}$ depending upon the pH of the aqueous medium.

In the case of Aluminum electrode, reactions are as follows:

Anode:



Cathode:



For the aluminum electrodes, $\text{Al}^{3+}_{(aq)}$ ions will immediately undergo further spontaneous reaction to generate corresponding hydroxides and polyhydroxides. Due to hydrolysis of Al^{3+} , $\text{Al}(\text{H}_2\text{O})_6^{3+}$, $\text{Al}(\text{H}_2\text{O})_5\text{OH}_2^{+}$, $\text{Al}(\text{H}_2\text{O})(\text{OH})_2^{2+}$ generated. This hydrolysis products produced many monomeric and polymeric substance such as, $\text{Al}(\text{OH})^{2+}$, $\text{Al}(\text{OH})^{2+}$, $\text{Al}_2(\text{OH})_2^{4+}$, $\text{Al}(\text{OH})_4^{+}$, $\text{Al}_6(\text{OH})_{15}^{3+}$, $\text{Al}_7(\text{OH})_{17}^{4+}$, $\text{Al}_8(\text{OH})_{20}^{4+}$, $\text{Al}_{13}\text{O}_4(\text{OH})_{24}^{7+}$, $\text{Al}_{13}(\text{OH})_{34}^{5+}$ [38].

Within the electrocoagulation reactor, several distinct electrochemical reactions are produced independently. These reactions are as follows:

- (i) Seeding: This is resulting from the anode reduction of metal anions that becomes very centers for larger, stable, insoluble complexes that precipitate as complex metal ions.
- (ii) Emulsion breaking: Due to the oxygen and hydrogen ions that bond into the water receptor sites of oil molecules creating a water in soluble complex separating water from oil, mud, dyes inks, etc.
- (iii) Halogen complexing: As the metal ions bind into a chlorinated hydrocarbon molecules resulting in a large insoluble complexes separating water from pesticides, herbicides, chlorinated PCB's, etc.
- (iv) Bleaching: As the oxygen ions produced in the reaction chamber oxidizes dyes, cyanides, bacteria, viruses, biohazards. Electron flooding of the water eliminates the polar effect of the water complex, allowing colloidal materials to precipitates and increase of electrons creates an osmotic pressure that raptures bacteria, cysts and viruses.
- (v) Oxidation reduction: These reactions are forced to their natural end point within the reaction tank which seeds up the natural process of nature that occurs in wet chemistry.
- (vi) Electrocoagulation induced pH: This is swings toward the neutral.

IV. Comparison of Different Processes

Electrocoagulation is most efficient method with less effected disadvantages. Data in Table no. (1) [43 -56] Indicated the efficiency of electrocoagulation compare to other process.

V. Advantages

- (i) EC requires simple equipment and is easy to operate.
- (ii) EC requires low initial investment with low operating cost.
- (iii) The electrolytic processes in the EC cell are controlled electrically and with no moving thus requiring less maintenance.
- (iv) EC does not require any chemicals. So there is no problem of neutralizing excess chemicals and no possibility of secondary pollution caused by chemical substances..
- (v) EC composed of mainly metallic oxides/hydroxides. Sludge formed by EC tends to be readily settable and easy to de-water, so low sludge generation can be done.
- (vi) EC flock tends to be much larger, contains less bound water, is acid-resistant and more stable, and therefore, can be separated faster by filtration.
- (vii) EC produces effluent with less total dissolved solids (TDS) content as compared with chemical treatments. If this water is reused, the low TDS level contributes to a lower water recovery cost.
- (viii) The EC process has the advantage of removing the smallest colloidal particles, because the applied electric field sets them in faster motion, thereby facilitating the coagulation.
- (ix) The gas bubbles produced during electrolysis can carry the pollutant to the top of the solution where it can be more easily concentrated, collected and removed.
- (x) After treatment EC gives palatable, clear, colorless odorless water with zero discharge.
- (xi) EC handles large variation in the waste streams with multiple contaminants.

(xii) The EC technique can be easily used in rural areas where electricity is not available, since a solar panel attached which may be sufficient to carry out the process.

VI. Disadvantages

- 1) In some EC systems, an impermeable formation of oxides film form on the cathode, so efficiency of electrocoagulation cell.
- 2) High conductivity of the waste water suspension is required.
- 3) Gelatinous hydroxide may tend to solubilised in some cases.
- 4) Due to oxidation, sacrificial anode dissolved in the waste water, so need to be regularly replaced.
- 5) The use of electricity may be expensive in some cases.

VII. Recent Improvements

The EC phenomenon has been known as an electrochemical technique for the last century. It has been used with varying degrees of success for treatment of water and wastewater obtained from various sources. In the treatment of wastewater by a hybrid electrocoagulation–flotation technique [41] by Al electrodes, different EC reactors to evaluate their water treatment performance and found out the best configurations to maximize the treatment efficiency. The EC reactors were configured with water up-flow or cross-flow arrangements. The bipolar electrodes were connected in series via the water, and the monopolar electrodes connected in parallel via copper connectors. The current efficiency (Φ) required for the production of dissolved Al^{3+} due to the passage of electrical charge Q (C) in a volume V (m^3) of water was calculated using Faraday's law:

$$\Phi = 3 \times F \times V / Q, (11)$$

Where F is the Faraday constant.

The specific electrical energy consumption (SEEC) was calculated as a function of the applied cell voltage (U):

$$SEEC[kWh (kg Al^{3+})^{-1}] = nFU/3.6 \times 10^3 M_{Al} \Phi, (12)$$

Where n is the number of moles of electrons per mole of the aluminum dissolved.

It was concluded that an up-flow configuration of the electro coagulator performed better than a horizontal flow configuration, with both bipolar and monopolar electrodes. Also, the performance of the EC process was found to be superior to that of conventional chemical coagulation with aluminum sulphate. As per [40], low frequency (25–75 Hz) sonic field at current densities of 0.1–0.4 $A m^{-2}$ to improve the performance of the EC cell with carbon steel electrodes. During this increase the quantity of iron hydroxides, and thereby enhance coagulation. It was assumed that the applied sonic field enhanced the rates of mass transport. Decreased the thickness of the diffuse double layer at the electrode surface. Activated the electrode surface by generating defects at the crystal lattices of the electrodes. Activated the ions in the reaction zone at the electrodes by ultra-sound waves. Increased the temperature at the electrode surface due to friction between the liquid and the surfaces.

However, disadvantages take place after applying the sonic field. Among other things the acoustic waves may destroy part of the colloidal iron hydroxides as well as the adsorption layer at the surface of the colloidal particles. One of the most important considerations in lowering the cost of the EC process is to minimize the IR-drop to enhance current efficiency. Evolution of oxygen at the anode represents an unwanted leakage of current, which reduces the overall current efficiency. This problem can be minimized through the choice of an anodic material that presents a high over potential for the oxygen evolution reaction near the anode. This high over potential permits the realization of anodic reactions, which are not possible with other materials and in particular, the oxidation of organic compounds with a very high current efficiency.

To achieve this goal, a number different configuration have used binary [41,42] & ternary alloys as well as carbon electrodes and titanium sheets coated with certain active oxides as anodes for electrochemical treatment of wastewater, in particular those containing organic dyes, phenols, chloro-substituted phenols, and tannery wastes. As per configuration of [48] the electrocoagulation of aqueous suspensions of ultrafine kaolin particles in a single stirred cell apparatus and in a continuously flowing system consisting of three cells in series. The coagulation rate was described by a second-order rate equation:

$$dc/dt = -k_1 c^2 (1 - e^{-k_2 t})^2, (13)$$

Where c is the concentration at time t ,

u the electrophoretic velocity of the particles,

$k_2 = u/x$ (x being the geometric parameter of the electrode size),

$k_1 = 4kT/3\mu$ (k is the Boltzmann's constant),

μ = the viscosity of the continuous medium.

This second-order rate equation incorporates the electrophoretic migration of particles, and subsequent release of discharged particles into the bulk. The constant terms in this equation were derived from the basic electrophoretic and coagulation phenomenon, which is dependent on the zeta potential of the suspended particles, the applied voltage, the initial concentration of the particles and the electrode geometry.

In the number of EC experiments with ultrafine kaolin particles in a single stirred cell with electrodes in parallel connections found reasonably similarity with the theoretically in a theoretical model involving the electrolysis voltage required in an EC process, the current density, conductivity of the water/wastewater, the interelectrode distance, and the surface of the electrodes. Experiments were carried out with aluminum electrodes to verify and confirm the theoretical model

and determine the constant terms used in the model. Two mathematical models, one applicable to non-passivated aluminum electrode and the other to passivated aluminum electrodes were proposed and experimentally verified.

The theoretical model is based on the fact that when current passes through the electrochemical reactor, it must overcome the equilibrium potential difference, anode over potential, cathode over potential and IR-drop of the solution. The electrolysis voltage U_0 (V) between electrodes may, therefore, be considered to consist of the following terms:

$$U_0 = E_{eq} + \eta_{a,a} + \eta_{a,c} + \eta_{a,p} + |\eta_{c,a}| + |\eta_{c,c}| + dkj, \quad (14)$$

where

E_{eq} = the equilibrium potential difference between the electrodes,

$\eta_{a,a}$ = the activation over potential at the anode,

$\eta_{a,c}$ = the concentration over potential at the anode,

$\eta_{a,p}$ = passive over potential at the anode,

$\eta_{a,a}$ = activation over potential,

$|\eta_{c,a}|$ = activation over potential at the cathode,

$|\eta_{c,c}|$ = concentration over potential at the cathode,

j = current density (A/m^2),

d = net distance between the electrodes (m),

κ = conductivity of the wastewater,

The oxidation at the anode, reduction at the cathode and hydrolysis reaction in the medium to be considered to evaluate different potential terms by using Tafel equation and Nernst-Planck equation and finally propose the following mathematical relationships for calculations of U_0 values:

$$U_0 = A + \eta_{a,p} + dkj + K_1 \ln j, \quad (15)$$

Where

U_0 = potential,

A and K_1 = constant terms,

J = current density (Am^{-2}),

D = net distance between the electrodes (m),

$\eta_{a,p}$ = anode passive potential (V)

κ = conductivity of the wastewater for a non-passivated electrode, the passive over potential can be neglected. For a passivated electrode the relationship can be rearranged to

$$U_0 = A + dkj + K_1 \ln j + K_2 j n \kappa m, \quad (16)$$

Where

K_2 = constant term.

A , K_1 , K_2 , m and n need to be experimentally determined.

Hybrid process:

Sometimes it becomes necessary to use two or more methods of treatment, i.e. hybrid processes, to ensure efficient treatment of wastewater. The EC technology can be designed into water treatment systems to include membrane separation, reverse osmosis, electro filtration, sludge dewatering, thermo-oxidation and other conventional technologies to enhance the recovery of fine particles and metal ions from wastewater. Removal of coloring materials from dyestuffs using EC with electroflotation has been done by have reported the uses of EC with dissolved air flotation (DAF) for treatments of urban wastewater. Continuous treatment of textile wastewater by combining electrochemical oxidation, coagulation and activated sludge has been mentioned by [58]. EC also been used in conjunction with filtration to remove silica and suspended solids that tend to foul reverse osmosis membranes [57,58].

VIII. Conclusion

Without doubt the provision of an adequate water supply suitable for a diversity of uses by world's growing population is one of the 21st century more pressing challenges. Even in the developed countries, the use of large scale, continuous throughput waste treatment plant is not complete solution. Electrocoagulation has successfully treated a wide range of polluted waste water. But the full potential of EC techniques as a waste water treatment is not yet to be fully realized due to following deficiencies in a number of following key areas:

- It is still an empirically optimized process that requires more fundamental knowledge for engineering design.
- No dominant reactor design exists, adequate scale-up parameters have not been defined, material of construction are varied.
- No widely applicable mechanistically based approach to the mathematical modeling of electrocoagulation reactors.
- Failure to fully appreciate that the performance of an electrocoagulation reactor is largely determined by the interaction that occur between the three foundation technologies of electrochemistry, coagulation and flotation.
- No generic solution to the problem of electrode passivation.

After all electrocoagulation has been used successfully to treat a wide range of polluted wastewaters. But the full potential of EC technique as a wastewater treatment is yet to be fully realized. It is still an empirically optimized process that requires more fundamental knowledge for engineering design. No dominant reactor design exists, adequate scale-up parameters have not been defined, and materials of construction are varied. This technology has excellent future because of numerous advantages and the nature of the changing strategic water needs in the world.

References

- [1] K. Rajeshwar, J.G. Ibanez, and G.M. Swain, *J. Appl. Electrochem.*, 24, 1994, 1077.
- [2] M.Y.A. Mollah, R. Schennach, J.R. Parga, and D.L. Cocke, *J. Hazard. Mater.* 84, 2001, 29.
- [3] M.Y.A. Mollah, P. Morkovsky, J.A.G. Gomes, M. Kesmez, J. Parga, and D.L. Cocke, *J. Hazard. Mater.* 114, 2004, 199.
- [4] V.L. Pogrebnaya, A.A. Klimenko, T.N. Bokovikova, E.P. Tsymbal, and N.P. Pronina, *Chem. Petrol. Eng.*, 31, 1995, 280.
- [5] Z.V.P. Murthy, C. Nancy, and A. Kant, *Sep. Sci. Technol.*, 42, 2007, 819.
- [6] X. Chen, G. Chen, and P.L. Yue, *Sep. Purif. Technol.*, 19, 2000, 65.
- [7] E.C. Beck, A.P. Giannini, and E.R. Ramirez, *Food Technol.*, 22, 1974, 18.
- [8] J. Lawrence, and L. Knieper, *Ind. Wastewater*, 1–2, 2000, 20.
- [9] N. Biswas, and G. Lazarescu, *Int. J. Environ. Stud.*, 38, 1991, 65.
- [10] P.stamberger, *J. Colloid Interface*, 1, 1946, 93.
- [11] J.S. Do, and M.L. Chen, *J. Appl. Electrochem.*, 24, 1994, 785.
- [12] J.G. Ibanez, M.M. Singh, and Z. Szafran, *J. Chem. Edu.*, 75, 1998,1040.
- [13] G. Vlyssides, M. Loizidou, P.K. Karlis, and A.A. Zorpas, *J. Hazard. Mater.* 70, 1999, 41.
- [14] G.M. Yalcin, and C. Dogcar, *Waste Manage.*, 22, 2002, 491.
- [15] Y. Xiong, P.J. Strunk, H. Xia, X. Zhu, and H.T. Karlsson, *Water Res.*, 35, 2001, 4226.
- [16] N. Mameri, A.R. Yeddou, H. Lounici, D. Belhocine, H. Grib, and B. Bariou, *Water Res.*, 32,,1998, 1604.
- [17] M. Panizza, C. Bocca, and G. Cerisola, *Water Res.*, 34, 2000, 2601.
- [18] T. Tsai, S.T. Lin, and Y.C. Shue, and P.L. Su, *Water Res.*, 31, 1997, 3073.
- [19] J.C. Donnini, J. Kan, T.A. Hassan, K.L. Kar, and *Can. J. Chem. Eng.*, 72, 1994, 667.
- [20] N.S. Abuzaid, A.A. Bukhari, and Z.M. Al-Hamouz, *Adv. Environ. Res.*, 6, 2002, 325.
- [21] R.R. Renk, *Energy Prog.*, 8, 1988, 205.
- [22] J. Szykarczuk, J. Kan, T.A. Hassan, and J.C. Donnini, *Clays Clay Miner.*, 42, 1994, 667.
- [23] M. Belongia, P.D. Harworth, J.C. Baygents, and S. Raghavan, *J. Electrochem. Soc.*, 146, 1999, 4124.
- [24] M.J. Matteson, R.L. Dobson, R.W. Glenn Jr., N.S. Kukunoor, H. Waits III, and E.R. Clayfield, *Colloid Surface, A*: 104, 1995, 101.
- [25] S. Koparal, and U.B. Ogutveren, *J. Hazard. Mater.* 89, 2002, 83.
- [26] W. Phutdhawong, S. Chowwanapoonpohn, and D. Buddhasukh, *Anal. Sci.*, 16, 2000, 1083.
- [27] N. Balasubramanian, and K. Madhavan, *Chem. Eng. Technol.*, 24, 2001, 855.
- [28] L.C. Chiang, J.E. Chang, and S.C. Tseng, *Water Sci. Technol.*, 36, 997, 123.
- [29] M.F. Pouet, and A. Grasmick, *Water Sci. Technol.* 31, 1995, 275.
- [30] G. Chen, *Sep. Purif. Technol.*, 38, 2004, 11.
- [31] M.F. Pouet, and A. Grasmick, *Water Sci. Technol.*, 31, 1995, 275.
- [32] A. Gurses, M. Yalcin, and C. Dogan, *Waste Manag.*, 22, 2002, 491.
- [33] M. Kobya, O.T. Can, and M. Bayramoglu, *J. Hazard. Mater.* 100, 2003, 163.
- [34] O.T. Can, M. Bayramoglu, and M. Kobya, *Ind. Eng. Chem. Res.*, 42, 2003, 3391.
- [35] N. Daneshvar, H. AshassSorkhabi, and A. Tizpar, *Separ. Purif. Technol.*, 31, 2003, 177.
- [36] O. Larue, E. Vorobiev, C. Vu, and B. Durand, *Separ. Purif. Technol.*, 31, 2003, 177.
- [37] O.Y. Pykhteev, A.A. Ofimov, L.N. Moskvina, and Russ. *J. Appl.Chem.*, 72, 1999, 9.
- [38] P.N. Johnson, and A. Amirtharajah, *J. AWWA*, 5, 1983, 232.
- [39] M. Rebhun, and M. Lurie, *Water Sci. Technol.*, 27, 1993, 1.
- [41] V.K. Kovatchva and M.D. Parlapanski, *Sono-electrocoagulation of iron hydroxides. Colloids Surf.* 149, 1999, 603–608.
- [42] Chen, G. Chen and P.L. Yue, *Anodic oxidation of dyes at novel Ti/B-diamond electrode. Chem Eng. Sci.* 58, 2003, 995–1001.
- [43] F. Li, S. Li, C. Zhang and H. Zhao, *Application of corrosive cell process in treatment of Printing and dyeing wastewater. Chem. Eng. Environ. Protect.* 15, 1995, 157–161.
- [44] Safia Moosvi, and Datta Madamwar, *Bioresource technology*, Volume 98(17), 2007, 3384-3392.
- [45] Deepak Pant, and Alok Adholeya, *Bioresource Technology*, Volume 98 (12), 2007, 2321-2334.
- [46] Samia M. Helmy, Shadia EI Rafie, and Moataser Y. Ghaly, *Desalination*, 158(1-3), 2003, 331-339.
- [47] Sanna Kotrappanavar Natraj, Kallapa M. Hosamani, and Tejrjaj M. Aminabhavi, *Water Research*, 40 (12), 2006, 349-356
- [48] Nathalie Meunier, Patrick Drogui, Camille Montane, Guy Mercier, and Jean Francois Blairs. *Jour.of Hazr. Matr.*, 137(1), 2006, 581-590.
- [49] R.P. Van Hille, G.A. Boshoff, P.D. Rose, and J.R. Duncan. *Resources, Conservation and Recycling.* 27 (1-2), 1999. 157 -167.
- [50] Samia M. Helmy, Shadia EI Rafie, Moataser and Y. Ghaly. *Desalination*, 158 (1-3), 2003, 331-339.
- [51] Ero Pehlivan, and Turkan Altum, *Jour. of Hazr. Matr.*, 140(1-2),, 2007, 299-307.
- [52] Naffa Adhoum, L. Monser, N. Bellakhal, and Jamel-Eddine Belgaied. *J. Hazard. Matr.* B112, 2004, 207-213
- [53] Ana M. Elicehe, Sergio M. Corvalm, and Inmaculada Ortiz, *Computers and Chem. Engg.*, 29 (6), 2005, 1483-1490.
- [54] S. Song, A. Lopez – Valdivieso, D.J. Hernandez Campos, C. Peng, M.G. Monroy – Fernandez, and I. Razo – Soto. *Water Research.* 40 (2), 2006, 364 – 372.
- [55] Jewel A.G. Gomes, Praveen Daida, Mehmet Kesmez, Michael Weir, Hector Moreno, Jose R. Parga, George Irwin, Hylton McWhinney, Tony Grady, and Eric Peterson David L. Cocke. *J. Hazard. Matr.* 139(2), 2007, 220-231.
- [56] Jose R. Parga, David L. Cocke, Jesus L. Valenzuela, Jewel A. Gomes, Mehmet Kesmez, George Irwin, Hector Moreno, and Michael Weir. *Jour. of Hazr. Matr.* 124[1-3], 2005, 247-254.
- [57] M.F. Pouet, and A. Grasmick, *Filtr. Sep.*, 31, 1994, 269.
- [58] M.F. Pouet, F. Persin, and M. Rumeau, *Water Sci. Tech.*, 25 (12), 1992, 247.

Figures and Tables

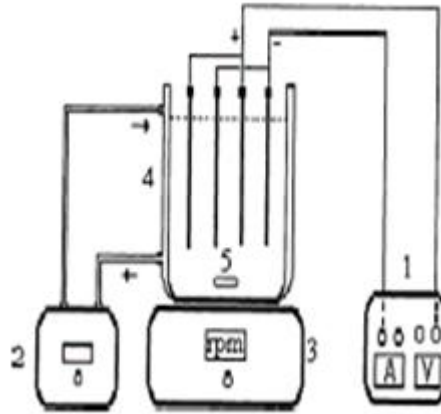
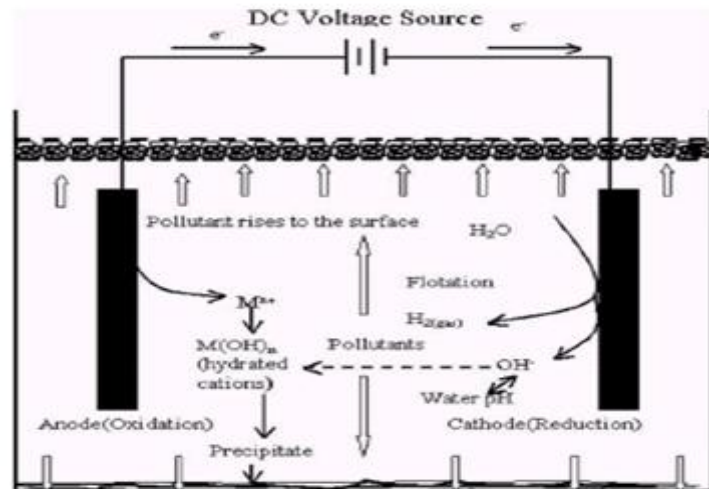
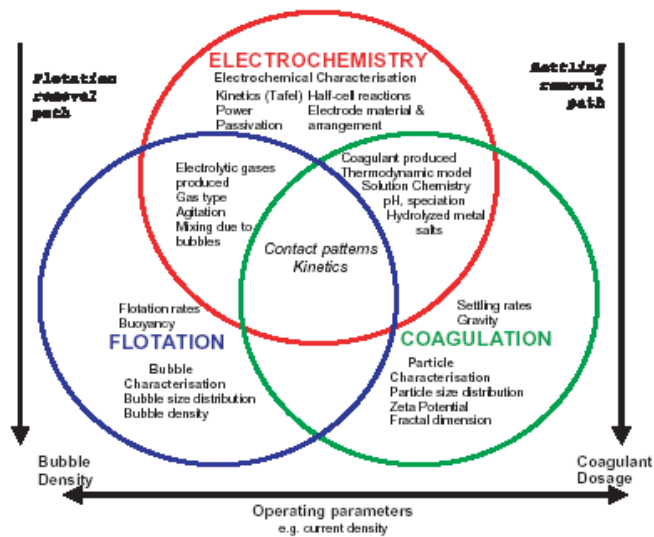


Fig. (1) Schematic diagram of experimental set-up”

- 1. Digital D.C Power Supply
- 2. Water circulator
- 3. Digital Magnetic Stirrer
- 4. Electrochemical Cell
- 5. Magnetic Bar Stirrer



“Fig.(2) Schematic diagram of bench-scale two-electrode electrocoagulation cell”



“Fig. (3) Conceptual framework for electrocoagulation as synthetic technology”

TABLE (1) Comparison data of different process

<i>Parameters</i>	<i>Chem. Coag.</i>	<i>Bio logical</i>	<i>Physico-chemical</i>	<i>Membrane & Ion exchange</i>	<i>Electro coagulation</i>	<i>References</i>
Color	89	100	77-100 Coag+Phent o oxidation	99.8 Membrane	100	43 - 47
COD	94	90 - 96	80-100 Coag+Phent o oxidation	99.9 Membrane	87.3 - 87.7	44 - 47
Pb	>99.8	95	> 80 Coag+Phent o oxidation	95 Ion exchange	98.8 ± 1.3	48 - 51
Cu	>99.8	95	>80 Coag+Phent o Oxidation	98 – 99 Ion exchange	> 99.9	48 - 52
Zn	>99.8	95	>80 Coag+Phent o oxidation	98 – 99 Ion exchange	> 99.9	48 - 52
Cr	>99.8	95	>80 Coag+pento oxidation	98 – 99 Membrane & Ion exchange	> 99.8	48 – 50,53
Ni	>99.8	95	>80 Coag+Phent o oxidation	99.8 Membrane	>99.8	48 - 51
Cd	>99.8	95	>80 Coag+Phent o Oxidation	99.9 Membrane	100	48 - 51
As	99	95	>80 Coag+Phent o Oxidation	90 Adsorption	>99.6	49,50,54, 55,56

Mercury Removal Using Fe –Fe Electrodes by Electrocoagulation

Satish I. Chaturvedi

Department of Chemical Engineering, SVM Institute of Technology, India

ABSTRACT: The performance of electrocoagulation is a promising electrochemical technique with iron sacrificed anode for waste water treatment on laboratory scale was done. Several parameters like initial metal concentration, pH, voltage, agitation and electrolyte concentration at different time were investigated to achieve a higher removal rate of mercury. Experiments were carried out with different initial metal concentration ranging from 30 ppm, 50 ppm and 100 ppm, pH ranging from 2.5 pH, 4.5 pH and 7.0 pH, Voltage vary from 6V, 9V and 12V, electrolyte concentration changes from 0.6667 g/lit., 1.333 g/lit. and 2.0 g/lit., agitation vary from 200 rpm, 400 rpm and 600 rpm with a constant spacing between two electrodes is 1.0 cm. Maximum mercury removal was achieved at the end of 40 minute operation. Total operating cost also calculated from the power cost and cost of electrode material. The method was found to be highly efficient and relatively fast compared to conventional existing techniques.

Keywords: Electrocoagulation, Heavy metals, Iron electrodes, Operating cost.

I. Introduction

Legislative regulation concerns with the discharge of waste water are strictly increase drastically, due to higher toxicity of metal ions. Different methods like precipitation, coagulation, sedimentation, adsorption, ion exchange and reverse osmosis [1, 2 and 3]. The difference between electrocoagulation and chemical coagulation is based on the delivered of iron ions [4]. In the electrocoagulation, coagulation and precipitation are not conducted through chemicals – known as coagulants – to the process, but via electrodes in the electrolytic cell [5]. Electrochemically is the most promising technologies to a clear environment with a broad range of technology to treat wastewater. Electrochemical consist of electrocoagulation and electrolysis, have been successfully developed for the treatment of different kind of industrial waste waters [6, 7 and 8]. In electrolysis oxidation, reduction and decomposition whereas electrocoagulation coagulation, adsorption, precipitation and floatation [9, 10 and 11] mechanisms employed to remove pollutant from waste waters. Since the turn of the 19th century, electrocoagulation widely applied for the treatment of waste water [12]. Electrocoagulation process bears merits such as safety, selectivity, versatility, amenability to automation, environmental compatibility and energy efficiency.. Electrocoagulation process is also characterized by simple and easy operated equipment, short operation time, none or negligible amounts of chemicals and low sludge production [13 and 14]. Electrocoagulation is a generation process of metallic hydroxide flocks by electro dissolution of sacrificial anode generally made of iron or aluminum [11]. The metal ion generation takes place at the anode and hydrogen gas is released from the cathode. Also, hydrogen gas is also float the flocculated particles from the water. The mechanism of electrocoagulation is highly dependent on the chemistry of aqueous medium, pH, particle size and chemical constituent concentrations will also influence the electrocoagulation process. Electrode assembly is the heart of the electrolytic cell. Different electrodes are utilized like, iron [15], aluminum [16], graphite, titanium [17], carbon [18] and mild steel [19]. Although, aluminum and iron are extensively used to clarify waste water [20]. They are cheap, readily available and proven effective [21].

The electrocoagulation has successfully been applied to the treatment of removal of arsenic [22], phosphate [23], sulfide, sulfate and sulfite [24], boron [25], fluoride [26], nitrate [27], chromate [28], restaurant waste water [29], Alcohol distillery waste water [30], treatment of copper, lead and cadmium in natural water and simulated waste water [31].

In addition, the following physico-chemical reaction may also took place in the electrocoagulation cell [31]. (i) cathodic reduction of impurities present in the waste water (ii) Discharge and coagulation of colloidal particles (iii) migration of ions due to electrophoretic action (iv) Due to generation of oxygen and hydrogen bubble electrofloatation of coagulated particles took place (v) reduction of metal ions at the cathode (vi) other chemical and electrochemical process.

The main objectives of the present work were to gain into some fundamental mechanisms and possible interactions influencing the removal process of mercury by electrocoagulation. The process was examined under different values of initial pH, initial concentration, electrolyte concentration, applied potential and agitation in order to determine optimum conditions.

II. Electrocoagulation Mechanism

This technique has recently attracted a great deal of attention. Electrocoagulation or enhanced coagulation accompanied through electrofloatation is an efficient electrochemical water and waste water treatment technology. Electrocoagulation consists of situ formation of coagulants due to electrodisolution of sacrificial anode Coagulants are responsible for aggregation as well as precipitation of suspended particles and simultaneously adsorption of dissolved pollutants. Tiny bubbles of hydrogen and oxygen generated at cathode and anode respectively collide with air bubbles and float the pollutant particles.

In electrocoagulation, iron is oxidized to iron hydroxide, Fe (OH) n , where n is 2 or 3. The following mechanisms have been proposed for the formation of Fe (OH) n [32]:

Mechanism: 1

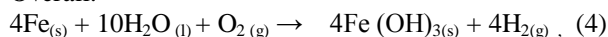
Anode:



Cathode:

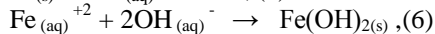
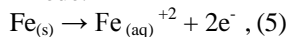


Overall:

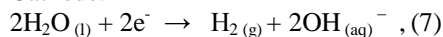


Mechanism: 2

Anode:



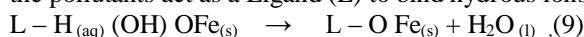
Cathode:



Overall:



The generated $\text{Fe}(\text{OH})_n$ remains in the aqueous solution as a gelatinous suspension, which can remove the pollutants either by complexation or electrostatic attraction followed by coagulation [32]. In the case of surface complexation the pollutants act as a Ligand (L) to bind hydrous ions:



Also, in many wastewaters which contain chlorides, so another strong oxidant of hypochlorite may be developed which is given as per following equation [33 and 34]:



Iron electrode oxidize and ferric ions generated and forms monomeric ions $\text{Fe}(\text{OH})_3$, and hydroxyl complexes like $\text{Fe}(\text{H}_2\text{O})_6^{3+}$, $\text{Fe}(\text{H}_2\text{O})_5^{2+}$, $\text{Fe}(\text{H}_2\text{O})_4(\text{OH})_2^{+}$, $\text{Fe}(\text{H}_2\text{O})_5\text{OH}^{2+}$, $\text{Fe}_2(\text{H}_2\text{O})_8(\text{OH})_2^{4+}$, $\text{Fe}_2(\text{H}_2\text{O})_6(\text{OH})_4^{4+}$ [35]. Generation of these complexes strongly depend upon pH [36]. The formation of these hydroxides, polyhydroxides, and polyhydroxy metallic are responsible for cause of coagulation which have affinity with dispersed as well as counter ions.

III. Experimental and Set up Procedure

3.1 Materials and methods

Electrocoagulation was carried out by preparing synthetic solution of 30 ppm, 50 ppm and 100 ppm concentration by dissolving the require quantity of mercury chloride in a conventional 1000 ml glass beaker. The net spacing between the electrodes are 10 mm in order to minimize the IR drop [36] which is shown in fig. (1). Fe plates of 140 mm x 18 mm x 2 mm were used as electrodes for electrocoagulation. The effective surface area of each electrode was 60 mm x 18 mm x 2 mm. The entire electrode assembly was fitted on non conducting wedges and hanged from the electrocoagulation cell. At beginning of the each run, 750 ml of desired concentration was poured into the reactor. Conductivity of the solution was improved by addition of sodium chloride as an electrolyte in order to reduce the IR – drop or solution resistance potential [36 and 37]. The added amount of sodium chloride was 0.6667 gm/lit, 1.333 gm/lit and 2.0 gm/lit. All chemicals were of analytical grade and supplied by Merck, Germany. All the experiments were carried out at room temperature. The electrodes were connected to D.C. power source in a monopolar mode. The electrical contacts were established with crocodile clips.

The electrode assembly was placed in the cell and the electrodes were connected to respective anode and cathode for a different time interval from 5 minute to 60 minute and voltage vary from 6V, 9V and 12V. All runs were performed at different stirring speed of 200 rpm, 400 rpm and 600 rpm. In each run 750 ml. HgCl_2 solution placed in the electrolytic cell with a pH range of 2.5 pH, 4.5 pH and 7.0 pH for a different electrolyte concentration of 0.6667 g/lit., 1.333 g/lit., 2.0 g/lit. The treated sample collected at different time interval. After each run, the power was switched off and electrodes were dismantled. Before each run, electrodes were washed thoroughly with water to remove any solid residues on the surfaces, dried and reweighed to calculate sacrificial electrodes consumption.

3.2 Chemical analysis

The pH was monitored with a high precision pH meter (micro process based pH system, model 1012 - E) which was equipped with a combined glass electrode. The initial pH of the solutions was adjusted by adding NaOH or H_2SO_4 solutions. Conductivity of the solution measured with electronic conductivity meter (micro process based conductivity meter, model 1601 - E) equipped with an immersion measurement probe. The total concentration of mercury in solution was determined with (ELCO, SL – 159) UV - vis spectrophotometer at 575 nm according to Beer – Lambert law. The mercury removal efficiency is calculated as follows: [15]

$$\text{CR} (\%) = \frac{\text{Co} - \text{Ce}}{\text{Co}} \times 100 \text{ , (11)}$$

Where CR is the removal efficiency, Co – mercury concentration at initial, Ce – mercury concentration at equilibrium.

IV. Result Analysis

4.1 Influence of electrocoagulation time

To explore the effect of operating time for electrolysis, optimum parameter maintained for initial pH 4.5, initial metal concentration 50 ppm, stirring rate 400 rpm, applied potential 9V and electrolyte concentration 1.333 gm/lit. to achieved 94.5% at 40 minute demonstrated in fig (2). The electrocoagulation process is controlled many parameters like pollutant concentration and composition, initial pH and conductivity. Additionally, electrode material applied potential, charge loading and coagulation time effect the process. During electrocoagulation, anodic and cathodic reduction occurs at positive and negative electrode respectively. Lively evolution of oxygen responsible of reduction the anode dissolution which is related with dissolved amount of iron. The released ions neutralized the particles charges so initiate the coagulation.

Initially, minor formation of oxygen at sacrificial anode competes with iron dissolution which reduced the dissolved amount of iron at the sacrificial anode which cause co-precipitation and sweeping effect and attributed to slower removal rate of mercury shown in table (1). Optimum removal efficiency gained at 40 minute with 94.5 % as formation of enough coagulant iron hydroxides concentration. But due to continuous electrocoagulation, some of hydroxides ions oxidized at anode. So generation of iron is reduced [38] and efficiency of removal of mercury decrease by about 12.2 % after 20 minute.

As electrocoagulation proceeding, is responsible for cause of increase of concentration ions and their hydroxide flocks [35] lead to increase of pH. Initially, in the electrocoagulation, slower increased of pH observed due to slower generation of hydroxide ion with increasing the solubility. But as electrocoagulation proceed, reduction of solubility was took place which cause ultimate rise of 43 % in pH of the solution with increasing the hydroxide ion generation. But rate of pH decrease slightly up to 6.44 units due to incremental improvement in the average OH/Fe mole ratio due to decline of solubility.

4.2 Effect of applied potential

It is well known that during electrocoagulation, current passing through the circuit has raised due to increased applied potential. To evaluate the optimum mercury removal efficiency, experiments were conducted at different applied potential such as 6V, 9V and 12V with the different optimum conditions such as initial pH 4.5, initial metal concentration 50 ppm, stirring rate 400 rpm and electrolyte concentration 1.333 gm/lit. to achieved as high as 94.5 % removal efficiency of mercury at 40 minute demonstrates in fig (3) with data in table (2). Also, it is fact that current not only determines the coagulant dosage rate [2, 7, 27] but also the bubble production rate, size and flocks growth which closely affect the mercury removal efficiency of mercury. As per [7, 27, 39, 40, 41] rise of mercury removal efficiency incurred as increase of current and current density. When applied potential rate is increased from 6V to 9V mercury removal efficiency increased from 85 % to 94.5 and then decreased at 12V about 27.2 % of optimum value of 9V. It seems that increasing the applied potential, more Fe⁺² and OH⁻ were generated in the electrochemical cell which enhance the coagulant dosage cause accelerated mercury removal at a optimum value of 94.5 % at 40 minute. Above the critical value, dissolution of Fe⁺² exceeded, leads to excessive generation of oxygen with consequently heat generation. Therefore, no or more Fe⁺² ions remain in the solution and decreased mercury removal about 14.7 %, 12.2 % and 13.4 % of critical value of 6V, 9V and 12V respectively [42].

4.3 Effect of agitation

Batch electrocoagulation experiments were conducted for different time and optimize the mercury removal efficiency at a different time interval from 5 minute to 60 minute with different rpm at 200, 400 and 600 illustrated in fig. (4). As stirring rate was increased from 200 rpm to 400 rpm rate of collision and mobility of ions were increased slowly increased with agitation. At critical value of 400 rpm flocks formation was higher which intimately associated with each other and precipitation became easier cause [41] significantly maximum mercury removal as high as 78.3 % and 14.3 % for 200 rpm and 600 rpm respectively. But at higher agitation, solubility of precipitates increase or some time unsuitable flocks formation took place which was leading reasons for decreasing 23.6 %, 12.2 % and 14.2 % the mercury removal efficiency for 6V, 9V and 12V respectively after critical value shown in table (3).

4.4 Cost estimation

Economic analysis includes consist different operating cost like electrodes cost, energy consumption cost, as well as labor, sludge transportation and disposal, maintenance and fixed costs. The later costs are largely independent of the type of the electrode material. For calculation of the operating cost (US \$/m³), energy consumption cost (US \$ KWh/m³) and electrodes material cost (US \$ Kg/m³) have been taken into account as a major cost for economic investigation.

Operating cost = a Cenergy + b Celectrodes

Where 'a' is the electrical energy price (US \$ KWh/m³) and 'b' is the electrode material price (US \$ /Kg Fe). Cost of electrode material (Kg Fe/m³ HgCl₂ solution) is calculated as per following equation by Faraday's law:

$$\text{Celectrodes} = \frac{I \times t \times Mw}{Z \times F \times v} \quad (12)$$

Where: I = Current (A)

t = Electrolysis time (s)

Mw = Molecular mass of Fe (g/mol)

F = Faraday's constant (c/mol)

Z = number of electron transfer

v = volume of HgCl₂ solution (m³)

The major cost of electrocoagulation is associated with electrical energy consumption during electrocoagulation shown in table (4). It is calculated in (KWh/m³ HgCl₂ solution) as per following equation :

$$C_{\text{energy}} = \frac{V \times I \times t_{\text{EC}}}{v} \quad (13)$$

Where: V = Cell voltage (V)

I = Current (A)

t_{EC} = electrolysis time (s)

v = Volume (m³) of HgCl₂ solution

Unit price a, b given for the Indian market April – 2008 was as follows:

- (1) electrical energy price 0.5570 US \$/ KWh
- (2) electrodes material price 1.7722 US \$/Kg for Fe

Cost due to electrical energy consumption and electrode material are calculated for different time shown in fig. (5) follows the data mention in table no. (4) in which both are increasing with time. In fig. (6), it seems that the operating cost shown in table (5) is also increased almost linearly with time due to increase in consumption of electrical energy as well as electrode material.

V. Conclusion

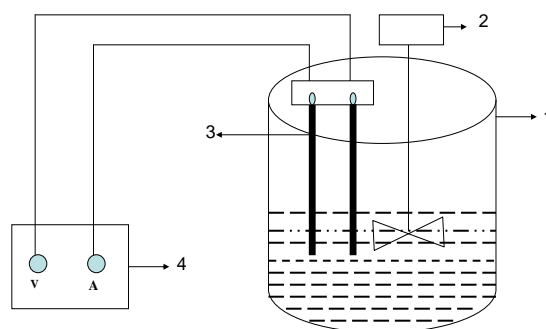
In this study, behavior of iron electrode in the electrocoagulation process has been investigated. On the base of wide range of experiments, different evidence was concluded. The removal rate of mercury was affected by different factors like – initial pH of the solution, electrolyte concentration, applied potential, initial concentration and agitation. By keeping optimum pH – 4.5, ppm – 50, voltage – 9V, agitation – 400 rpm and electrolytic concentration 1.333 g/lit., 94.5 % mercury removal achieved within 40 minute. In the electrocoagulation cell, due to formation of hydroxyl ions forms at the cathode. Removal rate of mercury start from slow rate and achieved a peak value then rate falls. During electrocoagulation, quick and effective mercury removal achieved.

References

- [1] N. Kongsricharoern and C. Polprasert, Electrochemical precipitation of chromium (Cr⁶⁺) from an electroplating waste water, Water Sci. Technol. 31 (1995), p.109 – 117.
- [2] N. Adhoum, L. Monser, N. Bellakhal and J. E. Belgaied, Treatment of electroplating waste water containing Cu²⁺, Zn²⁺, and Cr(VI) by electrocoagulation, J. Hazard. Mater, 112, 2004, 207 – 213.
- [3] N. Meunier, P. Drogué, C. Gourvence, G. Mercier, R. Hausler and J.F. Blais, Removal of metals in leachate from sewage sludge using electrochemical technology, Environ. Technol., 25, 2004, 235 – 245.
- [4] J. C. Donni, J. Kan, J. Szykarczuk, T. A. Hassan and K. L. Kar, The operating cost of electrocoagulation, Can. J. Chem. Eng., 72, 1994, 1007 – 1012.
- [5] A. S. Kopalal, The removal of salinity from product formation by conventional and electrochemical methods, Fresenius Environ. Bull., 12a (11), 2002, 1071 – 1077.
- [6] A. G. Vlyssides, P. Karlis, M. Loizidou, A. Zorpas and D. Arapoglou, Treatment of leachate from a domestic solid waste sanitary landfill by an electrolysis system, Environ. Technol., 22, 2001, 1467 – 1476.
- [7] C. T. Tsai, S. T. Lin, Y. C. Shue and P. L. Su, Electrolysis of soluble organic matter in leachate from landfills, Water res., 31, 1997, 3073 – 3081.
- [8] J. Naumczyk, L. Szpyrkowicz, D. M. De Feverri and F. Zillio – Grandi, Electrochemical treatment of tannery wastewater containing high strength pollutants, Trans. IChemE, 74 B, 1996, 59 – 68.
- [9] A. G. Vlyssides, P. K. Karlis and A.A. Zorpas, Electrochemical oxidation of noncyanide strippers wastes, Environ. Int., 25, 1999, 663 – 670.
- [10] J. Grimm, D. Bessarabov and R. Sanderson, Review of electro – assisted methods for water purification, Desalination, 115, 2008, 285 – 294.
- [11] K Rajeshwar, J. G. Ibanez and G. M. Swai, Electrochemistry and environment, J. Appl. Electrochem., 24, 1994, 1077 – 1091.
- [12] M.J. Matteson, R. L. Dobson, R.W. Glann, N.S. Kukunoor, W. H. Waits and E.J. Clayfield, Electrocoagulation and separation of aqueous suspensions of ultra fine particles, Colloids Surface, A 104, 1995, 101 – 109.
- [13] N.S. Abuzaid, A. Bukhari and Z. M. Al-Hamouz, Ground water coagulation using soluble stainless steel electrodes, Adv. Environ. Res., 6, 2002, 325 – 333.
- [14] H. Bergmann, A. Rittel, T. Lourtchouk, K. Schoeps and K. Bouzek, electrochemical treatment of cooling lubricants, Chem. Eng. Process., 42, 2003, 105 – 119.
- [15] Y. S. Yildiz, A. S. Kopalal, S. Irdemdez and B. Keskinler, Electrocoagulation of synthetically prepared waters containing high concentration of NOM using iron cast electrodes, J. Hazard. Mater, B 139, 2007, 373 – 380.
- [16] I. L. Hernandez, C. B. Diaz, G. R. Movales, B. Bilyeu and U. Nunez, A combined electrocoagulation – sorption process applied to mixed industrial waste water, J. Hazard. Mater, 144, 2007, 240 – 248.
- [17] M..Murugananthan, G. B. Raju and S. Prabhakar, Separation of pollutants from tannery effluents by electro floatation, Sep. purif. Technol., 40, 2004, 69 – 75.
- [18] A. A. Gallegos and D. Pletcher, The removal of low level organics via hydrogen peroxide formed in a reticulated vitreous carbon cathode cell, Part : the removal of phenols and related compounds from aqueous effluents, Electrochim. Acta, 44, 1999, 2483 – 2492.
- [19] A.K. Golder, N. Hridaya, A.N. Samanta and S. Ray, Electrocoagulation of methylene blue and eosin yellowish using mild steel electrodes, J.Hazard. Mater, 127, 2005, 134 – 140.

- [20] A. Bes-Pia, J.A. Mendoza-Roca, M.I. Alcaina-Miranda, A. Iborra-Clar and M.I. Iborra-Clar, Reuse Of wastewater of the textile industry after its treatment with a combination of physico-chemical treatment and membrane technologies, *Desalination*, 149, 2002, 169 – 174.
- [21] X. Chen, G. C. Chen P.L. Yue, Separation of pollutants from restaurant waste water by electrocoagulation, *Sep. Purif. Technol.*, 19, 2000, 65 – 76.
- [22] P. R. Kumar, S. Chaudhari, K. C. Khilar, and S. P. Mahajan, Removal of arsenic from water by electrocoagulation, *Chemosphere*, 55, 2004, 1245 – 1252.
- [23] N. Bektas, H. Akbulut, H. Inan, and A. Dimoglo, Removal of phosphate from aqueous solution by electro-coagulation, *J. Hazard. Mater. B* 106, 2004, 101 – 105.
- [24] T. Kim, C. Park, E. Shin and S. Kim, Decolorization of disperse and reactive dyes by continuous electrocoagulation process, *Desalination*, 150, 2002, 165 – 175.
- [25] A. E. Yilmaz, R. Boncukcuoglu, M. M. Kocakerim and B. Keskinler, The investigation of parameters affecting boron removal by electrocoagulation method, *J. Hazard. Mater. B* 125, 2005, 160 – 165.
- [26] N. Mameri, A. R. Yeddou, H. Lounici, D. Belhocine, H. Grib and Bariou, Defluoridation of septentrional of sahara water of North Africa by electrocoagulation process using bipolar aluminum electrodes, *Water Res.*, 32, 1998, 1604 – 1612.
- [27] A. S. Koparal and U. B. Ogutveren, Removal of nitrate from water by electro reduction and electrocoagulation, *J. Hazard. Mater. B* 89, 2002, 83 -94.
- [28] P. Gao, X. Chen, F. Shen and G. Chen, Removal of chromium (VI) from waste water by combined electrocoagulation – electroflotation without a filter, *Sep. Purif. Technol.*, 43, 2004, 117 – 123.
- [29] Z.V. P. Murthy, C. Nancy and Akash Kant, Separation of pollutants from restaurant wastewater by electrocoagulation, *Sep. Purif. Technol.*, 42, 2007, 819 – 833.
- [30] Y. Yavruz, EC and EF processes for the treatment of alcohol distillery waste water, *Sep. Purif. Technol.*, 53, 2006, 135 – 140.
- [31] C. Escobar, C. Soto – Salazar and M. I. Toral, Optimization of the electrocoagulation process for the removal of copper, lead and cadmium in natural water and simulated waste water, *J. Environ. Manage.*, 81, 2006, 381 – 391.
- [32] N. Modirshahla, M. A. Behnajady and S. kooshaiian, Investigation of the effect of different electrode connections on the removal efficiency of Tartrazine from aqueous solution by electrocoagulation, *Dyes pigments*, 7,4 2007, 249 – 257.
- [33] C. J. Israilides, A. G. Vlyssides, V. N. Mourafeti and G. Karvouni, Olive oil waste water treatment with use of an electrolysis system, *Bioresour. Technol.*, 61, 1997, 163 – 170.
- [34] L. Szypkiewicz, G. H. Kelsall, S. N. Kaul and M. De Faveri, Performance of electrochemical reactor for treatment of Tannery wastewater, *Chem. Eng. Sci.*, 56, 2001, 1579 – 1586.
- [35] N. Daneshvar, A. R. Khataee, A. R. Amani and M. H. Rasoulifard, Decolorization of C. I. Acid Yellow 23 solutions by electrocoagulation process : Investigation of operational parameters and evaluation of specific electrical energy consumption (SEEK), *J. Hazard. Mater.* 148, 2004, 566 – 572.
- [36] M. Y. A. Mollah, P. Morkovsky, J. A. G. Gomes, M. Kesmez, J. Parga and D. L. Cocke, Fundamental future and perspectives of electrocoagulation, *J. Hazard. Mater. B* 114, 2004, 199 – 210.
- [37] G. H. Chen, Electrochemical technologies in wastewater treatment, *Sep. Purif. Technol.*, 38, 2004, 11 – 41.
- [38] N. Daneshvar, H. Ashassi – Sorkhabi and A. Tizpar, Decolorization of II by electrocoagulation method, *Sep. Purif. Technol.*, 31, 2003, 153 – 162.
- [39] O. B. Ogutveren and S. Koparal, Electrocoagulation for oil – water emulsion treatment, *J. Environ. Sci. Health, A* 32, 1997, 2507 – 2520.
- [40] O. B. Ogutveren, E. Toru and S. Koparal, Removal of cyanide by anodic oxidation for wastewater treatment, *Water Res.*, 8(9/10), 1999, 1851 – 1856.
- [41] A. S. Koparal and O.B. Ogutveren, Removal of nitrate from aqueous solutions by electrodialysis, *Int. J. Environ. Stud.*, 3(59), 2002, 323 – 329.
- [42] I. Heidmann and W. Calmano, Removal of Cr (VI) from model wastewaters by electrocoagulation with Fe electrodes, *Sep. Purif. Technol.*, 61, 2008, 15 -21.

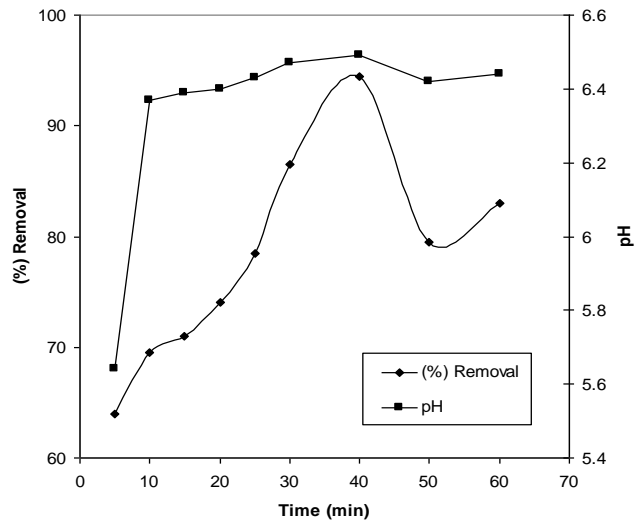
FIGURES AND TABLES



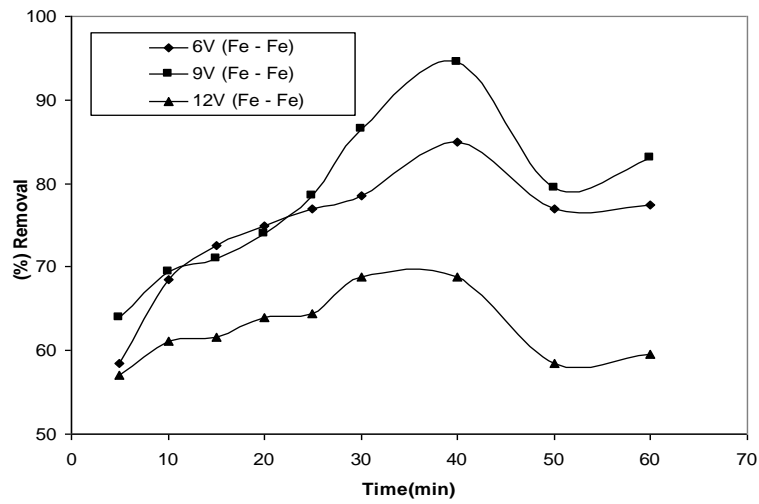
Schematic process arrangement

1. Electrolytic cell
2. Stirrer
3. Mild steel electrode pair
4. Power supply (V, Voltage regulator and A, current regulator)

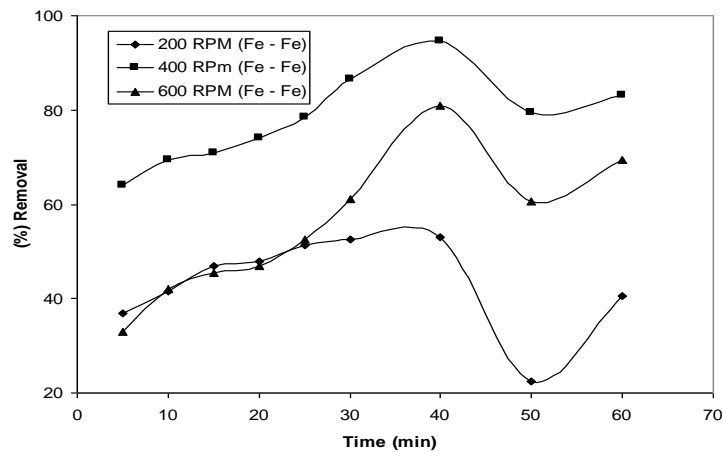
“Fig. (1) Electrolytic cell”



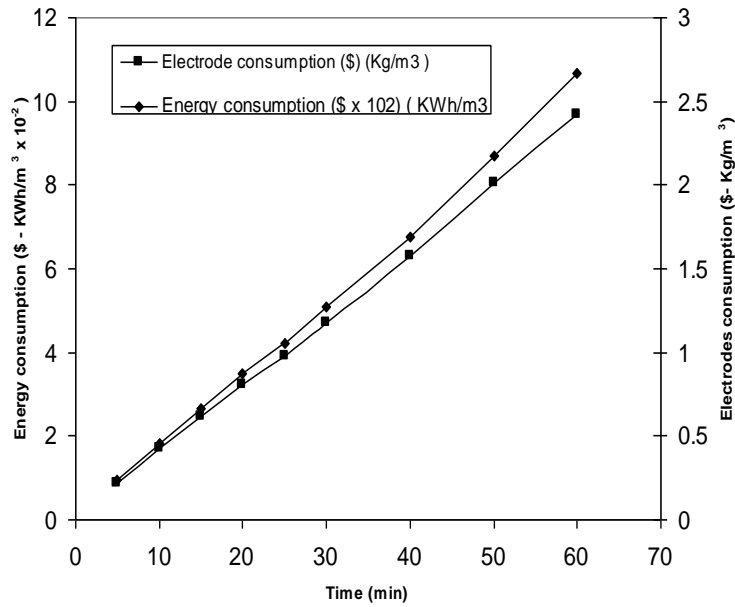
“Fig. (2) % Removal efficiency of mercury and pH with electrocoagulation Time ppm – 50, Voltage – 9V, Agitation – 400 rpm, Electrolyte concentration – 1.333 g/lit., pH – 4.5”



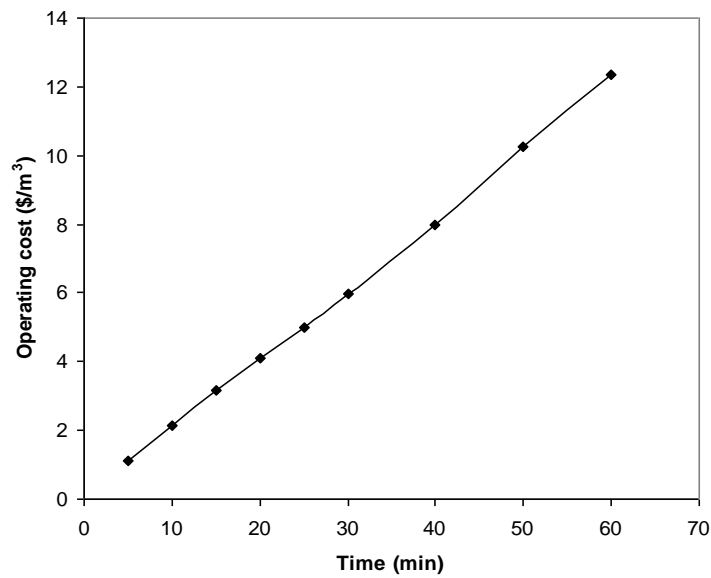
“Fig. (3) Effect of applied potential on the removal efficiency of mercury with Time. ppm – 50, Agitation – 400 rpm, Electrolyte concentration – 1.333 g/lit., pH – 4.5”



“Fig. (4) Effect of agitation on the removal efficiency of mercury with time. ppm – 50, electrolyte concentration 1.333 g/lit., Voltage – 9V, pH – 4.5”



“Fig. (5) Effect of electrolysis time on energy consumption (\$ x 10²) (KWh/m³) and electrode consumption (\$) (Kg/m³ of HgCl₂ solution). ppm – 50, Voltage – 9V, Agitation – 400 rpm, Electrolyte concentration – 1.333 g/lit., pH – 4.5”



“Fig. (6) Effect of electrolysis time on operating cost (\$/m³). ppm – 50, Voltage – 9V, Agitation – 400 rpm, Electrolyte concentration – 1.333 g/lit., pH – 4.5”

TABLE (1) % Removal efficiency of mercury and pH with electrocoagulation Time

<i>Time (min)</i>	<i>(%) Removal</i>	<i>pH</i>
5	64	5.64
10	69.5	6.37
15	71	6.39
20	74	6.4
25	78.5	6.43
30	86.5	6.47
40	94.5	6.49
50	79.5	6.42
60	83	6.44

TABLE (2) Effect of applied potential on the removal efficiency of mercury with Time

<i>Time (min)</i>	<i>(%) Removal</i>		
	<i>6 Volt</i>	<i>9 Volt</i>	<i>12 Volt</i>
5	58.5	64	57
10	68.5	69.5	61.2
15	72.5	71	61.6
20	75	74	64
25	77	78.5	64.4
30	78.5	86.5	68.8
40	85	94.5	68.8
50	77	79.5	58.5
60	77.5	83	59.6

TABLE (3) Effect of agitation on the removal efficiency of mercury with time.

<i>Time (min)</i>	<i>(%) Removal</i>		
	<i>200 RPM</i>	<i>400 RPM</i>	<i>600RPM</i>
5	37	64	33
10	41.6	69.5	42
15	46.8	71	45.5
20	48	74	47
25	51.4	78.5	52.5
30	52.5	86.5	61
40	53	94.5	81
50	22.5	79.5	60.5
60	40.5	83	69.5

TABLE (4) Effect of electrolysis time on energy consumption ($\$ \times 10^2$) (KWh/m^3) and electrode consumption ($\$$) (Kg/m^3)

<i>Time (min)</i>	<i>Energy consumption ($\\$ \times 10^2$) ($\text{KWh/m}^3$)</i>	<i>Electrode consumption ($\\$) (Kg/m^3)</i>
5	0.2338	0.8686
10	0.4566	1.6989
15	0.6684	2.4818
20	0.8688	3.2263
25	1.0583	3.9295
30	1.27	4.7154
40	1.6931	6.2872
50	2.1729	8.0658
60	2.6668	9.679

TABLE (5) Effect of electrolysis time on operating cost ($\$/\text{m}^3$).

Time (min)	Operating cost ($\$/\text{m}^3$)
5	1.074
10	2.1525
15	3.1502
20	4.0957
25	4.9879
30	5.9854
40	7.9803
50	10.2387
60	12.3458

Mercury Removal Using Al – Al Electrodes by Electrocoagulation

Satish I. Chaturvedi

Department of Chemical Engineering, SVM Institute of Technology, Bharuch, India

ABSTRACT: The attempt has been made to remove mercury from mercury containing waste water prepared synthetically by using sodium chloride as an electrolyte using sacrificial aluminum anode in a batch wise by electrocoagulation cell. The affect of applied potential, initial pH, initial concentration of solution, agitation, electrolyte concentration and energy consumption on percent removal of mercury have been investigated. The removal efficiency of mercury was achieved 98.5% under optimum condition in which solution pH was 4.5, applied potential 9 V, initial solution concentration 50 ppm, electrolyte concentration 1.333 g/lit. With a stirring speed 400 rpm.

Keywords: Aluminum chloride, applied potential, Electrocoagulation, Energy consumption, Optimization

I. Introduction

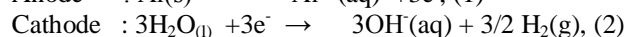
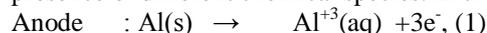
Electroplating or acid mine waste water generate different toxic substances like cyanides, alkaline cleaning agent, degreasing solvents, oil, fats and metals [1, 2]. Successful empirical studies [3, 4, 5, 6, 7, 8] show the successful treatment of waste water. Different techniques like adsorption, ion exchange, reverse osmosis and precipitation have been employed for the treatment of heavy metals. Effluent from metal plating and surface finishing generate higher concentration of metals in effluents. Due to high toxicity, discharge of waste water containing heavy metals are strictly regulated in the environment.

Since more than a century, electrocoagulation technique has been available. In last decades electrocoagulation [9, 10, 11, 12] consider an efficient method for the treatment of heavy metal containing solutions. Electrocoagulation is able to eliminate chemical oxygen demand [4,5,6,13], color [7], restaurant waste water [14], electroplating wastewater [3] and textile wastewaters [15,16,17,18]. The main objective of this study was examining some fundamental mechanisms and different aspects of electrocoagulation process influencing removal of mercury by electrocoagulation

II. Electrocoagulation

Electrocoagulation is an efficient method for water and waste water to destabilize the finely dispersed particles. Electrocoagulation consist of simple with reduction of equipments, easy operation and also decreased of sludge generation [19]. Different mechanisms like coagulation, absorption, adsorption, precipitation and flotation play an important role in the electrocoagulation process. The most common electrode material are aluminum and iron which are readily available, cheap and effective [20]. When direct current is applied, due to dissolution of aluminum electrode which act as a sacrificial anode, situ generation of Al^{+3} ions which act as a coagulants took place. These coagulants are responsible for destabilize finely dispersed particles in the vicinity of the anode surface and form flocks. Meanwhile, tiny bubble of H_2 produced at cathode.

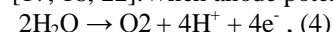
Due to dissolution of sacrificial electrode, various species generated [21] depending upon the pH of the solution and presence of different chemical species. In the case of aluminum, the main reactions are:



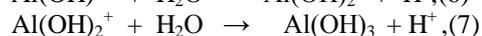
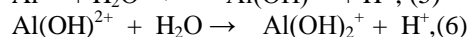
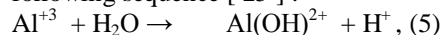
As per reaction (1) and (2), Al^{+3} and OH^- ions generated due to electrolytic dissolution of anode and form various monomeric species which follows complex precipitation kinetics and finally transform into $Al(OH)_3(s)$.



These "sweep flocks" $Al(OH)_3$ have large surface area and amorphous in nature. So quick adsorption of soluble organic compounds and trapping of colloids particles forms. Finally, these flocks eliminated due to sedimentation or H_2 floatation [17, 18, 22]. When anode potential is sufficiently high [3, 5, 20, 23, 24] secondary reaction may occur with oxygen evolution:



Due to spontaneous hydrolysis reaction, aluminum ion (Al^{+3}) as per eq. (1), generated different monomeric species as per following sequence [25]:



According to eq.(5), (6) and (7) anode vicinity appears as acidic while due to generation of H_2 as per eq.(2) cathode electrode vicinity became alkali.

III. Experimental set up

Electrocoagulation was performed in a cylindrical electrochemical cell in a batch wise with a pair of aluminum electrodes displayed in fig. (1) With a two facing of 10 mm. The dimension of each electrode was 14 cm. x 1.8 cm. x 0.2 cm.

with a effective area of each electrodes was 6cm. x 1.8 cm. x 0.2 cm. Waste water samples used in the experiments were prepared synthetically using $HgCl_2$ having 99.99 % of purity from Merck. All solutions used for electrocoagulation were prepared from analytical grade chemical reagent (Merck products). Experiments were conducted with temperature

around $\pm 28^{\circ}\text{C}$. The solution was stirred by an overhead stainless steel rod stirrer for homogeneity of the solution. After each run, the electrodes were washed thoroughly with dilute H_2SO_4 solution to remove oxide then washed with distilled water to remove any solid residues on the surfaces then dried and reweighed. The parameters chosen in the experiments whose range given in table no. (1). Electrodes were connected to a direct current power supply. Current passing through the circuit and applied potential were measured by using two digital multimeters as ampere meter and voltmeter respectively. Sodium chloride as supporting electrolyte was added to increase ionic conductivity of the solution. Besides its ionic contribution also reduce the adverse effect of anions like HCO_3^- , SO_4^{2-} . Electrolysis generated chlorine is also improved in water disinfection [26]. High precision pH meter (microprocessor based model 1012 – E) equipped with a combined glass electrode used for measurement of pH. Sulfuric acid or sodium hydroxide was used for changing the initial pH of the solution. A digital conductivity meter (model – 1601 E) equipped with an immersion measurement probe was used to measure the ionic conductivity of aqueous phase. The concentration of mercury determined by using a UV–vis spectrophotometer (Elco SL – 159) at 575 nm. Mercury removal efficiency is calculated as per following equation [27]:

$$\text{Mercury removal efficiency (\%)} = \frac{C_i - C_o}{C_i} \times 100, \quad (8)$$

C_i and C_o were the initial and present concentration (mg/lit.) of the mercury in the solution respectively.

IV. Results and discussion

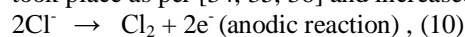
4.1 Effect of electrolyte concentration

Fig. (2) Shows the effect of without electrolyte concentration on removal efficiency of mercury with time. In the absence of electrolyte, conductivity of the solution and current density would be lower. So amount of the chloride ions in the solution decreased, which cause the increased of the total residence in electrocoagulation cell. As conductivity of the solution was less, generation of aluminum hydroxide was slower in the solution, which was responsible for lower removal efficiency of mercury. In the following table no. (2), Shows the effect of electrolyte concentration of absents to maximum concentration on removal efficiency of mercury with time.

Fig.(3) indicates the effect of NaCl concentration with respect to the time to achieved 98.5 % mercury removal. Low electrical conductivity of the solution cause maximum resistance between anode and cathode which is reduced on the base of high energy. By addition of sufficient quantity of NaCl in the solution overcome this problem and increase the conductivity and density of current would be increased as per [28]:

$$V = E_C - E_A - |\varepsilon_A| - |\varepsilon_C| - IR_{\text{cell}} - IR_{\text{circuit}}, \quad (9)$$

In addition of electrolyte increase of conductivity of the solution resulted into the reduction of the energy consumption [29, 30]. Also removal efficiency increase with increase in conductivity of the solution according [28, 31, 32]. According to reactions (10), (11) and (12) [33], when NaCl as electrolyte was added, formation of weak hypochlorous acid took place as per [34, 35, 36] and increased of chloride ion concentration as dissociation took place.



For lower concentration 0.6667 g/lit. There are not enough ions formed to conduct the current and probably lower efficiency of mercury removal observed [37]. As concentration of chloride ions increased 1.333 g/lit. in the solution, destroy the passivation layer and increase dissolution of electrode either by precipitation or incorporation of chloride ions into oxide film in the electrode dissolution [38]. As anodic dissolution of the electrode increased which cause blanketing oxide layer and attributed optimum 98.5 % removal rate of mercury? But at higher amount of Cl^- ions, solubility of mercury will be higher which reduced removal rate of mercury.

4.2 Effect of initial concentration

In the fig. (4), effect of initial concentration of mercury from 30 ppm to 100 ppm on removal efficiency with time is shown. Out of the different mechanisms for removal of mercury in electrocoagulation adsorption on to metallic hydroxide flocks has crucial important. Although at higher concentration there is certain limitation for adsorption capacity of flocks [37]. Concentration of ions and their flocks initiates at initial concentration – 30 ppm of solution turned towards into the removal rate of mercury. Optimization removal 98.5 % gain at 50 minute for 50 ppm concentration of mercury as adsorption capacity of flocks maximum. But above the concentration of 50 - ppm, adsorption capacity of flocks exhausted which was responsible for inactiveness of electrode effective surface. Meanwhile, at higher concentration of solution, generation of intermediate products increased which compete with mercury and water for active site on the electrodes [37] which leads to insolubility of aluminum hydroxide ions and declined mercury removal rate fall down. In the following table no. (3), Shows the effect of initial concentration on removal efficiency of mercury with time

4.3 Effect of applied potential

During electrocoagulation, applied potential is a crucial parameter on the performance of electrolytic cell. In this applied potential was varied by 6V, 9V, 12V at a constant pH 4.5, agitation 400 rpm, initial concentration 50 ppm, electrolyte concentration 1.333 g/lit. Shown in fig. (5). as per reaction (1) and (4) sacrificial metal dissolution and oxygen formation compete with each other respectively. According to faraday's law as per following eq. (14) [39]:

$$m = ItM, \quad (14)$$

ZF

m = amount of anode material dissolved (g)

I = current (A)

t = electrolysis time (s)

Z = no. of electrons involved in the reaction

F = Faraday's constant

The amount of dissolved sacrificial anode and generated hydroxyl ions are controlled by the applied current. After applied sufficient voltage, dissolution of sacrificial anode cause metal ions which were hydrolyzed and form a series of metallic hydroxide species. Electrostatic interparticles attraction increase enough as dispersed particles neutralized by these hydroxides species and encouraging agglomeration [40]. In the following table no.(4), Shows the effect of applied potential on removal efficiency of mercury with time. As applied potential increased for same initial pH, removal rate has increased according to [41, 42, 43, 44, 45]. In the early stage of electrocoagulation at voltage of 6V, suspended oxide particles were not able to destabilized and occur insufficient coagulation leads to slower removal rate of mercury. At critical voltage of 9V, optimum removal efficiency 98.5 % attributed as to surpass of effective Al^{+3} dissolution [46]. When voltage is exceed than this value, oxygen evolution as per eq. (4), lower the aluminum dissolution. Simultaneously, the oxygen promoted oxidation of Al to Al^{+3} . So, less or no aluminum ions are available [46] because abrupt decreased in mercury removal.

4.4 Effect of agitation

Electrocoagulation performed at different stirring speed of 200 rpm, 400 rpm and 600 rpm at optimum parameters of initial pH – 4.5, initial concentration – 50 ppm., voltage – 9V, electrolyte dosage 1.333 g./lit. For a different time vary from 5 minute to 60 minute shown in fig.(6). In the following table no. (5), Shows the effect of agitation on removal efficiency of mercury with time. During electrocoagulation, generation of aluminum hydroxides, different polymers with its complexes took place according to different criteria In the beginning of the electrocoagulation from 200 to 400 rpm, generation of coagulants were negligible which turned into slower removal rate of mercury. As rpm increased during electrocoagulation, aluminum hydroxide as a coagulant formed which leads to improved contact between mercury and different aluminum hydroxides and complexes, formed in the vicinity of an electrode [47] which was responsible for optimum 98.5 % removal rate of mercury at 50 minute. But at higher agitation, excess temperature took place which destroyed the aluminum oxide film on the electrodes surface and compact $Al(OH)_3$ flocks formed on the surface of the electrodes [48] and reduced the removal rate of mercury.

V. Conclusion

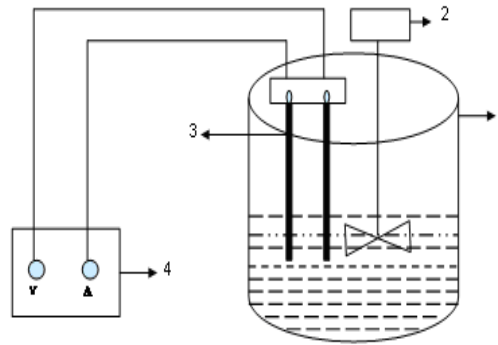
In this electrocoagulation, the behavior of aluminum electrodes has been find out based on the different parameters such as electrolyte concentration , electrolysis time, Initial pH, solution concentration, applied potential and agitation for removal of mercury containing wastewater prepared synthetically. Removal mechanism mainly due to the formation of hydroxyl ion as reduction of the cathodic surface. Also generation of aluminum ions based on the weight loss of electrodes. To destroyed the passive film at anode and by optimizing electrolyte concentration 1.333 g/lit., applied potential 9V, initial solution pH 4.5, initial solution concentration 50 ppm, agitation 400 rpm, removal efficiency of mercury achieved 98.5 % within 50 minutes. Thus the electrocoagulation method is efficient and faster method for removal of mercury at optimum conditions.

References

- [1] M.Hunsom, K.Pruksathorn, S.Damrongled, H. Vergnes and P.Duverneuil, Electrochemical treatment of heavy metals (Cu^{2+} , Cu^{6+} , Ni^{2+}) from industrial effluent and modeling of copper reduction, Water Res., 39, 2005, 610 – 616.
- [2] N. Kongsricharoern and C. Polprasert, Electrochemical precipitation of chromium (Cr^{6+}) from an electroplating waste – water, Water Sci. Technol., 31, 1995, 109 – 117.
- [3] N. Adhoum, L.Monser, N. Bellakhal and J. E.Belgaied, Treatment of electroplating wastewater containing Cu^{+2} , Zn^{+2} and $Cr(VI)$ by electrocoagulation, J. Hazard. Mater, 112, 2004, 207 – 213.
- [4] X H Xu and X F.Zhu, Treatment of refractory oily wastewater by electrocoagulation process, Chemosphere, 56, 2004 889 – 894.
- [5] G. H. Chen, X. M. Chen and P. L. Yue, Electrocoagulation and electroflotation of restaurant wastewater, J. Environ. Eng., ASCE 126, 2000, 858 – 863.
- [6] M. F. Pouet and A. Grasmick, Urban waste-water treatment by electrocoagulation and flotation, Water Sci. Technol., 31, 1995, 275 – 283.
- [7] J. Q. Jiang , N. Graham, C. Andre, G. H. Kelsall and N. Brandon, Laboratory study of electrocoagulation – flotation for water treatment, Water Res., 36, 2004, 69 – 75.
- [8] E. A. Vik., D. A. Carlson, A. S. Eikum and E. T. Gjessing, Electrocoagulation of potable water, Water Res., 18, 1984, 1355 – 1360.
- [9] J. Mrozowski and J. Zielinski, Studies of zinc and lead removal from industrial wastes by electrocoagulation. Environ. Prot. Eng., 9, 1983, 77 – 85.
- [10] G. Chen, Electrochemical technologies in wastewater treatment, Sep. Purif. Technol., 38, 2004, 11 – 41.
- [11] U. B. Ogutveren, N. Gonen and A. S. Kopalal, Removal of chromium from aqueous solutions and plating bath rinse by an electrochemical method, Int. J. Environ. Stud.,45, 1994, 81 – 87.
- [12] P. R. Kumar, S. Chaudhari, K. C. Khilar and S. P. Mahajan, Removal of arsenic from water by electrocoagulation, Chemosphers, 55, 2004, 1245 – 1252.
- [13] M. Murugananthan, G. B. Raju and S. Prabhakar, Separation of pollutants from tannery effluents by electroflotation, Sep. Purif. Technol., 40, 2004, 69 – 75.

- [14] Z. V. P. Murthy, C. Nancy and Akash Kant, Separation of pollutants from restaurant wastewater by electrocoagulation, *Sep. Sci. and Technol.*, 42, 2007, 819 – 833.
- [15] M. N. Pons, A. Alinsafi, M. Khemis, J. P. Leclerc, A. Yaacoubi, A. Benhammou and A. Nejmeddine, Electrocoagulation of reactive textiles dyes and textiles wastewater, *Chem. Eng. Process.*, 44, 2005, 461 – 470.
- [16] Y. M. Slokar and A. M. L. Marechal, Methods of decolorization of textile wastewaters, *Dyes Pigments*, 37, 1998, 335 – 356.
- [17] M. Kobya, O. T. Can, M. Bayramoglu and M. Sozbir, Operating cost analysis of electrocoagulation textile dye waste water, *Sep. Purif. Technol.*, 37, 2004, 117 – 125.
- [18] M. Kobya, O. T. Can and M. Bayramoglu, Treatment of textile wastewaters by electrocoagulation using iron and aluminum electrodes, *J. Hazard. Mater. B* 100, 2003, 117 – 125.
- [19] A. Gueres, M. Yalcm and C. Dogar, Electrocoagulation of some reactive dyes: a statistical investigation of some electrochemical variables, *Waste Manage*, 22, 2002, 491 – 499.
- [20] X. Chen, G. Chen and P. L. Yue, Separations of pollutants from restaurant wastewater by electrocoagulation, *Sep. Purif. Technol.*, 19, 2000, 65 – 76.
- [21] G. R. Morales, E.C.Medina, J.A.Cotero, B.Bilyeu and C.B.Diaz, Aluminum electrocoagulation with peroxide applied to wastewater from pasta and cookie processing, *Sep. Purif. Technol.*, 54, 2007, 124 – 129.
- [22] M. Kobya, O. T. Can and M. Bayramoglu, Decolorization of reactive dye solutions by electrocoagulation using aluminum electrodes, *Ind. Eng. Chem. Res.*, 42, 2003, 3391 – 3396.
- [23] M. Y. A. Mollah, P. Morkovsky, J. A. G. Gomes, M. Kesmez, J. Parga and D. L. Cocke, Fundamentals, present and future perspectives of electrocoagulation, *J. Hazard. Mater. B* 114, 2004, 199 – 210.
- [24] M. Kobya, H. Hiz, E. Senturk, C. Aydiner and E. Demirbas, Treatment of potato chips manufacturing wastewater by electrocoagulation, *Desalination*, 190, 2006, 201 – 211.
- [25] G. Mouedhen, M. Feki, M. D. P. Wery and H. F. Ayedi, Behavior of aluminum electrodes in electrocoagulation process, *J. Hazard. Mater.* 150, 2006, 124 – 135.
- [26] Y. Avsar, U. Kurt and T. Gonullu, Comparison of classical chemical and electrochemical processes for treating rose processing wastewater, *J. Hazard. Mater.* 148, 2007, 340 – 345.
- [27] N.Modirshahla, M. A. Behnajady and S. Kooshaiian, Investigation of the effect of different electrode connections on the removal efficiency of Tartrazine from aqueous solutions by electrocoagulation, *Dyes pigments*, 74, 2007, 249 – 257.
- [28] N. Daneshvar, H. Ashassi - Sorkhabi and A. Tipzar, Decolorization of orange II by electrocoagulation method, *Sep. Pur. Technol.*, 31, 2003, 153 – 162.
- [29] S. H. Lin and C. C. Chang, Treatment of landfill leachate by combined electro-Fenton oxidation and sequencing batch reactor method, *Water Res.*, 34, 2000, 4243 – 4249.
- [30] C. T. Wang, Decolorization of Congo red with three – dimensional flow - by packed – bed electrodes, *J. Environ. Sci. Health part A : Toxic / Hazard. Subst. Environ. Eng.*, 38, 2003, 399 – 413.
- [31] S.H. Lin and C. F. Peng, Treatment of textile waste water by electrochemical method, *Water Res.*, 28, 1994, 277 - 282.
- [32] S. H. Lin and C. F. Peng, Continuous treatment of textile wastewater by coagulation, electrochemical oxidation and activated sludge, *Water Res.*, 30, 1996, 587 – 592.
- [33] Y.S.Yildiz, A.S.Koparal, S.Irdemez and B.Keskinler, Electrocoagulation of synthetically prepared waters containing high concentration of NOM using iron cast electrodes, *J. Hazard. Mater.* 139, 2007, 373 – 380.
- [34] Y. Seida and Y. Nakno, Removal of humic substances by layered double hydroxide containing iron, *Water Res.*, 5, 2000, 1487 – 1494.
- [35] I. P. Teerman and M. R. Jekel, Adsorption of humic substances onto β -FeOOH and its chemical regeneration, *Water Sci. Technol.*, 9, 1999, 199 – 206.
- [36] A. S. Koparal, The removal of salinity from produced formation by conventional and electrochemical methods, *Fresenius Environ. Bull.*, 12a, 2002, 1071 – 1077.
- [37] N. Modirshahla and M. A. Behnajady and S. Mohammadi – Aghdam, Investigation of the effect of different electrodes and their connections on the removal efficiency of 4 – nitrophenol from aqueous solutions by electrocoagulation, *J. Hazard. Mater.*, 154, 2008, 778 – 786.
- [38] W. J. Lee and S. I. Pyun, Effect of hydroxide ion addition on anode dissolution of pure aluminum in chloride ion – containing solution, *Electrochim. Acta*, 44, 1999, 4041 – 4049.
- [39] M. Y. A. Mollah, P. Morkovsky, J. A. G. Gomes, M. Kesmez, J. Parga and D. L. Cocke, Fundamentals, present and future perspectives of electrocoagulation, *J. Hazard. Mater.* 114, 2004, 199 – 210.
- [40] M. Y. A. Mollah, R. Schennach, J. Parga, and D. L. Cocke, Electrocoagulation (EC) – science and applications, *J. Hazard. Mater. B* 84, 2001, 29 – 41.
- [41] U. B. Ogutveren and S. Koparal, Electrocoagulation for oil – water emulsion treatment, *J. Environ. Sci. Health, A* 32, 1997, 2507 – 2520.
- [42] C. T. Tsai, S. T. Lin, Y. C. Shue and P. L. Su, Electrolysis of soluble organic matter in leachate from landfills, *Water Res.*, 12, 1997, 3073 – 3081.
- [43] U. B. Ogutveren, E. Toru and S. Koparal, Removal of cyanide by anodic oxidation for wastewater treatment, *Water Res.*, 8, 1998, 1851 – 1856.
- [44] A. S. Koparal and U. B. Ogtuveren, Removal of nitrate from aqueous solutions by electrocoagulation, *J. Hazard. Mater. B* (89), 2002, 83 – 94.
- [45] A. S. Koparal and U. B. Ogtuveren, Removal of nitrate from aqueous solutions by electrodialysis, *Int. J. Environ. Stud.*, 3, 2002, 323 – 329.
- [46] I. Heidmann and W. Calmano, Removal of Cr(VI) From model wastewaters by electrocoagulation with Fe electrodes, *Sep. Purif. Technol.*, 61, 2008, 15 -21.
- [47] A. K. Golder, A. N. Samanta and S. Ray, Removal of trivalent chromium by electrocoagulation, *Sep. Purif. Technol.*, 53, 2007, 33 – 41.
- [48] G. Chen, Electrochemical technologies in wastewater treatment, *Sep. Purif. Technol.*, 38, 2004, 11 – 41.

Figures and Tables



Schematic process arrangement

- 1. Electrolytic cell
- 2. Stirrer
- 3. Aluminum - Aluminum electrode pair
- 4. Power supply (V, Voltage regulator and A, current regulator)

Fig. (1) Electrolytic cell

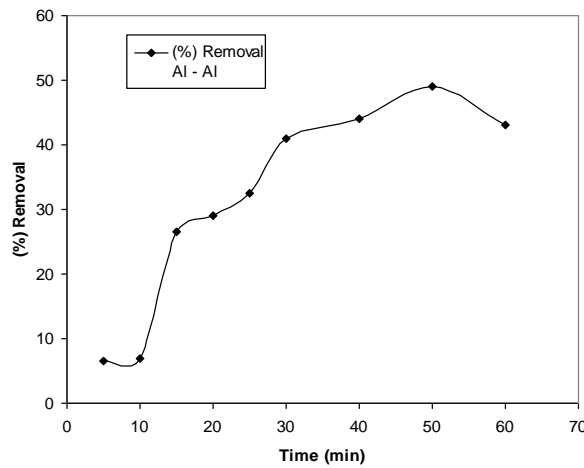


Fig. (2) Effect of without electrolyte concentration on the removal efficiency Of mercury with Time. Ppm – 50, Agitation – 400 rpm, Voltage – 9V, pH – 4.5

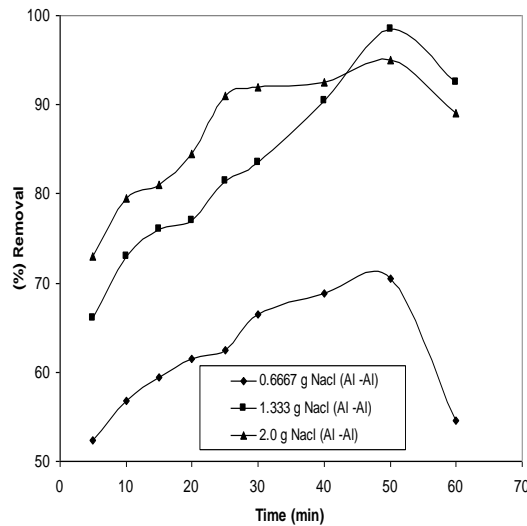
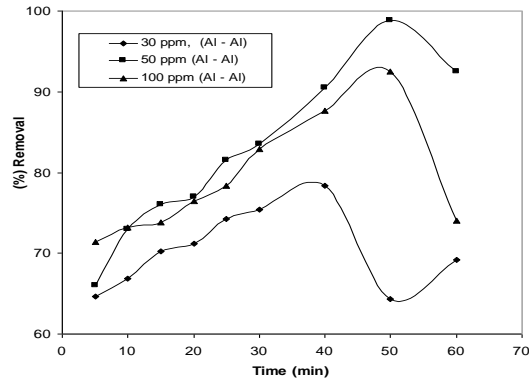
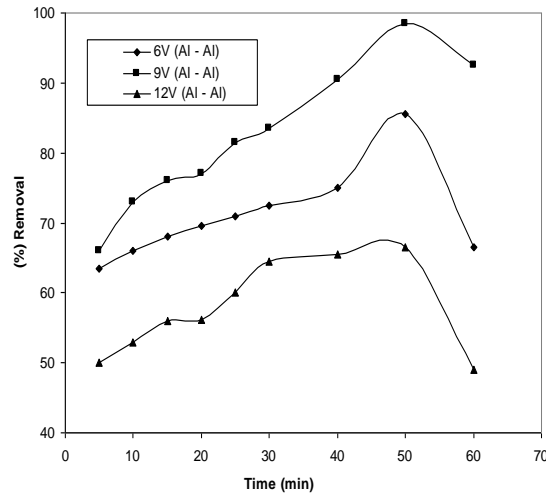


Fig. (3) Effect of electrolyte concentration on the removal efficiency Of mercury with Time. Ppm – 50, Agitation – 400 rpm, Voltage – 9V, pH – 4.5



“Fig. (4) Effect of initial concentration on the removal efficiency of mercury With Time. Voltage – 9V, Agitation – 400 rpm, Electrolyte concentration – 1.333 g/lit, pH – 4.5”



“Fig. (5) Effect of applied potential on the removal efficiency of mercury with Time. Ppm – 50, Agitation – 400 rpm, Electrolyte concentration – 1.333 g/lit., pH – 4.5”

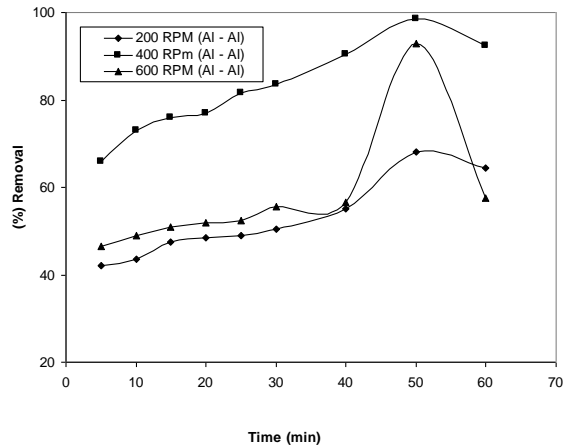


Fig. (6) Effect of agitation on the removal efficiency of mercury with Time. Ppm – 50, electrolyte concentration 1.333 g/lit., Voltage – 9V, pH – 4.5”

TABLE (1) Experimental parameters with Range

<i>Experimental parameters</i>	<i>Range</i>
Agitation (rpm)	0.6667, 1.333, 2.0
Concentration of supporting electrolyte (g/lit)	0.6667, 1.333, 2.0
pH	2.5, 4.5, 6.5
Mercury concentration (ppm)	30, 50, 100
Applied potential (V)	6,9,12
Agitation (rpm)	200, 400, 600

TABLE (2) Effect of electrolyte concentration on the (%) removal efficiency of mercury with Time.

Time (min)	(%) Removal efficiency of mercury			
	Without NaCl	0.6667 g NaCl/lit.	1.333 g NaCl/lit.	2.0 g NaCl/lit.
5	6.5	52.3	66	73
10	7	56.8	73	79.5
15	26.5	59.4	76	81
20	29	61.5	77	84.5
25	32.5	62.5	81.5	91
30	41	66.5	83.5	92
40	44	68.8	90.5	92.5
50	49	70.5	98.5	95
60	49	54.6	92.5	89

TABLE (3) Effect of initial concentration on the (%) removal efficiency of mercury with Time

Time (min)	(%) Removal efficiency of mercury		
	30 ppm	50 ppm	100 ppm
5	64.6	66	71.4
10	66.9	73	73.2
15	70.2	76	73.8
20	71.2	77	76.5
25	74.3	81.5	78.4
30	75.4	83.5	82.9
40	78.4	90.5	87.6
50	64.3	98.5	92.5
60	69.2	92.5	74

TABLE (4) Effect of applied potential on the (%) removal efficiency of mercury with Time

Time (min)	(%) Removal efficiency of mercury		
	6 Volt	9 Volt	12 Volt
5	63.5	66	50
10	66	73	53
15	68	76	56
20	69.5	77	56.2
25	71	81.5	60
30	72.5	83.5	64.4
40	75	90.5	65.5
50	85.5	98.5	66.5
60	66.5	92.5	49

TABLE (5) Effect of agitation on the (%) removal efficiency of mercury with Time

Time (min)	(%) Removal efficiency of mercury		
	200 RPM	400 RPM	600 RPM
5	42	66	46.5
10	43.6	73	49
15	47.4	76	51
20	48.5	77	52
25	49	81.5	52.5
30	50.5	83.5	55.5
40	55	90.5	56.5
50	68	98.5	93
60	64.5	92.5	57.5

English Teaching and Learning in the Digital Age

G. Padmavathi

Asst. Prof. of English, H&S Dept. Teegala Krishna Reddy Engineering College, Medbowli, Meerpet, Hyderabad
500097, India

The word 'innovation' is derived from Latin word 'innovare', which means to change something new. In other words it can be said that 'innovation' involves the practical implementation of new ideas.

Due to tremendous progress in information and communication technology, the scenario of contemporary teaching techniques is entirely changed. And the teacher of 21st century should shed traditional concepts and techniques of classroom teaching and should adopt the recent and innovative teaching techniques.

Teaching English depends on the potential excellence, skills and update knowledge of English teachers. The role of English teacher in present context has remarkably changed because of various factors such as social, cultural, economic and technology developments across the globe.

The subject of teaching English at this level is very wide and the difficulties the teacher faces are at large. Due to globalization the world is changing rapidly, hence a teacher has to improve and update knowledge of innovative techniques to meet the demand of changing era.

English language teachers must be innovative, imaginative, and resourceful and have thorough knowledge of the subject and adopt new techniques to change socio-economic status of the country.

Computer assisted language learning:

Language learning software was first created in 1960, concordance started in 1969, and the artificial intelligence programme specifically designed for language learning appeared in 1976. Computer games for language learning emerged in 1988, e-mail project were used by 1988. The internet knowledge resources were first reported in 1974.

Computer assisted language learning plays a vital role in teaching English at tertiary level. While computer has grown more powerful and multimedia has become more integrated, CALL. The major focus of CALL is on receptive skills. The internet is mainly a reading and listening to audio and video files. Though the limited access of CALL, it reached its full potential.

I. Blogs

Classroom outside the classroom:

Blog is derived from weblog. It is a diary or regular opinion columns posted on the internet. In blog, the writer posts diary entry which others can read and comment on it.

Weblogging is for learners' autonomy. The blogs are used in two main ways in English language teaching. The first, learners can be encouraged to write and post their blogs. If learners are learning to write journals or engaged in other form of extensive writing in the classroom, it is the right place to check their ability of writing. The learners are asked to post their blogs to create wider and more meaningful audience for their writing. The experience of

creating publicly available blogs may be motivating their learners and encourage to develop the new set of writing strategies.

The second, the most common in the language learning, the teacher can write the main blog entries, which learners can then comment on them. Even teacher can send assignments or projects to students on the taught topics, by which students can complete the work and send back to teachers. It is very easy for the teacher to access the work through the blog and students can rectify their mistakes. So, the blog can encourage teachers to control teaching outside the classroom.

II. Social networking

Social networking websites are started in 2003, and it is the most popular way to network. In July 2006, for instance, a social networking site- MySpace received more hits than Google (Gefer 2006). Other well known social networking sites include Face book, Friendster, Bebo and YouTube. In addition to general social networking sites, there are more specific sites, for instance, mytep allows English language teacher to network. Most social sites have group creation facilities which teachers can use to set up outside class discussion environment (Thelwall 2008) and YouTube and Flicter provide opportunities to improve communication skills as well as language learning. For example, learners can be encouraged to make a video of their presentation and post it in the public domain on YouTube and learners can use sharing sites to find and exchange resources with other learners (Godwin-Jones 2005).

III. Wikis

A wiki is a web based platform for collaborative writing. It is used within a private domain as well as public domain for collaborative. The important feature of wikis is particularly used for language learning which record of all drafts is. This emphasizes and focuses on the writing process as well as written products.

An example of a private wiki used for language learning can be found in Mak et al (forthcoming), who describe a wiki based project to produce a school brochure for parents at a Hong Kong secondary school within the public domain. Learners can be asked to be collaborative as class to produce a Wikipedia entry (McDonald 2007). Such project promotes peer to peer collaboration, increase motivation, empower learners to construct knowledge, and enable progress assessment (Zorko 2007).

IV. Massively Multi- Player Online Games

Game based learning has many faceted benefits motivation, critical thinking, and engagement in learning. Games can be either designed especially for language learning objectives from existing well-known games like the Sims (Purushotam 2005) within the latter paradigm: One of

the most promising approaches involving web 2.0 games, called massively multi player online games or MMPOG.

The first gives a platform for an online game for millions, and second is particularly user created virtual world where user can interact in much the same way with the real world. It is a very difficult task to engage the learner in extensive communication in English outside the classroom, but the games provide large scale opportunities for interaction.

V. Mobile Phone Assisted language learning

Mobile phones are considered as miniature computers because of its additional facilities like texting, gaming, email and recording.

Mobile Phone Assisted language learning covers PDAs, iPods and wireless computing. MPALL applications consist of mini lessons of grammar points, closed ended quizzes or games testing discrete language points available through SMS,

the web or downloads, the vocabulary lessons, short definitions of words with examples of use, recording lectures for better understanding, dictionary, and a communicative language learning games using actions.

The most important features of Mobile Phone Assisted language learning are- social interactivity, context portability, sensitivity, connectivity, individuality and immediacy.

Due to greater opportunities of Computer Assisted Language learning, more and more language learning is likely taking place outside classroom setting.

Digital age language learning:

The powerful information and communication technologies available have opened up new social and educational opportunities, creating new needs and requiring the development of new skills. 'The development of literacy and communication skills in new online media is critical to success in almost all walks of life.' (Shetzer and Warschauer 1999:171)

Digital age language learning, this new concept focuses on the need of adopting new technologies to incorporate digital literacy skills to language curriculum.

Digital age language teachers have four important responsibilities:

1. To know the availability of the online resources and to make language learning effective.
2. Context based selections of the resources according to students group and develops suitable activities that will create opportunities for enhancing both language and digital skills.
3. Need to teach the skills necessary to function in the digital age, including reading and writing digital text and communicating and publishing online.
4. Digital literacy skills are done seamlessly and in an integrated manner so that the language course is a coherent whole rather than a collection of loose components.

Some important characteristics of digital age:

1. Authentic resources and activities.
2. Online books.
3. Collaboration and communication.

4. Hypermedia.
5. Skills of integration.
6. Just in time learning.
7. Knowledge.
8. Language, style, registers.
9. Multimedia.
10. Netiquette.
11. Online tools.
12. Production.
13. Reading.
14. Spell checks.
15. Text manipulation.
16. Web page publication.

Language skills need to be combined with digital skills in order to be useful in the 21st century. Taking in to account both present and future needs of students will result in curricula and teaching that are up to date, interesting motivating and relevant for digital age.

The multimedia language lab:

Multimedia language lab is developed to respond to students for different learning styles. The basic purpose of language lab is to focus on sound, text images, videos, animation and interesting context that can be created and accessed from electronic devices such as computer, mp3 players, cell phones, and iPods. By using multimedia in the classroom, the students can better understand the lessons by cultivating self thinking ability with integration of four skills. Even this is useful for the learner to learn and stimulate retention by recorded classes and presentation.

This tool can develop all four skills of language. Silverman and Hins (2009) found that both English language learners and native speakers who used video clips to illustrate vocabulary items showed greater improvements in vocabulary knowledge than those who did not receive the multimedia instructions. Even students can improve their vocabulary by playing games and puzzles on computer.

1. Writing: On internet, there are many websites where one can get exposure to write article, short stories and poems. Students can write and get responses from peer group of experts for further developments.
2. Listening: By listening recorded talks of experts and native speakers, lectures of eminent persons and English sound track movies such as 'pride and prejudice' 'water lilies' 'ghost and plays of shakespeare's can enhance listening ability and improve their interest in learning. And listen native speaker records and make self correction by listening to the correct responses and learn proper pronunciation, stress and intonation by self control.
3. Speaking: Speaking skills are improved by getting instructions on soft skills and involving oneself in the talk show chart and many more group activities.

Language laboratory has following facilities to enhance learners' skills: online tutorials, teaching materials-audio recording, video recording, computer, LCD, soft skills' teaching software, external web location, games and quizzes, tests, interactive teaching tips for common errors and pronunciation, functional grammar, building vocabulary power & group discussion.

In the present scenario it is time to shed away our post colonial indignation and get into the right track of learning effective language skills.

VI. Audio-visual aids in teaching English

F. M. Noel rightly says, "Good instruction is the foundation of any educational programme. Audio-visual training aids are component parts of that foundation."

Teacher takes help of some instructional aides to teach English more efficiently and successfully. Prof. C.S. Bhandari opines, "Our aim of teaching English is to impart certain skills without making the process of teaching and learning monotonous."

Audio visual aids are effective tools to impart good education. These aids are divided as video, audio and audio-visual aids. Video refers as seeing, audio refers as hearing and audio-visual refers to combination of both.

These aids are CD, DVD, tape recorder, e-book, graphics, pictures, charts and are used to create the requisite interest and motivate the students to learn the language. The main purpose of audio-visual aids is to enable the teachers to make his teaching effective and interesting. Good models are presented before the students to teach effectively. In this way it can be said that audio-visual aids direct sensory experience to the students.

Classification of audio-visual aids:

- Bulletin board
- Flannel board/graphs
- Slides film strips
- Overhead projector
- Tape recorder/gramophone
- Radio
- T.V. / Video

VII. Context Based Approach

Context Based Approach is a substitute to conventional way of teaching grammar in classroom. It is a bridge between knowledge of English grammar and the use of English language in real life communication, instead of memorizing the rules and contextualize them. They can easily differentiate the structure and meaning. By doing so, learners would gradually recognize the right structure for the right context. An elementary exposure to English language and its basic components aims to help the undergraduate students, who are already exposed to the language. Context Based Approach is usage based one, which could be effectively used in CLT. The core objective of the approach is useful in real life communication. The ultimate purpose of the approach is to raise grammatical consciousness, an awareness of the communicative function of grammar, and ability to distinguish between different grammatical systems.

This broad umbrella definition fuses certain techniques of grammar translation method, structural approach to language and communication approach. Like in grammar translation method, students are asked to compare and contrast the meaning of the sentences, like in structural approach, students are asked to identify the right solution for the particular context by group work.

The advantage of using context based approach for teaching grammar is that students would comprehend why a particular rule is applied in a given structure and when best to use that structure in real life context. This would make the students confident of their communication as they would know exactly what they mean by using a particular grammar structure.

The purposed approach would give a boost to communicative approach and help to have command of the language in undergraduate college.

VIII. Conclusion

Due to globalization, English has got the status of global language, world language, and international language. English is a powerful market language and transaction of modernization. The changing scenario of English is impacted on English curriculum and teaching methodologies to cater the need of present era.

References

- [1] Gupta Deepti, 2005. ELT in India: "A Brief and Current overview," Asian EFL Journal Volume 7. Issue 1, Article 12.
- [2] Nunan David (1991) "Communicative tasks and the language curriculum," TESOL, Quarterly 25(2), 279-295.
- [3] Purushotma, R "You're not studying, you're just.....," Language Learning and Technology 9.1 (2005): 80-96.
- [4] Vyas A. Manish and Patel L. Yogesh "Teaching English as a second language- Anew Pedagogy for a New Century," PHI Learning Pvt Ltd. New Delhi (2009).

Author's Biography



G. Padmavathi, Asst.Prof.in Teegala Krishna Reddy Engineering College, M. A. and B.A. from OU Hyderabad. Her area of interest is on ELT and English Lit. Working as Editor for the college News letter and Souvenir.

Treatability Study of Tannery Effluent by Enhanced Primary Treatment

Saritha Banuraman¹, Meikandaan.T.P.²

Bharath Institute of Science and Technology, Bharath University, 173, Agaram Road, Selaiyur,
Chennai-600 073, India

Abstract: This project work has been focused on the study of enhanced primary treatment of tannery effluent by coagulants which includes analysis of physico-chemical parameters of tannery effluent as well as the treatment efficiency of alum, ferric sulphate and their combination (alum + ferric sulphate). Sample collection and analysis were performed using standard methods for the examination of water and wastewater (1998). Tannery effluent has been treated with the coagulants. The influences of pH and coagulant dosages were studied. Conditions were optimized according to the pollutant removal efficiencies measured in terms of reduction in concentration of total suspended solid (TSS), biological oxygen demand (BOD₅), chemical oxygen demand (COD) and Chromium(Cr). The reduced concentration of pollutants have been analyzed with industrial effluent discharge standards to determine the efficiency of coagulants in enhanced primary treatment of tannery effluent.

Keywords: alum, ferric sulphate, total suspended solid (TSS), biological oxygen demand (BOD₅), chemical oxygen demand (COD) and chromium (Cr)

I. Introduction

Industrial wastes are usually generated from different industrial processes, as a result the amount and toxicity of waste released from industrial activities varies with the industrial processes. Again, among all the industrial wastes tannery effluents are ranked as the highest pollutants (Shen, 1999). In developing countries, many industrial units are operating in a small and medium scale. These industrial units can generate a considerable pollution load by discharging untreated effluents directly into the environment.

Over the last few decades large scale usage of chemicals in various human activities has grown very fast, particularly in a country like India which has to go for rapid industrialization in order to sustain over growing large problem of population.

The current pattern of industrial activity alters the natural flow of materials and introduces novel chemicals into the environment. The released organic compounds and heavy metals are one of the key factors that exert negative influences on man and environment causing toxicity to plants and other forms of biotics and abiotics that are continually exposed to potentially toxic heavy metals.

But in recent years, the concentrated growth of this industry in certain localities has shown how the waste from this industry can cause irreversible damage to the water environment in the vicinity. In view of its peculiar pollution potential, and the increasing demand for good quality of water, both for domestic and other industrial purposes, it has become essential to treat the waste to a certain degree prior to its disposal. Tanning industry contributes significantly towards exports, employment generation and occupies an important role in Indian economy on the other hand, tannery wastes are ranked as the highest pollutants among all the industrial wastes. The damage to the environment by the hazardous tannery effluent is becoming an acute problem in the country.

The chrome tanning process results in toxic metals, especially chromium passing to wastewater and are not easily eliminated by ordinary treatment process. Tannery effluents are mainly characterized by high salinity, high organic loading and specific pollutants such as chromium. Various chemicals used in tanning are lime, sodium carbonate, sodium bicarbonate, common salt, sodium sulphate, chrome sulphate, fat liquors, vegetable oils and dyes. The tannery effluent was found to contain higher concentrations of total dissolved solids, chromium, chloride, ammonia, nitrate and sulphates when the samples were collected from the outlets of the industry. Besides these, chemicals such as zinc chloride, mercuric chloride and formaldehyde are used as disinfectants, sodium chloride in curing and as bleaching powder and sodium fluoride to prevent putrefaction, lime in liming, sodium sulphate, ammonium chloride, borax and hydrochloric acid in delimiting, sodium for decreasing and basic or acidic dyes in leather finishing.

Hence, the tannery effluent is always characterized by its strong colour (reddish dull brown), high BOD, high pH, and high dissolved solids. The other major chemical constituents of the waste from the tanning industry are sulphide and chromium. These chemicals mixed with water are discharged from the tanneries and pollute the ground water permanently and make it unfit for drinking, irrigation and general consumption. Therefore there lies an urgent need to determine the pollution levels in the effluent from these industries.

Treatment of tannery effluent is difficult and represents a serious environmental and technological problem due to presence of a series of chemicals with low biodegradability. So the treatment of tannery effluents is a matter of great concern in the country having leather tanning industry. As a result, a number of research work carried out around the world regarding the treatment of tannery effluents using different technology. Several studies have been carried out for the treatment of industrial effluents through coagulation and flocculation process (Shouli et al., 1992).

II. Materials and methods

2.1 Sampling

For the present investigation, the sample was collected at the discharge drain to sedimentation tank of Forward Leathers, Nagalkeni, Chromepet, Chennai. Tannery effluent was collected into plastic bottles which were thoroughly cleaned with nitric acid solution followed by repeated washing with distilled water and dried. After collection, physical appearance and pH were noted and preserved at 4°C. All the pollutant parameters were analyzed following the procedure as per the Standards Methods for the Examination of Water and Wastewater (APHA-AWWA-WPCF, 1998).

2.2 Analysis of physico-chemical parameters

All the pollutant parameters were analyzed following the procedure as per the Standards Methods for the Examination of Water and Wastewater (APHA-AWWA-WPCF, 1998) which is shown in table 2.1.

Table 2.1. Analysis of physico-chemical parameters

S.No.	Parameter	Method of analysis used
1	pH	pH meter
2	Turbidity	Digital Nephelometer
3	Total solids	Gravimetric Method
4	Total dissolved solids	Gravimetric Method
5	Total suspended solids	Gravimetric Method
6	Chlorides	Colorimetric Method
7	Biological oxygen demand	Microbiological Titration Method
8	Chemical oxygen demand	Closed Reflux Colorimetric Method
9	Chromium	Colorimetric Method
10	Weight	High precision balance

2.3 Physical and Chemical parameters of tannery effluent

Physical and chemical parameters of collected tannery effluent were analyzed by the method of analysis shown in table 2.1. And the observed values were tabulated in table 2.2.

Table 2.2 Physical and chemical parameters of tannery effluent

Parameter	Values
Appearance	Brownish
Odor	Objectionable
pH	6.2
Turbidity	207.5 NTU
Total solids	7500 mg/l
Total suspended solids	2550 mg/l
Total dissolved solids	4950 mg/l
Chlorides	1136 mg/l
BOD ₅	3480 mg/l
COD	5479 mg/l
Chromium	67 mg/l

2.4 Primary treatment by chemical coagulation

Coagulation is the process by which colloidal particles and very fine solid suspensions initially present in a wastewater are combined into larger agglomerates that can be separated via sedimentation, flocculation, filtration, centrifugation or other separation methods. Coagulation is commonly achieved by adding different types of chemicals (coagulants) to the wastewater to promote destabilization of the colloid dispersion and agglomeration of the resulting individual colloidal particles.

The addition of some common coagulants to a wastewater not only produces coagulation of colloids but also typically results in the precipitation of soluble compounds that can be present in the wastewater. In addition, coagulation can also produce the removal of particles larger than colloidal particles due to the entrapment of such particles in the flocs formed during coagulation.

2.5 Coagulants used

The coagulants alum, ferric sulphate and combination of alum and ferric sulphate were used for the experiment. Each of this coagulant weighed individually (15 g) and dissolved in the 1 litre of distilled water.

After rigorous mixing, different doses (20 to 110 mg/l) of coagulant solution were taken to treat 1 litre of tannery effluent. Mixed coagulants were added at the same time and at the same ratio.

The jar test is the most widely used method for evaluating and optimizing the flocculation process. This study consists of rapid mixing, slow mixing and sedimentation. The apparatus consists of four beakers to be agitated

simultaneously. Tannery effluent with coagulants are agitated in a flocculator at 100 rpm for 1 minute and then 30 rpm was quickly established for 10 mins. After slow mixing beakers were removed carefully from the flocculator and allowed to settle for 60 minster clear effluent from few mm below level of water was taken out for analysis.

III. Results and discussion

The Jar Test was done with coagulants. The amount of residual pollutant in effluent is measured at the end of each pH experiment (keeping dosage of coagulant constant) and optimum pH is fixed by observing maximum removal of pollutants and with that optimum pH, dosage were varied.

The optimum coagulation pH for alum is obtained by observing maximum percentage of pollutant removal which has been shown in Table 3.1 and figure 3.1.

Table 3.1. Optimum pH for alum

pH	% of removal rate of TSS	% of removal rate of BOD5	% of removal rate of COD	% of removal rate of Chromium
2	42	25	22	34
4	60	36	33	41
6	65	52	49	59
8	76	67	55	77
10	74	64	53	65
12	73	60	52	64

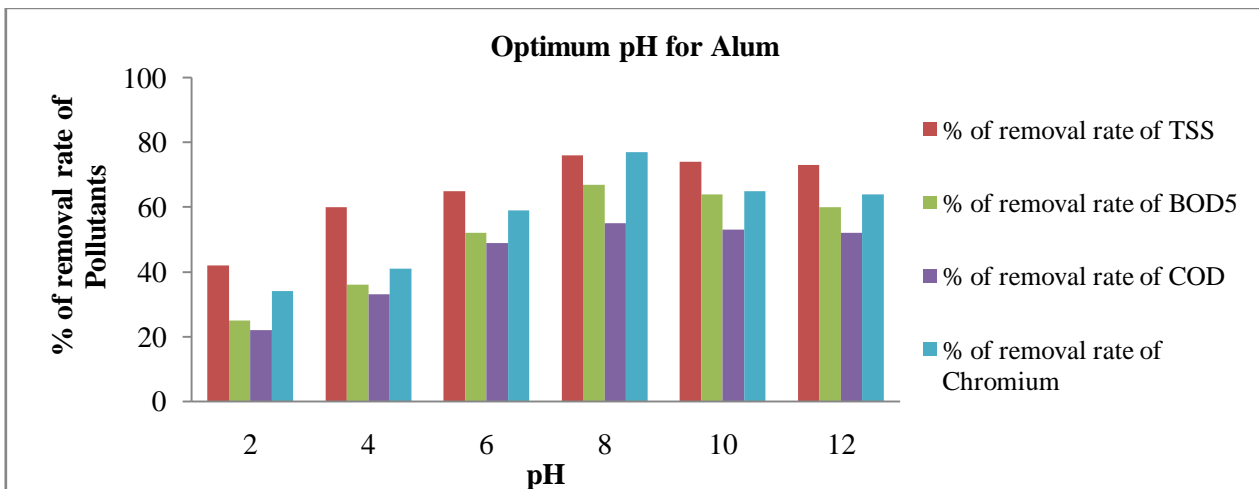


Figure 3.1. Optimum pH for Alum

The efficiency of the coagulants is clearly depicted by comparing the percentage of removal rate of pollutants from tannery effluent which has been shown in table 3.2 and figure 3.2.

Table 3.2. Comparison of % of removal rate of Total Suspended Solids (TSS) by coagulants

Dosage (mg/l)	Removal rate % of TSS of treated tannery effluent using Alum	Removal rate % of TSS of treated tannery effluent using Ferric sulphate	Removal rate % of TSS of treated tannery effluent using (Alum + Ferric sulphate)
20	15	12	28
30	28	25	44
40	32	30	55
50	39	37	62
60	49	47	80
70	76	69	95
80	91	86	95
90	89	87	93
100	88	87	92
110	87	87	88

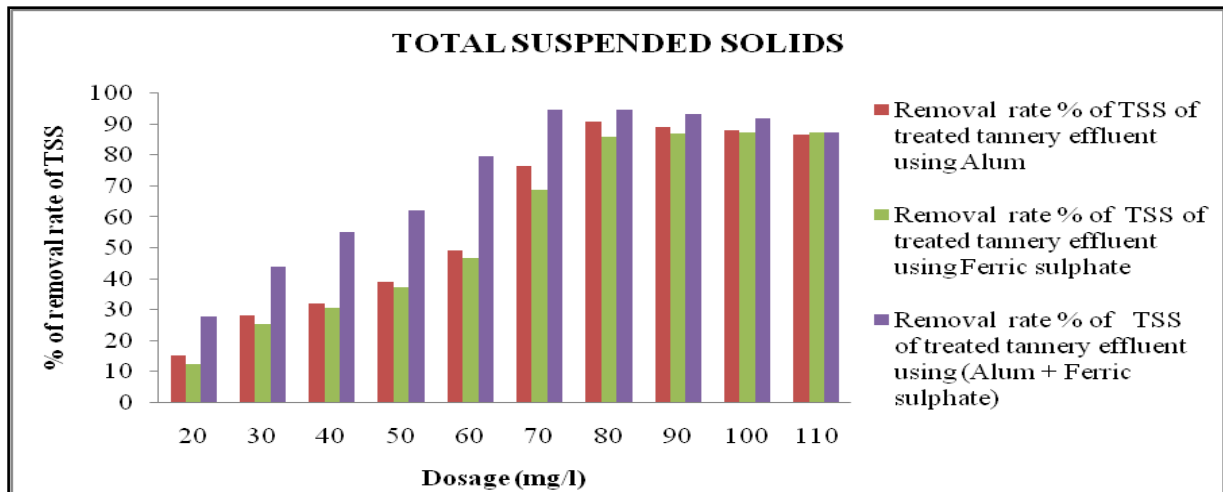


Figure 3.2. Comparison of % of removal rate of TSS by coagulants

IV. Conclusion

The study of tannery effluent by enhanced primary treatment has been carried out. After treatment with coagulants, the concentrations of pollutants were analyzed with industrial effluent discharge standards. From this study following conclusion has been made.

- The coagulants are effective for the treatment of tannery effluents.
- It is observed that pH8 is optimal for better efficiency of alum, ferric sulphate and their combination (alum ferric sulphate) for treatment of the tannery effluent taken for study.
- For alum dosage of 80 mg/l, 91% of TSS, 89% of BOD5, 78% of COD and 90% of Cr has been removed.
- For ferric sulphate dosage of 100 mg/l, 87% of TSS, 82% of BOD5, 71% of COD and 78% of Cr has been removed.
- For alum + ferric sulphate dosage of 70 mg/l, 95% of TSS, 91% of BOD5, 80% of COD and 92% of Cr has been removed.
- At optimum dosage, enhanced primary treatment with alum+ferric sulphate combination is effective for reduction of concentration of pollutants.
- National effluent discharge standards for total suspended solids, biological oxygen demand and chromium were met after enhanced primary treatment. However, COD content was high, emphasizing the need of secondary treatment for the tannery effluent.

Hence, from this study it has been concluded that alum+ferric sulphate coagulant combination is effective for reduction of concentration of pollutants from tannery effluent.

References

- [1] Aboulhassan, M. A. Yaacoubi, A. and Souabi, S. (2007) 'Pollution reduction and biodegradability index improvement of tannery effluents', Int. J. Environ. Sci. Tech., Vol.5, No.1, pp. 11-16.
- [2] APHA-AWWA-WPCF (1998) 'Standard methods for the examination of water and wastewater', 19th Ed., Washington DC.
- [3] Eckenfelder, (1989) 'Industrial water pollution control', pp. 92.
- [4] Haydar, S. Aziz, J.A. and Ahmad, M.S. (2007) 'Biological Treatment of Tannery Wastewater Using Activated Sludge Process', Pak. J. Eng. Appl. Sci., Vol.1, pp. 61-66.
- [5] Lofrano, G. Belgiorno, V. Gallo, M. Raimo, A. and Meriç, S. (2006) 'Toxicity reduction in leather tanning wastewater by improved coagulation flocculation process', Global Nest Journal, Vol. 8, No.2, pp. 151-158.
- [6] Metcalf and Eddy, 'Wastewater Engineering' (4th Ed.)
- [7] Nazmul Islam, K.M. Khaled Misbahuzzaman, Ahemd Kamruzzaman Majumder and Milan Chakrabarty, (2011) 'Efficiency of different coagulants combination for the treatment of tannery effluents - A case study of Bangladesh', African Journal of Environmental Science and Technology, Vol.5, No.6, pp. 409-419.
- [8] Shen, T.T. (1999) 'Industrial pollution prevention' Springer, (2nd Ed.), pp. 40.
- [9] Shouli, A.S. Bewtra, J.K. Biswas, N. (1992) 'Effectiveness of coagulation and flocculation processes in removal of selected volatile organic contaminants from wastewaters', Int. J. Environ. Stud., Vol.40, pp. 2-7.
- [10] Sajjad Haydar, Javed Anwar Aziz (2009) 'Characterization and treatability studies of tannery wastewater using chemically enhanced primary treatment (CEPT)—A case study of Saddiq Leather Works', Journal of Hazardous Materials, Vol. 163, No. 2-3, pp. 1076-1083.
- [11] Sajjad Haydar and Javed Anwar Aziz (2009) 'Coagulation- flocculation studies of tannery wastewater using combination of alum with cationic and anionic polymers', Journal of Hazardous Materials, Vol.68, pp. 1035-1040.
- [12] Song, Z. Williams, C.J. and Edyvean, R.G.J. (2004) 'Treatment of tannery wastewater by chemical coagulation', Desalination, Vol.164, No.3, pp. 249-259.
- [13] Zouboulis, A.I. Samaras, P. and Ntolia, A. (2006) Study of tannery wastewater treatment in a leather industry of the area of Kastoria, 2nd international conference, AQUA - 2006.

Experimental Investigation of IC Engine and Gassifier with Different Biomass Materials

Amit Shrivastava¹, Prof. S. K. Agrawal², Prof. C. S. Koli³

1. M. Tech Student (Thermal System & Design), SRCEM, Banmore

2. Asst.Prof&HOD, Mechanical Engineering, SRCEM, Banmore,

3. Asst.Prof. Mechanical Engineering, SRCEM, Banmore

Abstract: With recent price rise and scarcity of these fuels there has been a trend towards use of alternative energy sources like solar, wind, geothermal etc. However these energy resources have not been able to provide an economically viable solution for agricultural applications. Biomass materials are non-toxic, biodegradable, produced from renewable sources and contribute a minimal amount of net green house gases, such as CO₂, SO₂ and NO emissions to the atmosphere. Need of a suitable biomass material fuel for existing internal combustion engines is being desperately felt these days, when petroleum reserves are soon going to vanish from the surface of earth. Biomass fuel proposes one such option with its suitability as a replacement fuel for existing internal combustion engines, it becomes interesting to know performance of a dedicated IC engine with biodiesel fuel. Up to 50% Biomass material fuel blends in Gasifier can substitute wood without any modification in the engine. Hence, these blends of Vegetable waste may be considered as wood fuel substitutes.

Key Words: Biomass, Gasification, Wood, Vegetables waste

I. Introduction

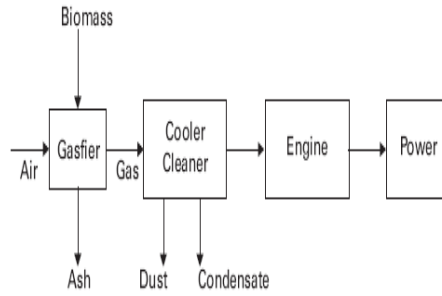
This study is relevant because efficient conversion processes are required for renewable resources in order to compare with fossil fuels. The topic is studied from a fundamental point of view with the help of thermodynamics. This comprises the first law, which states that energy can never be lost, and the second law, which states that the quality of energy will always degrade in irreversible processes. Biomass is thus regarded as a certain amount of work potential (that was previously fixed by photosynthesis), which decreases with every conversion step. The clue is to develop optimised processes, in which the work potential is largely retained, so that a high proportion of useful work is delivered. Gasification is a process that converts organic or fossil based carbonaceous material into carbon monoxide, Hydrogen, carbon dioxide and methane. This is achieved by reacting the material at high temperatures, without combustion, with a controlled amount of oxygen. The resulting gas mixture is called syngas or producer gas and is itself a fuel. Gasification is a method for extracting energy from many different types of organic material.

Vegetable waste pallets

Gasifier Model	Cosmo Cp-10
Mode of Operation (power mode)	Cold & Clean Gas
Gasifier Type	Down Draft
Rated Gas flow	25 m ³ /hr
Average gas calorific value	1000 k cal/m ³
Gasification Temperature	1000-1200 degree centigrade
Ash removal	Manual, once every six hours.
Fuel type & Size	Wood/woody waste with maximum dimension not exceeding 25 mm & 25 mm dia.
Permissible moisture content in Biomass	5-20% (Wet basis)
Biomass charging	Online batch mode, by topping up once every two to four hours
Rated Hourly consumption	Up to 17 kg.
Typical conversion efficiency	> 75%
Typical gas composition	CO- 19%, H ₂ -18%, CO ₂ -10%, CH ₄ - upto 3%, N ₂ -50%
Engine Genset	
Rated output (gross)	11 kWe
Rated output (net)	10 kWe
Specific Biomass Consumption	Less than 1.5 kg/kWhr

Vegetable Waste pellets are a type of fuel, generally made from compacted vegetable waste. The pellets are extremely dense and can be produced with a low humidity content (below 10%) that allows them to be burned with very high combustion efficiency. Pellets are produced by compressing the mixture of vegetable waste, wheat straw and cow dung which has first passed through a hammer mill to provide a uniform dough-like mass. This mass is fed to a press where it is squeezed through a Die having holes of the size required (normally 6 mm diameter, sometimes 8 mm or larger). The high pressure of the press causes the temperature of the vegetable waste to increase greatly.

Gasifier System for Power Generation



Experimental Setup

A downdraft gasifier of capacity 10KWe setup was installed in RGPV Energy Park to produce energy from various biomass materials. A three cylinder four stroke engine was purchased and installed with gasifier in Energy Park of Energy Department RGPV Bhopal to conduct experimental work for testing different biomass material fuels.



Procedure of experimentation

1. First start the water pump to fill water in tank. There should be sufficient water level in tank.
2. Fill the pieces of wood in gasifier chamber.
3. Give ignition to material in downdraft gasifier.
4. Initially the gas is exhausted to atmosphere.
5. Check the quality of gas by ignites a flame over gas.
6. If gas catches fire then take this gas in engine after cleaning.
7. Give self to engine.
8. After starting of engine check current and voltage on ammeter and voltmeter.
9. Give load when all conditions found normal.
10. This process continuously done for various fuels.

Technical Specification of Gasifier

A.C. Generator

Generator is a device which converts mechanical energy to electrical energy. A.C. Generator means Alternator; it consists of a Stator and a Rotor. The stator provides the armature winding whereas rotor provides the rotating magnetic field. When the Rotor is rotated by the prime-mover, the stator winding or conductor is cut by the magnetic flux of the rotor magnetic poles. Hence the EMF is induced in the stator conductors. The emf generated in the stator conductor is taken out from three leads connected to the stator winding.



Rating of Alternator

Rating	15 KVA
Phase	3
Pole	6
Connection	Star
AC Voltage	415V
Current	15A
Rotating speed	1500rpm
Ambient temperature	40 °C
Company name	Crompton Greaves Ltd

Results and Discussion

Repeated experimental work was done by using gasifier and three cylinder four stroke petrol engines and data was recorded. After collection of all data these data are represented in graphs & tables which are shown below

Subabool Wood Observation Table

S.No	Parameter	Value
1.	O ₂	14.5 ppm
2.	CO	2632 ppm
3.	NO	85 ppm
4.	SO ₂	49 ppm
5.	CxHy	4.82 ppm
6.	NOx	87 ppm
7.	Ta (°C)	32.5°C
8.	Tg (°C)	574.1°C
9.	Δt (°C)	541.6°C

Observation Table of Subabool Wood + Vegetable Waste Pallets (50%+50%)

S.No.	Parameter	Value
1.	O ₂	13 ppm
2.	CO	7986 ppm
3.	NO	232 ppm
4.	SO ₂	966 ppm
5.	CxHy	4.72 ppm
6.	NOx	239 ppm
7.	Ta (°C)	34.8°C
8.	Tg (°C)	727.3°C
9.	Δt (°C)	692.4°C

Engine Performance with Subabool Wood

S.No	Voltage	Amp	Frequency	Time	Consumption
1	420V	9A	50Hz	3.30 Hrs	20Kg/hr
2	420V	9A	50 Hz	3 Hrs	20Kg/hr
3	420V	8A	50 Hz	3.30 Hrs	20Kg/hr
4	420V	9A	50 Hz	3.30 Hrs	20Kg/hr
5	420V	10A	50Hz	4 Hrs	20Kg/hr

Engine Performance with Wood+ Pallets

S.No	Voltage	Amp	Frequ ency	Time	Consumptio n
1	420V	10A	50 Hz	4.30 Hrs	22Kg/hr
2	420V	10A	50 Hz	6 Hrs	22Kg/hr
3	420V	11A	50 Hz	6 Hrs	22Kg/hr
4	420V	12A	50 Hz	5 Hrs	22Kg/hr
5	420V	11A	50 Hz	6 Hrs	22Kg/hr

Calorific Value of subool wood=3540 Kcal/kg

Calorific value of vegetable waste pallets=2750 Kcal/kg

Calorific value of 50% Wood and 50% Vegetable Waste pallets= (3540+2750)/2 = 3145 Kcal/Kg

Mass of wood consumed in one hour=20 kg

Mass of wood+pallets consumed in one hour= 22 kg

Power= mass x calorific value

Power input to gasifier with wood

$P= 20 \times 3540 = 70800 \text{ kcal/hour} = 82325.58 \text{ Watts}$

Power input to gasifier with wood+

Vegetable waste pallets (50%+50%)

$P= 22 \times 3145 = 69190 \text{ kcal/hour}$

$= 80453.48 \text{ Watts}$

Flow of gas =21 Nm³/Hour

Average calorific value of gas=1000 Kcal/Nm³

Gasifier output Power= 21 x 1000=21000 Kcal/Hour

$=24418.60 \text{ Watts}$

Efficiency of Gasifier with wood

=Power Output/Power Input

$=24418.60/82325.58$

$=29.66\%$

Efficiency of Gasifier with wood+vegetable Waste Pallets (50%+50%)

= Power Output/Power Input

$=24418.60/80453.48$

$=30.35\%$

Efficiency of engine with wood

Power input to engine= 24418.60 Watts

Specific Biomass Consumption=Power of engine/fuel consumed

Specific Biomass consumption with wood

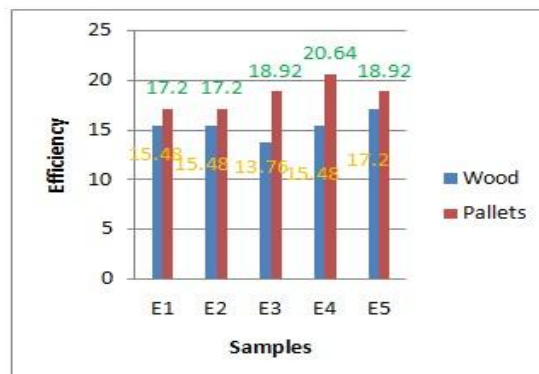
$=3780/19$

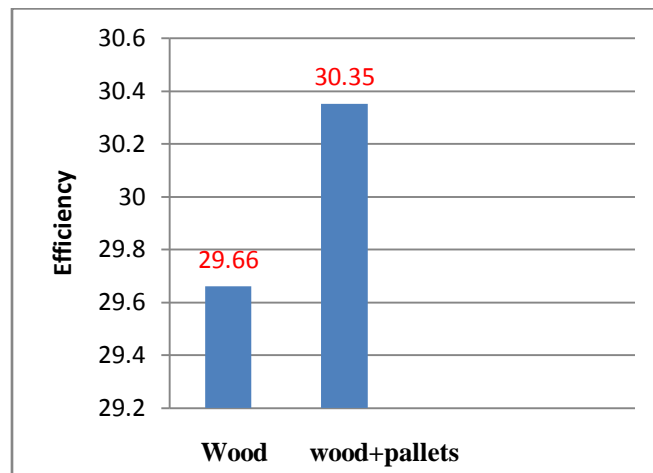
$=198.95 \text{ Watt/Kg}$

Specific Biomass consumption with wood+vegetable Waste Pallets (50%+50%)

$=4536/23$

$=197.22 \text{ Watt/Kg}$





Conclusion

1. The temperature of producer gas with Wood is 574.1°C and with wood + pallets is 727.3°C . This indicates that a wood+pallet is a better fuel than Subabool wood.
2. The efficiency of gasifier with wood is 29.66% and with wood + pallets is 30.35%. This shows that wood+pallets are a better fuel than Subabool wood.
3. Efficiency of engine with wood+vegetable waste is more so we can use vegetable waste with wood as a gasifier fuel.
4. Specific fuel consumption is less when we use wood+vegetable waste as fuel.

Future Scope

1. Analysis of composition of exhaust emission can be done with prolonged service with biomass material.
2. Performance of engine can be compared for various blends of biomass material. Present study is focused only to blend Subabool wood and vegetable waste biomass material.
3. By computation analysis performance parameters can be extrapolated and compared with experimental results.
4. Design changes can be studied and can be proposed after studying the problems encountered after prolonged service of engines with this biomass material fuel.
5. Emission studies can also be done.
6. Content of poisonous gases in producer gas can be reduced.

Social Benefits

1. This improves rural economy and employment through Biomass supply.
2. The plant will also encourage the concept of energy plantation thus resulting in greener environment resulting in more rainfall and reduction in ambient temperature.
3. The costs of installation per kW are about the same as for large power levels (of the order of hundreds of MWs) and the plant load factor is about the same as for large thermal power plants.
4. It improves the country's energy self-reliance and reduces the crippling oil import bill and saves enormous foreign exchange.

References

- [1] Huang Zhigang, Yang Renfa, et al (1981) Discussion on Light-duty Biogas-diesel Dual Fuel Engine, Internal Combustion Engine Engineering 1981, No2, p.64-70.
- [2] K. Sivakumar and N. Krishna Mohan Dept. of Mechanical Engineering, Annamalai University, Annamalai Nagar, Chidambaram-608 002, Tamil Nadu, India.
- [3] David Sutton Centre for Environmental Research, University of Limerick, Limerick, Ireland.
- [4] Wankhade, P.P. Dept. of Mech. Eng., SantGadge Baba Amravati Univ., Amravati, India.
- [5] Zhang Baozhao Xu Yicheng China National Rice Research Institute, Hangzhou, 310006, China.
- [6] G. Sridhar Indian Institute of Science Combustion Gasification and Propulsion Laboratory Bangalore, India.
- [7] Francisco V. Tinaut Department of Energy and Fluid Mechanics Engineering, University of Valladolid, Paseo del Cauce s/n, E-47011 Valladolid, Spain.
- [8] Department of Energy and Mineral Engineering, the Pennsylvania State University, University Park, Pa 16802, USA.
- [9] Chemical Engineering Group, Birla Institute of Technology and Science (BITS), PILANI-333 031, Rajasthan, India.
- [10] R.N. Singh, U. Jena, J.B. Patel, A.M. Sharma Thermo chemical Conversion Division, Sardar Patel Renewable energy Research Institute, Vallabh Vidyanagar, Gujarat 388120, India.
- [11] Reed, T.B. and A. Das, Handbook of Biomass Downdraft Gasifier Engine Systems. 1998: The Biomass Energy Foundation Press.
- [12] Zainal, Z.A., et al., Prediction of performance of a downdraft gasifier using equilibrium modelling for different biomass materials. Energy Conversion and Management, 2001. 42: p. 1499-1515.

- [13] V V N Kishore and C S Sinha. 'Gasifier Systems and Stirling Engines: Status and Prospects in India'. 'In Innovation in the Indian Power Sector: Technologies and Approaches'. L. Srivistava and R K New Delhi, 1991, pp 375-384.Pachauri (Eds), Tata McGraw Hill.
- [14] Heywood J.B (1988) Internal Combustion Engine Fundamentals, McGraw–Hill Book Company, New York. 5. C Wu, B Xu, X Yin and Z Luo. 'The Current State of Rice Hulls.
- [15] C Wu, S Zheng, Z Luo and X Yin. 'The Status and Future of Biomass Gasification and Power Generation System'. China-EU Renewable Energy Technology Conference, Brussels, March 1999.
- [16] Mukunda, H. S., Paul, P. J., Shrinivasa, U. and Rajan, N. K. S., Combustion of Wood Spheres – Experiments and Model Analysis, Proceedings of the 20th Symposium (International) on Combustion, 1984.

Removal of Ash Content from Indian Coal by Using Solvents

Biswajit Saha,¹ Chanchalmondal²

1, 2(Department of chemical engineering, Jadavpur University, West Bengal, India)

ABSTRACT: Coal is most important fossil fuel in world. Energy requirement of world is increasing in many fields day by day. The crude oil and coal are the main backbone of energy. Since the reserves of crude oil are decreasing day by day as a result the coal becomes the main sources of fossil fuel. Ash content of Indian coal is very high ranging from 15% to 55% [1]. Ash is an inorganic compound present into the coal defined as a mass of incombustible material remaining after complete combustion of coal as a percentage of the original mass of the coal. It is mainly due to the presence of silicon-di-oxide, Aluminium oxide, Ferric oxide and Calcium oxide. In this paper, the different experiments have been done using different solvents such as N-Methyl-2-Pyrrolidone (NMP), Furfural, Aniline, Acetic Acid and Toluene with different concentration. Comparative study of different solvents show NMP is the best solvent or extractant with respect to the removal of ash content from coal. The maximum reduction of ash content of coal is 72 % at 120^oC and 1 atmospheric pressure in presence of NMP as an extractant which has high chemical and thermal stability. NMP is recyclable and biodegradable and it is not a hazardous chemical. 65% of NMP was recovered by thermal distillation at 202^oC-206^oC and then using hot air oven remaining part of NMP was removed from mixture of NMP and coal dust.

Keywords: Coal dust, Extractant, Hot Air Oven, NMP (N-Methyl-2-pyrrolidone), Thermal Distillation

I. INTRODUCTION

This century coal is the heart in energy field. Global coal consumption grew by 7.6% in 2010 which is the fastest global energy rate since 2003 [7]. Coal represent at present about 70% of world's proven fossil fuel resources. Moreover coal is also a more delocalized resource; it has lower cost among the different fossil fuel [4]. Coal is classified mainly (a) Anthracite (b) Bituminous (c) Lignite. Among them Bituminous and Lignite has high ash contain.

Table-1: Bulk chemical composition of coal ash [5]

Component	Bituminous	Lignite
SiO ₂	20-60	15-45
Al ₂ O ₃	5-35	10-25
Fe ₂ O ₃	10-40	4-15
CaO	1-12	15-40
MgO	0-5	3-10

Indian coal has high ash content and is to be fallen into Bituminous and lignite category, so it is very poor in quality compare to other countries.

Table-2: Typical ash characteristics [1]

Compound (%)	India	Australia	Canada	S. Africa
SiO ₂	57.0	59.0	53.0	49.0
Al ₂ O ₃	27.0	28.5	30.5	30.1
Fe ₂ O ₃	10.0	3.6	4.8	6.9
CaO	1.7	1.35	3.9	5.5
MgO	0.63	0.75	0.4	1.3
Na ₂ O	0.35	0.65	0.9	0.8
SO ₃	0.56	0.9	2.5	3.6

The main utilization of coal is in power plant, currently 71% on India's electricity is generated from coal [13]. But ash content of coal creates a lot of problems including erosion, difficulty in pulverization, poor emissivity, flame temperature [10, 11] and also efficiency of thermal power station as a result the production cost of electricity is high. The low ash coal can reduce erosion rates by 50-60%, maintenance costs by 35% and increase thermal efficiencies as much as 4-5% [9,8] and also reduces amount of emitted fly ash and hazardous air pollutant precursors, improves health and safety and mitigates environmental degradation [12]. Coal purification process first started in U.S.A., Japan and other European countries [13].

The coal extract knows as solvent refined coal which can be used as such for various purposes or further processed

to obtain syncrudes and host of chemicals [2]. Cleaning of coal mainly divided into two processes (a) Mechanical (b) Chemical [1]. In India many researcher work on removal of ash from coal by various chemical and solvents like (a) Mixture of calcium fluoride and sulphuric acid (b) Anthracene oil (c) Sulphuric acid (d) Hydrochloric acid (e) Sodium Hydroxide (f) Mixture of NMP and Ethylene-di-oxide) [1,2,6,14]. But in this experiment a comparative study on performance to remove the ash content from Indian coal is shown among NMP, Aniline, Furfural, Acetic acid, Toluene as an extractant and recovery process of solvent is conducted by thermal distillation process.

II. MATERIAL AND METHOD

2.1 Preparation of samples

Four types of coal samples have been collected from different mines having different percentages of ash. The samples are leveled A, B, C and D and their ash contents are 4.7%, 26%, 37% and 51.1% respectively. The samples are properly grinded and have been passed through 72 mesh.

2.2 Experimental procedure

Five solvents such as NMP, Furfural, Aniline, Acetic acid and Toluene have been selected based on literature survey to remove ash from coal samples. Initially four samples, leveled A, B, C, and D are mixed with individual solvents in four different containers having same solvent to coal ratio. The coal added solvents has been heated at 120° C where a mechanical stirrer has been used as shown in figure 1 to ensure proper mixing for half an hour. After that the mixture has been sent to thermal distillation unit as shown in figure 2 to recover the solvents. Approximately 65% solvent has been recovered by this process the remaining part of solvent of mixture is removed by drying it in hot air oven and again the ash content of solvent refined coal [12] has been determined using proximate analysis. The same procedure has been repeated taking different solvent to coal ratio.



Fig. 1. Mechanical stirrer with continuous heating system



Fig. 2. Thermal Distillation column setup

III. RESULT AND DISCUSSION

Several experiments have been done using different solvents such as NMP, Aniline, Furfural, Acetic Acid and Toluene with their different concentrations to remove ash content of coal leveled A, B, C, and D.

3.1. Removal of ash of Sample leveled D.

The experimental results have been tabulated as shown in table 1 where first column shows the concentrations of solvents and remaining columns show the removal of ash contents in the respective solvents. These data have been plotted as shown in figure 3

Table : 3.1 Performance of 5 solvents on removal of ash content of sample labeled D

Concentration Coal: Solvent	Percentage removal of ash				
	NMP	Aniline	Furfural	Acetic Acid	Toluene
1:6	8%	6%	5%	1.2%	1.25%
1:10	18%	8%	7%	1.5%	1.55%
1:15	18%	8%	7%	1.5%	1.55%
1:19	18%	8%	7%	1.51%	1.55%
1:20	17.9%	7.9%	6.98%	1.51%	1.55%
1:22	17.9%	7.9%	6.98%	1.51%	1.56%

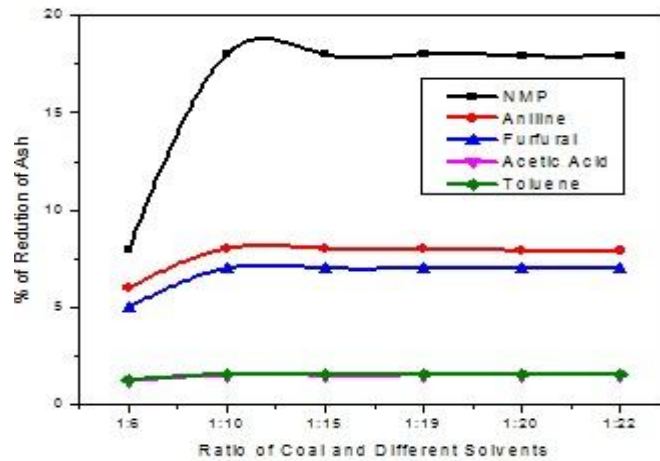


Fig. 3:- performance curve of different solvents on removal of ash of sample labeled D

It is evident from figure3 that NMP has a highest capacity to remove the ash compare to other four solvents. Reduction of ash is increased in case of NMP with increase of solvent concentration at a certain level . After that reduction of ash content is start to decrease with increase of solvent concentration. Maximum reduction of ash is found 18% with 1:10 concentration of NMP. The same trend is followed in case of Aniline and Furfural. But reduction of ash content is 8 & 7% respectively when the coal and solvent ratio is 1:10. It is clear from the figures that Acetic acid and Toluene show the same characteristics for the removal of ash from coal. The maximum reductions of ash are ranges from 1.50% to 1.55% and it is also almost constant at any concentrations of those solvents.

3.2. Removal of ash of Sample leveled C

The experimental results have been tabulated as shown in table 2 where first column shows the concentrations of solvents and remaining columns show the removal of ash contents in the respective solvents. These data have been plotted as shown in figure 4

Concentration Coal: Solvent	Percentage removal of ash				
	NMP	Aniline	Furfural	Acetic Acid	Toluene
1:6	3.5%	5.4%	5%	1.5%	1.30%
1:10	5.4%	6.75%	6.4%	1.86%	1.55%
1:20	11%	8.1%	7.5%	1.86%	1.55%
1:30	13.5%	11.35%	10.8%	1.86%	1.55%
1:40	20%	19%	19%	1.86%	1.54%
1:45	20%	19%	19%	1.85%	1.54%

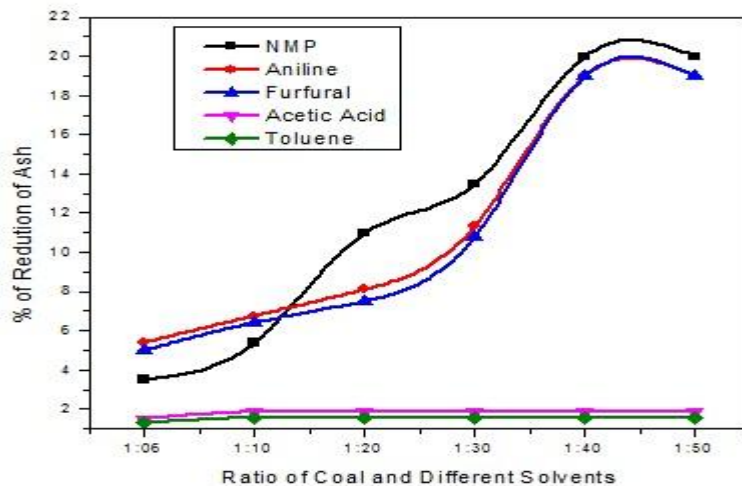


Fig. 4:- :- performance curve of different solvents on removal of ash of sample labeled C

It is evident from figure4 that, reduction of ash is increased in case of NMP with increase of solvent concentration at a certain level. After that reduction of ash content is start to decrease with increase of solvent concentration. Maximum reduction of ash is found 20% with 1:40 concentration of NMP. The same trend is followed in case of Aniline and Furfural.

But reduction of ash content is 19% both when the coal and solvent ratio is 1:40. It is clear from the figures that Acetic acid and Toluene show the same characteristics for the removal of ash from coal. The maximum reductions of ash are ranges from 1.55% to 1.86% and it is also almost constant at any concentrations of those solvents.

3.3. Removal of ash of Sample leveled B

The experimental results have been tabulated as shown in table 3 where first column shows the concentrations of solvents and remaining columns show the removal of ash contents in the respective solvents. These data have been plotted as shown in figure 5

Concentration Coal: Solvent	Percentage removal of ash				
	NMP	Aniline	Furfural	Acetic Acid	Toluene
1:6	9.6%	7.7%	7.4%	1.7%	1.67%
1:10	26%	14.7%	15%	1.8%	1.9%
1:20	26%	19%	18.5%	1.8%	1.9%
1:30	26%	19%	18.5%	1.8%	1.9%
1:40	25.96%	19%	18%	1.78%	1.89%
1:50	25.96%	18.9%	18%	1.79%	1.88%

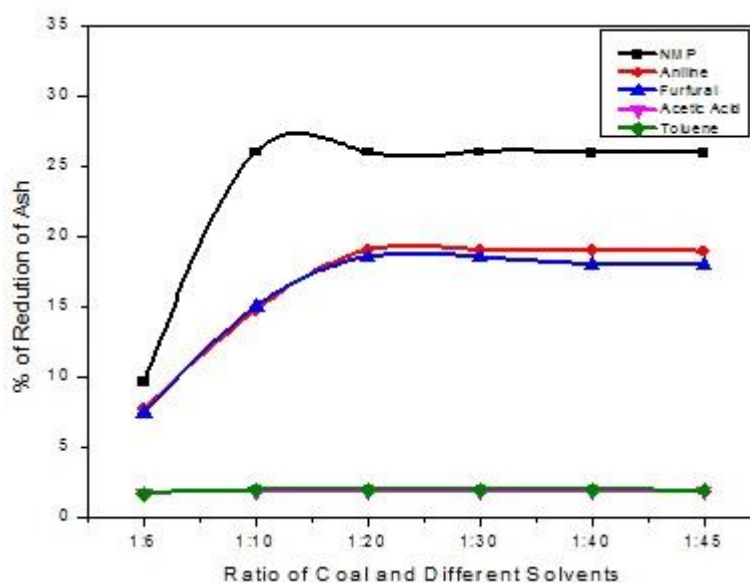


Fig. 5:- :- performance curve of different solvents on removal of ash of sample labeled B

It is evident from figure5 that NMP has a highest capacity to remove the ash compare to other four solvents. Reduction of ash is increased in case of NMP with increase of solvent concentration at a certain level . After that reduction of ash content is start to decrease with increase of solvent concentration. Maximum reduction of ash is found 26% with 1:10 concentration of NMP. The same trend is followed in case of Aniline and Furfural. But reduction of ash content is 14.7 & 15% respectively when the coal and solvent ratio is 1:10. It is clear from the figures that Acetic acid and Toluene show the same characteristics for the removal of ash from coal. The maximum reductions of ash are ranges from 1.8% to 1.9% and it is also almost constant at any concentrations of those solvents.

3.4. Removal of ash of Sample leveled A

The experimental results have been tabulated as shown in table 4 where first column shows the concentrations of solvents and remaining columns show the removal of ash contents in the respective solvents. These data have been plotted as shown in figure 6.

Concentration Coal: Solvent	Percentage removal of ash				
	NMP	Aniline	Furfural	Acetic Acid	Toluene
1:6	23.4%	25%	23%	1.75%	1.6%
1:10	72.34%	70.6%	64.46%	1.8%	1.8%
1:20	72.34%	71%	69%	1.8%	1.8%
1:30	72.34%	71%	69%	1.8%	1.8%
1:40	72.34%	69.9%	68.9%	1.79%	1.78%
1:50	72%	69.9%	68.5%	1.78%	1.79%

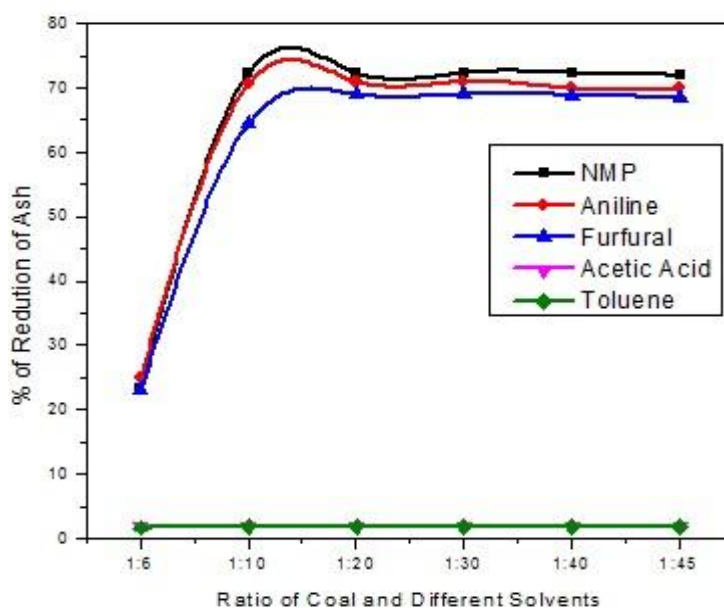


Fig. 6:- :- performance curve of different solvents on removal of ash of sample labeled A

It is evident from figure6 that NMP has a highest capacity to remove the ash compare to other four solvents. Reduction of ash is increased in case of NMP with increase of solvent concentration at a certain level . After that reduction of ash content is start to decrease with increase of solvent concentration. Maximum reduction of ash is found 72.34% with 1:10 concentration of NMP. The same trend is followed in case of Aniline and Furfural. But reduction of ash content is 70.6 & 64.46% respectively when the coal and solvent ratio is 1:10. It is clear from the figures that Acetic acid and Toluene show the same characteristics for the removal of ash from coal. The maximum reductions of ash is ranges between 1.75-1.8% it is also almost constant at any concentrations of those solvents

IV. CONCLUSION

This study shows that NMP is the best solvent to remove ash from coal compare to other four solvents such as Aniline, furfural, Acetic Acid and Toluene. Highest ash removal by NMP is 72.34% when coal and solvent ratio is 1:10. But there is a limitation to increase the concentration of NMP. Experimental result shows that after a certain value of concentration of NMP the ash removal is constant and there is no change in ash removal further increasing the concentration of NMP. So the value of this concentration where the removal of ash is constant is called critical concentration. Every solvent has its own critical concentration.

V. ACKNOWLEDGEMENTS

I greatly thankful to chemical engineering department of Jadavpur University for allocation this valuable project to me and help me by giving financial assistantship for done this project.

I also thank my project guide Dr. ChanchalMondal who gave me his valuable instruction for done this project very smoothly.

REFERENCES

Journal Papers:

- [1] Choudhury, R., Bhaktavatsalam, A.K , 1995 “Benification of Indian Coal by Chemical Technique” , Energy Converse anagement” , 38(2): 173-178
- [2] Choudhury, S.B., Brahmachari, B.B., Dwivedi S.R., Roy, A.K., Dasgupta, P.K., Chakra borty, M. Haque, R., 1996 “Solvent-refined coal from high ash non-coking coal &washery middling for use in metallurgical coke making part-1. Production, testing & characterisation”, Fuel processing technology, 47:203-213
- [3] Sato,Y., Kushiyama, S., Tatsumoto, K., Yamaguchi, H., 2004 “Up grading of low rank coal with solvent”, Fuel processing Technology, 85(14):1551-1564
- [4] Franco,A., Diaz, A.R., 2009 “The future challenges for “clean coal technology”: joining efficiency increase & pollutant emission control”, Energy, 34(3):348-354
- [5] Ahmaruzzaman, M., 2010 “A review on the utilization fly ash”, Process in energy and combustion science, 36(3): 327-363 4
- [6] Shivaprasad, K.H., Nagabhushana, M.M., Venkataiah, C., 2010 “Reduction of ash content in Raw coal using acid & alkali”, E-journal of Chemistry, 7(4):1254-1257
- [7] Liang, X.,Wang Z., Zhou, Z., Huang, Z., Zhou, J., Cen, K., 2013 “Up to date life cycle assessment & comparison study of clean coal power generation technology in China”, Journal of cleaner production, 39:24-31

Books:

- [8] “Impact of Coal Quality and Coal Beneficiation on Utility Boiler”, 2005 Coal Preparation Directory and Handbook, Copyright Coal Age and Coal Preparation Society of America. p23-33

Theses:

- [9] Hatt, R, 1997 ,“Washed Coal From a Utilization Perspective”, World Coal

Proceedings Papers:

- [10] Bickelhaupt, R. E. , 1979 ,“ A Technique for Predicting Fly Ash Resistivity” , The International Conference on Electrostatic Precipitation (ICESP X), pp. 1-10
- [11] Hatt, R., 1995, “Correlating the Slagging of a Utility Boiler with Coal Characteristics” Engineering Foundation Conference, Waterville Valley , New Hampshire, USA, pp-16-22
- [12] Annual report “Improving Efficiency of Coal Fired Plants in Developing Countries”, 2002-2003, Russia, International Energy Agency, (available online at :www.iea.org/media/workshops/2011/platformrussia/Fernandez.pdf)
- [13] “World Energy Investment Outlook-2003 Insights”, 2006, International Energy Agency, pg 319-323 (available online at : <http://www.worldenergyoutlook.org/media/weowebiste/2008-1994/weo2003.pdf>)
- [14] Meena, N.K., Singh, V.K., Golder, A.K., Chandaliya, V.K., Biswas, P.P., Das, C., 2010 “Improvent of coal properties using organic solvent”, CHEMCON-2010

A User-Friendly Image Sharing Scheme Using JPEG-LS Prediction and LSB Matching Function

Hung P. VO

Department of Engineering and Technology, Tra Vinh University, No. 126 National Road 53, Tra Vinh City, Tra Vinh Province, Viet Nam

Abstract: User-friendly secret sharing encrypts a secret image into n meaningful image shares or shadows first proposed by Thien and Lin in 2003. Their scheme can achieve the goal of secret image sharing with the additional capabilities of simple visual-management of shadows owing to representing of shadow images as shrunken version of the original image. After that, Yang *et al.* proposed an improved scheme in 2007 by using different primes for various blocks in Shamir's polynomial function. In this article, we propose a novel version of (t, n) -threshold user-friendly image sharing scheme which attempts to indicate prime number for encoding a t -pixel block based on JPEG-LS prediction technique and utilize LSB matching function to hide indicators of the prime numbers. The simulator presents that the proposed scheme attains the properties of user-friendly image sharing. In particular, reconstructed image is higher than that of the previous schemes in terms of the quality of image.

Keywords: image sharing, secret sharing, secret image sharing, user-friendly shadow

I. INTRODUCTION

With the advent of high-speed network infrastructure as well as low-cost computing and networking hardware, handling and processing digital information by computers and sharing them over internet has become more and more popular. Since communication via internet is considered insecurely communicated environment, demands for shielding communicated information is compulsory and necessary. So, security of digital data is an important issue in the design of communication systems. Data hiding techniques and secret sharing are used to secure confidentiality information while it is transmitted through unsecured communication channels. Unlike data hiding technique which provides a way of security for digital image data by embedding secret message in preselected meaningful images, called camouflage images [1-3].

However, the common weak point of them is that secret image is protected in a single information carrier. Once the carrier is damaged or destroyed, the secret image is lost. Differing from aforementioned methods, secret image sharing method provides protocol in which a dealer distributes secret data among a set of participants and only the number of the participants is important for recovering the secret information in the reconstructed phase. This mechanism is not only fault tolerance, but also fast transmission [6, 7]; such scheme is called a threshold secret sharing scheme.

The concept of secret sharing scheme was introduced in 1979 by Shamir [4], called the (t, n) -threshold scheme. Shamir's scheme is based on polynomial interpolation and the polynomial sharing function of degree $t-1$ is defined as $S(x) = s + a_1x + \dots + a_{t-1}x^{t-1} \pmod p$ to encode a secret number s into n shadows (denoted s_1, s_2, \dots, s_n), where p is the large prime number selected randomly and coefficients a_1, a_2, \dots, a_{t-1} are random numbers within $[0, p-1]$.

1.1. The shares s_1, s_2, \dots, s_n are produced as $s_i = S(x_i)$, for all $1 \leq i \leq n$, where x_1, x_2, \dots, x_n are pair distinct random values.

1.2. Given any t pairs $(x_i, s_i)_{i=1}^t$, the secret s can be derived using Lagrange's interpolation formula as

$$S(x) = \sum_{i=1}^t (s_i \times \prod_{j=1, j \neq i}^t \frac{x - x_j}{x_i - x_j}). \quad (1)$$

In 2002, Thien and Lin [6] extended the secret sharing scheme from number system to image system, and this is called (t, n) -threshold secret image sharing scheme. In the scheme, coefficients (s, a_1, \dots, a_{t-1}) of the Shamir's polynomial are considered as pixel values and the modulus p used in the function is set to 251. A secret image is encoded into n meaningless shadow images and distributed to n involved participants. The secret image may be only reconstructed without cooperation of at least a group of t authorized participants. Any number of shadows less than t cannot be used to reveal the secret image.

However, from the view point of security, the system may still expose the secret information to attackers since it is known that the shares are the noise-like shadow images which may attract malicious user's attention. To conquer this shortcoming, recently, many proposed secret image sharing with steganography schemes have been introduced which construct n pairs of secret shadows. The produced shadows then are embedded into cover images to generate n camouflage images [8-13]. These camouflage images look like cover images and do not draw attacker's attention while transmitted to involved participants via Internet. The constraint of above-mentioned schemes is that the size of cover image is more larger than that of shadow, so it is commonly not suitable for saved-bandwidth network applications. Besides, although the shadow images are no longer noise-like but it is still difficult to manage secret image from the view of image management.

Therefore, some recent literature has been devised to overcome the above weaknesses [14, 15]. In 2002, Thien and Lin [14] proposed an image-sharing mechanism with user-friendly shadow images. Consequently, the generated shadow images are like the reduction version of the original secret image. In 2007, Yang *et al.* [15] enhanced and extended the scheme based on $(t-1)$ -degree polynomial functions with different primes in encoding blocks. However, quality of the reconstructed images is still inferior, making them infeasible for medical, military, or artistic applications [11, 16-17].

This article presents a novel version of (t, n) user-friendly sharing scheme, capable of producing portrait-looking shadow images yet still having properties of a secretimage sharing. Particularly, each shadow image contains a slight amount of information from the original image, in which the contents of the shadow play the identification rather than restore the original secret image. Herein, the concept of Yang *et al.*'s image sharing using polynomial with different primes is used to ensure that each shadow image is a user-friendly share. However, the proposed scheme sets different prime numbers for encoding different blocks by using the JPEG-LS prediction technique [18-21]. Moreover, to prevent the original image degradation, LSB matching function [22] is utilized to hide indicators of the prime numbers.

The rest of this paper is organized as follows. Section 2 briefly reviews pertinent literature. Section 3 then describes the proposed scheme in detail. Section 4 summarizes the experimental results and discussions. Conclusions are finally drawn in Section 5.

II. RELATED WORKS

In this section, we briefly review the related techniques including the concept of JPEG-LS prediction, using LSB matching function for hiding indicators of the prime numbers and Yang *et al.*'s scheme in Subsections 2.1, 2.2 and 2.3, respectively.

2.1 JPEG-LS Prediction Technique

JPEG-LS technique [18-21] is the latest standard for lossless and near lossless image compression, abbreviated form of Joint Photographic Experts Group-Lossless Standard. The core algorithm behind JPEG-LS was developed by Hewlett Packard in 1990s, called Low Complexity Lossless Compression for Images (LOCO-I) [18]. The detailed design of the algorithm can be summarized in Equation (2) depending on the predictive template shown in Figure 1.

$$X = \begin{cases} \min(A, B) & \text{if } C \geq \max(A, B) \\ \max(A, B) & \text{if } C \leq \min(A, B) \\ A + B - C & \text{otherwise} \end{cases} \quad (2)$$

where $\min(A, B)$ and $\max(A, B)$ stand for the minimum and maximum values among pixels A and B , respectively.

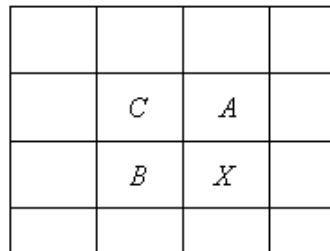


Figure 1. JPEG-LS predictive template

According to the Equation (2), predicted value X in Figure 1 will be A (B) when there is a vertical (horizontal) edge detection of the current pixel location X shown in Figure 2; or X will be $A + B - C$ when the neighboring pixels have comparable values.

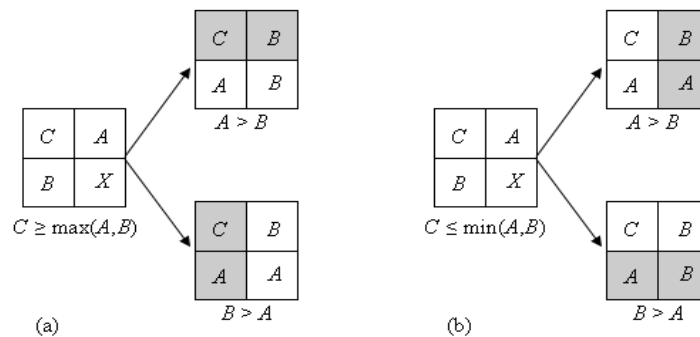


Figure 2. Edge detection flowcharts (a) $C \geq \max(A, B)$; (b) $C \leq \min(A, B)$

2.2 LSB Matching Function for data hiding

Unlike conventional LSB substitution, where secret message is embedded into cover image by replacing the LSBs of the cover image with message bits, LSB matching [22] does not simply replace the LSBs of the cover image with secret message bits. In 2009, Chan proposed LSB matching function for data hiding [23]. By adopting a one-dimension approach instead of two-dimension approach of the image, the LSBs of a sequence of image pixels are computed by XOR function (XF) defined in Equation (3) to be compatible with the message bits.

$$XF(y_i) = LSB\left(\left\lfloor \frac{y_{i-1}}{2} \right\rfloor\right) \oplus LSB(y_i), \quad (3)$$

Where y_i, y_{i-1} are pixel values at the location i and $i-1$, respectively. The operator \oplus is an exclusive OR operator and $LSB(.)$ is the least-significant-bit function. The LSBs compatible algorithm of sequential pixels with message bits is presented in Figure 3.

Input: Assume y_i, y_{i+1} are the values at the position $i, i+1$ in the sequential pixels and s_i, s_{i+1} are the secret message bits, respectively.

Output: y'_i, y'_{i+1} are stego pixels at the position i and $i+1$, respectively.

```

if  $LSB(y_i) \neq s_i$ 
{
     $y'_{i+1} = y_{i+1}$ 
    if  $XF(y'_{i+1}) = s_{i+1}$ 
         $y'_i = y_i - LSB(y_i) + \overline{LSB(y_i)}$ 
    else
        if  $LSB\left(\left\lfloor \frac{y_i-1}{2} \right\rfloor\right) = LSB\left(\left\lfloor \frac{y_i}{2} \right\rfloor\right)$ 
             $y'_i = y_i + 1$ 
        else
             $y'_i = y_i - 1$ 
}
    
```

Figure 3. Matching algorithm for pixel and message bit

2.3 Yang et al.'s user-friendly image sharing scheme

In their basic $(2, n)$ user-friendly image sharing using polynomials with different primes [15], the secret image is first divided into 2-pixel non-overlapping blocks. Then the dealer D choose a set of four primes $\{p_1, p_2, p_3, p_4\}$ satisfied by $p_1 < p_2 < p_3 < p_4 \leq 251$. In the sharing phase, each block of the secret image is encoded into shadows based on Shamir's polynomial function with different prime numbers. The prime number used to encode a block is determined according to the maximum distance in pixels of block with the last pixel in the previous block. For example, (P_{n-2}, P_{n-1}) and (P_n, P_{n+1}) are the previous and current two-pixel blocks, respectively. The pixel P_{\max} leading to the maximum distance from the current block to the previous block is defined as in (4):

$$P_{\max} = \begin{cases} P_n & \text{if } |P_n - P_{n-1}| > |P_{n+1} - P_{n-1}| \\ P_{n+1} & \text{otherwise} \end{cases} \quad (4)$$

The prime number is then determined according to P_{\max} . Additionally, the prime number for encoding the block needs to remember which is used to decode the block in the recovering phase. In each two-pixel block, the LSBs are adjusted as (00), (01), (10) or (11) to indicate the prime number p_1, p_2, p_3 , or p_4 , respectively, used in decoding the next block. The LSB of each pixel in the previous block is modified as follows:

$$\begin{cases} LSB(P_{n-2}) = 0, LSB(P_{n-1}) = 0 & \text{for } |P_{\max} - P_{n-1}| \leq (p_1 - 1)/2 \\ LSB(P_{n-2}) = 0, LSB(P_{n-1}) = 1 & \text{for } (p_1 - 1)/2 < |P_{\max} - P_{n-1}| \leq (p_2 - 1)/2 \\ LSB(P_{n-2}) = 1, LSB(P_{n-1}) = 0 & \text{for } (p_2 - 1)/2 < |P_{\max} - P_{n-1}| \leq (p_3 - 1)/2 \\ LSB(P_{n-2}) = 1, LSB(P_{n-1}) = 1 & \text{for } (p_3 - 1)/2 < |P_{\max} - P_{n-1}| \leq 250 \end{cases} \quad (5)$$

Subsequently, Shamir's polynomial function rewritten as in Equation (6) is applied on the current block.

$$S(x) = (a_0 + x \times a_1) \bmod p_j \quad \text{for } j = 1, 2, 3, 4, \quad (6)$$

Where the prime number p_j is determined by Equation (5), and the coefficients a_0 and a_1 are computed as follows:

$$\begin{cases} a_0 = (P_n - P_{n-1}) + (p_j - 1)/2 \\ a_1 = (P_{n+1} - P_{n-1}) + (p_j - 1)/2 \end{cases} \quad \text{for } j = 1, 2, 3, \quad (7)$$

$$\begin{cases} a_0 = \lfloor (P_n - P_{n-1})/2 \rfloor + (p_j - 1)/2 \\ a_1 = \lfloor (P_{n+1} - P_{n-1})/2 \rfloor + (p_j - 1)/2 \end{cases} \quad \text{for } j = 3. \quad (8)$$

Finally, shadow pixels \hat{P}_i ($1 \leq i \leq n$) can be found by locating the value that are closest to the average value of pixels in the current block, but also satisfy the constraint $\hat{P}_i \bmod p_j = s_i$.

The recovering procedure starts by determining the prime number from the previously recovered block and shadow pixels. Then, using Lagrange interpolation recovers coefficients a_0 and a_1 . After that, the original pixels P_n and P_{n+1} are restored through Equation (7) and (8).

III. PROPOSED SCHEME

Details of the proposed scheme are given in this section. There are two phases: Sharing and retrieving phase.

1.3. Sharing phase

Sharing phase consists of four sub-procedures that may be summarized as in Figure 4. Classification of primes is the first procedure used to identify prime number for encoding a block. Indications of primes are embedded in secret image on using LSB matching function in the second procedure. Modified secret image is partitioned into shadows by sharing algorithm which is presented in the third procedure. Because Shamir's secret sharing method is employed, shadows look like noisy images. Thus, to produce user-friendly share images, an association between the shadow value and the corresponding average value of block is executed in the fourth procedure.

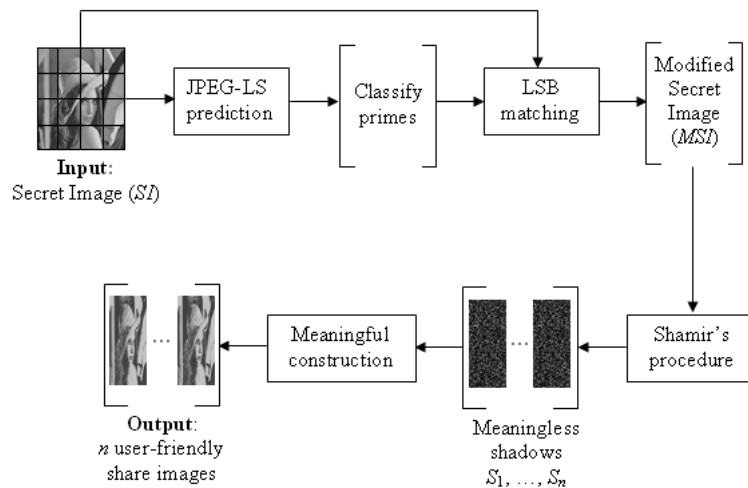


Figure 4. Flowchart of the sharing phase

1.3.1. Classification of primes procedure

To share an secret image (SI) size of ($M \times N$) pixels by using the proposed user-friendly (t, n)-threshold sharing system with various prime numbers, The dealer D first selects 2^t prime numbers (denoted as p_1, p_2, \dots, p_{2^t}) such that $p_1 < p_2 < \dots < p_{2^t} \leq 251$. These prime numbers used in encoding t -pixel non-overlapping blocks are classified according to the maximum distance of block in pixels. In contrast to scheme in [15], the proposed scheme uses the JPEG-LS prediction technique [18] to predict value of each pixel depending on the predictive pattern of pixels as in Figure 1 and Equation (2). By combining the predicted values and the current pixel value, the maximum distance of the m -th block (denoted as d_m) is defined as in (9):

$$d_m = \max(|P_m^i - X_m^i|) \quad \text{for } i = 1, 2, \dots, t, \quad (9)$$

Where P_m^i is the pixel value at the position i -th in the m -th block; X_m^i is the predicted value of pixel P_m^i . Next, the procedure is continued by identifying the prime number for block. The criterion to determine prime number for the m -th block, called p_m , is defined as follows:

$$p_m = \begin{cases} p_1 & \text{if } d_m < (p_1 - 3) / 2, \\ p_i & \text{if } (p_{i-1} - 3) / 2 \leq d_m < (p_i - 3) / 2, \text{ and } 2 \leq i < 2^t, \\ p_{2^t} & \text{otherwise.} \end{cases} \quad (10)$$

This example demonstrates the procedure, in which a (2, 4)-threshold scheme with four (2^2) chosen primes $\{p_1, p_2, p_3, p_4\} = \{17, 61, 131, 251\}$. A secret image SI and its predicted values are shown in Figure 5.

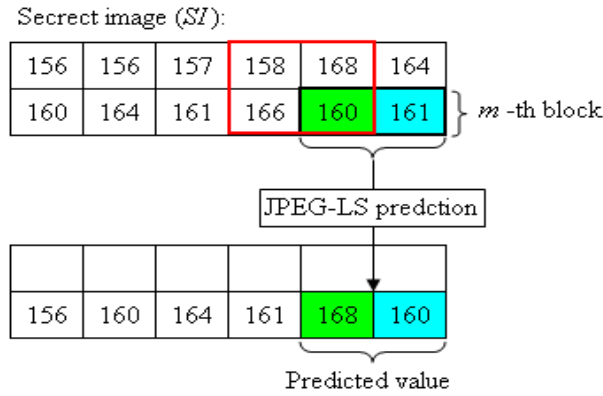


Figure 5. An example of a secret image SI and its predicted value

According to the Figure 5 and Equation (9), value d_m is computed ($d_m = \max (|160-168|, |161-160|) = 8$). Following the Equation (10), the prime number in encoding m -th block is determined ($p_m = p_2 = 61$).

1.3.2. Embedding the prime indicators procedure

Since Shamir’s framework is used in the second phase (recovering phase), the prime numbers necessitate to remember for later use. The prime number is encoded as $\{(0\dots00), (0\dots01)\dots \text{ or } (1\dots11)\}$ to indicate the prime numbers $\{p_1, p_2\dots \text{ or } p_{2^t}\}$. Other word, the indicator id_m of prime p_m is defined as Equation (11):

$$id_m = \begin{cases} (0\dots00) & \text{for } p_m = p_1 \\ (0\dots01) & \text{for } p_m = p_2 \\ \vdots \\ (1\dots11) & \text{for } p_m = p_{2^t} \end{cases} \quad (11)$$

This procedure would be continued by implementing the embedding indicators of primes into SI based on using LSB matching function [23], with the result that a matched secret image (MSI) is generated. In that, the LSBs of pixels in block indicate the prime number which is used in decoding the next block in the recovering phase. In other word, LSBs of pixels in the previous block of m -th block are compatible with the indicators of the prime number p_m . The matching procedure treat prime indications of block as a sequence bits and consider SI as one-dimensional rather than two-dimensional array. The flow chart of matching procedure in (t, n) -threshold proposed scheme is shown as in Figure 6.

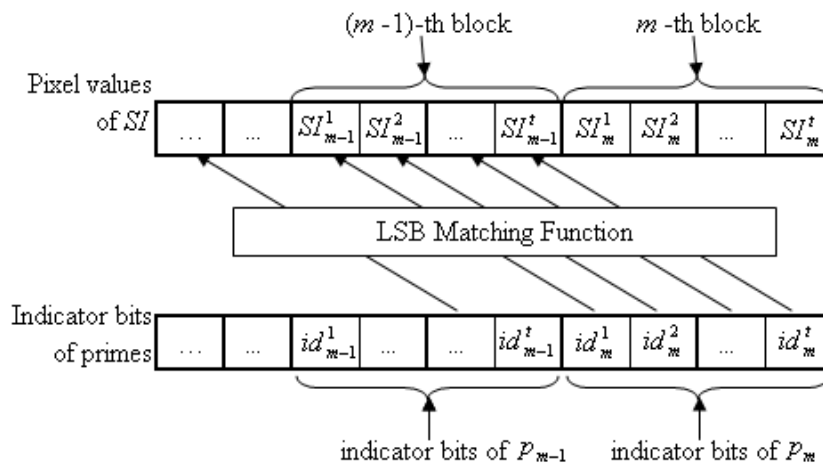


Figure 6. The flow chart of matching procedure in (t, n) -threshold system

The following example performs the effectiveness of the embedding procedure. As aforementioned, the prime numbers are longer used in the retrieving phase, the indicators of the prime $p_m = 61$ ($id_m = 01$) are embedded into the SI using XOR function. The process of embedding procedure is shown in Figure 7. The indicator bits ($id_m^1 = 0$ and $id_m^2 = 1$) of prime p_m are matched with the LSBs of two pixels in the previous block of m -th block, respectively.

As can be seen in the Figure 7, the values of $XF(MSI_{m-1}^1)$ and $XF(MSI_{m-1}^2)$ are not equal to id_m^1 and id_m^2 , respectively. And according to the pseudo-code shown in Figure 3, the pixel value MSI_{m-1}^2 is set as SI_{m-1}^2 , the pixel value MSI_{m-1}^1 is set as $SI_{m-1}^1 + 1$. Generally, in this case, if the conventional LSB replacement method is applied, there are two pixel values in SI are modified. In contrast, there is only one pixel in SI is adjusted in this method.

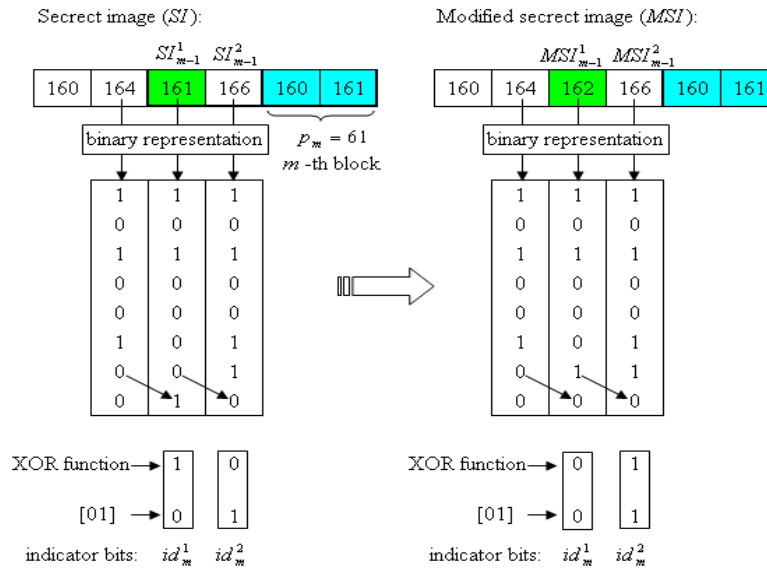


Figure 7. Embedding procedure

1.3.3. Partitioning procedure

Applying the Shamir's polynomial function of degree $(t-1)$, the procedure divides MSI into non-overlapping blocks, each of which contains t pixels. Unlike in the original polynomial, coefficients a_1, a_2, \dots, a_{t-1} are random numbers, the process of partitioning m -th block starts by computing the coefficients through the equation as follows:

$$\begin{cases} f_i = (MSI_m^i - PMSI_m^i) + (p_m - 1)/2 & \text{if } p_m \neq p_2', \text{ (for } 1 \leq i \leq t), \\ f_i = \lfloor (MSI_m^i - PMSI_m^i) / 2 \rfloor + (p_m - 1)/2 & \text{otherwise.} \end{cases} \quad (12)$$

where $PMSI_m^i$ is predicted value of i -th pixel MSI_m^i in m -th block. It means that the JPEG-LS prediction technique is one more time adopted on the MSI image. Then the coefficients f_i play as input values of the function:

$$S_m(x) = \sum_{i=1}^t f_i x^{i-1} \text{ mod } p_m \quad (13)$$

Now, n input values x_j ($1 \leq j \leq n$) are chosen freely and all x_j must be distinguished from each other. With each chosen x_j , a corresponding value of $S_m(x_j)$ is calculated by Equation (13).

Assume after the previous Subsection, the modified secret image (MSI) is obtained and apply the JPEG-LS prediction technique on MSI given as in Figure 8.

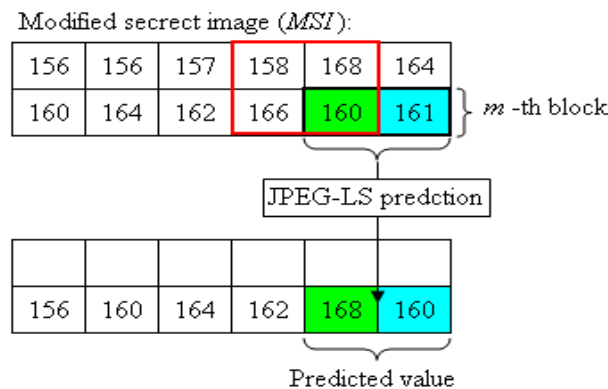


Figure 8. An example of MSI and its predicted values

To encode m -th block of MSI , the Equation (13) is implemented with the determined prime number $p_m=61$, in which the coefficients f_1 and f_2 equal to 22 and 31 (according to Equation (12), $f_1 = (160 - 168) + (61 - 1)/2 = 22$,

$f_2 = (161-160) + (61-1)/2 = 31$). For example $(x_1, x_2, x_3, x_4) = \{1, 2, 3, 4\}$ corresponds to the order of four involved participants. Block m is encoded into four packets: $S_m(x_1) = 53, S_m(x_2) = 23, S_m(x_3) = 54$ and $S_m(x_4) = 23$.

1.3.4. User-friendly Shadows construction procedure

Owing to using Shamir’s framework, generated shadow images look like noise which may attract the attention of the malicious users during transmission. Thus, this Subsection generates user-friendly shadow pixels \tilde{P}_m^j distributed to the j -th participant ($1 \leq j \leq n$). The process produced pixel \tilde{P}_m^j is an association between the value $S_m(x_j)$ and m -th block. The value of \tilde{P}_m^j have to satisfy two criteria:

- (i) $\tilde{P}_m^j = p_m \times k + S_m(x_j)$ where k is a non-negative integer,
- (ii) \tilde{P}_m^j is the closest value to the average value of m -th block.

Finally, the obtained value \tilde{P}_m^j is delivered to the j -th participant.

Following the above example, the process calculates the shadow \tilde{P}_m^1 for the participant 1 combined $S_m(x_1) = 53$ with the average value of pixels in block $m (\lfloor (160+161)/2 \rfloor = 160)$. The value \tilde{P}_m^1 is chosen 175 because $\{53, 114, 175, 236\}$ is the set of numbers which satisfies the form $61 \times k + 53$.

1.4. Retrieving phase

Retrieving phase consists of two sub-procedures: reconstruction and recovering which is summarized as in the Figure 9. The first sub-procedure is used to join t shadow images based on Lagrange interpolation. Second, recovering procedure reveals the original secret image. The details of these phase is presented below:

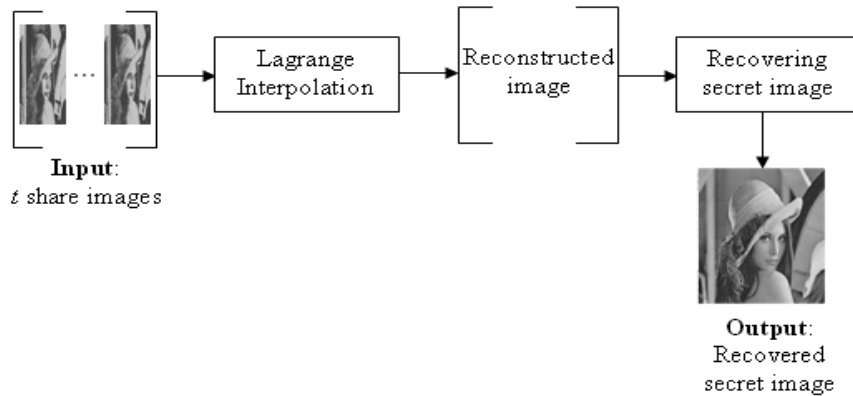


Figure 9. Flowchart of the retrieving phase

First of all, the reconstruction procedure is started by collecting the shadows from the authorized participants and determining the prime number from the initial shadow pixels. Any t of them will be sufficient to reconstruct image. According to the Equation (1), the coefficients f_1, f_2, \dots, f_t of the Equation (13) are solved. After that, the recovering original image is restored through the Equation (12).

IV. DISCUSSIONS AND EXPERIMENTAL RESULTS

Results of the tests executed to demonstrate the feasibility of the proposed scheme are presented in this section. A set of images of size 512×512 shown in Figure 10 is used as test images.

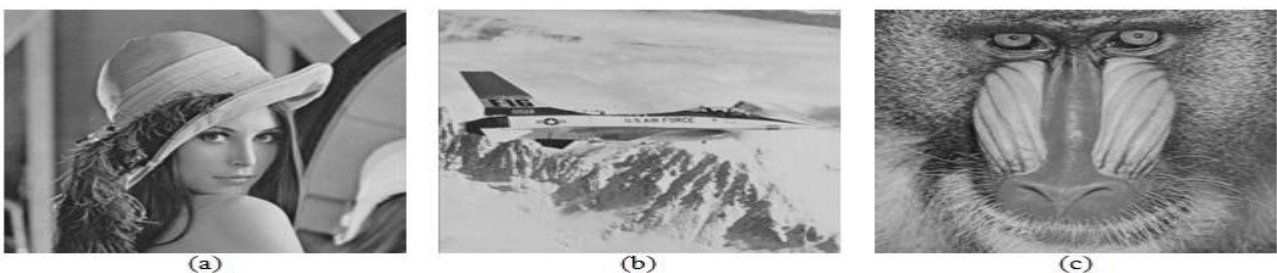


Figure 10. A set of test images of size 512×512: (a) Lena; (b) Jet; (c) Baboon

Proposed method uses a (t, n) -threshold sharing with different prime numbers to generate shadows. According to the Subsection 3.1.4, obtained value \tilde{P}_m^j is similarity to the corresponding pixel in m -th block of MSI . Furthermore, the size of each shadow image is $1/t$ the size of the secret image. On the other hand, according to the ensuring of the Shamir's method, even if $(n-t)$ shadows are lost or corrupted when transferred or stored, it is still possible to recover the secret image.

Therefore, it can be said that the characteristics of user-friendly image sharing are satisfied in the proposed scheme. Figure 11 presents the results obtained using a $(2, 4)$ -threshold scheme with chosen primes $\{p_1, p_2, p_3, p_4\} = \{17, 61, 131, 251\}$. The scheme encodes images shown in Figure 10 into four shadows separately; the obtained shadows in Figure 11 (a1)-(a4), (b1)-(b4), (c1)-(c4) are the results of the Figure 10 (a), (b), (c), respectively.



Figure 11. Obtained shadows from $(2, 4)$ -threshold user-friendly image sharing scheme with four different primes $\{p_1, p_2, p_3, p_4\} = \{17, 61, 131, 251\}$

Notably, each shadow image looks like a shrunken version of the original image. So, from the view point of image database manager, this similarity allows users to recognize each shadow image with its original image without any computation. Of course, this characteristic only provides to distinguish content among multiple shadow images. Because, too much detailed information of the secret image is omitted, illegal users cannot obtain a high-quality image from taking a single shadow image. The image quality of the reconstructed image is the peak signal-to-noise ration ($PSNR$) and is defined as

$$PSNR = 10 \times \log_{10} \left(\frac{255^2}{MSE} \right) \text{DB} \quad (14)$$

where MSE is the mean squared error between original image and recovered image. MSE is evaluated as follow:

$$MSE = \frac{1}{M \times N} \sum_i^M \sum_j^N (p_{i,j} - p'_{i,j})^2 \quad (15)$$

Where $(M \times N)$ is the size of an image; $p_{i,j}$ is the original pixel value; and $p'_{i,j}$ is the recovered pixel value.

Figure 12 shows images (a), (b) and (c) obtained by direct expansion images of the shadow images Figure 11 (a1), (b1) and (c1) to the size of the original image. The $PSNR$ values between these images and the original image are 27.62dB, 27.79 and 21.46dB respectively.



Figure 12. Results obtained by expanding a single shadow image to the size of original image: images (a), (b) and (c) obtained from Figure 11 (a1), (b1) and (c1)

In the revealing phase, proposed scheme uses Lagrange’s interpolation to restore the original image. Any two of shadow images are gathered, the original image can be reconstructed. Figure 13 (a), (b) and (c) are recovered from any two shadows of Figure 11 (a1)-(a4), (b1)-(b4) and (c1)-(c4), respectively.



Figure 13. Reconstructed images from any 2 shadow images

During the embedding procedure, in the sharing phase, hides indicators of prime numbers into secret image on using LSB matching function [23], which is used to limit the modification of the secret image. LSB of each pixel is matched with the indicator based on XOR function (Equation (3)). Yang *et al.*’s method uses the conventional LSB replacement which embeds indicators of primes into secret image by replacing the LSBs of the secret image with indicator bits. Besides, in the scheme of Yang *et al.*, the determination of prime numbers for a block fully depends on the last pixel of the previous block. The proposed scheme, by contrast, uses the JPEG-LS prediction technique that estimates accurately predicted pixel value. The proposed method rarely uses the equation like Equation (8) in Equation (12). Therefore, the proposed method can obtain better quality of the recovered images. Table 1 presents the image qualities of (2, 4)-threshold of the proposed scheme compared with those for two previous published user-friendly image sharing method. The values in Table 1 are the *PSNR* values of the recovered images. It reveals that the proposed scheme can reconstruct the original image with a higher quality than that of previous schemes.

Table 1. Qualities of the recovered images based on different user-friendly image-sharing schemes in a set of test images

	Thien <i>et al.</i> [14]	Yang <i>et al.</i> [15]	Proposed scheme
Lena	37.37	50.53	52.91
Jet	39.19	49.76	52.90
Baboon	34.75	49.17	52.89

Table 2. Comparison of the proposed scheme with others in terms of the average *PSNRs* value of expanded shadow images

	Thien <i>et al.</i> [14]	Yang <i>et al.</i> [15]	Proposed scheme
Lena	24.80	23.32	27.62
Jet	25.65	23.14	27.79
Baboon	20.55	18.52	21.46

The values shown in the Table 2 are the average *PSNRs* values of the expanded image and the original image by the proposed method and other schemes. Notably, the *PSNR* value of each shadow image is slightly higher than that of the schemes in [14] and [15]. The moderate quality of shadow images in the proposed scheme is convenient in images management, rather than recovering a high-quality image based on image-interpolation technique by illegal users.

V. CONCLUSIONS

This paper proposed a novel user-friendly image sharing method with different prime numbers that provides shadow images among authorized participants. Each participant receives a meaningful image looking like a shrunken version of the original image. The proposed scheme is based on Yang *et al.*’s framework. However, in this paper, the prime number is determined according to the predicted value which leads to the small prime number in encoding block. In addition, the indicators of prime numbers are embedded into secret image based on the XOR function that limits modification of original pixel value, so that a better visual quality of the reconstructed image is guaranteed in the proposed scheme.

References

- [1] W. Bender, D. Gruhl, N. Morimoto and A. Lu, "Techniques for data hiding," IBM Systems Journal, Vol. 35, pp. 312-336, 1996.
- [2] C. T. Hsu and J. L. Wu, "Hiding digital watermarks in images," IEEE Transactions of Image Processing, Vol. 8, pp. 58-68, 1999.
- [3] D. C. Wu and W. H. Tsai, "Data hiding in images via multiple-based number conversion and lossy compression," IEEE Transactions on Consumer Electronics Vol. 44, pp. 1406-1412, 1998.
- [4] A. Shamir, "How to share a secret," Communications of the ACM, Vol. 22, no. 11, pp. 612-613, 1979.
- [5] G. R. Blakley, "Safeguarding cryptographic keys," AFIPS 1979 National Computer Conference, Vol. 48, pp. 313-317, 1979.
- [6] C. C. Thien, J. C. Lin, "Secret image sharing," Computers and Graphics, Vol. 26, pp. 765-770, 2002.
- [7] S. K. Chen and J. C. Lin, "Fault-tolerant and progressive transmission of images," Pattern Recognition, Vol. 38, pp. 2466-2471, 2005.
- [8] C. C. Lin, W. H. Tsai, "Secret image sharing with steganography and authentication," Journal of Systems and Software, Vol. 73, pp. 405-414, 2004.
- [9] C. N. Yang, T. S. Chen, K. H. Yu, C. C. Wang, "Improvements of image sharing with steganography and authentication," Journal of Systems and Software, Vol. 80, pp. 1070-1076, 2007.
- [10] C. C. Chang, Y. P. Hsieh, C. H. Lin, "Sharing secrets in stego images with authentication," Pattern Recognition, Vol. 41, pp. 3130-3137, 2008.
- [11] P. Y. Lin and C. S. Chan, "Invertible secret image sharing with steganography," Pattern Recognition Letters, Vol. 31, pp. 1887-1893, 2010.
- [12] Z. Eslami and J. Z. Ahmadabadi, "Secret image sharing with authentication-chaining and dynamic embedding," Journal of Systems and Software, Vol. 84, pp. 803-809, 2011.
- [13] M. Ulutasa, G. Ulutas and V. V. Nabiyeva, "Medical image security and EPR hiding using Shamir's secret sharing scheme," Journal of Systems and Software, Vol. 84, pp. 341-353, 2011.
- [14] C. C. Thien and J. C. Lin, "An image-sharing method with user-friendly shadow images," IEEE Transactions on Circuits and Systems for Video Technology, Vol. 13, pp. 1161-1169, 2003.
- [15] C. N. Yang, K. H. Yu, and R. Lukac, "User-friendly image sharing using polynomials with different primes," International Journal of Imaging Systems and Technology Vol. 17, pp. 40-47, 2007.
- [16] Zhicheng Ni, Yun Q. Shi, Nirwan Ansari, Wei Su, Qibin, and Xiao Lin, "Robust lossless image data hiding designed for semi-fragile image authentication," IEEE Transactions on Circuits and Systems for Video Technology, Vol. 18, pp. 497-509, 2008.
- [17] Jun Tian, "Reversible data embedding using a difference expansion," IEEE Transactions on Circuits and Systems for Video Technology, Vol. 13, pp.890-896, 2003.
- [18] M. Weinberger, G. Seroussi, G. Shapiro, "The LOCO-I Lossless Image Compression Algorithm: Principles and Standardization into JPEG-LS," HPL-98-193, 1998.
- [19] B. Carpentieri, M. J. Weinberger and G. Seroussi, "Lossless compression of continuous-tone images," Proceeding of the IEEE, Vol. 88, 2000.
- [20] J. Jiang, B. Guo and S. Y. Yang, "Revisiting the JPEG-LS prediction scheme," IEE Proceedings- Vision, Image and Signal Processing, Vol. 147, pp. 575-580, 2000.
- [21] S. Bedi, E. A. Edirisinghe and G. Grecos, "Improvement to the JPEG-LS prediction scheme," Journal of Image and Vision Computing, Vol. 22, pp. 9-14, 2004.
- [22] J. Mielikainen, "LSB matching revisited," IEEE Signal Processing Letters, Vol. 13, pp. 285-287, 2006.
- [23] C. S. Chan, "On using LSB matching function for data hiding in pixels," Fundamenta Informaticae, Vol.96, pp. 49-59, 2009.

Effect of Cryogenic Treatment on Mechanical Properties of Cold Work Tool Steels

A D Wale,¹ Prof. V D Wakchaure²

¹Department of Mechanical Engineering, AVCOE Sangamner, Pune University, India

Abstract: In this paper effect of cryogenic treatment on mechanical properties of cold work tool steels at various combination of heat treatment cycle (process sequence) are studied. The material selected for these processes are AISI D2 and D3. Cryogenic treatment is commonly referred as cryotreatment, is an add-on process to the conventional heat treatment of tool steel. Cryogenic treatment improves hardness, microstructure of metal (retained austenite to martensite), dimensional stability and decreases residual stresses. The effects of these process sequences of cryotreatment on properties of tool steel were studied by conducting some laboratory tests. Study of microstructure characterization of different specimens is carried out using optical microscope. Also hardness measurement was done by using Vickers indentation method.

Keywords: Cryogenic treatments, hardness, microstructure, Phase transitions, Tool steel.

I. INTRODUCTION

Tool steel refers to a variety of carbon and alloy steels that are particularly well-suited to be made into tools. Their suitability comes from their distinctive hardness, resistance to abrasion, their ability to hold a cutting edge, and their resistance to deformation at elevated temperatures (red-hardness). Tool steels are used in cutting tools, punches, and other industrial tooling. Different tool steels are developed to resist wear at temperatures of forming and cutting applications.

Tool steels are broadly divided into six categories like cold work, shock resisting, hot work, high speed, water hardening, plastic mold and special-purpose tool steels. Among them, cold work tool steels are the most important category, as they are used for many types of tools, dies and other applications where high wear resistance and low cost are needed.[1]

Tool steel is generally used in a heat treated state. Conventional heat treatment gives hardness as well as toughness, wear resistance and ductility to steel. Even performed properly, conventional heat treating cannot remove all of the retained austenite (large, unstable particles of carbon carbide) from steel. The retained austenite as a soft phase in steels could reduce the product life and in working conditions, it can be transformed into martensite. This new martensite could cause several problems for working tools. This new martensite is very brittle and differs from the tempered one, which is used in tools.

Furthermore, this martensite causes micro cracks and reduces the product life. Regarding the problems mentioned above, the controlled transformation of retained austenite into martensite is essential to many types of component. In order to obtain this transformation the cold treatment is used.

Cold treatment is generally classified as either so called "sub-zero treatment" at temperatures down to about -80 °C or "deep cryogenic treatment" at liquid nitrogen temperature (-196°C). More recent evidence shows that the wear resistance is further enhanced by virtue of cryogenic treatment at liquid nitrogen temperature. Most researchers believed that there are two mechanisms to improve the mechanical properties of the work that has been treated cryogenically. The first mechanism is attributed to the transformation of retained austenite to martensite. The second is to initiate the nucleation sites for precipitating a large number of fine carbides in the matrix of martensite. [2, 3]

Cryogenic treatment commonly referred to as cryotreatment, is an add-on process to the conventional heat treatment of tool/die steel. It consists of controlled cooling of conventionally hardened steel specimens to some selected cryogenic temperature (-50°C to -196°C) and holding there for sufficiently long duration (20 to 75 h) before being heated back to the ambient temperature at a predetermined rate for subsequent tempering treatment. It is different from the age-old cold treatment, which is carried out in between -60°C and -80°C and without any significant duration of soaking at the lowest temperature of treatment. [4, 5, 6]

Due to the cryogenic treatment, the problems occurred in conventional heat treatment is reduced by controlled transformation of the retained austenite into martensite, which is essential to many types of component. Cryogenic treatment in tool steels causes the precipitation of finely dispersed carbides in martensite and also converts soft unstable austenite to martensite. Cryogenic treatment improves wear resistance, hardness, toughness, resistance to fatigue cracking, microstructure of metal (retained austenite to martensite), dimensional stability and decreases residual stresses. Also reduces tool consumption and down time for equipment setup thus leading to cost reduction of about 50%. Cryogenic treatment gives machining, grinding and polishing finish due to little soft austenite. The greatest improvement in properties is obtained by selecting proper heat treatment process sequence (cryogenic treatment in between quenching and tempering), soaking time (cryoprocess time), stabilization (keep at room temperature for one week after quenching), hardening temperature, heating and cooling rate. [7, 8, 9, 10].

II. EXPERIMENTAL METHODOLOGY

2.1 Material selection

AISI D2 and D3 tool steel materials are selected for studying effect of process sequence on behavior of cryotreated cold work tool steel at different process cycles. The chemical composition of specimen (dia.10mm, Height 35mm) was

analyzed in optical emission spectroscopy (OES). The machine used for the analysis of raw material chemical composition was named as Spectrophoto Analyzer [AS 200(Switzerland)].

2.2 Treatments

The material chosen in this work was given various treatments and treatment cycles indicated in fig.1 and table I. Specimens were subjected to conventional heat treatment and deep cryogenic treatment separately. Conventional heat treatment consist of hardening and tempering, while deep cryogenic treatment involve an additional low temperature treatment cycle to conventional heat treatment process.

TABLE I: Process sequence for both tool steel D2 & D3

Sr. No.	Group Name	Process Sequence
1	Group A	Conventional Heat Treated specimens (CHT)
2	Group B	Austenitizing Quenching Cryogenic (AQC)
3	Group C	Austenitizing Quenching Cryogenic tempering (AQCT)
4	Group D	Austenitizing Quenching Cryogenic tempering tempering (AQCTT)
5	Group E	Austenitizing Quenching tempering Cryogenic tempering (AQTCT)

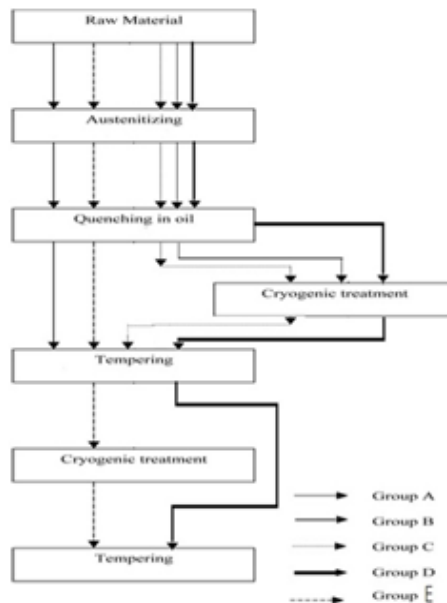


Figure 1: Flow chart for process sequence

2.2.1 Hardening

Pre heating at 720⁰C was done before hardening and Hardening at 1020⁰C was done in electrically heated protected atmosphere type furnace, for both the specimens of tool steel D2 & D3. Hardening was done at 1020⁰C to achieve the austenitization point & grain uniformity (Structural balance).

2.2.2 Quenching

Quenching is done at 500⁰C in oil, with continuous agitation, to avoid thermal shocks.

2.2.3 Tempering

Tempering was done in electrically heated protected atmosphere type furnace at 520⁰C to relieve the stresses.

2.2.4 Cryogenic Treatment

Cryogenic treatment was done on tool steel D2 & D3 at -185⁰C, for 10 hrs. The cryogenic treatment box was made by America Cryogenics.

III. EXPERIMENTAL SETUP FOR CRYOGENIC HEAT TREATMENT

Fig. 2 shows the schematic representation of Cryogenic Treatment equipment is used to obtain -125⁰C to -196⁰C temperature. It comprises an insulated box (Cryo-box), one motor with a circulating fan, one thermocouple to measure the

cryogenic temperature inside the box connected to a temperature controller and programmer, a liquid nitrogen tank and a solenoid valve for the gas inlet. The actual temperature of the mass loaded in the box is recorded by a thermocouple.

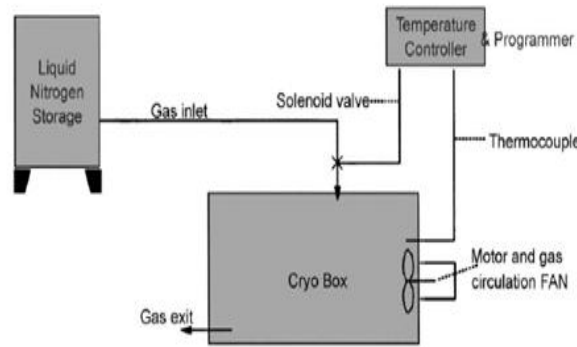


Figure 2: Block diagram of the cryogenic treatment equipment

IV. RESULTS OF CHEMICAL ANALYSIS

The composition of the raw material was analyzed in optical emission spectroscopy (OES). The machine used for the analysis of raw material chemical composition was named as Spectrophoto Analyzer [AS200 (Switzerland)].

V. MICROSTRUCTURAL CHARACTERIZATION

Microstructure examinations were carried out by using inverted optical microscope of Carl Zeiss AL350 at magnification 450X. Different phases like retained austenite, untendered martensite, tempered martensite were checked. Also secondary carbide sizes & shapes were checked.

VI. HARDNESS MEASUREMENT

For all hardness measurement, Vickers indentation method was used. The flat surface was prepared by polishing paper on 1/0. For D-2 and D3 steel material HV scale was used.

VII. RESULTS AND DISCUSSION

7.1 Results of chemical analysis of D2 and D3 raw material

The material considered for the study was obtained in the form of 10mm diameter rod & length 40mm of D2 & D3 tool steel.

TABLE II: The result of chemical analysis of D2 raw material

Carbon	Chromium	Manganese	Vanadium	Molybdenum	Iron
1.5	12.53	0.36	1.04	0.83	Remaining

TABLE III: The result of chemical analysis of D3 raw material

Carbon	Chromium	Manganese	Silicon	Iron
2.23	12.31	0.49	0.26	Remaining

7.2 Hardness study

The hardness values for all samples are shown in table no. IV. It is clear from the table that for D2 material CHT specimen has less hardness than cryotreated specimen but there is gradual decrease in hardness observed from AQC to AQCT. For D3 material CHT specimen has less hardness than cryotreated specimen but there is gradual increase in hardness observed from AQCT to AQTCT. The AQC specimen of D3 material has highest hardness.

TABLE IV: The hardness (HV) of the heat-treated D2 & D3 tool steel samples

Process	Hardness (HV)	
	D2	D3
Conventional Heat Treated specimens (CHT)	805	811.8
Austenitizing Quenching Cryogenic (AQC)	927	1022.3
Austenitizing Quenching Cryogenic tempering (AQCT)	916	724.3
Austenitizing Quenching Cryogenic tempering tempering (AQCTT)	841	731.5
Austenitizing Quenching tempering Cryogenic tempering (AQTCT)	828.7	767.3

7.3 Microstructure analysis

7.3.1 D2 Tool steel

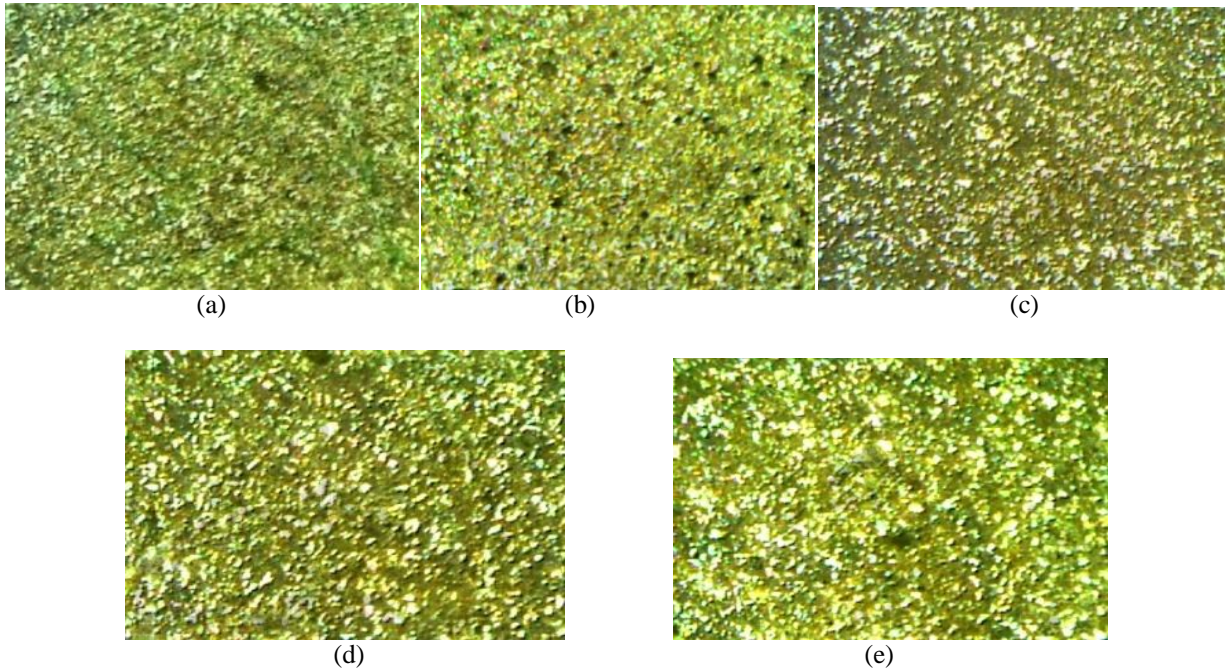


Figure 3 : Microstructure of various combinations of treatments for the specimen of D2 steel
 a) CHT b) AQC c) AQCT d) AQCTT e) AQTCT

Microstructure of various combinations of treatment for the specimen of D2 steel is shown in fig. 3(a-e). Fig 3(a) shows microstructure of CHT in which Globular shape carbides up to 9 micron and nodular shape carbides of 11X 4 micron size. Martensite etches dark. Untempered martensite observed is more up to 10% and retained austenite is seen up to 50%. Fig 3 (b) shows microstructure of AQC. The structure consists of globular carbides are up to 2 micron and nodular carbide are of 2x5 micron in size. Untempered martensite observed is below 2%. Massive carbides not seen and 95% unstable austenitic structure seen. Fig 3 (c) shows microstructure of AQCT. Globular and nodular shape carbide up to 10% is observed in 5 micron and 10x3 micron in size respectively. Untempered martensite observed is more up to 4%. Retained austenite is present up to 20% under tempered structure. Fig 3 (d) shows microstructure of AQCTT. Globular and nodular shape carbide up to 12% is observed in matrix of tempered martensite. Globular carbides are upto 3 micron and nodular carbide is of 14x5 micron in size. Untempered martensite observed is more up to 5% and retained austenite up to 50% under tempered structure. Fig 3 (e) shows microstructure of AQTCT. Nodular shape carbide up to 7% is of 13x6 micron in size, observed in matrix of tempered martensite. Untempered martensite observed is more up to 4%. Retained austenite up to 50%. under tempered structure. Microstructure of all combination treatment shows globular and nodular carbides are uniformly distributed in the austenite matrix.

7.3.2 D3 Tool Steel

Microstructure of various combinations of treatment for the specimen of D3 steel is shown in fig. 4(a-e). Fig. 4(a) shows microstructure of CHT in which Elliptical Globular shape carbide upto 20% of 3x6 micron in size are observed in matrix of tempered martensite. Untempered martensite observed is up to 7%. The structure is well distributed. Martensite etches dark. Globular and nodular carbides uniformly distributed in the tempered martensite matrix. 20% Retained austenite seen slightly under tempered structure. Fig 4 (b) shows microstructure of AQC. Globular and erratic shape carbide upto 4% are observed in matrix of tempered martensite. Globular carbides are up to 8 micron and erratic carbide are of 10x3 micron in size. Untempered martensite observed in trace amount. Martensite not etches dark. Globular and nodular carbides uniformly distributed in the austenite matrix. Massive carbides are not seen. Micro cracks visible. 95% unstable austenitic structure. Fig 4(c) shows microstructure of AQCT. More nodular shape carbide upto 15% are of 2x4 micron in size, observed in matrix of tempered martensite. Untempered martensite observed is more upto 20%. Martensite etches dark.

Globular and nodular carbides uniformly distributed in the tempered matrix. Retained austenite not seen. Fig 4 (d) shows microstructure of AQCTT. Nodular shape carbide up to 10% is of 3x5 micron in size, observed in matrix of tempered martensite. Untempered martensite observed is more upto 7%. Martensite etches dark. Globular and nodular carbides uniformly distributed in the tempered martensite matrix. Retained austenite not seen. Fig 4 (e) shows microstructure of AQTCT. Globular and erratic shape carbide upto 10% of 2x4 micron in size is observed in matrix of tempered martensite.

Untempered martensite observed is upto 5%. Martensite etches dark. Globular and nodular carbides uniformly distributed in the tempered martensite matrix. Retained austenite is not seen.

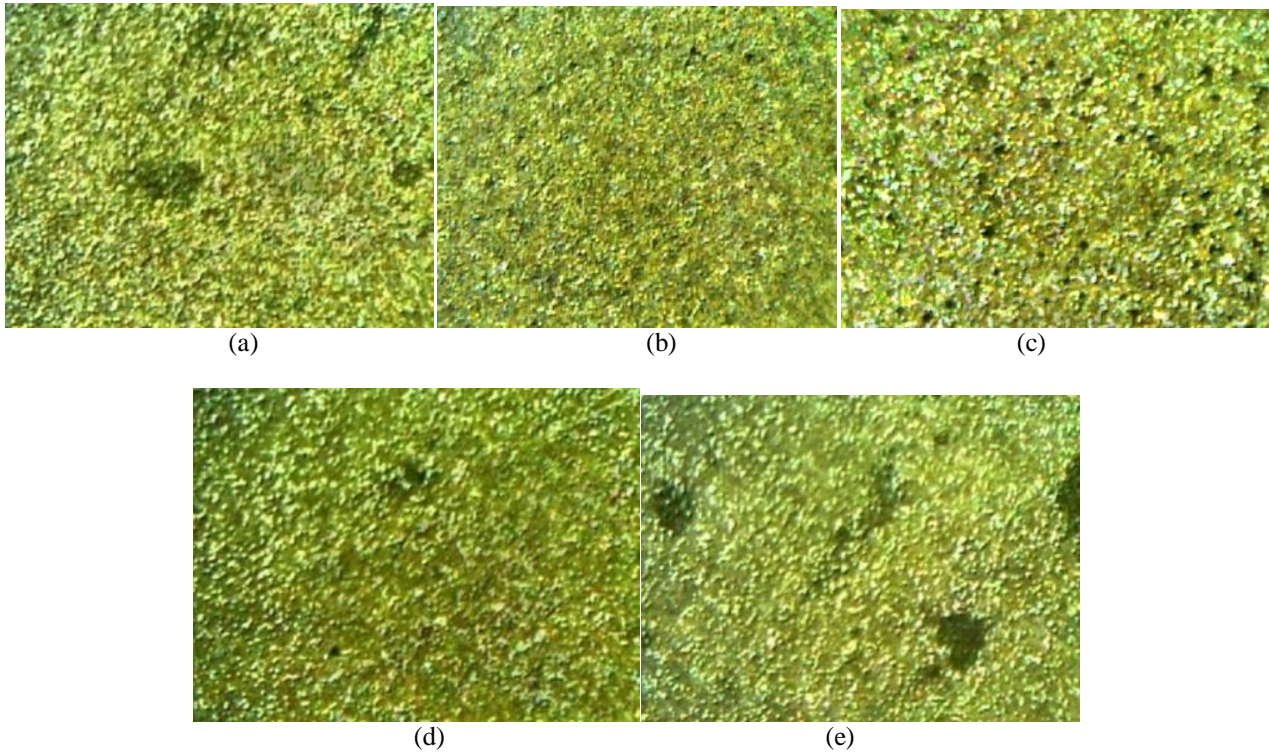


Figure 4 : Microstructure of various combinations of treatments for the specimen of D3 steel
a) CHT b) AQC c) AQCT d) AQCTT e) AQTCT

Microstructure of tool steel D2 & D3 were subjected to various combinations of treatments as described in table 1. In the process sequence Austenitizing Quenching Cryogenic tempering (AQCT), Austenitizing Quenching Cryogenic tempering tempering (AQCTT) & Austenitizing Quenching tempering Cryogenic tempering (AQTCT) for tool steel D3 retained austenite was not seen. For D2 tool steel in process sequence Austenitizing Quenching Cryogenic tempering (AQCT) retained austenite is up to 20%. In process Austenitizing Quenching Cryogenic tempering tempering (AQCTT) and Austenitizing Quenching tempering Cryogenic tempering (AQTCT) retained austenite is up to 50%. For D2 tool steel massive carbides not seen and 95% unstable austenitic structure is seen. Also the general shape of carbides observed was Globular, Nodular or elliptical.

VIII. CONCLUSION

Cryogenic treatment is add on process to conventional heat treatment process of tool steel. Cryogenic treatment improves microstructure of metal i.e. controlled transformation of retained austenite into martensite. For D3 tool steel retained austenite was not seen in the process sequence Austenitizing Quenching Cryogenic tempering (AQCT), Austenitizing Quenching Cryogenic tempering tempering (AQCTT) and Austenitizing Quenching tempering Cryogenic tempering (AQTCT). For D2 tool steel retained austenite is up to 20% in process sequence Austenitizing Quenching Cryogenic tempering (AQCT). Also retained austenite is up to 50% in process Austenitizing Quenching Cryogenic tempering tempering (AQCTT) and Austenitizing Quenching tempering Cryogenic tempering (AQTCT). The effect of cryogenic treatment on hardness shows that for D2 and D3 tool steel CHT specimen has less hardness than cryotreated specimen. But for D2 tool steel there is gradual decrease in hardness observed from AQC to AQTCT. For D3 tool steel there is gradual increase in hardness observed from AQCT to AQTCT and AQC specimen has highest hardness. The multiple tempering decreases hardness in D2 tool steel where as increases hardness in D3 tool steel. For D2 and D3 tool steel in process sequence Austenitizing Quenching Cryogenic (AQC) massive carbides not seen and 95% unstable austenitic structure is seen. But both tool steel have maximum hardness value for this process sequence. In D3 tool steel the micro cracks were observed on the untempered samples. The general shape of carbides observed was Globular, Nodular or elliptical. In D2 tool steel retained austenite is not totally converted to martensite where as in D3 tool steel retained austenite is totally converted to martensite.

IX. ACKNOWLEDGMENT

The author thanks Dr. G.J. Vikhe Patil (Principal), Prof. A. K. Mishra HOD (Mech. Dept.), Prof. V.S. Aher PG I/C. Prof. V.D.Wakchuare, Amrutvahini College of Engineering Sangamner, Mr.Deshmukh Sanjay, Unique Treatments Nashik, Mr.Patankar M.K. Nashik Engineering Cluster, Dr. Ghadge N.U., Nashik Cryogenic Services, Dr. Bhase P. G. Fan Services, Nashik, all my friends and all staff of mechanical department Amrutvahini Polytechnic for their help during this work.

REFERENCES

- [1] L. Bourithis, G.D. Papadimitriou, J. Sideris, Comparison of wear properties of tool steels AISI D2 and O1 with the same hardness, Tribology International ,39 , 2006, pp 479-489.
- [2] Fanju Meng, Kohsuke Tagashira, Ryo Azumu and Hideaki Sohma, Role of eta-carbide precipitations in the wear resistance improvements of Fe-12Cr-Mo-V-1.4C tool steel by cryogenic treatment , ISIJ international, 34, 1994, 205-210.
- [3] Chai Hung Sun, The effect of microstructure and the mechanical properties of AISI D2 tool steel by deep cryogenic treatment, Tatung University, Thesis for MS, July 2006.
- [4] D. Das, A.K. Dutta, K.K. Ray, Correlation of microstructure with wear behavior of deep cryogenically treated AISI D2 steel, Wear, 267, 2009, 1371-1380.
- [5] D. Das, A.K. Dutta, K.K. Ray, Optimization of the duration of cryogenic processing to maximize wear resistance of AISI D2 steel, Cryogenics, 49, 2009, 176-184.
- [6] D. Das, A.K. Dutta, K.K. Ray, On the enhancement of wear resistance of tool steels by cryogenic treatment, Philosophical Magazine Letters , 88 (11),2008, 801-811.
- [7] A. Molinari, M. Pellizzari, S. Gialanella, G. Staffelini, K. H. Stiansy, Effect of deep cryogenic treatment on the mechanical properties of tool steels, Journal of Materials Processing Technology ,118 ,2001, 350-355.
- [8] N.B. Dhokey, S. Nirbhavne, Dry sliding wear of cryotreated multiple tempered D-3 tool steel, Materials Processing Technology ,209 ,2009, 1484-1490.
- [9] A. Akhbarizadeh, A. Shafyei, M.A. Golozar, Effects of cryogenic treatment on wear behavior of D6 tool steel, Materials and Design, 30,2009, 3259–3264.
- [10] Cord Henrik Surberg, Paul Stratton, and Klaus Lingenhole, The effect of some heat treatment parameters on the dimensional stability of AISI D2, Cryogenics, 48 ,2008, 42-47.
- [11] T. Yugandhar, P.K. Krishnan, C.V. Bhaskar Rao and R. Kalidas, Cryogenic treatment and its effect on tool steel, 6th International Tooling conference, 671-683.
- [12] D. Mohan Lal, S. Renganarayanan, A. Kalanidhi, Cryogenic treatment to augment wear resistance of tool and die steels, Cryogenics ,41,2001 , 149-155.

Ultrasonic Investigation of Binary Mixtures on Stearates and Methyl Ethyl Ketone

r. Kavitha,¹ s. Jayakumar,² v. Kannappan,³ r. Uma⁴

1. Research scholar, Department of Chemistry, Pachaiyappa's College, Chennai – 30.

2. Assoc Prof., Department of Physics, Vivekananda College, Mylapore, Chennai – 04.

3. Assoc Prof., Department of Chemistry (Retd.), Presidency College, Chennai – 05.

4. Assoc. Prof., Department of Chemistry, Pachaiyappa's College, Chennai – 30.

ABSTRACT: We report the measurements of ultrasonic velocity in the binary mixtures of zinc stearate - methyl ethyl ketone and calcium stearate - methyl ethyl ketone at 303 K. It is used to evaluate the different thermo acoustical parameters along with the excess properties, the experimental data obtained is fitted with the models and percentage deviation is calculated. From the light of these parameters molecular interaction such as existence of strong molecular association and weak interaction among the participating mixtures has been observed in the present study.

Keywords: Stearates, stabilizer, solvent, positive and negative deviation, excess properties.

I. INTRODUCTION

The velocity of sound in a compound is closely related to many other physical and chemical properties [1]. The self – association of liquids and solids become one of the interesting effects characterizing the solvent. It is especially important when the structure of the solvent plays a crucial role in the studied field [2]. The interest arises, because of the fact that the mixing behaviour of a binary mixture of type A – B is highly dependent upon the geometry, size and structure of both the components [3]. When component A is stearate and the component B is solvent containing aliphatic component, then the molecular interactions of either structure breaking or structure making types are possible. The structure breaking interactions involve mainly the disruptions in the dipolar association in the species. However, the specific interactions that result in the formation of new associated species. For many purposes, it is necessary to know the volumes and compressibility's of the solutions relative to their corresponding values at infinite dilution. The determination of such quantities requires the extrapolation of experimental data in very dilute solutions. Zinc stearate $(C_{18}H_{35}O_2)_2Zn$ and calcium stearate $(C_{17}H_{34}COO)_2Ca$ are the stabilizers used, a soap of zinc and calcium that repels water. It is the most powerful mold release agent among all metal soaps. It contains no electrolyte and has a hydrophobic effect. Its main application areas are the plastics and rubber industry where it is used as a releasing agent and lubricant which can be easily incorporated. Methyl ethyl ketone is used as glue solvents. The polarity, dipole moment, polarizability and hydrogen bonding of a solvent determines what type of components it is able to dissolve and with what other solvents or liquid compounds it is miscible. Therefore, the measurements of physico-chemical property data on such mixtures will be useful in the process engineering. The results have been discussed in terms of molecular interactions. The values of ultrasonic velocity (U), density (ρ) and viscosity (η) for the pure components is given in Table 1.

From the experimental values, a few acoustical parameters such as adiabatic compressibility (β), acoustical impedance (Z), molar sound velocity (R), Wada's constant (W), molar volume (V_m), free volume (V_f), intermolecular free length (L_f), internal pressure (π), absorption coefficient (α/f^2) viscous relaxation time (τ), degree of intermolecular attraction (α), excess ultrasonic velocity (U^E), excess adiabatic compressibility (β^E), excess acoustical impedance (Z^E), excess free length (L_f^E) and excess molar volume (V_m^E) were derived over the entire mole fraction range. Ultrasonic velocities have also been evaluated theoretically with the help of Impedance relation, Nomoto relation, Van Dael & Vangeel relation and Junjie relation. The suitability of these theories and equations were checked by comparing theoretical values of ultrasonic speeds with the values obtained experimentally. Literature survey showed that no measurements have been previously reported for the mixtures reported in this paper.

II. MATERIALS AND METHODS

The chemicals used were of analytical grade and obtained from E.Merck Company. Thermostatically controlled well-stirred water bath whose temperature was maintained to ± 0.01 K accuracy was used for all the measurements. Binary mixtures were prepared by weighing in airtight bottles; the possible uncertainty in the concentration is estimated to be less than ± 0.0001 . Densities of pure components and their mixtures were determined by using a $1 \times 10^{-5} \text{ m}^3$ double arm pycnometer. The density values from triplicate replication at the temperature of 303 K were reproducible within $\pm 2 \times 10^{-2} \text{ kg m}^{-3}$. The uncertainty in density and excess molar volume values were found to be $\pm 4 \times 10^{-2} \text{ kg m}^{-3}$ and $\pm 0.001 \times 10^{-6} \text{ m}^3 \text{ mol}^{-1}$ respectively. Ostwald's viscometer having capacity of about 15 ml and the capillary having a length of about 90 mm and 0.5 mm internal diameter has been used to measure the flow times of pure liquids and liquid mixtures and it was calibrated with benzene (density $\approx 0.8738 \text{ g cm}^{-3}$) and doubly distilled water (density $\approx 0.9970 \text{ g cm}^{-3}$) at 303 K. The flow time of pure liquids and liquid mixtures were repeated for five times. The uncertainty of viscosity was $\pm 0.005 \times 10^{-3} \text{ m Pas}$. Speed of sound was measured by using a variable path, single crystal interferometer. (United scientific company, India), working at 2 MHz frequency. The interferometer was calibrated using toluene. Measurement of speed of sound through

medium was based on the accurate determination of the wavelength of ultrasonic waves of known frequency produced by quartz crystal in the measuring cell. The interferometer cell was filled with the test liquid, and water was circulated around the measuring cell from a thermostat. The uncertainty was estimated to be 0.1ms^{-1} .

The adiabatic compressibility (β_s) was calculated by the equation

$$\beta = 1/\rho U^2 \quad (1)$$

Where ρ the density of mixture and U is the ultrasonic velocity of the mixture.

The acoustical impedance (Z) was calculated by the equation,

$$Z = \rho U \quad (2)$$

The molar sound velocity (R) was calculated by the equation

$$R = (M_{\text{eff}} / \rho) U^{1/3} \quad (3)$$

The molar compressibility or Wada's constant (W), was calculated by the equation

$$W = (M / \rho) \beta^{-1/7} \quad (4)$$

The intermolecular free length (L_f) was calculated by the equation

$$L_f = k \beta^{1/2} \quad (5)$$

Where $K = 1.98 \times 10^{-6}$, the Jacobson constant (Jacobson 1952).

The Free volume was calculated by the equation

$$V_f = (M_{\text{eff}} U / K \eta)^{3/2} \quad (6)$$

Where $K = 4.28 \times 10^9$ for all liquids which is a temperature independent constant.

The internal pressure was calculated by the equation

$$\pi = \{bRT / (V^2 V_f)^{1/3}\} \quad (7)$$

b is a packing factor, R is a gas constant, V_f is free volume and T is temperature.

The absorption coefficient was calculated by the equation

$$(\alpha/f^2) = (8\pi^2 \eta / 3\rho U^3) \quad (8)$$

The viscous relaxation time was calculated by the equation

$$\tau = (4\eta / 3\rho U^2) \quad (9)$$

The degree of intermolecular attraction (α) was calculated by the equation

$$\alpha = (u^2 / u_{\text{im}}^2) - 1 \quad (10)$$

Where $u_{\text{im}}^2 = 1 / \{(x_1 M_1 + x_2 M_2)(x_1 / M_1 u_1^2 + x_2 / M_2 u_2^2)\}$

The U^E , β^E , Z^E , L_f^E , and V_m^E were derived over the entire mole fraction range by using the general equation

$$A^E = A - (X_1 A_1 + (1-X_1) A_2) \quad (11)$$

Where A is the corresponding parameters (U , β , Z , L_f , and V_m) of binary mixture and A_1 and A_2 are the corresponding pure component values.

The sound velocity can be correlated with the relation called Impedance relation which is represented as $U_{\text{IM}} =$

$$(X_1 Z_1 + X_2 Z_2) / (X_1 \rho_1 + X_2 \rho_2) \quad (12)$$

Where X , Z , ρ denote the mole fraction, acoustic impedance and density of the component respectively.

Nomoto derived an empirical formula for the sound velocity in binary mixture. It is given by the equation

$$U_{\text{NR}} = [R/V]^3 = \left\{ \frac{(X_1 R_1 + X_2 R_2)}{(X_1 V_1 + X_2 V_2)} \right\}^3 \quad (13)$$

Where X , R , V denote the mole fraction, molar sound velocity and molar volume at temperature T of the component. The acoustical behaviour of binary mixture was studied in detail by Van deal et al. The expression for sound velocity (U_{IMR}) of binary mixtures can be obtained from equation

$$U_{\text{IMR}} = \left\{ \frac{[1/(X_1 M_1 + X_2 M_2)]}{[X_1 / M_1 U_1^2 + X_2 / M_2 U_2^2]} \right\}^{1/2} \quad (14)$$

Where X, M and U are the mole fraction, molecular weight and sound velocity of component. Junjie derived an empirical formula for the sound velocity in binary mixture. It is given by the equation

$$U_{jun} = \left\{ \frac{(X_1 V_1 + X_2 V_2)}{(X_1 M_1 + X_2 M_2)^{1/2}} \left[\frac{X_1 V_1}{\rho_1 U_1^2} + \frac{X_2 V_2}{\rho_2 U_2^2} \right]^{-1/2} \right\} \quad (15)$$

Where X, V, M, ρ denote the mole fraction, molar volume, molecular weight and density of the components. The percentage deviation of the experimental velocity from the theoretical value is given by the equation

$$\text{Percentage deviation in velocity} = \frac{U_{Theo} - U_{Expt}}{U_{Theo}} \times 100 \quad (16)$$

III. RESULTS AND DISCUSSION

The ultrasonic velocity, density and viscosity data for the pure components at 303 K are given below:

Table 1: Comparison of density, ultrasonic velocity and viscosity data at 303 K

Component	U m/s	ρ Kg/m ³	η X 10 ⁻¹ Nsm ⁻²
Zinc stearate	1404	1133	-
Calcium stearate	1310	1145	-
Methyl ethyl ketone	1170	805	3.97

Table 2 gives the measured and acoustic parameters such as ultrasonic velocities (U), density (ρ), viscosity (η), adiabatic compressibility (B), acoustical impedance (Z), molar sound velocity (R), molar compressibility (W), molar volume (V_m), free volume (V_f), Table 3 gives the thermodynamic properties like intermolecular free length (L_f), internal pressure (π), absorption coefficient (α/f²), viscous relaxation time (τ), degree of intermolecular attraction (α), Table 4 gives the excess parameters like excess ultrasonic velocity (U^E), excess adiabatic compressibility (B^E), excess acoustical impedance (Z^E), excess free length (L_f^E), excess molar volume (V_m^E), Table 5 gives the theoretical values of ultrasonic velocity calculated from Impedance, Nomoto, Van Dael & Vangeel and Junjie's relation along with the experimental ultrasonic velocity and percentage deviation for the binary mixtures zinc stearate - methyl ethyl ketone and calcium stearate - methyl ethyl ketone over the entire composition range at 303 K.

Table 2: Measured and acoustic parameters of binary mixtures at 303 K

Conc of stearate	U ms ⁻¹	ρ Kgm ⁻³	η / 10 ⁻¹ Nsm ⁻²	β / 10 ⁻¹⁰ Kg ⁻¹ ms ⁻²	Z / 10 ⁶ Kg m ⁻² s ⁻¹	R	W	V _m / 10 ⁻¹ m ³ mole ⁻¹	V _f / 10 ⁻⁷ m ³ mole ⁻¹
zinc stearate – methyl ethyl ketone									
0.01	1276	811.3	4.09	7.57	1.04	0.97	1.80	0.895	3.84
0.02	1292	817.6	4.26	7.33	1.06	0.97	1.80	0.894	3.73
0.03	1352	823.9	4.43	6.64	1.11	0.99	1.83	0.893	3.81
0.04	1372	830.2	4.60	6.40	1.14	0.99	1.84	0.893	3.72
0.05	1388	836.6	4.77	6.20	1.16	0.99	1.84	0.892	3.62
0.06	1400	842.9	4.94	6.05	1.18	1.00	1.85	0.891	3.51
0.07	1412	849.2	5.12	5.91	1.20	1.00	1.85	0.890	3.40
0.08	1576	855.5	5.29	4.71	1.35	1.04	1.91	0.889	3.85
0.09	1584	861.8	5.47	4.62	1.37	1.04	1.92	0.889	3.73
0.1	1596	868.2	5.65	4.52	1.39	1.04	1.92	0.888	3.62
calcium stearate – methyl ethyl ketone									
0.01	1188	811.0	3.43	8.74	0.964	0.95	1.76	0.895	4.50
0.02	1212	817.1	3.59	8.33	0.990	0.95	1.77	0.894	4.37
0.03	1220	823.2	3.75	8.16	1.00	0.95	1.78	0.893	4.17
0.04	1384	829.2	3.92	6.30	1.15	0.99	1.84	0.893	4.78
0.05	1400	835.3	4.08	6.11	1.17	1.00	1.85	0.892	4.62
0.06	1412	841.4	4.25	5.96	1.19	1.00	1.85	0.891	4.44
0.07	1414	847.4	4.42	5.90	1.20	1.00	1.85	0.890	4.24
0.08	1428	853.5	4.59	5.75	1.22	1.00	1.86	0.889	4.10
0.09	1432	859.6	4.76	5.67	1.23	1.00	1.86	0.889	3.94
0.1	1464	865.6	4.93	5.39	1.27	1.01	1.87	0.888	3.89

Table 3: Thermodynamic parameters of binary mixtures at 303 K

Conc of stearate	$L_f / 10^{-11}$ m	$\pi / 10^6$ atm	$\alpha/f^2 / 10^{-12}$ $m^{-1}s^2$	$\tau / 10^{-10}$ s	$\alpha / 10^{-1}$ m
zinc stearate – methyl ethyl ketone					
0.01	5.46	3.46	6.39	4.13	1.97
0.02	5.30	3.50	6.35	4.16	2.34
0.03	5.11	3.48	5.72	3.92	3.60
0.04	5.02	3.51	5.64	3.92	4.09
0.05	4.94	3.54	5.60	3.94	4.50
0.06	4.88	3.58	5.62	3.99	4.84
0.07	4.82	3.62	5.63	4.03	5.18
0.08	4.30	3.48	4.16	3.32	9.02
0.09	4.27	3.52	4.20	3.37	9.32
0.1	4.22	3.55	4.21	3.41	9.73
calcium stearate – methyl ethyl ketone					
0.01	5.86	3.29	6.64	4.00	0.370
0.02	5.73	3.32	6.49	3.99	0.855
0.03	5.67	3.37	6.60	4.08	1.06
0.04	4.98	3.23	4.68	3.29	4.32
0.05	4.90	3.27	4.68	3.32	4.73
0.06	4.84	3.31	4.71	3.38	5.07
0.07	4.82	3.36	4.85	3.47	5.19
0.08	4.76	3.40	4.85	3.51	5.58
0.09	4.73	3.45	4.96	3.60	5.75
0.1	4.61	3.47	4.77	3.55	6.55

Table 4: Excess parameters of binary mixtures like U^E , β^E , Z^E , L_f^E and v_m^E at 303 K

Conc of stearate	U^E ms^{-1}	$\beta^E / 10^{-10}$ $Kg^{-1}ms^{-2}$	$Z^E / 10^5$ $Kg m^{-2}s^{-1}$	$L_f^E / 10^{-12}$ m	$V_m^E / 10^{-3}$ $m^3 mole^{-1}$
zinc stearate – methyl ethyl ketone					
0.01	106	-1.50	0.928	-5.16	-0.499
0.02	122	-1.74	1.13	-6.03	-0.998
0.03	181	-2.42	1.70	-8.60	-1.50
0.04	201	-2.66	1.95	-9.52	-1.99
0.05	217	-2.85	2.16	-10.3	-2.49
0.06	229	-3.00	2.35	-10.9	-2.98
0.07	241	-3.14	2.53	-11.4	-3.48
0.08	404	-4.34	4.02	-16.6	-3.97
0.09	412	-4.41	4.18	-17.0	-4.46
0.1	424	-4.51	4.38	-17.4	-4.95
calcium stearate – methyl ethyl ketone					
0.01	18	-0.335	0.212	-1.11	-0.472
0.02	42	-0.736	0.475	-2.47	-0.947
0.03	50	-0.902	0.610	-3.05	-1.42
0.04	214	-2.77	2.04	-9.93	-1.89
0.05	229	-2.95	2.25	-10.7	-2.36
0.06	241	-3.09	2.43	-11.2	-2.83
0.07	243	-3.15	2.53	-11.5	-3.30
0.08	257	-3.30	2.73	-12.1	-3.77
0.09	261	-3.37	2.85	-12.4	-4.24
0.1	293	-3.65	3.21	-13.6	-4.71

Table 5: Experimental velocities and theoretical velocities along with the percentage deviation of binary mixtures at 303 K

Conc of stearate	Ultrasonic velocity U / ms^{-1}			% Deviation					
	EXPT	Imp	Nom	VDV	Junjie's	Imp	Nom	VDV	Junjie's
zinc stearate – methyl ethyl ketone									

0.01	1276	1170	1171	1166	1170	-9.032	-8.946	-9.393	-9.029
0.02	1292	1171	1172	1163	1171	-10.372	-10.199	-11.100	-10.366
0.03	1352	1171	1174	1159	1171	-15.469	-15.199	-16.608	-15.458
0.04	1372	1171	1175	1156	1171	-17.147	-16.785	-18.684	-17.132
0.05	1388	1171	1176	1153	1172	-18.484	-18.029	-20.421	-18.464
0.06	1400	1172	1177	1149	1172	-19.479	-18.933	-21.816	-19.453
0.07	1412	1172	1178	1146	1172	-20.473	-19.835	-23.214	-20.441
0.08	1576	1172	1179	1143	1173	-34.433	-33.625	-37.918	-34.390
0.09	1584	1173	1181	1139	1173	-35.082	-34.175	-39.011	-35.031
0.1	1596	1173	1182	1136	1173	-36.072	-35.064	-40.457	-36.013
calcium stearate – methyl ethyl ketone									
0.01	1188	1170	1171	1167	1170	-1.523	-1.477	-1.832	-1.534
0.02	1212	1170	1171	1163	1170	-3.558	-3.465	-4.189	-3.580
0.03	1220	1171	1172	1160	1170	-4.226	-4.086	-5.177	-4.257
0.04	1384	1171	1173	1157	1170	-18.219	-18.008	-19.653	-18.265
0.05	1400	1171	1173	1153	1170	-19.568	-19.303	-21.374	-19.625
0.06	1412	1171	1174	1150	1170	-20.574	-20.256	-22.754	-20.642
0.07	1414	1171	1175	1147	1170	-20.727	-20.358	-23.267	-20.804
0.08	1428	1171	1175	1144	1171	-21.904	-21.481	-24.827	-21.991
0.09	1432	1172	1176	1141	1171	-22.227	-21.754	-25.513	-22.323
0.1	1464	1172	1177	1138	1171	-24.940	-24.406	-28.661	-25.046

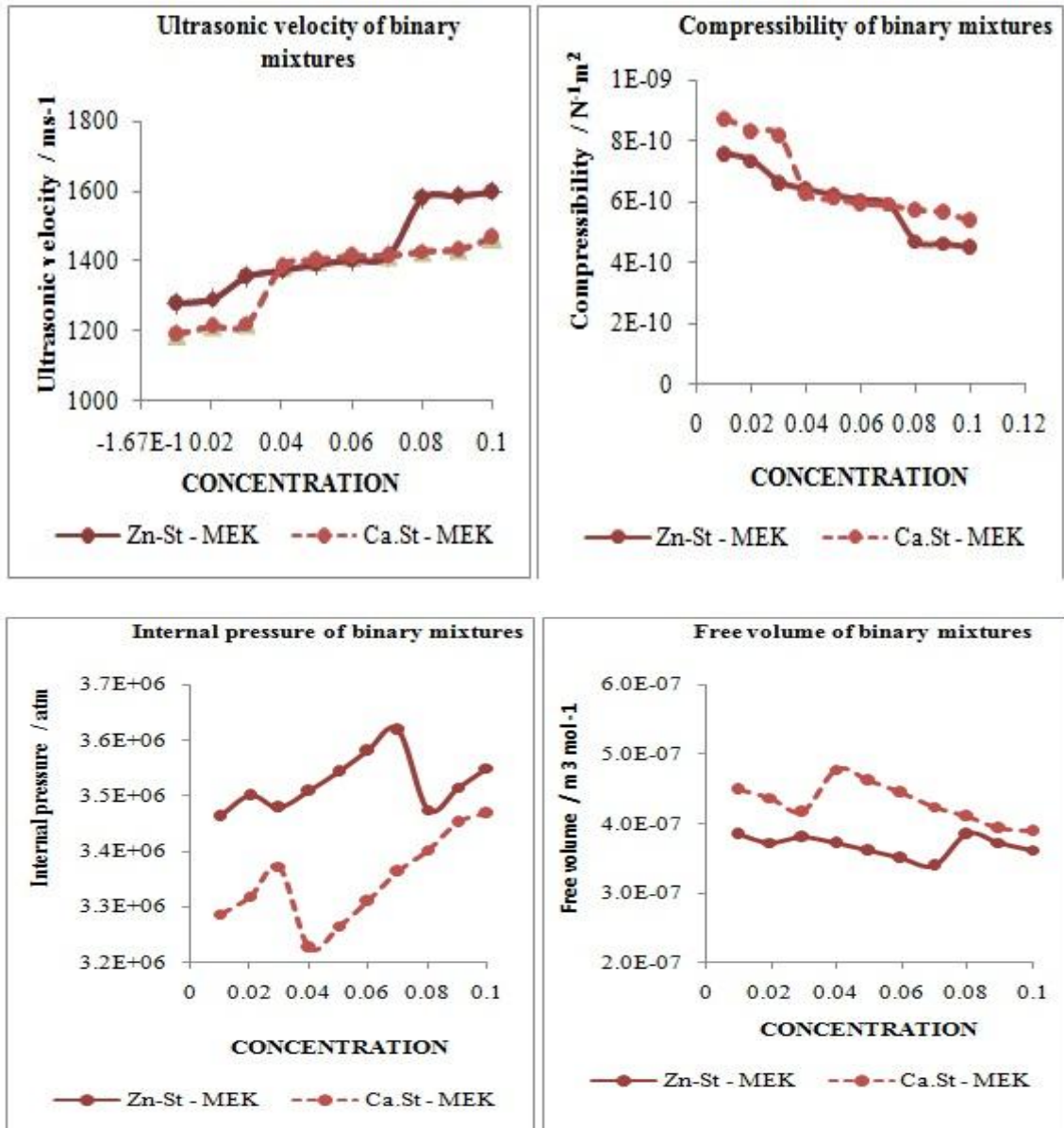


Fig. 1 Computed parameters of zinc stearate – MEK and calcium stearate – MEK at 303 K

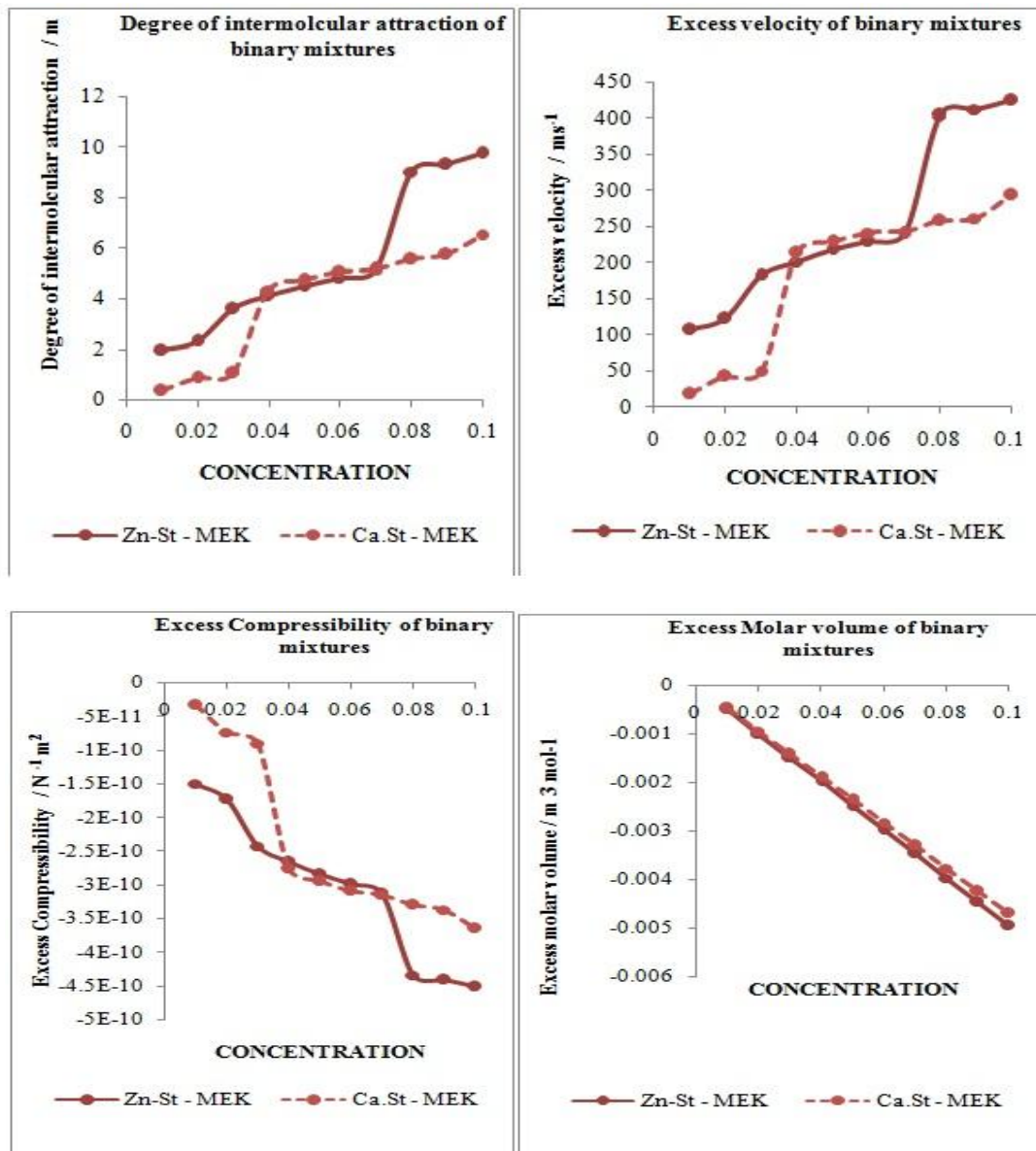


Fig. 2 Excess parameters of zinc stearate – MEK and calcium stearate – MEK at 303 K

The ultrasonic velocity values (U) increases linearly with increase in concentration of stearates zinc stearate, calcium stearate in addition to methyl ethyl ketone. Increase in concentration of either zinc stearate or calcium stearate favours increase in ultrasonic velocity due to decrease in space between chains inside the structure of material, thus decrease in spacing may be attributed to increase in cross linking between chains which consequently cause increase in rigidity of the material. When kinetic elements of adjacent chains have high mobility, cross linkages prevent the moving part of adjacent chains increase effectiveness of intermolecular interaction. This may result in a growth in the modulus of elasticity of stearates and ultrasonic velocity with increase in cross linkage factor. However, ultrasonic velocity increases as stearates behave as weak electrolytes in dilute solution and ionize into simple metal cations as either Zn^{2+} and $RCOO^-$ or Ca^{2+} and $RCOO^-$. Methyl ethyl ketone used in the present study depends upon polarity, increase in polarity due to the high electro negativity increases molecular motion leading to solute – solvent interaction [4]. It is observed that slight increase in addition of zinc stearate with methyl ethyl ketone than with calcium stearate – methyl ethyl ketone, but after 0.04M concentration, it shows similar trend of increase with increase in stearate concentration. The density values (ρ) increases with increase in concentration predicts that there is greater molecular interaction between the two components [5]. The viscosity values (η) increases with increase in concentration which give some reliable information in the study of molecular interaction [6]. As concentration increases, association increases or steric crowding is more so that the intermolecular interaction between the molecules is weakened.

The adiabatic compressibility (β) exhibits an exact reverse trend as that of ultrasonic velocity. The disruption of stearates by solvents and weak interaction between unlike molecules leave the binary mixtures more compressible. When stearates are added to methyl ethyl ketone, it attracts certain solvent molecules towards itself by wrenching the molecule from bulk of the solvent due to the force of electrostriction. The available solvent molecules for the next incoming component get decreased and every solvent has a limit for the compression as limiting compressibility value. The

compressibility of solvent is greater than that of solution and it decreases with increase in concentration of solution [7] shows non – linear variation in both zinc stearate – methyl ethyl ketone and calcium stearate – methyl ethyl ketone. Acoustic impedance increases with increase in stearate concentration due to the interaction between stearate and solvent molecules which increases intermolecular distance making relatively wider gaps between the molecules and becoming the main cause of impediment in the propagation of ultrasonic waves. It is observed that linear increase in acoustic impedance with increase in concentration of either zinc stearate or calcium stearate confirms the presence of molecular association between solute – solvent molecules through intermolecular hydrogen bonding [8]. Rao constant (R) and Wada's constant (W) shows linear variation and almost it is constant with increase in concentration which indicates the presence of solute – solvent interaction. In mixtures zinc stearate – methyl ethyl ketone and calcium stearate – methyl ethyl ketone, decrease in the free volume is observed. It also confirms the increasing order of symmetry and presence of close packing nature in the systems.

The intermolecular free length (L_f) also follows the same trend as that of adiabatic compressibility. The decrease in free length with increase in ultrasonic velocity along with increase in concentration of zinc stearate or calcium stearate in binary mixtures leads to increase in intermolecular force, which strengthens the idea of molecular association in each system [9]. In both the binary mixtures zinc stearate – methyl ethyl ketone and calcium stearate – methyl ethyl ketone greater free length is predicted.

For the binary mixtures zinc stearate – methyl ethyl ketone and calcium stearate – methyl ethyl ketone, the association between like molecules is weak unlike molecular interaction at specific concentration which leads to the very low contribution to the internal pressure values. The change in the values of internal pressure is very low which suggests that weak interaction is present and which is almost concentration independent. Increase in internal pressure with decrease in free volume along with increase in concentration of stearate suggest the close packing of the molecules inside the shield, which may be brought about by increase in magnitude of interactions.

The absorption coefficient values (α/f^2) in binary mixtures zinc stearate – methyl ethyl ketone and calcium stearate – methyl ethyl ketone decreases and increases with variation in concentration. The values of relaxation time are calculated shows both increase and decrease with increase in concentration of either zinc stearate or calcium stearate to methyl ethyl ketone. Intermolecular attraction is the study of the structural variation and the nature of interaction occurring in the system. Maximum value confirms the presence of intermolecular interaction in system. In addition of zinc stearate – methyl ethyl ketone and calcium stearate – methyl ethyl ketone interaction parameter (α) value increases with increase in concentration shows molecular interaction between them [10]. Large positive value of interaction parameter yields weakening of molecular forces. The strengthening of molecular forces is represented by negative values of molecular interaction parameter.

The computed values of excess parameters for the mixtures at temperature 303 K are given in Table 5 and the plots of excess parameters versus concentration are shown in Fig.1 & 2. The excess velocity shows positive deviations which predict the weak interaction due to dispersion force. It shows non linear variation for zinc stearate – methyl ethyl ketone and calcium stearate –methyl ethyl ketone, predicting specific intermolecular interaction between them, leads to strong association due to rupture of cohesion and growing adhesion forms dipole – dipole interaction. Non linear increase and decrease values are observed with respect to the concentration of stearates. In all binary mixtures, it shows large deviation at high concentration implies that the specific interaction dominate over the dispersive interaction between unlike molecules. However decrease in excess compressibility with increase in ultrasonic velocity suggests that there may be strong intermolecular hydrogen bond existing between them making the binary mixture less compressible indicate significant interaction [11]. The negative excess free length values investigated are resultant of several opposing factors such as strong molecular interaction through charge transfer, dipole – induced dipole and dipole – dipole interaction, interstitial accommodation and orientation ordering lead to a more compact structure.

It was reported that the positive deviation in excess ultrasonic velocity and excess impedance indicates the presence of strong interactions between component molecules in the mixture. Excess impedance increases with increase in concentration of either zinc stearate or calcium stearate with addition of solvents confirms the strong molecular interaction.

Excess values may be affected by three factors, first factors explains the specific forces between molecules such as hydrogen bond, charge transfer complex shows large negative deviation. The second factor deals with the physical intermolecular forces, including electrostatic forces between charged particles, between a permanent dipole, induction forces between a permanent dipole and an induced dipole, force of attraction and repulsion between non polar molecules favouring physical intermolecular force shows both positive and negative deviation. The third factor deals with the structural characteristics of the component arising from geometrical fitting of one component into other structure due to the differences in shape and size of the components. Excess molar volume shows negative deviation in the binary mixtures and linear decrease with increase in concentration of either zinc stearate or calcium stearate. Increase in chain length and increase in polarizability decreases excess molar volume that can be attributed to strong unlike interactions between molecules.

The experimental and theoretical velocities calculated by using various empirical relations are presented in Tables 5 for the binary mixtures at temperature 303 K. It is assumed that all the liquid molecules are spherical in shape which is not true every time, it is supposed that volume does not change on mixing. The deviation factor from the calculated and experimental values of ultrasonic velocity is reasonable and provides very good agreement with experimental value. The observed deviation of theoretical values of velocity from the experimental values should be rather treated as evidence of molecular interaction which takes place between the component molecules in the binary system. Deviation is larger in Van Dael and Vangeel relation due to strengthening among unlike molecules. At all concentrations experimental ultrasonic velocity is found to be in good agreement with theoretical Nomo to velocity which is due to weak dipolar dispersive interaction between like molecules. The agreement between experimental and theoretical velocity follows the order

$U_{Nom} > U_{Jun} > U_{Imp} > U_{Vdv}$. Thus the observed deviation of theoretical values of velocity from the experimental values shows that the molecular interaction is taking place between the solute molecules in stearate and solvent [12]. Comparatively zinc stearate – methyl ethyl ketone shows maximum deviation that confirms strong molecular interaction and calcium stearate – methyl ethyl ketone shows least deviation revealing weak interaction among them. The less deviation in Nomoto's relation suggests that the interactions are due to dipole – dipole, dipole – induced dipole between like molecules. At all concentrations Van Dael and Vangeel velocity value shows maximum deviation. This may not be due to the weak dipolar and dispersive interactions between the like molecules. As the availability of free dipoles increases, the dipole induced dipole interaction dominates [13-14].

IV. CONCLUSION

The present investigation of stabilizers zinc stearate, calcium stearate with solvent methyl ethyl ketone and its experimental values of ultrasonic velocity, density and viscosity for the binary mixtures of zinc stearate - methyl ethyl ketone and calcium stearate - methyl ethyl ketone at 303 K are measured. When aliphatic ketone methyl ethyl ketone is added to either zinc stearate or calcium stearate, interaction is less. It may be due to the reason that both are aliphatic components.

zinc stearate – methyl ethyl ketone \approx calcium stearate – methyl ethyl ketone

Among the binary mixtures, solvents in addition to zinc stearate show maximum molecular interaction than with calcium stearate may be due to the presence of zinc ion. The theoretical velocities obtained by various theories also well reflect the existing interactions. From these data, thermodynamic excess functions have been calculated and correlated using standard relations like Impedance relation, Nomo to relation, Van Dael & Vangeel and Junjie theory. The sign and magnitude of these quantities have been discussed in terms of dipole – induced dipole interactions between the mixing components.

REFERENCES

- [1] Gouw T H and Vlugter Ultrasonic sound velocity, (1964) 524.
- [2] Jaroslaw Wawer, Anna Placzek, Dorota Warminska, Waclaw Grzybkowski J. Mol. Liq., 149 (2009) 37.
- [3] G W Marks J. Acoust. Soc. Am. 41 (1967) 103
- [4] Nath G and Paikaray R Indian J. Phys., 83(9) (2009) 1309.
- [5] Vasantharani P, Pandiyan V and Kannappan A N Asian Journal of Applied Sciences 2(2) (2009) 169.
- [6] George Ritzoulis Can. J. Chem., 67 (1989) 1105.
- [7] Sethu Raman M, Ponnuswamy V, Kolandaivel P and Perumal K J. Mol. Liq., 135 (2007) 46.
- [8] Syamala V, Siva Kumar K and Vekateswarlu P J. Mol. Liq., 136 (2007) 29.
- [9] Madhu Rastogi, Aashees Awasthi, Manisha Gupta and Shukla J P J. Mol. Liq., 107/1-3(2003) 185.
- [10] Pandey J D, Sanguri V, Dwivedi D K and Tiwari K K J. Mol. Liq, 135 (2007) 65.
- [11] Amalendu Pal and Rekha Gaba Journal of Molecular Liquids, 144 (1-2) (2009) 50.
- [12] Nadhibatla V Sastry, Rakesh R Thakor and Mitesh C Patel Journal of Molecular liquids. 144 (2009) 13.
- [13] R Kumar, S Jayakumar and V Kannappan, Indian Journal of Pure & Applied Physics, Vol. 46. March 2008, pp. 169 – 175.
- [14] Ulagendran, R Kumar, S Jayakumar and V Kannappan. Journal of Molecular liquids, 148 (2009) pp. 67 – 72.

Engineering Properties of Kaolinitic Clay with Potencial Use in Drugs and Cosmetics

M. G. Silva-Valenzuela,¹ C. M. Matos,² L. A. Shah,³ F.M. S. Carvalho,⁴

I. J. Sayeg,⁵ F. R. Valenzuela-Diaz⁶

¹Polytechnic School, University of São Paulo, Brazil.

²University Center Estacio Radial of São Paulo, Brazil.

³Institute of Physics & Electronics, University of Peshawar, Pakistan

⁴Intituto de Geoscience, University of São Paulo, Brazil.

ABSTRACT: The Clays are one of the oldest raw materials available. They are minerals abundant around the world and, currently, when the societies are more interested in environmentally correct products, clays appear as an important alternative, because they are environmentally-friendly materials. In this study, our objective is to describe some properties of one Brazilian kaolin clay for use in drugs and cosmetics. The kaolin sample was characterized by X-ray diffraction, optical microscopy, scanning electron microscopy, swelling capacity and cation-exchange capacity. Our results show that the analyzed kaolin sample has potential for use in cosmetics.

I. INTRODUCTION

Clays are a powerful and abundant material in nature, presenting several properties which may justify ~~you~~ their use in many industrial applications. They can be used as a raw material in several industry segments, such as civil construction and oil wells, chemical, white ceramic, food, drugs and cosmetics, filler for polymers, and others [1, 2]. For each application the engineering properties of the clays must be carefully designed to obtain the desired result.

Clays are usually defined as natural materials presenting fine granulometry. Often, these materials exhibit a lamellar structure as a consequence of the crystalline arrangement formed by the silicon and aluminum oxides, which are the main components of clays. These structures displayed by these materials, tetrahedral for silicon oxide and octahedral for aluminum oxide combine to form a unique structural arrangement in which sheets of tetrahedral and octahedral overlap each other, leading to structural changes such as 2:1 (one octahedral sheet between two octahedral sheets) and 1:1 (one tetrahedral sheet to one octahedral sheet) that characterize the various clay minerals [3, 4]. Bentonite and kaolin clays, the most studied clays, presenting structure 2:1 and 1:1, respectively. The searched engineering properties in these clays are related to their structures, and may be described by chemical composition, granulometric distribution, swelling capacity, morphology, plasticity, resistance, and cation-exchange capacity. Besides the main clay minerals expected to be found in given clay, other clay minerals, accessory minerals, and unwanted components [5], can be found in natural clays, in a composition that may invalidate their use in industrial applications such as pharmaceuticals and cosmetics. In this way, the degree of purity of the clay is an important property for various applications. [6]. On the other hand, the mineralogical standard presented by clay can maximize its use for a particular application.

The clays, as minerals originated from volcanic eruptions usually, weathering or hydrothermal alteration of crystalline rocks (Fig. 1), may contain in addition to the characteristic clay minerals, trace elements which might be toxic to health depending on their quantity in sample (e.g., Pb, Cd, Hg and others), and accessory minerals or impurities such as quartz, feldspar, mica, pyrite and carbonates, or rutile in varying concentrations. Therefore, depending on their final application, the clay must undergo a process of purification to remove undesirable impurities and ensure the reproducibility of results.

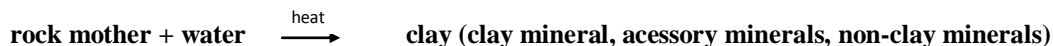


Figure 1. General Scheme of formation of clays and clay minerals.

The kaolin clay, also known as "china clay" is chemically a hydrous aluminum silicate characterized as very fine powder, chemical inertness and lamellar structure (1: 1). In addition, its properties such as color, softness, and small particle size make it a suitable material for various industrial applications.

Kaolins with high purity, in their natural or modified form, are used in the formulations of drugs and cosmetics, primarily as inert charges, but they can also to act as active ingredients, used in medicines for stomach disorders and cosmetic muds. [7].

In this work, we describe the characterization and main engineering properties of a Brazilian kaolin clay to investigate its potential for use in drugs and cosmetics.

II. EXPERIMENTAL

II. 1. Material

In this paper we used a sample of kaolin from São Paulo, Brazil. The sample as received, crude sample, presented white color and was dried at 60°C before use.

II.2. X-ray diffraction (XRD)

The X-ray diffractogram for the sample of kaolin clay was obtained by powder method, using X-ray diffraction from Philips apparatus, X'PERT MPD model, operating in Cu K α radiation, at 40kV and 40 mA, at a scan speed $2\theta/s = 0.020$ and step of 1s, to observe the presence of characteristic clay minerals and accessory minerals.

II.3. Optical microscopy

For this analysis, 1.0 g of sample was added to 50 mL of deionized water, under mechanical agitation during 15 minutes. After shaking the dispersion was transferred to a glass slide of 18 x 18 mm in size, and taken to an oven at 60°C, overnight. The slide containing dry sample was analyzed by optical microscopy in Zeiss Stemi-2000C equipment.

II.4. Scanning electron microscopy (SEM)

Scanning electron microscopy of sample was performed in a LEO 440 device, equipped with Si(Li) solid state detector in X-ray energy dispersive spectrometry, to access the morphology of the kaolin, which was placed on stub, coated with gold in EMITECH K550 sputter coater.

II.5. Swelling capacity

The swelling performance of crude clay has been evaluated based on Foster method [8]. Shortly, 1.0 g of sample has been slowly added to 100 mL graduated cylinders containing 50 mL of deionized water, 10% solutions of sodium lauryl ether sulphate (SLES) and cethyl trimethylammonium chloride (CTAC), and allowed to stand overnight.

III. RESULTS

The result of swelling test for the sample was 2 mL/g, indicating that the sample presents no swelling capacity in the analyzed solvents. However, this was expected due the 1:1 structure of the kaolin clays. Micrographies by SEM showed that the sample is essentially constituted by lamellar structures (Fig. 2). The X-ray diffractogram of the sample (Fig. 3a) revealed the existence of peaks at $d_{001}=7.14 \text{ \AA}$ and $d_{001}=3.5 \text{ \AA}$ for the kaolinite clay mineral, peak at $d_{001}=10.0 \text{ \AA}$ attributed to mineral mica, and peak at $d_{001}=3.3 \text{ \AA}$ related to quartz. By optical microscopy we observe that the analyzed kaolin sample presents a white powder with some silver points, probably related to mica mineral (Fig. 3b).

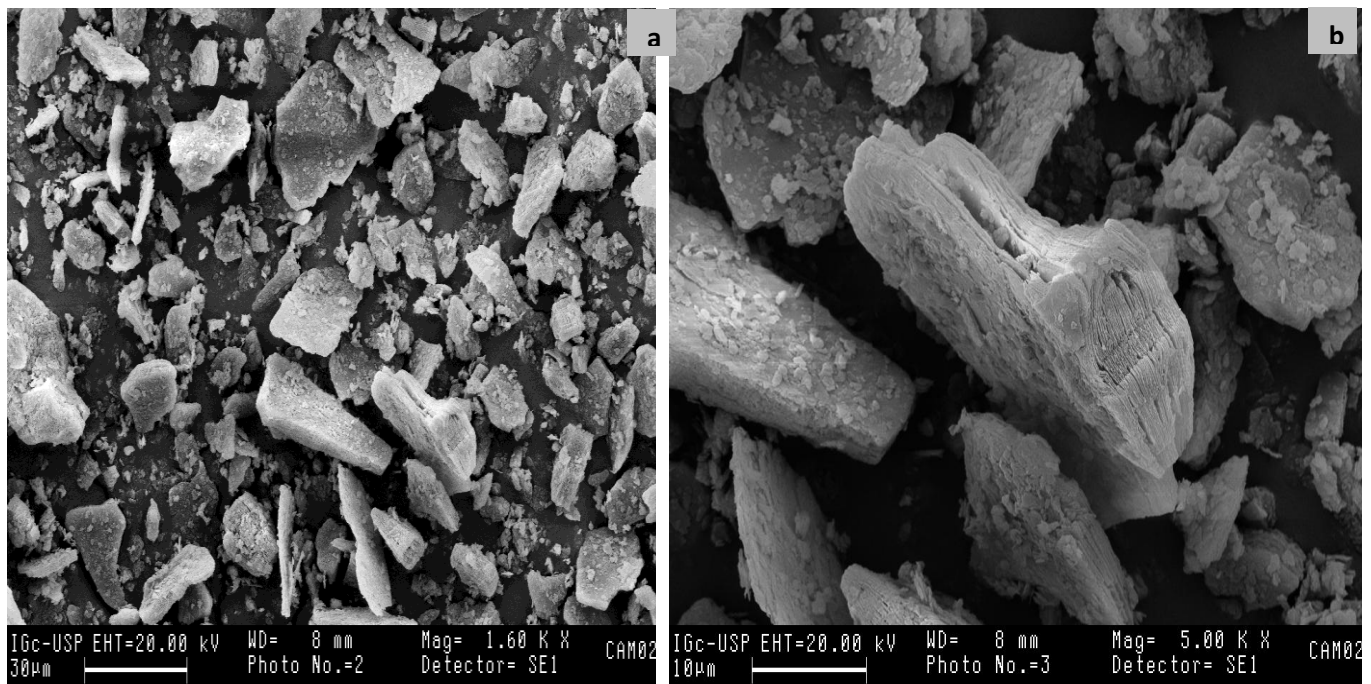


Figure 2. Images of kaolin clay by SEM showing lamellar structure, with different increases: a) 1600X; b)5000X.

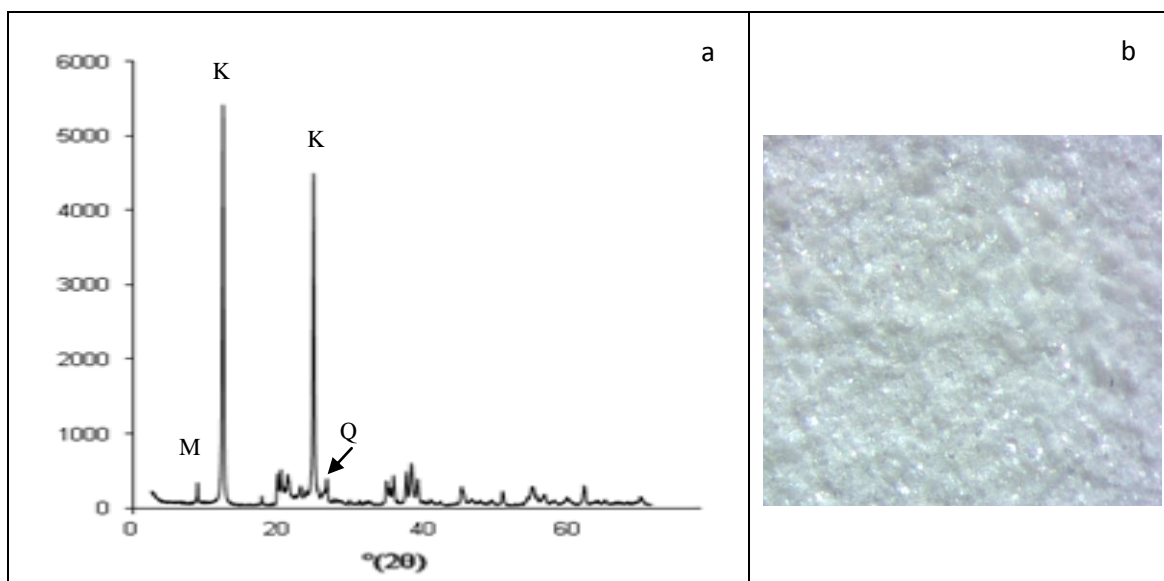


Figure 3. Shows XRD diffractogram (a) and image by optical microscopy (b) for kaolin sample (M=mica, K=kaolin, Q=quartz).

IV. CONCLUSION

Our results showing that the analyzed sample is mainly constituted by kaolinite clay in major concentration, and mica in minor concentration, what was confirmed by optical microscopy. This clay composition might be adequate for some applications of kaolin in cosmetics, since mica is added to some formulations of lotions and emulsions in order to donate brightness. In addition, the analysis by scanning electron microscopy revealed that the kaolin sample analyzed in this work is constituted of kaolinite clay mineral, as evidenced by the lamellar structure observed in the micrographies. These described properties indicate that the sample presents potential to use in cosmetic. However, purification proceedings, and other characterizations, must be performed to ensure its use both in cosmetics as topical drugs.

V. ACKNOWLEDGMENT

We are grateful to FAPESP for financial support.

REFERENCES

- [1] H.H. Murray, in Applied clay mineralogy-occurrences, processing and application of kaolins, bentonites, palygorskyte sepiolite, and common clays, in Development and clay science, 2 (Amsterdam: Elsevier, 2007)85-110.
- [2] A.R.V. Silva and H.C. Ferreira, Argilas bentoníticas: conceitos, estruturas, propriedades, usos industriais, reservas, produção e produtores/fornecedores nacionais e internacionais. Revista Eletrônica de Materiais e Processos, 2 (2008)26-29.
- [3] Grim, R. E. Clay Mineralogy (New York: McGraw Hill, , 1962).
- [4] F.R. Valenzuela-Díaz, P. Souza-Santos and H. Souza-Santos, A importância das argilas industriais brasileiras II. Química Industrial, 44 (1992)31-35.
- [5] K. A. Carrado, S. Decarreau, S. Petit, F. Bergaya and G. Lagaly, Synthetic clay minerals and purification of natural clays, in F. Bergaya, B.K.G. Theng and G. Lagaly (Eds), Handbook of clay science, 1 (Elsevier, 2006) 115-139.
- [6] M.G. Silva-Valenzuela, F.M.S. Carvalho, I.J. Sayeg, L.G. Sant'Anna, F.R. Valenzuela-Díaz, Purification and characterization of a natural Brazilian clay blend. Materials Science Forum 727-728 (2012) 1439-1443.
- [7] A. López-Galindo, C. Viseras, P. Cerezo, Compositional, technical and safety specifications of clays to be used as pharmaceutical and cosmetic products. Applied Clay Sciences, 36(2007)51-63.
- [8] M.D. Foster, Geochemical studies of Clay minerals II – Relation between ionic substitution and swelling in montmorillonites. American Mineralogy 38(1956)994-1006.

Protection of Web Application against Sql Injection Attacks

Sonam Panda,¹ Ramani S²

VIT University, Vellore, India

Abstract: SQL injection attack is the most common attack in websites now-a-days. Some malicious codes gets injected to the database by unauthorized users and because of this attack, the actual database can be stolen or destroyed or modified or the device can be taken control by the hacker. The main cause of this type of attacks is poor coding by the developers. Hence, the login phase is more vulnerable to SQL injection attack and prevention technique should be applied on this phase to secure the database. In this paper, some predefined methods are discussed and hybrid encryption method is applied in the database to avoid attack on login phase. This applied hybrid encryption method is a combination of Advanced Encryption Standard (AES) and Rabin cryptosystem. These two level encryption methods are applied to a system where faculty's information are kept and the designing of this system are done by using PHP and MYSQL.

Keywords: SQL injection attack, hybrid encryption, AES, Rabin, PHP

I. Introduction

With the rising use of internet, web application vulnerability has been increasing effectively. SQL injection attack is an easiest method of attack in which attackers inject some SQL codes to the original code in the database to get sensitive information or to destroy the information. History says SQL injection attack has been there around for years and now this is a popular method to exploit the security system.

Different techniques and methods have been developed and used to protect the database. But still attackers use this method very often because they are finding it easy to type a few deformed SQL commands into the front-end as well as back-end application. Types of SQL injection are tautologies, illegal/ logically in corrected queries, union queries, piggy backed queries, blind injection, timing attacks etc. [3][4]. Attackers inject codes using tautology statements into the authentication phase to enter into the database, which says 1=1 is always true and so the injected query becomes true even if the wrong username and password are being entered. Similarly they use logically incorrect queries to get an error message and this message works as a hint for them to find out some information. Single quotes, double quotes and backslashes are generally used in query to make these incorrect codes work correctly. Union operator is used while injecting codes to join the injected query to the original query. Piggy backed queries are those which use semicolons with injected codes to make duplicate codes work along with original ones. Hackers use blind SQL injection attack by asking some true or false questions if error messages are costumed by programmer. To make a delay in operation, attackers use timing attack and by taking the advantage of

this, attacker hacks the username and password with the use of BENCHMARKS.

Cryptography is an absolutely necessary field that ensures the security of database. By applying encryption method, database attacks can be prevented. Encryption of data helps to change the data into a format that is not readable [1]. Without the proper key, this format can't be deciphered even if attacker hacks the information. Application of encryption in login phase makes it difficult for unauthorized users to access the database. Indrani Balasundaram et al. (2011) proposed a query encryption method using hybrid encryption in which two layer of encryption was applied i.e. AES and RSA encryption [2]. The method of encryption which combines a symmetric and an asymmetric encryption method to take the advantages of each type of method is called hybrid encryption method. In symmetric key encryption, one common key is used by sender and receiver where as in asymmetric key encryption, two keys are used (a public key and a private key). This paper proposes a technique which is similar to previous paper but here Rabin encryption method is applied instead of RSA as Rabin cryptosystem is said to be a good replacement of RSA cryptosystem. Between these two, AES is a symmetric key cryptography where Rabin cryptosystem is an asymmetric or public key cryptography.

The other part of the paper includes related work about SQL injection attack, work done, implementation and discussion and conclusion respectively.

II. Related work

Ettore Merlo et al. (2006) presented an approach which detects insider and outsider threat in SQL injection attack and the implementation was done in PHP [8]. Hasan Kadhem et al. (2009) proposed mixed cryptography to encrypt database [6]. Atefeh Tajpour et al. (2010) did a survey on all types of SQL injection attacks and prevention methods and evaluated all approaches [5]. Indrani Balasundaram et al. (2011) proposed a hybrid encryption (PSQLIA-HBE) to prevent SQL injection attack where they used AES encryption and RSA cryptosystem in the login and verification phase to make the authentication scheme more secure.

III. Work Done

Some predefined methods like quote block function, regular expressions, parameterized queries are used to avoid quotes and strings because their presence have important roles in SQL injection attacks. Especially in PHP, there are predefined codes using these methods to escape from SQL injection attacks [7]. So these are used in this project and for preventing greater exploitation encryption methods are used.

The model proposed by Indrani Balasundaram et al. is used in this paper also. The only difference is that here, Rabin cryptosystem is used instead of RSA cryptosystem

as it is a good replacement to RSA. So, basically the system model is an adaption of previously proposed model. The system model includes three phases i.e. registration phase, login phase and verification phase.

1. In registration phase, a new user registers his/her name by selecting unique username and password and the data get sent to server and when server receives the username and password, it saves these information in the database in a table and along these data; server keeps a unique key for each username generated by the server itself. Then server sends back a confirmation request to the client.

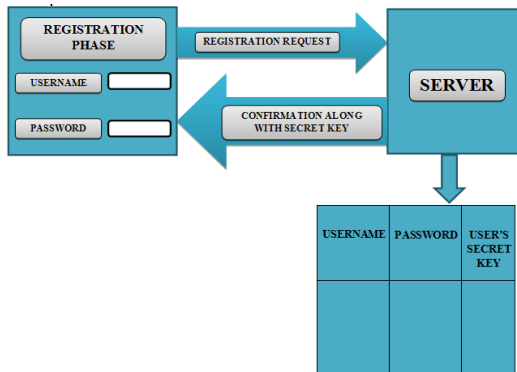


Fig 1: model of registration phase

2. In login phase, when a registered user tries to login, the username and password get encrypted by applying AES encryption algorithm which uses user's secret key. After that, a query gets generated automatically using the encrypted username and password. Then Rabin encryption is used to encrypt the query where server's public key is used to encrypt the query and once it gets encrypted it is sent to the server.

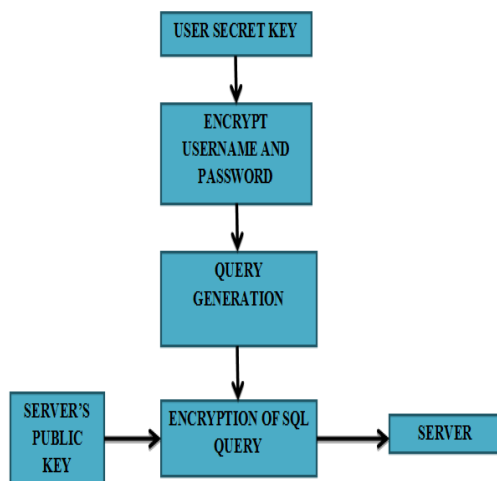


Fig 2: model of login phase

3. In verification phase, when server receives the query, it uses Rabin decryption method to decrypt the query where the server's private keys are used. Server then checks the username and password and again the username and password gets decrypted using AES decryption algorithm. After getting decrypted, if the

username and password match to the database table, the login request gets accepted.

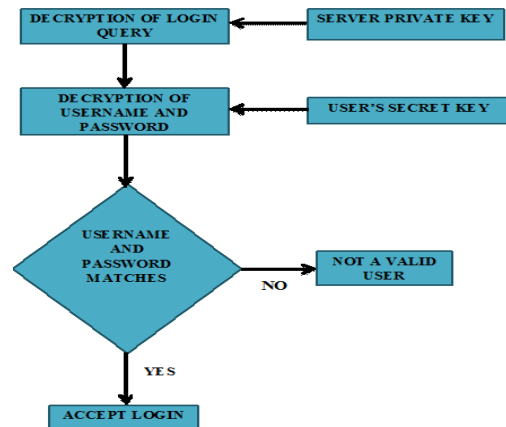


Fig 3: model of verification phase

A little more work is added i.e. after login, a user can search for the faculty's information. The faculty information contains the faculty name, employee id, school name, course title, time, date; slot etc. and one can search by the employee id to know about the information related to the id.

IV. Implementation

The whole implementation is done in windows operating system and the code is developed by using HTML, PHP and MYSQL. PHP has its own predefined commands such as 'mysql_real_escape_string' and 'stripslashes' which are used in this project. So first part of the paper includes a little survey based on predefined function. Net Beans IDE 7.0 and Wamp Server are used for the implementation.

In second part, the system model is an adaption of the model proposed by Indrani Balasundaram et al. (2011). They have implemented the model using core java but here PHP and MYSQL are used. In database, separate tables are there for AES encryption, Rabin encryption, Rabin decryption and AES decryption and all tables have a common column i.e. id. For example,

id	username	password	name	secret_key
1	sonam	123	sonam	202cb962ac59075b964b07152d234b70

Fig 4: Secret Key Generation after Registration

username	password	enc_user	enc_pass	id
sonam	123	95ae5805f83382917a23395abe51cd5	14311c8f75014f193758083b38ac7fde4	1

Fig 5: Sample Example of AES Encryption in Database

The third part consists of four tables i.e. school, faculty, course and slot. All these tables are connected to each other by primary key. So when user searches by giving any employee id, it retrieves the related information. This system is to provide information to students as well as teachers when they need.

V. Conclusion and Future Work

In this paper, various types of SQL injection attacks as well as predefined prevention methods are discussed. Then the hybrid encryption method is used which includes AES encryption and Rabin's cryptosystem. The reason behind the use of two layer of encryption is that it will be more secured. SQL query is generated and encrypted by Rabin's cryptosystem because even if hackers hack the information and decode the AES encryption part, it will still be more difficult for them to know about the encrypted query. Between Rabin and RSA, it is difficult to say which cryptosystem is better. So Rabin encryption is applied in this paper because it is a good alternative to RSA and in some cases Rabin is a little faster than RSA. This proposed method is an attempt to add some more security to databases to avoid SQL injection attack.

References

- [1] Berhrouz A Forouzan et al., Cryptography and Network Security, New Delhi: McGraw-Hill
- [2] Indrani Balasundaram et al. "An authentication scheme for preventing SQL injection attack using hybrid encryption (PSQLIA-HBE)" Euro journal publishing, 2011.
- [3] XuePing-Chen "SQL injection attack and guard technical research" 2011.
- [4] Varian Luong "Intrusion detection and prevention system: SQL injection attacks", 2010.
- [5] Atefeh Tajpour et al. "Evaluation of SQL Injection Detection and Prevention Techniques" Second International Conference on Computational Intelligence, 2010.
- [6] Hasan Kadhem et al. "A Novel Framework for Database Security based on Mixed Cryptography" Fourth International Conference on Internet and Web Applications and Services, 2009.
- [7] Ettore Merlo et al. "Automated protection of PHP applications against SQL injection attacks" IEEE 2007.
- [8] Ettore Merlo et al. "Insider and outsider threat sensitive SQL injection vulnerability analysis in PHP" IEEE 2006.

An Experimental Study on Diesel Engine Performances Using Biodiesel from Used Frying Oil

Pravin V. Jadhav,¹ Vinod M. Wankar²

1, 2 Department of Mechanical Engineering, Priyadarshini college of Engineering, Nagpur, India

Abstract: The paper contains study of diesel engine performance using bio-diesel from waste frying oil. Biodiesel is produced from used frying oil which is obtained from local restaurant and hotels by transesterification process. In the present study neat biodiesel as well as blends of varying proportions of bio-diesel and diesel were used to run C.I. engine. It is found that viscosity of bio-diesel was more which affects the performance of diesel engine. Expectable thermal efficiencies and specific fuel consumption (SFC) were achieved with blends without any operational difficulties. In the present work performance of diesel engine using varying blends of biodiesel like B20, B60 and B100 i.e. neat biodiesel is tested.

Keyword: biodiesel, C.I. engine, SFC, transesterification, emission

I. INTRODUCTION

Due to global depletion of world petroleum reserves and the impact of environmental pollution of increasing exhaust emission there is an urgent need for suitable alternative fuel. The various alternative fuel options researched for diesel are mainly biogas producer gas, methanol, ethanol and vegetable oil. Out of this vegetable oil is one of the promising fuels for diesel engine. An idea of using vegetable oil as fuel for diesel engine is very old as Dr. Rudolph Diesel used peanut oil in one of his engine at Paris exposition in the year 1900. The interest in vegetable oil revalued again in 1973 after energy crises situation and much edible oil as well as non edible oil like sunflower, soybean peanuts etc. were tested. But considering fodder value of edible oil the waste frying oil is started testing for its suitability with diesel fuel. There are huge amount of used frying oil from restaurant, hotels that has no proper used. As this oil are available at low cost and using this oil for biodiesel will ensure better use of both money and used fried oil which otherwise going to waste. Research conducted all over the world using biodiesel and biodiesel blends. Diesel engine were fueled with B20, B50 and B100 or neat biodiesel fuel, from all the result it is evident blends with diesel gives better performance related of engine performance as well as exhaust emission. So studies of blends are very important.

II. Experimental Setup

The setup consists of a single cylinder, four strokes, Diesel engine connected to eddy current type dynamometer for loading. Provision is made for interfacing airflow, fuel flow, temperatures, Speed and Torque measurement. The set up has stand-alone panel box consisting of air box, fuel tank, manometer, fuel measuring unit, transmitters for air and fuel flow measurements.

The biodiesel was prepared from used frying oil collected from local restaurants, hotels by transesterification process. The blends used for testing are B20, B60 and B100. Comparison of fuel property between diesel and bio-diesel given in table 1

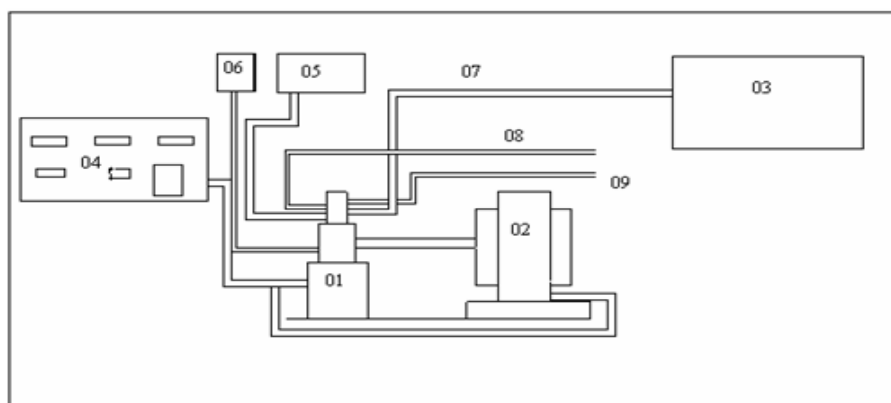


Fig: 1 Experimental setup four stroke single cylinder diesel engine

- | | |
|--------------------------|---|
| 1: Engine | 2: Dynamometer |
| 3: Gas Analyser | 4: Digital display of mass of fuel, mass of air, Various Temperature and Dynamometer Control Knob |
| 5: Air Tank | 6: Fuel Tank |
| 7: Exhaust Gas Pipe Line | 8 : Water In |
| 9 : Water Out | |

Table: 1 Comparative analysis of fuel properties using fried oil biodiesel and diesel.

Fuel properties	Diesel	Biodiesel
Density (gm/cc)	0.845	0.9
Viscosity (cSt)	3.0	5.7
Flash point (°C)	32	140
Cetane no.	48	55
Calorific value (KJ/Kg)	42000-46000	38000-42000

Main differences between diesel fuel, ester fuel and vegetable oil are the viscosity, certain number and heat content. The viscosity of diesel is about 3.0g/cc and that of fried oil biodiesel is 5.7g/cc. The viscosity of a fuel is important because it affects the atomization of the fuel being injected into the engine combustion chamber. A small fuel drop is desired so complete combustion occurs. A high viscosity fuel, such as raw oil, will produce a larger drop of fuel in an engine combustion chamber, which may not burn as clean as a fuel produces a smaller drop. Unburned oxidized fuel will build up in the engine around valves, injector tips and on piston and ring. Biodiesel has a viscosity much smaller drop, which burns cleaner. Rating varies considerably among the listed fuels, and is a measure of the self-ignition quality of the fuel. Diesel fuel usually has Cetane rating between 45 and 50 while vegetable oil 35 to 45. Biodiesel is usually 50 to 60. The quality affects engine performance, cold starting, warm up and engine combustion roughness. Cetane rating is to the volatility of the fuel where more volatile fuels have higher rating. A high cetane fuel also may lead to combustion and smoke if the fuel ignites too soon by not allowing enough time for the fuel to mix with air for combustion. The energy content of the fuels also varies. Diesel fuel typically contains about 42000-46000 while vegetable oil and biodiesel contain about 38000-42000KJ/Kg.

Test engine:

Test is carried on Kirloskar diesel DM103 having compression ratio 17.5:1 rated power of 10 BHP at rated speed of 1500 rpm – The engine is coupled with eddy current dynamometer for loading.

III. Result and Discussion

The CI engine is tested at various loads starting from no load condition to rated load condition the test is conducted at constant speed equal to rated engine speed. The engine did not have any initial starting difficulties during operation using neat biodiesel from waste fried oil and its blend with diesel.

Engine performance:

Brake Thermal Efficiency:

Fig. 2 shows the engine performance at various load starting from no load to full load. There is a small deviation in brake thermal efficiency for biodiesel that with diesel. The brake power developed is reduced in biodiesel as compared to diesel. The brake thermal efficiency decreases slightly. As the amount of biodiesel increases, the brake thermal efficiency decreases. This happened due to higher viscosity & lower heat content of biodiesel.

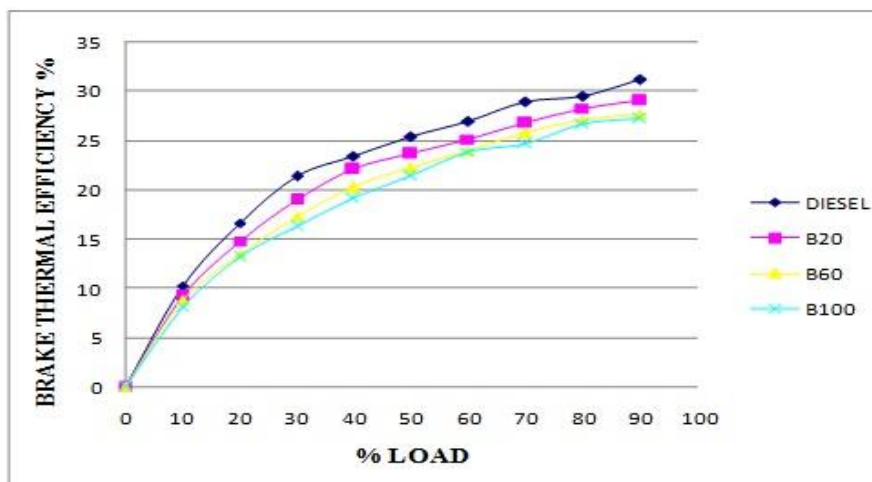


Fig. 2 BTE v/s Load

Break Sp. Fuel consumption:

Fig.3 shows brake specific fuel consumption of the engine against load. The Sp. Fuel consumption is higher in biodiesel; as compared to diesel. The reason is that fuel has lower calorific value. As a result to produce the same amount of energy, more amount of biodiesel is consumed. As the percentage of biodiesel in blend increases the BSFC increases.

IV. CONCLUSION

The exhaust performance characteristics of waste fried oil biodiesel and its blends with diesel have been compared with diesel performance. The results of study are as follows.

- i) The properties of biodiesel from waste fried oil are comparable with diesel fuel.
- ii) The waste fried oil biodiesel shows similar trends for brake thermal efficiency with slight reduction in the brake thermal efficiency. For B20 it is very close to that for diesel.
- iii) Brake specific fuel consumption (BSFC) for biodiesel from waste fried oil is higher because of lower heating values. The Sp. Fuel consumption increases with blending proportion for waste fried oil.

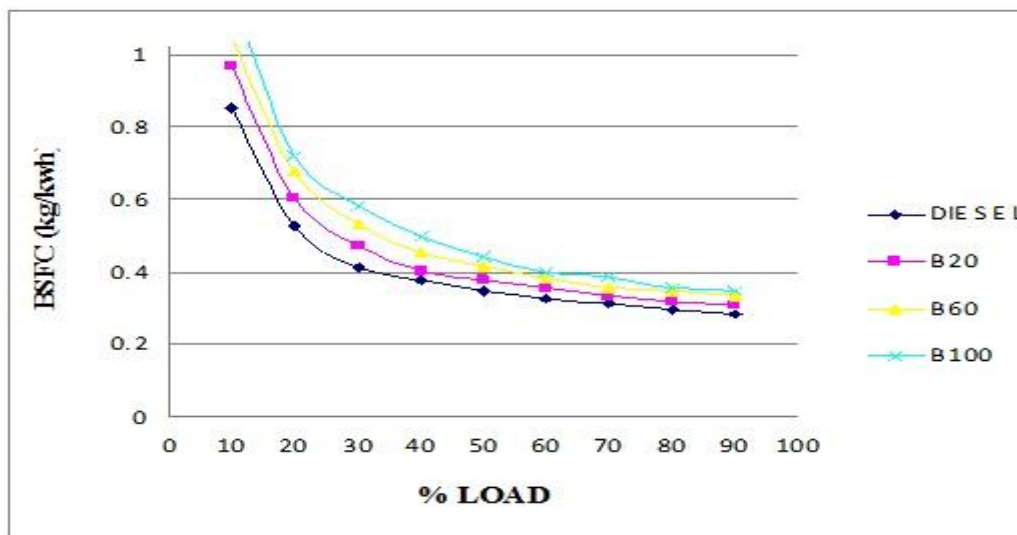


Fig 3 BSFC v/s Load (%)

REFERENCES

- [1] G Lakshmi Narayana Rao, S Sampath, K Rajagopal "Experimental Studies on the Combustion and Emission Characteristics of a Diesel Engine Fuelled with Used Cooking Oil Methyl Ester and its Diesel Blends" International Journal of Applied Science, Engineering and Technology 4;2 © www.waset.org Spring 2008
- [2] Nagao Totani, Kumiko Tsuji, Ayako Yamaguchi "Effects of deteriorated frying oil on Wistar Rats" Oleo Sci. 55 (6), 291-297 (2006)
- [3] M. Mittelbach, S. Gangl "Long storage stability of biodiesel made from rapeseed and used frying oil". JACOS, Vol., 78, no. 6 (2001)
- [4] A.Serdari, K. Fragioudakis, S. Kalligeros, S. Stounas, E. Lois "Impact of using biodiesels of different origin additives on the performance of a stationary diesel engine". Transaction of the ASME Vol. 122, 624-631, (2000).
- [5] Y. Zhang, M.A. Dube, D.D. McLean, M. Kates "Biodiesel production from waste cooking oil: 1. Process design and technological assessment" Bioresource Technology 89, 1-16, (2003)
- [6] Kapila Wadumesthrige, Jeremiah C. Smith, John R. Wilson, Steven O. Salley, K. Y. Simon Ng "Investigation of the Parameters Affecting the Cetane Number of Biodiesel" J Am Oil Chem Soc 85:1073-1081,(2008)
- [7] Matt Johnston, and Tracey Holloway "A global potential of national biodiesel production potential." Environ. Sci. technol. 41(23), 7967-7973, (2007)
- [8] Anh N. Phan, and Tan M. Phan "Biodiesel production from waste cooking oils." Science direct, 87 (17-18), 3490-349, (2008)
- [9] Arjun B. Chhetry, K. Chris Watts, M. Rafiqul Islam "Waste cooking oil as alternative feedstock for biodiesel production." Energies, 1, 3-18; 2008
- [10] Divya Bajpai V.K Tyagi "Biodiesel: Source, Production, Composition, Properties and Its Benefits."J.Oleo.Sci.. 55 (10), 487-502, (2006)
- [11] C.V. Sudhir, N.Y. Sharma and P.Mohanani "Potential of waste cooking oils as biodiesel feed stock". Emirates Journal for Engineering Research, 12 (3), 69-75 (2007)

Dynamic Analysis of Delaminated Sandwich Composites

Nisha A S,¹ Saraswathy B²

¹(Department of Civil Engineering, NSS College of Engineering, University of Calicut, Kerala, India

²(Department of Civil Engineering, TKM College of Engineering, Kerala University, Kerala, India

ABSTRACT: The analytical formulation for free vibration of sandwich beams consisting of two different layers and is split along the interface with single and multiple delaminations is presented here. The influence of the delamination size and location on the natural frequency is investigated experimentally for beams with single delamination and the results agree well with present analytical formulation. Modal analysis has also been conducted using finite element package ANSYS and has been compared with the experimental results. It is observed that the delamination reduces the natural frequency and change the mode shape. To identify the exact location and extent of delamination, strain plots are used.

Keywords: Debond, Delamination, Free Vibration, Mode Shapes, Natural Frequency

I. Introduction

Composite materials have fully established themselves as workable engineering materials and are now quite extensively used in various engineering applications wherein weight saving is of paramount importance. However composites are very sensitive to the anomalies induced during their fabrication or service life. These materials are prone to damages such as fibre breakage, matrix cracking and delamination. Delamination is the critical parameter for laminates under compression and one of the most common failure modes in composite laminates. Delamination reduces the load-carrying capability of the structure and can thus lead to an early failure. Delamination can promote early failure by interacting with other failure modes. The presence of delamination in a composite structure affects its integrity as well as its mechanical properties such as stiffness and compressive strength. Vibration based methods are a new approach for damage detection and are more globally sensitive to damage than localized methods such as ultrasonic and thermography methods.

Ahmed [1] presented a finite element analysis technique which includes the effect of transverse shear deformation for sandwich beams without any debond Wang et al [2] examined the free vibration of an isotropic beam split by a through-width delamination. They analyzed the beam as four joined Euler- Bernoulli beams, which were assumed to vibrate 'freely' without touching each other. This was later improved by Mujumdar and Suryanarayanan [3] who then proposed a solution based on the assumption that the delaminated beams were constrained to have identical transverse displacement. Their solution compared favorably with their experiments on homogeneous, isotropic beams with single delaminations. But multiple delaminations further weaken a sandwich beam and cause a shift in natural frequencies. An increased number of delaminations also considerably complicate the problem and hence no analytical solution has been studied in detail so far. In the present study, the formulation of Mujumdar and Suryanarayanan [3] has been extended for beams with multiple delaminations. Pandey and Biswas [4] used mode shape curvature method for damage assessment in composites. This methodology is modified using strain plots for identifying the location and extent of delamination in the present study.

II. Analytical formulation

Fig 1 shows a beam with two arbitrarily located through-width delaminations. The beam is assumed to be homogeneous and isotropic. For the analysis, beam has been subdivided into seven regions, namely two delaminated regions and three integral regions. The delamination region itself is made up of two separate component segments above and below the plane of delamination, joined at their ends to the integral segments. Each segment is modeled as an Euler beam. It is assumed that transverse displacement of the delaminated layers is identical and there is no natural gap between the delaminated layers.

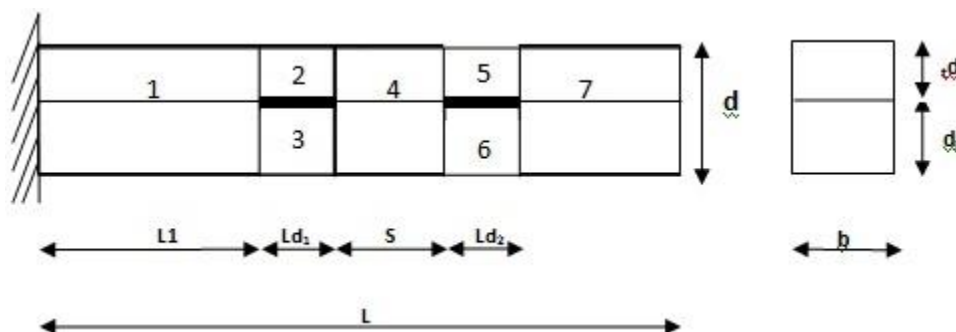


Fig .1 Model of multiple debonded two layered sandwich beam

The governing equations of transverse equilibrium for the intact regions are,

$$\frac{\partial^4 w_i}{\partial x^4} + \frac{\rho A}{EI} \frac{\partial^2 w_i}{\partial t^2} = 0, \quad i=1,4,7 \dots \dots \dots (1)$$

In the case of delaminated segments 2 and 3, the governing equation can be written as

$$\frac{\partial^4 w_2}{\partial x^4} + \frac{\rho(A_2 + A_3)}{E(I_2 + I_3)} \frac{\partial^2 w_2}{\partial t^2} = 0, \quad \text{since } w_2 = w_3. (2)$$

Similarly for delaminated segments 5 and 6, the governing equation can be written as

$$\frac{\partial^4 w_5}{\partial x^4} + \frac{\rho(A_5 + A_6)}{E(I_5 + I_6)} \frac{\partial^2 w_5}{\partial t^2} = 0, \quad \text{since } w_5 = w_6. (3)$$

$$\text{Assume harmonic function } w_i(x, t) = W_i(x)e^{i\omega t} (4)$$

where ω is the natural frequency and W_i is the mode shape.

Substituting Eq.(4) in Eqs.(1), (2), (3) and introducing non-dimensional variable $\xi = \frac{x}{L}$, we can obtain the generalized solutions of the Eqs.(1), (2) and (3) as

$$W_1(\psi) = A_1 \cosh(\lambda\psi) + A_2 \sinh(\lambda\psi) + A_3 \cos(\lambda\psi) + A_4 \sin(\lambda\psi) (5)$$

$$W_2(\psi) = A_5 \cosh(\lambda_{d1}\psi) + A_6 \sinh(\lambda_{d1}\psi) + A_7 \cos(\lambda_{d1}\psi) + A_8 \sin(\lambda_{d1}\psi) (6)$$

$$W_4(\psi) = A_9 \cosh(\lambda\psi) + A_{10} \sinh(\lambda\psi) + A_{11} \cos(\lambda\psi) + A_{12} \sin(\lambda\psi) (7)$$

$$W_5(\psi) = A_{13} \cosh(\lambda_{d2}\psi) + A_{14} \sinh(\lambda_{d2}\psi) + A_{15} \cos(\lambda_{d2}\psi) + A_{16} \sin(\lambda_{d2}\psi) (8)$$

$$W_7(\psi) = A_{17} \cosh(\lambda\psi) + A_{18} \sinh(\lambda\psi) + A_{19} \cos(\lambda\psi) + A_{20} \sin(\lambda\psi) (9)$$

$$\text{where } \lambda = \left[\frac{\rho A \omega^2 L^4}{EI} \right]^{1/4}, \quad \lambda_{d1} = \lambda \left[\frac{I}{I_2 + I_3} \right]^{1/4} \quad \text{and} \quad \lambda_{d2} = \lambda \left[\frac{I}{I_5 + I_6} \right]^{1/4} (10)$$

The 20 unknown coefficients A_1 to A_{20} can be determined using appropriate boundary conditions of intact regions and continuity/equilibrium conditions at delamination boundaries.

The boundary conditions for a cantilever beam are as given below:

$$1. \text{ The deflection at the fixed end is zero, ie. at } \psi = 0, W_1 = 0 (11)$$

$$2. \text{ The slope at the fixed end is zero, ie. at } \psi = 0, \frac{dW_1}{dx_1} = 0 (12)$$

$$3. \text{ The bending moment at the free end is zero, ie. at } x=L; \psi = 1, \frac{d^2W_7}{dx_7^2} = 0 (13)$$

$$4. \text{ The shear force at the free end is zero, ie. at } x=L; \psi = 1, \frac{d^3W_7}{dx_7^3} = 0 (14)$$

The Continuity/Equilibrium conditions are as given below:

At the delamination boundary, $x=L_1, \psi = \frac{L_1}{L} = \psi_1$. Applying the compatibility conditions, the following equations are derived.

$$1. \text{ Deflection compatibility states that } W_1(\psi_1) = W_2(\psi_1) (15)$$

$$2. \text{ Slope compatibility states that } W_1'(\psi_1) = W_2'(\psi_1) (16)$$

3. Bending moment compatibility condition states that

$$EIW_1''(\psi_1) = E(I_2 + I_3)W_2''(\psi_1) \quad (17)$$

4. Shear force compatibility condition states that

$$EIW_1'''(\psi_1) = E(I_2 + I_3)W_2'''(\psi_1) \quad (18)$$

At the delamination boundary, $\psi = \psi_2 = \frac{L_1 + L_{d1}}{L}$, applying compatibility conditions, the following equations are derived.

5. Deflection compatibility states that $W_2(\psi_2) = W_4(\psi_2)$ (19)

6. Slope compatibility states that $W_2'(\psi_2) = W_4'(\psi_2)$ (20)

7. Bending moment compatibility condition states that

$$EIW_4''(\psi_2) = E(I_2 + I_3)W_2''(\psi_2) \quad (21)$$

8. Shear force compatibility condition states that

$$EIW_4'''(\psi_2) = E(I_2 + I_3)W_2'''(\psi_2) \quad (22)$$

Similarly at the second delamination boundaries, we can get 8 more equations. This forms a set of 20 homogeneous equations for 20 unknown coefficients. Solving the eigen value problem, we obtain the natural frequencies and mode shapes.

The above formulation has been used for finding the natural frequencies of beams with different end conditions, viz. both ends fixed and both ends free.

III. Finite Element Analysis

The finite element models used for the present study are generated using a meshing application developed in Visual Basic. A single keypoint is created at the ends of the delamination and two keypoints are created anywhere along the delamination using this program as in Fig 2. The volumes above the delaminated region are defined using one of the two keypoints and the volumes below are defined using the other keypoint. This ensures no connectivity between the volumes above and below the delaminated region and thus it behaves as a delaminated beam. Layered brick element of SOLID45 is used for the modeling of sandwich composite beams. It is an 8-noded layered structural solid element. The element has three translational degrees of freedom per node in the nodal x, y, and z directions [5].

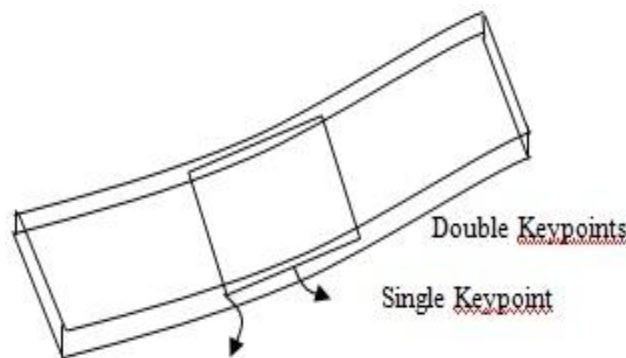


Fig 2. Delamination Modeling in FEM

IV. Experimental Study

An experimental study is carried out to show the validity of the analytical results obtained. The beam specimens are made by bonding thin aluminum strips using a very thin epoxy film adhesive. The delamination is simulated by bonding only a part of the beam surfaces to create unbonded regions at various locations. Delaminations are created by inserting telephone sheet of 50 microns along the width for the required length (50 mm) of delamination.

In order to incorporate the effect of central layer delaminations, the thickness for each aluminium strip is kept as 2mm. The beams are of sizes 300mm×25mm×2mm each. The delamination length of the manufactured specimens is kept as 50 mm.



Fig 3. Two layered metallic beam specimens with 50 mm delaminations

A piezoelectric accelerometer (Model 8730AE500, SNC190699 manufactured by Kistler) with a measuring range of ± 500 g, and sensitivity 9.52mV/g is used for testing. The instrumented hammer is Bruel & Kjaer (Model No. 8202) equipment along with a force gauge (Model No 8200) with an output sensitivity of 9.52mV/g. Weight of the hammer is 280 grams. A PC based 2 channel FFT analyzer is connected to the PC through data acquisition card (PC I MCA card, manufactured by OROS).

Transfer functions only are measured. Frequency versus Phase angle and Frequency versus Amplitude graphs are obtained. The beams are tested for two different boundary conditions, viz. clamped-free and free-free.

V. Results and Discussions

The experimental results obtained for the composite beam specimens with single delamination are found in good agreement with the present analysis results as given in Table 1. Hence the present model can be used for studying the dynamics of debonded sandwich beams. The finite element analysis results are also found to be comparable. The length of delamination is kept constant and the location is varied, near to the fixed end (0.25L-0.4L), middle (0.5L-0.7L) and towards the free end (0.75L-0.9L).

Table 1. Comparison of natural frequency of beams with single debond (50mm)

Specimen details	First mode frequency (Hz)					
	Cantilever			Free- Free		
	Experimental	Analytical	FEM	Experimental	Analytical	FEM
Intact	35.25	35.95	35.39	198.75	215.60	225.00
Debond 0.25L-0.4L	31.25	30.25	32.25	196.25	213.80	223.00
0.50L-0.7L	33.75	33.73	35.30	198.75	215.36	224.00
0.75L-0.9L	34.75	35.80	35.30	195.00	207.75	222.35

The variation in natural frequency for various percentages of debonding lengths for a cantilever beam is given in Table 2 from which it is clear that the presence of debonding reduces the natural frequencies of the composite beam.

Table 2 Natural frequencies for various debonding lengths for a cantilever beam

Size of delamination	Frequency		
	First mode	Second mode	Third mode
Nil	35.393	221.62	619.74
10%	35.358	219.04	601.9
20%	35.122	204.13	540.13
30%	34.515	180.19	513.57
40%	33.447	160.62	508.83
50%	31.967	149.92	435.75
60%	30.25	146.33	304.27
70%	28.506	146.03	224.42
80%	26.908	144.48	172.32
90%	25.559	136.47	139.95

To study the effect of location of debonding on the modal parameters, various parametric studies are conducted by providing a constant delamination length, 50mm at three different locations along the longitudinal directions as shown in

Table 3. The variation in natural frequency with the debond location is as shown in Fig 4. It can be concluded that the debond has a minimum effect on modal frequency if it is towards the free end of the cantilever and has the maximum decrease when it is near to the fixity. Thus, the same bonding length has different effects, with respect to the change in location.

Table 3 Effect of the location of debonding on natural frequency for a cantilever beam

Debond location	First mode frequency (Hz)
Intact beam	35.393
(1) Near to the fixity (debond 25-75mm)	35.236
(2) Left of the centre (debond 100-150mm)	35.263
(3) Right of the centre (debond 150-200mm)	35.301
(4) Near the free end (debond 225-275mm)	35.370

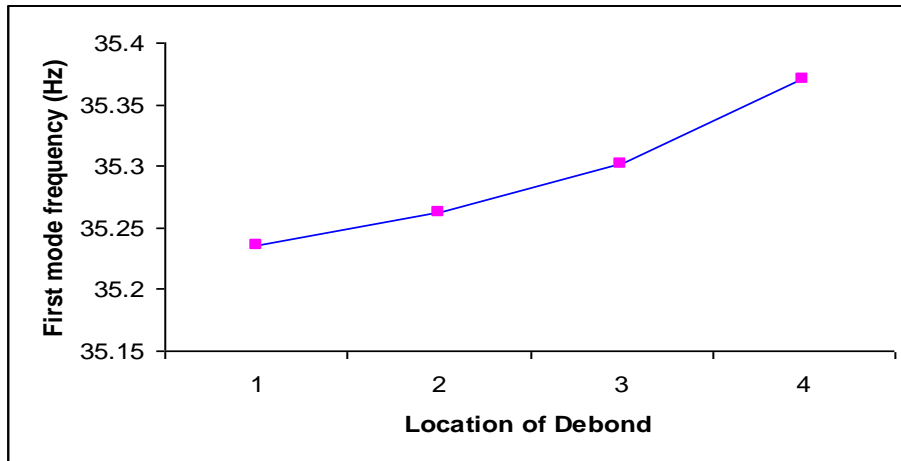


Fig 4. First mode frequency Vs Location of debonds

The mode shapes for the first mode of the cantilever beam, for various debonding lengths (60 mm, 120 mm and 180 mm) are shown along with that for an intact beam in Fig 5.

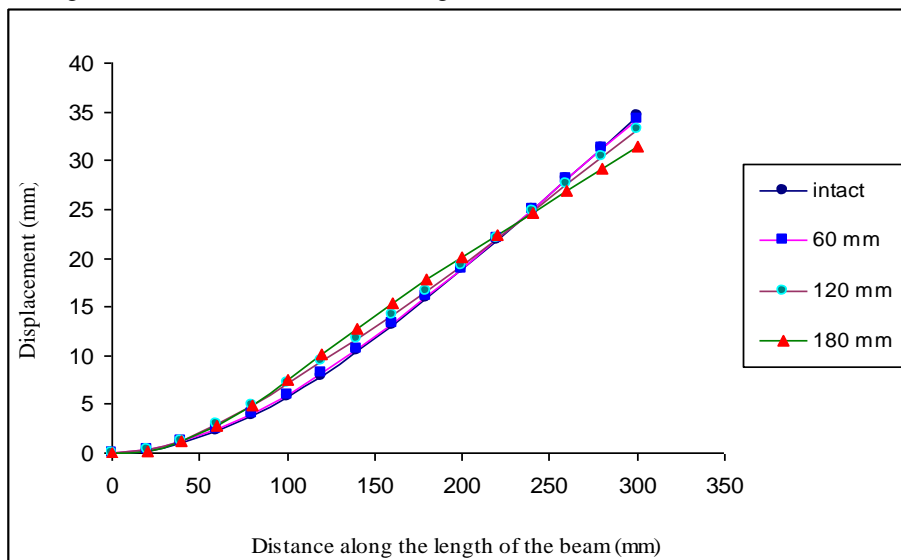


Fig 5. Mode shapes of intact and debonded beam

It can be seen that when the debonding length is very small, the mode shape is identical for both intact and debonded beams. A significant change in mode shape is observed only for larger delaminations. Hence to identify the exact location and extent of damage in sandwich composite beams, the strain plots can be used. Fig 6 represents the variation of longitudinal strain for a debond of 50% of total beam length starting extending from 10 mm to 140 mm.

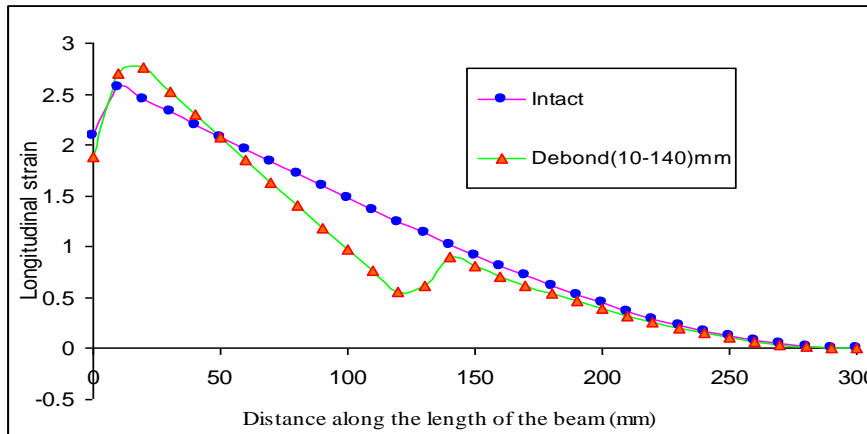


Fig 6 Strain plot of an intact beam and a debonded beam

Table 4 shows the natural frequencies of a double delaminated cantilever beam obtained using the present analytical formulations. The length of first debond (L_{d1}) and its location (L_1) is kept same in all the cases. The length of the second delamination (L_{d2}) and the distance between the two debonds (s) is varied.

Table 4 natural frequencies of beam with multiple (two) delaminations

		$L_1=10\text{ mm}, L_{d1}=50\text{ mm}$					
L_{d2}	S	5 mm	10 mm	15 mm	20 mm	50 mm	100 mm
	Frequency (Hz)						
10 mm		22.27	22.27	22.27	22.43	22.59	22.91
20 mm		21.48	21.64	21.79	21.80	22.27	22.75
50 mm		20.20	20.52	20.68	20.84	21.63	22.59
100 mm		19.41	19.57	19.88	20.04	21.32	22.60

It is observed that the presence of a second debond does not produce a considerable reduction in natural frequencies compared to that of a beam with single debond. It is clear that as the spacing between two similar debonds is greater than the length of the debond, there is no reasonable change in frequency values and mode shapes. Hence for identifying the exact location of multiple debonds also, the strain plots can be effectively used.

VI. Conclusions

An analytical solution for the free vibration of two layered sandwich beam with multiple delaminations is presented. The influence of the delamination sizes and locations on the natural frequency as well as the mode shapes is investigated experimentally for beams with single delamination and the results agree well with present analytical formulation. In multiple delaminated beams, the effect of a second debond is felt only when it is very close to the first one. It is found that for small debonding lengths (less than 30% of the length of the beam), the changes in mode shapes and reduction in natural frequencies compared to that of an intact beam are not significant. But the variations of longitudinal strains for a delaminated beam suffers more irregularities at the delamination location and hence this feature can be effectively used for identifying the extent and location of debond.

REFERENCES

Journal Papers:

- [1] Ahmed K.M, Static and dynamic analysis of sandwich structures by the method of finite elements, Journal of Sound and Vibration, 18(1), 1971, 75-91.
- [2] Wang JTS, Liu YY, Gibby JA., Vibration of split beams, Journal of Sound and Vibration, 84, 1982, 491-502.
- [3] Mujumdar PM, Suryanarayanan S, Flexural vibrations of beams with delaminations, Journal of Sound and Vibration, 125, 1988, 441-61.
- [4] Pandey A.K, M. Biswas and M.M. Samman, Damage detection from changes in curvature mode shapes, Journal of sound and vibration, 145(2), 1991, 321-332.
- [5] ANSYS Manuals

Hgrid: An Economical Model for Mass-Health Care System Using Latest Technology (Grid Computing)

S.Kanchana Devi,¹ Dr.S.Govindarajan²

1, 2Department of Computer Applications, SRM University, India

ABSTRACT: The large Hospitals and healthcare institutions consist of different Medical equipments and computers hardware software resources scattered across their campus. Rarely these resources are totally utilized to their fullest capacities and most of the times they remain idle. This situation seems to be alright for the rich and developed countries. Definitely for developing countries like India, we cannot afford huge investments in Computer Hardware's, embedded equipments (which are generally costlier), system software (including proprietary systems) and Application software based on expert systems. In order to efficiently and enormously utilize the resources across the health centres/hospitals/medical universities, the grid computing technology deployed in massive health care maintenance requirements

I. Introduction

This Paper analyse the need for health grid, the architectural framework is designed to develop a health grid system for kattankulathur campus.

II. Need for the Study

Most of the Health centres and medical institutions have powerful collection of computing resources and health related instruments on their campus for use in areas from high performance computing to general access medical laboratories(in the form of image processing, preserving health parameters of individuals, availability of drugs, blood banks and other treatment related facilities). However, these resources are rarely used to their fullest potential. Due to paucity of funds and exponential increase in patient registrations, most often it is required to ensure the minimum facilities to reach the needy patients. Therefore, it is mandatory to search and find out the right technology to ensure the full utilization of the computing resources to be passed on to the needy and poor patient by exploiting the computing power to the maximum possible extent. Though the telemedicine system through internet emerges now, the important aspects of secured access & Information are lacking as per most of the users. Moreover, the internet based systems are more vulnerable to spam and viruses. Therefore, the requirement boils down to find out a system of making optimal usage of these resources to different patients by deploying appropriate current state of our technology. The vast requirements are confined to not only to multi speciality hospitals, but also to various major healthcare institutions attached to medical colleges, private banking centres and universities too.

III. Objectives

Keeping the above needs in mind, the objective of this paper is to device an Architectural framework for Health

Care system to utilize the human knowledge power and other hospital resources effectively. The term "Health grids" means that encompassing the Grid Computing technology on the Internet based health care system. Grid infrastructure comprises applications, services or middleware components that deal with the specific problems arising in the processing of biomedical data.

IV. Hypotheses

The large Hospitals and medical institutions has limited computing resources, but are scattered at different departments at different places. To achieve our stated objectives, the possible hypotheses is to frame optimal usage of all these resources (Including massive storages intermittently required by different departments surgeons)through the latest cutting edge technology of grid computing.

V. Scope of research

This framework provides resource utilization in a proper way across multiple industries including health enters& Engineering industries. Researchers can use grid computing processing power to hunt for new viruses, search for new drugs, model disease outbreaks, image the body's organs and determine treatments for patients. Doctors can gain access to relevant health data regardless of where it is stored. Patients can receive a more individualized form of healthcare. Healthcare workers are better able to collaborate and share large amounts of information.

V.1 for a healthcare Professional/Biomedical Researcher

From the individualised care point of view, for the clinicians to make the best diagnosis and decide on treatment all the relevant health information of the patient needs to be available and transparently accessible to them regardless of the location where it is stored. Moreover, computer-aided tools are now essential for interpreting patient-specific data in order to determine the most suitable therapy from the diagnosis.

To store and process medical images, genetic information and other patient data, a large amount of computing power is needed. Large computing resources are also needed for keeping statistics of patient records, for knowledge extraction using data mining, and for the simulation of organisms and diseases using complex biomedical models. Grid technology has undoubtedly much to offer medical professionals, as illustrated by the following examples. The delivery of medical information and certain services through the internet is familiar. In health grid computing, we seek an extension of the concept

to consider how to provide large scale services to the user on demand. Some case study quoted by SHARE PROJECT Supporting and Structuring Health grid activities & Research in Europe, Developing a Roadmap [3].

- 1) Consider a radiologist who needs to manipulate an image: we want to provide a set of services, some of which may require heavy processing, making them available on her desktop 'transparently', as if they were programs simply running on her computer.
- 2) Consider a public health service which monitors certain infectious diseases and has to trigger an alert in case of a suspected epidemic. The identification of unusual patterns would in many cases be the critical step to halting the problem.
- 3) Consider a surgical simulation prior to maxillofacial surgery, to determine how the patient's face may appear after one manoeuvre versus another, the presence of sufficient tissue to allow the operation or to demand transplantation, and even to involve the patient in the decision.
- 4) Consider a 'neglected disease' like malaria. Malaria is neglected by the pharmaceutical industry because there is no prospect of profit in it. Relatively little progress has been made towards the eradication of this well understood disease, notwithstanding substantial investments of public funds in research projects. In silico lead generation may possibly be coupled with investment in plant by the poorer nations that suffer from it to lead to a locally sustainable solution.
- 5) Consider the possibility of linking genomic information to imaging in diseases like juvenile idiopathic arthritis. The genome will indicate susceptibility long before the disease is expressed, but equally, signs picked up from imaging may obviate the need for genetic screening, thus avoiding some of the most acute problems associated with it.
- 6) Consider more abstractly the nature of evidence based practice, the volume of scientific literature that provides the evidence base and the accumulation of evidence from practice that occurs as a matter of routine healthcare. How can these be integrated?. How can they be used without violating any ethical restrictions on use of data, confidentiality, privacy, security? How can they be shared without violating any data protection laws?

These are simple examples of foreseeable beneficial advances within the next generation of developments. For the radiologist or the maxillofacial surgeon, the services described would be important new tools, while for the provider of such services the underlying grid would be an ideal e-market place. For the public health service concerned with infectious diseases or the academic unit concerned with neglected diseases, health grids would provide power and flexibility beyond what could be achieved using traditional approaches. For a group of physicians seeking to improved treatment through research, grid offers a completely new concept.

VI. Socio-Economic benefits

Modern healthcare services are expected to be available around the clock, seven days a week, so that systems with pervasive access and near-absolute fault

tolerance are indispensable. However, it is difficult for these applications to run non-stop with a high quality of service. Grids could help by providing a platform of collaboration, allowing the linking centres which co-operate to achieve better continuity and quality of service. Medical staff will then be able to share experience, knowledge and 'second opinion' with other internal and external staff. The distributed architecture of grids with the availability of high-bandwidth networks responds well to the requirements of healthcare provision. There are also optimistic stakeholders' views towards medical research, healthcare and computing capabilities combined to better satisfy the patient

Health grids promise many benefits to mobile patients as well as citizens. It could help a travelling individual to receive the right treatment in an emergency situation, thanks to the ability of the grid to facilitate communication between the local hospital of the patient and the admitting hospital far away in order to exchange necessary health related information.

VII. Research Questions

What is the nature of implementation of Grid computing technology over the healthcare maintenance? , What are the technologies trade off the architectural components? [3], what are the Socio economical benefits of the health grid system?

VIII. Architectural Model

This section describes the logical representation of the architectural model. The Grid System designed for the health centre is "campus grid" which is one of the types of grid. Health grid architectural framework designed consists of several sub systems. The sub systems are described as grid layers such as application (Higher) layer, Management (Middle) Layer, Computing (Low) layer. Highest layer is application layer deals with clinical applications and consists of user interfaces, next is management that and routing requests and responses, manages job queue along with job scheduling algorithms and methodologies, allocating resources for the job queue. The Third layer is Computing layer which is responsible for mapping the resources to the jobs and controls the execution. The groups are virtual nodes of health grid system.

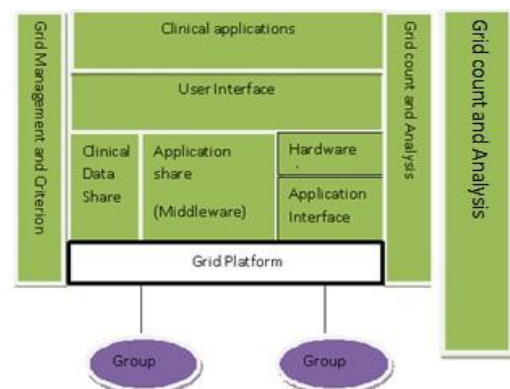


Figure1. Health grid system Architecture

The Grid is connected to the three layer architecture through Globus Toolkit which provides the grid Environment. The group could be able to complete the jobs adjusted run automatically according to the user's need and return the result to users. Integrations are intended to be transparent and seamless to the developer. The group is mainly responsible for two functions: the management function of works and the management function of system adjustment. The work management function include shading over interface, management interface and the parallel work management; the system management function includes system supervision, the allotment strategy, the management of works PRI and SLA management.

The Overall architecture is bounded by the Grid Management and criterion component that enables Grid

authentication, resource authorization, and security concerns.

VIII.1 Technologies to build the architecture

Based on the architectural model the grid topology is defined as specified in figure.2. This section specifies the physical structure of campus grid and the table provides various technologies can be used to build the model for healthcare system.

VIII.2 Architectural Tradeoffs for Health grid resources

The following table list the technologies available to enable the activity of each Component in the physical topological structure specified at figure 2.

S.No	Component in the Architecture of campus grid	Technology
1	Grid Management Centre (Resource Management, job scheduling, files management)	Cluster Installation- At head node. 1.Rocks is based on Redhat Linux, Provides less flexibility, easy to install [9] 2.Alternate is OSCAR(Open Source Cluster Application Resource) gives more flexible management but complex to install[5]
2	Local Scheduler- Load balancing, file staging, and other administrative task	1.PBS[8] 2. LSF 3.Condor 4.Computing centre software(CCS)
3	Grid Architecture, Resource Identification, Authorization, Authentication and security	1.Globus Toolkit 4.0, 2.latest Globus Toolkit 5.0[10], 3.Gridshib[25]
4	Grid Portal	1.Jetspear is a IBM product, provides out-of-box web portal for enterprise settings[6] 2.Jetspeed is an open source Apache product built as an enterprise information portal 3.Gridspear is an open source project that is part of grid lab[35]
5	Portlets	1.Gridportlets are JSR-168 complaint are compatible with all portlets 2. The Open Grid Computing Environment (OGCE) [39] develops open source portlets with the intention for them to be used under multiple portal frameworks.

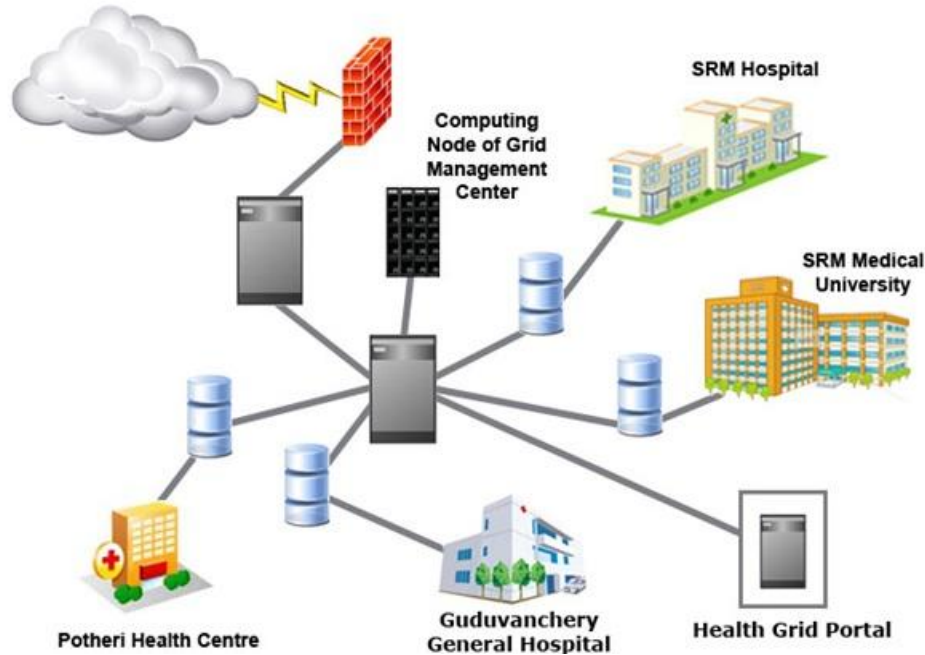


Figure 2: Campus Grid Topology Structure

The Globus Toolkit [10] has become widely accepted as the standard tool for building grid architecture and boasts success stories including GriPhyN [11], Open Science Grid [12], TeraGrid [13], and NEES grid [14]. The Globus Toolkit provides identification, authentication, authorization, and security for connecting the resources of the grid, as shown in Figure 2. The infrastructure allows for strict local control of a given resource but still allows users from anywhere to perform a variety of tasks related to resource and service discovery, file management, system and job monitoring, and job submission.

VIII.3 Health grid physical structure

Geographically the Hospitals, health centres and the medical institutions are situated at different places. This paper designed a topological structure to establish and to show the communication manner in between the layers. There is a control node which logically controls the grid environment to which the other health nodes are connected by network structure. Web portal for the Health grid is enabling the raw and processed information.

The Grid network is connected to internet provided with grid security. The network routers are routing the requests and responses in between the nodes.

IX. Socio-economic recommendations

This section discusses the socio economic requirement for the successful development and implementation of campus grid for health centres and medical institutions across Kattankulathur region and in future across the country.

IX.1 Trust and Acceptance from society.

Trust is a very important element in any interaction between the different members of a society. In the market context, trust is crucial for successful business to business collaborations. Similarly, in a health grid domain a good collaboration will not be achieved unless a trust relationship exists between the different users and stakeholders. Pilot projects and prototype applications, which are an inherent part of the technology health grid, need to be future oriented in the sense that the ultimate routine operation users have to be persuaded both of their value and their applicability, i.e. their ability to fit into real clinical or research workflows. This has to be taken seriously from the very beginning, even in proof-of-technology demonstrators. The goal should always be to give users, especially clinicians, tools that they would consider using with patients in real healthcare situations. Trust and acceptance can be greatly enhanced by the establishment of appropriate ethics committee structures to advice on the observance of ethical principles.

IX. 2 Cross-Organisational Interoperability.

The effective deployment of knowledge grids will crucially depend on collaboration between institutions, meaning more than “simple” access to each others’ data and computing resources. This collaboration requires the utilization of human resources and in some cases a significant strategic re-orientation and re-organisation of working processes and even management structures. Particular attention should be given to flexibility of government regulated budgets and reimbursement schemes.

X. Future work and Conclusion

In this paper, the architectural model has been designed and the technologies can be used to deploy the system are stated. The security establishment for campus grid

is analysed from distributed systems security and developed for this system. Implementing the campus grid for the hospitals helps to utilize the man power and other computational and medical devices effectively across the country and across the universe through different exclusive architectures. The future work of this paper could be actual implementation in such a way that generating clusters, development of forms, reports along with the data and establish resource security. United Kingdom [3] started the development of health grid on 2002 itself. Though the noise of health grid echoes in India, there is no architectural model available for health grid as of now. The main advantage of this model is the cost effectiveness.

References

JOURNALS

- [1] Jing Wang 1, Zhimin Yang1, Weili Kou11 Department of Computing, Shandong University, Weihai, P.R, China," A Solution for Building Campus Grid", IEEE Transactions.
- [2] Mark Olive, Hanene Rahmouni and Tony Solomonides, "A European Healthgrid "Journal of Medical Internet research, European Commission, Information Society and Media.

THESES

- [3] Research and technology development on telematics systems in health care. Annual technical report on RTD in health care. CEC DG XIII. Brussels: AIM, 1993.
- [4] e-Science talk project www.gridtalk.org/Documents/ehealth.pdf

CONFERENCE PROCEEDINGS

- [5] Krishna Nadiminti and Rajkumar Buyya, The University of Melbourne, "Enterprise Grid computing: State-of-the-Art", 2009, Computer Science-Technology and Applications, 2009. Proceedings of IFCSTA '09. V1, PP160 – 163
- [6] V. Welch, T. Barton, K. Keahey, and F. Siebenlist, "Attributes, Anonymity, and Access: Shibboleth and Globus Integration to Facilitate Grid Collaboration," presented at 4th Annual PKI R&D Workshop, Gaithersburg, MD, 2005.

- [9] Multi Conference on Systemic, Cybernetics and Informatics, Or-lando, Florida, 2002.
- [9] The GridPort Toolkit, October 2005, <http://gridport.net>.
- [10] Altair PBS Professional, October 2005, <http://www.altair.com/software/pbspro.htm>
- [11] IBM LoadLeveler, October 2005, <http://www-03.ibm.com/servers/eserver/clusters/software/loadleveler.html>
- [12] Computing Center Software, October 2005, <http://wwwcs.upb.de/pc2/projects/ccs>.
- [13] The Globus Toolkit, October 2005, <http://globus.org/toolkit/about.html>.
- [14] Grid Physics Network, October 2005, <http://www.griphyn.org>.
- [15] Open Science Grid, October 2005, <http://www.opensciencegrid.org>.
- [16] TeraGrid, October 2005, <http://www.teragrid.org>.
- [17] NEESgrid, October 2005, <http://www.neesgrid.org>.
- [18] Condor-C, October 2005, http://cs.wisc.edu/condor/manual/v6.7.8/5_4Condor_C.html
- [19] GridLab: A Grid Application Toolkit and Testbed, October 2005, <http://gridlab.org>.
- [21] Sun ONE Portal Server, November 2005, http://docs.sun.com/app/docs/coll/S1_PortalServer_61.
- [22] Research and technology development on telematics systems in health care. Annual technical report on RTD in health care. CEC DG XIII. Brussels: AIM, 1993.
- [23] e-Science talk project www.gridtalk.org/Documents/ehealth.pdf

URLs

- [7] OpenPBS, October 2005, <http://www.openpbs.org>.
- [8] T. Naughton and S. L. Scott, "The Penguin in the Pail - OSCAR Cluster Installation Tool," presented at 6th World

Effect of Additives on Electrical Resistivity of Pulp Black Liquor-Sawdust Blends

Rasha A. Ahmed,¹ Amal H. Abdel Kader²

^{1,2} Kingdom of Saudi Arabia, Taif University, Faculty of science, Chemistry dept., ²National Research Center, Cellulose and Paper Dept., ¹Forensic Chemistry Laboratories, Medico Legal Department, Ministry of Justice, Cairo, Egypt.

Abstract: Unlike the large scale paper mills which use the pulp black liquor (PBL) for recovery of chemicals, the small and medium mills usually throw away the black liquor after pulping, leading to pollution problems. Furthermore, sawdust wastes (SDW) produced from factories leads to a big problem. The objective of this study is to determine the effect of natural binders (wax and starch) on the thermal conductivity and electrical resistivity of black liquor-sawdust composites. Surface analysis of samples was studied. Results from Cyclic voltammetry and electrochemical impedance spectroscopy techniques demonstrated that addition of starch and wax increases electrical resistivity of black liquor-sawdust composites.

Keywords: black liquor, natural binders, surface analysis, thermal conductivity, electrochemical impedance.

I. Introduction

Approximately 7 tones of black liquor are produced in the manufacture of one tone of pulp [1, 2]. Black liquor is an effluent from alkaline pulping of lignocellulosic raw materials, which is an intermediate step in the manufacturing of paper [3]. In large paper mills, the black liquor so produced is combusted, after concentration, in a specially designed boiler to derive energy [4-7]. One of the main ingredients in black liquor is lignin, which is the material in trees that binds wood fibers together and makes them rigid, and which must be removed from wood fibers to create paper [8-12].

The weak black liquor has a solid content of approximately 15% by weight, which is too low for combustion. To raise the solid content in the liquor, it is being evaporated by a sequence of concentrators. When the resulting strong black liquor reaches the recovery unit (boiler or gasifier) it has a solid content of around 75%. Chemically, black liquor is a mixture of several basic elements where the largest fractions are carbon, oxygen, sodium and sulfur.

Sawdust is a by-product from sawmills. Wood chips screening is defined as finely divided wood material which has passed through the screens prior to pulping, *i.e.* wood material smaller than the accepted size for chips. The quality of sawdust depends on the saw type, method of sawing, type of tree used, and the storage method of logs including temperature, moisture and season [13-18]. Thus, sawdust and chips screenings from different mills can be very heterogeneous raw materials.

An adhesive is a substance capable of holding materials together by surface attachment with the ability to sustain the designed load requirement without deformation or failure. For an adhesive to be effective, there are two major characteristic requirements. The adhesive must be capable of impacting adequate bond between the two materials by principle of resistance to load shear, which implies creep static or time independent deformation under sustained load. Other desired requirements are ease of application, reasonable setting time, resistance to moisture, aging, heat and fungal attack, non-staining and gap filling. Traditionally, adhesives of natural origin have been used to repair and adhere black liquor-sawdust material, particularly, starch paste, Arabic gum, and animal glue or gelatin. These adhesives are expected to remain relatively reversible over time. Wax (Fig.1) has been used as an adhesive since the beginning of time. It refers to a class of organic chemical compounds that are plastic (malleable) near ambient temperatures. Characteristically, they melt above 45 °C to give a low viscosity liquid. Waxes are insoluble in water but soluble in organic and nonpolar solvents. Its molecular structure is branched and circular, making it an excellent adhesive. Wax is great gap filler, adheres instantly and is not toxic unless it is burned. It works on any material, porous or non porous. It is acid free and will not wrinkle fine papers. Wax can act as an elastomer, and tackifying agent provides excellent hot-melt adhesive and bond strength, it improves moisture resistance and wettability.

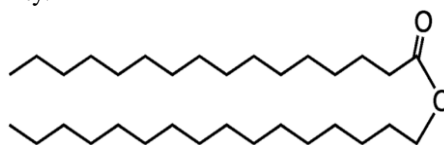


Fig. 1. Wax structure

Starch or amyllum, Fig. 2, is a carbohydrate consisting of a large number of glucose units joined by glycosidic bonds. This polysaccharide is produced by all green plants as an energy store. It is found in many processes either as an

adhesive or thickener. The fine, smooth texture, non-staining, non-poisonous nature of starch and the good stability of the product with time makes it a desirable choice particularly for domestic uses.

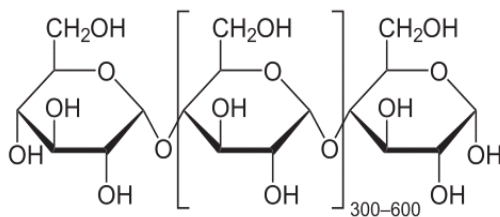


Fig. 2. Starch structure

Electrochemical impedance spectroscopy (EIS) has been used extensively to characterize the electrical properties of desired materials as a function of frequency. The EIS results are used to interpret impedance spectra in terms of resistance and capacitance associated with the physicochemical properties of desired samples [19-25]. To our knowledge, there are very few studies reporting the use of impedance in studying the thermal conductivity and electric resistivity of PBL.

The major purpose of this paper is to study the thermal conductivity and electrical resistivity of two wastes (PBL and SDW), hoping to decrease the pollution problem obtained from these wastes by using them as an active materials for the production of eco-friendly insulating composites using synthetic and natural binders such as wax and starch paste.

First, the morphology of PBL in present and absent of additives was studied using SEM and FT-IR. Secondly, electrochemical impedance and cyclic voltammetry techniques were used to measure the effect of additives on the thermal conductivity and electrical resistivity of the PBL samples.

II. Experimental procedures

2.1.1. Reagent and materials

A waste of pulp black liquor (PBL) from paper industry was provided by paper factory, sawdust waste (SDW) was provided by wood and furniture factories. Three samples were prepared using pulp black liquor waste (PBL) as solid residue after filtration and drying (blank), mixing it with fine sawdust wastes and wax as a binder to produce the second sample (BLSW), finally it mixed with sawdust and natural binder starch paste to produce the third sample (BLSS).

2.1.2. Characteristics of black liquor

The composition of the (PBL) produced during the pulping process in different plants may not be the same, even if the same pulping process is used. However, black liquor consists generally of lignin, hemicelluloses, cellulose, and silica. Minor constituents such as fats, wax, resins, mucilage, and gums. Harada et al., [26] exist in small portions. The elemental analysis of black liquor is 36.4% C, 18.6% Na, 4.8% S, 3.5% H, 2.02% K, 0.24% Cl, 0.14% N, 34.30 % O. [27, 28].

2.2. Instrumental and experimental set-up

The electrodes for the electrochemical studies were fabricated as follows: 10.0 mg of synthesized samples (PBL, BLSW, BLSS) were pressed on an empty electrode with a 1cm² geometrical area. The measurements were carried out with a potentiostat/galvanostat Autolab PGSTAT 73022. EIS measurements were done at an open circuit potential with applied 10 mV sinusoidal perturbations in the 100 kHz to 0.1 mHz frequency range, taking 7 steps per decade. For this purpose, a conventional three-electrode cell was used, composed of Ag/AgCl reference electrode, a platinum wire as the counter electrode, and the empty electrode disc (diameter: 2.5 mm) as the working electrode. The tests were carried in 0.1 M Briton Robinson (B-R) buffer pH 3.5.

Scanning electron microscope (SEM) (Philips, XI 30) was used for characterization of the homogeneity of the coatings where the samples were coated with gold before SEM examination. JASCO 300-E Fourier transform infrared (FT-IR) spectrometer was used to analyze changes in the chemical structure of the samples. The IR spectra were carried out using the potassium bromide pellet technique in the wave number region 4000–400 cm⁻¹.

III. Results and discussion

3.1. Surface morphology

3.1.1. Scanning Electron Microscopy (SEM)

The SEM was done to show the external surface of samples and the interference between composites at different magnifications. Fig. 3(A) shows the SEM images of the blank sample (PBL), where large number of pores and cavities were observed. The cavities on the surface of PBL result in its electric conductivity. After relatively mild mixing of wax and starch was applied to PBL, SEM of BLSW and BLSS samples in Fig. 3B and C, respectively, reveals that both samples are homogenous compact layers in which the pores are filled, and distributed uniformly. The good network of interconnected pores increases the electric resistivity of the PBL due to the presence of wax and starch which act as a great gap filler. It also increases bond strength between black liquor and sawdust wastes.

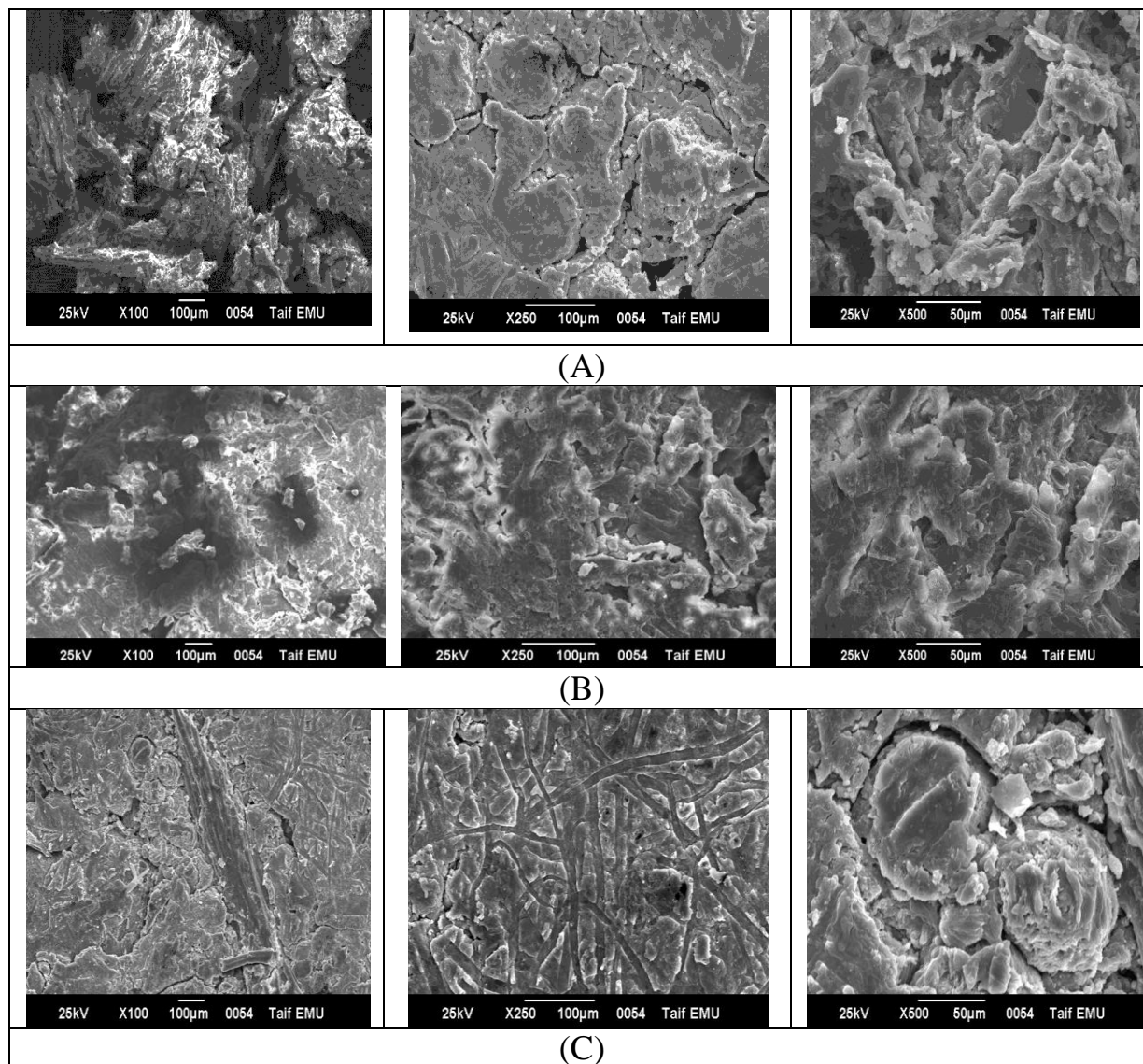


Fig. 3. SEM micrographs showing the surface of PBL(A), BLSW(B), BLSS (C) (magnification 100, 250 and 500 μm).

3.1.2. Comparison of IR Spectra

A full, detailed IR transmission spectrum for the three samples was obtained, and is presented in Fig. 4.

The IR spectrum of PBL Fig. 4(A) shows, the appearance of bands at $1597-1457\text{ cm}^{-1}$ for the aromatic skeletal vibration of the PBL, The characteristic bands of black liquor were assigned according to the literature, as shown in Table 1.

In contrast, if we look at the IR spectra of BLSW Fig. 4(B), significant features seen include: Appearance of a band at 1222 cm^{-1} which can be assigned to C-O stretching. Progression of weak band at 1118 cm^{-1} for C-OH stretch is noticed. Other frequency present at 782 cm^{-1} for CH_2 rocking assigned to wax structure.

Spectrum of BLSS Fig. 4(C), for the modified black liquor with starch was obtained. The absorption region at 1029 cm^{-1} relates to C-C and C-O stretching modes of the polysaccharide backbone [29, 30]. Appearance of a band at 1380 cm^{-1} assigned to bending modes of O-C-H, C-C-H, and C-O-H angles [30]. Other frequencies, which are not seen before, are observed at 622 and 445 cm^{-1} .

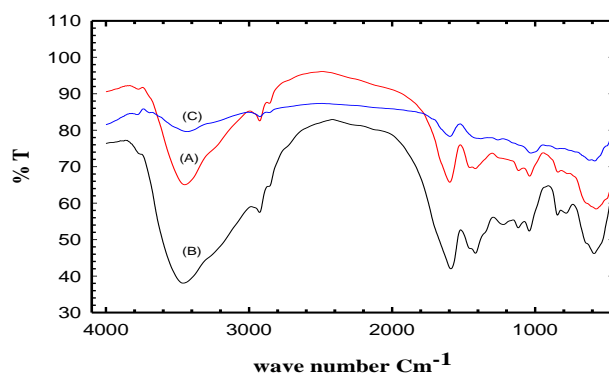


Fig. 4. FTIR spectrum of PBL (A), BLSW (B), and BLSS (C)

Table (1) lists the assignment of the different IR bands of samples.

Maximum band position (cm ⁻¹)	Band origin
3450-3694	OH stretching (H- bonded)
2924- 2926	CH stretching of methyl or methylene group.
2858	CH vibration of methyl of methoxy group.
1457.9	CH stretching of methyl or methylene group.
1417-1419	CH vibration of methyl group.
1029-1041	OH stretching of primary alcohol.
844	Aromatic C-H out of plane bending.

IV. Electrochemical study

4.1. Electrochemical behavior of the black liquor – sawdust blends

Cyclic voltammetry measurements were performed over a potential range of -2 to 2 V/s) to examine the electrochemical characteristics of black liquor – sawdust blends. Fig. 5(A) shows the cyclic voltammogram of black liquor and sawdust in 0.1 mol L^{-1} B-R (pH 3.4) at 288 K. One anodic broad peak current at -0.12 V with a high charging current during the potential sweep is observed. This attributed to the flow of electric charges through the pulp black liquor (blank), which in turn increases the electric conductivity and decreases resistivity of the sample. The flow of electric charges is expected from the contribution of a high pore diameter of PBL and the conjugated structure of black liquor.

However, Fig. 5(B, C) shows the cyclic voltammogram of black liquor, sawdust with wax and starch, respectively, in 0.1 mol L^{-1} B-R (pH 3.4) at 288 K. In presence of wax or starch, the charged current decreases which attributed to the physical properties of both blends as insulating material which fill the porous film of the black liquor, and retarded the movement of electric charges and thus decreases the current. Generally, the porous structure with a high pores diameters in pulp black liquor sample (PBL) can accommodate more electrolytes and increases electrochemical activation, but the addition of wax or starch to black liquor and sawdust composite decreases their conductivity and becomes more insulation. These data comes in a good agreement with the SEM images.

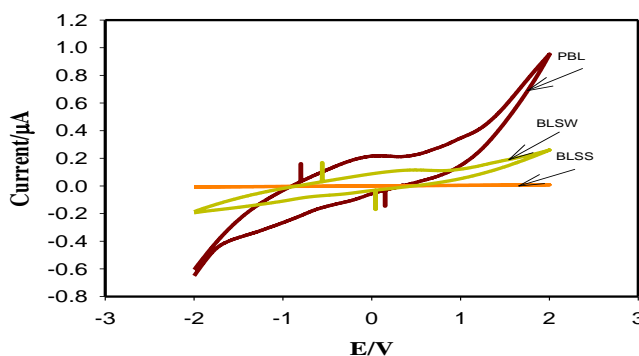


Fig. 5. Cyclic voltammograms of black liquor (PBL), BLSW, and BLSS in 0.1 mol L^{-1} B-R (pH 3.4) at 288 K

4.2. Electrochemical impedance analysis
4.2.1. Effect of additives

To evaluate the effect of wax and starch paste on the conductivity and resistivity of the black liquor composite, electrochemical impedance were investigated in absence and presence of these additives. EIS data were obtained for the black liquor composite electrodes at AC frequency varying between 100 kHz and 0.1 mHz at open circuit potential in B-R buffer (pH=3.4) at 318 K. Fig. 6 shows a typical Nyquist plot, that is plot of imaginary part of the modulus Z'' vs. real one Z' , for black liquor (PBL) (A), BLSW (B), and BLSS (C). The impedance spectra include semicircles; the large diameter semicircle indicates the higher electron transfer resistance of black liquor sawdust in present of starch paste, in which it confirmed with the cyclic voltammetry technique. However, the diameter of the semicircle decreases in BLSW sample indicating the flow of electric current through that composite. This attributed to wax structure which affected by temperature and permit electron transfer faster than that in starch composite. The presence of starch in PBL perform more stable product. On the other hand, in absence of additives, the diameter of semicircle diminished markedly. Thus, the charge transfer resistance of electro oxidation of pulp black liquor (PBL) increases greatly, and the charge transfer rate is enhanced.

In general, Additives provides excellent adhesive and high bond strength, Moreover they improve electrical resistivity of PBL at room temperature.

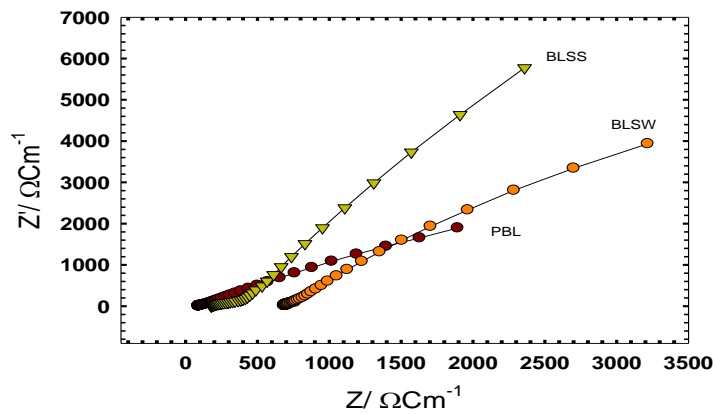


Fig. 6. A typical impedance spectrum for PBL, BLSW and BLSS at 343 K.

4.2.2. Effect of temperature

To evaluate the effect of raising temperature on the conductivity and resistivity of the black liquor composite, electrochemical impedance were investigated at temperature range from 288 K to 343 K for PBL, BLSW, and BLSS. Nyquist plot for pulp black liquor (PBL) at different temperatures is shown in Fig. 7. The large diameter semicircle indicates that the charge transfer rate is sluggish and causes the high resistivity of the composite at 288 K.

However, after rising the temperature, the diameter of semicircle diminishes markedly. Thus, the charge transfer resistance of PBL decreases greatly, and the charge transfer rate is enhanced. The data proves that increasing temperature increases the diameter of these pores and, facilitates the electron transfer across these pores, which make PBL more conductive at higher temperatures. The same behavior is noticed in BLSW, and BLSS. By increasing temperature above 300 K wax melt and separated from its composite causing flow of electricity. However, the more stable BLSS composite retain its behavior to some extent at higher temperature.

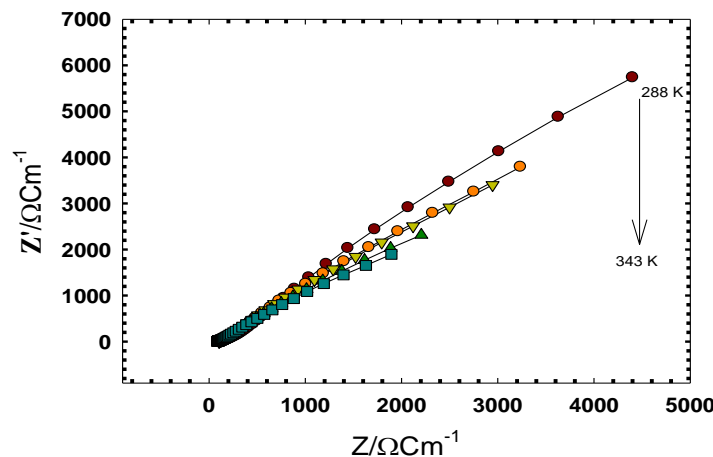


Fig. 7. Nyquist plot for black liquor and saw dust (PBL) at different temperatures

V. Conclusion

In previous references, the morphology and properties of PBL has studied in absence and presence of additives, but the investigations of the porosity as well as thermal conductivity and electrical resistivity of PBL using electrochemical technique are absent. In this paper, the effect of additives (wax and starch) on the porosity, conductivity, and resistivity of PBL-SD has been studied by electrochemical technique, and electrochemical impedance spectroscopy, and confirmed by surface analysis.

VI. Acknowledgments

We gratefully acknowledge Chemistry Department (University of Taif, kingdom of Saudi Arabia) for financial support to carry out the above investigations.

References

- [1] P. Stenius, ed. *Forest Products Chemistry. Papermaking Science and Technology*. 3. Helsinki, Finland: Fapet OY. (2000) pp. 62–78. ISBN 952-5216-03-9.
- [2] J. Biermann, Christopher. *Essentials of Pulping and Papermaking*. San Diego: Academic Press, Inc. (1993) ISBN 0-12-097360-X.
- [3] D. Clayton, D. Easty, D. Einspahr, W. Lonsky. Chemical reactions of wood constituents. In: Grace TM, Leopold B, Malcolm EW, Kocurek MJ, editors. *Pulp and paper manufacture*. vol. 5. Alkaline Pulping. Atlanta: TAPPI Press, (1992) p. 38.
- [4] V. Venkatesh, N. Nguyen. Evaporation and concentration of black liquor. In: Green RP, Hough G, editors. *Chemical recovery in the alkaline pulping processes*. Atlanta: TAPPI Press, (1992) p. 5–12.
- [5] . N. Adams, and W. J. Fredrick “Kraft Recovery Boiler Physical and Chemical Processes”, (1988) American Paper Institute.
- [6] M. Baucher, C. Halpin, M. Petit Conil, W. Boerjan. Lignin, genetic engineering and impact on pulping. *Critical Reviews in Biochemistry and Molecular Biology*, 38 (2003) 305–50.
- [7] L. Guang, L. Yangsheng, N. Jinren, S. Hanchang, Q. Yi Treatability of kraft spent liquor by microfiltration and ultrafiltration. *Desalination*, 160 (2004) 131–41.
- [8] G. Q. Lu, T. Toyama., H. J. Kim, I. Naruse., K. Ohtake.; Proc. The 3rd International Symposium on Coal Combustion, Beijing, China, (1995) 37-44.
- [9] G. Q. Lu, T. Toyama., H. J. Kim., I. Naruse., K. Ohtake., M. Kamide.; *Kagaku Kogaku Ronbunshu*, 23 (1997) 404-412.
- [10] G. Q. Lu, T. Toyama, H. J. Kim, I. Naruse, K. Ohtake, M. Kamide, *Kagaku Kogaku Ronbunshu*, 23 (1997) 954-961.
- [11] P. Bernath, S. A. Siquefield, L. L. Baxter, G. Sclippa, C. M. Rohlfling and M. Barfield “In situ analysis of ash deposits from black liquor combustion” *Vibrational Spectroscopy* 16 (1998) 95–103.
- [12] H. J. Kim, G. Q. Glu, T. Jili and M. Hisadakata “Binding and desulfurization characteristics of pulp black liquor in biocoal briquettes”, *Environmental Science Technology*, 36 (2002) 607-1612.
- [13] C. Yang, G. Cao, Y. Li, X. Zhang, H. Ren, X. Wang, et al. A constructed alkaline consortium and its dynamics in treating alkaline black liquor with very high pollution load. (2008) *PLoS One*, 3.
- [14] C. Yang, Y. Niu, H. Su, Z. Wang, F. Tao, X. Wang, et al. A novel microbial habitat of alkaline black liquor with very high pollution load: microbial diversity and the key members in application potentials. *Bioresour Technology*, 101 (2010) 1737–1744.
- [15] C. Yang, Z. Wang, Y. Li, Y. Niu, M. Du, X. He, et al. Metabolic versatility of halotolerant and alkaliphilic strains of *Halomonas* isolated from alkaline black liquor. *Bioresour Technology*, 101 (2010) 6778–6784.
- [16] O. Isomäki, Tutkimus sahanpurun perusominaisuksista. *Paper Puu*, 52 (1970) 571–584.
- [17] P. Rantasuo, Framställning av sågspånscellulosa med Enso-Bauer M&D-kokare. *Norsk Skogind*, 30 (1976) 186–188.
- [18] J. Liiri, Sahanpurun keittoprosessin ja sen lämpötilasäädettävyyden tutkiminen jatkuvatoimisella Enso-Bauer M & D –keittimellä, M.Sc. Thesis, Lappeenranta University of Technology, Lappeenranta, Finland., (1979) pp.70
- [19] T. E. Kerner, et al. Electrical impedance spectroscopy of the breast: Clinical imaging results in 26 subjects. *IEEE Transactions on Medical Imaging*, 21 (2002) 638–645.
- [20] E. Gersing, Impedance spectroscopy on living tissue for determination of the state of organs. *Bioelectrochemistry and Bioenergetics*, 45 (1998) 145–149.
- [21] L. K. Pan, , H. T. Huang, & C. Q. Sun, Dielectric relaxation and transition of porous silicon. *Journal of Applied Physics*, 94 (2003) 2695–2700.
- [22] K. Prabakar, & S. P. Mallikarjun Rao, Complex impedance spectroscopy studies on fatigued soft and hard PZT ceramics. *Journal of Alloys and Compounds*, 437 (2007) 302–310.
- [23] Li, Xiaobei, Impedance spectroscopy for manufacturing control of material physical properties, (2003) Masters Thesis, Department of Electrical Engineering, University of Washington).
- [24] M. I. N. Zhang, D. G. Stout, & J. H. M. Willison, Electrical impedance analysis in plant tissues: Symplasmic resistance and membrane capacitance in the Hayden model. *Journal of Experimental Botany*, 41 (1990) 371–380.
- [25] M. I. N. Zhang, & J. H. M. Willison, Electrical impedance analysis in plant tissues: A double shell model. *Journal of Experimental Botany*, 42 (1991) 1465–1475.
- [26] C. Harada, Y. Saito, Y. Nakamura, H. Minato. The effect of sodium hydroxide treatment of rice straw on in situ disappearance of hemicellulose and lignin in its cell wall. *Animal Science Journal*, 72 (2001) 19–25.
- [27] M.L. Hassan, A.A.M.A. Nada. Utilization of lignocellulosic fibers in molded polyester composites. *Journal of Applied Polymer Science*, 87. (2003) 653–60.
- [28] S. A. El-Mekkawi, I. M. Ismail, M M. El-Attar, A. A. Fahmy, S. Samia Mohammed, “Utilization of black liquor as concrete admixture and set retarder aid” (2011) *Journal of Advanced Research*, 17 February.
- [29] R.H. Wilson, and P.S. Belton, A Fourier-transform infrared study of wheat starch gels. *Carbohydrate Research*, 180 (1988) 339-344.
- [30] V. Bellon-Maurel,, C. Vallat, , and D. Goffinet, Quantitative analysis of individual sugars during starch hydrolysis by FT-IR/ATR spectrometry. Part I: Multivariate calibration study-repeatability and reproducibility. *Applied Spectroscopy*, 49 (1995) 556-562.

Ring-Oscillator-Based Injection-Locked Frequency Divider with Vernier Method

Hasan Almasi,¹ Mostafa Yargholi,² Saeed Fathi Ghiri³

^{1, 2, 3}Department of Electrical Engineering Faculty of Engineering, University of Zanjan, Zanjan, Iran

Abstract: Frequency synthesizers are one of the most critical blocks for multi-standard multi-band systems. This paper presents a low power and wide locking range Injection frequency divider. Ring-oscillator-based injection-locked frequency divider has merits of compact and low power devices. Two injection-locked frequency dividers, with divide-by-3 and divide-by-5 operations respectively, were simulated by TSMC 0.18 μm CMOS technology to verify the proposed design. The locked ranges of divide-by-3 and divide-by-5 are 1.9 GHz and 1.4 GHz, with 0.25mw and 0.93mw power consumption at 1 V supply voltage, respectively.

Keywords: Differential injection, frequency divider, ring oscillator, wide tuning range, low power, Vernier.

I. INTRODUCTION

A frequency divider is widely used for quadrature signal generators and high frequency systems such as frequency synthesizers. The inductance/capacitance (LC) resonator-based injection-locked frequency divider (ILFD) [1] is widely used because of high frequency operation. However, its locking range is generally narrow. In the recent years, the ILFDs have attracted much attention due to their high frequency and lower power consumption [2, 3]. The ILFDs are based on the injection-locked oscillators. There are two types of ILFDs. The former is LC-oscillator-based ILFD, which can operate at very high frequency with low power consumption, but its locking range is narrow and the area is too large due to the LC tank. The latter type of ILFD can be based on RC ring oscillator, which has the merits of low power, large locked range, and small area. In the last years, lots of researchers have focused on ring-oscillator-based ILFDs [2–4]. Ref. [4] and [5] both demonstrated that multi-phase injection with a specific phase difference can maximize the locking range of the ring-oscillator-based ILFD. Ring oscillators, on the other hand, occupy extremely small area. In addition, they generally have a larger locking range because of their lower quality factor (Q). Although the phase noise of traditional ring oscillators is high, the noise performance improves dramatically when locked to a clean reference. A drawback is that, in general the exact multi-phase inputs are difficult to be obtained directly in conventional LC differential voltage-controlled oscillator (VCO). In addition, the locking range will become worse if the phase difference of inputs departs from the optimum value [6]. We use single injection instead of multi-phase injection in this paper to achieve a wide locked range for ring oscillator frequency divider.

II. BACKGROUND

As multi-standard multi-band systems emerge in today wireless market, one of the most critical blocks to be realized is the frequency synthesizer, which at least must satisfy two main criteria: operating over a wide range of frequencies and low power consumption. Locking of injection based oscillator is a well-known and deeply studied phenomenon. When an external signal is applied to an oscillator, the oscillator stops to be an autonomous circuit and synchronizes to the external signal. The conditions under which this phenomenon happens have been deeply investigated by Adler in 1946 [7], and by many other authors [8, 9]. Consider the conceptual block of a free-running oscillator shown in Fig. 1(a): it consist of a gain block $f(v_o)$ and a linear filter $h(t)$. The Barkausen's amplitude and phase criteria define the conditions under which the oscillation can be sustained at a given frequency ω . Those conditions are presented by denoting:

$$|F(\omega) H(\omega)| = 1 \quad (1)$$

$$\angle F(\omega) H(\omega) = 2\pi \quad (2)$$

Where $F(\omega)$ and $H(\omega)$ are the transfer function of the filter and the gain block respectively. Suppose that the gain block is capable to set its gain in such a way which (1) can be satisfied at any frequency, then, oscillation happens at the frequency, ω_0 , where the phase of the filter satisfies (2). ω_0 is the oscillator's natural frequency, which is the oscillation frequency of the oscillator when any external signal is applied to it.

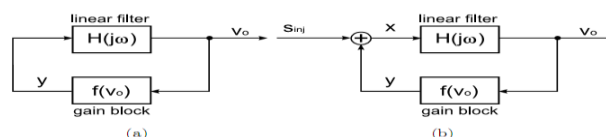


Figure 1: (a) Block diagram of a free-running oscillator. (b)Block diagram of an injection locked oscillator.

As illustrate in Fig. 1(b), the external signal s_{inj} at frequency ω_{inj} is applied to the oscillator. The signal X that feeds the linear filter is sum of the feedback signal Y and the injection signal s_{inj} . Then the total phase shift across the loop at ω_0 is not any longer 2π , because of the extra phase shift introduced by s_{inj} , and the oscillation cannot be sustained at that frequency. However, under particular conditions the phase response of the filter at the frequency ω_{inj} compensates this extra phase shift and the Barkhausen's phase criterion is satisfied at ω_{inj} , instead of ω_0 . It is said that the oscillator is injection locked by s_{inj} and its oscillation frequency moves from the natural frequency ω_0 to the injection frequency ω_{inj} [7, 10]. The range of frequencies $\omega_0 \pm \omega_L$ where synchronization occurs defines the locking range of the oscillator. ω_L depends on the strength of the injecting signal s_{inj} , and the selectivity of filter, it's usually results in a small fraction of ω_0 .

III. DESIGN CONSIDERATIONS OF THE ILFD

The design consideration of the ILFD includes the operating frequency, power consumption and locking range. The operating frequency of the ILFD is set by the speed of both blocks, the injector and the frequency selective block. Ring-oscillator-based ILFDs (Ring-ILFDs) feature wide locking ranges, small silicon area and large division module [3-11]. Ring-ILFDs' operation frequencies are mainly depend on the dimension of the devices and the power consumption. Although the phase noise of the conventional ring-oscillator is poor, the noise performance of ring-ILFDs can be further improved by injecting a clean signal [9]. In order to widen the locking range, to overcome process, voltage, and temperature (PVT) variations, the multiple-input injection technique for Ring-ILFDs with even division ratios has been proposed in [5] and [8]. However, the locking range of Ring-ILFDs with odd division ratios can rarely overcome the PVT variations. Usually when the number of ring-oscillator stages increases, the locking range becomes smaller severely [12]. Since low division ratios can decrease the speed and power in the following building blocks, to widen the locking range of large odd-division-module Ring-ILFDs still desired.

For conventional single-phase injection, the locking range of the ILFD is narrow since the extra phase shift around the loop is generated by only one injection. For multi-phase injection, the extra phase shift can be provided by multiple injection currents. The locking range of this ILFD will be widened if the phase of the injections progress with the ring oscillator's intrinsic delays. However, as mentioned previously, the requirement of specific multi-phase inputs makes this technique impractical in low power application [13]. We analyse the proposed divide-by-3 ILFD, as shown in Fig. 2, to demonstrate the base of our idea. The concept of this prototype can be applied to other ring-oscillator-based ILFDs. Each node v_i ($i = 1, 2, 3$) is connected to every other node in the ring oscillator through an injection transistor to form a symmetrical injection circuit.

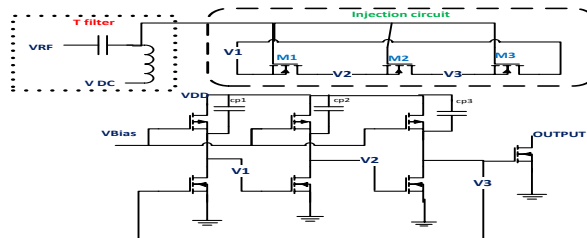


Figure 2: Schematic of proposed divide-by-3 ILFD

RF signal apply to V_{inj} node by T filter block, where all gate injection transistors (M_i) connected there. Bias voltage (V_{DC}) is necessary for injection circuit driver. Bias Tee used for this work, salience that must said elevate of quality bias tee circuit. In this schematic DC voltage (V_{Bias}) is used for inverter stage PMOS gate bias; this node can be used for control of frequency operation. C_{pi} represents the parasitic capacitance in the node V_i . In the qualitative analysis, the injection transistor can be treated as a mixer. Assume that the injection voltage is introduced as:

$$V_{inj} = V_{dc} + A_{inj} \cos(\omega_{inj} t + \theta_{inj}) \quad (3)$$

Where V_{dc} and A_{inj} are the dc voltage, amplitude, and phase of injection signal, respectively. The voltage at each oscillation node V_i ($i=1, 2, 3$) in Fig. 2 is $\cos(\omega t + \theta_i)$, where $\theta_i = (i - 1)(2\pi/3)$, is angle of $2\pi/3$ with different i . Thus, the injection current (generated by M_i through mixing) can be described as:

$$I_{inj,i} = \sum_{m=0}^{\infty} \sum_{n=0}^{\infty} a_{mn} \cos(m\omega_{inj} t + m\theta_{inj}) \times \cos(n\omega t + n\theta_{ds,i}) \quad (4)$$

Where a_{mn} is an intermediation transconductance coefficient of the mixer, and in the case of divide-by-3? We have considered only the fundamental current because other harmonics will be suppressed by the intrinsic low-pass filter in the loop of ring oscillator, so the fundamental current is, For simplicity, only the terms with $m=0, n=1$ and $m=1, n=2, 4$, are taken into consideration. Therefore, Eq. (4) expanded as:

$$I_{inj,i} = \frac{a_{01}}{2} \cos(\omega t + \theta_{ds,i}) + \frac{a_{12}}{2} \cos(\omega t + \theta_{inj} - 2\theta_{ds,i}) + \frac{a_{14}}{2} \cos(\omega t - \theta_{inj} + 4\theta_{ds,i}) \quad (5)$$

For each in Eq. (5), the parameters, a_{01}, a_{12}, a_{14} are the same, and only $\theta_{ds,i}$ is different, and have the same amplitude and form the angle of $\theta_{ds,i}$ with each other. To simplify the qualitative analysis, we assume that the current flows from drain to source. The total current injected into the node V_i will be

$$|I_{inj_tot,i}| = \sqrt{3}|I_{inj,i}| \quad (6)$$

Where the angle between each $I_{inj_tot,i}$ is also $\frac{2\pi}{3}$. Therefore, the phase of the total injection currents progress with the intrinsic phase in the ILFD.

Fortunately, the number of injection transistors in our proposed N -stage ILFD is $N(N-1)/2$, which increases rapidly with N . Therefore, even while the division ratio is large, the injection efficiency will not degrade severely since much more currents can be injected into the ILFD.

We assume that the injection current $I_{inj,i}$ is much smaller than the oscillation current, $I_{osc,i}$. By using the same method in [13], the one-sided locking range for our proposed divide-by-3 ILFD at the fundamental frequency can be derived as:

$$\frac{\Delta\omega}{\omega_0} \leq 4 \left| \frac{I_{inj}}{I_{osc}} \right| \cdot \left(1 - 3 \left| \frac{I_{inj}}{I_{osc}} \right|^2 \right)^{-\frac{1}{2}} \quad (7)$$

In addition we have substituted the NMOS transistors in Fig.2 which is proposed by Yi et al [13], with Vernier inverter circuit. The resultant circuit scheme is the same as fig. 2 for divide-by-3 frequency dividers. For the divide-by-5 frequency divider, the circuit scheme is like fig. 3. The proposed circuit is faster than the circuit which is proposed in [13].

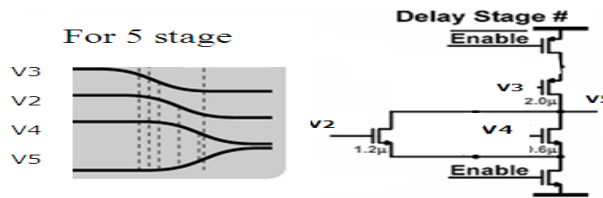


Figure 3: Vernier method inverter

Vernier method is usually used for designing high-speed oscillator. The frequencies that can be achieved by this method increase by increasing the number of successive stages (vernier) of the ring oscillator. This is noteworthy that the increase performance of the proposed method is optimized for more than 3 stage rings; in other words in the higher frequencies application, this way is better than other methods. Fig. 4 show this method, we applied signals from outputs of before stages to input of current inverter stage that increase speed of rising and falling time in vernier inverter, such as Fig.4(b). As demonstrated in Fig. 4(a), loop of several inverter stages considered as ring oscillator.

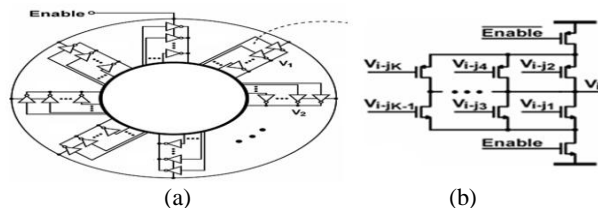


Figure 4: Schematic of frequency divider using Vernier method.

IV. SIMULATION RESULTS

Two circuits, three and five stage of vernier ring as illustrated in Fig.2 and Fig. 4(b), have been designed and simulated by TSMC 0.18 μm CMOS technology. Fig. 4(b) demonstrated schematic of inverter with more than one input from vernier method.

In both ILFDs, the single-end delay cell is designed as a NMOS inverter with a PMOS current-source load. A simple open-drain NMOS inverter is used for the output buffer. Note that the bodies of all NMOS (PMOS) transistors are connected to ground (VDD). The external bias voltages of PMOS load, V_{Bias} , is used to tune ILFD's free running frequency. To realize a large modulation conductance of injection transistors, the DC voltage of injection signal, V_{DC} , is set to 0.3 V as the optimize value. The supply voltage V_{DD} is set to 1V, and can be further reduced to 0.8 V.

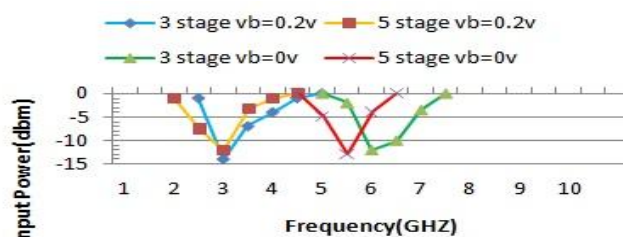


Figure 5: Measured input sensitivity of proposed ILFDs

The input sensitivity (that is very mainstay at quality of L and C input filter) of divide-by-3 ILFD and divide-by-5 ILFD operating at 1 V supply voltage are depicted in Fig. 5. When $V_{Bias}=0$ V, the locking frequency is from 5.6 to 7.5 GHz and the power consumption is 0.25 mw for divide-by-3 ILFD.

In divide-by-5 ILFD, thanks to the 10 injection transistors, its locking frequency is from 5 to 6.4 GHz and the power consumption is 0.93 mw while $VDD=1V$. Table 1 illustrated the results in different proposed ILFDs.

FOM is maximum operating frequency/ power [2] which is a good criterion for comparing oscillators. The higher FOM shows the better performance of an oscillator. We have calculated the FOM for several proposed methods in the literature. These results are shown in table 1. The results illustrate that our proposed scheme has the best FOM.

Table1. Comparison results with other RC ILFDs in CMOS technology.

Ref.	Tech. μ m	VDD (v)	Div. Ratio	Locking Freq. (GHz)	Power (mw)	FOM* (GHz/mw)
[6]	0.18	1.0	3	2.51-3.50	0.4	8.75
[7]	0.18	1.8	3	4.85-5.7	12.51	0.46
[8]	0.18	1.8	3	8.28-11.4	12.5	0.92
[9]	0.18	1.8	3	1.2-4.9	0.74	6.62
	0.18	1.8	7	1.4-4.4	0.88	5
[10]	0.065	1.2	7	4.1-5.1	0.516	9.88
[11]	0.13	1.5	3	24-30.8	13	2.27
<i>This work</i>	0.18	1	3	5.6-7.5	0.25	30
	0.18	1	5	5-6.4	0.93	6.88

V. CONCLUSION

In this paper, we improve the locking range in conventional single-phase injection ILFD by introducing symmetrical injection structure. Analysis reveals that the proposed design can realize multi-phase injection with only single-phase input. Two ILFDs, with division ratio of 3 and 5, respectively, were designed and simulation to verify our analysis. Measurement results show that our design can achieve a reasonable performance with low power and small area due to absence of inductors in our design. The locked ranges of divide-by-3 and divide-by-5 dividers are 1.9 GHz and 1.4 GHz, while dissipating 0.25mw and 0.93mw at 1 V supply voltage, respectively.

REFERENCES

- [1] H. R. Rategh, and T. H. Lee, Super harmonic injection-locked frequency dividers, *IEEE J. Solid-State Circuits*, vol. 34, no. 6, pp. 813–821, Jun. 1999.
- [2] K. Yamamoto, and M. Fujishima, A 44- μ W 4.3-GHz injection locked frequency divider with 2.3-GHz locking range, *IEEE J. Solid-State Circuits*, vol. 40, no. 3, pp. 671–677, Mar. 2005.
- [3] S. Seo, H. Seo, S. Jeon, and J.-S. Rieh, A 20–30 GHz divide-by-3 ring-oscillator-based injection locked frequency divider with a wide locking range, *Microwave Opt. Tech. Lett.*, vol. 53, no. 4, pp. 839–841, Apr. 2011.
- [4] J.-C. Chien, and L.-H. Lu, Analysis and design of wideband injection-locked ring oscillators with multiple-input injection, *IEEE J. Solid-State Circuits*, vol. 42, no. 9, pp. 1906–1915, Sep. 2007.
- [5] A. Mirzaei, M. Heidari, R. Bagheri, and A. Abidi, Multi-phase injection widens lock range of ring-oscillator-based frequency dividers, *IEEE J. Solid-State Circuits*, vol. 43, no. 3, pp. 656–671, Mar. 2008.
- [6] A. Tedesco, A. Bonfanti, L. Panseri, and A. Lacaita, A 11-15 GHz CMOS 2 Frequency divider for broad-band I/Q generation, *IEEE Microwave Wireless Component Letters*, vol. 15, no. 11, pp. 724–726, Nov. 2005.
- [7] R. Adler, A study of locking phenomena in oscillators, in *Proceedings of the IRE*, vol. 34, no. 6, pp. 351–357, Jun. 1946.
- [8] A. Mirzaei, M. E. Heidari, R. Bagheri, S. Chehrizi, and A. A. Abidi, The quadrature LC oscillator: A complete portrait based on injection locking, *IEEE J. Solid-State Circuits*, vol. 42, no. 9, pp. 1916–1932, 2007.
- [9] S. Verma, H. R. Rategh, and T. H. Lee, A unified model for injection-locked frequency dividers, *IEEE J. Solid-State Circuits*, vol. 38, no. 6, pp. 1015–1027, 2003.
- [10] B. Razavi, A study of injection locking and pulling in oscillators, *IEEE J. Solid-State Circuits*, vol. 39, no. 9, pp. 1415–1424, Sep. 2004.
- [11] Karsilayan, A Fully Differential Low-Power Divide-by-8 Injection-Locked Frequency Divider up to 18GHz, *IEEE J. of Solid-State Circuits*, vol. 42, no. 3, pp. 583-591, Mar. 2007.
- [12] W. Chen, and C. Kuo, 18 GHz and 7 GHz super harmonic injection locked dividers in 0.25- μ m CMOS technology, in *Proc. ESSCIRC*, pp. 89–92, 2002.
- [13] X. Yi, Ch. Ch. Boon, M. A. Do, K. S. Yeo, and W. M. Lim, Design of Ring-Oscillator-Based Injection-Locked Frequency Dividers With Single Phase Inputs. *IEEE Microwave and wireless components letters*, vol. 21, no. 10, PP. 559-561, 2011.

Experimental Analysis on Multi Hole Nozzle Jet Pump

Jagadeshwar Kandula¹, M Vijay Kumar²

1, 2(Asst Professor, Mechanical Engineering, K L University, Guntur, Andhra Pradesh, India)

ABSTRACT: Water is central to survival, without water human, plant and animal life would be impossible. Therefore supply of water has become one of the fundamental requirements of any society and the need to transfer water has generated the design of various forms of mechanical devices, which can be categorized as pumps. Jet pump is a device that performs its pumping action by the transfer of energy from a high velocity supply jet to one of low velocity suction flow. These two flows mix in the mixing tube and the kinetic energy of the combined flow is converted partially into the pressure energy in the diffuser. The optimization of the design of multi hole nozzle jet pump with various pitch circle diameter (PCD) and five different diameter mixing tubes.

The area ratios chosen have been modified and the final area ratios used were $R = 0.20, 0.28, 0.36, 0.43$ & 0.50 . From the graphs, head ratio at zero discharge ratios (N_o), discharge ratio at zero head ratio (M_o) and slope of $M-N$ (m) curve were noted along with the extrapolated values of maximum efficiency (η_{bep}), optimum discharge ratio (M_{opt}), and optimum head ratio (N_{opt}) and tabulated. In order to distinguish these nozzle plates from these charts one can conclude that efficiency is higher at lower pitch circle diameter, lower mixing tube diameter and higher area ratios. In the range of experiments conducted highest maximum efficiency was obtained for an area ratio of 0.43 with 2 holes on 13 PCD with 25.9 mm mixing tube.

Keywords: Area ratios, Mixing tube, Multi hole nozzle, Nozzle plates, Pitch circle diameter (PCD)

I. INTRODUCTION

Pumps are hydraulic machinery that converts mechanical energy to fluid energy to increase the hydraulic energy in the flow. Pumps are devices that transfer energy from an external source to liquid in order to move the liquid from one location to another. This process will increase the energy of the liquid as it leaves the pump. In other words “Pumping is the addition of energy to liquid, which is normally used for the purpose of moving the liquid from one place to other or to do any other work”. Jet pump is a device, Layout and Measuring Arrangement of Test Setup as shown in Fig.1, which performs its pumping action by the transfer of energy from a high velocity supply jet to one of low velocity suction flow. These two flows mix in the mixing tube and the kinetic energy of the combined flow is converted into the pressure energy in the diffuser

The applications of jet pump are Deep well pumping, Booster pumping, Dredging, Sediment transportation, Priming of large sumps and Siphons. They are also useful in Reactor coolant circulation, Aircraft fuel pumping, Condensate pumping in space power systems, Recirculation and mixing in process industries, Steam jet refrigeration and Tunnel ventilation. The main advantage of the jet pump compared to the Rotodynamic pumps is offset installation. Possibility of the offset installation is a unique feature of jet pump. It can be installed away from the source of water up to a distance of 90 meters or even more. The only limitation of the jet pump is its comparatively lower efficiency.

The following processes take place in a jet pump

- a. Pressure energy of the fluid from supply pipe is converted into kinetic energy in the driving nozzle.
- b. Suction fluid induces through suction pipe as the pressure falls in the driving nozzle.
- c. The flow from driving nozzle and suction stream combines by turbulent mixing in the mixing tube of jet pump.
- d. Kinetic energy of the combined fluid in mixing tube is converted into pressure energy in the diffuser and
- e. The resultant fluid is then delivered in the delivery pipe.

II. EXPERIMENTAL SETUP

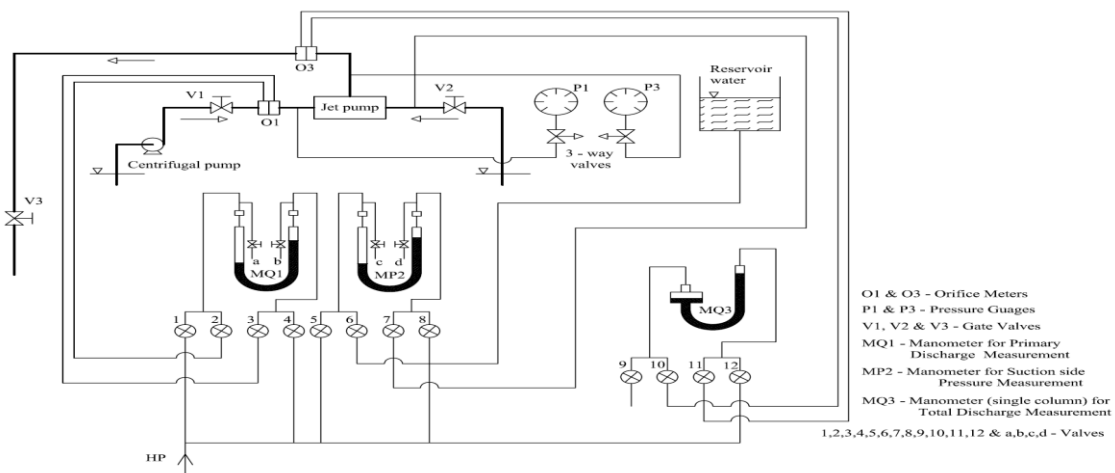


Fig.1 Layout and Measuring Arrangement of Test Setup

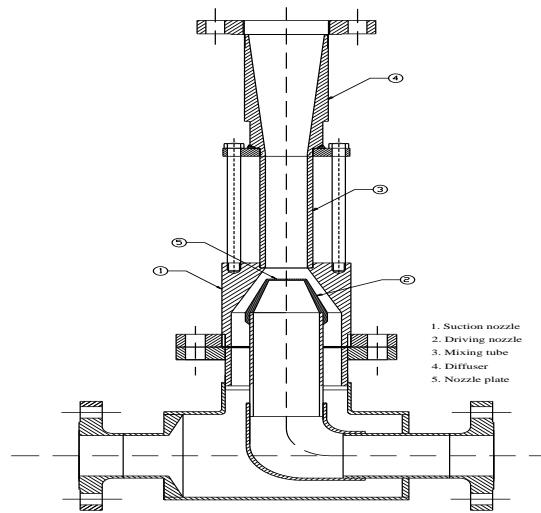


Fig.2 Cross Sectional view of View of The Jet Pump

The performance of a jet pump is graphically represented by Head ratio (N) as a function of Discharge ratio (M) and Efficiency (η) as a function of Discharge ratio (M). The graph indicates that as the discharge ratio increases the head ratio decreases. The slope of the M-N curve depends on the area ratio of the jet pump. In case of discharge ratio versus efficiency, the curve increases till the maximum efficiency then it drops. If the pump is running with cavitation its performance drops drastically at one discharge ratio. The Cross Sectional view of View of The Jet Pump as shown in Fig.2 and Arrangement of holes on various multi holes nozzle plates are shown in Fig.3.

The main objective of this project work is to conduct an experimental study on the performance characteristics of the multi hole nozzle jet pump with number of holes ranging from two to six. This project work includes the optimization of the design of multi hole nozzle jet pump with various pitch circle diameters and mixing tubes.

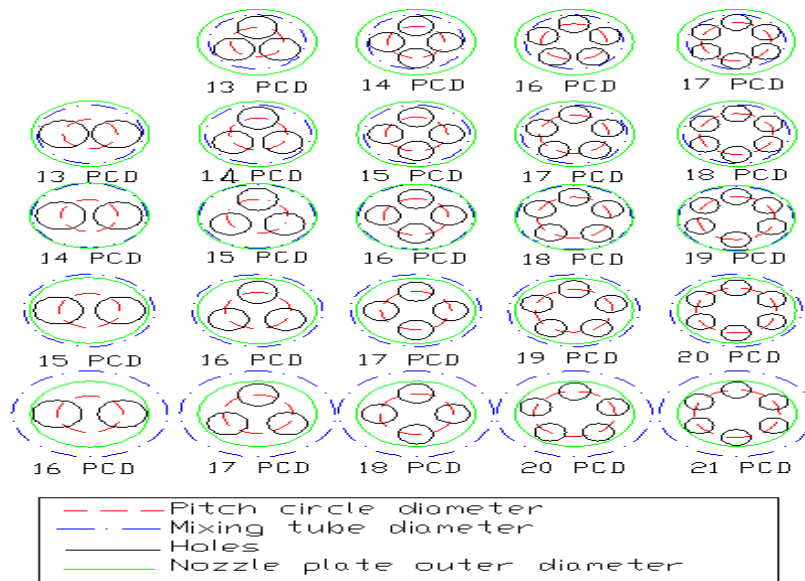


Fig.3 Arrangement of holes on various multi holes

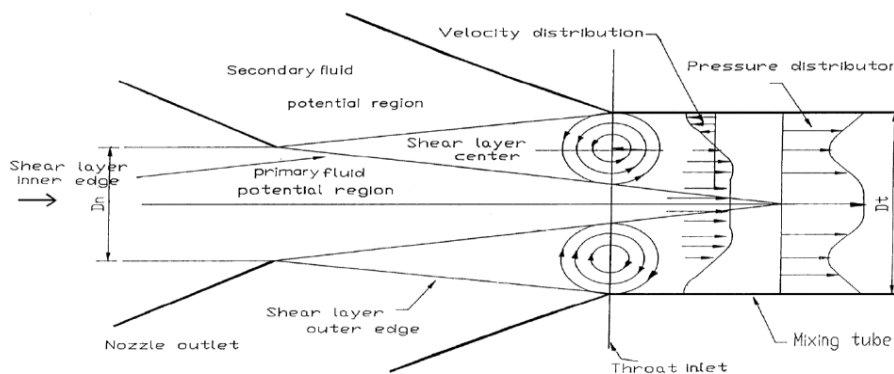


Fig.4 Schematic representation of the flow pattern between the nozzle outlet and the throat inlet

III. EQUATIONS

Area Ratio (R): It is the ratio of driving nozzle area and mixing tube throat area and is given by

$$R = \frac{A_n}{A_t} = \left(\frac{d_n}{d_t} \right)^2 \quad (1)$$

Discharge Ratio (M): It is the ratio between suction flow rate and primary flow rate of jet pump.

$$M = \frac{Q_2}{Q_1} \quad (2)$$

Head Ratio (N)

It is the ratio between net jet pump head and net driving head of the jet pump.

Jet pump supply head H_1 is given by

$$H_1 = \frac{p_1}{\gamma} + \frac{v_1^2}{2g} + z_1 \quad (3), \quad H_2 = \frac{p_2}{\gamma} + \frac{v_2^2}{2g} + z_2 \quad (4)$$

Jet pump delivery head H_3 is given by

$$H_3 = \frac{p_3}{\gamma} + \frac{v_3^2}{2g} + z_3 \quad (5), \quad N = \frac{H_3 - H_2}{H_1 - H_3} \quad (6)$$

Efficiency of Jet Pump (η)

It is defined as the ratio of energy increase of suction stream (output energy) to the energy decrease of driving stream (input energy).

$$\eta = \left(\frac{Q_2}{Q_1} \right) \times \left(\frac{H_3 - H_2}{H_1 - H_3} \right) = M \times N \quad (7)$$

IV. RESULTS

Plots of head ratio (N) Vs discharge ratio (M) are shown in Fig.5a to Fig 9a for various No. of holes. The legend of the Figures refer to No. of holes-PCD-mixing tube diameter. In all the plots M-N curves are fitted as a straight line by the method of least squares.

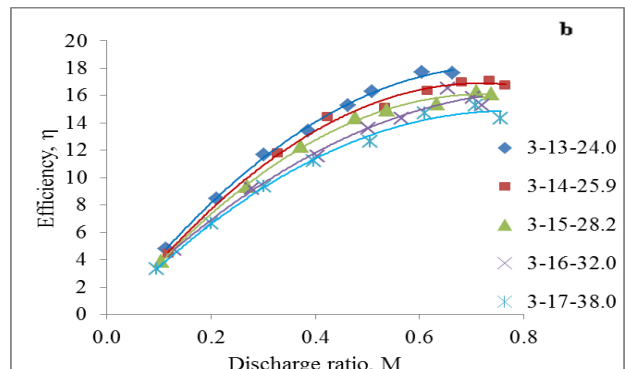
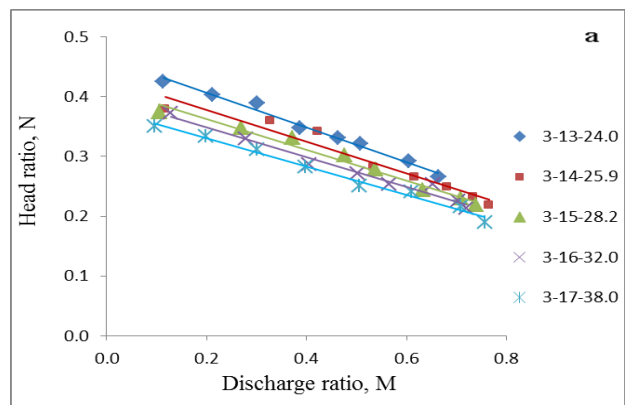
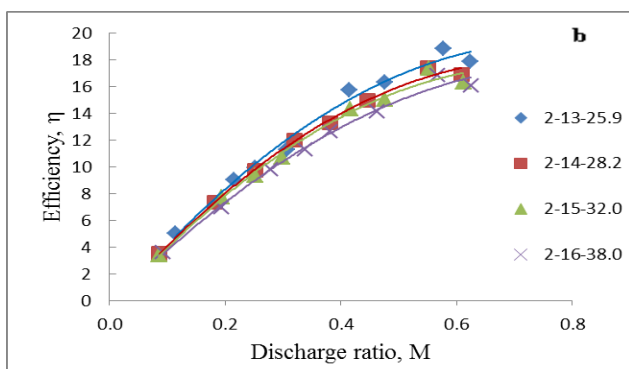
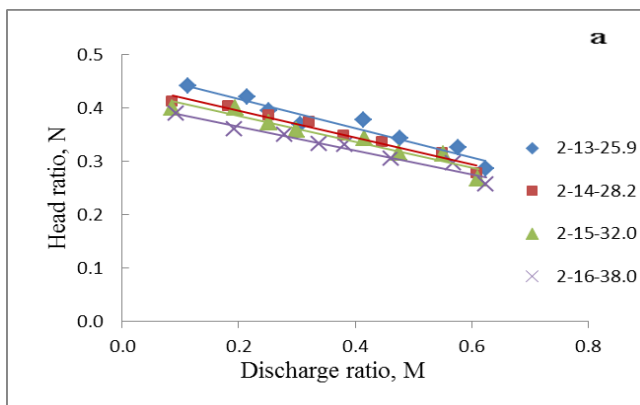


Fig.5 Performance characteristics of Jet Pump with 2 holes

Fig.6 Performance characteristics of Jet Pump with 3 holes

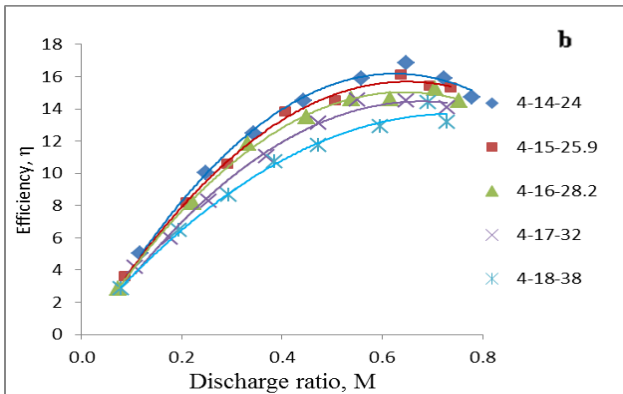
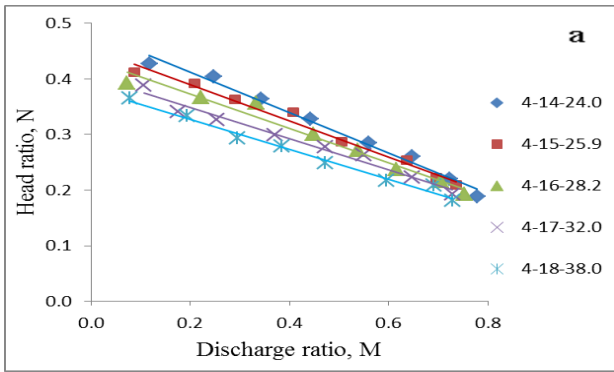


Fig.7 Performance characteristics of Jet Pump with 4 holes

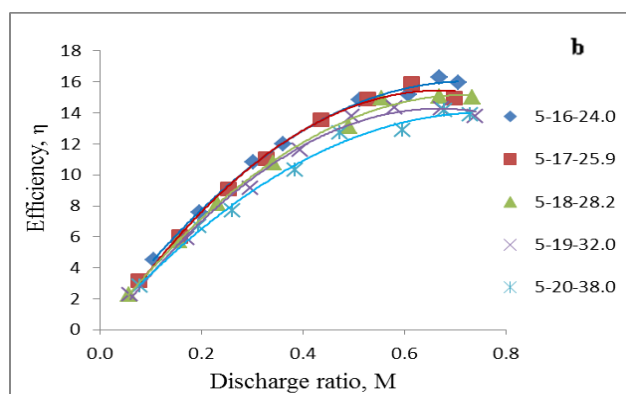
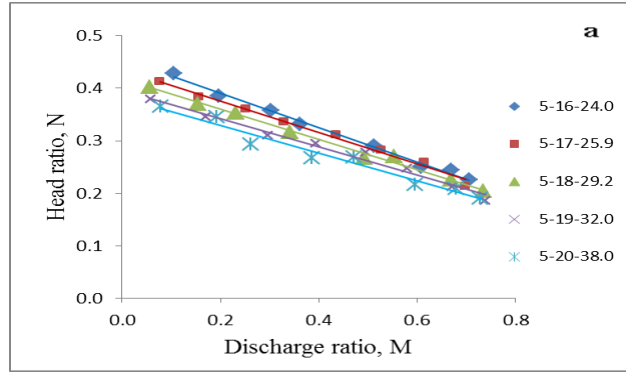


Fig.8 Performance characteristics Of Jet pump with 5 holes

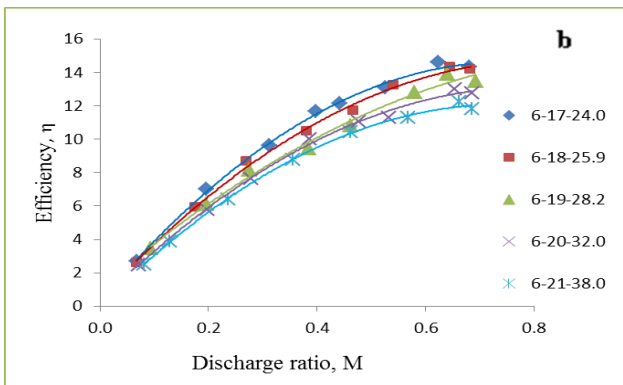
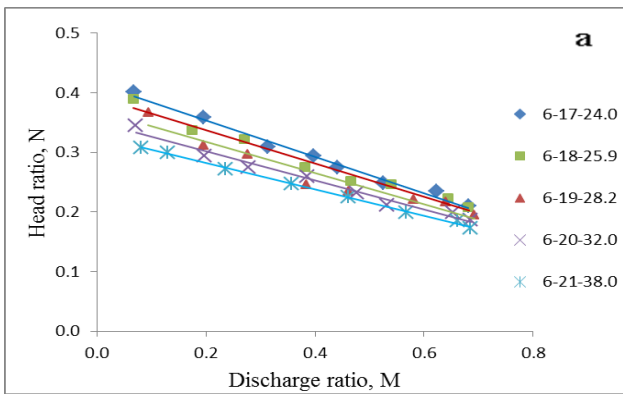


Fig.9 Performance characteristics of Jet pump with 6 holes

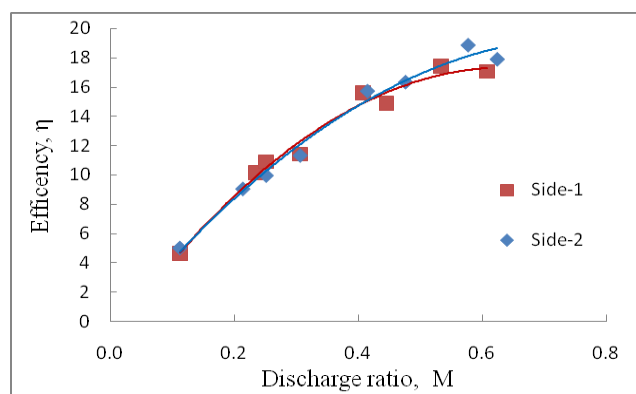


Fig.10 Effect of manufacturing inaccuracy

Shown Fig.10 each time after taking the readings of one nozzle plate, the nozzle plate was reversed and the experiment was repeated. This was because of the considerable variation noticed of the jet pump performance for two cases which might be due to manufacturing inaccuracy in drilling holes on the plates. So after taking the readings on both sides, jet pump performance was determined and the side of the nozzle plate which exhibited higher efficiency was chosen as the right one.

Table.1 Performance parameters for all the Nozzle Plates

S.NO	Dh(mm)	Z	Dp	Dm(mm)	M0	N0	m	Mbep	Nbep	ημαξ %
1	12	2	13	25.9	1.738	0.471	-0.271	0.85	0.24	20.46
2	12	2	14	28.2	1.777	0.446	-0.251	0.9	0.22	19.81
3	12	2	15	32	1.797	0.433	-0.241	0.95	0.2	19.38
4	12	2	16	38	1.839	0.41	-0.223	0.9	0.21	18.84
5	9.8	3	13	24	1.611	0.464	-0.288	0.8	0.234	18.69
6	9.8	3	14	25.9	1.623	0.43	-0.265	0.8	0.218	17.44
7	9.8	3	15	28.2	1.611	0.414	-0.257	0.8	0.208	16.67
8	9.8	3	16	32	1.611	0.398	-0.247	0.8	0.2	15.97
9	9.8	3	17	38	1.595	0.378	-0.237	0.8	0.188	15.07
10	8.5	4	14	24	1.337	0.484	-0.362	0.65	0.249	16.17
11	8.5	4	15	25.9	1.401	0.454	-0.324	0.7	0.227	15.9
12	8.5	4	16	28.2	1.409	0.434	-0.308	0.7	0.218	15.29
13	8.5	4	17	32	1.414	0.41	-0.29	0.7	0.209	14.61
14	8.5	4	18	38	1.448	0.404	-0.279	0.7	0.191	13.35
15	7.6	5	16	24	1.397	0.454	-0.325	0.7	0.227	15.86
16	7.6	5	17	25.9	1.455	0.435	-0.299	0.75	0.211	15.81
17	7.6	5	18	28.2	1.455	0.416	-0.286	0.7	0.216	15.11
18	7.6	5	19	32	1.479	0.395	-0.267	0.75	0.195	14.61
19	7.6	5	20	38	1.443	0.381	-0.264	0.7	0.196	13.73
20	6.9	6	17	24	1.361	0.415	-0.305	0.7	0.202	14.11
21	6.9	6	18	25.9	1.409	0.393	-0.279	0.7	0.198	13.84
22	6.9	6	19	28.2	1.418	0.37	-0.261	0.7	0.187	13.11
23	6.9	6	20	32	1.44	0.35	-0.243	0.7	0.18	12.59
24	6.9	6	21	38	1.482	0.326	-0.22	0.65	0.18	11.68

In all plots of M Vs N shown in Fig. 5a to Fig.9a head ratio (N) and discharge ratio (M) are related as a straight line and an equation of first order of the following form is obtained.

$$N = (m \times M) + N_0 \tag{9}$$

Where, m is the slope of the M-N curve, N₀ is the head ratio at discharge ratio = 0, From this equation, M values at N = 0 is calculated and indicated as M₀

$$M_{bep} = (-N_0/2m) \tag{10}$$

Where, M_{bep} = Discharge ratio at best efficiency point

$$N_{bep} = (N_0/2) \tag{11}$$

Where, N_{bep} = Head ratio at best efficiency point

Product of M and N is nothing but efficiency. Values of M and N corresponding to best efficiency point were used to determine maximum efficiency.

$$\eta_{max} = M_{bep} \times N_{bep} \tag{12}$$

It may be observed from this table that maximum efficiency decreases as PCD increases for a given No. of holes. Further, for a given No. of holes maximum efficiency decreases as the No. of holes increases as the PCD increases, there is an increase in maximum efficiency, slope (m), M_{bep}, N_{bep}, N₀ and M₀. In the range of experiments conducted highest maximum efficiency was obtained for 2 holes on 13 PCD with 25.9 mm mixing tube.

V. CONCLUSIONS

- ❖ A small manufacturing error in the nozzle plate holes results in a considerable change in performance of the jet pump.
- ❖ Jet pump with multihole nozzle having smaller No. of holes with smaller PCD and smaller mixing tube diameter gives higher efficiency
- ❖ In the range of experiments conducted highest maximum efficiency was obtained for an area ratio of 0.43 with 2 holes on 13 PCD with 25.9 mm mixing tube.

VI. SCOPE FOR FURTHER WORK

- ❖ The performance of jet pump for various area ratios can be done by changing the mixing tube design.

REFERENCES

- [1] Gosline, J.E. and O'Brien, M.P., 1934, 'The Water Jet pump', University of California Publications in Engineering, .3, pp.167-190.
- [2] IS 2952 Part I, 1964, 'Indian Standards Recommendations for methods of measurements of fluid flow by means of orifice plates and nozzles- Incompressible fluids'. Bureau of Indian Standards, New Delhi.
- [3] Muller, N.H.G. 1964, 'Water jet pump', Proc. ASCE, J1.Hyd. Div., 90, pp 83-113.
- [4] Narui, H. and Harda, S., 1979, 'Cavitation in water jet pumps', Bull. Of the JSME, .22, (166), pp.562-569
- [5] Stepanoff, A.J., 1957, 'Centrifugal and axial flow pumps', 2nd Edi. John Wiley and Sons, New York.
- [6] Mikail, S., Morcos, S.M., and Shaheen, Y.A, 1988 "Experimental Investigations of a Slurry Jet Pump", Proc. Third International Symposium on Liquid-Solid Flows, ASME, Winter Annual Meeting, Chicago, Illinois,
- [7] Fish, G., 1970 "The Solids –Handlin Jet Pump", Hydrotransport 1, First International Conference on the Hydraulic Transport of Solids in Pipes, (BHRA) Held at the University of Warwick, U.K.

Experimental Studies of Automotive Disc Brake Noise and Vibration: A Review

Amr M. Rabia,¹ Nouby M. Ghazaly,² M. M. Salem,³ Ali M. Abd-El-Tawwab⁴
Automotive and Tractor Eng. Dept., Minia University, El-Minia - 61111, Egypt

ABSTRACT: In the last few decades, there have been extensive studies on analysis and investigation of disc brake vibrations done by many researchers around the world on the possibility of eliminating brake vibration to improve vehicle users' comfort. Despite these efforts, still no general solution exists. Therefore, it is one of the most important issues that require a detailed and in-depth study for investigation brake noise and vibration. Research on brake noise and vibration has been conducted using theoretical, experimental and numerical approaches. Experimental methods can provide real measured data and they are trustworthy. This paper aims to focus on experimental investigations and summarized recent studies on automotive disc brake noise and vibration for measuring instable frequencies and mode shapes for the system in vibration and to verify possible numerical solutions. Finally, the critical areas where further research directions are needed for reducing vibration of disc brake are suggested in the conclusions.

Keywords: Noise and vibration, experimental investigations, automotive disc brake.

I. INTRODUCTION

Since vehicle comfort has become such an important factor to indicate the quality of a passenger car, eliminating or reducing the noise and vibration of a vehicle structure and system seems to provide a leading edge in the market to vehicle manufacturers. With progress made towards other aspects of vehicle design refinement against vehicle vibration and noise through improvement, refinement in brake vibration and noise is inevitable. Research into understanding brake noise and vibration has been ongoing over the last 50 years or more. Initially drum brakes were studied due to their extensive use in early automotive brake systems. However, disc brake systems have been common place on passenger vehicles since the 1960s and are used more extensively in modern vehicles. It follows that research into brake noise and vibration became focused more onto disc brake systems. A schematic of a disc brake assembly is shown in Figure 1. A large flat circular plate disc, referred to as the brake rotor, is mounted to the wheel axle and rotates with the applied to the piston, the inner pad is forced against the brake rotor. The caliper housing itself "floats", i.e. is free to slide back and forth in the direction of the wheel axis, and moves in the opposite direction to the piston. Fingers on the caliper force the outer pad into contact with the other side of the rotor clamping it between the pads. The caliper assembly is constrained by the anchor bracket from moving about the wheel axis; hence a braking torque is generated. Variations to this arrangement exist, some including fixed calipers with pistons that act on both the inner and outer pads directly, but the sliding caliper is used on the majority of automotive brake systems.

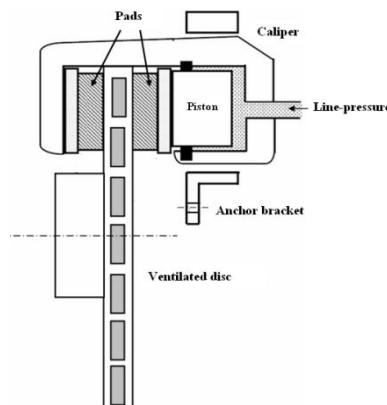


Figure 1 Schematic of a sliding disc brake caliper.

The rotor disc materials of a disc brake system are normally made from gray cast iron due to its excellent heat conductivity, good damping capacity and high strength [1–3]. Generally, the friction materials may be classified into four categories, metallic, metal ceramic, asbestos filled resin composites and asbestos-free composites. The friction pad materials are required to provide a stable coefficient of friction and a low wear rate at various operating speeds, pressures, temperatures, and environmental conditions [4–7]. Furthermore, these materials must also be compatible with the rotor material in order to reduce its extensive wear, vibration, and noise during braking [4].

There are many considerations in analyzing noise and vibration in automotive disc brake systems. During disc brake engagement, the brake lining rubs against the rotor and the kinetic energy is dissipated in the related friction process as a heat. This kinetic energy is transferred into the energy of the contact asperities, particles, and atoms [8]. Then, the energy of

the motion of asperities, particles, and atoms translates into vibration and generates a sound wave [9]. The growth of friction layers affects the contact stiffness considerably and may cause the system to become instable [10]. Hoffmann and Gaul reported that surface properties (such as surface topography, roughness characterizations, physical properties of the interface, and the debris materials between the surfaces) may play significant role for the generation of vibration and noise [11]. A large number of papers have been published which contain models describing brake noise and vibration. There are typically three methods available to investigate brake vibration and noise, i.e., through experimental methods or analytical methods or numerical methods. Experimental methods can provide real measured data and they are trustworthy. Experimental approaches have been used to measure the brake frequencies and mode shapes for the system in vibration and to verify possible solutions that can eliminate or significantly reduce brake noise and vibration. This paper begins with an introduction to the automotive disc brake system, to give an overview of disc brake components and their function. A review of brake vibration literature is then presented that explains the disc brake vibration generated by friction. The scientific findings are categorized into the experimental investigations that have been employed to examine vibration problems.

II. EXPERIMENTAL APPROACHES

Over the years, experimental approaches using brake dynamometers or on-road tests have been widely used to examine the brake noise and vibration, to investigate the effects of different parameters and operating conditions, to understand the characteristics of the brake system during a vibration event and to verify possible solutions that can eliminate or reduce the vibration occurrence. The brake noise and vibration dynamometer has become the main testing platform for identifying propensity to generate noise during braking and for investigating brake vibration problems. There are two designs for the brake dynamometer. The first design is an inertia-type brake dynamometer that has flywheel attached to it and can be used to measure vibration at negative velocity slope. The second design is a drag-type brake dynamometer that can only test brake vibration at a constant speed.

It was typical to use a microphone and an accelerometer to capture sound intensity and vibration behaviour during vibration generation. Tarter [12] used these available tools to conduct a series of tests on noise and vibration with modified disc, friction material and pad contact geometry. From his experimental investigation, it was observed that slotted disc could eliminate squeal vibration while changes in friction material and pad contact geometry could have a significant effect in squeal vibration reduction.

Ichiba and Nagasawa [13] attempted to describe the cause of disc brake vibration using brake test rig. Small accelerometers were installed in the back plate, the disc and the friction material in order to measure its vibrational characteristics. They concluded that squeal vibration generation was dependent on the ratio of change in frictional force rather than in the friction - velocity characteristics where the exciting energy was derived from the fluctuations in surface pressure.

Felske et al. [14] were one of the first groups to use holographic interferometry to view the vibration modes on a self-excited disc brake. They present interferograms for two types of brake; a yoke and a fist type. The disc interferograms presented are self-excited (Double Pulsed Holography) and artificially excited (Time Averaged Holography). They suggested that the audible noise from a brake system comes from the pad and caliper, and not the disc as the noise from this destructively interferes in air.

Vadari et al. [15] discussed the future direction of disc brake noise testing. The discussion was focused on the on-vehicle data acquisition, integrated brake noise measurement system and dynamometer testing. They suggested the need for continued development of standardized methods for identifying and counting noise occurrences both on-and-off the road. The critical step to a true understanding of brake noise generation was to remove any subjective measurements from the counting process and adopting reliable and repeated descriptions of the brake noise propensity of a particular design. This could be achieved by using more robust on vehicle data acquisition, a simple and reliable brake noise dynamometer and a correct tool to visualise noise and vibration behaviour.

Bettge and Starcevic [16] carried out an experimental work on many samples of pads and discs using white light interferometry. They measured the topography of the surfaces quantitatively. They computed the distributions of area, height and slope of the contact patches. They described the influence of friction power and testing time. Their results show that high braking power leads to larger contact patches on the surface of the brake pads, the height of contact patches also increased and the contact patches are tilted towards the sliding direction.

Senatore et al. [17] conducted an experimental work on brake and clutch facing samples in sliding motion at different levels of loading, slip speed and sliding acceleration. They performed short time experiments using Pin-on-disc sliding contact in the laboratory test stand. They obtained a comprehensive view of the influence of the main sliding parameters by means of an artificial neural network. They investigated the not weak influence of the sliding acceleration to improve the friction coefficient prediction during transient operations. They concluded that the higher the sliding acceleration, the higher the friction coefficient. The materials have exhibited nearly linear dependence of the friction coefficient on the pressure contact in the studied ranges.

Nishiwaki et al. [18] examined the out-of-plane deformation of a rotating disc using the doubled pulsed technique in order to visualise the vibration pattern of the disc and pad when squeal vibration occurs. Their results show that squeal vibration was generated when both the rotating disc and pads vibrated in bending mode. They also concluded that squeal phenomena were strongly influenced by the natural frequencies and mode shapes of the disc.

Oliviera et al. [19] carried out an experimental work on brake squeal vibration instability. They investigated the dynamical and squeal vibration behaviors of a brake setup. They identified several characteristics that lead to instabilities

and correlated them with the operating parameters. Their results indicated that the pad dynamics have a key role in the selection of the squealing modes at one of the out-of-plane eigen frequency of the system. They found that squeal vibration occurs at frequencies close to natural frequencies of the coupled system. In addition, the in-plane dynamics of the pad plays a key role in the squeal vibration mode selection. Squeal vibration does not require that a stick-slip limit cycle is established. Squeal vibration frequency is not globally affected by changes in relative velocity.

Oberst and Lai [20] conducted an experimental work using a noise dynamometer to determine the influence of geometrical parameters of brake pads on vibration. They evaluated the experimental results with a noise index and ranked for warm and cold brake stops. They analyzed the data using statistical description based on population distributions and a correlation analysis. They performed the correlation analysis between the time-averaged friction coefficient and peak sound pressure data by applying a semblance analysis and a joint recurrence quantification analysis. They compared linear measures with nonlinear measures based on statistical from the underlying joint recurrence plots. Their results indicated that pads with a single vertical slots or a single slot perform better than pads with no slots or double vertical slots.

Kemmer [21] experimentally investigated the friction layer between pad and disc and modeled it as a granular medium. In his simulations, he found the contact stiffness of the granular friction layer to be directly dependent on the particles' diameter, the shear modulus of the particles' material, the friction coefficient for the interactions among the particles, the normal force, and inversely dependent on the friction layer's thickness. With his experiments, he showed that for one friction material, higher pressures lead to smaller wear debris particles.

Fieldhouse and Steel [22] summarized an experimental work on varying mechanically induced offset center of pressure between the pad and rotor. They investigated the propensity of a brake to generate noise over a range of temperatures and pressures. Their results indicated that a mechanical instability which is not influenced by temperature or pressure is possible within a brake system. Such a mechanical instability is caused by 'spragging' of the system, which would encourage low-frequency noise generation. Pad abutment is important with a trailing abutment being found to be the most stable arrangement. The co-planar forces acting on the pad tend to promote a leading offset. At minimum friction for the pad-caliper abutment interface the offset tends towards the critical offset value. To promote stability a disc brake requires a high friction coefficient between pad abutment and caliper mounting bracket and a low friction material coefficient. The position of the mounting plane for the caliper carrier bracket is important because of its influence over the spragging angle. It needs to be as close to the plane of the disc rubbing surface as possible.

Eriksson et al. [23] conducted an experimental research in friction behavior and squeal vibration generation for four different disc brake pads at low speeds. They studied the influence of speed and pressure variation. The test included braking with continuously increasing and decreasing brake pressure at constant speed and vice versa. Their results indicated that no squeal vibrations were generated below a coefficient of friction of 0.4. Braking conditions with a high coefficient of friction were related to more frequent squeal vibration generation.

JOE et al. [24] carried out a theoretical and experimental work on a floating caliper disc brake system using a linear, lumped, and distributed parameter model. They investigated the dynamic stability by using the complex eigenvalues. Their work was done with a constant friction coefficient. Their results indicated that a small error between experimental and theoretical natural frequencies, the mode of the disc is significantly responsible of the frequencies of the disc brake vibration and noise as well as the mode of each component. The system is more unstable if the friction coefficient, lining stiffness, length of the pads, and thickness of the lining are large, the system is more stable if the Young's modulus and the mass of the disc and pads are large.

Abu Bakar and Ouyang [25] summarized a theoretical and an experimental study on wear prediction of friction material in a disc brake system. They investigated wear established on the surfaces of a new pair of brake pads under different duration of brake. They developed a three-dimensional finite element model of a real disc brake considering the real surface topography of the friction material. Their results indicated that the contact area of a new frictional material increases and initial rough surfaces later become smoother as wear progresses. The leading edge is prone to more wear than the trailing edge. The simulation result showed a reasonably good correlation with the experimental results in the static contact pressure distribution, and height distributions. Good agreement found between the unstable frequency predicting in the stability analysis and the vibration frequency recorded in the experiment.

Meziane et al. [26] carried out a theoretical and experimental work on a pad-disc tribometer. They did simulations for the pad-disc system to allow describing the instability phenomena that occur during the interface of two bodies in contact. They used a coulomb's friction law at the contact surface with constant coefficient. They showed the importance of the pad poisson's ratio in the occurrence of the unstable state. Their results indicated that the contact surface of the pad can stick, slip or separate locally from the surface of the disc when instability occurs; these slip-stick-separation type contact waves generate impact forces that cause vibration. These waves give rise to periodic shocks in time and frequency, of which the fundamental frequency corresponds to a pad mode. This unstable mode is obtained by calculating the eigen modes and eigen frequencies of the system at rest and without taking friction into account. They reported that Poisson's ratio of the pad plays a basic role in the stability of the system since the latter becomes unstable beyond a threshold value.

Triches et al. [27] conducted a research to reduce noise from the disc brake systems using constrained layer damping. They studied the characterization of the noise generation via the brake dynamometer Figure 2. They measured the Pad, rotor and caliper Frequency Response Functions (FRF's) by exciting each component with an impact hammer, and measuring the acceleration response with a small accelerometer. They carried out a modal analysis for rotor which supported by a foam block, in order to simulate the free-free boundary condition. They studied the behavior of brake

components under pressure and temperature. They developed and tested an insulator bonded in the back plate. Their results indicated that a strong noise frequency around 7 kHz occur at a temperature of 150o and a pressure of 25 bar. The final dynamometer test showed reduction about of 20dB for some frequencies.

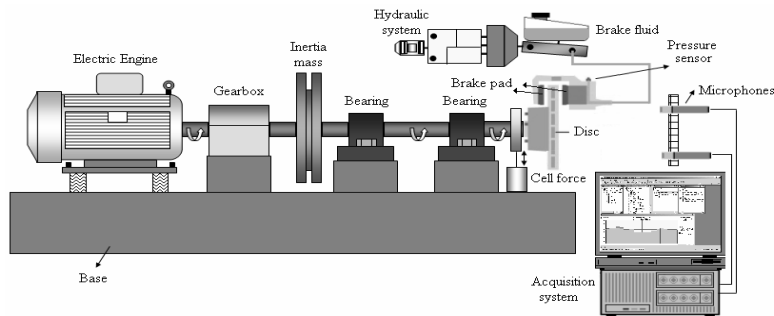


Figure 2 Components of an inertial dynamometer.

Oliviero Giannini et al. [28] carried out an experimental work to characterize the vibration and noise. They designed and built a laboratory brake for controlling experimental studies of noise emission in automotive brake as shown in Figure 3. They developed a relationship between modal and operational parameters of the system and emitted sound. They measured the relationship between the frequency of vibration emission and normal load. Their results indicated that an increase of the stiffness of the caliper affects the frequency of the vibration emission, shifting each zone to higher frequencies, but the motion of the whole system remains qualitatively the same.

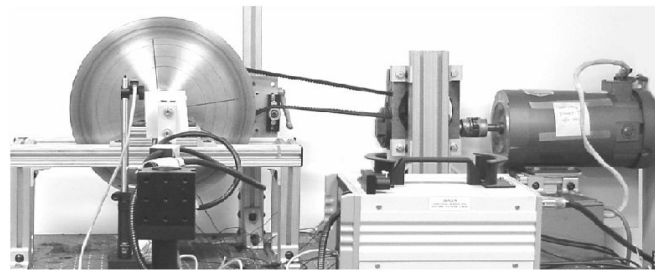


Figure 3 laboratory brake rig.

III. CONCLUSION

From the number of papers that have been published and summarized in this review, it is suggested that disc brake noise and vibration still continues to be a major concern for the automotive industry despite the efforts to reduce its occurrence during the past decades. Experimental methods will still play an important role for a number of reasons. Firstly, they offer more effective analysis tools than numerical methods. Secondly, diagnosis of the cause of brake vibration problems can often only be found by experimentation. Moreover, they can provide real measured data and they are trustworthy. Finally, the verification of solutions to noise and vibration problems can be achieved through experimental tests under different braking operating conditions. The previous experimental results reveal that there are numerous factors that influence the occurrence of vibration and noise in automotive disc brakes including materials and geometry of brake components, component interaction and many operating and environmental condition. All of these issues suggest that there is a strong need for further research to enhance our understanding of various parameters behind vibration generation.

IV. ACKNOWLEDGEMENTS

The authors would like to thank the FAW industry Group, manufacturing and trading of friction products in Egypt and Minia University for their continuous support in the research work.

REFERENCES

Journal Papers:

- [1] P.J. Blau, and J.C. McLaughlin, Effects of water films and sliding speed on the frictional behavior of truck disc brake materials, *Tribol Int* 36, 2003, 709–15.
- [2] K.W. Liew, and N.S.M. El-Tayeb, The effect of rotor disc material on tribo behavior of automotive brake pad materials, *Surf Rev Lett* 15(5), 2008, 625–33.
- [3] M. Eriksson, F. Bergman, and S. Jacobson, on the nature of tribological contact in automotive brakes, *Wear* 252(1–2), 2002, 26–36.
- [4] S.J. Kim, and H. Jang, Friction and wear of friction materials containing two different phenolic resins reinforced with aramid pulp, *Tribol Int* 33, 2000, 477–84.
- [5] M.G. Jacko, and S.K. Rhee, Brake linings and clutch facings, Kirk – Othmer encyclopedia of chemical technology, 4th ed., 4. New York: Wiley; 1992.
- [6] M.G. Jacko, P.H.S. Tsang, and S.K. Rhee, Automotive friction materials evolution during the past decade, *Wear* 100, 1984, 503–515.

- [7] M.H. Cho, S.J. Kim, D. Kim, and H. Jang, Effects of ingredients on tribological characteristics of a brake lining: an experimental case study, *Wear* 258, 2005, 1682–7.
- [8] F. Chen, and C. A. Tan, and R. L. Quaglia, Disc brake squeal-mechanism, analysis, evaluation and reduction/prevention, Warrendale, Pa.: 2006, SAE International.
- [9] I. Singer, and H. Pollock, Fundamentals of friction, Kluwer Academic publishers, Barunlage, Harx, Germany, 1992.
- [10] M. Paliwal, Development of a friction layer model for the brake pad-rotor interface for noise and vibration, Southern Illinois University at Carbondale, Ph.D. thesis, 2003.
- [11] N. P. Hoffmann, and L. Gaul, Friction induced vibrations of brake: research fields and activities, SAE international (08BC-0033), 2008.
- [12] J. H. Tarter, Disc brake squeal, S.A.E. Technical Paper 830530, 1983.
- [13] N. Ishihara, M. Nishiwaki, and H. Shimizu, Experimental analysis of low frequency brake squeal noise, S.A.E. Technical Paper 962128, 1996.
- [14] A. Felske, G. Hoppe, and H. Matthai, Oscillations In Squealing Disk Brakes – Analysis Of Vibration Modes By Holographic Interferometry, SAE Paper No. 780333, 1978.
- [15] V. Vadari, and M. Albright, An introduction to brake noise engineering, sound and vibration, Vol35-7, Roush Industries Inc., Livonia, Michigan, 2001.
- [16] D. Bettge and J. Starcevic, Topographic properties of the contact zones of wear surfaces in disc brakes, *Wear*, Vol. 254, 2003, 195-202.
- [17] A. Senatore , V. D’Agostino , R.DiGiuda and V. Petrone , Experimental investigation and neural network prediction of brakes and clutch material frictional behavior considering the sliding acceleration influence, *Tribology International*, Vol. 44, 2011, 1199-1207.
- [18] M. Nishiwaki, H. Harada, H. Okamura, and T. Ikeuchi, Study on disc brake squeal, S.A.E. Technical Paper: 890864, 1989.
- [19] G. Oliviera, A. Akay and F. Massi, Experimental analysis of brake squeal noise on a laboratory brake setup, *Journal of Sound and Vibration*, Vol. 292, 2006, 1-20.
- [20] S.Oberst and J.C.S. Lai, Statistical analysis of brake squeal noise, *Journal of Sound and Vibration*, Vol. 330, 2011, 2978-2994.
- [21] H. A. Kemmer, Investigation of the Friction Behavior of Automotive Brakes through Experiments and Tribological Modeling, PhD thesis, Universität Paderborn / Robert Bosch GmbH, Schriftenreihe ISBN 3-00-011230-8, 2002.
- [22] J. D. Fieldhouse and W. P. Steel, A study of brake noise and the influence of the centre of pressure at the disc/pad interface, the coefficient of friction and caliper mounting geometry, *Automobile Engineering*, part D, Vol. 217, 2003.
- [23] M. Eriksson and S. Jacobson, Friction behaviour and squeal generation of disc brake sat low speeds, *Proc Instn Mech Engrs*, Part D, Vol 215, 2001.
- [24] Y.-G. JOE, B.-G.CHA, H.-J SIM, H.-J. LEE and J.-E. OH, Analysis Of Disc Brake Instability Due To Friction-Induced Vibration Using A Distributed Parameter Model, *International Journal of Automotive Technology*, Vol. 9, No. 2, 2008, PP. 161-171.
- [25] A. Abu Bakar and H. Ouyang, Wear prediction of friction material and brake squeal using the finite element method, *Wear*, Vol. 246, 2008, 1069-1076.
- [26] A. Meziane , S. D’Errico , L. Baillet and B. Laulagent, Instabilities generated by friction in a pad-disc system during the braking process, *Tribology International*, Vol. 40, 2007, 1127-1136.
- [27] M. Triches Jr, S. N. Y. Gerges and R. Jordan, Reduction of squeal noise from disc brake systems using constrained layer damping, *J. of the Braz. Soc. of Mech. Sci. & Eng*, Vol. I, No. 3, 2004, 340-348.
- [28] G. Oliviero, X. Zhaoshun, and A. Akay, A laboratory brake for the study of automotive brake noise, IMAC-XX: Conference & Exposition on Structural Dynamics, 2002, pp. 548-551.

Biographies



Amr M. Rabia is an assistant lecturer in Automotive and Tractor Eng. Dept., Minia University, Egypt. He received his B.Sc. from Automotive and Tractor Eng. Dept., Minia University, Egypt in 2007. Presently, he is pursuing M.Sc. in Minia University. His areas of interests are finite element methods, noise and vibrations of vehicle.



Nouby M. Ghazaly is an assistant Professor in Automotive and Tractor Eng. Dept., Minia University, Egypt. He obtained his PhD from Anna University, Chennai, India in 2011. He has to his credit more than 22 research papers in the areas of vehicle dynamics, noise and vibrations and finite element methods. He is a Technical Committee Member and a Reviewer of several international journals and conferences. He is currently serving as a consulting engineer of ATALON for testing and consulting engineers, India.



Ali M. Abd-El-Tawwab is an Associate Professor and Head of Automotive and Tractor Eng. Dept., Minia University, Egypt. He has many international and notional journal and conference papers to his credit. he has around 26 years of experience in teaching and research in the areas of Vehicle Ride Comfort, Active Suspension System Design and Control, Noise and Vibration Control, Computer Programming, Vehicle Mathematical Modeling and Vehicle Performance.

Performance Analysis of Multicarrier SPWM Strategies for Three Phase Z - Source Seven Level Cascaded Inverter

V. Arun,¹ B. Shanthi,² S. P. Natarajan³

¹Department of EEE, Arunai Engineering College, Thiruvannamalai, Tamilnadu, India

²Centralised Instrumentation and Service Laboratory, Annamalai University, Chidambaram, Tamilnadu, India

³Department of EIE, Annamalai University, Chidambaram, Tamilnadu, India

ABSTRACT: This paper presents multicarrier PWM strategies for three phase cascaded seven level Z-source inverter. Multilevel inverters possess the advantage of reduced harmonics, high-power capability and high-voltage level. Impedance network in the cascaded multilevel inverter circuit will perform boost operation. This paper focuses on multicarrier sinusoidal pulse width modulation (MCSPWM) strategy for the three phase seven level Z source cascaded inverter. Performance parameters of three phase seven level Z source cascaded inverter have been analyzed. A simulation model of three phase seven level Z source cascaded inverter developed using MATLAB/SIMULINK and its performance has been analyzed.

Keywords: APOD, CO, POD, PD, SPWM.

I. INTRODUCTION

Multilevel inverters have become an attractive choice as a partial solution to the improvement of the global conversion chain efficiency. Multilevel inverter is a switching converter where the appropriate control of an arrangement of switching devices allows combining diverse input voltages to synthesize a sinusoidal output voltage waveform. Carrara et al [1] discussed various multilevel PWM methods and theoretical analysis of PWM strategies. Huang et al [2] proposed Z-source inverter for residential photovoltaic applications. Loh et al [3] have used pulse-width modulated strategies for Z-source neutral point clamped inverter. Various pulse-width modulated strategies for Z source inverter was discussed by Loh et al [4]. Different control strategies for Z-source neutral-point-clamped Inverter and also for cascaded MLI were discussed in [5,6]. Malinowski et al [7] analysed various cascaded multilevel inverters. Three level Z source inverter topology was introduced by Peng in [8]. Rendusara et al [9] analysed common mode voltage and PWM strategies for adjustable speed drive. Shanthi and Natarajan [10] discussed various unipolar PWM strategies for single phase five level cascaded inverter. Zhou et al [11] discussed Z source inverter based single phase uninterruptible power supply.

II. Z-SOURCE SEVEN LEVEL CASCADED INVERTER

Figure 1 shows the two-port network that consists of an inductors (L_1 , L_2) and capacitors (C_1 , C_2) and connected in X shape is employed to provide an impedance source (Z Source) coupling the inverter to the dc source.

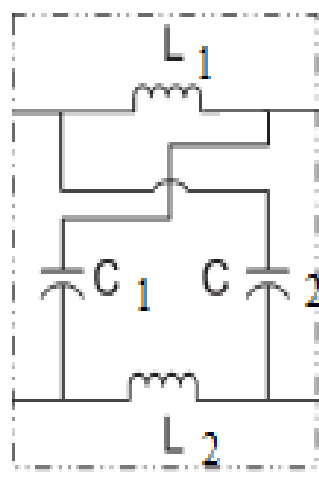


Figure 1 Impedance Network

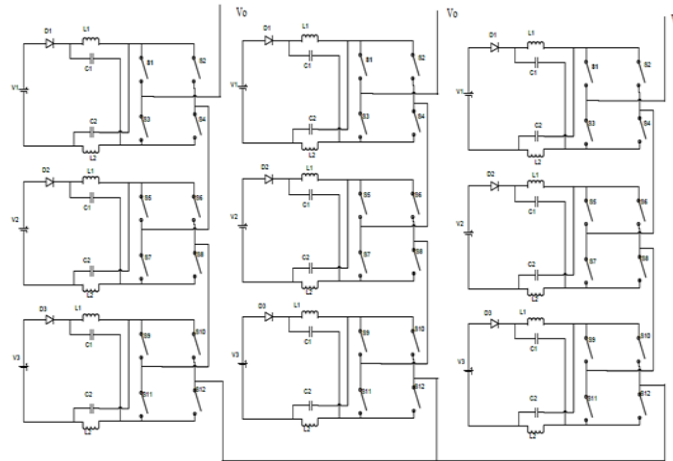


Figure 2 Three phase Seven Level Z source cascaded inverter

Figure 2 shows the seven level Z source cascaded inverter. The inverter topology is based on the series connection of single-phase inverters with separate impedance dc sources. The resulting phase voltage is synthesized by the addition of the voltages generated by the different cells. The number of output voltage levels are $2n+1$, where n is the number of cells. The ac output of each H-bridge is connected in series such that the synthesized output voltage waveform is the sum of all the individual H-bridge outputs.

III. MULTICARRIER PWM STRATEGY

Multicarrier PWM strategy is the widely adopted modulation strategy for MLI. It is similar to that of the sinusoidal PWM strategy except for the fact that several carriers are used. Multicarrier PWM is one in which several triangular carrier signals are compared with one sinusoidal modulating signal. The number of carriers required to produce m -level output is $m-1$. All carriers have the same peak to peak amplitude A_c and same frequency f_c except for VF. The reference waveform has peak to peak amplitude of A_m and a frequency f_m . The reference is continuously compared with each of the carrier signals and whenever the reference is greater than the carrier signal, pulse is generated. There are many carrier arrangements to implement the PWM strategies. In this work the following strategies were carried out.

- Phase disposition PWM strategy.
- Phase opposition disposition PWM strategy.
- Alternate phase opposition disposition PWM strategy.
- Carrier overlapping PWM strategy.
- Variable frequency PWM strategy.

The frequency ratio m_f is as follows: $m_f = f_c / f_m$

III.a. Phase Disposition PWM strategy (PDPWM).

Fig. 3 shows the sinusoidal pulse width modulation of an m -level inverter, $(m-1)$ carriers with the same frequency f_c and same amplitude A_c are positioned such that the bands they occupy are contiguous. If the reference wave is more than a carrier signal, then the active devices corresponding to that carrier are switched on. Otherwise, the devices switch off.

Amplitude of modulation index $m_a = 2A_m / (m-1)A_c$

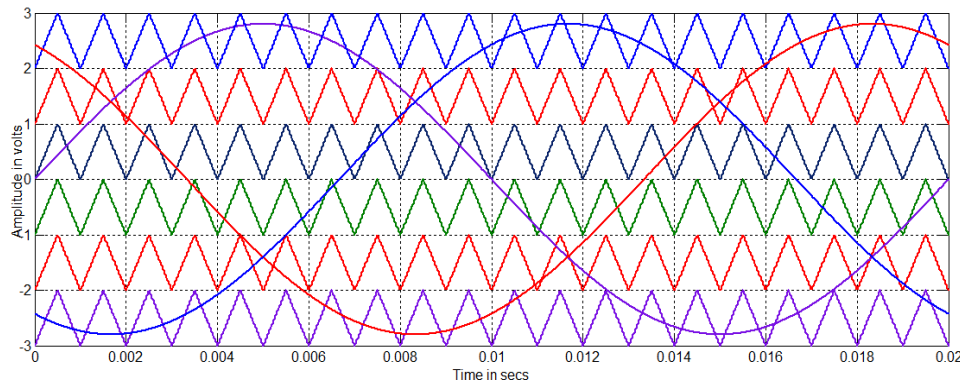


Figure 3 Carrier arrangement for PDPWM strategy ($m_a=0.9$ and $m_f=20$)

III.b. Phase Opposition Disposition PWM strategy (PODPWM).

In POD strategy the carrier waveforms above the zero reference are in phase. The carrier waveforms below are also in phase, but are 180 degrees phase shifted from those above zero as shown in Fig.4.

Amplitude of modulation index $m_a = 2A_m / (m-1)A_c$

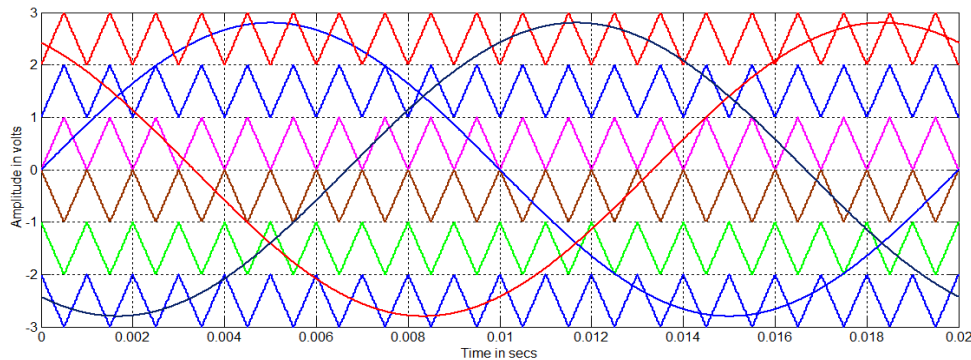


Figure 4 Carrier arrangement for PODPWM strategy ($m_a=0.9$ and $m_f=20$)

III.c. Alternate Phase Opposition Disposition PWM strategy (APODWM)

In APOD strategy the carriers of same amplitude are phase displaced from each other by 180 degrees alternately. The carrier arrangement is shown in Fig.5.

Amplitude of modulation index $m_a = 2A_m / (m-1)A_c$

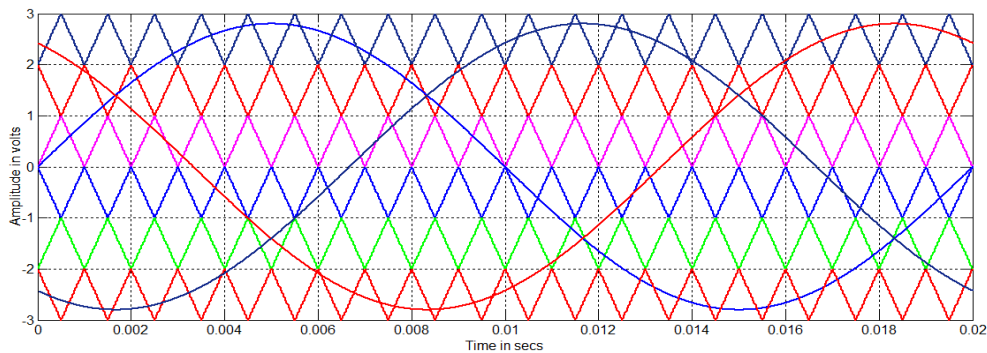


Figure 5 Carrier arrangement for APOD PWM strategy ($m_a=0.9$ and $m_f=20$)

III.d. Carrier Overlapping PWM strategy (COPWM).

In COPWM strategy, carriers with the same frequency f_c and same peak-to-peak amplitude A_c are disposed such that the bands they occupy are overlap each other; the overlapping vertical distance between each carrier is $A_c/2$. The reference waveform is centered in the middle of the carrier set as in Fig.6.

The amplitude modulation index m_a for carrier overlapping method as follows:

$$m_a = A_m / 2A_c$$

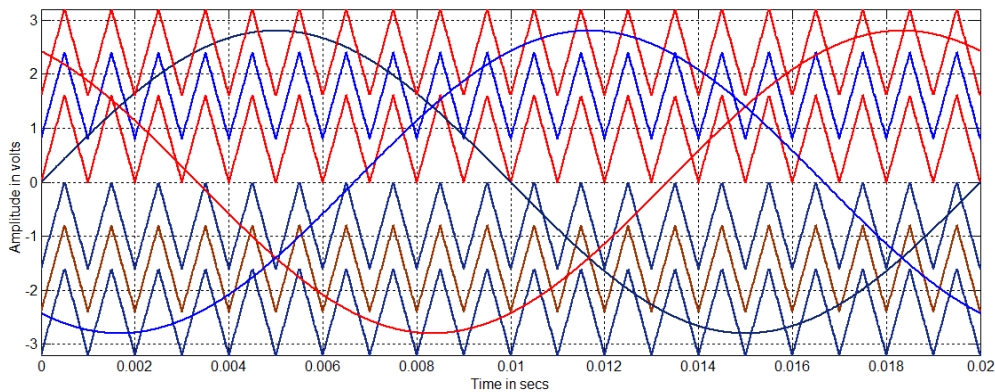


Figure 6 Carrier arrangement for COPWM strategy ($m_a=0.9$ and $m_f=20$)

III.e. Variable frequency PWM strategy (VFPWM)

The number of switching for upper and lower devices of chosen MLI is much more than that of intermediate switches in other PWM using constant frequency carriers. In order to equalize the number of switching for all the switches, variable frequency PWM strategy is used.

$$\text{Modulation index } m_a = 2A_m / (m-1)A_c$$

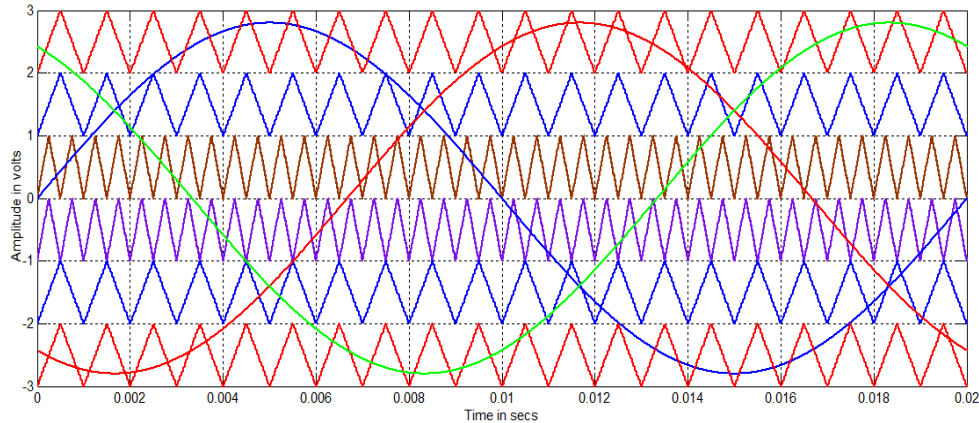


Figure 7 Carrier arrangement for VFPWM strategy ($m_a=0.9$ and $m_{f1}=20, m_{f2}=40$)

IV. SIMULATION RESULTS

The Z-source cascaded seven level inverter is modeled in SIMULINK using power system block set. Switching signals for cascaded multilevel inverter using MCSPWM strategies are simulated. Simulations are performed for different values of m_a ranging from 0.8 to 1 and the corresponding %THD are measured using the FFT block and their values are listed in Table I. Figure 8-17 show the simulated output voltage of Z source CMLI and their harmonic spectra. Figure 8 displays the seven level output voltage generated by PDPWM switching strategy and its FFT plot is shown in Figure 9. Figure 10 shows the seven level output voltage generated by PODPWM strategy and its FFT plot is shown in Figure 11. Figure 12 shows the seven level output voltage generated by APODPWM strategy and its FFT plot is shown in Figure 13. Figure 14 shows the seven level output voltage generated by COPWM strategy and its FFT plot is shown in Figure 15. Figure 16 shows the seven level output voltage generated by VFPWM strategy and its FFT plot is shown in Figure 17. Tables II and III displayed the V_{RMS} (fundamental) of the output voltage and Crest Factor (CF) for various modulation indices of Z-Source seven level cascaded inverter respectively.

The following parameter values are used for simulation: $V_1=50V$, $V_2=50V$, $V_3=50V$, R (load) = 100 ohms, $f_c=1000$ Hz and $f_m=50$ Hz.

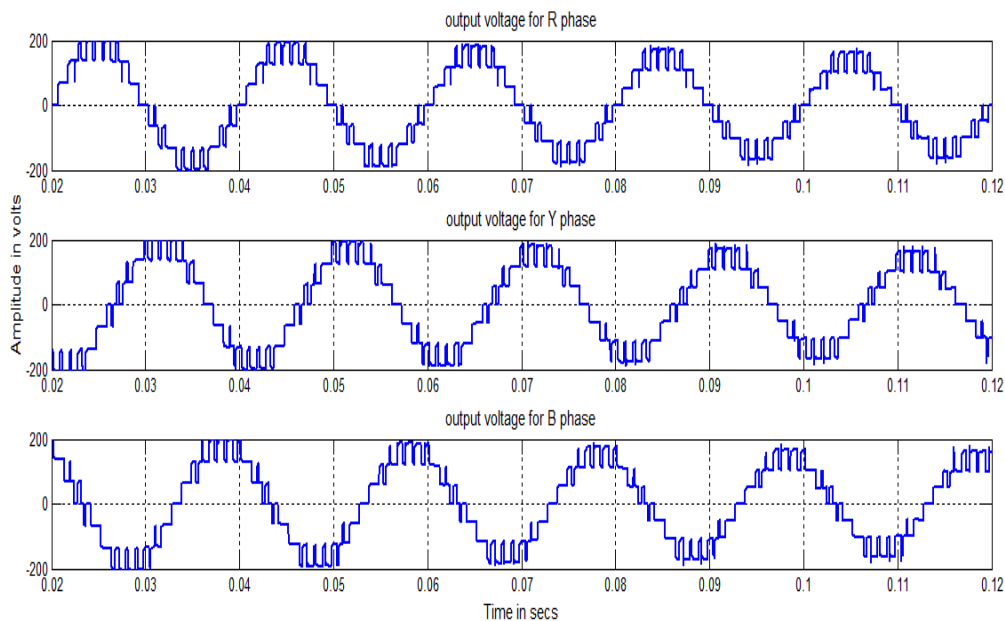


Figure 8 Output voltage generated by PDPWM

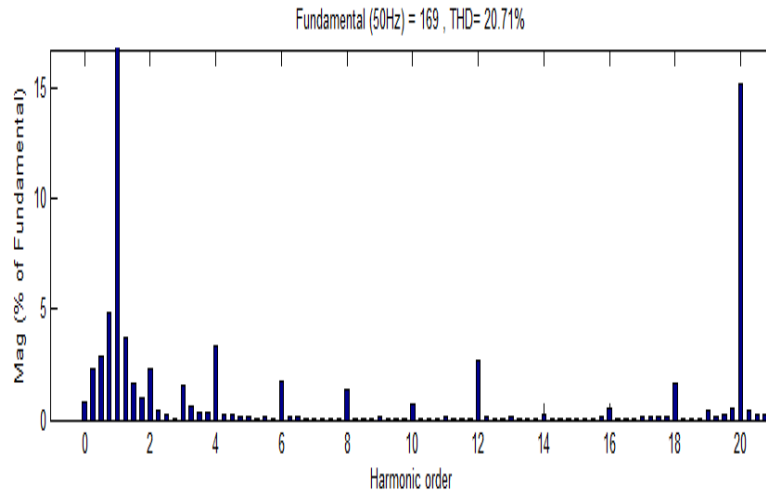


Figure 9 FFT plot for output voltage of PDPWM

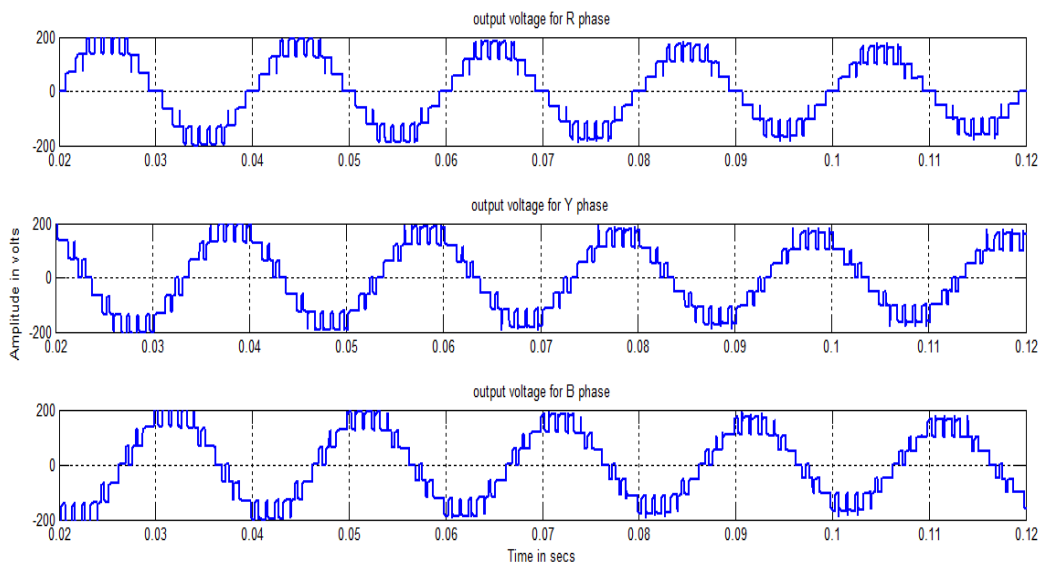


Figure 10 Output voltage generated by PODPWM

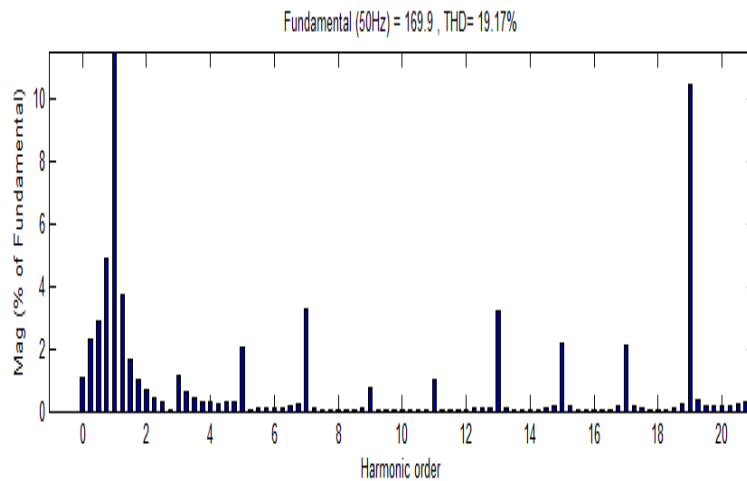


Figure 11 FFT plot for output voltage of PODPWM

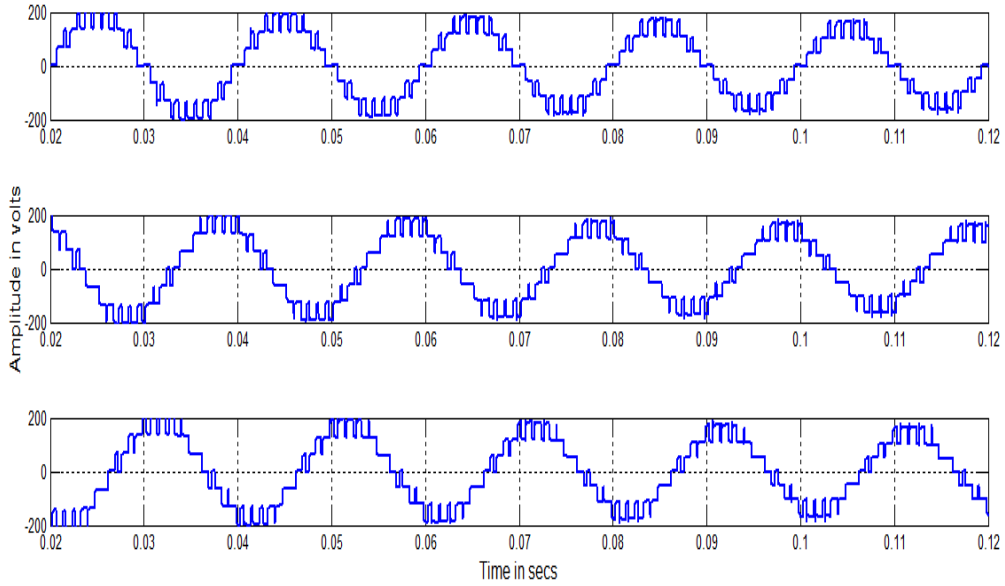


Figure 12 Output voltage generated by APODPWM

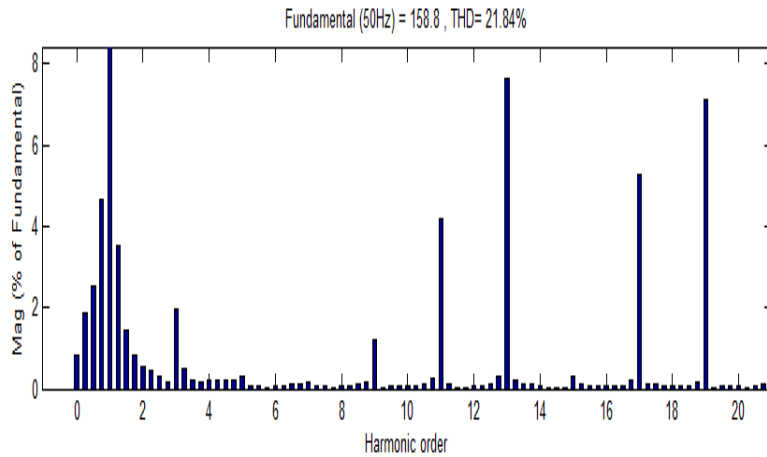


Figure 13 FFT plot for output voltage of APODPWM

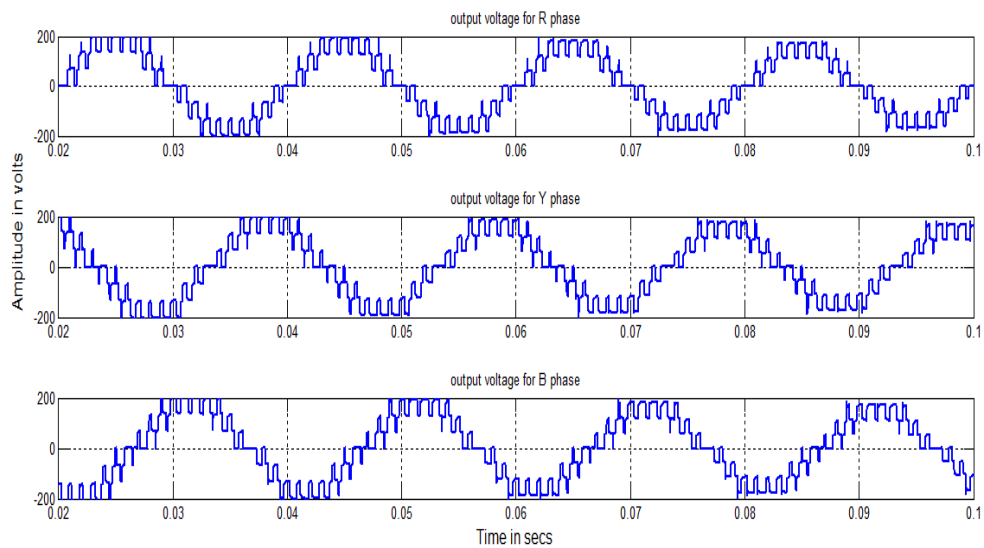


Figure 14 Output voltage generated by CODPWM

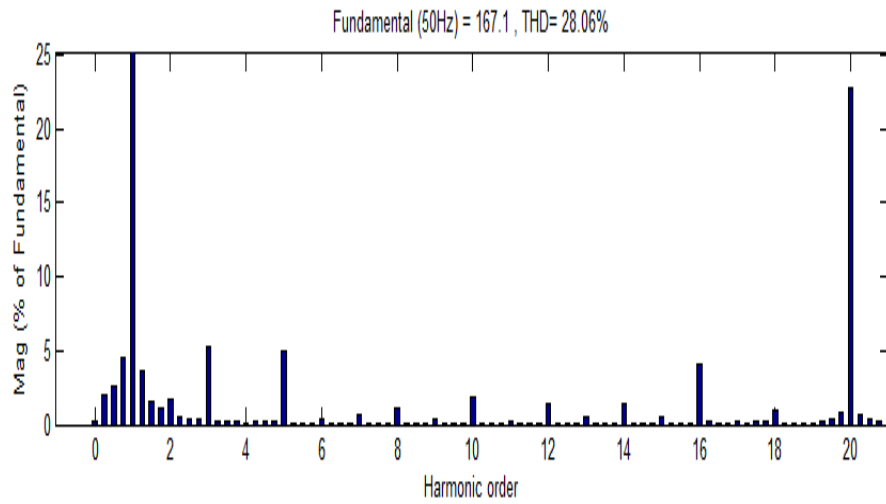


Figure 15 FFT plot for output voltage of COPWM

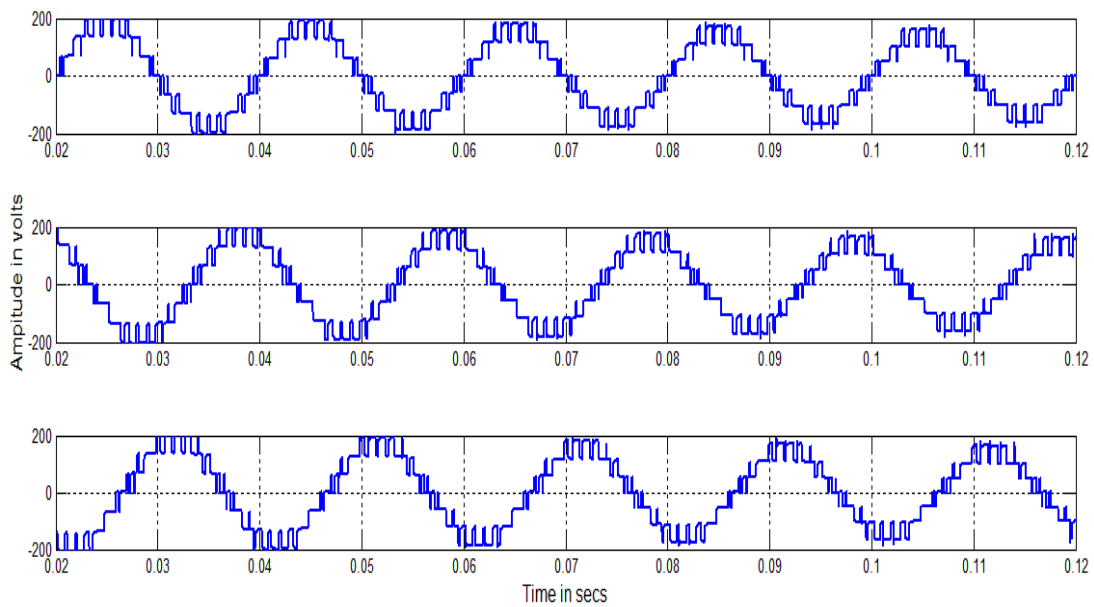


Figure 16 Output voltage generated by VFPWM

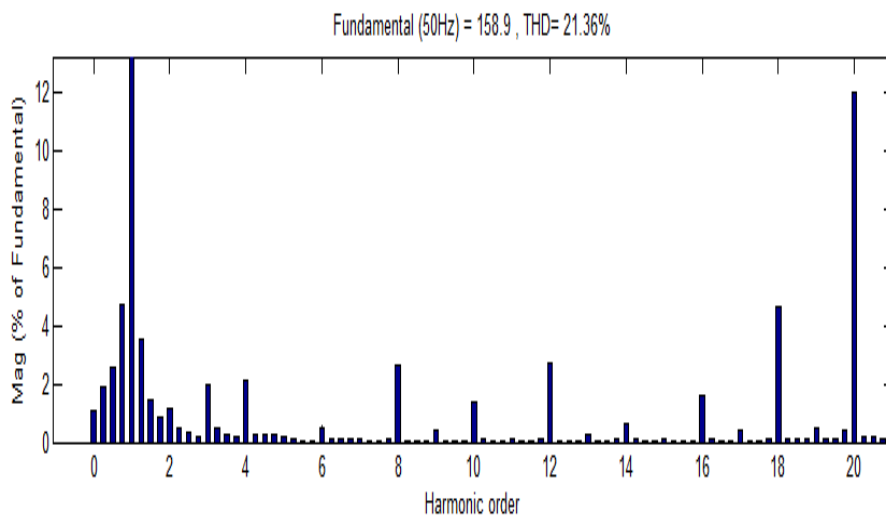


Figure 17 FFT plot for output voltage of VFPWM

TABLE I.
 % THD For Different Modulation Indices

m_a	PD	POD	APOD	CO	VF
1	17.34	15.70	18.22	25.38	17.94
0.8	20.71	19.17	21.84	28.06	21.36
0.9	23.11	22.01	22.87	32.04	23.78

TABLE II.
 V_{RMS} (Fundamental) For Different Modulation Indices

m_a	PD	POD	APOD	CO	VF
1	126.2	126.3	118.3	123.8	118.2
0.8	119.5	120.1	112.3	118.1	112.4
0.9	112.5	112.5	105.9	110.8	106

TABLE III.
 Crest Factor for Different Modulation Indices

m_a	PD	POD	APOD	CO	VF
1	1.4136	1.4140	1.4150	1.4135	1.4145
0.8	1.4142	1.4146	1.4140	1.4149	1.4137
0.9	1.4142	1.4133	1.4145	1.4142	1.4141

V. CONCLUSION

In this paper, MCSPWM strategy for three phase Z source seven level cascaded inverter have been presented. Z source multilevel inverter gives higher output voltage through its Z source network. Performance factors like %THD, V_{RMS} and CF have been measured, presented and analyzed. It is found that the PODPWM strategy provides lower %THD and higher V_{RMS} and less number of dominant harmonics than the other strategies. DC source can be replaced by renewable energy sources and this Z source seven level cascaded inverter can be used for distributed generation systems.

REFERENCES

- [1] G.Carrara, S.Gardella, M. Marchesoni, R. Salutati, and G. Sciuotto, "A new multilevel PWM method: A theoretical analysis," IEEE Trans.Power Electron., vol. 7, no. 4, pp. 497–505, Jul. 1992.
- [2] Y. Huang, M. Shen, and F. Z. Peng, "A Z-source inverter for residential photovoltaic systems," IEEE Trans.Power Electron., vol. 21, no. 6, pp. 1776–1782, Nov. 2006.
- [3] P. C. Loh, S. Y. Feng, F. Blaabjerg, and K. N. Soon, "Pulse-width modulated Z-source neutral-point-clamped inverter," IEEE Trans. Ind. Appl., vol. 43, no. 5, pp. 1054–1061, Sep./Oct. 2007.
- [4] P. C. Loh, F. Blaabjerg, S. Y. Feng, and K. N. Soon, "Pulse-width modulated Z-source neutral-point-clamped inverter," in Proc. IEEE APEC'06, 2006, pp. 431–437.
- [5] P. C. Loh, F. Blaabjerg, and C. P. Wong, "Comparative evaluation of pulse-width modulation strategies for Z-source neutral-point-clamped inverter," in Proc. IEEE PESC'06, 2006, pp. 1316–1322.
- [6] P. C. Loh, D. G. Holmes, Y. Fukuta, and T. A. Lipo, "Reduced common mode modulation strategies for cascaded multilevel inverters," IEEE Trans. Ind. Appl., vol. 39, no. 5, pp. 1386–1395, Sep./Oct. 2003.
- [7] M. Malinowski, K. Gopakumar, J. Rodriguez, and M. A. Pérez, "A Survey on Cascaded Multilevel Inverters," IEEE Transactions on Industrial Electronics, vol. 57, no. 7, pp. 2197–2206, 2010.
- [8] F. Z. Peng, "Z-source inverter," IEEE Trans. Ind. Appl., vol. 39, no. 2, pp. 504–510, Mar./Apr. 2003.
- [9] D. A. Rendusara, E. Cengelci, P. N. Enjeti, V. R. Stefanovic, and J. W. Gray, "Analysis of common mode voltage – 'neutral shift' in medium voltage PWM adjustable speed drive (MV-ASD) systems," IEEE Trans. Power Electron, vol. 15, no. 6, pp. 1124–1133, Nov. 2000.
- [10] B. Shanthi and S.P. Natarajan, "Comparative study on various unipolar PWM strategies for single phase five level cascaded inverter," International Journal of Power Electronics (IJEPELEC), Special issue on: Power Converters: Modelling, Simulation, Analysis, Topologies, Secondary issues and Applications, Inder Science Publication, Switzerland, pp.36-50, 2009.
- [11] Z. J. Zhou, X. Zhang, P. Xu, and W. X. Shen, "Single-phase uninterruptible power supply based on Z-source inverter," IEEE Trans. Ind. Electron., vol. 55, no. 8, pp. 2997–3004, Aug. 2008.

Implementing Re-Active Power Compensation Technique in Long Transmission System (750 Km) By Using Shunt Facts Control Device with Mat Lab Simlink Tool

Dabberu.Venkateswara Rao,¹ Bodi.Srikanth²

1, 2(Department of Electrical & Electronics Engineering, KL University, India

ABSTRACT: This paper attempts to implementation and simulation of the Fuzzy logic control of firing angle for SVC in order to achieve better, smooth and adaptive control of reactive power by using facts technology, Flexible AC transmission system (FACTS) is a technology, The FACTS technology is a promising technology to achieve complete deregulation of Power System i.e. Generation, Transmission and Distribution as complete individual units, which is based on power electronic devices, used to enhance the existing transmission capabilities in order to make the transmission system flexible and independent operation. The loading capability of transmission system can also be enhanced nearer to the thermal limits without affecting the stability. Complete close-loop smooth control of reactive power can be achieved using shunt connected FACTS devices. Static VAR Compensator (SVC) is one of the shunt connected FACTS device, which can be utilized for the purpose of reactive power compensation. Intelligent FACTS devices make them adaptable and hence it is emerging in the present state of art..Implementing re-active power compensation technique is carried out for long Transmission line and the compensation is placed at the receiving end (load end).

Keyword: FACTS, Tcr, and Tsr, Fuzzy Logic

I. INTRODUCTION

He reactive power generation and absorption in power T system is essential since the reactive power is very precious in keeping the voltage of power system stable. The main elements for generation and absorption of reactive power are transmission line, transformers and alternators. The transmission line distributed parameters throughout the line, on light loads or at no loads become predominant and consequently the line supplies charging VAR (generates reactive power). In order to maintain the terminal voltage at the load bus adequate, reactive reserves are needed. FACTS devices like SVC can supply or absorb the reactive power at receiving end bus or at load end bus in transmission system, which helps in achieving better economy in power transfer.

In this paper long Transmission line is simulated using 4π line segments by keeping the sending end voltage constant. The receiving end voltage fluctuations were observed for different loads. In order to maintain the receiving end voltage constant, shunt inductor and capacitor is added for different loading conditions. SVC is simulated by means of fixed capacitor and thyristor controlled reactor (FC-TCR) which is placed at the receiving end. The firing angle control circuit is designed and the firing angles are varied for various loading Conditions to make the receiving end voltage equal to sending end voltage. Fuzzy logic

controller is designed to achieve the firing angles for SVC such that it maintains a flat voltage profile. All the results thus obtained, were verified and were utilized in framing of fuzzy rule base in order to achieve better reactive power compensation for the long Transmission line. Based on observed results for load voltage variations for different values of load resistance, inductance and capacitance a fuzzy controller is designed which controls the firing angle of SVC in order to automatically maintain the receiving end voltage constant.

II. OPERATING PRINCIPLES And implementing Of Static var compensator

An elementary single phase thyristor controlled reactor [1] (TCR) shown in Fig.1 consists of a fixed (usually air core) reactor of inductance L and a two anti parallel SCRs. The device brought into conduction by simultaneous application of gate pulses to SCRs of the same polarity. In addition, it will automatically block immediately after the ac current crosses zero, unless the gate signal is reapplied. The current in the reactor can be controlled from maximum (SCR closed) to zero (SCR open) by the method of firing delay angle control. That is, the SCR conduction delayed with respect to the peak of the applied voltage in each half-cycle, and thus the duration of the current conduction interval is controlled.

This method of current control is illustrated separately for the positive and negative current cycles in Fig.2 where the applied voltage V and the reactor current $i_L(\alpha)$ at zero delay angle (switch fully closed) and at an arbitrary α delay angle are shown. When $\alpha = 0$, the SCR closes at the crest of the applied voltage and evidently the resulting current in the reactor will be the same as that obtained in steady state with a permanently closed switch.

III. Indentations and Equations

When the gating of the SCR is delayed by an angle α ($0 \leq \alpha \leq \pi/2$) with respect to the crest of the voltage, the current in the reactor can be expressed [1] as follows

$$V(t) = V \cos \omega t \quad (1)$$

$$i_L = (1/L) \int_{\alpha}^{\omega t} V(t) dt = (V/\omega L) (\sin \omega t - \sin \alpha) \quad (2)$$

Since the SCR, by definition, opens as the current reaches zero, is valid for the interval $\alpha \leq \omega t \leq \pi - \alpha$. For subsequent negative half-cycle intervals, the sign of the terms in equation (1) becomes opposite.

In the above equation (1) the term $(V/\omega L) \sin \alpha = 0$ is offset which is shifted down for positive and up for negative current half-cycles obtained at $\alpha = 0$, as illustrated in Fig.2. Since the SCRs automatically turns off at the

instant of current zero crossing of SCR this process actually controls the conduction intervals (or angle) of the SCR. That is, the delay angle α defines the prevailing conduction angle σ ($\sigma = \pi - 2\alpha$). Thus, as the delay angle α increases, the corresponding increasing offset results in the reduction of the conduction angle σ of the SCR, and the consequent reduction of the reactor current. At the maximum delay of $\alpha = \pi / 2$, the offset also reaches its maximum of $V/\omega L$, at which both the conduction angle and the reactor current becomes zero. The two parameters, delay angle α and conduction angle σ are equivalent and therefore TCR can be characterized by either of them; their use is simply a matter of preference. For this reason, expression related to the TCR can be found in the literature both in terms of α and σ [1].

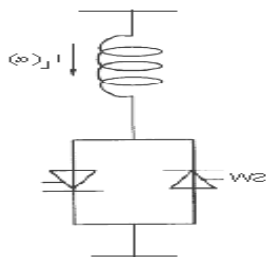


Fig. 1. Basic Thyristor Controlled Reactor

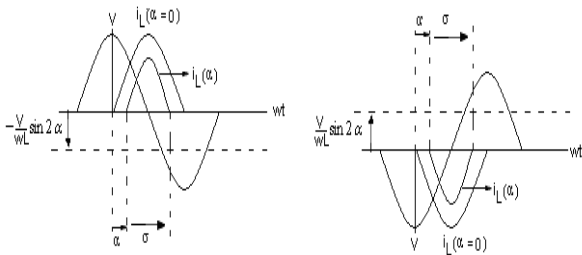


Fig.2. firing delay angle

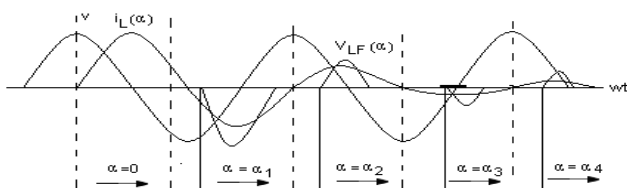


Fig. 3. Operating waveforms

It is evident that the magnitude of the current in the reactor varied continuously by delay angle control from maximum ($\alpha=0$) to zero ($\alpha=\pi/2$) shown in Fig.3, where the reactor current $i_L(\alpha)$ together with its fundamental component $i_{LF}(\alpha)$ are shown at various delay angles α [1]. However the adjustment of the current in reactor can take place only once in each-half cycle, in the zero to $\pi/2$ interval [1]. This restriction result in a delay of the attainable current control. The worst-case delay, when changing the current from maximum to zero (or vice versa), is a half-cycle of the applied ac voltage. The amplitude $I_{LF}(\alpha)$ of the fundamental reactor current $i_{LF}(\alpha)$ can be expressed as a function of angle α [1].

$$I_{LF}(\alpha) = V/\omega L (1 - (2/\pi)\alpha - (1/\pi)\sin(2\alpha)) \quad (3)$$

Where V is the amplitude of the applied voltage, L is the inductance of the thyristor-controlled reactor and ω is the angular frequency of the applied voltage. The variation of the amplitude $I_{LF}(\alpha)$, normalized to the maximum current I_{LFmax} , ($I_{LFmax} = V/\omega L$), is shown plotted against delay angle α shown in Fig.4.

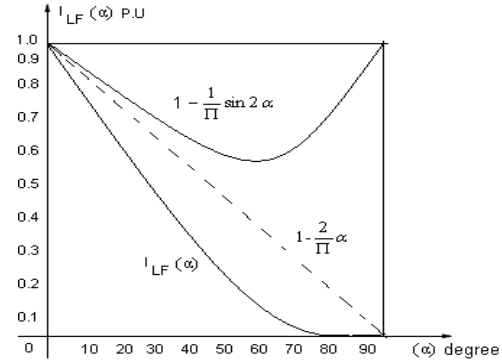


Fig.4. Amplitude variation of the fundamental TCR current with the delay angle (α)

It is clear from Fig.4 the TCR can control the fundamental current continuously from zero (SCR open) to a maximum (SCR closed) as if it was a variable reactive admittance. Thus, an effective reactance admittance, $B_L(\alpha)$, for the TCR can be defined. This admittance, as a function of angle α is obtained as:

$$B_L(\alpha) = 1/\omega L (1 - (2/\pi)\alpha - (1/\pi)\sin(2\alpha)) \quad (4)$$

Evidently, the admittance $B_L(\alpha)$ varies with α in the same manner as the fundamental current $I_{LF}(\alpha)$. The meaning of equation (4) is that at each delay angle α an effective admittance $B_L(\alpha)$ can be defined which determines the magnitude of the fundamental current, $I_{LF}(\alpha)$, in the TCR at a given applied voltage V . In practice, the maximal magnitude of the applied voltage and that of the corresponding current limited by the ratings of the power components (reactor and SCRs) used. Thus, a practical TCR can be operated anywhere in a defined V-I area, the boundaries of which are determined by its maximum attainable admittance, voltage and current ratings as illustrated in the Fig.5a. The TCR limits are established by design from actual operating requirements. If the TCR switching is restricted to a fixed delay angle, usually $\alpha = 0$, then it becomes a thyristor switched reactor (TSR). The TSR provide a fixed inductive admittance and thus, when connected to the ac system, the reactive current in it will be proportion to the applied voltage as the V - I plot in the Fig.5b.

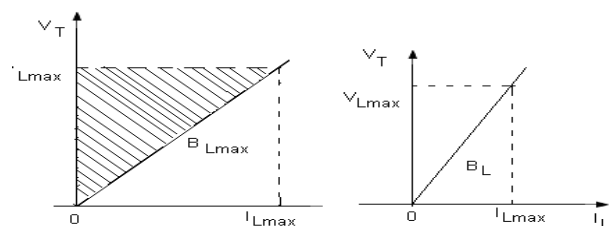


Fig.5. Operating V-I area of (a) For TCR and (b) For TSR

V_{Lmax} = voltage limit, I_{Lmax} = current limit

B_{Lmax} = max admittance of TCR,
 B_L = admittance of reactor

A basic VAR generator arrangement using a fixed capacitor with a thyristor-controlled reactor (FC-TCR) shown in Fig.6 [1].The current in the reactor is varied by the previously discussed method of firing delay angle control. A filter network that has the necessary capacitive impedance at the fundamental frequency to generate the reactive power required usually substitutes the fixed capacitor in practice, fully or partially, but it provides low impedance at selected frequencies to shunt the dominant harmonics produced by the TCR.

The fixed capacitor thyristor-controlled reactor type VAR generator may be considered essentially to consist of a variable reactor (controlled by a delay angle α) and a fixed capacitor. With an overall VAR demand versus VAR output characteristic as shown in Fig.7 in constant capacitive VAR generator (Q_c) of the fixed capacitor is opposed by the variable VAR absorption (Q_L) of the thyristor controlled reactor, to yield the total VAR output (Q) required. At the maximum capacitive VAR output, the thyristor-controlled reactor is off ($\alpha=90^\circ$). To decrease the capacitive output, decreasing delay angle α . At zero VAR output increases the current in the reactor, the capacitive and inductive current becomes equal and thus the capacitive and inductive VARs cancel out. With a further decrease of angle α , the inductive current becomes larger than the capacitive current, resulting in a net inductive VAR output. At zero delay angle, the thyristor-controlled reactor conducts current over the full 180° interval, resulting in maximum inductive VAR output that is equal to the difference between the VARs generated by the capacitor and those absorbed by the fully conducting reactor.

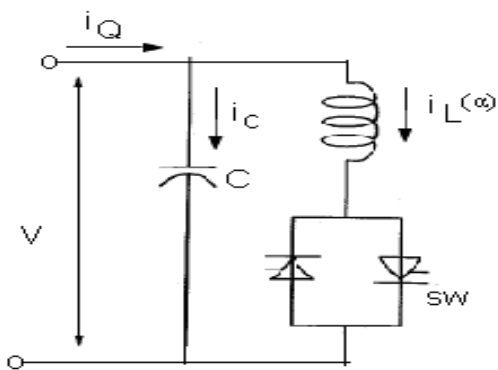


Fig.6. basic FC-TCR type static generator

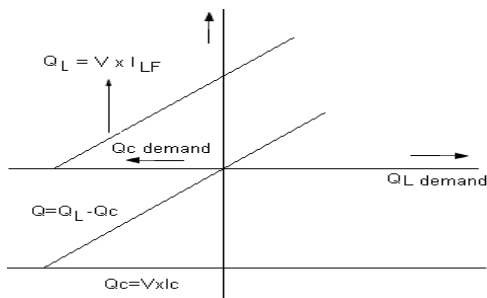


Fig.7. VAR demand versus VAR output characteristic

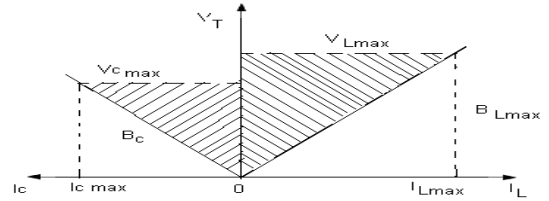


Fig.8. V-I characteristics of the FC-TCR type VAR Generator

In Fig.8 the voltage defines the V-I operating area of the FC-TCR VAR generator and current rating of the major power components. In the dynamic V-I Characteristics of SVC along with the Load lines showed in the Fig.9 the load characteristics assumed straight lines for Dynamic studies as easily seen that the voltage improved with compensation when compared without compensation.

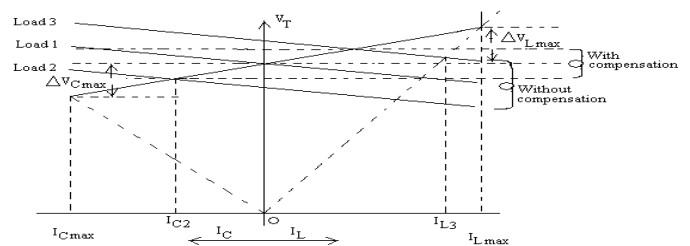


Fig.9. Dynamic V-I Characteristics of SVC with Load lines

- V_{Cmax} = voltage limit of capacitor
- B_C = admittance of capacitor
- V_{Lmax} = voltage limit of TCR
- I_{Cmax} = capacitive current limit
- I_{Lmax} = inductive current limit
- B_{Lmax} = max inductive admittance

IV. FIGURES and Tables

IV.1 SVC WITH OUT FUZZY

This below implementation block diagram gives clear explanation of svc without fuzzy logic, this experiment result is use to refer reactive power compensation technique, after that same test is conducted with fuzzy and take the readings of table III respectively.

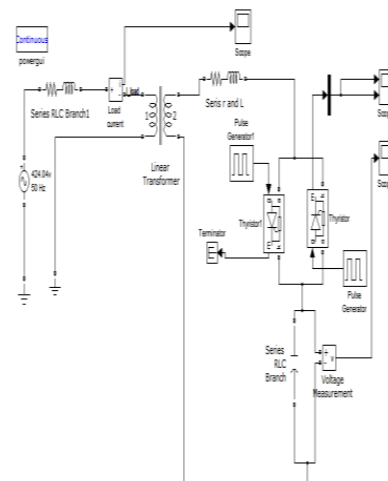


Fig.10. svc for 750 kv transmission line without fuzzy

IV.2 FUZZY LOGIC CONTROLLER

Fuzzy logic is a new control approach with great potential for real time applications [2] [3]. Fig.10 shows the structure of the fuzzy logic controller (FIS-Fuzzy inference system) in MATLAB Fuzzy logic toolbox. [5][6]. Load voltage and load current taken as input to fuzzy system. For a closed loop control, error input can be selected as current, voltage or impedance, according to control type. To get the linearity triangular membership function is taken with 50% overlap. The output of fuzzy controller taken as the control signal and the pulse generator provides synchronous firing pulses to thyristors as shown in fig.12. The Fuzzy Logic is a rule based controller, where a set of rules represents a control decision mechanism to correct the effect of certain causes coming from power system. In fuzzy logic, the five linguistic variables expressed by fuzzy sets defined on their respective universes of discourse. Table-I shows the suggested membership function rules of FC-TCR controller. The rule of this table can be chosen based on practical experience and simulation results observed from the behavior of the system around its stable equilibrium points.

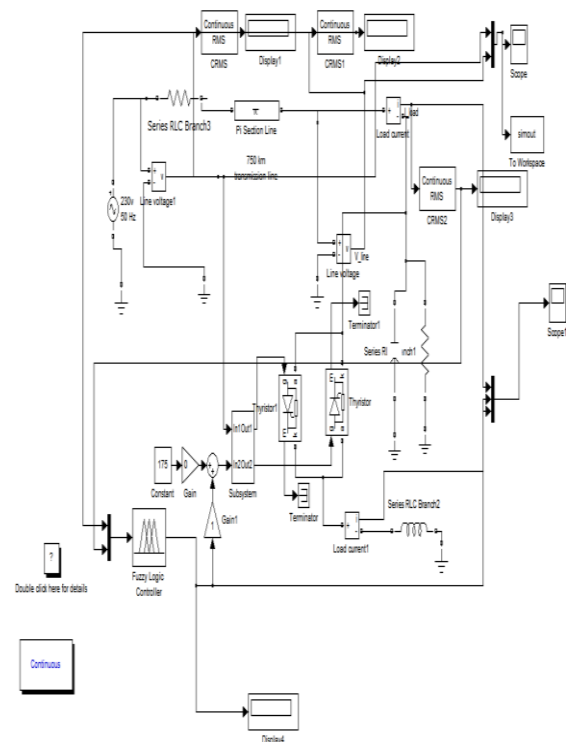


Fig.11. Structure of fuzzy logic controller

Table I. Membership function rules

		Load voltage				
		NL	NM	P	PM	PB
Load current	NL	PB	PB	NM	NM	NL
	NM	PB	PB	NM	P	NL
	P	P	PM	NM	NM	P
	PM	NM	P	NM	NM	PM
	PB	NL	NM	NM	NL	NL

IV. 3 LONG TRANSMISSION LINE

An available simple two-bus artificial transmission (750 km) line model of 4 π line segments with 750 km,

distributed parameters were used in this study. The line inductance 0.1mH /km, capacitance 0.01 μ f/km and the line resistance 0.001 Ω were used. Each π section is of 187km, 187km, 188km and 188 km. Supply voltage is 230V - 50 Hz having source internal resistance of 1 Ω connected to node A. Static load is connected at receiving end B .The load resistance was varied to obtain the voltage variations at the receiving end. A shunt branch consisting of inductor and capacitor is added to compensate the reactive power of transmission line. With the change of load and due to Ferranti effect, the variations in voltages are observed at receiving end B of transmission line. The practical values of shunt elements are varied for different loading conditions to get both sending and receiving end voltages equal. As shown in Table II.

Table II compensated practical values Of inductor and capacitor

S.N O	Load Resistance Ω	Compensating Inductance	Compensating Capacitance (μ f)
1.	500	0.8 H	1
2.	400	0.9H	1
3.	300	0.19H	2
4.	200	0.18 H	5
5.	150	0.19H	5
6.	100	0.22H	8
7.	50	0.14	8.5
8.	40	0.14	9.0
9.	30	0.14	10
10.	20	0.14	12

A. FIRING CIRCUIT DESIGN

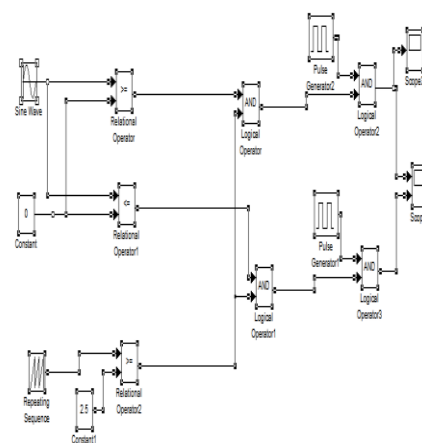


Fig 12 firing pulse generating circuit

Table III TEST RESULT

Load voltage before and after compensation The transmission line without any compensation was not satisfying the essential condition of maintaining the voltage within the reasonable limits. The effect of increasing load was to reduce the voltage level at the load end. At light

loads, the load voltage is greater than the sending end voltage as the reactive power generated is greater than absorbed. At higher loads the load voltage drops, as the reactive power absorbed is greater than generated, as shown in Table III. Fig.13 and Fig.14 indicates unequal voltage profiles. Fig.16 clearly shows the firing angle and inductor current control.

Tr Line Parameters for Lt=10mh/km Ct=0.1µf/km R.=0.001Ω		Before compensation For Vs= 230V (p-p)		After Compensation For L=0.19H C=8µ f For Vs= 230 (P-P)		
R Ω	Vs (rms) Volts	VR (rms) Volts	IR rms Amp	VR (rms) Volts	IR (rms) Amp	α.
500	162.6	270.80	0.54	162.1	2.032	90
400	162.6	268.10	0.67	162.4	2.036	100
300	162.6	268.00	0.89	162.	2.099	102
200	162.6	261.10	1.30	162.7	2.182	103
180	162.6	258.10	1.43	162.4	2.198	105
160	162.6	256.10	1.59	162.3	2.232	106
140	162.6	250.30	1.78	162.8	2.299	108
120	162.6	243.80	2.03	161.8	2.357	109
100	162.6	234.20	2.34	162.4	2.459	112
80	162.6	219.50	2.74	163.3	2.651	117
60	162.6	195.80	3.26	162.3	3.071	128

Simulation Results

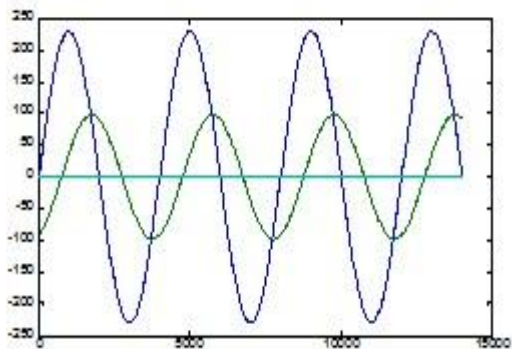


Fig.13. Uncompensated voltage for heavy load

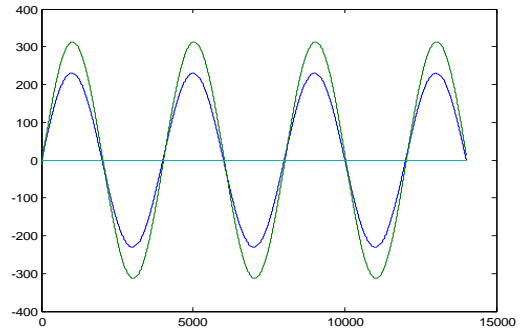


Fig.14. Uncompensated voltage for light load

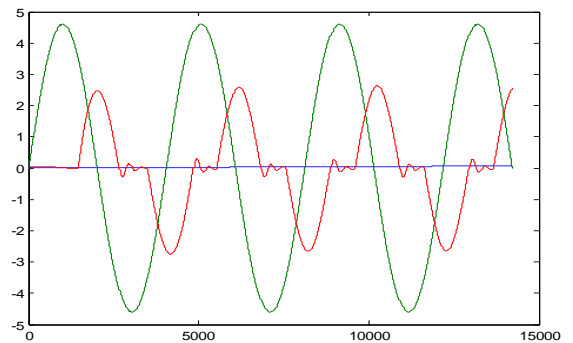


Fig.15. Inductor Current for firing angle 165 deg

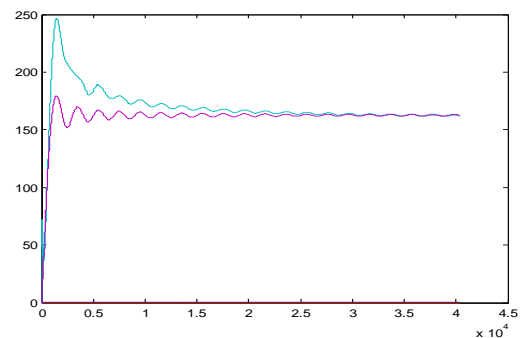


Fig.16. Compensated $V_R = V_S$ (RMS voltage) for $R=200\Omega$

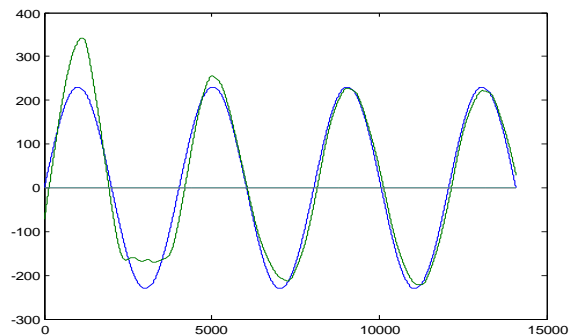


Fig17. Compensated $V_R = V_S$ (instantaneous voltage) For $R=200\Omega$

V. CONCLUSION

This paper presents an “online Fuzzy control scheme for SVC” and it can be concluded that the use of fuzzy controlled SVC (FC-TCR) compensating device with the firing angle control is continuous, effective and it is a

simplest way of controlling the reactive power of transmission line. It is observed that SVC device was able to compensate both over and under voltages. Compensating voltages are shown in Fig.17 and Fig.18. The use of fuzzy logic has facilitated the closed loop control of system, by designing a set of rules, which decides the firing angle given to SVC to attain the required voltage. With MATLAB simulations and actual testing it is observed that SVC (FC-TCR) provides an effective reactive power control irrespective of load variations.

ACKNOWLEDGEMENTS

use of fuzzy controlled SVC (FC-TCR) compensating device with the firing angle control is continuous, effective and it is a simplest way of controlling the reactive power of transmission line.

REFERENCES

Journal Papers:

- [1] S.M.Sadeghzadeh M. Ehsan Improvement of Transient Stability Limit in Power System Transmission Lines Using Fuzzy Control of FACTS Devices ,IEEE Transactions on Power System Vol.13 No.3 ,August 1998Books:
- [2] Understanding FACTS Concepts and Technology Of flexible AC Transmission Systems by (Narain. G. Hingorani IEEE Press USA 1980).

Chapters in Books:

- [3] Timothy J Ross, Fuzzy Logic with Engineering Applications (McGraw-Hill, Inc, New York, 1997).

Theses:

- [4] Bart Kosko, Neural Networks and Fuzzy Systems A Dynamical Systems Approach to Machine Intelligence Prentice-Hall of India New Delhi, June 1994.

Proceedings Papers:

- [5] Chuen Chien Lee "Fuzzy Logic in Control Systems: Fuzzy Logic Controller". Part I and Part II. IEEE R. IEEE transactions on system, man, and cybernetics, vol.20 March/April1990 Electrical Engineering Dept Pontifica Universidad Catolica De CHILE

AUTHORS BIOGRAPHY



Dabiru.Venkateswara Rao, his education qualification is B.Tech(EEE),M.Tech (Power Systems and Power Electronics), His worked in the area of power transmission and distribution systems.Present He is working as an Senior Electrical Engineer in ABB Power Industry at Rourkala,orisa,India.His area of interests are modern fuzzy logic control of power systems



Bodi Srikanth has worked in the area of power systems with modern FACTS controllers. He is working as an Assistant Professor in the Department of Electrical and Electronics Engineering, andhrapradesh, India. His areas of interests are fuzzy logic Applications in Modern Power Electronics application systems

Healthcare Information System – A Web Based Spatial and Aspatial Helpdesk

Shoba P

M Tech Geo-Informatics, University of Madras, India

ABSTRACT: Healthcare related Information is a most expected area focused by the people, Organization and government. This is the system or a Website established and considered as an information system provided by the particular hospital to the user, hence it's also termed as Hospital Information System. Information sharing with respect to spatial and Non-spatial forms through web will enable the user to have complete health related information such as Routing facility within the hospital where no labels and numbers are placed properly, Shortest routing Algorithm form blood banks to hospitals, E-doctor service (where user can clear the doubts, ask queries and prescription through web), Important medical terms, First Aid help desk, National health schemes, Ambulance services available etc. Open GIS is a best tool for accompanying the spatial routing task. System has followed 2 Tier Architecture in the development of E-doctor service where the consistent database will be maintained by the hospital server to update the queries instantly by the user. Spatial Routing will facilitate the user to find out the path from the entrance where they are standing to the appropriate building.

Keywords: Web mapping, Spatial Routing, E-Doctor, First aid help desk, Blog service, PostgreSQL

I. INTRODUCTION

Healthcare information System is an emerging need of common people which has to be concentrated by the Government since the requirement rate of the people getting peak level now a days. The System is the one which accepts any form of input from the user, process it, and can provide desired output after processing the input. This project named as Health care Information System dealt with Spatial and Aspatial (which is also known as Non-spatial Information) information of Health related scenario. Spatial Information provides routing facility (Dynamic Web maps) where as Aspatial Information facilitates E-doctor, Blood banks details, National schemes announced by the government, emergency contacts, first aid helpdesk functions etc. There are more than ten Open Source technologies were used in structuring health care information System. One of the core Technologies used in this project is GIS (Geo-graphical Information System), a tool for capturing, manipulating, analyzing and modeling spatial as well as aspatial data with respect to real world entity. There are some commercial software's are available like Arc Map for handling spatial and aspatial data. But maps and associated information are meaningful only if it's accessible and operable by a layman. This can be done by publishing maps on the web with some interactive tools. Using Commercial software's to publish the maps on the internet is highly expensive and more technical skill is available to understand the working flow. To overcome from this issue there is an exploring technology which is getting updated every day called open source Web GIS is available to everyone at free of cost. Main Characteristics of open source are transparency (Source code can be downloaded by the user), Platform neutral (open source software can be installed at any Operating System environment), no licensing issue (the user will not be interrupted by asking license and all), Easy to upgrade, easy to learn (Documents are clearly provided which can make the user to learn the web processes quickly), and ensure more security etc but all are based on OGC Standards. The database which is capable of storing, manipulating, querying and retrieving data (Spatial and Aspatial) is PostgreSQL, and this the one used throughout the project work. On the whole it's a complete website handling spatial and non-spatial data to provide the user friendly page which in turn directs the person to the appropriate respond.

II. NEED OF THE STUDY

The existing hospital website is static which makes it less interactive. It doesn't have database connectivity. Moreover patients didn't have an access to the details of the hospital, services, and functions through the site, hence they were not updated about the latest events and placement drives. And mainly it didn't focus on spatial page development popularly known as web mapping which provides excellent routing system spatially with many tools embedded with it. In order to make the site dynamic and more interactive and effective, a database link to our hospital website and web mapping technologies are linked with the website. More Aesthetic styles are created for spatial entities using SLD Cookbook in geoserver to make the map which is shown on the web page more clearly to the people who use the system. The proposed spatial helpdesk has developed using the two tier architecture which uses the following languages and Technologies.

1. Geoserver 2.2
2. Mapserver 6.0.3
3. MapScript
4. Apache
5. PostgreSQL 9.2
6. QGIS (Quantum GIS) 1.7.4
7. PHP (Hypertext Preprocessor)
8. JQuery

9. JavaScript
10. OpenLayers
11. Geoext
12. XML (Extensible Markup Language)
13. HTML (Hyper Text Markup Language)
14. Flash
15. CSS (Cascading Style Sheet)
16. Photoshop

All technologies mentioned above are an open source technology. Any time developer can download it and use without any interruptions. Most frequently these open source applications are getting updated with new innovations with appropriate documents. This makes the developer to update the system frequently with more advancement.

III. AIM

To develop a complete website with the combination of spatial (Web Mapping) and aspatial pages for Healthcare information System to provide health related services to common people.

IV. OBJECTIVE

1. To develop the routing Algorithm to find out the shortest route from important blood banks to the government hospitals around Chennai with the aid of PostgreSQL, PHP, OpenLayers, MapScript, Mapserver, JavaScript, QGIS, Photoshop and HTML.
2. To develop a Dynamic Interactive web map for providing route from the entrance of the hospital to the appropriate building using Geoext, JavaScript, XML, Geoserver and QGIS.
3. To create an E-Doctor Section by establishing connection between database and user page using PostgreSQL and PHP.
4. To develop a complete website to integrate the spatial web map page and Aspatial helpdesk page using HTML, flash, CSS, PHP and JQuery.

V. STUDY AREA

Stanley Hospital, Chennai.

It's located in 13.09758 Latitude and 80.29456 Longitude. Stanley hospital extents from has an area of 22,343 m². Stanley Government Hospital, one of the oldest and pioneering hospital for excellence in India. The seed for this institution was sown as early as 1740, The East India Company first created the medical department. The hospital has an out-patient attendance of around 5000 patients per day. A unique feature is its 8-story surgical complex equipped to perform up to 40 surgeries simultaneously, and a separate pediatrics block with all specialties under one roof. RSRM hospital is also attached for obstetrics and Gynecology care. The three well known departments of the Stanley Medical Hospitals are Surgical Gastroenterology, Urology and the Institute of Hand Rehabilitation and Plastic Surgery. The Institute for Research and Rehabilitation of Hand and the Department of Plastic Surgery (IRRH & DPS) is one of the best centers in Southeast Asia. The Department of Surgical Gastroenterology was the first in India to perform a successful liver transplant, Surgical Gastroenterologist and the first among Hospitals/ Hospital Departments in India to obtain the ISO 9001 certification. The Department of Urology performs up to fifty kidney transplants a year.

Study area selection is significant because this is the main factor which will make the project effective and successful. So initially a small survey has been took in government hospitals of Chennai where the area is large and the people have been suffering in finding the required department since the label and numbers are not that much visible and proper. Stanley is a government hospital, where people are very much suffering in finding the departments and this is the hospital which is not even having website for providing healthcare information at free of cost. So the project mainly concentrates on website creation for Stanley hospital which is also incorporates interactive web map routing system.

VI. METHODOLOGY

6.1 DATA COLLECTION

Data has been collected from the Stanley hospital by taking Google imagery and GPS on hand. Routes are collected as a linear segment from GPS. Mean while various routes inside the hospital boundary, departments, and blocks are also traced on the map. Building blocks and associated attributes like department name, working hour, number of floors, department in each floor etc are noted manually and this information have been entered as a Aspatial data while creating spatial information of those collected earlier. Area and extent has been calculated in QGIS. Chennai Data such as Road network, Point of Interest, and boundary are collected from cloudmade website.

6.2 COMPONENTS OF WEB FORM

- Home Page Design
- First aid Helpdesk
- Emergency Contacts
- Blood Banks Details
- Ambulance contacts

- Important Medical Terminology
- National Health scheme
- Spatial Touch Design also known as Interactive Web mapping Service
- Route Planner, comes under web shortest route algorithm
- Blog Page design
- E-Doctor Design
- Satellite View of the hospital
- Spatial Help Desk – an Overview

6.3 ARCHITECTURAL MODEL

The project operates on 2 tier Architecture principle. Client and Server are the two tiers. This architecture is also called Client-Server architecture because of the two components: The client that runs the application and the server that handles the database back-end. When the client starts it establishes a connection to the server and communicates as needed with the server while running the client. The client computer usually can't see the database directly and can only access the data by starting the client. This means that the data on the server is much more secure. Now users are unable to change or delete data unless they have specific user rights to do so. The client-server solution also allows multiple users to access the database at the same time as long as they are accessing data in different parts of the database. One other huge benefit is that the server is processing data that allows the client to work on the presentation and business logic only. This mean that the client and the server is sharing the workload and by scaling the server to be more powerful than the client, you are usually able to load many clients to the server allowing more users to work on the system at the same time.

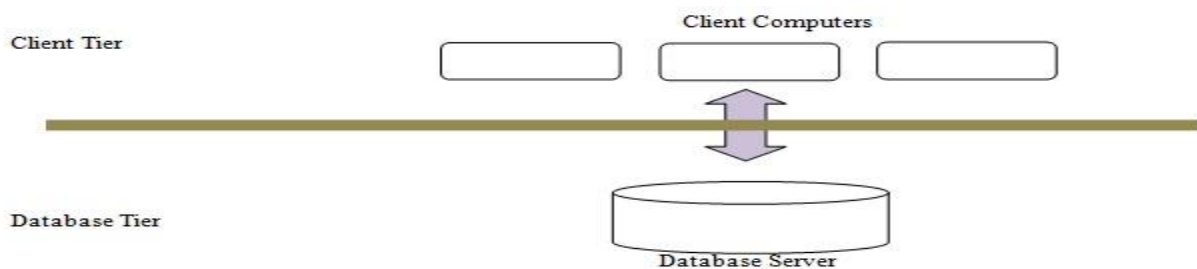


Figure 1

6.4 GENERAL WORK FLOW

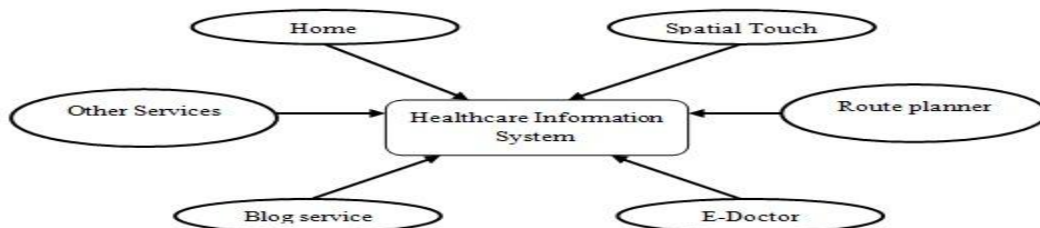


Figure 2

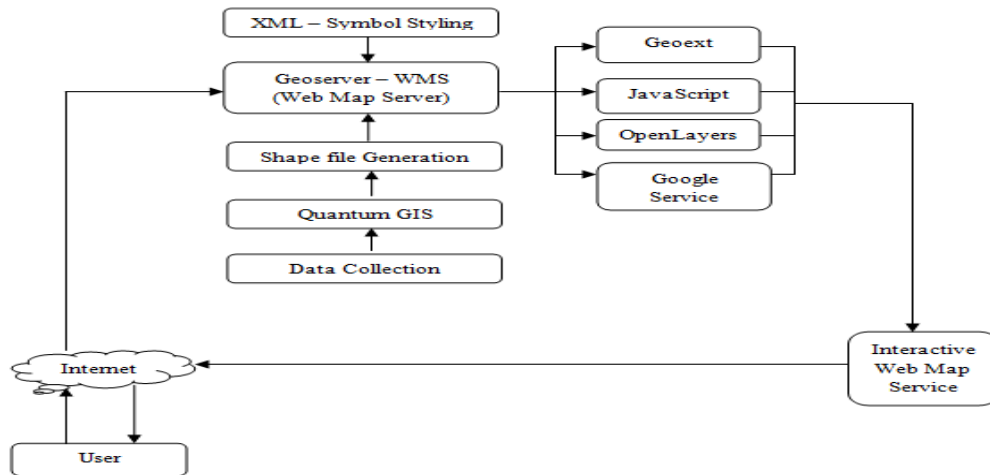
6.5 HOME PAGE DESIGN

The home page of a website is the first page that a user perceives upon entering the website URL at the browser address area. It forms the abstract of the entire website. Photoshop is used in the design of logo placed at the top of the web page. HTML, CSS (Cascading style sheets), JQuery and Flash scripts are written for designing the webpage. The Page Consists of several health information such as First aid helpdesk for providing first aid guidelines in the case of emergency, Medical terminology which should be known by the common people, Ambulance services around Chennai, Emergency contacts, Blood banks details, Some updated Government scheme which is not known to the people, and spatial helpdesk to guide the people about the spatial web map service so that everyone can understand how to operate this system to obtain efficient information with respect to spatial and aspatial data. Home page is shown in figure 3. Other services like Emergency contacts, blood bank details, government scheme are available in every page/ function at bottom.

6.6 WEB MAPPING DESIGN

It's named as Spatial Touch function. Generally this web mapping application is developed to aid people who suffer very much to find the way from the entrance to the corresponding department in case of emergency. This one click application will make people to know the path and location of the desired department by clicking only once on the page which in turn deviate the view from Aspatial to spatial map. QGIS application is used in developing spatial data of hospital

blocks, route inside the hospital, outer road, railway line and boundary as shown in figure 4 and figure 9. Once a request is sent from the user to GeoServer for the data to render in the map viewer, then the data can be transmitted from server to user as a as an image (via a Web Mapping Service (WMS)). Spatial Web map shows the direction from where the people are standing and the route to the appropriate building. It's an Interactive web map where user can inquire the map to know the details of road, building and its function, railway line etc. They can also remove the map from the legend panel, add the map from the server, option provided at the right panel, refresh and back to the spatial touch. The technologies used in the development of web maps are specified below.



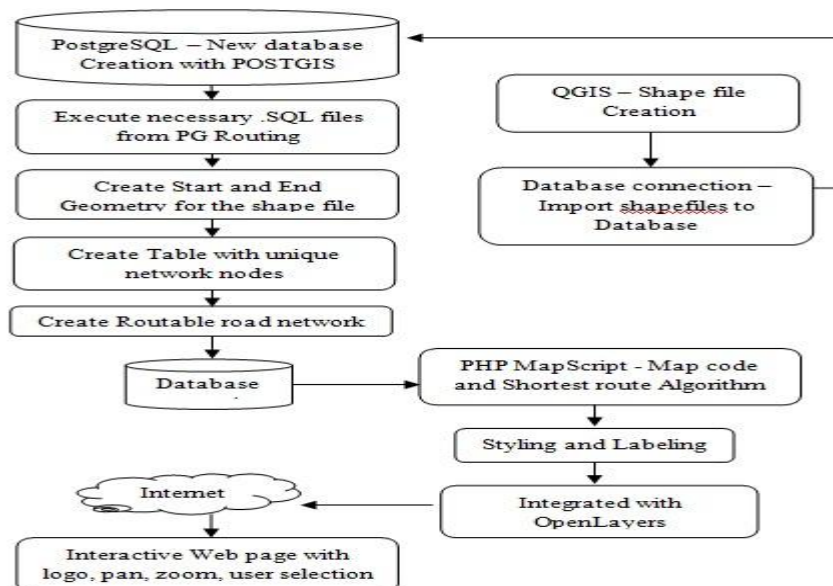
Flow Chart 1: Spatial Touch System Flow Diagram

6.7 ROUTE PLANNER

Route Planner is a section where shortest route algorithm has been incorporated to show the shortest route from the important blood banks to the hospitals with transfusion department. PGRouting has been installed in the database such that the all 802 functions are taken their place in the appropriate database required for running routing algorithm. This Installation has been done by running three sql files as mentioned below

- routing_core.sql
- routing_core_wrappers.sql
- routing_topology.sql

QGIS is used in the creation of shape files of Chennai road network, hospitals with transfusion medicine, blood banks and bust stop as shown in figure. The road network and shape files are converted to a database file and loaded in the database where the PGRouting functions are installed. The PHP MapScript coding for publishing base maps and shortest route are put together in OpenLayers JavaScript to make a page as an interactive one. Each time, at user query, the database has been connected and shortest route geometry has been retrieved and plotted as a line on the web. Finally 4 Google service such as Google street, Google physical, Google hybrid and Google Satellite have been called to make the web map user friendly. The complete route planner has been shown in figure 7.



Flow chart 2: Route Planner System flow Diagram

6.8 E-DOCTOR

E-doctor is an important service which would be act as online doctor where people may ask their doubts, queries, even prescription from the effective doctors through online. If the doctors think that the query is significant, the suggestions are posted in blog section. This Service has been developed by establishing connection between database (server) and Web page from where the people can shoot their questions. PHP plays a vital role to accomplish this task. Through this connection the submitted query has been getting updated in the DB which is located in the hospital server. Since the query updation has been taken place to the appropriate department, only authorized can access the database by providing password authentication to the database. E –Doctor web page shown in figure 5.

6.9 BLOG SERVICE

Blog service is generated using simple HTML and CSS functionalities. This section is for updating the suggestion from query asked, latest inventions, etc.. If the doctors think that the question raised from the person is significant, and everybody should know about it, then the answer from the doctors will be posted in the blog. Latest inventions in medical field are also updated frequently in the blog. The blog service page is shown in figure 6.

VII. RESULT AND DISCUSSION

7.1 SYSTEM TESTING

Testing is a set activity that can be planned and conducted systematically. Testing begins at the module level and work towards the integration of entire computers based system. Nothing is complete without testing, as it is vital success of the system. The testing process steps are mentioned below

7.1.1 Integrated Testing

7.1.2 Output Testing

7.1.1 INTEGRATED TESTING

Spatial and aspatial data are integrated in this system. While conversion of spatial data to database file, the cross checking or testing is necessary since the conversion creates the geom field in the database. While providing link from Aspatial web page to spatial webpage there must be adequate level of integrated testing is necessary. This application is browser sensitive, means it can able to run all the functions effectively only on the Internet explorer.

7.1.2 OUTPUT TESTING

This is the final step in testing. In this the entire system was tested as a whole with all forms, code, modules and class modules. This form of testing is popularly known as Black Box testing or system testing.

Black Box testing methods focus on the functional requirement of the software. That is, Black Box testing enables to derive sets of input conditions that will fully exercise all functional requirements for a program. Black Box testing attempts to find errors in the following categories; incorrect or missing functions, interface errors, errors in data structures or external database access, performance errors and initialization errors and termination errors.

The prototype visualization tool has developed successfully which enable users to spatially visualize hospital Information within a web browser, without the need for any additional software, or software training. The complex workings of the system are hidden from the user and the automatic rendering design used in this system enables users with no prior knowledge of GIS to visualize their data and immediately gain some understanding of the spatial structure of their data. In comparison to that of commercial closed source software, open source is more complicated to initially implement. Although there is no specific dedicated customer support service, the support and advice provided by users in the open source community through forums and mailing lists is extensive, and there is a large community devoted to help and share ideas which can inspire "out of the box" thinking on solutions which may not be possible in closed source applications. The System developed can also be placed at the hospital entrance to meet the user's routing need in the case of emergency.

Although the Information System are integrated with spatial and Aspatial web pages there are some unavoidable limitations present. Some tools developed in the open source environment may be browser dependent and some may not be. So there is a need of crucial knowledge to finalize the browser from where it has to take move. Some of the Information like Doctors at OP, Timing, Oxygen supply storage, and Patients incoming record should have been included in the system since it's a system deployed by the hospital.

VIII. FIGURES / WEBPAGES



Figure 3



Figure 4



Figure 5



Figure 6

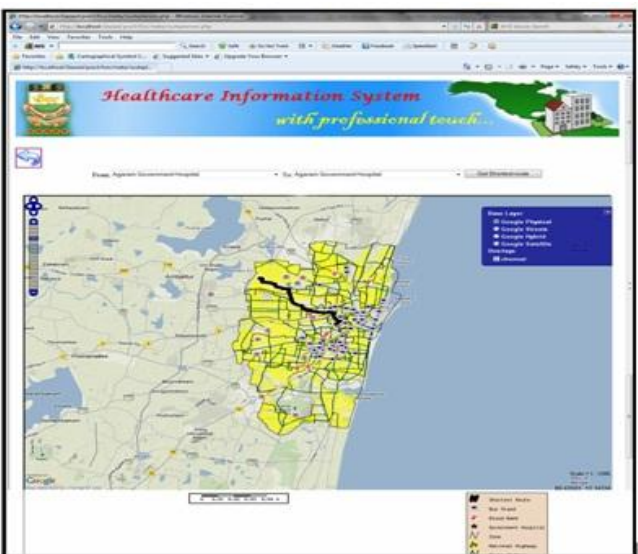


Figure 7

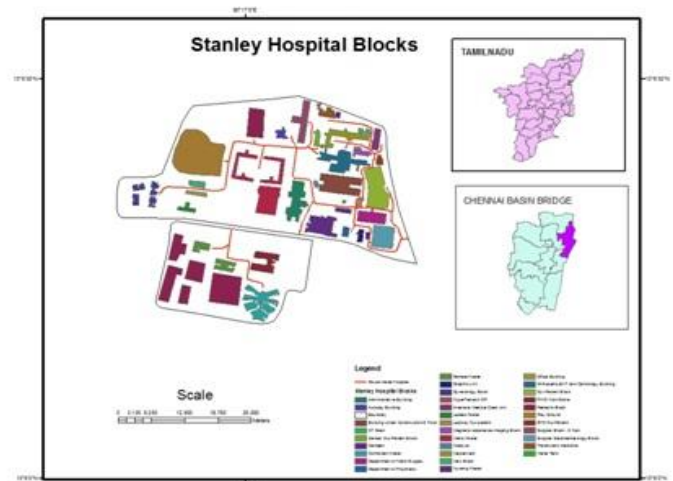


Figure 8

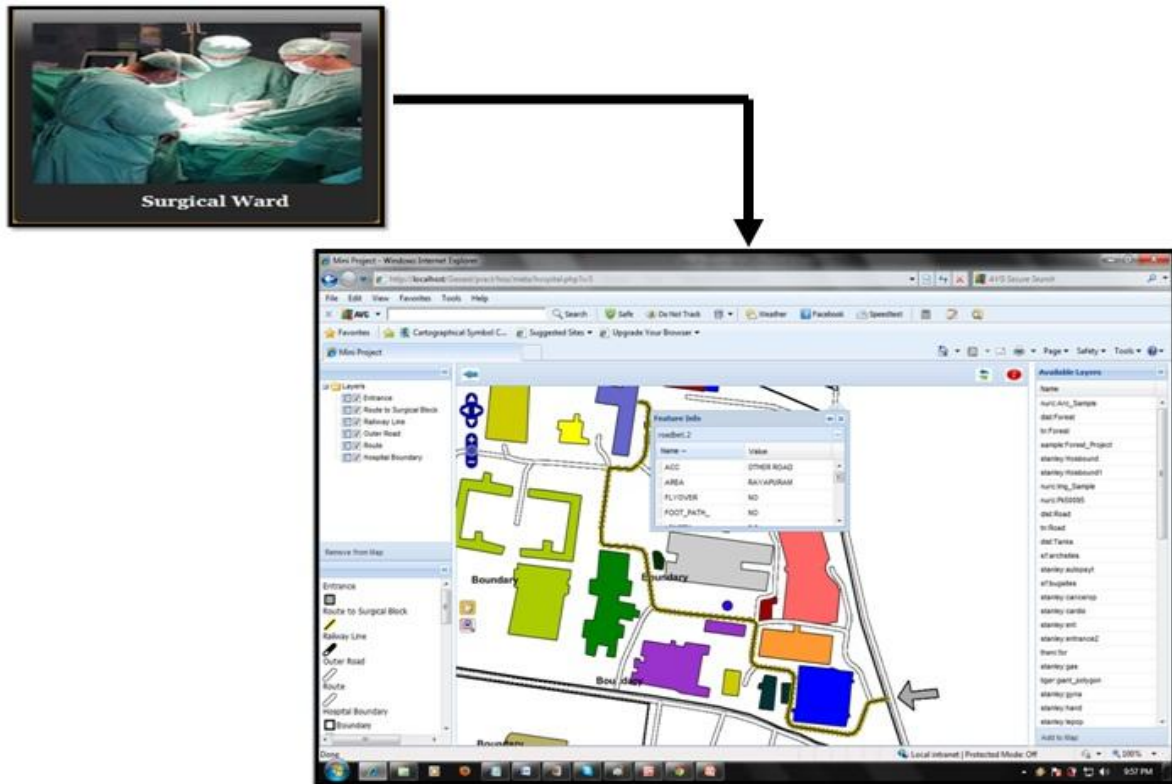


Figure 9

IX. ACKNOWLEDGEMENTS

I would like to express my sincere gratitude to Mrs.Mahalakshmi Narayanan, Principal System Analyst in National Informatics Centre for providing her support during my work.

I also extend my sincere appreciation to Ms.Bhuvanawari, Senior Programmer who provided the valuable suggestion and precious time in accomplishing this work.

I also thank all the staff members and my friends for the help to furnish this work.

REFERENCES

- [1] Open-Source web-based geographical information system for health exposure assessment by Barry Evans and Clive E Sabel 2012
- [2] Interactive web-based mapping: bridging technology and data for health by Linda High field, Jutas Arthasarnpravit, Cecelia A Ottenweller and Arnaud Dasprez 2011
- [3] Web-based GIS: the vector-borne disease airline importation risk (VBD-AIR) tool by Zhuojie Huang, Aniruddha Das, Youliang Qiu and Andrew J Tatem 2012
- [4] Web Map by University of Virginia
- [5] Columbia University Medical Centre
- [6] Online GIS services for mapping and sharing disease information by Sheng Gao, Darka Mioc, Francois Anton, Xiaolun Yi3 and David J Coleman 2008
- [7] Towards Web-based representation and processing of health information by Sheng Gao1, Darka Mioc, Xiaolun Yi, Francois Anton, Eddie Oldfield and David J Coleman 2009

Influence of Strong Acids (Hydrochloric and Sulphuric) In Water on Properties of Natural Admixture Cements

D. Sreehari Rao,¹ Prof. I.V.Ramana Reddy²

¹ Assistant Professor, Department of Civil Engineering, College of Engineering, S. V. University, Tirupati, Andhra Pradesh-517 502, INDIA.

² Professor, Department of Civil Engineering, College of Engineering, S. V. University, Tirupati, Andhra Pradesh-517 502, INDIA.

ABSTRACT: Admixtures and the water have an important role on application of concrete. The study is aimed at investigating the effect of strong acids as mixing water on setting times, soundness and compressive strength of admixture cements. This paper therefore presents the result and findings of an experimental research on the influence of strong acids on setting and strength development of admixture cements. In the research PPC plus 10% silica fume was added by weight and cubes were casted with deionised water and deionised water containing strong acids of HCl and H₂SO₄. The results shows the HCl and H₂SO₄ in deionised water accelerate the initial and final setting times in all concentrations. Both HCl and H₂SO₄ in deionised water decrease the compressive strength from early age (3-days) to the maximum age (2years). In the present work analysis the hydration characteristics of the admixture cements using the techniques of X-ray diffraction analysis and useful conclusions are obtained regarding the influence of strong acids.

Key words: PPC, Silica fume, setting times, strength development, X-ray diffraction

The presence of acids in water changes the properties of concrete in setting times as well as strength. Water is an essential ingredient of concrete as it effectively participates in the chemical reactions with natural admixture cements like natural pozzolana and other supplementary cementitious materials (Silica fume). Pozzolans are commonly used as an addition to Portland cement to increase the long-term strength and other material properties. Concrete is not only material that is risk to physical and chemical process of deterioration associated with water. Therefore, it will be desirable to review, in general, the characteristics of water that make it the principal agent of destruction of material. The I.S.Code 456-2000 also specifies the minimum pH-value as 6.0 and also permissible limits for solids in the water to fit for construction purposes. The code has not specified the limits to the individual components like acidic substances. The use of natural and economical materials seems to be one of the possible solutions for the future. The development of an economical cement concrete with interesting properties in the fresh and hardened state will certainly help and encourage the use of this material in the construction industry. Hence, in the present investigation to find the effects and quality of water on setting and strength properties of admixture cement. The effect of strong acidic substances on setting, hardening and strength development of admixture cement are not known much. Hence, an investigation is carried out on setting time, soundness and strength of admixture cements.

I. Materials and Methods

Materials: The details of various materials used in the experimental investigation are presented below.

Cement: The cement used in the present investigation is of 43 grade Pozzolana Portland Cement manufactured by ACC Ltd.

Fine aggregate: The fine aggregate used in this investigation is the river sand obtained from Swarnamukhi River near Tirupati, Chittoor district in Andhra Pradesh.

Silica fume: Silica fume used in the present study was obtained from Elkem India Pvt. Ltd., Mumbai.

Water: Deionised water spiked with strong acidic substances (H₂SO₄ and HCl) with different concentration is used in mixing water.

Experimental System: The following equipment is used for casting and testing of specimens: (i) Cube moulds, (ii) 200T U.T.M(Universal Testing Machine) for cube compressive strength determination,(iii)Vicat's apparatus including moulds conforming to IS4031(part-5)-1988 for setting times, (iv)Le-Chatelier's equipment to determine the soundness of cement and (v) cement cubes prepared with water containing, H₂SO₄ in the concentration of 50 mg/L,150 mg/L,200 mg/L,500 mg/L and 800mg/L and HCl, in the concentration of 50 mg/L,150 mg/L,200 mg/L,500 mg/L and 800mg/L, in mixing water.

Setting time: Vicat's apparatus conforming IS4031(part-5) 1988 consist of a frame to which a movable rod having an indicator is attached which gives the penetration, weighing 100g and having diameter and length of 10mm and 50mm respectively. Vicat's apparatus included three attachments-square needle for initial setting time, plunger for determining normal consistency and needle with annular collar for final setting time.

Compressive Strength: The test specimens for determination of compressive strength of admixture cement prepared using standard metallic cube moulds adopting IS procedure for the compactions. The cubes were demoulded after 24hours of casting and cured in water having similar quality as used in preparation of mix. The cubes are tested for compressive strength for short term and long term. The

compressive strength is computed as the average value of the three samples.

II. Results and Discussion

The results of the present investigation are presented both in tabular and graphical forms. In order to facilitate the analysis, interpretation of the results is carried out at each phase of the experimental work. This interpretation of the results obtained is based on the current knowledge available in the literature as well as on the nature of result obtained. The significance of the result is assessed with reference to the standards specified by the relevant I S codes;

1. The averages of both the initial and final setting times of three cement samples prepared with mixing water containing typical chemical or biological component of varying concentrations under consideration is compared with those of the cement specimens prepared with deionised water. If the difference is less than 30 minutes, the change is considered to be negligible or insignificant and if it is more than 30 minutes, the change is considered to be significant.
2. The average compressive strength of at least three cubes prepared with water under consideration is compared with that of three similar cubes prepared with deionised water. If the difference in the strength is less than 10%, it is considered to be insignificant and if it is greater than 10%, it is considered to be significant.

**Setting time:
 Hydrochloric Acid (HCl):**

The effect of hydrochloric acid on the initial and final setting times is shown in Fig 1. Both initial and final setting got retarded with increase in hydrochloric acid concentration in deionised water. The retardation for initial and final setting times is significant (i.e., more than 30 minutes), when the hydrochloric acid content exceeds 150mg/l and 200 mg/l respectively. When the acid content is 800 mg/l, the initial setting time is about 192 minutes, which is 64 minutes more than that of the control mix. Similarly a difference of 44 minutes is observed in the case of final setting time.

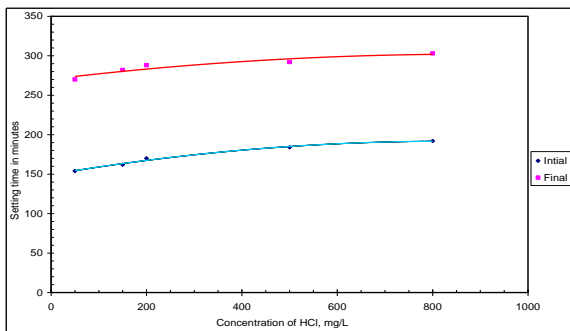


Fig.1 Variation of Setting times of admixture cement (PPC cement + 10% Silica fume) corresponding to various concentrations of HCl in deionised water.

Sulphuric Acid (H₂SO₄):

The effect of sulphuric acid on the initial and final setting times is shown in Fig 2. Both initial and final setting got retarded with an increase in sulphuric acid concentration in the deionised water. The retardation for initial setting time is significant, when the sulphuric acid concentration exceeds 150 mg/L respectively. When sulphuric acid content is 800 mg/L, initial setting time is 202 minutes which is 74 minutes more than that of control mix; similarly difference of 53 minutes is observed in the case of final setting time.

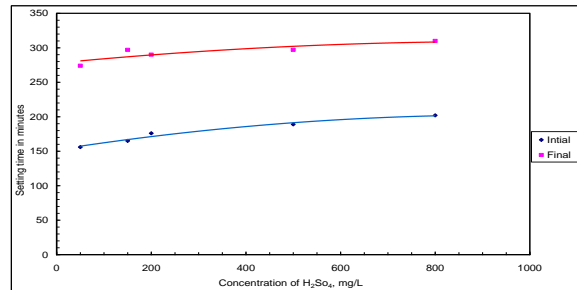


Fig.2. Variation of Setting times of admixture cement (PPC cement + 10% Silica fume) corresponding to various concentrations of H₂SO₄ in deionised water.

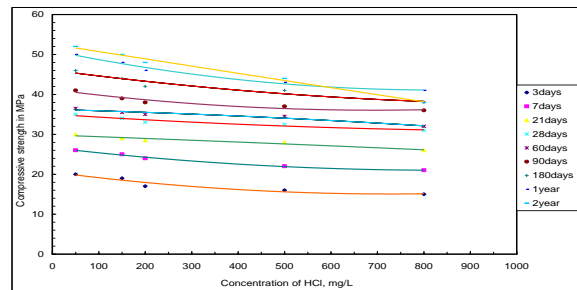


Fig.3. Variation of compressive strength of admixture cement (PPC cement + 10% Silica fume) mortar cubes at different ages corresponding to various concentrations of HCl in deionised water.

The effect of HCl on the compressive strength of admixture cement mortar is presented in Fig 3. Continuous decrease in compressive strength of the cement mortar cubes prepared with HCl acid solution is observed as the acid concentration increases till the maximum concentration (800 mg/L) tested.

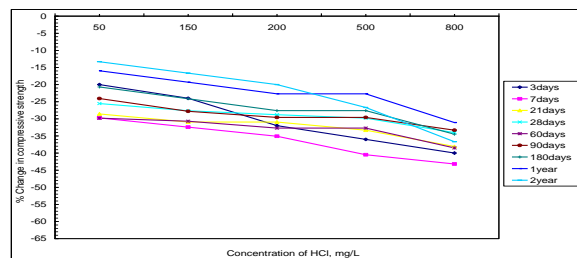


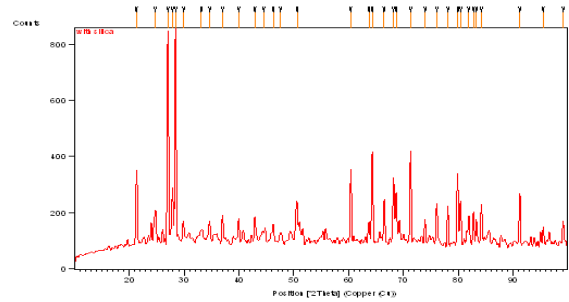
Fig.4. Percentage variation of compressive strength of admixture cement (PPC cement + 10% Silica fume) mortar cubes at different ages corresponding to various concentrations of HCl in deionised water.

The percent change in compressive strength is presented in Fig 4. Although there is decrease in the

compressive strength of cement mortar cube of all age samples, significant decrease is observed in all age samples. The rate of decrease in compressive strength also gradually increases with the increase in the concentration of the HCl as well as age. For the 3-day sample, significant decrease in strength starts at 200 mg/L. Similarly, for 28-day, 60-day, 90-day, 180-day, 1-year and 2-year samples, significant decrease in strength starts at 200 mg/L, 500 mg/L concentrations respectively and the trend continues up to the maximum concentration. 2-year sample shows the maximum decrease in compressive strength with increase in concentration of HCl. When HCl concentration is 800 mg/L, the decrease in compressive strength is 36.70 % than that of the control mix.

compressive strength is 35 % when compared with that of the control mix.

III. X-RAY DIFFRACTION



Peak List

Pos.[°2Th]	Height[ct]	FWHM[°2Th]	d- _o	Rel.Int.[
21.2999	284.22	0.2854	4.1681	34.84
24.6774	108.28	0.4955	3.60474	13.27
27.044	808.37	0.2522	3.29443	99.08
27.8776	207.59	0.2099	3.19779	25.45
28.4259	815.83	0.2414	3.13734	100
29.8629	61.46	0.017	2.98956	7.53
33.171	21.87	1.773	2.69859	2.68
34.6229	69.14	0.3235	2.58867	8.48
36.999	95.41	0.3082	2.42769	11.69
39.9368	86.14	0.2457	2.25562	10.56
42.9052	94.01	0.2153	2.10619	11.52
44.5205	26.66	1.9653	2.03345	3.27
46.209	62.09	0.3433	1.963	7.61
47.5966	1.82	0.0013	1.90896	0.22
50.5851	112.53	0.5774	1.80296	13.79
60.3873	271.37	0.2481	1.53164	33.26
63.6841	71.39	0.2107	1.46006	8.75
64.2899	349.65	0.2524	1.44776	42.86
66.4734	167.42	0.2302	1.4054	20.52
68.16	278.63	0.1668	1.37467	34.15
68.6174	127.28	0.8095	1.36662	15.6
71.3241	356.41	0.2348	1.32126	43.69
73.9238	51.08	0.6812	1.28109	6.26
76.0972	158.41	0.2823	1.24982	19.42
78.0615	135.48	0.2351	1.22321	16.61
79.882	266.63	0.2495	1.19985	32.68
80.4209	154.97	0.2624	1.19316	18.99
81.8855	95.91	0.3066	1.17548	11.76
82.7426	103.41	0.2265	1.16547	12.68
83.3019	89.55	0.202	1.15906	10.98
84.2383	135.62	0.2587	1.14854	16.62
91.1915	195.95	0.2402	1.07822	24.02
95.4305	30.71	0.952	1.04121	3.76
99.0816	87.25	0.2877	1.0124	10.69

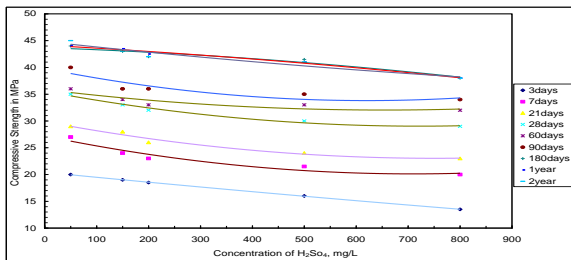


Fig.5. Variation of compressive strength of admixture cement (PPC cement + 10% Silica fume) mortar cubes at different ages corresponding to various concentrations of H₂SO₄ in deionised water.

The effect of H₂SO₄ on the compressive strength of cement mortar cubes is presented in Fig.5. Decrease in compressive strength of the cement mortar cubes prepared with H₂SO₄ solution is observed as the sulphuric acid concentration increases, the maximum concentration being 800 mg/l.

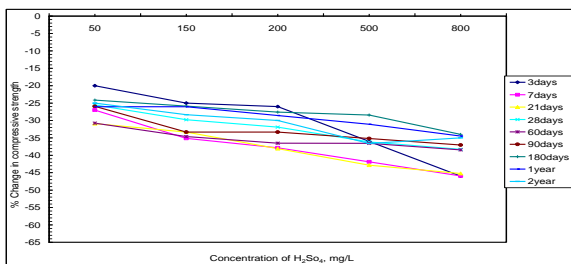
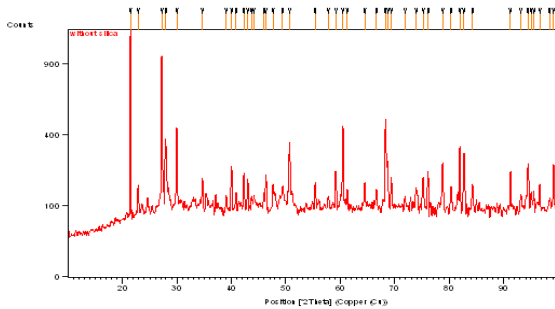


Fig.6 Percent variation of compressive strength of admixture cement (PPC cement + 10% Silica fume) mortar cubes at different ages corresponding to various concentrations of H₂SO₄ in deionised water.

The percent change in compressive strength of mortar cubes prepared with various concentration of H₂SO₄ in deionised water is shown in Fig 6. Although there is decrease in the compressive strength of cement mortar cube of all age samples, significant decrease is observed in all age samples. The rate of decrease in compressive strength is normally varies with the increase in the concentration of the H₂SO₄ as well as age. And the trend continues up to the maximum concentration. 2-year sample shows the maximum decrease in compressive strength with increase in concentration of H₂SO₄. When H₂SO₄ concentration is 800 mg/L, the decrease in

Fig.a. X-ray diffraction pattern of powdered admixture cement (PPC cement +10% silica fume) mortar cube prepared with deionised water.

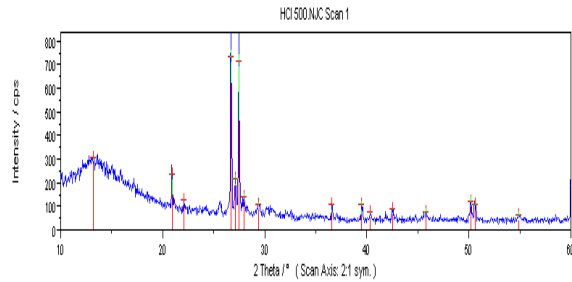


Peak List

Pos.[°2Th	Height[ct	FWHM[°2Th	d-	Rel.Int.[
21.437	1171.43	0.3008	4.1418	100.00
22.888	86.60	0.1805	3.8824	7.39
27.210	897.90	0.2406	3.2747	76.65
27.914	284.63	0.2406	3.1937	24.30
29.965	345.90	0.3008	2.9796	29.53
34.701	91.95	0.2406	2.583	7.85
39.052	45.30	0.361	2.3047	3.87
40.027	156.15	0.2406	2.2508	13.33
40.831	93.60	0.122	2.2082	7.99
42.307	120.72	0.3008	2.1346	10.31
42.999	92.95	0.1805	2.1018	7.93
43.745	64.71	0.1498	2.0677	5.52
44.137	62.00	0.1389	2.0502	5.29
46.003	89.30	0.1348	1.9713	7.62
46.352	116.21	0.1805	1.9573	9.92
47.667	76.26	0.361	1.9063	6.51
49.402	88.41	0.3519	1.8433	7.55
50.675	254.95	0.2406	1.8	21.76
55.387	84.72	0.2406	1.6575	7.23
57.805	70.69	0.1562	1.5938	6.03
59.194	128.95	0.2406	1.5596	11.01
60.475	358.90	0.2406	1.5296	30.64
61.274	103.90	0.101	1.5116	8.87
64.471	86.67	0.2406	1.4441	7.40
66.641	56.12	0.361	1.4023	4.79
68.282	396.76	0.2406	1.3725	33.87
68.742	241.70	1.6638	1.3645	20.63
69.355	100.93	0.2406	1.3539	8.62
71.922	61.25	0.1721	1.3118	5.23
73.960	57.10	0.4813	1.2806	4.87
75.247	106.14	0.3008	1.2618	9.06
76.135	132.14	0.1805	1.2493	11.28
78.772	171.85	0.2406	1.214	14.67
80.324	75.96	0.3008	1.1944	6.48
81.939	251.31	0.2406	1.1749	21.45
82.719	221.84	0.3008	1.1657	18.94

84.281	85.40	0.2406	1.1481	7.29
91.240	137.60	0.2406	1.0778	11.75
93.175	50.58	0.361	1.0604	4.32
94.473	171.35	0.3008	1.0492	14.63
95.057	91.55	0.1539	1.0443	7.82
95.516	106.10	0.1072	1.0405	9.06
96.651	87.40	0.2406	1.0313	7.46
98.430	77.50	0.1145	1.0173	6.62
99.141	168.76	0.2406	1.012	14.41

Fig.b. X-ray diffraction pattern of powdered PPC mortar cube prepared with deionised water.



No	d_Fit (Å)	Ang-parab	Ang-COG	Low Limit	Upp. Limit	I-net	I-bgr	FWH M	2-Theta
1	6.5094	13.592 2	13.228 3	10.050 0	20.800 0	308.41	0.00	7.1856	13.592 2
2	4.2462	20.903 8	20.907 6	17.250 0	22.000 0	238.14	0.00	0.1787	20.903 8
3	4.0188	22.100 7	22.088 1	21.050 0	25.450 0	125.72	0.00	18.740 3	22.100 7
4	3.3367	26.695 4	26.699 1	26.250 0	26.900 0	736.76	0.00	0.1412	26.695 4
5	3.2835	27.136 1	27.122 2	26.900 0	27.300 0	219.26	0.00	0.2423	27.136 1
6	3.2452	27.462 6	27.459 5	27.250 0	27.650 0	712.83	0.00	0.1377	27.462 6
7	3.1857	27.985 7	27.980 3	27.650 0	29.250 0	143.40	0.00	1.0316	27.985 7
8	3.0315	29.440 3	29.397 0	28.350 0	30.100 0	108.48	0.00	25.979 4	29.440 3
9	2.4530	36.603 8	36.590 3	34.250 0	39.400 0	107.85	0.00	0.2121	36.603 8
10	2.2781	39.526 2	39.498 7	37.150 0	40.250 0	108.91	0.00	0.2735	39.526 2
11	2.2334	40.351 4	40.336 4	39.700 0	41.750 0	73.72	0.00	0.8347	40.351 4
12	2.1240	42.527 3	42.522 9	41.900 0	45.750 0	88.66	0.00	0.2558	42.527 3
13	1.9802	45.785 4	45.799 5	42.600 0	49.950 0	76.19	0.00	1.1762	45.785 4
14	1.8162	50.191 2	50.202 5	45.900 0	50.450 0	118.21	0.00	0.3999	50.191 2
15	1.8025	50.600 0	50.598 8	50.300 0	54.800 0	106.00	0.00	0.3325	50.600 0
16	1.6709	54.905 4	54.906 9	50.800 0	59.850 0	65.67	0.00	1.8828	54.905 4

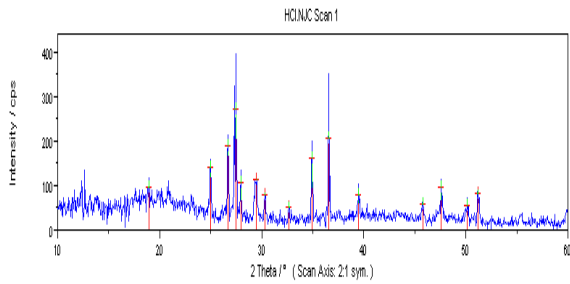


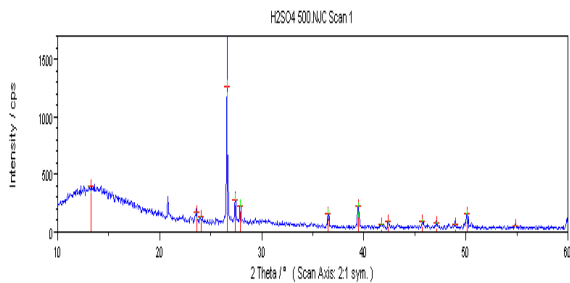
Fig.7. Powdered X- Ray diffraction pattern for the cement mortar cubes prepared with HCl (500 mg/L and 800 mg/L) in deionised water.

Powdered X- Ray diffraction pattern for the admixture cement (PPC+10% Silica fume) mortar cubes prepared with HCl (500 mg/L and 800 mg/L) in deionised water is shown in fig.7.

The comparison of this pattern with that for deionised water indicates the formation compounds α -C2S hydrate ($\text{Ca}_2(\text{HSiO}_4)(\text{OH})$), CaCl_2 and AlCl_3 which are evident from the presence of sets of d-spacing's 1.670Å for ($\text{Ca}_2(\text{HSiO}_4)(\text{OH})$), 6.509Å, 4.246Å and 3.245Å for CaCl_2 and 3.336Å for AlCl_3 respectively, which are absent in the matter for the control mix (Fig a and Fig b).

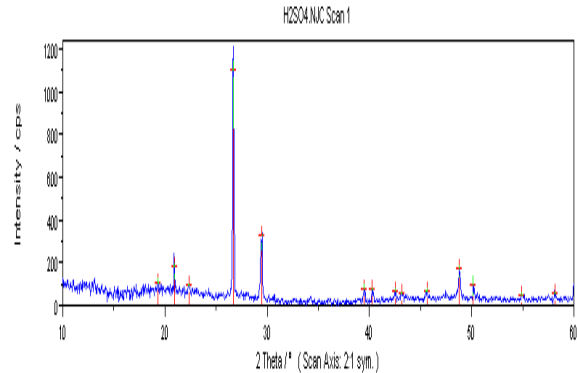
The possible chemical reaction upon the hydration of cement with mixing water containing HCl is $3\text{Cao} + \text{Al}_2\text{O}_3 + \text{SiO}_2 + 8 \text{HCl} \rightarrow \text{Ca}_2(\text{HSiO}_4)(\text{OH}) + \text{CaCl}_2 + 2\text{AlCl}_3 + 2\text{H}_2\text{O}$

The reason for the retardation of setting time of cement could be attributed to the formation of α -C₂S hydrate ($\text{Ca}_2(\text{HSiO}_4)(\text{OH})$). The reaction of cement with water containing HCl leads to the formation of chlorides of calcium and aluminum in addition to α -C₂S Hydrate ($\text{Ca}_2(\text{HSiO}_4)(\text{OH})$). Among these, chlorides of calcium and aluminum are soluble. Even silica forms a colloidal solution. Significant decrease in compressive strength at longer duration, i.e., 21-day onwards, could be due to the formation of soluble chlorides.



N	d_Fit	Ang-	Ang-	Low	Upp.	I-net	I-bgr	FWH	2-
1	6.752	13.10	13.27	10.10	20.70	397.6	0.00	7.977	13.10
2	3.769	23.58	23.60	23.05	25.45	173.8	0.00	0.542	23.58
3	3.709	23.96	24.03	23.70	26.25	126.6	0.00	17.15	23.96
4	3.347	26.60	26.60	26.25	27.15	1256.	0.00	0.134	26.60
5	3.250	27.41	27.39	26.80	27.75	282.6	0.00	0.212	27.41
6	3.195	27.89	27.90	27.60	34.75	225.7	0.00	0.243	27.89
7	2.457	36.53	36.50	34.25	39.30	159.6	0.00	0.183	36.53
8	2.281	39.46	39.44	39.00	39.85	223.3	0.00	0.213	39.46

9	2.161	41.76	41.75	39.65	42.25	72.00	0.00	0.665	41.76
10	2.129	42.41	42.38	41.90	43.20	88.80	0.00	0.291	42.41
11	1.981	45.75	45.75	42.80	47.00	96.80	0.00	0.336	45.75
12	1.927	47.10	47.11	45.95	48.20	81.67	0.00	0.424	47.10
13	1.859	48.94	48.95	47.35	49.75	72.34	0.00	0.749	48.94
14	1.819	50.09	50.10	49.65	51.35	154.0	0.00	0.332	50.09
15	1.672	54.85	54.90	53.80	58.30	57.20	0.00	1.877	54.85



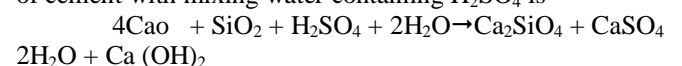
N	d_Fit	Ang-	Ang-	Low	Upp.	I-net	I-bgr	FWH	2-
1	4.5955	19.298	19.314	16.850	20.800	107.32	69.6	0.7462	19.298
2	4.2453	20.908	20.909	16.850	22.300	182.13	36.3	0.1398	20.908
3	3.9720	22.364	22.363	21.050	24.800	95.87	25.4	0.6246	22.364
4	3.3403	26.665	26.683	26.500	26.850	1104.1	32.4	0.1423	26.665
5	3.0306	29.449	29.457	29.150	29.650	327.98	34.9	0.1813	29.449
6	2.2798	39.495	39.504	39.300	39.700	79.13	16.7	0.2497	39.495
7	2.2356	40.310	40.284	40.150	40.500	73.18	14.1	0.2290	40.310
8	2.1244	42.518	42.512	41.850	43.100	63.51	6.62	0.3539	42.518
9	2.0944	43.159	43.202	42.650	45.400	53.93	4.13	0.6775	43.159
10	1.9870	45.618	45.653	45.250	48.600	67.13	0.00	0.5764	45.618
11	1.8644	48.806	48.778	48.150	49.300	175.24	0.00	0.2658	48.806
12	1.8171	50.165	50.156	49.700	50.900	95.75	0.00	0.2424	50.165
13	1.6707	54.910	54.912	53.650	58.000	53.12	0.00	0.5028	54.910
14	1.5852	58.148	58.140	57.950	59.850	60.55	0.00	0.3299	58.148

Fig.8. Powdered X- Ray diffraction pattern for the admixture cement (PPC+10% Silica fume) mortar cubes prepared with H₂SO₄ (500 mg/L and 800 mg/L) in deionised water.

Powdered X- Ray diffraction pattern for the admixture cement (PPC+10% Silica fume) mortar cubes prepared with H₂SO₄ (500 mg/L and 800 mg/L) in deionised water is shown in fig.8.

The comparison of this pattern with that cubes prepared with deionised water indicates the formation of α -C₂S (α -Ca₂SiO₄), CaSO₄·2H₂O and Ca(OH)₂ compounds which are evident from the presence of sets of d-spacing's 3.195Å, 1.981Å and 1.672Å for α -Ca₂SiO₄, 4.245Å and 1.817Å for CaSO₄·2H₂O and 3.195Å and 2.457Å for Ca(OH)₂ respectively, which are absent in the matter for the control mix (Fig a and Fig b).

The possible chemical reaction upon the hydration of cement with mixing water containing H₂SO₄ is



The possible reason for the retardation of setting of cement is the formation of $\text{CaSO}_4 \cdot 2\text{H}_2\text{O}$. If the cement is mixed with H_2SO_4 , it leads to formation of gypsum and calcium hydroxide, in addition to α -Dicalcium silicate ($\alpha\text{-Ca}_2\text{SiO}_4$). Among these, sulphate of calcium is soluble. Even silica forms a colloidal solution. Significant decrease in compressive strength at shorter duration may be due to the formation of soluble sulphates.

The sulphate-bearing water penetrates the hardened cement paste and the final damage to the hardened cement paste is due to the formation of voluminous water-rich calcium compounds. Calcium sulphate formation goes through a process leading to the reduction of stiffness and strength; this is followed by expansion and cracking, and eventual transformation of the material into a mushy or non cohesive mass at longer periods.

IV. Effect of Strong Acids

The strong acidic compounds generally present in water are HCl and H_2SO_4 . The effects of these at various concentrations in deionised water on the initial and final setting times of cement and on the compressive strength of cement mortar cubes were already discussed in the above sub sections. The behavior of strong acidic compounds is elucidated in a comprehensive manner as follows:

Both HCl and H_2SO_4 in deionised water retard the initial as well as final setting times phenomena at all concentrations (Fig 1. and Fig 2.).

HCl in deionised water decreases the compressive strength of mortar cubes, the decrease being significant only at ages varying from 3-day to 2-year samples. H_2SO_4 also decreases compressive strength at all ages, is significant only at ages varying from 3-day to 2-year samples (Figs 3 to 6).

By comparing all these results of strong acidic compounds with those of the control mix, it is evident that both HCl and H_2SO_4 affect the compressive strength negatively. This negative effect increases with respect to increase in concentration as well as duration. Hence, both HCl and H_2SO_4 are the most critical compounds against which a lot of care should be taken if they exist in the mixing water and their concentrations should not be more than 50 mg/L.

It is evident that between these two, the effect of H_2SO_4 is the more critical, against which great care is mandatory. Reaction with HCl leads to the formation of chlorides of calcium and aluminum, which are soluble. But the reaction with H_2SO_4 leads to formation of calcium sulphate and calcium hydroxide. Sulphate-bearing water penetrates the hardened cement paste and forms voluminous calcium compounds. Reduction in stiffness and strength along with expansion and cracking finally transforms the materials into a non cohesive mass at long duration. It is observed from the results that the strength of 2-year sample made with HCl is 36.67 %, which is comparatively higher than that of H_2SO_4 which is 35%.

V. CONCLUSIONS

1. Presence of HCl in water retards significantly the initial and final setting in concentrations more than 200mg/L. Its concentration higher than 200mg/L results in significant decrease in compressive strength.
2. Presence of H_2SO_4 in water retards significantly the initial and final setting in concentrations more than 200mg/L. Its concentration higher than 200mg/L results in significant decrease in compressive strength.
3. Strong acidic substances like HCl and H_2SO_4 in water reduce the compressive strength significantly with respect to increasing concentration as well as age. Thus, care to be taken while using such water for cement mortar and concrete.

REFERENCES

- [1] Fidestol, (2001): Use of Microsilica Concrete Indian Concrete Journal.
- [2] IS 516:1959: Methods of Test for Strength of Concrete.
- [3] IS 650:1966: Standard Sand for Testing of Cement (First Revision), Indian Standards Institution, New Delhi.
- [4] Mehta, P.K. (1983): Pozzolanic and Cementitious by Products as Mineral Admixtures for Concrete - A Critical Review, Proceedings of ACI Special Publication, ACI-SP-79, pp. 1-43.
- [5] Mehta, P.K. (1984): Testing and Correlation of Fly Ash Properties with Respect of Pozzolanic Behaviour, CS-3314, Electrical Power Research Institute (EPRI), Palo Alto California, Jan.
- [6] Mehta, P.K. (1988): Pozzolanic and Cementitious Bi-products in Concrete- another Look, ACI-SP-114, Vol. 1, pp. 1-43.

3-Chromatic Cubic Graphs with Complementary Connected Domination Number Three

Selvam Avadayappan,¹ S. Kalaimathy,² G. Mahadevan³

^{1,2} Department of Mathematics, VHNSN College, Virudhunagar - 626001, India.

³ Department of Mathematics, Gandhi gram Rural University, Gandhi gram - 624302, India.

Abstract: Let $G(V, E)$ be a graph. A subset S of V is called a dominating set of G if every vertex in $V-S$ is adjacent to at least one vertex in S . The domination number $\gamma(G)$ is the minimum cardinality taken over all such dominating sets in G . A subset S of V is said to be a complementary connected dominating set (ccd-set) if S is a dominating set and $\langle V-S \rangle$ is connected. The chromatic number χ is the minimum number of colours required to colour all the vertices such that no two adjacent vertices receive the same colour. In this paper, we characterize the r -regular graphs with $\gamma_{cc} = \chi = 2$ and the 3-regular graphs with $\gamma_{cc} = \chi = 3$.

Keywords: Dominating set, domination number, complementary connected domination number, chromatic number, regular graphs and cubic graphs.

AMS Subject Classification Code: 05C (primary).

I. INTRODUCTION

Throughout this paper, by a graph we mean a finite, simple, connected and undirected graph $G(V, E)$. The number of vertices in G is denoted by n . We denote a cycle on n vertices by C_n . Δ denotes the maximum degree in G . If S is a subset of V , then $\langle S \rangle$ denotes the induced subgraph of G induced by S . For any two subsets V_1 and V_2 of V , let $E(V_1, V_2)$ denote the set of all edges with one end in V_1 and the other in V_2 . The girth of G is the length of a shortest cycle in G if exists, otherwise it is infinite. The terms which are not defined here can be found in [3].

A subset S of V is called a dominating set of G if every vertex in $V-S$ is adjacent to at least one vertex in S . The domination number $\gamma(G)$ of G is the minimum number of vertices in a dominating set G . Various types of dominating set and domination number have been introduced and studied by several authors [1], [4], [5], [6], [7], [8], [9], [10], [11], [12], [13] and [16]. Many graph theoretic parameters such as χ , α , β etc. have been compared and combined with $\gamma(G)$. Paulraj Joseph and Arumugam discussed the relationship between domination number and connectivity in [14], as well as domination number and chromatic number in [15].

T. Tamizhchelvam and B. Jayaprasad [17] have introduced the complementary connected domination number. A subset S of V is said to be a complementary connected dominating set (ccd-set) of G if S is a dominating set and $\langle V-S \rangle$ is connected. The minimum cardinality of S is called the complementary connected domination number and is denoted by γ_{cc} .

For example, the graph H_1 shown in Figure 1, has $\gamma_{cc} = 3$. Here $S = \{v_2, v_4, v_7\}$ is a γ_{cc} -set of H_1 . For the graph H_2 shown in Figure 1, $\gamma_{cc} = 4$ and $S = \{v_1, v_2, v_3, v_6\}$ is a γ_{cc} -set of H_2 .

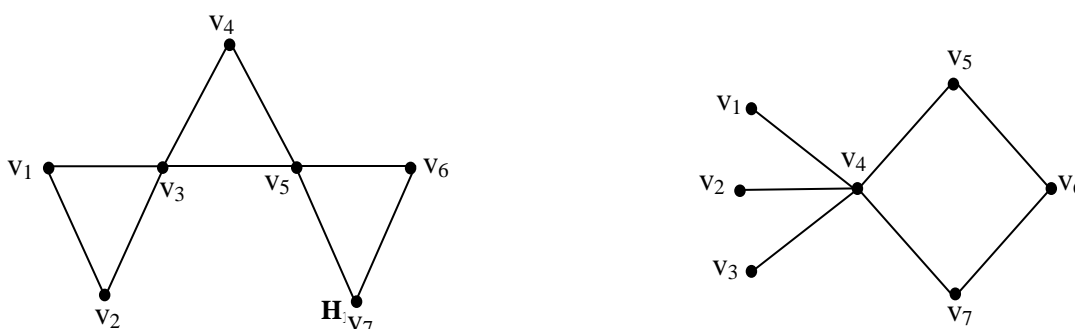
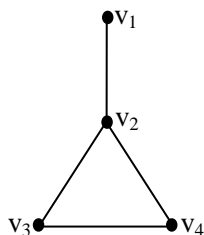


Figure 1

Note that a graph may have more than one γ_{cc} -set. For example, $S_1 = \{v_1, v_4, v_6\}$ is also a γ_{cc} -set of H_1 . In [17], the following results have been obtained:

1. For $n > 3$, $\gamma_{cc}(P_n) = n - 2$.
 2. For $n \geq 3$, $\gamma_{cc}(C_n) = n - 2$.
 3. For $n \geq 1$, $\gamma_{cc}(K_{1, m}) = m$.
 4. For any graph G , $\gamma(G) \leq \gamma_{cc}(G)$ and the inequality is strict.
- For example, consider the graph G shown in Figure 2. Here $\gamma(G) = 1$ where as $\gamma_{cc}(G) = 2$.



G
Figure 2

In fact, we can easily note that for any integer $i \geq 0$, there exists a graph G with $\gamma_{cc}(G) - \gamma(G) = i$.

5. If P_k ($k \geq 4$) is a subgraph of the graph G , then $\gamma_{cc}(G) \leq n - 2$.

6. Let G be a graph with $n \geq 3$. Then there exists a γ_{cc} -set S of G which contains all pendant vertices of G .

7. If $\gamma_{cc}(G) \leq n - 2$, then any γ_{cc} -set S of G contains all pendant vertices of G .

8. For any connected graph G with n vertices and m edges, $\left\lceil \frac{n}{\Delta + 1} \right\rceil \leq \gamma_{cc} \leq 2m - n + 1$.

Let $P_k(m_1, m_2)$ where $k \geq 2$ and $m_1, m_2 \geq 1$ be the graph obtained by identifying the centers of the stars K_{1,m_1} and K_{1,m_2} at the ends of a path P_k respectively. The graph $C_3(m_1, m_2, 0)$ is obtained from C_3 by identifying the centers of the stars K_{1,m_1} and K_{1,m_2} at any two vertices of C_3 respectively.

For example, the graphs $P_4(3, 2)$ and $C_3(4, 1, 0)$ are shown in Figure 3.

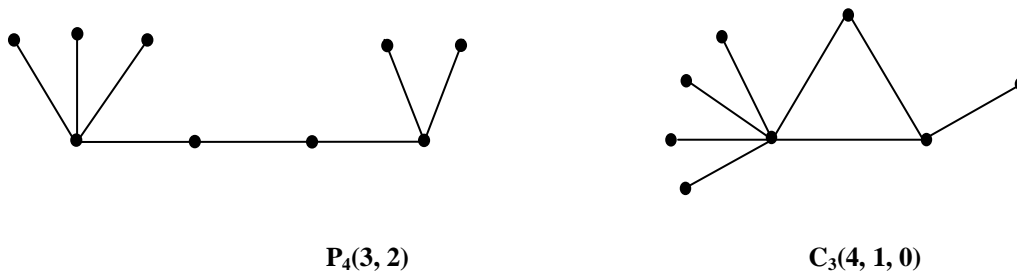


Figure 3

In [2], S. Avadayappan and C.S. Senthilkumar have characterized the graphs with $\gamma_{cc} = n - 2$. More precisely, they have proved that for any graph G , $\gamma_{cc}(G) = n - 2$ if and only if G is isomorphic to any one of the following graphs: (i) $P_k(m_1, m_2)$ where $k \geq 2$, $m_1, m_2 \geq 1$, (ii) C_n , $n \geq 3$, and (iii) $C_3(m_1, m_2, 0)$ where $m_1, m_2 \geq 0$.

II. Complementary Connected Domination Number

In this section, we characterize the graphs with $\gamma_{cc} = \chi = 2$ and hence the r -regular graphs with $\gamma_{cc} = \chi = 2$. Let G be a bipartite graph with bipartition (X, Y) where $X = \{u_1, u_2, \dots, u_m\}$ and $Y = \{v_1, v_2, \dots, v_n\}$. Then $G_{u,v}$ is the graph obtained from G by adding two new vertices u and v and the new edges $uv_i, 1 \leq i \leq n; vu_j, 1 \leq j \leq m$. Take $G_{u,v}^* = G_{u,v} + uv$.

It is clear that $G_{u,v}$ and $G_{u,v}^*$ are bipartite graphs.

For example, the graph G and the corresponding graphs $G_{u,v}$ and $G_{u,v}^*$ are shown in Figure 4.

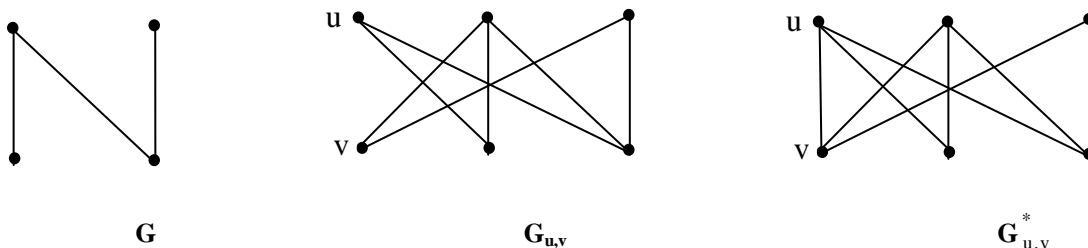


Figure 4

It is easy to note that for the graphs $G_{u,v}$ and $G_{u,v}^*$, $\gamma_{cc} = 2$. In fact, the converse is also true which is proved in the next theorem.

Theorem 1 Let G be a graph. Then $\gamma_{cc} = \chi = 2$ if and only if $G \cong H_{u,v}$ or $H_{u,v}^*$ for some connected bipartite graph H .

Proof Suppose $\gamma_{cc} = \chi = 2$. Then G is a bipartite graph with bipartition, say, (X, Y) . Let $S = \{u, v\}$ be a γ_{cc} -set. Then clearly both u and v cannot be in the same partition. Now, consider the bipartite graph $H = G - S$. If u and v are not adjacent in G , then $G \cong H_{u,v}$. Otherwise, $G \cong H_{u,v}^*$. The converse part is obvious. Hence the theorem. ■

The next theorem shows that there are only two r -regular graphs for which $\gamma_{cc} = \chi = 2$.

Theorem 2 Let G be an r -regular graph. Then $\gamma_{cc} = \chi = 2$ if and only if $G \cong K_{r,r}$ or $K_{r+1,r+1}-F$.

Proof Let G be an r -regular graph on n vertices with $\gamma_{cc} = \chi = 2$.

Then $2 = \gamma_{cc} \geq \left\lceil \frac{n}{\Delta+1} \right\rceil = \left\lceil \frac{n}{r+1} \right\rceil$. This implies $n \leq 2r + 2$. But $\chi = 2$ and hence G is a bipartite graph with bipartition (X, Y) .

Since G is r -regular, $|X| = |Y|$ and thus $n = 2r$ or $2r + 2$. If $n = 2r$, then clearly $G \cong K_{r,r}$. If $n = 2r + 2$, then $|X| = |Y| = r + 1$ and so each vertex in X is not adjacent to exactly one vertex in Y and vice versa. Thus $G \cong K_{r+1,r+1} - F$. The converse part is trivial. ■

2. 2 - REGULAR AND 3 - REGULAR GRAPHS

Let G be a connected 2-regular graph. Then clearly G is a cycle. Moreover, for even cycles $\chi = 2$ where as for odd cycles, $\chi = 3$. Hence for cycles if $\gamma_{cc} = \chi$ then $\gamma_{cc} = 2$ or 3. But we have $\gamma_{cc}(C_n) = n - 2$, for $n \geq 3$. If $\gamma_{cc}(C_n) = 2$, then $n = 4$ and so $G \cong C_4$ and if $\gamma_{cc}(C_n) = 3$, then $G \cong C_5$. Thus, $G \cong C_4$ or C_5 . Therefore, we can conclude that C_4 and C_5 are the only connected 2-regular graphs for which $\gamma_{cc} = \chi$. Next, we characterize the 3-regular graphs for which $\gamma_{cc} = \chi = 3$. To attain this we need Lemma 1.

Lemma 1 Let G be an r -regular graph on $2r + 2$ vertices. If $\gamma_{cc}(G) = 2$, then there exist two non adjacent vertices u and v such that $N(u) \cap N(v) = \emptyset$.

Proof Let G be an r -regular graph on $2r+2$ vertices. Suppose $\gamma_{cc}(G) = 2$. Let $S = \{u, v\}$ be a γ_{cc} -set. Then $V(G) = N[u] \cup N[v]$. If u and v are adjacent, then $|N[u] \cup N[v]| \leq 2r$, which is a contradiction. Thus u and v are not adjacent. If $N(u) \cap N(v) \neq \emptyset$, then we get $|N[u] \cup N[v]| \leq 2r+1$, a contradiction. Hence, $N(u) \cap N(v) = \emptyset$. Thus there are two non adjacent vertices u and v such that $N(u) \cap N(v) = \emptyset$. Hence the theorem. ■

Lemma 2 There does not exist a 3-regular graph on 6 vertices with $\gamma_{cc}(G) = \chi(G) = 3$.

Proof Let G be a 3-regular graph on 6 vertices with $\gamma_{cc} = \chi = 3$. Then the girth of G is 3 or 4. If it is 3, then $G \cong C_3 \times P_2$. Otherwise, $G \cong K_{3,3}$. But $\gamma_{cc}(C_3 \times P_2) = \gamma_{cc}(K_{3,3}) = 2$, which is a contradiction. ■
 For further discussion, we need a list of graphs shown in Figure 5.

Lemma 3 Let G be a 3-regular graph on 8 vertices. Then $\gamma_{cc}(G) = \chi(G) = 3$ if and only if $G \cong G_1$ or G_2 .

Proof Let G be a 3-regular graph on 8 vertices with $\gamma_{cc} = \chi = 3$. Then G has 12 edges. Let v_1, v_2, \dots, v_8 be the vertices of G and let $S = \{v_6, v_7, v_8\}$ be a γ_{cc} -set. Take $V_s = V - S$. Since S is a γ_{cc} -set, $\langle V_s \rangle$ is connected. Also $\Delta(V_s) = 2$ and hence $\langle V_s \rangle$ is either P_5 or C_5 .

Case (i) If $\langle V_s \rangle$ is isomorphic to C_5 , then $|E(V_s, S)| = 5$. This implies that $\langle S \rangle$ has 2 edges and 3 vertices. Therefore, $\langle S \rangle = P_3 = v_6v_7v_8$. Without loss of generality, we can assume that v_7 is adjacent to v_1 . If $N(v_6) = \{v_4, v_5, v_7\}$, then $N(v_8) = \{v_2, v_3, v_7\}$ and the resultant graph has $\gamma_{cc} = 2$ with $S = \{v_5, v_8\}$, a contradiction. When the neighbours of v_6 are $\{v_3, v_5, v_7\}$ (or $\{v_2, v_5, v_7\}$), we get the graph G_2 (or G_1).

Case (ii) $\langle V_s \rangle \cong P_5$. In this case $|E(V_s, S)| = 7$. Thus, $\langle S \rangle$ has only one edge. That is, $\langle S \rangle = P_2 \cup K_1$. Without loss of generality, we can assume that v_8 is the isolated vertex in $\langle S \rangle$. Then it is enough to deal the case in which $N(v_6)$ and $N(v_8)$ have a common neighbour or the case in which $N(v_7)$ and $N(v_8)$ have a common neighbour. In the remaining cases, by Lemma 1, we get $\gamma_{cc} = 2$, which is impossible.

Suppose the neighbours of v_8 are $\{v_1, v_2, v_5\}$. When $N(v_7) = \{v_1, v_3, v_6\}$, the given graph has $\gamma_{cc} = 2$ with $S = \{v_2, v_6\}$ which is impossible. And the graph G_1 is obtained when the neighbours of v_7 are $\{v_1, v_4, v_6\}$. On the other side, let $\{v_1, v_3, v_5\}$ be the neighbours of v_8 . If $N(v_7) = \{v_1, v_2, v_6\}$, then $N(v_6) = \{v_4, v_5, v_7\}$. Here $\{v_1, v_4\}$ is a ccd set, a contradiction. If $N(v_7) = \{v_1, v_4, v_6\}$, then the resultant graph is G_2 .

Conversely, since for $i = 1, 2$, $\text{rad}(G_i) = \text{diam}(G_i) = 2$, any two non adjacent vertices have a common neighbour and thus $\gamma_{cc} \neq 2$. Also it is easy to see that $\gamma_{cc}(G_1) = \gamma_{cc}(G_2) = 3$. In addition, it is clear that $\chi(G_1) = \chi(G_2) = 3$. This completes the lemma. ■

Lemma 4 Let G be a 3 - regular graph on 10 vertices. Then $\gamma_{cc}(G) = \chi(G) = 3$ if and only if $G \cong G_i$, $3 \leq i \leq 17$.

Proof Let G be a 3-regular graph on 10 vertices for which $\gamma_{cc}(G) = \chi(G) = 3$. Then G contains 15 edges. Let v_i , $1 \leq i \leq 10$ be the vertices of G and let $S = \{v_8, v_9, v_{10}\}$ be a γ_{cc} - set. Since G is 3-regular and by the definition of a γ_{cc} - set, every vertex in $\langle V_S \rangle$ has degree 1 or 2. Hence $\langle V_S \rangle$ is isomorphic to C_7 or P_7 .

Case (i) $\langle V_S \rangle \cong C_7$.

Since G is 3-regular, $|E(V_S, S)| = 7$. Then $\langle S \rangle$ contains only one edge as G has 15 edges. Thus $\langle S \rangle = P_2 \cup K_1$ in which v_{10} is the isolated vertex.

Let the three consecutive vertices of C_7 , say, v_1, v_2, v_3 be the neighbours of v_{10} . Now, the vertex v_4 belongs to either v_9 or v_8 . Without loss of generality, take $v_4 \in N(v_9)$. If $N(v_9) = \{v_4, v_5, v_8\}$, then $N(v_8) = \{v_6, v_7, v_9\}$ and the resultant graph is G_9 . When the neighbours of v_9 are $\{v_4, v_6, v_8\}$ (or $\{v_4, v_7, v_8\}$), we get the graph G_{16} (or G_6). In a similar way, we can deal the case when $v_4 \in N(v_{10})$.

Let $N(v_{10}) = \{v_1, v_2, v_4\}$ and let $v_3 \in N(v_9)$. If we take the neighbours of v_9 as $\{v_3, v_5, v_8\}$, $\{v_3, v_6, v_8\}$ or $\{v_3, v_7, v_8\}$, then we get the graphs G_3 , G_5 and G_7 respectively.

Let $N(v_{10}) = \{v_1, v_2, v_5\}$. Without loss of generality, let $v_3 \in N(v_9)$. Then the neighbours of v_9 are $\{v_3, v_4, v_8\}$, $\{v_3, v_6, v_8\}$ or $\{v_3, v_7, v_8\}$ and so we get the graphs respectively G_{12} , G_5 and G_4 .

Let $N(v_{10}) = \{v_1, v_3, v_5\}$. Take $v_3 \in N(v_9)$. If $N(v_9)$ are $\{v_2, v_4, v_8\}$, $\{v_2, v_6, v_8\}$ or $\{v_4, v_6, v_9\}$, then we get the graphs G_4 , G_{10} and G_{14} respectively.

Case (ii) $\langle V_S \rangle \cong P_7$.

Since G is 3-regular, $|E(V_S, S)| = 9$. Thus $\langle S \rangle$ has no edge, that is $\langle S \rangle \cong K_3^c$.

Let $N(v_{10}) = \{v_1, v_2, v_3\}$. Then $N(v_7) = \{v_6, v_8, v_9\}$. Without loss of generality, we can take $v_1 \in N(v_9)$. One can easily check that if the neighbours of v_9 are $\{v_1, v_4, v_7\}$, $\{v_1, v_5, v_7\}$ or $\{v_4, v_6, v_7\}$, the corresponding graphs are isomorphic to G_8 , G_6 and G_9 respectively.

Now, we consider the three consecutive internal vertices in P_7 are adjacent to a vertex, say v_{10} in $\langle S \rangle$. That is $N(v_{10}) = \{v_2, v_3, v_4\}$. This implies that $N(v_1) = \{v_2, v_8, v_9\}$ and $N(v_8) = \{v_1, v_6, v_7\}$. And the only possibility is that $N(v_9) = \{v_1, v_5, v_7\}$. In this case, we get the graph isomorphic to G_6 .

Take $N(v_{10}) = \{v_1, v_2, v_4\}$. If the neighbours of v_9 are $\{v_1, v_5, v_7\}$ (or $\{v_1, v_6, v_7\}$), then we get the graph isomorphic to G_7 (or G_3). The remaining possibilities are already discussed in the earlier cases.

Now, consider $N(v_{10}) = \{v_2, v_3, v_5\}$. This forces that $N(v_1) = \{v_2, v_8, v_9\}$ and $N(v_7) = \{v_6, v_8, v_9\}$. The only possibility is that $N(v_9) = \{v_1, v_4, v_7\}$, and the resultant graph is isomorphic to G_7 .

Let $N(v_{10}) = \{v_3, v_4, v_6\}$. This implies that $N(v_1) = \{v_2, v_8, v_9\}$ and $N(v_7) = \{v_4, v_8, v_9\}$. Then $N(v_9) = \{v_1, v_2, v_7\}$ and the resultant graph is isomorphic to G_3 .

Let $N(v_{10}) = \{v_4, v_5, v_7\}$. By leaving the repeated cases, we get the graph G_7 when the neighbours of v_9 are $\{v_1, v_2, v_6\}$ or $\{v_1, v_2, v_7\}$.

Suppose, $N(v_{10}) = \{v_1, v_2, v_5\}$. This implies that $N(v_1) = \{v_6, v_8, v_9\}$. When the neighbours of v_9 are $\{v_1, v_4, v_7\}$ or $\{v_1, v_6, v_7\}$, we get the graph isomorphic to G_{13} or G_{12} . The remaining cases have been dealt already.

Let $N(v_{10}) = \{v_2, v_3, v_6\}$. This forces that $N(v_1) = \{v_2, v_8, v_9\}$ and $N(v_7) = \{v_6, v_8, v_9\}$. The only possibility is $N(v_9) = \{v_1, v_4, v_7\}$ and so we get the resultant graph isomorphic to G_5 .

Let $N(v_{10}) = \{v_3, v_4, v_7\}$. This gives $N(v_1) = \{v_2, v_8, v_9\}$. By omitting the repeated cases, we get the graphs isomorphic to G_{12} and G_{17} , when the neighbours of v_9 are $\{v_1, v_2, v_5\}$ (or $\{v_1, v_2, v_7\}$) and $\{v_1, v_2, v_6\}$ respectively.

Let $N(v_{10}) = \{v_1, v_2, v_6\}$ which implies that $N(v_7) = \{v_6, v_8, v_9\}$. The only case is that if $N(v_9) = \{v_1, v_4, v_7\}$, then we get the graph isomorphic to G_5 .

Let $N(v_{10}) = \{v_2, v_3, v_7\}$. This forces that $N(v_1) = \{v_2, v_8, v_9\}$. If $N(v_9) = \{v_1, v_4, v_6\}$ (or $\{v_1, v_4, v_7\}$), then the corresponding resultant graph is isomorphic to G_5 (or G_{13}).

Let $N(v_{10}) = \{v_1, v_2, v_7\}$. The only possibility is that $N(v_9) = \{v_1, v_4, v_6\}$, and so the resultant graph is isomorphic to G_4 .

Suppose $N(v_{10}) = \{v_2, v_4, v_6\}$. This implies that $N(v_1) = \{v_2, v_8, v_9\}$ and $N(v_7) = \{v_6, v_8, v_9\}$. The only case left is that $N(v_9) = \{v_1, v_3, v_7\}$ and $N(v_8) = \{v_1, v_5, v_7\}$. In this case, we get $\chi = 2$, a contradiction.

Let the neighbours of v_{10} be $\{v_1, v_3, v_6\}$. This forces that $N(v_7) = \{v_6, v_8, v_9\}$. By leaving the repeated possibilities, we get the isomorphic graphs G_{11} or G_{10} , when $N(v_9) = \{v_1, v_4, v_7\}$ or $\{v_1, v_5, v_7\}$ respectively.

Let $N(v_{10}) = \{v_2, v_4, v_7\}$. Then $N(v_7) = \{v_2, v_8, v_9\}$ and hence $N(v_9) = \{v_1, v_3, v_6\}$. Then we get the graph isomorphic to G_{10} .

Conversely, suppose $\gamma_{cc} = 2$ and let $\{v_i, v_s\}$ be a γ_{cc} - set. Then, $|N(v_i) \cup N(v_s)| \leq 8$ a contradiction, since G has 10 vertices. Thus $\gamma_{cc} \neq 2$. Also it is clear that $\gamma_{cc}(G_i) = 3$, for all $3 \leq i \leq 17$. Moreover, one can easily verify that $\chi(G_i) = 3$, for all i , $3 \leq i \leq 17$.

Hence the lemma ■

Lemma 5 Let G be a 3-regular graph on 12 vertices. Then $\gamma_{cc}(G) = \chi(G) = 3$ if and only if $G \cong G_i$, $18 \leq i \leq 42$.

Proof Let G be a 3-regular graph on 12 vertices for which $\gamma_{cc}(G) = \chi(G) = 3$. Then G contains 18 edges. Let $\{v_i / i = 1, 2, \dots, 12\}$ be the vertex set of G and let $S = \{v_{10}, v_{11}, v_{12}\}$ be a γ_{cc} -set. Since G is 3-regular and since S is a dominating set, every vertex in $\langle V_S \rangle$ is of degree 1 or 2. Therefore $\langle V_S \rangle$ is isomorphic to P_9 or C_9 . If $\langle V_S \rangle \cong P_9$, then $|E(V_S, S)| = 11$, which is impossible as G contains 18 edges. This forces that $\langle V_S \rangle \cong C_9$. In this case, $|E(V_S, S)| = 9$ which means that $\langle S \rangle$ contains no edge. That is, $\langle S \rangle$ is isomorphic to K_3^c .

Case (i) let the neighbours of v_{12} be three consecutive vertices of C_9 say, v_1, v_2, v_3 . Now, the vertex v_4 belongs to either $N(v_{10})$ or $N(v_{11})$. Without loss of generality, we can assume that $v_4 \in N(v_{11})$. If $N(v_{11}) = \{v_4, v_5, v_6\}$, then $N(v_{10}) = \{v_7, v_8, v_9\}$ which gives the graph isomorphic to G_{38} . In a similar way, one can easily check that if the neighbours of v_{11} are $\{v_4, v_5, v_7\}$, $\{v_4, v_5, v_8\}$ (or $\{v_4, v_6, v_7\}$), $\{v_4, v_5, v_9\}$ (or $\{v_4, v_8, v_9\}$), $\{v_4, v_6, v_8\}$, $\{v_4, v_6, v_9\}$ (or $\{v_4, v_7, v_9\}$) and $\{v_4, v_7, v_8\}$ the corresponding graphs are isomorphic to $G_{26}, G_{35}, G_{25}, G_{29}, G_{30}$ and G_{39} respectively.

Case(ii) Let $\{v_1, v_2, v_4\}$ be the neighbours of v_{12} and let $v_3 \in N(v_{11})$. Then we get the graphs isomorphic to $G_{27}, G_{22}, G_{23}, G_{28}, G_{19}$ and G_{36} when we take the neighbours of v_{11} as $\{v_3, v_5, v_7\}$, $\{v_3, v_5, v_8\}$, $\{v_3, v_6, v_7\}$, $\{v_3, v_6, v_8\}$, $\{v_3, v_6, v_9\}$ and $\{v_3, v_7, v_8\}$ respectively. The case when $v_3 \in N(v_{10})$ follows in a similar manner. By case(i), we can omit the remaining cases in which one of the vertices of v_{11} and v_{10} have the three consecutive neighbours.

Case(iii) Let $N(v_{12}) = \{v_1, v_2, v_5\}$. Without loss of generality, assume that $v_3 \in N(v_{11})$. Then the neighbours of v_{11} can be $\{v_3, v_6, v_7\}$, $\{v_3, v_6, v_8\}$, $\{v_3, v_6, v_9\}$, $\{v_3, v_7, v_8\}$ or $\{v_3, v_7, v_9\}$. The corresponding graphs are isomorphic to $G_{31}, G_{24}, G_{20}, G_{33}$ and G_{32} respectively.

Case(iv) Let $N(v_{12}) = \{v_1, v_2, v_6\}$. Let $N(v_{11})$ contain v_3 . Then the neighbours of v_{11} are $\{v_3, v_4, v_8\}$, $\{v_3, v_5, v_8\}$ or $\{v_3, v_7, v_8\}$. Thus the graphs are G_{34}, G_{41} or G_{40} respectively.

Case(v) Suppose $N(v_{12}) = \{v_1, v_3, v_5\}$. Without loss of generality, let v_2 belong to $N(v_{11})$. Then we get the isomorphic graphs G_{37} and G_{42} respective to the neighbours of v_{11} which are $\{v_2, v_6, v_8\}$ and $\{v_2, v_7, v_9\}$.

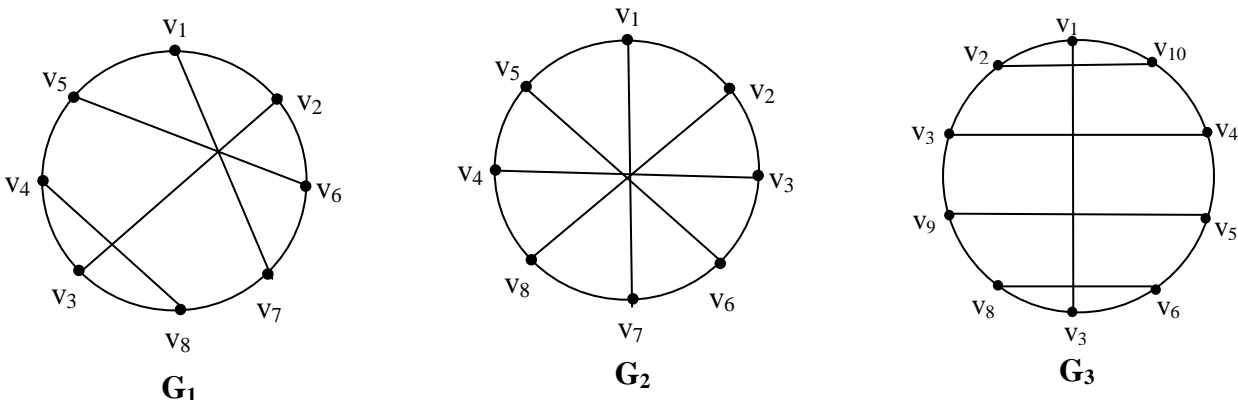
Case(vi) Let $N(v_{12}) = \{v_1, v_3, v_6\}$. Then the neighbours of v_{11} are $\{v_2, v_5, v_8\}$ and so we get the graph isomorphic to G_{21} . The remaining possibilities have been dealt in the earlier cases.

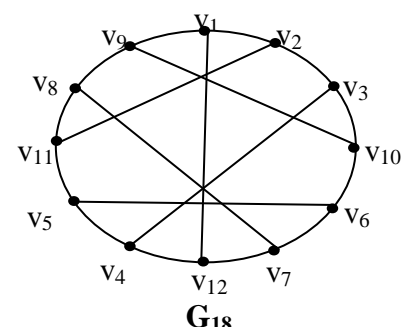
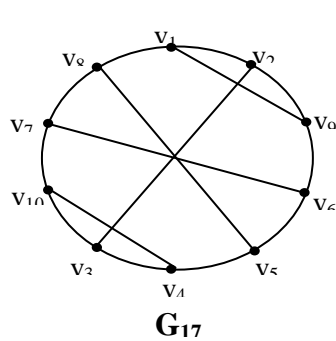
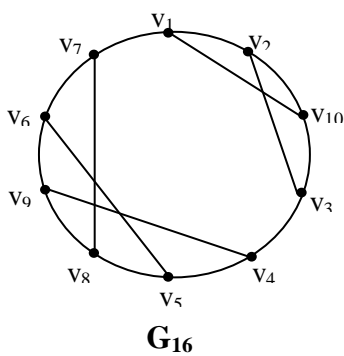
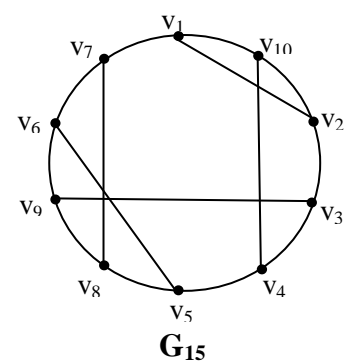
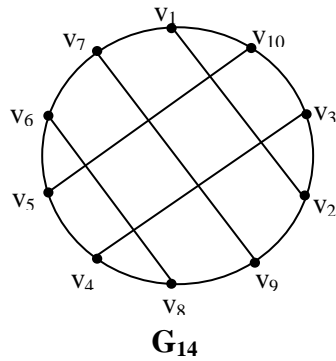
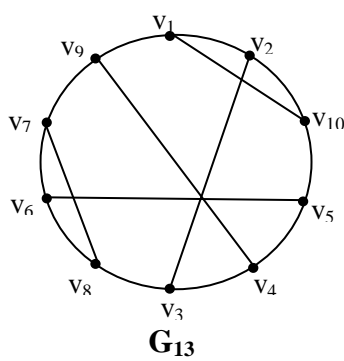
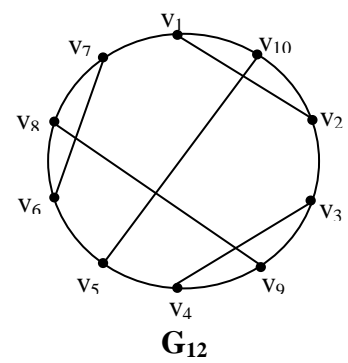
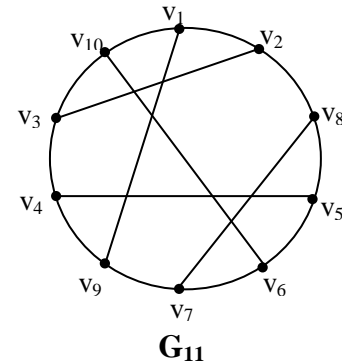
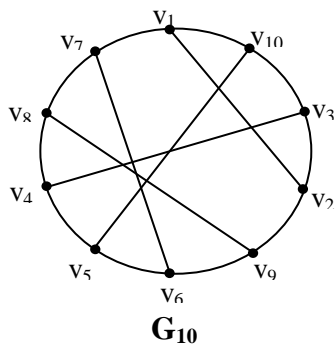
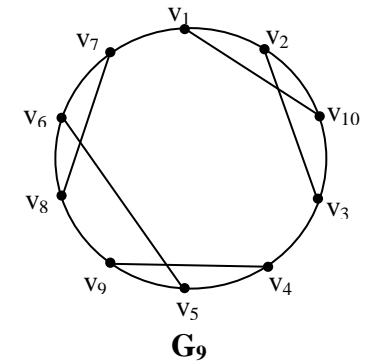
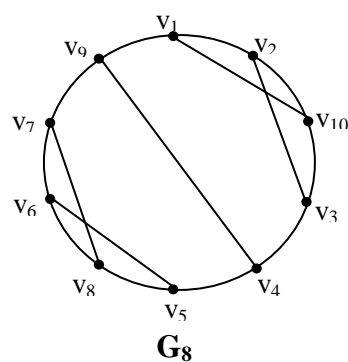
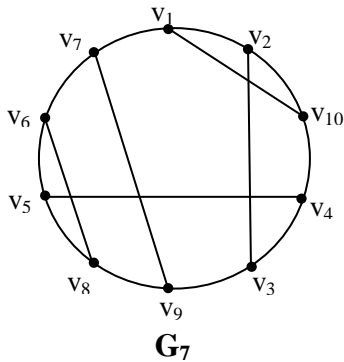
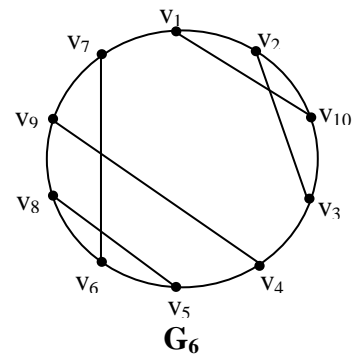
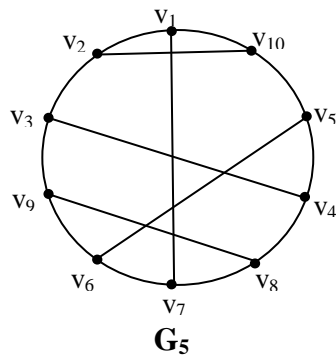
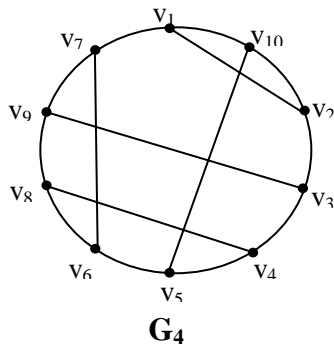
Case(vii) Let the neighbours of v_{12} be $\{v_1, v_4, v_7\}$. By leaving the repeated possibilities, we get the only case that $N(v_{11}) = \{v_2, v_5, v_8\}$. Then the resultant graph is isomorphic to G_{18} .

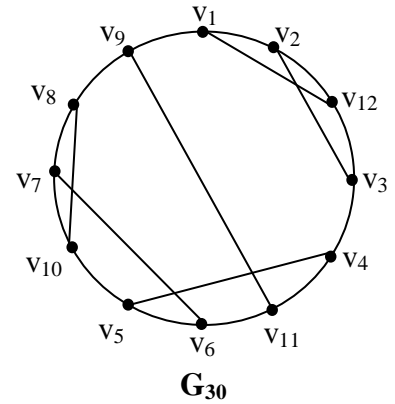
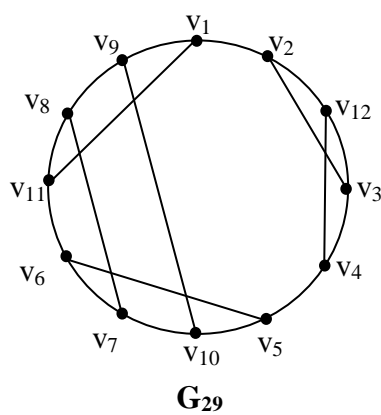
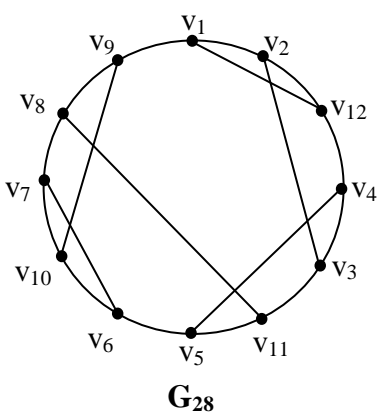
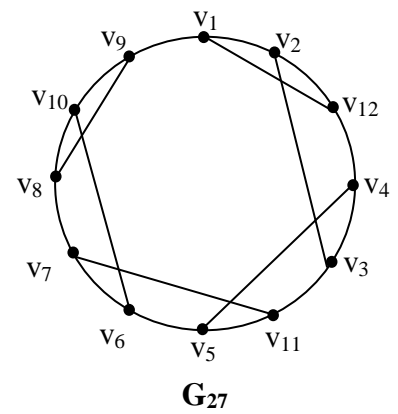
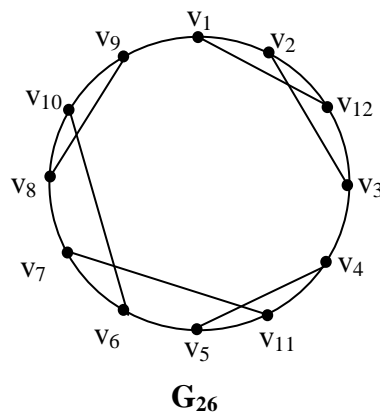
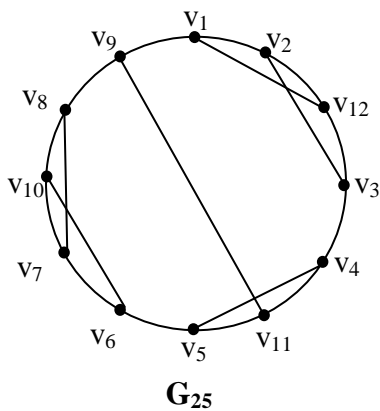
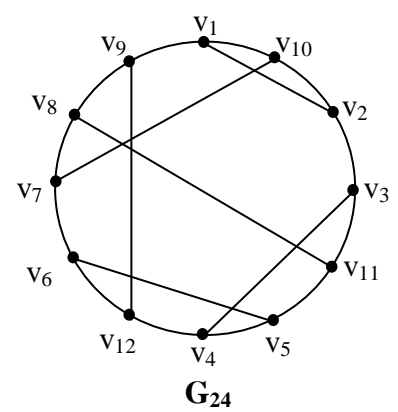
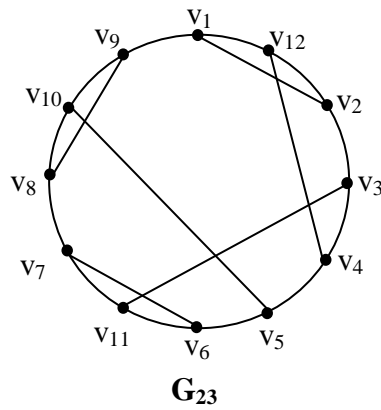
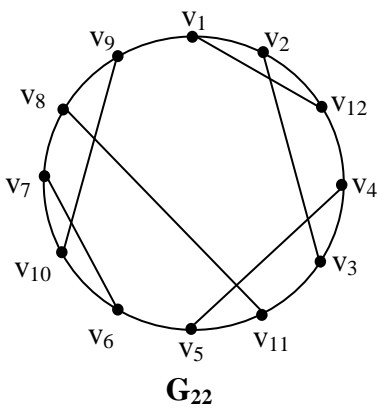
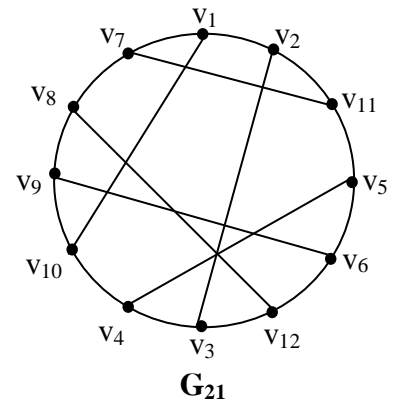
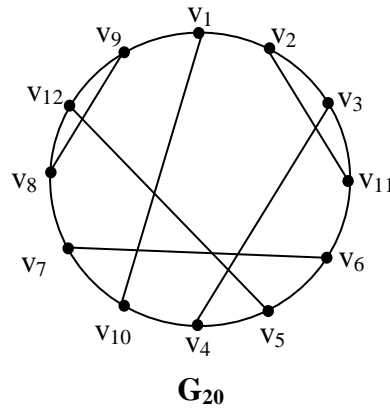
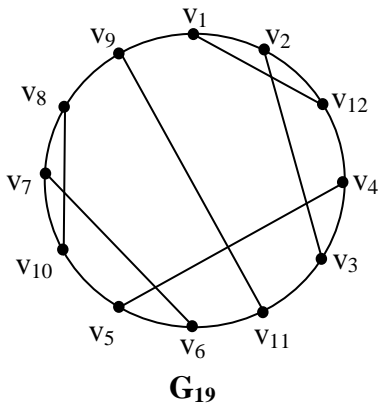
Conversely, it is easy to verify that each G_i has a ccd-set with three elements and so $\gamma_{cc}(G_i) \leq 3$. In addition, each G_i is a 3-regular graph on 12 vertices. Therefore $\gamma_{cc}(G_i) \geq \left\lceil \frac{n}{\Delta + 1} \right\rceil = 3$. This means that $\gamma_{cc}(G_i) = 3$, for all i , $18 \leq i \leq 42$. Also, one can easily check that $\chi(G_i) = 3$, for all i , $18 \leq i \leq 42$. Hence $\gamma_{cc}(G_i) = \chi(G_i) = 3$, for all i , $18 \leq i \leq 42$. Thus the converse follows. ■

Theorem 3 Let G be a 3-regular graph. Then $\gamma_{cc} = \chi = 3$ if and only if $G \cong G_i$, for $1 \leq i \leq 42$.

Proof Let G be any one of the above 42 graphs. Then it can be easily verified that $\gamma_{cc} = \chi = 3$. Conversely, we know that $3 = \gamma_{cc} \geq \left\lceil \frac{n}{\Delta + 1} \right\rceil = \left\lceil \frac{n}{4} \right\rceil$. This implies that $n \leq 12$. Since G is 3-regular, $n = 6, 8, 10$ and 12 . Now the result follows from the Lemmas 2, 3, 4 and 5.







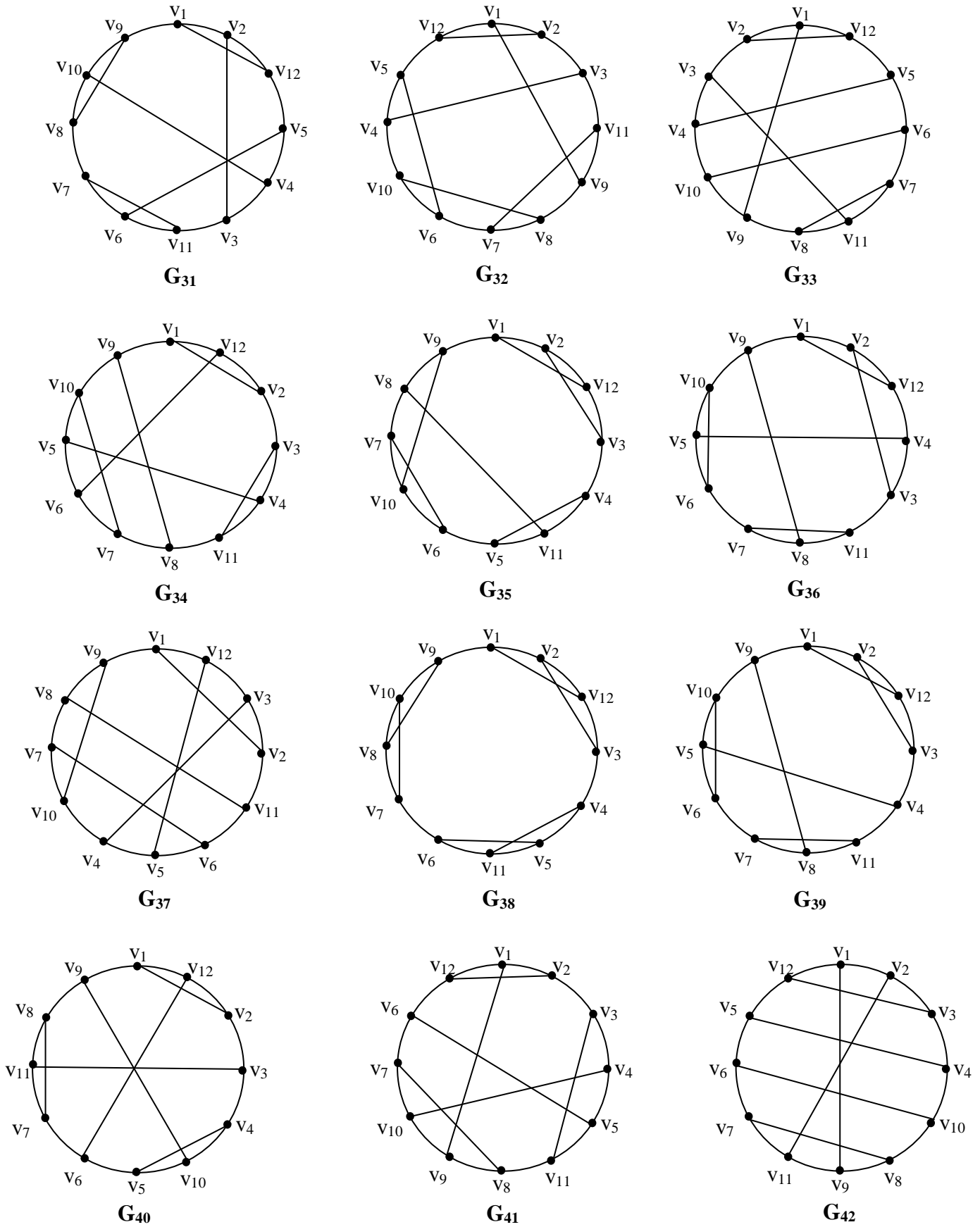


Figure 5

REFERENCES

- [1] Arumugam. S, ThuraiSwamy, *Total domination in graphs*, Ars Combinatoria, 43(1996), 89-92.
- [2] Selvam Avadayappan and C. S. Senthilkumar, *Characterisation of graphs on domination parameters*, Ars Combinatoria, 103(2012), 423-431.
- [3] R. Balakrishnan and K. Renganathan, *A text book of graph theory*, Springer-verlag, New York, Inc (1999).
- [4] E. J. Cockayne and S. T. Hedetniemi, *towards a theory of domination in graphs*, Networks 7 (1997), 247-261.
- [5] Teresa W. Haynes, *Paired domination in graphs*, Congr. Numer 150 (2001).
- [6] Mahadevan G, Selvam Avadayappan, Mydeen bibi A., *Double Domination Number and Chromatic Number of a Graph*, Narosa Publication, (2007), 182-190.
- [7] Mahadevan G, Selvam Avadayappan, Mydeen bibi A., *Cubic Graphs with Equal Two Domination Number and Chromatic Number*, International Journal Information Technology and Knowledge Management, ISSN 0973-4414, Vol.4, No. 2 (2011), 379-383.
- [8] Mahadevan G, Selvam Avadayappan, Mydeen bibi A., *Characterization of Two Domination Number and Chromatic Number of a Graph*, International Journal of Computational Science and Mathematics, ISSN 0974-3189, Vol 3, No 2 (2011), 245-254.
- [9] Mahadevan G, Selvam Avadayappan, Mydeen bibi A., *Extended Results on Two Domination Number and Chromatic Number of a Graph*, International Journal of Mathematics and Soft Computing, ISSN 2249-3328 Vol.1, No.1 (2011), 47-57.
- [10] Mahadevan G, Selvam A, Hajmeeral M, *On efficient domination number and chromatic number of a graph I* , International Journal of Physical Sciences, Vol 21(1)M, (2009), 1-8.
- [11] Mahadevan G, Selvam Avadayappan. A and Hajmeeral M, *Further results on dom strong domination number of the graph*, International Journal of Algorithms, Computing and Mathematics, Vol 3, No 1, (2010), 23-30.
- [12] Mahadevan G, Selvam Avadayappan. A and Hajmeeral.M and Latha Venkateswari.U, *Further characterization of connected efficient domination number of a graph*, International Journal of Combinatorial Graph theory and applications, Vol 3, No 1, Jan-Jun 2010, 29-39.
- [13] Teresa W. Haynes, Stephen T. Hedetniemi and Peter J. Slater, *Fundamentals of domination in graphs*, Marcel deckker, New York (1998).
- [14] J. Paulraj Joseph and S. Arumugam, *Domination and connectivity in graphs*, International Journal of Management and Systems Vol 8 No. 3 (1992), 233-236.
- [15] J. Paulraj Joseph and S. Arumugam, *Domination and colouring in graphs*, International Journal of Management and Systems 11 (1999), 177-182.
- [16] J. Paulraj Joseph, Selvam Avadayappan and G. Mahadevan, *Induced complementary perfect dominating number of a graph*, Mathematical and Computational Models, Dec (2005) 425-435.
- [17] T. Tamizh Chelvam and B. Jaya Prasad, *Complementary connected domination number of a graph*, International Journal of Management and Systems 18 (2002), No. 22, 147-153.

On The Number of Zeros of a Polynomial inside the Unit Disk

M. H. Gulzar

Department of Mathematics University of Kashmir, Srinagar 190006

Abstract: In this paper we find an upper bound for the number of zeros of a polynomial inside the unit disk, when the coefficients of the polynomial or their real and imaginary parts are restricted to certain conditions.

Mathematics Subject Classification: 30C10, 30C15

Key-words and phrases: Polynomial, Unit disk, Zero.

I. Introduction and Statement of Results

Regarding the number of zeros of a polynomial inside the unit disk, the following results were recently proved by M. H. Gulzar [2]:

Theorem A: Let $P(z) = \sum_{j=0}^n a_j z^j$ be a polynomial of degree n such that for some $\rho \geq 0$,

$$\rho + a_n \geq a_{n-1} \geq \dots \geq a_1 \geq a_0.$$

Then the number of zeros of $P(z)$ in $\frac{|a_0|}{M_1} \leq |z| \leq \delta, 0 < \delta < 1$ does not exceed

$$\frac{1}{\log \frac{1}{\delta}} \log \frac{2\rho + |a_n| + a_n + |a_0| - a_0}{|a_0|},$$

Where $M_1 = 2\rho + |a_n| + a_n - a_0$.

Theorem B: Let $P(z) = \sum_{j=0}^n a_j z^j$ be a polynomial of degree n with complex coefficients .If

$\text{Re } a_j = \alpha_j, \text{Im } a_j = \beta_j, j = 0, 1, \dots, n$, and for some $\rho \geq 0$,

$$\rho + \alpha_n \geq \alpha_{n-1} \geq \dots \geq \alpha_1 \geq \alpha_0,$$

then the number of zeros of $P(z)$ in $\frac{|a_0|}{M_2} \leq |z| \leq \delta, 0 < \delta < 1$, does not exceed

$$\frac{1}{\log \frac{1}{\delta}} \log \frac{2\rho + |\alpha_n| + \alpha_n + |\alpha_0| - \alpha_0 + 2 \sum_{j=0}^n |\beta_j|}{|a_0|},$$

Where $M_2 = 2\rho + |\alpha_n| + \alpha_n - \alpha_0 + |\beta_0| + 2 \sum_{j=1}^n |\beta_j|$.

Theorem C: Let $P(z) = \sum_{j=0}^n a_j z^j$ be a polynomial of degree n with complex coefficients .If

$\text{Re } a_j = \alpha_j, \text{Im } a_j = \beta_j, j = 0, 1, \dots, n$, and for some $\rho \geq 0$,

$$\rho + \beta_n \geq \beta_{n-1} \geq \dots \geq \beta_1 \geq \beta_0,$$

then the number of zeros of $P(z)$ in $\frac{|a_0|}{M_3} \leq |z| \leq \delta, 0 < \delta < 1$, does not exceed

$$\frac{1}{\log \frac{1}{\delta}} \log \frac{2\rho + |\beta_n| + \beta_n + |\beta_0| - \beta_0 + 2\sum_{j=0}^n |\alpha_j|}{|a_0|},$$

Where $M_3 = 2\rho + |\beta_n| + \beta_n - \beta_0 + |\alpha_0| + 2\sum_{j=1}^n |\alpha_j|$.

Theorem D. Let $P(z) = \sum_{j=0}^n a_j z^j$ be a polynomial of degree n with complex coefficients such that

$$|\arg a_j - \beta| \leq \alpha \leq \frac{\pi}{2}, j = 0, 1, \dots, n, \text{ for some real } \beta$$

and

$$|\rho + a_n| \geq |a_{n-1}| \geq \dots \geq |a_1| \geq |a_0|, \text{ for some } \rho \geq 0.$$

Then the number of zeros of $P(z)$ in $\frac{|a_0|}{M_4} \leq |z| \leq \delta, 0 < \delta < 1$, does not exceed

$$\frac{1}{\log \frac{1}{\delta}} \log \frac{(\rho + |a_n|)(\cos \alpha + \sin \alpha + 1) - |a_0|(\cos \alpha - \sin \alpha - 1) + 2 \sin \alpha \sum_{j=1}^{n-1} |a_j|}{|a_0|},$$

where

$$M_4 = (\rho + |a_n|)(\cos \alpha + \sin \alpha + 1) - |a_0|(\cos \alpha - \sin \alpha) + 2 \sin \alpha \sum_{j=1}^{n-1} |a_j|$$

In this paper, we prove certain generalizations of the above results. In fact, we prove the following :

Theorem 1: Let $P(z) = \sum_{j=0}^n a_j z^j$ be a polynomial of degree n with $\operatorname{Re}(a_j) = \alpha_j$ and $\operatorname{Im}(a_j) = \beta_j, j=0,1,2,\dots,n$. If

for some real numbers $\lambda, \rho \geq 0, 1 \leq k \leq n, \alpha_{n-k} \neq 0, \alpha_{n-k-1} > \alpha_{n-k}$,

$$\rho + \alpha_n \geq \alpha_{n-1} \geq \dots \alpha_{n-k+1} \geq \lambda \alpha_{n-k} \geq \alpha_{n-k-1} \geq \dots \geq \alpha_1 \geq \alpha_0,$$

then the number of zeros of $P(z)$ in $\frac{|a_0|}{M_5} \leq |z| \leq \delta, 0 < \delta < 1$, does not exceed

$$\frac{1}{\log \frac{1}{\delta}} \log \frac{2\rho + |\alpha_n| + \alpha_n + (\lambda - 1)\alpha_{n-k} + |\lambda - 1||\alpha_{n-k}| - \alpha_0 + |\alpha_0| + 2\sum_{j=0}^n |\beta_j|}{|a_0|},$$

where $M_5 = 2\rho + |\alpha_n| + \alpha_n + (\lambda - 1)\alpha_{n-k} + |\lambda - 1||\alpha_{n-k}| - \alpha_0 + |\beta_0| + 2\sum_{j=1}^n |\beta_j|$,

and if $\alpha_{n-k} > \alpha_{n-k+1}$, then the number of zeros of $P(z)$ in $\frac{|a_0|}{M_6} \leq |z| \leq \delta, 0 < \delta < 1$, does not exceed

$$\frac{1}{\log \frac{1}{\delta}} \log \frac{2\rho + |\alpha_n| + \alpha_n + (1 - \lambda)\alpha_{n-k} + |1 - \lambda||\alpha_{n-k}| - \alpha_0 + |\alpha_0| + 2\sum_{j=0}^n |\beta_j|}{|a_0|},$$

where $M_6 = 2\rho + |\alpha_n| + \alpha_n + (1 - \lambda)\alpha_{n-k} + |1 - \lambda||\alpha_{n-k}| - \alpha_0 + |\beta_0| + 2\sum_{j=1}^n |\beta_j|$.

Remark 1: Taking $\lambda = 1$, Theorem 1 reduces to Theorem B.

Remark 2: If a_j are real i.e. $\beta_j = 0$ for all j , Theorem 1 gives the following result which reduces to Theorem A by taking $\lambda = 1$:

Theorem 2: Let $P(z) = \sum_{j=0}^n a_j z^j$ be a polynomial of degree n . If for some real numbers $\lambda, \rho \geq 0$,

$$1 \leq k \leq n, a_{n-k} \neq 0, a_{n-k-1} > a_{n-k},$$

$$\rho + a_n \geq a_{n-1} \geq \dots \geq a_{n-k+1} \geq \lambda a_{n-k} \geq a_{n-k-1} \geq \dots \geq a_1 \geq a_0,$$

then the number of zeros of $P(z)$ in $\frac{|a_0|}{M_7} \leq |z| \leq \delta, 0 < \delta < 1$, does not exceed

$$\frac{1}{\log \frac{1}{\delta}} \log \frac{2\rho + |a_n| + a_n + (\lambda - 1)a_{n-k} + |\lambda - 1||a_{n-k}| - a_0 + |a_0|}{|a_0|},$$

where $M_7 = 2\rho + |a_n| + a_n + (\lambda - 1)a_{n-k} + |\lambda - 1||a_{n-k}| - a_0$,

and if $a_{n-k} > a_{n-k+1}$, then the number of zeros of $P(z)$ in $\frac{|a_0|}{M_8} \leq |z| \leq \delta, 0 < \delta < 1$, does not exceed

$$\frac{1}{\log \frac{1}{\delta}} \log \frac{2\rho + |a_n| + a_n + (1 - \lambda)a_{n-k} + |1 - \lambda||a_{n-k}| - a_0 + |a_0|}{|a_0|},$$

where $M_8 = 2\rho + |a_n| + a_n + (1 - \lambda)a_{n-k} + |1 - \lambda||a_{n-k}| - a_0$.

Applying Theorem 1 to the polynomial $-iP(z)$, we get the following result, which reduces to Theorem C by taking $\lambda = 1$:

Theorem 3: Let $P(z) = \sum_{j=0}^n a_j z^j$ be a polynomial of degree n with $\text{Re}(a_j) = \alpha_j$ and $\text{Im}(a_j) = \beta_j, j=0,1,2,\dots,n$. If

$$\text{for some real numbers } \lambda, \rho \geq 0, 1 \leq k \leq n, \beta_{n-k} \neq 0, \beta_{n-k-1} > \beta_{n-k},$$

$$\rho + \beta_n \geq \beta_{n-1} \geq \dots \geq \beta_{n-k+1} \geq \lambda \beta_{n-k} \geq \beta_{n-k-1} \geq \dots \geq \beta_1 \geq \beta_0,$$

then the number of zeros of $P(z)$ in $\frac{|a_0|}{M_9} \leq |z| \leq \delta, 0 < \delta < 1$, does not exceed

$$\frac{1}{\log \frac{1}{\delta}} \log \frac{2\rho + |\beta_n| + \beta_n + (\lambda - 1)\beta_{n-k} + |\lambda - 1||\beta_{n-k}| - \beta_0 + |\beta_0| + 2 \sum_{j=0}^n |\alpha_j|}{|a_0|},$$

where $M_9 = 2\rho + |\beta_n| + \beta_n + (\lambda - 1)\beta_{n-k} + |\lambda - 1||\beta_{n-k}| - \beta_0 + |\alpha_0| + 2 \sum_{j=1}^n |\alpha_j|$,

and if $\beta_{n-k} > \beta_{n-k+1}$, then the number of zeros of $P(z)$ in $\frac{|a_0|}{M_{10}} \leq |z| \leq \delta, 0 < \delta < 1$, does not exceed

$$\frac{1}{\log \frac{1}{\delta}} \log \frac{2\rho + |\beta_n| + \beta_n + (1 - \lambda)\beta_{n-k} + |1 - \lambda||\beta_{n-k}| - \beta_0 + |\beta_0| + 2 \sum_{j=0}^n |\alpha_j|}{|a_0|},$$

where $M_{10} = 2\rho + |\beta_n| + \beta_n + (1 - \lambda)\beta_{n-k} + |1 - \lambda||\beta_{n-k}| - \beta_0 + |\alpha_0| + 2 \sum_{j=1}^n |\alpha_j|$.

Theorem 4: Let $P(z) = \sum_{j=0}^n a_j z^j$ be a polynomial of degree n . If for some real numbers $\lambda > 0, \rho \geq 0, 1 \leq k \leq n, a_{n-k} \neq 0,$

$$|\rho + a_n| \geq |a_{n-1}| \geq \dots \geq |a_{n-k+1}| \geq \lambda |a_{n-k}| \geq |a_{n-k-1}| \geq \dots \geq |a_1| \geq |a_0|,$$

and for some real $\beta, |\arg a_j - \beta| \leq \alpha \leq \frac{\pi}{2}, j = 0, 1, \dots, n$ and $|a_{n-k-1}| > |a_{n-k}|$, i.e. $\lambda > 1$, then the number of zeros of

$P(z)$ in $\frac{|a_0|}{M_{11}} \leq |z| \leq \delta, 0 < \delta < 1$, does not exceed

$$\frac{1}{\log \frac{1}{\delta}} \log \frac{[(\rho + |a_n|(\cos \alpha + \sin \alpha + 1) - |a_{n-k}|(\cos \alpha - \sin \alpha - \lambda \cos \alpha - \lambda \sin \alpha - \lambda + 1) - |a_0|(\cos \alpha - \sin \alpha - 1) + 2 \sin \alpha \sum_{j=1, j \neq n-k}^{n-1} |a_j|)]}{|a_0|}}$$

where $M_{11} = (\rho + |a_n|(\cos \alpha + \sin \alpha + 1) - |a_{n-k}|(\cos \alpha - \sin \alpha - \lambda \cos \alpha - \lambda \sin \alpha - \lambda + 1) - |a_0|(\cos \alpha - \sin \alpha) + 2 \sin \alpha \sum_{j=1, j \neq n-k}^{n-1} |a_j|$

and if $|a_{n-k}| > |a_{n-k+1}|$, i.e. $\lambda < 1$, then the number of zeros of $P(z)$ in $\frac{|a_0|}{M_{12}} \leq |z| \leq \delta, 0 < \delta < 1$, does not exceed

$$\frac{1}{\log \frac{1}{\delta}} \log \frac{[(\rho + |a_n|(\cos \alpha + \sin \alpha + 1) + |a_{n-k}|(\cos \alpha + \sin \alpha - \lambda \cos \alpha + \lambda \sin \alpha + 1 - \lambda) - |a_0|(\cos \alpha - \sin \alpha - 1) + 2 \sin \alpha \sum_{j=1, j \neq n-k}^{n-1} |a_j|)]}{|a_0|}} \quad \text{Where}$$

$M_{12} = (\rho + |a_n|(\cos \alpha + \sin \alpha + 1) + |a_{n-k}|(\cos \alpha + \sin \alpha - \lambda \cos \alpha + \lambda \sin \alpha + 1 - \lambda) - |a_0|(\cos \alpha - \sin \alpha) + 2 \sin \alpha \sum_{j=1, j \neq n-k}^{n-1} |a_j|$.

Remark 4: Taking $\lambda = 1$, Theorem 4 reduces to Theorem D.

II. Lemmas

For the proofs of the above results, we need the following results:

Lemma 1.: Let $P(z) = \sum_{j=0}^n a_j z^j$ be a polynomial of degree n with complex coefficients such that

$|\arg a_j - \beta| \leq \alpha \leq \frac{\pi}{2}, j = 0, 1, \dots, n$, for some real β , then for some $t > 0$,

$$|ta_j - a_{j-1}| \leq [t|a_j| - |a_{j-1}|] \cos \alpha + [t|a_j| + |a_{j-1}|] \sin \alpha.$$

The proof of lemma 1 follows from a lemma due to Govil and Rahman [1].

Lemma 2. If $p(z)$ is regular, $p(0) \neq 0$ and $|p(z)| \leq M$ in $|z| \leq 1$, then the number of zeros of $p(z)$ in $|z| \leq \delta, 0 < \delta < 1$, does not exceed $\frac{1}{\log \frac{1}{\delta}} \log \frac{M}{|p(0)|}$ (see [4], p171).

III. Proofs of Theorems

Proof of Theorem 1: Consider the polynomial

$$\begin{aligned} F(z) &= (1-z)P(z) \\ &= (1-z)(a_n z^n + a_{n-1} z^{n-1} + \dots + a_1 z + a_0) \\ &= -a_n z^{n+1} + (a_n - a_{n-1})z^n + \dots + (a_{n-k+1} - a_{n-k})z^{n-k+1} + (a_{n-k} - a_{n-k-1})z^{n-k} \\ &\quad + (a_{n-k-1} - a_{n-k-2})z^{n-k-1} + \dots + (a_1 - a_0)z + a_0 \\ &= -(\alpha_n + i\beta_n)z^{n+1} + (\alpha_n - \alpha_{n-1})z^n + \dots + (\alpha_{n-k+1} - \alpha_{n-k})z^{n-k+1} \\ &\quad + (\alpha_{n-k} - \alpha_{n-k-1})z^{n-k} + (\alpha_{n-k-1} - \alpha_{n-k-2})z^{n-k-1} + \dots + (\alpha_1 - \alpha_0)z + \alpha_0 \\ &\quad + i \sum_{j=1}^n (\beta_j - \beta_{j-1})z^j + i\beta_0 \end{aligned}$$

If $\alpha_{n-k-1} > \alpha_{n-k}$, then

$$\begin{aligned} F(z) &= -(\alpha_n + i\beta_n)z^{n+1} - \rho z^n + (\rho + \alpha_n - \alpha_{n-1})z^n + \dots + (\alpha_{n-k+1} - \alpha_{n-k})z^{n-k+1} \\ &\quad + (\lambda\alpha_{n-k} - \alpha_{n-k-1})z^{n-k} - (\lambda-1)\alpha_{n-k}z^{n-k} + (\alpha_{n-k-1} - \alpha_{n-k-2})z^{n-k-1} + \dots \\ &\quad + (\alpha_1 - \alpha_0)z + \alpha_0 + i \sum_{j=1}^n (\beta_j - \beta_{j-1})z^j + i\beta_0. \end{aligned}$$

For $|z| \leq 1$,

$$\begin{aligned} |F(z)| &\leq |\alpha_n| + \rho + \rho + \alpha_n - \alpha_{n-1} + \dots + \alpha_{n-k+1} - \alpha_{n-k} + \lambda\alpha_{n-k} - \alpha_{n-k-1} + |\lambda-1||\alpha_{n-k}| \\ &\quad + \alpha_{n-k-1} - \alpha_{n-k-2} + \dots + \alpha_1 - \alpha_0 + |\alpha_0| + 2 \sum_{j=0}^n |\beta_j| \\ &= 2\rho + |\alpha_n| + \alpha_n + (\lambda-1)\alpha_{n-k} + |\lambda-1||\alpha_{n-k}| - \alpha_0 + |\alpha_0| + 2 \sum_{j=0}^n |\beta_j| \end{aligned}$$

Hence by Lemma 2, the number of zeros of $F(z)$ in $|z| \leq \delta, 0 < \delta < 1$, does not exceed

$$\frac{1}{\log \frac{1}{\delta}} \log \frac{2\rho + |\alpha_n| + \alpha_n + (\lambda-1)\alpha_{n-k} + |\lambda-1||\alpha_{n-k}| - \alpha_0 + |\alpha_0| + 2 \sum_{j=0}^n |\beta_j|}{|\alpha_0|}.$$

On the other hand, let

$$\begin{aligned} Q(z) &= -a_n z^{n+1} + (a_n - a_{n-1})z^n + \dots + (a_{n-k+1} - a_{n-k})z^{n-k+1} + (a_{n-k} - a_{n-k-1})z^{n-k} \\ &\quad + (a_{n-k-1} - a_{n-k-2})z^{n-k-1} + \dots + (a_1 - a_0)z \end{aligned}$$

For $|z| \leq 1$,

$$\begin{aligned} |Q(z)| &\leq |\alpha_n| + \rho + \rho + \alpha_n - \alpha_{n-1} + \dots + \alpha_{n-k+1} - \alpha_{n-k} + \lambda\alpha_{n-k} - \alpha_{n-k-1} + |\lambda-1||\alpha_{n-k}| \\ &\quad + \alpha_{n-k-1} - \alpha_{n-k-2} + \dots + \alpha_1 - \alpha_0 + |\beta_0| + 2 \sum_{j=1}^n |\beta_j| \\ &= 2\rho + |\alpha_n| + \alpha_n + (\lambda-1)\alpha_{n-k} + |\lambda-1||\alpha_{n-k}| - \alpha_0 + |\beta_0| + 2 \sum_{j=1}^n |\beta_j| = M_5. \end{aligned}$$

Since $Q(0)=0$, we have, by Rouché's theorem,

$$|Q(z)| \leq M_5 |z|, \text{ for } |z| \leq 1.$$

Thus

$$|F(z)| = |a_0 + Q(z)|$$

$$\geq |a_0| - |Q(z)|$$

$$\geq |a_0| - M_5 |z|$$

$$> 0$$

$$\text{if } |z| < \frac{|a_0|}{M_5}.$$

This shows that $F(z)$ has no zero in $|z| < \frac{|a_0|}{M_5}$. Consequently it follows that the number of zeros of $F(z)$ and hence $P(z)$ in

$$\frac{|a_0|}{M_5} \leq |z| \leq \delta, 0 < \delta < 1, \text{ does not exceed}$$

$$\frac{1}{\log \frac{1}{\delta}} \log \frac{2\rho + |\alpha_n| + \alpha_n + (\lambda - 1)\alpha_{n-k} + |\lambda - 1| |\alpha_{n-k}| - \alpha_0 + |\alpha_0| + 2 \sum_{j=0}^n |\beta_j|}{|a_0|}$$

If $\alpha_{n-k} > \alpha_{n-k+1}$, then

$$\begin{aligned} F(z) = & -(\alpha_n + i\beta_n)z^{n+1} - \rho z^n + (\rho + \alpha_n - \alpha_{n-1})z^n + \dots + (\alpha_{n-k+1} - \lambda\alpha_{n-k})z^{n-k+1} \\ & + (\alpha_{n-k} - \alpha_{n-k-1})z^{n-k} - (1-\lambda)\alpha_{n-k}z^{n-k+1} + (\alpha_{n-k-1} - \alpha_{n-k-2})z^{n-k-1} + \dots \\ & + (\alpha_1 - \alpha_0)z + \alpha_0 + i \sum_{j=1}^n (\beta_j - \beta_{j-1})z^j + i\beta_0. \end{aligned}$$

For $|z| \leq 1$,

$$\begin{aligned} |F(z)| \leq & |\alpha_n| + \rho + \rho + \alpha_n - \alpha_{n-1} + \dots + \alpha_{n-k+1} - \lambda\alpha_{n-k} + \alpha_{n-k} - \alpha_{n-k-1} + |1-\lambda| |\alpha_{n-k}| \\ & + \alpha_{n-k-1} - \alpha_{n-k-2} + \dots + \alpha_1 - \alpha_0 + |\alpha_0| + 2 \sum_{j=0}^n |\beta_j| \\ = & 2\rho + |\alpha_n| + \alpha_n + (1-\lambda)\alpha_{n-k} + |1-\lambda| |\alpha_{n-k}| - \alpha_0 + |\alpha_0| + 2 \sum_{j=0}^n |\beta_j| \end{aligned}$$

Hence by Lemma 2, the number of zeros of $F(z)$ in $|z| \leq \delta, 0 < \delta < 1$, does not exceed

$$\frac{1}{\log \frac{1}{\delta}} \log \frac{2\rho + |\alpha_n| + \alpha_n + (1-\lambda)\alpha_{n-k} + |1-\lambda| |\alpha_{n-k}| - \alpha_0 + |\alpha_0| + 2 \sum_{j=0}^n |\beta_j|}{|a_0|}.$$

On the other hand, let

$$\begin{aligned} Q(z) = & -a_n z^{n+1} + (a_n - a_{n-1})z^n + \dots + (a_{n-k+1} - a_{n-k})z^{n-k+1} + (a_{n-k} - a_{n-k-1})z^{n-k} \\ & + (a_{n-k-1} - a_{n-k-2})z^{n-k-1} + \dots + (a_1 - a_0)z \end{aligned}$$

$$\begin{aligned}
 &= -(\alpha_n + i\beta_n)z^{n+1} - \rho z^n + (\rho + \alpha_n - \alpha_{n-1})z^n + \dots + (\alpha_{n-k+1} - \lambda\alpha_{n-k})z^{n-k+1} \\
 &+ (\alpha_{n-k} - \alpha_{n-k-1})z^{n-k} - (1-\lambda)a_{n-k}z^{n-k+1} + (\alpha_{n-k-1} - \alpha_{n-k-2})z^{n-k-1} + \dots \\
 &+ (\alpha_1 - \alpha_0)z + i\sum_{j=1}^n (\beta_j - \beta_{j-1})z^j
 \end{aligned}$$

For $|z| \leq 1$,

$$\begin{aligned}
 |Q(z)| &\leq |\alpha_n| + \rho + \rho + \alpha_n - \alpha_{n-1} + \dots + \alpha_{n-k+1} - \lambda\alpha_{n-k} + \alpha_{n-k} - \alpha_{n-k-1} + |1 - \lambda||\alpha_{n-k}| \\
 &+ \alpha_{n-k-1} - \alpha_{n-k-2} + \dots + \alpha_1 - \alpha_0 + |\beta_0| + 2\sum_{j=1}^n |\beta_j| \\
 &= 2\rho + |\alpha_n| + \alpha_n + (1-\lambda) + |1 - \lambda||\alpha_{n-k}| - \alpha_0 + |\beta_0| + 2\sum_{j=1}^n |\beta_j| = M_6.
 \end{aligned}$$

Since $Q(0)=0$, we have, by Rouché's theorem,

$$|Q(z)| \leq M|z|, \text{ for } |z| \leq 1.$$

Thus

$$|F(z)| = |a_0 + Q(z)|$$

$$\geq |a_0| - |Q(z)|$$

$$\geq |a_0| - M_6|z|$$

$$> 0$$

$$\text{if } |z| < \frac{|a_0|}{M_6}.$$

This shows that $F(z)$ has no zero in $|z| < \frac{|a_0|}{M_6}$. Consequently it follows that the number of zeros of $F(z)$ and hence $P(z)$ in

$$\frac{|a_0|}{M_6} \leq |z| \leq \delta, 0 < \delta < 1, \text{ does not exceed}$$

$$\frac{1}{\log \frac{1}{\delta}} \log \frac{2\rho + |\alpha_n| + \alpha_n + (1-\lambda)\alpha_{n-k} + |1 - \lambda||\alpha_{n-k}| - \alpha_0 + |\alpha_0| + 2\sum_{j=0}^n |\beta_j|}{|a_0|}.$$

That proves Theorem 1.

Proof of Theorem 4: Consider the polynomial

$$F(z) = (1-z)P(z)$$

$$= (1-z)(a_n z^n + a_{n-1} z^{n-1} + \dots + a_1 z + a_0)$$

$$\begin{aligned}
 &= -a_n z^{n+1} + (a_n - a_{n-1})z^n + \dots + (a_{n-k+1} - a_{n-k})z^{n-k+1} + (a_{n-k} - a_{n-k-1})z^{n-k} \\
 &+ (a_{n-k-1} - a_{n-k-2})z^{n-k-1} + \dots + (a_1 - a_0)z + a_0
 \end{aligned}$$

If $|a_{n-k-1}| > |a_{n-k}|$, i.e. $\lambda > 1$, then

$$\begin{aligned}
 F(z) &= -a_n z^{n+1} - \rho z^n + (\rho + a_n - a_{n-1})z^n + \dots + (a_{n-k+1} - a_{n-k})z^{n-k+1} \\
 &+ (\lambda a_{n-k} - a_{n-k-1})z^{n-k} - (\lambda - 1)a_{n-k}z^{n-k} + (a_{n-k-1} - a_{n-k-2})z^{n-k-1} + \dots \\
 &+ (a_1 - a_0)z + a_0
 \end{aligned}$$

so that for $|z| \leq 1$, we have by using Lemma 1,

$$|F(z)| \leq |a_n| + \rho + |\rho + a_n - a_{n-1}| + \dots + |a_{n-k+1} - a_{n-k}| + |\lambda a_{n-k} - a_{n-k-1}|$$

$$\begin{aligned}
 & + |\lambda - 1| |a_{n-k}| + |a_{n-k-1} - a_{n-k-2}| + \dots + |a_1 - a_0| + |a_0| \\
 & \leq |a_n| + \rho + (|\rho + a_n| - |a_{n-1}|) \cos \alpha + (|\rho + a_n| + |a_{n-1}|) \sin \alpha + \dots \\
 & \quad + (|a_{n-k+1}| - |a_{n-k}|) \cos \alpha + (|a_{n-k+1}| + |a_{n-k}|) \sin \alpha + (\lambda - 1) |a_{n-k}| \\
 & \quad + (\lambda |a_{n-k}| - |a_{n-k-1}|) \cos \alpha + (\lambda |a_{n-k}| + |a_{n-k-1}|) \sin \alpha \\
 & \quad + (|a_{n-k-1}| - |a_{n-k-2}|) \cos \alpha + (|a_{n-k-1}| + |a_{n-k-2}|) \sin \alpha + \dots \\
 & \quad + (|a_1| - |a_0|) \cos \alpha + (|a_1| + |a_0|) \sin \alpha + |a_0| \\
 & \leq (\rho + |a_n|)(\cos \alpha + \sin \alpha + 1) - |a_{n-k}|(\cos \alpha - \sin \alpha - \lambda \cos \alpha - \lambda \sin \alpha - \lambda + 1) \\
 & \quad - |a_0|(\cos \alpha - \sin \alpha - 1) + 2 \sin \alpha \sum_{j=1, j \neq n-k}^{n-1} |a_j|
 \end{aligned}$$

Hence, by Lemma 2, the number of zeros of $F(z)$ in $|z| \leq \delta, 0 < \delta < 1$, does not exceed

$$\frac{1}{\log \frac{1}{\delta}} \log \frac{[(\rho + |a_n|)(\cos \alpha + \sin \alpha + 1) - |a_{n-k}|(\cos \alpha - \sin \alpha - \lambda \cos \alpha - \lambda \sin \alpha - \lambda + 1) - |a_0|(\cos \alpha - \sin \alpha - 1) + 2 \sin \alpha \sum_{j=1, j \neq n-k}^{n-1} |a_j|]}{|a_0|}$$

On the other hand,

let

$$\begin{aligned}
 Q(z) = & -a_n z^{n+1} + (a_n - a_{n-1})z^n + \dots + (a_{n-k+1} - a_{n-k})z^{n-k+1} + (a_{n-k} - a_{n-k-1})z^{n-k} \\
 & + (a_{n-k-1} - a_{n-k-2})z^{n-k-1} + \dots + (a_1 - a_0)z
 \end{aligned}$$

For $|z| \leq 1$,

$$\begin{aligned}
 |Q(z)| & \leq (\rho + |a_n|)(\cos \alpha + \sin \alpha + 1) - |a_{n-k}|(\cos \alpha - \sin \alpha - \lambda \cos \alpha - \lambda \sin \alpha - \lambda + 1) \\
 & \quad - |a_0|(\cos \alpha - \sin \alpha) + 2 \sin \alpha \sum_{j=1, j \neq n-k}^{n-1} |a_j| \\
 & = M_{11}.
 \end{aligned}$$

Since $Q(0)=0$, we have, by Rouché's Theorem,

$$|Q(z)| \leq M_{11}|z|, \text{ for } |z| \leq 1.$$

Thus, for $|z| \leq 1$,

$$\begin{aligned}
 |F(z)| & = |a_0 + Q(z)| \\
 & \geq |a_0| - |Q(z)| \\
 & \geq |a_0| - M_{11}|z| \\
 & > 0
 \end{aligned}$$

if $|z| < \frac{|a_0|}{M_{11}}$.

This shows that $F(z)$ has all its zeros z with $|z| \leq 1$ in $|z| \geq \frac{|a_0|}{M_{11}}$.

Thus, the number of zeros of $F(z)$ and hence $P(z)$ in $\frac{|a_0|}{M_{11}} \leq |z| \leq \delta, 0 < \delta < 1$, does not exceed

$$\frac{1}{\log \frac{1}{\delta}} \log \frac{[(\rho + |a_n|)(\cos \alpha + \sin \alpha + 1) - |a_{n-k}|(\cos \alpha - \sin \alpha - \lambda \cos \alpha - \lambda \sin \alpha - \lambda + 1) - |a_0|(\cos \alpha - \sin \alpha - 1) + 2 \sin \alpha \sum_{j=1, j \neq n-k}^{n-1} |a_j|]}{|a_0|}}$$

If $|a_{n-k}| > |a_{n-k+1}|$, i.e. $\lambda < 1$, then

$$F(z) = -a_n z^{n+1} - \rho z^n + (\rho + a_n - a_{n-1})z^n + \dots + (a_{n-k+1} - \lambda a_{n-k})z^{n-k+1} + (a_{n-k} - a_{n-k-1})z^{n-k} - (1-\lambda)a_{n-k}z^{n-k+1} + (a_{n-k-1} - a_{n-k-2})z^{n-k-1} + \dots + (a_1 - a_0)z + a_0$$

so that for $|z| \leq 1$, we have by Lemma 1,

$$\begin{aligned} |F(z)| &\leq |a_n| + \rho + |\rho + a_n - a_{n-1}| + \dots + |a_{n-k+1} - \lambda a_{n-k}| + |a_{n-k} - a_{n-k-1}| \\ &\quad + |1 - \lambda||a_{n-k}| + |a_{n-k-1} - a_{n-k-2}| + \dots + |a_1 - a_0| + |a_0| \\ &\leq |a_n| + \rho + (|\rho + a_n| - |a_{n-1}|)\cos \alpha + (|\rho + a_n| + |a_{n-1}|)\sin \alpha + \dots \\ &\quad + (|a_{n-k+1}| - \lambda|a_{n-k}|)\cos \alpha + (|a_{n-k+1}| + \lambda|a_{n-k}|)\sin \alpha + |1 - \lambda||a_{n-k}| \\ &\quad + (|a_{n-k}| - |a_{n-k-1}|)\cos \alpha + (|a_{n-k}| + |a_{n-k-1}|)\sin \alpha \\ &\quad + (|a_{n-k-1}| - |a_{n-k-2}|)\cos \alpha + (|a_{n-k-1}| + |a_{n-k-2}|)\sin \alpha + \dots \\ &\quad + (|a_1| - |a_0|)\cos \alpha + (|a_1| + |a_0|)\sin \alpha + |a_0| \\ &\leq (\rho + |a_n|)(\cos \alpha + \sin \alpha + 1) + |a_{n-k}|(\cos \alpha + \sin \alpha - \lambda \cos \alpha + \lambda \sin \alpha + 1 - \lambda) \\ &\quad - |a_0|(\cos \alpha - \sin \alpha - 1) + 2 \sin \alpha \sum_{j=1, j \neq n-k}^{n-1} |a_j| \end{aligned}$$

Hence, by Lemma 2, the number of zeros of $F(z)$ in $|z| \leq \delta, 0 < \delta < 1$, does not exceed

$$\frac{1}{\log \frac{1}{\delta}} \log \frac{[(\rho + |a_n|)(\cos \alpha + \sin \alpha + 1) + |a_{n-k}|(\cos \alpha + \sin \alpha - \lambda \cos \alpha + \lambda \sin \alpha + 1 - \lambda) - |a_0|(\cos \alpha - \sin \alpha - 1) + 2 \sin \alpha \sum_{j=1, j \neq n-k}^{n-1} |a_j|]}{|a_0|}}$$

On the other hand, let

$$Q(z) = -a_n z^{n+1} + (a_n - a_{n-1})z^n + \dots + (a_{n-k+1} - a_{n-k})z^{n-k+1} + (a_{n-k} - a_{n-k-1})z^{n-k} + (a_{n-k-1} - a_{n-k-2})z^{n-k-1} + \dots + (a_1 - a_0)z$$

For $|z| \leq 1$, by using Lemma 1,

$$\begin{aligned} |Q(z)| &\leq (\rho + |a_n|)(\cos \alpha + \sin \alpha + 1) + |a_{n-k}|(\cos \alpha + \sin \alpha - \lambda \cos \alpha + \lambda \sin \alpha + 1 - \lambda) \\ &\quad - |a_0|(\cos \alpha - \sin \alpha) + 2 \sin \alpha \sum_{j=1, j \neq n-k}^{n-1} |a_j| \\ &= M_{12}. \end{aligned}$$

Since $Q(0)=0$, we have, by Rouché's Theorem,

$$|Q(z)| \leq M_{12}|z|, \text{ for } |z| \leq 1.$$

Thus, for $|z| \leq 1$,

$$\begin{aligned}
 |F(z)| &= |a_0 + Q(z)| \\
 &\geq |a_0| - |Q(z)| \\
 &\geq |a_0| - M_{12}|z| \\
 &> 0 \\
 \text{if } |z| &< \frac{|a_0|}{M_{12}}.
 \end{aligned}$$

This shows that F(z) has all its zeros z with $|z| \leq 1$ in $|z| \geq \frac{|a_0|}{M_{12}}$.

Thus, the number of zeros of F(z) and hence P(z) in $\frac{|a_0|}{M_{12}} \leq |z| \leq \delta, 0 < \delta < 1$, does not exceed

$$\frac{1}{\log \frac{1}{\delta}} \log \frac{[(\rho + |a_n|(\cos \alpha + \sin \alpha + 1) + |a_{n-k}|(\cos \alpha + \sin \alpha - \lambda \cos \alpha + \lambda \sin \alpha + 1 - \lambda) - |a_0|(\cos \alpha - \sin \alpha - 1) + 2 \sin \alpha \sum_{j=1, j \neq n-k}^{n-1} |a_j|)]}{|a_0|}$$

That proves Theorem 4.

References

- [1] N.K.Govil and Q.I.Rahman, On the Enestrom-Keakeya Theorem, Tohoku Math.J.20 (1968), 126-136.
- [2] M. H. Gulzar, on the number of Zeros of a polynomial in a prescribed Region, Research Journal of Pure Algebra-2(2), 2012, 1-11.
- [3] E C. Titchmarsh, The Theory of Functions, 2nd edition, Oxford University Press, London, 1939.

Use of Hydrocarbons and Other Blends as Refrigerant

Mohd. Aasim Nazeer Ahmad Quraishi,¹ U. S. Wankhede²

¹M. Tech. IV Semester, Heat Power Engineering, G. H. Rasoni College of Engineering, Nagpur-440016,

²Professor, Mechanical Engineering Department, G. H. Rasoni College of Engineering, Nagpur-440016.

Abstract: This paper presents a study of different environmental friendly refrigerants of either hydrocarbon or Hydro fluoro carbons (HFC) class. Hydrocarbons (HCs) have zero ODP and very low GWP whereas HFCs have zero ODP but a quite higher GWP. Almost in all the cases, when R-134a was replaced with HCs the COP of the system was improved, ON time ratio and energy consumption was reduced. Due to a higher value of latent heat of HCs, the amount of refrigerant charge was also reduced as compared with HFC-134a. When hydro chloro fluoro carbons (HCFCs) were replaced with HFCs the system delivered a poor performance with increased energy consumption. When nano particles were added to the refrigerant, system delivered better performance with reduced energy consumption than that of pure refrigerant.

Keywords: TEWI, ON time ratio, Pull down time.

I. Introduction

The most commonly used refrigerants in the late 1800s and in the early 1900s were natural refrigerants such as ammonia, carbon dioxide, sulphur dioxide and methyl chloride. All these refrigerants were found to be toxic or hazardous. In 1928, a safer class of alternative refrigerants became available with the invention of chlorofluorocarbons (CFCs) and hydro chloro fluorocarbons (HCFCs). CFCs and HCFCs have many suitable properties such as stability, non-toxicity, non-flammable, good material compatibility and good thermodynamic properties, which led to their common wide spread use by both consumers and industries around the globe, especially as refrigerants in air-conditioning and refrigeration systems.

Results from many researches show that ozone layer is being depleted due to the presence of chlorine in the stratosphere. The general consensus for the cause of this is that CFCs and HCFCs are large class of chlorine containing chemicals, which migrate to the stratosphere where they react with ozone. Later, chlorine atoms continue to convert more ozone to oxygen. The discovery of the depletion of the earth's ozone layer, which shields the earth's surface from UV radiation, has resulted in a series of international treaties demanding a gradual phase out of halogenated fluids. The CFCs have been banned in developed countries since 1996, and in 2030, producing and using of CFCs will be prohibited completely in the entire world. Also, the partially halogenated HCFCs are bound to be prohibited in the near future.

The researches are going on to find out some alternate refrigerants which does not harm to the environment and the protective ozone layer. Research has shown that hydrocarbons are good alternative to existing refrigerants.

II. Refrigerants under Considerations

Hydrocarbons, propane (R-290) and isobutane (R-600a) were among the first refrigerants, but due to their flammability and safety purposes, their use was abandoned and the direction of researches was shifted towards a safer and inert class of refrigerants. Thus the use of HCs as a refrigerant is not a new technology. Since 15 years, hydrocarbon and their blends are again being used at commercial scale [1].

Isobutane (R-600a) is the most frequently used hydrocarbon refrigerant. In Europe it is the most dominating refrigerant in domestic refrigerators. In 2004, the use of isobutane and its blend was 33% in domestic refrigerators and freezers at global level. Propane (R-290) and propene (R-1270) are widely being used in heat pumps, air conditioners and commercial refrigeration systems. Butane (R-600) is also under consideration but it has not been used commercially. Pentane and pentene also have the potential to be used as refrigerant and they are to be considered as the replacement to R-11 in centrifugal systems [2].

PROPERTIES OF REFRIGERANTS AT 40°C

Ref.	No.	Formula	M (kg/kmol)	T _{bp} (°C)	T _{tr} (°C)	T _{cr} (°C)	h _{fg} (kJ/kg)	ρ _l (kg/m ³)	ρ _v (kg/m ³)
Isobutane	R600a	CH ₃ -(CH ₃) ₃	58.12	-11.67	-159.59	134.67	311.4	530.0	13.667
Propane	R290	CH ₃ -CH ₂ -CH ₃	44.096	-42.09	-187.67	96.675	306.51	467.07	30.202
Propene	R1270	CH ₂ =CH-CH ₃	42.08	-47.69	-185.2	92.42	303.14	476.66	35.708
R134a	R134a	CF ₃ -CH ₂ F	102.03	-26.074	-103.3	101.06	163.02	1146.7	50.085
R22	R22	CHClF ₂	86.468	-40.81	-157.42	96.145	166.6	1128.5	66.193
Ammonia	R717	NH ₃	17.03	-33.327	-77.655	132.25	1099.31	579.44	12.034

Ref.	Refrigerant name	no.	Refrigerant number
Formula	Chemical formula	M	Molecular weight
T_{bp}	Normal boiling point	T_{tr}	Triple point
T_{cr}	Critical temperature	h_{fg}	Latent heat of vaporization
ρ_l	Liquid density	ρ_v	Vapor density

III. Literature Survey

a) Replacement of R-22 with HFCs

A trial was performed by Rocca and Panno [3] to replace R22 with new HFC refrigerants and the performance was compared with R-22. The plant working efficiency was first estimated with R-22 and then with three new HFC refrigerants, R-417a, R-422a and R-422d. The experimental results showed that R-22 has the least energy consumption among all the refrigerants under trial. Results also reveal that the three HFC refrigerants can replace R-22 without any change in lubricant or without any modification in the system and the accessories. These refrigerants also provide the safe and reliable working conditions. The results also verified that despite these advantages, the performance of the new tested HFCs was not as efficient as with R-22.

Experimentation was made to replace R-22 with a new refrigerant R-422d by Aprea et al. [4]. The experiment was carried out under three different operating conditions. The experimental results showed that COP of the system with R-422d was 20% lower than that of using R-22, the reason behind is high vapor density that also leads to lower cooling capacity and increased energy consumption. The discharge pressure was 15% higher than that of R-22 but it was under design limit. The discharge temperature was 20°C lower which offers a longer compressor life. The improvement in heat exchange by condenser in order to improve the performance was carried out by using a fan. Increasing the fan speed only by 20% improved COP in the range of 14.5–23.5%.

Llopis et al. [5] replaced R-22 by two refrigerants HFC-422a and HFC-417b in medium and low evaporating temperatures. The test was conducted in a two stage refrigerating plant equipped with subcooling. The evaporator and condenser temperature range were -31°C to 17°C and 30°C to 48°C respectively. The experimental results showed that with the use of new refrigerants, the refrigerant mass flow rate need to be incremented. The new refrigerants also lead to lower specific refrigerating effect that tends to reduced cooling capacity. This reduction in the plant capacity was much more than expected from the theoretical analysis.

b) Replacement of R-134a with other HFCs

Bolaji [6] carried out a trial on domestic refrigerator designed to work with R-134a and replaced it by R-152a and R-32 which have zero ODP and low GWP. The performance with the new refrigerant was evaluated and compared with R-134a. The result showed that the average COP obtained with R-152a was 4.7% higher while average COP with R-32 was 8.5% lower as compared to R-134a. The energy consumption by the system was also reduced. The compressor consumed 4.0% and 3.2% lesser energy with R-152a as compared to the energy consumption with R-134a and R-32 respectively. The design temperature and pull down time using R-152a and R-134a were achieved earlier than using R-32. The discharge pressure of R-152a was about 0.8% less than that of R-134a while the discharge pressure using R-32 was the highest with average value of 8.1% and 7.2% higher than those of R-134a and R-152a respectively. In general, the system performed better than the other two refrigerants this shows that R-152a can be used to replace R-134a in domestic refrigerators.

A trial was made by Khorshid et al. [7] on domestic refrigerator to replace R-134a by two different blends one as R-134a (6.61%), R-32 (5.64%) and R-152a (87.75%) and the other as R-32 (15.34%), R-600a (8.79%) and R-152a (75.87%). The results of the test show that COP was improved by 11.93% and 2.07% by using the former and latter respectively as compared with R-134a. The new refrigerant blends have zero ODP and low GWP of the order of 242 and 200 respectively.

IV. Replacement of R-134a with HCs

Jwo et al. [8] used a blend of R-290 and R-600a instead of R-134a. The experiment was performed on a 440 liters domestic refrigerator. During test refrigerant R-134a was replaced with varied mass of hydrocarbon blends. The results show that refrigerating effect was improved by using hydrocarbon blends. The refrigerator which was designed to work with 150 gm of R-134a gave best result with 90 gm of hydrocarbon refrigerant that implies a reduction of 40% in refrigerant charge. The design temperature was obtained quicker when the mixture of R-290 and R-600a was used that reduced the individual working time, hence the total working time per month was lesser than by using R-134a. On average, the new refrigerant mixture offers a better refrigerating behavior and reduces the energy consumption by 4.4%.

Rasti et al. [9] substituted R-134a with R-436a (mixture of R-290 and R-600a with a mass ratio of 56/44) in a 238 liter domestic refrigerator without any modification in the system. The compressor was charged with different amount of R-436a. The various results of the experiment showed that the refrigerant R-436a has better performance compared to R-134a considering various parameters. The ON time ratio was reduced by 13% when R-436a was used. The energy consumption per day was reduced by 5.3%. The refrigerant charge required in case of R-134a was 105g and the optimum amount of refrigerant for R-436a was 55g which implies a saving of 48% in refrigerant charge. The evaporator inlet temperature was reduced by 3.5°C. The energy efficiency index was raised from E to D. The results also showed that Total Equivalent Warming Impact (TEWI) of R-436a is 11.8% lesser than R-134a. Thus R-436a appears to be a good replacement for R-134a.

Sattar et al. [10] used a domestic refrigerator to conduct trial which was designed to work with R-134a. The trial was conducted to check the possibility of using hydrocarbons as refrigerants. Pure butane, isobutane and mixture of butane, isobutane and propane were used as alternate refrigerants. The performance of the system was compared with R-134a. The compressor consumed 3% and 2% lesser energy when iso butane and butane were used at 28°C ambient condition. The amount of refrigerant charge with R-134a was 140 gm and it was reduced to 70 gm with the pure hydrocarbon and its blends which exhibits a saving of 50% in refrigerant charge. The trials were performed without any alteration in the system that shows the possibility of using hydrocarbons and their blends without any modification.

V. Replacement of Pure Refrigerant with Nano Refrigerant

Shengshan Bi et al. [11] made use of TiO₂-R600a nano refrigerant in a domestic refrigerator without any system modification. The experimentation was performed using TiO₂-R600a with 0.1 g/lit and 0.5 g/lit of TiO₂ nano particles concentrations. The performance was compared with pure R-600a. The design temperatures were obtained at a quicker rate with TiO₂-R600a nano refrigerant. The energy consumptions were reduced by 5.94% and 9.60% with the concentrations as 0.1 g/lit and 0.5 g/lit of TiO₂ nano particles respectively. All the results obtained exhibited that TiO₂-R600a nano refrigerant worked safely and normally in the refrigerator with better performance than pure R-600a system. Thus TiO₂-R600a nano refrigerant may be used in domestic refrigerator with better performance and lower energy consumption without any alteration of the system.

Saidur et al. [12] conducted experiment with HFC-134a in domestic refrigerator with TiO₂ nano particles. The results showed that this nano refrigerant gave better performance. The energy consumption of HFC-134a refrigerant using mineral oil and nano particles mixture as lubricant was lesser than with pure HFC-134a and it saved 26.1% energy with 0.1% mass fraction TiO₂ nano particles compared to the HFC-134a. 60% HFC-134a with mineral oil and 0.1% wt Al₂O₃ nano particles gave optimal performance. The power consumption was reduced by 2.4% and the COP was improved by 4.4%. It has been identified that fundamental properties of nano fluids change drastically and depend upon the concentration of suspension of the nano particles in the base fluid.

VI. Conclusions

As per the Kyoto and Montreal protocols, the harmful refrigerants are to be phased out and are to be replaced with alternate environmental friendly refrigerants. The objective of this paper is to evaluate different environmental friendly refrigerant. On the basis of collecting information, the following conclusions may be drawn.

HFCs can replace R-22 without any modification in the system. Despite having the advantage of zero ODP, the system delivers the poor performance with increased energy consumption as compared with R-22. Hydrocarbons and their various blends may replace R-134a without any system modifications. COP of the system is improved with reduced energy consumption. ON time ratio and pull down time are also reduced. The system requires to be charged with 40% to 50% lesser amount of refrigerant due to a quite higher value of latent heat of hydrocarbons.

When nano particles are added to the refrigerants, thermo physical properties change drastically and depend on the concentration of the nano particles. Nano refrigerant can be used in the refrigeration system without any modifications. The system delivers better performance than with pure refrigerant; the energy consumption is also reduced. However optimum blend composition for maximum performance of the system is not much studied. Research work for deciding the concentration of blends has to be undertaken to have better performance of the system.

References

- [1] Jose M. Corberan, Jacobo Segurado, Daniel Colbourne, Jose Gonzalvez, Review of standards for the use of hydrocarbon refrigerants in A/C, heat pump and refrigeration equipment, *International Journal of Refrigeration* 31 (2008) 748–756.
- [2] Bjorn Palm, Hydrocarbons as refrigerants in small heat pump and refrigeration systems – A review, *International Journal of Refrigeration* 31 (2008) 552–563.
- [3] Vincenzo La Rocca, Giuseppe Panno, Experimental performance evaluation of a vapour compression refrigerating plant when replacing R22 with alternative refrigerants *Applied Energy* 88 (2011) 2809–2815.
- [4] Ciro Aprea, Angelo Maiorino, Rita Mastrullo, Change in energy performance as a result of a R-422d retrofit: An experimental analysis for a vapor compression refrigeration plant for a walk in cooler, *Applied Energy* 88, (2011) 4742–4748.
- [5] R. Llopis, R. Cabello, D. Sánchez, E. Torella, J. Patino, J. G. Sánchez, Experimental evaluation of HCFC-22 replacement by the drop-in fluids HFC-422a and HFC-417b for low temperature refrigeration applications, *Applied Thermal Engineering* 31 (2011) 1323–1331.
- [6] B. O. Bolaji, Experimental study of R152a and R32 to replace R134a in a domestic refrigerator, *Energy* 35 (2010) 3793–3798.
- [7] E. Khorshid, B. Alshiraan, A. Alsairafi, A. Alzemi, A. Allahddad, Performance investigation on new refrigerant mixture (2011).
- [8] Ching Song Jwo, Chen-Ching Ting, Wei-Ru Wang, Efficiency analysis of home refrigerators by replacing hydrocarbon refrigerants, *Measurement* 42 (2009) 697–701.
- [9] M. Rasti M.S. Hatamipour, S.F. Aghmiri, M. Tavakoli, Enhancement of domestic refrigerator's energy efficiency index using a hydrocarbon mixture refrigerant, *Measurement* 45 (2012) 1807–1813.
- [10] M. A. Sattar, R. Saidur, H. H. Masjuki, Performance investigation of domestic refrigerator using pure hydrocarbons and blends of hydrocarbons as refrigerants, *World Academy of Science, Engineering and Technology* 29 (2007) 223–228.
- [11] Shengshan Bi, Kai Guo, Zhigang Liu, Jiangtao Wu, Performance of a domestic refrigerator using TiO₂-R600a nano-refrigerant as working fluid, *Energy Conversion and Management* 52 (2011) 733–737.
- [12] R. Saidur, S.N. Kazi, M.S. Hossain, M.M. Rahman, H.A. Mohammed, A review on the performance of nano particles suspended with refrigerants and lubricating oils in refrigeration systems, *Renewable and Sustainable Energy Reviews* 15 (2011) 310–323.

Effect of Addition of Polymer on the Properties of Waste Plastic Fibre Reinforced Concrete-An Experimental Investigation

Prahallada M.C,¹ Prakash K.B²

¹Professor, Department of Civil Engineering, Christ University Faculty of Engineering, Bangalore-560074
Karnataka, INDIA.

²Prakash K.B. Principal, Government College of Engineering, Devagiri, Haveri-581110, Karnataka, INDIA

Abstract: Recycling technology or reusing technology is not a new technology. Since civilization, man, in one form or the other, is recycling some of the materials for his convenience. Today, the recycling technology is gaining importance because of the reasons of growing quantity of wastes and to save natural resources. As the population is growing, the quantity of waste on this earth is also growing. The greedy nature of man has doubled the quantity of wastes. These wastes are causing an endangering pollution of the environment pollution of their environment. Some of wastes are polluting the environment instantaneously after their release and some of the wastes are polluting the environment slowly. Waste plastic is one of the major environmental pollutants. Plastic is a non bio-degradable material or it is a non-perishable material. It cannot be destroyed easily. Any efforts of destroying it again results in environmental pollution. The main objective of this paper is to throw some light on the effective use of waste plastics in concrete. The effect of addition of waste plastics in the form of fibres into the concrete along with some polymer has been studied in this paper. The strength characteristics of waste plastic fibre reinforced concrete with different percentages of polymer have been found experimentally.

Keywords: Polymer, Fibre reinforced concrete, Waste plastic fibre, Strength and Workability characteristics

I. Introduction

Many efforts are being continuously made to bring down the environmental pollution on this mother earth. The breathing air which sustains the life is being polluted; the drinking water which ushers life into all living beings is being polluted; the mother earth/soil which supports all living beings is being polluted; the hearing sound which is a communication media is being polluted: the edible food which nourishes the living beings is being polluted. Pollution has not left any area. It is spreading its tentacles in all walks of life

As the population is growing, the quantity of waste on this earth is also growing. The greedy nature of man has doubled the quantity of wastes. These wastes are causing an endangering pollution of the environment pollution of their environment. Some of wastes are polluting the environment instantaneously after their release and some of the wastes are polluting the environment slowly.

Many of the wastes and especially the industrial wastes are causing enormous pollution of the environment, among them, the noteworthy are Fly ash, Blast furnace slag, Silica fume, Stone crusher dust, etc. The safe disposal of these industrial wastes has become a major problem to the industrialists as well as to the environmentalists.

In today's circumstances, plastic has become one of the major environmental pollutants. Plastic is a non-bio-degradable material or, it is a non-perishable material. It cannot be destroyed easily. Any efforts of destroying it again results in environmental pollution. Plastics have entered every conceivable field like medical, agricultural, automobile and of course households. They come in handy on account of their useful properties like being light weight and economical. They are one of the useful materials ever created by man. Engineers have shaped plastics that are as rigid as steel or as soft as cotton or sponge. The word plastic comes from the Greek word "Plastikos" which means able to be shaped. Chemically plastics are polymers. A polymer is a substance which contains a particular molecular group repeated hundreds of times linked together in definite pattern. There are hundreds of different plastics. But basically they belong to two primary groups namely "thermosetting Plastics" and Thermo Plastics"

Engineers have created hundreds of different plastics and each has its own properties. Plastic parts are replacing metals in aero planes, cars and other mechanical devices. Airplane wings are now made of plastics which reduce the weight of air craft and there by reduces fuel consumption. Plastic has also replaced metals in building construction materials such as pipes because they are weight and do not corrode. Plastic fibre and fabrics have replaced natural fibres like cotton, silk and wool. We have nylon, linen, polyester fabrics which are more durable. Plastic fibres are excellent for clothing, carpeting and upholstery. The only drawback of plastics is that they are not environmental friendly, because they are non-bio-degradable material. That is why environmentalists have raised big hue and cry against their use. Even though plastic is making wonders in all the fields, it is endangering the environment. It is causing environmental pollution. Plastics cannot be perished. It cannot be dumped in soil. If dumped in soil it causes the soil pollution. It cannot be dumped in water. If dumped in water it causes water pollution.

When the waste plastic did not find any place in America and Europe, they dumped million tonnes of waste plastic in Atlantic and Pacific oceans. This has resulted in many accidents of ships and the death of much aquatic life. It cannot be burnt also. If burnt it causes air pollution by releasing many toxic gases. Many metropolitan and industrial cities of the world have become population less due to the environmental problem caused by the plastic. Thus plastic is causing tremendous environmental pollution. Many researches are going on for uses of this plastic in a safe manner.

II. Experimental work

2.1 Materials Used

- Cement: Ordinary Portland Cement-53 grade was used having a specific gravity of 3.15 and it satisfies the requirements of IS: 12269-1987 specifications.
- Fine aggregates: Locally available sand collected from the bed of river Bhadra was used as fine aggregate. The sand used was having fineness modulus 2.96 and conformed to grading zone-III as per IS: 383-1970 specification.
- Coarse aggregates: The crushed stone aggregate were collected from the local quarry. The coarse aggregates used in the experimentation were 10mm and down size aggregate and tested as per IS: 383-1970 and 2386-1963 (I, II and III) specifications. The aggregates used were having fineness modulus 1.9.
- Recycled aggregates: The recycled aggregates were collected from demolished concrete slabs, beams & columns. The recycled aggregates used in the experimentation were 10mm and down size aggregates and tested as per IS: 383 -1970 and 2386 (I, II and III). The aggregates were having fineness modulus of 1.75.
- Fibres: The waste plastic fibres were obtained by cutting waste plastic pots, buckets, cans, drums and utensils. The waste plastic fibres obtained were all recycled plastics. The fibres were cut from steel wire cutter and it is labour oriented. The thickness of waste plastic fibres was 1mm and its breadth was kept 5mm and these fibres were straight. The different volume fraction of fibres and suitable aspect ratio were selected and used in this investigation
- Water: Ordinary potable water free from organic content, turbidity and salts was used for mixing and for curing throughout the investigation.
- Superplasticizer: To impart the additional desired properties, a superplasticizer (Conplast SP-430) was used. The dosage of super plasticizer adopted in the experimentation was 1% (by weight of cement).
- Polymer: Nafufill BB2 polymer was used in the experimentation manufactured by MC. Bauchemie (India) Pvt. Ltd. Mumbai. The dosage of polymer adopted in the experimentation were 0%, 2%, 4%, 6%, 8% and 10%.

2.2 Experimental Procedure

The main objective of this experimental investigation is to find out the effect of addition of polymer on the workability and strength characteristics of waste plastic fibre reinforced concrete. The results are compared with polymer concrete without waste plastic fibres.

Concrete was prepared by a design mix proportion of 1: 1.435: 2.46 with a W/C ratio of 0.48 which correspond to M20 grade of concrete. The different percentage addition of polymer adopted in the experimental programme are 0%, 2%, 4%, 6%, 8% and 10%. Waste plastic fibres having an aspect ratio 50 (thickness = 1mm, length = 30mm and breadth = 5mm) were added in the dry mix at the rate of 1.5% (by volume fraction). The required percentage of polymer was added and machine mixed. All the specimens were cast with and without waste plastic fibres and tested after 28 days of curing as per IS specifications. When the mix was wet the workability test like slump test, compaction factor test and flow tests were carried out. After 28 days of water curing the specimens were weighed for their density and tested for their strength. The different strength parameters of waste plastic fibre reinforced concrete like compressive strength, tensile strength, flexural strength and impact strength were found for different percentage addition/replacement of cement by Micro silica-600 as the case may be. The compressive strength tests were conducted as per IS: 516-1959 on specimens of size 150 x 150 x 150 mm. The tensile strength tests were conducted as per IS: 5816-1999 on specimens of diameter 150 mm and length 300mm. Indirect tension test (Brazilian test) was conducted on tensile strength test specimens. Flexural strength tests were conducted as per IS: 516-1959 on specimens of size 100 x 100 x 500mm. Two point loading was adopted on a span of 400 mm, while conducting the flexural strength test. The impact strength tests were conducted as per ACI committee-544 on the panels of size 250 x 250 x 30 mm. A mild steel ball weighing 1.216 kg was dropped from a height of one meter on the impact specimen, which was kept on the floor. The care was taken to see that the ball was dropped at the center point of specimen every time. The number of blows required to cause first crack and final failure were noted. From these numbers of blows, the impact energy was calculated as follows.

$$\begin{aligned}\text{Impact energy} &= mghN \\ &= w/g \times g \times h \times N \\ &= whN \text{ (N-m)}\end{aligned}$$

Where, m = mass of the ball

w = weight of the ball = 1.216 kg

g = acceleration due to gravity

h = height of the drop = 1m

N = average number of blows to cause the failure.

III. Experimental results

The following tables give the details of the experimental results

3.1 Compressive strength test results -The following Table No. 3.1.1 and 3.1.2 gives the compressive strength test results of polymer concrete with and without waste plastic fibres.

Table 3.1.1: Compressive strength test results of polymer concrete with waste plastic fibres

Percentage addition of polymer	Specimen identification	Weight of specimen (N)	Density (kN/m ³)	Average density (kN/m ³)	Failure load (kN)	Compressive strength (MPa)	Average compressive strength (MPa)	Percentage increase or decrease of compressive strength w. r. t reference mix
0 (Ref mix)	A	76	22.52	22.52	640	28.44	28.74	---
	A	76	22.52		640	28.44		
	A	76	22.52		660	29.33		
2	B	75	22.23	22.23	690	30.66	30.52	+ 6
	B	75	22.23		680	30.22		
	B	75	22.23		690	30.66		
4	C	76	22.52	22.52	720	32	32.44	+ 13
	C	76	22.52		740	32.88		
	C	76	22.52		730	32.44		
6	D	74	21.93	21.93	740	32.88	33.48	+ 16
	D	74	21.93		760	33.77		
	D	74	21.93		760	33.77		
8	E	72	21.33	21.53	760	33.77	34.52	+ 20
	E	72	21.33		770	34.22		
	E	74	21.93		800	35.55		
10	F	74	21.93	21.93	710	31.55	31.7	+ 10
	F	74	21.93		720	32		
	F	74	21.93		710	31.55		

Table 3.1.2: Compressive strength test results of polymer concrete without waste plastic fibres

Percentage addition of polymer	Specimen identification	Weight of specimen (N)	Density (kN/m ³)	Average density (kN/m ³)	Failure load (kN)	Compressive strength (MPa)	Average compressive strength (MPa)	Percentage increase or decrease of compressive strength w. r. t reference mix
0 (Ref mix)	A1	73	21.63	21.43	585	26	25.73	---
	A1	72	21.33		580	25.78		
	A1	72	21.33		572	25.42		
2	B1	72	21.33	21.13	595	26.44	26.07	+ 1
	B1	71	21.04		585	26		
	B1	71	21.04		580	25.77		
4	C1	72	21.33	21.34	660	29.34	29.5	+ 15
	C1	71	21.04		675	30		
	C1	73	21.63		656	29.15		
6	D1	71	21.04	21.04	700	31.12	31.62	+ 23
	D1	71	21.04		710	31.55		
	D1	71	21.04		724	32.17		
8	E1	71	21.04	20.94	730	32.45	32.6	+ 27
	E1	70	20.74		730	32.45		
	E1	71	21.04		740	32.89		
10	F1	70	20.74	20.94	650	28.89	29.04	+ 13
	F1	71	21.04		660	29.34		
	F1	71	21.04		650	28.89		

The above results can be depicted in the form of graph as shown fig 3.1

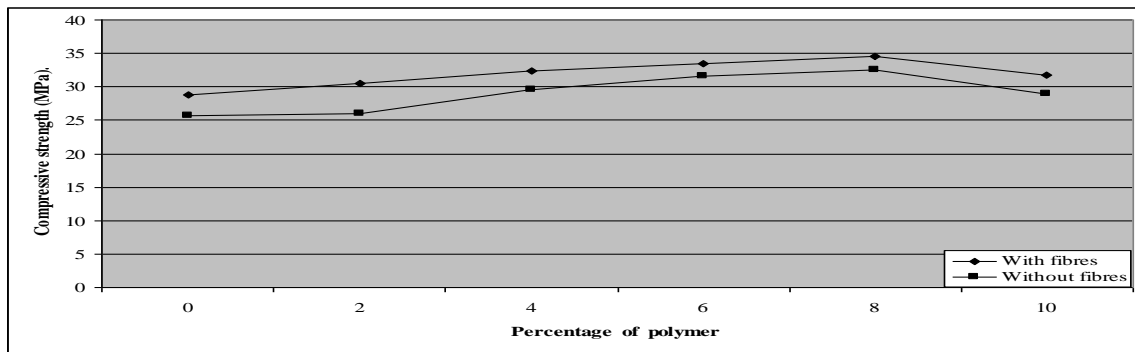


Fig.3.1: Variation of compressive strength test results of concrete with and without waste plastic fibres for different percentage addition of polymer

3.2 Tensile strength test results -The following Table No. 3.2.1 and 3.2.2 gives the tensile strength test results of polymer concrete with and without waste plastic fibres.

Table 3.2.1: Tensile strength test results of polymer concrete with waste plastic fibres

Percentage addition of polymer	Specimen identification	Failure load (kN)	Tensile strength (MPa)	Average tensile strength (MPa)	Percentage increase or decrease of tensile strength w. r. t reference mix
0 (Ref mix)	A	240	3.39	3.82	---
	A	280	3.96		
	A	290	4.1		
2	B	280	3.96	3.96	+ 4
	B	300	4.24		
	B	260	3.67		
4	C	290	4.1	4.29	+ 12
	C	320	4.52		
	C	300	4.24		
6	D	340	4.81	4.67	+ 22
	D	320	4.52		
	D	330	4.66		
8	E	360	5.09	5.04	+ 32
	E	360	5.09		
	E	350	4.95		
10	F	300	4.24	4.52	+ 18
	F	330	4.66		
	F	330	4.66		

Table 3.2.2: Tensile strength test results of polymer concrete without waste plastic fibres

Percentage addition of polymer	Specimen identification	Failure load (kN)	Tensile strength (MPa)	Average tensile strength (MPa)	Percentage increase or decrease of tensile strength w. r. t reference mix
0 (Ref mix)	A	175	2.47	2.5	---
	A	175	2.47		
	A	180	2.54		
2	B	195	2.76	2.7	+ 8
	B	190	2.68		
	B	190	2.68		
4	C	215	3.04	3.15	+ 26
	C	220	3.11		
	C	233	3.29		
6	D	280	3.96	3.92	+ 57
	D	275	3.9		
	D	275	3.9		
8	E	295	4.17	4.17	+ 67
	E	300	4.24		
	E	290	4.1		
10	F	262	3.66	3.53	+ 41
	F	240	3.4		
	F	250	3.53		

The above results can be depicted in the form of graph as shown fig 3.2

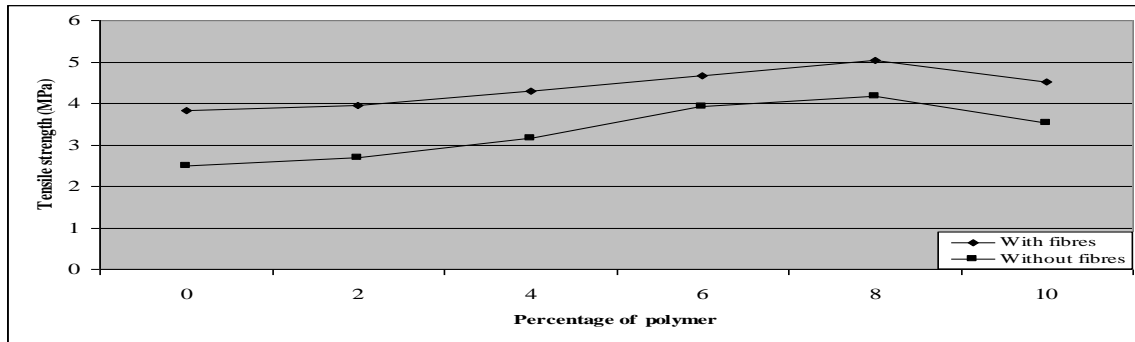


Fig.3.2: Variation of tensile strength test results of concrete with and without waste plastic fibres for different percentage addition of polymer

3.3 Flexural strength test results -The following Table No. 3.3.1 and 3.3.2 gives the flexural strength test results of polymer concrete with and without waste plastic fibres

Table 3.3.1: Flexural strength test results of polymer concrete with waste plastic fibres

Percentage addition of polymer	Specimen identification	Failure load (kN)	Flexural strength (MPa)	Average flexural strength (MPa)	Percentage increase or decrease of flexural strength w. r. t reference mix
0 (Ref mix)	A	13.8	5.52	5.53	---
	A	13.8	5.52		
	A	13.9	5.56		
2	B	14.3	5.72	5.61	+ 2
	B	14	5.6		
	B	13.8	5.52		
4	C	14.5	5.8	5.73	+ 4
	C	14.3	5.72		
	C	14.2	5.68		
6	D	14.7	5.88	5.85	+ 6
	D	14.5	5.8		
	D	14.7	5.88		
8	E	14.8	5.92	5.95	+ 8
	E	14.9	5.96		
	E	14.9	5.96		
10	F	14.1	5.64	5.69	+ 3
	F	14.4	5.76		
	F	14.2	5.68		

Table 3.3.2: Flexural strength test results of polymer concrete without waste plastic fibres

Percentage addition of polymer	Specimen identification	Failure load (kN)	Flexural strength (MPa)	Average flexural strength (MPa)	Percentage increase or decrease of flexural strength w. r. t reference mix
0 (Ref mix)	A1	9.6	3.84	3.78	---
	A1	9.4	3.76		
	A1	9.4	3.76		
2	B1	10.6	4.24	4.21	+ 11
	B1	10.52	4.2		
	B1	10.5	4.2		
4	C1	11.5	4.6	4.7	+ 24
	C1	11.9	4.76		
	C1	11.8	4.72		
6	D1	13	5.2	5.1	+ 35
	D1	12.8	5.12		
	D1	12.5	5		
8	E1	14	5.6	5.62	+ 49
	E1	14	5.6		
	E1	14.2	5.68		
10	F1	12.5	5	4.8	+ 27
	F1	11.5	4.6		
	F1	12	4.8		

The above results can be depicted in the form of graph as shown fig 3.3

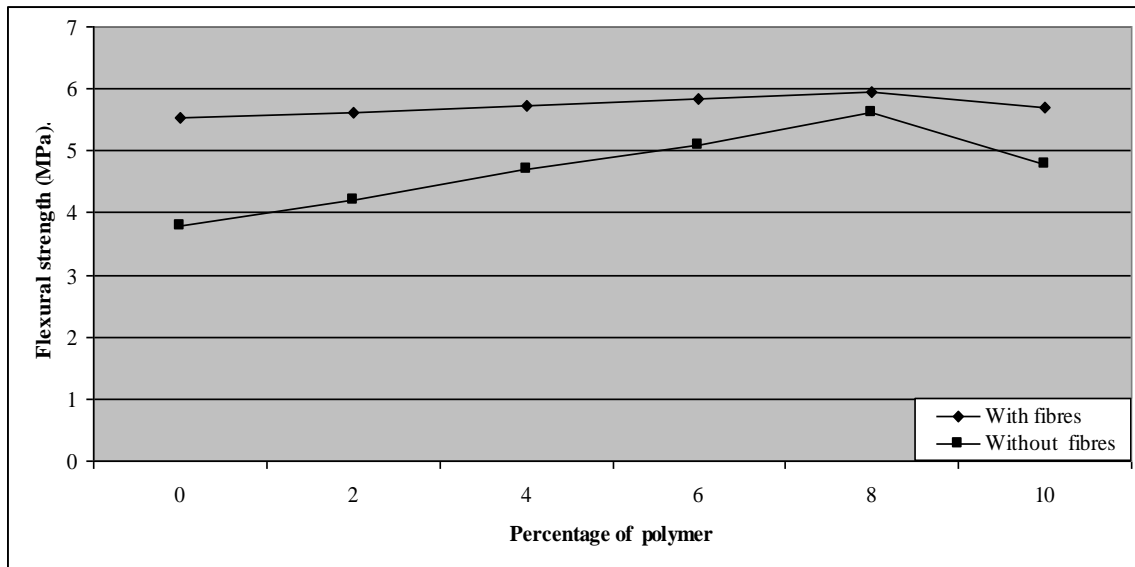


Fig 3.3: Variation of flexural strength test results of concrete with and without waste plastic fibres for different percentage addition of polymer

3.4 Impact strength test results - The following Table No. 3.4.1 and 3.4.2 gives the impact strength test results of polymer concrete with waste plastic fibres

Table 3.4.1: Impact strength test results of polymer concrete with waste plastic fibres

Percentage addition of polymer	Specimen identification	Number of blows required to cause		Average number of blows required to cause		Impact strength (N-m) required to cause		Percentage increase or decrease of impact strength w. r. t reference mix	
		first crack	final failure	first crack	final failure	first crack	final failure	first crack	final failure
0 (Ref mix)	A	6	20	4.34	19.34	52.77	235.17	---	---
	A	4	21						
	A	3	17						
2	B	6	22	5.67	22.34	68.94	271.65	+ 31	+ 16
	B	4	21						
	B	7	24						
4	C	7	24	7	25	85.12	304	+ 61	+ 29
	C	8	28						
	C	6	23						
6	D	10	26	10.67	27	129.74	328.32	+ 146	+ 40
	D	12	30						
	D	10	25						
8	E	12	30	12.67	31	154.06	376.96	+ 192	+ 60
	E	13	33						
	E	13	30						
10	F	9	26	8.34	25.67	101.41	312.14	+ 92	+ 33
	F	8	26						
	F	8	25						

Table 3.4.2: Impact strength test results of polymer concrete without waste plastic fibres

Percentage addition of polymer	Specimen identification	Number of blows required to cause		Average number of blows required to cause		Impact strength (N-m) required to cause		Percentage increase or decrease of impact strength w. r. t reference mix	
		first crack	final failure	first crack	final failure	first crack	final failure	first crack	final failure
0 (Ref mix)	A1	3	16	3.34	16.34	41.61	198.7	---	---
	A1	4	17						
	A1	3	16						
2	B1	4	18	4	18.34	48.64	223	+ 17	+ 12
	B1	4	18						
	B1	4	19						
4	C1	6	24	5.67	22.67	68.94	275.66	+ 66	+ 39
	C1	5	22						
	C1	6	22						
6	D1	7	24	7.34	24.34	89.25	296	+ 115	+ 49
	D1	8	25						
	D1	7	24						
8	E1	9	25	9.34	25.67	113.57	312.14	+ 173	+ 57
	E1	10	27						
	E1	9	25						
10	F1	8	24	7.67	24	93.26	291.84	+ 124	+ 47
	F1	8	23						
	F1	7	25						

The above results can be depicted in the form of graph as shown fig 3.4

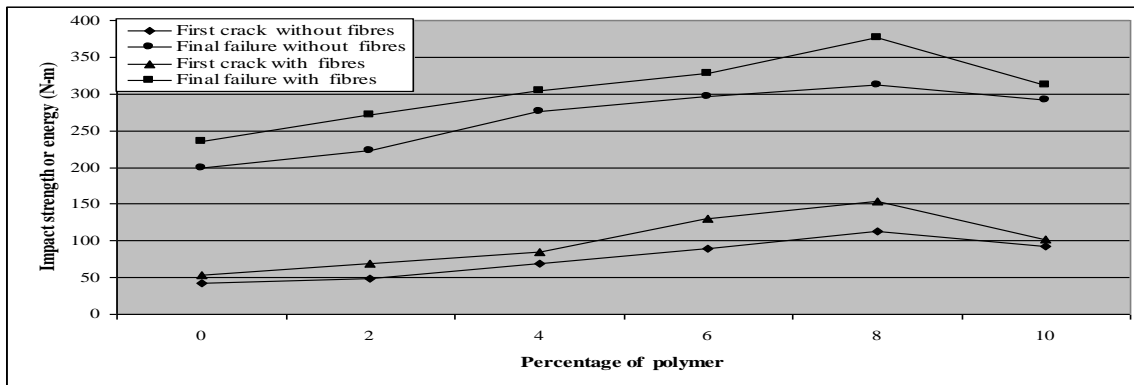


Fig 3.4: Variation of impact strength test results of concrete with and without waste plastic fibres for different percentage addition of polymer

3.5 Workability test results -The following Table No 3.5.1 gives the overall results of workability of polymer concrete with and without waste plastic fibres

Table 3.5.1: Workability of polymer concrete with and without waste plastic fibres

Percentage addition of polymer	Workability of concrete with waste plastic fibres			Workability of concrete without waste plastic fibres		
	Slump (mm)	Compaction factor	Percentage flow	Slump (mm)	Compaction factor	Percentage flow
0 (Ref. mix)	0	0.8	7.9	0	0.8	8.2
2	0	0.8	11.8	0	0.81	12.5
4	0	0.81	17.1	0	0.82	18
6	0	0.84	18.4	0	0.84	19
8	0	0.85	22.3	0	0.86	22.8
10	0	0.82	20.5	0	0.83	21

The above results can be depicted in the form of graph as shown fig 3.5 to 3.7

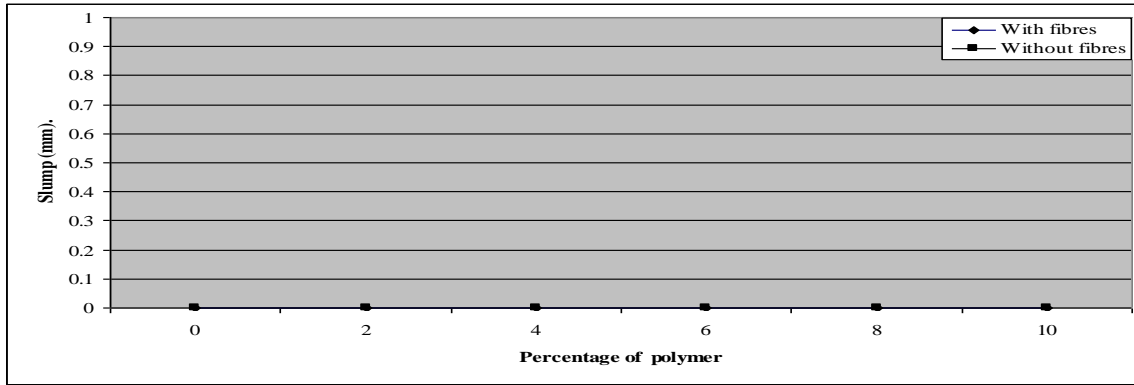


Fig 3.5: Variation of slump of concrete with and without waste plastic fibres for with different percentage addition of polymer

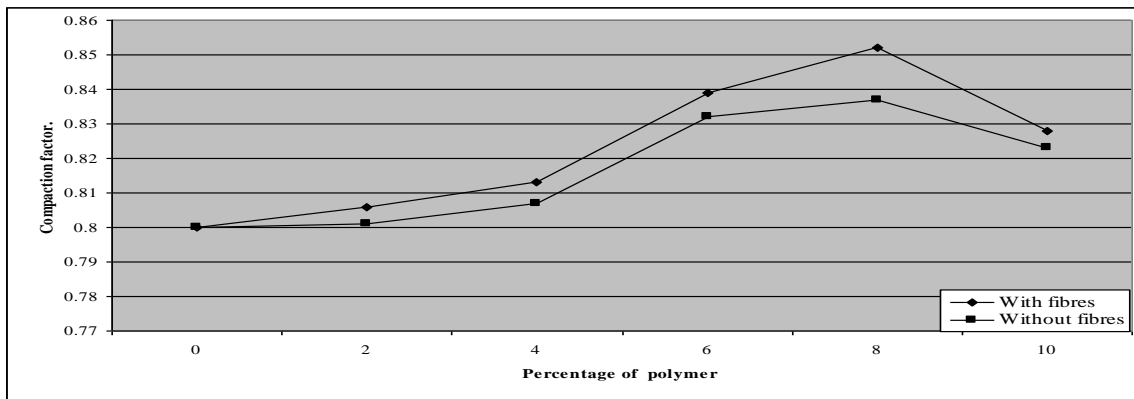


Fig 3.6: Variation of compaction factor of concrete with and without waste plastic fibres for different percentage addition of polymer

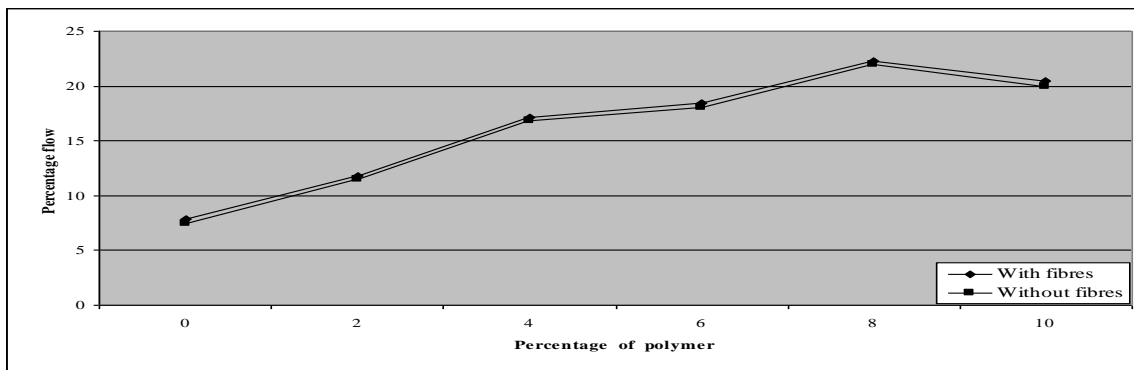


Fig 3.7: Variation of percentage flow of concrete with and without waste plastic fibres for different percentage addition of polymer

IV. Observations and Discussions

Based on the experimental results the following observations are made

- Both the concretes with waste plastic fibres and without waste plastic fibres show an increasing trend in the compressive strength from 0% addition of polymer up to 8% addition. After 8% of addition of polymer the compressive strength starts decreasing i.e., the maximum compressive strength is obtained when 8% polymer is added. Therefore, the higher compressive strength can be achieved when 8% polymer is added and the percentage increase in the compressive strength is 20% and 27% respectively for concrete with and without waste plastic fibres. Both the concretes with waste plastic fibres and without waste plastic fibres show an increasing trend in the tensile strength from 0% addition of polymer up to 8% addition. After 8% of addition of polymer the tensile strength starts decreasing i.e., the maximum tensile strength is obtained when 8% polymer is added. Therefore, the higher tensile strength can be achieved when 8% polymer is added and the percentage increase in the tensile strength is 32% and 67% respectively for concrete with and without waste plastic fibres. Both the concretes with waste plastic fibres and without waste plastic fibres show an increasing trend in the flexural strength from 0% addition of polymer up to 8% addition. After 8% of addition of polymer, the flexural strength starts decreasing i.e., the maximum flexural strength is obtained when 8% polymer is added. Therefore, the higher flexural

strength can be achieved when 8% polymer is added and the percentage increase in the flexural strength is 8% and 49% respectively for concrete with and without waste plastic fibres.

Both the concretes with waste plastic fibres and without waste plastic fibres show an increasing trend in the impact strength from 0% addition of polymer upto 8% addition. After 8% of addition of polymer the impact strength starts decreasing i.e., the maximum impact strength is obtained when 8% polymer is added. Therefore, the higher impact strength can be achieved when 8% polymer is added and the percentage increase in the impact strength for final failure 60% and 59% respectively for concrete with and without waste plastic fibres.

This may be due to the fact that addition of 8% polymer may induce more workability and make the mix more homogeneous there by producing higher strength properties.

Thus it can be concluded that addition of 8% polymer can produce higher strengths in concrete with or without waste plastic fibres.

- 2 It has been observed that the strength properties (compressive strength, tensile strength, flexural strength, and impact strength) of polymer concrete with waste plastic fibres are higher as compared to the polymer concrete without waste plastic fibres.

This may be due to the fact that the addition of waste plastic fibres certainly induces desirable strength properties by arresting the cracks.

Thus it can be concluded that the strength properties of polymer concrete can be enhanced by adding waste plastic fibres into it.

- 3 It has been observed that the workability of waste plastic fibre reinforced concrete increases upto 8% addition of polymer. After 8% the workability decreases. Therefore, the maximum workability is achieved with the addition of 8% polymer. This is true for concretes with and without waste plastic fibres.

This may be due to the fact that more than 8% addition of polymer may induce stiffness to concrete there by reducing the workability characteristics.

Thus it can be concluded that addition of 8% polymer can produce good workability properties to concrete with or without waste plastic fibres.

4. It has been observed that the workability values of concrete with waste plastic fibres are less as compared to concrete without waste plastic fibres. This is true for all the percentage addition of polymers.

This is obviously due to the fact that the addition of waste plastic fibres obstructs the flow and reduces the workability.

Thus it can be concluded that the workability of polymer concrete with waste plastic fibres is less as compared to workability of polymer concrete without waste plastic fibres.

5. It is observed from the literature (Neelamagum.M et al.,) that the Glass fibre reinforced concrete with polymer impregnation show marginally increases in the strength properties. However the addition of polymer in waste plastic fibre reinforced concrete has yielded better strength characteristics as compared to Glass fibre reinforced concrete.

V. Conclusions

1. Addition of 8% polymer can produce higher strength characteristics in concrete with or without waste plastic fibres.
2. The strength properties of polymer concrete can be enhanced by adding waste plastic fibres into it.
3. Addition of 8% polymer can produce good workability properties to concrete with or without waste plastic fibres.
4. Workability of polymer concrete with waste plastic fibres is less as compared to workability of polymer concrete without waste plastic fibres.

VI. Acknowledgements

The authors would like to thank Vice-Chancellor, Christ University, Fr. Benny Thomas, Director and Dr. Iven Jose, Associate Dean, Christ University Faculty of Engineering, Bangalore for their constant encouragement.

References

- [1] Nataraj M.C., Dhang.M. Gupta, A.P., "Behaviour of steel fibre reinforced concrete under compression", proceedings of the International Symposium on innovative world of concrete, Calcutta, India.
- [2] Neelamegam, M. and Venkateshwarlu, B., "Properties of Glass Fibre Reinforced Cement Composites with and without Polymer Impregnation", Proceedings of the International Symposium on Fibre Reinforced Concrete, December 16-19, 1987, Madras, India, pp.3.67-3.82.
- [3] Praksah K. B., and Prahallada, M .C., " Investigations on various Aspect ratios of the waste plastic fibre reinforced concrete" technical journal New Building Materials and Construction world, July 2001.
- [4] Ramakrishna "Materials and properties of fibre reinforced concrete", Proceedings of International Symposium on FRC, 19 December 1987, Madras, India.

A Novel Way to Stabilize Electricity Demand-Supply Ratio in Market

Shubhadeep A. Basak,¹ Nilesh D. Bankar²

^{1,2} 3rd year, Dept. of Electrical Engineering, Government College of Engineering, Amravati, India

Abstract: Presently, the demand-supply gap in electricity is very monstrous and the common man can use only a few percentage of the generated electricity. A decentralized approach has been taken in this study to understand the prevalent demand-supply gap in electricity in the Indian market. The roots of this gap have been thoroughly viewed from every possible angle. Circumnavigating the entire electricity market readily brings out the flaws and drawbacks in it resulting in a very bleak scenario. Quality control factors are also considered to the minutest detail. So, a new method of supply chain marketing in the electricity sector is proposed.

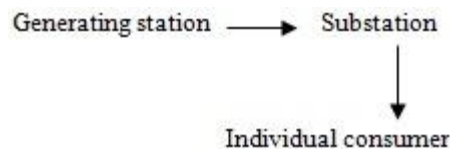
Keywords: Capacitor banks, Insulator, LASER technology, Optical Sensors, Spatial coherence.

I. Introduction

The first demonstration of electric light in Kolkata was conducted on 24th July, 1879 by PW Fleury & Co. followed by Bombay in 1882.^[1] The first hydroelectric installation in India was in Darjeeling in 1897^[2]. After 115 years of first installation of hydroelectric plant in India in Darjeeling in 1897, the electricity sector in India has an installed capacity of 207.85 Gigawatt (GW) as of September 2012, the world's fifth largest^[3]. Thermal power plants constitute about 66% of the installed capacity, hydroelectric about 19% and rest is a combination of wind, small hydro, biomass, waste-to-electricity, and nuclear. If we compare the scenario with other countries of the world, we will find that in India the coal-fired plants account for 56% of India's installed electricity capacity; the same is 92% of South Africa's, 77% of China's and 76% of Australia's. The renewal hydropower constitutes 19%, renewal energy about 12% and natural gas about 9%^[4,5]. In December 2011, it was estimated that over 300 million Indian citizens had no access to electricity. Over one third of India's rural population lacked electricity, as did 6% of the urban population. Those who had access to electricity in India, the supply was intermittent and unreliable. In 2010, blackouts and power shedding interrupted irrigation and manufacturing across the country^[6,7]. The per capita consumption of electricity in India is reported to be 778 kWh^[4] which is quite less compared to worldwide per capita annual average of 2600 kWh and 6200 kWh in European Union^[7].

India currently suffers from a major shortage of electricity generation capacity, even though it is the world's fourth largest energy consumer after United States, China and Russia. The International Energy Agency estimates India needs an investment of at least \$135 billion to provide universal access of electricity to its population. Gap between peak electricity demand and supply is 12%. Though 80% of rural areas have been connected to electricity, less than 45% of rural households have access to electricity. The transmission and distribution losses are 35-45% compared to the world average of less than 15%. In simple words, out of every 100 units produced, 33 units are lost during transmission and distribution.

In the present electricity distribution system, a grid (power transmission system) consists of two infrastructures: the high-voltage transmission systems, which carry electricity from the power plants and transmit it hundreds of miles away, and the lower-voltage distribution systems, which draw electricity from the transmission lines and distribute it to individual customers.



High voltage is used for transmission lines to minimize electrical losses; however, high voltage is impractical for distribution lines. Electricity distribution is the penultimate process in the delivery of electric power, i.e. the part between transmission and user purchase from an electricity retailer. It is generally considered to include medium-voltage (less than 50kV) power lines, low-voltage electrical substations and pole-mounted transformers, low-voltage (less than 1000V) distribution wiring and sometimes electricity meters. This interface features transformers that "step down" the transmission voltages to lower voltages for the distribution systems. Transformers located along the distribution lines further step down the voltage for household use. Thus, transmission and distribution losses need to be minimised in order to achieve high efficiency.

II. Objective

For the past two decades, India had to face increasing deficit in power supply, both for meeting its normal energy requirements as well as its peak load demand. The problem is acute during peak hours and summers, and necessitates planned load shedding by many utilities to maintain the grid in a healthy state. The average all-India shortages in 2009-10 were at 10 per cent in terms of normal energy requirement and about 13 per cent in terms of peak load^[9]. With the shortage

at both the normal and the peak levels, Indian power industry does not exhibit much cyclicity. Further, with assured returns, the margins of players and their profitability is almost independent of the economic cycles. Electricity is the most important component of primary energy. India's electricity consumption has grown at an average rate of 7.3 per cent during the period 2002-07. Consumption has increased at a faster rate since 2002-03, reflecting buoyant industrial demand. Industrial consumers are the largest group of electricity consumers, followed by the domestic, agricultural and commercial consumers, respectively. In April 2012 according to Central Electricity Authority (CEA), the gap between electricity generation and demand in India touched 8.2% and the highest shortfall was observed in Meghalaya at 28.1% whereas the shortfall witnessed by western region was 11.4% and South India was 15.5% respectively^[10]. In India, electricity losses during transmission and distribution were 24% in 2010 and losses due to consumer theft or billing deficiencies added another 10-15%^[11]. In 2004, it has been reported that theft of electricity in India caused a nationwide loss of \$4.5 billion^[12]. India's per capita electricity consumption increased from 178 kWh in 1985-86 to 704.4 kWh in 2007-08. Over the period, 2001-08, per capita consumption has increased at an average rate of 4.45 per cent. It is still much lower compared to the international standards. The aim of our paper is that according to our proposed system, the gap between demand and supply will be reduced.

III. Actual Method

Here, as we see in the present system, it requires a two step process for its completion. Usually copper wires are used for conduction. Our proposed system is:

3.1 Use of LASER to detect power theft

A laser is a device that emits light (electromagnetic radiation) through a process of optical amplification based on the stimulated emission of photons. The term "laser" is an acronym for Light Amplification by Stimulated Emission of Radiation. The emitted laser light is very useful for its high degree of spatial and temporal coherence, unattainable using other technologies. Spatial coherence is detected through the output being a narrow beam which is diffraction-limited, often called as "pencil beam." Laser beams can be focused to very tiny spots, achieving a very high irradiance or they can be launched into a beam of very low divergence in order to concentrate their power at a large distance.^{[13][14]}

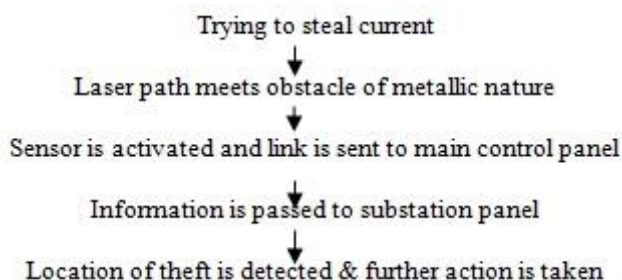
An Infrared (IR) LASER emits light with a longer wavelength than visible light, measured from the nominal edge of visible red light at 0.74micrometres (μm), and extending to 300 μm . These wavelengths correspond to a frequency range of approximately 1 to 400 THz^[13] and include most of the thermal radiation emitted by objects near room temperature. Microscopically, IR light is typically emitted or absorbed by molecules when they change their rotational-vibrational movements. Far infrared laser (FIR laser, terahertz laser) is a laser with output wavelength in far infrared part of the electromagnetic spectrum, between 30-1000 μm (300 GHz - 10 THz). It is one of the possible sources of terahertz radiation.

FIR lasers can be used in terahertz time-domain spectroscopy, terahertz imaging as well in fusion plasma physics diagnostics. They can be used to detect explosives and chemical warfare agents, by the means of infrared spectroscopy or to evaluate the plasma densities by the means of interferometry techniques. But near infrared Lasers have wavelengths of 1-5 μm .^[15]

Initially at the electricity generating plant, infrared laser generators are connected around the bus bars. The bars are kept as an axis; Infrared laser is generated at the starting point of the bus bar which can go upto a very large distance. Here, near infrared laser is used because for its short wavelength, large distance can be covered by it.

3.1.1 CROSS-SECTIONAL VIEW OF OUR PROPOSED MODEL

Thus in this arrangement (Fig.1), the laser beams surround the conductors carrying the electric current. The Laser generators will be connected to optical sensors which in turn will be connected to a control panel. The laser selected is such that it will only detect a metallic object and nothing other than that. When somebody connects a wire to the conductor for stealing electricity, the path of the Laser will be blocked by that wire. So, the some sensor becomes activated and goes into operation. It sends information about the fault and location of theft to the personnel sitting in the main control panel. He will pass this information to the substation control panel.



The LASER generated by one arrangement can travel only a definite amount of distance. So, after some distance, recharging is required. Thus, after few kilometres we require another laser operator to generate the next beam of light. In this way, the invisible laser beam will cover the entire length of conductor.

3.2 Use of dielectrics to reduce transmission losses

A dielectric is an electrical insulator that is polarized by an applied electric field. When a dielectric is placed in an electric field, electric charges do not flow through the material, as in a conductor, but only slightly shift from their average equilibrium positions causing dielectric polarization. Because of this dielectric polarization, positive charges are displaced toward the field and negative charges shift in the opposite direction. This creates an internal electric field which reduces the overall field within the dielectric itself. If a dielectric is composed of weakly bonded molecules, those molecules not only become polarized, but also reorient so that their symmetry axis aligns to the field.

Although the term "insulator" implies low electrical conduction, "dielectric" is typically used to describe materials with a high polarizability. The latter is expressed by a number called the dielectric constant. A common, yet notable example of a dielectric is the electrically insulating material between the metallic plates of a capacitor. The polarization of the dielectric by the applied electric field increases the capacitor's surface charge. The dielectric properties are concerned with the storage and dissipation of electric and magnetic energy in materials. It is important to explain various phenomena in electronics, optics, and physics. To increase the efficiency of electricity transmission we have to increase the power factor. For increasing the power factor we can use capacitor banks. Capacitor banks (Fig.2) contain dielectric material. As we know that by the property of dielectric materials we can reduce the transmission losses. So if we use good quality of dielectric material, we can reduce the transmission losses.^[16]

IV. Figures and Tables

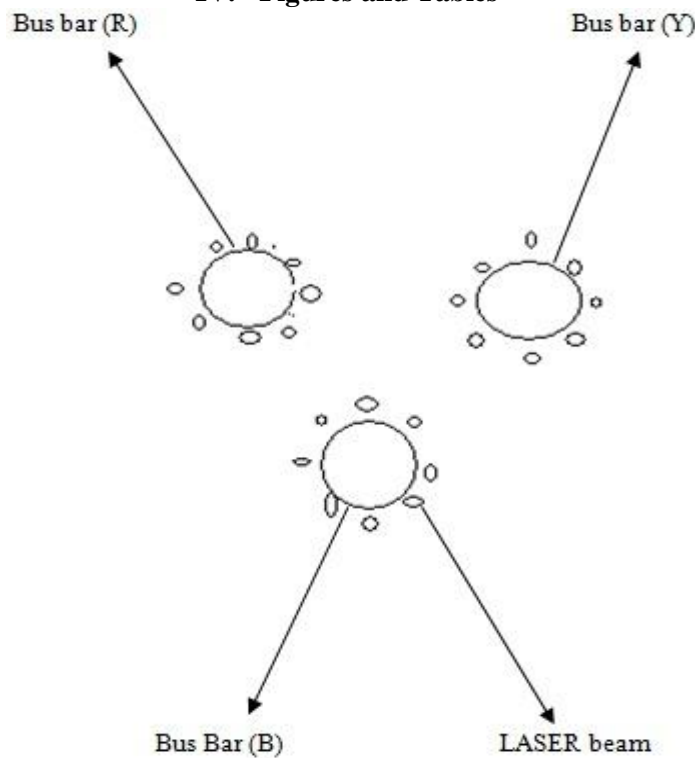


Fig.1. Proposed Model



Fig.2. Capacitor Bank

V. Summary

The laser technology used here provides an ideal model for the security of electric current against possible stealing threads. Power thefts constitute a large proportion of the total yearly losses.

Electricity Demand and Supply Source: CEA

FY	Energy				Peak Demand			
	(MU)				(MW)			
	Demand	Availability	Shortage	%	Demand	Met	Shortage	%
2002-03	545,983	497,890	48,093	8.8	81,492	71,547	9,945	12.2
2003-04	559,264	519,398	39,866	7.1	84,574	75,066	9,508	11.2
2004-05	591,373	548,115	43,258	7.3	87,906	77,652	10,254	11.7
2005-06	631,024	578,511	52,513	8.3	93,214	81,792	11,422	12.3
2006-07	693,057	624,716	68,341	9.9	100,715	86,818	13,897	13.8
2007-08	737,052	664,660	72,392	9.8	108,866	90,793	18,073	16.6
2008-09	777,039	691,038	86,001	11.1	109,809	96,785	13,024	11.9
2009-10	830,594	746,644	83,950	10.1	118,472	102,725	15,747	13.3

By the use of capacitors the expected I^2R losses can be reduced. Here the capacitors store charge and increases the active component of power. In capacitor banks the dielectric materials are used to reduce the transmission losses. If we use high purity dielectric material, the losses can be minimized to a very very low value.

VI. Conclusion

Now in the present market scenario we can see that the economics of power distribution is not viable for sustained long term growth and development. On one hand the demand always goes on increasing while on the other, the supply cannot keep pace with the rising demand. Thus the demand supply gap goes on increasing. This is further aggravated by the situations like fuel shortages, strikes, non-operating units of the power plant etc.. But the disadvantages are also to be taken into account. It includes the cost of production of LASER beam, special equipments required to maintain it and its applicability in dense areas. But it can be applied on a trial basis in selected markets and the maintenance costs should be calculated. If it becomes feasible, it can be expanded to other areas. Thus our proposed method presents an idea to reduce the losses, so that the supply becomes almost proportional to demand. Hence, the market can be stabilized to a great extent.

References

- [1] "Let there be light" (http://www.telegraphindia.com/1090426/jsp/calcutta/story_10866828.jsp). The Telegraph April 26, 2009.
- [2] Darjeeling Hydro Power System (<http://www.theiet.org/resources/library/archives/featured/darjeeling.cfm>)
- [3] "ALL INDIA REGIONWISE GENERATING INSTALLED CAPACITY OF POWER" (http://www.cea.nic.in/reports/monthly/executive_rep/jun12/8.pdf) Central Electricity Authority, Ministry of Power, Government of India, June 2012. http://www.cea.nic.in/reports/monthly/executive_rep/jun12/8.pdf
- [4] Power Sector at a Glance ALL INDIA. (http://www.powermin.nic.in/indian_electricity_scenario/introduction.htm) Ministry of Power, Government of India, June 2012. http://www.powermin.nic.in/indian_electricity_scenario/introduction.htm
- [5] World Coal Institute – India "The coal resource, a comprehensive overview of coal" (<http://www.worldcoal.org/pages/content/index.asp?PageID=402>) World Coal Institute, March 2009 (<http://www.worldcoal.org/pages/content/index.asp?PageID=402>)
- [6] "For India, a Power Failure Looms" <http://online.wsj.com/article/SB10001424052970203550304577136283175793516.html>) The Wall Street Journal. 2 January 2012. <http://online.wsj.com/article/SB10001424052970203550304577136283175793516.html>
- [7] Uwe Remme et al. (February 2011). "Technology development prospects for the Indian power sector" (http://www.iea.org/papers/2011/technology_development_india.pdf)
- [8] "World Energy Outlook 2011: Energy for All" (http://www.iea.org/papers/2011/weo2011_energy_for_all.pdf) International Energy Agency. October 2011. http://www.iea.org/papers/2011/weo2011_energy_for_all.pdf
- [9] <http://www.spartastrategy.com/blog/2011/07/indias-energy-dem-and-supply-deficit/>
- [10] <http://economictimes.indiatimes.com/articleshow/13395891.cms>
- [11] Yoginder Alagh, Former Minister of Power and Science Technology of India (2011). "Transmission and Distribution of Electricity in India Regulation, Investment and Efficiency" (<http://www.oecd.org/dataoecd/35/33/46235043.pdf>) OECD <http://www.oecd.org/dataoecd/35/33/46235043.pdf>
- [12] "Reforming the Power Sector: Controlling Electricity Theft and improving Revenue" (http://rru.worldbank.org/documents/publicpolicyjournal/272bhatia_Gulati.pdf) (PDF). The World Bank http://rru.worldbank.org/documents/publicpolicyjournal/272bhatia_Gulati.pdf
- [13] Gould, R. Gordon (1959). "The LASER, Light Amplification by Stimulated Emission of Radiation". In Franken, P.A. and Sands, R.H. (Eds). The Ann Arbor Conference on Optical Pumping, the University of Michigan, 15 June through 18 June 1959. p.128
- [14] "Laser" Reference.com. Retrieved May 15, 2008.
- [15] en.wikipedia.org/wiki/Far-infrared_laser.
- [16] en.wikipedia.org/wiki/Dielectric.

A Survey on Different Clustering Algorithms in Data Mining Technique

P. IndiraPriya,¹ Dr. D.K.Ghosh²

¹Tagore Engineering College, Chennai, India

²V.S.B. Engineering College, Karur, India

ABSTRACT: Fast retrieval of the relevant information from databases has always been a significant issue. There are many techniques are developed for this purpose; In among data clustering is one of the major technique. The process of creating vital information from a huge amount of data is learning. It can be classified into two such as supervised learning and unsupervised learning. Clustering is a kind of unsupervised data mining technique. It describes the general working behavior, the methodologies followed by these approaches and the parameters which affect the performance of these algorithms. In classifying web pages, the similarity between web pages is a very important feature. The main objective of this paper is to gather more core concepts and techniques in the large subset of cluster analysis.

Keywords: Clustering, Unsupervised Learning Web Pages, Classifications.

I. Introduction

Now a day, people come across a huge amount of information and store or represent it as data. One of the vital means in dealing with these data is to classify or group them into a set of categories or clusters. Clustering involves creating groups of objects that are similar, and those that are dissimilar. The clustering problem lies in finding groups of similar objects in the data. The similarity between the objects is measured with the use of a similarity function. Clustering is especially useful for organizing documents, to improve retrieval and support browsing. Clustering is often confused with classification, but there is some difference between the two. In classification, the objects are assigned to pre defined classes, whereas in clustering the classes are also to be defined. To be Precise, Data Clustering is a technique in which, the information that is logically similar is physically stored together. In order to increase the efficiency in the database system the numbers of disk accesses are to be minimized. In clustering, objects having similar properties are placed in one class, and a single access to the disk makes the entire class available. Clustering algorithms can be applied in many areas, for instance, marketing, biology, libraries, insurance, city-planning, earthquakes, and www document classification.

1.1 Clustering

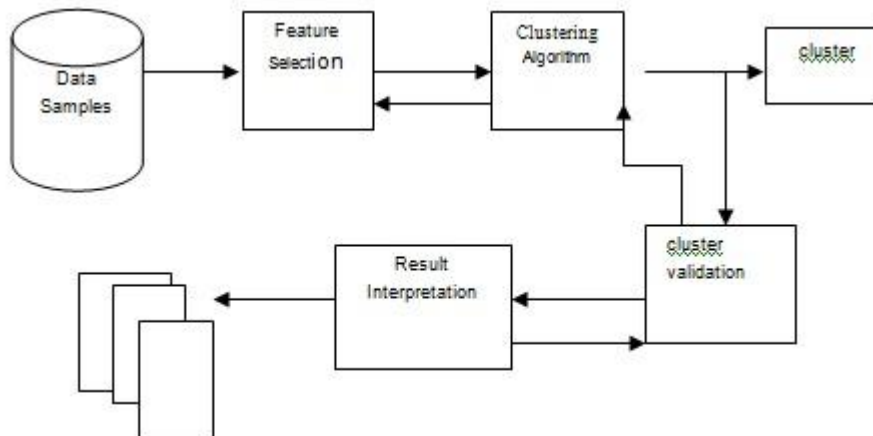
Clustering can be considered the most important unsupervised learning problem; so, as with every other problem of this kind, it deals with finding a structure in a collection of unlabeled data. The process of organizing objects into groups whose members are similar in some way is a cluster. A collection of objects which are “similar” between them and are “dissimilar” to the objects belonging to other clusters. Two important topics are: (1) Different ways to group a set of objects into a set cluster (2) types of Clusters.

The analysis of cluster is to identify and classifies objects, individuals or variables, on the basis of the similarities. It seeks to minimize within-group variance and maximize between-group variance. The result of the cluster analysis is a number of heterogeneous groups with homogeneous contents. The individuals within a single group are similar rather than substantial differences between the groups.

The Cluster analysis groups data objects based only on the information found in the data that describes the objects and their relationships. The goal is that the objects within a group be similar (or related) to one another and different from (or unrelated to) the objects in the other groups. The greater similarity (or homogeneity) of clustering is within a group, and the greater the difference between groups, the better or more distinct the clustering [8]. Data may be thought of as points in a space where the axes correspond to the variables. The cluster analysis divides the space into regions, characteristic of the groups found in the data. The main advantage of a clustered solution is automatic recovery from failure, that is, recovery without user intervention. The disadvantages of clustering are complexity and inability to recover from database corruption. An ordered list of objects, which have some common characteristics of cluster. The objects belong to an interval $[a, b]$, in our case $[0, 1]$ [2]. The distance between two clusters involves some or all elements of the two clusters. The clustering method determines how the distance should be computed [1]. A similarity measure $SIMILAR(D_i, D_j)$ can be used to represent the similarity between the documents. Typical similarity generates values of 0 for documents exhibiting no agreement among the assigned indexed terms, and 1 when perfect agreement is detected. Intermediate values are obtained for cases of partial agreement [1]. If the similarity measure is computed for all pairs of documents (D_i, D_j) except when $i=j$, an average value AVERAGE SIMILARITY is obtainable. Specifically, $AVERAGE\ SIMILARITY = \frac{1}{n(n-1)} \sum_{i \neq j} SIMILAR(D_i, D_j)$, where $i=1,2,\dots,n$ and $j=1,2,\dots,n$ and $i < j$. The lowest possible input value of similarity is required to join two objects in one cluster. The similarity between objects calculated by the function $SIMILAR(D_i, D_j)$, represented in the form of a matrix is called a similarity matrix. The dissimilarity coefficient of two clusters is defined as the distance between them. The smaller the value of the dissimilarity coefficient, the more similar the two clusters are.

The first document or object of a cluster is defined as the initiator of that cluster, i.e., similarity of every incoming object's is compared with the initiator. The initiator is called the cluster seed. The procedure of the cluster analysis with four basic steps is as follows:

1) **Feature selection or extraction.** As pointed out by Jain *et al.* [5], [6] and Bishop [7], feature selection chooses distinguishing features from a set of candidates, while feature extraction utilizes some transformations to generate useful and novel features from the original ones. An elegant selection of features can greatly decrease the workload, and simplify the subsequent design process. Generally, ideal features should be of use in distinguishing patterns belonging to different clusters, immune to noise, easy to extract and interpret. An elaborate discussion on feature extraction, in the context of data visualization and dimensionality reduction. More information on feature selection can be found in [7], [5], and [9].



Knowledge

2) **Clustering algorithm design or selection.** This step is usually combined with the selection of a corresponding proximity measure, and the construction of a criterion function. Patterns are grouped according to whether they resemble one another. Obviously, the proximity measure directly affects the formation of the resulting clusters. Almost all clustering algorithms are explicitly or implicitly connected to some definition of the proximity measure. Some algorithms even work directly on the proximity matrix. Once a proximity measure is chosen, the construction of a clustering criterion function makes the partition of clusters an optimization problem, which is well defined mathematically, and has rich solutions in the literature. Clustering is ubiquitous, and a wealth of clustering algorithms has been developed to solve different problems in specific fields. It has been very difficult to develop a unified framework for reasoning about it (clustering) at a technical level, and profoundly diverse approaches to clustering [10], as proved through an impossibility theorem. Therefore, it is important to carefully investigate the characteristics of the problem on hand, in order to select or design an appropriate clustering strategy.

3) **Cluster validation.** Given a data set, each clustering algorithm can always generate a division, no matter whether the structure exists or not. Moreover, different approaches usually lead to different clusters; and even for the same algorithm, parameter identification or the presentation order of the input patterns may affect the final results. Therefore, effective evaluation standards and criteria are important to provide the users with a degree of confidence, for the clustering results derived from the used algorithms. These assessments should be objective and have no preferences to any algorithm. Also, they should be useful for answering questions like how many clusters are hidden in the data, whether the clusters obtained are meaningful or just artifacts of the algorithms. Generally, there are three categories of testing criteria: external indices, internal indices, and relative indices. These are defined on three types of clustering structures, known as partitional clustering, hierarchical clustering, and individual clusters [11]. Tests for a situation, where no clustering structure exists in the data, are also considered [12], but seldom used, since users are confident of the presence of clusters. External indices are based on some pre specified structure, which is a reflection of prior information on the data, and used as a standard to validate the clustering solutions. Internal tests are not dependent on external information (prior knowledge). On the contrary, they examine the clustering structure directly from the original data. Relative criteria place the emphasis on the comparison of different clustering structures, in order to provide a reference, to decide which one may best reveal the characteristics of the objects. Shall not survey the topic in depth, but refer interested readers to [13], [14]. Approaches to fuzzy clustering validity are reported in [16], [17], [18].

4) **Results interpretation.** The ultimate goal of clustering is to provide users with meaningful insights into the original data, so that they can effectively solve the problems encountered. Experts in the relevant fields interpret the data partition. Further analyzes, even experiments, may be required to guarantee the reliability of the extracted knowledge.

1.2 Classification

Classification plays a vital role in many information management and retrieval tasks. On the Web, the classification of page content is essential to focused crawling, to the assisted development of web directories, to topic-specific web link analysis, and to the analysis of the topical structure of the Web. Web page classification can also help improve the quality of web search. Web page classification, also known as web page categorization, is the process of assigning a web page to one or more predefined category labels. Classification is often posed as a supervised learning problem (Mitchell 1997) in which a set of labeled data is used to train a classifier, which can be applied to label future examples.

The general problem of web page classification can be divided into multiple sub-problems: subject, functional, sentiment, and other types of classification. Subject classification concerns the subject or topic of a Web page. For example, judging whether a page is about “arts”, “business” or “sports” is an instance of subject classification. Functional classification cares about the role that the Web page plays. For example, deciding a page to be a “personal homepage”, “course page” or “admission page” is an instance of functional classification. Sentiment classification focuses on the opinion that is presented in a web page, i.e., the author’s attitude about some particular topic. Other types of classification include genre classification (e.g., (zu Eissen and Stein 2004)), search engine spam classification (e.g., (Gyongyi and Garcia-Molina 2005b; Castillo, Donato, Gionis, Murdock, and Silvestri 2007)) and so on.

Based on the number of classes in the problem, classification can be divided into binary classification and multi-class classification, where binary classification categorizes instances into exactly one of two classes; multi-class classification deals with more than two classes. Based on the number of classes that can be assigned to an instance, classification can be divided into single-label classification and multi-label classification. In single-label classification, one and only one class label is to be assigned to each instance, while in multi-label classification; more than one class can be assigned to an instance. If a problem is multi-class, say four-class classification, it means four classes are involved, say Arts, Business, Computers, and Sports. It can be either single-label, where exactly one class label can be assigned to an instance, or multi-label, where an instance can belong to any one, two, or all of the classes. Based on the type of class assignment, classification can be divided into hard classification and soft classification. In hard classification, an instance can either be or not be in a particular class, without an intermediate state; while in soft classification, an instance can be predicted to be in some class with some likelihood (often a probability distribution across all classes).

Based on the organization of categories, web page classification can also be divided into flat classification and hierarchical classification. In flat classification, categories are considered parallel, i.e., one category does not supersede another, while in hierarchical classification, the categories are organized in a hierarchical tree-like structure, in which each category may have a number of subcategories.

Clustering can be in the form of classification, in that it creates a labeling of objects with class (cluster) labels. Classification means a supervised classification; i.e., new, unlabeled objects are assigned a class label using developed objects with known class labels. The term segmentation and partitioning are sometimes used as synonyms for clustering. The partitioning is often used in connection with techniques that divide graphs into sub graphs and that are not strongly connected to clustering. Segmentation often refers to the division of data into group using simple techniques; eg., an image can be split into segments based only on pixel intensity and color, or people can be divided into groups based on their income. Clustering is a type of classification imposed on a finite set of objects. The relationship between objects is represented in a proximity matrix, in which rows and columns correspond to objects. The proximity matrix is the one and only input to a clustering algorithm.

In this paper, various clustering algorithms in data mining are discussed. A new approach for to improve the prediction accuracy of the clustering algorithms is proposed.

II. Approaches

2.1 Types of Clustering Algorithms

Clustering is a division of data into groups of similar objects [3]. The clustering algorithm can be divided into five categories, viz, Hierarchical, Partition, Spectral, Grid based and Density based clustering algorithms.

2.1.1 Hierarchical Clustering Algorithm

The hierarchical clustering algorithm is a group of data objects forming a tree shaped structure. It can be broadly classified into agglomerative hierarchical clustering and divisive hierarchical clustering. In the agglomerative approach, which is also called as the bottom up approach, each data point is considered to be a separate cluster, and on each iteration the clusters are merged, based on a criterion. The merging can be done by using the single link, complete link, centroid or wards method. In the divisive approach all data points are considered as a single cluster, and they are split into a number of clusters, based on certain criteria, and this is called as the top down approach. Examples of this algorithms are LEGCLUST [22], BRICH [19] (Balance Iterative Reducing and Clustering using Hierarchies), CURE (Cluster Using REpresentatives) [20], and Chameleon [1].

The construction of a hierarchical agglomerative classification can be achieved by the following general algorithm.

1. Find the 2 closest objects and merge them into a cluster
2. Find and merge the next two closest points, where a point is either an individual object or a cluster of objects.
3. If more than one cluster remains, return to step 2.

Individual methods are characterized by the definition used for the identification of the closest pair of points, and by the means used to describe the new cluster when two clusters are merged. There are some general approaches to the implementation of this algorithm; these being stored matrix and stored data, are discussed below:

- In the second matrix approach, an $N \times N$ matrix containing all pair wise distance values is first created, and updated as new clusters are formed. This approach has at least an $O(n^2)$ time requirement, rising to $O(n^3)$ if a simple serial scan of dissimilarity matrix is used to identify the points, which need to be fused in each agglomeration, a serious limitation for large N .
- The stored data approach requires the recalculation of the pair wise dissimilarity values for each of the $N-1$ agglomerations, and the $O(N)$ space requirement is therefore achieved at the expense of an $O(N^2)$ time requirement.

The advantages of hierarchical clustering include embedded flexibility regarding the level of granularity, and ease of handling of any forms of similarity or distance. Consequently, its applicability to any attributes types and its logical structure, make it easy to read and interpret. The disadvantages of hierarchical clustering are related to the vagueness of termination criteria, the fact that most hierarchical algorithms do not revisit once constructed, (intermediate) clusters with the purpose of their improvement; and that they are relatively unstable and unreliable, i.e., the first combination or separation of objects, which may be based on a small difference in the criterion, will constrain the rest of the analysis.

2.1.2 Spectral Clustering Algorithm

Spectral clustering refers to a class of techniques, which relies on the Eigen structure of a similarity matrix. Clusters are formed by partitioning data points using the similarity matrix. Any spectral clustering algorithm will have three main stages [23]. They are preprocessing, spectral mapping and post mapping. Preprocessing deals with the construction of the similarity matrix. Spectral Mapping deals with the construction of Eigen vectors for the similarity matrix. Post Processing deals with the grouping of data points.

The advantages of the spectral clustering algorithm are: strong assumptions on the cluster shape are not made; it is simple to implement and objective; it does not consider local optima; it is statistically consistent and works faster. The major drawback of this approach is that it exhibits high computational complexity. For large data set it requires $O(n^3)$, where n is the number of data points [17]. Examples of this algorithm are, SM(Shi and Malik) algorithm, KVV (Kannan, Vempala and Vetta) algorithm, and NJW (Ng, Jordan and Weiss) algorithm [22].

2.1.3 Grid based Clustering Algorithm

The grid based algorithm quantizes the object space into a finite number of cells, that forms a grid structure [1]. Operations are done on these grids. The advantage of this method is its lower processing time. Clustering complexity is based on the number of populated grid cells, and does not depend on the number of objects in the dataset. The major features of this algorithm are, no distance computations, Clustering is performed on summarized data points, Shapes are limited to the union of grid-cells, and the complexity of the algorithm is usually $O(\text{Number of populated grid-cells})$. STING [1] is an example of this algorithm.

2.1.4 Density based Clustering Algorithm

The density based algorithm allows the given cluster to continue to grow as long as the density in the neighborhood exceeds a certain threshold [4]. This algorithm is suitable for handling noise in the dataset. The following points are enumerated as the features of this algorithm: it handles clusters of arbitrary shape, Handles noise, needs only one scan of the input dataset, and the density parameters to be initialized. DBSCAN, DENCLUE and OPTICS [4] are examples of this algorithm.

Density-Based Connectivity

The crucial concepts of this section are density and connectivity, both measured in terms of local distribution of nearest neighbors.

The algorithm DBSCAN (Density Based Spatial Clustering of Applications with Noise) targeting low-dimensional spatial data is the major representative of this category.

Two input parameters and Min Pts are used to define:

- 1) An ϵ -neighborhood $N_\epsilon(x) = \{y \mid d(x, y) \leq \epsilon\}$ of the point x ,
- 2) A core object (a point with a neighborhood consisting of more than Min Pts points)
- 3) A concept of a point y density-reachable from a core object x (a finite sequence of core objects between x and y exists such that each next belongs to an ϵ -neighborhood of its predecessor)
- 4) A density-connectivity of two points x, y (they should be density-reachable from a common core object).

Density Functions

Hinneburg & Keim [1998] shifted the emphasis from computing densities pinned to data points to computing density functions defined over the underlying attribute space. They proposed the algorithm DENCLUE (DENSITY-based CLustering Using a Density Function). Along with DBCLASD, it has a firm mathematical foundation. DENCLUE uses a density function.

$$f^D(x) = \sum_{y \in D} f(x, y) \quad (1)$$

That is the superposition of several influence functions. When the f -term depends on x, y , the formula can be recognized as a convolution with a kernel. Examples include a square wave function $f(x, y) = \Theta(\|x - y\| / \sigma)$ equal to 1, if the distance between x and y is less than or equal to σ , and a Gaussian influence function $f(x, y) = e^{-\|x-y\|^2 / 2\sigma^2}$. This provides a high level of generality: the first example leads to DBSCAN, the second one to k -means clusters! Both examples depend on parameter σ . Restricting the summation to $D = \{y : \|x - y\| < k \sigma\} \subset X$ enables a practical implementation. DENCLUE concentrates on the local maxima of the density functions called density-attractors, and uses the flavor of the gradient hill-climbing technique for finding them. In addition to center-defined clusters, arbitrary-shape clusters are defined as continuations along sequences of points whose local densities are no less than the prescribed threshold ϵ . The algorithm is stable with respect to outliers and authors show how to choose parameters ϵ and σ . DENCLUE scales well, since at its initial stage it builds a map of hyper-rectangle cubes with an edge length 2σ . For this reason, the algorithm can be classified as a grid-based method.

The advantages of this density function in clustering are, that it does not require a-priori specification of the number of clusters, is able to identify noise data while clustering, and the DBSCAN algorithm is able to find arbitrarily sized and arbitrarily shaped clusters. The disadvantages of this density function in clustering are that the DBSCAN algorithm fails in the case of varying density clusters and in the case of a neck type of dataset.

2.1.5 Partition Clustering Algorithm

Partitioning methods generally result in a set of M clusters, each object belonging to one cluster. Each cluster may be represented by a centroid or a cluster representative; this is some sort of a summary description of all the objects contained in a cluster. The precise form of this description will depend on the type of the object which is being clustered. In cases where real-valued data is available, the arithmetic mean of the attribute vectors for all objects within a cluster provides an appropriate representative; alternative types of centroid may be required in other cases; e.g., a cluster of documents can be represented by a list of those keywords that occur in some minimum number of documents within a cluster. If the number of clusters is large, the centroids can be further clustered to produce a hierarchy within a dataset. The partition clustering algorithm splits the data points into k partition, where each partition represents a cluster. The partition is done based on certain objective functions. One such criterion function is minimizing the square error criterion which is computed as,

$$E = \sum \sum \|p - m_i\|^2 \quad (2)$$

Where p is the point in a cluster and m_i is the mean of the cluster. The cluster should exhibit two properties; they are (1) each group must contain at least one object (2) each object must belong to exactly one group. The main drawback of this algorithm [3] is whenever a point is close to the center of another cluster; it gives a poor result due to overlapping of the data points.

Single Pass is a very simple partition method; it creates a partitioned dataset in three steps. First, it makes the first object the centroid for the first cluster. For the next object, it calculates the similarity, S , with each existing cluster centroid, using some similarity coefficient. Finally, if the highest calculated S is greater than some specified threshold value, it adds the object to the corresponding cluster, and re-determines the centroid; otherwise, it uses the object to initiate a new cluster. If any objects remain to be clustered, it returns to step 2.

As its name implies, this method requires only one pass through the dataset; the time requirements are typically of the order $O(N \log N)$ for order $O(\log N)$ clusters. This makes it a very efficient clustering method for a serial processor. A disadvantage is that the resulting clusters are not independent of the order in which the documents are processed, with the first clusters formed usually being larger than those created later in the clustering run.

K -Means Clustering Algorithm is one of the partition based clustering algorithms. The advantages of the simple K means algorithm. That it is easy to implement and works with any of the standard norms. It allows straight forward parallelization; and it is insensitive with respect to data ordering. The disadvantages of the K means algorithm are as follows. The results strongly depend on the initial guess of the centroids. The local optimum (computed for a cluster) does not need to be a global optimum (overall clustering of a data set). It is not obvious what the good number K is in each case, and the process is, with respect to the outlier.

2.2 Soft Clustering

2.2.1 Fuzzy K Means Clustering

Fuzzy clustering allows each feature vector to belong to more than one cluster with different membership degrees (between 0 and 1), and vague or fuzzy boundaries between clusters. Fuzzy clustering is often used in modeling (fuzzy modeling, neural networks, rule-based systems), where the clusters are sought as a structural setup for the ensuing modelling activities. In this case, the viewpoints can be formed as some points that are located at the boundaries of the range of input variables, so that we achieve a comprehensive "coverage" of the input space, and this way, the models "spanned" over these information granules can be highly representative. The clusters exhibit a certain "crowding" tendency. It is very unlikely to see the clusters positioned at the extreme values of the input variables and, thus, represent these regions when it comes to the construction of the model. To elaborate on this effect in more detail and high light its implications to system modeling, let us

consider a rule-based model that is governed by the rules of the form if \mathbf{x} is A_i . . . then y is B_i and if \mathbf{x} is A_c . . . then y is B_c , where A_i and B_i are fuzzy sets, that are defined in the input and output spaces, respectively. Quite commonly, these fuzzy sets are developed through fuzzy clustering, and the centers of the clusters (prototypes) are the modes of the fuzzy sets A_i and B_i . Alluding to the prototypes formed through clustering, we note that they are formed in the aggregate input–output space, i.e., $[v_i, m_i]$. Three difficulties exist in fuzzy clustering. First, the optimal number of clusters K to be created, has to be determined (the number of clusters cannot always be defined *a priori* and a good cluster validity criterion has to be found). Second, the character and location of the cluster prototypes (centers) is not necessarily known *a priori*, and initial guesses have to be made. Third, the data characterized by large variability in the cluster shape, cluster density, and the number of points (feature vectors) in different clusters, have to be handled.

2.2.2 Fuzzy C Means Clustering

This algorithm works by assigning the membership to each data point corresponding to each cluster center, on the basis of the distance between the cluster center and the data point. The nearer data is to the cluster center, the more is its membership towards the particular cluster center. Clearly, the summation of the membership of each data point should be equal to one. The advantages of this clustering algorithm are it gives the best result for an overlapped data set, and a comparatively better than k-means algorithm. Unlike the k-means, where the data point must exclusively belong to one cluster center, here the data point is assigned a membership to each cluster center, as a result of which the data point may belong to more than one cluster center. The disadvantages of the clustering algorithm are, Apriori specification of the number of clusters; with a lower value of β get a better result but at the expense of more number of iterations and the Euclidean distance measures can unequally weight underlying factors.

2.2.3 New Weighted Fuzzy C Means Clustering

A new weighted fuzzy C-means (NW-FCM) algorithm was proposed by Chih-Cheng Hung et al [26]; it is used to improve the performance of both the FCM models for high dimensional multiclass pattern recognition problems. The methodology used in NW-FCM is the concept of the weighted mean from the non parametric weighted feature extraction (NWFE) and the cluster mean from the discriminate analysis feature extraction (DAFE).

2.3 Neural Network Based Clustering

Neural networks-based clustering has been dominated by SOFMs, and the adaptive resonance theory (ART), both of which are reviewed here. The objective of SOFM is to represent high-dimensional input patterns with prototype vectors that can be visualized in a usually two-dimensional lattice structure [21]. Each unit in the lattice is called a neuron, and the adjacent neurons are connected to each other, which gives a clear topology of how the network fits itself in to the input space. The input patterns are fully connected to all neurons via adaptable weights, and during the training process, the neighboring input patterns are projected into the lattice, corresponding to the adjacent neurons. In this sense, some authors prefer to think of SOFM as a method to display the latent data structure in a visual way rather than a clustering approach [24].

The merits of neural network based clustering are, the input space density approximation and independence of the order of input patterns and SOFM need to predefine the size of the lattice, i.e., the number of clusters, which is unknown in most circumstances. The de Merits of this neural network based clustering is, it may suffer from input space density misrepresentation [25], where areas of low pattern density may be over-represented, and areas of high density under-represented.

2.4 Genetic Based Clustering Algorithms

2.4.1 Genetic K-Means Algorithm

K. Krishna and M. Narasimha Murty proposed a novel hybrid genetic algorithm (GA) that finds a globally optimal partition of a given data into a specified number of clusters. GAs used earlier in clustering, employ either an expensive crossover operator to generate valid child chromosomes from parent chromosomes, or a costly fitness function or both. To circumvent these expensive operations, they hybridized the GA with a classical gradient descent algorithm used in clustering, viz., the K-means algorithm. Hence, the name genetic K-means algorithm (GKA). They defined the K-means operator, one-step of the K-means algorithm, and used it in GKA as a search operator, instead of crossover. They also defined a biased mutation operator specific to clustering, called distance-based-mutation. Using the finite Markov chain theory, they proved that the GKA converges to a global optimum. It is observed in the simulations that the GKA converges to the best known optimum, corresponding to the given data, in concurrence with the convergence result. It is also observed that the GKA searches faster than some of the other evolutionary algorithms used for clustering. The advantage of the genetic k means clustering algorithm is that it is faster than some of the other clustering algorithms.

2.4.2 Immune Genetic Algorithm based Fuzzy K-means Clustering Algorithm

Chengjie Gu et al [27] proposed a Fuzzy Kernel K Means clustering method based on the immune Genetic algorithm (IGA-FKMM). The Dependence of the fuzzy k means clustering on the distribution of sample was eliminated, with the introduction of the kernel function in this approach. The immune genetic algorithm has been used to suppress fluctuations that occurred at later evolution and to avoid the local optimum. This algorithm provides the global optimum and higher cluster accuracy.

2.4.3 Immune Genetic Algorithm based Novel Weighted Fuzzy C-means Clustering Algorithm

A Novel Weighted Fuzzy C-Means clustering method, based on the Immune Genetic Algorithm (IGA-NWFCM) was proposed by S.Ganapthy et al [28] for effective intrusion detection. Hence, it improves the performance of the existing techniques to solve the high dimensional multiclass problems. Moreover, the probability of obtaining the global value is increased by the application of the immune genetic algorithm. It provides high classification accuracy, stability, and probability of gaining the global optimum value.

III. Comparative Analysis

The computational complexity of some typical and classical clustering algorithms in Table 1 with several newly proposed approaches specifically designed to deal with large-scale data sets.

Table 1 Computational Complexity of Clustering Algorithms

Clustering Algorithm	Complexity	Capability of tackling high dimensional data
K – means	$O(NKd)$ time $O(N+ K)$ (space)	No
Fuzzy c means	Near $O(N)$	No
Hierarchical clustering	$O(N^2)$ (time) $O(N^2)$ (space)	No
CLARA	$O(K(40+K)^2+K(N-K))^+$ (time)	No
CLARANS	Quadratic in total performance	No
BIRCH	$O(N)$ (time)	No
DBSCAN	$O(N \log N)$ (time)	No
CURE	$O(N_{sample}^2 \log N_{sample})$ (time) $O(N_{sample})$ (space)	Yes

IV. Proposed Approach

The goal of clustering is to determine the intrinsic grouping in a set of unlabeled data. But how does one decide what constitutes a good clustering? It can be shown that there is no absolute “best” criterion, which would be independent of the final aim of the clustering. Consequently, it is the user who must supply this criterion, in such a way that the result of the clustering will suit this needs. For instance, it could be interested in finding representatives for homogeneous groups (data reduction), in finding “natural clusters”, and describe their unknown properties (“natural” data types), in finding useful and suitable groupings (“useful” data classes) or in finding unusual data objects (outlier detection).

In this review, the clustering scalability and efficiency of various clustering algorithm have been analyzed. This system propose a different Clustering algorithms for data sets appearing in statistics, computer science, and machine learning, and illustrate their applications in some benchmark data sets, the traveling salesman problem, and bioinformatics, a new field attracting intensive efforts. The results of different clustering depict the efficiency of the method. Because of the computation overhead in constructing dissimilarity matrix. There is also some scope for applying the clustering procedure to large datasets. In large datasets, the clustering efficiency is degraded and also need to improve time and scalability values. So to probe novel approaches for making efficient clustering schemas.

V. Conclusion

The cluster analysis examines unlabeled data, by either constructing a hierarchical structure, or forming a set of groups, according to a pre specified number. In this paper, an attempt has been made to give the basic concept of clustering, by first providing the definition of different clustering algorithms and some related terms. The soft clustering technique and hierarchical method of clustering were explained. The main focus was on these clustering algorithms, and a review of a wide variety of approaches that are mentioned in the literature. These algorithms evolve from different research communities, and these methods reveal that each of them has advantages and disadvantages. The drawback of the k-means algorithm is to find the optimal k value and initial centroid for each cluster. This is overcome by applying concepts, such as fuzzy algorithm.

References

- [1], Jiawei Han, MichelineKamber, "Data Mining Concepts and Techniques" Elsevier Publication.
- [2], AthmanBouguettaya "On Line Clustering", IEEE Transaction on Knowledge and Data Engineering Volume 8, No. 2, April 1996.
- [3], P. Berkhin, 2002. Survey of Clustering Data Mining Techniques. Ttechnical report, AccrueSoftware, San Jose, Calif.
- [4], Jiawei Han, Micheline Kamber, "Data Mining Concepts and Techniques" Elsevier Publication.
- [5], A. Jain, R. Duin, and J. Mao, "Statistical pattern recognition: A review," IEEE Trans. Pattern Anal. Mach.Intell., vol. 22, no. 1, pp. 4–37, 2000.
- [6], A. Jain, M. Murty, and P. Flynn, "Data clustering: A review," ACM Comput. Surv., vol. 31, no. 3, pp. 264–323, 1999
- [7], Bishop, Neural Networks for Pattern Recognition. New York: Oxford Univ. Press, 1995.
- [8], Bruce Moxon "Defining Data Mining, The Hows and Whys of Data Mining, and How It Differs From Other Analytical Techniques" Online Addition of DBMS Data Warehouse Supplement, August 1996.
- [9], Handbook of Pattern Recognition and Computer Vision, C. Chen, L. Pau, and P. Wang, Eds., World Scientific, Singapore, 1993, pp. 61–124. J. Sklansky and W. Siedlecki, "Large-scale feature selection".
- [10], J. Kleinberg, "An impossibility theorem for clustering," in Proc. 2002 Conf. Advances in Neural Information Processing Systems, vol. 15, 2002, pp. 463–470.
- [11], A. Jain and R. Dubes, Algorithms for Clustering Data. Englewood Cliffs, NJ: Prentice-Hall, 1988.
- [12], A. Gordon, "Cluster validation," in Data Science, Classification, and Related Methods, C. Hayashi, N. Ohsumi, K. Yajima, Y. Tanaka, H. Bock, and Y. Bada, Eds. New York: Springer-Verlag, 1998, pp. 22–39.
- [13], Handbook of Pattern Recognition and Computer Vision, C. Chen, L. Pau, and P.Wang, Eds.,World Scientific, Singapore, 1993, pp. 3–32. R. Dubes, "Cluster analysis and related issue".
- [14], A. Gordon, "Cluster validation," in Data Science, Classification, and Related Methods, C. Hayashi, N. Ohsumi, K. Yajima, Y. Tanaka, H. Bock, and Y. Bada, Eds. New York: Springer-Verlag, 1998, pp. 22–39.
- [15], S. Bandyopadhyay and U. Maulik, "Nonparametric genetic clustering: Comparison of validity indices," IEEE Trans. Syst., Man, Cybern. C, Appl. Rev., vol. 31, no. 1, pp. 120–125, Feb. 2001.
- [16], R. Davé and R. Krishnapuram, "Robust clustering methods: A unified view," IEEE Trans. Fuzzy Syst., vol. 5, no. 2, pp. 270–293, May 1997.
- [17], A. Geva, "Hierarchical unsupervised fuzzy clustering," IEEE Trans. Fuzzy Syst., vol. 7, no. 6, pp. 723–733, Dec. 1999.
- [18], R. Hammah and J. Curran, "Validity measures for the fuzzy cluster analysis of orientations," IEEE Trans. Pattern Anal. Mach. Intell., vol. 22, no. 12, pp. 1467–1472, Dec. 2000.
- [19], M. Livny, R.Ramakrishnan, T. Zhang, 1996. BIRCH: An Efficient Clustering Method for VeryLarge Databases. Proceeding ACMSIGMOD Workshop on Research Issues on Data Mining andKnowledge Discovery: 103-114.
- [20], S. Guha, R. Rastogi, and K. Shim, 1998. CURE: An Efficient Clustering Algorithm for Large Databases. Proc. ACM Int'l Conf. Management of Data: 73-84.
- [21], T. Kohonen, "The self-organizing map," Proc. IEEE, vol. 78, no. 9, pp.1464–1480, Sep. 1990.
- [22], Santos, J.M, de SA, J.M, Alexandre, L.A, 2008. LEGClust- A Clustering Algorithm based on Layered Entropic subgraph. Pattern Analysis and Machine Intelligence, IEEE Transactions: 62-75.
- [23], M Meila, D Verma, 2001. Comparison of spectral clustering algorithm. University of Washington, Technical report
- [24], N. Pal, J. Bezdek, and E. Tsao, "Generalized clustering networks andKohonen's self-organizing scheme," IEEE Trans. Neural Netw., vol. 4, no. 4, pp. 549–557, Jul. 1993.
- [25], S. Haykin, Neural Networks: A Comprehensive Foundation, 2nd ed. Englewood Cliffs, NJ: Prentice-Hall, 1999.
- [26], Chih-Cheng Hung, Sameer Kulkarni, Bor-Chen Kuo, "A New Weighted Fuzzy C-Means Clustering Algorithm for Remotely Sensed Image Classification", IEEE Journal of Selected Topics in Signal Processing, Vol. 5, No.3, pp. 543-553, 2011.
- [27], Chengjie GU, Shunyi ZHANG, Kai LIU, He Huang, "Fuzzy Kernal K-Means Clustering Method Based on Immune Genetic Algorithm", Journal of Computational Information Systems, Vol. 7, No. 1, pp. 221-231, 2011.
- [28], S.Ganapathy, K.Kulothungan, P.Yogesh, A.Kannan, " A Novel Weighted Fuzzy C-Means Clustering Based on Immune Genetic Algorithm for Intrusion Detection", Proceeding Engineering, Elsevier, Vol. 38, pp. 1750-1757, 2012.

Power Management in Optimized Link State Routing (OLSR) Protocol

Dharam Vir,¹ Dr. S.K.Agarwal,² Dr. S.A.Imam³

^{1,2}Department of Electronics Engg, YMCA University of Science & Technology, Faridabad, India

³Department of Electronics & Comm. Engg., Jamia Millia Islamia, New Delhi, India

Abstract: In most pioneering topics in computer communications is wireless networking. One area in wireless networking is mobile ad hoc networking. The concept of mobile ad hoc networking is based on the fact that users can communicate with each other in network, without any form of centralized administration. In a mobile ad hoc network, nodes are often powered by batteries. Every message can send and every computation performed drains the battery life. One solution for power conservation in mobile ad hoc network is power management. This means that routing decisions made by the routing protocol should be based on the power-status of the nodes. Nodes with low batteries will be less preferably for forwarding packets than nodes with full batteries, thus increasing the life of the nodes. A routing protocol should try to minimize control traffic, such as periodic update messages to improve the lifetime of the nodes and network. Power management in wireless networks deals with the process of managing energy resources by means of controlling the battery discharge, adjusting the transmission power, and scheduling of power sources. We efforts to solve this problem here we can describe the power management issues in mobile nodes to modified Optimized Link State Routing (OLSR) protocol and it was designed on QualNet 5.0 simulator. The modification is done in effect of power management issue in modified OLSR and existing OLSR routing protocol with the metrics like power consumes in all three modes transmit, received and ideal modes, TC message received, Hello message received, signal received and forward to MAC, signal received but with errors and power consumption have been used. For simulation purpose QualNet5.0 has been used as the tool.

Keywords: Ad hoc wireless Networks, Power Management, Optimized Link State Routing (OLSR), QualNet 5.0 simulator.

I. INTRODUCTION

Wireless sensor networks (WSN's) have attracted a great deal of research attention due to their wide-range of prospective applications. Applications of wireless sensor networks contain battlefield surveillance, medical monitoring, biological detection, inventory tracking and home security. This type of network consists of collection of nodes and each node has limited battery power capacity. There may be many possible routes available between two nodes over which data can be able to flow. Assume that each node generated some information and this information needs to be delivered to a destination node. Any node in the network can easily transmit their data packet to a distance node, if it has enough battery power. If any node is far from its neighbour node then large amount of transmission power is required to transmit the data from source to destination. After every transmission, remaining power of this node decreases and some amounts of data transmission of this node will be eliminated from the network because of empty battery power and in similar situation there will be a condition that no node is available for data transmission and overall lifetime of network will decreases [1].

Existing power awareness routing protocols can generally classified as a power management or power control protocol. In IEEE 802.11 there is already a type of power management implemented. The implantation of power awareness routing in this task is only focusing on power control management schemes. However, to make power management schemes for mobile ad hoc networks is most effective, an efficient message routing algorithms, coupled with good solutions for optimizing power consumption during the transmit, received and idle modes of data. In power control routing protocols several metrics can be used to optimize power management in routing. Minimizing the energy consumed for each message is an evident solution that optimizes locally the power consumption. An effective routing protocol should not only focus on individual nodes in the system but also focus on the system as a whole. The nodes have high residual power but the system is not connected because some critical nodes have been depleted of power. Different routing schemes can be utilized, but the two most extreme solutions to power awareness routing for a message are [1] [2]:

- Compute a path that maximizes the minimal power consumption; the path that requires the least power to transmit and receive a message, hereby keeping the power consumption needed to communicate as low as possible [3].
- Compute a path that maximizes the minimal residual power in the network; the path according to the residual energy of the nodes, hereby maximizing the lifetime of all nodes and the lifetime of the network.

In particular, Section II presents the need for power management in mobile ad-hoc networks and optimization of power. Section III briefly discusses the MANET routing protocols and functionality of Optimized Link State Routing (OLSR). Section IV Simulation platform and models, result analysis are discussed in Section V. Finally, Section VI conclusion and future work.

II. NEED FOR POWER MANAGEMENT IN MANETS

The nodes in an ad hoc wireless network are constrained but limited battery power for their operation. Hence, power management is an important issue in ad hoc networks. Power management is the process of managing power resources by means of controlling the battery recharge, adjusting the transmission power, and scheduling of power sources so as to increase the lifetime of the nodes of an ad hoc wireless network. The power efficiency of a node is defined as the ratio of the amount of data delivered but the node to the total power finished [3] [12].

The reasons for power management in ad hoc wireless networks are:

- Increasing gap between the power consumption and requirements of power availability, so need to the power management.
- Difficult to replace or recharge the batteries. Hence, power conservation is necessary in such scenarios.
- The relay traffic allowed through a destination node is more, and then it may leads to a faster depletion of the power source for that node.
- The best possible value for the transmission power increases the number of real-time transmissions.
- Power control is essential to maintain the required signal to interference ratio at the receiver and to increase the channel capability.
- Power consumption of a wireless radio depends on the operation mode. Four types of operation modes of a radio can be categorized: (i) transmit mode, (ii) receive mode, (iii) idle mode, and (iv) sleep mode.
- Batteries are likely to increase the size and weight of a mobile node, to reduce the size of the battery, power management techniques are necessary to utilize the maximum battery capacity in the best potential way.
- The power level of a battery is finite and limits the lifetime of a node. Every message sent and every computation performed drains the battery, need to power management in network.

A. Classification of Power Management Schemes:

To increase the life of an ad hoc wireless network, it is required to be aware of the capabilities and limitations of the power resources of the nodes. For longer lifetime of the node can be achieved by increasing the battery capacity. Increasing the capacity of the battery at the nodes can be achieved by either battery management, which concerns the internal characteristics of the battery, or power management, which deals with maximum utilization of battery capacity [4].

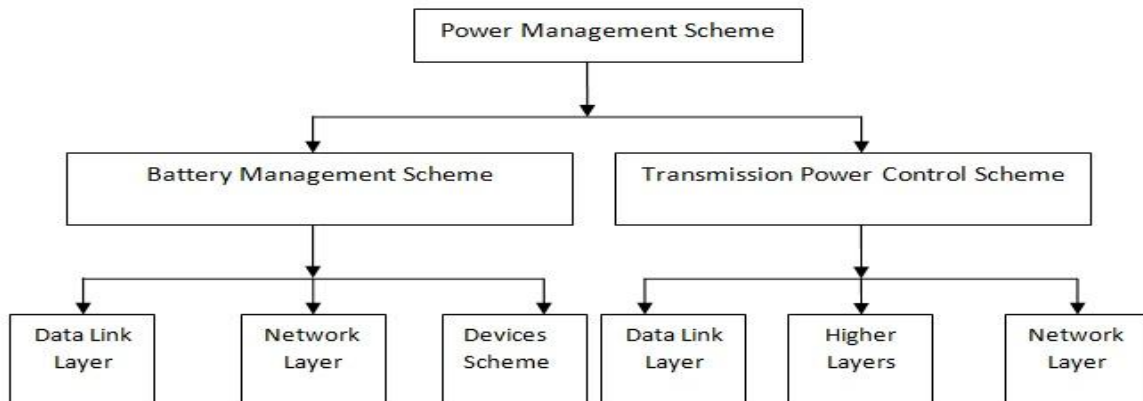


Fig. 1 Classification of Power Management Schemes

The routing protocol must be designed such a way to reduce the amount of information exchanged among the nodes, since communication incurs loss of power. Increase in the number of communication tasks also increases the traffic in the network, which results in loss of data, retransmissions, and hence more energy consumption. The power consumption occurs at the network layer is because of communication and calculation operations. The power conserved in communication operations is due to transmit-receive module present in the source and destination nodes [4] [11].

B. Optimization of power [3][8]:

In mobile ad hoc networking the optimization of power consumption can be divided according to functionality into:

- The maximum power utilized for the transmission of a message.
- The maximum power utilized for the reception of a message;
- The minimum power utilized while the system is idle.
- Reducing the access amount of data transmitted across the network.
- Lower the transceiver duty cycle range.
- Lower the frequency of data transmission.
- Reduce the frame overhead.
- Implementation of reliable power management techniques.
- Reduce redundant transmission.

- Reduce calculation overhead.
- For powerful routing protocol, reduce the number of retransmission across the network can be controlled effectively.
- Evaluating node density, congestion and network availability.
- For utilizing effective routing algorithm, network life time and energy will be conserved and redundant transmission will be reduced [13].

We suggest two corresponding optimization technique for control and manage the power consumption in ad-hoc networks:

- Optimized minimum power consumption during the idle time by switching to sleep mode; this is known as Power Management [5].
- Optimized minimum power consumption during communication, that is, while the system is transmitting and receiving messages; this is known as Power Control [5] [14].

III. MOBILE AD HOC NETWORK ROUTING PROTOCOLS

There are lots of ways to classify the MANET routing protocols depending on how the protocols to hold the packet and to deliver from source to destination. But Routing protocols are broadly classified into three types such as Proactive, Reactive and Hybrid protocols.

A. Proactive Protocols

These types of protocols are also called table driven protocols in which, the route to all the nodes is maintained in routing table. Packets are transferred over the predefined route specified in the routing table. These protocols have lower latency because all the routes are maintained at all the times. Example of Proactive protocols: Bellman Ford, DSDV, EIGRP (Enhanced Interior Gateway Routing Protocol) OLSR (Optimized Link State Routing) [6] [7].

B. Reactive Protocols

These types of protocols are also called as On Demand Routing Protocols where the routes are not predefined for routing. A Source node calls for the route discovery phase to determine a new route whenever a transmission is needed. This is a repetitive technique until it reaches the destination. Reactive techniques have smaller routing overheads but higher latency. Example of Reactive Protocols: DSR, AODV, DYMO etc [5].

C. Hybrid Protocols

Hybrid protocol is the combinations of reactive and proactive protocols and takes advantages of these two protocols and as a result, routes are found rapidly in the routing zone. Example Protocol: ZRP (Zone Routing Protocol) [10].

1) OPTIMIZED LINK STATE PROTOCOL:

The Optimized Link State Routing (OLSR) protocol, developed by the French National Institute for Research in Computer Science and Control (INRIA), was developed for mobile ad-hoc networks. It operates in a table-driven and proactive manner, i.e., topology information is exchanged between the nodes on periodic basis. Its main objective is to minimize the control traffic by selecting a small number of nodes, known as Multi Point Relays (MPR) for flooding topological information. In route calculation, these MPR nodes are used to form an optimal route from a given node to any destination in the network. This routing protocol is particularly suited for a large and dense network. OLSR generally proposes four types of periodic control messages, namely [6] [15]:

- Hello messages
- Topology Control (TC) messages
- Multiple Interface Declaration (MID) messages
- Host and Network Association (HNA) messages.

a) Hello messages:

OLSR [18] uses two kinds of the control messages: Hello and Topology Control (TC). Hello messages are periodically exchanged within the one-hop neighborhood to obtain the neighborhood information. Using this neighborhood information, each node in the network selects a subset of one-hop away neighbors known as the MPR set. In the MPR set, all two-hop away neighbors are reachable through any member of the MPR set. Hello messages are used for finding the information about the link status and the host's neighbours. With the Hello message the Multipoint Relay (MPR) Selector set is constructed which describes which neighbours has chosen this host to act as MPR and from this information the host can calculate its own set of the MPRs. the Hello messages are sent only one hop away but the TC messages are broadcasted throughout the entire network. TC messages are used for broadcasting information about own advertised neighbours which includes at least the MPR Selector list.

b) Topology Control (TC) messages:

TC messages are generated and retransmitted for flooding topological information in the whole network only through MPR nodes. Also, MID and HNA messages are relayed only by MPR nodes. Therefore, OLSR optimizes the control traffic overhead by minimizing the size of the MPR set. An MPR member generates and retransmits TC messages. These messages provide each node in the network with sufficient link-state information to allow route calculation [17] [18].

c) Multiple Interface Declaration (MID) messages:

MID messages are generated by an OLSR node with multiple OLSR interfaces to notify other OLSR nodes about its interfaces participating in the OLSR routing domain. There is also Multiple Interface Declaration (MID) messages which are used for informing other host that the announcing host can have multiple OLSR interface addresses. The MID message is broadcasted throughout the entire network only by MPRs [18].

Apart from these OLSR control messages, a node associated with OLSR MANET and non-OLSR MANET periodically issues HNA messages notifying the connected non-OLSR Networks. These HNA messages are also flooded throughout the OLSR domain by the MPR nodes so that the external routes are learned by all the OLSR nodes.

Table 1 Description of OLSR parameters:

Parameters	Description
OLSR-HELLO-INTERVAL	Specifies the time interval between two consecutive HELLO messages within one-hop neighborhood to obtain the neighborhood information.
OLSR-TC-INTERVAL	Specifies the time interval between two consecutive TC messages.
OLSR-MID-INTERVAL	Specifies the time interval between two consecutive MID messages. MID messages will be broadcasted only when an OLSR node has multiple OLSR interfaces.
OLSR-HNA-INTERVAL	Specifies the time interval between two consecutive HNA messages. HNA messages will be broadcasted only when an OLSR node has non-OLSR interface.

So the topological changes cause the flooding of the topological information to all available hosts in the network. To reduce the possible overhead in the network protocol uses Multipoint Relays (MPR). The idea of MPR is to reduce flooding of broadcasts by reducing the same broadcast in some regions in the network, more details about MPR can be found later in this chapter. Another reduce is to provide the shortest path. The reducing the time interval for the control messages transmission can bring more reactivity to the topological changes.

d) Host and Network Association (HNA) messages:

There is also a “Host and Network Association” (HNA) message which provides the external routing information by giving the possibility for routing to the external addresses. The HNA message provides information about the network- and the net mask addresses, so that OLSR host can consider that the announcing host can act as a gateway to the announcing set of addresses. The HNA is considered as a generalized version of the TC message with only difference that the TC message can inform about route canceling while HNA message information is removed only after expiration time [9].

(1) Multipoint Relays Selection:

In this section the proposed algorithm for the selection of Multipoint Relay set is described. This algorithm is found from [9]. Hello message can be chosen to act as MPR. The neighbour must be symmetric in order to become an MPR. Proposed algorithm for selecting Multipoint Relay set:

- Take all the symmetric one hop neighbours which are willing to act as an MPR.
- Calculate for every neighbour host a degree, which is a number of the symmetric neighbours, that are two hops way from the calculating source and does not include the source or its one hop neighbours.
- Add the neighbour symmetric host to the MPR set. If it is the only neighbour from which is possible to get to the specific two hop neighbour, then remove the chosen host neighbours from the two hop neighbour set.
- If there are still some hosts in the two hop neighbour set, then calculate the reach ability of the each one hop neighbour, meaning the number of the two hop neighbours, that are yet uncovered by MPR set.
- Repeat previous step until the two hop neighbours set is empty.
- For the optimization, set the hosts in the MPR set in the increasing order basing on the willingness. If one host is taken away and all the two hop neighbours,

(2) Topology Information [15]:

In order to exchange the topological information and build the topology information base the host that were selected as MPR need to sent the topology control (TC) message. The TC messages are broadcasted throughout the network and only MPR are allowed to forward TC messages. The TC messages are generated and broadcasted periodically in the network. The TC message is sent by a host in order to advertise own links in the network. The host must send at least the links of its MPR selector set. The TC message includes the own set of advertised links and the sequence number of each message.

(3) Control traffic [15]:

All OLSR control traffic is to be transmitted over UDP. This traffic is to be broadcasted when using IPv4, but no broadcast address is specified.

(4) Routing Table Calculations:

The host maintains the routing table, the routing table entries have following information: destination address, next address, number of hops to the destination and local interface address. Next address indicates the next hop host. The information is got from the topological set (from the TC messages) and from the local link information base (from the Hello messages) [15].

IV. SIMULATION PLATFORM AND MODELS

In QualNet 5.0 [16] [17], a precise network topology is referred to as a scenario. A scenario allows the user to denote all the network components and environment under which the network will operate. This includes: terrain details, channel propagation effects including path loss, battery model, fading, and shadowing, wired and wireless subnets, network devices such as hubs, switches and routers, the whole protocol stack selection of standards or user-configured network components, and applications running on the network. In this work QualNet 5.0 network simulator has been used to design modify OLSR routing protocol or an existing OLSR routing protocol of mobile ad-hoc networks. The physical medium used is 802.11 PHY with a data rate of 2 Mbps. The MAC protocol used is the 802.11 MAC protocol, configured for MANET mode. In this work wireless module of IEEE 802.11b is used to enable mobility of the wireless nodes. IEEE 802.11b support more accurate wireless models for propagation, path loss, multi-path fading and reception on wireless networks. The simulations are carried out for network densities of 100 nodes respectively in 10 intervals. The area considered for the above network densities are 1500m * 1500m. Simulations scenarios is design for modification in OLSR and existing OLSR routing protocol for power management with the metrics like power consumes in all three modes transmit, received and ideal modes, TC message received, Hello message received, signal received and forward to MAC, signal received but with errors. The parameters and description is given in table1. Fig. 2 shows the running designed scenario for modify OLSR routing protocol with number of CBR's and nodes.

Table 2: Traffic and Mobility parameters for modified OLSR routing protocol.

Parameter	Short Description	Value/Type
Topological Area	Represents topology or arrangement of mobile nodes. Determined in x & y axis. Also known as network size or dimensional area. Measured in	1500 *1500 m ²
No. of nodes	Nodes are communication devices or routers.	1-100
Pause time	The maximum amount of time, a node stays before a new direction and speed is selected	10, 20, 40
Max. speed	Maximum mobility speed of a node. Measured in meter/second.	20 m/s
Transmission range	Radio transmission range allows a mobile node to send & receive radio signals. Measured in meters	250 m
Mobility pattern	Define movement of nodes, which is characterized by speed, direction, and rate of change	Random way point
Application	Denote the traffic type to be used i.e. CBR stands for constant bit rate. Used for real time traffic.	CBR
PHY	PHY stands for physical layer. 802.11b is basically IEEE wireless standard	802.11b
Packet size	Node sends & receives data in the form of packet. Measured in kilobytes.	512 kB
Packet transmission rate	Every traffic source sends a packet at specific rate that is measured in packet/second.	2 Packets/second
Simulation time	Total duration for which simulation runs.	400 s
No. of CBR	Total number of CBR connections that can be established among different mobile nodes for communication.	10
Nodes	Mobile or fixed routers with wireless receivers or wireless transmitters which are free to move arbitrarily	100
Battery Model	Battery rate capacity effect: the model which precisely estimates non-linearity effect of rated capacity versus discharge current load.	Linear Model
Start/ End Time	Time when the conversation ends. If end time is specified as 0, then conversation continue until the end of simulation.	Variable
Simulation time	Length of simulation and time when scenario complete task.	1800 seconds

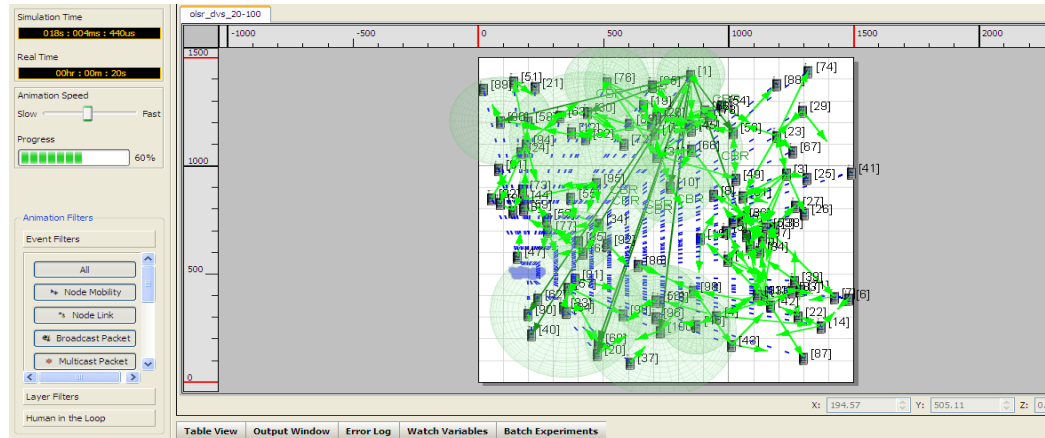


Fig. 2 Snapshot of running designed scenario for modifies OLSR routing protocol with number of CBR's and nodes.

V. RESULT AND ANALYSIS

A. TC Message Received:

Specifies the time interval between two consecutive TC messages. The TC messages are broadcasted throughout the network and only MPR are allowed to forward TC messages. The TC messages are generated and broadcasted periodically in the network. Host can increase its transmission rate to become more sensible to the possible link failures. When the change in the MPR Selector set is noticed, it indicates that the link failure has happened and the host must transmit the new TC message as soon as possible

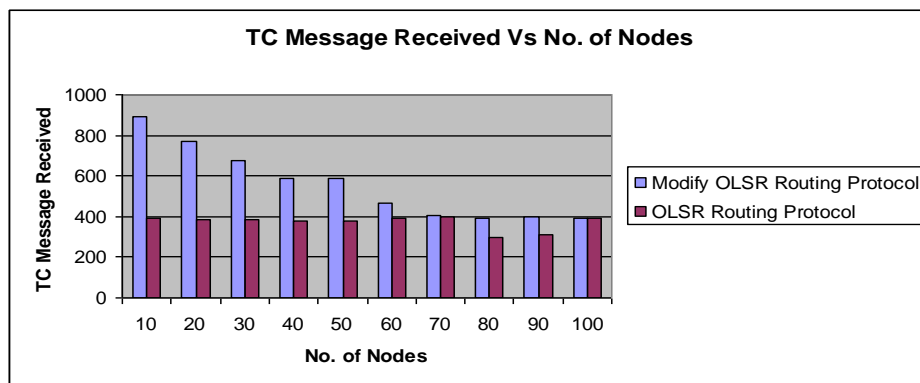


Fig. 3 TC Message received with varying nodes and OLSR routing protocols.

- Fig. 3 shows the impact variation of TC Message received with in modified OLSR routing protocol as parameter and also variation in no. of nodes. Following inference can be made:
- By observation from graph and analysis of designed scenario observation efforts trying minimize the link failures between nodes, so lifetime of nodes increases, and also saves power consumption. Hence overall performance of power may increases. In modified OLSR link failure less as compare OLSR routing.
- The maximum transmission rates also increase in modified OLSR and consume less power by OLSR.

B. Hello Message Received:

Specifies the time interval between two consecutive HELLO messages within one-hop neighborhood to obtain the neighborhood information.

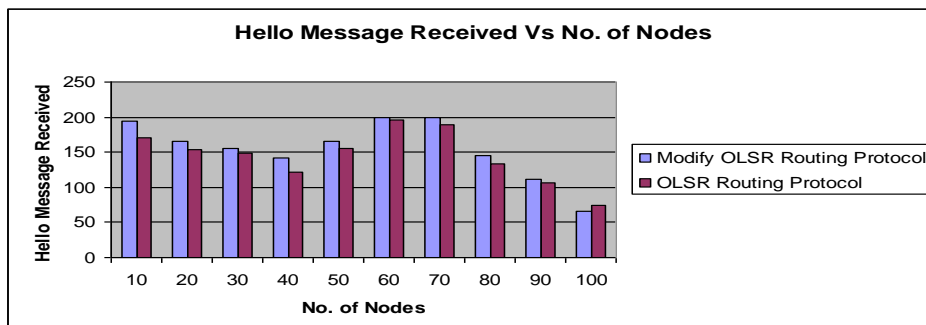


Fig. 4 Hello Message received with varying nodes and OLSR routing protocols.

- Fig. 4 shows the impact variation of Hello message received with in modified OLSR routing protocol as parameter and also variation in no. of nodes. Following inference can be made:
- By observation from graph and analysis of designed scenario observation efforts for trying minimize the time interval between the nodes for sending information, so lifetime and scalability of nodes increases, and also saves power consumption. In modified OLSR the message send ratio increases with time and also increases message sending ratio as compare OLSR routing.

C. Signal Received but with errors:

Number of incoming signals the radio failed to receive. PHY model is a simple radio model that supports either Signal-to-Noise Ratio (SNR) or Bit Error Rate (BER) based reception.

- Fig. 5 shows the impact variation of Signal Received but with errors in modified OLSR routing protocol as parameter and also variation in no. of nodes. Following inference can be made:
- By observation from graph and analysis of designed scenario observation efforts for trying minimize the errors when 1 mbps data received from source node to destination. In modified OLSR the errors less then as compare OLSR routing.

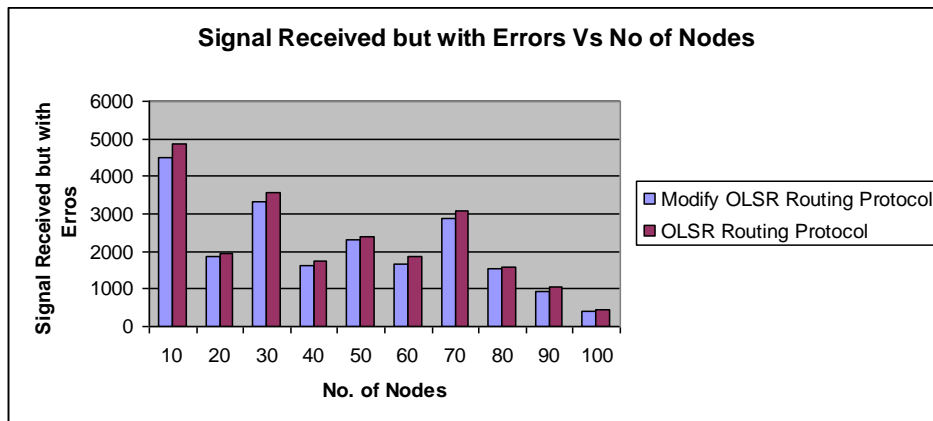


Fig. 5 Signal received but with errors with varying nodes and OLSR routing protocols.

D. Signal Received and Forwards to MAC:

Number of incoming signals successfully received and forwarded to MAC.

- Fig. 6 shows the impact variation of Signal received and forwards to MAC in modified OLSR routing protocol as parameter and also variation in no. of nodes. Following inference can be made:
- By observation from graph and analysis of designed scenario observation efforts for trying incoming signals received from source node to destination node are successfully received and forwarded to MAC. In modified OLSR the received signals more then as compare OLSR routing.

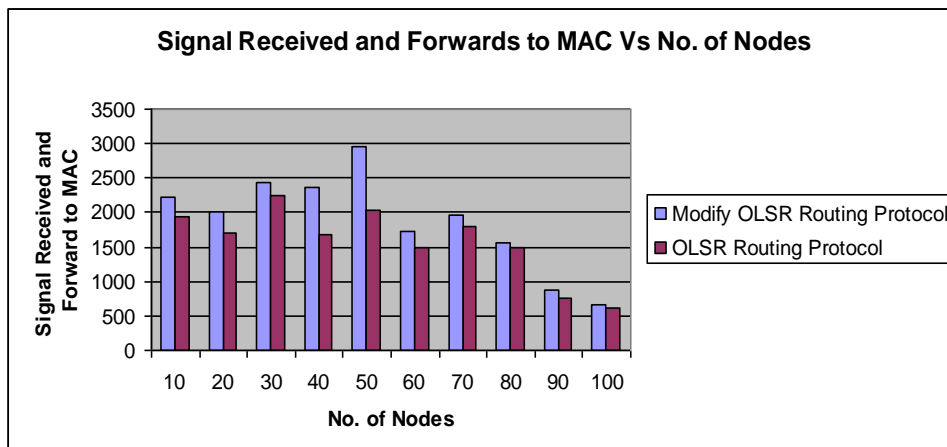


Fig. 6 Signal received and forwards to MAC with varying nodes and OLSR routing protocols.

Power Consumption:

This is the ratio of the average power consumed in each node to total power. The lifetime, scalability, response time and effective sampling frequency, all of these parameters of the wireless sensor network depend upon the power. Power failure regularly breaks in the network. Energy is required for maintaining the individual health of the nodes, during receiving the packets and transmitting the data as well.

E. Power Consumed in Transmit Mode:

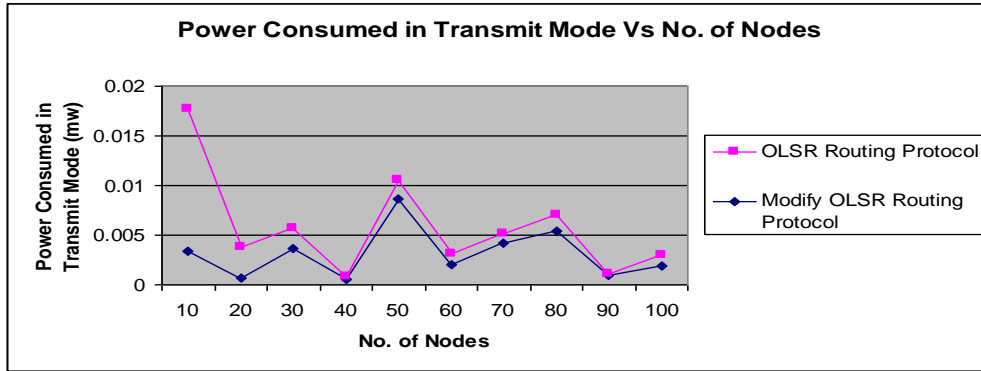


Fig. 7 Power consumed in transmit mode with varying nodes and OLSR routing protocols.

- Fig. 7 shows the impact variation of Power consumption in transmit mode with modified OLSR routing protocol as parameter and also variation in no. of nodes. Following inference can be made:
- By observation from graph and running scenario the maximum power consumed when distance of nodes is longer, hence overall performance of power manage of modified OLSR consumes less power as compare OLSR routing.
- The maximum power consumes by OLSR which is tailed by manage OLSR routing protocol.

F. Power Consumed in Received Mode:

- Fig. 8 shows the impact variation of Power consumption in transmit mode with modified OLSR routing protocol as parameter and also variation in no. of nodes. Following inference can be made:
- On analyzing the results for energy consumption in receive mode it has been concluded that modified OLSR consumes less power as compare to OLSR routing protocol.
- Maximum average power consumes when long distance nodes communicate each other as observing graph and scenario in figure 2.

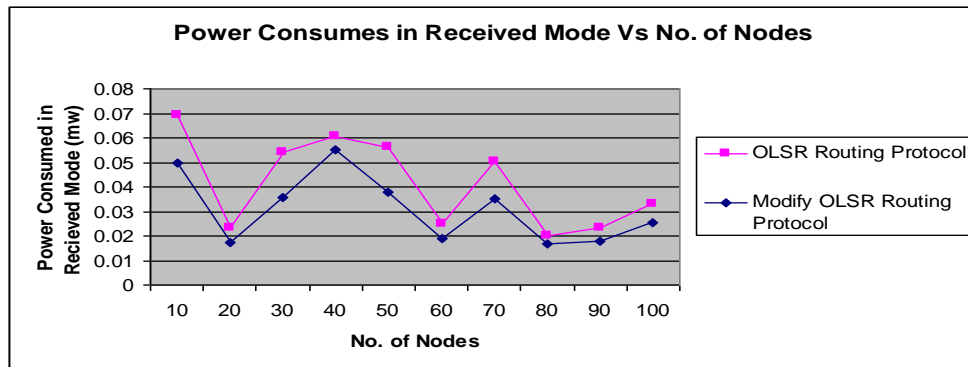


Fig. 8 Power consumed in received mode with varying nodes and OLSR routing protocols.

G. Power Consumed in Ideal Mode:

- Fig. 9 shows the impact variation of Power consumption in transmit mode with modified OLSR routing protocol as parameter and also variation in no. of nodes. Following inference can be made:

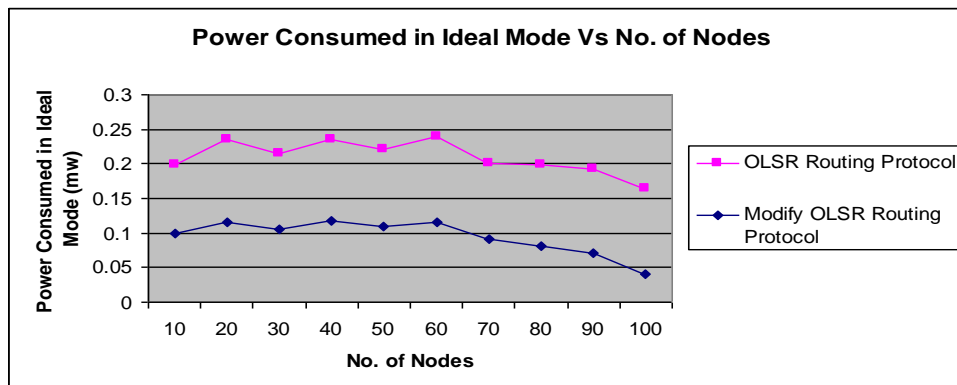


Fig. 9 Power consumed in ideal mode with varying nodes and OLSR routing protocols

- By observation from graph and running scenario the over all power consumed when distance of nodes is longer, hence overall performance of power manage by modified OLSR consumes less power as compare OLSR routing.
- The maximum power consumes by OLSR which is tailed by manage OLSR routing protocol.

VI. CONCLUSION

In this article, the important issue of power management in Optimized Link State Routing (OLSR), mobile ad-hoc wireless network is discussed. Since mobile nodes have limited battery lives, mobile networks should consume battery power more efficiently to maximize the network life, battery power capacity, transmission power consumption, stability of routes etc. We efforts to solve the problem of reduce the power consumption through power management issues in mobile ah hoc network by modified Optimized Link State Routing (OLSR) protocol and results shown as above. The modified OLSR routing protocol to minimize control traffic, periodic TC messages update, remaining battery power capacity, controlling the battery discharge to improve the power consumption in all modes. The future scope of this protocol is to successfully simulate it for a very large network and implement it with a voice application. For feature work we proposed to reduce the power consumption in Reactive routing protocol is tested with less number of packets and only for packet level power consumption for a very large network.

REFERENCES

- [1] Al-Maashri A. and M.Ould-Khaoua. 2006. "Performance Analysis of MANET Routing Protocols in the Presence of Self-Similar Traffic", In Proceedings of the 31st IEEE Conference on Local Computer Networks, Tampa, Florida, USA. pp. 803-806.
- [2] V. Raghunathan, C. Schurgers, S. Park, and M. B. Srivastava. Energy-aware wireless microsensor networks. IEEE Signal Processing Magazine, 19:40–50, 2002.
- [3] Azzedine Boukerche "Performance Evaluation of Routing Protocols for Ad Hoc Wireless Networks", Mobile Networks and Applications 9, 333–342, 2004 ONT K1N- 6N5, Canada
- [4] S.W. Arms, C.P. Townsend, D.L. Churchill, J.H. Galbreath, S.W. Mundell , "Power Management for Energy Harvesting Wireless Sensors " SPIE Int'l Symposium on Smart Structures & Smart Materials.
- [5] Kuppusamy, P.Thirunavukkarasu, K. Kalavathi B.; "A study and comparison of OLSR, AODV and TORA routing protocols in ad hoc networks" 2011 3rd IEEE international Conference on Electronics Computer Technology (ICECT), Issue Date: 8-10 April 2011 On page(s): 143 – 147.
- [6] Muktadir A.H.A. 2007. "Energy Consumption study of OLSR and DYMO MANET Routing Protocols" in Urban Area, National Conference on Communication and Information Security, Daffodil International University, Dhaka, Bangladesh. Pp.133-136.
- [7] Reddy P.C. and P.C. Reddy. 2006. "Performance Analysis of Ad Hoc Network Routing Protocols", Academic Open Internet Journal, Volume 17.
- [8] HuseyinOzgun Tan and Ibrahim Korpeoglu, "Power Efficient Data Gathering and Aggregation in Wireless Sensor Networks"
- [9] R.L.Cruz and A.R.Santhanam, "Optimal Routing, Link Scheduling, and power control in Multi-Hop Networks", Proceedings of INFOCOM 2003, vol. 1, pp. 702-711, April 2003.
- [10] C.K Toh, "Maximizing Battery Life Routing to Support Ubiquitous Mobile Computing in Wireless Ad Hoc Networks", IEEE Communications Magazine, vol.39, no.6, pp. 138-147, June 2001.
- [11] Yunxia Chen, Student Member, IEEE, and Qing Zhao, Member, IEEE "On the Lifetime of Wireless Sensor Networks" IEEE Communications Letters, VOL. 9, NO. 11, November 2005.
- [12] Murthy and Garcia-Luna-Aceves, "An Efficient Routing Protocol for Wireless Networks", ACM Mobile Networks and App. J., Special Issue on Routing in Mobile Communication Networks, Oct. 1996, pp. 183-97.
- [13] Xu, Heidemann, Estrin, "Adaptive Energy-Conserving Routing for Multihop Ad Hoc Networks", 2000
- [14] V. Rishiwal, M. Yadav and S. Verma, "Power Aware Routing to support Real Time Traffic in Mobile Ad-hoc Networks", International Conference on Emerging Trends in Engg & Tech., IEEE, pp. 223-227, 2008
- [15] Clausen, T., Jacquet, P, Optimized Link State Routing Protocol, IETF Internet Draft, Jan2003, <http://menetou.inria.fr/draft-ietf-manet-olsr-11.txt>
- [16] QualNet documentation, "QualNet 5.0 Model Library:Wireless"; <http://www.scalablenetworks.com>,
- [17] "Qualnet 5.0," <http://www.scalable-networks.com>,
- [18] Wireless routing protocols www.wikipedia.com

Measurement of Soil Parameters by Using Penetrometer Needle Apparatus

Mahmoud M. Abu zeid,¹ Amr M. Radwan,² Emad A. Osman,³
Ahmed M. Abu-bakr,⁴ Ahmed M. Hassan⁵

¹Research student PhD, Civil Engineering Department, South Valley University, Egypt,

²Professor, Civil Engineering Department, Helwan University, Egypt.

³Professor, Civil Engineering Department, Minia University, Egypt.

^{4,5}Associate Professor, Civil Engineering Department, Minia University, Egypt,

ABSTRACT: In this research a simple practical was applied to determine soil parameters using penetrometer needle apparatus. Penetration tests were performed on both coarse and fine sands. Different sands densities and penetration disk diameter were applied in the tests. Correlations between applied normal stresses and resulting penetration distances were obtained. Correlations between soil densities and applied stresses were then determined. These correlations were used to estimate different soil parameters.

Keywords: Penetration, sand, friction angle, normal stress, density, Young's modulus.

I. INTRODUCTION

The history of the penetrometers dates back to 1846 when a French engineer Collin developed a 1 mm diameter needle shaped penetrometer to estimate the cohesion of different clay types (Sanglerat, 1972). Several types were used thereafter to cope with different types of soil and guarantee reproducibility of results. There are two general types of hand-held penetrometers: Static and Dynamic penetrometers. Both measure soil resistance to vertical penetration of a probe or disk, the distinction between the two types lies in how force is applied to the disk. The static penetrometer measures the force required to push a metal disk through the soil at a constant velocity. The force is usually measured by a load cell or strain gauge (e.g. proving ring) coupled with an analog dial or pressure transducer for readout (Herrick and Jones, 2002). As the operator pushes down the penetrometer, the note keeper records cone index values for each depth increment to evaluate the depth and thickness of compacted layers. disk indices depend on disk properties (high and size) and soil properties, e.g. bulk density, texture, and soil moisture (ASAE b, 1999; Herrick and Jones, 2002). Soil behavior under disk penetration involves a combination of cutting, compression, shear or plastic failures, or any combination of these (Gill, 1968). Various approaches (Farrell and Greacen, 1965; Rohani and Baladi, 1981; Tollner and Verma, 1984; Tollner et al, 1987; Yu and Mitchel, 1998) studied the soil responses in cone penetration including: (i) bearing capacity theory, (ii) cavity expansion theory, (iii) steady state deformation, (iv) finite element (FE) analysis, and (v) laboratory experimental methods. The main objective of this research is to develop a practical method to estimate soil parameter using penetration method. To assess this objective laboratory tests were applied. In the laboratory testing stage, laboratory tests on sandy soil and imposing densities different comparative and get them on the dry densities the sand user and conduct laboratory tests of various such as , Grain Size Analysis, Specific Gravity Test, Direct Shear Test and Stress – Strain modulus, two types of sandy soil (fine and coarse sand) were used in this laboratory work in which relationships between normal stress and penetrating distance at different dry densities using the following procedure. Samples of each kind from sand were prepared for the purpose of performing the handled penetrometer needle tests. These samples were prepared in relative density molds.

II. EXPERIMENTAL WORK

2.1. Sample Preparation

Two types of air dry fine and coarse sand were used in this laboratory work. Samples were compacted to different densities in a circular mould 15 cm diameter and 15 cm high. Fine sand samples were prepared at seven different dry densities and five dry densities for coarse sand is shown in Fig. (1).

2.2 Penetrometer Needle Apparatus

The apparatus basically consists of a needle attached to a spring - loaded plunger through a shank. An array of interchangeable needle tips is available, to facilitate the measurement of a wide range of penetration resistance values. A calibration of penetration against dry unit weight and water content was obtained by pushing the needle in to specially prepared samples for which these values are known and noting the penetration. The penetration of needle and the penetration resistance may be shown on a graduated scale on the shank and the stem of handle respectively. Against the penetration resistance, the corresponding values of water content and dry unit weight are obtained from the calibration curve. Proctor-type penetrometer is a device that is used to determine the strength of the soil in terms of its distance to penetration. It is commonly used in characterization of the soil by off-road mobility experts and scientists it consists of a different types of rings, cone and spherical shapes in measuring penetration distance with different dry density for cohesion less soils and for use with needles of larger areas. Small stem graduated at 12.5 mm intervals, to indicate the depth of penetration and for use with needless of smaller areas. The stem is calibrated 150 lbf * 2lbf division, one needle point set comprising one each of

2.5 , 2.0 , 1.5 and 1.3 cm diameter and 1 cm height for all rings In addition to the cone diameter of 2 cm and a height of 2 cm. Complete as above in a wooden carrying case. mounted on a 22 mm long 12.6 mm penetrating shaft, connected to a 32 mm diameter and 278 mm long pipe (pressure shaft), enclosing a 25 3 mm mean diameter, 3.3 mm diameter of the wire and 243 mm long compression spring, with a connecting nut. This nut equally connects a 210 mm long and 12.6 mm diameter pressure shaft. The handle is a 305 mm long and 21.5 mm diameter pipe which is connected to the pressure shaft. This tool is designed to allow at least a maximum force of 2000 kPa and can be operated in a vertical position. The design is limited by the fact that resistance increases with increasing depth due to the increase contact area with the ring, Description of component parts and shape of the apparatus is shown in Fig. (2).



Fig (1): Model Used in Laboratory penetration Test



Fig (2): Shape of penitrometer needle apparatus

III. RESULTS AND ANALYSIS

Common handle penitrometer was used to perform penetration tests on coarse and fine sand. Five densities were used for coarse sand samples, whereas seven densities were used for fine sand samples as explained above.

3.1 Tests performed on coarse sand

Table (1) shows penetration distance and normal stress regarding a density of 1.76 g/cm³ for different disk diameters.

Table (1): Results of Penetrating Distance and Normal Stress at Dry Density 1.76 g/cm³

Disk diameters	Penetrating distance (cm)	Normal stress (kg/cm ²)				
		Trial 1	Trial 2	Trial 3	Trial 4	average
2.5 cm	9	13.27	13.37	13.06	13.47	13.29
	8	9.19	9.50	9.39	8.98	9.26
	7	7.15	7.25	7.45	7.04	7.22
	6	6.84	6.94	6.94	6.84	6.89
	5	4.39	4.49	4.59	4.39	4.47
	4	2.66	2.55	2.76	2.55	1.13
2.0 cm	9	16.56	16.4	16.56	16.09	16.4
	8	11.47	11.15	11.31	11.47	11.35
	7	8.315	8.76	9.08	8.92	8.92
	6	8.59	8.44	8.44	8.59	8.52
	5	5.57	5.42	5.26	5.73	5.50
	4	3.35	3.19	3.19	3.5	3.31
1.5 cm	9	22.05	21.75	21.75	22.32	21.97
	8	15.26	15.26	15.54	14.69	15.19
	7	11.87	11.30	11.08	12.15	11.60
	6	11.30	11.30	11.00	10.75	11.09
	5	7.35	7.35	7.06	7.63	7.35

	4	4.52	4.52	4.24	3.96	4.31
1.3 cm	9	25.94	26.32	25.94	26.69	26.22
	8	18.05	18.42	17.67	18.42	18.14
	7	13.91	13.91	13.54	14.29	13.91
	6	13.16	13.16	9.61	9.61	11.39
	5	8.65	8.27	8.65	7.90	8.37
	4	5.27	4.89	5.27	5.64	5.27
cone	9	15.75	15.85	15.56	15.97	15.63
	8	10.91	11.25	11.14	10.73	11.01
	7	8.49	8.60	8.80	8.39	8.57
	6	8.11	5.74	8.24	8.14	8.18
	5	5.21	5.31	5.41	5.21	5.29
	4	3.16	3.05	3.26	3.05	3.13

By plotting the results of normal stress values against that of different penetration distance from 4 cm to 9 cm, a reliable correlation were obtained as shown in Fig (3). The values of coefficient of determination associated with the following best – fitted equation for 2.5 cm diameter disk are

$$y = 2.157(x) - 6.978$$

$$R^2 = 0.951$$

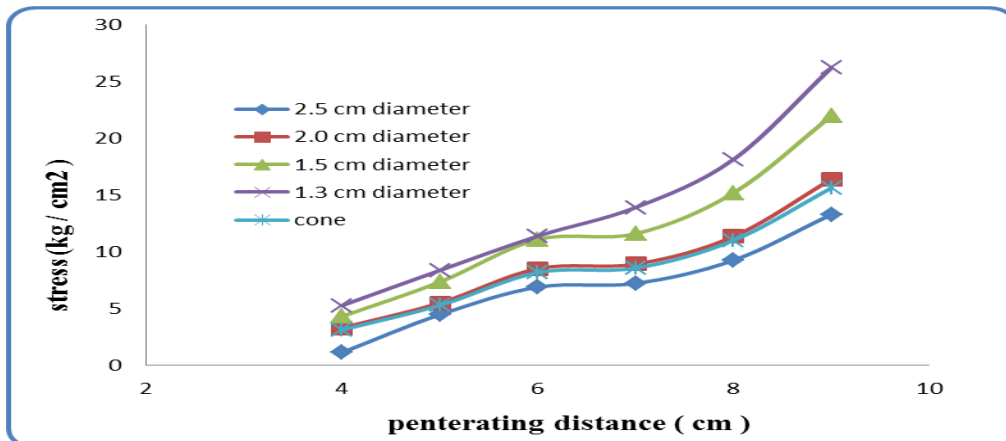


Fig (3): Correlation between normal stress and penetration distance at dry density 1.76 g/cm^3

Figure (3) indicates that normal stress increases with increases of penetration distance. The results showed linear correlation with acceptable coefficient of determination.

Similar correlations were determined for disk diameters of 2.0, 1.5, 1.2, and cone. The linear correlations for these disk diameters are:

2.0 cm diameter disk

$$y = 2.382(x) - 6.488$$

$$R^2 = 0.945$$

1.5 cm diameter disk

$$y = 3.209(x) - 8.943$$

$$R^2 = 0.942$$

1.3 cm diameter disk

$$y = 2.382(x) - 6.488$$

$$R^2 = 0.945$$

Cone

$$y = 2.287(x) - 6.231$$

$$R^2 = 0.95$$

Similar correlations were obtained for samples of other used densities. All Correlations above indicates that normal stress increases with increases of penetration distance.

The previously explained penetration/stress correlations were used to obtain a correlation between soil density and normal stress. Fig (4) Shows correlations between dry density and normal stress for different disk diameters for each penetration distance. These correlations may be used to estimate soil density directly by knowing penetration distance corresponding to used disk diameter and resulting normal stress.

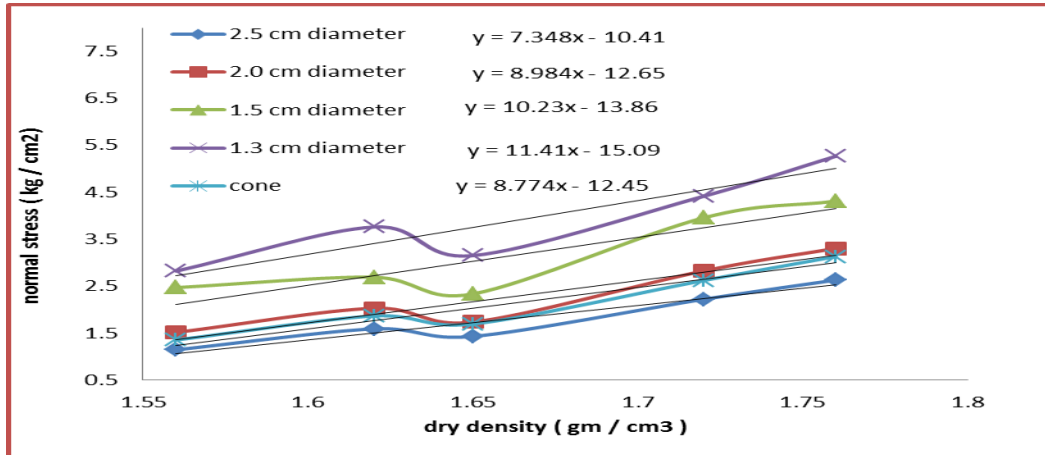


Fig (4) Correlation between normal stress and dry density at 4 cm penetration distance with different diameters of disk

3.2 Tests performed on fine sand

Table (2) shows penetration distance and normal stress regarding a density of 1.63 g/cm³ for different disk diameters.

Table (2) Results of Penetrating Distance and Normal Stress at Dry Density 1.63 g/cm³

Disk diameters	Penetrating distance (cm)	Normal stress (kg/cm ²)				
		Trial 1	Trial 2	Trial 3	Trial 4	average
2.5 cm	9	4.895	4.895	4.895	4.695	4.845
	8	3.47	3.57	3.47	3.265	3.82
	7	3.165	3.165	3.06	3.06	3.115
	6	2.855	2.96	2.855	2.55	2.805
	5	1.735	1.835	1.735	1.635	1.735
	4	0.92	1.02	1.02	0.92	0.97
2.0 cm	9	6.21	6.21	5.89	5.89	6.05
	8	4.295	4.295	3.98	4.14	4.18
	7	3.98	3.98	3.505	3.505	3.745
	6	3.66	3.345	3.345	3.66	3.505
	5	2.23	2.39	2.23	1.91	2.19
	4	1.115	1.115	1.115	1.115	1.115
1.5 cm	9	8.19	8.19	7.625	7.625	7.91
	8	5.93	5.645	5.645	5.365	5.645
	7	5.365	5.085	4.8	5.365	5.155
	6	4.8	4.8	4.235	4.235	4.52
	5	2.825	3.105	3.39	2.825	3.035
	4	1.975	1.975	2.54	1.975	2.115
1.3 cm	9	9.775	9.775	9.025	9.025	9.4
	8	6.765	6.765	7.145	7.145	6.955
	7	6.39	6.39	6.015	6.015	6.205
	6	5.64	5.64	4.885	5.265	5.36
	5	3.385	3.76	3.76	4.135	3.76
	4	2.63	2.63	2.63	2.63	2.63
cone	9	5.81	5.795	5.685	5.485	5.69375
	8	4.12	4.22	4.12	3.915	4.09375
	7	3.76	3.765	3.66	3.66	3.71125
	6	3.39	3.51	3.405	3.1	3.35125
	5	2.06	2.135	2.035	1.935	2.04125
	4	1.09	1.17	1.17	1.07	1.125

By plotting the results of normal stress values with that of different penetration distance from 4 cm to 9 cm, a reliable correlation were obtained as shown in Fig (5). The values of coefficient of determination associated with the following best – fitted equation are:

$$y = 0.741(x) - 1.935$$

$$R^2 = 0.984$$

Fig (5) indicates that normal stress increases with increases of penetration distance. The result is linear correlation with acceptable coefficient of determination.

Similar correlations were determined for disk diameters of 2.0, 1.5, 1.2, and cone, as shown in Fig (5).the linear correlations for these disk diameters are:

2.0 cm diameter disk

$$y = 0.882(x) - 2.271$$

$$R2 = 0.944$$

1.5 cm diameter disk

$$y = 1.069(x) - 2.223$$

$$R2 = 0.958$$

1.3 cm diameter disk

$$y = 1.265(x) - 2.505$$

$$R2 = 0.971$$

Cone

$$y = 0.838(x) - 2.116$$

$$R2 = 0.959$$

All Correlations above indicates that normal stress increases with increases of penetration distance.

The previously explained penetration/stress correlations were also used to obtain a correlation between soil density and normal stress. Fig (4) Shows correlations between dry density and normal stress for different disk diameters for each penetration distance. These correlations may be used to estimate soil density directly by knowing penetration distance corresponding to used disk diameter and resulting normal stress.

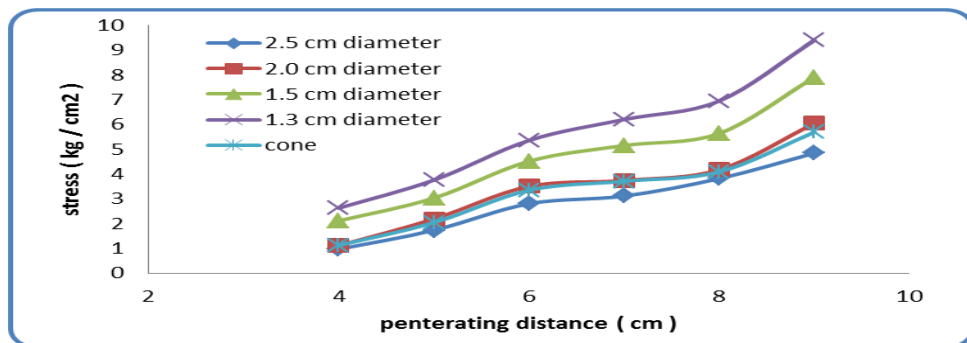


Fig (5): Correlation between normal stress and penetration distance with cone at dry density 1.63 g/cm³

3.3 Correlation between soil density and normal stresses

The previously explained penetration/stress correlations were used to obtain a correlation between soil density and normal stress. Fig (6) show correlations between dry density and normal stress for different disk diameters for each penetration distance. These correlations may be used to estimate soil density directly by knowing penetration distance corresponding to used disk diameter and resulting normal stress, but we'll show one penetration distance.

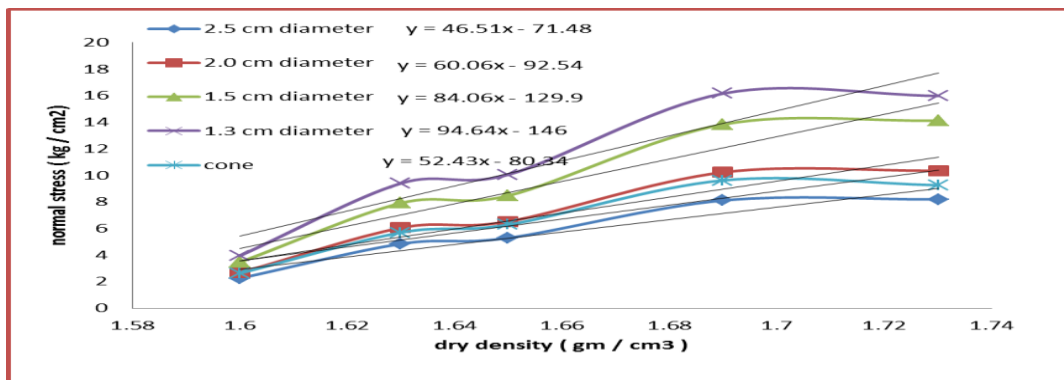


Fig (6): Correlation between normal stress and dry density at 9 cm penetration distance with different disk diameters

3.4 Estimation of soil parameters

Table (3) shows the result of laboratory tests which were alleged to all densities used in research so as to estimate the internal friction angle and young's modulus. Been drawing a relationship between density and internal friction angle and it is to know the angle of friction of any density within existing densities in Figures (7) and (8) respectively.

Table (3): Results of Young's Modulus and Friction Angle for Sandy Soil

Dry density (gm/cm ³)	m _v	E _{oed} = (1/m _v)	E(kg/cm ²)	Φ(degrees)
1.79	0.0016	612	510	40
1.75	0.0016	598.8	499	39
1.73	0.0017	574.8	479	38
1.71	0.0019	525.6	438	37
1.69	0.002	489.6	408	36
1.68	0.0021	465.6	388	36
1.67	0.0022	452.4	377	35
1.65	0.0025	404.4	337	34
1.63	0.0028	355.2	296	33
1.62	0.0029	342	285	32
1.6	0.0034	294	245	32
1.56	0.0039	256.8	214	31

$$E_{oed} = (1/m_v)$$

$$E_{oed} = E (1-\nu) / (1+\nu) (1-2 \nu)$$

Where:

m_v = coefficient of volumetric compressibility.

E = young's modulus

ν = poisons ratio in this research assumed 0.25

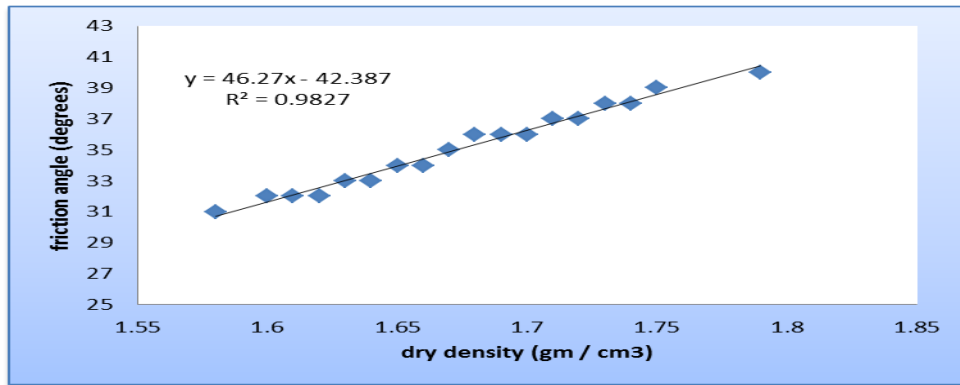


Fig (7): Correlation between friction angle and dry density for sandy soil

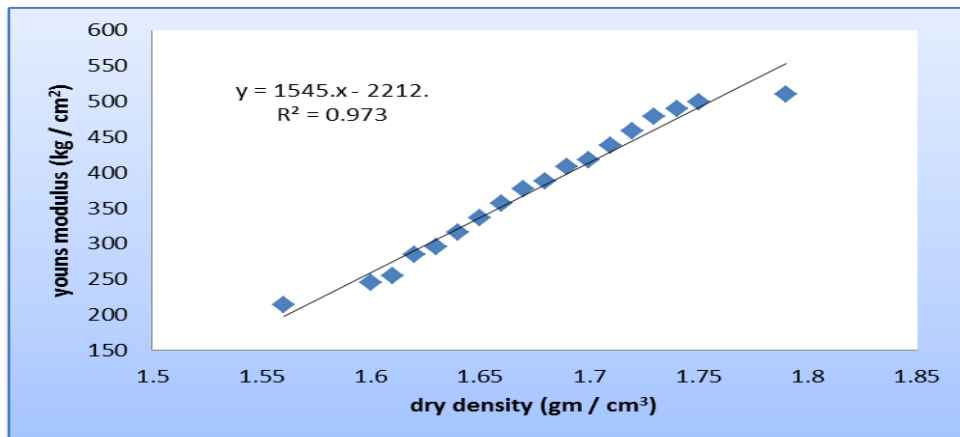


Fig (8): Correlation between dry density and Young's modulus for sandy soil

IV. CONCLUSIONS

Based on laboratory and field tests results, the following conclusions can be drawn, for sandy soil with Correlation between normal stress and penetration distance with different rings (cm) diameter at different dry density (gm / cm^3) for coarse sand , Correlation between Normal Stress and Dry Density at different Penetration Distance with Different Diameters of Rings for coarse sand, Correlation between normal stress and penetration distance with different rings (cm) diameter at different dry density (gm / cm^3) for fine sand and Correlation between Normal Stress and Dry Density at different Penetration Distance with Different Diameters of Rings for fine sand.

References

- [1] ASAE Standards, 46th Ed. 1999a. ASAE S313.3, Soil cone penetrometer. St. Joseph, Mich.: ASAE.
- [2] ASAE 1999b. ASAE EP542. Procedures for using and reporting data obtained with the soil cone penetrometer. St. Joseph, Mich.: ASAE.
- [3] Godwin,R.J.,N.L.Warner, and D..L.O. Smith. 1991. The development of a dynamic drop-cone device for the assessment of soil strength and the effects of machinerytraffic. J. Agric. Eng. Res. 48:123–131.
- [4] Herrick, J. E. and Jones, T. L. 2002. A dynamic cone penetrometer for measuring soil penetration resistance, Soil Sci. Soc. Am. J. 66:1320–1324
- [5] Perumpral, J.V. 1987. Cone penetrometer applications—A review. Trans. ASAE 30:939–944.
- [6] Raper, R. L., B. H. Washington, and J. D. Jarrell. 1999. A tractor-mounted multiple-probe soil cone penetrometer. Applied Engineering in Agriculture 15(4): 287-290.
- [7] Raper, R. L. and A. K. Sharma 2004 .Soil moisture effects on energy requirements and Soil dis ruption of subsoiling a coastal plain soil,Transactions of the ASAE Vol.
- [8] Sanglerat, G. 1972. The penetrometer and soil exploration. Interpretation of penetration diagrams-theory and practice. Transportation Research Board. 500 Fifth St. NW, Washington DC, 2001, National Academy of Sciences.
- [9] Tollner, E.W. and Verma, B.P., 1987. Lubricated and nonlubricated cone penetrometer comparison in six soils. Trans. ASAE 30(6), 1611-1618.

Determination of the Vulnerability of Water Supply Aquifers in Parts of Imo River Basin, South-Eastern Nigeria: The Case of Benin Formation

Ikechukwu Boniface Ijeh

Department of Physics, College of Natural and Applied Sciences, Michael Okpara University of Agriculture, Umudike. PMB 7267, Umuahia, Abia State, Nigeria.

ABSTRACT: Eight locations in the study area were investigated to obtain data on the depth to water table, net recharge, aquifer media, soil media, topography, impact of the vadose zone and hydraulic conductivity. These parameters are denoted by the acronym, DRASTIC, an empirical groundwater model that estimates groundwater contamination vulnerability of aquifer systems based on the hydrogeological settings of the area. This was used to develop a vulnerability map for the study area. The vulnerability map shows that areas within Benin Formation have generally moderate vulnerability to pollution.

Keywords: Aquifer Media, DRASTIC, Net Recharge, Soil Media, Topography, Vulnerability, Water Table.

I. INTRODUCTION

The Imo River Basin is based on a bedrock of a sequence of sedimentary rocks of about 5480m thick and with ages ranging from Upper Cretaceous to Recent (Uma, 1986)¹. It is known to contain several aquiferous units. The proportion of sandstones to shales varies from formation to formation and sometimes from place to place within the same formation. The interlayering of sandy and shaly units form complex aquifer systems that are respectively localized in the formations, such that it is almost impossible for aquifers to cross formation boundaries. This is because the regional stratigraphy and the general trends of the geologic formations feature sharp changes in lithology which prevent hydraulic continuity (Uma, 1989)². The characteristics of these aquifers such as transmissivity, hydraulic conductivity and storage potentials are not clearly understood. Since the mid 1980's, some researchers from the academia have carried out geological/geochemical investigations. Uma (1986) carried out a study on the ground resources of the Imo River Basin using hydro-geological data from existing boreholes. He concluded that three aquifer systems (shallow, middle and deep) exist in the area (Uma, 1989). Geophysical investigations on groundwater resources in the Imo River Basin were also carried out in different sections of the basin. While the contributions made by these workers are remarkable, more work still needs to be done, particularly in the area of vulnerability of the aquifer systems. The present study is aimed at investigating the vulnerability of the hydro-geological character in Ameki and Imo shale Formations to pollution. Vulnerability assessment is more meaningful in areas where water resources are under stress due to industrial or agricultural activities, as it can provide valuable information for planning prevention of further deterioration of the environment (³Mendoza et al., 2006; ⁴Antonakos et al., 2007).

1.1 The Study Area

Figure 1 show the location map of the Imo River Basin where the study area is situated. The study area (Figure 2) lies between latitudes 5°05'N and 5°37' and longitudes 7°00' and 7°30'. The Benin Formation (Miocene to Recent) covers more than half of the area of the Imo River Basin. It consists of sands, sandstones, and gravels, with intercalations of clay and sandy clay. The sands are fine-medium-coarse grained and poorly sorted (⁵Whiteman, 1982; and ⁶Uma and Egboka, 1985). Petrographic study on several thin sections (⁷Onyeagocha, 1980) show that quartz makes up more than 95% of all grains, but ⁸Asseez (1976) and ⁹Avbovbo (1978) indicated a possible presence of more percentage of other skeletal materials including feldspar. This formation has very low dip to the south and south-west. The youngest deposits in the basin are alluvium of recent age found mainly at the estuary of the Imo River at the Atlantic Ocean and on the flood plains of the river.

The Imo River Basin has a large amount of recharge; estimated at 2.5 billion m³ per annum, coming mainly from direct infiltration of precipitation. Average annual rainfall is about 2000mm (¹⁰Onwuegbuche, 1993). The Benin Formation is by far the most aquiferous unit, consisting mainly of massive continental sands, sandstones, and gravels. It has a very extensive deep unconfined aquifer which covers more than half of the Imo River Basin. The aquifer consists of thick complex interbedded units of fine, medium and coarse-grained quartz sands and gravels (Uma, 1989).

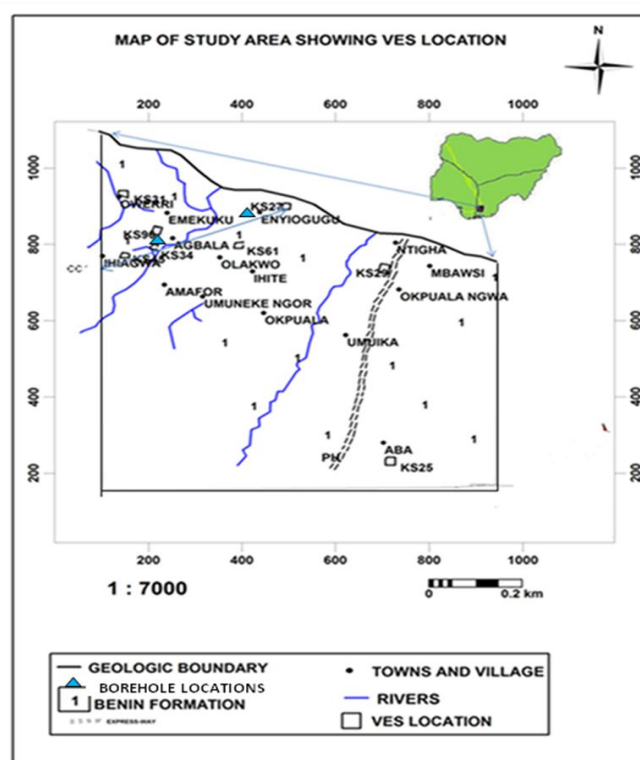
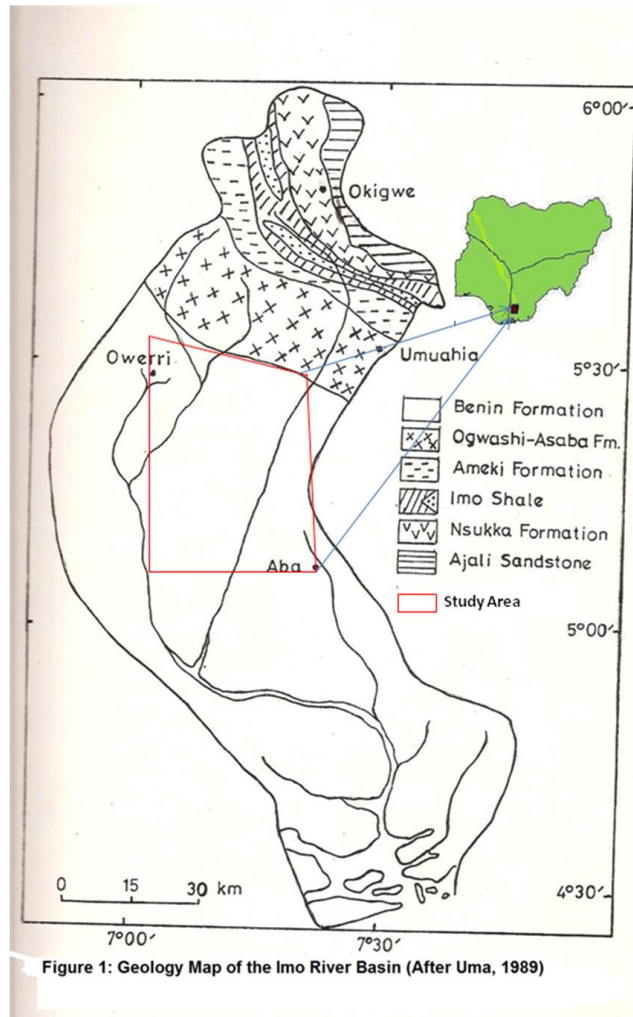


Figure 2: Map of the Study Area showing VES locations

II. METHODOLOGY

The DRASTIC model was developed in USA for the purpose of protecting groundwater resources (¹¹Aller et al., 1985; ¹²Aller, 1987). DRASTIC is an empirical groundwater model that estimates groundwater contamination vulnerability of aquifer systems based on the hydro geological settings of the area. A hydro geological setting is defined as mappable unit with common hydro geological characteristics (¹³Engel et al., 1996). The DRASTIC model was used to develop the groundwater vulnerability map for the study area. The generic model was used to determine the weights and the ratings. The model employs a numerical ranking system that assigns relative weights to various parameters. The acronym DRASTIC is derived from the seven factors considered in the method, which are **D**epth to water table [**D**], **R**echarge [**R**], **A**quifer media [**A**], **S**oil media [**S**], **T**opography [**T**], **I**mpact of the vadose [**I**] and **C**onductivity [**C**]. Each DRASTIC factor is assigned a weight based on its relative significance in affecting pollution potential. The ratings range from 1 – 10 and weights from 1-5. The DRASTIC Index [**DI**], a measure of pollution potential, is computed by summation of the products of ratings and weights of each factor. The final result for each hydrogeological setting is a numerical value, called DRASTIC index. The higher the value is, the more susceptible the area is to groundwater pollution.

Depth to the Water Table

The depth to the water table is the distance from the ground to the water table. This determines the depth of material through which a contaminant must travel before reaching the aquifer. The presence of low permeability layers, which confine aquifers, limits the travel of contaminants into an aquifer. There is a greater chance for attenuation to occur as the depth to water increases because, deeper water levels imply longer travel distances. The depth to the water table was obtained from Table 4.1 and converted to feet to determine the DRASTIC rating.

Net Recharge

Net recharge represents the amount of water per unit area of land, which penetrates the land and reaches the water table. Recharge water is the means by which leaching and contaminants are transported vertically to the water table and horizontally within the aquifer. The greater the recharge rate, the greater the potential for groundwater pollution. The net recharge was taken to be about 12% of the average annual rainfall (¹⁴Navulur, 1996).

Aquifer Media

An aquifer is defined as a permeable geologic unit that will yield useful quantities of water. The aquifer medium influences the amount of effective surface area of materials with which contaminants may come in contact. The larger the grain size and the more the fractures or openings within the aquifer, the higher the permeability and the lower the attenuation capacity of pollutants in the aquifer media. Only unconfined aquifer was considered, for which the DRASTIC model is valid (Aller et al., 1987). The aquifer media was obtained by taking depths at which water was struck and correlating those depths with the lithological description of the VES result or strata description to identify the aquifer media.

Soil Media

Soil media refers to the uppermost portion of the vadose zone characterized by significant biological activity. It was considered as the upper weathered zone of the earth, which averages a depth of one meter or less from the ground surface. Soil has a significant impact on the amount of recharge which can infiltrate into the ground and hence on the ability of contaminant to move vertically into the vadose zone. The smaller the grain size, the less the pollution potential. Soil media was obtained from the soil map of the study area.

Topography Map

Topography refers to the variability of slope of the land surface. Topography helps control the likelihood that a pollutant will run off or pool and remain on the surface in one area long enough to infiltrate. The study area was found to be relatively flat with topography ranging from 0% - 3%. The topography was estimated from a topographic contour map.

Impact of the Vadose Zone

The vadose zone is defined as the zone above the water table which is unsaturated or discontinuously saturated. This zone determines the attenuation characteristics of the material below typical soil horizon and above the water table. The impact of the vadose zone was obtained by using the lithological description or strata description resulting from the VES data analysis.

Hydraulic Conductivity

Hydraulic conductivity refers to the ability of the aquifer material to transmit water, which in turn, controls the rate at which groundwater will flow under a given gradient. The values of the hydraulic conductivity were derived from the Dar Zarrouk parameters (transverse unit resistance and longitudinal conductance in porous media) obtained from the VES data (¹⁵Niswaw and Singhal, 1981). The hydraulic conductivities were converted from m/day to gpd/ft^2 before application in finding the DRASIC Index. $1 \text{ gal/day/ft}^2 = 0.0408 \text{ m/day}$.

Eight vertical electrical sounding results coupled with the geology of the study area were used to determine such parameters as the depth to the water table, the aquifer media, the soil media and the impact of the vadose zone. The VES sounding locations, as represented by northings and eastings, were used in geo-referencing. The GIS software, ArchView 3.2a, was

used to generate the Groundwater Vulnerability Map. Estimates for the vulnerability indices spatial distribution were determined by applying appropriate GIS overlay functions.

III. RESULTS AND DISCUSSIONS

The deduced DRASTIC parameters were used to compute the DRASTIC Index at the various VES points and these are given in Table 1. This was then used to generate the Groundwater Vulnerability Map (GVM) for the study area. Fig. 3 shows the vulnerability map of the study area. The map shows that most of the areas in Benin Formation have moderate vulnerability because the overburden is largely fine, medium and coarse grained sand. Fig. 4 shows the vulnerability map of parts of Imo River Basin covering Imo Shale (4), Ameki Formation (3), Ogwashi-Asaba Formation (2), and Benin Formation (1). This helps to compare the respective degrees of vulnerability of the different formations. Areas of low vulnerability have drastic index of <120; areas of moderate vulnerability have drastic index of 121-140; while high vulnerability is >140. Higher vulnerabilities can be observed around the south east of the study area, around Aba. Low vulnerabilities can be observed at areas around Obibiezena and Naze.

TABLE 1: Calculated DRASTIC Index for the Study Area.

VES #	LOCATION	NORTHINGS	EASTINGS	D _r	D _w	R _r	R _w	A _r	A _w	S _r	S _w	T _r	T _w	I _r	I _w	C _r	C _w	DI
KS25	FAULKS RD, ABA	125638	544503	5	5	9	4	8	3	6	2	10	1	5	5	4	3	144
KS27	OBOKWU NGURU	164201	530389	1	5	9	4	8	3	6	2	8	1	8	5	4	3	137
KS29	UMUIKE LOWA	153926	546313	3	5	9	4	5	3	6	2	9	1	9	5	2	3	138
KS31	100 WORKS L/O OWERRI	168585	510539	5	5	9	4	8	3	6	2	10	1	1	5	8	3	136
KS34	OBIBIEZENA	156051	511975	1	5	9	4	8	3	6	2	10	1	1	5	8	3	116
KS45	UMUOMA	155685	509897	1	5	9	4	3	3	3	2	10	1	3	5	4	3	93
KS61	UMUOHIAGU	157988	523336	1	5	9	4	8	3	6	2	10	1	8	5	2	3	133
KS90	NAZE	159633	512175	5	5	9	4	8	3	6	2	8	1	1	5	6	3	128

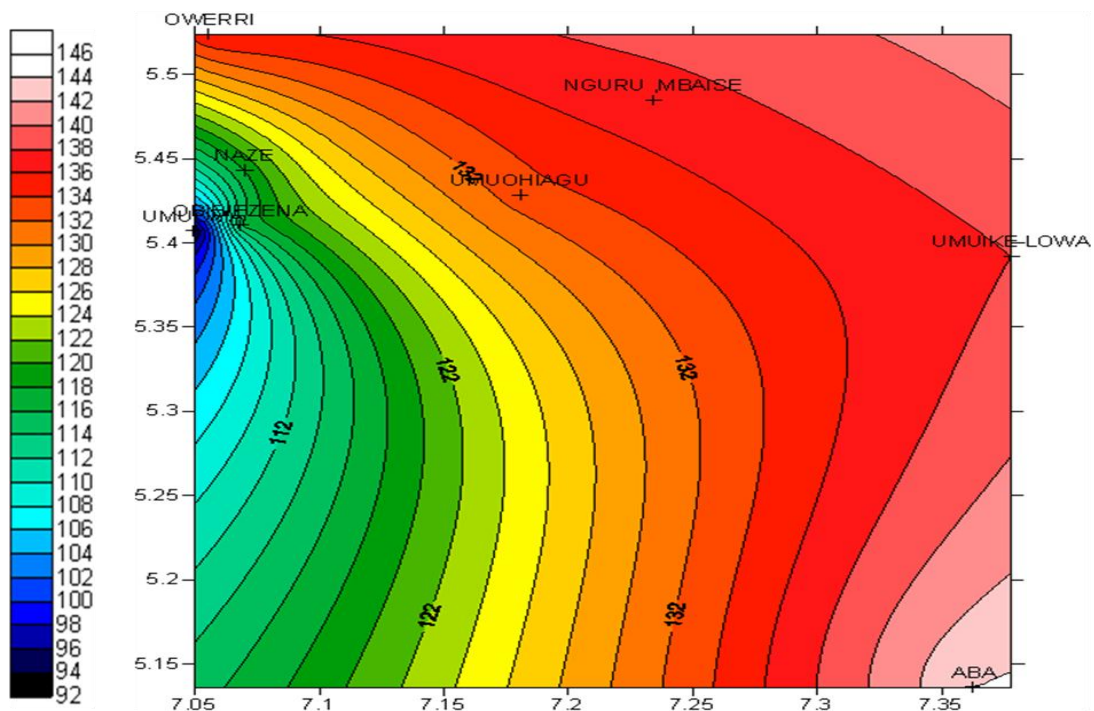


Figure 3 :Vulnerability Map of Benin Formation

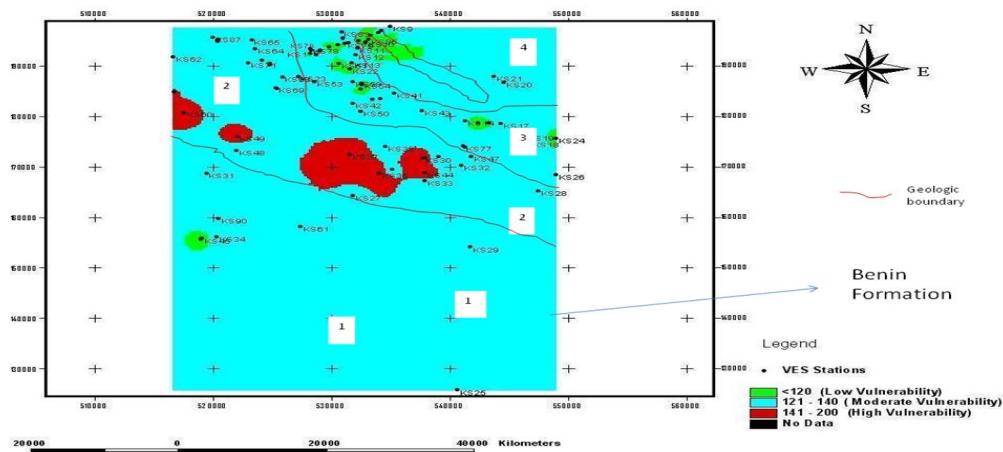


Figure 4: The Vulnerability Map of Parts of Imo River Basin

IV. CONCLUSION

The study area consists of coastal plain sands with relatively high permeability, so most of the area is moderately vulnerable. The DRASTIC model proved to be useful in the assessment of the vulnerability of the formation studied.

V. ACKNOWLEDGEMENTS

The author wishes to acknowledge with gratitude the Anambra-Imo River Basin Authority, the Imo State Rural Water Supply Agency, and UNICEF Owerri for giving us access to their information resources. Special thanks to Engr. Emeka Udokporo of FLAB Engineering and Mr. A. O. Kanu of the Abia State Water Board, who made a lot of useful material available and helped in many other ways; also Mr. R. C. Oty of the Anambra- Imo River Basin Authority, and Mr. R. N. Ibe of the Ministry of Public Utilities, Owerri for their tremendous help in the work.

REFERENCES

- [1] Uma, K. O. (1986); Analysis of Transmissivity and Hydraulic Conductivity of Sandy Aquifers of the Imo River Basin. Unpl. Ph.D. Thesis, University of Nigeria, Nsukka.
- [2] Uma, K.O., (1989); An appraisal of the groundwater resources of the Imo River Basin, Nigeria. Journal of Mining and Geology Vol. 25 Nos 1&2, pp.305-31
- [3] Mendoza JA, Barmen G (2006). Assessment of groundwater vulnerability in the Rio Artiguas basin, Nicaragua. Environ. Geol., 50:569-580.
- [4] Antonakos AK, Lambrakis NJ (2007). Development and testing of three hybrid methods for the assessment of aquifer vulnerability to nitrates, based on the drastic model, an example from NE Korinthia, Greece. J. Hydrol., 333: 288-304.
- [5] Whitman, A.,(1982); Nigeria: Its Petroleum Geology Resources and Potentials, Vol.2, Graham and Trotman Publ., London SWIVIDE.
- [6] Uma, K. O. and Egboka, B. C. E., (1985); Groundwater potentials of Owerri and its environs. Nig. Journal of Min. Geol., Vol. 22, pp.57-64.
- [7] Onyeagocha, A. C. (1980); Petrography and depositional environment of the Benin Formation. Nigerian. Journal of Mining and Geology. 17, pp.147-151.
- [8] Asseez, L. O., (1976); Review of the Stratigraphy, Sedimentation and Structure of the Niger Delta. In: C.A. Kogbe (ed.) Geology of Nigeria. Elizabethan Publ. Co. Lagos.
- [9] Aybovbo, A. A., (1978); Tertiary Lithostratigraphy of Niger Delta Bull. Am. Assoc. Pet. Geol., V.6, p.295- 306.
- [10] Onwuegbuche, A. A., (1993); Geoelectrical investigations in the Imo River Basin Nigeria. Unpublished Ph.D thesis. Department of Physics, University of Calabar. Pp.2-62.
- [11] Aller, L., Bennet T., Lehr J.H., Petty R.J., and Hackett G. (1985); DRASTIC: "A standardized system for evaluating groundwater pollution potential using hydro geological settings."U.S. Environmental Protection Agency, Ada, Ok, EPA/600/2-87-036, 455p.
- [12] Aller, L., (1987); "DRASTIC": A Standardized System for Evaluating Groundwater Pollution Potential Using Hydro geological Settings. EPA 600/2-87-035. U.S. Environmental Protection Agency, Ada, Oklahoma.
- [13] Engel, B., Navulur, K., Cooper, B., Hahn, L. (1996); Estimating Groundwater Vulnerability to Non-point Source Pollution from Nitrates and Pesticides on a Regional Scale. IAHS Publications, No. 235, pp.521-526.
- [14] Navulur, K. C. S., (1996); Groundwater evaluation to non-point source nitrate pollution for large areas using GIS. Ph.D. thesis, Purdue University, West Lafayette, Indianapolis, USA.
- [15] Niswaw, S. and Singhal, D.C., (1981); Estimation of Aquifer Transmissivity from Dar-zarrouk parameters in porous media. Journal of Hydrology, Vol. 50 pp. 393-399.

A Survey on Implementation of Smart Grid in Iran

Alireza Akoushideh,¹ Mehrdad Zobeiri,² Babak Mazloom-Nezhad Maybodi³

^{1,3}Electrical and Computer Department, Shahid Beheshti University G. C, Tehran, Iran

²Department of Engineering Islamic Azad University, Garmsar Branch, Iran

ABSTRACT: Recently, importance of power consumption, green house gas and renewable energy sources proposed an international requirement, Smart Grids. Advance metering Infra-structure (AMI) and smart meters are fundamental elements of this new field. This new system has ability to configure, manage and process the gathered information and produce graphs and necessary reports.

In this paper, smart networks and its advantages are discussed especially in Iran. Furthermore, a survey about Smart metering implementation in Iran is done which debate about standardization, metering unit's specifications, localization and other aspects of implementation method.

Keywords: AMI, AMR, Smart grid, Smart metering.

I. INTRODUCTION

High quality Electricity generation for Digital Society, optimum combination of generation methods using clean energies and attaining at least 1000kwh till 2050 is priority of world electricity industry[1]. Production of digital tools, which are sensitive to quality of electricity, will increase five times till 2020. Electrical and hybrid cars will be produced more and CO₂ emission is necessary to be reduced. Also, entrance of many small distributed generators makes revolution on electricity's network and its component communication.

Xcel Energy announced that they have successfully implemented the Ventyx Smart Grid Operations Solution in Boulder, Colorado. This implementation is the first fully integrated Smart Grid city in the world. The Ventyx Solution will make it possible to convert the data from the Smart Grid into actual information that will assist both utility providers, and consumers alike, in making energy-related decisions. Ventyx is the largest private software, data and advisory services provider for the energy industry and Xcel Energy is a major U.S. electricity and natural gas company[2].

Control of 4000MW load peak, 3% increase of renewable energy's stations by construction of 2000MW renewable power plant and 3000MW distributed generators and other objectives, which are mentioned in book one, objectives of Iran Department of Energy, display deep changes in expansion of electricity network. It means smart grid, smart metering and new management is necessary. Three main parts of this research are (a) Definition of AMR, AMI, generic benefit of smart metering. (b) Smart metering implementation steps which are done and (c) Propose a Smart metering implementation road map. In the following, smart networks definition, AMR and AMI are in section II. Advantages of smart grid are discussed in section III. Smart grid in Iran, Goals of AMI implementation and current project are in section IV. In section V, road map of smart

metering is mentioned. Discussion and conclusion of research are in section VI.

II. SMART NETWORKS

A smart network is defined as an energy network where there is a pervasive information and communications technology overlay that effectively enables integrated management of the creation, transport, storage and consumption of energy. Specific emphasis is placed on the application of digital technology to provide accessible, flexible, reliable and economically sustainable electrical energy to users. Fig. 1 depicts plan of a smart network.

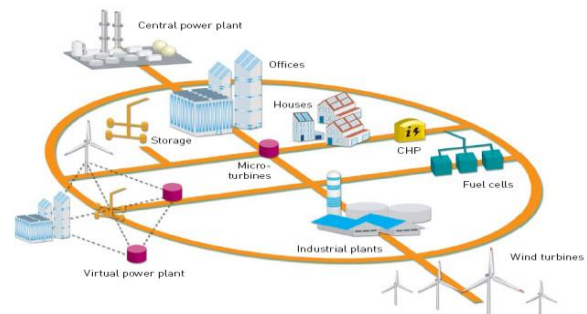


Figure 1. Smart network plan[3]

There are two definitions in Smart grid or network, Automatic Meter Reading (AMR) and Advanced Meter Infra-structure (AMI) which are described in the following.

A. Automatic Meter Reading (AMR)

Automatic meter reading, or AMR, is the technology of automatically collecting consumption, diagnostic, and status data from water meter or energy metering devices (gas, electric) and transferring that data to a central database for billing, troubleshooting, and analyzing. This technology mainly saves utility providers the expense of periodic trips to each physical location to read a meter. Another advantage is that billing can be based on near real-time consumption rather than on estimates based on past or predicted consumption. This timely information coupled with analysis can help both utility providers and customers control better the use and production of electric energy, gas usage, or water consumption. AMR technologies include handheld, mobile and network technologies based on telephony platforms (wired and wireless), radio frequency (RF), or power line transmission.

B. Advanced Metering Infrastructure (AMI)

AMIs are systems that measure, collect, and analyze energy usage, and communicate with metering devices such as electricity meters, gas meters, heat meters, and water meters, either on request or on a schedule. These

systems include hardware, software, communications, consumer energy displays and controllers, customer associated systems, Meter Data Management (MDM) software, and supplier business systems. The network between the measurement devices and business systems allows collection and distribution of information to customers, suppliers, utility companies, and service providers. This enables these businesses to participate in demand response services. Consumers can use information provided by the system to change their normal consumption patterns to take advantage of lower prices. Pricing can be used to curb growth of peak consumption. AMI differs from traditional automatic meter reading (AMR) in that it enables two-way communications with the meter. Systems only capable of meter readings do not qualify as AMI systems[4].

III. ADVANTAGE OF SMART GRID

The benefits most often associated with an AMI and AMR investment are documented and include[5]:

- Improving the accuracy of billing information by reducing the number of estimated meter reads, immediate validation and verification of the accuracy of current usage information, verification that customers are indeed to the appropriate rate schedule; and more timely identification of potential metering problems.
- Early identification of potential revenue integrity issues such as theft; or in the case of a water utility, improved identification of system leaks or improper customer usage (i.e. night time watering of lawns during periods of restrictions);
- Verification of the efficacy of the Utility's load management programs; and an overall improvement in customer satisfaction as the utility is now able to provide customers with better information concerning their usage and cost patterns.

More advanced benefits of AMI and AMR investments comes from integrating AMI and AMR information with other utility operating systems to improve overall management and operation of the utility system. These benefits may be derived from:

- A better understanding of customer usage characteristics; which can then be used in a predictive manner.
- More accurate (real time) characterization of the operating condition of the distribution network that can result in earlier identification that an outage has either occurred or is imminent on the system.

IV. SMART GRID IN IRAN[6]

Iran Energy Efficiency Organization, responsible for implementation and deployment of Smart Metering project (FAHAM) in Iran, started the first phase of the project by selecting contractors through a tender that was executed successfully on 11 Dec 2011. The winners are thereby authorized for installing 1000000 smart meters in five separate distinct and predefined areas under the supervision of Tehran metropolitan, Alborz province, Zanjan province, Booshehr province, and Mashhad and Ahvaz Power distribution utilities. FAHAM is considered as the greatest ICT project in electric industry of Iran. The notable aspects of this project with various stakeholders and

using successful projects experience of other countries, led us to employ EPC method to implement this project in Iran.

A. Goals and Benefits of AMI implementation in Iran

There are economical, social and environmental benefits of AMI Implementation in Iran which are mentioned in the following.

1) Economical benefits

- Reducing non-technical losses
- Demand management (tariff management)
- Improving consumption patterns through the information shared with the customer
- Improving the payment system
- Reducing total costs of meter's reading, operation and maintenance, and customer's disconnection and reconnection
- Preparation for electricity retail markets

2) Social benefits

- No need for periodic trips to each physical location to read the meters
- Establishment of appropriate services for developing the electronic government
- Increasing electricity sale options with different prices
- Power delivery with higher quality and reliability
- Reducing cost of electricity due to reduced operating costs
- Increasing billing accuracy and speed by eliminating the human error factor
- Providing better customer service
- Creating customer's participation in consumption management and costs reduction

3) Environmental benefits

- Reducing polluted gas and CO2 emissions
- Reducing consumption through network energy management and reducing network losses
- Demand management through sharing the information with customers

B. FAHAM project

Some businesses, which FAHAM project need to perform correctly, are:

- Correcting customer's consumption pattern
- Preparing for complete elimination
- Applying energy management by the network operator in normal and critical conditions
- Improving meter readings and billing processes
- Reducing non-technical losses as well as monitoring technical losses in distribution network
- Improving the quality of service, reducing duration of power cuts and supervision on electric power quality
- Developing distributed generation and clean energy usage
- Possibility of electricity pre-sale and establishing electricity retail markets
- Optimizing operation and maintenance costs
- Providing appropriate management of water and gas meters

V. SMART METERING IMPLEMENTATION ROAD MAP IN IRAN

A. Standardization

In order to cope with the challenges of an increasing deployment of innovative technologies and to foster the interconnectivity between these technologies, compilation features performance of smart metering system or standardization is an important step of smart metering implementation which has to be offered by responsible organization such as IEEE-SA.

The European Commission has mandated the European standardization organizations, i.e. CEN, CENELEC and ETSI, to adopt a set of standards for smart grids. Resulting from the mandate M/490, these standards will be a key step for the deployment of smart grids in Europe [CEN/ CENELEC/ ETSI, 2011][7].

A minimum common set of functionalities for smart metering has been put forward by the European Commission with the aim of enabling member states to identify common means of achieving cost efficiencies (and inefficiencies) in their rollout plans. The functionality set, developed jointly by the European Commission's directorates of Energy and Information Society and Media, comprises 10 functionalities. These were determined based on comments from member states in response to an initial list of 13 functionalities based on the ERGEG Guidelines of Good Practice on Regulatory Aspects of Smart Metering for Electricity and Gas. These ten functionalities are[8]:

1) For the customer

- Provides readings from the meter to the customer and to equipment that he may have installed
- Updates these readings frequently enough to allow the information to be used to achieve energy savings.

2) For the meter operator

- Allows remote reading of meter registers by the meter operator
- Provides two-way communication between the meter and external networks for maintenance and control of the meter
- Allows readings to be taken frequently enough to allow the information to be used for network planning.

3) For commercial aspects of energy supply

- Supports advanced tariff systems, including multiple tariffs, time of use registers, block tariff registers, remote tariff control, etc. as applicable
- Allows remote on/off control of the supply and/or flow or power limitation.

4) For security and privacy:

- Provides secure data communications
- Fraud prevention and detection.

5) To allow distributed generation:

- Provides import/export and reactive metering.
The three functionalities on which there was limited consensus are:
- For the customer: Provides the readings in a form easily understood by the untrained consumer, and with

calculations enabling final customers to better control their energy consumption, e.g. in terms of cost, as averages, as comparisons to other periods, etc.

- For the meter operator: Provides for the monitoring of power quality
- For commercial aspects of energy supply: Supports energy supply by prepayment and on credit.

The approximately two-thirds of European member states that have not yet undertaken smart meter cost-benefit analyses are recommended when they do so to use this set of common functionalities.

The functionality set also could serve member states, the metering industry and utilities as a solid basis for their respective investments, facilitate rollout associated procurement, and provide regulators with European reference definitions, the document states.

B. Short-term courses and seminars of smart metering systems

The custodians this field such as FAHAM, universities, related associations and so on should make regular seminars to clear smart metering for experts, managers students and peoples. Fortunately, some short-term courses[6] and Conference such as SEGT2012[9] have been started. Topics of SEGT2012 conference are:

- Power and Energy System Applications (Generation, Transmission, Distribution, Markets, Operations, and Planning)
- Monitoring and Power Quality
- Distributed Generation, Energy Storages, and Micro grids
- Automation and Management of Electrical Energy Systems
- Reliability, Demand Response, Load Management and Forecasting
- Wide-area Metering, Monitoring, Control, and Protection
- Smart Grids Impacts on Fault Management (Protection Infrastructure, Emergency Response, and System Restoration)
- Electric Transportation and Vehicles
- Smart Grid Regulation and Standards
- Required Supporting Communications, Control and Information Systems
- Smart Sensors and Advanced Metering Infrastructure
- Information Technology, Database Management, and Cyber-Physical Systems Security

C. Contractor support

It is necessary to support smart grid's contractors on producing, importing, design and implementation. By this method, contractors work better and Department of Energy will get to its objects completely.

D. Defining of smart metering equipment's specifications

An electrical smart metering tool shall include Built-in or modular communication units to receive or send on-line commands using generic protocols for using in all regions of country. In the following some technical specification are mentioned.

1) RS232 Standard

In telecommunications, RS-232 is the traditional name for a series of standards for serial binary single-ended data and control signals connecting between a DTE (Data Terminal Equipment) and a DCE (Data Circuit-terminating Equipment). It is commonly used in computer serial ports[10].

2) RS-485

This protocol also known as TIA/EIA-485 or RS-485 is a standard defining the electrical characteristics of drivers and receivers for use in balanced digital multipoint systems. The standard is published by the Telecommunications Industry Association/Electronic Industries Alliance (TIA/EIA)[11].

3) PSTN

The public switched telephone network (PSTN) is the network of the world's public circuit-switched telephone networks. It consists of telephone lines, fiber optic cables, microwave transmission links, cellular networks, communications satellites, and undersea telephone cables, all inter-connected by switching centers, thus allowing any telephone in the world to communicate with any other.

4) GSM

Global System for Mobile Communications, is a standard set developed by the European Telecommunications Standards Institute (ETSI) [12] to describe technologies for second generation (2G) digital cellular networks.

5) GPRS

General packet radio service (GPRS) is a packet oriented mobile data service on the 2G and 3G cellular communication system's global system for mobile communications (GSM). GPRS was originally standardized by European Telecommunications Standards Institute (ETSI) in response to the earlier CDPD and i-mode packet-switched cellular technologies[12, 13].

6) Ethernet

This protocol is a family of computer networking technologies for local area networks (LANs). Ethernet was commercially introduced in 1980 and standardized in 1985 as IEEE 802.3. Ethernet has largely replaced competing wired LAN technologies. Since its commercial release, Ethernet has retained a good degree of compatibility. Features such as the 48-bit MAC address and Ethernet frame format have influenced other networking protocols.

7) M-Bus

Meter-Bus[14] is a European standard (EN 13757-2 physical and link layer, EN 13757-3 application layer) for the remote reading of gas or electricity meters. M-Bus is also usable for other types of consumption meters. The M-Bus interface is made for communication on two wires, making it very cost effective. A radio variant of M-Bus (Wireless M-Bus) is also specified in EN 13757-4.

Furthermore communication protocols, Hardware modules which seem benefit for AMI are Data Concentrator, In-Home-Unit-Display, Automation software.

VI. DISCUSSION AND CONCLUSION

Although there is a regulatory framework on implementation of Smart grid, but communication technology and electrical and physical environment is important. Therefore, it's necessary to localize generic smart metering implementation rules. Therefore, it is necessary to localize implementation methods of smart grid in each province of Iran. In the following, practical steps are proposed[15].

- a) Formation of committees such as restructuring, DG, micro-grid, IT and automation based on society-economical studies.
- b) Importance and aspects of smart grid such as fault following, loss reducing, reliability, supporting of renewable energy sources and asset management using AMI are defined in committees.
- c) Division of project to practical phases such as:
 - Internet and library based research on electrical smart grid and advanced metering units
 - Possibility of distributed generation source in region
 - Research on current network and necessities of AMI implementation
 - Smart grid simulation, society-economical analysis, study of results and proposals.

It seems the members of this project should have proficiency on reliability, smart metering and DG, power system programming. Furthermore, having power network software such as DigSILENT[16] and so on is necessary for this executive-research project.

Therefore, target of this project will be (a) recognition of DG sources, (b) recognition of appropriate to places advanced metering instruments, (c) recognition of technical and economical benefits of smart metering in region. Another result of using smart metering is making of a base for modification of consumption patterns and full implementation of targeted subsidies[1].

Finally, considering the situation, synchronizing of benefit factors and Legal obligations are effective factors for implementation of smart grid.

REFERENCES

- [1] Amvaj-e-bartar, Iranian monthly magazine of Electrical Engineering. Available: <http://www.amvaj-e-bartar.com>
- [2] J. Cohen-Donnelly. (2009). Consumer Energy Report. Available: <http://www.consumerenergyreport.com/2009/09/11/boulder-colorado-worlds-first-smart-grid-city/>
- [3] G. Nicholson, "Smart Networks : Transforming Energy Networks," October 2010.
- [4] Synaptitude Consulting, Smart Grid Energy Definitions and Glossary. Available: http://www.synaptitudeconsulting.com/knowledge/smart_grid_center/
- [5] Bringing the Complete AMI Advantage to a Broader Group of Utility Customers. Available: <http://www.nextgenpe.com/>
- [6] Iran Energy Efficiency Organization, IEEO-SABA. Available: <http://hooshmand.saba.org.ir>
- [7] Strategic Energy Technologies Information System (SETIS). Available: <http://setis.ec.europa.eu/newsroom-items-folder/electricity-grids>
- [8] Common functionalities proposed for smart metering in Europe Available: www.metering.com

- [9] Smart Electrical Grids Technology, SEGT 2012 .Available:
http://segt.org/Contact_e.aspx
- [10] "EIA standard RS-232-C: Interface between Data Terminal Equipment and Data Communication Equipment Employing Serial Binary Data Interchange," ed. Washington: Electronic Industries Association. Engineering Dept. , 1969.
- [11] M. Soltero, J. Zhang, and C. Cockril, "RS-422 and RS-485 Standards Overview and System Configurations," ed: Texas Instruments Incorporated, June 2002–Revised May 2010.
- [12] The European Telecommunications Standards Institute. Available: <http://www.etsi.org/WebSite/homepage.aspx>
- [13] The Mobile Broadband Standard. Available: <http://www.3gpp.org/>
- [14] The valid M-Bus standard. Available: <http://www.m-bus.com/>
- [15] "Proposal of a 5-year research project for Isfahan Regional Electricity ", Available: www.erec.co.ir.
- [16] DIGSILENT GmbH. Available:
<http://www.digsilent.de/index.php/index-en.html>

Factors Affecting Rail Transportation by Enhancing the Quality of Railway, Increasing Safety and Reducing Accidents

Iman Ikani,¹ Nima Ikani²

¹Islamic Azad University, South Tehran Branch

²Islamic Azad University, Chalous Branch

Abstract: The present study tries to investigate some shortcomings and inefficiencies in rail transportation systems. It also tries to suggest an appropriate strategy to improve lines and technical buildings in order to have a safe and high-speed rail system. It is worth noting that using the knowledge and experience of some skilled and experienced people can solve many problems. There are many factors to promote the quality of railroads such as environmental factors, line geometry, atmospheric conditions, etc and each of these factors has an important role in enhancing safety. By considering these factors, we can now reach a high-quality bed and high-speed lines.

Due to the several years of railway history and dramatic effects of climate change in different regions and the increased traffic of rail vehicles, it is the time to predict and perform some arrangements for the safe passage of floodwater and sediment in some establishments such as bridges. There was no passage of water in these bridges within a few years but today there is a good passage of high-discharge floodwater. These bridges were considered ordinary bridges a few decades ago and had not any significant problem for the passage of water and flood but they have created many difficulties in keeping and moving trains in recent years.

Keywords: process and movement, enhancing quality, Line and technical buildings

1. introduction

According to a hundred-year history of railroad in Iran, we observed many failures and difficulties and tried to solve them during these years. Today we have a railroad which is the result of trial and error. We were able to meet many shortcomings using the experiences of developed countries in order to have an appropriate and usable railroad. Thus we need the knowledge and updated skills in order to enhance the safety and quality of lines.

2. Factors affecting the quality of lines

Here there are some important points that have to be addressed. Inspired by the experience and knowledge of qualified individuals, upgraded lines can be achieved.

1. Removing the connection inside the tunnel: we can prevent the repeated impacts which cause damage to facilities such as tunnels, bridges which also cause the displacement of Malone on the tunnel hull, because their healthcare and control were considered always by the Lines and technical buildings staff. (figure 1)



Figure 1 – removing the connection using hermit welding

2. Removing the connection on bridges: connections on bridges, whether Farboton bridges or metal chassis bridges cause impacts from wheels into the junction. This impact hits to the bridge configuration and bridge slab. Its repetition and continuity in the long term crushes the slab. Seaton the side base and impacts on the side base. It can also lose the Threading of Malone in Farboton bridges. These impacts also affect on screws and rivet in metal chassis bridges and also cause the movement of bridge components on each other. These impacts cause irreparable damages to the junction of chassis on the side slab which are different from each other. (figure 2)

3.



Figure 2– removing the connection using Thermit welding

4. changes in environmental and climatic conditions



Due to the several years' of railway history and dramatic effects of climate change in different regions and the increased traffic of rail vehicles, it is the time to identify these areas and predict and perform arrangements for the safe passage of sediments through some bridges. (Figure 3 and 4) for example the sulfur bridge which is located at 800+933 Km in Tabriz–Razi which has created difficulties in maintaining and the movement of trains in recent years. Perhaps it was a typical bridge a few decades ago and did not have any significant problem against the water and flood passage.

Figure 3–Blocking the bridge opening when material collapsed in the monsoon rains

Figure 4-dredging the blocked bridge opening

A landslide which is occurred by changing environmental conditions and increasing rainfall is another environmental change which brings problems in risk-prone areas for train travel. (Figure 5) the operations of reconstruction and infrastructure are usually not performed in thrust areas. The reason is that the rush for lines to communicate each other is not usually standard. And this provides the frequency of this problem in the next few years.



Figure 5-landslides on the road

Trenches which have hard and impenetrable layer during construction of lines are another environmental factor. These trenches have been changed and collapsed during the time due to the Weathering factors. (Figure 6) today there is an urge to maintain and control daily the trenches which is so expensive, While we can solve this problem and promote the train travel security by identifying these areas and Widening and decreasing the height of the trenches which are always risky.

Figure 6– trenches collapsed due to the erosion

Another factor that may cause problem during the time and under environmental conditions is the inlet and outlet of tunnels which have begun and ended in a small trench for various reasons. (Figure 7) the erosion of the trench above the tunnel and falling rocks on the line, is one of the risky areas in the railway system. However, by identifying and detecting and by lengthening the tunnels for about 20 to 50 meters the risk will go away.





Figure 7-Input and Output trenches of the tunnel

5. monitoring and coordination with other organizations

Another factor in lines security is monitoring and coordination with other organizations, For example establishing the traveled way in the downstream of the railway line which causes the destruction of embankments or the removal of material from the mountain foot and trench foot. Due to climatic conditions, such as rivers and mountains, and having crossed both ways in one place, this issue may cause injuries and it is impossible to compensate it in the next few years if the executives of the traveled way ignore the ideas of the line experts at the time of making contract and Surveying. For example at 933+050 Km of Tabriz-Razi, the river bed height was increased due to the trenching of roads and throwing rocks in the river. (Figure 8) After a few years' the height reached to the Sulfur Bridge opening because the river was full of sediments and it became another factor for filling this bridge with sediments. It caused a lack of movement for these sediments in the bridge, while it was possible to prevent such a problem at the beginning by providing a useful approach in establishing the traveled way.



Figure 8 - filling the opening of sediments due to trenching

6. converting at-grade passageways into grade passageways

At-grade passageways are key points on the rail system. Most of the time there are accidents and disasters due to the train collision with road vehicles. This may lead to the train stop and disruption. Recently some operations have been conducted in converting at-grade passageways into grade passageways which is an important step to establish security in the movement of trains.

7. Controlling Operations of Railways

The line measuring machines is one factor in line controlling which is done according to the amount of traffic in each axis. This increases the quality lines, provided that the defects detected by the device can be removed by the maintenance areas and groups. Resolving the problem should be done carefully and this is an important issue related to a domain. (Figure 9). In the case of landslides, a surveyor group should be sent to those areas. Also the authorities should report any increase in connections or shakes from line to the vehicles. These are warning that the areas should be controlled, it is necessary to give a report in order to troubleshoot the problem and to return the line into its initial state.

Figure 9—Controlling line and needle parameters (width, disability, Deylam, away) as manual and mechanized

8. Maintenance of Building

New materials that can be used to perform maintenance task on the lines is another factor to enhance the Linequality. For example it strengthens the quality of concretetraversesand it may result in a better performance. Thus specialarrangements shouldbe made due to the weather conditionsandtemperatureandfreezingtemperature which are effective factors of concretedegradation. And enough accuracy shouldbetakenin thetransportand handling of the traverse.

9. embankment geometry:

Theembankmentgeometry form is the most importantfactorin establishing the line. (Figure 10).For example sidewalk on both sides of the line are responsible for traveler's traffic during the route. The sidewalk height prevents the entry of rainfall; it also prevents the subsidence of line due to the Loosening under the traverses. Allitemslisted in this section are factors that have asignificantimpactonworseningthedamage of the line. Adperson in chargeofthetechnical buildings should monitor and inspect and pays attentiontothesepoints.



Figure 10-Geometry of the embankment

10. protective walls:

Protective walls including crater walls, tunnel opening walls and coastal wall sare the other factor in enhancing the line security. These walls mustbecontrolled. The risk of damage ontheline should be reduced by discharging behind retaining wallsand inspecting foundationsandbasement of surety walls and also by controlling the flood at the coastal walls.

11. human factors

According tothe government policyof divestingthe public sectorto the private sector, it is likely to have newrecession inthecorrect maintenance waywith the arrival of newcomers who have no experience.It may causeirreversibledangerandinjuryonthebody of organization.So as we haverecentlywitnessed, the formation of educationalclasses and theircontinuity can preventaccidentsand playan importantrole in performing the issues.

Re-using experienced people and experts with updated knowledge can be useful in overcoming the problems and enhancing the quality of train traveling alongside the lines. Thiswillcreatethe necessaryincentives forindividualsand will provide areas forimprovementand progressthisorganization.On the other hand job securityis somethingthatcan makemotivationin theperson and he would besuccessfulinhis affairs. We hope to have defect-freeandhigh quality Maintenanceofflines andtechnical buildings which is oneof factorsoftherailwayin a near future to serve our valuable and importantcommunity.

3. conclusion

According to the description of the factors the tin crease quality and reduce accidents, we can conclude that enhancing the trafficsafetyin trainsusing technical knowledge and experience is an important principle that executives must keep in mind in order to become successful in implementinglargeprojects.Using experienced people with high technical knowledge and providing solutions and using the knowledge of the leading countries in therailindustryand purchasing machinery and materials with international standards we can pass one hundred yearswithina short time and we can develop this industry inourown country.

References

- [1] From many years ofexperienceinTabriz-Raziline and collaborating in lengtheningthetunnelproject– participating in the embankment repair and installing line in thrust areas...
- [2] website

Human Brain with Emr of Cell Phone

¹G.A. Bhalerao ²Prof. R.G. Zope ³G.B. Khaire ⁴B.P. Tambe

^{1,3,4}M.E. Student, Pune University, M.H., India

²Professor, Dept of E & TC SRES COE Kopergaon, Pune University, M.H., India

ABSTRACT: Electromagnetic radiation produce by cell phone and the relationship with the human's health is not a new matter. From the time when the used of mobile (cell) phone had increased rapidly over the long-ago, people are becoming more concern with their health when dealing with the electromagnetic radiation. This type of radiation would leads to heating of body tissue at particular rate called the thermal radiation. Thermal radiation, it depends on the signal frequency of the energy, the power density of the radio frequency field that beats the body and the polarization of wave, the result of thermal distribution image generated by cell phone towards human head from thermal imaging camera. The analysis is conducted in a laboratory with average of 45 minutes talking hour with two different types of mobile phone having internal and external antenna.

Keywords: Air tube Headsets, DARPA, EMR, Radio frequency, SAR, Thermal Camera,

I. INTRODUCTION

The cell phone is an important device in our life. The number of mobile phone users has increased recently. Approximately there are around 1.6 billion cell phone users throughout the world and the numbers are increasing [6]. Cell phone radio frequency used to exchange a few words has the ability to penetrate through semi-solid substances like meat, and living tissue to a distance proportional to its power density [11]. It also can cause dielectric heating effect or thermal effect [6]. Thermal effect is basically the temperature rise in the body cause of energy absorption from oscillating electric fields or electromagnetic radiation [3]. Thermal radiation is generated when heat from the movement of charged particles within atoms of the cell phone's case is converted to electromagnetic radiation. Thermal radiation of the cell phone also related to the specific absorption rate (SAR). It is defined as the rate of radio frequency (RF) power absorbed per unit mass by any part of the body. SAR values are dependent on the separation distance between the body and the cell phone. The nearer the distances of the radiation to the human head, the higher the SAR values [2]. RF is emitted by the cell phone antenna. An antenna is a transducer designed to transmit or receive electromagnetic waves [3]. Studies show that RF radiation has the ability to cause biological damage through heating effects [5]. Moreover it has been observed by cell phone users that symptoms like headaches, earaches, blurring of vision, short term memory loss, numbing, irritated, burning sensations, bad sleep, electromagnetic reaction, exhaustion and nervousness [4]. Thermal effect has been reported to cause temperature rise at the skin near ear skull region. In Europe, the European Union Council has adopted the recommendations made by International Commission on Non Ionizing Radiation Protection. These recommendations set a SAR limit of 2.0 W/kg in 10g of

The results taken by University Malaysia Sarawak, Malaysia, Faculty of Engineering show that an increased of heat especially at the place near the ear skull after 45 minutes of operation. When comparing both different types of mobile phone, mobile phone with external antenna produce more heat compared to mobile phone with internal antenna. By considering the result and thermal camera invented by DARPA (Defense Advanced Research Project Agency) it will possible to disconnect call /switch off cell phone when temperature inside head increased due to radiation.

1.1 ELECTROMAGNETIC RADIATION

The World Health Organization (WHO) defines electromagnetic fields on its WebPages dedicated to the concerns regarding the increasing presence of this form of radiation. In essence, an electromagnetic field is comprised of two components, one being an electric field generated by differences in voltage and another being a magnetic field generated by the flow of current. The field propagates at the speed of light (300,000 kilometers per second or 186,000 miles per second) in waves of a certain length that oscillate at a certain frequency (number of oscillations or cycles per second). In the electromagnetic range, gamma rays given off by radioactive materials, cosmic rays, and X-rays are all dangerous to humans and other organisms because of the relatively high energy "quanta" (packets) they carry (high frequency or short-wavelength waves). Such rays lead to "dangerous radiation" (ionizing; i.e., with an ability to break bonds between molecules). Mobile phone systems also act in the electromagnetic range (sometimes referred to as "microwave" or "radiofrequency"), however, the frequency (energy "quanta") of the longer-wavelength waves associated with this technology is lower (and therefore safer to humans) and regarded as "non-ionizing"

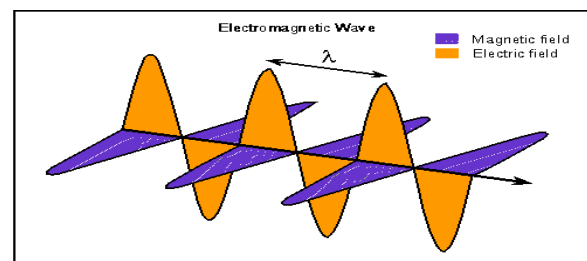


Figure 1.1: Electromagnetic Radiations

1.2 TYPES OF ELECTROMAGNETIC RADIATION

Ionizing radiation - This type of radiation contains enough electromagnetic energy to strip atoms and molecules from the tissue and alter chemical reactions in the body. Gamma rays and X-rays are two forms of ionizing radiation. We know they cause damage, which is why we wear a lead vest when X-rays are taken of our bodies.

Non-ionizing radiation - Non-ionizing radiation is typically safe. It causes some heating effect, but usually not enough to cause any type of long-term damage to tissue. Radio-frequency energy, visible light and microwave radiation are considered non-ionizing. Electromagnetic Spectrum

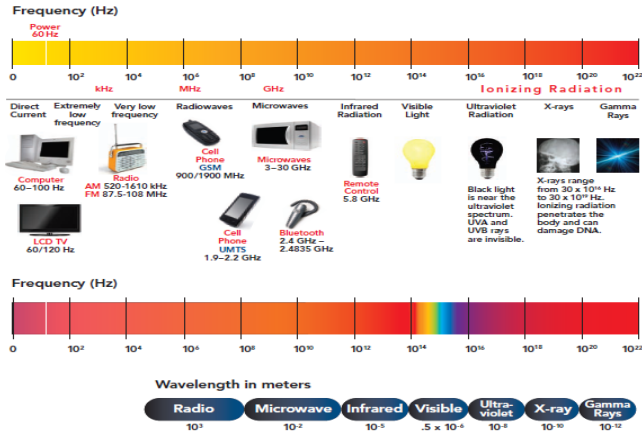


Figure 1.2: Electromagnetic radiation types.

II LITERATURE REVIEW

2.1 GLOBAL SYSTEM FOR MOBILE COMMUNICATION (GSM)

Global system for mobile communication (GSM) is a digital wireless communication protocol for mobile phones and was developed in the early 1980's. GSM also provided useful features like security, authentication and the invention of the SIM card. GSM networks operate in four different frequency ranges which are 900 MHz band, 1800 MHz band, 850 MHz band and 1900 MHz band. GSM 900 and GSM 1800 standard is the most commonly used standard. 850 MHz band and 1900 MHz band is introduced because the 900 MHz and 1800 MHz frequency bands were already allocated. GSM 1800 standard provide more bandwidth and less power requirements than GSM 900 MHz. The transmission power in the mobile phone is limited to a maximum of 2 watts in GSM 850 and GSM 900 while maximum power of 1 watt in GSM 1800 and GSM 1900. The specifications of GSM 900 and GSM 1800 are shown in Table 2.1.

Table 2.1: Specification of the GSM 900 and GSM 1800

Specification	GSM 900	GSM 1800
Downlink Frequencies	935-960 MHz	1710-1785 MHz
Uplink Frequencies	890-915 MHz	1805-1880 MHz
Channel Spacing	200 kHz	200 kHz
Modulation	GMSK	GMSK
Typical Mobile Transmit Power	2W	1W
Maximum Base station transmit power	320W	20W
Maximum Distance	35 km	8 km
Speech Encoding	LPC (13 kbit)	LPC (13 kbit)
Bit rate	270 kbps	270 kbps

2.2 RADIO FREQUENCY AND SAR

Radio frequency has the ability to penetrate through semi-solid substances like meat, and living tissue to a distance proportional to its power density. This ability will cause dielectric heating on the tissue of the human

body. Dielectric heating also calls thermal effect. Thermal effects are the temperature rise in the body cause of energy absorption from oscillating electric fields. The force produced by an electric field on charged objects will generate electric currents. Thermal effect from the high intensity radio frequency of mobile phone will cause heating at the skin near the ear skull region. Temperature at the skin will continuously increase until it is balanced at certain level when the heat will then be absorbed by the flow of blood to others part of body. Several minutes was taken for the radiated skin part temperature to reach the equilibrium temperature. The equilibrium temperature will be determined by calculating the average power absorbed which also called Specific Absorption Rate (SAR). Figure 2.1 shows the continuous of high intensity radiation of radio frequency toward the skin near the ear skull region [9].

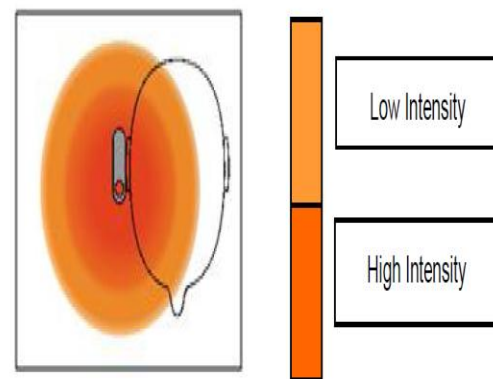


Figure 2.1: High Intensity Radiation of Radio Frequency toward the Skin near the Ear Skull Region

Specific Absorption Rate (SAR) is a dissymmetric quantity which is defined as the rate of RF power absorbed per unit mass by any part of the body. SAR value commonly is determined either 1g or 10g of simulated biological tissue in the shape of a cube. SAR value normally specified at the maximum transmission power. Transmission power will be higher when the mobile phone is used at the area with very low field strength of received signals [11]. SAR values are dependent on the separation distance of the body and the mobile phones. As the distance of the body and mobile phones is closed, the SAR values will be higher and vice versa.

2.2 BASIC THERMAL CAMERA

All thermal cameras consist of the same basic elements as shown in figure 2.2:

- A lens made of special material that focuses thermal energy onto a detector.
- A detector that is sensitive to IR energy.
- Electronics and signal processing elements that translate the energy gathered by the detector and convert it into a video signal that can be displayed on a monitor

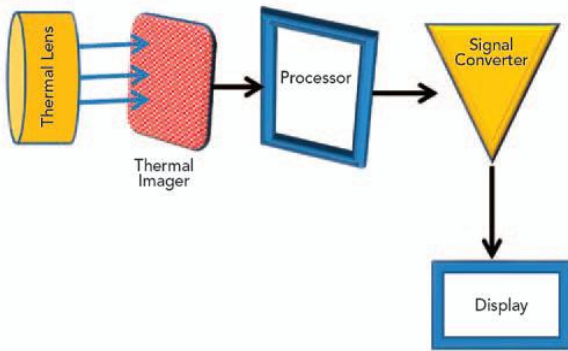


Figure 2.2: Basic block diagram for Thermal Camera.

IR energy barely passes through conventional lens glass, so thermal cameras have to use lenses made out of different materials that are expensive compared to standard glass. Two of the most commonly used lens materials are germanium and zinc selenide. Both of these materials are highly transmissive of IR radiation, meaning that thermal energy passes through them with great efficiency. Germanium has the highest index of refraction of any commonly used IR transmitting materials. It is a very popular material for systems operating in the 3-5 or 8-12 μm spectral regions. Germanium blocks ultraviolet (UV) and visible light up to about 2 μm . It is the best material for transmitting allowing up to 95% of the energy to flow through the lens. However, germanium has the property of thermal runaway, meaning that the transmission factor decreases as temperature increases. Because of this feature, thermal cameras incorporating germanium lens material should be used in areas at temperatures below 158° F (70°C).

2.4 LIMITING EXPOSURE TO HARMFUL CELL PHONE RADIATION

By means of following tips it is somewhat possible to minimize the risk of radiation towards human being

1. Turn on loud speaker.
2. SMS's only.
3. Select the offline mode.
4. From left ear to right ear.
5. Avoid narrow space.
6. Note the signal.
7. Do not stay long.
8. Reduce play around with the Smartphone.
9. Keep your cell phone when not connected.
10. Do not pocket the phone.
11. Do not put the phone in bed.
12. Buy cell phone with low radiation rating.
13. Avoid children
14. Use an Air Tube Headset

2.5 DARPA (DEFENSE ADVANCED RESEARCH PROJECT AGENCY) INVENTION

Thermal imaging shows how the world looks at infrared wavelengths of 8 to 12 micrometers. At those wavelengths, people, warm-blooded animals, and operating engines glow brightly against the cooler background of plants and soil. Firefighters use thermal imaging cameras to identify dangerous hot spots. Soldiers use them to check what might be lurking in the brush, especially in dim light.

But today's thermal imaging cameras are big and expensive standard military versions resemble binoculars and cost thousands of dollars. Civilian models used by firefighters and contractors cost \$1000 or more and may weigh a few kilograms. Key problems are the high cost, large size, and power requirements of the infrared-sensitive sensors needed to record images at wavelengths about 20 times longer than visible light. To overcome those problems, DARPA is paying Raytheon Vision Systems \$13.4 million over three years to develop ways to make the sensors small and cheap enough to be integrated into phones. Soon every US soldier could have a thermal imaging camera in their back pocket.

2.6 ENVI-BROWN TUBE AIRCOM TECHNOLOGY BLUETUBE-AIRTUBE-RF3 HEADSET

"With regards to the advice that hands-free kits be used, there are conflicting results. Some studies suggest that radiation exposure, if it exists, could actually be higher because the ear piece is closer to the brain... Advice on the use of hands-free kits is being revised and national guidelines are due to be published later this year." - Martin Whild, Assistant Information Officer for the National Radiological Protection Board which advises both the public and government on the risks of radiation. (Evening Times London, England April 30, 2004) The Anti-Radiation Air-tube Headset offers the safest alternative on the marketplace today as shown in figure 2.4.



Figure 2.4: Blue tube/Air tube Headsets

The Anti-Radiation Air-tube headset incorporates a few features that other headsets simply don't have: a special AirCom sound-delivery tube that may reduce electromagnetic radiation, a tangle-free cord, only available with tangle free chord in ear bud style, and a unique earpiece system.

2.7 BLOCK SYSTEM TO DISCONNECT CALL WHEN TEMP. INSIDE HEAD ABOVE SPECIFIED LIMIT

On the basis of thermal image camera invented by DARPA, by means of its small size like button of shirt it will possible to make use of it in cell phone to measure temperature inside brain. Then by means of electronic circuit the measure temperature will compare with the standard one and if it is greater than standard then either disconnect the call or switch off cell phone.

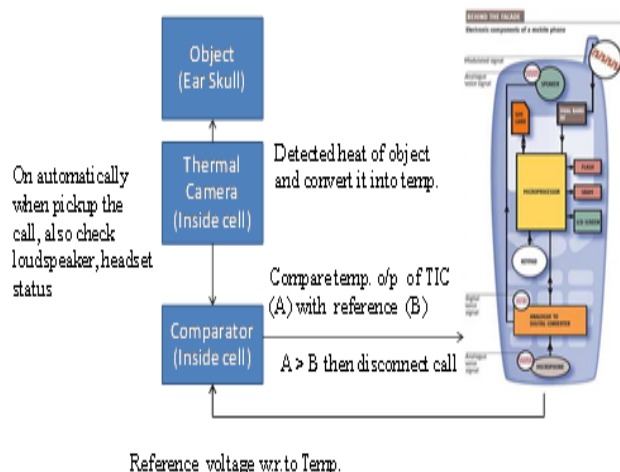


Figure 2.5: Block Diagram to disconnect call when brain temperature above normal range.

As shown in figure 2.5., when call will be pickup, Thermal Camera inside cell phone will turn on automatically, if loud speaker is not switch on and considering that cell phone hold near ear. Loud speaker on means consider cell phone won't near ear. When Thermal Image Camera switch on it will detect the heat of object in front of it and convert it into temperature. Then this temperature in terms of voltage compare with reference voltage with respect to temperature in comparator. If object temperature is greater than reference (i.e. normal range at which tissue will not burn) the output of comparator goes low/high as per logic. This output will be use for turn of RF switch (i.e. disconnect incoming call).

III CONCLUSION

The analysis done by University Malaysia Sarawak, Malaysia faculties that the human head can absorbed the radiation from the mobile phone easily. This radiation is so-called the thermal radiation where the human head temperature increase significantly as the talking hour (period of time using the mobile phone) increased. Mobile hand phone with external antenna and serving GSM 900 shows high increase after 15 minutes operation compared to mobile phone with internal antenna and serving GSM 1800. Features study will on the basis of thermal image camera invented by DARPA, by means of its small size like button of shirt it will possible to make use of it in cell phone to measure temperature inside brain. Then by means of electronic circuit the measure temperature will compare with the standard one and if it is greater than standard then either disconnect the call or switch off cell phone.

REFERENCES

- [1] V. F. Fusco, Foundations of antenna theory and techniques. Harlow: Prentice Hall, 2005.
- [2] C. Kargel, Infrared thermal imaging to measure local temperature rises caused by handheld mobile phones, IEEE Transaction on Instrumentation and Measurement, vol. 54, no. 4, pp. 1513-1519, 2005.
- [3] R. F. Safe - What is RF radiation? [Online]. Retrieved 31 July 2008. Available: http://www.rfsafe.com/research/rf_radiation/what_is_rf/intr_o.htm.
- [4] D. Coggon. (2006). Health risk from mobile phone base stations. [Online]. Retrieved 18 August 2008. Available: <http://oem.bmj.com/cgi/content/full/63/5/298>.
- [5] BBC - Mobile phone safety. [Online]. Retrieved 28 August 2008. Available: <http://www.bbc.co.uk/science/hottopics/mobilephones/safety.shtml>.
- [6] Better Health Channel - Mobile phones and your health. [Online]. Retrieved 28 August 2009. Available: http://www.betterhealth.vic.gov.au/bhcv2/bhcarticles.nsf/pages/Mobile_phones_and_your_health.
- [7] Government must inform us of cell phone risk Joel M. Moskowitz, Open Forum, San Francisco Chronicle, April 28, 2010 <http://sfgate.com/cgi-bin/article.cgi?f=c/a/2010/04/28/EDMB1D58TC.DTL>
- [8] Journal of Exposure Science and Environmental Epidemiology advance online publication 16 June 2010; doi: 10.1038/jes.2010.12.
- [9] ARPANSA - Australian radiation protection and nuclear safety agency: Mobile telephone scientific background. [Online]. Retrieved 29 July 2010. Available: <http://www.arpansa.gov.au/mobilephones/mobiles1.cfm>.
- [10] International Journal of Network and Mobile Technologies ISSN 1832-6758 Electronic Version VOL 1 / ISSUE 2 / NOVEMBER 2010 © 2010 INTI University College
- [11] Cell Phone Radiation and Health Recommendations Joel M. Markowitz, Ph.D., Director Center for Family and Community Health, School of Public Health University of California, Berkeley May 11, 2011

Website

American Cancer Society (www.cancer.org)
National Cancer Institute (www.cancer.gov)

Performance Characteristics of Four Stroke Single Cylinder Diesel Engine With 10% Iso Butanol at Different Injection Pressures

K.keerthi,¹ Kiran.C.kariankal,² S.sravya³
^{1,2,3}Mechanical engineering, SR engineering college, JNTU, AP, India

ABSTRACT: Biodiesel with additives is attracting increased attention for performance and emission improvement of diesel engines. Higher fuel injection pressure is an effective way to improve the performance and reduce Particulate Matter (PM) emissions. In this present work, Isobutanol as an additive to the diesel and biodiesel blends was investigated experimentally in a direct injection diesel engine to evaluate performance, combustion and emissions at different injection pressures such as 200,225,250 and 275 bars respectively. Isobutanol was added as 10% by volume to diesel-biodiesel blends. From experimental results it was found that injection pressure could be increased up to 250 bar when the engine operates with biodiesel-diesel blends with isobutanol as an additive. At this increased pressure, brake thermal efficiency and fuel economy were improved with increasing blend percentage. Carbon Monoxide (CO) emissions and smoke opacity were reduced significantly while Nitrogen Oxides (NO_x) emissions increased marginally.

Keywords: Biodiesel; Brake thermal efficiency; Emissions; Injection pressure; Isobutanol

I. INTRODUCTION

Fuel injection pressure in diesel engine plays an important role in engine performance. Higher injection pressure decreases fuel particle diameter which aids in better formation of mixing of fuel to air during ignition period, as a result of which engine performance will increase. High-pressure injection in combination with small orifice can achieve lean combustion which allows better fuel atomization, evaporation and improved emissions [1]. High injection pressure also reduces soot emissions [2]. The effect of injection pressure on performance of Direct Injection (DI) diesel engine shows the best performance at 220 bar and better fuel economy at 200 bar respectively [3]. In turbocharged diesel engines, high injection pressures for O₂, SO₂, and CO₂, while low injection pressure for NO_x and smoke level are preferred for decreasing emissions [4]. The problem of higher NO_x emissions at high injection pressures can be addressed by the addition of Carbon dioxide (CO₂) as diluents to the diesel [5]. Injection pressure variation is also investigated on various diesel-biodiesel blends by researchers. Higher injection pressures are preferred for biodiesel for effective atomization and mixing, since the viscosity of biodiesel is higher than diesel which causes problems in atomization and mixing. Optimum fuel injection pressure for linseed methyl ester was found to be 240 bar, based on comparable thermal efficiency, reduction in carbon monoxide, unburned hydrocarbons and smoke emissions. However oxides of nitrogen increase at higher injection pressures [6]. Diesel-Karajan biodiesel blends at fuel injection pressure of 210 bar demonstrate that the Hydro Carbon (HC) emissions decrease by 25 % and NO_x emissions decrease by 30 to 39 % respectively [7]. Hone oil can be blended with diesel up to 30% when the engine is operated at increased injection pressures [8]. Biodiesel-diesel blends in a turbocharged, high-pressure common rail diesel engines increase thermal efficiency and NO_x emission while Hydrocarbon, CO and CO₂ emissions reduce significantly [9]. Bio-Ethanol at higher injection pressures reduces emissions without comprising the performance [10]. Hone oil-diesel blends show the better injector opening pressure of 240 bar for improving the brake thermal efficiency and emissions [11]. Diesel-methanol blends with the increased injection pressure from 180 bar to 220 bar reduce smoke, unburned hydrocarbon, and carbon monoxide emissions, while combustion efficiency, nitrogen oxides and carbon dioxide emissions increase [12]. Recent studies show that additives have become indispensable tools for performance and emission improvement. Oxygenates are the candidates for reducing particulate matter. Oxygenates like ethanol, I-propanol, I-butanol and I-pentanol improve performance parameters and reduce exhaust emissions [13, 14]. Gasoline-ethanol blends with additives such as cyclooctanol, cycloheptanol increase brake thermal efficiency when compared to gasoline with reduction in CO, CO₂ and NO_x while HC and O₂ increase moderately [15]. Gasoline with additives like ethanol and ethanol-isobutanol increase the brake power, volumetric and brake thermal efficiencies and fuel consumption. The CO and HC decreased while the NO_x concentration increased [16]. Bio-additives (matter extracted from palm oil) as gasoline additives showed improvement in fuel economy and exhaust emissions of SI engine [17]. Methyl-ester of Jatropha oil diesel blends with Multi-DM-32 diesel additive showed comparable efficiencies, lower smoke, CO₂ and CO [18]. The addition of Di Methyl Carbonate (DMC) to diesel fuel increases efficiency marginally with reduction in NO_x emissions while PM and soot emissions decrease considerably [19, 20]. Ethanol addition to diesel-biodiesel blends increases brake thermal efficiency with reduction in carbon monoxide and smoke emissions and at the same time hydrocarbons, oxides of nitrogen and carbon dioxide emissions increase[21].Some researchers have used cetane improvers and some others have used additives in coated engines. Addition of di-tertiary-butyl peroxide and the conventional cetane improver, ethyl hexyls' nitrate additives to diesel fuel reduced all regulated and unregulated emissions including NO_x emissions [22]. Additives with coated engines improved efficiency, in addition to the increase in cylinder pressure, reduction in NO_x and maximum heat release rate. Thermal Barrier Coated (TBC) DI diesel engine with fuel additives reduced the smoke density and NO_x emission of the engine exhaust [23]. 1-4 dioxins, as an additive to the diesel fuel showed the potential to reduce smoke density with slight increase in NO_x and drop in fuel economy for a normal engine.

2.5% improvement of brake thermal efficiency and smoke reduction of 19% were observed when compared to neat diesel for TBC engines [24]. P-series glycol ethers were effective in reducing hydrocarbon, carbon monoxide, and particulate matter emissions [25]. Isobutanol–diesel fuel blends containing 5, 10, 15 and 20% isobutanol show marginal decrease in brake power and increase BSFC in proportion to the isobutanol content in the blends. It was also observed that slight improvement in BTE with the blend containing 10% isobutanol. CO emissions decrease with the use of the blends, while HC emissions increase compared to diesel fuel [26].

Present work attempts to investigate performance, combustion and emission characteristics of diesel engine with isobutanol as an additive to the diesel-biodiesel blends at different injection pressures from 200 bar to 275 bar. Since isobutanol has higher energy density and lower Reid Vapor Pressure (RVP) it can be used as a potential fuel additive to petroleum fuels.

II. Experimental Set-Up and Procedure

2.1 Experimental Set-up

The engine shown in Fig.1 for investigation on fish oil biodiesel-diesel blends to evaluate the performance and emission characteristics was a computerized single cylinder four stroke, naturally aspirated direct injection and water cooled diesel engine. The specifications of the test engine are given in Table 1. It was directly coupled to an eddy current dynamometer. The engine and the dynamometer were interfaced to a control panel which was connected to a computer. Engine Soft version 2.4 was used for recording the test parameters such as fuel flow rate, temperatures, air flow rate, load etc, and for calculating the engine performance characteristics such as brake thermal efficiency, brake specific fuel consumption.



Table1. Specifications of the test engine

Particulars	Specifications
Make	Kirloskar
Rated power	3.7 k(5hp)
Bore	80 mm
Stroke length	110 mm
Swept volume	562 cc
Compression ratio	16.5:1
Rated speed	1500 rpm

2.2 Test Fuels

For experimental investigation, biodiesel derived from fish oil was mixed with diesel in varying proportions such as 20%, 30% and 40% by volume and isobutanol as an additive was added as 10% by volume to all the blends designated as B20, B30 and B40 (i.e. B20 indicates biodiesel 20%, isobutanol 10% and remaining proportion diesel by volume respectively). Table.2 shows the properties of isobutanol.

Table 2. Properties of Isobutanol

Property	Range
Flash point, open cup, °C	37.7
Specific gravity, 20/20°C	0.8030
Viscosity at 20°C (Centipoises)	3.95
Auto ignition temperature, °C	440
Surface tension at 20°C, ((dynes/cm)	22.94
Heat of combustion, kJ/kg	36162

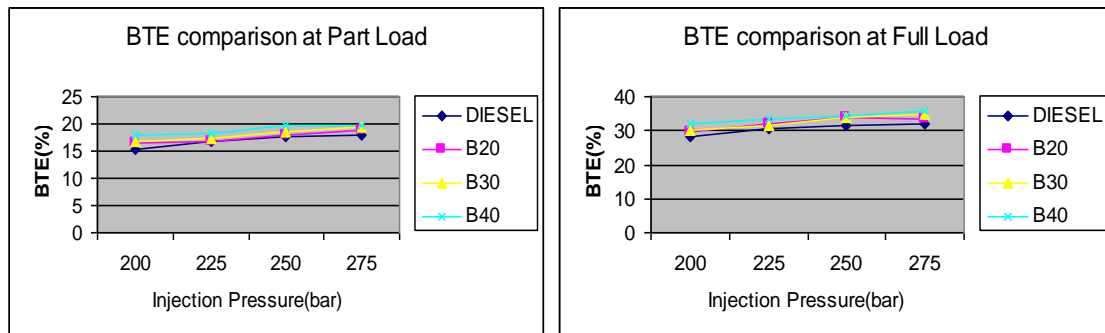
2.3 Experimental Procedure

The entire engine experiments were conducted at a rated speed of 1500 rpm with an injection timing of 27° before Top Dead Center (TDC). The engine was allowed to run till the steady state is reached. Then the engine was loaded in terms of 0%, 25%, 50%, 75% and 100% load. At each load, the experiments are conducted by varying the injection pressure from 200 to 275 bars. The first stage of experiments was performed with pure diesel at different loads from no-load to full load (20 N-m) by varying injection pressure from 200 bar to 275 bars with an interval of 25 bars. The engine loads were adjusted by an eddy current dynamometer. The second stage of experiments was conducted using various blends of diesel-biodiesel with isobutanol as an additive with same injection pressures and same operating conditions. All the performance and combustion characteristics readings were recorded online while exhaust emissions CO, and NO_x were recorded by the flue gas analyzer (FGA533) and smoke opacity was measured with Hart ridge smoke meter (OMS103).

III. Results and Discussion

3.1 Performance analysis

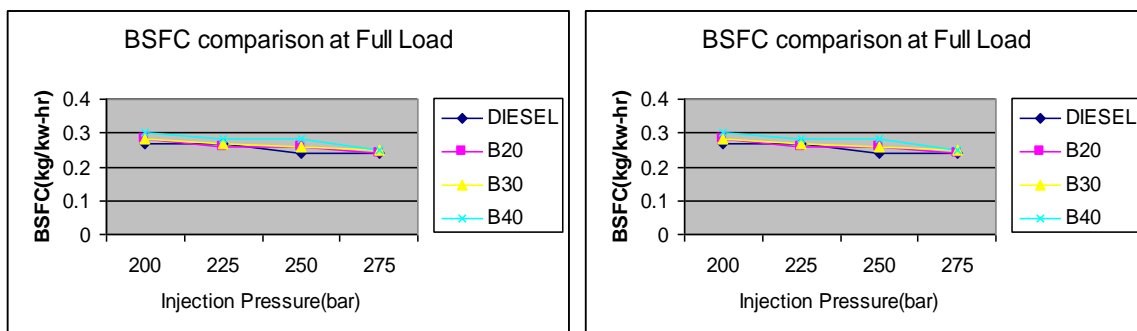
Performance parameters such as BTE and BSFC results of diesel and blends are shown in figures 2 and 3. Figure 2(a) and (b) shows the variation of BTE with injection pressure for different fuels at part load and at full load respectively. Figure 2(a) shows that at part load BTE increases considerably from 200 to 250 bars, and thereafter the increase is insignificant. This may be attributed to the improved spray characteristics, better atomization and better fuel and air mixing as a result of increased injection pressure. This will lead to improved combustion process and in turn improved efficiency. However higher injection pressures (i.e. more than 250bar) lead to smallest diameter of fuel droplet and affect the spray pattern and penetration which lowers the performance [27]. Figure 2(b) shows that at full load only marginal improvement in BTE was observed. Blends with isobutanol maintain better BTE than diesel. Figure 3(a) and (b) shows the variation of Brake Specific Fuel Consumption (BSFC) with injection pressure for different fuels. Figure 3(a) shows that at part load operation, BSFC of the blends was considerably higher than diesel and Figure 3(b) shows that at full load it was slightly more when compared to diesel. The reason for this tendency is slight decrease in energy content of the blended fuel when isobutanol was added. It can also be observed that the BSFC of all the blends including diesel decreases with increase in injection pressure. The reason for decrease in BSFC with increase in injection pressure is due to complete combustion of fuel. Higher injection pressures assist in better mixing of fuel with air [28]



2. A) BTE at Part Load

2. b) BTE at Full Load

Figure2. Variation of Brake Thermal Efficiency with Injection Pressure for different fuel blends



3. A) BSFC at Part Load

3. b) BSFC at Full Load

Figure 3. Variation of Brake Specific Fuel Consumption with Injection Pressure for different fuel blends

3.2 Combustion analysis

Combustion analysis such as cylinder pressure versus crank angle is shown in figure 4. Figure 4(a), (b), (c) and (d) shows the variation of cylinder pressure with crank angle at 200 bar, 225 bar, 250 bar and 275 bar injection pressures respectively for different fuels at 20N-m load. It can be seen from these figures that the cylinder pressure of the blends was lower than diesel at all injection pressures. The reason for decrease in cylinder pressure with the blends was due to the fact that the isobutanol has lower cetane number and heating value which lowers the combustion the pressure, these results are

also identical with the literature [29]. And also cylinder pressure of the blends including diesel increases with increase in injection pressure up to 250 bar after that it decreases slightly at 275 bar.

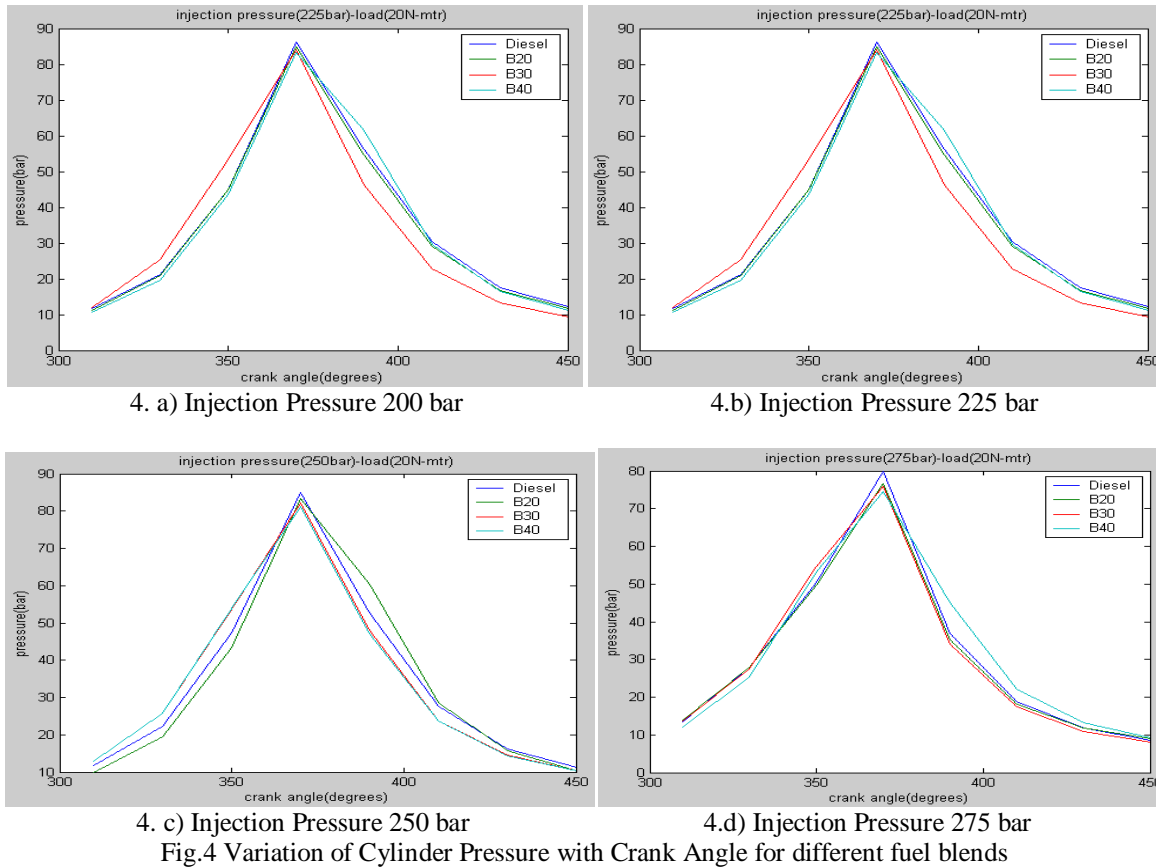


Fig.4 Variation of Cylinder Pressure with Crank Angle for different fuel blends

3.3 Emission Analysis

Exhaust emission results such as CO, NO_x and smoke are shown in figures 5 to 7. Figure 5(a) and (b) shows the variation of CO emissions with injection pressure for different fuels both at part load and full load respectively. Figure 5(a) shows that, CO emissions at part load decrease up to 225 bar and thereafter the variation was insignificant, while at full load as shown in Figure 5(b) significant reductions were observed with the blends than the diesel. The reasons for reduction in CO emissions were oxygen content of the blends enhances the fuel air mixing and isobutanol has lower C/H ratio and also it causes the leaning effect on the blends resulting in lower CO emissions. The effect of injection pressure at full load on CO emissions was significant than at part load operation. Figure 6(a) and (b) shows the variation of NO_x emissions with injection pressure for different fuels both at part load and full load respectively. NO_x emissions are lower for the blends when compared to diesel at all injection pressures. However they increase with increase in injection pressure. The rate of increase in NO_x is higher at higher injection pressures when compared to that of lower injection pressures. The formation of NO_x is a temperature dependent phenomenon, at higher injection pressures the increase in NO_x level is due to faster combustion and higher temperatures reached in the cycle [30]. Isobutanol has lower heating value and oxygen content which results in lower combustion temperatures and consequently NO_x emissions decrease [31]. Figure 7(a) and (b) shows the variation of Smoke opacity with injection pressure for different fuels. Smoke density decreases significantly with the addition of isobutanol to the blends and it decreases further with increase in injection pressure. However slight variation was observed with the increase in blend percentage. The results of NO_x and smoke also compare with the results of [32].

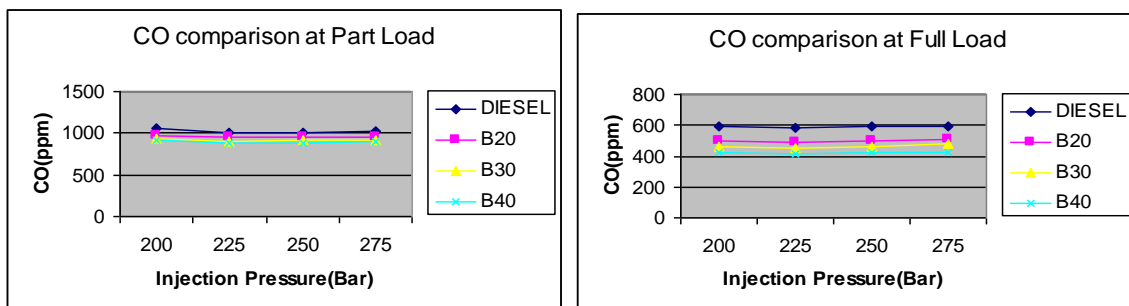
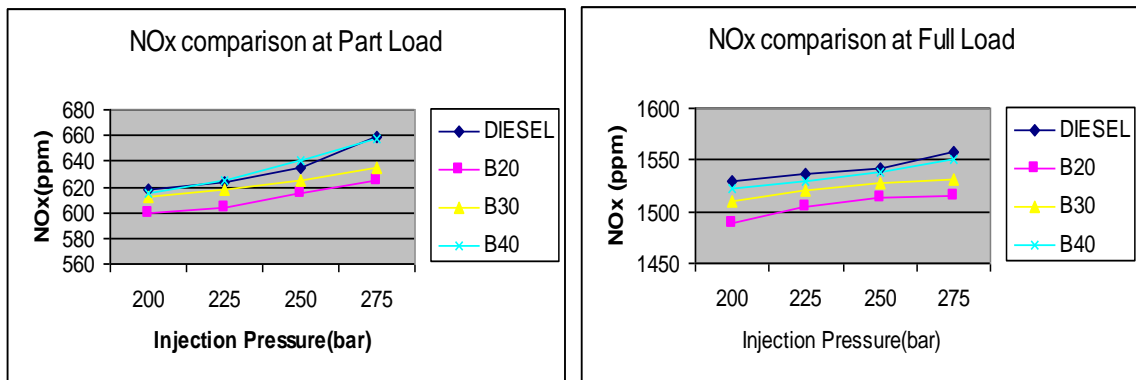
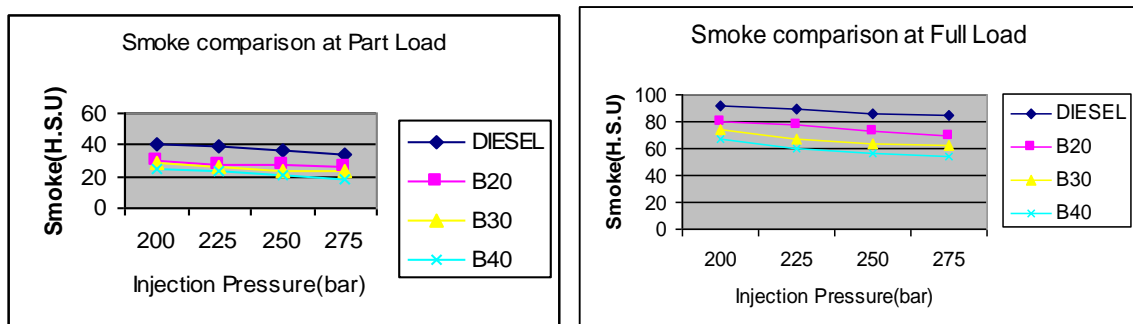


Fig.5 Variation of CO emissions with Injection Pressure for different fuel blends



6. a) Part Load
 6.b) Full Load
 Fig.6 Variation of NO_x emissions with Injection Pressure for different fuel blends



7. a) Part Load
 7.b) Full Load
 Fig.7 Variation of Smoke Density with Injection Pressure for different fuel blends

IV. CONCLUSION

The conclusions derived from present experimental investigation to evaluate performance, combustion and emission characteristics on four stroke single cylinder diesel engine fuelled with diesel-biodiesel blends with isobutanol as an additive at different injection pressures are summarized as follows:

1. Brake thermal efficiency increased with all blends when compared to the conventional diesel fuel. Maximum Brake thermal efficiency obtained was 33.5% with B40 blend with 10% isobutanol against 28% with conventional diesel.
2. Brake specific fuel consumption decreased with the blends with isobutanol when compared with diesel fuel.
3. Cylinder pressure of the blends increase with increase in injection pressure.
4. CO emissions and smoke density decrease significantly with the blends and isobutanol and further decrease with the increasing injection pressure when compared with diesel. NO_x emissions decrease marginally with the blends and isobutanol which however increase with injection pressure

REFERENCES

- [1] Prashanth Karra. And Song Charng Kong. Diesel Emission Characteristics Using High Injection Pressure with Converging Nozzles in a Medium-Duty Engine. SAE Paper Number, 2008-01-1085.
- [2] Sukumar Puhan, Jegan, R. Balasubramanian, K. and Nagarajan, G. Effect of injection pressure on performance, emission and combustion characteristics of high linolenic linseed oil methyl ester in a DI diesel engine. Renewable Energy, 2009, 34, 1227–1233.
- [3] Rosli Abu Bakar. Semin. and Abdul Rahim Ismail. Fuel Injection Pressure Effect on Performance of Direct Injection Diesel Engines. American Journal of Applied Sciences, 2008 5 (3): 197-202.
- [4] Ismet Celykten. An experimental investigation of the effect of the injection pressure on engine performance and exhaust emission in indirect injection diesel engines. Applied Thermal Engineering, 2003, 23, 2051–2060.
- [5] Can Cinar, Tolga Topgul, Murat Ciniviz, and Can Hasimoglu. Effects of injection pressure and intake CO₂ concentration on performance and emission parameters of an IDI turbocharged diesel engine. Applied Thermal Engineering, 2005, 25, 1854–1862.
- [6] Nagarhalli, M.V. and Nandedkar, V.M. Effect of injection pressure on emission and performance characteristics of Karanja biodiesel and its blends in C.I. Engine. International Journal of Applied Engineering Research, 2011, Volume 1, no 4.
- [7] Venkanna, B.K. Swati B. Wadawadagi, and Venkataramana Reddy, C. Effect of Injection Pressure on Performance, Emission and Combustion Characteristics of Direct Injection Diesel Engine Running on Blends of Pongamia Pinnata Linn Oil (Honge oil) and Diesel Fuel. The CIGR Ejournal, 2009, Manuscript number 1316. Vol. XI.
- [8] Wang, X.G. Zheng, B. Huang, Z.H. Zhang, N. Zhang, Y.J. and Hu, E.J. Performance and emissions of a turbocharged, high-pressure common rail diesel engine operating on biodiesel/diesel blends. Proc. IMechE Part D: J. Automobile Engineering, 2010, Vol. 225.
- [9] Paolo Sementa. Bianca Maria Vaglieco. And Francesco Catapano. Influence of the Injection Pressure on the Combustion Performance and Emissions of Small GDI Engine Fuelled with Bio-Ethanol. SAE Paper Number: 2011-37-0007.
- [10] Won, H.W. and Peters, N. Optimizing the injection pressure for cluster nozzle concepts in a direct injection diesel engine. International Journal of Engine Research, 2010, 11: 163-175.

- [11] Venkanna, Krishnamurthy, Belagur, Vekataramana, and Reddy, Chittimini., Effect Of Injector Opening Pressures On The Performance, Emission And Combustion Characteristics Of DI Diesel Engine Running on Honne Oil and Diesel Fuel Blend. *Thermal Science International Scientific Journal*, 2010, Volume 14, Issue 4, Pages 1051 – 1061.
- [12] Mustafa Canakci, Cenk Sayin, Ahmet Necati Ozsezen, and Ali Turkcan. Effect of Injection Pressure on the Combustion, Performance, and Emission Characteristics of a Diesel Engine Fueled with Methanol-blended Diesel Fuel. *Energy Fuels*, 2009, 23 (6), pp 2908–2920.
- [13] Ryo, Michikawauchi, Shiro, Tanno, Yasushi, Ito, and Mutsumi, Kanda. Combustion Improvement of Diesel Engine by Alcohol Addition - Investigation of Port Injection Method and Blended Fuel Method. *SAE International Journal of Fuels Lubricants*, 2011, 4:48-57.
- [14] Sivalakshmi, S. and Balusamy, T. Effects of oxygenated Organic Compounds-neem Oil Blends on the Performance and Exhaust Emissions of a DI Diesel Engine. SAE Paper Number: 2011-01-0331.
- [15] Ananda Srinivasan, C. and Saravanan, C.G. Study of Combustion Characteristics of an SI Engine Fuelled with Ethanol and Oxygenated Fuel Additives. *Journal of Sustainable Energy & Environment*, 2010, 85-91.
- [16] Balaji, D. Govindarajan, P. and Venkatesan. 2010. Influence of isobutanol blend in spark ignition engine Performance and emissions operated with gasoline and Ethanol. *International Journal of Engineering Science and Technology*, 2010, Vol. 2(7), 2859-2868.
- [17] YAO, ChunDe, ZHANG, ZhiHui, XU, YuanLi, and HUANG, Yu. Experimental investigation of effects of bio-additives on fuel economy of the gasoline engine. *Science in China Series E: Technological Sciences*.
- [18] HanumanthaRao, Y.V. RamSudheer, Voleti, SitaramaRaju, A.V. and Nageswara Reddy, P. Experimental investigations on jatropa biodiesel and additive in diesel engine. *Indian Journal of Science and Technology*, 2009, Vol.2, No 4.
- [19] Zhang, G.D. Liu, H. Xia, X.X. Zhang, W.G. and Fang, J.H. Effects of dimethyl carbonate fuel additive on diesel engine performances. *Proc. IMechE Part D: J. Automobile Engineering*, 2005, D13904, Vol. 219.
- [20] Nibin, T. Sathiyagnanam, A.P. Sivaprakasam, S. and Saravanan, C.G. Investigation on Emission Characteristics of a Diesel Engine using Oxygenated Fuel Additive. *IE(I) Journal MC*, 2005, Vol 86.
- [21] Venkata Subbaiah, G. Raja Gopal, K. Syed Altaf Hussain, Durga Prasad, B. and Tirupathi Reddy, K. Rice Bran Oil Biodiesel As an Additive In Diesel-Ethanol Blends For Diesel Engines. *Ijrras*, 2010, 3(3).
- [22] Manish Nandi, K. The Performance of Di-tertiary-Butyl Peroxide as Cetane Improver in Diesel Fuels. ARCO Chemical Company, Newtown Square, PA 19073.
- [23] Sathiyagnanam, A.P. Saravanan, C.G. and Dhandapani, S. Effect of Thermal-Barrier Coating plus Fuel Additive for Reducing Emission from DI Diesel Engine. *Proceedings of the World Congress on Engineering*, 2010, Vol II WCE 2010, June 30 - July 2, 2010, London, U.K.
- [24] SundarRaj, C. Sendilvelan, S. and Arul, S. Performance of a Thermally Insulated Constant Speed Diesel Engine with Dioxane Blended Fuels. *Global Journal of Researches in Engineering*, 2010, Vol. 10 Issue 2 (Ver 1.0).
- [25] Karas, L.J. Kesling, H.S. Jr, Liotta, F.J. Jr. and Nandi, M.K. Low Emission Oxygenated Diesel Fuel. 3801 West Chester Pike Newtown Square, PA 19073-2387. ARCO Chemical Company Research and Development.
- [26] Murat, Karabektas, and Murat, Hosoz. Performance and emission characteristics of a diesel engine using isobutanol–diesel fuel blends. *Renewable Energy*, 2009, Volume 34, Issue 6, Pages 1554-1559.
- [27] Venkanna, B.K., Swati, B., Wadawadagi, Venkataramana Reddy, C., Effect of Injection Pressure on Performance, Emission and Combustion Characteristics of Direct Injection Diesel Engine Running on Blends of Pongamia Pinnata Linn Oil (Honge oil) and Diesel Fuel. *Agricultural Engineering international: The CIGR Ejournal*, 1316. Vol. XI. May, 2009.
- [28] Sanjay Patil, Akarte, M.M., Effect of Injection Pressure on CI Engine Performance Fuelled with Biodiesel and its blends. *International Journal of Scientific & Engineering Research*, Volume 3, Issue 3, March 2012.
- [29] K. Venkateswarlu, B.S.R. Murthy, and V.V. Subbarao., An Experimental Investigation on Performance, Combustion and Emission Characteristics of Diesel-Biodiesel Blends with Isobutanol as an Additive. SAE Technical Paper number: 2012-28-0011, DOI: 10.4271/2012-28-0011.
- [30] Hariharan, V.S., Vijayakumar Reddy, K., Effect of injection pressure on diesel engine performance with Sea lemon oil. *Indian Journal of Science and Technology*, Vol. 4, No. 8, 2011.
- [31] Xiaolei Gu, Guo Li, Xue Jiang, Zuohua Huang, and Chia-fon Lee., Experimental study on the performance of and emissions from a low-speed light-duty diesel engine fueled with *n*-butanol–diesel and isobutanol–diesel blends. *Proceedings of the Institution of Mechanical Engineers, Part D: Journal of Automobile Engineering* 0954407012453231 first published on August 13, 2012.
- [32] Yakup Icinur, Duran Altiparmak., Effect of fuel cetane number and injection pressure on a DI Diesel engine performance and emissions. *Energy Conversion and Management*, Volume 44, Issue 3, February 2003, Pages 389–397.

The effects of isobutanol- and *n*-butanol-enriched diesel fuel on the diesel engine performance and emissions are investigated. Neat diesel, 15% isobutanol–85% diesel, 30% isobutanol–70% diesel, 15% *n*-butanol–85% diesel, and 30% *n*-butanol–70% diesel blends are investigated in this study. The tests were carried out at light and medium loads and a fixed low engine speed, and by using various combinations of the exhaust gas recirculation rate and the injection timing to investigate the effect of the molecular structure difference on soot formation. The results show that *n*-butanol–diesel blends give a longer ignition delay than isobutanol–diesel blends do. Hence isobutanol has a higher peak cylinder pressure and a higher premixed heat release rate than *n*-butanol does. Adding butanol (isobutanol and/or *n*-butanol) to diesel fuel is able to decrease the soot emissions substantially, while the change in the nitrogen oxide emissions varies slightly. Soot emissions from *n*-butanol–diesel blends are lower than those from isobutanol–diesel blends. Introducing exhaust gas recirculation and retarding the injection timing are effective approaches to decrease the nitrogen oxide emissions. However, a high exhaust gas recirculation rate leads to a loss in the fuel efficiency. The combination of a low exhaust gas recirculation rate, later injection and butanol blends can achieve low-temperature combustion and simultaneously decrease the nitrogen oxide and soot emissions.

On Chip Bus Tracer Based On Reverse Encoding In Soc

Blessy Babu ¹, Karthika Manilal ²

¹PG Scholar, Dept. of Electronics and Communication Engg, TKM Institute of Technology, Kollam, Kerala, India
²Asst. Professor, Dept. of Electronics and Communication Engg, TKM Institute of Technology, Kollam, Kerala, India

Abstract: System on chip (SoC) is the integration of different components in to a single chip targeting a specific application. Real-time observability of the internal chip signals is crucial to SoC debugging, the obvious choice would be to use chip pins to observe them. However, this method is difficult to implement in the presence of high frequency internal clocks and limitation of the chip pins. A solution to this problem is to embed a bus tracer in SoC to capture bus signal, and to store the trace in on-chip storage (trace memory). The size of bus trace increases rapidly as the numbers of transactions are more. In order to reduce the trace size, compression is necessary. These compression mechanisms include slice compression, differential compression and dictionary based compression. The compression algorithms use forward encoding method i.e. first data is recorded as uncompressed and all others are encoded. Trace memory is a circular buffer, so in case of wrapping around this may result in loss of data and affects the decompression flow. Therefore a new reverse encoding method is used that results in efficient circular buffer utilization. To capture the bus signals, an on-chip communication architecture based on WISHBONE bus, with four masters and four slaves is designed and the hardware tracer based on reverse encoding is integrated to this. This is coded using VHDL, simulated using ModelSim 6.4c and synthesized using Xilinx ISE tool.

I. INTRODUCTION

The growing complexity and shorter time to market constraint makes verification and debugging a major hurdle in shortening development cycle of system on chip.

In contrast to software debugging, hardware debugging methods provides insight to observability of internal state system and real time behavior in SoC. The limitation of this approach is unavailability of dedicated pins and increased gap of internal and external frequencies while moving trace out of chip. This leads to demand for on chip debugging units. The main problem dealing with the on chip debug units is that execution trace in SoC is large and hence for storing these much data results in increased cost of hardware implementation and data acquisition systems. The solution to this problem is to integrate a tracer in to the bus, which is the communication architecture in SoC, to capture and compress signal in real time and store them in an on-chip trace memory. The traced data can then be decompressed on the software terminal for performance analysis, bus utilization and verification.

Trace collection is controlled by user defined signal condition. They are two types of traces forward trace and backward trace. As shown in figure 1 the forward/backward trace refers to trace captured before/after a triggering event. The forward trace is used for diagnosing errors at known time periods and backward trace is used for detecting the system Backward trace Event trigger Forward trace

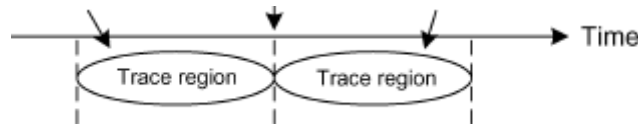


Fig.1. Difference between forward trace and backward trace

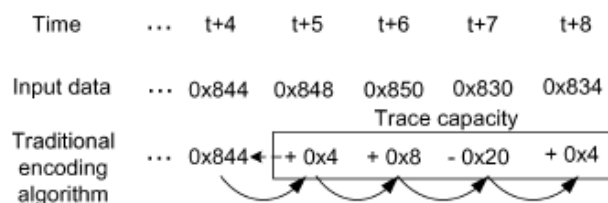


Fig.2. forward encoding differential compression algorithm malfunctioning.

Traces which are collected are stored in a trace memory; since capacity is limited it is usually used as circular buffer. In case of backward trace, signals are continuously collected, so when trace memory is full, wrapping around occurs i.e., initial data become overwritten. This causes a problem when the trace needs to be compressed.

For example, Fig.2 shows traditional differential compression algorithm that make use of forward encoding. It works as follows. First datum is recorded as uncompressed; when second datum comes it is encoded with respect to first, ie, difference between the first and second is stored. When third datum comes it is encoded with respect to second and so on. The problem occurs when first data become overwritten due to wrapping around in circular buffer. This initial data is in uncompressed format and all other dates are encoded with respect to that .Therefore when it is lost all other data's becomes useless ie, they cannot be decompressed.

In this paper a reverse encoding algorithm is proposed. This algorithm is applied to different popular compression algorithms and demonstrated in an on WISHBONE bus for SoC. The tracer supports both forward and backward trace with effective circular buffer utilization in addition to good compression ratios and small hardware overhead. This paper is organized as follows. Section II discusses related work regarding tracers. Section III presents the proposed algorithm. Section IV introduces architecture of on chip bus tracer. In Section VI, the experimental results are discussed. Section VIII concludes this paper.

II. RELATED WORKS

The execution traces in SoC is large so there needs a large amount of memory for storing these data's. This results the need of reduction/compression techniques. They techniques are divided into lossy and lossless approaches.

Lossy approach has the advantage of high compression ratio [3]. The idea is to capture only the erroneous signals in a trace buffer to increase the trace-buffer utilization. Here a three pass methodology is used. During the first pass, the rough error rate is measured, in the second pass, a set of suspect clock cycles where errors may be present is determined, and then in the third pass, the trace buffer captures only during the suspect clock cycles. In this manner, the effective observation window of the trace buffer can be expanded significantly, by up to orders of magnitude. This greatly increases the effectiveness of a given size trace buffer and can rapidly speed up the debug process.. But it is not suitable for real time on chip bus tracing

Lossless data compression algorithms can be classified into two main categories statistical coding algorithms and dictionary coding algorithms [5] Statistical based compression algorithms, such as Huffman coding or arithmetic coding can lead to an optimal average code length and hence good compression ratio. For the real-time requirement and the fact that debug data is not known a-priori these static methods are not suitable. The second category of data compression algorithms is the dictionary-based compression algorithms. The compression in these methods is achieved by encoding a symbol or a sequence of consecutive symbols into shorter code words which are represented by indices to the dictionary locations. But this approaches face difficulty when wrapping around occurs because they use forward encoding algorithm.

For effective debugging they must support both forward and backward trace. The logic analyzers [7] support forward trace but they have no compression ability and backward trace capability.

In ARM ETM [6] and NEXUS interface, data filtering is used to increase trace depth. They use a branch target technique to compress instruction address: it ignores consecutive address and stores only branch and target address. The hardware overhead of these works is small since

the filtering mechanism is simple to implement in hardware. However, the effectiveness of these techniques is mainly limited by the average basic block size, which is roughly around four or five instructions per basic block,

Periodical triggering supports both forward and backward trace[4]. Here trace memory is divided into small segments using a ping pong organization. These segments are compressed separately hence destruction of one segment does not affect another. But has a disadvantage of more uncompressed data. Utilization ratio can be increased by increasing the segments but it reduces the compression ratio.

III. REVERSE ENCODING ALGORITHM

To overcome the disadvantage of data loss due to wrapping around in circular buffer a reverse encoding is applied to different compression algorithms in trace reduction stage.. In this newest data is set to uncompressed and all other preceding datum's are encoded with respect to the newest so when first data is removed, it doesn't affect the decompression because it is only a encoded value not the initial uncompressed data. As in reverse encoding, there is a difference from Fig.2.i.e.0x834 is set as uncompressed and all others are encoded with respect to that.

IV. SYSTEM ARCHITECTURE

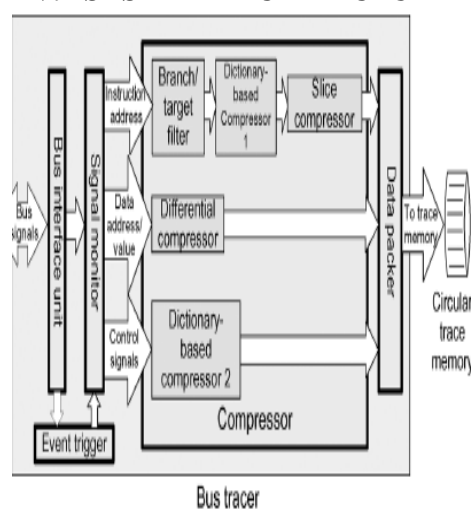


Fig.3. Bus tracer hardware architecture

Fig. 3 shows the hardware architecture of the bus tracer. It has two major functional modules (1) signal monitor/tracing and (2) trace compression. Signal monitor consist of event trigger, bus interface unit and signal monitor. Bus interface unit handles bus requests and collects the bus signal for storing, signal monitor synchronizes the signals and pass these signals to data reduction stage, where reverse encoding is applied. Event trigger module is configurable and controls trigger condition of start/stop a trace. When triggered the bus tracer starts capturing signals and stops until another trigger happens. Finally, the data packer packs the compressed data and writes them to the circular trace memory.

As shown in Fig. 3 bus signals are classified into three, instruction address, data address/value, and control signals. Instruction addresses are processed in three steps. First is to record only the non sequential jumping address. In virtual of the computer program usually having the property of spatial locality, each adjacent address pattern often is increased by a sequential offset .Hence, we can choose to only record the adjacent address pattern increased by a non-sequential offset, also called branch jump address, so as to eliminate the most address information. Secondly such branch/target addresses repeat several times because most programs are recursive. Therefore, dictionary-based compressor is used to reduce these repeated addresses. Third, the higher part between two adjacent address patterns is almost similar. Hence, if we can make the similarity between the current address and the previous address to be eliminated, the compression ratio may be rising dramatically. So the dictionary contents from dictionary-based compressor 1 are further compressed by a slice compressor. For control signals, we use dictionary-based compressor 2 (shown in Fig. 3). Because the variety of transfer types in a system is usually small, the same transfer types appear frequently. Therefore, the control signal patterns indicating the transfer types also appear frequently, which enables the dictionary-based method to reduce the size of the repeated signal patterns. The signal variations on data bus (data address and data value buses) are not regular that compared with program address bus. Using the differential approach based on subtraction is the convenience way to reduce the data bus trace size and the hardware cost of subtraction module is small.

The following sections show how to apply our reverse-encoding algorithm to the compression methods used in this bus tracer

A. Differential Compression

Compared to forward encoding, reverse encoding differ in following areas (1) since forward encoding records the first datum as uncompressed while reverse encoding records last datum as uncompressed (2) forward encoding relates the present datum to the previous datum while the reverse encoding relates the present datum to the next datum. The encoded results of both forward and reverse encoding are same because absolute difference is not changed after interchanging the minuend and the subtrahend.

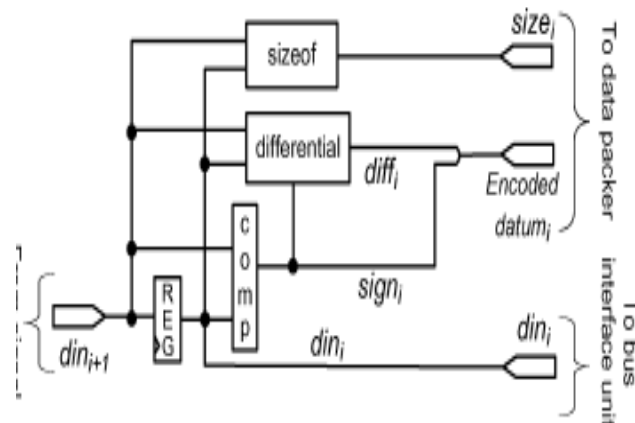


Fig. 4. Differential compressor hardware based on reverse encoding

Fig. 4 shows the differential compressor hardware based on reverse encoding. The present datum is represented as $dini$ and next datum is represented as $dini+1$, $dini+1$ is obtained by delaying the input data with a register *REG*. For each cycle three outputs are generated: 1) the absolute difference, which is obtained by subtracting the present datum from the next datum ; 2) the sign magnitude, which is obtained by comparing the two data, that results in identifying whether the result is positive or negative ; and 3) $size_i$ which indicates the number of meaningful bits of the difference. The reason for representing the difference as the absolute value and a signed magnitude is because the high-order bits of the absolute difference are usually zeros and can be discarded. The absolute difference and the sign magnitude are further packed together to form the final encoded datum . Finally, the data packer module stores the meaningful low-order bits of the encoded datum according to the size. In addition, to record the last datum in uncompressed format, we can read it from the register *REG* when the trace stops. Therefore, the register *REG* is implemented as the interface register of the tracer so that it can access via the bus.

B. Slice Compression

The basic principle of slice compression is that the higher parts between two adjacent branch/target address data are almost similar. Hence, by the elimination of the similar parts, the compression ratio can be raised. Table I shows an example of forward-/reverse-encoding slice compression for a set of instruction addresses. In the forward encoding, the first address is kept uncompressed. The succeeding address is encoded as its differential bits from the preceding address, .eg., 0x0300_6120 is encoded as 0x120 since the difference between 0x0300_6120 and 0x0300_6600 is 0x120. For reverse encoding, the reference direction is reversed; the last address is kept uncompressed while the previous ones are encoded based on the uncompressed last address.

Time	Original address	Forward encoding	Reverse encoding
t	0x0300_6600	0x0300_6600	0x600
t+1	0x0300_6120	0x120	0x20
t+2	0x0300_6130	0x30	0x300_6130
t+3	0x0080_4020	0x080_4020	0x020
t+4	0x0080_4400	0x400	0x0080_4400

Table I
 Example of slice compression for forward/reverse encoding

The implementation of the reverse-encoding slice compression is similar to that of the differential compression, as shown in Fig. 4. The only difference is that the *sizeof*, *differential*, and *comp* modules now compare the bit difference of two data.

C. Dictionary-Based Compression

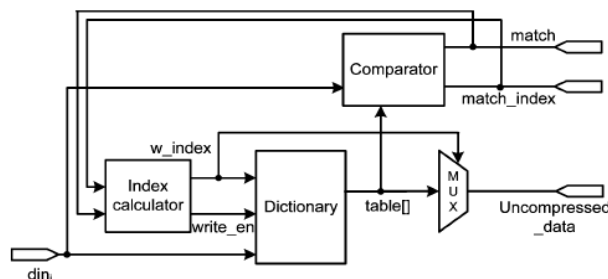


Fig.5. Dictionary compressor hardware based on forward encoding

In dictionary based compression the idea is to map the data to a table keeping frequently appeared data, and record the table index instead of the data to reduce size. Fig. 5 shows the hardware architecture of forward encoding dictionary compression. For each input datum, the comparator compares the datum with the data in the dictionary. If the datum is not in the table (Match=Miss), the datum is written into the table and also recorded in a trace. Otherwise, the index of the hit table entry (Match=Hit) is recorded instead of the datum. But the problem associated with this is that when wrapping around occurs, the uncompressed datum might be overwritten, resulting in data loss. Consider a example that we are sending a series of data's a1, a2, a3, a4, a5, a6.a1 to a3 has the same value as do a4 to a6. At first cycle, since the table is empty, input datum does not match with any table entry (known as a Miss). Therefore, it is inserted into the table and immediately recorded in an uncompressed format. At second and third cycle, a2 and a3 are the same; hence they are encoded as the indexes, respectively. At fourth clock cycle, a4 replaces a1 because a4 is different from a1 (known as a Miss) and the table has only one entry, replaces. In this encoding algorithm, when a1 is overwritten, a2 and a3 cannot be decompressed.

Reverse encoding based dictionary compression can eliminate this problem. Concept of reverse encoding is that, the recording of a1 is delayed: It is only recorded until it is replaced with a4. As a result, the encoded data are placed before the uncompressed datum .With this order, the wrapping around does not cause data loss since the encoded data are lost before the related uncompressed data.

Fig.6. shows the dictionary-based compressor hardware based on reverse encoding. The input datum is compared with the data in the dictionary (din1) by the comparator. If there is a match, then the comparator sends the matched entry number (match index) to the data packer. If not, the input datum is inserted in the dictionary according to the index (w_index) calculated by the index calculator. At the same time, the replaced datum (replaced data) is output to the slice compressor for the further processing.

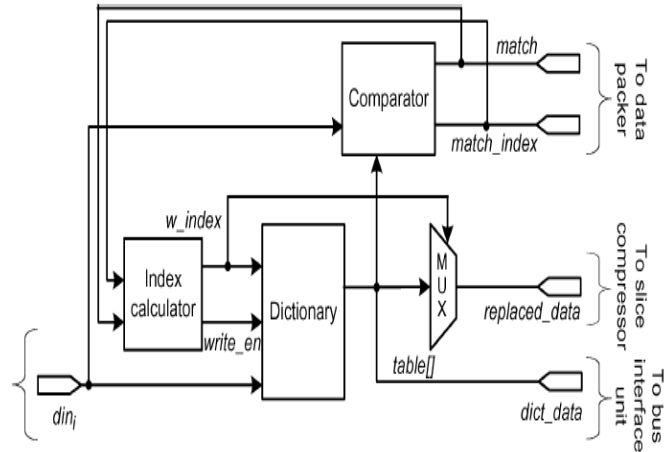


Fig.6. Dictionary compressor hardware based on reverse encoding

Main difference between forward and reverse encoding is that when data's are placed in dictionary they are not immediately recorded, it is recorded only when the data's are replaced.

V. DATA PACKER

Data packer receives the compressed data from the compression module, processes them, and writes them to the circular trace memory. It is responsible for: packet management and circular buffer management. For packet management, since the compressed data length and type are variable, every compressed data needs a header for interpretation. Therefore, this step generates a proper header and attaches it to each compressed datum. Fig.7 shows data packet example. Last packet contains the uncompressed date hence decompression starts from this. since the decompression works in a backward order, in order to interpret the content of a packet, the header is placed at the end of a packet so that the header can be read first before the trace data. It is obtained by reversing the bit order of a packet, since the sub headers should also be read before the compressed data.

VI. SIMULATION RESULTS

As an experimental study a communication architecture based on wishbone in SoC is designed consisting of four masters and four slaves .Master 1 is designed as processor and slaves as memories and the bus tracer based on reverse encoding is integrated to this architecture for tracing the processors program memory. Fig.8, Fig.9, Fig.10 shows results of master 1 communication to external memory

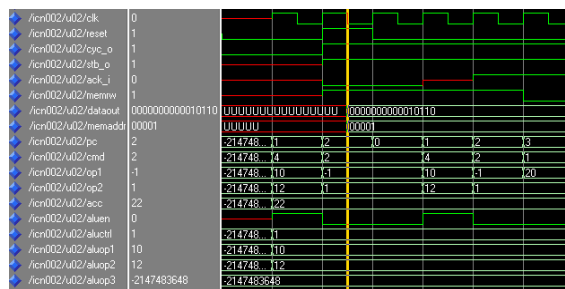


Fig.8.Simulation result of master 1 during write operation

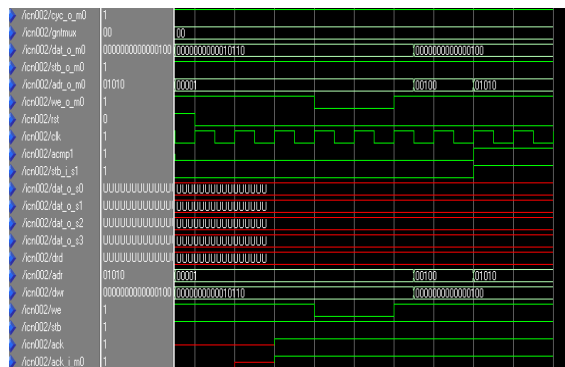


Fig.9. Simulation result of wishbone bus during write operation

The whole architecture is modeled using VHDL. Simulation was done using Modelsim XE III 6.4 and is synthesized using Xilinx ISE 9.2i

V. CONCLUSION

During design implementation stage and final chip testing bus signal tracing (bus tracer) can help designer to debug and analyze hardware-software design. Traditional tracers use forward-encoding compression algorithms to reduce the data size. However, such algorithms are not suitable for a backward trace with a circular buffer. So a reverse encoding based bus tracer is proposed that support both forward and backward trace. This tracer is integrated on wishbone bus consisting of four masters and four slaves. The result shows that this tracer can achieve good circular buffer utilization.

REFERENCES

- [1] Fu-Ching Yang, "Reverse encoding based on chip bus tracer for effective circular buffer utilization", IEEE Trans. vlsi, vol. 18, no. 50, pp. 732–739, 2010.
- [2] Ayas kantha swain, "Design and verification of wishbone bus interface for system on chip integration", 2010 annual IEEE India conference
- [3] J.-S. Yang and N. A. Touba, "Expanding trace buffer observation window for in-system silicon debug through selective capture," in Proc. IEEE 26th VLSI Test Symp., Apr. 27–May 1 2008, pp. 345–351.
- [4] Y.-T. Lin, W.-C. Shiue, and I.-J. Huang, "A multi-resolution AHB bus tracer for read-time compression of forward/backward traces in a circular buffer," in Proc. DAC, Jul. 2008, pp. 862–865.
- [5] E. Anis and N. Nicolici, "On using lossless compression of debug data in embedded logic analysis," in Proc. IEEE Int. Test Conf., Oct. 2007, pp. 1–10.
- [6] ARM, Ltd., Cambridge, U.K., "Embedded trace macrocell architecture specification," 2002. [Online]. Available: <http://infocenter.arm.com/>
- [7] Altera Corporation, San Jose, CA, "Signal Tap embedded logic analyzer mega function," 2001. [Online]. Available: <http://www.altera.com/literature/ds/dssignal.pdf>

Success Factors for Build Operate Transfer (BOT) Power Plant Projects in Iran

Aminah Binti Yusof,¹ Bahman Salami²

¹(Associate Professor, Faculty of Civil Engineering, Universiti Teknologi Malaysia, Malaysia)

²(PhD Candidate, Faculty of Civil Engineering, Universiti Teknologi Malaysia, Malaysia)

Abstract: Iranian electric power industry has adopted Build Operate Transfer (BOT) approach in a number of projects as an alternative to utilize private sector investment. Therefore, some power plant projects have been successfully implemented through BOT such as South Isfahan power plant as a first BOT power plant; in contrast, some of them have been failed in the procurement process. Thus, there is a need for improving procurement approaches for future BOT projects. This study identifies and analysis various success factors in BOT power plant projects in Iran. The research methodology that has been utilized including literature review, and survey questionnaire have distributed to BOT experts. Hence, this research establishes success factors for BOT power plant project in Iran comprise of 33 factors. All 33 success factors are considered as important factors in BOT infrastructure projects; moreover, there is a good agreement in significance of success factors between government organization, consultants, and concessionaires.

Keywords: Success Factors, Power Plant, BOT, Iran

I. INTRODUCTION

The desire to attain the sustainability, in terms of economic, social and environmental demands the innovative project undertaking. The innovative approach involves private sector especially in funding the project. In 80th decade, many Asian countries started privatization of infrastructure to improve public facilities and increase the life level [1], [2], [3], [4], [5]. The attractiveness of Build Operate and Transfer (BOT) approach has increased in developing countries due to the advantages offered by the approach. The main advantage is the chances of government to utilize private sector's investment, management, and technology. Previous studies have assessed the market potential for producing the power, absorbing foreign and local investment engaged in BOT procurement.

On the other hand, some BOT infrastructure projects have been failed around the world. Therefore, government and promoters should notice to the 1 success factors in these projects. There are some existing researches in CSFs of BOT projects around the world such as [6], [7], [8]. These studies have been done in CSFs of BOT projects only in China while it needs to identify CSFs in other countries that have utilized BOT approach in their infrastructure projects. Therefore, since there is no study to date in CSFs in BOT power plant projects in Iran, the research in this area will help both government organization and concessionaire. This paper identifies critical success factors (CSFs) in BOT power plant projects in Iran.

II. BOT POWER PLANT IN IRAN

After changing economic trends in Iran, and with particular attention to the utilization of non-government sector resources, Iran's Ministry of Energy started to attract local and foreign investment by BOT and BOO methods to implement infrastructure projects in power industry. The first power plant project proposed for private sector investment in construction of power plant was in Kerman province in 1995. However it was dropped after the withdrawal of investor. Then, in 1999, Parehsar power plant project in Gilan province proposed as an international tender was selected to be an international consortium; however, the project was stopped due to the structural problems in the implementation process. Since cancellation of that project, many projects came into negotiation but none of them reached to the stage of implementation.

Thus, the authorities in charge of the Iranian power industry and MAPNA Company initiated to remove the existing impediments in the way of the execution of such plans by creating a new project [9]. Until now, South Isfahan Power Plant has been identified as a pioneer and first Iranian IPP project. Given the nature of the project, the direct-negotiation-procedure was selected for the assignment of works. The South Isfahan BOT project was thus launched. This project is the first BOT Power Plant project that has been put into operation in the Iranian power industry. In this regard, a pre-agreement was signed between Iran Power Development Corporation (IPDC) and MAPNA International Company in 2002. The period of time specified for construction period was 3 years, and 20 years for the commercial operation period following the Commercial Operation Date (COD) of the power plant. Recently, the government has decided to transfer the majority of the power plant to the private sector; therefore, the government encourages the private sector to utilize Build Own Operate (BOO) approach in power plant project. BOO is similar to BOT but without transferring to government, commonly used in Australia at the beginning [10]. Table I illustrates BOT and BOO power plant projects in Iran.

Table I: A list of power projects via BOT and BOO approaches in Iran

<i>Project Name</i>	<i>Type of Power</i>	<i>Method of Investment</i>	<i>Capacity (MW)</i>	<i>Project Investment Value (million €)</i>	<i>Concession Period</i>	<i>Status</i>
South Isfahan	Gas	BOT	954	320	20	In Operation
Fars	Gas	BOT	972	550	20	In Operation
Parehsar	Combined Cycle	BOT	968	550	20	In Construction
South Isfahan	Steam	BOT	480	----	20	In Planning
Mianeh	Combined Cycle	BOT	1000	----	20	In Planning
Rafsanjan	Combined Cycle	BOT	1000	----	20	In Planning
Rudeshur	Gas	BOO	2000	700	----	In Operation
Asaluyeh2	Gas	BOO	1000	350	----	In Operation
Ferdos	Gas	BOO	1000	350	----	In Operation
Kahnuj2	Combined Cycle	BOO	50	31	----	In Operation
Noshahr	Combined Cycle	BOO	50	31	----	In Operation
Ali Abad	Gas	BOO	1000	350	----	In Operation
Khoramshar	Gas	BOO	1500	525	----	In Construction
Genaveh	Combined Cycle	BOO	500	310	----	In Construction
Khoram	Combined Cycle	BOO	1000	620	----	In Construction
Kahnuj1	Combined Cycle	BOO	1000	620	----	In Construction
Islam Abad	Combined Cycle	BOO	500	310	----	In Construction
Yazd2	Combined Cycle	BOO	500	310	----	In Construction
Isfahan2	Combined Cycle	BOO	500	310	----	In Construction

III. RESEARCH METHODOLOGY

3.1. The procedure

The quantitative research methodology was employed in this research. Therefore, the research methodology was considered for this study in two stages:

- The first stage was a widespread literature review and interview with BOT experts to identify the success factors in BOT projects. The most significant reviewed previous researches included [11], [6], [12], [13], [14], [7], [15], [16], [17], [8], [18]. The CSFs related to BOT projects were identified and recognized success factors with the most agreement by these researchers as a benchmark for further researches. Hence, 33 success factors were identified in BOT infrastructure projects.
- The second stage was a survey questionnaire to government organizations, consultants, and concessionaires conducted to evaluate the criticality of the listed CSFs.

3.2. The survey sample

The questionnaire explored some barriers that BOT power plant project encounter them. Therefore, the questionnaire was conducted with BOT participants involved in the Iranian electric power industry. For this purpose, the questionnaire was distributed to government organization, consultants, and concessionaires. A total of 142 questionnaires were distributed to BOT and BOO experts according to three above categories. They were dispersed only by the researcher, person by person, in order to help them if it is necessary. Moreover, this method of questionnaire distribution makes direct access to the respondents to ensure that the respondents realize the requirements of the questionnaire. The direct method is significant in encouraging respondent to answer the detailed questionnaire. A total of 129 questionnaires were gathered. From this number, 123 questionnaires were considered as valid questionnaires for analysis (Table II).

Table II: Distributed, returned, and missing questionnaire comparison

<i>Description</i>	<i>Quantity</i>	<i>Percentage (%)</i>
Questionnaire distributed	142	100
Questionnaire returned	129	91
Questionnaire valid and	123	86.5
Missing	19	13.5

The questionnaire was written in English language, but it was translated to Persian language because the study area was in Iran, and questionnaires were distributed among Iranian experts in BOT projects and also to facilitate easier reading and compatibility of understanding. The Likert scale was selected to obtain weight of 33 success factors to BOT power plant project in Iran. In this type of question, the respondents answer based on the amount of importance where 1 represented “not important”, 2 “less important”, 3 “important”, and 4 “most important”.

3.3. Data Analysis

The respondents are grouped into their position in organization or company including Managing Director, Project Manager, Technical Manager, Financial Manager, Planning Manager, and Junior Manager. These questionnaires’ results are considered as reliable and valid, since the majority of the respondents were in positions of senior or middle manager. Table III illustrates the position of respondents in their organization or company.

Table III: Position of respondents in their organization/company

	<i>Managing Director</i>	<i>Project Manager</i>	<i>Technical Manager</i>	<i>Financial Manager</i>	<i>Planning Manager</i>	<i>Junior Manager</i>	<i>Total</i>
Public Sector	-----	18	3	-----	6	15	42
Concessionaires	-----	15	3	6	6	18	48
Consultants	3	15	6	-----	6	3	33
Total	3	48	12	6	18	36	123

On the other hand, these questionnaires’ results are considered as reliable and valid in terms of their academic qualification. It means that 49 percent (60 people) of respondents approximately possess the Bachelor Degree and 51 percent (63 people) possess the Master Degree. Figure 1 shows number of respondents’ academic qualification in three categories.

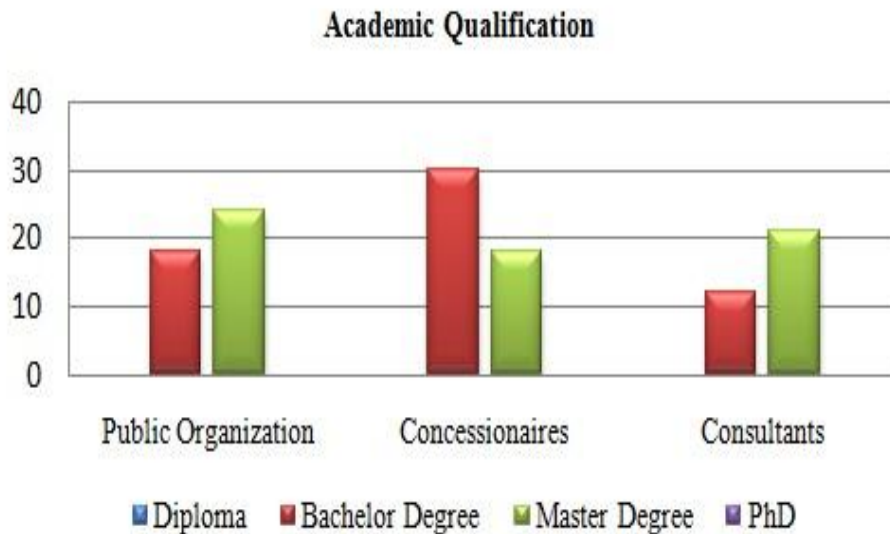


Figure1. Academic qualification of respondents

In order to increase the reliability and validity of data collection, all respondents were selected through experts who had experience in BOT infrastructure projects in Iran. In public organization, 15 respondents have 6-10 years experience in BOT power plant projects and 9 respondents have less than 6 years experience in this field. It means that 78.5 percent of the respondents have more than 6 years experience in BOT projects. Moreover, in concessionaires, 33 respondents have 6-10 years experience in BOT power plant projects and 12 respondents have less than 6 years experience in this field. It clearly seems that the majority of respondents (75%) have experience in BOT project more than 6 years. Finally, in consultants’ category, around half of the respondents (45.5%) have more than 6 years experience in BOT power plant projects in Iran. Therefore, it corroborates to obtain high-quality data to ensure regarding the reliability and validity of data collection. Figure 2 illustrates the experience of respondents in BOT infrastructure projects.

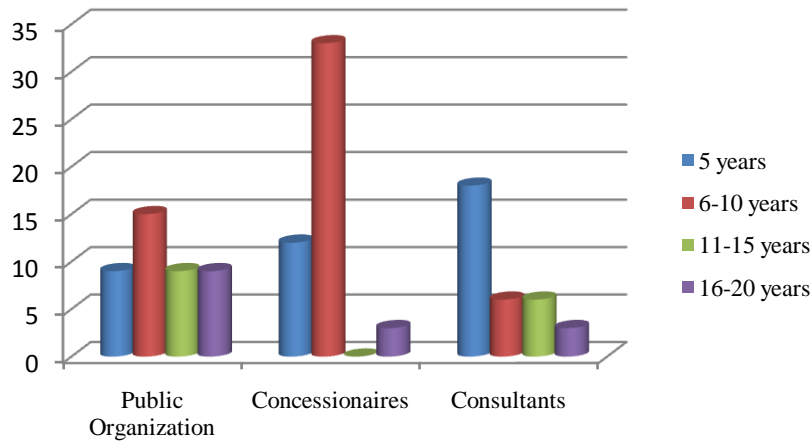


Figure2. Experience of respondents in BOT infrastructure projects

On the other hand, in public organization, 15 respondents have collaborated in 2-5 BOT power plant projects, 9 respondents in 6-10 projects and also 12 respondents in more than 11 projects. It means that 85 percent of respondents have cooperated in more than 2 BOT power plant projects. In concessionaires' category, 18 respondents have been involved only one BOT power plant projects, 27 respondents in 2-5 projects, and 3 respondents in 6-10 projects. Therefore, this refers to 62.5 percent cooperation of the respondents in more than 2 BOT power plant projects. Furthermore, in consultants' category, 21 respondents have worked in 2-5 BOT power plant projects, 3 respondents in 6-10 projects, and 3 respondents in more than 11 projects. This implies to 82 percent collaboration of the respondents in more than 2 BOT power plant projects. Finally, it is concluded that the majority of the respondents (75%) have totally been involved in more than 2 BOT power plant projects. The respondents' participation in BOT infrastructure projects in Iran is indicated in Figure 3.

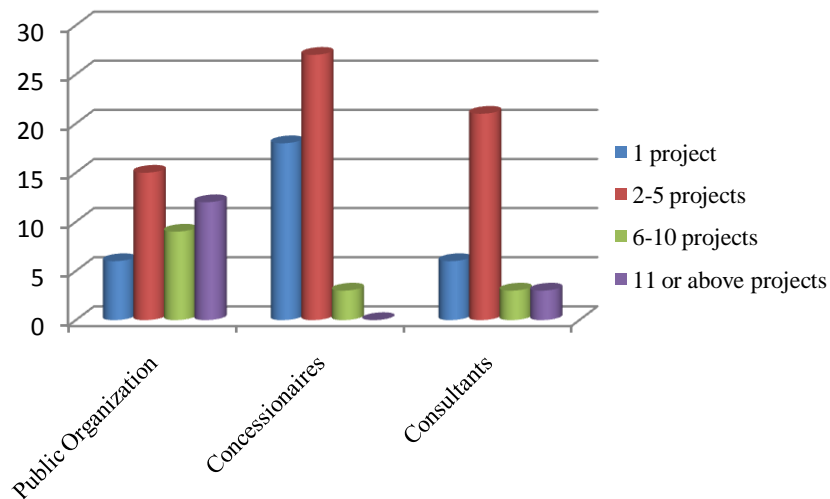


Figure3. Respondents' participation in BOT projects

The method utilized in this research was one-way ANOVA data analysis. This method is used where we have one independent variable with three or more levels (groups) and one dependent continuous variable. As mentioned earlier, there are three categories of the respondents including government organization, concessionaires, and consultants. This method of analysis is also utilized to show the differences or similarities of their comments.

IV. FINDING AND DISCUSSION

Thirty three success factors have been considered to recognize respondents' ideas in these three classifications including consultants (33 persons), the government organization (42 persons), and concessionaires (48 persons). The mean scores of assigned by consultants to Appropriate project identification, Stable political situation, Favorable legislation regulation, and Well-organized and committed public agency are greater than 3.50. This indicates that these three factors are

the most important factors in view of consultants (Table IV). On the other hand, the mean scores of twenty nine sub-factors have been considered between 2.50 to 3.50. These sub-factors comprise of Favorable project management, Attractive financial package, Reasonable risk allocation, Government support, Commitment and responsibility of public and private sectors, Competitive and transparent procurement process, Experience with BOT project by public sector, Utilize local company in project company, Technology transfer, and Concrete concession agreement, Select suitable consortium, Overhauling guarantees, Sound environment impact, Training local staff, A multidisciplinary and multinational team, Short concession period, Good relationship with government, Public safety, Social support, Profit sharing with government, Special guarantees by the government, Select suitable subcontractor, Standardization of engineering contract, Multilateral investment guarantees agency insurance, Technical solution advance, Quality control and supervision, Capability to lead project by government, Operation in good condition, and Financial market availability. This refers to the significance of these 29 success factors in view of consultants. Therefore, in their viewpoint, all thirty three success factors are regarded as important or the most important factors because their mean scores are greater than 2.50.

Moreover, in government organization, the success factor of Attractive financial package has the highest mean score (3.67) and is considered as the most important through all thirty three sub-factors. This is followed by Stable political situation (score of 3.64), Favorable legislation regulation (score of 3.62), Reasonable risk allocation (score of 3.59), and Favorable project management (score of 3.51) by considering of mean score more than 3.50. Furthermore, the mean scores of twenty eight factors have been considered between 2.50 to 3.50. These factors comprise of Appropriate project identification, Technical solution advance, Technology transfer, Utilize local company in project company, Reasonable risk allocation, Commitment & responsibility of public & private sectors, Concrete concession agreement, Select suitable consortium, Government support, Overhauling guarantees, Profit sharing with government, Good relationship with government, Training local staff, Quality control and supervision, Sound environment impact, Select suitable subcontractor, A multidisciplinary and multinational team, Standardization of engineering contract, Short concession period, Competitive & transparent procurement process, Public safety, Experience with BOT project by public sector, Multilateral investment guarantees agency insurance, Capability to lead project by government, Special guarantees by the government, Well-organized & committed public agency, Operation in good condition, Social support, and Financial market availability. This implies that these 28 aforementioned success factors are important in view of government organization. Therefore, in their viewpoint, all thirty three critical success sub-factors are also regarded as important or the most important factors because of their mean scores greater than 2.50.

Furthermore, in category of concessionaires, the success factors of Capability to lead project by government has the highest mean score (3.63) and is considered the most important through of all thirty three sub-factors. The mean scores assigned to Stable political situation, Favorable legislation regulation, and Appropriate project identification are greater than 3.50. In other words, this indicates the importance of these three factors through others in concessionaires' viewpoint. Moreover, the mean scores of twenty nine factors consist of Experience with BOT project by public sector, Competitive and transparent procurement process, Special guarantees by the government, Commitment and responsibility of public and private sectors, Social support, Utilize local company in project company, Government support, Concrete concession agreement, Select suitable consortium, Technology transfer, Standardization of engineering contract, Good relationship with government, Favorable project management, Profit sharing with government, Technical solution advance, Sound environment impact, Quality control and supervision, Training local staff, A multidisciplinary and multinational team, Public safety, Reasonable risk allocation, Select suitable subcontractor, Overhauling guarantees, Attractive financial package, Multilateral investment guarantees agency insurance, Well-organized & committed public agency, Short concession period, Operation in good condition, and Financial market availability have been considered between 2.50 to 3.50. This implies that these 29 success factors are important in view of concessionaires. Therefore, because of the mean scores of all 33 success factors greater than 2.50, they are concerned as important or the most important factors in view of the concessionaires.

In Table IV, from the analysis, it is concluded that the most important sub-factors (rank 1) in viewpoint of three categories respondents are Appropriate project identification" for consultants, Attractive financial package for a government organization, and Capability to lead the project by government for concessionaires. Appropriate project identification is the most important success factors in project procurement system in consultants' view because it needs to utilize especial experts in BOT projects by the government. While, government organization respondents pointed to the attractive financial package as the most significant factors in BOT projects because they have concentrated on the best financial proposal by concessionaires to solve their limited budget. In contrast, concessionaires noticed to the government's ability to lead projects because it is more important to success the infrastructure projects in their viewpoint. The least important factor (rank 33) belongs to Financial market availability for all three classifications of the respondents. In other words, all respondents believe that financial market availability does not play significant role as the success factor in BOT infrastructure projects.

Eventually, although there are some differences in rank, the mean scores are very close and more than 2.50. Hence, all 33 success factors are considered as important factors in BOT infrastructure projects. There is no important difference between consultants, government organization, and concessionaires in respect of the success factors in BOT infrastructure projects according to the statistical results (significance) because significant indexes are more than 0.05 [19].

Table IV: Views of consultants, government organization, and concessionaires about success factors in BOT projects

Success Factors	Consultants (N=33)			Government Organization (N=42)			Concessionaires (N=48)			Significance
	Mean	S.D.	Rank	Mean	S.D.	Rank	Mean	S.D.	Rank	
Appropriate project identification	3.70	0.60	1	3.41	0.63	6	3.53	0.65	4	0.827
Stable political situation	3.67	0.54	2	3.64	0.58	2	3.60	0.57	2	0.887
Favorable legislation regulation	3.64	0.55	3	3.62	0.58	3	3.58	0.61	3	0.916
Well-organized & committed public agency	3.54	0.88	4	3.02	0.87	30	3.04	0.85	30	0.776
Favorable project management	3.49	0.51	5	3.51	0.55	5	3.19	0.58	18	0.850
Attractive financial package	3.47	0.69	6	3.67	0.49	1	3.06	0.73	28	0.900
Reasonable risk allocation	3.44	0.71	7	3.59	0.75	4	3.13	0.76	24	0.767
Government support	3.42	0.78	8	3.26	0.73	13	3.31	0.72	10	0.834
Commitment & responsibility of public & private sectors	3.40	0.61	9	3.31	0.64	10	3.33	0.60	8	0.835
Competitive & transparent procurement process	3.38	0.70	10	3.07	0.71	24	3.39	0.71	6	0.952
Experience with BOT project by public sector	3.35	0.77	11	3.07	0.78	26	3.41	0.80	5	0.787
Utilize local company in project company	3.30	0.68	12	3.33	0.69	9	3.31	0.70	9	0.980
Concrete concession agreement	3.27	0.67	14	3.31	0.68	11	3.29	0.68	12	0.973
Technology transfer	3.27	0.63	13	3.36	0.66	8	3.25	0.67	14	0.774
Select suitable consortium	3.24	0.66	15	3.29	0.67	12	3.27	0.68	13	0.962
Overhauling guarantees	3.22	0.61	16	3.23	0.63	14	3.11	0.65	27	0.947
Sound environment impact	3.21	0.60	17	3.14	0.68	19	3.17	0.69	19	0.904
Good relationship with government	3.18	0.77	21	3.19	0.74	16	3.20	0.74	16	0.987
Short concession period	3.18	0.73	20	3.10	0.69	23	2.96	0.77	31	0.384
Training local staff	3.18	0.58	18	3.17	0.62	17	3.15	0.68	21	0.968
A multidisciplinary and multinational team	3.18	0.58	19	3.12	0.67	21	3.15	0.68	22	0.918
Public safety	3.15	0.67	22	3.07	0.75	25	3.13	0.70	25	0.880
Social support	3.13	0.70	23	2.71	0.67	32	3.31	0.65	11	0.853
Special guarantees by the government	3.12	0.70	25	3.02	0.72	29	3.36	0.74	7	0.838
Profit sharing with government	3.12	0.60	24	3.19	0.64	15	3.19	0.64	17	0.869
Select suitable subcontractor	3.11	0.60	26	3.12	0.62	20	3.12	0.63	26	0.980
Multilateral investment guarantees agency insurance	3.10	0.77	28	3.05	0.73	27	3.04	0.77	29	0.955
Standardization of engineering contract	3.10	0.53	27	3.11	0.57	22	3.24	0.61	15	0.852
Technical solution advance	3.09	0.58	29	3.36	0.65	7	3.17	0.63	20	0.863
Quality control and supervision	3.06	0.61	30	3.14	0.65	18	3.15	0.65	23	0.812
Capability to lead project by government	3.00	0.75	31	3.05	0.82	28	3.63	0.77	1	0.915
Operation in good condition	2.91	0.88	32	2.83	0.88	31	2.79	0.90	32	0.842
Financial market availability	2.79	0.86	33	2.57	0.89	33	2.66	0.90	33	0.259

V. CONCLUSION

BOT approach has a key role in rapid development of Iranian electric power industry to provide energy for massive demand in economic growth. According to extensive literature review, this research establishes success factors for BOT power plant project in Iran comprise of 33 factors.

In This study, 123 valid questionnaires were received from the respondents including government organization, consultants, and concessionaires. These questionnaires' results are considered as reliable and valid since the majority of the respondents were in positions of senior or middle manager. Moreover, majority of the respondents had BOT experience more than 6 years in government organization and concessionaires.

From the analysis, the mean scores of assigned by consultants to Appropriate project identification, Stable political situation, Favorable legislation regulation, and Well-organized & committed public agency are greater than 3.50. This indicates that these three factors are the most important factors in view of the consultants. For government organization, the success factor of Attractive financial package has the highest mean score (3.67) and is considered the most important through all thirty three sub-factors. Capability to lead the project by government with highest mean scores (3.63) is considered as the most important factors through all 33 success factors by concessionaires. The assigned mean scores to Stable political situation, Favorable legislation regulation, and Appropriate project identification are greater than 3.50. Despite the difference in ranking, the mean scores are very close and more than 2.50. Therefore, the respondents believe that all thirty three success factors are important in BOT infrastructure projects. There are no significant differences between consultants, government organization, and concessionaires in respect of the success factors in BOT power plant projects in Iran.

REFERENCES

- [1] Toan. T.N., Ozawa. K. (2007). Evaluation of procurement systems for BOT infrastructure projects in Asian countries. University of Tokyo.
- [2] Ahadzi, M. and Bowles, G. (2004). Public-private partnerships and contract negotiations: an empirical study. *Construction Management and Economics*. 22(November), 967-78.
- [3] Chen, M.S., Lu, H.F., Lin, H.W. (2006). Are the nonprofit organizations suitable to engage in BOT or BLT scheme? A feasible analysis for the relationship of private and nonprofit sectors. *International Journal of Project Management*. 24 (6), 244-252.
- [4] Zhang. X.Q., Kumaraswamy. M.M., (2001). BOT-based approaches to infrastructure development in China. *Journal of Construction Engineering and Management*. 7 (1), 18-25.
- [5] Wang. S.Q., Tiong. R.L.K, Ting. S.K., Chew. D., and Ashley. D. (1998). Evaluation and competitive tendering of BOT power plant project in china. *Journal of Construction Engineering and Management*. 124(4), 333-341.
- [6] Qiao, L., Wang, S.Q., Tiong, R.L.K., and Chan, T.S. (2002). Critical success factors for BOT infrastructure projects in China. *The Journal of Structured Finance*. 8 (1), 40-52.
- [7] Zhang. X.Q.,(2005). Critical success factors for public-private partnerships in infrastructure development. *Journal of Construction Engineering and Management*. 131 (1), 3-14.
- [8] Zhao. Z.Y; Zuo. J, Zillance. G, Wang. X.W. (2009). Critical success factors for BOT electric power projects in China: Thermal power versus wind power. *Renewable Energy*. 35, 1283-1291.
- [9] Mansourzadeh, H. (2007). South Isfahan Gas Power Plant: The First IPP in Iran. Tehran.
- [10] Cheung, E. (2009). Developing a best practice framework for implementing public private partnership (PPP) in Hong Kong. Queensland University of Technology.
- [11] Tiong, R.L.k. (1996). CSFs in competitive tendering and negotiation model for BOT projects. *Journal of Construction Engineering and Management*. 122(3), 205-211.
- [12] Qiao, L., Wang, S.Q., Tiong, R.L.K., and Chan, T.S. (2001). Framework for critical success factors of BOT projects in China. *The Journal of Structured Finance*. 7 (1), 35-51.
- [13] Nijkamp, P., Van der Burch, M., and Vindigni, G. (2002). A comparative institutional evaluation of public private partnerships in Dutch urban land-use and revitalization projects. *Urban Stud*. 39(10), 1865-1880.
- [14] Jamali, D. (2004). Success and failure mechanisms of public private partnerships (PPPs) in developing countries: Insights from the Lebanese context. *Int. J. Public Sector Management*. 17(5), 414-430.
- [15] Hardcastle, C., Edwards, P.J., Akintoye, A. and Li, B. (2006), Critical success factors for PP/PFI projects in the UK construction industry: a factor analysis approach.
- [16] El-Gohary, N. M., Osman, H., and El-Diraby, T. E. (2006). Stakeholder management for public private partnerships. *International Journal of Project Management*. 24, 595-604.
- [17] Chen, C. and Doloi, H. (2008). BOT application in China: Driving and impeding factors. *International Journal of Project Management*. 26, 388-398.
- [18] Chan, A.P.C. Lam, P.T.I Chan, D.W.M. Cheung, E. Ke, y. (2010). Critical Success Factors for PPPs in Infrastructure Developments: Chinese Perspective. *Journal of Construction Engineering and Management*. 136 (5), 484-494.
- [19] Pallant, J. (2007). SPSS Survival Manual (third edition). Mc Graw Hill. New York.

Detecting and Localizing Color Text in Natural Scene Images Using Region Based & Connected Component Method

Mohanabharathi.R,¹ Surender.K,² Selvi.C³

^{1, 2, 3} Asst. Professor /Department of Computer Science and Engineering Selvam College of Technology, Namakkal.

Abstract: Large amounts of information are embedded in natural scenes which are often required to be automatically recognized and processed. This requires automatic detection, segmentation and recognition of visual text entities in natural scene images. In this paper, we present a hybrid approach to detect color texts in natural scene images. The approaches used in this project are region based and connected component based approach. A text region detector is designed to estimate the probabilities of text position and scale, which helps to segment candidate text components with an efficient local binarization algorithm. To combine unary component properties and binary contextual component relationships, a conditional random field (CRF) model with supervised parameter learning is proposed. Finally, text components are grouped into text lines/words with a learning-based energy minimization method. In our proposed system, a selective metric-based clustering is used to extract textual information in real-world images, thus enabling the processing of character segmentation into individual components to increase final recognition rates. This project is evaluated on natural scene image dataset.

Keywords: Conditional random field (CRF); connected component analysis (CCA); text detection; text localization.

I. INTRODUCTION

Image processing is a physical process used to convert an image signal into a physical image. Fig.1 shows, Image acquisition is the first process in image processing that is used to acquire digital image. Image enhancement is the simplest and most appealing areas of digital image processing. The idea behind enhancement techniques is to bring out detail that is obscured, or simply to highlight certain features of interest in an image. Recognition is the process that assigns a label to an object based on its descriptors. This is the act of determining the properties of represented region for processing the images. Information Extraction (IE) is a type of information retrieval whose goal is to automatically extract structured information from unstructured and/or semi-structured machine-readable documents. In most of the cases, this activity concerns processing human language texts by means of Natural Language Processing (NLP). Recent activities in multimedia document processing like automatic annotation and concept extraction out of images/audio/video could be seen as information extraction. [2] [3]

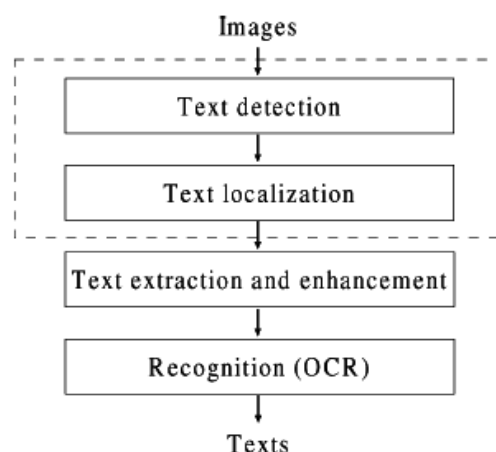


Fig.1.Text information extraction

Existing system presented a hybrid approach to robustly detect and localize texts in natural scene images by taking advantages of both region-based and CC-based methods. This system consists of three stages are the pre-processing stage, the connected component analysis stage and text grouping. At the pre-processing stage, a text region detector is designed to detect text regions in each layer of the image pyramid and project the text confidence and scale information back to the original image, scale-adaptive local binarization is then applied to generate candidate text components. At the connected component analysis stage, [4][5][7] a CRF model combining unary component properties and binary contextual component relationships is used to filter out non-text components. At the last stage, neighboring text components are linked with a learning-based minimum spanning tree (MST) algorithm and between-line/word edges are cut off with an energy minimization model to group text components into text lines or words. And also describes the binary contextual component relationships, in addition to the unary component properties, are integrated in a CRF model, whose parameters are jointly

optimized by supervised learning. But this approach fails on some hard-to-segment texts. Although the existing methods have reported promising localization performance, there still remain several problems to solve. For region-based methods, the speed is relatively slow and the performance is sensitive to text alignment orientation. On the other hand, CC-based methods cannot segment text components accurately without prior knowledge of text position and scale. Here, designing fast and reliable connected component analyzer is difficult since there are many non-text components which are easily confused with texts when analyzed individually.

This paper is organised as follows: Section II briefly reviews the related work. Section III describes the preprocessing of image. Section IV explains the connected component analysis using CRF model. Section V describes the text line/word grouping method. Clustering based method for text extraction and character segmentation is discussed in section VI. Experimental results and conclusion are presented in section VII.

II. RELATED WORKS

Most region-based methods are based on observations that text regions have distinct characteristics from non-text regions such as the distribution of gradient strength and texture properties. Generally, a region-based method consists of two stages: 1) text detection to estimate text existing confidence in local image regions by classification, and 2) text localization to cluster local text regions into text blocks, and text verification to remove non-text regions for further processing.

An earlier method proposed by Wu *et al.* [44] uses a set of Gaussian derivative filters to extract texture features from local image regions. With the corresponding filter responses, all image pixels are assigned to one of three classes (“text”, “non text” and “complex background”), then c-means clustering and morphological operators are used to group text pixels into text regions.

Li *et al.* [16] proposed an algorithm for detecting texts in video by using first- and second-order moments of wavelet decomposition responses as local region features classified by a neural network classifier. Text regions are then merged at each pyramid layer and further projected back to the original image map.

Recently, Weinman *et al.* [14] use a CRF model for patch-based text detection. This method justifies the benefit of adding contextual information to traditional local region-based text detection methods. Their experimental results show that this method can deal with texts of variable scales and alignment orientations. To speed up text detection, Chen and Yuille [5] proposed a fast text detector using a cascade AdaBoost classifier, whose weak learners are selected from a feature pool containing gray-level, gradient and edge features. Detected text regions are then merged into text blocks, from which text components are segmented by local binarization. Their results on the ICDAR 2005 competition dataset [15] show that this method performs competitively and is more than 10 times faster than the other methods.

Unlike region-based methods, CC-based methods are based on observations that texts can be seen as a set of connected components, each of which has distinct geometric features, and neighboring components have close spatial and geometric relationships. These methods normally consist of three stages: 1) CC extraction to segment candidate text components from images; 2) CC analysis to filter out non-text components using heuristic rules or classifiers; and 3) post-processing to group text components into text blocks (e.g., words and lines).

The method of Liu *et al.* [17] extracts candidate CCs based on edge contour features and removes non-text components by wavelet feature analysis. Within each text component region, a GMM is used for binarization by fitting the gray-level distributions of the foreground and background pixel clusters. Zhang *et al.* [19] presented a Markov random field (MRF) method for exploring the neighboring information of components. The candidate text components are initially segmented with a mean-shift process. After building up a component adjacency graph, a MRF model integrating a first-order component term and a higher-order contextual term is used for labeling components as “text” or “non-text”. For multilingual text localization, Liu *et al.* proposed a method [18] which employs a GMM to fit third-order neighboring information of components using a specific training criterion: maximum minimum similarity (MMS). Their experiments show good performance on their multilingual image datasets.

III. PRE-PROCESSING

In this module, preprocessing stage of the overall process is discussed. At the preprocessing stage, a text region detector is designed to detect text regions in each layer of the image pyramid and project the text confidence and scale information back to the original image, scale-adaptive local binarization is then applied to generate candidate text components. To extract and utilize local text region information, a text region detector is designed by integrating a widely used feature descriptor: Histogram of oriented gradients (HOG) and waldboost classifier to estimate the text confidence and the corresponding scale, based on which candidate text components can be segmented and analyzed accurately. Initially, the original color image is converted into a gray level image. To measure the text confidence for each image patch in a window, no matter it is accepted or rejected. [2] [3] [9] [10] The posterior probability of a label y_i , $y_i \in \{\text{'text'}, \text{'non-text'}\}$ conditioned on its detection state, s_i , $s_i \in \{\text{'accepted'}, \text{'rejected'}\}$ at the stage t , can be estimated based on the Bayes formula as defined as

$$\begin{aligned}
 P_t(y_i|s_i) &= \frac{P_t(s_i|y_i)P_t(y_i)}{\sum_{y_i} P_t(s_i|y_i)P_t(y_i)} \\
 &= \frac{P_t(s_i|y_i)P_{t-1}(y_i|\text{accepted})}{\sum_{y_i} P_t(s_i|y_i)P_{t-1}(y_i|\text{accepted})},
 \end{aligned}$$

Where all the stage likelihoods $P_t(s_i/y_i)$ are calculated on a validation dataset during training. The text scale map is used in local binarization for adaptively segmenting candidate CCs and the confidence map is used later in CCA for component classification. The formula to binarize each pixel x is

$$b(x) = \begin{cases} 0, & \text{if } gray(x) < \mu_r(x) - k \cdot \sigma_r(x); \\ 255, & \text{if } gray(x) > \mu_r(x) + k \cdot \sigma_r(x); \\ 100, & \text{otherwise,} \end{cases}$$

Here $\mu_r(x)$ and $\sigma_r(x)$ are mean and standard deviation with radius r . Figure 3 shows the example of preprocessing stage. They calculate the radius from the text scale map which is more stable under noisy conditions. After local binarization assume that within each local region, gray-level values of foreground pixels are higher or lower than the average intensity.

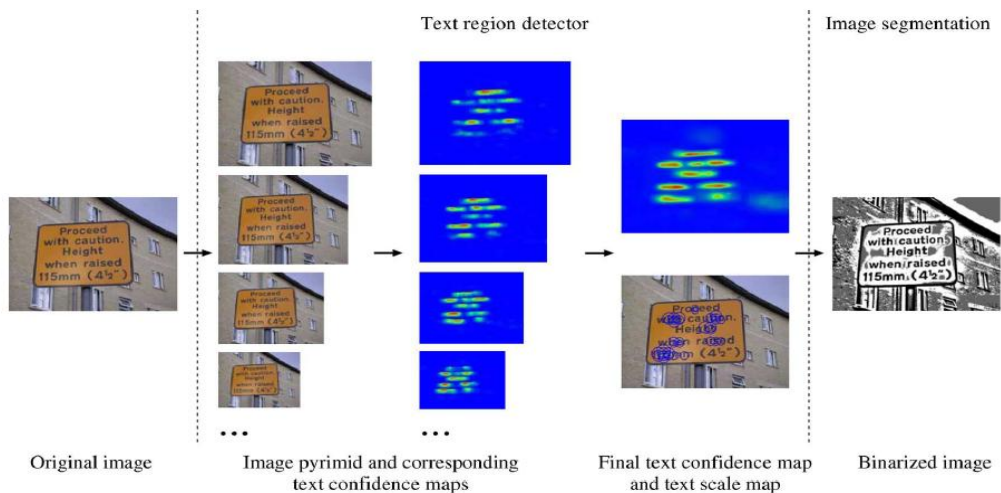


Fig.3.Example of preprocessing stage

IV. CONNECTED COMPONENT ANALYSIS

This module presents the connected component analysis (CCA) stage using a CRF model combining unary component properties and binary contextual component relationships is used to filter out non-text components. Conditional random field (CRF) [4] [7] is proposed model to assign candidate components as one of the two classes (“text” and “non-text”) by considering both unary component properties and binary contextual component relationships. CRF is a probabilistic graphical model which has been widely used in many areas such as natural language processing. Next considering that neighboring text components normally have similar width or height, build up a component neighborhood graph by defining a component linkage rule. And also use the CRF model to explore contextual component relationships as well as unary component properties. During the test process, to alleviate the computation overhead of graph inference, some apparent non-text components are first removed by using thresholds on unary component features. The thresholds are set to safely accept almost all text components in the training set.

V. TEXT GROUPING METHOD

To group text components into text regions are lines and words, a learning-based method by clustering nearing components into a tree with a minimum spanning tree (MST) algorithm and cutting off between-line (word) edges with an energy minimization model is designed. Cluster text components into a tree with MST based on a learned distance metric, which is defined between two components as a linear combination of some features. With the initial component tree built with the MST algorithm, between-line/word edges need to be cut to partition the tree into subtrees, each of which corresponds to a text unit. Finally, text words corresponding to partitioned subtrees can be extracted and the ones containing too small components are removed as noises. With the initial component tree built with the MST algorithm, between-line/word edges need to be cut to partition the tree into subtrees, each of which corresponds to a text unit (line or word).

A .Text Line Partition

A method to formulate the edge cutting in the tree is proposed as a learning-based energy minimization problem. In the component tree, each edge is assigned one of two labels: “linked” and “cut”, and each subtree corresponding to a text line are separated by cutting the “cut” edges. The objective of the proposed method is to find the optimal edge labels such that the total energy of the separated subtrees is minimal. The total text line energy is defined as

$$E(L) = \sum_{i=1}^N W_{line} \cdot F_i,$$

Where N is the number of subtrees (text lines), F_i is the feature vector of a text line, and W_{line} is the vector of combining weights.

B. Text Word Partition

For comparing our system with previous methods which reported word localization results, further partition text lines into words using a similar process as line partition. The major difference lies in the word-level features, which are defined as: 1) word number; 2) component centroid distances of cut edges; 3) component bounding box distances of cut edges; 4) bounding box distances between words separated by cut edges; 5) the ratio between the component centroid distance of the cut edge and the average component centroid distance of the edges within separated words; and 6) bounding box distance ratio between the cut edge and edges within separated words.

VI. SELECTIVE METRIC-BASED CLUSTERING USING LOG-GABOR FILTERS

This module discuss about the selective metric based clustering using log-Gabor filter. Hence, our selective metric-based clustering is integrated into a dynamic method suitable for text extraction and character segmentation. This method uses several metrics to merge similar color together for an efficient text-driven segmentation in the RGB color space. However, color information by itself is not sufficient to solve all natural scene issues; hence complement it with intensity and spatial information obtained using Log-Gabor filters, thus enabling the processing of character segmentation into individual components to increase final recognition rates. Our selective metric-based clustering uses mainly color information for text extraction and our system fails for natural scene images having embossed characters. In this case, foreground and background have the same color presenting partial shadows around characters due to the relief but not enough to separate textual foreground from background in a discriminative way as displayed.

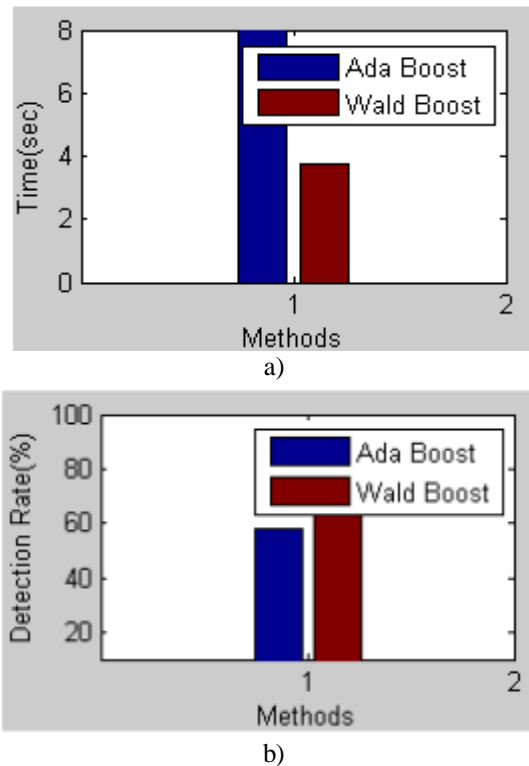


Fig.3. Comparison between adaboost and waldbost classifier a) Execution Time b) Detection Rate

Gray-level information with the simultaneous use of a priori information on characters could be a solution to handle these cases. Next we propose a new text validation measure M to find the most textual foreground cluster over the two remaining clusters. Based on properties of connected components of each cluster, spatial information is already added at this point to find the main textual cluster. The proposed validation measure, M, is based on the largest regularity of connected components of text compared to those of noise and background. And also we use Log-Gabor filters that present globally high responses to characters. Hence, in order to choose efficiently which clustering distance is better to handle text text extraction, we perform an average of pixel values inside each mask. The mask which has the highest average is chosen as the final segmentation.

VII. RESULT AND CONCLUSION

From the results its incurred that waldboost classifier has better execution time and detection rate of text, when compared with previously used adaboost classifier in preprocessing stage .Hence this classifier can be used for text recognition to be integrated with text localization for complete text information extraction.

REFERENCES

- [1] D. T. Chen, J.-M. Odobez, and H. Bourlard, "Text detection and recognition in images and video frames," *Pattern Recogn.*, vol. 37, no. 5, pp. 595–608, 2004.
- [2] X. L. Chen, J. Yang, J. Zhang, and A. Waibel, "Automatic detection and recognition of signs from natural scenes," *IEEE Trans. Image Process.*, vol. 13, no. 1, pp. 87–99, Jan. 2004.
- [3] X. R. Chen and A. L. Yuille, "Detecting and reading text in natural scenes," in *Proc. IEEE Conf. Computer Vision and Pattern Recognition (CVPR'04)*, Washington, DC, 2004, pp. 366–373.
- [4] N. Dalal and B. Triggs, "Histograms of oriented gradients for human detection," in *Proc. IEEE Conf. Computer Vision and Pattern Recognition (CVPR'05)*, San Diego, CA, 2005, pp. 886–893.
- [5] S. L. Feng, R. Manmatha, and A. McCallum, "Exploring the use of conditional random field models and HMMs for historical handwritten document recognition," in *Proc. Washington, DC, 2006*, pp. 30–37.
- [6] J. Gllavata, R. Ewerth, and B. Freisleben, "Text detection in images based on unsupervised classification of high-frequency wavelet coefficients," in *Proc. 17th Int. Conf. Pattern Recognition (ICPR'04)*, Cambridge, U.K., 2004, pp. 425–428.
- [7] J. M. Hammersley and P. Clifford, *Markov Field on Finite Graphs and Lattices*, 1971, unpublished. [10] X.-B. Jin, C.-L. Liu, and X. Hou, "Regularized margin-based conditional log-likelihood loss for prototype learning," *Pattern Recogn.*, vol. 43, no. 7, pp. 2428–2438, 2010.
- [8] Y. Jin and S. Geman, "Context and hierarchy in a probabilistic image model," in *Proc. IEEE Conf. Computer Vision and Pattern Recognition (CVPR'06)*, New York, NY, 2006, pp. 2145–2152.
- [9] B.-H. Juang and S. Katagiri, "Discriminative learning for minimum error classification," *IEEE Trans. Signal Process.*, vol. 40, pp. 3043–3054, 1992.
- [10] K. Jung, K. I. Kim, and A. K. Jain, "Text information extraction in images and video: A survey," *Pattern Recogn.*, vol. 37, no. 5, pp. 977–997, 2004.
- [11] K. I. Kim, K. Jung, and J. H. Kim, "Texture-based approach for text detection in images using support vector machines and continuously adaptive mean shift algorithm," *IEEE Trans. Pattern Anal. Mach. Intell.*, vol. 25, no. 12, pp. 1631–1639, 2003.
- [12] A Hybrid Approach to Detect and Localize Texts in Natural Scene Images Yi-Feng Pan, Xinwen Hou, and Cheng-Lin Liu, Senior Member
- [13] V. Wu, R. Manmatha, and E. M. Riseman, "Finding text in images," in *Proc. 2nd ACM Int. Conf. Digital Libraries (DL'97)*, New York, NY, 1997, pp. 3–12.
- [14] J. Weinman, A. Hanson, and A. McCallum, "Sign detection in natural images with conditional random fields," in *Proc. 14th IEEE Workshop on Machine Learning for Signal Processing (MLSP'04)*, São Luís, Brazil, 2004, pp. 549–558.
- [15] S. M. Lucas, "ICDAR 2005 text locating competition results," in *Proc. 8th Int. Conf. Document Analysis and Recognition (ICDAR'05)*, Seoul, South Korea, 2005, pp. 80–84.
- [16] H. P. Li, D. Doermann, and O. Kia, "Automatic text detection and tracking in digital video," *IEEE Trans. Image Process.*, vol. 9, pp. 147–156, Jan. 2000.
- [17] Y. X. Liu, S. Goto, and T. Ikenaga, "A contour-based robust algorithm for text detection in color images," *IEICE Trans. Inf. Syst.*, vol. E89-D, no. 3, pp. 1221–1230, 2006.
- [18] X. B. Liu, H. Fu, and Y. D. Jia, "Gaussian mixture modeling and learning of neighboring characters for multilingual text extraction in images," *Pattern Recogn.*, vol. 41, no. 2, pp. 484–493, 2008.
- [19] D.-Q. Zhang and S.-F. Chang, "Learning to detect scene text using a higher-order MRF with belief propagation," in *Proc. IEEE Conf. Computer Vision and Pattern Recognition Workshop s (CVPRW'04)*, Washington, DC, 2004, pp. 101–108.
- [20] Y.-F. Pan, X. W. Hou, and C.-L. Liu, "A robust system to detect and localize texts in natural scene images," in *Proc. 8th IAPR Workshop on Document Analysis Syetems (DAS'08)*, Nara, Japan, 2008, pp. 35–42.

High Heat Flux Micro-Electronics Cooling

P.D. Giradkar,¹ U.S.Wankhede²

¹Student, III Semester, M. Tech, Heat Power Engineering, G. H. Raisoni College of Engineering, Nagpur

²Professor, Mechanical Engineering Department, G. H. Raisoni College of Engineering, Nagpur

Abstract: The temperature of an electronics device rises fairly linearly with increasing device heat flux. This relationship is especially problematic for defense electronics, where heat dissipation is projected to exceed $1000\text{W}/\text{cm}^2$ in the near future. This paper study explored the benefit of cooling the electronics device using indirect refrigeration cooling system. In this system the heat sink in a primary pumped liquid loop, reject heat to a secondary refrigeration loop. It was being explored for two phase cooling of ultra high power electronic component. For effective and efficient thermal management of electronic systems active control methods desired to suppress inherent flow instability especially in transient applications. The inclusion of the vapor compression cycle in the two loop system elevates the temperature difference between the refrigerant and the ambient cooling media, resulting in increased system cooling capacity.

Keywords: High heat flux Refrigeration system Two-loop cooling

I. Introduction

Recent liquid cooling research efforts have culminated in numerous cooling solutions that are capable of tackling mostly the $50\text{-}150\text{ W}/\text{cm}^2$ range Mudawar et al. [1]. Defense electronics represent a specialized class of devices that have for the most part followed the heat dissipation trends of commercial devices. However, a new generation of devices for defense radars and directed-energy laser and microwave weapons are approaching $1000\text{ W}/\text{cm}^2$ [1], which exceeds the capabilities of today's most advanced liquid cooling solutions. This trend was the primary motivation for the present study. The goal here was to develop advanced thermal management schemes that can remove very large heat fluxes from advanced defense electronics while maintaining device temperatures below 125°C . The large transient heat loads were imposed and needed to be efficiently and effectively dissipated. Conventional cooling solutions were inadequate for dynamic thermal managements of compact electronic systems. Two-phase cooling technology can provide effective schemes to address some of the high-heat-flux electronics cooling challenges was described by Lee and Mudawar [2].

The difficulty in implementing even the most aggressive liquid cooling scheme was that, for a given resistance between the device and coolant and fixed coolant temperature, the device temperature increases fairly linearly with increasing heat dissipation rate. This relationship could easily bring the temperature of the device above its maximum limit when dissipating high heat fluxes. For a device operating slightly below its maximum temperature limit, dissipating increasing amounts of heat requires reducing the temperature of the liquid coolant. This trend would ultimately drop the coolant temperature below ambient temperature, requiring the use of a refrigeration system to sustain the cooling. Further reducing the coolant temperature allows the device to operate well below its maximum temperature limit. This latter benefit, coupled with enhanced reliability and device performance, was the primary reason behind the recent introduction of a number of commercial systems that capitalize on low temperature cooling. Due to the inherent subcooled boiling advantage, two-loop cooling systems have been demonstrated to be far more effective at dissipating high-power heat fluxes. Such systems can provide the flexibility of choosing different working fluids and pressure levels in the primary and secondary loops, and also offer the scalability for the removal of multiple distributed heat loads with a centralized chiller.

For many years cooling technology has played a key role in enabling and facilitating the packaging and performance improvements in each new generation of computers. The role of internal and external thermal resistance in module level cooling was discussed in terms of heat removal from chips and module. The use of air-cooled heat sinks and liquid-cooled cold plates to improve module cooling is addressed by Richard et al.[3]. Immersion cooling as a scheme to accommodate high heat flux at the chip level was also discussed. Cooling at the system level was discussed in terms of air, hybrid, liquid, and refrigeration-cooled systems. The growing problem of data center thermal management was also considered. To achieve the holistic design it will be necessary to develop advanced modeling tools to integrate the electrical, thermal, and mechanical aspects of package and product function, while providing enhanced usability & minimizing interface incompatibilities.

II. Direct Versus Indirect Liquid Cooling

A) TWO PHASE SPRAY COOLING

Due to resistances of the different layers of materials separating the chip from the liquid coolant, a relatively large temperature gradient is incurred when dissipating high heat fluxes in indirect liquid cooling.. These resistances may be completely eliminated by direct liquid cooling of the chip. However, having liquid come in direct contact with the chip's surface limits cooling options to a few dielectric and inert coolants. Unfortunately, the thermo physical properties of these coolants are quite inferior to those of common coolants such as water/ethylene glycol. Direct liquid cooling is therefore advantageous only when its convective thermal resistance is smaller than the sum of the convective, conductive and contact resistances of the indirect cooling. Because heat spreading plays a minor role in a direct cooling system, high-flux chips may be packaged quite close to one another, greatly reducing both the weight and the volume of the cooling system. Given the

inferior thermo physical properties of dielectric coolants and the strong dependence of cooling performance on convective resistance, the viability of a direct cooling system is highly dependent on the ability to achieve very large convective heat transfer coefficients. This goal can be realized by adopting a highly effective liquid cooling configuration (e.g., spray, jet impingement, micro channel flow) and also by capitalizing on the benefits of phase change was discussed by Mudawar et al.[1].

B) TWO PHASE MICROCHANNEL COOLING

The use of low temperature refrigeration to maintain low device temperatures while dissipating high heat fluxes. Both direct and indirect refrigeration cooling configurations were examined. In the direct cooling system, a micro-channel heat sink serves as an evaporator in a conventional vapor compression cycle using R134a as working fluid. In the indirect cooling system, HFE 7100 used to cool the heat sink in a liquid loop that rejects the heat to a secondary refrigeration loop. Found some Key from the study are as follows by Lee and Mudawar [2].

- (a) Two drastically different flow behaviors were observed Because of compressor performance constraints, mostly high void fraction two-phase flow patterns prevail in the R134a system, dominated by saturated boiling. On the other hand, the indirect refrigeration cooling system facilitates highly subcooled boiling inside the micro-channel heat sink.
- (b) Different pressure drop trends were observed. With R134a saturated boiling, pressure drop increases with increasing heat flux, but this increase becomes milder as most of the flow was converted to vapor. Pressure drop with HFE 7100 subcooled boiling first decreases with increasing heat flux because of decreasing viscosity in the single-phase liquid region. Pressure drop begins increasing following the commencement of boiling. Increasing mass velocity at high fluxes actually decreases pressure drop because of a reduction in void fraction.
- (c) The convective heat transfer coefficient for the R134a and HFE 7100 systems follow opposite trends relative to Thermodynamic equilibrium quality. For R134a (Refrigerant) the heat transfer coefficient was highest near $x_e = 0$ and decreases monotonically with increasing x_e . On the other hand, the convective heat transfer coefficient for HFE 7100 increases with increasing x_e below $x_e = 0$. Highest h values are about equal for the two fluids.
- (d) While the R134a system can produce fairly large h values, its cooling performance is limited by low CHF. Because of its high CHF, the indirect cooling system better suited for high-flux heat dissipation. Tests with this system yielded cooling heat fluxes as high as 840 W/cm^2 without encountering CHF.
- (e) The results from both systems provide a global understanding of the cooling behavior of micro-channel heat sinks. These results are combined to construct a map of performance trends relative to mass velocity, sub cooling, pressure, and surface tension. Extreme conditions of near-saturated flow, low mass velocity, low pressure and high surface tension point to 'micro-channel' behavior, where macro-channel flow pattern maps fail to apply, instabilities are prominent, and CHF is quite low. On the other hand, systems with high mass velocity, high sub cooling, high pressure and low surface tension are far more stable and yield very high CHF values; two-phase flow in these systems follows the fluid flow and heat transfer behavior, as well as the flow pattern maps of micro channel.

III. Direct cooling system

MEMS device uses the electro hydrodynamic principles to pump and form an ultra thin film over a heated surface that requires cooling. It applied an electric field to a set of interdigitated inclined electrodes to pump and form a thin film and to remove heat by thin film evaporation process. Cooling rates of 35 W/cm^2 were obtained at a superheat of 19°C . This smart cooling system will allow the direct attachment of a small, self-contained cooling device to the backside of an electronic component and can controllably remove heat from the electronic component describe by Darabi and Ekula [4].

Trutassanawin et al. [5] designed, built and evaluated the performance of aminiaturescale refrigeration system (MSRS) suitable for electronics cooling applications. Their MSRS had the following components: a commercial small-scale compressor, a micro channel condenser, a manual needle valve as the expansion device, a cold plate micro channel evaporator, a heat spreader and two compressor cooling fans. A suction accumulator to avoid liquid flow to the compressor, an oil filter to return oil to the compressor and guarantee good lubrication, and heat sources to simulate the chips were also installed. HFC134a was the working fluid. System performance measurements were conducted at evaporator temperatures from 10°C to 20°C and condenser temperatures from 40°C to 60°C . The cooling capacity of the system varied from 121 W to 268 W with a COP of 1.9-3.2 at pressure ratios of 1.9-3.2. Their MSRS was able to dissipate CPU heat fluxes of approximately $40\text{-}75 \text{ W/cm}^2$ and keep the junction temperature below 85°C for a chip size of 1.9 cm^2 . It was concluded that a new compressor design for electronics cooling applications was needed to achieve better performance of the system (the most significant losses occurred in the compressor, which was not designed for the operating conditions of electronics cooling). It was also recommended to study the development of an automatic expansion device and a suitable control strategy for the MSRS.

Experimental measurements and numerical results were used to assess the thermal performance of the heat sink in relation to the performance of the refrigeration cycle. It provides several important thermal benefits such as high-flux dissipation, low surface-to-coolant resistance, and most importantly low device temperature. Higher heat transfer coefficients are possible with greater mass velocities. However, greater mass velocities are typically associated with wet compression conditions corresponding to evaporator exit quality below unity and liquid entrainment at the compressor inlet. Wet compression compromises compressor performance and reliability as well as refrigeration cycle efficiency. Wet compression must therefore be minimized by maintaining only slightly superheated conditions at the compressor inlet, or using a wet compression tolerant compressor. Another thermal disadvantage of a superheated evaporator outlet is the likelihood of a

localized increase in the solid wall temperature towards the outlet, which can cause large thermal stresses at the same location. Practical solutions therefore needed to develop systems which were both wet compression tolerant and that include adaptive flow control to maintain the desired evaporator outlet quality describe by Lee and Mudawar [6].

IV. Impinging Jet Cooling System

A) SINGAL PHASE IMPINGING JET

Spray cooling has been identified as a potential solution that can dissipate 150–200 W/cm². While maintaining the chip temperature below 125 °C. Mudawar et al. [1] explores the viability and implementation of this cooling scheme. First, commercial coolants are assessed for their suitability to this application in terms of thermal, environmental, and safety concerns and material compatibility. In this assessment, HFE-7100 identified as the optimum coolant in all performance categories. Next, spray models are used to determine the HFE-7100 spray conditions that meet such stringent heat dissipation requirements. These findings are verified experimentally, demonstrating that spray cooling is a viable thermal management solution for hybrid vehicle electronics.

Jemmy et al. [7] adopts bi-technologies: single phase impinging jet and mini channels heat exchanger. The system has the cooling capacity of 200 W over a single chip with a hydraulic diameter of 12 mm. The equivalent heat flux was 177 W/cm². The cooling system maintains the chip_s surface temperature below 95°C maximum when the ambient temperature is 30°C. De-ionized water is the working fluid of the system. For the impinging jet, two different nozzles are designed and tested. The hydraulic diameters (d_N) are 0.5 mm and 0.8 mm. The corresponding volume flow rates are 280 ml/min and 348 ml/min. Mini channels heat exchanger has 6 (six) copper tubes with the inner diameter of 1.27 mm and the total length of about 1 m. The cooling system has a mini diaphragm pump and a DC electric fan with the maximum power consumptions of 8.4 W and 0.96 W respectively. The coefficient of performance of the system is 21.4

Amon et al. [8]. Described the development of EDIFICE, an integrated evaporative spray cooling device micro-fabricated in silicon for package-level cooling of high-heat flux electronics. It combines efficient phase-change heat transfer utilizing latent heat of vaporization of dielectric coolants and on-chip control to provide localized, adaptive, on-demand cooling. To satisfy temporal and spatial heat removal requirements, it contains built-in software to provide on-demand cooling achieved through the control of droplet sizes, impingement frequencies and impingement locations based on the on-chip sensing of temperature, thermal gradients and dielectric film thickness. Basic experiments to develop and characterize micro-nozzles are reported, as well as experiments with chip surface texturing to improve spreading and boiling behavior. Current work on the project involves the fabrication of an actual miniature EDIFICE device and its testing and characterization in real electronics.

V. Two-phase cooling systems

Two-phase cooling systems with high subcooled boiling had various flow boiling instabilities. Flow boiling oscillations may modify the hydrodynamics of the flow, introduce severe structural vibrations, generate acoustic noise, and can jeopardize the structural integrity of the system. But, most importantly, flow oscillations can lead to not hinder the thermal performance as premature initiation of the CHF condition. On the other hand, most of the existing studies focus on removing the heat at the device level, while active cooling at the system level had not received much attention especially for transient applications. Recently, these critical operational issues had been recognized and recommended by Garimella et al. [9]. For future research: New “concepts for dampening or elimination of potential two-phase loop flow instabilities, and concepts for two-phase loop feedback flow control” are needed in active and transient thermal management of next generation military, automotive, and harsh-environment electronic systems.

Knowledge about flow instabilities was particularly important for better design, control, and performance prediction of any two-phase system, especially the design of large/fast transient electronics cooling systems [2,9]. In the two-loop refrigeration system, flow boiling instability was one of the biggest operation problems for effective and efficient dynamic thermal management of electronics. Which provides additional physical insight about two-phase thermal-fluid dynamics and proposes new concepts for model-based active flow instability analysis and control in transient electronics cooling systems under critical heat flux constraints. Advanced flow instability control strategies are based on dynamic thermal-fluid models. For boiling microchannel systems, no dynamic thermal-fluid model is widely accepted for transient and active thermal management study. Therefore, Zhanga et al. [10] use conventional-scale two phase flow models to evaluate general analysis and control methodologies, which could be extended to microchannel thermal-fluid systems.

Some alternative cooling approaches such as heat pipes, liquid immersion, jet impingement and sprays, thermoelectric & refrigeration mentioned by Trutassanawin et al. [5]. For refrigeration, the following possible advantages were cited: (i) one of the only methods which can work at a high ambient temperature, (ii) chip to fluid thermal resistances are considerably lower, resulting in lower junction temperatures, which could lead to higher heat fluxes being dissipated, and (iii) lower junction temperatures can also increase the microprocessor’s performance and increase the chip’s reliability. Possible “disadvantages” were characterized to be: (i) an increase in the complexity and cost, (ii) possible increase in the cooling system volume and (iii) uncertainties in the system reliability (moving parts in the compressor).

VI. Hybrid two-phase cooling cycle

Three micro-evaporator cooling cycles, one with a pump, one with a compressor and a hybrid of the two together, was proposed by Braz et al. [11] for cooling a computer blade server. The hybrid cycle is characterized by the interchangeability between the first two cycles, where the decision on the cycle to operate is based on the season (necessity or economical benefit for heat recovery) or the maintenance of cycle's driver. The main characteristics of each cycle are presented as well as the details of the micro-evaporator cooler for the blade's CPU. Analysis of the cycle overall efficiency and the potential for heat recovery shows that the best cycle to use depends mainly on the end application of the heat recovered. Four refrigerants were evaluated as the possible working fluids for cooling the microprocessors. HFC134a and HFC245fa were found to be the best choices for the desired application.

Thermal designers of data centers and server manufacturers are showing a greater concern regarding the cooling of the new generation data centers, which consume considerably more electricity and dissipate much more waste heat, a situation that is creating a re-thinking about the most effective cooling systems for the future beyond conventional air cooling of the chips/servers. A potential significantly better solution is to make use of on-chip two-phase cooling, which, besides improving the cooling performance at the chip level, also adds the capability to reuse the waste heat in a convenient manner, since higher evaporating and condensing temperatures of the two-phase cooling system (from 60 to 95^oC) are possible with such a new green cooling technology. In the present project, two such two-phase cooling cycles using micro-evaporation technology were experimentally evaluated with specific attention being paid to (i) controllability of the two-phase cooling system, (ii) energy consumption and (iii) overall exergetic efficiency. The controllers were evaluated by tracking and disturbance rejection tests, which were shown to be efficient and effective. The average temperatures of the chips were maintained below the limit of 85 ^oC for all tests evaluated in steady state and transient conditions. In general, simple SISO strategies were sufficient to attain the requirements of control. Regarding energy and exergy analyses, the experimental results showed that both systems can be thermodynamically improved since only about 10% of the exergy supplied is in fact recovered in the condenser describe by Braz et al. [12].

A hybrid two-phase cooling cycle has been proposed and simulated by Braz et al.[13] to cool micro processors and auxiliary electronics of blade server boards with two-phase evaporating flow in the micro evaporator cooling elements. A simulation code was developed and 5 cases were simulated considering 3 different working fluids, HFC134a, HFO1234ze and water and different internal diameters of the pipes and elbows joining the components. The results showed that the liquid water cooling cycle has a pumping power consumption 5.5 times that obtained for the two-phase HFC134a cooling cycle, both considering a liquid pump as the driver of the fluid. When compared with the HFO1234ze cooling cycle the difference drops to 4.4 times. The simulation of the vapor compression cooling cycle showed higher pumping power consumption when compared with the other cycles simulated. However, this cycle can be justified when the waste heat at the condenser is recovered for applications such as district heating and preheating of boiler feed water. An exergy analyses of the cooling cycles, regarding the potential of exergy recovery at the condenser, showed a low overall exergetic efficiency (lower than 50%), meaning that improvements can be done to increase the thermodynamic performance of the cycles. When looking at local effects, such analyses showed that the driver and the ME+MP_{AE} are the components with the lowest exergetic efficiency and would be the main components to be improved in terms of thermodynamic design. It was also shown that the overall exergetic efficiency of the vapor compression cooling cycle is strongly influenced by the compressor overall efficiency, which showed to be more exergetically efficient than the liquid pumping cooling cycle for an overall efficiency higher than 67%. A case study was developed to investigate the potential savings in energy a datacenter can make by implementing on-chip cooling with waste heat recovery. As an application for the waste heat, a coal fired power plant was analyzed. The results showed that, when compared with traditional air cooling systems, the energy consumption of the datacenter could be reduced by as much as 50% when using a liquid pumping cycle and 41% when using a vapor compression cycle. The overall consumption can be reduced even further if the recovered energy was sold to a secondary application, such as a thermal power plant. Power plant thermal efficiency improvements in the order of 2.2% are possible if datacenter waste heat was incorporated in the power plant's feed water. This could imply huge savings in terms of fuel as well as carbon tax due to a reduced carbon footprint.

A comparison of existing and predicted future miniature refrigeration systems reveals that of currently existing systems, only thermoelectric coolers (TECs) are commercially available. Ten years from now, however, it was likely that several types of mesoscale refrigerators will become available, including the vapor compression, Stirling, pulse tube, reverse Brayton, and orption refrigerators, in addition to improved TECs. Existing TECs are limited in their cooling capacity, due in part to their low efficiencies. These low efficiencies, which means that the coefficient of performance (COP) was less than one, results in more work having to be input to the TEC, compared to the amount of heat that the TEC can pump. Since both heat and work are dissipated at the hot end of the TEC (the "condenser"), this creates a thermal bottleneck between the hot end of the TEC and the ambient air heat sink. Thus, the performance of the TEC is much more sensitive to the thermal resistance between the TEC and the ambient air, compared to the thermal resistance between the chip and the TEC had been discussed by Phelan et al.[14].

After analyzing various cycle, it recognize that conventional vapor-compression cycle was cascaded with a pumped-loop cycle, which directly cools the electronic chip had better performance seen by Phelan et al. [15]. No superheating of the refrigerant in the primary cycle is required. As a result this type of cycle consumes a very low amount of power (0.2 kW), and it was best amongst the four cycles from an energy point of view. Evaporator exit quality, the energy consumption reduction enjoyed by the two-loop system becomes insignificant. Thus, there has to be a critical evaporator exit quality where use of a conventional or single-loop system may be a better choice. It can be seen that the two-loop system is

more efficient than the single-loop system up to an exit quality of 0.89. For higher exit quality the single-loop system is a better choice because of the reduction in the energy required to heat the two-phase refrigerant mixture. For high-heat flux electronics cooling the two-loop system performs better than the conventional vapor compression system or the other systems investigated.

Zhang et al.[16] were conducted experiments to investigate the effect of temperature oscillation on startup behavior and operating performance in a miniature LHP with flat evaporator of 8 mm thick. The evaporator with sintered copper powder wick is in series structure with compensation chamber and made of copper. Water is the working fluid. It is found that the LHP is able to start up at heat load of 15W with temperature oscillation. And the oscillating frequency of temperature rises and amplitude decreases with increasing heat load. Due to insufficient driving force and phase distribution of working fluid in the compensation chamber under different heat load in LHP temperature oscillation takes place. The development of unstable operation in the LHP was the reflection of the re-distribution of working fluid in the loop while the hydrodynamic and thermal equilibrium of the loop is broken and re-built repeatedly. For specific heat load, high operating temperature can improve the operating stability of LHP due to large capillary force.

VII. Summary

- 1) Micro channels: As this technique have greater industrial acceptance, it improved capability in both experimentation and analytical modeling. Specific issues include measurement of experimental heat loss, better understanding of inlet and exit plenum effects, better understanding of the conditions for the transition between macro channel transport and micro channel transport, control of flow instabilities in phase-change schemes, improved prediction of critical heat flux, and development of better heat transfer fluids.
- 2) Liquid cooling: Liquid cooling systems of different Forms, from spray cooling to heat pipe spreaders and thermosyphons, have been implemented in applications As varied as gaming systems and military electronics. Particular attention must be paid to containment and fluid Compatibility issues especially in the context of overall Cooling systems cost, as well as to the importance of judicious fluid fill ratios in heat pipes and thermosyphons Especially at high heat fluxes. Phase-change immersion cooling, while appropriate for prior-generation supercomputers, has not yet been embraced by system designers because of a lack of understanding of the boiling process, the role of enhanced surfaces, incipience hysteresis issues, and low critical heat flux values for dielectric fluids.
- 3) Compression refrigeration cooling: This staple of server thermal management systems being contemplated for mobile computing systems and desktop applications through the use of micro refrigeration systems. Some challenges include condensation issues, the need for extremely high reliability, and battery life. Challenges at the data center level include the need for improved site-specific design of cooling capability and the need for dynamic matching of local and global thermal parameters.
- 4) Air cooling: There is room for continued performance gains in air cooling through optimal design of heat sinks and air flows, and for a delineation of air cooling limits under different sets of constraints. Work continues in branching radial fins, skived heat sinks, ionic prime-movers, and active cooling with piezo-actuated jets. Recent EU tightening of fan noise limits further constrains fluid velocity. Jet impingement cooling continues to be viable for several applications. Need to pursue hybrid solutions that incorporate air cooling with heat pipes and thermoelectrics.

VIII. Recommendations for future research

- 1) Research in microscale cooling systems must continue at the present rate in order to meet the ever increasing cooling Requirements due to advances in electronics and optical devices.
- 2) Research areas must achieve a good balance between fundamental studies, analytical models, and verifiable experimentation for ALL components of the microscale system design.
- 3) Research teams must acquire the multidisciplinary skills required for true integration of the cooling system into electronic packages and devices.
- 4) Researchers must work in close collaboration with industry to reduce the time between experimentation and implementation of cooling approaches. Particular attention must be paid to cost drivers such as the mass of the thermal management system.
- 5) A library of cooling solutions covering the range of technologies, and preferably scalable from handhelds to servers and data centers, must emerge

IX. Conclusions

In order to diffuse high heat flux from chip heat sources and reduce thermal resistance at the chip-to-sink interface, there is a need to develop low cost, higher thermal conductivity, packaging materials such as adhesives, thermal pastes and thermal spreaders. Advanced cooling technology in the form of heat pipes and vapor chambers are already widely used. Further advances in these technologies as well as thermoelectric cooling technology, direct liquid cooling technology, high-performance air-cooled heat sinks and air movers are also needed. To achieve the holistic design referred to above, it will be necessary to develop advanced modeling tools to integrate the electrical, thermal, and mechanical aspects of package and product function, while providing enhanced usability and minimizing interface incompatibilities.

REFERENCES

- [1] I. Mudawar, D.Bharathan, K.Kelly, and S.Narumanchi, "Two-Phase Spray Cooling of Hybrid Vehicle Electronics", (2009).
- [2] Lee, J and Mudawar, I., "Low-temperature two-phase micro channel cooling for high-heat-flux thermal management of defense electronics", (2008).
- [3] Richard C. Chu, Robert E. Simons, Michael J. Ellsworth, Roger R. Schmidt, and Vincent Cozzolino, "Review of Cooling Technologies for Computer Products", IEEE (2004)
- [4] J. Darabi and K. Ekula," Development of a chip-integrated micro cooling device"(2003)
- [5] Trutassanawin,S., Groll,E.A., Garimella,S.V., Cremaschi, "Experimental Investigation of a Miniature-Scale Refrigeration Systems for Electronics Cooling", IEEE (2006).
- [6] Jaeseon Lee and Issam Mudawar, "Implementation of Microchannel Evaporator for High-Heat-Flux Refrigeration Cooling Applications", ASME, (2006)
- [7] Jemmy S. Bintoro, Aliakbar Akbarzadeh, Masataka Mochizuki, "A closed-loop electronics cooling by implementing single phase impinging jet and mini channels heat exchanger", Applied Thermal Engineering 25 (2005) 2740–2753
- [8] Cristina H. Amon "Mems-based thermal management of high heat flux devices EDIFICE: embedded droplet impingement for integrated cooling of electronics"(2001).
- [9] Garimella, S.V., Fleischer, A.S., Murthy, J.Y., et al., "Thermal challenges in next generation electronic systems" (2008).
- [10] TieJun Zhanga , John T. Wena , b, Yoav Pelesa, Juan Catanoa, "Two-phase refrigerant flow instability analysis and active control in transient electronics cooling systems" , (2010)
- [11] Jackson Braz Marcinichen, John Richard Thome, Bruno Miche, "Cooling of microprocessors with micro-evaporation: A novel two-phase cooling cycle" (2010)
- [12] Jackson Braz Marcinichen, Jonathan A. Olivier, Vinicius de Oliveira, John R. Thome, "A review of on-chip micro-evaporation: Experimental evaluation of liquid pumping and vapor compression driven cooling systems and control", (2011).
- [13] Jackson Braz Marcinichen, Jonathan Albert Olivier, John Richard Thome, "On-chip two-phase cooling of datacenters: Cooling system and energy recovery evaluation", (2012).
- [14] Patrick E. Phelan, Victor A. Chiriach, and Tien-Yu Tom Lee, "Current and Future Miniature Refrigeration Cooling Technologies for High Power Microelectronics", IEEE (2002).
- [15] P.E.Phelan, Y.Gupta, H.Tyagi, & R. PrashJ. Cattano, G.Michna, R.Zhou, J.Wen, M. Jensen, & Y.Peleser, "Optimization of refrigeration systems for high-heat-flux Microelectronics" (2008)
- [16] XianfengZhang ,Jiepeng Huo, Shuangfeng Wang, "Experimental investigation on temperature oscillation in miniature loop heat pipe with flat evaporator" (2011).

Weak Triple Connected Domination Number of a Graph

G. Mahadevan¹ V. G. Bhagavathi Ammal² Selvam Avadayappan³ T. Subramanian⁴

¹Dept. of Mathematics, Gandhi gram Rural Institute Deemed University, Gandhi gram – 624302

²PG. Dept. of Mathematics, Sree Ayyappa College for Women, Chunkankadai, Nagercoil – 629302

³Dept. of Mathematics, VHNSN College, Virudhunagar – 626001

⁴Dept. of Mathematics, Anna University: Tirunelveli Region, Tirunelveli. 627007

Abstract: Recently the concept of triple connected graphs with real life application was introduced in [14] by considering the existence of a path containing any three vertices of a graph G . In [3], G. Mahadevan et. al., introduced triple connected domination number of a graph. Also in [10], the authors introduced the concept of strong triple connected domination number of a graph. A subset S of V of a nontrivial graph G is said to be triple connected dominating set, if S is a dominating set and the induced sub graph $\langle S \rangle$ is triple connected. The minimum cardinality taken over all triple connected dominating sets is called the triple connected domination number and is denoted by γ_{tc} . A subset S of V of a nontrivial graph G is said to be strong triple connected dominating set, if S is a strong dominating set and the induced sub graph $\langle S \rangle$ is triple connected. The minimum cardinality taken over all strong triple connected dominating sets is called the strong triple connected domination number and is denoted by γ_{stc} . In this paper we introduce the concept of weak triple connected domination number of a graph. Let $G = (V, E)$ a graph. A set $D \subseteq V$ is a weak dominating set of G if for every vertex $y \in V - D$ there is a vertex $x \in D$ with $xy \in E$ and $d(y, G) \geq d(x, G)$. The weak domination number $\gamma_w(G)$ is defined as the minimum cardinality of a weak dominating set. A subset S of V of a nontrivial graph G is said to be weak triple connected dominating set, if S is a weak dominating set and the induced sub graph $\langle S \rangle$ is triple connected. The minimum cardinality taken over all weak triple connected dominating sets is called the weak triple connected domination number and is denoted by γ_{wtc} . We determine this number for some standard graphs and obtain bounds for general graph. Its relationship with other graph theoretical parameters are also investigated.

Keywords: Domination Number, Triple connected graph, Weak Triple connected domination number
AMS Subject Classification: 05C 69

I. Introduction

By a graph we mean a finite, simple, connected and undirected graph $G(V, E)$, where V denotes its vertex set and E its edge set. Unless otherwise stated, the graph G has p vertices and q edges. Degree of a vertex v is denoted by $d(v)$, the maximum degree of a graph G is denoted by $\Delta(G)$. We denote a cycle on p vertices by C_p , a path on p vertices by P_p , and a complete graph on p vertices by K_p . A graph G is connected if any two vertices of G are connected by a path. A maximal connected sub graph of a graph G is called a component of G . The number of components of G is denoted by $\omega(G)$. The complement \bar{G} of G is the graph with vertex set V in which two vertices are adjacent if and only if they are not adjacent in G . A tree is a connected acyclic graph. A bipartite graph (or bigraph) is a graph whose vertex set can be divided into two disjoint sets V_1 and V_2 such that every edge has one end in V_1 and another end in V_2 . A complete bipartite graph is a bipartite graph where every vertex of V_1 is adjacent to every vertex in V_2 . The complete bipartite graph with partitions of order $|V_1|=m$ and $|V_2|=n$, is denoted by $K_{m,n}$. A star, denoted by $K_{1,p-1}$ is a tree with one root vertex and $p-1$ pendant vertices. A cut-vertex (cut edge) of a graph G is a vertex (edge) whose removal increases the number of components. A vertex cut, or separating set of a connected graph G is a set of vertices whose removal results in a disconnected. The connectivity or vertex connectivity of a graph G , denoted by $\kappa(G)$ (where G is not complete) is the size of a smallest vertex cut. The chromatic number of a graph G , denoted by $\chi(G)$ is the smallest number of colors needed to colour all the vertices of a graph G in which adjacent vertices receive different colour. For any real number x , $[x]$ denotes the largest integer less than or equal to x . A Nordhaus-Gaddum-type result is a (tight) lower or upper bound on the sum or product of a parameter of a graph and its complement. Terms not defined here are used in the sense of [2].

A subset S of V is called a dominating set of G if every vertex in $V - S$ is adjacent to at least one vertex in S . The domination number $\gamma(G)$ of G is the minimum cardinality taken over all dominating sets in G . A dominating set S of a connected graph G is said to be a connected dominating set of G if the induced sub graph $\langle S \rangle$ is connected. The minimum cardinality taken over all connected dominating sets is the connected domination number and is denoted by γ_c . A subset S of V is called a weak dominating set of G , if for every vertex $y \in V(G) - D$ there is a vertex $x \in D$ with $xy \in E(G)$ and $d(y, G) \geq d(x, G)$. The weak domination number $\gamma_w(G)$ is defined as the minimum cardinality of a weak domination set. One can get a comprehensive survey of results on various types of domination number of a graph in [17, 18, 19].

Many authors have introduced different types of domination parameters by imposing conditions on the dominating set [15, 16]. Recently, the concept of triple connected graphs has been introduced by Paulraj Joseph J. et. al., [14] by considering the existence of a path containing any three vertices of G . They have studied the properties of triple connected graphs and established many results on them. A graph G is said to be triple connected if any three vertices lie on a path in G . All paths, cycles, complete graphs and wheels are some standard examples of triple connected graphs. In [3] Mahadevan G. et. al., introduced triple connected domination number of a graph and found many results on them.

A subset S of V of a nontrivial connected graph G is said to be triple connected dominating set, if S is a dominating set and the induced sub graph $\langle S \rangle$ is triple connected. The minimum cardinality taken over all triple connected dominating sets is called the triple connected domination number of G and is denoted by $\gamma_{tc}(G)$.

In [4, 5, 6, 7, 8, 9] Mahadevan G. et. al., introduced complementary triple connected domination number, paired triple connected domination number, complementary perfect triple connected domination number, triple connected two domination number, restrained triple connected domination number, dom strong triple connected domination number of a graph. In [10], the same author also introduced strong triple connected domination of a graph which is communicated to a journal for publication.

In this paper, we use this idea to develop the concept of weak triple connected dominating set and weak triple connected domination number of a graph

Notation 1.1 Let G be a connected graph with m vertices v_1, v_2, \dots, v_m . The graph obtained from G by attaching n_1 times a pendant vertex of P_1 on the vertex v_1 , n_2 times a pendant vertex of P_2 on the vertex v_2 and so on, is denoted by $G(n_1P_1, n_2P_2, n_3P_3, \dots, n_mP_m)$ where $n_i, l_i \geq 0$ and $1 \leq i \leq m$.

Example 1.2 Let $v_1, v_2, v_3, v_4, v_5, v_6$ be the vertices of K_6 . The graph $K_6(P_2, 3P_2, P_3, P_2, P_4, P_2)$ is obtained from K_6 by attaching 1 time a pendant vertex of P_2 on v_1 , 3 time a pendant vertex of P_2 on v_2 , 1 time a pendant vertex of P_3 on v_3 and 1 time a pendant vertex of P_2 on v_4 , 1 time a pendant vertex of P_4 on v_5 , 1 time a pendant vertex of P_2 on v_6 and is shown in Figure 1.1.

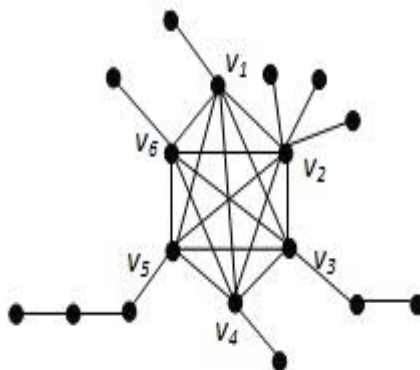


Figure 1.1: $K_6(P_2, 3P_2, P_3, 2P_4)$

II. Weak Triple connected domination number

Definition 2.1 A subset S of V of a nontrivial graph G is said to be a weak triple connected dominating set, if S is a weak dominating set and the induced subgraph $\langle S \rangle$ is triple connected. The minimum cardinality taken over all weak triple connected dominating sets is called the weak triple connected domination number of G and is denoted by $\gamma_{wtc}(G)$. Any weak triple connected dominating set with γ_{wtc} vertices is called a γ_{wtc} -set of G .

Example 2.2 for the graph G_1 in Figure 2.1, $S = \{v_1, v_2, v_3\}$ forms a γ_{wtc} -set of G . Hence $\gamma_{wtc}(G_1) = 3$.

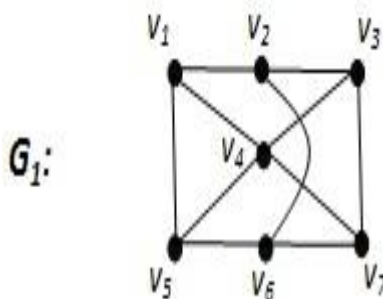


Figure 2.1

Observation 2.3 Weak triple connected dominating set (wtcd set) does not exist for all graphs and if it exists, then $\gamma_{wtc}(G) \geq 3$.

Example 2.4 for the graph G_2 in Figure 2.2, any minimum triple connected dominating set must contain the v_5 and any triple connected dominating set containing v_5 is not a weak triple connected and hence γ_{wtc} does not exist.

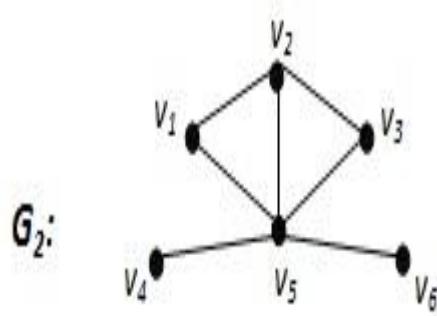


Figure 2.2: Graph with no wtcd set

Throughout this paper we consider only connected graphs for which weak triple connected dominating set exists.

Observation 2.5 The complement of the weak triple connected dominating set need not be a weak triple connected dominating set.

Observation 2.6 every weak triple connected dominating set is a triple dominating set but not conversely.

Observation 2.7 every weak triple connected dominating set is a dominating set but not conversely.

Observation 2.8 For any connected graph G , $\gamma_{tc}(G) \leq \gamma_{wtc}(G)$ and for K_p , ($p > 3$) the bound is sharp.

Exact value for some standard graphs:

- 1) For any cycle of order $p > 3$, $\gamma_{wtc}(C_p) = \begin{cases} 3 & \text{if } p < 5 \\ p - 2 & \text{if } p \geq 5. \end{cases}$
- 2) For any complete graph of order $p > 3$, $\gamma_{wtc}(K_p) = 3$.

Theorem 2.9 For any connected graph G with $p > 3$, we have $3 \leq \gamma_{wtc}(G) \leq p - 1$ and the bounds are sharp.

Proof the lower and upper bounds follows from Definition 2.1. For the cycle C_4 , the lower bound is attained and for K_4 , the upper bound is attained.

Theorem 2.10 For a connected graph G with 4 vertices, $\gamma_{wtc}(G) = p - 1$ if and only if G is isomorphic to $G \cong C_4, K_4, K_4 - \{e\}$.

Proof Suppose $G \cong C_4, K_4 - \{e\}, K_4$, then $\gamma_{wtc}(G) = 3 = p - 1$. Conversely, let G be a connected graph with p vertices such that $\gamma_{wtc}(G) = p - 1$. Let $S = \{v_1, v_2, v_3\}$ be a γ_{wtc} -set of G and $V - S = \{v_4\}$. Since S is a γ_{wtc} -set of G , $\langle S \rangle = P_3$ or C_3 .

Case(i) $\langle S \rangle = P_3 = v_1 v_2 v_3$.

Since G is connected, v_4 is adjacent to v_1 (or v_3) or v_4 is adjacent to v_2 . Hence $G \cong P_4$ or $K_{1,3}$, but for both the graphs a γ_{wtc} -set does not exists. By increasing the degrees, no graph exists.

Case(ii) $\langle S \rangle = C_3 = v_1 v_2 v_3 v_1$.

Since G is connected, v_4 is adjacent to v_1 (or v_2 or v_3). Hence $G \cong C_3(P_2)$, but for $C_3(P_2)$ γ_{wtc} -set does not exists. On increasing the degree, $G \cong C_4, K_4, K_4 - \{e\}$.

The Nordhaus – Gaddum type result is given below:

Theorem 2.24 Let G be a graph such that G and \bar{G} have no isolates of order $p > 3$. Then

- (i) $\gamma_{wtc}(G) + \gamma_{wtc}(\bar{G}) \leq 2(p - 1)$
- (ii) $\gamma_{wtc}(G) \cdot \gamma_{wtc}(\bar{G}) \leq (p - 1)^2$ and the bound is sharp.

Proof The bound directly follows from Theorem 2.9. For the cycle C_4 , both the bounds are attained.

III. Relation with Other Graph Theoretical Parameters

Theorem 3.1 For any connected graph G with $p > 3$ vertices, $\gamma_{wtc}(G) + \kappa(G) \leq 2p - 2$ and the bound is sharp if and only if $G \cong K_4$.

Proof Let G be a connected graph with $p > 3$ vertices. We know that $\kappa(G) \leq p - 1$ and by Theorem 2.9, $\gamma_{wtc}(G) \leq p - 1$. Hence $\gamma_{wtc}(G) + \kappa(G) \leq 2p - 2$. Suppose G is isomorphic to K_4 . Then clearly $\gamma_{wtc}(G) + \kappa(G) = 2p - 2$. Conversely, Let $\gamma_{wtc}(G) + \kappa(G) = 2p - 2$. This is possible only if $\gamma_{wtc}(G) = p - 1$ and $\kappa(G) = p - 1$. But $\kappa(G) = p - 1$, and so $G \cong K_p$ for which $\gamma_{wtc}(G) = 3 = p - 1$ so that $p = 4$. Hence $G \cong K_4$.

Theorem 3.2 for any connected graph G with $p > 3$ vertices, $\gamma_{wtc}(G) + \chi(G) \leq 2p - 1$ and the bound is sharp if and only if $G \cong K_4$.

Proof Let G be a connected graph with $p > 3$ vertices. We know that $\chi(G) \leq p$ and by Theorem 2.9, $\gamma_{wtc}(G) \leq p - 1$. Hence $\gamma_{wtc}(G) + \chi(G) \leq 2p - 1$. Suppose G is isomorphic to K_4 . Then clearly $\gamma_{wtc}(G) + \chi(G) = 2p - 1$. Conversely, let $\gamma_{wtc}(G) + \chi(G) = 2p - 1$. This is possible only if $\gamma_{wtc}(G) = p - 1$ and $\chi(G) = p$. Since $\chi(G) = p$, G is isomorphic to K_p for which $\gamma_{wtc}(G) = 3 = p - 1$ so that $p = 4$. Hence $G \cong K_4$.

Theorem 3.3 for any connected graph G with $p > 3$ vertices, $\gamma_{wtc}(G) + \Delta(G) \leq 2p - 2$ and the bound is sharp.

Proof Let G be a connected graph with $p > 3$ vertices. We know that $\Delta(G) \leq p - 1$ and by Theorem 2.9, $\gamma_{wtc}(G) \leq p - 1$. Hence $\gamma_{wtc}(G) + \Delta(G) \leq 2p - 2$. For K_4 , the bound is sharp.

REFERENCES

- [1] Acharya.B.D, (1980): The strong domination number of a graph and related concepts, *J.Math.Phys.Sci*,14 pp 471-475.
- [2] John Adrian Bondy, Murty U.S.R. (2009): *Graph Theory*, Springer, 2008.
- [3] Mahadevan G., Selvam A., Paulraj Joseph J., and Subramanian T. (2012): Triple connected domination number of a graph, *International J.Math. Combin.* Vol.3, 93-104.
- [4] Mahadevan G., Selvam A., Paulraj Joseph J., Ayisha B., and Subramanian T. (2012): Complementary triple connected domination number of a graph, Accepted for publication in *Advances and Applications in Discrete Mathematics*, ISSN 0974-1658.
- [5] Mahadevan G, Selvam Avadayappan, Mydeen bibi A., Subramanian T. (2012): Complementary perfect triple connected domination number of a graph, *International Journal of Engineering Research and Application*, ISSN 2248- 9622, Vol.2, Issue 5, Sep –Oct, pp 260-265.
- [6] Mahadevan. G, Selvam Avadayappan, Nagarajan. A, Rajeswari. A, Subramanian. T. (2012): Paired Triple connected domination number of a graph, *International Journal of Computational Engineering Research*, Vol. 2, Issue 5, Sep. 2012, pp. 1333-1338.
- [7] Mahadevan G., Selvam A., Ayisha B., and Subramanian T. (2012): Triple connected two domination number of a graph, *International Journal of Computational Engineering Research* Vol. 2, Issue 6, Oct. 2012, pp.101-104.
- [8] Mahadevan G., Selvam A., Bhagavathi Ammal V. G, and Subramanian T. (2012): Restrained triple connected domination number of a graph, *International Journal of Engineering Research and Application*, ISSN 2248-9622, Vol. 2, Issue 6, Nov – dec. 2012, pp.225-229.
- [9] Mahadevan G., Selvam Avadayappan., Hajmeeral. M., and Subramanian T. (2012): Dom strong triple connected domination number of a graph, *American Journal of Mathematics and Mathematical Sciences*, ISSN 2278-0874, Vol. 1, Issue No. 2, July – dec.2012, pp.29-37.
- [10] Mahadevan G., Selvam A., Bhagavathi Ammal V. G, and Subramanian T. (2012): strong triple connected domination number of a graph, Accepted for publication in *International Journal of Computational Engineering Research*.
- [11] Nordhaus E. A. and Gaddum J. W. (1956): On complementary graphs, *Amer. Math. Monthly*, 63: 175–177.
- [12] Paulraj Joseph J. and Arumugam. S. (1992): Domination and connectivity in graphs, *International Journal of Management Systems*, 8 (3): 233–236.
- [13] Paulraj Joseph J. and Arumugam. S. (1997): Domination and coloring in graphs, *International Journal of Management Systems*, 8 (1): 37–44.
- [14] Paulraj Joseph J., Angel Jebitha M.K., Chithra Devi P. and Sudhana G. (2012): Triple connected graphs, *Indian Journal of Mathematics and Mathematical Sciences*, ISSN 0973-3329, Vol. 8, No.1, pp 61-75.
- [15] Paulraj Joseph J. and Mahadevan G. (2006): On complementary perfect domination number of a graph, *Acta Ciencia Indica*, Vol. XXXI M, No. 2: 847–853.
- [16] Sampathkumar, E.; Walikar, HB (1979): The connected domination number of a graph, *J.Math. Phys. Sci* 13 (6): 607–613.
- [17] Sampathkumar E and Puspaltha.L (1996): Strong weak domination and domination balance in a graph, *discrete math.* 161, pp 235-242.
- [18] Teresa W. Haynes, Stephen T. Hedetniemi and Peter J. Slater (1998): *Domination in graphs*, Advanced Topics, Marcel Dekker, New York.
- [19] Teresa W. Haynes, Stephen T. Hedetniemi and Peter J. Slater (1998): *Fundamentals of domination in graphs*, Marcel Dekker, New York.

Ground water nitrate removal by using 'Chitosan' as an adsorbent

Dr.I.D.Patil,¹ Dr. M. Husain,² Er.V.R.Rahane³

¹ Head, Deptt. Of Biotechnology, SSBT's COET, Bambhori, Jalgaon, Maharashtra, India

² Head, Deptt. Of Civil Engineering, SSBT's COET, Bambhori, Jalgaon, Maharashtra, India

³ Asst. Prof., Amrutvahini College of Engineering, Sangamner, Maharashtra, India

ABSTRACT: Environmental pollution is the most terrible ecological crisis to which we are subjected today. Today the environment has become foul, contaminated, undesirable, and therefore harmful for the health of living organisms, including man. The most common contaminant identified in ground water is dissolved nitrogen in the form of Nitrate (NO_3). Decomposition of organic matter present in soils leaching, of soluble fertilizers, human and animal excreta are the source of nitrate in subsurface waters. This research work is for to find preventive measures to avoid the nitrate pollution. This paper explains suitability of naturally available adsorbent i.e. 'Chitosan' for removal of nitrates from water is studied. The work is for the use of Chitosan in the different forms and concentrations to achieve the task.

Keywords: Adsorption, Chitosan, Ground water, Nitrates, pH

I. INTRODUCTION

Water is a common chemical substance that is essential for the survival of all known forms of life. About 97% of earth's water is saline and is contained in oceans. Remaining 3% is fresh water. About 68.7% of fresh water is trapped in the ice caps and glaciers, while 30.1 % of fresh water exists in the form of groundwater, 0.3 % in surface water and 0.9% in other form.

Nitrate is a chemical, like salt. We get nitrate in food and in water. Usually, water is a fairly minor source of nitrate. However, sometimes water has high levels of nitrate - then it is a significant source. Nitrates are naturally present in many foods like carrots and spinach. Nitrate (NO_3^-) is a water-soluble molecule made up of nitrogen and oxygen. It is formed when nitrogen from ammonia or other sources combines with oxygenated water. Nitrate is a natural constituent of plants and is found in vegetables at varying levels depending on the amount of fertilizer applied and on other growing conditions. According to the World Health Organization, most adults ingest 20-70 milligrams of nitrate-nitrogen per day with most of this coming from foods like lettuce, celery, beets, and spinach. When foods containing nitrate are eaten as part of a balanced diet the nitrate exposure is not thought to be harmful.

Nitrate is formed when nitrogen from ammonia or other sources combines with oxygenated water. Nitrate is a natural constituent of plants and is found in vegetables at varying levels depending on the amount of fertilizer applied and on other growing conditions.

1.1 Sources of Nitrates Pollution in Groundwater:

Cultivation in areas where the soil layer is relatively thin, or has poor nutrient buffering capacity, or where there are changes in land use;

- Over fertilization of crop for intensification of agricultural activity;
- Spread cultivation of crops which require high fertilizers doses and which leave the soil bare over long periods (maize, tobacco and vegetables);
- Drainage systems which lead to drainage of fertilizers;
- Intensive agricultural rotation cycles involving frequent plugging and extensive areas of bare soils during winters;
- Organic fertilizers from animal husbandry;
- Increased urbanization.

1.2 Problems Associated With High Nitrate Levels:

If the level is 10 mg/l or higher do not use the water to feed your baby. Infants who are fed water that is high in nitrate can develop a condition that doctors call methemoglobinemia. The condition is also called "blue baby syndrome" because the skin appears blue-gray or lavender in color. Although many studies have been performed attempting to link stomach and gastrointestinal cancer due to nitrate intake

II. OBJECTIVE OF THE STUDY

- 1) To investigate the groundwater pollution status in the study area.
- 2) To study the suitability of water for domestic use.
- 3) To study the suitability of different forms chitosan as an adsorbent for removal of nitrates.

III. METHODOLOGY

3.1 Sample Collection:

The region we selected is having mixed cultures of irrigation and cropping pattern. Also the area is having industries and the fields around the disposing area are irrigated by the wells which are being contaminated. Also some areas are irrigated by the river water was also selected for the nitrate concentration.

About 130 water samples of groundwater from areas over the agricultural belt in Sangamner taluka region of Ahmednagar District, Maharashtra were randomly collected over the period of six months. All samples were collected in 1 lit polythene bottles and carried to the laboratory for analysis.

3.2 Methods of Nitrate Determination:

- 1) Spectrophotometer
- 2) IS code method
- 3) Nitrates kit

In this experimental work Spectrophotometer method was used for determination of nitrate concentration in groundwater samples collected.

3.3 Methods for Nitrate Removal from Water:

There are various methods and materials with the help of with nitrate can be removed from water. There are two options for achieving safe nitrate levels. First of all there are non-treatment techniques that consist of blending drinking waters, or changing water sources. The second alternative is the use of treatment processes, such as ion exchange, reverse osmosis, biological de-nitrification and chemical reduction to actually remove portions of the pollutant.

These are following various treatment processes for removal of nitrate:

- Nitrate removal from water using conifer tissues.
- Removal of nitrates and ammonium ions from water using natural sorbent as zeolite (clinoptilolite).
- The removal of nitrate from water by chitosan.(proposed)

However, among the treatment process listed above we have used chitosan as an adsorbent in powder and liquid form for removal of nitrate from source water.

3.3.1 Chitosan:

Chitin and chitosan are nitrogenous polysaccharides that are made up of acetyl glucosamine and glucosamine units. In fact, these two polymers have exactly the same basic chemical structure: (1→4)-2-acetamido-2-deoxy-β-D-glucan and(1→4)-2-amino-2-deoxy-β-D-glucan, respectively. The chemical structure of chitosan is shown in fig. no.1. The difference between them is the deacetylation degree (DD) and their respective solubility in dilute acidic media. Sorlier et al., (2001) considered that chitosan is the only derivative to be soluble at a DD above 40%. Chitosan is a biodegradable, nontoxic extract from shellfish shells used in a variety of water purification applications. Chitosan is derived from chitin (pronounced ky-tin), nature's second most abundant biopolymer and primary constituent of shellfish shells, insect exoskeletons, and fungi cell walls. Chitosan is so safe that it is used in commercial aquariums to clarify the water in the aquarium exhibits and it is also used to clarify public pools and spas. In addition to its safety record, the secret of its success is the way in which it interacts with sediment particles. Chitosan creates a fibrous web linking sediment particles together in a three-dimensional matrix. When this matrix enters a sand filter it is caught in the sand but allows the water through, but other polymers and coagulants form a gelatinous flock that rapidly clogs filters. Chitosan allows extremely long filtration cycles at sediment loading rates that are well above industry standards. Characteristics of Chitosan are shown in table no.1.

IV. EXPERIMENTAL WORK & ANALYSIS

This experimental research work is within two phase by using chitosan in powder and liquid form for removal of nitrate.

Phase 1: Removal of nitrates using chitosan in the powder form:

The feasibility of removal of nitrates by chitosan was tested by using chitosan in the powder form. 0.5, 1 and 1.5 g of chitosan powder was added separately to 250 ml sample of groundwater. Graph No.1 shows change in nitrate level with varying dosage of chitosan in powder form.

This suggests that chitosan is an efficient disinfectant in its native form (powder). There was no change in the fluoride concentration after treating the groundwater sample with chitosan in powder form. The other observation was that, the use of chitosan in powder form imparted turbidity to the treated water.

Phase 2: Removal of nitrates using chitosan in solution form:

In phase-2, chitosan was used in solution form. 3% acetic acid solution was prepared by diluting 3ml of acetic acid to 100 ml with distilled water. Desired quantity of Chitosan powder was then weighed and dissolved in this acetic acid solution to obtain chitosan solution. Two sets of chitosan solution were prepared. One set was prepared by dissolving 0.01g of chitosan and the other, by dissolving 0.05g of chitosan powder. Chitosan dissolved completely to give a colourless solution. The chitosan solutions were then used in different volumes. 1ml, 5ml and 10ml of the two chitosan solutions were added separately to every 250ml of the groundwater sample. Graph No.2 shows change in nitrate level with varying dosage of chitosan solution.

A significant reduction in the nitrate nitrogen concentration was observed. The use of chitosan in solution showed better results in comparison to the use of the same in powder form. Another important observation was that there was no significant increase in turbidity. The treated solution was rather clear. But there was a reduction in pH of the treated water with an increase in the chitosan solution dosage. A pH of 5.27 was obtained the least, obtained with 10ml of chitosan solution.

The chitosan solution containing 0.05g of chitosan was also found to give good results. There were significant reductions in the concentration of nitrates. The pH dropped to 5.31 in the water sample treated with 10ml of chitosan solution.

V. CONCLUSIONS

1. The use of chitosan in powder form, to treat water, showed positive results. Nitrate removal was significant. But, chitosan powder rendered the water turbid which may be aesthetically objectionable. It showed better results in the lowest concentration used i.e. 0.5g/250ml sample.
2. Use of chitosan in solution form showed better results in comparison with the performance of the same in powder form. The quantity of chitosan powder consumed was meager and therefore economically more feasible.
3. Chitosan in solution was found to remove hardness and chlorides and there were significant reductions in nitrate and fluoride concentrations. Disinfection efficiency was 99.5%.
4. Unlike in the powder form, the solution form did not impart turbidity to the treated water but there was a steep decrease in the pH with an increase in the chitosan solution dosage.

REFERENCES

[1] APHA (American Public Health Association) 1985 Standard methods for the examination of water and waste water (16th edn), APHA, American Water Works Association and Water Pollution Control Federation, Washington DC, USA.
 [2] Mishra, A., Ray, C., and Kolpin, D. (2004). "Use of Qualitative and Quantitative information in Neural Networks for Assessing Agricultural Chemical Contamination of Domestic Wells." J. Hydrol. Eng., 9(6), 502–511.
 [3] S.Fetouani., M. Sbaa, M. Vanclooster, B. Bendra, Agricultural Water Management, Volume 95, Issue 2, February 2008, Pages 133–142
 [4] Annouar, S.; M. Mountadar; A. Soufiane; A. Elmidaoui; M.A. Menkouchi Sahli; M. Kahlaoui, Unit of Analytical Chemistry of the Environmental Faculty of Sciences, El Jadida, Morocco. Desalination Strategies in South Mediterranean Countries, Vol 168 No 1-3, p 185, 15 Aug 2004
 [5] F. Lasserrea, M. Razaacka., O. Bantonb "Mapping groundwater contamination risk using GIS and groundwater modelling. A case study from the Gaza Strip, Palestine" Arabian Journal of eosciences, April 2011, Volume 4, Issue 3-4, pp 483-494
 [6] N. SRINIVASA RAO, Impact of clayey soils on nitrate pollution in the groundwater of the lower Vanisadhara River basin, India (2005)131:8(1194) Hydrological Sciences—Journal—des Sciences Hydrologiques, 43(5) October 2008
 [7] Huang, Y. and Zhang, T. (2005). "Modeling of Nitrate Adsorption and Reduction in Fe0 -Packed Columns through Impulse Loading Tests." J. Environ. Eng., 131(8), 1194–1202.
 [8] Iital, Arvo; Pachel, Karin; Deelstra, Johannes. Estonia., Environmental Science and Policy vol. 11 issue 2 April, 2008.pp. 185-193.
 [9] George J. Kraft*, Will Stites, (2003) Nitrate impacts on groundwater from irrigated-vegetable systems in a humid north-central US sand plain Agriculture, Ecosystems and Environment 100 63–74.

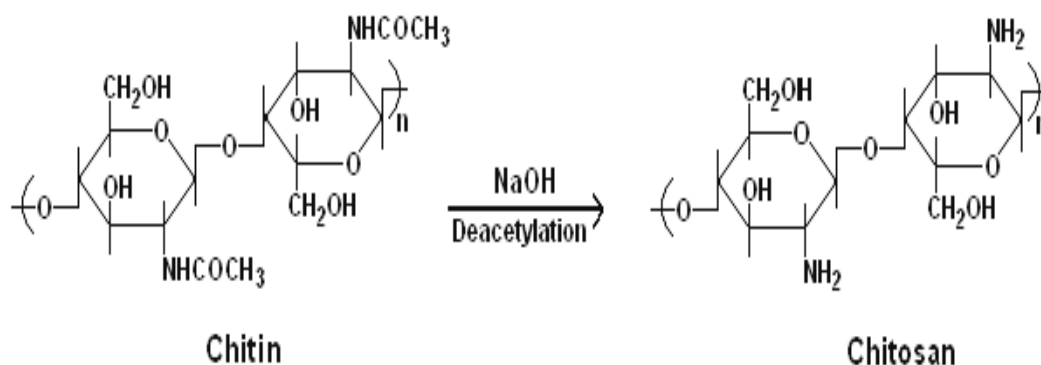
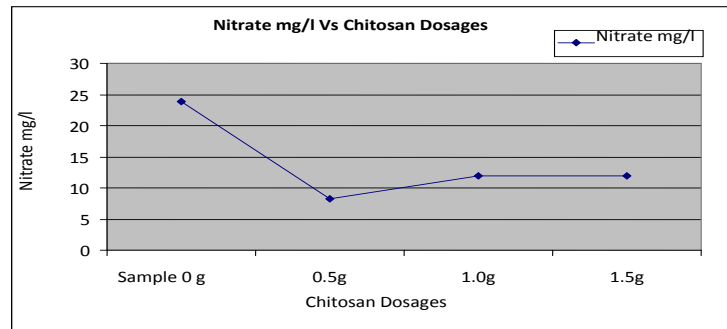


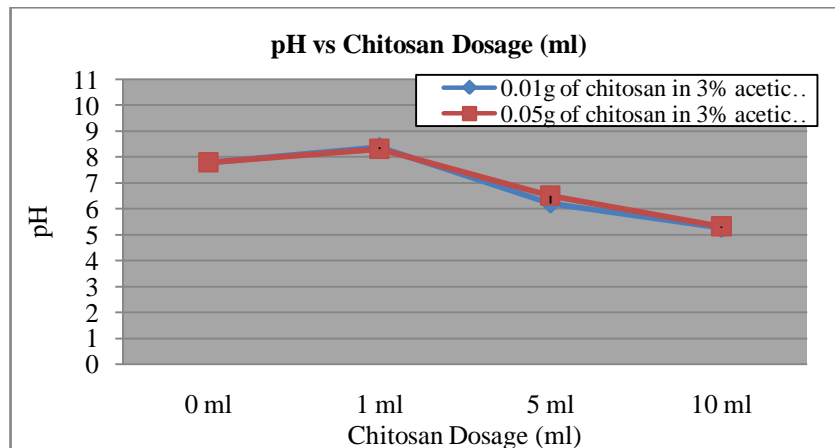
Fig No.1 Scheme of Chemical Deactivation of Chitin to Produce Chitosan

Table No.1-Characteristics of Chitosan

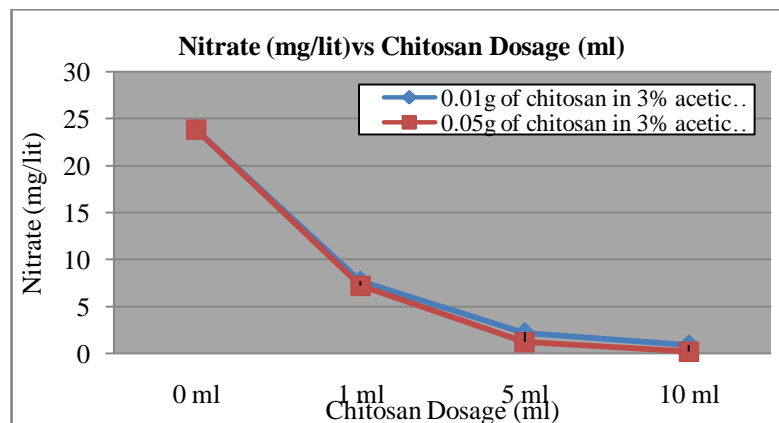
Item	Characteristic
1. Appearance	Yellowish
2. particle size	Mesh no.60
3. ash content	0.83%
4. moisture content	8.5%
5. deacetylation degree(%DAC)	86%
6. Solution(1% in 1% acetic acid)	
Insoluble	0.59%
Viscosity	152 cps
7. Heavy metals	0 ppm
Total Plate count	50
Yeast and Mould	20
E.coli	Nil
Salmonelia	Nil



Graph 1 Profile of nitrate Vs Chitosan dosage



Graph 2 Profile of pH versus Chitosan Dosage in solution form (Phase- 2).



Graph 3 Profile of Nitrate versus Chitosan Dosage in solution form (Phase- 2).

A Teaching Methodology for Introductory Programming Courses using Alice

Ozgur Aktunc

Department of Engineering, St. Mary's University, San Antonio, United States

Abstract: Enrollment numbers and retention rates have been decreasing in technology programs in United States of America, particularly for underrepresented minority groups. At St. Mary's University, we started an Engineering Summer Program (ESP) that consists of programming and robotics sessions for high school students. The programming courses offer an opportunity for many students to write a computer program for the first time in their lives. In these courses we are using a popular instructional tool for teaching programming called Alice. Alice is a 3D interactive environment that has visual and narrative aspects. Our objectives include motivating the students to start programming, keeping the frustration levels to a minimum, which is a common problem for new programmers, and increasing the students' problem solving skills. In this paper, we present a survey of the common challenges faced in introductory programming courses, the objectives of these courses, and our approach to start programming using Alice with a transition to Java, a popular object-oriented language.

Keywords: Introductory programming, education, teaching methodology, Alice, Java.

I. INTRODUCTION

Introductory programming courses are part of Computer Science (CS), Computer Engineering (CE), Computer Information Systems (CIS), and many engineering curricula. Programs generally offer two to four programming courses consisting of fundamentals of programming, object-oriented programming (C++ and Java), and applications of popular languages.

The discussion of what needs to be taught in introductory programming courses has existed since the early seventies. Gries suggested that an introductory course should be concerned with three aspects of programming [1]:

- How to solve problems.
- How to develop an algorithmic solution to a problem.
- How to verify that an algorithm is correct.

Despite the advances in the availability of resources to teach programming courses, the fundamental issue of teaching problem solving using algorithms is still the main challenge for instructors. While we do not want to delve into the reasons for lack of problem solving skills in engineering and CS students, we would like to emphasize the importance of teaching problem solving. We adopt Polya's [2] four-phase process as our guideline to teach problem solving:

1. Understand the problem.
2. Devise a plan.
3. Carry out the plan.
4. Look back (reflect).

Polya's work has been adapted by many educators. Barnette et al. [3] applied Polya's four-phase process of problem solving to programming:

1. Understand the problem.

- a. Knowing the boundaries of the problem.
- b. Knowing the constraints of the solution.
- c. Knowing what actions are allowed.

2. Devise a plan.

- a. Organize thought to develop a detailed algorithm.
- b. Use tools, such as outlining and pseudo code.

3. Implement the plan.

- a. Carry out the steps in the algorithm.
- b. Translate the problem into a language understandable by the device to be used.

4. Test the plan.

- a. Did the solution yield appropriate results?
- b. Can the solution be improved?

Introductory programming courses should help students gain problem solving skills while they become familiar with computers and programming languages. Palumbo [4] published a review of literature regarding the connection between

learning programming languages and problem solving skills. Palumbo discussed the transferability of the skills learned in programming courses to problem solving skills. For engineering students, learning to apply acquired skills and expertise to a new problem solving domain is a crucial benefit of programming courses.

Many techniques and tools have been used to teach programming in the last four decades. The transition from procedural languages, Fortran and Pascal, to object-oriented languages, Java and C++, has led to the increase in the number of new tools. The tools that help beginners learn to program can be classified as [5]:

- Visual programming tools.
- Narrative tools.
- Flow-model tools.
- Specialized realization tools.
- Tiered language tools.

In the following sections, we will review the challenges faced in teaching programming courses and introduce our pedagogy to overcome some of these challenges.

II. CHALLENGES OF TEACHING INTRODUCTORY PROGRAMMING COURSES

Our literature survey indicated numerous challenges instructors face while teaching programming courses [6, 7]:

- Wide variation in the students' backgrounds.
- Majority of the students find programming to be a difficult and complex cognitive task.
- Excessive amount of time spent teaching the language syntax. Spending too much time learning the syntax without context is detrimental to students' success.
- Most programming environments are also confusing as they were developed for professional software engineers, making them difficult for first year students.
- Inability to see the execution of the program before correcting the syntax and execution errors.
- Lack of motivation to learn programming, as the programming profession is considered boring by many students.

It is difficult to propose a simple solution to overcome these challenges. We will summarize some of the ideas proposed in the literature, followed by our own approach to improve teaching methods.

One of the first issues that an instructor has to make a decision about is the choice of a programming language. Teaching the syntax of the language chosen is one of the pedagogical objectives of the instructor. However, instructors should place a higher priority on improving students' problem solving and design skills. We agree with the perspective of Al-Imamy et al. [8] that the choice of programming language is less important than the issues of what to teach, how to teach it, and finding the balance between knowledge of the syntax, design skills, and problem solving skills.

The majority of the software community agrees that object-oriented programming is a good tool for teaching the fundamentals of programming. Object-oriented paradigm supports concepts, such as well-structured programming, modularization, and program design. It also supports techniques, such as programming in teams, maintenance of large systems, and software reuse, which are vital in today's business world. We believe that object-oriented programming should be taught first in the introductory programming courses. The reason for doing this is the issue of paradigm shift. Learning to program in an object-oriented style seems to be very difficult after being used to programming in a procedural style. Research shows that becoming familiar with an object-oriented language, having started out with procedural programming, may take from 6 to 18 months [9]. On the other hand, students do not seem to have as much difficulty understanding object-oriented principles when they learn them first.

Programming is central to the computing curricula. CS, CE, and CIS curricula all require instruction in computer programming. Many students in these programs perceive programming as difficult and socially isolating. Students' psychological barriers towards programming are as challenging to overcome as the technical issues we mentioned earlier. Programming courses must be redesigned to be more suitable for the new generation of students who have grown up with computers, gaming, and interactive user interfaces [10]. Students get discouraged when "programming the solution of a problem" is harder for them than "working it out in their head". Current programming environments are not designed to help the students to transform their algorithmic solution to programs.

Another issue that higher education institutes face is that women and minorities are underrepresented in programming and computer related jobs and schools. To improve their representation, new approaches are needed to teach programming courses and increase these groups' confidence in their knowledge as it influences their perseverance [11]. Whether taken at a high school or an undergraduate institution, the first programming course has a lasting effect on students. A positive course experience leaves students with good programming habits, the ability to learn on their own, and a favorable impression of programming as a profession [12].

Engineering or computer science summer programs available to middle and high school students have successfully introduced programming to these groups. Evidence shows that students participating in these programs have increased confidence in their programming ability, understand basic programming concepts, and understand the relationship between algorithms and programs [13]. The author of this paper started an initiative at St. Mary's University to have an engineering summer program in 2010 offering programming and robotics courses to high school students. This summer program introduces the engineering profession to underrepresented groups in conjunction with teaching programming and robotics.

III. OUR PEDAGOGY FOR TEACHING INTRODUCTORY PROGRAMMING COURSES

One of the most popular instructional tools for teaching programming is called Alice. Alice is a 3D interactive environment that has visual and narrative aspects. Alice is an open-source software written in Java. It supports creating animations and building virtual worlds through a user interface where the user can drag and drop basic programming blocks to create programs (Figure 1). Alice allows students to choose from many objects, such as animals or buildings, and create their virtual world based on these predefined objects. Students can create their programs by dragging the statements/expressions into the main window instead of having to write code. This mechanism helps to avoid syntax errors that are known to discourage new programmers. The interface allows students to change the properties of their objects and create their own methods and functions (Figure 2). Students can also create animations and make their virtual world interactive using keyboard and mouse inputs. The output of the program can be easily accessed anytime, without the need for compiling, by using the play button. This brings up an animation window where the student can watch his/her animation at different speeds. The visual output allows the students to see both the results of their program immediately and the building blocks of the program.

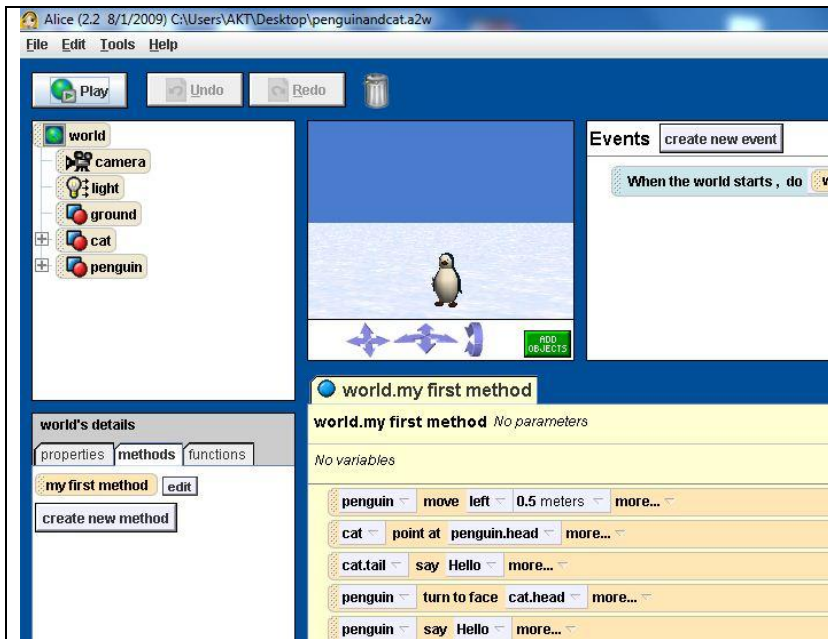


Figure 1. Alice's graphical user interface



Figure 2. Alice's method editing interface

It is well-known in education that the use of visual stimuli increases student comprehension significantly. A program's internal state and flow of execution can be represented visually by Alice [14]. The animations where characters play out a scene or a virtual world where objects respond to mouse and keyboard inputs are more appealing than text-based programs. Alice is very helpful for instructors that teach the basics of object-oriented paradigm. Students can add objects to their virtual world, add or modify properties of these objects, and create their own methods. Previous research showed that using Alice sustains student interest and involvement [15, 16]. Alice gives the students an intuitive feel for object-oriented concepts that makes the transition to object-oriented languages, such as Java and C++, easier.

We follow an inquiry-based approach where students receive basic instructions to use Alice and are expected to identify the procedures and do the implementation themselves. Programming workshops should not be strictly cookbook type practices where students have step-by-step instructions on how to select objects and choose the methods for the objects. The cookbook type instruction may result in students leaving the workshop with animations and stories without any idea of their significance and the underlying concepts. Evidence shows that students' research skills, problem solving abilities, and self-confidence in programming improve significantly with inquiry-based instruction [17].

IV. FUTURE STUDY

Our Engineering Summer Program at St. Mary's University provides us with invaluable data regarding the use of Alice software. We hold surveys for each session to record the students' opinions. We plan to do a comparative study based on our ESP survey results and our programming course surveys collected from our freshman courses. We also have plans to incorporate Alice into our beginning programming course at the freshman level. Our approach will begin with teaching object-oriented basics using Alice, followed by a transition to Java language. In our software engineering program at St. Mary's University, this introductory programming course is followed by an object-oriented design course and a higher level Java and applications course.

V. CONCLUSION

Alice is undoubtedly a useful tool for teaching introductory programming. Alice is currently being used successfully in numerous undergraduate and high school programs. However, the instructors should define the learning objectives of the course based on the object-oriented paradigm, not on Alice alone. Focusing exclusively on one tool would distract both the instructor and the students from the main objectives of a programming course. Alice is limited in terms of the applications that can be created, mainly animations and virtual worlds. Alice should be used to teach the basic concepts of programming and these concepts should be applied to high level languages, such as Java, that do not have the limitations of Alice. The transition from Alice to Java allows students to compare and repeat these fundamental concepts and strengthen their understanding. The combination of Alice and Java gives students a solid programming background and prepares them for higher level programming courses.

References

- [1] D. Gries, What should we teach in an introductory programming course? Proceedings of the Fourth SIGCSE Technical Symposium on Computer Science Education, New York, NY, 1974, 81-89.
- [2] G. Polya, How to solve it, 2nd edition (Princeton, NJ: Princeton University Press, 1957).
- [3] N. D. Barnette, W. D. McQuain, and M. A. Keenan, Programming in C++, course notes, Computer Science Department, Virginia Tech University, 1999.
- [4] D. Palumbo, Programming language/problem solving research: A review of relevant issues, Review of Educational Research, Vol. 60, 1990, 65-89.
- [5] K. Powers, P. Gross, S. Cooper, M. McNally, K. J. Goldman, V. Proulx, and M. Carlisle, Tools for teaching introductory programming: what works?, SIGCSE Bulletin, Vol. 38, 2006, 560-561.
- [6] A. Azad and F. Kohun, Considerations for Selecting a Programming Language to Teach Perspective Teachers, Alice Symposium, Duke University, Durham, NC, 2009.
- [7] D. Goulet and D. Slater, Alice and the introductory programming course: An invitation to dialogue, Information Systems Education Journal, Vol. 7, 2009.
- [8] S. Al-Imamy, J. Alizadeh, and M. A. Nour, On the development of a programming teaching tool: The effect of teaching by templates on the learning process, Journal of Information Technology Education, Vol. 5, 2006.
- [9] M. Kolling, The problem of teaching object-oriented programming, part 1: Languages, Journal of Object-Oriented Programming, Vol. 11, No. 8, 1999, 8-15.
- [10] B. McKenzie, Introductory Programming with Alice as a Gateway to the Computing Profession, Proceedings of the 23rd Annual Conference for Information Systems Educators, 2006.
- [11] B. L. Wellman, J. Davis, and M. Anderson, Alice and robotics in introductory CS courses, the Fifth Richard Tapia celebration of diversity in computing conference: intellect, initiatives, insight, and innovations, 2009, 98-102.
- [12] M. O. Pendergast, Teaching introductory programming to IS students, Journal of Information Technology Education, Vol. 5, 2006, 491-515.
- [13] B. Moskal, D. Lurie, and S. Cooper, Evaluating the effectiveness of a new instructional approach, Proceedings of the 35th SIGCSE Technical Symposium on Computer Science Education, 2004, 75-79.
- [14] D. Parsons, Programming osmosis: Knowledge transfer from imperative to visual programming environments, 20th Annual Conference of the National Advisory Committee on Computing Qualifications, 2007.
- [15] T. Wang, W. Mei, S. Lin, S. Chiu, and J. M. Lin, Teaching programming concepts to high school students with Alice, Proceedings of the 39th IEEE International Conference on Frontiers in Education Conference, 2009, 955-960.
- [16] T. Daly, Using introductory programming tools to teach programming concepts: A literature review, The Journal for Computing Teachers, 2009.
- [17] P. Brickman, C. Gormally, B. Hallar, and N. Armstrong, Effects of Inquiry-based Learning on Students' Science Literacy Skills and Confidence, International Journal for the Scholarship of Teaching and Learning, Vol. 3, No. 2, 2009.

A Survey on Authentication for Grayscale Images Based On Visual Cryptographic Technique

B. Priyanka¹, E. Purushottam,²

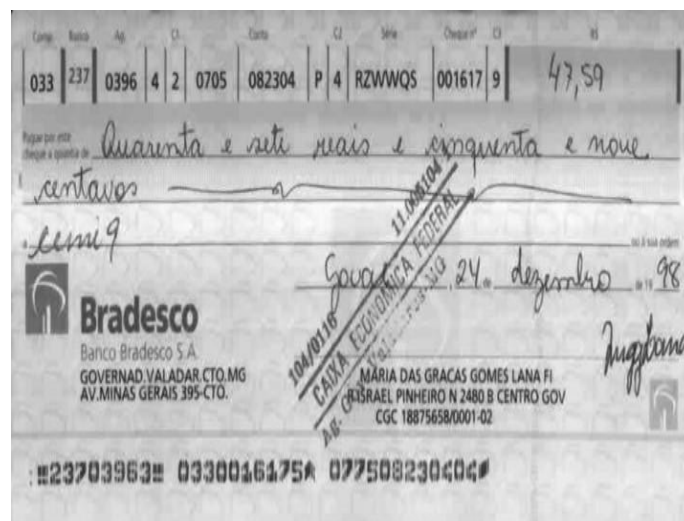
Abstract: A new digital watermarking technique as authentication method based on secret sharing sharing method for color images was proposed. The image is transformed in to binarized block form in which the watermark is embedded for authentication purpose and then the image is divided into several shares using shamir secret sharing scheme, which reconstructs the secret by using reverse Shamir secret sharing scheme and is been proceeded for authentication process i.e to check the watermark embedded in the image.

Key Words: digital watermarking, secret, Shamir secret sharing, image authentication.

I. INTRODUCTION

Digital information is a form of preserving data for which authentication is necessary to overcome the tampering attacks. In multimedia applications, it is necessary to authenticate the source image which might be subjected to tampering. So, for such content authentication watermarking technique is used. It is one among the emerging fields that are used for content authentication. As, the content authentication is being the hottest topics now a days, it is necessary to assure that the delivering of image to somewhere is delivered as it is. However, with the fast advance of digital technologies it is easy to make the modifications to the images. Thus integrity of image become a serious concern. To solve those image authentication problem particularly digitized documents, digital signatures, tables, texts, etc., whose security must be protected. In this paper we are performing image authentication of grayscale images. Grayscale image has two gray values i.e foreground and background. Grayscale images look like binary ones. So, we can call a grayscale image as binary like grayscale image. Binary image consists of two colors black and white. Using binary images can cause some problems. As the binary images are simple in nature many unpleasant strokes can encounters. So using grayscale images can solve the problem of visual quality which the binary one cannot does.

Many conventional methods have been proposed for authentication of grayscale images. In our proposed method, the image is first watermarked and divided into shares using Shamir secret sharing scheme. Later, those shares are reconstructed using inverse Shamir secret sharing scheme and watermark has been extracted if the image is authentic. Data loss during transmission are marked as gray blocks.



Grayscale cheque image

II. DIGITAL WATERMARKING

Digital watermarking is a technique for inserting a watermark into an image, which is been later extracted or detected for identification and authentication purposes. A watermark is a form of text or image that is been embedded in to the paper for its evidence of authenticity. The extension of this concept is Digital watermarking. Watermarks are of two kinds: visible and invisible. It is related to steganography but, in watermarking technique the information that is hidden is usually related to the cover object. It is used for content authentication and copyright protection.

Digital watermarking is defined as the digital signal that is embedded in audio, video or image with some information related to those and which cannot be eliminated easily.

The process to embed a watermark is done in three steps:

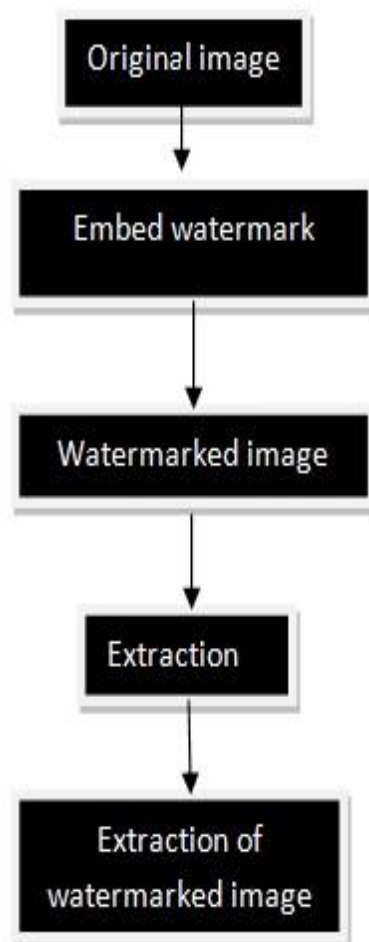
- 1. Embedding watermark:** In this algorithm it accepts the data to be embedded and produces watermark signal.
- 2. Attack on image:** The watermark signal is transmitted and during transformation the attacker may or may not modify the image. If there is a modification then it is said to be an attack.
- 3. Detection of watermark:** This algorithm is applied when the attacked signal to extract watermark from it. If the signal undergoes any modification then the information is also carried in the copy. If suppose, the signal doesn't undergo any modification the watermark is present and it can be extracted.

We first embed the watermark in to the original or cover image and make it a watermarked image and then after transformation we extract the watermark and check whether it has been undergone any sort of manipulations or attacks. Finally, we extract the watermark from the image to prove its authenticity. To avoid illegal access to the watermark a secret key as shown in the figure is used during the embedding process and extraction process of watermark.

Watermarking techniques are used for copyright protection, broadcast monitoring, authentication, tamper detection and digital finger printing, content protection, content labeling.

A watermark may be:

- 1. Robust:** As the names mentioned it is strong and overcomes several processing attacks. For example: filtering, compression
- 2. Fragile:** It is distorted under slight changes.
- 3. Semi-fragile:** It breaks under the changes performed by the user i.e exceeding specific threshold.



Block diagram of watermarking

III. SECRET SHARING METHOD

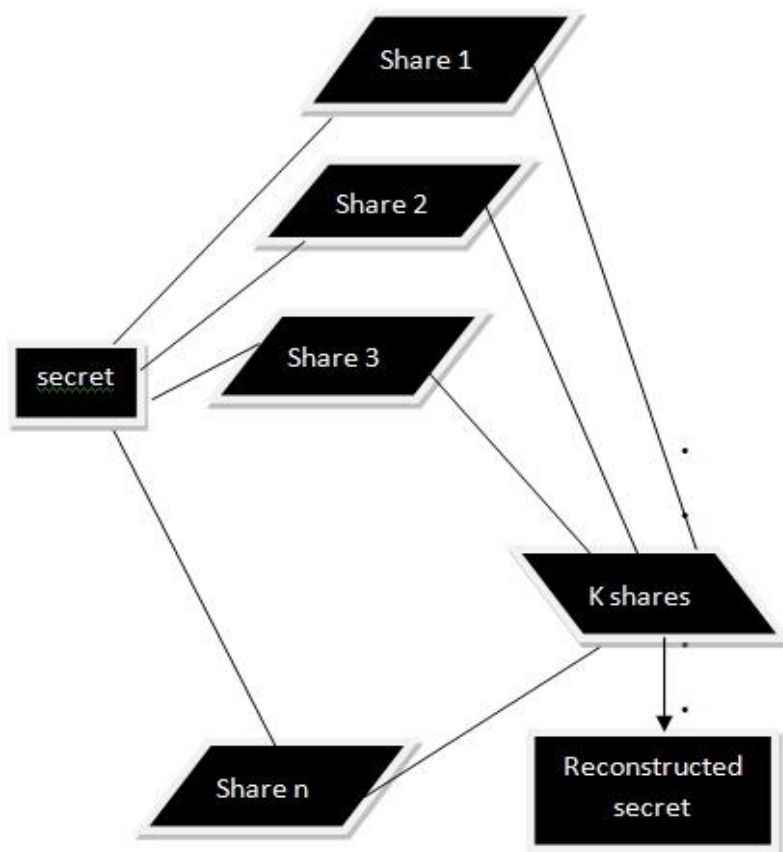
During decades some scientists (eleven) are working on a secret project. They wish to lock up the documents and details of the secret project in a cabinet so that the cabinet can be opened if and only if six or more of the scientists are present. So, What is the smallest number of locks needed to open the documents? What is the smallest number of keys to the locks each scientist must carry to view the documents?

The method of secret sharing is sharing a secret among group of participants. It is come to know that previously there are some eleven scientists who are working on a secret project for which they wanted to lockup their documents regarding the project with some secret code. So there the problem arises. They want those documents to be enclosed to the cabinet only if six or more scientists opens it with their individual secret key share. It means cabinet consisting of eleven members having their own individual unique secret key. But in order to access the documents of project a single secret share key not sufficient and at the same time it is not necessary to have all eleven secret share keys to open the documents. So for this Shamir proposed an algorithm named Shamir secret sharing algorithm where a single secret is shared among group of participants. Here participants are the authorized users who access to the data.

The algorithm goes in the following manner:

1. Divide the data d in to n pieces i.e $d_1, d_2, d_3, d_4, \dots, d_n$
2. It is distributed among n participants.
3. The secret or data can be reconstruct able only if k pieces are present.
4. Even $k-1$ pieces are not acceptable.

So he proposed a scheme called (k,n) threshold scheme. Where k is the minimal number of users or participants to reconstruct the key and n is the total number of divided pieces of data or secret. For example: a company wants to sign the checks by the executives in a digitized manner. At the same time company's signature must be secret, so the if we give the company's signature to all the executives then it is pruned to privacy attacks. So in order to solve this problem they are using (k,n) threshold scheme i.e they are putting a minimal number of key as 3 i.e $(3,n)$ they are given a magnetic card with that. The company president is given 3 keys, vice president is given 2 keys and the executive is given a single one. So in order to prune to any attacks the executive must have still 2 keys and the vice president must have still one more key.



Secret sharing method

IV. PROPOSED METHOD

Original image is authenticated by embedding a watermark which is invisible. Later, the image is divided into shares using Shamir secret sharing method and the divided shares are transferred and by using inverse Shamir secret sharing method we form the original image and the watermark is extracted from that image to authenticate.

Embedding watermark: An image A is selected form set of standard images and let it be the base image on which a watermark is embedded.

Algorithm:

- Step 1:** Let B be a grayscale image to be watermarked.
- Step 2:** Use a pseudo-random number generator with a known seed to generate a set of non repeating pseudo-random locations L within the grayscale image B .
- Step 3:** Clear all pixels of B that belong to L , obtaining B^* .
- Step 4:** Compute the fingerprint $H .H(B^*)$.
- Step 5:** perform exclusive-or H for getting the marked fingerprint H^* .
- Step 6:** Encrypt H^* with the secret key or private key thus generating the MAC/DS S .
- Step 7:** Insert S into the set of pixels L , generating the watermarked image B

Dividing the shares: We apply (k,n) threshold secret scheme for dividing the watermark image into shares. The following is the algorithm for dividing the watermark image in to shares.

Algorithm:

- Step 1:** Take secret d in the form of an integer, number n of participants, and threshold $k \leq n$.
- Step 2:** Choose a random prime number p larger than d .
- Step 3:** Select $k-1$ integer values $c_1, c_2, c_3, \dots, \dots, c_{k-1}$ range of 0 through $p-1$.
- Step 4:** Select n distinct real values $x_1, x_2, x_3, \dots, \dots, x_n$
- Step 5:** Use the following $(k-1)$ degree polynomial to compute n function values $F(x_i)$, called partial shares for $i=1,2, \dots, n$ i.e

$$F(x_i) = (d + c_1x_i + c_2x_i^2 + \dots + c_{k-1}x_i^{k-1}) \text{ mod } p$$
- Step 6:** Deliver the two-tuple $(x_i, F(x_i))$ as a share to the i participant where $i=1,2,3, \dots, n$.

Reconstructing the shares: We reconstruct the shares by applying inverse Shamir secret sharing scheme. The following is the algorithm reconstructing the watermarked image.

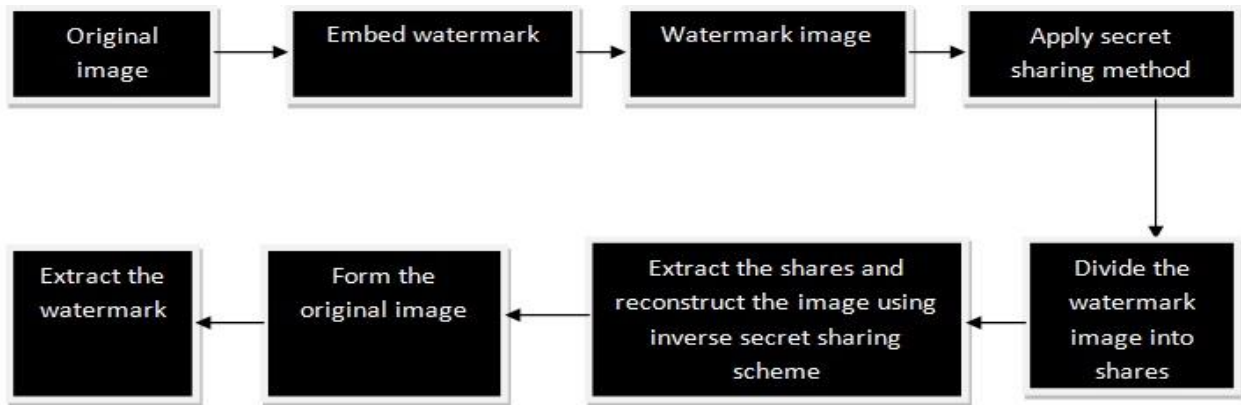
Algorithm :

- Step 1:** k shares collected from the n participants and the prime number p with both k and p
- Step 2:** Use the k shares $(x_1, F(x_1)), (x_2, F(x_2)), \dots, (x_k, F(x_k))$ to $F(x_j) = (d + c_1 + c_2x_j^2 + \dots + c_{k-1}x_j^{k-1}) \text{ mod } p$ where $j=1,2, \dots, k$
- Step 3:** Solve the k equations above by Lagrange's interpolation to obtain d as follows

$$d = (-1)^{k-1} [F(x_1) \frac{x_2 x_3 \dots x_k}{x_1 - x_2 (x_1 - x_3) \dots (x_1 - x_k)} + F(x_2) \frac{x_1 x_3 \dots x_k}{(x_2 - x_1)(x_2 - x_3) \dots (x_2 - x_k)} + \dots + F(x_k) \frac{x_1 x_2 \dots x_{k-1}}{(x_k - x_1)(x_k - x_2) \dots (x_k - x_{k-1})}] \text{ mod } p$$

Step 4: Compute c_1 through c_{k-1} by expanding the following equality and comparing the result with Step 2 while regarding variable x in the equality below to be x_j

$$F(x) = [F(x_1) \frac{(x - x_2)(x - x_3) \dots (x - x_k)}{(x_1 - x_2)(x_1 - x_3) \dots (x_1 - x_k)} + F(x_2) \frac{(x - x_1)(x - x_3) \dots (x - x_k)}{(x_2 - x_1)(x_2 - x_3) \dots (x_2 - x_k)} + \dots + F(x_k) \frac{(x - x_1)(x - x_2) \dots (x - x_{k-1})}{(x_k - x_1)(x_k - x_2) \dots (x_k - x_{k-1})}] \text{ mod } p$$

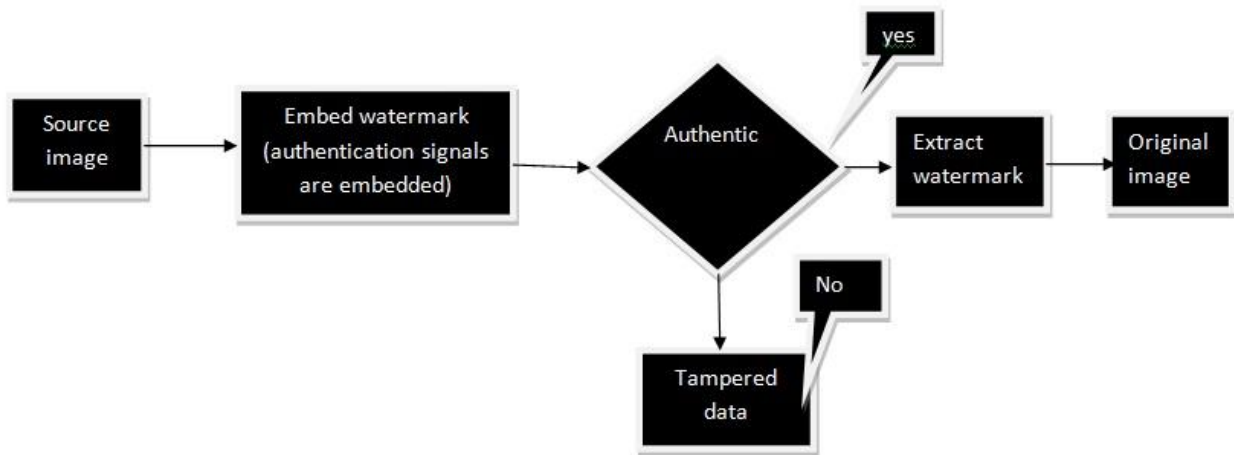


Process for authentication of grayscale cheque image

Extraction of watermark:

Algorithm:

- Step 1:** Let X be a watermarked image. Use the same pseudorandom number that has been applied in insertion process to generate again the same set of non repeating pseudo-random locations L where the watermark has been inserted.
- Step 2:** Let X^* be the image obtained from X by clearing all pixels in L . Using the same hashing function H compute the fingerprint $H.H(X^*)$.
- Step 3:** Extract the watermark from X by scanning pixels in L and decrypt the result using the secret key and obtain the decrypted data D .
- Step 4:** By applying exclusive-or H with D , obtaining the check image C .
- Step 5:** If C and A are equal, the watermark is verified. Otherwise, the image X has been modified. The following is the procedure for authentication.



V. EXPERIMENTAL RESULTS

The following are the experimental results performed on grayscale cheque image. A cover image is taken and performed the authentication process. Firstly, embed a water in to the image by using algorithm 1.



(a)



(b)

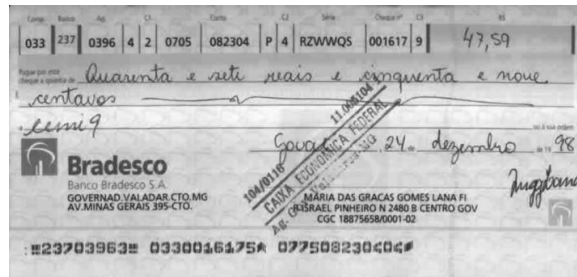
Experimental results for cheque image (a) cover image or original image (b) embedded watermark image

Later, the image is divided in to shares using Shamir secret sharing method. The shares are reconstructed using inverse Shamir secret sharing scheme and form a original or cover image. Then, check for the watermark embedded in the image. The image is said to be authentic if watermark is present. Extract the watermark. There occurs, a loss of data during the transmission process, which is marked as gray blocks as shown in the figure. If there is no data loss during transmission the original image is recovered.

The following are the figures related to the image with tampering i.e the tampering is shown in the form of gray blocks and without tampering i.e original or cover image.



(c)



(d)

(c) Image with tampering shown in the form of gray blocks (d) original or cover image without tampering.

VI. CONCLUSION

In, this paper a new image authentication using secret sharing method is proposed. The grayscale cheque image is watermarked first and that watermark is divided in to shares using Shamir secret sharing method. Later, the shares are reconstructed using inverse Shamir secret sharing scheme and the watermark is extracted. Data loss during the transmission is shown in the form of gray blocks. This can be performed for color images also.

On $G^{\#}P$ -Continuous Maps In Topological Spaces

K. Alli,¹ S. Pious missier,² A. Subramanian³

^{1,3}P.G.Department of Mathematics, The M. D. T. Hindu College, Tirunelveli, Tamil Nadu (India)-627010,

²P.G.Department of Mathematics, V. O. Chidambaram College, Thoothukudi, Tamil Nadu (India)-628008,

Abstract: The aim of this paper is to introduce and study $g^{\#}p$ -continuous maps. Basic characterizations and several properties concerning them are obtained. Further, $g^{\#}p$ -irresolute map is also defined. Some of the properties are investigated.
1991 AMS Classification: 54A05, 54D10.

Keywords: $g^{\#}$ - closed set, $g^{\#}p$ -closed set, $g^{\#}p$ -continuous maps and $g^{\#}p$ -irresolute maps.

I. INTRODUCTION

N.Levine [16] introduced the class of g -closed sets. M.K.R.S.Veerakumar introduced several generalized closed sets namely, g^* -closed sets, $g^{\#}$ -closed sets, g^*p -closed sets, g^*p -continuous maps, g^*p -irresolute maps and their properties. The authors [26] have already introduced $g^{\#}p$ -closed sets and their properties. In this paper we study the new class of map called as $g^{\#}p$ -continuous maps. Different characterizations of the introduced concepts are also found. In this direction $g^{\#}p$ -irresolute maps are defined and some of their properties are studied by giving some counter example.

II. PRELIMINARIES

Throughout this paper (X, τ) (or X) represent topological spaces on which no separation axioms are assumed unless otherwise mentioned. For a subset A of a space (X, τ) , $cl(A)$, $int(A)$ and $C(A)$ denote the closure of A , the interior of A and the complement of A respectively.

We recall the following definitions which are useful in the sequel.

Definition 2.1:

A subset A of a space (X, τ) is called

- (i) a semi-open set [17] if $A \subseteq cl(int(A))$ and a semi-closed [17] set if $int(cl(A)) \subseteq A$.
- (ii) a preopen set [21] if $A \subseteq int(cl(A))$ and a preclosed [21] set if $cl(int(A)) \subseteq A$.
- (iii) an α -open set [23] if $A \subseteq int(cl(int(A)))$ and an α -closed [23] set if $cl(int(cl(A))) \subseteq A$.
- (iv) a semi-preopen set [2] ($=\beta$ -open [1]) if $A \subseteq cl(int(cl(A)))$ and a semi-preclosed set [2] ($=\beta$ -closed [1]) if $int(cl(int(A))) \subseteq A$ and
- (v) a regular open [15] set if $A = int(cl(A))$ and a regular closed [15] set if $cl(int(A)) = A$.

The semi-closure (resp. preclosure, α -closure, semi-preclosure) of a subset A of a space (X, τ) is the intersection of all semi-closed (resp. preclosed, α -closed, semi-preclosed) sets that contain A and is denoted by $scl(A)$ (resp. $pcl(A)$, $\alpha cl(A)$, $spcl(A)$).

Definition 2.2:

A subset A of a space (X, τ) is called

- (i) a generalized closed (briefly g -closed) set [16] if $cl(A) \subseteq U$ whenever $A \subseteq U$ and U is open in (X, τ) .
- (ii) a semi-generalized closed (briefly sg -closed) set [6] if $scl(A) \subseteq U$ whenever $A \subseteq U$ and U is semi-open in (X, τ) . The complement of a sg -closed set is called a sg -open [6] set.
- (iii) a generalized semi-closed (briefly gs -closed) set [4] if $scl(A) \subseteq U$ whenever $A \subseteq U$ and U is open in (X, τ) .
- (iv) an α -generalized closed (briefly αg -closed) set [18] if $\alpha cl(A) \subseteq U$ whenever $A \subseteq U$ and U is open in (X, τ) .
- (v) a generalized α -closed (briefly $g\alpha$ -closed) set [19] if $\alpha cl(A) \subseteq U$ whenever $A \subseteq U$ and U is α -open in (X, τ) . The complement of a $g\alpha$ -closed set is called a $g\alpha$ -open [7] set.
- (vi) a generalized preclosed (briefly gp -closed) set [20] if $pcl(A) \subseteq U$ whenever $A \subseteq U$ and U is open in (X, τ) .
- (vii) a generalized semi-preclosed (briefly gsp -closed) set [10] if $spcl(A) \subseteq U$ whenever $A \subseteq U$ and U is open in (X, τ) .
- (viii) a generalized preregular closed (briefly gpr -closed) set [13] if $pcl(A) \subseteq U$ whenever $A \subseteq U$ and U is regular open in (X, τ) .
- (ix) a $g^{\#}$ -closed set [27] if $cl(A) \subseteq U$ whenever $A \subseteq U$ and U is αg -open in (X, τ) .
- (x) a g^*p -pre closed set [28] (briefly g^*p -closed) set if $pcl(A) \subseteq U$ whenever $A \subseteq U$ and U is a g -open set in (X, τ) .
- (xi) a $g^{\#}p$ -pre closed set [26] (briefly $g^{\#}p$ -closed) set if $pcl(A) \subseteq U$ whenever $A \subseteq U$ and U is a $g^{\#}$ -open set in (X, τ) .

Definition 2.3:

- A function $f: (X, \tau) \rightarrow (Y, \sigma)$ is said to be
- (i) Semi-continuous [17] if $f^{-1}(V)$ is semi-open in (X, τ) for every open set V of (Y, σ) .
 - (ii) Pre-continuous [21] if $f^{-1}(V)$ is preclosed in (X, τ) for every closed set V of (Y, σ) .
 - (iii) α -continuous [22] if $f^{-1}(V)$ is α -closed in (X, τ) for every closed set V of (Y, σ) .
 - (iv) β -continuous [1] if $f^{-1}(V)$ is semi-preopen in (X, τ) for every open set V of (Y, σ) .
 - (v) g -continuous [5] if $f^{-1}(V)$ is g -closed in (X, τ) for every closed set V of (Y, σ) .
 - (vi) sg -continuous [25] if $f^{-1}(V)$ is sg -closed in (X, τ) for every closed set V of (Y, σ) .
 - (vii) gs -continuous [8] if $f^{-1}(V)$ is gs -closed in (X, τ) for every closed set V of (Y, σ) .
 - (viii) $g\alpha$ -continuous [19] if $f^{-1}(V)$ is $g\alpha$ -closed in (X, τ) for every closed set V of (Y, σ) .
 - (ix) αg -continuous [13] if $f^{-1}(V)$ is αg -closed in (X, τ) for every closed set V of (Y, σ) .
 - (x) gsp -continuous [10] if $f^{-1}(V)$ is gsp -closed in (X, τ) for every closed set V of (Y, σ) .
 - (xi) gp -continuous [24] if $f^{-1}(V)$ is gp -closed in (X, τ) for every closed set V of (Y, σ) .
 - (xii) gpr -continuous [13] if $f^{-1}(V)$ is gpr -closed in (X, τ) for every closed set V of (Y, σ) .
 - (xiii) gc -irresolute [5] if $f^{-1}(V)$ is g -closed in (X, τ) for every g -closed set V of (Y, σ) .
 - (xiv) gp -irresolute [3] if $f^{-1}(V)$ is gp -closed in (X, τ) for every gp -closed set V of (Y, σ) .
 - (xv) gsp -irresolute [10] if $f^{-1}(V)$ is gsp -closed in (X, τ) for every gsp -closed set V of (Y, σ) .
 - (xvi) p -open [14] if $f(U)$ is preopen in (Y, σ) for every preopen set U in (X, τ) .
 - (xvii) pre- α -open [7] if $f(U)$ is α -closed in (Y, σ) for every α -closed set U in (X, τ) .
 - (xviii) $g^\#$ -continuous [27] if $f^{-1}(V)$ is $g^\#$ -closed in (X, τ) for every closed set V of (Y, σ) .
 - (xix) $g^\#$ -irresolute [27] if $f^{-1}(V)$ is $g^\#$ -closed in (X, τ) for every $g^\#$ -closed set V of (Y, σ) .
 - (xx) g^*p -continuous [28] if $f^{-1}(V)$ is g^*p -closed in (X, τ) for every closed set V of (Y, σ) .
 - (xxi) g^*p -irresolute [28] if $f^{-1}(V)$ is g^*p -closed in (X, τ) for every g^*p -closed set V of (Y, σ) .

Definition 2.4:

- A space (X, τ) is called a
- (i) $T_{1/2}$ space [16] if every g -closed set is closed.
 - (ii) semi- $T_{1/2}$ space [6] if every sg -closed set is semi-closed.
 - (iii) semi-pre- $T_{1/2}$ space [10] if every gsp -closed set is semi-preclosed.
 - (iv) preregular $T_{1/2}$ space [13] if every gpr -closed set is preclosed.
 - (v) $T_p^\#$ space [26] if every $g^\#p$ -closed set is closed.
 - (vi) $T_p^\#$ space [26] if every gp -closed set is $g^\#p$ -closed
 - (vii) $T_p^{\#\#}$ space [26] if every $g^\#p$ -closed set is $g\alpha$ -closed.
 - (viii) ${}_aT_p^\#$ space [26] if every $g^\#p$ -closed set is preclosed.
 - (ix) ${}_aT_p^{\#\#}$ space [26] if every $g^\#p$ -closed set is α -closed.

III. $g^\#$ -PRE –CONTINUOUS MAPS AND $g^\#$ -PRE- IRRESOLUTE MAPS

We introduce the following definition

Definition 3.1:

A function $f: (X, \tau) \rightarrow (Y, \sigma)$ is said to be $g^\#p$ -continuous if $f^{-1}(V)$ is a $g^\#p$ -closed set of (X, τ) for every closed set V of (Y, σ) .

Theorem 3.2:

- (i) Every pre-continuous map [resp. α -continuous, $g\alpha$ -continuous and every continuous map] is $g^\#p$ -continuous .
- (ii) Every $g^\#p$ -continuous map is gpr -continuous and gsp -continuous.

Proof: Follows from the theorem 3.02 [26]

the converse of the theorem 3.2 need not be true as can be seen from the following examples.

Example 3.3:

Let $X = \{a, b, c\} = Y, \tau = \{ \emptyset, X, \{a\}, \{a, c\} \}$ and $\sigma = \{ \emptyset, Y, \{a\}, \{b\}, \{a, b\}, \{a, c\} \}$. Define $f: (X, \tau) \rightarrow (Y, \sigma)$ by $f(a)=a, f(b)=c$ and $f(c)=b$. f is not a pre-continuous map, since $\{a, c\}$ is a closed set of (Y, σ) but $f^{-1}\{a, c\} = \{a, b\}$ is not a preclosed set of (X, τ) . But it is $g^\#p$ -continuous map.

Example 3.4:

Let $X = \{a, b, c\} = Y, \tau = \{ \emptyset, X, \{a\}, \{a, b\} \}$. Define $g: (X, \tau) \rightarrow (X, \tau)$ by $g(a)=b, g(b)=c$ and $g(c)=a$. g is not a $g^\#p$ -continuous map, since $\{b, c\}$ is a closed set of (X, τ) but $g^{-1}(\{b, c\}) = \{a, b\}$ is not a $g^\#p$ -closed set of (X, τ) . But it is gpr -continuous.

Example 3.5:

Let $X = \{a, b, c\} = Y, \tau = \{ \emptyset, X, \{a\}, \{b\}, \{a, b\} \}$ and $\sigma = \{ X, \emptyset, \{b, c\}, \{b\} \}$. Define $g: (X, \tau) \rightarrow (Y, \sigma)$ by $g(a)=a, g(b)=b$ and $g(c)=c$. g is not a $g^\#p$ -continuous map, since $\{a\}$ is a closed set of (Y, σ) but $g^{-1}(\{a\}) = \{a\}$ is not a $g^\#p$ -closed set of (X, τ) . But it is gsp -continuous.

Thus the class of $g^{\#}p$ -continuous maps properly contains the classes of pre-continuous maps, $g\alpha$ -continuous maps, α -continuous maps and the class of continuous maps. Next we show that the class of $g^{\#}p$ -continuous maps is properly contained in the classes of gpr -continuous and gsp -continuous maps.

Theorem 3.6:

- (i) $g^{\#}p$ -continuity is independent of semi-continuity and β -continuity.
- (ii) $g^{\#}p$ -continuity is independent of gs -continuity and sg -continuity.

Example 3.7:

Let $X=\{a,b,c\}=Y, \tau=\{\emptyset, X, \{a\}\}$. Define $f:(X, \tau)\rightarrow(Y, \tau)$ by $f(a)=b, f(b)=c$ and $f(c)=a$. f is $g^{\#}p$ -continuous but not β -continuity and semi-continuity maps.

Example 3.8:

Let $X=\{a,b,c\}=Y, \tau=\{\emptyset, X, \{a\}, \{b\}, \{a,b\}\}$ and $\sigma=\{\emptyset, Y, \{a,b\}\}$. Define $h:(X, \tau)\rightarrow(Y, \sigma)$ by $h(a)=c, h(b)=b$ and $h(c)=a$. h is not $g^{\#}p$ -continuous map, since $\{c\}$ is a closed set of (Y, σ) but $h^{-1}\{c\}=\{a\}$ is not a $g^{\#}p$ -closed set of (X, τ) . But it is semi-continuous and β -continuous map.

Example 3.9:

Let $X=\{a,b,c\}, \tau=\{\emptyset, X, \{a,b\}\}$. Define $\theta:(X, \tau)\rightarrow(X, \tau)$ by $\theta(a)=c, \theta(b)=b, \theta(c)=a$. θ is a $g^{\#}p$ -continuous map but it is not gs -continuous and sg -continuous.

Example 3.10:

Let X, Y, τ as in the example 3.8 and $\sigma=\{\emptyset, Y, \{a\}, \{a,c\}\}$. Define $h:(X, \tau)\rightarrow(Y, \sigma)$ by $h(a)=b, h(b)=c$ and $h(c)=a$. h is not $g^{\#}p$ -continuous map, since $\{b\}$ is a closed set of (Y, σ) but $h^{-1}\{b\}=\{a\}$ is not a $g^{\#}p$ -closed set of (X, τ) . But it is gs -continuous and sg -continuous maps.

Remark 3.11:

Composition of two $g^{\#}p$ -continuous maps need not be $g^{\#}p$ -continuous maps as seen in the following example.

Example 3.12:

Let $X=\{a,b,c\}=Y=Z, \tau=\{\emptyset, X, \{a\}, \{b\}, \{a,b\}\}$ and $\sigma=\{\emptyset, Y, \{a\}, \{a,c\}\}$ and $\eta=\{\emptyset, Z, \{a\}, \{b\}, \{a,b\}, \{a,c\}\}$. Define $f:(X, \tau)\rightarrow(Y, \sigma)$ by $f(a)=c, f(b)=a, f(c)=b$. Define $g:(Y, \sigma)\rightarrow(Z, \eta)$ by $g(a)=a, g(b)=c, g(c)=b$. Clearly f and g are $g^{\#}p$ -continuous maps. $g \circ f:(X, \tau)\rightarrow(Z, \eta)$ is not $g^{\#}p$ -continuous, since $\{b\}$ is a closed set of (Z, η) but $(g \circ f)^{-1}(\{b\})=f^{-1}(g^{-1}\{b\})=f^{-1}(\{c\})=\{a\}$ is not a $g^{\#}p$ -closed set of (X, τ) .

We introduce the following definition.

Definition 3.13:

A function $f:(X, \tau)\rightarrow(Y, \sigma)$ is said to be $g^{\#}p$ -irresolute if $f^{-1}(V)$ is a $g^{\#}p$ -closed set of (X, τ) for every $g^{\#}p$ -closed set V of (Y, σ) .

Clearly every $g^{\#}p$ -irresolute map is $g^{\#}p$ -continuous. The converse is not true as it can be seen by the following example.

Example 3.14:

Let X, Y, τ, σ and f be as in the above example 3.12. f is not $g^{\#}p$ -irresolute, since $\{c\}$ is a $g^{\#}p$ -closed set of (Y, σ) but $f^{-1}(\{c\})=\{a\}$ is not a $g^{\#}p$ -closed set of (X, τ) . But it is $g^{\#}p$ -continuous.

Theorem 3.15:

Let $f:(X, \tau)\rightarrow(Y, \sigma)$ and $g:(Y, \sigma)\rightarrow(Z, \eta)$ be any two functions. Then

- (i) $g \circ f:(X, \tau)\rightarrow(Z, \eta)$ is $g^{\#}p$ -continuous if g is continuous and f is $g^{\#}p$ -continuous.
- (ii) $g \circ f:(X, \tau)\rightarrow(Z, \eta)$ is $g^{\#}p$ -irresolute if g is $g^{\#}p$ -irresolute and f is $g^{\#}p$ -irresolute.
- (iii) $g \circ f:(X, \tau)\rightarrow(Z, \eta)$ is $g^{\#}p$ -continuous if g is $g^{\#}p$ -continuous and f is $g^{\#}p$ -irresolute.

The proof is obvious from the definitions 3.1 and 3.13.

Theorem 3.16:

Let $f:(X, \tau)\rightarrow(Y, \sigma)$ be a bijective $g^{\#}p$ -irresolute and p -open map. Then $f(A)$ is $g^{\#}p$ -closed in (Y, σ) for every $g^{\#}p$ -closed set A of (X, τ) .

Proof: Let A be a $g^{\#}p$ -closed set of (X, τ) . Let V be a $g^{\#}p$ -open set of (Y, σ) containing $f(A)$. Since f is $g^{\#}p$ -irresolute, then $f^{-1}(V)$ is a $g^{\#}p$ -open set of (X, τ) . Since $A \subseteq f^{-1}(V)$ and A is $g^{\#}p$ -closed, then $pcl(A) \subseteq f^{-1}(V)$. Then $f(pcl(A)) \subseteq V$. Then $f(pcl(A)) = pcl(f(pcl(A)))$ since f is a bijection and p -open map. Now $pcl(f(A)) \subseteq pcl(f(pcl(A))) = f(pcl(A)) \subseteq V$. Hence $f(A)$ is a $g^{\#}p$ -closed set in (Y, σ) .

Theorem 3.17:

Let $(X, \tau) \rightarrow (Y, \sigma)$ be a $g^{\#}p$ -continuous map.

- (i) If (X, τ) is a $T_p^{\#}$ space, then f is continuous.
- (ii) If (X, τ) is a $T_p^{\#\#}$ space, then f is $g\alpha$ -continuous.
- (iii) If (X, τ) is a ${}_{\alpha}T_p^{\#}$ space, then f is pre-continuous.
- (iv) If (X, τ) is a ${}_{\alpha}T_p^{\#\#}$ space, then f is α -continuous.

Theorem 3.18:

Let $(X, \tau) \rightarrow (Y, \sigma)$ be a gp -continuous map. If (X, τ) is a ${}^{\#}T_p$ space, then f is $g^{\#}p$ -continuous.

Theorem 3.19:

Let $(X, \tau) \rightarrow (Y, \sigma)$ be a gsp -continuous map. If (X, τ) is a ${}^{\#}_s T_p$ space, then f is $g^{\#}p$ -continuous.

Theorem 3.20:

Let $(X, \tau) \rightarrow (Y, \sigma)$ be onto, $g^{\#}p$ -irresolute and closed. If (X, τ) is a $T_p^{\#}$ space, then (Y, σ) is also a $T_p^{\#}$ space.
Proof: Let A be a $g^{\#}p$ -closed set of (Y, σ) . Since f is $g^{\#}p$ -irresolute, then $f^{-1}(A)$ is $g^{\#}p$ -closed in (X, τ) . Since (X, τ) is a $T_p^{\#}$ space, then $f^{-1}(A)$ is closed in (X, τ) . Since f is closed and onto, then $A = f(f^{-1}(A))$ is closed in (Y, σ) . Hence (Y, σ) is also a $T_p^{\#}$ space.

Definition 3.21:

A function $f: (X, \tau) \rightarrow (Y, \sigma)$ is said to be pre- $g^{\#}p$ -closed if $f(U)$ is $g^{\#}p$ -closed in (Y, σ) for every $g^{\#}p$ -closed set U in (X, τ) .

Definition 3.22:

A function $f: (X, \tau) \rightarrow (Y, \sigma)$ is said to be pre- $g\alpha$ -closed if $f(U)$ is $g\alpha$ -closed in (Y, σ) for every $g\alpha$ -closed set U in (X, τ) .

Theorem 3.23:

Let $(X, \tau) \rightarrow (Y, \sigma)$ be onto, $g^{\#}p$ -irresolute and pre- $g\alpha$ -closed. If (X, τ) is a $T_p^{\#\#}$ space, then (Y, σ) is also a $T_p^{\#\#}$ space.
Proof: Let A be a $g^{\#}p$ -closed set of (Y, σ) . Since f is $g^{\#}p$ -irresolute, then $f^{-1}(A)$ is $g^{\#}p$ -closed in (X, τ) . Since (X, τ) is a $T_p^{\#\#}$ space, then $f^{-1}(A)$ is $g\alpha$ -closed in (X, τ) . Since f is pre- $g\alpha$ -closed and onto, then $A = f(f^{-1}(A))$ is $g\alpha$ -closed in (Y, σ) . Hence (Y, σ) is also a $T_p^{\#\#}$ space.

Theorem 3.24:

Let $(X, \tau) \rightarrow (Y, \sigma)$ be onto, $g^{\#}p$ -irresolute and p -closed. If (X, τ) is an ${}_{\alpha}T_p^{\#}$ space, then (Y, σ) is also an ${}_{\alpha}T_p^{\#}$ space.

Theorem 3.25:

Let $(X, \tau) \rightarrow (Y, \sigma)$ be onto, $g^{\#}p$ -irresolute and pre- α -closed. If (X, τ) is an ${}_{\alpha}T_p^{\#\#}$ space, then (Y, σ) is also an ${}_{\alpha}T_p^{\#\#}$ space.

Theorem 3.26:

Let $(X, \tau) \rightarrow (Y, \sigma)$ be onto, gp -irresolute and pre- $g^{\#}p$ -closed. If (X, τ) is a ${}^{\#}T_p$ space, then (Y, σ) is also a ${}^{\#}T_p$ space.

REFERENCES

- [1] Abd El-Monsef ,M.E., El-Deeb ,S.N and Mahmud ,R.A., β -open sets and β -continuous mappings, Bull. Fac. Sci. Assiut Univ., 12 (1983), 77-90.
- [2] Andrijević,D., Semi-preopen sets, Mat. Vesnik, 38(1)(1986), 24-32.
- [3] Arockiarani,I, Balachandran, K and J.Dontchev., Some characterizations of gp -irresolute and gp -continuous maps between topological spaces, Mem. Fac. Sci. Kochi Univ. Ser.A. Math., 20 (1999), 93-104.
- [4] Arya,S.P and Nour,T., Characterizations of s -normal spaces, Indian J. Pure. Appl. Math., 21(8) (1990), 717-719.
- [5] Balachandran,K., Sundaram,P and Maki,H., On generalized continuous maps in topological spaces, Mem. Fac. Sci. Kochi Univ. Ser.A. Math., 12(1991), 5-13.
- [6] Bhattacharya ,P and Lahiri,B.K., Semi-generalized closed sets in topology, Indian J. Math., 29(3)(1987), 375-382.
- [7] Devi,R., Balachandran,K and Maki,H., Generalized α -closed maps and α -generalized closed maps, Indian J. Pure. Appl. Math., 29(1) (1998), 37-49.
- [8] Devi, R., Maki,H and Balachandran,K., Semi-generalized homeomorphisms and generalized semi-Homeomorphisms, Indian J. Pure. Appl. Math., 26 (3) (1995), 271-284.
- [9] Dontchev,J., On door spaces, Indian J. Pure. Appl. Math., 26(9)(1995), 873-881.
- [10] Dontchev,J., On generalizing semi-preopen sets, Mem. Fac. Sci. Kochi Univ. Ser.A. Math., 16 (1995), 35-48.
- [11] Dontchev, J., On some separation axioms associated with the α -topology, Mem. Fac. Sci. Kochi Univ. Ser.A. Math, 18 (1997), 31-35.
- [12] Dunham, W., $T_{1/2}$ spaces, Kyungpook Math. J., 17 (1977), 161-169.
- [13] Gnanambal, Y., On generalized preregular closed sets in topological spaces, Indian J. Pure. Appl. Math., 28(3)(1997), 351-360.
- [14] Janković,D.S., A note on mappings of extremally disconnected spaces, Acta Math. Hung., 46(1985), 83-92.
- [15] Kuratowski,C., Topology I, Hafner, New York,1958.

- [16] Levine,N., Generalized closed sets in topology, Rend. Circ. Math. Palermo, 19(2) (1970), 89-96.
- [17] Levine,N., Semi-open sets and semi-continuity in topological spaces, Amer. Math. Monthly, 70 (1963), 36-41.
- [18] Maki,H., Devi,R., and Balachandran,K., Associated topologies of generalized α -closed sets and α - generalized closed sets, Mem. Fac. Sci. Kochi Univ. Ser.A. Math., 15(1994), 51-63.
- [19] Maki,H., Devi,R., and Balachandran,K., Generalized α -closed sets in topology, Bull. Fukuoka Univ. Ed. Part III, 42 (1993), 13-21.
- [20] Maki,H., Umehara,J and Noiri,T., Every topological space is pre- $T_{1/2}$ space, Mem. Fac. Sci. Kochi Univ. Ser.A. Math., 17 (1996), 33-42.
- [21] Mashhour, A.S., Abd El-Monsef, M.E and El-Deeb,S.N., On pre-continuous and weak pre- continuous mappings, Proc. Math. and Phys. Soc. Egypt, 53(1982), 47-53.
- [22] Mashhour,A.S.,Hasanein,IA and El-Deeb,S.N., α -continuous and α -open mappings, Acta Math Hung., 41(3-4)(1983), 213-218.
- [23] Njåstad,O., On some classes of nearly open sets, Pacific J. Math., 15(1965), 961-970.
- [24] Noiri,T., Maki,H and Umehara,J., Generalized preclosed functions, Mem. Fac. Sci. Kochi Univ. Ser.A. Math., 19 (1998), 13-20.
- [25] Sundaram, P., Maki,H and Balachandran,K., Semi-generalized continuous maps and semi- $T_{1/2}$ spaces, Bull. Fukuoka Univ. Ed. Part III, 40 (1991), 33-40.
- [26] Pious Missier,S., Alli,K and Subramanian,A., $g^{\#}$ -p-closed sets in a topological spaces, IJMA (accepted).
- [27] Veera kumar, M.K.R.S., $g^{\#}$ -closed sets in topological spaces, Mem.Fac.Sci.Kochi Univ.Ser.A.Math 24(2003), 1-13.
- [28] Veera kumar, M.K.R.S., g -preclosed sets Acta ciencia Indica (Maths) Meerut XXVIII (M)(1) 2002.

A Combined Model of Bayesian Network and Spatial Markov Kernel for Multiclass Image Segmentation and Categorization

Anurekha G¹, Dr. Ramamoorthy S²

¹Final Year Student, M.Tech CSE Department, Dr.M.G.R.Educational and Research Institute University, Tamil Nadu, India

²Principal, Kodaikannal Institute of Technology, Kodaikannal, Tamil Nadu, India

Abstract: We propose a new Bayesian Network model that segments the region of interest from the image and categorize the segmented image. A Bayesian Network is constructed from an over segmentation to model the statistical dependencies among edge segments, vertices, corners and blobs. The proposed interactive image segmentation involves active user intervention for interactive image segmentation while existing interactive segmentation approaches are often passively depend on the user to provide exact intervention. Image categorization is done based on the Spatial Markov Kernel (SMK) that categorizes the segmented image.

Index Terms: Bayesian Network, Image Segmentation, Interactive image segmentation, Image Categorization, Spatial Markov Kernel algorithm

I. Introduction

For some applications, such as image recognition or compression, we cannot process the whole image directly for the reason that it is inefficient and unpractical. Image segmentation (IS) and categorization is a difficult problem in computer vision. IS aims at partitioning an image into constituent regions of interest and identify category of the segmented image. Data-driven approaches sometimes fail to produce accurate segmentation when the image contains shadow, occlusion, cluttering, low contrast area, or noise. The existing systems including the clustering method, region growing, active contours, normalized cuts [1], graph-cut-based approaches [2], Markov random fields (MRFs), etc. adopts Data-Driven approach and thus the Bayesian network model is adopted for accurate image segmentation.

The term image categorization refers to the labeling of images into one of a number of predefined categories. Although this is usually not a very difficult task for humans, it has proved to be an extremely difficult problem for machines (or computer programs). The existing works of image categorization are done with regions and colors they are low level categorization of images which doesn't offer a much accurate result when the background and the foreground are in the same color or dimension so to overcome this Spatial Markov Kernel is used.

II. Overview of the Approach

The aim of the proposed system is to segment the region of interest and categorize the segmented image based on the available dataset. The overall approach of the proposed system is clearly portrait in the flow chart diagram "Fig 1". The steps involved in this system are

1. Input the image to be segmented with the outline image. Outline image is the user intervention image that details the region to be segmented from the whole image
2. Construct the over segmented image correlating the statistical dependencies among edge segments, vertices and corners
3. Construct a Bayesian network with region, edge, vertex measurements as nodes
4. Segmentation is carried out by matching the pixels
5. If the user is satisfied with segmented output it is classified further else re-segmentation is carried out
6. The segmented output with its category is output to the user.

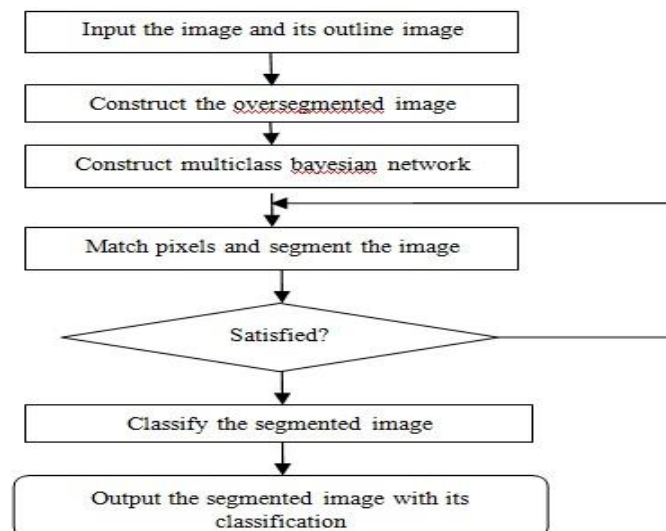


Fig 1 flow chart of proposed system

The over segmentation of the image is obtained from standard image segmentation approach like watershed segmentation [3], normalized cut, and anisotropic diffusion. In our experiment we have used watershed segmentation to obtain the over segmentation image.

III. Multiclass Image Segmentation

Multiclass image segmentation can be done in two different ways

1. We can design a series of BN models for segmenting each class versus the background. Applying these models will generate a multiclass segmentation.
2. We can extend the binary nodes (especially the region nodes) in the BN to discrete nodes with multiple states, allowing distinguishing multiple object classes.

The second method is followed in our experiments i.e. by extending the region node to discrete nodes with multiple states.

IV. Image Categorization Algorithm

1. Given a multiclass image categorization problem, the strategy of training an Support Vector Machine[4] (SVM) classifier is one against the rest for our SMK2 and one against one for our SMK1
2. we need to compute our SMK2 C times to solve an image categorization problem with C categories based on the one-against-the-rest strategy, whereas our SMK1 can be commonly adopted for all the binary classification sub problems
3. An image with $X \times Y$ blocks can be denoted as a sequence $Q = q1,1q1,2, \dots, q1,Y q2,1q2,2, \dots, q2,Y \dots, qX,Y$, where $q_{x,y} \in S$ ($1 \leq x \leq X, 1 \leq y \leq Y$) is the visual keyword automatically assigned to block (x, y) in the image.
4. Let $Q_{x,y}$ denote the sequence of states from block $(1, 1)$ to block (x, y) in a row wise raster scan on the regular grid

SMK 1:

The basic idea of defining a kernel is to map the 2-D sequence Q of an image into a high-dimensional feature space: $Q \rightarrow \Phi(Q)$. If an SMC model $\lambda^{(Q)}$ is estimated via MLE for each image (or each sequence) Q , the feature mapping Φ can be given as

$$\Phi(Q) = \lambda^{(Q)} = \{\pi^{(Q)}, H^{(Q)}, V^{(Q)}\} \quad (1)$$

That is, each sequence Q is now represented by the model parameters of an SMC.

We focus on capturing spatial dependence between states (visual keywords), we only consider the horizontal and vertical transition matrices in $\Phi(Q)$. Moreover, to make the computation more efficient, the feature mapping Φ is then defined as

$$\Phi(Q) = \{h_{ij}^{(Q)} + v_{ij}^{(Q)} / 2\}_{1 \leq i, j \leq M} \quad (2)$$

The feature mapping Φ has been defined; our SMK1 function in the feature space (determined by Φ) can be given as

$$K(Q, \tilde{Q}) = K_{\text{orig}}(\Phi(Q), \Phi(\tilde{Q})) \quad (3)$$

Where Q and \tilde{Q} are two sequences and K_{orig} can be any kind of an original kernel. In our experiments, the Gaussian kernel is used as K_{orig}

SMK 2:

Let $\lambda_0 = \{\pi_0, H_0 = \{h_{ij}^0\}_{M \times M}, V_0 = \{v_{ij}^0\}_{M \times M}\}$ be the SMC model estimated for a category. The feature mapping Φ for a sequence Q can be defined based on the following Fisher score:

$$\Phi(Q) = \frac{\partial \log P(Q|\lambda)}{\partial \lambda} \Bigg|_{\lambda=\lambda_0} \quad (4)$$

Where $\lambda = \{\pi, H, V\}$ denotes an arbitrary SMC model. Since we focus on capturing the spatial dependence between states (visual keywords), only the horizontal and vertical transition

matrices (i.e., H and V) are used to define $\Phi(Q)$ in the following. To make sure that the two transition matrices $H = \{h_{ij}\}_{M \times M}$ and $V = \{v_{ij}\}_{M \times M}$ satisfy the probability constraint conditions (i.e., $\sum_{j=1}^M h_{ij} = 1$ and $\sum_{j=1}^M v_{ij} = 1$), we take into account the following substitutions:

$$h_{ij} = e^{\alpha_{ij}} / \sum_{j'=1}^M e^{\alpha_{ij'}} \quad (5)$$

$$v_{ij} = e^{\beta_{ij}} / \sum_{j'=1}^M e^{\beta_{ij'}} \quad (6)$$

where $-\infty < \alpha_{ij}$, and $\beta_{ij} < +\infty$.

The feature mapping used by SMK1, we finally take into account the following Φ for the SMK2 function

$$\Phi(Q) = \{(\nabla_i^{(Q)} + \nabla_{\beta_{ij}}^{(Q)})/2\}_{1 \leq i, j \leq m} \quad (7)$$

V. Experimental Setup

Our proposed model is implemented by MATLAB version 7 and tested. An example with the jaguar image is given below. The outline image is given as input along the jaguar image for segmentation fig (3) and fig (2).



Fig 2: input image

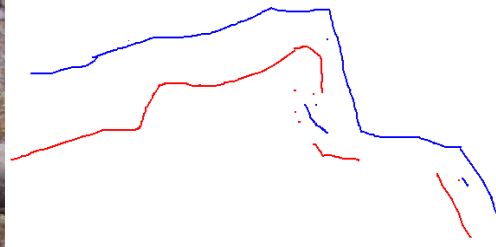


Fig 3: outline image

The user intervention i.e. the region to segment is given through the outline image. The region above the blue colored lines are ignored and the pixels that matches with the blue line is considered and segmentation is carried out. Initially the oversegmented image is generated. Outline image over oversegmented image and oversegmented image is shown in the fig (4) and fig (5) respectively

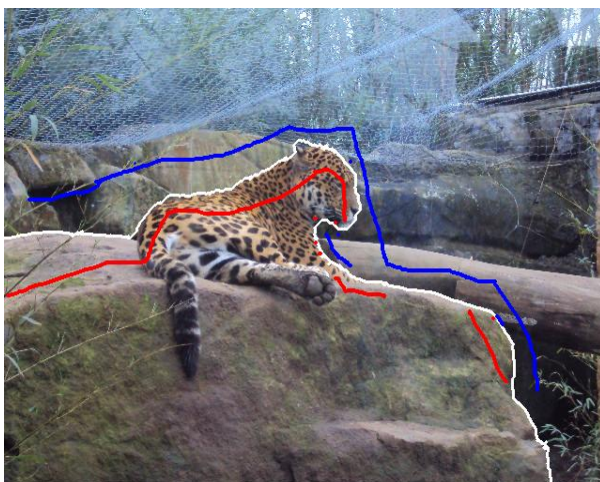


Fig 4: outline over oversegmented image

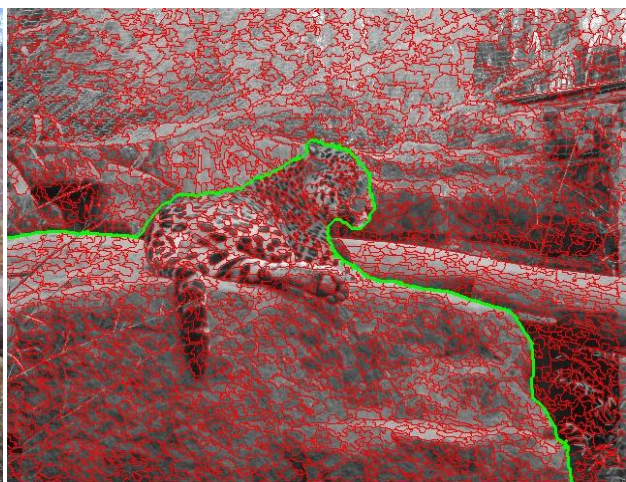


Fig 5: oversegmented image

The fig(6) and fig(7) shows the segmented region and its background region which is the required output of our system.



Fig 6: Segmented image



Fig 7: Background image

The segmented image is then categorized based on the information available in the database. The output after the segmented image categorization is given in fig (8)



The image is categorized as
Jaguar
Rock
Grass

Fig 8: Output image

VI. Conclusion

In this paper, we first propose a Multiclass image segmentation with image categorization based on Bayesian Network. The Bayesian Network systematically encodes the relationships among regions, edge segments, vertices, angles, and their measurements. The advantages of our proposed system is

1. Implementation of multiclass image segmentation and categorization.
2. It provides a systematic way to model the image segmentation problem in a probabilistic manner.
3. It is very convenient to incorporate new knowledge into the model due to the expressive and inference power of Bayesian Networks.
4. The user's intervention can be easily incorporated into the Bayesian Network as new evidence in an incremental way unlike other IS methods

The accuracy obtained by our model is 93.5%. Finally, although our model focuses on Multiclass Image segmentation and categorization the model is designed for dataset other than medical images which will be studied in our future along with the connectivity constraints.

References

- [1] J. Shi and J. Malik, "Normalized cuts and image segmentation," *IEEE Trans. Pattern Anal. Mach. Intell.*, vol. 22, no. 8, pp. 888–905, Aug.2000.
- [2] D. Freedman and T. Zhang, "Interactive graph cut based segmentation with shape priors," in *Proc. IEEE Conf. Comput. Vis. Pattern Recognit.*, 2005, pp. 755–762.
- [3] L. Vincent and P. Soille, "Watersheds in digital spaces: An efficient algorithm based on immersion simulations," *IEEE Trans. Pattern Anal. Mach. Intell.*, vol. 13, no. 6, pp. 583–598, Jun. 1991.
- [4] S. Tong and D. Koller, "Support vector machine active learning with applications to text classification," *J. Mach. Learning Res.*, vol. 2, pp. 45–66, 2000.
- [5] E. Mortensen and J. Jia, "A Bayesian network framework for real-time object selection," in *Workshop Percept. Org. Comput. Vis.*, 2004, p. 44.
- [6] A. Vailaya, M. Figueiredo, A. Jain, and H.-J. Zhang, "Image classification for content-based indexing," *IEEE Trans. Image Process.*, vol. 10, no. 1, pp. 117–130, Jan. 2001.

The (G'/G) - Expansion Method for Finding Traveling Wave Solutions of Some Nonlinear Pdes in Mathematical Physics

J.F.Alzaidy

Mathematics Department, Faculty of Science, Taif University, Kingdom of Saudi Arabia

Abstract: In the present paper, we construct the traveling wave solutions involving parameters of some nonlinear PDEs in mathematical physics; namely the variable coefficients KdV (vcKdV) equation, the modified dispersive water wave (MDWW) equations and the symmetrically coupled KdV equations by using a simple method which is called the $\left(\frac{G'}{G}\right)$ -expansion method, where $G = G(\xi)$ satisfies the second order linear ordinary differential equation. When the parameters are taken special values, the solitary waves are derived from the traveling waves. The traveling wave solutions are expressed by hyperbolic, trigonometric and rational functions. This method is more powerful and will be used in further works to establish more entirely new solutions for other kinds of nonlinear PDEs arising in mathematical physics.

Keywords: The (G'/G) expansion method; traveling wave solutions; the variable coefficients KdV (vcKdV) equation; the modified dispersive water wave (MDWW) equations; symmetrically coupled KdV equations, solitary wave solutions.

AMS Subject Classifications: 35K99; 35P05; 35P99.

I. Introduction

In recent years, the exact solutions of nonlinear PDEs have been investigated by many authors (see for example [1-30]) who are interested in nonlinear physical phenomena. Many effective methods have been presented ,such as inverse scattering transform method [1], Bäcklund transformation [2], Darboux transformation [3], Hirota bilinear method [4], variable separation approach [5], various tanh methods [6–9], homogeneous balance method [10] , similarity reductions method [11,12] , the reduction mKdV equation method [13], the tri-function method [14,15], the projective Riccati equation method [16], the Weierstrass elliptic function method [17], the Sine- Cosine method [18,19], the Jacobi elliptic function expansion [20,21], the complex hyperbolic function method [22], the truncated Painlevé expansion [23], the F-expansion method [24], the rank analysis method [25] and so on.

In the present paper, we shall use a simple method which is called the $\left(\frac{G'}{G}\right)$ -expansion method [26,27]. This method is firstly proposed by the Chinese Mathematicians Wang et al [28] for which the traveling wave solutions of nonlinear equations are obtained. The main idea of this method is that the traveling wave solutions of nonlinear equations can be expressed by a polynomial in $\left(\frac{G'}{G}\right)$, where $G = G(\xi)$ satisfies the second order linear ordinary differential equation $G''(\xi) + \lambda G'(\xi) + \mu G(\xi) = 0$, where $\xi = k(x - ct)$, where λ, μ, k and c are constants . The degree of this polynomial can be determined by considering the homogeneous balance between the highest order derivatives and the nonlinear terms appearing in the given nonlinear equations .The coefficients of this polynomial can be obtained by solving a set of algebraic equations resulted from the process of using the proposed method. This new method will play an important role in expressing the traveling wave solutions for nonlinear evolution equations via the vcKdV equation, the MDWW equations and the symmetrically coupled KdV equations in terms of hyperbolic, trigonometric and rational functions.

II. Description of the $\left(\frac{G'}{G}\right)$ - expansion method

Suppose we have the following nonlinear PDE:

$$P(u, u_t, u_x, u_{tt}, u_{xx}, u_{xt}, \dots) = 0, \quad (1)$$

Where $u = u(x, t)$ is an unknown function, P is a polynomial in $u = u(x, t)$ and its various partial derivatives in which the highest order derivatives and nonlinear terms are involved. In the following we give the main steps of a deformation method:

Setp1. Suppose that

$$u(x, t) = u(\xi), \quad \xi = \xi(x, t). \quad (2)$$

The traveling wave variable (2) permits us reducing (1) to an ODE for $u = u(\xi)$ in the form:

$$P(u, u', u'', \dots) = 0, \quad (3)$$

where $' = \frac{d}{d\xi}$.

Setp2. Suppose that the solution Eq.(3) can be expressed by a polynomial in $\left(\frac{G'}{G}\right)$ as follows:

$$u(\xi) = \sum_{i=0}^n a_i \left(\frac{G'}{G}\right)^i, \tag{4}$$

While $G = G(\xi)$ satisfies the second order linear differential equation in the form:

$$G''(\xi) + \lambda G'(\xi) + \mu G(\xi) = 0, \tag{5}$$

Where $a_i (i = 0, 1, \dots, n)$, λ and μ are constants to be determined later.

Setp3. The positive integer " n " can be determined by considering the homogeneous balance between the highest derivative term and the nonlinear terms appearing in Eq.(3). Therefore, we can get the value of n in Eq.(4).

Setp4. Substituting Eq.(4) into Eq.(3) and using Eq.(5), collecting all terms with the same power of $\left(\frac{G'}{G}\right)$ together and then equating each coefficient of the resulted polynomial to zero, yield a set of algebraic equations for a_i, λ, μ, c and k .

Setp5. Solving the algebraic equations by use of Maple or Mathematica, we obtain values for a_i, λ, μ, c and k .

Setp6. Since the general solutions of Eq. (5) have been well known for us, then substituting the obtained coefficients and the general solution of Eq. (5) into Eq. (4), we have the travelling wave solutions of the nonlinear PDE (1).

III. Applications of the method

In this section, we apply the $\left(\frac{G'}{G}\right)$ -expansion method to construct the traveling wave solutions for some nonlinear PDEs, namely the cvKdV equation, the MDWW equations and the symmetrically coupled KdV equations which are very important nonlinear evolution equations in mathematical physics and have been paid attention by many researchers.

3.1. Example1. The cvKdV equation

We start with the cvKdV equation [29] in the form:

$$u_t + f(t)uu_x + g(t)u_{xxx} = 0, \tag{6}$$

Where $f(t) \neq 0, g(t) \neq 0$ are some given functions. This equation is well-known as a model equation describing the propagation of weakly-nonlinear weakly-dispersive waves in inhomogeneous media.. Obtaining exact solutions for non-linear differential equations have long been one of the central themes of perpetual interest in mathematics and physics. To study the travelling wave solutions of Eq. (6), we take the following transformation

$$u(x, t) = u(\xi), \quad \xi = x + \frac{\omega}{\alpha} \int_0^t g(\hat{t}) d\hat{t}, \tag{7}$$

Where ω the wave is speed and α is a constant. By using Eq. (7), Eq.(6) is converted into an ODE

$$\frac{\omega}{\alpha} u' + 2uu' + u''' = 0, \tag{8}$$

Where the functions $f(t)$ and $g(t)$ in Eq.(6) should satisfy the condition

$$f(t) = 2g(t). \tag{9}$$

Integrating Eq.(8) with respect to ξ once and taking the constant of integration to be zero, we obtain

$$\frac{\omega}{\alpha} u + u^2 + u'' = 0, \tag{10}$$

Suppose that the solution of ODE (10) can be expressed by polynomial in terms of $\left(\frac{G'}{G}\right)$ as follows:

$$u(\xi) = \sum_{i=0}^n a_i \left(\frac{G'}{G}\right)^i, \tag{11}$$

Where $a_i (i = 0, 1, \dots, n)$ are arbitrary constants, while $G(\xi)$ satisfies the second order linear ODE (5). Considering the homogeneous balance between the highest order derivatives and the nonlinear terms in Eq. (10), we get $n = 2$. Thus, we have

$$u(\xi) = a_0 + a_1 \left(\frac{G'}{G}\right) + a_2 \left(\frac{G'}{G}\right)^2, \tag{12}$$

Where a_0, a_1 and a_2 are constants to be determined later. Substituting Eq.(12) with Eq.(5) into Eq.(10) and collecting all terms with the same power of $\left(\frac{G'}{G}\right)$. Setting each coefficients of this polynomial to be zero, we have the following system of algebraic equations:

$$\begin{aligned}
 \left(\frac{G'}{G}\right)^0 &: \frac{\omega a_0}{\alpha} + a_0^2 + \lambda \mu a_1 + 2\mu^2 a_2 = 0, \\
 \left(\frac{G'}{G}\right)^1 &: \lambda^2 a_1 + 2\mu a_1 + \frac{\omega a_1}{\alpha} + 2a_0 a_1 + 6\lambda \mu a_2 = 0, \\
 \left(\frac{G'}{G}\right)^2 &: 3\lambda a_1 + a_1^2 + 4\lambda^2 a_2 + 8\mu a_2 + \frac{\omega a_2}{\alpha} + 2a_0 a_2 = 0, \\
 \left(\frac{G'}{G}\right)^3 &: 2a_1 + 10\lambda a_2 + 2a_1 a_2 = 0, \\
 \left(\frac{G'}{G}\right)^4 &: 6a_2 + a_2^2 = 0,
 \end{aligned} \tag{13}$$

On solving the above algebraic Eqs. (13) By using the Maple or Mathematica, we have

$$a_0 = -6\mu, \quad a_1 = -6\lambda, \quad a_2 = -6, \quad \omega = -\alpha M, \tag{14}$$

Where $M = \lambda^2 - 4\mu$.

Substituting Eq. (14) into Eq.(12) yields

$$u(\xi) = -6\mu - 6\lambda \left(\frac{G'}{G}\right) - 6 \left(\frac{G'}{G}\right)^2, \tag{15}$$

Where

$$\xi = x - M \int_0^t g(\hat{t}) d\hat{t}. \tag{16}$$

On solving Eq.(5), we deduce that

$$\frac{G'}{G} = \begin{cases} \frac{1}{2}\sqrt{M} \left(\frac{A \cosh\left(\frac{1}{2}\sqrt{M}\xi\right) + B \sinh\left(\frac{1}{2}\sqrt{M}\xi\right)}{A \sinh\left(\frac{1}{2}\sqrt{M}\xi\right) + B \cosh\left(\frac{1}{2}\sqrt{M}\xi\right)} \right) - \frac{\lambda}{2} & \text{if } M > 0, \\ \frac{1}{2}\sqrt{-M} \left(\frac{-A \sin\left(\frac{1}{2}\sqrt{-M}\xi\right) + B \cos\left(\frac{1}{2}\sqrt{-M}\xi\right)}{A \cos\left(\frac{1}{2}\sqrt{-M}\xi\right) + B \sin\left(\frac{1}{2}\sqrt{-M}\xi\right)} \right) - \frac{\lambda}{2} & \text{if } M < 0, \\ \frac{B}{B\xi + A} - \frac{\lambda}{2} & \text{if } M = 0, \end{cases} \tag{17}$$

Where A and B are arbitrary constants and $M = \lambda^2 - 4\mu$.

On substituting Eq.(17) into Eq.(15), we deduce the following three types of traveling wave solutions:

Case1. If $M > 0$, Then we have the hyperbolic solution

$$u(\xi) = \frac{3M}{2} \left[1 - \left(\frac{A \cosh\left(\frac{1}{2}\sqrt{M}\xi\right) + B \sinh\left(\frac{1}{2}\sqrt{M}\xi\right)}{A \sinh\left(\frac{1}{2}\sqrt{M}\xi\right) + B \cosh\left(\frac{1}{2}\sqrt{M}\xi\right)} \right)^2 \right], \tag{18}$$

Case2. If $M < 0$, Then we have the trigonometric solution

$$u(\xi) = \frac{3M}{2} \left[1 + \left(\frac{-A \sin\left(\frac{1}{2}\sqrt{-M}\xi\right) + B \cos\left(\frac{1}{2}\sqrt{-M}\xi\right)}{A \cos\left(\frac{1}{2}\sqrt{-M}\xi\right) + B \sin\left(\frac{1}{2}\sqrt{-M}\xi\right)} \right)^2 \right], \tag{19}$$

Case3. If $M = 0$, Then we have the the rational solution

$$u(\xi) = \frac{3}{2}\lambda^2 - 6 \left[\mu + \left(\frac{B}{B\xi + A} \right)^2 \right], \tag{20}$$

In particular, if we set $B = 0, A \neq 0, \lambda > 0, \mu = 0$, in Eq.(18), then we get

$$u(\xi) = -\frac{3\lambda^2}{2} \operatorname{csch}^2\left(\frac{\lambda}{2}\xi\right), \tag{21}$$

While, if $B \neq 0, \lambda > 0, A^2 > B^2$ and $\mu = 0$, then we deduce that:

$$u(\xi) = \frac{3\lambda^2}{2} \operatorname{sech}^2\left(\frac{\lambda}{2}\xi + \xi_0\right), \tag{22}$$

Where $\xi_0 = \tanh^{-1}\left(\frac{A}{B}\right)$. The solutions (21) and (22) represent the solitary wave solutions of Eq. (6).

3.2. Example 2. The MDWW equation

In this subsection, we study the MDWW equations [30] in the forms:

$$u_t = -\frac{1}{4}v_{xx} + \frac{1}{2}(uv)_x, \tag{23}$$

$$v_t = -u_{xx} - 2uu_x + \frac{3}{2}vv_x. \tag{24}$$

The traveling wave variables below

$$u(x, t) = u(\xi), \quad v(x, t) = v(\xi), \quad \xi = k(x + \omega t), \tag{25}$$

permit us converting the equations (23) and (24) into ODEs for $u(x, t) = u(\xi)$ and $v(x, t) = v(\xi)$ as follows:

$$-\frac{1}{4}kv'' + \frac{1}{2}(uv)' - \omega u' = 0, \tag{26}$$

$$-ku'' - 2uu' + \frac{3}{2}vv' - \omega v' = 0, \tag{27}$$

Where k and ω are the wave number and the wave speed, respectively. On integrating Eqs.(26) and (27) with respect to ξ once, yields

$$k_1 - \frac{1}{4}kv' + \frac{1}{2}(uv) - \omega u = 0, \tag{28}$$

$$k_2 - ku' - u^2 + \frac{3}{4}v^2 - \omega v = 0, \tag{29}$$

Where k_1 and k_2 is an integration constants.

Suppose that the solutions of the ODEs (28) and (29) can be expressed by polynomials in terms of $\left(\frac{G'}{G}\right)$ as follows:

$$u(\xi) = \sum_{i=0}^n a_i \left(\frac{G'}{G}\right)^i, \tag{30}$$

$$v(\xi) = \sum_{i=0}^m b_i \left(\frac{G'}{G}\right)^i. \tag{31}$$

Where $a_i (i = 0, 1, \dots, n)$ and $b_i (i = 0, 1, \dots, m)$ are arbitrary constants, while $G(\xi)$ satisfies the second order linear ODE (5). Considering the homogeneous balance between the highest order derivatives and the nonlinear terms in Eqs.(28) and (29), we get $n = m = 1$. Thus, we have

$$u(\xi) = a_0 + a_1 \left(\frac{G'}{G}\right), \quad a_1 \neq 0, \tag{32}$$

$$v(\xi) = b_0 + b_1 \left(\frac{G'}{G}\right), \quad b_1 \neq 0, \tag{33}$$

Where a_0, a_1, b_0 and b_1 are arbitrary constants to be determined later. Substituting Eqs.(32),(33) with Eq.(5) into Eqs.(28) and (29), collecting all terms with the same power of $\left(\frac{G'}{G}\right)$ and setting them to zero, we have the following system of algebraic equations:

$$\left(\frac{G'}{G}\right)^0 : \omega a_0 + \frac{a_0 b_0}{2} + \frac{1}{4}k\mu b_1 + k_1 = 0,$$

$$\left(\frac{G'}{G}\right)^1 : \omega a_1 + \frac{a_1 b_0}{2} + \frac{1}{4}k\lambda b_1 + \frac{a_0 b_1}{2} = 0,$$

$$\left(\frac{G'}{G}\right)^2 : \frac{kb_1}{4} + \frac{a_1 b_1}{2} = 0,$$

$$\begin{aligned} \left(\frac{G'}{G}\right)^0 &: -a_0^2 + k\mu a_1 + \omega b_0 + \frac{3b_0^2}{4} + k_2 = 0, \\ \left(\frac{G'}{G}\right)^1 &: k\lambda a_1 - 2a_0 a_1 + \omega b_1 + \frac{3b_0 b_1}{2} = 0, \\ \left(\frac{G'}{G}\right)^2 &: k a_1 - a_1^2 + \frac{3b_1^2}{4} = 0. \end{aligned} \tag{34}$$

Solving the above algebraic Eqs.(34) by using the Maple or Mathematica, yields

$$\begin{aligned} a_0 &= \frac{1}{2}(\lambda a_1 - \omega), & a_1 &= a_1, & b_0 &= \lambda a_1 - \omega, & b_1 &= 2a_1, \\ k_1 &= \frac{1}{4}(\omega^2 - M a_1^2), & k_1 &= \frac{1}{2}(\omega^2 - M a_1^2), & k &= -2a_1. \end{aligned} \tag{35}$$

Substituting Eq.(35) into Eqs.(32) and (33) we obtain

$$u(\xi) = \frac{1}{2}(\lambda a_1 - \omega) + a_1 \left(\frac{G'}{G}\right), \tag{36}$$

$$v(\xi) = \lambda a_1 - \omega + 2a_1 \left(\frac{G'}{G}\right), \tag{37}$$

where

$$\xi = -2a_1(x + \omega t). \tag{38}$$

From Eqs.(17),(36) and (37), we deduce the following three types of traveling wave solutions:

Case1. If $M > 0$, then we have the hyperbolic solution

$$u(\xi) = \frac{1}{2} \left[a_1 \sqrt{M} \left(\frac{A \cosh\left(\frac{1}{2}\sqrt{M}\xi\right) + B \sinh\left(\frac{1}{2}\sqrt{M}\xi\right)}{A \sinh\left(\frac{1}{2}\sqrt{M}\xi\right) + B \cosh\left(\frac{1}{2}\sqrt{M}\xi\right)} \right) - \omega \right], \tag{39}$$

$$v(\xi) = a_1 \sqrt{M} \left(\frac{A \cosh\left(\frac{1}{2}\sqrt{M}\xi\right) + B \sinh\left(\frac{1}{2}\sqrt{M}\xi\right)}{A \sinh\left(\frac{1}{2}\sqrt{M}\xi\right) + B \cosh\left(\frac{1}{2}\sqrt{M}\xi\right)} \right) - \omega. \tag{40}$$

Case2. If $M < 0$, then we have the trigonometric solution

$$u(\xi) = \frac{1}{2} \left[a_1 \sqrt{-M} \left(\frac{-A \sin\left(\frac{1}{2}\sqrt{-M}\xi\right) + B \cos\left(\frac{1}{2}\sqrt{-M}\xi\right)}{A \cos\left(\frac{1}{2}\sqrt{-M}\xi\right) + B \sin\left(\frac{1}{2}\sqrt{-M}\xi\right)} \right) - \omega \right], \tag{41}$$

$$v(\xi) = a_1 \sqrt{-M} \left(\frac{-A \sin\left(\frac{1}{2}\sqrt{-M}\xi\right) + B \cos\left(\frac{1}{2}\sqrt{-M}\xi\right)}{A \cos\left(\frac{1}{2}\sqrt{-M}\xi\right) + B \sin\left(\frac{1}{2}\sqrt{-M}\xi\right)} \right) - \omega. \tag{42}$$

Case3. If $M = 0$, then we have the rational solution

$$u(\xi) = a_1 \left(\frac{B}{B\xi + A} \right) - \frac{\omega}{2}, \tag{43}$$

$$v(\xi) = 2a_1 \left(\frac{B}{B\xi + A} \right) - \omega. \tag{44}$$

In particular if $B = 0$, $A \neq 0$, $\lambda > 0$ and $\mu = 0$, then we deduce from Eqs.(39) and (40) that:

$$u(\xi) = \frac{1}{2} \left[a_1 \lambda \coth\left(\frac{\lambda}{2}\xi\right) - \omega \right], \tag{45}$$

$$v(\xi) = a_1 \lambda \coth\left(\frac{\lambda}{2}\xi\right) - \omega, \tag{46}$$

While, if $B \neq 0$, $A^2 > B^2$, $\lambda > 0$ and $\mu = 0$, then we deduce that:

$$u(\xi) = \frac{1}{2} \left[a_1 \lambda \tanh\left(\frac{\lambda}{2}\xi + \xi_0\right) - \omega \right], \tag{47}$$

$$v(\xi) = a_1 \lambda \tanh\left(\frac{\lambda}{2} \xi + \xi_0\right) - \omega, \tag{48}$$

Where $\xi_0 = \tanh^{-1}\left(\frac{A}{B}\right)$. The solutions (45)- (48) represent the solitary wave solutions of Eqs.(23) and (24).

3.3. Example 3. The symmetrically coupled KdV equations

In this subsection, we consider the symmetrically coupled KdV equations [31] in the forms:

$$u_t = u_{xxx} + v_{xxx} + 6uu_x + 4uv_x + 2u_x v = 0, \tag{49}$$

$$v_t = u_{xxx} + v_{xxx} + 6vv_x + 4vu_x + 2v_x u = 0. \tag{50}$$

The traveling wave variable (25) permits us converting Eqs.(49) and (50) into the following ODEs:

$$-\omega u' + k^2(u''' + v''') + 6uu' + 4uv' + 2u'v = 0, \tag{51}$$

$$-\omega v' + k^2(u''' + v''') + 6vv' + 4vu' + 2v'u = 0. \tag{52}$$

Considering the homogeneous balance between highest order derivatives and nonlinear terms in Eqs.(51) and (52), we have

$$u(\xi) = a_0 + a_1 \left(\frac{G'}{G}\right) + a_2 \left(\frac{G'}{G}\right)^2, \quad a_2 \neq 0, \tag{53}$$

$$v(\xi) = b_0 + b_1 \left(\frac{G'}{G}\right) + b_2 \left(\frac{G'}{G}\right)^2, \quad b_2 \neq 0, \tag{54}$$

Where a_0, a_1, a_2, b_0, b_1 and b_2 are arbitrary constants to be determined later. Substituting Eqs.(53) and (54) with Eq.(5) into Eqs.(51) and (52), collecting all terms with the same power of $\left(\frac{G'}{G}\right)$ and setting them to zero, we have the following system of algebraic equations:

$$\begin{aligned} \left(\frac{G'}{G}\right)^0 : & -k^2 \lambda^2 \mu a_1 - 2k^2 \mu^2 a_1 + \mu \omega a_1 - 6\mu a_0 a_1 - 6k^2 \lambda \mu^2 a_2 - k^2 \lambda^2 \mu b_1 - 2k^2 \mu^2 b_1 - 4\mu a_0 b_1 - 6k^2 \lambda \mu^2 b_2 = 0, \\ \left(\frac{G'}{G}\right)^1 : & -k^2 \lambda^3 a_1 - 8k^2 \lambda \mu a_1 + \lambda \omega a_1 - 6\lambda a_0 a_1 - 6\mu a_1^2 - 14k^2 \lambda^2 \mu a_2 - 16k^2 \mu^2 a_2 + 2\mu \omega a_2 - 12\mu a_0 a_2 - k^2 \lambda^3 b_1 - \\ & 8k^2 \lambda \mu b_1 - 4\lambda a_0 b_1 - 6\mu a_1 b_1 - 14k^2 \lambda^2 \mu b_2 - 16k^2 \mu^2 b_2 - 8\mu a_0 b_2 = 0, \\ \left(\frac{G'}{G}\right)^2 : & -7k^2 \lambda^2 a_1 - 8k^2 \mu a_1 + \omega a_1 - 6a_0 a_1 - 6\lambda a_1^2 - 8k^2 \lambda^3 a_2 - 52k^2 \lambda \mu a_2 + 2\lambda \omega a_2 - 12\lambda a_0 a_2 - 18\mu a_1 a_2 - \\ & 7k^2 \lambda^2 b_1 - 8k^2 \mu b_1 - 4a_0 b_1 - 6\lambda a_1 b_1 - 8\mu a_2 b_1 - 8k^2 \lambda^3 b_2 - 52k^2 \lambda \mu b_2 - 8\lambda a_0 b_2 - 10\mu a_1 b_2 = 0, \\ \left(\frac{G'}{G}\right)^3 : & -12k^2 \lambda a_1 - 6a_1^2 - 38k^2 \lambda^2 a_2 - 40k^2 \mu a_2 + 2\omega a_2 - 12a_0 a_2 - 18\lambda a_1 a_2 - 12\mu a_2^2 - 12k^2 \lambda b_1 - 6a_1 b_1 - \\ & 8\lambda a_2 b_1 - 38k^2 \lambda^2 b_2 - 40k^2 \mu b_2 - 8a_0 b_2 - 10\lambda a_1 b_2 - 12\mu a_2 b_2 = 0, \\ \left(\frac{G'}{G}\right)^4 : & -6k^2 a_1 - 54k^2 \lambda a_2 - 18a_1 a_2 - 12\lambda a_2^2 - 6k^2 b_1 - 8a_2 b_1 - 54k^2 \lambda b_2 - 10a_1 b_2 - 12\lambda a_2 b_2 = 0, \\ \left(\frac{G'}{G}\right)^5 : & -24k^2 a_2 - 12a_2^2 - 24k^2 b_2 - 12a_2 b_2 = 0, \\ \left(\frac{G'}{G}\right)^0 : & -k^2 \lambda^2 \mu a_1 - 2k^2 \mu^2 a_1 - 6k^2 \lambda \mu^2 a_2 - k^2 \lambda^2 \mu b_1 - 2k^2 \mu^2 b_1 + \mu \omega b_1 - 2\mu a_0 b_1 - 6k^2 \lambda \mu^2 b_2 = 0, \\ \left(\frac{G'}{G}\right)^1 : & -k^2 \lambda^3 a_1 - 8k^2 \lambda \mu a_1 - 14k^2 \lambda^2 \mu a_2 - 16k^2 \mu^2 a_2 - k^2 \lambda^3 b_1 - 8k^2 \lambda \mu b_1 + \lambda \omega b_1 - 2\lambda a_0 b_1 - 6\mu a_1 b_1 - 6\mu b_1^2 - \\ & 14k^2 \lambda^2 \mu b_2 - 16k^2 \mu^2 b_2 + 2\mu \omega b_2 - 4\mu a_0 b_2 = 0, \\ \left(\frac{G'}{G}\right)^2 : & -7k^2 \lambda^2 a_1 - 8k^2 \mu a_1 - 8k^2 \lambda^3 a_2 - 52k^2 \lambda \mu a_2 - 7k^2 \lambda^2 b_1 - 8k^2 \mu b_1 + \omega b_1 - 2a_0 b_1 - 6\lambda a_1 b_1 - 10\mu a_2 b_1 - \\ & 6\lambda b_1^2 - 8k^2 \lambda^3 b_2 - 52k^2 \lambda \mu b_2 + 2\lambda \omega b_2 - 4\lambda a_0 b_2 - 8\mu a_1 b_2 - 18\mu b_1 b_2 = 0, \\ \left(\frac{G'}{G}\right)^3 : & -12k^2 \lambda a_1 - 38k^2 \lambda^2 a_2 - 40k^2 \mu a_2 - 12k^2 \lambda b_1 - 6a_1 b_1 - 10\lambda a_2 b_1 - 6b_1^2 - 38k^2 \lambda^2 b_2 - 40k^2 \mu b_2 + 2\omega b_2 - \\ & 4a_0 b_2 - 8\lambda a_1 b_2 - 12\mu a_2 b_2 - 18\lambda b_1 b_2 - 12\mu b_2^2 = 0, \\ \left(\frac{G'}{G}\right)^4 : & -6k^2 a_1 - 54k^2 \lambda a_2 - 6k^2 b_1 - 10a_2 b_1 - 54k^2 \lambda b_2 - 8a_1 b_2 - 12\lambda a_2 b_2 - 18b_1 b_2 - 12\lambda b_2^2 = 0, \\ \left(\frac{G'}{G}\right)^5 : & -24k^2 a_2 - 24k^2 b_2 - 12a_2 b_2 - 12b_2^2 = 0. \end{aligned} \tag{55}$$

Solving the above algebraic Eqs.(55) by using the Maple or Mathematica, we have

$$a_0 = b_0 = 0, \quad a_1 = -\frac{\omega\lambda}{\lambda^2 + 8\mu}, \quad a_2 = -\frac{\omega}{\lambda^2 + 8\mu}, \quad b_1 = -\frac{\omega\lambda}{\lambda^2 + 8\mu}, \quad (56)$$

$$b_2 = -\frac{\omega}{\lambda^2 + 8\mu}, \quad k = \pm \sqrt{\frac{\omega}{2\lambda^2 + 16\mu}}.$$

Substituting Eq.(56) into Eqs.(53) and (54) yields

$$u(\xi) = -\frac{\omega\lambda}{\lambda^2 + 8\mu} \left(\frac{G'}{G}\right) - \frac{\omega}{\lambda^2 + 8\mu} \left(\frac{G'}{G}\right)^2, \quad (57)$$

$$v(\xi) = -\frac{\omega\lambda}{\lambda^2 + 8\mu_1} \left(\frac{G'}{G}\right) - \frac{\omega}{\lambda^2 + 8\mu} \left(\frac{G'}{G}\right)^2, \quad (58)$$

Where

$$\xi = \pm \sqrt{\frac{\omega}{2\lambda^2 + 16\mu}} (x + \omega t). \quad (59)$$

From Eqs. (17), (57) and (58), we deduce the following three types of traveling wave solutions:

Case 1. If $M > 0$, Then we have the hyperbolic solution

$$u(\xi) = \frac{\omega}{4(\lambda^2 + 8\mu)} \left[\lambda^2 - M \left(\frac{A \cosh\left(\frac{1}{2}\sqrt{M}\xi\right) + B \sinh\left(\frac{1}{2}\sqrt{M}\xi\right)}{A \sinh\left(\frac{1}{2}\sqrt{M}\xi\right) + B \cosh\left(\frac{1}{2}\sqrt{M}\xi\right)} \right)^2 \right], \quad (60)$$

$$v(\xi) = \frac{\omega}{4(\lambda^2 + 8\mu)} \left[\lambda^2 - M \left(\frac{A \cosh\left(\frac{1}{2}\sqrt{M}\xi\right) + B \sinh\left(\frac{1}{2}\sqrt{M}\xi\right)}{A \sinh\left(\frac{1}{2}\sqrt{M}\xi\right) + B \cosh\left(\frac{1}{2}\sqrt{M}\xi\right)} \right)^2 \right]. \quad (61)$$

Case2. If $M < 0$, Then we have the trigonometric solution

$$u(\xi) = \frac{\omega}{4(\lambda^2 + 8\mu)} \left[\lambda^2 + M \left(\frac{A \cosh\left(\frac{1}{2}\sqrt{M}\xi\right) + B \sinh\left(\frac{1}{2}\sqrt{M}\xi\right)}{A \sinh\left(\frac{1}{2}\sqrt{M}\xi\right) + B \cosh\left(\frac{1}{2}\sqrt{M}\xi\right)} \right)^2 \right], \quad (62)$$

$$v(\xi) = \frac{\omega}{4(\lambda^2 + 8\mu)} \left[\lambda^2 + M \left(\frac{A \cosh\left(\frac{1}{2}\sqrt{M}\xi\right) + B \sinh\left(\frac{1}{2}\sqrt{M}\xi\right)}{A \sinh\left(\frac{1}{2}\sqrt{M}\xi\right) + B \cosh\left(\frac{1}{2}\sqrt{M}\xi\right)} \right)^2 \right]. \quad (63)$$

Case3. If $M = 0$, Then we have the rational solution

$$u(\xi) = \frac{\omega}{4(\lambda^2 + 8\mu)} \left[\lambda^2 - 4 \left(\frac{B}{B\xi + A} \right)^2 \right], \quad (64)$$

$$v(\xi) = \frac{\omega}{4(\lambda^2 + 8\mu)} \left[\lambda^2 - 4 \left(\frac{B}{B\xi + A} \right)^2 \right]. \quad (65)$$

In particular if $B = 0, A \neq 0, \lambda > 0$ and $\mu = 0$, then we deduce from Eq.(60) and Eq.(61) that:

$$u(\xi) = \frac{-\omega}{4} \operatorname{csch}^2\left(\frac{\lambda}{2}\xi\right), \quad (66)$$

$$v(\xi) = \frac{-\omega}{4} \operatorname{csch}^2\left(\frac{\lambda}{2}\xi\right), \quad (67)$$

while, if $B \neq 0, A^2 > B^2, \lambda > 0$ and $\mu = 0$, then we deduce that:

$$u(\xi) = \frac{\omega}{4} \operatorname{sech}^2\left(\frac{\lambda}{2}\xi + \xi_0\right), \quad (68)$$

$$v(\xi) = \frac{\omega}{4} \operatorname{sech}^2\left(\frac{\lambda}{2}\xi + \xi_0\right), \quad (69)$$

Where $\xi_0 = \tanh^{-1}\left(\frac{A}{B}\right)$. The solutions (66) - (69) represent the solitary wave solutions of Eqs. (49) and (50).

IV. Conclusion

In this work, we have seen that three types of traveling wave solutions in terms of hyperbolic, trigonometric and rational functions for the vcKdV equation, the MDWW equations and the symmetrically coupled KdV equations are successfully found out by using the $\left(\frac{G'}{G}\right)$ -expansion method. From our results obtained in this paper, we conclude that the $\left(\frac{G'}{G}\right)$ -expansion method is powerful, effective and convenient. The performance of this method is reliable, simple and gives many new solutions. The $\left(\frac{G'}{G}\right)$ -expansion method has more advantages: It is direct and concise. Also, the solutions of the proposed nonlinear evolution equations in this paper have many potential applications in physics and engineering. Finally, this method provides a powerful mathematical tool to obtain more general exact solutions of a great many nonlinear PDEs in mathematical physics.

References

- [1] M. J. Ablowitz and P.A. Clarkson, Soliton, Nonlinear Evolution Equations and Inverse Scattering, Cambridge University Press, Cambridge, 1991.
- [2] C. H. GU Et AL., Soliton Theory and Its Application, Zhejiang Science and Technology Press, Zhejiang, 1990.
- [3] V. B. Matveev and M.A. Salle, Darboux Transformation and Soliton, Springer, Berlin, 1991.
- [4] R. Hirota, the Direct Method in Soliton Theory, Cambridge University Press, Cambridge, 2004.
- [5] S.Y. Lou, J.Z. Lu, Special solutions from variable separation approach: Davey-Stewartson equation, J. Phys. A: Math. Gen. 29 (1996) 4209.
- [6] E. J. Parkes and B.R. Duffy, Travelling solitary wave solutions to a compound KdV-Burgers equation, Phys. Lett. A 229 (1997) 217.
- [7] E. Fan, Extended tanh-function method and its applications to nonlinear equations, Phys. Lett. A 277 (2000) 212.
- [8] Z. Y. Yan, New explicit travelling wave solutions for two new integrable coupled nonlinear evolution equations, Phys. Lett. A 292 (2001) 100.
- [9] Y. Chen, Y. Zheng, Generalized extended tanh-function method to construct new explicit exact solutions for the approximate equations for long water waves, Int. J. Mod. Phys. C 14 (4) (2003) 601.
- [10] M. L. Wang, Application of a homogeneous balance method to exact solutions of nonlinear equations in mathematical physics, Phys. Lett. A 216 (1996) 67.
- [11] G. W. Bluman and S. Kumei, Symmetries and Differential Equations, Springer-Verlag, New York, 1989.
- [12] P. J. Olver, Applications of Lie Groups to Differential Equations, Springer-Verlag, New York, 1986.
- [13] Z. Y. Yan, A reduction mKdV method with symbolic computation to construct new doubly- periodic solutions for nonlinear wave equations, Int. J. Mod. Phys. C, 14 (2003) 661.
- [14] Z. Y. Yan, The new tri-function method to multiple exact solutions of nonlinear wave equations, Physica Scripta, 78 (2008) 035001.
- [15] Z. Y. Yan, Periodic, solitary and rational wave solutions of the 3D extended quantum Zakharov– Kuznetsov equation in dense quantum plasmas, Physics Letters A, 373 (2009) 2432.
- [16] D. C. Lu and B. J. Hong, New exact solutions for the (2+1)-dimensional Generalized Broer-Kaup system, Appl. Math. Comput, 199(2008)572.
- [17] A. V. Porubov, Periodical solution to the nonlinear dissipative equation for surface waves in a convecting liquid, Phys. Lett. A, 221 (1996) 391.
- [18] M. Wazwaz, The tanh and sine- cosine method for compact and noncompact solutions of nonlinear Klein Gordon equation, Appl. Math. Comput, 167 (2005)1179.
- [19] Z. Y. Yan and H. Q. Zhang, New explicit solitary wave solutions and periodic wave solutions for Whitham–Broer–Kaup equation in shallow water, Phys. Lett. A, 285 (2001) 355.
- [20] D. C. Lu, Jacobi elliptic functions solutions for two variant Boussinesq equations, Chaos, Solitons and Fractals, 24 (2005) 1373.
- [21] Z. Y. Yan, Abundant families of Jacobi elliptic functions of the (2+1) dimensional integrable Davey- Stewartson-type equation via a new method, Chaos, Solitons and Fractals, 18 (2003) 299.
- [22] C. L. Bai and H. Zhao, Generalized method to construct the solitonic solutions to (3+1)- dimensional nonlinear equation, Phys. Lett. A, 354 (2006) 428.
- [23] F. Cariello and M. Tabor, Similarity reductions from extended Painleve' expansions for nonintegrable evolution equations, Physica D, 53 (1991) 59.
- [24] M. Wang and X. Li, Extended F-expansion and periodic wave solutions for the generalized Zakharov equations, Phys. Lett. A, 343 (2005) 48.
- [25] X. Feng, Exploratory approach to explicit solution of nonlinear evolution equations, Int. J. Theor. Phys, 39 (2000) 222.
- [26] E. M. E. Zayed and K.A.Gepreel, The $\left(\frac{G'}{G}\right)$ -expansion method for finding traveling wave solutions of nonlinear PDEs in mathematical physics, J. Math. Phys., 50 (2009) 013502.
- [27] A. Bekir, Application of the $\left(\frac{G'}{G}\right)$ - expansion method for nonlinear evolution equations, Phys. Lett A, 372 (2008) 3400.
- [28] M. Wang, X. Li and J.Zhang, The $\left(\frac{G'}{G}\right)$ -expansion method and traveling wave solutions of nonlinear evolution equations in mathematical physics, Phys. Lett A, 372 (2008) 417.
- [29] G.A. El and R. H. J. Grimshaw, Generation of undular bores in the shelves of slowly- varying solitary waves, Chaos, 12 (2002)1015.
- [30] M. Alabdullatif and H. A. Abdusalam, New exact travelling wave solutions for some famous nonlinear partial differential equations using the improved tanh-function method, Int. J. Comput. Math,83 (2006)741.
- [31] J. P. Wang, A List of 1+1 Dimensional Intergable Equations and Their Properties, J .Nonlinear Mathematical Physics,9 (2002)228.

Vibration Analysis of Composite Plate

Sharayu U. Ratnaparkhi,¹ S.S. Sarnobat²

^{1,2}Department of Production Engineering, D.Y. Patil College of Engineering, Pune, India,

Abstract: Most of the structural components are generally subjected to dynamic loadings in their Working life. Very often these components may have to perform in severe dynamic environment where in the maximum damage results from the resonant vibrations. Susceptibility to fracture of materials due to vibration is determined from stress and frequency. Maximum amplitude of the vibration must be in the limited for the safety of the structure. Hence vibration analysis has become very important in designing a structure to know in advance its response and to take necessary steps to control the structural vibrations and its amplitudes. The present study involves extensive experimental works to investigate the free vibration of woven fiber Glass/Epoxy composite plates in free-free boundary conditions. The specimens of woven glass fiber and epoxy matrix composite plates are manufactured by the hand-layup technique. Elastic parameters of the plate are also determined experimentally by tensile testing of specimens. An experimental investigation is carried out using modal analysis technique, to obtain the Natural frequencies. Also, this experiment is used to validate the results obtained from the FEA using Ansys. The effects of different parameters including aspect ratio, and fiber orientation of woven fiber composite plates are studied in free-free boundary conditions in details. This study may provide valuable information for researchers and engineers in design applications.

Keywords: Finite element Analysis, Frequency Response function, Modal Analysis, Woven composite,

I. Introduction

Literature review is focused on the different types of analysis of composite materials [1]. Due to the requirement of high performance material in aerospace and marine structures, the prospect of future research of composite material, such as FRP (Fibre Reinforced Plastic) is very bright. Analysis of natural frequency and properties of composite plate has started from 40 years ago. The combination of different materials has been used for many thousands of years to achieve better performance requirements. There are nowadays many examples in the aeronautical and automobile industries, and yet the application of composite materials is still growing, including now areas such as nautical industries, sporting goods, civil and aerospace construction. The affects of different parameters on natural frequency is important analysis.

In this present work, Vibration analysis of Glass/Epoxy composite plate under Free Free boundary condition is carried out for analyze the effect of factors such as No. of layers, Fiber orientation angle and aspect ratio on the natural frequency.

1.1 Scope

The scope of the study includes the following:

- Fabrication of Woven Roving Glass/Epoxy composite plates less than 7 mm thickness
- Experimental Modal analysis work carried out on FFT analyzer.
- Affecting parameters are Fiber orientation angle and Aspect ratio

II. Methodology

In the present study, it is very necessary to develop proper composite plate fabrication method. In this hand layup fabrication method is developed. Proper experimental plan is necessary to achieve good results in conducting research. Simulation is carried out using Ansys Software. FRF results, DOE data, and simulation results are compared.

2.1 Experimentation

2.1.1 Geometrical Property

In choosing the types of specimens to construct and test, woven fibered Glass/Epoxy composite plates are taken. Seven woven fibre Glass/Epoxy composite plates are taken. Plates prepared to cast as free one by hand layup. The maximum length of plate is 25 cm. The average thickness of all specimens was measured by a screw gauge having a least count of 0.01mm.

2.1.2 Fabrication Method

The resin serves as the matrix for the reinforcing glass fibers, much as concrete acts as the matrix for steel reinforcing rods. The percentage of fibre and matrix was 50:50 in weight. Contact moulding in an open mould by hand lay-up was used to combine plies of WR in the prescribed sequence. A flat plywood rigid platform was selected. A plastic sheet was kept on the plywood platform and a thin film of polyvinyl alcohol was applied as a releasing agent by use of spray gun. Laminating starts with the application of a gel coat (epoxy and hardener) deposited on the mould by brush, whose main purpose was to provide a smooth external surface and to protect the fibers from direct exposure to the environment. Ply was cut from roll of woven roving. Layers of reinforcement were placed on the mould at top of the gel coat and gel coat was applied again by brush. Any air which may be entrapped was removed using serrated steel rollers.[3]

2.1.3 Determination of Material Constants

The characteristics of woven fiber Glass/Epoxy composite plate which can be defined completely by two material constants: E and ν . For material characterization of composites, laminate having 8 layers is manufactured to evaluate the material constants.[2] The constants are determined experimentally by performing tensile tests on specimens as described in ASTM standard: D 638-08 and D 3039/D 3039M – 2006. The specimens were cut from the plates themselves by diamond cutter or by hex saw. After cutting in the hex saw, it was polished in the polishing machine. At least three replicate sample specimens were tested and mean values adopted.

2.2 Testing

2.2.1 Test Setup

The connections of Data acquisition system, computer, and accelerometer, amplifier, modal hammer, and cables to the system are done as per the guidance manual. The plate was excited in a selected point by means of a small impact hammer. The plate is at Free-Free condition as shown in fig.

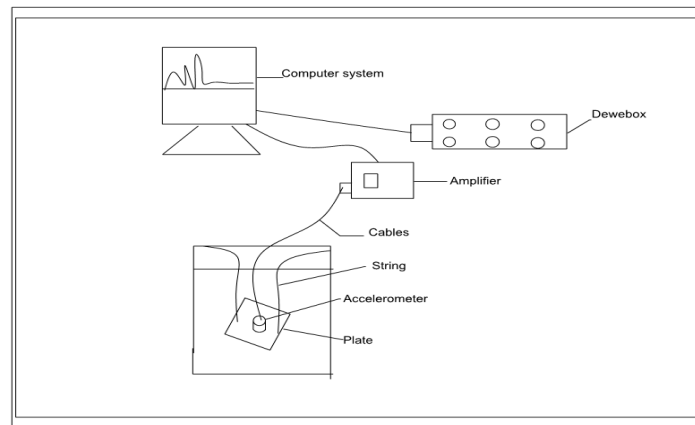


Fig. Schematic of experimental setup

2.2.2 Test procedure

The resulting vibrations of the plate in a select point are measured by an accelerometer. The accelerometer is mounted by means of bees wax. The signal was then subsequently input to the second channel of the analyzer, where its frequency spectrum was also obtained. The response point was kept fixed at a particular point and the location of excitation was varied throughout the plate. Both input and output signals are investigated by means of FFT and resulting frequency response functions are transmitted to a computer for modal parameter extraction. The output from the analyzer was displayed on the analyzer screen by using DEWESoft 6 software. Various forms of Frequency Response Functions (FRF) are directly measured.

2.3 Ansys FEA Model

FEA involves three stages of activity:

- Preprocessing,
- Processing and
- Post processing.

In this study, finite element analysis is conducted using ANSYS software. To model the composite plate Linear layer Shell 99 element is used and it is modal analysis. The plate is at free free boundary condition. Degrees of freedom are UX, UY, UZ, ROTX, ROTY, ROTZ.

III. Data Analysis

Plate	Mode no.	Experimental Frequency (Hz)	Simulation Frequency (Hz)	Error (%)
Glass/Epoxy plate with aspect ratio 1:1	1	224.6	210.7	6.18
	2	576	618.0	7.29
	3	1298	1197	7.78

Plate	Mode no.	Experimental Frequency (Hz)	Simulation Frequency (Hz)	Error (%)
Glass/Epoxy plate with aspect ratio 1:1.5	1	332	283	14.75
	2	791	881	10.21
	3	1562	1467	6.11

Plate	Mode no.	Experimental Frequency (Hz)	Simulation Frequency (Hz)	Error (%)
Glass/Epoxy plate with aspect ratio 1:2	1	400.4	308	21
	2	927.7	960	3.61
	3	1845	1787	3.14

Plate	Mode no.	Experimental Frequency (Hz)	Simulation Frequency (Hz)	Error (%)
Glass/Epoxy plate with aspect ratio [45/-45] orientation	1	224.6	223.86	0.32
	2	478	584	18.15
	3	1093	1037	5.12

Plate	Mode no.	Experimental Frequency (Hz)	Simulation Frequency (Hz)	Error (%)
Glass/Epoxy plate with aspect ratio [30/-60] orientation	1	255.13	262	2.67
	2	661	634	3.36
	3	1296	1214	6.3

IV. Result And Discussion

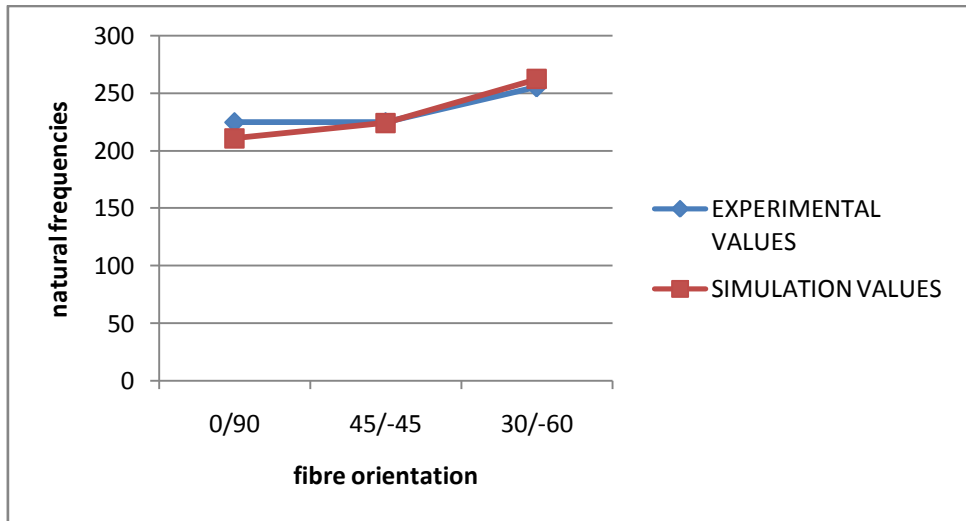


Fig. Effect of Fiber orientation on Natural frequencies.

Fiber orientation Vs Natural frequency graph. It shows lower value for [45/-45] fiber orientation. And increased frequency for [30/-60]. The maximum error for comparison between experimental and simulation is 6%.

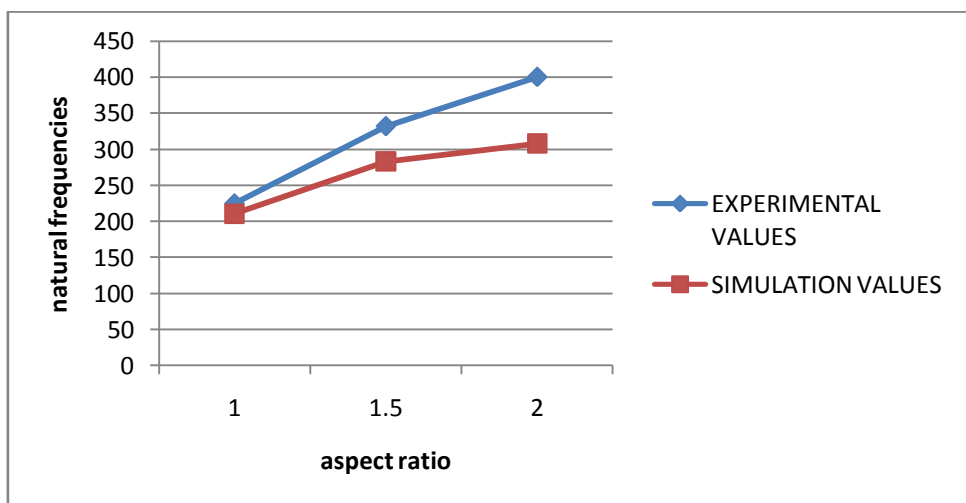


Fig. Effect of Aspect ratio on Natural frequency.

Natural frequency increases with increase in aspect ratio. It gives parabolic curve. The error may occur due to un-damped natural frequency is considered in the program and damping was present in the system.

4.1 Result Discussion

Natural frequencies of woven fiber Glass/Epoxy composite plates are measured by data acquisition system for free-free boundary condition. There are three different parameters such as aspect ratio of plate and fiber orientation. The program developed by FEA is used to measure the natural frequencies of those plates. experimental values and simulation study are compared with each other. In experimental result, natural mode of frequency sometimes varies within a range as shown in Tables. It shows that an approximate agreement with the FEA based program. As the mode no increases, the percentage error between experimental value and programming value decreases. But the differences between compared results are reasonable. The reasons for differences are may be:

The standard size of the specimen is dog-boned shape. There may be variation of elastic properties of the plate, as the sample cut from the plate was different from the plate used in the case vibration testing.

Tensile properties may vary with specimen preparation and with speed and environment of testing. Present specimens couldn't align in the centre of the jaw, because there is a diamond shaped hole where slippage was occurred. Specimens were fixed one of the sides of the jaw. So, there may be a chance of decrease of elastic modulus (Young's modulus).

V. Conclusion

5.1 Parametric Study

The Glass/ Epoxy laminated composite plates are manufactured and modal testing is done for free-free boundary condition by using Data acquisition System. Frequency Response Functions are obtained by FFT. Quantitative results are presented to show the effects of different parameters like aspect ratio and fibre orientation.

The experimental frequency data is in fair agreement with the program computation. The Percentage of error between experimental value and ANSYS package is within 15%. The difference is probably due to uncertainty in elastic properties and other described reasons. For Free-free boundary condition it is found that the natural frequency of plate increases with the increasing of aspect ratio. Natural frequency decreases as the ply orientation increases up to [45/-45] and again increases up to [30/-60].

5.2 Future scope

The present approach is devoted that the major affecting parameter on natural frequency. As the composite material are made of two or more distinct phase materials. Manufacturing consideration plays an important role in design part. I have to analyse the affect of different fabrication factors such as curing time, curing temperature and volume fraction ratio so as to optimise the fabrication process.

VI. ACKNOWLEDGMENT

This project work is supported by Prof. S. S. Sarnobat (D.Y.Patil college of Engg. Pune) and R.I.T, Sakrale.

REFERENCES

Journal papers:

- [1] Y.X. Zhang, C.H. Yang "Recent developments in finite element analysis for laminated composite plates." Composite Structures 88 (2009) 147-157
- [2] B.N Singh, A.K.S Bisht, M.K.Pandit, K.K Shukla "Non linear vibration analysis of composite plates with material uncertainties: A Monte Carlo Simulation approach", Journal of sound and vibration 324 (2009)126-138
- [3] Faruk Firat Calim, "Free and forced vibrations of non-uniform composite beams", Composite Structures 88 (2009) 413-423.

Books:

- [4] Robert M. Jones, Mechanics of composite material (Virginia Polytechnic Institute and state university, Taylor and Francis)

Effect of Hardness, Tensile and Wear Behavior of Al-4.5wt%Cu Alloy/Flyash/SiC Metal Matrix Composites

G.N.Lokesh,¹ M.Ramachandra,² K.V.Mahendra,³ T.Sreenith⁴

^{1,4}Department of Mechanical Engineering, Acharya Institute of Technology, Bangalore-560090, India

²Department of Mechanical Engineering, BMS College of Engineering, Bangalore-560019, India

³Department of Mechanical Engineering, Jyothy Institute of Technology, Bangalore-560062, India

Abstract: Metal-matrix composites (MMCs) have emerged as potential alternatives to conventional alloys in high-strength and stiffness applications. In the present investigation Al-4.5wt.%Cu alloy reinforced flyash and SiC particulates were casted by liquid metal stirring casting technique. The 2wt.%flyash with 2, 4, 6wt.%SiC and 4wt.%flyash with 2, 4, 6wt.%SiC were reinforced in Al-4.5wt.%Cu matrix. The composites were tested for hardness, tensile strength and dry sliding wear behavior. The results show improved hardness, tensile strength and wear resistance with increase in percentage of reinforcements. Optical micrograph indicates better bonding between matrix, flyash and SiC particle with no fracture initiation at matrix particle interface.

Keywords: Flyash, Liquid stir casting, Metal matrix composite, Wear

I. INTRODUCTION

The unique properties of the particulate reinforced composite materials are to a great extent dependent on the unique nature on the matrix-particle interface. The requirement for strong, light and stiff materials has extended an interest in MMCs. During the past three decades, MMCs have received substantial attention because of their improved strength, high elastic modulus and increased wear resistance over conventional base alloys. The wide scale introduction of MMCs has been increasing simultaneously with the technological development. Increased attention has been directed toward particulate metal matrix composite for tribological applications due to the advantages of MMCs such as good sliding wear resistance, high load carrying capacity and low density [1]. MMCs are also used in many different fields besides aerospace applications [2]. The ceramic fiber and particulate- reinforced MMCs have been used to improve the wear resistance in automotive and aircraft brakes [3], and diesel piston engines [4]. The coal combustion waste product flyash produced by thermal power plants, is an increasingly urgent problem associated with their storage and disposal [5]. On the other hand, fly ash presents a unique natural source of the particulate material for light-weight low-cost composites [6]. This is because of the combination of its low price along with low density, attractive physical and mechanical properties, and advantageous spherical shape, which is very expensive to produce it in an artificial way. Therefore, information on the reactivity of fly ash with different molten metals is of high practical importance. SiC reinforced aluminum alloy composites are the typical candidates for engineering applications in aerospace, military and civil manufacturing industries due to their enhanced mechanical properties over the corresponding aluminum alloys such as high strength, stiffness, hardness, wear resistance and fatigue resistance [7-9]. Thus in this paper composites produced with different weight percentage of both flyash and SiC reinforced in Al-4.5wt%Cu base alloy through stir casting route. Influence of reinforcement on hardness, ultimate tensile strength and wear properties are studied. Micro photographs using optical microscope has been carried out to investigate the particle-matrix interface.

II. EXPERIMENTAL WORK

A stir casting setup which consisted of a resistance furnace and a stirrer assembly is used to synthesis the composite. Al-4.5wt. %Cu alloy commercially prepared was melted in a resistance heated muffle furnace and casted in a clay graphite crucible. Table 1 shows the chemical composition of base alloy, analysed by optical emission spectrometer.

Table1. The chemical composition of the matrix alloy (wt. %)

Cu	Mg	Si	Fe	Mn	Ni	Pb	Sn	Ti	Zn	Al
4.51	0.061	0.52	0.59	0.13	0.06	0.03	0.02	0.012	0.12	balance

The temperature of the melting is increased to 750°C and it is degassed by cleansed with hexachloroethane tablets. The density of flyash measured is 2.1g/cm³ with the particle size varying between 49 and 60µm. SiC particle size which is used to fabricate the composite had an average of 65 µm and density is 3.2g/cm³. The Al-Cu alloy flyash/SiC composite was prepared by stir casting route. The flyash particles were preheated to 210°C for two hours to remove moisture. Also the dies were preheated to 150 °C for 2-3 hours. Then the molten metal was stirred to create a vortex as shown in Fig 1 and then the reinforcements were added. The stirrer is maintained approximately 450rpm throughout the process. The stirring was continued for another 1min even after the completion of particle feeding. The temperature was also monitored simultaneously during stirring the molten metal. The mixture was poured into the mold and the time taken to fill the mold

was 6.1 seconds for base alloy and 9.3 seconds for 4wt% flyash, 6wt% SiC reinforcements. The maximum duration of mixing was 3min. The clearance of the stirrer from the bottom of the crucible was approximately 10 mm with the melt depth of 120 mm. The stirred dispersed molten metal was poured into preheated S.G. iron moulds and cooled to room temperature.

Composites produced were subjected to T6 heat treatment. The castings were heated to 450°C for 12 hours, quenched in 100°C water and reheated to 150°C for 16hours. Then the samples were allowed to cool in the furnace temperature.



Fig. 1. The molten metal was stirred to create a vortex

Hardness measurements were performed using a Brinell hardness tester with a load of 10kgf. Hardness values were averaged over five measurements taken at different points on the cross-section. Tensile tests were carried out using samples prepared according to ASTM D3479-1982 standard. These tests were conducted using a computerized universal testing machine (UTM) with 100KN capacity. Figure 2 shows the tensile specimens after the conduction of test in UTM.



Fig. 2. Composite specimens after tensile test

Wear test were carried out under dry sliding condition on a pin-on-disc apparatus. A steel disc (AISI D2) was used as counter surface and composites were made into pins having 6mm diameter and 30mm in height. The pins were made to slide on the steel disc at 60minutes duration under the loads of 10, 15 and 20N. A hardened steel disc (60HRC) was used as the counter face. Photographs were taken for a polished section of each sample from optical microscope to examine the effect of the percentage of particle on the wear behavior of the composites,

III. RESULTS AND DISCUSSION

3.1. Hardness

Hardness tests were performed on as cast and composites to know the effect of flyash and SiC in matrix material. Hardness of MMCs is increased with increased weight percentage of flyash and SiC particle then that of its parent metal. It is evident from figure 3 that the hardness of Al-4.5wt. %Cu alloy increased by the addition of 4wt. % flyash and up to 6wt. % SiC. This may be due to the harder ceramic particle of SiC and hard flyash particulates. The strengthening of the composite can be due to dispersion strengthening as well as due to particle reinforcement. Thus flyash as filler in Aluminium casting reduces cost, decreases density and increase hardness which are need in various industrial like automotive applications.

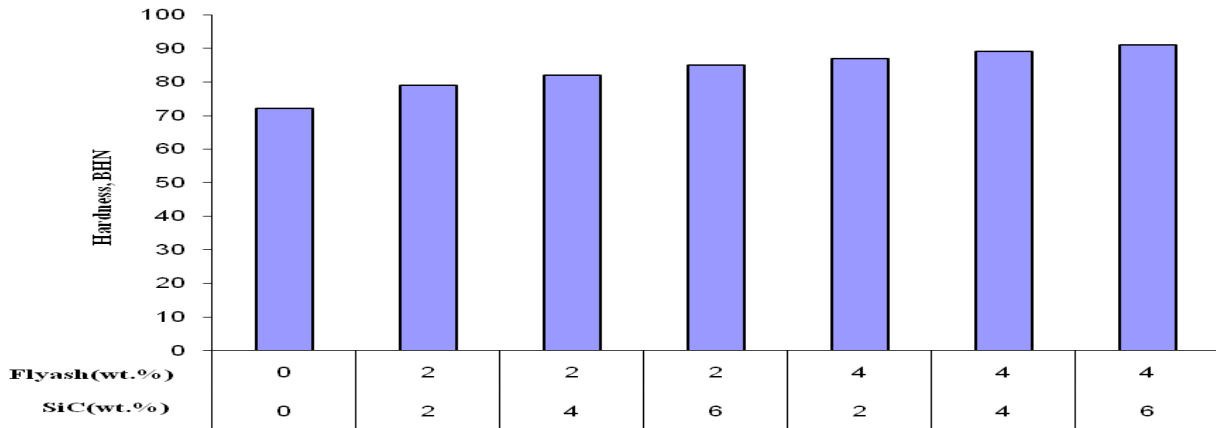


Fig. 3. Brinell hardness number of Al-4.5wt%Cu reinforced Flyash and SiC particulates

3.2. Tensile strength

Tensile properties indicate that the flyash and SiC addition leads to improvement in the ultimate tensile strength. The size range of the particle is very wide. Figure 4 shows the effect of flyash and SiC particulate content on tensile behaviour of the composites. The size ranges of the flyash indicate that the composite prepared can be considered as dispersion strengthened as well as particle reinforced composite. It is observed that the ultimate strength (UTS) of matrix alloy is increased with increase in percentage of flyash and SiC reinforcements. This may be due to segregation of particles and finer grain structure of the castings.

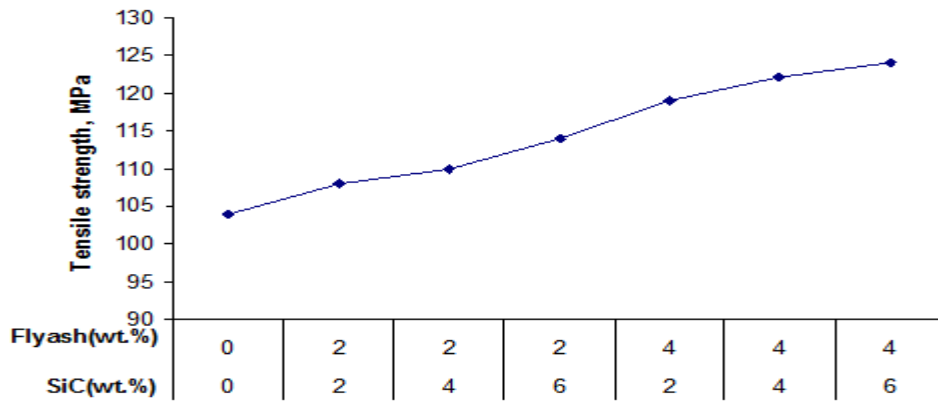


Fig. 4. Ultimate tensile strength of Al-4.5wt%Cu reinforced Flyash and SiC particulates

3.3. Wear behaviour

Dry sliding wear behaviour of matrix alloy reinforced flyash and SiC shows reasonable increase in wear resistance. It is observed that addition of 4wt. % flyash and 6wt. % SiC shows lesser wear than other composites. Figure (5, 6 & 7) shows the weight loss during wear test for different weight percentage of Al-4.5wt.%Cu alloy and Al-4.5wt.%Cu alloy reinforced flyash and SiC MMCs. The highest weight loss is distinct for matrix alloy and linearly the weight loss decreased by increasing the percentage of reinforcements. The wear resistance of the composites is considerably improved due to the addition of 6wt.% SiC particle. Also presence of 4wt.% flyash strengthen the matrix and hence more wear resistance is observed and therefore volume of wear debris increase with increasing normal load resulting in greater wear loss.

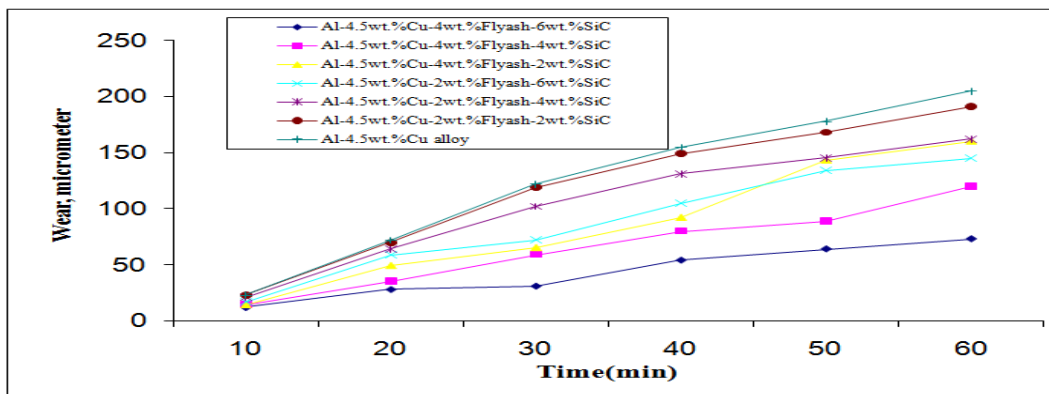


Fig. 5. Wear vs. time at various percentage of flyash and SiC at 10 N load of castings

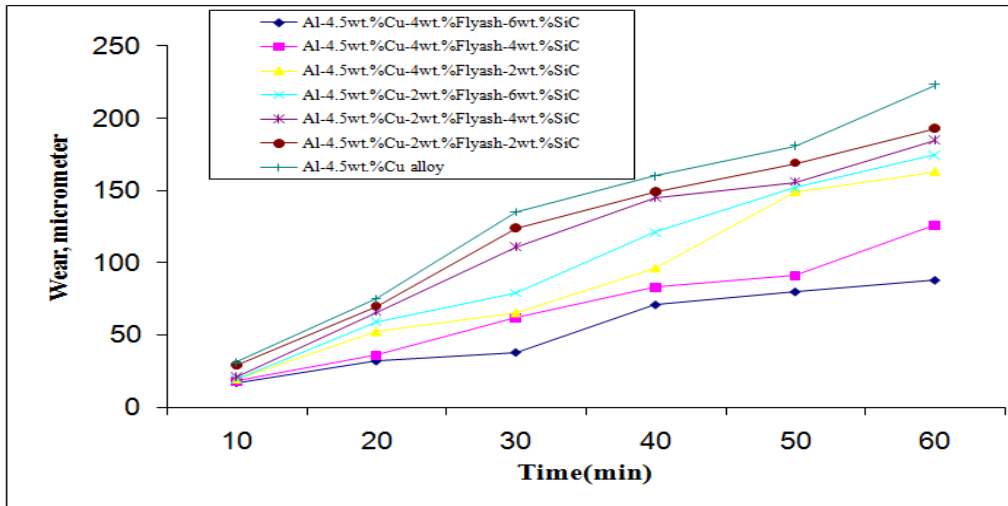


Fig. 6. Wear vs. time at various percentage of flyash and SiC at 15 N load of castings

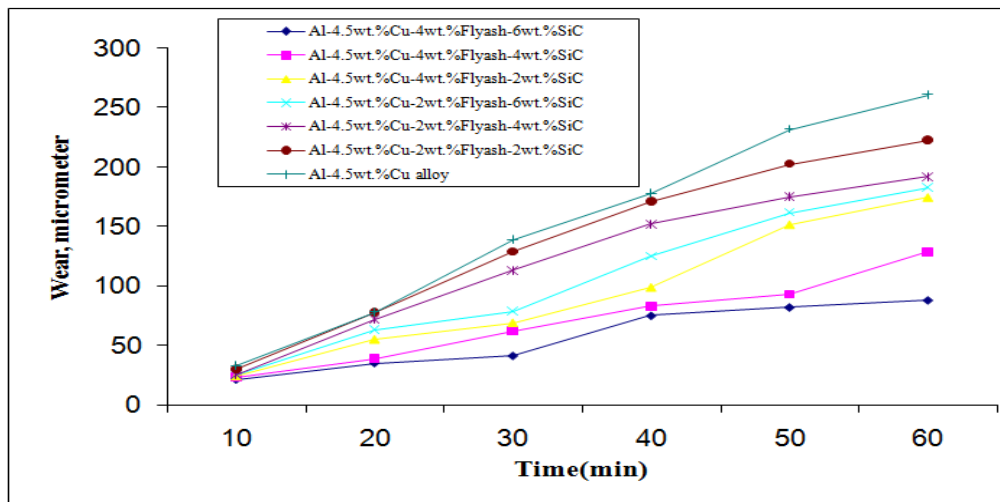


Fig. 7. Wear vs. time at various percentage of flyash and SiC at 20 N load of castings

3.4. Microstructure

Figure (8, 9 and 10) shows the microphotographs of worn surface of 4wt. % flyash, 6wt. % SiC MMCs under normal load of 10, 15 and 20N. It can be seen in Figures that the presence of grooves of varying sizes was observed frequently on the worn surface. The worn debris particles are likely to act as third body abrasive particles. The flyash and SiC particles trapped between the specimen and counterface cause microploughing on the contact surface of the composite. At higher applied loads, higher wear rates are observed. The wearing surface is characterized by a significant transfer of material between the sliding surfaces. Flyash and SiC could be dispersed inside the matrix alloy with better bonding due to which the wear resistance occurred. In all the normal loads the flyash and SiC particles embedded in the matrix is visible showing uniform distribution of reinforcements. Also from worn surface it is observed that matrix alloy reinforced upto 4wt. % flyash and 6wt. % SiC for maximum load of 20N, there is no fracture initiation at matrix particle interface.

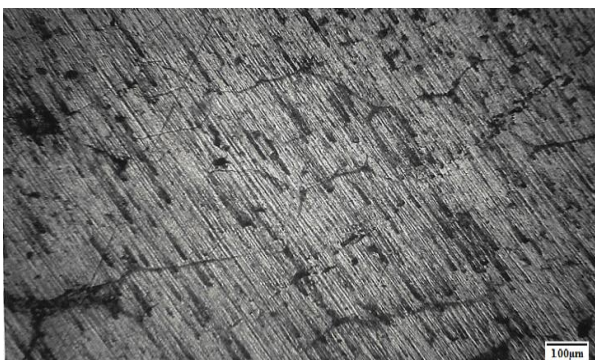


Fig. 8. Optical micrograph of worn sample of matrix alloy reinforced 4% flyash, 6% SiC at 10N load

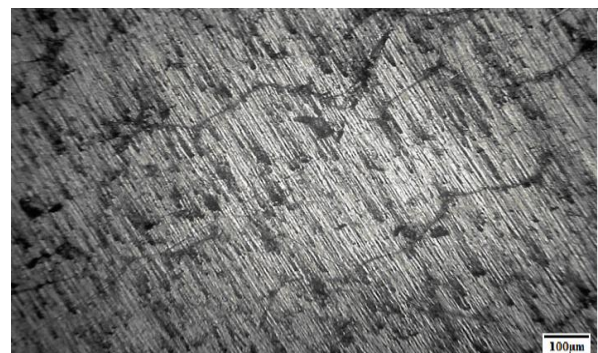


Fig. 9. Optical micrograph of worn sample of matrix alloy reinforced 4% flyash, 6% SiC at 15N load



Fig. 10. Optical micrograph of worn sample of matrix alloy reinforced 4%flyash, 6%SiC at 20N load

IV. CONCLUSION

The results from the experimental work conclude that flyash up to 4% and SiC up to 6% by weight can be successfully added to Al-4.5wt.%Cu alloy by stir casting route to produce composites. Addition of flyash and SiC improves the hardness of the composite. Ultimate tensile strength increases with an increase of flyash and SiC particulates. The wear resistance increases with an increased percentage of flyash and SiC. Optical micro photographs shows better bonding between matrix, flyash and SiC with no fracture observed at matrix particle interface.

V. ACKNOWLEDGEMENTS

The author is greatly thankful to Department of mechanical engineering of BMS College of Engineering Bangalore, and Jyothy Institute of Technology, Bangalore, India, for providing the facility to conduct experiments. Also author acknowledge M/S. Grindwell Norton Ltd, Renigunta, Andhra Pradesh, for providing SiC particulates for research work.

REFERENCES

- [1] M. Muratoglu and M. Aksoy, *Materials Science and Engineering A282* (2000), pp 91–99.
- [2] Zhangwei Wang, Min Song, Chao Sun, Yuehui He, *Materials Science and Engineering A 528* (2011), pp1131–1137.
- [3] T.L. Ho, in: W.A. Glasser (Ed.), *Wear of Materials*, American Society of Mechanical Engineers, (1977), pp. 70–76.
- [4] R. Munro, *International Congress and Exposition, Detroit, MI, 28 February–4 March 1983*, SAE Tech Paper 830067.
- [5] J. Sobczak, N. Sobczak and P.K. Rohatgi, in: R. Ciach (Ed.), *Advanced Light Alloys and Composites*, NATO ASI Series, vol. 59, Kluwer Academic Publishers, Dordrecht, The Netherlands, (1998), pp 109.
- [6] J. Sobczak, N. Sobczak, G. Przystas, *Utilization of Waste Materials in Foundry Industry on Example of Fly Ashes. State of the Art and Application Perspectives*, Foundry Research Institute, Cracow, Poland, (1999).
- [7] J.M. Torralba, C.E. da Costa, F. Velasco, *J. Mater. Proc. Technol.*, 133 (2003), pp 203–206.
- [8] Shyong, J. H., and Derby, B, *Materials Science and Engineering*, (1995) A 197, pp11-18.
- [9] N. Chawla, Y.L. Shen, *Adv. Eng. Mater.* 3 (2001), pp 357–370.

Increase of Salt Fog Corrosion Resistance of Plasma Nitrided Steel by Pulsed Plasma Post-Oxidation

J.C. Díaz-Guillén,¹ J.S. Zamarripa-Piña,² E. E. Granda-Gutiérrez,³
M. A. González-Albarrán,⁴ J.A. Díaz-Guillén,⁵ S.I. Pérez-Aguilar,⁶
J.Candelas-Ramírez⁷

^{1, 2, 3, 4, 6, 7} Corporación Mexicana de Investigación en Materiales S.A. de C.V., Saltillo, Coahuila. México.

⁵ División de Estudios de Posgrado e Investigación. Instituto Tecnológico de Saltillo. Saltillo, Coahuila. México

Abstract: Plasma nitriding has demonstrated to be a good alternative to increase surface hardness, wear and abrasion resistance of AISI 4340 steel. Unfortunately, corrosion resistance of the obtained nitrided layer is poor as a consequence of its high grade of porosity. In the present work, pulsed plasma post-oxidation process is analyzed as an alternative technique to increase corrosion resistance of plasma nitrided AISI 4340. The effect of post-oxidation process duration (15, 30 and 60 minutes) on the corrosion performance of samples when they are exposed to a rich chloride fog under controlled temperature and pressure conditions was evaluated. Results showed that post-oxidized during 15 minutes samples have the best corrosion performance. After 21 h of exposition to 3.5 % NaCl fog, the presence of red rust on post-oxidized during 15 minutes samples was reduced to around 1/16 part of the only nitrided sample. According with scanning electron microscopy and X-ray diffraction analysis, the increase in the corrosion resistance of post-oxidized samples is related to the occurrence of an oxidized thin layer constituted mainly by magnetite kind iron oxide.

Keywords: Plasma nitriding, plasma post-oxidation, salt fog corrosion.

I. INTRODUCTION

Ni-Cr-Mo steel AISI 4340 is a commonly used alloy which is characterized by its remarkable strength, ductility and toughness obtained as a consequence of its good tempering properties [1]. Because of its structural acceptable performance, AISI 4340 is widely used for fabrication of parts and components in automotive, aerospace as well as metal mechanics industries. In this sense, pieces as shafts, bolts, rods, reels, rotors and gears can be fabricated using this alloy. Despite its good mechanical properties, the lifetime of this alloy is not long enough, because of its low corrosion resistance and poor tribological properties [2].

In order to increase the lifetime of pieces and accessories fabricated using AISI 4340 steel, through optimization of corrosion and tribological performance, several coatings [3] and thermochemical treatments [4] have been applied on this alloy. In recent years, it has been demonstrated that ion nitriding, a plasma assisted surface modification thermochemical treatment, is an attractive technique which promotes the increase in hardness, wear and fatigue properties of several iron alloys [5, 6, 7].

Nitriding process results in the formation of a compounds layer followed by a nitrogen diffusion zone. The compounds layer is mainly constituted by a combination of iron nitrides ($\text{Fe}_{2,3}\text{N}$ and/or Fe_4N) and the diffusion zone is composed of nitrogen saturated ferrite together with dispersed precipitates of iron and alloy element nitrides [8]. Both regions are responsible for improvement of previously enounced properties. Nitrided layer improve significantly the tribological surface properties of nitrided pieces but it has a porous structure that limits the corrosion resistance of nitrided steels. In this way, increasing of corrosion properties is still an opportunity area for integral improvement of the surface properties of metal alloys.

In order to increase both, mechanical and corrosion properties of nitrided iron alloys, some complementary processes have been proposed, highlighting oxidation through air furnace process [9] and DC conventional plasma [10]. Post-oxidation treatments produce a thin oxide layer on compounds layer, which covers and seals micro-pores and improves the corrosion resistance of nitrided steel [11,12]. Currently, some researches are focused in the study of the influence of post-oxidation process parameters on properties and performance of these nitrided post-oxidized layers. It has been emphasized the fact that the post-oxidation process has to be controlled to avoid the formation of hematite (Fe_2O_3) and to produce layers with high content of magnetite (Fe_3O_4), a compound of high chemical stability which is highly corrosion resistant [13,14].

With the aim to contribute to the study of influence of processing parameters during post-oxidation process, on corrosion performance of plasma nitrided low alloy AISI 4340 steel, in the present work it is proposed the pulsed plasma post-oxidation process as an alternative to improve the corrosion performance of this alloy. It is analyzed the influence of plasma post-oxidation process duration, in a pulsed DC glow discharge, on corrosion performance of post-oxidized samples when they are exposed to a 3.5% NaCl fog. (Procedure ASTM B177, Standard practice for operating salt spray apparatus).

II. MATERIALS AND METHODS

AISI 4340 samples (4 x 4 x 0.5 cm) from a commercial source were used in the present study. Table 1 shows the chemical composition of samples which was obtained through infrared detection for carbon and sulfur and X-Ray spectroscopy for the rest of elements.

Table 1. Chemical composition of substrates used in this study

Element	C	S	Mn	P	Si	Cr	Ni	Mo	Cu	Fe
Weight %	0.38	0.017	0.63	0.008	0.19	0.80	1.64	0.20	0.14	Balance

Previous plasma treatment, samples were ground using different grades of SiC emery paper (120, 240, 320, 400, 600 progressively) and polished with a 0.5 µm diamond suspension. After that, samples were subjected to a cleaning stage in an acetone ultrasonic bath, in order to remove dust or oil from the surface.

Pulsed plasma nitriding was carried out using a DC pulsed glow discharge sustained in a 50% N₂ 50% H₂ gas mixture at 2 torr. The next parameters were kept constant: temperature 520 °C, processing time 3 hr, discharge voltage 800V and frequency of 1000 Hz. Pulsed plasma post oxidation process was carried out immediately after nitriding by changing in processing conditions. The DC discharge used during post-oxidation stage was kept using a gas mixture 20% O₂ 80% N₂ at 1.5 Torr using a frequency of 1000 Hz at 400°C. Processing time during post oxidation process was manipulated for values of 15, 30, and 60 minutes.

Both, nitriding and post-oxidizing process were carried out using an own design processing equipment [15] which consists of a vacuum chamber containing a central cathode biased by negative high voltage pulses. Plasma is generated and sustained by an IGBT (Insulated Gate Bipolar Transistor) based DC pulsed power supply unit, which provides precise adjustments of discharge current, pulse frequency and duty cycle. An auxiliary heating system offers full control over the sample temperature, which is measured by a K-type thermocouple directly fastened on the samples. Mass flow controllers allow the precise control of pressure and gas mixture inside the vacuum chamber.

Once duplex nitriding post-oxidizing process was concluded, samples were cross sectioned, polished, and etched with 5% Nital reagent to reveal the modified surface region. Scanning electron microscopy (SEM) was used to analyze morphological changes on surface and cross section of the samples. Crystalline phases occurring on the surface of modified samples were identified by the use of X-ray diffraction technique (XRD). XRD patterns were obtained in a Philips X'Pert diffractometer, using a Cu Kα radiation (λ=1.5406 nm), 45 kV and 40 mA. Scanning was carried out from 34° to 50° 2θ with a step of 0.016° and step duration of 20 s.

Corrosion performance of nitrided post-oxidized samples under influence of a rich chloride fog was evaluated in agreement with procedure specified by standard ASTM B-117. This practice provides a controlled corrosive environment which has been utilized to produce relative corrosion resistance information for specimens of metals and coated metals exposed in a given test chamber. Untreated, nitrided and nitrided post-oxidized samples were exposed to a salt fog for 72 hr. A periodic evaluation of the corrosion grade of surface samples was carried out at 2, 4, 6, 21, 23, 25, 27, 48 and 72 hr. Corrosion performance test parameters are listed at table 2.

Table 2. Salt spray test parameters.

Test parameter	Condition
Cabinet temperature	35 °C
Tower temperature	50 °C
Tower pressure	96.53 kPa (14psi)
Solution pH	6.96
Average of specific gravity	1,040 g/mL
Collection rate	1.68 mL/h
Exposition angle	30° to the vertical
Grade water	ASTM D 1193, Type IV
Exposition time	72 hours

III. RESULTS AND ANALYSIS

Figure 1 shows 2000X SEM surface views of a) Plasma nitrided and b) Plasma nitrided post-oxidized during 15 minutes samples. The surface morphology of pulsed plasma nitrided sample is characterized by edged particles with well-defined boundaries. This morphology has been reported for low alloy steels processed by plasma surface treatment as active screen plasma nitriding [16] and it has been related to sputtering phenomenon intensity [3,17]. However, post-oxidized sample (Figure 1b) exhibits comparatively a more homogeneous appearance with decreased in edged particles quantity leading to a less rough surface which could be related to the formation of an oxides layer resulting from the post-oxidation process. It have been reported for post-oxidation process that an adherent oxide phases fill and seal the holes between particles of nitrided surfaces, which could have a positive effect on corrosion resistance improvement [18].

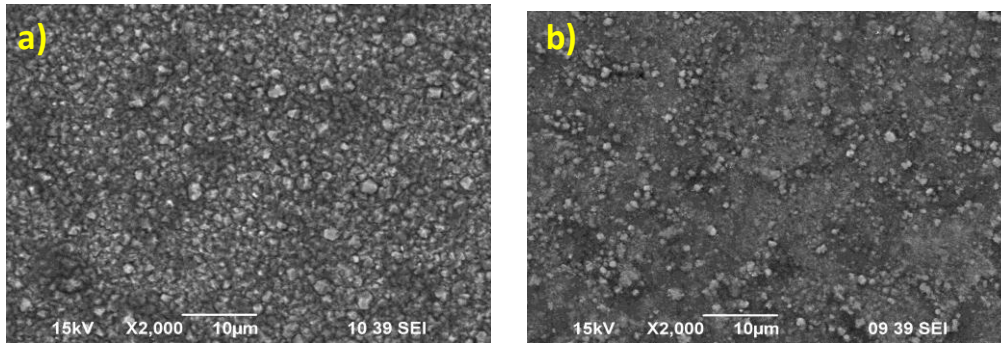


Figure 1. Representative SEM surface views of a) Plasma nitrided and b) Plasma nitrided post-oxidized samples.

Figure 2 shows a SEM cross view of duplex, nitrided post-oxidized during 15 minutes sample. The presence of an oxidized layer on the nitrided surface, which fill and seal the holes of nitrided sample, can be confirmed through this cross view. It can be appreciated a bi-layer arrangement constituted by a thin oxide layer on a thicker nitrided layer. Both, oxidized and nitrided layer are not chemical etched by Nital reagent. This bi-layer arrangement was observed for all evaluated samples; however it was evident the influence of post-oxidation time on oxidized layer thickness: 325 nm (± 28), 431 nm (± 50) and 722 nm (± 118) were measured for samples post-oxidized during 15, 30 y 60 minutes respectively.

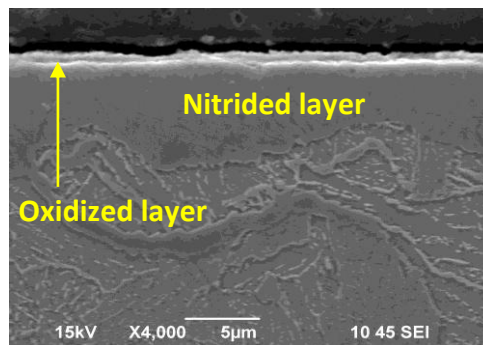


Figure 2. SEM cross view of nitrided post-oxidized sample for 15 minutes.

X-Ray diffraction patterns for untreated, nitrided and nitrided post-oxidized during 15 minutes samples are showed at figure 3. Plasma nitriding promoted a high attenuation of the reflections related to α -Fe giving rise to appearance of reflections located at 41.09° and 47.74° 2 theta associated to γ' - Fe_4N monophasic layer. Similarly, the post-oxidation treatment promotes the clear appearance of reflection located at 35.90° and 43.64° 2 theta, which are characteristics of kind magnetite iron oxide. It is important to remark that, for iron alloys oxidation process, the presence of high content of magnetite layers instead of hematite is preferred, mainly due to the well-known high corrosion performance of magnetite phase [13, 14]. In this sense, this work shows optimal processing condition for getting rich magnetite layers.

Both crystalline phases, γ' - Fe_4N and Fe_3O_4 , occur for all evaluated post-oxidation periods. However, additional to appearance of magnetite as a consequence of oxidation process, there is evident the occurrences of Fe_3N iron nitride. This phenomenon has been reported previously and it has been related to Fe_4N decomposition chemical reaction, because the presence of oxygen, to produce kind magnetite iron oxide through the reaction $3\text{Fe}_4\text{N} + 2\text{O}_2 = 3\text{Fe}_3\text{N} + \text{Fe}_3\text{O}_4$ [14].

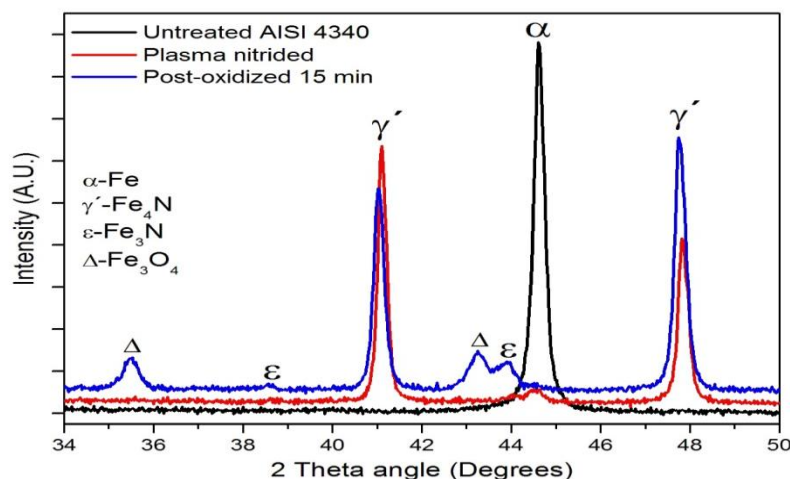


Figure 3. X-ray diffraction patterns for untreated, nitrided and nitrided post oxidized during 15 minutes samples.

Figure 4 shows the influence of post-oxidation process duration on samples corrosion performance, tested under rich chloride fog in agreement with procedure ASTM B117 and under conditions previously described. It can be seen that both, nitrided and nitrided post-oxidized samples show lower corrosion rate that untreated sample (evaluated through red rust presence on the surface of the samples). Moreover, it is evident that corrosion susceptibility of nitrided post-oxidized samples is considerably lower than only nitrided sample, which is much more evident after 21 hour test. Thus, after 21 h exposed to rich chloride fog, untreated and plasma nitrided samples showed presence of red rust on 90 and 80% of their surface respectively. However, for nitrided post-oxidized samples after 21 h test, presence of red rust on 5, 40 and 45% of the samples surface was detected for oxidation periods of 15, 30 and 60 minutes respectively. Figure 5 shows surface views of the samples: untreated, nitrided and nitrided post-oxidized during 15, 30 and 60 minutes.

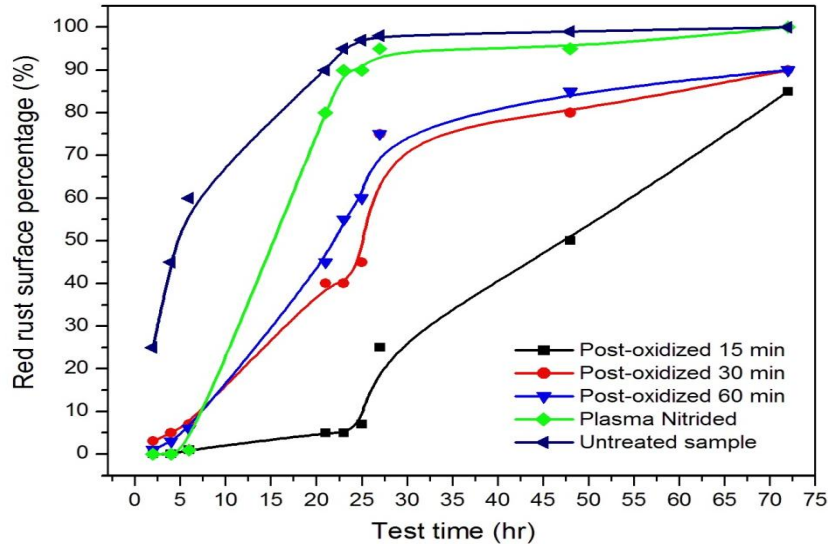


Figure 4. Influence of post-oxidation process duration on corrosion performance of evaluated samples.



Figure 5. Surface pictures of samples after 21h exposed to rich chloride fog. a) Untreated, b) nitrided, and post-oxidized during c) 15, d) 30 and e) 60 minutes.

In a previously work we reported that for the case of nitrided post-oxidized AISI 1045 steel, after 30 minutes of oxidation at 400°C, oxidized layer shows a cracking phenomenon which could be attributed to its thicker thickness and to the embrittlement of oxidized layer due to oxygen oversaturation [19]. In this sense, samples exhibiting any superficial cracking could be result in the exposition of fog of little surface sections without oxidized layer, which would result in the evident decrease in the corrosion performance.

Corrosion performance results show that show that 15 minutes of post-oxidation process is enough time to reduce the corrosion rate to around 1/16 part of the only nitrided sample corrosion rate. This fact represents a considerable increase in corrosion resistance of samples post-oxidized during 15 minutes respect samples processed during 30 and 60 minutes, which can be directly translated to an important energy and time saving.

It is important to emphasized that after 72 hour test, the better corrosion performance of post-oxidized samples respect untreated and nitrided samples is still evident. Thus, after 72 h test, untreated and nitrided samples shown presence of red rust on 100% of its surfaces while post-oxidized samples showed presence of this red rust on 85, 90 and 90% of its surface for samples post-oxidized during 15, 30 and 60 minutes respectively.

IV. CONCLUSION

In the present work the influence of pulsed plasma post-oxidation process on crystalline phase's composition and corrosion performance of plasma nitrided AISI 4340 steel was evaluated. Results analysis let us to conclude that:

Pulsed plasma nitriding promotes the modification of surface morphology from mirror polished (untreated sample) to a surface characterized by edged particles and well defined boundaries. As a consequence of the post-oxidation process, the quantity of edged particles was reduced leading to a less rough surface; the latter could be related to the formation of a homogeneous oxidized layer. Plasma post-oxidation process of nitrided AISI 4340 steel promotes the occurrence of a surface constituted by a magnetite thin layer on a thicker nitrided layer. The oxidized layer is characterized by presence of kind Fe_4N and Fe_3N iron nitrides.

The corrosion performance of the samples exposed to a salt fog was significantly better in the case of the oxidized samples compared with nitrided samples. After 21 h test, plasma nitrided sample showed red rust on 80% of its surface while samples post oxidized during 15 minutes showed only 5% of its surface with the occurrence of this red rust. This fact represent a decrease in corrosion rate of sample post-oxidized during 15 minutes to 1/16 part respect only nitrided sample.

REFERENCES

- [1] ASM International. ASM International Handbook Volume 1. Properties and selection: irons steel and high performance alloys. 10 th edition USA
- [2] R.C. Souza, H.J.C. Voorwald and M.O.H. Cioffi. Fatigue strength of HVOF sprayed Cr3C2–25NiCr and WC-10Ni on AISI 4340 steel. *Surface and Coatings Technology*. 203, 2008, 191-198.
- [3] H.J.C. Voorwald, L.F.S. Vieira, M.O.H. Cioffi. Evaluation of WC-10Ni thermal spraying coating by HVOF on the fatigue and corrosion AISI 4340 steel. *Procedia Engineering*. 2, 2010, 331-340
- [4] Sule Yildiz, Kahraman Sirin, Erdinc Kaluc. Effect of the ion nitriding surface hardening process on fatigue behavior of AISI 4340 steel. *Materials Characterization* 59, 2008, 351-358
- [5] Asadi Z.S., Mahboubi F. Effect of component's geometry on the plasma nitriding behavior of AISI 4340 steel. *Journal of Materials and Design* 34, 2012, 516-521
- [6] A. Akbari, R. Mohammadzadeh, C. Templier, J.P. Riviere. Effect of the initial microstructure on the plasma nitriding behavior of AISI M2 high speed steel. *Surface and Coatings Technology*, 204, 2010, 4114-4120
- [7] J.C. Stinville, P. Villechaise, C. Templier, J.P. Riviere, M. Droue. Plasma nitriding of 316L austenitic stainless steel: Experimental investigation of fatigue life and surface evolution. *Surface and Coatings Technology*, 204, 2010, 1947-1951
- [8] K. Ozbaysal, O. T. Inal. Thermodynamics and structure of solidification in the fusion zone of CO₂ laser welds of 15-5 PH stainless steel. *Materials Science Engineering*. 78, 1986, 179-191.
- [9] Yucl Birol. Effect of post-oxidation treatment on thermal fatigue behaviour of plasma nitrided hot work tool steel at elevated temperatures. *Surface and Coatings Technology*. 205, 2011, 2763-2769
- [10] N. Yasavol, F. Mahboubi. *Materials and Design* 38, 2012, 59-XX
- [11] M. Zlatanovic, N Popovic, Z. Bogdanov, S.Zlatanovic. Pulsed plasma-oxidation of nitrided steel samples. *Surface and Coatings Technology*. 174-175, 2003, 1220-1224
- [12] F. Borgioli, E. Galvanetto, A. Fossati, T. Bacci. Glow-discharge nitriding and post-oxidising treatments of AISI H11 steel. *Surface and Coatings Technology*. 162, 2003, 61-66
- [13] F. Mahboubi, M. Fattah. Duplex treatment of plasma nitriding and plasma oxidation of plain carbon steel. *Vacuum*. 79, 2005, 1-6
- [14] Yang. Li, Liang Wang, Dandan Zhang, Lie Shen. Improvement of corrosion resistance of nitrided low alloy steel by plasma post-oxidation. *Applied Surface Science*. 256, 2010, 4149-4152
- [15] Díaz Guillén J C, Campa Castilla A, Pérez Aguilar S I, Granda Gutiérrez E E, Garza Gómez A, Candelas Ramírez J, Méndez Méndez R. Effect of duty cycle on surface properties of AISI 4340 using a pulsed plasma nitriding process. *Superficies y Vacío*. 21, 2009, 1-4
- [16] Z.Sotani Asadi, F. Mahboubi. Effect of component's geometry on the plasma nitriding behavior of AISI 4340 steel. *Materials and Design*. 34, 2012, 516-521
- [17] H.J.C. Voorwald, L.F.S. Vieira, M.O.H. Cioffi. *Procedia Engineering* 2, 2010, 331-340
- [18] Zhao C, Li C.X, Dong H, Beel T. Study on the active screen plasma nitriding and its nitriding mechanism. *Surface and Coatings Technology*. 201, 2006, 2320-2325
- [19] Alireza Esfahani, Mahmoud Heydarzadeh Sohi, Jafar Rassizadehghani, Farzad Mahboubi. Effect of treating atmosphere in plasma post-oxidation of nitro carburized AISI 5115 steel. *Vacuum*, 82, 2008, 346-351
- [20] Díaz Guillén J. C., Granda Gutiérrez. E. E., Campa Castilla A., Pérez Aguilar S. I., Garza Gómez A., Candelas Ramírez J. Modificación superficial de un acero AISI 1045 mediante un proceso dúplex nitruración y post- oxidación en un plasma CD pulsado. *Superficies y Vacío* 25(3), 2012, 166-170.

Impact Analysis on Car Bumper by varying speeds using Materials ABS Plastic and Poly Ether Imide by Finite Element Analysis software Solid works

Pradeep Kumar Uddandapu

Assistant Professor ,Dept of Mechanical Engineering, K.S.R.M College of Engg, Kadapa, Andhra Pradesh, India

Abstract: Bumper is one of the main parts which are used as protection for passengers from front and rear collision. The aim of this study was to analyze and study the structure and material employed for car bumper in one of the car manufacturer. In this study, the most important variables like material, structures, shapes and impact conditions are studied for analysis of the bumper beam in order to improve the crashworthiness during collision. The simulation of a bumper is characterized by impact modeling using Pro/Engineer, impact analysis is done by SOILD WORKS according to the speed that is 13.3 m sec^{-1} (48 km h^{-1}) given in order to analyze the results. This speed is according to regulations of Federal Motor Vehicle Safety Standards, FMVSS 208- Occupant Crash Protection whereby the purpose and scope of this standard specifies requirements to afford impact protection for passengers. In this research, analysis is done for speed according to regulations and also by changing the speeds. Simulation using Finite Element Analysis software, which is SOILD WORKS, was conducted. The material used for bumper is CARBON FIBER-REINFORCED POLY-ETHER-IMIDE PEI and ABS Plastic.

Keywords: Pro-E, Solid works, meshing, bumper, stress, displacement, strain

I. INTRODUCTION

An automobile's bumper is the front-most or rear-most part, ostensibly designed to allow the car to sustain an impact without damage to the vehicle's safety systems. They are not capable of reducing injury to vehicle occupants in high-speed impacts, but are increasingly being designed to mitigate injury to pedestrians struck by cars. Front and rear bumpers became standard equipment on all cars in 1925. What were then simple metal beams attached to the front and rear of a car have evolved into complex, engineered components that are integral to the protection of the vehicle in low-speed collisions.

Today's plastic auto bumpers and fascia systems are aesthetically pleasing, while offering advantages to both designers and drivers. The majority of modern plastic car bumper system fascias are made of thermoplastic olefins (TPOs), polycarbonates, polyesters, polypropylene, polyurethanes, polyamides, or blends of these with, for instance, glass fibers, for strength and structural rigidity.

The use of plastic in auto bumpers and fascias gives designers a tremendous amount of freedom when it comes to styling a prototype vehicle, or improving an existing model. Plastic can be styled for both aesthetic and functional reasons in many ways without greatly affecting the cost of production. Plastic bumpers contain reinforcements that allow them to be as impact-resistant as metals while being less expensive to replace than their metal equivalents.

Plastic car bumpers generally expand at the same rate as metal bumpers under normal driving temperatures and do not usually require special fixtures to keep them in place. Some of the plastic products used in making auto bumpers and fascias can be recycled. This enables the manufacturer to reuse scrap material in a cost-effective manner. A new recycling program uses painted TPO scrap to produce new bumper fascias through an innovative and major recycling breakthrough process that removes paint from salvage yard plastic. Tests reveal post-industrial recycled TPO performs exactly like virgin material, converting hundreds of thousands of pounds of material destined for landfills into workable grade-A material, and reducing material costs for manufacturers.

Why has bumper effectiveness been reduced in preventing damage in a minor collision? One reason could be that statutory bumper standards were made quite loose. As a result, many of today's bumpers allow cars to be damaged more easily.

II. Design Of Car Bumper By Pro-E Software

Pro/Engineer is a software application within the CAID/CAD/CAM/CAE category, along with other similar products currently on the market. Pro/Engineer is a parametric, feature-based modeling architecture incorporated into a single database philosophy with advanced rule-based design capabilities. The capabilities of the product can be split into the three main heading of Engineering Design, Analysis and Manufacturing. This data is then documented in a standard 2D production drawing or the 3D drawing standard ASME Y14.41-2003.

Modeling of car bumper is done with help of Pro-e software and dimensions are selected from one of car bumper. As the impact is more for the front portion of bumper only outer dimensions of car bumper has been considered for modeling, Slots provided in middle of car bumper is used for reducing drag effect in car bumper.



Figure: 1

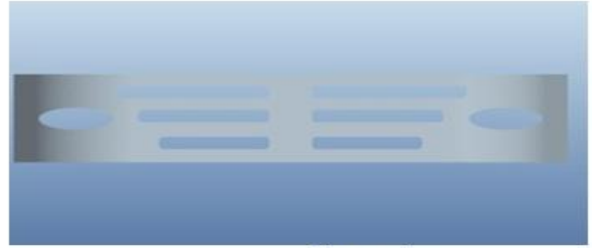


Figure: 2

III. Analysis Of Car Bumper With Fea Software Solid Works

Cosmos works is useful software for design analysis in mechanical engineering. That's an introduction for you who would like to learn more about COSMOS Works. COSMOS Works is a design analysis automation application fully integrated with Solid Works. This software uses the Finite Element Method (FEM) to simulate the working conditions of your designs and predict their behavior. FEM requires the solution of large systems of equations. Powered by fast solvers, COSMOS Works makes it possible for designers to quickly check the integrity of their designs and search for the optimum solution.

A product development cycle typically includes the following steps: 1 Build your model in the Solid Works CAD system 2 Prototype the design. 3 Test the prototype in the field. 4 Evaluate the results of the field tests. 5 Modify the design based on the field test results. Analysis Steps: You complete a study by performing the following steps: • Create a study defining its analysis type and options. If needed, define parameters of your study. Parameters could be a model dimension, a material property, a force value, or any other entity that you want to investigate its impact on the design. Analysis Background: Linear Static Analysis Frequency Analysis Linear zed Buckling Analysis Thermal Analysis Optimization Studies, Material property, Material Models, Linear Elastic Isotropic, Plotting Results, Describes how to generate a result plot and result tools. Listing Results, Overview of the results that can be listed, Graphing Results, Shows you how to graph results, Results of Structural Studies, Lists results available from structural studies, Results of Thermal Studies. Lists results available from thermal studies, Reports, explains the study report utility. Stress Check. Lists the basics of checking stress results and different criteria used in the checking

MESHING OF CAR BUMPER

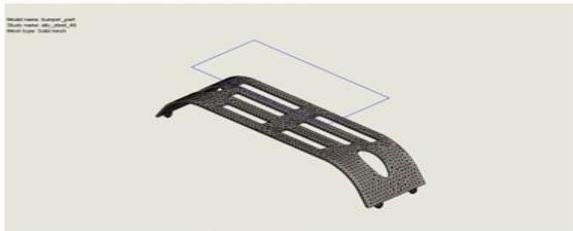


Figure 3

ABS Plastic

Model name: bumper_part Current Configuration: Default	
Solid Bodies	
Treated As	Volumetric Properties
Solid Body	Mass:17.9998 lb
	Volume:488.464 in ³
	Density:0.0368498 lb/in ³
	Weight:17.9876 lbf

Table.1

Setup Information

Type	Velocity at impact
Analysis type	Drop Test
Mesh type	Solid Mesh
Velocity Magnitude	13.3 m/sec
Impact Velocity Reference	Plane1
Gravity	9.81 m/s ²
Gravity Reference	Front Plane
Parallel to reference plane	Top Plane
Friction Coefficient	0
Target Stiffness	Rigid target

Table.2

Units

Unit system:	SI (MKS),FPS
Length/Displacement	mm
Temperature	Kelvin
Angular velocity	Rad/sec
Pressure/Stress	N/m ²

Table.3

Material Properties ABS Plastic

Name : ABS Plastic
 Model Type : Linear Elastic Isotropic
 Default failure : Max Von Mises Stress
 Tensile strength : $3e+007$ N/m²
 Elastic modulus : $2e+009$ N/m²
 Poisson's ratio : 0.394
 Mass density : 1020 kg/m³
 Shear modulus : $3.189e+008$ N/m²

Name	Type	Min	Max
Stress1	VON: von Mises Stress	1.79916e-016 N/mm ² (MPa) Node: 11391	25.4296 N/mm ² (MPa) Node: 307

Table.4 & Figure.4

Name	Type	Min	Max
Displacement1	URES: Resultant Displacement	0.00170703 mm Node: 7857	0.2977 mm Node: 901

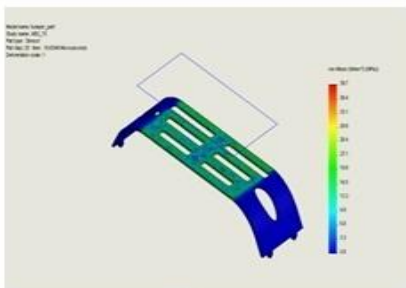
Table.5 & Figure.5

Name	Type	Min	Max
Strain1	ESTRN: Equivalent Strain	0 Element: 8041	0.00865195 Element: 545

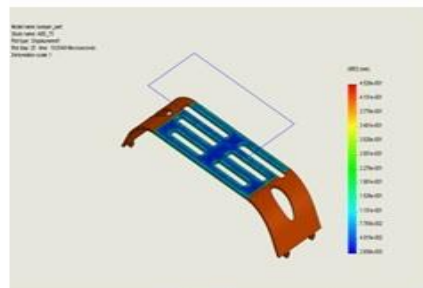
Table.6 & Figure.6

For 75 KM/hr ABS Plastic

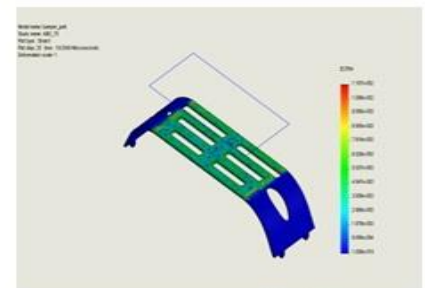
Stress1 MIN 3.60887e-016 N/mm² Node: 11712 MAX 39.6692 N/mm² Node: 307
 Displacement1 MIN 0.00265575 mm Node: 7857 MAX 0.452602 mm Node: 3614
 Strain MIN 0 Element: 8041 MAX 0.0118735 Element: 1732



Stress
Figure.7



Displacement
Figure.8



Strain
Figure.9

POLY-ETHER-IMIDE PEI

 Model name: bumper_part Current Configuration: Default	
Solid Bodies	
Treated As	Volumetric Properties
Solid Body	Mass:26.1174 lb Volume:488.464 in ³ Density:0.0534684 lb/in ³ Weight:26.0997 lbf

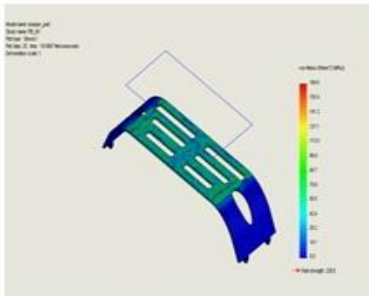
Table.7& Figure.10

Material Properties PEI

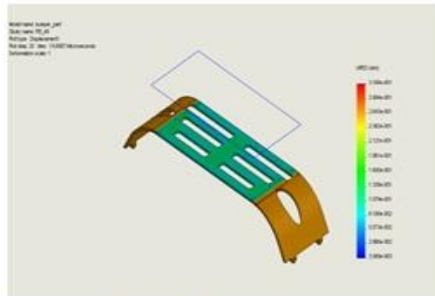
Name : PEI
 Model Type : Linear Elastic Isotropic
 Default failure : Max Von Mises Stress
 Yield strength : $2.3e+008$ N/m²
 Tensile strength : $2.41e+008$ N/m²
 Elastic modulus : $3.38e+010$ N/m²
 Poisson's ratio : 0.4
 Mass density : 1480 kg/m³
 Shear modulus : $3.189e+008$ N/m²

For 48 KM/hr PEI Plastic

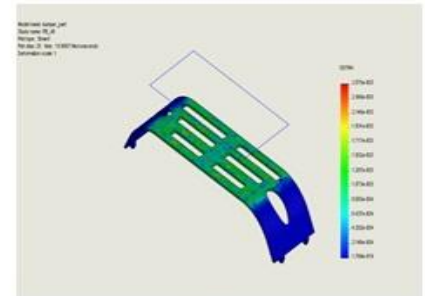
Stress1 MIN 1.00086e-014 N/mm² Node: 1569 MAX 169.485 N/mm² Node: 14495 Displacement1 MIN 0.00358896 mm Node: 15102: MAX 0.31642 mm Node: 1091
 Strain MIN 0 Element: 8041 MAX 0.00257491 Element: 6554



Stress
Figure.11



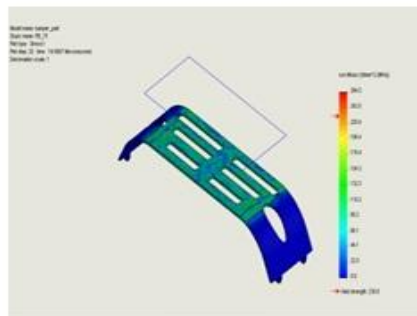
Displacement
Figure.12



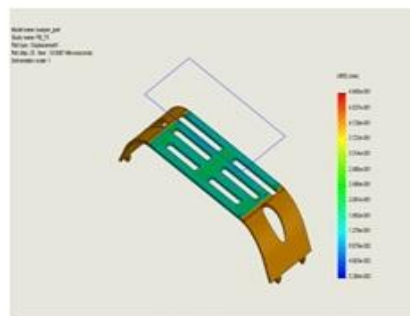
Strain
Figure.13

For 75 KM/hr PEI Plastic

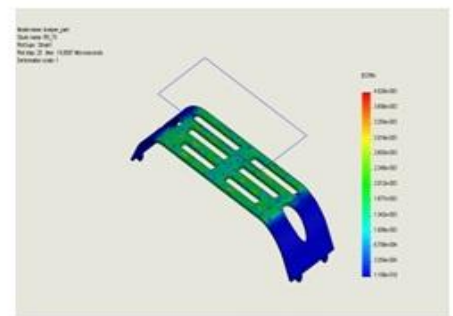
Stress1 MIN 1.11257e-014 N/mm² Node: 16808 MAX 264.538 N/mm² Node: 14495
 Displacement1 MIN 0.00526361 mm Node: 15102 MAX 0.494451 mm Node: 1091
 Strain MIN 0 Element: 8041 MAX 0.00402493 Element: 6554



Stress
Figure.14



Displacement
Figure.15



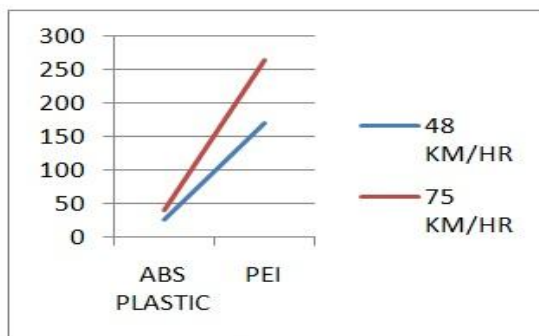
Strain
Figure.16

IV. Results and Discussions

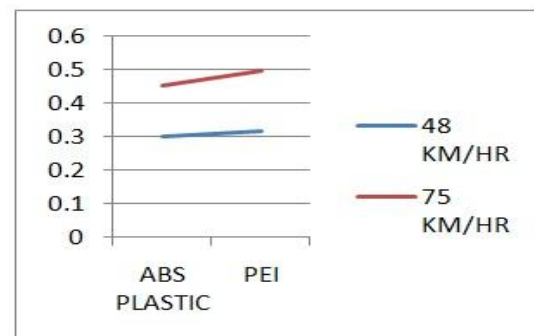
Observing the graphs of stress and Displacement, values of Abs plastic are less than PEI, The ABS Plastic has good impact resistance when compared to PEI.

		STRESS N/mm ²	DISP mm	STRAIN
ABS PLASTIC	48 Km/hr	25.4296	0.297715	0.00865195
	75 Km/hr	39.6692	0.452602	0.0118735
PEI	48 Km/hr	169.485	0.31642	0.0025749
	75 Km/hr	264.538	0.494451	0.0040249

Table.8



Graph.1 Materials Vs Stress



Graph.2 Materials Vs Displacement

V. Conclusion

Modeling of a car bumper is done using 3D modeling software Pro/Engineer. Impact analysis is done on the car bumper for different speeds of 48Km/hr, 75Km/hr. The analysis is also carried on the car bumper for different materials ABS Plastic and Carbon Fiber-Reinforced Poly-Ether-Imide PEI. At Present the material used for car bumper is steel. Steel is replacing with ABS Plastic and Carbon fiber -Reinforced Poly-Ether-Imide PEI. The density of ABS Plastic and PEI is less than that of steel; thereby the overall weight of car bumper is reduced.

By observing the Impact Analysis results like Stress, Displacement and strain , the stress values are less for ABS Plastic and PEI than steel. By comparing the results of ABS Plastic and PEI, the stress values are less for ABS Plastic than PEI. ABS Plastic is better for utilization comparing PEI.

References

- [1] H. S. Park, X. P. Dang, A. Roderburg, "Development of Plastic Front Panels Of Green Cars" CIRP Journal of Manufacturing & Technology vol 26 Pages 35-53
- [2] Kuziak .R. Kawalla, R.waengler.s. "Advanced high strength materials for automotive industry A review" Journal of Archives of Civil & Mechanical engineering .volume 8 issue2, 2008-12-30 ,Pages 103-117
- [3] Falai chen , Bert Juttler, "Geometric Modeling & Processing", Journal on CAD, volume 42 issue1 pages 1- 15
- [4] David H. Allen "Structural Analysis, Aerospace" Journal on Encyclopedia of Physical science and technology 3rd edition 2003
- [5] Japan.s.Daniel.L. and Theodor .k.2005. "Finite Element Analysis of Beams", Journal of Impact engg. Vol 31, Pages 861-876., Pages 155-173.
- [6] OLBISI olagoke (1997) "Hand book of Thermo Plastics", Marcel Dekker, New York.
- [8] Dominick v. rosato, "Plastics Engineering", Manufacturing & Data Hand Book
- [9] Donald v .rosato, "Plastics Engineering", Manufacturing & Data Hand Book

An Idea of Multi-Functional Storage Reservoirs in Mountain Regions

Jan Jaremski

Rzeszow University of Technology, Rzeszow, Poland

Abstract: The paper presents possibilities of construction of multi-functional reservoir in mountain regions, especially those with soft rocks. Construction of relatively small reservoir instead of big ones and taking the area configuration into account allows eliminating expensive embankments and insists to construction of cofferdams. The cofferdam can be formed of the occurring rock eluvium. Such idea was analyzed for the south of Poland. At present we can observe the climate changes accompanied by increase of the weather dynamics and unusual intensity of extreme phenomena. Mineralogical composition of rocks or their eluvia occurring in the considered area is usually not taken into account while forecasting of such phenomena. The proposed tests on determination of the eluvium areas especially susceptible to formation of mud avalanches in the mountains sites.

Keywords: flysch eluvium, reservoir, rock eluvium, mud avalanches, swelling

I. INTRODUCTION

The climate variation has been observed recently. They are accompanied by increase of the weather dynamics and unusual intensity of extreme phenomena. Precipitations are very intense and they are accompanied by landslides and mud avalanches, or long-lasting droughts. A lack of suitable retention causes a fast flow of discharge water to the seas. Mineralogical composition of rocks or their eluvia occurring in the considered area is usually not taken into account while forecasting of such phenomena. Colloidal activity, a state of colloidal bonding and crystallization strongly influence formation of avalanches, strength of the mixtures and reversibility of their reactions with participation of clay minerals.

Polish water resources are rather poor in comparison with other European countries. 1600 m³ falls to one person in a typical year; in a dry year it is below 1450 m³ [1]. In Spain such number is twice higher, and for all Europe this number equals to 4500 m³. Retention ability of Polish reservoirs equals to 6% of the mean flow of the surface water per year. Moreover, it does not prevent against periodical excess of deficit of water. Our water resources vary at different seasons and their distribution is not uniform. The Podkarpacie region, especially its mountain part, belongs to the regions where the water resources are the most poor. Only 20% of all the underground water of that region occur in its mountain part. In this region there is a lack of rich aquiferous layers because of an unique geological structure, i.e. the laminar Carpathian flysch. It is water-permeable (there are no faults and dislocations), so in this region there are very good conditions for small flood pools. Such conditions allow for high surface flows which can be significantly slowed down owing to renaturization of the flows and so-called "small retention". The program of "small retention" gives the best results in mountain and forest areas, for example the Bieszczady mountains in the south of Poland. "Small retention" satisfies most requirements connected with ecological methods of water economics, and if it is correctly realized, it can help in improvement of natural values of ecosystems []. The Podkarpacie region belongs to the mountains range of the Carpathian arc and the fall before the Carpathians. The region is very diversified considering its configurations and geological structure. Such diversification influences hydrography, climate, soils, flora and fauna etc.

Intense precipitations in the summer are very important for the idea of construction of flood pools. The mountain part of the region belongs to the Carpathian climate with thermal conditions varying depending on the site height. Geological and hydrogeological conditions of the region in its mountain part are really suitable for the flood pools. The eastern Carpathians are built of flysch formations, weathered in their top layer. The eluvia usually occur as dust or dust clays. The external part of the massif contains flysch formations (Fig. 1), i.e. sandstone, mudstone, menillites, etc. [14].



Fig. 1. Outcrops of the Carpathian Flysch

The Bieszczady Mountains are the area where there are very good conditions for the considered reservoirs because of favourable tectonics and its effects. It appears from the tests realized in the Podkarpacie region it appears that the eluvia occurring under the surface are of a high volume, and from mineralogical tests it results that they are suitable for location of reservoirs because they guarantee the maximum tightness. Thus, construction of small earth dams or rock-fill dams probably

will not require application of additional sealing elements. The eluvium of suitable parameters will play that role. The eluvia in the layers located just under the surface usually occur as dust or dust clays.

Generally speaking, in the flysch formations of the Podkarpacie region there are no advanced aquiferous layers. The minimum surface permeability is also an effect of mineralogical structure of the surface layers. Under moderate swelling, illite minerals seal the site surface and increase intensity of the surface flow. In a consequence, even relatively low precipitations cause a flood situation at many water-courses and rivers in the Podkarpacie region. Thus, construction of multi-functional pools of small retention on the limited areas protects the water-courses of the Podkarpacie region against the results of floods. The proposed idea increases pure water resources, influences beauty of the region. It also changes geotechnical conditions and improves stabilization of slopes, protects against landslides.

The proposed idea seems to be reasonable because in 1995 in Japan 360 such reservoirs were built in the mountains, and the country was protected against floods. At the same time, suitable amount of water was delivered for rice growing (Japan is an important exporter of rice at present).

Let us note that the considered pools are located in the mountains, and the cofferdams baffling the valleys are made of soil concrete because of a large amount of montmorillonite in the rock eluvia. In the past in Andalusia the Moor engineers built the reservoirs used for the purposes of agriculture, and this area of Spain developed very quickly. Let us remember that the proposed pools should be supplied by water flowing from the eastern Carpathians being an enclave of unique environmental conditions.

Water-bearing character of the flysch rocks is connected with their slots – it results from their low porosity, i.e. from 0.02 to 0.1. The flow in the interporous spaces is difficult because of their small dimensions; moreover they are filled with the weathered illite fraction, susceptible to shrinkage and swelling, decreasing water absorbability of the flysch, sometimes to zero. Water absorbability gets worse as the depth of layer deposits rises. Resources of underground water is very low, there are no water-bearing layers. Water is stopped and occurs only in the cracked rocks. Under such conditions, precipitation waters can easily flow to the water-courses, and next to the fall before the Carpathians where they supply the reservoir of underground waters. From that reservoir they flow through the underground gutters to the basin of the Dniestr River. Minimal surface permeability is also an effect of mineralogical structure of surface layers, i.e. illite and smectite minerals. Because of swelling, these minerals seal the surface and increase intensity of the surface run-off. In a consequence, even relatively small amount of precipitations cause floods at many rivers and water-courses of the Podkarpacie region.

Climate variation causes serious rain-storms which are very dangerous for inhabitants of the Podkarpacie region. Such storm took place on the 26th July, 2005 near locality Zagórz. Some villages were flooded in a very short time. The mentioned above example of Japan also proves that the proposed solution seems to be reasonable.

II. THE PREDICTED KINDS OF FLOOD POOLS

Rational management of water resources in the Podkarpacie region requires minimization of their variation at time and space (periods of drought and flood). Thus, retention must be developed in the area of the basin. Construction of small multi-functional pools is recommended. In management of each pool one function here is usually dominating (flood protection, touristic, ecological or energy function and so on), and other tasks are assigned as that main function. In practice, there are pools satisfying two or three main economic tasks at the same time depending on local needs. .

There is no one official classification of flood pools. So-called “small retention” includes all the microreservoirs, and small pools positively influencing the environment [10]. Small pools are usually of total volume to 0.1 of million m³ and the maximum swell height 5 m. They are built one by one, or in a cascade system [12]. All the cascade is usually used for energetic purposes. The systems of small retention pools are proposed instead of one big reservoir. In Bieszczady mountains there are many river valleys (Fig.2) which are good places for the proposed flood pools. In the past many people lived in those valleys, at present they uninhabited.

According to the proposed concept, reservoirs – depending on their location – can be flood pools, equalizing tanks, they can also be auxiliary reservoirs near big flood pools [3]. Some reservoirs should play the role of flow reservoirs formed as a result of partition of water-courses. Dry reservoirs are also provided as anti-flood protection. They will be accumulate the flowing eluvium or organic products.



Fig. 2. An exemplary site for a reservoir in the Bieszczady Mountains

In the considered region, the intense precipitations, of big slopes of the ground and the flysch substrate cause intense run-off of the weathered flysch layer, sometimes being like an avalanche. The rubble occurring in the reservoirs and flumes of water-courses causes that they become more and more shallow. Thus, construction of dry reservoirs is. In the considered area there are unusual conditions of flysch weathering, especially biological weathering. Such conditions are a result of rich afforestation. Generally speaking, in the considered region plan dry reservoirs it will be possible to plan dry reservoirs where will be accumulate the flowing weathered eluvia or organic products. Such places will be the programmed enclave of the intense development of flora and fauna and, we can also expect favourable humus processes.

III. APPLICATION OF FLYSCH ELUVIA FOR CONSTRUCTION OF COFFERDAMS

From the investigations on landslides in the Podkarpacie area it appears that the eluvia existing under the site surface are of a large thickness. From mineralogical tests it results that such eluvia are very good for location of reservoirs because they provide the maximum tightness. Thus, construction of small earth dams will not require additional sealing elements. This role should be played by a layer of eluvium of suitable parameters.

Experience obtained while investigations on marl eluvia as well as the elaborated test methods were applied for investigations of the Carpathian flysch and dust soils occurring in the river terraces, grounds of loess massif, illite clays and baidelite clays [4,5]. These grounds are susceptible to moisture changes accompanied by shrinkage and swelling as well as petrification. This property is strictly connected with presence of illite in mineralogical composition of the considered media. Even a very small amount of that mineral influences joints of the basic minerals.

The samples prepared of eluvium shales were tested and next the obtained results were compared with the results obtained for the samples from river valleys treated as the accumulated sediment of the flysch eluvium [5]. The test were carried out in order to estimate usability of flysch eluvia for construction of cofferdams by identification of clayey minerals. Differentiation of these minerals is important because the contents of smectite groups exerts an unfavourable influence on setting and hardening of ground concrete [11]. As for the considered ground media, their basic geotechnical parameters were tested and special attention was paid to swelling tests allowing to distinguish clayey minerals. Before the swelling tests, physical, chemical and strength tests as well as mineralogical tests of the considered media were carried out [4, 6]. Recognition of the grounds was based on chemical and mineralogical compositions by means of fluorescence, X-ray diffractometry and scanning microscopy. Moreover, derivatographic analysis was realized. Recognition of microstructure of the clays with so-called hidden swelling parameter were carried out by means of scanning microscopy. The mentioned tests of chemical composition (Fig.3) show the presence of potassium which occurs only in illite. It was proved by tests realized by means of the scanning electron microscope (SEM).

The tests of flysch swelling, swelling clay or the media with so-called hidden swelling parameter used the method described previously [8]. This method allows for cheap tests of flysch eluvia and estimation of their usability. Identification of illite in the flysch eluvium allows to qualify it as a material for construction of cofferdams because of moderate shrinkage and swelling as well as favourable petrification and sealing properties. Moreover, the proposed tests could help in selection of places for reservoir location into taking a proper tightness of the ground account.

Presence of illite being an aluminosilicate responsible for eluvium petrification allows for application of flysch chips and flysch eluvia for construction of earth cofferdams according to the proposed construction of multi-functional pools in the Bieszczady Mountains [3]. In Japan, the flood pools were located in the mountains and the cofferdams in the valleys where the ground-concrete is made. The eluvia occurring in Japan contain montmorillonites, so formation of cofferdams is difficult, because it is necessary to add much cement to the eluvia. It is also necessary to take care of ground-concrete because of formation of scratches caused by shrinkage of montmorillonite [13].

Construction of cofferdams using flysch chips and flysch eluvia is considered for each reservoir in Bieszczady, depending on its geological structure. Of course, a suitable amount of clayey minerals for petrification and sealing is necessary. If there are no enough illite minerals in the eluvium, we must consider a solution using geotextiles and sealing foils for cofferdams, and materials offered by such firms as Tensar International Corporation, Ten Cate Geosynthetics and Geobrug.

IV. THE PROPOSED TESTS FOR DETERMINATION OF THE ELUVIUM AREAS ESPECIALLY SUSCEPTIBLE TO FORMATION OF MUD AVALANCHES IN THE MOUNTAINS SITES

Experience obtained in the while works on marl eluvia [2,4,7], and the elaborated test methods were used during tests of Carpathian flysch and dust soils occurring in river terraces generated as a result of the eluvia accumulation [5,11].

The samples prepared from the shale eluvia were tested and compared with the samples from the river valleys, treated as the accumulated sediment of the flysch eluvium. The basic geotechnical parameters of the considered ground media were tested. Special attention was paid to swelling tests allowing to identify clayey minerals. At present, the author is engaged in works connected with the causes of mud avalanches formation. In such cases, hydraulic conditions and influence of mineralogical composition should be taken into account. Tests of susceptibility of the soft rocks for formation of the mud avalanches could be limited to drawing of eluvium samples occurring at the slope. The samples should be subjected to swelling tests by means of the method given in the some previous papers [4,8,11]. This simple method allows to identify clayey minerals responsible for swelling, occurring in the rocks. While tests we use the presence of endothermic maxima – the temperature points at which the heated sample loses contents of bound water. The author found that minerals from the groups of monmorillonite and illite (causing swelling) lost that water at the temperature up to 200 degrees, and kaolinite – at 600 degree. Thus, the comminuted eluvium sample prepared to the standard swelling test and free

from water, subjected to the swelling test manifests swelling up to tens %. Under such conditions, the kaolinite sample swells up to some %. Let us remember that montmorillonites soak to 700%, while kaolinite soaks to 90%.

4.1 THE PROPOSED METHOD OF EXAMINATION OF CLAY MINERALS

Application of the method of swelling ability test, given in the author's earlier works [2,4,8] was proposed as method of determining the content of illite and smectite minerals. It has been proved so far that it is just these minerals that are responsible for moisture changes, extreme strength parameters and processes of petrification and maximum moisturizing. Tests were carried out on the material taken from the deposit of different breakups, and samples were grouped in accordance with the diameter of sieve meshes. With the method of successive trials, it has been found that the most stable and real results are obtained by conducting the tests in the following way [11]:

1. The material undergoes a preliminary air-drying in the case of water content so that it can be sifted through the of $\varnothing=0.76$ mm
2. the material thus prepared is subjected to moisture content near to the plasticity limit (during the trial of roller bursts at the first or second instant) and is subjected to working (just like a typical "dough")
3. forming the material into the "cake" – like shape of 10 mm in height
4. then , samples with the diameter $\varnothing=50$ mm and 65 mm and the height of 10 mm and 20 mm are cut by means of a ring
5. the samples thus prepared are weighed and dried in a drier at a temperature of 200 C for the period from two hours until reaching constant weight
6. after drying and cooling process the samples are weighed to determine their water content
7. the samples are subjected for the examination of swelling minerals in the apparatus testing unbounded swelling
8. After swelling has been defined the final moisture is determined.

The considered test informs us about the amounts and kinds of swelling minerals in the point of sampling. Thus, we get also the data concerning ability of the tested rock medium to water stoppage and moisture degree, as well as the maximum moisture occurring under natural conditions.

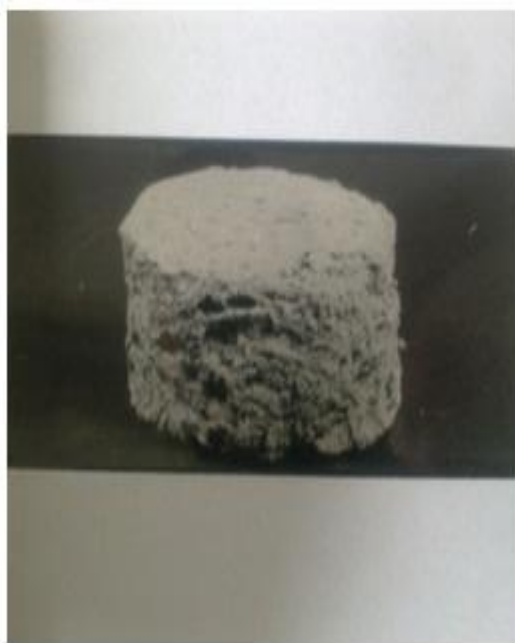


Fig.3.Examples of rocks samples after the investigation

After swelling, the sample moisture is the maximum moisture, under which we get the worst numerical values of the strength parameters. Under such conditions, landslides are possible. In our analysis, soft rocks are treated as mixtures containing much clayey minerals. In the case of occurrence of greater contents of montmorillonite, greater amount of moisture is present and it is accompanied by fluidization and formation of mud avalanches. Similarly, content of the swelling minerals in higher parts of mountains causes their collecting in the rock slots. Then, possibility of landslides and rock falls increases.

The swelling investigations were preceded by physical, chemical and strength tests of the considered media. Recognition of such soils were based on tests of chemical and mineralogical composition by means of fluorescence and X-ray diffraction method. Moreover, derivatographic analyses were performed. Tests of clay structure with so-called swelling parameter were realized by means of scanning microscopy (SEM) utilization of SEM, derivatogram method, fluorescence, diffraction method.

Simple analyses and tests according to the discussed swelling tests allow to identify sites which can be easily subjected to mud avalanches and rock falls. Such information are very useful for the site management.

VI. CONCLUSIONS

- 6.1. Suitable geological (soft rocks) structure allows for cheap construction of reservoirs. Dislocations and fault fissures filled with weathering materials because of their mineralogical structure, i.e. swelling minerals cause self-sealing of the bottom. A lack of water-bearing layers eliminates uncontrolled outlet of water to the ground.
- 6.2. Distinct improvement of protection against floods is an advantage of the proposed solution (see the mentioned solution in Japan). At present, intense precipitations are transported to water-courses and rivers because they cannot percolate to the ground (it is favourable for reservoir structure).
- 6.3. Water supply for inhabitants of a given region and water collecting in reservoirs can be very important in the future. Large amount of water of high quality should be a valuable good. Water resources could influence future development of many regions.
- 6.4. Construction of the considered reservoirs is rather cheap because it is possible to introduce unified earth cofferdams using ground-concrete as a construction material.
- 6.5. Introduction of the considered reservoirs could help in generation of new places of employment (construction and service, tourists' service)
- 6.6. Some reservoirs could be used in energetics.

REFERENS

- [1] Bogacz – Rygas M : (2007) Aspekty ekologiczne stosowania nowych rozwiązań odprowadzania wód opadowych i ich zagospodarowanie(in polish),. Wavin Metalplast-Buk.Kielce.
- [2] Jaremski J.:(1994) Influence of physical and chemical processes occurring in eluvium of the Opole marls and their influence on the geotechnical parameters, Proceedings of the 7th International Congress IAEG, Lisboa , A.A Balkema, 859-868.
- [3] Jaremski J.:(2007) O niektórych aspektach budowy wielofunkcyjnych zbiorników retencyjnych w części górzyskiej województwa podkarpackiego. Cywilizacja i żywioty, (in polish), seria: Monografie Instytutu Meteorologii i Gospodarki Wodnej, Warszawa.
- [4] Jaremski J.:(1995) Proposal for a method determining value of the maximum swelling of soil by example of the Opole marls eluvium and illite clays. Proc. of 8th Int. Cong. on Rock Mechanics, Tokyo, A.A.Balkema.
- [5] Jaremski J.:(2004) The influence of changes of weathering water content on the formation of landslides in the Carpathian Flysch. Proc. of 9th Australia New Zealand Conference on Geomechanics, Auckland – February 2004, New Zealand Geotechnical Society Inc.
- [6] Jaremski J.:(2005), The influence of physical and chemical processes occurring in the weathered Opole marls on the geotechnical parameters, Publishing House of Rzeszów University of Technology, 2005,p. 98.
- [7] Jaremski J.(1991), Creep property of Opole marls weathering on the base of the model laboratory research and the research “ in situ” , Proceedings of the 7th International Congress on Rocks Mechanics, Aachen, A.A. Balkema, 1991, 269-273.
- [8] Jaremski J :(1994) Proposal for method of stating the value of maximum swelling of the soil on the example of Opole marls eluvium. Proc. 3th Int. Conf. on Trop. Resid. Soils., Maseru, A.A.Balkema,
- [9] Jaremski J :(1990) Analysis of swelling of marl eluvium of water infiltration. Proc. 6th Int. Cong. IAEG. Amsterdam, A.A. Balkema, Rotterdam.
- [10] Jaremski J.:(2010) Aspekty geotechniczne w ochronie zasobów wodnych województwa podkarpackiego. Inżynieria Morska i Geotechnika (in polish), nr. 1. Gdańsk 2010.
- [11] Jaremski J.:(2010), Influence of moisture changes on physico - chemical processes and geotechnical parameters in soft rocks, Studia Geotechnica et Mechanica, Vol. XXXII, No. 1, 2010
- [12] Mioduszewski W.:(2008) Mała retencja w lasach elementem kształtowania i ochrony zasobów wodnych. Studia i Materiały Centrum Edukacji Przyrodniczo-Leśnej R. 10. Zeszyt 2 (18) (in polish) .
- [13] WAKIZAKA Y.:(1994) Influence of montmorillonite group Bering aggregates on concrete. 7th International IAEG Congress, A.A. Balkema 1994, s. 3285-3294.
- [14] Zabuski L., Thiel K., Bober L.(1999), Landslides in Polish Carpathian Flysch, (in polish), IBWN PAN, Gdańsk, p. 172.

Structural Analysis of NAB Propeller Replaced With Composite Material

M.L.Pavan Kishore,¹ R.K.Behera,² Sreenivasulu Bezawada³

¹Research Scholar, Department of Mechanical Engineering, NIT Rourkela, Odisha, INDIA

²Professor, Department of Mechanical Engineering, NIT Rourkela, Odisha, INDIA,

³Assistant professor, Department of Mechanical Engineering, MITS, Madanapalle, Andhra pradesh, INDIA

Abstract : The present work deals with modeling and analyzing the propeller blade of a underwater vehicle for their strength. A propeller is a complex geometry which requires high end modeling software. The solid model of propeller is developed in CATIA V5 R17. Hexa solid mesh is generated for the model using HYPER MESH. Static, Modal analysis of both NAB and composite propeller are carried out in ANSYS software. The stresses obtained are well within the limit of elastic property of the materials. The deflection for composite propeller blade as well as for NAB was determined. On comparison which shows that by changing the layup sequence further composite materials can be made much stiffer than NAB propeller.

Keywords: Boundary conditions, Deformation, Elements, Nodes, Meshed model

I. INTRODUCTION

Ships and under water vehicles like submarines, torpedoes and submersibles etc., uses propeller as propulsion. The blade geometry and its design is more complex involving many controlling parameters. The strength analysis of such complex 3D blades with conventional formulas will give less accurate values. In such cases numerical analysis (Finite Element Analysis) gives comparable results with experimental values.

In the present project the propeller blade material is replaced from Nickel Aluminum Bronze (NAB) metal to a fiber reinforced composite material (FRP) for ship propeller. This complex analysis can be easily solved by finite element method techniques. The structural analysis is done for the four bladed solid NAB as well as Composite propeller. The structural analysis includes the evaluation of static and dynamic analysis for the propeller blades Eigen value analysis are performed. To compare the results. The goal of this work is to design, and evaluate the performance of the composite Propeller with that of the NAB propeller.

The first approach to strength problem was made by Taylor(1) who considered propeller as a cantilever rigidly fixed at the boss. then stresses were evaluated following the theory of simple bending using section of the blade by a cylinder. The measurements of deflection and the stresses on model blades subjected to simulated loads was carried out by I.E. collony (2) combining both the theoretical and experimental investigations. The main sources of propeller blade failure are resolved systematically by Changsuplee (3) carried out Fem analysis to determine the blade strength.

The distribution of thrust and torque along the radius to compare actual performance of a propeller with the calculated performance was given by George (4). W.J Colclough (5) the advantage of using a fiber reinforced material as a composite over the propeller blade from other materials. Christopher Leyens (6) discussed two different materials and design approached for the purpose of reduced weight and increased strength and stiffness. Gau-Feng Lin [7] et.al, carried out stress calculations for a fiber reinforced composite thruster blade. Jinsoo cho[8] developed a numerical optimization technique to determine the optimum propeller blade shape for efficiency improvement. Charles Dai[17] et.al., discusses preliminary propeller design strategy, numerical Optimization, knowledge based systems and geometric algorithms in general and in specific as applied to the design of a particular propeller. Based on above discussions replacement of NAB propeller blade was done to replace with composite material for strength analysis. paper. (10)

II. MODELING OF A B-SERIES PROPELLER BLADE

In order to model a propeller blade of particular series type airfoil points of specific type are required .In present work a B-series standard airfoil points are chosen for the modeling. The outline airfoil points and propeller blade are modeled in Solid works 2010 and the hub and filleting portion of blade are done in catia V5R17. since the propeller blade consisting of various radii are located through corresponding pitch angles. Then all rotated sections are projected onto a right circular cylinder of respective radii as shown in fig below. Then by using multi section surface option, the blade is modeled.

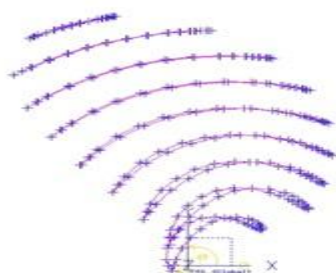


Figure1. construction of hydrofoils by

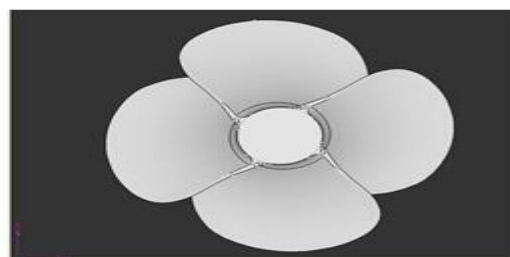


Fig2. Solid model of NAB propeller joining of points on surface of the blade

2.1. Hyper mesh as a tool for Meshing

The solid model of the propeller blade along with hub is imported to HYPERMESH 11.0 and solid mesh is generated for the model. The model with and without mesh are shown in figure below. Boundary conditions are applied to meshed model. The contact surface between hub and shaft is fixed in all degrees of freedom. Thrust of 332.14 N is uniformly distributed in the region between the sections at 0.7R and 0.75R on face side of blade, since it is the maximum loading condition zone on each blade as per the George [7] work. The loading condition is as shown in figure 4.8. Quality checks are verified for the meshed model. Jacobian, war page and aspect ratio are within permissible limits. Solid45 element type is chosen for NAB and solid46element is chosen for composite material.



Fig3.Composite Propeller

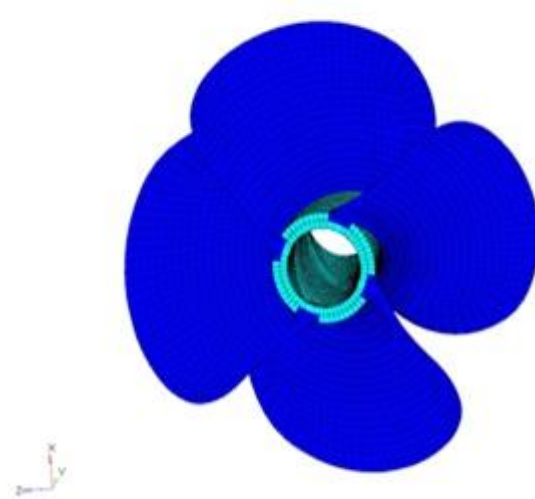


Fig4.Meshed model

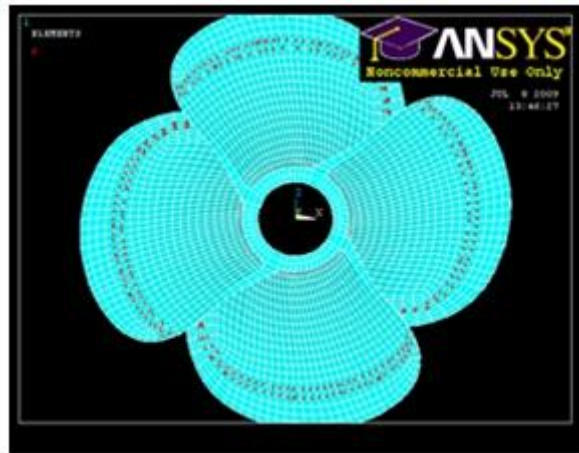


Fig5.Load Distribution at 0.75R

Table1.Material properties for NAB

Yield strength	178.3 mpa
Young's modulus	1.21x1e5 mpa
Poisson's ratio	0.34
Density	0.07556g/cc
Hardness	152-190 BHN
Melting point	650°c

Table2.Material properties for composite

RGlass roving UD/Epoxy	S2Glass fabric/Epoxy	Carbon UD/Epoxy
$E_x=53.1\text{Gpa}$	$E_x=22.925\text{Gpa}$	$E_x=142\text{Gpa}$
$E_y=12.4\text{Gpa}$	$E_y=22.925\text{Gpa}$	$E_y=10\text{Gpa}$
$E_z=12.4\text{Gpa}$	$E_z=12.4\text{Gpa}$	$E_z=10\text{Gpa}$
$N_{UXY}=0.16$	$N_{UXY}=0.12$	$N_{UXY}=0.16$
$N_{UYZ}=0.16$	$N_{UYZ}=0.2$	$N_{UYZ}=0.2$
$N_{UZX}=0.28$	$N_{UZX}=0.2$	$N_{UZX}=0.16$
$G_{xy}=6.6\text{Gpa}$	$G_{xy}=4.7\text{Gpa}$	$G_{xy}=5.2\text{Gpa}$
$G_{yz}=4.14\text{Gpa}$	$G_{yz}=4.2\text{Gpa}$	$G_{yz}=3.8\text{Gpa}$
$G_{zx}=4.14\text{Gpa}$	$G_{zx}=4.2\text{Gpa}$	$G_{zx}=6\text{Gpa}$
density = 2gm/cc	density=1.8gm/cc	density=1.6gm/cc

III. RESULTS AND DISSCUSSIONS

3.1. Static Analysis of NAB Propeller

The thrust of 332.17N is applied on face side of the blade in the region between 0.7R and 0.75R. The intersection of hub and shaft point's deformations in all directions are fixed. The thrust is produced because of the pressure difference between the face and back sides of propeller blades. This pressure difference also causes rolling movement of the underwater vehicle. This rolling movement is nullified by the forward propeller which rotates in other direction (reverse direction of aft propeller). The propeller blade is considered as cantilever beam i.e. fixed at one end and free at other end. The deformation pattern for aluminum propeller is shown in figure 6.1. The maximum deflection was found as 0.597 mm . Similar to the cantilever beam the deflection is maximum at free end.

The Von mises stress on the basis of shear distortion energy theory also calculated in the present analysis. The maximum von mises stress induced for aluminum blade is 125.484 N/mm² as shown in figure 7.0 which exceeds the allowable strength of aluminum i.e 178N/mm² that may cause failure. The stresses are greatest near to the mid chord of the blade-hub intersection with smaller stress magnitude toward the tip and edges of the blade. Figure 5,6 shows induced deformations and stresses in NAB and composite propeller.

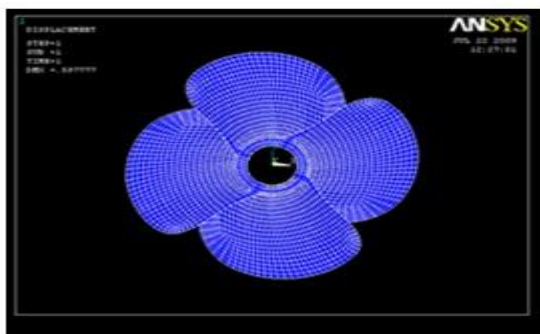


Fig5.Deformed model for NAB

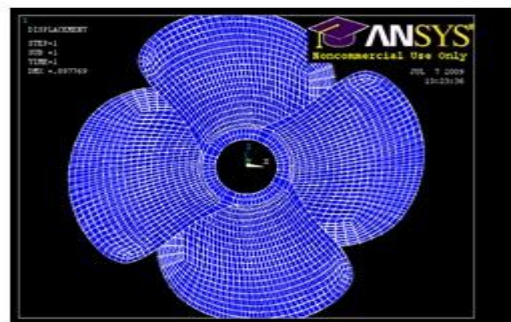


Fig6.Deformed model for Composite

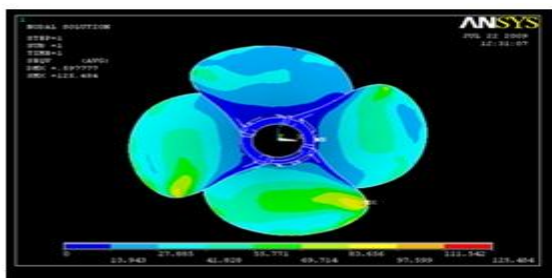


Fig7.Von Mises Stress for NAB

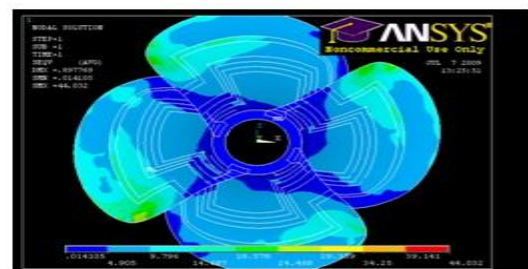


Fig8. Von Mises Stress for Composite

Table4. Comparison of NAB vs. Composite Propeller:

Deformation(mm)	0.597	0.897
Von misses Stress(MPa)	125.484	44.032
X component stress(MPa)	60.932	21.52
Y component stress(MPa)	23.641	11.947
Z component stress(MPa)	75538	17.543

3.2 Eigen value analysis of propeller blade

The required boundary conditions and density are given for extracting the first ten mode shapes of both aluminum and composite propeller blade. Type of analysis is changed to model and First ten mode shapes are obtained. By using Block Lanczos method the Eigen value analysis is carried out for NAB and composite propeller. This analysis helps in finding out the response due to loading the natural frequency and the corresponding mode shapes in the form of Eigen vectors of the propeller blade. This analysis also represents the undamped free vibration of the propeller blade in absence of damping and applied loads. First ten natural frequencies are obtained for Nickel-Aluminum-Bronze (NAB) and composite propeller.

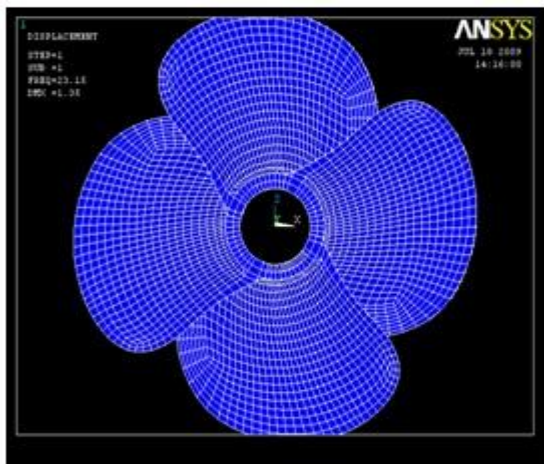


Fig9. First Mode shape for NAB

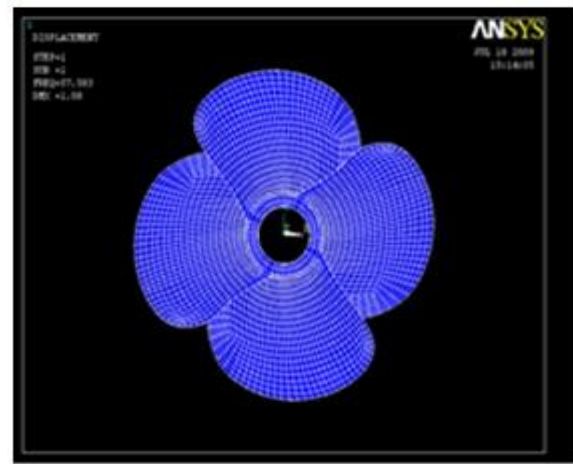


Fig10. First Mode shape for Composite

Table5. Natural frequencies of Both NAB & Composite Material

S.No	Eigen value analysis for Nickel-Aluminum-Bronze(NAB)in Hz	Eigen value analysis for composite propeller in Hz
1	23.159	57.583
2.	30.119	59.270
3.	30.973	59.706
4.	31.327	59.706
5.	50.735	65.222
6.	58.530	65.788
7.	61.356	65.788
8.	63.777	67.984
9.	66.102	84.627
10.	68.805	85.755

IV. CONCLUSIONS

1. The deflection for composite propeller blade was found to be around 0.897mm for all layers which is same as than that of NAB propeller i.e. 0.597mm, which shows that by changing the layup sequence further composite materials can be made much stiffer than aluminum propeller.
2. Maximum induced von mises stress for aluminum was found to be 125.484 N/mm² which is greater than composite propeller i.e. 47.4618 N/mm².
3. Eigen value analysis results showed that the natural frequencies of composite propeller were 22 % more than Nickel Aluminum Bronze (NAB) propeller.
4. Eigen value analysis results show that the first critical speed of composite propeller is 57 Hz and next critical speed is 59 Hz.
5. Eigen value analysis results show that the first critical speed of NAB propeller is 23 Hz and next critical speed is 30 Hz

REFERENCES

- [1] Taylor, D.w, "The Speed and Power and Ships", Washington, 1933
- [2] J.E.Conolly, "Strength Of Propellers", reads in London at a meeting of the royal intuition of naval architects on dec 1,1960,pp 139-160
- [3] Chang-sup lee, yong-jik kim,gun-do kim and in-sik nho. "Case Study On The Structural Failure Of Marine Propeller Blades" Aeronautical Journal, Jan 1972, pp87-98
- [4] George W.Stickle and John L.Crigler., "Propeller analysis from experimental data" report No.712, pp 147-164.
- [5] W.J.Colclough and J.G.Russel. "The Development Of A Composite Propeller Blade With A CFRP Spar" Aeronautical Journal, Jan 1972, pp53-57
- [6] Christoph Layens, Frank Kocian , Joachim hausmann., "Materials And Design Concepts For High Performance Compressor Components", plastics and polymers, Dec 1973, pp312-327
- [7] Gau-Feng Lin "Three Dimensional Stress Analysis of a Fiber Reinforced Composite Thruster Blade", the society of naval architects and marine engineers ,1991
- [8] Jinsoo Cho and Seung-Chul Lee, "Propeller Blade Shape Optimization For Efficiency Improvement ",Computer and Fluids, Vol.27, pp 407-419
- [9] 9. Charles Dai, Stephen Hanbric, lawerence mulvihill. "A Prototype Marine Propulstur Design Tool Using Artificial Intelligence And Numerical Optimization Techniques " ,Sname transations, Vol 102, 1994, pp 57-69.

Elemental Composition of Fine Particulate Matters from the Exhaust Emission of Jeepneys Plying the Route of Taft Avenue, Manila, Philippines

Maria Cecilia D. Galvez,¹ Heidi C. Jayo,² Edgar A. Vallar,³ Vernon R. Morris⁴

^{1,2,3}Physics Department, De La Salle University, 2401 Taft Avenue, Malate, Manila, Philippines 1004

⁴National Oceanic and Atmospheric Administration Center for Atmospheric Sciences, Howard University, Washington, DC 20001

Abstract: Elemental composition of fine particulate matters coming from the vehicular exhaust emission of jeepneys plying the route of Taft Avenue, Manila, Philippines was identified using SEM/EDX technique. SEM images of each fine particulate matter were also taken for morphological analysis. Elements that were revealed by EDX include Ca, Cl, Co, Cu, Cr, Fe, Mn, Pb, Hg, Ni, P, Na, S, Si, K, V, Mn, Ni, Zn, and Sn. Hazardous elements such as Co, Cl and Cr were detected in more than 50% of the particulate matter (PM) analyzed. The PM analyzed from jeepney 1, which was manufactured in 1980 contained the most number of hazardous elements that have a high frequency of occurrence. These include Pb and Hg which were found only in one or two PM in jeepneys 2 and 3. But for jeepney 1 traces of Pb and Hg were detected in more than 50% of the PM. Another hazardous element that was found only in the PM coming jeepney 1 is Se.

Keywords: jeepney, diesel, fine particulate matter, SEM/EDX, elemental composition

I. INTRODUCTION

Air pollution is one of the major environmental problems in the Philippines, especially in urban areas like Metro Manila which is densely-populated. Atmospheric particulate matter (PM) remains to be one of the major pollutants produced from human activities. They are classified according to size because of the different diameters that are associated with particles of different diameter. Fine Particulate Matters or PM_{2.5} are particles that are 2.5µm or less. These particles could be also called respirable particles because it could penetrate the respiratory system further compared to other particles of larger diameters. PM_{2.5} particles are primarily formed by chemical reactions in the atmosphere and through fuel combustion which come from motor vehicles, power generation, industrial facilities, residential fire places, wood stoves and agricultural burning. In the Philippines, based from the 2006 National Emission Inventory, the transport sector is the major source of air pollution in the country wherein 65% of air pollutants come from them. Most Filipinos take public transport (PT) with an estimate of about 70% of the total person trips taking PT with as high as 80% in highly urbanized cities. The most popular public transport in the Philippines is the jeepney and there are 227,493 jeepneys providing PT services throughout the country [1]. Jeepneys are predominantly fueled by diesel and most of the diesel engines are second hand and some are more than 20 years old. Diesel vehicles emit significant amount of nitrogen oxides (NOX) and also are a major source of fine particle emissions in urban locations. PM emissions in general are very hazardous and diesel PM, especially, is likely to cause cancer [2]. Hence, characterization of the composition of fine particulate emissions from diesel vehicles is very important. One method of characterizing fine particulate matter is using the Scanning Electron Microscope (SEM) with Energy Dispersive X-ray (EDX). SEM/EDX is a powerful tool in studying the size, shape, morphology, chemical and elemental composition of particulate matter. It can give us information whether the particles' origin is anthropogenic or created by natural processes. The elemental composition of atmospheric particles is sometimes more useful than their bulk elemental composition with a view to establish their origin and their potential effects on human health [3]. In the Philippines, no study has been made on the elemental composition of fine particulate matter coming from the exhaust emissions of jeepneys considering that it is the most popular means of transportation in the country and this public transport comprise 71% of the total number of vehicles registered in the country. In this study, we present to the best of our knowledge the first study on the elemental composition of fine particulate matters that came from the exhaust emissions of jeepneys plying the route of Taft Avenue, Manila, Philippines. The elemental composition and morphology of the PM was analyzed using SEM/EDX and air sampling using a personal cascade impactor is used to collect the PM.

II. AIR SAMPLING USING A PERSONAL CASCADE IMPACTOR AND SCANNING ELECTRON MICROSCOPY

The personal 2-stage low-volume cascade impactor was made from aluminum and had a nozzle diameter of 0.4 mm. Figure 1 shows the cascade impactor plugged in with a plastic tube connecting it to the vacuum pump with a pressure gauge and flow meter. A 9V battery was used to power the vacuum pump. The flow meter was used to monitor the flow rate which is set to 4-5 L/min and the pressure gauge was used to monitor the pressure. The cascade impactor setup is placed directly in front of the tailpipe exhaust of the jeepney. Particles were impacted on an 8-mm diameter aluminum foil. The filters were prepared using a thoroughly cleaned and sonicated 8-mm hole puncher. A small amount of ethanol was applied to the aluminum foil filter after it was cut to a diameter of 8 mm to remove impurities. Morphological features and elemental composition of individual particles were analyzed with a SEM (JSM 5310 JEOL) equipped with an EDX (Oxford) Analyser. Particle size was estimated from the direct appearance of individual particles in the scanning electron micrograph.

SEM/EDX was done according to the standard operating procedure for sample preparation and analysis of particulate matter samples by scanning electron microscopy. Scanning Electron Microscope was operated at acceleration voltage of 15 kV. The SEM images and analytical data of trace elements concentration were recorded with a Link Isis 3.0 software system with a SemAfore 5.0 SA20 Scan Digitizer for digital imaging. The instrument acquires either single spot spectrum or area spectrum, in this way it is possible to identify a single particle analysis and the mean values of the constituents from a group of particles.

III. RESULTS AND DISCUSSION

3.1. SEM/EDX Results of the Blank Aluminum Foil

To differentiate the elements from PM and the aluminum foil were the PM were deposited, the EDX spectra of blank Al foils prepared in the same way as the Al foils used for the personal cascade impactor was also obtained. Figure 2 shows the blank SEM image of Al foil and the corresponding EDX spectra. In the EDX spectra, of the aforementioned Al foil, aside from Al the only other element present is Oxygen (O). This indicates that the Al foils that were prepared for impaction of fine particulate matters were not contaminated by other foreign particles



Fig. 1. The two-stage personal cascade impactor.

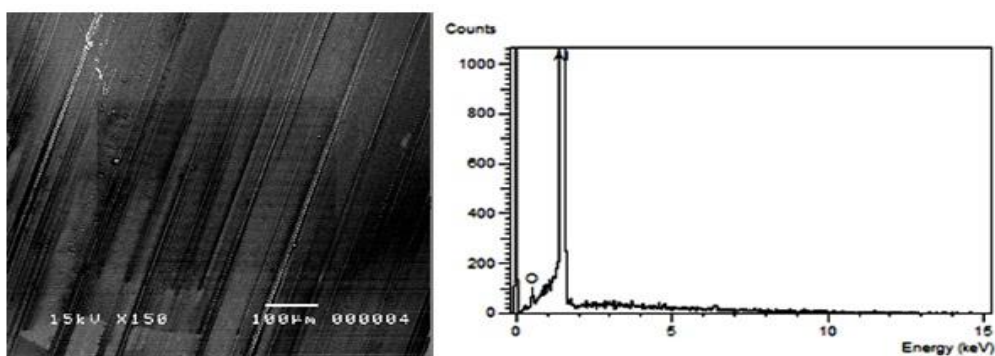


Fig. 2. SEM image of a blank Aluminum Foil Filter at a magnification of 150x with the corresponding EDS area spectrum.

3.2. SEM/EDX Results of the Fine Particulate Matter from Exhaust Emission of Jeepneys

Three jeepneys were used in this study differing in manufacturing year, 1980, 2003, and 2006, which will be referred to as jeepney 1, jeepney 2, and jeepney 3, respectively. Twenty (20) particles with a diameter not greater than 2.5 μm were selected for each jeep for analysis and detection of elemental composition and concentration. Figure 3 shows the SEM image and the EDS spectrum of some PM analyzed in the study. As can be seen from fig. 3, particles have different morphologies. We observed agglomerates, aggregates, floccules, sphere, strips, triangle, and irregularly shaped carbonaceous particles. From fig. 3, it can also be seen that PM with different morphologies have different elemental composition. EDX analysis of the PM collected for the three jeepneys revealed the presence of hazardous air pollutants, as classified by US/EPA, such as Cl, Co, Cr, Mn, Pb, Hg, Ni, and P. Figure 4 shows a box plot of the concentration in wt% of elements detected on the PM collected from the exhaust emissions of (a) jeepney 1, (b) jeepney2, and (c) jeepney 3. As can be seen from fig. 4, the major elements in all the PM for all the three jeeps are C and O. PM from jeepney 1, the oldest jeep, contains the most number of elements with high frequency of occurrence. The hazardous element, Se, was detected only in jeepney 1 with concentration of 1 wt % to 15 wt % which means that in some PM it is a major element. In a recent study by Atikul et. al, Se could not be traced to the gasoline itself but traceable to the engine chambers and emissions from other mechanical activities within the operation zones of the engine [4]. However, the mean concentration of Fe is lower for jeepney 1 compared to jeepneys 2 and 3. Another source of Fe in diesel exhaust PM is the lubricating oil. Si is also a minor

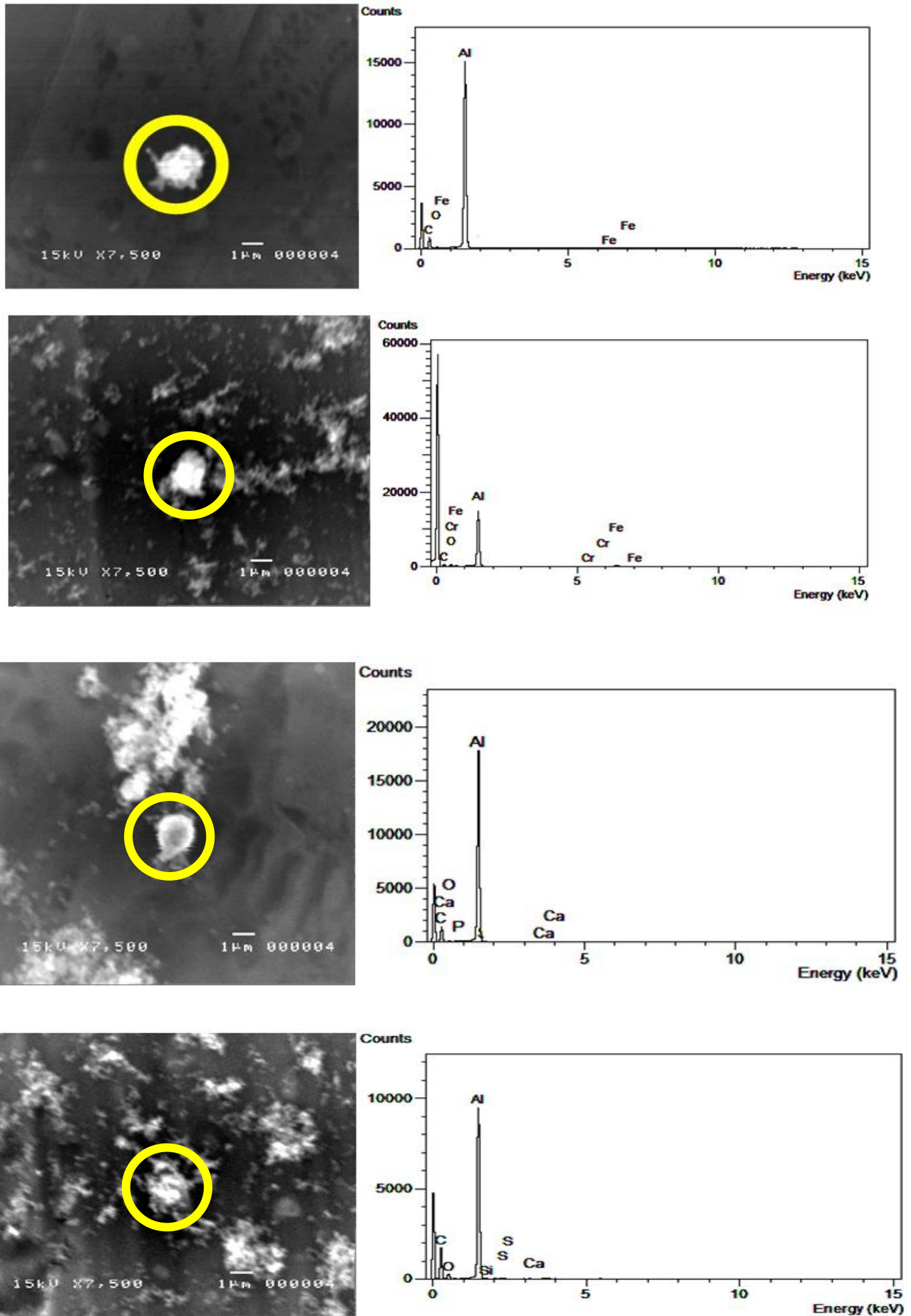


Fig. 3. SEM image of a PM_{2.5} collected from the exhaust emissions of jeepneys and the corresponding EDS spectrum. The magnification used is 7500x.

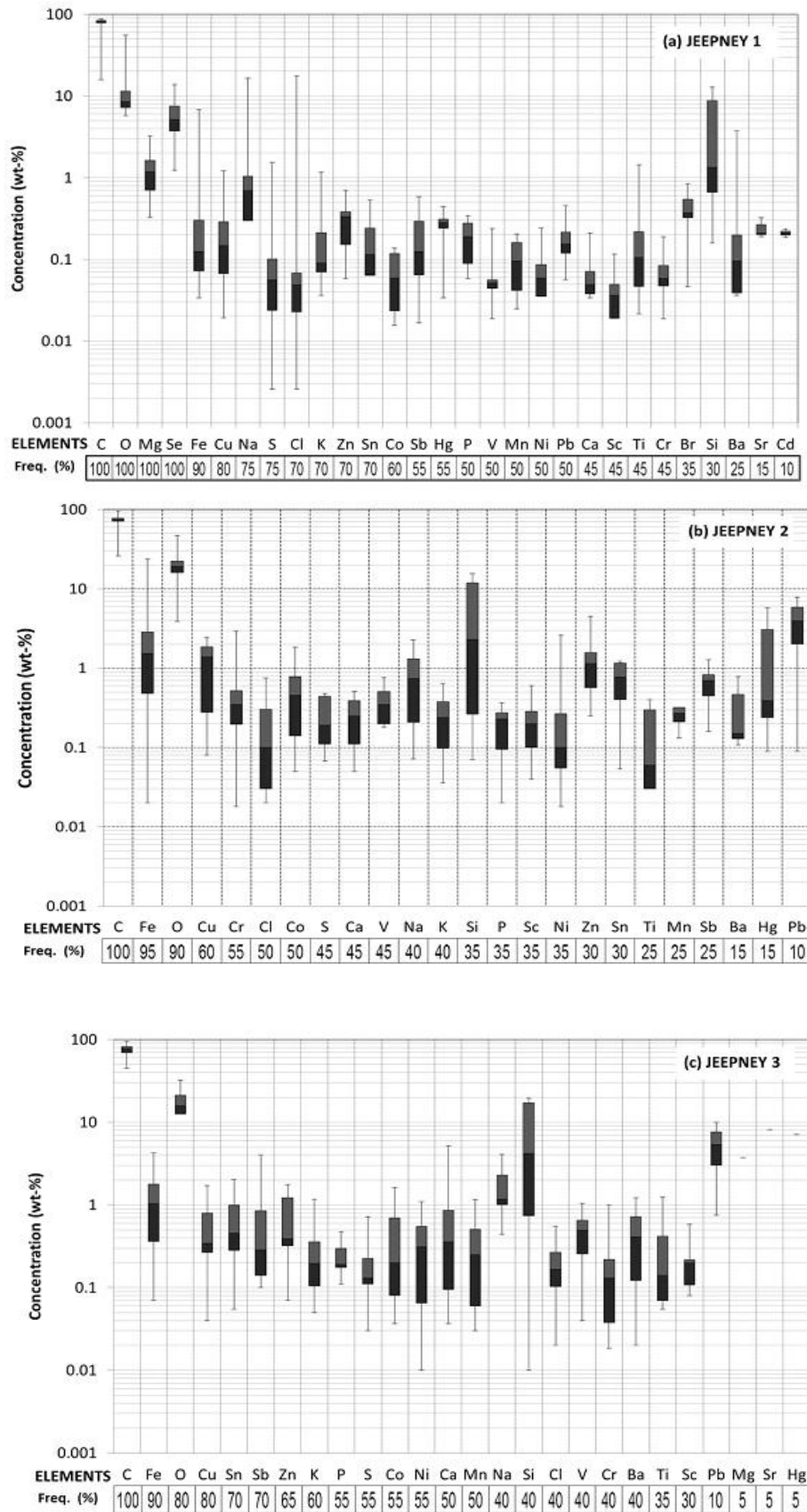


Fig. 4. Concentration (in wt%) of elements found in fine particulate matters collected from the exhaust emissions of (a) Jeepney 1; (b) Jeepney 2; (c) Jeepney 3.

element in all the three jeeps occurring in one-third of all the particles analyzed for each jeepney. It may have come from sintered silicon nitride that is used in automobile industry as a material for engine parts. More than 40% of the particles analyzed for all the jeepneys contain trace amounts of Cu, Co, Cl, Cr, Ca, Na, S, K, and V. Hazardous elements, Mn, Ni, Zn,

and Sn were detected in more than 50% of the PM in jeepneys 1 and 3 in trace amounts. Several engine lubricating oil additives include metallo-organic compounds resulting in some metal oxide emissions including such metals as P, Zn, Cr, and Ca, and fuel additives can result to emission of Cu and Fe and some other metals [5]. Among the three jeepneys, jeepney 1 contains the most number of hazardous elements with high frequency of occurrence. In 2001, leaded gasoline was phased out but in spite of this, trace amounts of Pb and Hg were detected in 50% of the PM of jeepney 1 whereas it was only detected in just one or two PM of jeepneys 1 and 2. Jeepney 1 was manufactured in 1980. Ar, Ba, Co, and Sr are inorganic exhaust components that are products of engine and component wear, or are trace contaminants of the fuel and/or lubricant oil which usually vaporize in the combustion chamber and then "plate" themselves to particles in the exhaust stream [6].

IV. Conclusion

Elemental composition of fine particulate matters from the exhaust emission of jeepneys, which uses second hand diesel engine, was determined using SEM/EDX technique. Several hazardous elements were detected in minor or trace amounts in most of the fine PM collected for all the three jeepneys. Morphological images from the SEM revealed various shapes and sizes of PM from diesel exhaust emissions of the three jeepneys. Most of the PM had sizes less than 2.5 μm which is typical for diesel particulate matter. The major element is C for all the PM analyzed. EDX analysis of the PM from all the three jeepneys revealed the presence of several elements like Ca, Cl, Co, Cu, Cr, Fe, Mn, Pb, Hg, Ni, P, Na, S, Si, K, V, Mn, Ni, Zn, and Sn. Hazardous elements such as Co, Cl and Cr were detected in more than 50% of the PM analyzed. The PM analyzed from jeepney 1 contained the most number of hazardous elements that have a high frequency of occurrence. These include Pb and Hg which were found only in one or two PM in jeepneys 2 and 3. But for jeepney 1 traces of Pb and Hg were detected in more than 50% of the PM. In April 2000, Pb was completely phased out in Metro Manila. But since jeepney 1 was manufactured in 1980, that could have explained the presence of Pb in its PM emission. Another hazardous element that was found only in the PM coming jeepney 1 is Se. Again this could have been due to the age of the engine. This element could serve as tracer for very old jeepneys that were still on the streets of Manila.

REFERENCES

- [1] R. F. Regidor, C. M. Montalbo, Jr., M. S. G. Napalang, H. O. Palmiano, R. G. Sigua, N. C. Tiglao, K. N. Vergel, Formulation of a National Environmentally Sustainable Transport Strategy for the Philippines-Final Report, United Nations Centre for Regional Development, May 2011. Available: <http://ncts.upd.edu.ph/est/>
- [2] A Roadmap for Cleaner Fuels and Vehicles in Asia, Asian Development Bank and Clean Air Initiative for Asian Cities Center Inc., 2007.
- [3] A. Srivastava, V. K. Jain, and A. Srivastava, SEM-EDX analysis of various sizes aerosols in Delhi India, Environ Monit Assess, 150, 2009, 405–416. DOI 10.1007/s10661-008-0239-0.
- [4] F.A. Atiku, P.O. Ikeh, U.Z. Faruk, A.U. Itodo, B.G. DanShehu and M.M. Ambursa, Physicochemical Analysis of Discharged Particulate from Power Generating Engines, Advances in Applied Science Research, vol. 2, no. 3, 2011, 287-294.
- [5] P. Anyon, S. Brown, D. Pattison, J. B. Anderson, N. Trompp, G. Walls, Toxic Emissions from Diesel Vehicles in Australia, Environment Australia, Commonwealth of Australia, April 2003.
- [6] R. K. Krieger, J. M. Brooks, G. A. Shiroma, D. J. Ames, and P. D. Venturini, Part A. Public Exposure To, Sources and Emissions of Diesel Exhaust in California, Report to the Air Resources Board on the Proposed Identification of Diesel Exhaust as a Toxic Air Contaminant, 1998.

A Review on Performance Analysis of Air-Cooled Condenser under Various Atmospheric Conditions

Manish Baweja,¹ Dr.V.N Bartaria²

¹M.E, Scholar HPT LNCT Bhopal, MP, India.

² Professor & HOD, Mechanical Engg. LNCT Bhopal, MP, India.

Abstract: Air Cooled condensers were first introduced in US power industry in early 1970's, but only during last 10-15 years number of installations greatly increased largely due to growing attention being paid to environmental safety. Also, growing demand for water for both domestic and industrial use has brought an increased interest in use of Air Cooled condensers. This is a review paper which studies the performance of Air-cooled condenser under various operating conditions it is found that there is degradation in performance of air cooled condenser under high ambient temperatures and windy conditions. The heat rejection rate of ACC also depends on surface condition of fins and thus its performance is reduced due to external fouling of finned tubes due to weather conditions and by internal fouling from condensate (Ammonia corrosion).

A Hybrid (dry/wet) dephlegmator achieves major enhancement in performance when ambient temperatures are high. Also shading of condensers is done for air-conditioning units to mitigate the adverse effect of high ambient temperatures due to solar radiation. Now a day's wind walls are used to reduce the effect of high wind velocity .second option is to increase the fan speed Fin cleaning plays an important role in heat rejection. External cleaning improves air side heat transfer coefficient. In order to improve the performance of an ACC Flat tubes inclined at some angle to horizontal can also be used in place of conventional circular horizontal tubes so that an improvement in heat transfer rate occurs.

Keywords: Air cooled condensers, Ambient temperatures, Fin cleaning, Heat transfer. Performance analysis,

I. Introduction

A condenser is a heat transfer device or unit used to condense a substance from its gaseous to its liquid state, typically by cooling it. In doing so, the latent heat is given up by the substance, and will transfer to the condenser coolant. Condensers are typically heat exchangers which have various designs and come in many sizes ranging from rather small (hand-held) to very large industrial-scale units used in plant processes. For example, a refrigerator uses a Condenser to get rid of heat extracted from the interior of the unit to the outside air. Condensers are used in air conditioning, industrial chemical processes .Such as distillation, steam power plants and other heat-exchange systems. Use of cooling water or surrounding air as the coolant is common in many condensers. The main use of a condenser is to receive exhausted steam from a steam engine or turbine and condense the steam. The benefit being that the energy which would be exhausted to the atmosphere is utilized .A steam condenser generally condenses the steam to a pressure significantly below atmospheric. This allows the turbine or engine to do more work. The condenser also converts the discharge steam back to feed water which is returned to the steam generator or boiler. In the condenser the latent heat of condensation is conducted to the cooling medium flowing through the cooling tubes.

CONDENSERS USED IN POWERPLANT:

1. Steam Condenser
2. Air Cooled Condenser

STEAM CONDENSER OR WATER COOLED CONDENSER

It is a device or an appliance in which steam condenses and heat released by steam is absorbed by water. A steam condenser is a device which condenses the steam at the exhaust of turbine. It serves two important functions. Firstly, it creates a very low pressure at the exhaust of turbine, thus permitting expansion of the steam in the prime mover to very low pressure. This helps converting heat energy of steam into mechanical energy in the prime mover. Secondly, the condensed steam can be used as feed water to the boiler.

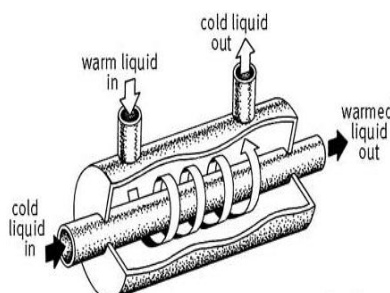


Fig 1. Water Cooled Condenser

There are two principal types of Steam Condensers

- a). Jet condensers
- b). Surface condenser

a).Jet condensers: In a jet condenser, cooling water and exhausted steam are together. Therefore, the temperature of cooling water and condensate is the same when leaving the condenser. Advantages of this type of condenser are low initial cost, less flow area required, less cooling water required and low maintenance charges. However its disadvantage is condensate is wasted and high power is required for pumping water.

b) Surface condenser: In a surface condenser, there is no direct contact between cooling water and exhausted steam. It consists of a bank of horizontal tubes enclosed in a cast iron shell. The cooling water flows through the tubes and exhausted steam over the surface of the tubes. The steam gives up its heat to water and is itself condensed. Advantage of this type of condenser are : condensate can be used as feed water, less pumping power required and creation of better vacuum at the turbine exhaust. However, disadvantage of this type of condenser are high initial cost, requires large floor area and high maintenance charges. The surface condenser is used for the majority of steam engine & steam turbine applications.

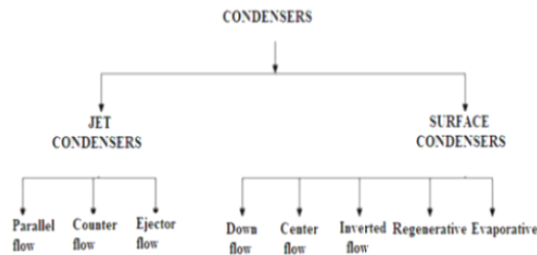


Fig 2. Types of Water Cooled Condenser

AIR COOLED CONDENSER

An Air cooled condenser, is simply a pressure vessel which cools a circulating fluid within finned tubes by forcing ambient air over the exterior of the tubes. A common example of an Air cooled condenser is car radiator Air cooled heat exchangers are used for two primary reasons.

- i. They increase plant efficiency
- ii. They are a good solution as compared to cooling towers and shell and tube heat exchangers because they do not require an auxiliary water supply (water lost due to drift and evaporation, plus no water treatment chemicals are required).

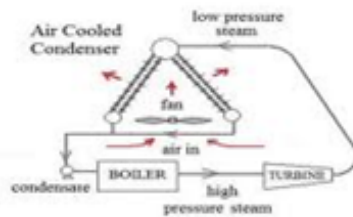


Fig 3.Basic Air Cooled Condenser cycle

An air-cooled heat exchanger can be as small as your car radiator or large enough to cover several acres of land, as is the case on air coolers for large power plants the air-cooled heat exchangers are mostly used when the plant location and the ambient Conditions do not allow an easy and economic use of other cooling systems

The most evident advantages of air-cooled Condensers are:

- a) No problem arising from thermal and chemical pollution of cooling fluids
- b) Flexibility for any plant location and plot plan arrangement because equipment requiring cooling need not be near a supply of cooling water.
- c) Reduction of maintenance costs
- d) Easy installation
- e) Lower environmental impact than water cooled condenser due to the elimination of an auxiliary water supply resulting in water saving
- f) No use of water treatment chemicals and no need for fire protection system.

Air-cooled finned-tube condensers are widely used in refrigeration and air-conditioning applications. For the same amount of heat transfer, the operation of air cooled condensers is more economic as compared with water cooled condensers typically air-cooled condensers are of the round tube and fin type. To improve the performance of air-cooled condensers

multiple techniques can be achieved such as enhancements on inner pipe surface, changing the tube geometry from round to flat shape and external fins.

FOULING TENDENCIES OF AIR COOLED CONDENSER

The external surfaces of the finned tubes on air-cooled condensers are very prone to fouling from pollen, dust, insects, leaves, plastic bags, bird carcasses, etc. Not only is the air flow affected but also the heat transfer coefficient, the deterioration in performance increasing unit operating costs. In severe cases, fouling can also limit the power generation capacity of the turbo generator. To improve the heat removal capacity of an air-cooled condenser under conditions of high ambient air temperature, operators will sometimes spray water on the heat exchanger to reduce surface temperature. Unfortunately, depending on the quality of water used, this sometimes leads to new scale formation on the tube fins and, again, reduces the heat transfer rate if the deposits are allowed to accumulate.

CLEANING TECHNIQUES FOR AIR COOLED CONDENSER

The three main methods for cleaning the external surfaces of air cooled condensers are as Follows:

- Fire hose
- High pressure Hand lance
- Semi-Automated cleaning Machine

1. Fire hose

Even though the volume of water consumed high, the washing effect of Fire hose is low due to low pressure involved. The galvanized surfaces of tubes and Fins are not damaged by this method the process is Labor and time intensive, and only a small improvement in performance even if surface seems to be optically clean. The reason is only a portion of fouling material is washed off and rest is pressed between fin tubes and cannot be washed off by this method. Again, the plant must be taken out of service and scaffolding erected in order that cleaning can be performed.

II. High pressure Hand lance

This method offers low water consumption and high water pressure .unfortunately the later can cause the galvanized surfaces to become damaged or Fins to be snapped off. As with the use of fire hose this method offers a small improvement in performance and once the fouling material has been compressed, It hinders heat transfer and obstructs air flow. Unfortunately, in order to perform cleaning the plant must be taken out of service and scaffolding erected.

III. Automated Cleaning Machine

The Automated cleaning Machine uses a significant volume of water, but at pressure that while allowing for effective surface cleaning avoids damaging galvanized surfaces and fins .An important advantage of automated cleaning method is that cleaning can be performed during operation while the unit is still online.

IV. Literature Survey

[1] A Study was performed on Performance Characteristics of an Air-Cooled Condenser under Ambient Conditions in December 2011. In this study effects of air flow pattern as well as ambient conditions were studied. Unfortunately ACC becomes less effective under high ambient temperature and windy conditions. Fin cleaning plays a vital role in heat rejection. External cleaning improves air side heat transfer coefficient. Ambient conditions affect the steam temperature and heat rejection rate. It is observed that rise in wind velocity decreases thermal effectiveness of ACC up to considerable level. Ambient temperature not only affects performance of ACC at the same time turbine back pressure also increases with rise in ambient temperature. Skirts are effective solution to reduce the effect of wind on volumetric effectiveness. Hot air recirculation increases with wind velocity. Now a day's wind walls are used to reduce this effect. Second option is to increase fan speed. It counter affects on electrical power consumption.

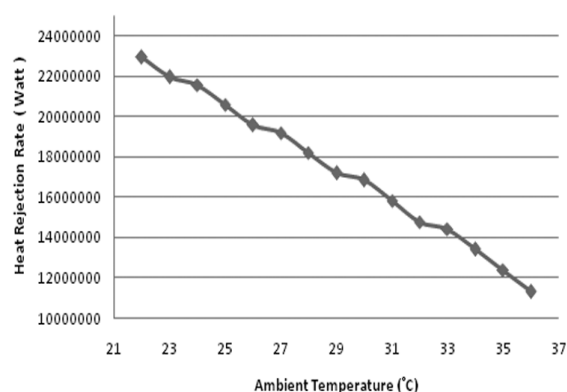


Fig. 4 Heat Rejection for various Ambient Temperatures. (Courtesy: Nirma Institute of technology - NUI CONE – 2011)

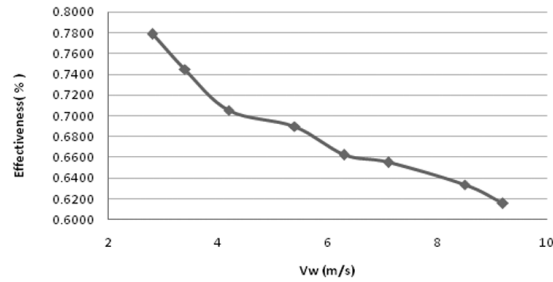


Fig.5. Effectiveness at different Wind Velocities
 (Courtesy: Nirma Institute Of technology - NUiCONE – 2011)

[2] A study was performed to evaluate the performance characteristics of a power plant incorporating a steam turbine and a direct air-cooled dry/wet condenser operating at different ambient temperatures. The proposed cooling system uses existing A-frame air-cooled condenser (ACC) technology and through the introduction of a hybrid (dry/wet) dephlegmator achieves measurable enhancement in cooling performance when ambient temperatures are high. [3] In this study they found that air-conditioning system with air cooled condensers, the condensing unit has to be kept in open for easy access to outdoor air in order to efficiently dissipate heat, During Daytime the solar radiation falling on the surface of the condenser and high ambient temperature can be detrimental for the energy performance. They studied the effectiveness of shading the condensing unit to mitigate the adverse effect of high ambient temperatures due to solar radiation .and analyzed that the theoretical increase in COP due to shading is found to be within 2.5%. [4] Heat transfer by convection in air cooled condensers is studied and improved in this work. In order to enhance the performance of air cooled condensers, it is important to take into consideration both of condensation inside condenser tubes and convection outside, where the enhancement in convection side is the dominant one. Aluminum extruded micro-channel flat tubes improve the performance of condensation more than conventional circular tubes but still has potential for air side improving. So the enhancement of convective heat transfer in air side is achieved in this study by inclination of the flat tubes by a certain angle with respect to horizontal in two cases.

V. Conclusion

The primary focus of this study is to evaluate the performance of Air-cooled condenser under various conditions. The performances of air-cooled condenser decreases with increase in ambient temperatures and high wind conditions. Hybrid (dry/wet) dephlegmator achieves measurable enhancement in cooling performance when ambient temperatures are high. Wind-walls are used to reduce the effect of wind .fan speed can also be increased. Changing the Shading the ACC of air-conditioned unit helps to reduce the high ambient temperature due to solar radiation. Shape of finned tubes from circular to flat and adjusting their inclination also helps in increasing heat transfer rate. Various techniques are also used to clean the tubes to increase heat transfer rate.

References

- [1] A. Rupeshkumar V. Ramani, B. Amitesh Paul, D. Anjana D. Saparia Nirma University Ahmadabad (December 2011) Performance Characteristics of an Air-Cooled Condenser under Ambient Conditions. NUiCONE 2011
- [2] Johan Adam Heynes and D.G Kroger University of Stellenbosch (December 2008) enhancement in cooling performance using a Dry/Wet Dephlegmator when ambient temperatures are high.
- [3] EA.I.ElSherbini and G. P. Maheshwari Building and Energy Technologies Department Kuwait Institute for Scientific Research (October-2010). ESL-IC-10-10-52 Effectiveness of Shading Air-Cooled Condensers of Air-Conditioning Systems.
- [4] M.M.Awad, H.M.Mostafa, G. I. Sultan, A.Elbooz, A.M.K.El-ghonemy Faculty of Engineering, Mansoura University, Egypt (2007). Alexandria Engineering Journal, Vol42, No-4, July 2003 Enhancement in heat transfer by changing tube geometry.

Calibration Estimator Using Different Distance Measures in Stratified Random Sampling

Dr. Nursel Koyuncu,¹ Prof. Dr. Cem Kadilar²
^{1,2}Hacettepe University, Department of Statistics, Beytepe, Ankara, Turkey

Abstract: Calibration estimators of finite population mean with different weights are considered. We define some new weights by using various loss functions. The estimators derived are compared by simulation.

Keywords: Calibration, Auxiliary information, stratified random sampling.

I. INTRODUCTION

Calibration estimation adjust the original design weights to incorporate the known population totals of auxiliary variables. The calibration weights are chosen to minimize a given distance measure and these weights satisfy the constraints related auxiliary variable information. In survey sampling many authors, such as Deville and Sarndal (1992), Estevao and Sarndal (2000), Arnab and Singh (2005), Farrell and Singh (2005), Kim and Park (2010) etc., defined some calibration estimators using different constraints. In stratified random sampling, calibration approach is used to get optimum strata weights. Tracy et al. (2003), Kim et al. (2007) and Koyuncu (2012) define some calibration estimators in stratified random sampling. In this study, under the stratified random sampling scheme some new weights for population mean under the different distance measures are proposed.

II. NOTATIONS and CALIBRATION ESTIMATORS

Consider a finite population $U = (u_1, u_2, \dots, u_N)$ of size N and let Y and X , respectively, be the study and auxiliary variables associated with each unit u_j ($j=1, 2, \dots, N$) of the population. Let the population of size, N , is stratified into L strata with the h -th stratum containing N_h units, where $h = 1, 2, \dots, L$ such that $\sum_{h=1}^L N_h = N$. A simple random sample of size n_h is drawn without replacement from the h -th stratum such that $\sum_{h=1}^L n_h = n$. Let (y_{hi}, x_{hi}) denote observed values of y and x on the i -th unit of the h -th stratum, where $i = 1, 2, \dots, N_h$ and $h = 1, 2, \dots, L$. Under this stratified random sampling scheme, the classical unbiased estimator of the population mean is given by ,

$$\bar{y}_{st} = \sum_{h=1}^L W_h \bar{y}_h \tag{1.1}$$

where $W_h = \frac{N_h}{N}$ is the stratum weight. The calibration estimator for stratified random sampling is defined Tracy et al. (2003) given by

$$\bar{y}_{st}(Tr) = \sum_{h=1}^L \Omega_h \bar{y}_h \tag{1.2}$$

where Ω_h are the weights minimize the distance measure. In this study we consider following distance measures

$$L_1 = \sum_{h=1}^L \frac{(\Omega_h - W_h)^2}{Q_h W_h} \tag{1.3}$$

$$L_2 = \sum_{h=1}^L 2 \frac{(\sqrt{\Omega_h} - \sqrt{W_h})^2}{Q_h} \tag{1.4}$$

$$L_3 = \sum_{h=1}^L \frac{1}{Q_h} \left(\frac{\Omega_h}{W_h} - 1 \right)^2 \tag{1.5}$$

$$L_4 = \sum_{h=1}^L \frac{1}{Q_h} \left(\frac{\sqrt{\Omega_h}}{\sqrt{W_h}} - 1 \right)^2 \tag{1.6}$$

and satisfy the calibration constraint:

$$\sum_{h=1}^L \Omega_h \bar{x}_h = \sum_{h=1}^L W_h \bar{X}_h \tag{1.7}$$

Case 1: The Lagrange function for the weights Ω_h , which satisfy the calibration equation in (1.7) and minimize the loss function given in equation (1.3) is given by

$$\Delta_1 = \sum_{h=1}^L \frac{(\Omega_h - W_h)^2}{Q_h W_h} - 2\lambda \left(\sum_{h=1}^L \Omega_h \bar{x}_h - \sum_{h=1}^L W_h \bar{X}_h \right) \tag{1.8}$$

Setting $\frac{\partial \Delta_1}{\partial \Omega_h} = 0$, we have

$$\Omega_h = W_h + \lambda \bar{x}_h Q_h W_h \tag{1.9}$$

On substituting weights in (1.7) and solving for lambda we have

$$\lambda = \frac{\sum_{h=1}^L W_h \bar{X}_h - \sum_{h=1}^L W_h \bar{x}_h}{\sum_{h=1}^L Q_h W_h \bar{x}_h^2} \tag{1.10}$$

Substituting (1.10) in (1.9) we get the weights as

$$\Omega_h = W_h + \frac{\sum_{h=1}^L W_h \bar{X}_h - \sum_{h=1}^L W_h \bar{x}_h}{\sum_{h=1}^L Q_h W_h \bar{x}_h^2} \bar{x}_h Q_h W_h \tag{1.11}$$

Substituting (1.11) in (1.2) we have

$$\bar{y}_{st}(Tr1) = \sum_{h=1}^L W_h \bar{y}_h + \frac{\sum_{h=1}^L W_h \bar{X}_h - \sum_{h=1}^L W_h \bar{x}_h}{\sum_{h=1}^L Q_h W_h \bar{x}_h^2} \sum_{h=1}^L Q_h W_h \bar{x}_h \bar{y}_h \tag{1.12}$$

Case 2: The Lagrange function for the weights Ω_h , which satisfy the calibration equation in (1.7) and minimize the loss function given in equation (1.4) is given by

$$\Delta_2 = \sum_{h=1}^L 2 \frac{(\sqrt{\Omega_h} - \sqrt{W_h})^2}{Q_h} - 2\lambda \left(\sum_{h=1}^L \Omega_h \bar{x}_h - \sum_{h=1}^L W_h \bar{X}_h \right) \tag{1.13}$$

Setting $\frac{\partial \Delta_2}{\partial \Omega_h} = 0$, we have

$$\Omega_h = \frac{W_h}{(1 - \lambda \bar{x}_h Q_h)^2} \tag{1.14}$$

Solving (1.14) for lambda, we obtain

$$\lambda = \frac{\bar{x}_h \Omega_h}{\frac{\Omega_h^{3/2} \bar{x}_h^2 Q_h}{(\sqrt{\Omega_h} - \sqrt{W_h})}} \tag{1.15}$$

Case 3: The Lagrange function for the weights Ω_h , which satisfy the calibration equation in (1.7) and minimize the loss function given in equation (1.5) is given by

$$\Delta_3 = \sum_{h=1}^L \frac{1}{Q_h} \left(\frac{\Omega_h}{W_h} - 1 \right)^2 - 2\lambda \left(\sum_{h=1}^L \Omega_h \bar{x}_h - \sum_{h=1}^L W_h \bar{X}_h \right) \quad (1.16)$$

Setting $\frac{\partial \Delta_3}{\partial \Omega_h} = 0$, we have

$$\Omega_h = W_h + \lambda W_h^2 \bar{x}_h Q_h \quad (1.17)$$

Substituting (1.17) in (1.7) and solving for lambda we have

$$\lambda = \frac{\sum_{h=1}^L W_h \bar{X}_h - \sum_{h=1}^L W_h \bar{x}_h}{\sum_{h=1}^L W_h^2 \bar{x}_h^2 Q_h} \quad (1.18)$$

Substituting (1.18) in (1.17) we get the weights as

$$\Omega_h = W_h + \frac{\sum_{h=1}^L W_h \bar{X}_h - \sum_{h=1}^L W_h \bar{x}_h}{\sum_{h=1}^L W_h^2 \bar{x}_h^2 Q_h} W_h^2 \bar{x}_h Q_h \quad (1.19)$$

Substituting (1.19) in (1.2) we have

$$\bar{y}_{st}(Tr3) = \sum_{h=1}^L \left(W_h \bar{y}_h + \frac{\sum_{h=1}^L W_h \bar{X}_h - \sum_{h=1}^L W_h \bar{x}_h}{\sum_{h=1}^L W_h^2 \bar{x}_h^2 Q_h} W_h^2 Q_h \bar{x}_h \bar{y}_h \right) \quad (1.20)$$

Case 4: The Lagrange function for the weights Ω_h , which satisfy the calibration equation in (1.7) and minimize the loss function given in equation (1.6) is given by

$$\Delta_4 = \sum_{h=1}^L \frac{1}{Q_h} \left(\frac{\sqrt{\Omega_h}}{\sqrt{W_h}} - 1 \right)^2 - 2\lambda \left(\sum_{h=1}^L \Omega_h \bar{x}_h - \sum_{h=1}^L W_h \bar{X}_h \right) \quad (1.21)$$

Setting $\frac{\partial \Delta_4}{\partial \Omega_h} = 0$ we have

$$\Omega_h = \frac{W_h}{(1 - 2\lambda \bar{x}_h Q_h W_h)^2} \quad (1.22)$$

Solving (1.22) for lambda, we obtain

$$\lambda = \frac{\Omega_h \bar{x}_h}{2Q_h W_h \Omega_h^{3/2} \bar{x}_h^2 \sqrt{\Omega_h} \pm \sqrt{W_h}} \quad (1.23)$$

III. SIMULATION STUDY

To study the performance of the proposed estimator, we generated four different artificial populations where x_{hi}^* and y_{hi}^* values are from different distributions as given in Table 1. To get different level of correlations between study and auxiliary variables, we applied some transformations given in Table 2. Every population consists of three strata having 100 units. We selected 5000 times $n_h = 30, 20, 40$ units from each stratum, respectively. The correlation coefficients between study and auxiliary variables for each stratum are taken as $\rho_{xy1} = 0.5, \rho_{xy2} = 0.7$, and $\rho_{xy3} = 0.9$, respectively. The quantities $S_{1x} = 4.5, S_{2x} = 6.2, S_{3x} = 8.4$, and $S_{1y} = S_{2y} = S_{3y} = 4.8$ were fixed in each stratum (see Tracy et al. 2003, Koyuncu (2012)). We calculated empirical mean square error and relative efficiency using following formulas:

$$MSE(\bar{y}_{st}(\alpha)) = \frac{\sum_{k=1}^N [\bar{y}_{st}(\alpha) - \bar{Y}]^2}{\binom{N}{n}}, \quad \alpha = Tr1, Tr3$$

It should be mentioned that in the case of distance function L_2 and L_4 , the iterative procedure for finding weights from the Lagrange equations doesn't converge for all selected samples. (See Pumputis (2005)). So we didn't give simulation results for L_2 and L_4 .

The simulation study shows that calibration estimator using distance measure L_1 are highly efficient than using distance measure L_3 .

IV. CONCLUSION

In this study we derived some new weights using different distance measures theoretically in stratified random sampling. The performance of the weights are compared with a simulation study.

REFERENCES

- [1] Arnab, R., Singh, S., 2005, A note on variance estimation for the generalized regression predictor, Australian and New Zealand Journal of Statistics, 47, 2, 231–234.
- [2] Deville, J.C., Sarndal, C.E., 1992, Calibration estimators in survey sampling, Journal of the American Statistical Association, 87, 376-382.
- [3] Estevao, V.M., Sarndal, C.E., 2000, A functional form approach to calibration, Journal of Official Statistics, 16, 379-399.
- [4] Farrell, P.J., Singh, S., 2005, Model-assisted higher order calibration of estimators of variance, Australian and New Zealand Journal of Statistics, 47, 3, 375–383.
- [5] Kim, J.M., Sungur, E.A., Heo T.Y., 2007, Calibration approach estimators in stratified sampling, Statistics and Probability Letters, 77, 1, 99-103.
- [6] Kim, J.K., Park, M., 2010, Calibration estimation in survey sampling, International Statistical Review, 78, 1, 21-29.
- [7] Koyuncu, N., 2012, Application of Calibration Method to Estimators in Sampling Theory, Hacettepe University Department of Statistics, PhD. Thesis.
- [8] Pumputis D. Calibrated estimators under different distance measures. Proceedings of the Workshop on Survey Sampling Theory and Methodology, 2005, p. 137–141. ISBN 9955-588-87-X.
- [9] Tracy, D.S., Singh, S., Arnab, R., 2003, Note on calibration in stratified and double sampling, Survey Methodology, 29, 99–104.

Table 1: Parameters and distributions of study and auxiliary variables

Parameters and distributions of the study variable	Parameters and distributions of the auxiliary variable
1. Population, $h = 1, 2, 3$	
$f(y_{hi}^*) = \frac{1}{\Gamma(1.5)} y_{hi}^{*1.5-1} e^{-y_{hi}^*}$	$f(x_{hi}^*) = \frac{1}{\Gamma(0.3)} x_{hi}^{*0.3-1} e^{-x_{hi}^*}$
2. Population, $h = 1, 2, 3$	
$f(y_{hi}^*) = \frac{1}{\Gamma(0.3)} y_{hi}^{*0.3-1} e^{-y_{hi}^*}$	$f(x_{hi}^*) = \frac{1}{\sqrt{2\pi}} e^{-\frac{x_{hi}^{*2}}{2}}$
3. Population, $h = 1, 2, 3$	
$f(y_{hi}^*) = \frac{1}{\sqrt{2\pi}} e^{-\frac{y_{hi}^{*2}}{2}}$	$f(x_{hi}^*) = \frac{1}{\Gamma(0.3)} x_{hi}^{*0.3-1} e^{-x_{hi}^*}$
4. Population, $h = 1, 2, 3$	
$f(y_{hi}^*) = \frac{1}{\sqrt{2\pi}} e^{-\frac{y_{hi}^{*2}}{2}}$	$f(x_{hi}^*) = \frac{1}{\sqrt{2\pi}} e^{-\frac{x_{hi}^{*2}}{2}}$

Table2: Properties of strata

Strata	Study Variable	Auxiliary Variable
1. Stratum	$y_{1i} = 50 + y_{1i}^*$	$x_{1i} = 15 + \sqrt{(1 - \rho_{xy1}^2)}x_{1i}^* + \rho_{xy1} \frac{S_{1x}}{S_{1y}} y_{1i}^*$
2. Stratum	$y_{2i} = 150 + y_{2i}^*$	$x_{2i} = 100 + \sqrt{(1 - \rho_{xy2}^2)}x_{2i}^* + \rho_{xy2} \frac{S_{2x}}{S_{2y}} y_{2i}^*$
3. Stratum	$y_{3i} = 100 + y_{3i}^*$	$x_{3i} = 200 + \sqrt{(1 - \rho_{xy3}^2)}x_{3i}^* + \rho_{xy3} \frac{S_{3x}}{S_{3y}} y_{3i}^*$

Table3: Mean Square Error of Estimators

	1. Population	2. Population	3. Population	4. Population
$\bar{y}_{st}(Tr1)$	249721461	254676687	246856254	251629447
$\bar{y}_{st}(Tr3)$	328969173	335131390	325711652	331650409

A Proposal of a model for the organization of Energy-efficient products

Sejdo Ferati

Department of Engineering, University of Applied Sciences Brandenburg, Germany

Abstract: The article deals with the production of energy-efficient products. It shows a way that could be used from the product determining over the organization of the process up to the realization of a product ready for use. The description of the steps will be carried out with the help of a model.

Keywords: Customer requirements, Energy efficiency, Energy-efficient product, Energy management, Product Idea

I. INTRODUCTION

Before a product is manufactured, an enterprise must provide certain preliminary works. It has to determine what the product is supposed to be used, for which demands it is supposed to cope with, which share of the market it should prove, whether the market needs the product, which sales strategy could be applied, whether parts must be bought from other suppliers and above all, whether it can be manufactured economically and last but not least, is a non-polluting and energy-efficient way of production possible. Due to the requirements at the product a strategy must be elaborated for the production process. Here the model for the creation of energy-efficient products starts. With the help of the flow model the requirements for the organization of the process are illustrated.

II. RECOMMENDATION OF A MODEL FOR THE DESIGN OF ENERGY-EFFICIENT PRODUCTS

At the beginning of the implementation of an idea for a new product always stands the product determining, followed by development and construction. During the phase of the product determining not only the product itself has to be considered, but also the application according to rules and the level of strain. Since the entirety of the processes is very complex, it is named product process.

Normally the objectives of the enterprise and the customer and market requirements are basis for the realization of a product idea. For this purpose the courses within the enterprise must be adapted onto the energy-efficient product that has to be designed. In large-scale enterprises those processes of product determining and realization have already been realized with former products and are based on repeatedly proven logical course structures and on harmonized processes of product determining, realization and support service. The complexity which is necessary in order to manufacture an energy-efficient product results from the product definition. This product definition is the fundament for all future decisions and defines, whether the product is supposed to become a simple, useful product or rather a product that should fulfill high-quality functions. In this way the decision is taken which extent and degree of complexity the manufacturing process will have and which share of the market the product is supposed to achieve.

Since every product is specific, also the flowchart must be tailored to every product separately. The flowchart shows the most important phases of the realization of the product with all single measures. With the help of furcations special features can be demonstrated. In the flowchart the word "process" is used frequently. In this way the manufacturing process and the product process are in brief meant. When a mass-production shall take place the manufacturing process must be elaborated very detailed since otherwise the error rate increases itself correspondingly. Simultaneously the qualification of the workers must be improved.

The projected flowchart is created in stages and follows in its classification the methodology of the VDI (The Association of German Engineers) Guidelines 2221. Accordingly the product is manufactured in an iterative process which corresponds to a stepped, progressive procedure (according to product and number of items). This procedure is in step with actual practice.

At the beginning of every process there is the idea. In the VDI Guidelines 2220 the course of the product planning as well as the upstream activities of the product determining are illustrated. The result of all measures for the product determining is the dutybook which, however, is not an inflexible flowchart. If it turns out that after creation of the dutybook new findings were added, these are integrated into the dutybook. If a principle-solution was reached, changes at the product are not possible. For the protection of the quality and to avoid errors methods of the preventive quality management can be used (according to VDI 2247) during the entire life cycle in all phases of the flowchart.

According to VDI Guidelines 2221 a flowchart contains all organizationally technical measures concerning planning, development and construction of technical products. The management makes the corresponding decisions for the priority of the energy efficiency. The interaction between product, product technology and fabrication techniques is expressed in the flowchart. Through intermediate measurements in different stages of the product (at the laboratory pattern, at the functional pattern and at the manufacturing pattern) errors can still be repaired in the course process.

References to the flowchart:

The flowchart ends with the finishing of the energy-efficient product while the life expectancy of the product ends only with the recycling of the product. During the processes of product determining and product realization should already attached importance to the fact that the product will be recycled energy-efficiently.

With the help of a solution catalog (by putting together the typical functions of all products in the company) a fast access can be carried out since it contains different realization possibilities, empirical values and calculation instructions for the products.

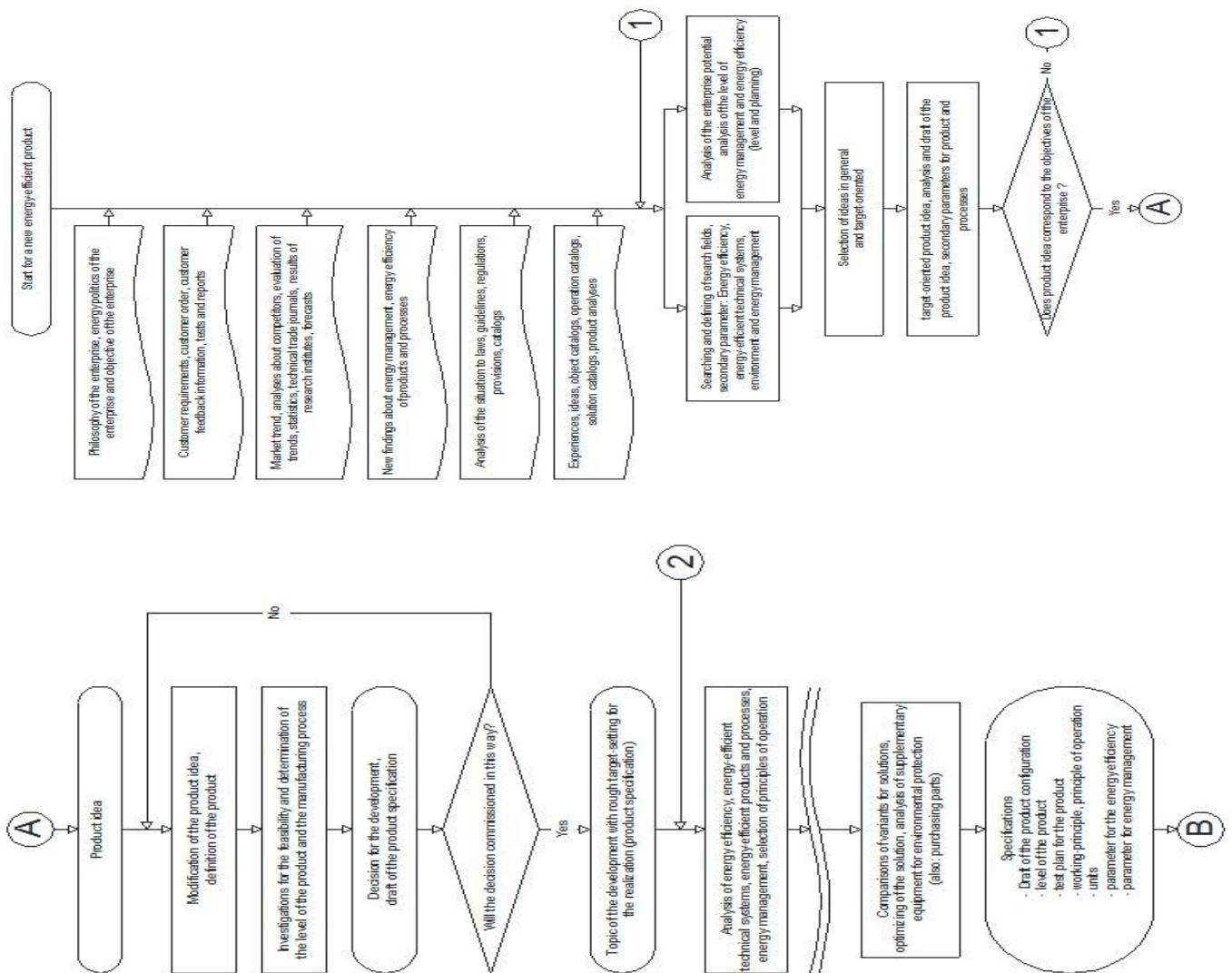
The object catalog on the other hand contains – independently of the task - solutions and calculations for one object/ one subject. This catalog should be split up into machine elements and manufacturing processes and can be used for the creation of solution variants.

The operation catalog contains experiences, instructions in calculations for different functions which can be realized with a product and solutions.

Functional or object plans are suitable as support during the product configuration. They must be compiled during the phases of product determining and product realization. Thus the compulsion of thinking over all phases during the process arises. The results are recorded in the field report.

In order to manufacture energy-efficient products, knowledge from different sectors as environmental protection, energy efficiency (Renewable energies law, Energy saving rule), ergonomics, design, etc. is necessary. As a result of a product development on the one hand products with practical functions must arise, however, on the other hand these products must not endanger the health of the human being. During the organization of a product its aesthetic function is also important. Indeed the appearance of a product is not always the main aim of the realization of the product. Nevertheless it should also be of high-quality, in a customer-oriented way and innovatively.

The product configuration is a complex process and therefore requires a flowchart tailored in particular to every single product.



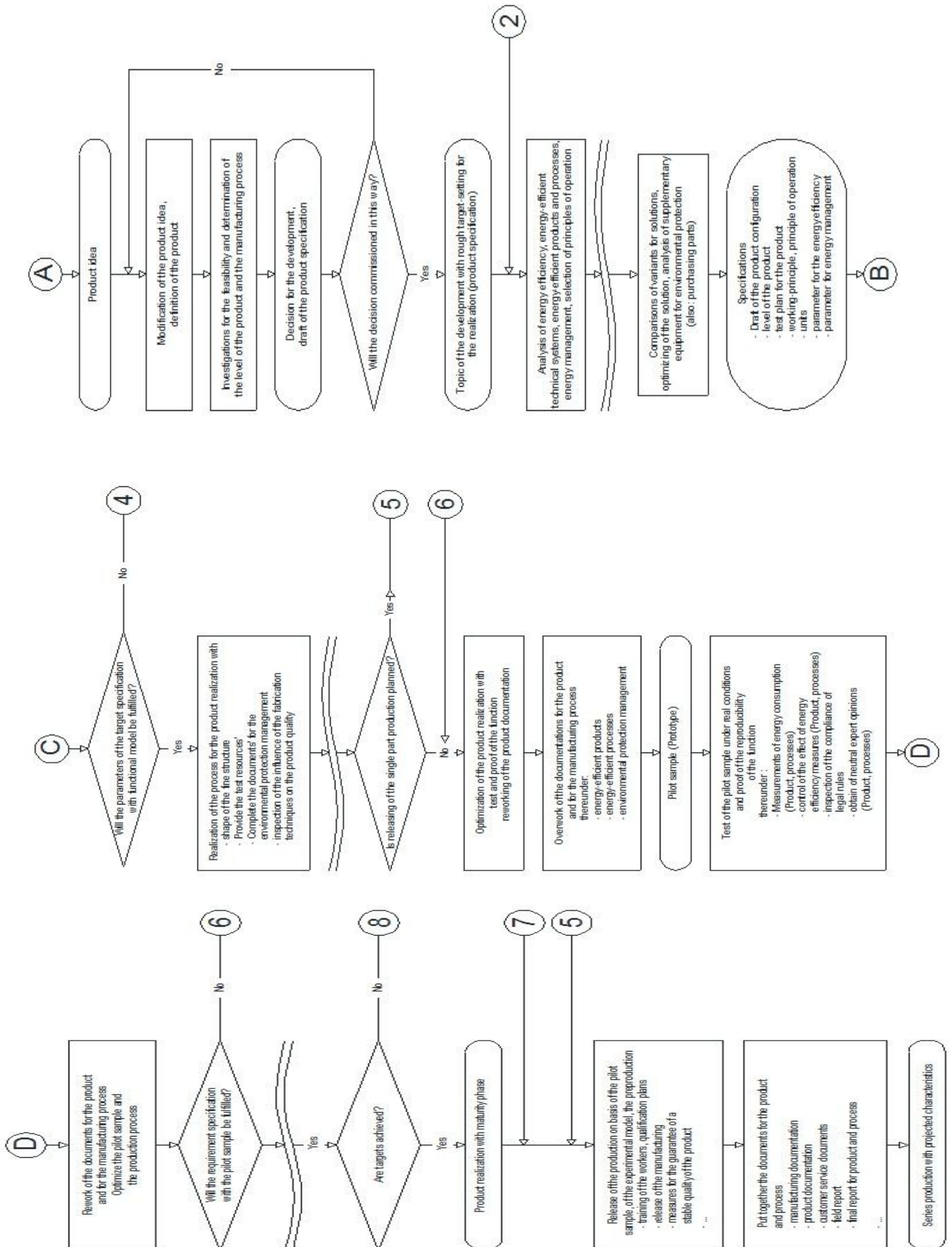


Fig. 1: Flowchart for the production of a new energy-efficient product

III. Conclusion

The organization of a new product is a comprehensive process which requires a complex approach. For every new product a separately designed flowchart for this product has to be elaborated. Attention has to be paid to the respective factors of the enterprise, the market and the legislation. This model was developed in particular for energy-efficient products. It can be adjusted correspondingly if certain conditions change.

REFERENCES

- [1] Dratwa, F., u.a.: Energiewirtschaft in Europa. Berlin: Springer-Verlag, 2010
- [2] Förtsch, G., Meinholz, H.: Handbuch Betriebliches Umweltmanagement. 1. Auflage (Wiesbaden: Vieweg + Teubner Verlag | Springer Fachmedien, 2011)
- [3] Kaltschmitt, M., Streicher, W., Wiese, A. (Hrsg.): Erneuerbare Energien. 4. Auflage (Berlin: Springer-Verlag, 2006)
- [4] Pehnt, M. (Hrsg.): Energieeffizienz. 1. korr. Nachdruck (Berlin: Springer-Verlag, 2010)
- [5] Pelte, D.: Die Zukunft unserer Energieversorgung. 1. Auflage (Wiesbaden: Vieweg + Teubner | GWV Fachverlage GmbH, 2010)
- [6] Pöschk, J. (Hrsg.): Energieeffizienz in Gebäuden. Jahrbuch 2011 (Berlin: VME- Verlag und Medienservice Energie, 2011)
- [7] Recknagel, H., Sprenger, E., Schramek, E.: Taschenbuch für Heizung + Klimatechnik. 74. Auflage (München: Oldenburg Industrie Verlag GmbH, 2009)
- [8] Schieferdecker, B. (Hrsg.): Energiemanagement-Tools. Berlin: Springer-Verlag, 2006)
- [9] Unger, J., Hurtado, A.: Alternative Energietechnik. 4. Überarb. Auflage (Wiesbaden: Vieweg + Teubner | GWV Fachverlage GmbH, 2011)
- [10] DIN EN ISO 50001 (12/2011): Energiemanagementsysteme
- [11] VDI 2220 – 05/1980): Produktplanung, Ablauf, Begriffe und Organisation
- [12] VDI 2221 – (05/1993): Methodik zum Entwickeln und Konstruieren technischer Systeme und Produkte
- [13] VDI 2247 – Entwurf (03/1994): Qualitätsmanagement in der Produktentwicklung
- [14] VDI 4602 – Blatt 1 (10/2007): Energiemanagement Begriffe
- [15] VDI 4602 – Blatt 2 (01/2011): Energiemanagement Beispiele

AUTHOR

Sejdo Ferati received his M.Sc. from the Faculty of Technical Sciences in Novi Sad, Serbia, his M.Eng. from the Beuth Hochschule für Technik (University of Applied Sciences) in Berlin, Germany and his Dr. degree from the Comenius University in Bratislava, Slovakia.

He is honorary professor at the Fachhochschule Brandenburg (University of Applied Sciences) in Brandenburg an der Havel, Germany.

He is Member of The Association of German Engineers (VDI)

Comparative Study for MCDS and DSR Which Are Used For Packet Forwarding In Ad Hoc Network

Prof. Nirmala Chouhan Thorwe,¹ Dr. Dinesh. M. Yadav,² Manoj Chouhan³

^{1,2}Computer Engineering/BSIOTR – Pune

³Shri Vaishnav Institute of Technology and Science –Indore

Abstract: this paper provides a brief overview of the operation of the DSR protocol; providing only enough detail that the reader can understand the analysis of DSR And comparative study of MCDS and DSR which is used for better understanding of step by step packet forwarding in to the Ad Hoc network. MCDS algorithm and DSR Protocol both are used in Ad hoc networking. In DSR, Blind broadcasting is used.

By using MCDS overcome from the limitation of DSR. It's proved comparative result on every step which is helpful for identify variation in packet forwarding.

Keywords: Ad hoc, DSR, MCDS, Blind broadcasting, packet forwarding.

I. Introduction

The routes that DSR discovers and uses are source routes. That is, the sender learns the complete, ordered sequence of network hops necessary to reach the destination, and, at a conceptual level, each packet to be routed carries this list of hops in its header. The key advantage of a source routing design is that intermediate nodes do not need to maintain up-to-date routing information in order to route the packets that they forward, since the packets themselves already contain all the routing decisions. MCDS provides solution for Blind broadcast in DSR.

II. Route Discovery in DSR

Route Discovery works by flooding a request through the network in a controlled manner, seeking a route to some target destination. In its simplest form, a source node A attempting to discover a route to a destination node D broadcasts a ROUTE REQUEST packet that is re-broadcast by intermediate nodes until it reaches D, which then answers by returning a ROUTE REPLY packet to A. Many optimizations to this basic mechanism are used to limit the frequency and spread of Route Discovery attempts. The controlled flood approach used by DSR works well in wired networks, but it is particularly well-suited to the nature of many wireless networks, where the communication channel between nodes is often inherently broadcast.

A single transmission of a ROUTE REQUEST is all that is needed to re-propagate the REQUEST to all of a node's neighbors. Figure 1.1 illustrates a simple Route Discovery. Before originating the ROUTE REQUEST, node A chooses a *request id* to place into the REQUEST such that the pair <originating address, request id > is globally unique. As the REQUEST propagates, each host adds its own address to a route being recorded in the packet, before broadcasting the REQUEST on to its neighbors (any host within range of its wireless transmission). When receiving a REQUEST, if a host has recently seen this request id or if it finds its own address already recorded in the route, it discards that copy of the REQUEST and does not propagate that copy further.

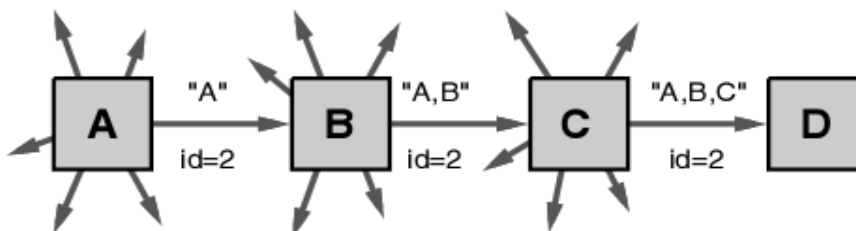


Figure 1.1 Basic operation of Route Discovery.

As a result of the duplicate check in the recorded source route, the algorithm for Route Discovery explicitly prohibits ROUTEREQUESTS from looping in the network. This is an important correctness property and is responsible for the loop-free property of DSR. The use of request ids represents a simple optimization that results in the ROUTE REQUESTs primarily spreading outwards from the originator, as shown in Figure 1.2, and curtails the number of REQUEST packets that circle around the originator.

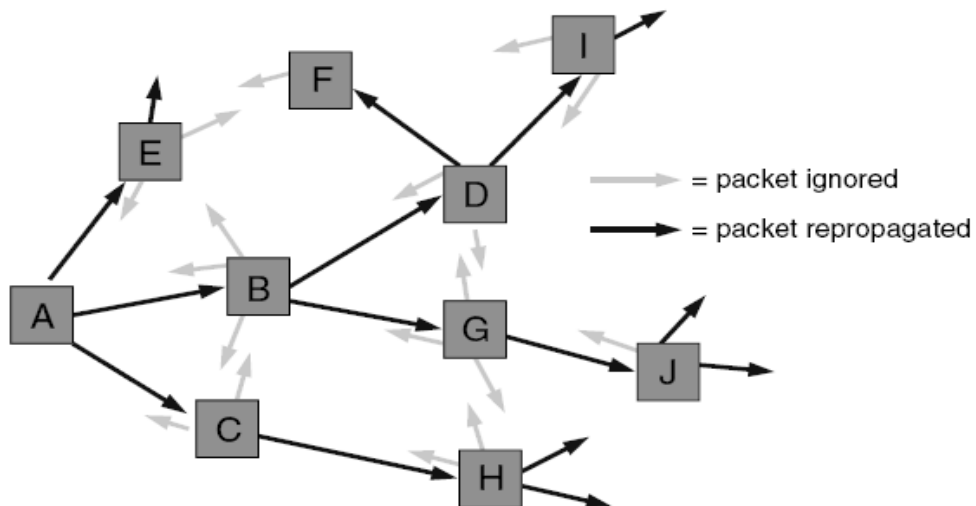


Figure 1.2 the use of request ids constrains the propagation of ROUTE

As an optimization, the protocol will still function correctly if the request ids are either not used or not cached long enough to prevent lateral movement of an outward propagating ROUTE REQUEST, though the overhead will REQUESTs into an organized outward-moving wave-front. While propagating a ROUTE REQUEST, nodes obey the normal rules for processing the Hop-Count or Time-to-Live field in the IP header of the packet carrying the ROUTE REQUEST. This mechanism can be used to implement a wide variety of “expanding ring” search strategies for the target, in which the hop limit is gradually increased in subsequent retransmissions of the ROUTE REQUEST for the target.

III. Proposed Solution MCDS

MCDS in mobile ad hoc network is treated as a virtual backbone for whole network. A virtual backbone structure on the ad-hoc network will be useful, in order to support unicast, multicast, and fault-tolerant routing within the ad-hoc network. This virtual backbone differs from the wired backbone of cellular network. The hosts in the MCDS maintain local copies of the global topology of the network, along with shortest paths between all pairs of nodes. Finding a minimal CDS for a connected graph is an NP-hard problem. For a small graph, we can enumerate all possible cases to find a minimal solution. However, this approach is not feasible for larger graphs.

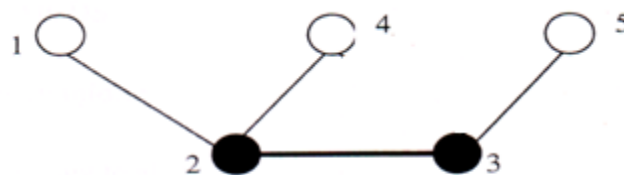


Fig 3.1 Two MCDS nodes in Ad Hoc Network

The algorithm for finding the MCDS can be classified into two categories:-

Finding a minimal CDS for a connected graph is an NP-hard problem. For a small graph, we can enumerate all possible cases to find a minimal solution. However, this approach is not feasible for larger graphs. Different approximation algorithms to find a minimal CDS have been proposed. Generally, they are divided into two classes:

- Global information based algorithms
- Local information based algorithms

Algorithms that use all information in the network are called global algorithms. The global algorithms assume that nodes keep identical copies of the entire topology. This is always true in a proactive link state routing protocol. Local algorithms utilize only local neighbor information.

The global algorithm finds a dominating set ‘c’ in the first phase by selecting the node with the largest effective degree and stopping when ‘C’ covers all nodes, (The effective degree is the number of neighbors not in ‘c’). ‘C’ may contain several disconnected components. In the second phase, CDS tries to use the minimum number of extra nodes to connect the components of ‘C’ to form a CDS. In this phase, links are assigned weights. If a link connects two non-CDS nodes that are in

the same component, this link is assigned weights of infinity. The weight for other links is the number of end points that are not in C^* . The lightest links are chosen to connect components. This phase ends when a CDS is found.

The different global algorithms, start at the node with the highest degree. It extends the set of selected CDS nodes by including the nodes adjacent to the current set that have the largest number of uncovered neighbors or two-hop uncovered neighbors until no uncovered nodes is left. The local algorithms are implemented in a distributed manner. This algorithms assumes that all nodes know all the other nodes that are within their two-hop range and that nodes have unique IDs. In the first phase, a nodes is selected as a potential member of the CDS if and only if it has two non-adjacent neighbors.

Nodes broadcast if they elect themselves as members of the potential CDS. Two extensions are used in the second phase to reduce the size of the CDS. A node stays in the CDS unless a neighbor CDS node with a larger ID covers its entire neighbor set. As an extension, if two adjacent CDS neighbors with larger IDs cover the neighbor set of a node, this node may change itself to a non-CDS node.

To determine routes with the MCDS, global knowledge of G is gathered into all the MCDS nodes and compute shortest paths based on local copies of G (akin to the link state approach restricted to MCDS Nodes. In general, the routes determined by the MCDS nodes do not pass through the MCDS.

However, the MCDS can handle routes in two situations:

- When a non-MCDS edge or node fails, the MCDS provides an immediate backup route to use while another shortest path is found, and
- The MCDS can be used for multicast and broadcast routing.

At a high level of abstraction, the MCDS based routing algorithm consists of the following steps to determine routes:

- Compute the MCDS.
- Gather topology information from non-MCDS nodes to MCDS nodes.
- Broadcast topology to all MCDS nodes.
- Determine routes. Each node runs an all pairs shortest path algorithm on its local copy of graph.
- Propagate information out to non- MCDS nodes.
- Send periodic maintenance update. Every T second for some large value of T , the MCDS nodes repeat the topology broadcast step. This periodic broadcast ensures that the MCDS nodes recognize drastic topology changes.

IV. Testing set

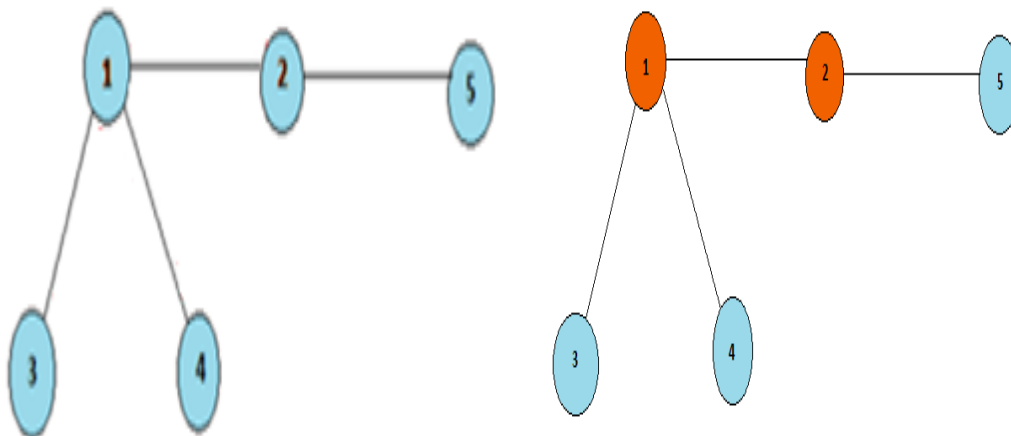


Fig 4.1 (a) DSR

(b)MCDS

4.1 Connection between nodes represented by table for algorithm-II: -

(1 indicate connection and 0 indicate no connection between nodes)

	1	2	3	4	5
1	0	1	1	1	0
2	1	0	0	0	1
3	1	0	0	0	0
4	1	0	0	0	0
5	0	1	0	0	0

Table 4.1 Connections between nodes.

4.2 Value analysis for Node 1:-

Source node	Destination	DSR	MCDS
1	1	0	0
	2	3	1
	3	3	1
	4	3	1
	5	5	2

Table 4.2.1 Packet forwarding from NODE 1

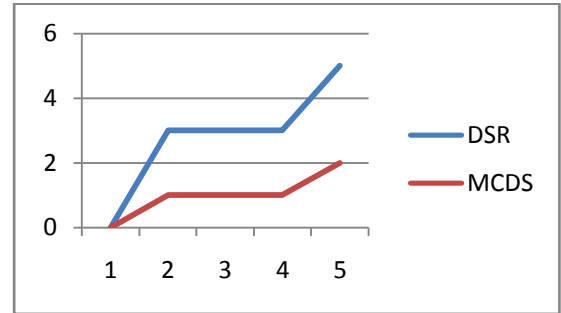


Fig. 4.2.1 Packet forwarding from NODE 1

4.3 Value analysis for Node2:-

Source node	Destination	DSR	MCDS
2	1	2	1
	2	0	0
	3	5	2
	4	5	2
	5	2	1

Table 4.3.1 Packet forwarding from NODE 2

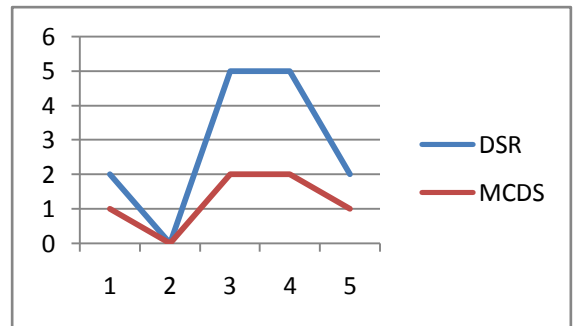


Fig. 4.3.1 Packet forwarding from NODE 2

4.4 Value analysis for Node 3 :-

Source node	Destination	DSR	MCDS
3	1	1	1
	2	3	2
	3	0	0
	4	6	2
	5	6	3

Table 4.4.1 Packet forwarding from NODE3

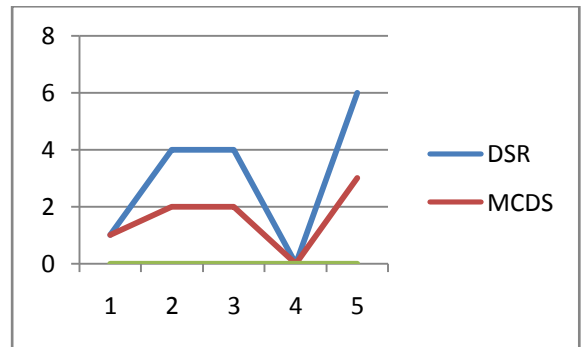


Fig. 4.4.1 Packet forwarding from NODE 3

4.5 Value analysis for Node 4 :-

Source node	Destination	DSR	MCDS
4	1	1	1
	2	4	2
	3	4	2
	4	0	0
	5	6	3

Table 4.5.1 Packet forwarding from NODE 4

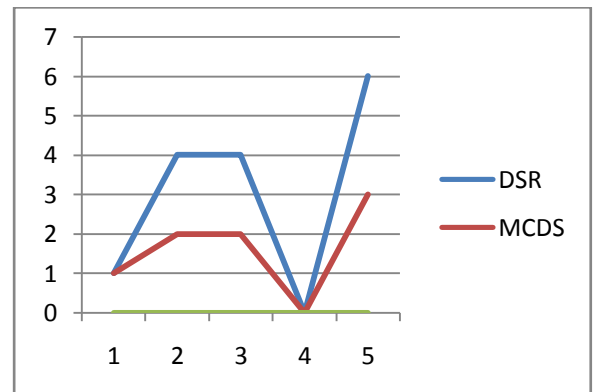


Fig. 4.5.1 Packet forwarding from NODE 4

4.6 Value analysis for Node 4 :-

Source node	Destination	DSR	MCDS
5	1	2	2
	2	1	1
	3	6	3
	4	6	3
	5	0	0

Table 4.6.1 Packet forwarding from NODE 5

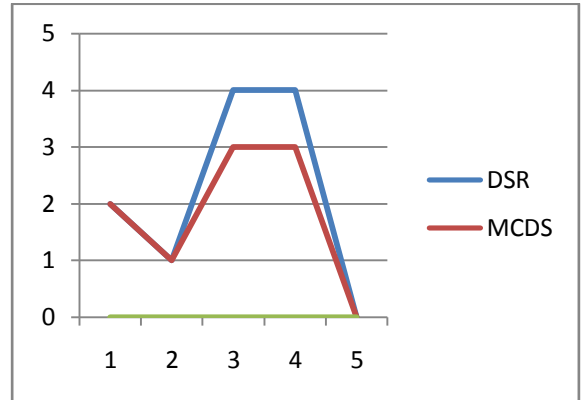


Fig. 4.6.1 Packet forwarding from NODE 5

V. All routing Analysis

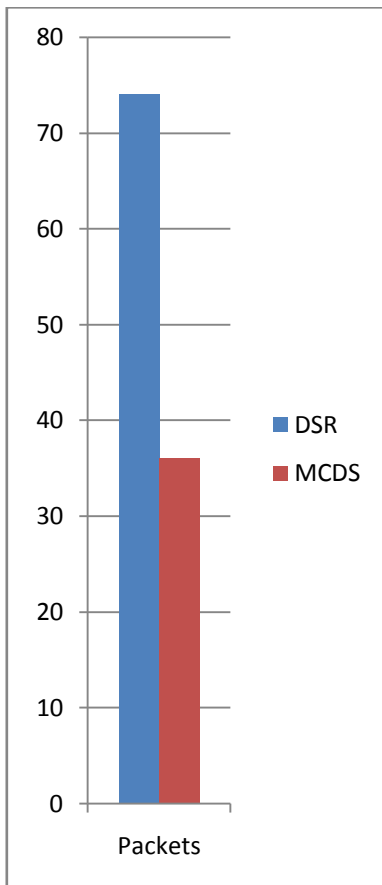


Table 5.1 Total Packet forwarding

Total Number of forwarding	DSR	MCDS
Packets	74	36

Fig 5.1 Results

VI. Conclusions

When the performance of DSR, in terms of packet loss rate and routing protocol overhead, is compared with that of three other routing protocols are DSDV, TORA, DSR, AODV designed for use in multi-hop ad hoc networks, DSR significantly outperforms the other protocols across a wide range of scenarios. If DSR protocol use MCDS algorithm for routing in ad hoc network then it is possible to significant reduction of overhead by using the MCDS to reduce redundancy due to blind broadcasts in DSR protocol. In DSR 74 packet forwarding is needed and in MCDS 36. With the help of resulting packet ratio, DSR with MCDS is better than simple DSR.

6.1 Various advantages of applying DSR on MCDS are:-

1. Total number of Nodes: - Fig 6.1.1 shows that the number of nodes in reaching from source to destination can be reduced

2. Time: - The above example helps to reduce the extra time required during route discovery to find the path from source to destination. Instead the path is already maintained by the MCDS members of the graph.

3. Broadcasting: - The Source need not broadcast the route request to all its neighbors; instead it can send the request only to the MCDS neighbors.

4. Bandwidth consumption: - The packet header size grows with the route length resulting in more bandwidth utilization. Thus, by applying DSR over MCDS, there is a significant reduction in total number of nodes, thereby reducing the bandwidth consumption.

6.2 Limitation

For example if a wireless ad hoc network is in form of a graph as shown in figure(a) then MCDS obtained by using algorithm in this like figure(b) where, black nodes is minimal connected dominating set. But practically it is not possible case for figure (a).

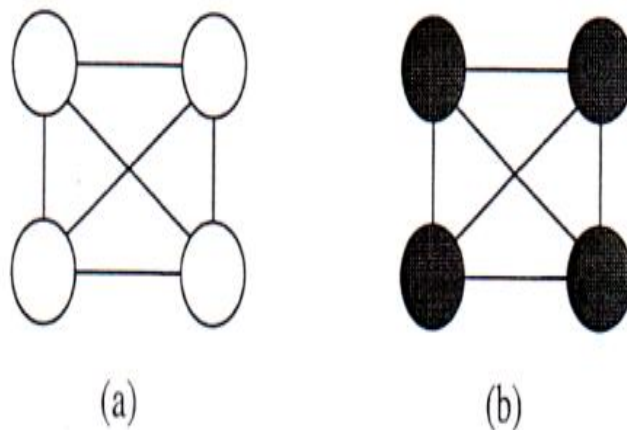


Fig 6.2.1

6.3 Future Scope

Numerous areas for future research can be described using this report. The various areas are:-

1 Node mobility:-The topology change is one of the most important issues in ad hoc network. Various researches can be done in this field.

2 Multi hop:-All the research work has been done considering the nodes at 1 hop or 2 hop distance. The efforts can be made to apply the work done in the cases of multi hop distance

While many challenges remain to be resolved before large scale MANETs can be widely deployed, small-scale mobile ad hoc networks will soon appear. If the above mentioned scopes can be successfully applied to the ad hoc networks this field will act as a boom to the wireless transmission.

REFERENCES

- [1] A Distributed approach for computing the minimum connected dominating set in ad hoc networks by Kais Mnif, Bo Rond and Michel Kadoch
- [2] David B. Johnson, David A. Maltz, and Josh Broch. DSR The Dynamic Source Routing Protocol for Multihop Wireless Ad Hoc Networks. In Ad Hoc Networking, edited by Charles E. Perkins, chapter 5, pages 139–172. Addison-Wesley, 2001.
- [3] David B. Johnson, David A. Maltz, Yih-Chun Hu, and Jorjeta Jetcheva. The Dynamic Source Routing Protocol for Mobile Ad Hoc Networks. Internet-Draft, draft-ietf-manet-dsr-04.txt, November 2000. Work in progress.
- [4] David A. Maltz. Resource Management in Multi-hop Ad Hoc Networks. Technical Report CMU CS TR00-150, School of Computer Science, Carnegie Mellon University, November 1999. Available from <http://www.monarch.cs.cmu.edu/papers.html>.
- [5] M. Scott Corson and Anthony Ephremides. A Distributed Routing Algorithm for Mobile Wireless Networks. Wireless Networks, 1(1):61–81, February 1995.
- [6] National Science Foundation. Research Priorities in Wireless and Mobile Communications and Networking: Report of a Workshop Held March 24–26, 1997, Airlie House, Virginia. Available at <http://www.cise.nsf.gov/anir/www.html>.
- [7] Rajendra V. Boppana and Satyadeva P. Konduru. An Adaptive Distance Vector Routing Algorithm for Mobile, Ad Hoc Networks. In Proceedings of IEEE INFOCOM 2001, pages 1753–1762, Anchorage, Alaska, April 2001.
- [8] IEEE Computer Society LAN MAN Standards Committee. Wireless LAN Medium Access Control (MAC) and Physical Layer (PHY) Specifications, IEEE STD 802.11-1999. The Institute of Electrical and Electronics Engineers, New York, New York, 1999.

- [9] John Jubin and Janet D. Tornow. The DARPA Packet Radio Network Protocols. Proceedings of the IEEE, 75(1):21–32, January 1987.
- [10] Stephen E. Deering and Robert M. Hinden. Internet Protocol, Version 6 (IPv6) Specification. RFC 2460, December 1998.
- [11] Charles E. Perkins and Pravin Bhagwat. Highly Dynamic Destination-Sequenced Distance-Vector Routing (DSDV) for Mobile Computers. In Proceedings of the SIGCOMM '94 Conference on Communications Architectures, Protocols and Applications, pages 234–244, August 1994. A revised version of the paper is available from <http://www.cs.umd.edu/projects/mcml/pub.html>.
- [12] On-Demand Multicast Routing in Ad Hoc Networks with Unidirectional Links Jorjeta G. Jetcheva and David B. Johnson December 15, 2004 CMU-CS-04-175 School of Computer Science Computer Science Department Carnegie Mellon University Pittsburgh, PA 15213
- [13] Vincent D. Park and M. Scott Corson. A Highly Adaptive Distributed Routing Algorithm for Mobile Wireless Networks. In Proceedings of INFOCOM'97, pages 1405–1413, April 1997.
- [14] Vincent D. Park and M. Scott Corson. Temporally-Ordered Routing Algorithm (TORA) Version 1: Functional Specification. Internet-Draft, draft-ietf-manet-tora-spec-01.txt, August 1998. Work in progress.
- [15] M. S. Corson, S. Papademetriou, P. Papadopoulos, V. Park, and A. Qayyum. An Internet MANET Encapsulation Protocol (IMEP) Specification. Internet-Draft, draft-ietf-manet-imep-spec-01.txt, August 1998. Work in progress.
- [16] David B. Johnson and David A. Maltz. Dynamic Source Routing in Ad Hoc Wireless Networks. In Mobile Computing, edited by Tomasz Imielinski and Hank Korth, chapter 5, pages 153–181. Kluwer Academic Publishers, 1996.
- [17] David A. Maltz, Josh Broch, and David B. Johnson. Experiences Designing and Building a Multi-Hop Wireless Ad Hoc Network Testbed. Technical Report 99-116, School of Computer Science, Carnegie Mellon University, March 1999. Available from <http://www.monarch.cs.cmu.edu/papers.html>.
- [18] Charles Perkins, editor. IP Mobility Support. Internet Request For Comments RFC 2002, October 1996.
- [19] Josh Broch, David A. Maltz, and David B. Johnson. Supporting Hierarchy and Heterogeneous Interfaces in Multi-Hop Wireless Ad Hoc Networks. In Proceedings of the Workshop on Mobile Computing held in conjunction with The International Symposium on Parallel Architectures, Algorithms, and Networks, pages 370–375, Perth, Australia, June 1999.
- [20] Elizabeth M. Royer and C.K. Toh. “A Review of current routing protocols for ad-hoc mobile wireless networks, ‘ IN IEEE personal communication magazing, pp. 46-55, April 1999

ATC Determination for Different Transactions Using ACPTDF

Saloni,¹ Meenakshi Dhakla²

¹Department of Electrical and Electronics Engineering, B.M.I.E.T Sonapat/M.D.U., India

²Department of Electrical Engineering, D.C.R.U.S.T., Murthal., India

Abstract: A fair competition needs open access and non-discriminatory operation of the transmission network. Open access to the transmission system places an emphasis on the intensive use interconnected network reliably, which requires knowledge of the network capability. Available Transfer Capability (ATC) is a measure of the remaining power transfer capability of the transmission network for further transactions. Available transfer capability in the transmission network has become essential quantity to be declared well in advance for its commercial use in a competitive electricity market. The assessment of ATC using AC Power transfer distribution factors (AC PTDFs) based approach has been used for single and simultaneous transactions using power transfer sensitivity and jacobian calculated with N-R method. The AC PTDFs are derived using sensitivity based approach for the system intact case. A study of ATC determination using AC Power Transfer Distribution Factor (AC PTDF). We predicted the AC PTDF is different for different transactions and ATC is also different with the help of MATLAB Programming. Simultaneous and single transactions have been carried out on IEEE 24 bus RTS for the assessment of ATC. The solutions obtained are quite encouraging and useful in the present restructuring environment.

Keywords: Available Transfer Capability (ATC), AC Power Transfer Distribution Factor (ACPTDF)

I. INTRODUCTION

Available transfer capability in the transmission network has become essential quantity to be declared well in advance for its commercial use in a competitive electricity market. Electric power industries throughout the world have been restructured to introduce competition among the market participants and bring several competitive opportunities. A fair competition needs open access and non-discriminatory operation of the transmission network. Open access to the transmission system places an emphasis on the intensive use of the interconnected network reliably, which requires knowledge of the network capability. Available Transfer Capability (ATC) is a measure of the remaining power transfer capability of the transmission network for further transactions. Its fast computation using DC load flow based approach is used worldwide for on line implementation. Many authors have proposed the ATC calculation based on DC/AC load flow approach. AC PTDF based approach has been proposed for multi-transaction cases using power transfer sensitivity and Jacobian calculated with three different methods. The methods can be implemented for any number of transactions occurring simultaneously.

The linear dc power transfer distribution factors (DC PTDF) based on dc power flow method, is possibly the only allocation technique presently in widespread use to

allocate MW flows on the lines for a transaction in the system. However, this has a poor accuracy due to the assumptions involved in the dc power flow model.

In a fast decoupled power flow model for transmission allocation has been suggested, which is based on linearizing ac power flow equations and using incremental steps based on current power flow state. However, it does not allocate losses to individual transactions. In a physical flow-based transmission loss allocation scheme based on expressing loss explicitly in terms of all transactions in a power system network was proposed. However, error between the system losses evaluated by ac load flow (ACLF) and the losses using the methodology based on were relatively high, ranging from 10% to 16%.

The ac power transfer distribution factors, computed at a base case, have been used to find various transmission system quantities for a change in MW transactions at different operating conditions.

II. ATC PRINCIPLES

Available Transfer Capability (ATC) is a measure of the transfer capability remaining in the physical transmission network for further commercial activity over and above already committed uses. Mathematically, ATC is defined as the Total Transfer Capability (TTC) less the Transmission Reliability Margin (TRM), less the sum of existing transmission commitments (which includes retail customer service) and the Capacity Benefit Margin (CBM).

2.1 TOTAL TRANSFER CAPABILITY (TTC): is defined as the amount of electric power that can be transferred over the interconnected transmission network in a reliable manner while meeting all of a specific set of defined pre- and post-contingency system conditions.

Transfer Capability is different from 'Transmission Capacity', which usually refers to the thermal limit or rating of a particular transmission element or component. The capability to meet load (transfer capability) would however depend on several other factors such as spatial distribution and diversity of generation/load, network configuration. Thus, the individual transmission line capacities or ratings cannot be arithmetically added to determine the transfer capability of a transmission path or interface.

2.2 TRANSMISSION RELIABILITY MARGIN (TRM): is defined as that amount of transmission transfer capability necessary to ensure that the interconnected transmission network is secure under a reasonable range of uncertainties in system conditions.

2.3 CAPACITY BENEFIT MARGIN (CBM): is defined as that amount of transmission transfer capability reserved by load serving entities to ensure access to generation from interconnected systems to meet generation reliability requirements.

III. ATC PRINCIPLES

The following Available Transfer Capability (ATC) Principles govern the development of the definition and determination of ATC and related terms. All transmission provider and user entities are expected to abide by these Principles.

3.1 ATC calculations must produce commercially viable results. ATCs produced by the calculations must give a reasonable and dependable indication of transfer capabilities available to the electric power market.

3.2 ATC calculations must recognize time-variant power flow conditions on the entire interconnected transmission network. In addition, the effects of simultaneous transfers and parallel path flows throughout the network must be addressed from a reliability viewpoint.

3.3 ATC calculations must recognize the dependency of ATC on the points of electric power injection, the directions of transfers across the interconnected transmission network, and the points of power extraction. All entities must provide sufficient information necessary for the calculation of ATC.

3.4 Regional or wide-area coordination is necessary to develop and post information that reasonably reflects the ATCs of the interconnected transmission network.

3.5 ATC calculations must conform to NERC, Regional, sub regional, power pool, and individual system reliability planning and operating policies, criteria, or guides.

3.6 The determination of ATC must accommodate reasonable uncertainties in system conditions and provide operating flexibility to ensure the secure operation of the interconnected network.

The calculation of transfer capability is generally based on computer simulations of the operation of the interconnected transmission network under a specific set of assumed operating conditions. These simulations are typically performed "off line," well before the systems approach that operational state. Each simulation represents a single "snapshot" of the operation of the interconnected network based on the projections of many factors. As such, they are viewed as reasonable indicators of network performance and available transfer capability.

IV. AC POWER TRANSFER DISTRIBUTION FACTOR

Consider a transaction P_{mn} between a seller bus, m and buyer bus, n. Further consider a line, 'l' carrying a part of the transaction power. Let the line be connected between a bus-i and a bus-j. For a change in real power transaction between the above seller and buyer say by ΔP_{mn} , if the change in transmission line quantity P_{ij} is ΔP_{ij} , the AC power transfer distribution factors can be defined as:

$$ACPTDF_{ij,mn} = \frac{\Delta P_{ij}}{\Delta P_{mn}}$$

V. METHODOLOGY

For a transaction among the buyer and seller buses by ΔP_{mn} , if the change in the transmission line quantity is ΔP_{ij} , the AC power transfer distribution factors can be defined as,

$$ACPTDF_{ij,mn} = \frac{\Delta P_{ij}}{\Delta P_{mn}} \quad (1)$$

For Power Transfer Distribution Factor calculation using AC load approach, the power flow sensitivity and Jacobian of power injection equations is required. The Jacobian can be calculated using N-R load flow based approach. The power flow equations in polar form can be represented as:

$$P_i = \sum_{j=1}^n |V_i| |V_j| |Y_{ij}| \cos(\theta_{ij} - \delta_i + \delta_j) \quad (2)$$

$$Q_i = \sum_{j=1}^n |V_i| |V_j| |Y_{ij}| \sin(\theta_{ij} - \delta_i + \delta_j) \quad (3)$$

Where n be the total no of buses P_i and Q_i are the real and reactive power injected at any bus i

$|V_i|$, $|V_j|$ are the voltage magnitudes at the buses respectively, δ_i , δ_j are the voltage angles at the buses i and bus j, and $|Y_{ij}|$, θ_{ij} are taken from Y_{bus} .

Using Taylor series expansion, the change in power flows at any bus i can be formulated in terms of Jacobian as:

$$\begin{bmatrix} \Delta P \\ \Delta Q \end{bmatrix} = \begin{bmatrix} J_1 & J_2 \\ J_3 & J_4 \end{bmatrix} \begin{bmatrix} \Delta \delta \\ \Delta |V| \end{bmatrix} \quad (4)$$

Where

$$[J_1] = \frac{\partial P}{\partial \delta}, [J_2] = \frac{\partial P}{\partial |V|}, [J_3] = \frac{\partial Q}{\partial \delta}, [J_4] = \frac{\partial Q}{\partial |V|} \quad (5)$$

The change in the angle and voltage magnitude can be determined as:

$$\begin{bmatrix} \Delta \delta \\ \Delta |V| \end{bmatrix} = \begin{bmatrix} J_1 & J_2 \\ J_3 & J_4 \end{bmatrix}^{-1} \begin{bmatrix} \Delta P \\ \Delta Q \end{bmatrix} \quad (6)$$

Using N-R load flow analysis bus voltage magnitudes and angles can be evaluated. For calculation of AC Power Transfer Distribution Factors, Jacobian and power flow sensitivity can be calculated. The power flow sensitivity can be determined using the power flow equations for real power.

The real power flow (P_{ij}) in a line-k, connected between buses i and j, can be written as:

$$P_{ij} = V_i V_j Y_{ij} \cos(\theta_{ij} + \delta_j - \delta_i) - V_i^2 Y_{ij} \cos \theta_{ij} \quad (7)$$

Where V_i and δ_i are the voltage magnitude and angle at bus- i. Y_{ij} And θ_{ij} magnitude and angle of ij^{th} element of $[Y_{Bus}]$.

Using Taylor's series approximation and ignoring higher order terms, change in real power can be written as:

$$\Delta P_{ij} = \frac{\partial P_{ij}}{\partial \delta_i} \Delta \delta_i + \frac{\partial P_{ij}}{\partial \delta_j} \Delta \delta_j + \frac{\partial P_{ij}}{\partial V_i} \Delta V_i + \frac{\partial P_{ij}}{\partial V_j} \Delta V_j \quad (8)$$

The sensitivity coefficients appearing in (7) can be obtained using the partial derivatives of real power flow (6) with respect to variables δ and V as:

$$\frac{\partial P_{ij}}{\partial \delta_{ij}} = V_i V_j Y_{ij} \sin(\theta_{ij} + \delta_j - \delta_i) \quad (9)$$

$$\frac{\partial P_{ij}}{\partial \delta_{ij}} = -V_i V_j Y_{ij} \sin(\theta_{ij} + \delta_j - \delta_i) \quad (10)$$

$$\frac{\partial P_{ij}}{\partial v_i} = V_j Y_{ij} \cos(\theta_{ij} + \delta_j - \delta_i) - 2 V_i Y_{ij} \cos \theta_{ij} \quad (11)$$

$$\frac{\partial P_{ij}}{\partial v_j} = V_i Y_{ij} \cos(\theta_{ij} + \delta_j - \delta_i) \quad (12)$$

The sensitivity of power flow equation can be written in the compact matrix form as:

$$\Delta P_{ij} = \begin{bmatrix} \frac{\partial P_{ij}}{\partial \delta_2}, \dots, \frac{\partial P_{ij}}{\partial \delta_n}, \frac{\partial P_{ij}}{\partial v_{g+1}}, \dots, \frac{\partial P_{ij}}{\partial v_n} \end{bmatrix} \begin{bmatrix} \Delta \delta_2 \\ \vdots \\ \Delta \delta_n \\ \Delta |V_{g+1}| \\ \vdots \\ \Delta |V_n| \end{bmatrix} \quad (13)$$

Where $\begin{bmatrix} \frac{\partial P_{ij}}{\partial \delta_2}, \dots, \frac{\partial P_{ij}}{\partial \delta_n}, \frac{\partial P_{ij}}{\partial v_{g+1}}, \dots, \frac{\partial P_{ij}}{\partial v_n} \end{bmatrix}$

Is line power flow sensitivity corresponding to angle and voltage magnitude. For a single transaction case between seller bus m and buyer bus n, the change in power transactions can be substituted at position of bus m and bus n as:

$$\Delta P_m = +P_t$$

$$\Delta P_n = -P_t$$

$$\Delta P_{ij} = \begin{bmatrix} \frac{\partial P_{ij}}{\partial \delta_2}, \dots, \frac{\partial P_{ij}}{\partial \delta_n}, \frac{\partial P_{ij}}{\partial v_{g+1}}, \dots, \frac{\partial P_{ij}}{\partial v_n} \end{bmatrix} [J]^{-1} \begin{bmatrix} 0 \\ \vdots \\ +P_t \\ 0 \\ \vdots \\ -P_t \\ 0 \end{bmatrix} =$$

$$ACPTDF_t * P_t \quad (14)$$

So, ACPTDFs for the transaction between seller bus m to buyer bus n can be represented as:

$$ACPTDF_{ij,mn} = \begin{bmatrix} \frac{\partial P_{ij}}{\partial \delta_2}, \dots, \frac{\partial P_{ij}}{\partial \delta_n}, \frac{\partial P_{ij}}{\partial v_{g+1}}, \dots, \frac{\partial P_{ij}}{\partial v_n} \end{bmatrix} [J]^{-1} \begin{bmatrix} 0 \\ \vdots \\ +1 \\ 0 \\ \vdots \\ -1 \\ 0 \end{bmatrix} \quad (15)$$

ACPTDFs are obtained for each line for particular transaction between seller and buyer bus. In the present work, the method of N-R Jacobian based approach (J_{N-R}) have considered for ACPTDFs determination.

4.1 N-R Jacobian based Approach

The power flow change can be expressed corresponding to line flow sensitivities with angle and voltage and change in angle and voltages can be obtained from N-R approach as:

$$\Delta P_{ij} = \begin{bmatrix} \frac{\partial P_{ij}}{\partial \delta_2}, \dots, \frac{\partial P_{ij}}{\partial \delta_n}, \frac{\partial P_{ij}}{\partial v_{g+1}}, \dots, \frac{\partial P_{ij}}{\partial v_n} \end{bmatrix} [J_{N-R}]^{-1} \begin{bmatrix} 0 \\ \vdots \\ +\Delta P_t \\ 0 \\ \vdots \\ -\Delta P_t \\ 0 \end{bmatrix} =$$

$$ACPTDF_t * P_t$$

$$ACPTDF_{ij,mn} = \begin{bmatrix} \frac{\partial P_{ij}}{\partial \delta_2}, \dots, \frac{\partial P_{ij}}{\partial \delta_n}, \frac{\partial P_{ij}}{\partial v_{g+1}}, \dots, \frac{\partial P_{ij}}{\partial v_n} \end{bmatrix} [J_{N-R}]^{-1} \begin{bmatrix} 0 \\ \vdots \\ +1 \\ 0 \\ \vdots \\ -1 \\ 0 \end{bmatrix} \quad (16)$$

Both Jacobian and line flow sensitivity factors are taken without considering any assumptions.

4.2 ATC Determination for Intact System Methodology remains same for calculation of ATC. The method of N-R Jacobian method provide different Jacobin and line flow sensitivity factors which are used for calculation of AC Power Transfer Distribution Factors. Real power flows in base case obtained from N-R approach and line limits as a given data are utilized for ATC determination.

Now P_{ij-mn}^{max} for any transaction seller bus m to buyer bus n can be obtained as:

$$P_{ij-mn}^{max} = \begin{cases} \frac{Limit_{ij}^{max} - P_{ij}}{ACPTDF_{ij,mn}} ; ACPTDF_{ij,mn} > 0 \\ \infty \text{ (infinite)} ; ACPTDF_{ij,mn} = 0 \\ \frac{-Limit_{ij}^{max} - P_{ij}}{ACPTDF_{ij,mn}} ; ACPTDF_{ij,mn} < 0 \end{cases} \quad (18)$$

Where P_{ij} is the real power flow through any line $i-j$, $Limit_{ij}^{max}$ is thermal limit of any line $i-j$, P_{ij-mn}^{max} is the maximum allowable transaction amount from bus/zone m to bus/zone n constrained by the line flow limit from bus/zone i to bus/zone j . For the given transaction, the ATC can be defined and obtained as:

$$ATC_{min} = \min\{P_{ij}^{max} | j \in N_1\} \quad (19)$$

Where, N_1 is the total number of lines in the system?

VI. RESULTS

In this chapter, discuss about the results of Available Transfer Capability (ATC) with respect to AC Power Transfer Distribution Factors (ACPTDFs) for different transactions. The results of ACPTDFs for all the lines and its ATC. The results have been determined for IEEE RTS 24 bus system. The results include PTFD calculations for intact system in case of all transactions. Based on the PTFDs, ATC have been calculated for all transaction cases. The ACPTDF is shown in Figure 1 for all the lines and the ATC for T1 is 7.57. ATC for T2 and T3 are 2.83 and 2.76 respectively.

ATC is calculated for IEEE RTS 24 bus system. ATC has been obtained for different transactions taken as single transaction and simultaneous transactions. These transactions have been categorized as:

T₁: Transaction between seller buses 23 to buyer bus 15 (Figure 1).

T₂: Transaction between seller buses 10 to buyer bus 3 (Figure 2).

T₃: Transaction between seller bus 23, 10 to buyer bus 15, 3 (simultaneous transaction) (Figure 3).

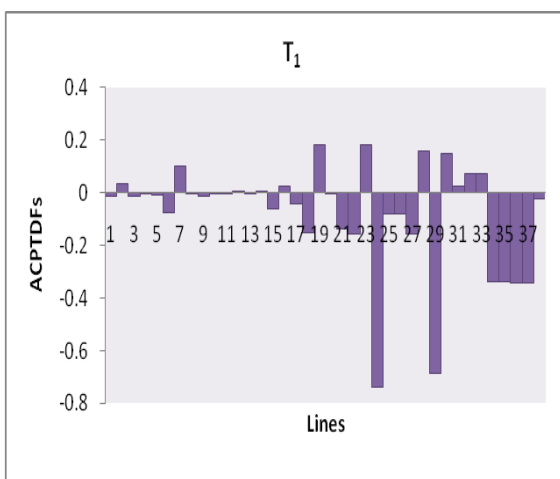


Fig. 1 Bar graph of ACPTDF for all the lines for T₁

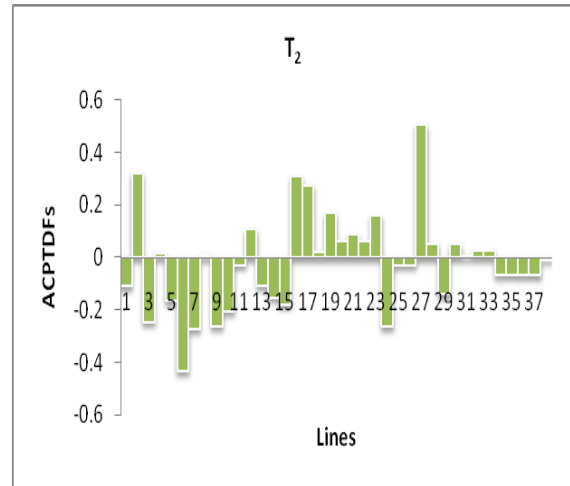


Fig. 2 Bar graph of ACPTDF for all the lines for T₂.

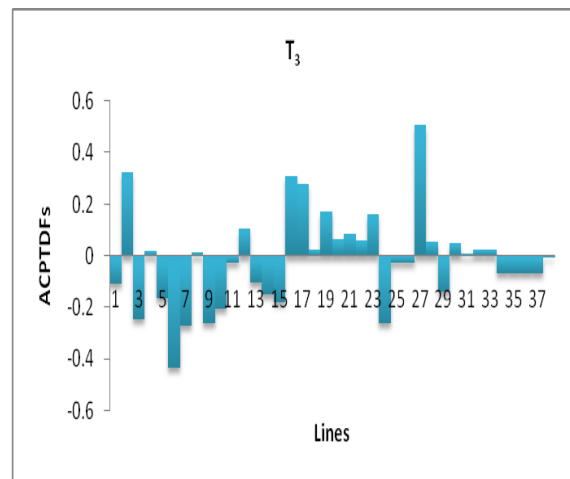


Fig. 3 Bar graph of ACPTDF for all the lines for T₃.

REFERENCES

- [1] North American Electric Reliability Council (NERC), "Available Transfer Capability Definitions and Determination", NERC Report, June 1996.
- [2] Venkatesh, Dr. Paramasivam; Gnanadass, Ramachandran; and Padhy, Dr. Narayana Prasad (2004), "Available Transfer Capability Determination Using Power Transfer Distribution Factors", International Journal of Emerging Electric Power Systems: Vol. 1: Iss. 2, Article 1009.
- [3] G. C. Ejebe, J. G. Waight, M. Santos-Nieto and W. F. Tinney, "Fast Calculation of Linear Available Transfer Capability", IEEE Trans. on Power Systems, vol. 15, no. 3, Aug. 2000, pp. 1112-1116.
- [4] G. Hamoud, "Assessment of Available Transfer Capability of Transmission Systems", IEEE Trans. on Power Systems, vol. 15, no. 1, Feb. 2000, pp. 27-32.
- [5] Narasimha Rao, K., Amarnath, J. and Kiran Kumar, K., Kamakshiah, S. S., "Available Transfer Capability Calculations Using Neural Networks in Deregulated Power", 2008 International Conference on Condition Monitoring and Diagnosis, Beijing, China, April 21-24, 2008.
- [6] Yajing Gao, Jin Yang, Ming Zhou, and Gengyin Li, "Available Transfer Capability Assessment of AC/DC Transmission System", 2010 International Conference on Power System Technology.
- [7] A. Kumar, S. C. Srivastava, and S. N. Singh, "Available Transfer Capability Assessment in a Competitive Electricity Market Using a Bifurcation Approach", IEE Proc. on

- Generation, Transmission and Distribution, vol. 151, no. 2, March 2004, pp. 133 – 140.
- [8] Mohamed Shaaban, Yixin Ni, Felix F. Wu, “Available Transfer Capability Evaluation by Decomposition”, Vol. No. 0-7803-7173-9/01/\$10.00 © 2001 IEEE.
- [9] Ashwani Kumar, S. C.Srivastava, “AC Power Transfer Distribution Factors for Allocating Power Transactions in a Deregulated Market”, IEEE Power Engineering Review, July 2002.
- [10] A. Kumar, S. C. Srivastava, and S. N. Singh, “Available Transfer Capability (ATC) Determination in Competitive Electricity Market Using AC Distribution Factors”, Electric Power Components and Systems, vol. 32, June 2004, pp. 927-939.
- [11] Hsiao-Dong Chiang, Alexander J. Flueck, Kirit S. Shah, Neal Balu, “CPFLOW: A Practical Tool for Tracing Power System Steady-State Stationary Behaviour Due to Load and Generation Variations”, IEEE Transactions on Power Systems, Vol. 10, No. 2, May 1995.
- [12] IEEE Reliability Test System, A report prepared by the Reliability Test System Task Force of the Applications of Probability Methods Subcommittee, IEEE Trans. on Power Apparatus and Systems, vol. PAS-98, pp. 2047-2054, Nov.-Dec. 1979.
- [13] Jitendra Kumar and Ashwani Kumar, “ACPTDF for Multi-transactions and ATC Determination in Deregulated Markets”, International Journal of Electrical and Computer Engineering (IJECE), Vol.1, No.1, September 2011, pp. 71~84, ISSN: 2088-8708.
- [14] Fernando L. Alvarado, “Solving Power Flow Problems with a Matlab Implementation of the Power System Applications Data Dictionary”, Proceedings of the 32nd Hawaii International Conference on System Sciences – 1999.

Emailing System as the basis for making automation of email System

Manumeet Mukund¹, Rana Majumdar²

¹Final Year Student (M.Tech.), Computer Science and Engineering, Amity University, UP, India

²Asst. Prof., IT Department, Amity University, UP, India

Abstract: This thesis presents an analysis of a capability to employ email System as the basis for making automation of email System. My project covers all the aspects of the related database technologies, such as JSP with SQL Server 2000 architecture to help determine how enterprises can implement this approach in the real insecure world, with commercial off-the-self products, to meet their needs. There were many concerns about using the JSP and servlets with SQL Server 2000 as the basis for using records of database, due to a trusted environment. By using appropriate trusted parts, when really necessary, and new technologies, we can find secure solutions for creating, storing and disseminating records.

The potential benefits of automating the service of email System is extensive especially with regard to better utilization of time, efficiency, space and safety. Now, new advances in technology have brought a practical system within reach. This project discusses the potential benefits of email automation, the associated technology requirements, and cost/benefit trades.

In order to implement the above, products, such as JSP and SQL Server 2000, are used. These are not only available free, easily testable and commonly used, but they provide us with a great interoperability among almost all the GUI platforms. The implementation can also be done by using other competitive technologies or platforms or can even use similar or related commercial products.

I. INTRODUCTION

EMailing system is a web application, which can be developed by using various web technologies such as ASP.NET, VC++, PHP and JSP etc. Computer and communication technologies have brought revolutionary changes in the information acquisition, processing, storage, retrieval and propagation. Keeping in view of the latest trend in Information Technologies (IT), I have developed windows-based software called EMailing system, which provides the total solutions for Intranet communication. EMailing system is designed using Client-Server Architecture, which imparts extra strength to storage capacity, multiple accesses to single database, backup and restore facilities. This software has been designed after a comprehensive study of different related functions practiced by several mail servers. The user-friendly GUI software is quiet easy to work with.

EMailing system is a mail tracing utility. It can receive mails from mail account and can send mail to other mail users. It can handle received mail efficiently with tracking each mail, its recipients and messages. It also has reporting of these mails. Mail accounts can be added and removed very easily and has many more features. It can also edit, modify, erase or view any user's mail account or can assign any user any authenticity or can change the preference of mails to and from users.

II. FIGURES AND TABLES

DFDs

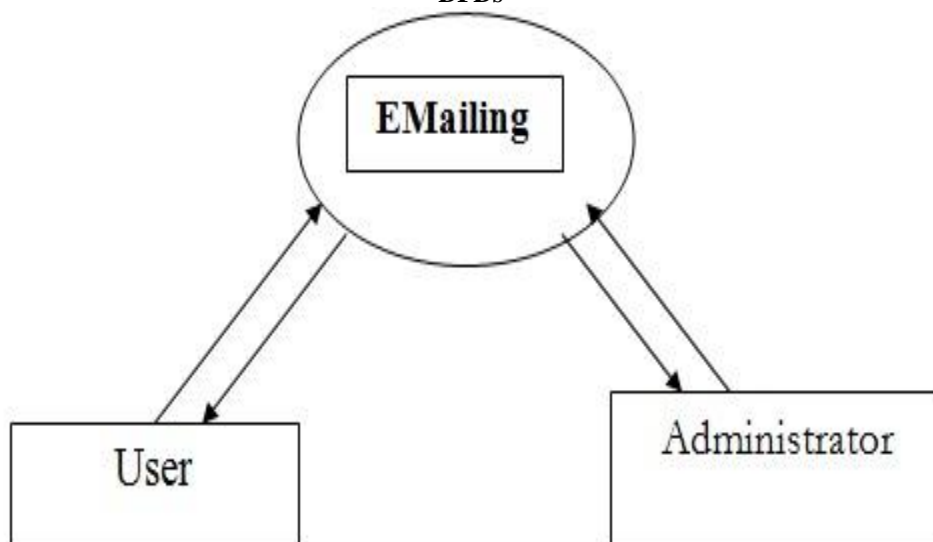


Fig (1): Physical Context Diagram for EMailing System:

Note: The Administrator is only a conceptual part of the system. The system is fully automated in itself.

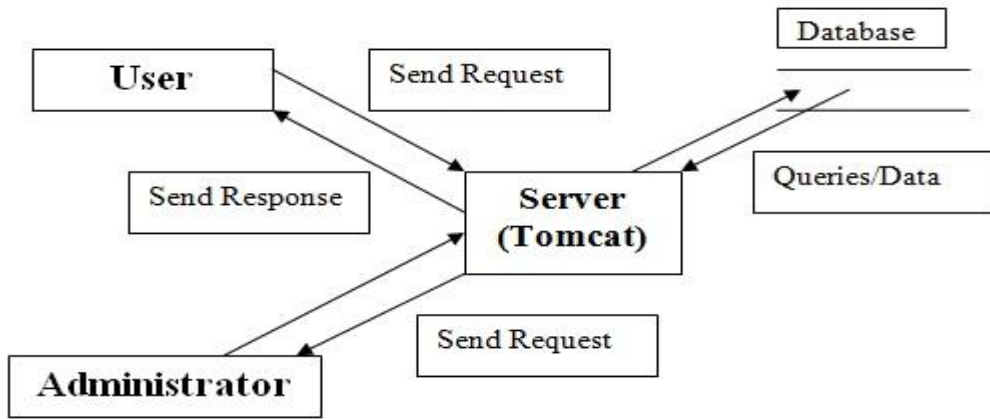


Fig (2): First Level Logical Diagram for Emailing System:

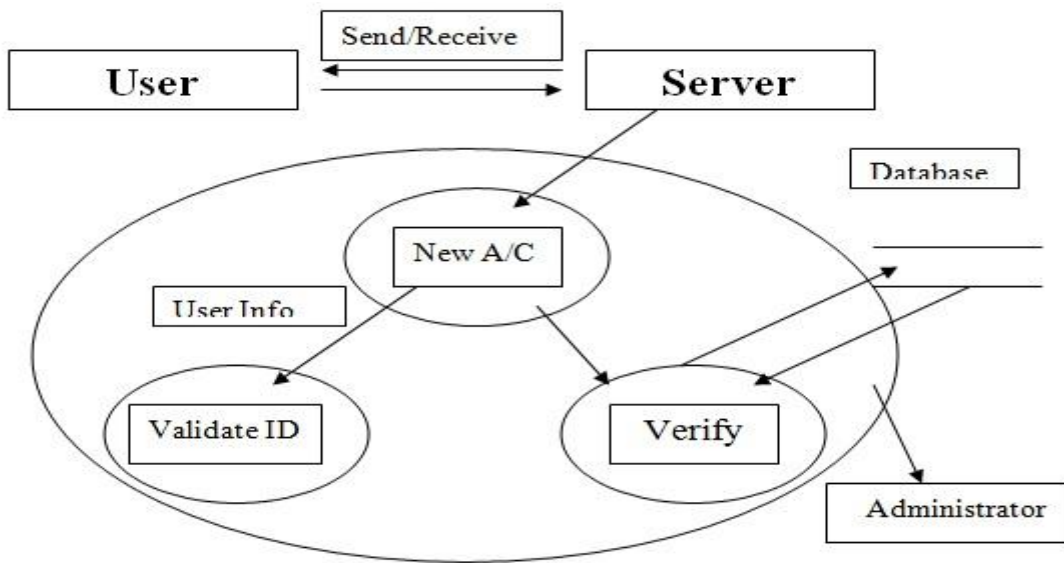


Fig (3): Second Level Logical Diagram for Emailing System

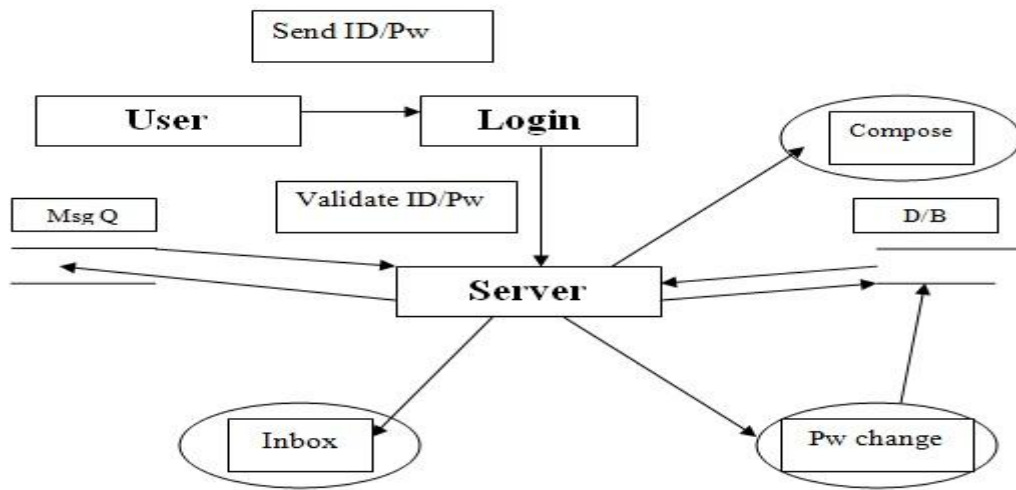


Fig (4): Third Level Logical Diagram for Emailing System:

Mail table

Field name	Data type
uid	varchar(20)
mdate	datetime
msub	varchar(50)
msize	numeric
mailin	varchar(1000)
mailout	varchar(1000)

User

Field name	Data type
uid	varchar(20)
pass	varchar(20)
seq	varchar(100)
ans	varchar(100)
occu	varchar(50)

III. CONCLUSION

The EMail system is developed on the top of SQL Server 2000 RDBMS using Integrated Development Environment provided by Java. It is Windows based software, which provides multiprogramming and multi-tasking environment. Thus EMail system is using built in security and recovery feature of SQL Server 2000 RDBMS. Also since the 'EMail system' is developed using Java (JSP) and therefore it has used event driven and modular programming style. Thus it facilitates for extendibility i.e. activities for new establishment can be easily added without affecting the main program with less effort and cost. An email System capable of delivering on the promises outlined above would necessarily have to be sophisticated and presumably involve substantial electronics, computers, and software. But, EMail system is a very time critical function. We certainly aren't going to deploy a new system that we couldn't prove is more accurate and timely than the existing system. At the same time, cost is going to be a major factor.

To explore this issue, let's examine some other transportation systems. The elevator was first automated in approximately 1940. Because elevators are mechanically guided except for one degree of freedom and other simplifying circumstances, automation could be accomplished without electronics, much less computers. Train automation is somewhat more difficult but also involves mechanical guidance. Mechanically guided email Systems have actually been proposed but would be much too limited.

Keep in mind that the potential benefits of EMail system are large. The savings in time, cost, efficiency, promptness, and reduced manpower burden, man-to-man enquiry will justify rather large development and deployment costs.

EMail system is "network enabled" to connect to any other service center of the same company and "web enabled" to enable the customers to get the status of their mails from any part of the world.

IV. ACKNOWLEDGEMENT

With profound sense of gratitude and regard, I convey my sincere thanks to my guide and mentor, for their valuable guidance and the confidence they instilled in me, that helped me in successful completion of the project report.

This acknowledgement would be incomplete without thanking the college faculty, who helped me in all possible ways with their wholehearted co-operation.

Last but not the least I am ever grateful to my friends for their help and support in completing my project

REFERENCES

Books

- [1] Ram Krishnamurthy, Java Programming
- [2] Wrox Publication, Professional Java Server Programming
- [3] Hans Bergstein, Java Server Pages
- [4] SAMS Publication, JSP in 21 days

Jatau Isaac Katuka,¹ Yahaya Shagaiya Daniel,² Bako Sunday Samuel³
^{1,2,3} Department of Mathematical Sciences, Kaduna State University, Nigeria.

Abstract: The transmission control protocol (TCP) is the most predominant transport layer protocol in the Internet today. It transports more than 90% percent of the traffic on the Internet. Its reliability, end-to-end congestion control mechanism, byte-stream transport mechanism, and, above all, its elegant and simple design have not only contributed to the success of the Internet, but also have made TCP an influencing protocol in the design of many of the other protocols and applications. Its adaptability to the congestion in the network has been an important feature leading to graceful degradation of the services offered by the network at times of extreme congestion. TCP in its traditional form was designed and optimized only for wired networks. This protocol is mainly known because of its feature of providing reliable delivery of packets from source to destination. In TCP, reliability is achieved by retransmitting lost packets. Since TCP is widely used today and the efficient integration of mobile adhoc networks (MANETs) with the Internet is paramount wherever possible, it is essential to have mechanisms that can improve TCP's performance in MANETs. In this paper, we describe the challenges of standard TCP in MANETs. We also proposed some techniques to improve TCP performance, advantages and disadvantages of the proposed techniques.

Keyword: Mobile Adhoc Networks (MANETs), Mobility, TCP Feedback, Medium Access Control (MAC), Transmission Control Protocol (TCP), Wireless Networks.

I. Introduction

The wireless arena has been experiencing exponential growth. We have seen great advances in network infrastructures growing availability of wireless applications, and the emergence of omnipresent wireless devices such as portable or handheld computers, Personal Digital Assistant (PDA), and all cell phones, all getting more powerful in their capabilities. These devices are now playing an ever-increasing important role in our lives. To mention only a few examples, mobile users can rely on their cellular phones to check e-mail and browse the internet; travellers with portable computers can surf the internet from airports, railway stations, cafes, and other public locations; tourists can use GPS terminals installed inside rental cars to view driving maps and locate tourist attraction; and at home, a family can synchronize data and transfer files between portable devices and desktops. Wireless internetworks are inevitable in future. Wireless links have high bit error rate, high latencies, and low bandwidth as compared to a wired link. The bit error is high because of its vulnerability to interference by Gaussian and stray noise and signals. TCP on wireless triggers congestion avoidance mechanisms, wherein the congestion window is reduced exponentially, thereby reducing the effective window size. The exponential decrease is to avoid further packet loss at the router. TCP is a reliable, end-to-end, connection-oriented transport layer protocol that provides a byte-stream-based service [the stream of bytes from the application layer is split into TCP segments, the length of each segment limited by a maximum segment size (MSS)]. The major responsibilities of TCP include congestion control, flow control, in-order delivery of packets, and reliable transportation of packets. Congestion control deals with excess traffic in the network which may lead to degradation in the performance of the network, whereas flow control controls the per-flow traffic such that the receiver capacity is not exceeded. TCP regulates the number of packets sent to the network by expanding and shrinking the congestion window. The TCP sender starts the session with a congestion window value of one MSS. It sends out one MSS and waits for the ACK. Once the ACK is received within the retransmission timeout (RTO) period, the congestion window is doubled and two MSSs are originated. This doubling of the congestion window with every successful acknowledgment of all the segments in the current congestion window, is called *slow-start* (a more appropriate name would be *exponential start*, as it actually grows exponentially) and it continues until the congestion window reaches the *slow-start threshold*. This linear growth, which continues until the congestion window reaches the receiver window (which is advertised by the TCP receiver and carries the information about the receiver's buffer size), is called *congestion avoidance*, as it tries to avoid increasing the congestion window exponentially, which will surely worsen the congestion in the network. TCP updates the RTO period with the current round-trip delay calculated on the arrival of every ACK packet. If the ACK packet does not arrive within the RTO period, then it assumes that the packet is lost. TCP assumes that the packet loss is due to the congestion in the network and it invokes the congestion control mechanism. The TCP sender reduces the slow-start threshold to half the current congestion window or two MSSs whichever is larger, resets the congestion window size to one MSS, activates the slow-start algorithm, and resets the RTO with an exponential back-off value which doubles with every subsequent retransmission. The slow-start process further doubles the congestion window with every successfully acknowledged window and, upon reaching the slow-start threshold, it enters into the congestion avoidance phase. The TCP sender also assumes a packet loss if it receives three consecutive duplicate ACKs (DUPACKs). Upon reception of three DUPACKs, the TCP sender retransmits the oldest unacknowledged segment. This is called the *fast retransmit* scheme. When the TCP receiver receives out-of-order packets, it generates DUPACKs to indicate to the TCP sender about the sequence number of the last in-order segment received successfully.

II. MANETs Application

Because MANETs are flexible networks that can be setup anywhere at any time without infrastructure, including pre-configuration or administration, people have come to realize the commercial potential and advantages that MANETs can bring. Historically, MANETs have primarily been used for tactical network-related applications to improve battle field communications and survivability. The dynamic nature of military operations means it is not possible to rely on access to a fixed preplaced communication infrastructure on the battle field. Pure wireless communication also has the limitation that radio signals are subject to interference and radio frequencies higher than 100MHz rarely propagate beyond Line of Sight (LOS). MANETs creates a suitable framework to address these issues, provides a mobile wireless distributed multihop wireless network without preplaced infrastructure, and provide connectivity beyond LOS. Although early MANETs applications and deployments were military oriented, non-military applications have grown substantially since then and have become the main focus of today. The introduction of technologies such as Bluetooth [8], IEEE 802.11[12], and Hyperlan[10] greatly facilitate the deployment of adhoc technology outside the military domain.

Applications	Description/Services
Tactical Networks	Military communication, operations Automated Battle fields
Sensor Networks	Collection of embedded sensor devices used to collect real-time data to automate everyday functions. Data highly correlated in time and space, e.g. remote sensors for weather, earth activities etc.
Emergency services	Search-and-rescue operations as well as disaster recovery e.g. early retrieval and transmission of patient data from/to the hospital
Commercial environments	E-Commerce e.g. electronic payments from anywhere
Home and enterprise networking	Home/office wireless networking (WLAN) e.g. shared whiteboard application, use PDA to print anywhere etc.
Educational applications	Setup virtual classrooms or conference rooms, setup adhoc communication during conferences, meetings, or lectures
Entertainment	Multiuser games, robotic pets, etc.
Location-aware services	Follow-on services, e.g. automatic call forwarding, transmission of the actual workspace to the current location.

Table 1. Mobile Adhoc Network Applications

III. TCP's challenges in MANETs

The performance of *TCP* degrades in MANETs, because *TCP* has to face challenges due to several reasons. Most of the progress made in *TCP* is centered on error recovery and congestion control. Representative innovations include fast transmissions and recovery[3], selective acknowledgements[6], random early detection(RED, [5]) in routers, and explicit congestion notification (ECN, [4]). *TCP* assumes that network congestion has happened whenever a packet is lost. It then invokes appropriate congestion control actions including window size reduction. Although this assumption is reasonable for wired networks, it is questionable for wireless networks especially MANETs. Below are the challenges faced when deploying *TCP* over MANETs?

1.1 Media Access Control (MAC)

In MANETs, use of broadcasting and shared transmission media introduces a non-negligible probability of packet collisions and media contention. In addition, with half-duplex radio collision detection is not possible, which severely reduces channel utilization as well as throughput, and brings new challenges to conventional CSMA/CD-based and MAC protocols in general. Among the top issues are hidden-terminal and exposed-terminal problems. The hidden-terminal problem occurs when two or more terminals, say A and B cannot detect each other's transmissions due to being outside of each other transmission range but their transmission ranges are not disjoint. A collision may occur when terminal A and B start transmitting towards the same receiver, terminal C as shown in fig.1 below. The exposed-terminal problem results from situations in which a permissible transmission from mobile station (sender) to another station has to be delayed due to the irrelevant transmission range. Fig. 1 below depicts a typical scenario in which the exposed-terminal problem may occur. It is worth noting that hidden-terminal and exposed-terminal problems are correlated with the transmission range. By increasing the transmission range, the hidden-terminal problem occurs less frequently. On the other hand, the exposed-terminal problem becomes more important as the transmission range identifies the area affected by a single transmission.

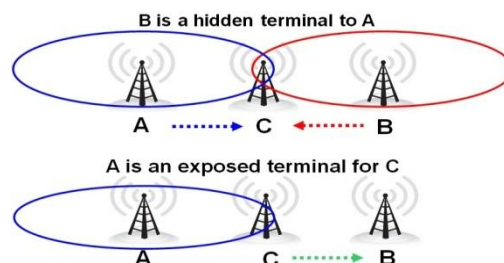


Fig. 1. Hidden-terminal and Exposed-terminal Problems

- 1.2 Power Constraint:** Because batteries carried by each mobile node have limited power, processing power is limited, which in turn limits services and applications that can be supported by each node. This becomes a bigger issue in MANETs because each node is acting as both an end system and a router at the same time, additional energy is required to forward packets from other nodes. *TCP* must use this scarce energy resource in an efficient manner by minimizing the number of unnecessary transmissions at the transport layer as well as at the link layer.
- 1.3 Mobility:** MANETs experience dynamic changes in network topology because of the unrestricted mobility of the nodes in the network. The topology changes lead to frequent changes in the connectivity of wireless links and hence the route to a particular destination may need to be recomputed very often. The responsibility of finding a route and reestablishing it once it gets broken is attached to the network layer. Once a path is broken, the routing protocol initiates a route reestablishment process. This route reestablishment process takes a significant amount of time to obtain a new route to the destination. The route reestablishment time is a function of the number of nodes in the network, transmission ranges of nodes, current topology of the network, bandwidth of the channel, traffic load in the network, and the nature of the routing protocol. If the route reestablishment time is greater than the *RTO* period of the *TCP* sender, then the *TCP* sender assumes congestion in the network, retransmits the lost packets, and initiates the congestion control algorithm. These retransmissions can lead to wastage of bandwidth and battery power. Eventually, when a new route is found, the *TCP* throughput continues to be low for some time, as it has to build up the congestion window since the traditional *TCP* undergoes a slow start.
- 1.4 Multipath Fading:** It is found that the *TCP* throughput degrades rapidly with an increase in path length in string (linear chain) topology MANETs. The possibility of a path break increases with path length. Given that the probability of a link break is p_l , the probability of a path break (p_b) for a path of length k can be obtained as $P_b = 1 - (1 - p_l)^k$. Hence as the path length increases, the probability of a path break increases, resulting in the degradation of the throughput in the network. However, it is doubted by some researcher[15] whether IEEE 802.11 works well in multi-hop adhoc networks, particularly when *TCP* is used as the transport layer protocol. Existing research work [7] has shown that *TCP* performance decreases drastically as the hop count becomes bigger and bigger.
- 1.5 Misinterpretation of congestion window:** *TCP* considers the congestion window as a measure of the rate of transmission that is acceptable to the network and the receiver. In MANETs, the congestion control mechanism are invoked when the network gets partitioned or when a path break occurs. This reduces the congestion window and increases the *RTO* period. When the route is reconfigured, the congestion window may not reflect the transmission rate acceptable to the new route, as the new route may actually accept a much higher transmission rate. Hence, when there are frequent path breaks, the congestion window may not reflect the maximum transmission rate acceptable to the network and the receiver.
- 1.6 Asymmetric link behavior:** The wireless link between a base station and a mobile terminal is asymmetric in nature. Compared with the base station, the mobile terminal has a limited power, processing capability, and buffer space. Asymmetry may manifest in several forms like bandwidth, loss rate asymmetry, and route asymmetry. The radio channel used in MANETs has different properties such as location-dependent contention, environmental effects on propagation, and directional properties leading to asymmetric links. The directional links can result in delivery of a packet to a node, but failure in the delivery of the acknowledgment back to the sender. It is possible for a bidirectional link to become uni-directional for a while. This can also lead to *TCP* invoking the congestion control algorithm and several retransmissions. For example, in multi-rate IEEE 802.11 protocol versions, senders may use the Auto-Rate-Feedback (ARF) algorithm for transmission rates after selection [1].
- 1.7 Uni-directional path:** Standard *TCP* relies on end-to-end ACK for ensuring reliability. Since the ACK packet is very short compared to a data segment, ACKs consume much less bandwidth in wired networks. In MANETs, every *TCP* ACK packet requires *RTS-CTS-Data-ACK* exchange in case IEEE 802.11 is used as the underlying *MAC* protocol. This can lead to an additional overhead of more than 70 bytes if there are no retransmissions. This can lead to significant bandwidth consumption on the reverse path, which may or may not contend with the forward path. If the reverse path contends with the forward path, it can lead to the reduction in the throughput of the forward path. Some routing protocols select the forward path to be also used as the reverse path, whereas certain other routing protocols may use an entirely different or partially different path for the ACKs. A path break on an entirely different reverse path can affect the performance of the network as much as a path break in the forward path.
- 1.8 Multipath routing:** In wired networks, route failures occur rarely while in MANETs, they are frequent events. The main cause of route failures is node mobility since nodes can move arbitrarily. There exists a set of QoS routing and best-effort routing protocols that use multiple paths between a source-destination pair. There are several advantages in using multipath routing. Some of these advantages include the reduction in route computing time, the high resilience to path breaks, high call acceptance ratio, and better security. For *TCP*, these advantages may add to throughput degradation. These can lead to a significant amount of out-of-order packets, which in turn generates a set of duplicate acknowledgments (DUPACKs) which cause additional power consumption and invocation of congestion control. In

[2], Lundgren et al. have conducted experiments and have subsequently conducted that the origin of this problem is heterogeneous transmission rates, the absence of an acknowledgment for broadcast packets, small packet size of Hello messages, and fluctuations of wireless links.

1.9 Network partitioning and remerging: The randomly moving nodes in MANETs can lead to network partitions. As long as the *TCP* sender, the *TCP* receiver, and all the intermediate nodes in the path between the *TCP* sender and the *TCP* receiver remain in the same partition, the *TCP* connection will remain intact. It is likely that the sender and receiver of the *TCP* session will remain in different partitions and, in certain cases, that only the intermediate nodes are affected by the network partitioning.

1.10 The use of sliding-window-based transmission: *TCP* uses a sliding window for flow control. The transmission of packets is decided by the size of the window, and when the ACKs arrive from a destination, further packets are transmitted. This avoids the use of individual fine-grained timers for transmission of each *TCP* flow. Such a design is preferred in order to improve scalability of the protocol in high-bandwidth networks such as the Internet where millions of *TCP* connections may be established with some heavily loaded servers. The use of a sliding window can also contribute to degraded performance in bandwidth-constrained MANETs where the *MAC* layer protocol may not exhibit short-term and long-term fairness. For example, the popular *MAC* protocols such as *CSMA/CA* protocol show short-term unfairness, where a node that has captured the channel has a higher probability of capturing the channel again. This unfairness can lead to a number of *TCP* ACK packets being delivered to the *TCP* sender in succession, leading to a burstiness in traffic due to the subsequent transmission of *TCP* segments.

IV. Proposed Methods to Improve *TCP* over MANETs

The quest to overcome the drawback of *TCP* over MANETs cannot be over emphasized. Lots of research has been done to improve the performance of *TCP* over MANETs and subsequently lots of approaches have been proposed. We categorically classify these approaches as follows:

1.11 TCP Feedback: *TCP Feedback (TCP-F)* [9] proposes modifications to the traditional *TCP* for improving performance in MANETs. It uses a feedback-based approach. *TCP-F* requires the support of a reliable link layer and a routing protocol that can provide feedback to the *TCP* sender about the path breaks. The routing protocol is expected to repair the broken path within a reasonable time period. *TCP-F* aims to minimize the throughput degradation resulting from the frequent path breaks that occur in MANETs. During a *TCP* session, there could be several path breaks resulting in considerable packet loss and path reestablishment delay. Upon detection of packet loss, the sender in a *TCP* session invokes the congestion control algorithm leading to the exponential back-off of retransmission timers and a decrease in congestion window size. This was discussed earlier in this chapter. In *TCP-F*, an intermediate node, upon detection of a path break, originates a route failure notification (*RFN*) packet. This *RFN* packet is routed toward the sender of the *TCP* session. The *TCP* sender's information is expected to be obtained from the *TCP* packets being forwarded by the node. The intermediate node that originates the *RFN* packet is called the failure point (*FP*). The *FP* maintains information about all the *RFNs* it has originated so far. Every intermediate node that forwards the *RFN* packet understands the route failure, updates its routing table accordingly, and avoids forwarding any more packets on that route. If any of the intermediate nodes that receive *RFN* has an alternate route to the same destination, then it discards the *RFN* packet and uses the alternate path for forwarding further data packets, thus reducing the control overhead involved in the route reconfiguration process. Otherwise, it forwards the *RFN* toward the source node. When a *TCP* sender receives an *RFN* packet, it goes into a state called *snooze*. In the *snooze* state, a sender stops sending any more packets to the destination, cancels all the timers, freezes its congestion window, freezes the retransmission timer, and sets up a route failure timer. This route failure timer is dependent on the routing protocol, network size, and the network dynamics and is to be taken as the worst-case route reconfiguration time. When the route failure timer expires, the *TCP* sender changes from the *snooze* state to the *connected* state. As soon as a node receives an *RRN* packet, it transmits all the packets in its buffer, assuming that the network is back to its original state. This can also take care of all the packets that were not acknowledged or lost during transit due to the path break. In fact, such a step avoids going through the slow-start process that would otherwise have occurred immediately after a period of congestion. The route failure timer set after receiving the *RFN* packet ensures that the sender does not remain in the *snooze* state indefinitely. Once the route failure timer expires, the sender goes back to the *connected* state in which it reactivates the frozen timers and starts sending the buffered and unacknowledged packets. This can also take care of the loss of the *RRN* packet due to any possible subsequent congestion. *TCP-F* permits the *TCP* congestion control algorithm to be in effect when the sender is not in the *snooze* state, thus making it sensitive to congestion in the network.

Advantages and Disadvantages

TCP-F provides a simple feedback-based solution to minimize the problems arising out of frequent path breaks in MANETs. At the same time, it also permits the *TCP* congestion control mechanism to respond to congestion in the network. *TCP-F* depends on the intermediate nodes' ability to detect route failures and the routing protocols' capability to reestablish a broken path within a reasonably short duration. Also, the *FP* should be able to obtain the correct path (the path

which the packet traversed) to the TCP-F sender for sending the RFN packet. This is simple with a routing protocol that uses source routing [*i.e.*, dynamic source routing (DSR)]. If a route to the sender is not available at the FP, then additional control packets may need to be generated for routing the RFN packet. TCP-F has an additional state compared to the traditional TCP state machine, and hence its implementation requires modifications to the existing TCP libraries. Another disadvantage of TCP-F is that the congestion window used after a new route is obtained may not reflect the achievable transmission rate acceptable to the network and the TCP-F receiver.

4.2 TCP with Explicit Link Failure Notification

Holland and Vaidya proposed the use of *TCP* with explicit link failure notification (TCP-ELFN) [11] for improving *TCP* performance in ad hoc wireless networks. This is similar to *TCP-F*, except for the handling of explicit link failure notification (ELFN) and the use of *TCP* probe packets for detecting the route reestablishment. The *ELFN* is originated by the node detecting a path break upon detection of a link failure to the *TCP* sender. This can be implemented in two ways: (i) by sending an ICMP destination unreachable (DUR) message to the sender, or (ii) by piggy-backing this information on the RouteError message that is sent to the sender. Once the *TCP* sender receives the *ELFN* packet, it disables its retransmission timers and enters a standby state. In this state, it periodically originates probe packets to see if a new route is reestablished. Upon reception of an ACK by the *TCP* receiver for the probe packets, it leaves the standby state, restores the retransmission timers, and continues to function as normal.

Advantages and Disadvantages

TCP-ELFN improves the *TCP* performance by decoupling the path break information from the congestion information by the use of *ELFN*. It is less dependent on the routing protocol and requires only link failure notification about the path break. The disadvantages of TCP-ELFN include the following: (i) when the network is temporarily partitioned, the path failure may last longer and this can lead to the origination of periodic probe packets consuming bandwidth and power and (ii) the congestion window used after a new route is obtained may not reflect the achievable transmission rate acceptable to the network and the *TCP* receiver.

4.3 TCP-Bus: *TCP* with buffering capability and sequence information (*TCP-Bus*) is similar to the *TCP-F* and *TCP-ELFN* in its use of feedback information from an intermediate node on detection of a path break. But *TCP-Bus* is more dependent on the routing protocol compared to *TCP-F* and *TCP-ELFN*. *TCP-Bus* was proposed, with associativity-based routing (*ABR*) [11] protocol as the routing scheme. Hence, it makes use of some of the special messages such as localized query (*LQ*) and *REPLY*, defined as part of *ABR* for finding a partial path. These messages are modified to carry *TCP* connection and segment information. Upon detection of a path break, an upstream intermediate node [called pivot node (*PN*)] originates an explicit route disconnection notification (*ERDN*) message. This *ERDN* packet is propagated to the *TCP-Bus* sender and, upon reception of it, the *TCP-Bus* sender stops transmission and freezes all timers and windows as in *TCP-F*. The packets in transit at the intermediate nodes from the *TCP-Bus* sender to the *PN* are buffered until a new partial path from the *PN* to the *TCP-Bus* receiver is obtained by the *PN*. In order to avoid unnecessary retransmissions, the timers for the buffered packets at the *TCP-Bus* sender and at the intermediate nodes up to *PN* use timeout values proportional to the round-trip time (*RTT*). The intermediate nodes between the *TCP-Bus* sender and the *PN* can request the *TCP-Bus* sender to selectively retransmit any of the lost packets. Upon detection of a path break, the downstream node originates a route notification (*RN*) packet to the *TCP-Bus* receiver, which is forwarded by all the downstream nodes in the path. An intermediate node that receives an *RN* packet discards all packets belonging to that flow. The *ERDN* packet is propagated to the *TCP-Bus* sender in a reliable way by using an implicit acknowledgment and retransmission mechanism. The *PN* includes the sequence number of the *TCP* segment belonging to the flow that is currently at the head of its queue in the *ERDN* packet. The *PN* also attempts to find a new partial route to the *TCP-Bus* receiver, and the availability of such a partial path to destination is intimated to the *TCP-Bus* sender through an explicit route successful notification (*ERSN*) packet. *TCP-Bus* utilizes the route reconfiguration mechanism of *ABR* to obtain the partial route to the destination. Due to this, other routing protocols may require changes to support *TCP-Bus*. The *LQ* and *REPLY* messages are modified to carry *TCP* segment information, including the last successfully received segment at the destination. The *LQ* packet carries the sequence number of the segment at the head of the queue buffered at the *PN* and the *REPLY* carries the sequence number of the last successful segment the *TCP-Bus* receiver received. This enables the *TCP-Bus* receiver to understand the packets lost in transition and those buffered at the intermediate nodes. This is used to avoid fast retransmission requests usually generated by the *TCP-Bus* receiver when it notices an out-of-order packet delivery. Upon a successful *LQ-REPLY* process to obtain a new route to the *TCP-Bus* receiver, *PN* informs the *TCP-Bus* sender of the new partial path using the *ERSN* packet. When the *TCP-Bus* sender receives an *ERSN* packet, it resumes the data transmission. Since there is a chance for *ERSN* packet loss due to congestion in the network, it needs to be sent reliably. The *TCP-Bus* sender also periodically originates probe packets to check the availability of a path to the destination.

Advantages and Disadvantages

The advantages of *TCP-Bus* include performance improvement and avoidance of fast retransmission due to the use of buffering, sequence numbering, and selective acknowledgment. *TCP-Bus* also takes advantage of the underlying routing protocols, especially the on-demand routing protocols such as *ABR*. The disadvantages of *TCP-Bus* include the

increased dependency on the routing protocol and the buffering at the intermediate nodes. The failure of intermediate nodes that buffer the packets may lead to loss of packets and performance degradation. The dependency of *TCP-Bus* on the routing protocol may degrade its performance with other routing protocols that do not have similar control messages as in *ABR*.

4.4 Ad Hoc TCP: Similar to *TCP-F* and *TCP-ELFN*, ad hoc *TCP (ATCP)* [14] also uses a network layer feedback mechanism to make the *TCP* sender aware of the status of the network path over which the *TCP* packets are propagated. Based on the feedback information received from the intermediate nodes, the *TCP* sender changes its state to the persist state, congestion control state, or the retransmit state. When an intermediate node finds that the network is partitioned, then the *TCP* sender state is changed to the persist state where it avoids unnecessary retransmissions. When *ATCP* puts *TCP* in the persist state, it sets *TCP*'s congestion window size to one in order to ensure that *TCP* does not continue using the old congestion window value. This forces *TCP* to probe the correct value of the congestion window to be used for the new route. If an intermediate node loses a packet due to error, then the *ATCP* at the *TCP* sender immediately retransmits it without invoking the congestion control algorithm. In order to be compatible with widely deployed *TCP*-based networks, *ATCP* provides this feature without modifying the traditional *TCP*. *ATCP* is implemented as a thin layer residing between the *IP* and *TCP* protocols. The *ATCP* layer essentially makes use of the explicit congestion notification (*ECN*) for maintenance of the states. In summary, *ATCP* tries to perform the activities listed in Table 2.

Event	Action
Packet loss due to high <i>BER</i>	Retransmits the lost packets without reducing congestion window
Route recomputation delay	Makes the <i>TCP</i> sender go to persist state and stop transmission until new route has been found
Transient partitions	Makes the <i>TCP</i> sender go to persist state and stop transmission until new route has been found
Out-of-order packet delivery due to multipath routing	Maintains <i>TCP</i> sender unaware of this and retransmits the packets from <i>TCP</i> buffer
Change in route	Recomputes the congestion window

Table 2. The actions taken by *ATCP*

Advantages and Disadvantages

Two major advantages of *ATCP* are (i) it maintains the end-to-end semantics of *TCP* and (ii) it is compatible with traditional *TCP*. These advantages permit *ATCP* to work seamlessly with the Internet. In addition, *ATCP* provides a feasible and efficient solution to improve throughput of *TCP* in MANETs. The disadvantages of *ATCP* include (i) the dependency on the network layer protocol to detect the route changes and partitions, which not all routing protocols may implement and (ii) the addition of a thin *ATCP* layer to the *TCP/IP* protocol stack that requires changes in the interface functions currently being used.

4.5 Split TCP: One of the major issues that affects the performance of *TCP* over MANETs is the degradation of throughput with increasing path length, as discussed early in this chapter. The short connections generally obtain much higher throughput than long connections. This can also lead to unfairness among *TCP* sessions, where one session may obtain much higher throughput than other sessions. This unfairness problem is further worsened by the use of *MAC* protocols such as *IEEE 802.11*, which are found to give a higher throughput for certain link-level sessions, leading to an effect known as *channel capture* effect. This effect leads to certain flows capturing the channel for longer time durations, thereby reducing throughput for other flows. The channel capture effect can also lead to low overall system throughput. *Split-TCP* [16] provides a unique solution to this problem by splitting the transport layer objectives into congestion control and end-to-end reliability. The congestion control is mostly a local phenomenon due to the result of high contention and high traffic load in a local region. In the MANET environment, this demands local solutions. At the same time, reliability is an end-to-end requirement and needs end-to-end acknowledgments. In addition to splitting the congestion control and reliability objectives, *split-TCP* splits a long *TCP* connection into a set of short concatenated *TCP* connections (called segments or zones) with a number of selected intermediate nodes (known as proxy nodes) as terminating points of these short connections

Advantages and Disadvantages

Split-TCP has the following advantages: (i) improved throughput, (ii) improved throughput fairness, and (iii) lessened impact of mobility. Throughput improvement is due to the reduction in the effective transmission path length (number of hops in a zone or a path segment). *TCP* throughput degrades with increasing path length. *Split-TCP* has shorter concatenated path segments, each operating at its own transmission rate, and hence the throughput is increased. This also leads to improved throughput fairness in the system. Since in *split-TCP*, the path segment length can be shorter than the end-to-end path length, the effect of mobility on throughput is lessened. The disadvantages of *split-TCP* can be listed as

follows: (i) It requires modifications to *TCP* protocol, (ii) the end-to-end connection handling of traditional *TCP* is violated, and (iii) the failure of proxy nodes can lead to throughput degradation. The traditional *TCP* has end-to-end semantics, where the intermediate nodes do not process *TCP* packets, whereas in split-*TCP*, the intermediate nodes need to process the *TCP* packets and hence, in addition to the loss of end-to-end semantics, certain security schemes that require *IP* payload encryption cannot be used. During frequent path breaks or during frequent node failures, the performance of split-*TCP* may be affected.

V. Conclusion

TCP is a reliable transport protocol tuned to perform well in traditional networks made up of links with low bit-error rates. Networks with higher bit-error rates, such as those with wireless links and mobile hosts, violate many of the assumptions made by *TCP*, causing degraded end-to-end performance. In this paper, we describe several protocols that improve *TCP* performance in wireless networks. Table 3 illustrates comparison of the different proposed methods based on mechanisms used for increasing efficiency. Different approaches have been taken to tackle the problems, but the right changes is dependent on where the single or multiple modification needs to be done.

Issue	TCP-F	TCP-ELFN	TCP-BuS	ATCP	Split-TCP
Packet loss due to <i>BER</i> or collision	Same as <i>TCP</i>	Same as <i>TCP</i>	Same as <i>TCP</i>	Retransmits the lost packets without involving congestion control	Same as <i>TCP</i>
Path breaks	<i>RFN</i> is sent to the <i>TCP</i> sender and state changes to snooze	<i>ELFN</i> is sent to the <i>TCP</i> sender and state changes to standby	<i>ERDN</i> is sent to the <i>TCP</i> sender, state changes to snooze, <i>ICMPDUR</i> is sent to the <i>TCP</i> sender, and <i>ATCP</i> puts <i>TCP</i> into persist state	Same as <i>TCP</i>	Same as <i>TCP</i>
Out-of-order packets	Same as <i>TCP</i>	Same as <i>TCP</i>	Out-of-order packets reached after a path recovery are handled	<i>ATCP</i> reorders packets and hence <i>TCP</i> avoids sending duplicates	Same as <i>TCP</i>
Congestion	Same as <i>TCP</i>	Same as <i>TCP</i>	Explicit messages such as <i>ICMP</i> source quench are used	<i>ECN</i> is used to notify <i>TCP</i> sender. Congestion control is same as <i>TCP</i>	Since connection is split, the congestion control is handled within a zone by proxy nodes
Congestion window after path reestablishment	Same as before the path break	Same as before the path break	Same as before the path break	Recomputed for new route	Proxy nodes maintain congestion window and handle congestion
Explicit path break notification	Yes	Yes	Yes	Yes	No
Explicit path reestablishment notification	Yes	No	Yes	No	No
Dependency on routing protocol	Yes	Yes	Yes	Yes	No
End-to-end semantics	Yes	Yes	Yes	Yes	No
Packets buffered at intermediate nodes	No	No	Yes	No	Yes

Table 3. A comparison of *TCP* solutions for MANETs

References

- [1] A. Kerman and L. Monteban, "Wavelan 11: A High – Performance Wireless LAN for the Unlicensed Band," Bell Labs Tech. J. Summer 1997, pp 118-33.
- [2] H. Lungren, E. Nordstro, and C. Tschudin, "Coping with Communication Gray Zones in IEEE 802.11 b-Based Adhoc Networks," Proc. Acm Wksp. Wireless Mobile Multimedia, Atlanta, GA, USA, Sept. 2002, pp. 49-55.
- [3] W. Stevens, "TCP Slow Start, Congestion Avoidance, Fast Retransmit, and Fast Recovery Algorithms," RFC 2001, Jan. 1997.
- [4] K. Ramakrishnan, S. Floyd and D. Black, "The Addition of Explicit Congestion Notification to IP," RFC 3168, Sept. 2001.
- [5] S. Floyd, V. Jacobson, "Random Early Detection Gateways for Congestion Avoidance," IEEE/ACM Transaction on Networking, Vol 1, no. 4, Aug. 1993.
- [6] M. Mathis, J. Mahdavi, S. Floyd and A. Romanow, "TCP Selective Acknowledgment Options," RFC 2018, Oct. 1996.
- [7] M. Gerla, K. Tang, and R. Bagrodia, "TCP Performance in Wireless Multihop Networks," In Proceedings of IEEE WMCSA 1999.
- [8] "Bluetooth Special Interest Group," Web site: <http://www.bluetooth.com>
- [9] K. Chandran, S. Raghunathan, S. Venkatesan, and R. Prakash, "A Feedback Based Scheme for Improving TCP Performance in Adhoc Wireless Networks," IEEE Personal Communications, 8(1): 34-39, Feb. 2001.
- [10] "Broadband Radio Access Networks (BRAN): High Performance Local Area Network (HYPERLAN) Type 2," Tech. Rep. 101 683 V1.1.1, ETSI.
- [11] G. Holland, and N.H. Vaidya, "Analysis of TCP Performance Over Mobile Adhoc Networks," MOBICOM' 99, Seattle, Aug. 1999.
- [12] "IEEE 802.11 WLAN Standard," Web site: <http://standards.ieee.org/getieee802.11>
- [13] C. Toh, "Associativity-Based Routing for Adhoc Mobile Networks," J. Wireless Pers. Commun., Vol. 4, no. 2, Mar. 1992.
- [14] J. Lui, and S. Singh, "ATCP: TCP for Mobile Adhoc Networks," IEEE JSAC, Vol. 19. No. 7, pp. 1300-1315, Jul. 2001.
- [15] S. Xu, and T. Saadawi, "Does the IEEE 802.11 MAC Protocol Work Well in Multihop Wireless Adhoc Networks?," IEEE Communi. Magazine, pp. 130-137, June 2001.
- [16] S. Kopparty et al., "Split TCP for Mobile Adhoc Networks," Proc. IEEE GLOBECOM, Taiwan, Nov. 2002

Ray-tracing model and Monte Carlo simulation for the design of the concentrating solar simulator reflector

Marco Bortolini,¹ Mauro Gamberi,² Alessandro Graziani³
^{1,2,3}Department of Management and Engineering, University of Padova, Italy

Abstract: Solar simulators are common laboratory devices to artificially reproduce the Sun emission spectrum. Their use in optic tests allows to study the effect of the solar radiation on both materials and components. This paper focuses on the effective design of the ellipsoidal reflector for concentrating solar simulators. A ray-tracing analytic model integrated to Monte Carlo simulation is proposed as an effective approach to optimize the reflector geometric configuration and to maximize the target incident radiation level and flux distribution. The developed model reproduces the ray trajectories from the source to the target and it includes the physical and optic phenomena affecting the light rays, e.g. absorption, deviation, reflection, distortion, etc. A realistic case study for the effective design of the ellipsoidal reflector for a single source small scale simulator, integrating a commercial xenon short arc lamp, is proposed to both validate and apply the proposed approach. Several scenarios are tested and the main obtained evidences are summarized.

Keywords: Ellipsoid, Monte Carlo simulation, Ray-tracing, Reflector surface, Solar simulator.

I. INTRODUCTION

Solar simulators provide a luminous flux approximating natural sunlight spectrum. Their basic structure includes a metal support frame, a light source, e.g. high flux arc lamp with power supplier, igniter and electronic load, and a reflective surface to properly orient the emitted rays lighting the target area. The reflector shape allows the system to generate a concentrated or non-concentrated light beam through an ellipsoidal or parabolic reflector. Fig. 1 shows a 3D scheme of a concentrating solar simulator, highlighting its functional modules.

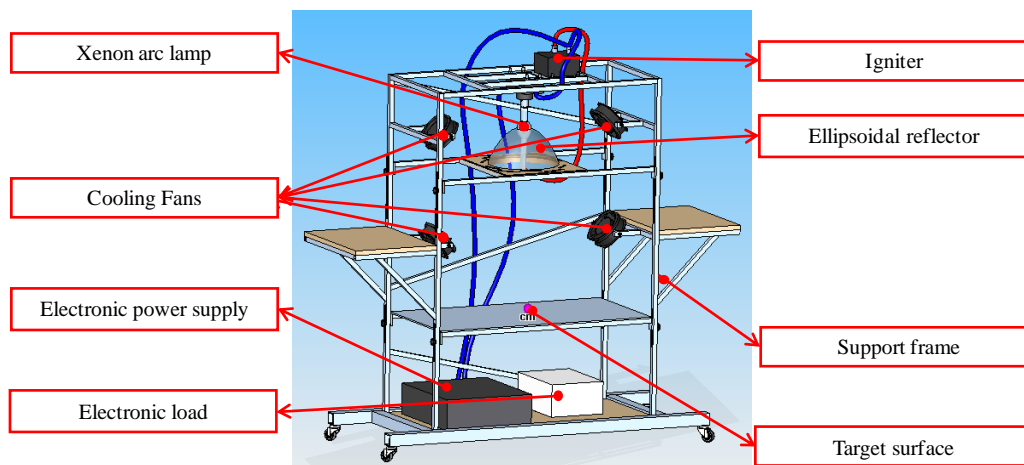


Figure 1: Single Source Solar Simulator, Functional Modules.

The relevance of such systems, in laboratory tests and analyses, is frequently discussed by the recent literature presenting several applications for a wide set of research fields. Petrash et al. [1] both review the topic and describe a 11000 suns high-flux solar simulator. Domínguez et al. [2, 3], Pravettoni et al. [4], Rehn and Hartwig [5], Hussain et al. [6] and Meng et al. [7] present different studies about the design and development of high flux solar simulators applied to both concentrating and non-concentrating photovoltaic systems.

Amoh [8] and Meng et al. [9] describe the design of solar simulators to test multi-junction solar cells for terrestrial and space applications. Kreuger et al. [10] develop a 45kW solar simulator for high-temperature solar thermal and thermo-chemical researches, while Codd et al. [11] present a low cost high flux simulator to study the optical melting and light absorption behavior of molten salts. All contributions focus on the relevance of the proper design of the system to achieve high performances in both flux intensity and uniformity on the target area. The mirror reflective surface represents a crucial component to gain these purposes. An accurate shape design and simulation of the physical and optic properties is essential before the simulator construction [12].

Ray-tracing algorithms are recognized as effective approaches to test the performances of different configurations of the reflective surface [1, 13-15].

This paper presents a ray-tracing model integrated to a Monte Carlo simulation to effectively design the ellipsoidal reflector of a single source concentrating solar simulator. The proposed model analytically reproduces the ray trajectories

from the source to the target and it includes the physical and optic phenomena and the distortions affecting the light rays. Furthermore, the ray-tracing model integration to the Monte Carlo simulation allows to test and compare several configurations of the reflector geometry and to study the most performing shape. This paper discusses such an approach and applies it to a realistic case study. The design of the reflector for a small scale solar simulator based on a commercial xenon short arc lamp is assessed. Particularly, the description of the implemented steps is provided together with the analysis of the simulated scenarios. Finally, the major outcomes are presented and properly commented.

The proposed approach goal is to support the designer of solar simulator optic systems with an integrated and easy-use method to rapidly test a system geometry before the prototyping phase and laboratory validation. An integrated approach to gain this purpose is of strong interest for both scientists and practitioners and its development is frequently encouraged.

The reminder of the present paper is organized as follows: Section II describes the steps of the developed ray-tracing model, while Section III introduces the Monte Carlo analysis and the aforementioned case study to design the ellipsoidal reflector of a single source concentrating solar simulator. The obtained results are presented and widely discussed in Section IV. Finally, Section V concludes this paper providing suggestions for further research.

II. RAY-TRACING MODEL

In geometrical optics, the foci of an ellipsoid of revolution are conjugate points [1]. If no distortion effects occur, each ray emitted by a punctiform source located in one of the foci passes through the other after a single specular reflection. According to this principle, the concentrating solar simulators are designed. The light source, i.e. the yellow spot in Fig. 2, reproducing the Sun emission spectrum and the target surface, i.e. the blue spot in Fig. 2, are located in correspondence of the two foci of an ellipsoidal surface, while the reflector lies on a portion of such an area and it is limited by a truncation section as depicted in Fig. 2 presenting the overall geometry of the system.

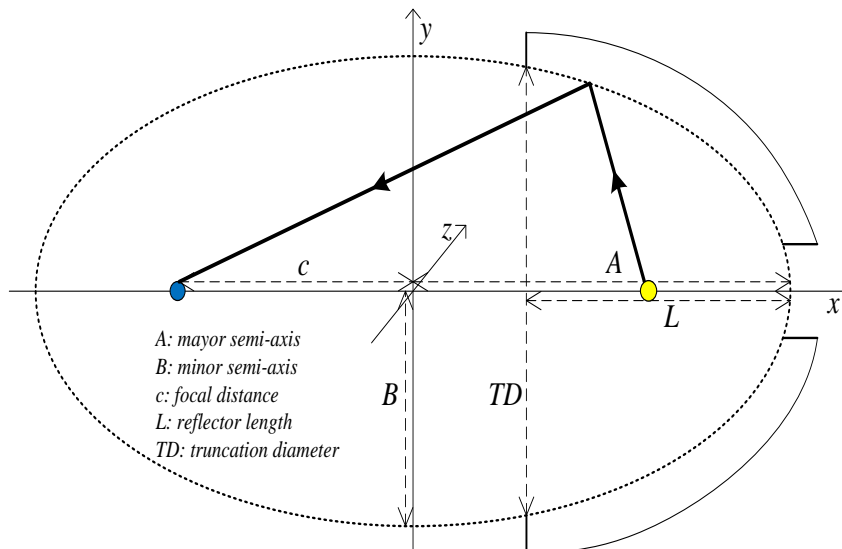


Figure 2: Single Source Solar Simulator Geometry and Notations.

Considering the operative contexts, the following conditions and phenomena contribute to reduce the global system radiation transfer efficiency, expressed as the ratio between the light flux that reaches the target and the global emitted flux.

- The finite area of the light source;
- The absorption phenomena caused by the presence of the quartz bulb, the electrodes and the reflective surface;
- The deviation and distortion phenomena caused by the specular dispersion errors of the reflective surface;
- The losses caused by the rays falling out of the reflector shape.

Such conditions cannot be neglected in the solar simulator design. Their impact in reducing the system performances is strongly correlated to the features of the emitting source, the target shape and, particularly, to the reflector characteristics. From this perspective, a model approaching this issue from an analytic point of view is of crucial interest.

The proposed ray-tracing approach faces this topic and it studies the ray trajectories, predicting the system global performances for a given configuration of the source, the reflector and the target surface. The next Fig. 3 shows the ray-tracing model flow-chart. It summarizes the step sequence of the proposed approach together with the stages in which the losses in the transfer efficiency generally occur.

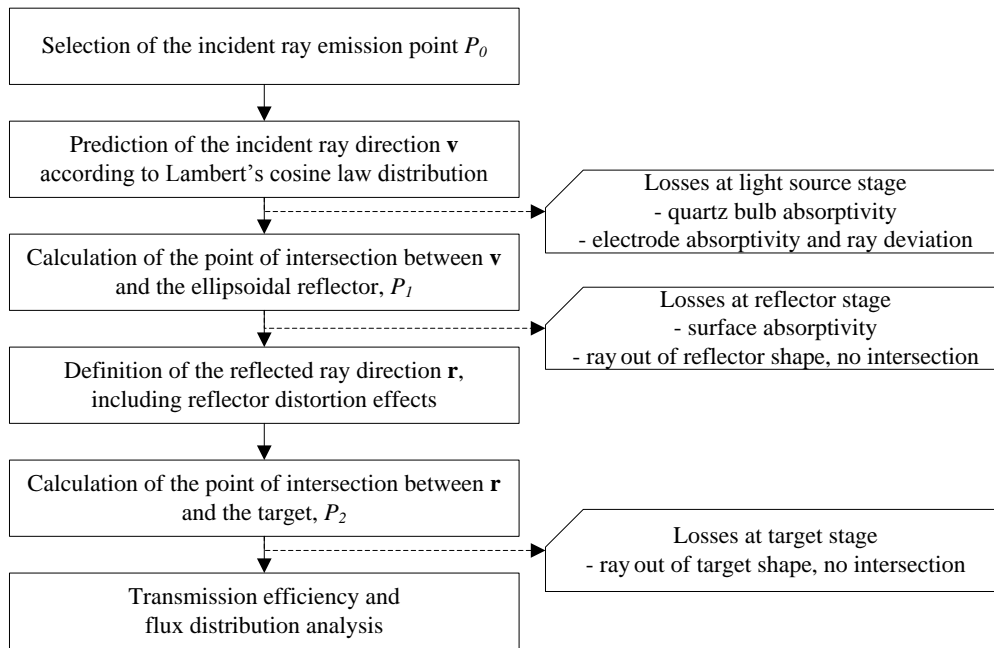


Figure 3: Ray-Tracing Model Flow-Chart.

According to the major literature [1, 2, 10] the light source is assumed to emit isotropic radiation uniformly from its surface. Consequently, the emission point, P_0 , is randomly located on the whole source surface. The incident ray direction, \mathbf{v} , is defined following the Lambert's cosine law distribution, as in (1) [16].

$$\mathbf{v} \times \mathbf{n} = \cos(\sin^{-1}\sqrt{U}) = \sqrt{1-U} \quad (1)$$

where \mathbf{n} is the normal direction to the emitting surface, in P_0 , and U a random number drawn from a [0, 1] uniform distribution. The quartz bulb and electrodes absorption phenomena are considered introducing two coefficients, i.e. the bulb and the electrodes absorption coefficients, reducing the emitted rays and decreasing the system efficiency, i.e. the losses at the light source stage.

For each emitted ray, the point of intersection with the ellipsoidal surface, P_1 , is calculated. If P_1 falls out of the reflector shape or it falls in the hole, close to the ellipsoid vertex, necessary to install the light source, the ray is considered lost and the process finishes. Otherwise, two possibilities occur. Generally, the mirror reflects the ray but, in few cases, an absorption phenomenon occurs and the ray is not reflected at all. In such a circumstance, modeled considering a further absorption coefficient, the process ends, i.e. the losses at the reflector stage.

Finally, considering the reflected rays, their direction, \mathbf{r} , is calculated. The vector \mathbf{r} is affected by the distortion effects caused by the specular dispersion errors of the reflective surface. As widely discussed by Cooper and Steinfeld [15], the geometric surface errors modify the normal vector, \mathbf{k} , to the ellipsoid surface. The authors identify two angular components of the dispersion error, i.e. the azimuthal angular component, θ_{err} , and the circumferential component, φ_{err} . By applying the, so called, Rayleigh method they outline the following expressions to estimate them:

$$\theta_{err} = \sqrt{2} \cdot \sigma_{err} \cdot \sqrt{-\ln U} \quad (2)$$

$$\varphi_{err} = 2\pi U \quad (3)$$

where σ_{err} is the standard deviation of the dispersion azimuthal angular error distribution, including all distortion effects, and U a random number drawn from a [0,1] uniform distribution. As a consequence, to estimate the direction of \mathbf{k} , in the point of intersection P_1 , the theoretic normal vector \mathbf{k}' needs to be twofold rotated. The rotation angles are θ_{err} and, then, φ_{err} . The former rotation is around a vector orthogonal to the plane where the major ellipse lies, while the latter rotation is around \mathbf{k}' .

The prediction of the normal vector to the reflective surface, in P_1 , allows to calculate the reflected ray direction, \mathbf{r} , according to (4) [16].

$$\mathbf{r} = \mathbf{v} - 2 \cdot (\mathbf{k} \times \mathbf{v}) \times \mathbf{k} \quad (4)$$

The point of intersection between \mathbf{r} and the plane where the target lies allows to find the coordinates of the common point P_2 . If P_2 is inside the target area the ray correctly hits the target, otherwise the ray is lost and the transfer efficiency decreases, i.e. the losses at the target stage. This study does not consider multiple reflection phenomena.

Finally, the distance and mutual position between P_2 and the ellipsoid focus point allows to study the radiative incident flux distribution on the target area.

III. MONTE CARLO SIMULATION

Several geometric and optic parameters affect the global transfer efficiency of solar simulator systems. A list of them, classified according to the physical component they belong to, is provided in the following.

Light source (generally an high flux arc lamp)

- Shape and dimensions;
- Emission light spectrum;
- Emission surface shape and dimensions, e.g. sphere, cylinder, etc.;
- Emission direction distribution;
- Absorption coefficients of quartz bulb and electrodes (if present);
- Interference angle of electrodes (if present).

Ellipsoidal reflective surface

- Reflector shape, identified by the two ellipsoid semi-axes or by the major semi-axis and the truncation diameter;
- Reflector length;
- Absorption coefficient;
- Standard deviation of the dispersion azimuthal angular error distribution.

Target surface

- Shape, e.g. circular, squared, rectangular;
- Dimensions;
- Relative position toward the ellipsoid.

For a given a set of the previous parameters, the geometric and optical features of the solar simulator are univocally identified and the ray-tracing model, described in previous Section II, is applicable to study the global performances of the system. In particular, the simulation of a large number of the emitted light rays allows to assess the expected distribution of the light on the target and to estimate the system global transfer efficiency. Such a simulation is feasible through the well-known Monte Carlo simulative approach when integrated to the described ray-tracing model.

Finally, varying one or several of the previous parameters, through a multi-scenario analysis, the best configuration of the system can be identified. Such a strategy is adopted in the realistic case study described in the following paragraph.

3.1 CASE STUDY. DESIGN OF A SINGLE SOURCE CONCENTRATING SOLAR SIMULATOR

The following case study provides an empirical application of the proposed approach. The design of a small-scale single source concentrating solar simulator is assessed. The system overall structure is similar to that proposed in previous Fig. 1. In particular, the emitting source is a commercial OSRAM XBO® 3000W/HTC OFR xenon short arc lamp with a luminous flux of 130000lumen and an average luminance of 85000cd/cm² [17]. The target area is assumed squared, centered on the ellipsoid focus point and its dimensions are of 50×50mm. Such features are assumed constant, while several configurations of the reflector shape, corresponding to different sets of the aforementioned parameters, are tested and the performances compared.

Further details about the considered high flux arc lamp are in Table 1 and represented in Fig. 4. The quartz bulb absorption coefficient is of 4% and the electrode absorption coefficient is of 98%.

Table 1: Geometric Features of the Emitting Source. Notations Refer to Fig. 4.

Lamp length (overall)	l_1	398mm
Lamp length	l_2	350mm
Lamp cathode length	a	165mm
Electrode gap (cold)	eo	6mm
Bulb diameter	d	60mm
Electrode interference angles	ϑ_1	30°
	ϑ_2	20°

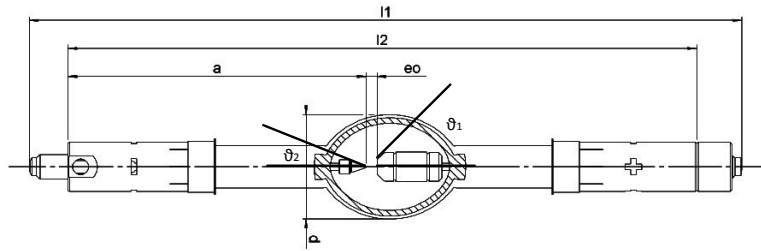


Figure 4: High Flux Arc Lamp Geometry.

Considering the ellipsoidal mirror reflector, the next Table 2 summarizes the tested scenarios corresponding to different geometric shapes and optic performances. The ranges of variation and the incremental steps for four of the most relevant parameters are presented.

Table 2: Tested Configurations for the Ellipsoidal Reflector [mm]. Refer to Fig. 2 for Notations.

	Min value	Max value	Step
<i>A</i>	200	1000	100
<i>TD</i>	100	2 <i>A</i>	50
σ_{err}	0.005	0.01	0.005
<i>L</i>	$A - \sqrt{A^2 - TD^2}/4$	<i>A</i>	50

Furthermore, a constant mirror absorption coefficient of 4% is considered in the analysis. 3840 scenarios appear and are simulated, i.e. multi-scenario analysis. For each scenario, $N = 5 \times 10^5$ emitted rays are traced and the results collected.

IV. RESULTS AND DISCUSSION

The measurement of the performances for each simulated scenario is assessed collecting the following data:

- N_A , number of the rays absorbed by the light source;
- N_H , number of the rays lost due to the presence of the hole used to install the light source;
- N_L , number of the rays falling out of the reflector shape;
- N_R , number of the rays absorbed by the mirror reflector;
- N_T , number of the reflected rays hitting the target;
- N_O , number of the reflected rays that do not hit the target.

Such a data allow to calculate the following key performance indicators highlighting the impact of the reflector features on the solar simulator efficiency:

- Losses due to the reflector shape, i.e. the ellipsoid shape and eccentricity, the hole and the truncation diameters;

$$\xi_1 = \frac{N_H + N_L}{N - N_A} \tag{5}$$

- Losses due to the optic and distortion effects caused by the reflector surface error distribution;

$$\xi_2 = \frac{N_R + N_O}{N - N_A - N_H - N_L} \tag{6}$$

- Global reflector transfer efficiency;

$$\eta = (1 - \xi_1) \cdot (1 - \xi_2) = \frac{N_T}{N - N_A} \tag{7}$$

- Statistical distribution of the reflected rays on the target surface, i.e. the mean distance M_D and its standard deviation σ_D between the point of intersection P_2 and the target center.

The Table 3 shows a subset of the obtained results for the tested scenarios presenting the twenty best and worst cases. In addition to the previous notations, ε indicates the ellipsoidal reflector eccentricity, as in (8), and included in the [0,1] range.

$$\varepsilon = \sqrt{1 - B^2/A^2} \tag{8}$$

Furthermore, Fig. 5 shows an example of radiative flux map. It considers the best of the simulated scenarios. The squared dashed line identifies the target surface whereas all dots inside the square are the rays hitting the target. The other dots are the rays causing the losses at the target stage.

Table 3: Multi Scenario Analysis Results. Twenty Best and Worst Scenarios.

Rank	A	TD	σ_{err}	L	B	ϵ	N_A	%	N_H	%	N_L	%	N_R	%	N_T	%	N_o	%	ξ_1	ξ_2	η	M_D	σ_D
1	600	650	0.005	600	325	0.841	65506	B.10%	5585	1.12%	6771	1.35%	16942	3.39%	401501	80.30%	3695	0.74%	2.844%	4.889%	92.407%	8.284	6.387
2	700	700	0.005	700	350	0.866	65865	B.17%	6287	1.26%	719	0.14%	16935	3.39%	399723	79.94%	10471	2.09%	1.614%	6.416%	92.073%	9.867	7.265
3	700	750	0.005	700	375	0.844	65477	B.10%	2107	0.42%	5849	1.17%	17211	3.44%	399732	79.95%	9624	1.92%	1.831%	6.291%	91.993%	9.622	7.147
4	600	600	0.005	600	300	0.866	65943	B.19%	13355	2.67%	702	0.14%	16782	3.36%	399052	79.81%	4166	0.83%	3.239%	4.988%	91.935%	8.521	6.205
5	600	700	0.005	600	350	0.812	65936	B.19%	1491	0.30%	13675	2.74%	16838	3.37%	398989	79.80%	3071	0.61%	3.494%	4.753%	91.919%	8.077	7.453
6	500	550	0.005	500	275	0.835	65626	B.13%	12034	2.41%	7907	1.58%	16699	3.34%	396935	79.39%	799	0.16%	4.591%	4.222%	91.381%	6.918	5.108
7	500	600	0.005	500	300	0.800	65623	B.12%	4064	0.81%	16235	3.25%	16688	3.34%	396752	79.35%	638	0.13%	4.673%	4.184%	91.338%	6.705	5.281
8	700	800	0.005	700	400	0.821	65424	B.08%	499	0.10%	11629	2.33%	17004	3.40%	396659	79.33%	8785	1.76%	2.791%	6.105%	91.275%	9.462	7.226
9	600	650	0.005	550	326	0.839	65174	B.03%	5308	1.06%	13451	2.69%	16698	3.34%	395752	79.15%	3617	0.72%	4.314%	4.883%	91.044%	8.298	6.631
10	700	700	0.005	650	351	0.865	65824	B.16%	6088	1.22%	5619	1.12%	16789	3.36%	395000	79.00%	10680	2.14%	2.696%	6.502%	90.977%	9.868	7.868
11	700	750	0.005	650	376	0.844	65819	B.16%	1925	0.39%	11180	2.24%	16775	3.36%	394742	78.95%	9559	1.91%	3.018%	6.254%	90.916%	9.661	12.983
12	600	600	0.005	550	301	0.865	65393	B.08%	13003	2.60%	6290	1.26%	16493	3.30%	394753	78.95%	4068	0.81%	4.439%	4.951%	90.830%	8.508	6.197
13	800	800	0.005	800	400	0.866	65306	B.06%	2336	0.47%	744	0.15%	17232	3.45%	394171	78.83%	20211	4.04%	0.709%	8.675%	90.678%	11.228	8.321
14	600	750	0.005	600	375	0.781	65675	B.14%	286	0.06%	21051	4.21%	16654	3.33%	393652	78.73%	2682	0.54%	4.913%	4.682%	90.635%	7.923	10.472
15	800	850	0.005	800	425	0.847	65715	B.14%	659	0.13%	5146	1.03%	17002	3.40%	392510	78.50%	18968	3.79%	1.337%	8.395%	90.381%	11.004	8.655
16	600	700	0.005	550	351	0.811	65720	B.14%	1407	0.28%	21106	4.22%	16375	3.28%	392244	78.45%	3148	0.63%	5.184%	4.741%	90.321%	8.074	6.300
17	700	850	0.005	700	425	0.795	65720	B.14%	211	0.04%	17598	3.52%	16642	3.33%	392119	78.42%	7710	1.54%	4.101%	5.847%	90.292%	9.232	10.141
18	700	650	0.005	650	326	0.885	65836	B.17%	13360	2.67%	584	0.12%	16704	3.34%	391884	78.38%	11632	2.33%	3.212%	6.743%	90.262%	10.109	7.391
19	700	650	0.005	700	325	0.886	65749	B.15%	13333	2.67%	512	0.10%	16895	3.38%	391933	78.39%	11578	2.32%	3.188%	6.773%	90.255%	10.112	7.375
20	500	500	0.005	500	250	0.866	65597	B.12%	24369	4.87%	722	0.14%	16449	3.29%	391887	78.38%	976	0.20%	5.776%	4.257%	90.213%	7.188	6.463
3821	600	450	0.005	50	563	0.346	65447	B.09%	35	0.007%	409130	81.83%	1016	0.20%	24347	4.87%	25	0.01%	94.158%	4.100%	5.603%	53.826	4427
3822	600	450	0.01	50	563	0.346	65927	B.19%	23	0.005%	408554	81.71%	1053	0.21%	22152	4.43%	2291	0.46%	94.126%	13.166%	5.103%	128.611	23924
3823	1000	850	0.005	100	975	0.222	65157	B.03%	11	0.002%	411962	82.39%	897	0.18%	21344	4.27%	629	0.13%	94.741%	6.672%	4.908%	92.488	5811
3824	800	500	0.005	50	718	0.440	65429	B.09%	22	0.004%	412160	82.43%	911	0.18%	21118	4.22%	360	0.07%	94.848%	5.677%	4.860%	43.496	2531
3825	900	800	0.01	100	873	0.243	65717	B.14%	11	0.002%	406282	81.26%	1085	0.22%	20798	4.16%	6107	1.22%	93.555%	25.695%	4.789%	383.653	150438
3826	1000	1050	0.01	150	997	0.082	66030	B.21%	8	0.002%	406182	81.24%	1177	0.24%	20351	4.07%	6252	1.25%	93.599%	26.742%	4.689%	199.142	7646
3827	900	500	0.01	50	761	0.535	65500	B.10%	23	0.005%	407282	81.46%	1145	0.23%	17951	3.59%	8099	1.62%	93.741%	33.992%	4.131%	58.225	2676
3828	1000	500	0.01	50	801	0.599	65804	B.16%	12	0.002%	403926	80.79%	1218	0.24%	17887	3.58%	11153	2.23%	93.031%	40.885%	4.120%	28.040	65
3829	800	500	0.01	50	718	0.440	65880	B.18%	27	0.005%	411665	82.33%	937	0.19%	16543	3.31%	4948	0.99%	94.834%	26.240%	3.811%	75.963	5461
3830	1000	550	0.005	50	881	0.474	66168	B.23%	12	0.002%	415741	83.15%	730	0.15%	16257	3.25%	1092	0.22%	95.833%	10.078%	3.747%	53.311	5468
3831	1000	850	0.01	100	975	0.222	65330	B.07%	12	0.002%	412098	82.42%	871	0.17%	15910	3.18%	5779	1.16%	94.810%	29.477%	3.660%	256.684	37704
3832	700	500	0.005	50	674	0.272	65630	B.13%	19	0.004%	419413	83.88%	589	0.12%	14309	2.86%	40	0.01%	96.561%	4.211%	3.294%	71.500	12637
3833	900	550	0.005	50	837	0.368	65986	B.20%	18	0.004%	420144	84.03%	543	0.11%	12947	2.59%	362	0.07%	96.808%	6.533%	2.983%	55.009	2629
3834	700	500	0.01	50	674	0.272	65828	B.17%	14	0.003%	418994	83.80%	585	0.12%	12729	2.55%	1850	0.37%	96.507%	16.058%	2.932%	100.957	3266
3835	1000	550	0.01	50	881	0.474	65808	B.16%	16	0.003%	416421	83.28%	687	0.14%	11242	2.25%	5826	1.17%	95.911%	36.683%	2.589%	91.629	6668
3836	900	550	0.01	50	837	0.368	65775	B.16%	16	0.003%	420351	84.07%	558	0.11%	9775	1.96%	3525	0.71%	96.809%	29.463%	2.251%	135.650	13985
3837	1000	600	0.005	50	961	0.277	65848	B.17%	8	0.002%	427627	85.53%	269	0.05%	6052	1.21%	196	0.04%	98.499%	7.135%	1.394%	101.737	18564
3838	800	550	0.005	50	790	0.156	65524	B.10%	11	0.002%	428332	85.67%	236	0.05%	5867	1.17%	30	0.01%	98.588%	4.337%	1.350%	87.917	8513
3839	800	550	0.01	50	790	0.156	65207	B.04%	7	0.011%	428814	85.76%	251	0.05%	4882	0.98%	839	0.17%	98.626%	18.252%	1.123%	195.014	16000
3840	1000	600	0.01	50	961	0.277	65586	B.12%	11	0.002%	427651	85.53%	296	0.06%	4658	0.93%	1798	0.36%	98.446%	31.013%	1.072%	226.342	40309

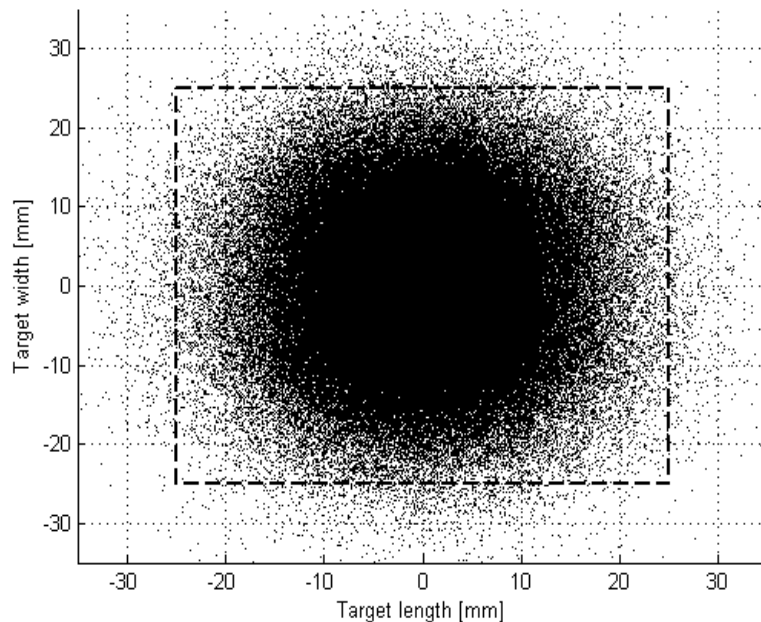


Figure 5: Radiative Flux Map for the Best Scenario.

The values of the global transfer efficiency vary from 92.407% of the best scenario to 1.072% of the worst case. Consequently, a first relevant outcome of the analysis is the heavily influence of the reflector design on the solar simulator performances.

Considering the best scenarios, the ξ_1 and ξ_2 loss indices present values lower than 9%, and the large amount of the reflected rays are concentrated close to the target, i.e. the mean distance between the rays and the ellipsoid focus point, M_D , is close to 10mm and the standard deviation, σ_D , is included between [5,13]mm. On the contrary, the most relevant cause for the performance decrease is the reflector shape losses. With reference to the worst scenarios, high values of ξ_1 , i.e. greater

than 93%, are always experienced, while ξ_2 does not present a regular trend. Such losses depend on the length of the reflector, i.e. the aforementioned parameter L . All the worst scenarios present little values for such a parameter, e.g. 50-100mm, so that the majority of the emitted rays is lost because no intersection with the mirror surface occurs. The high number of the rays falling out of the reflector shape, N_L , included between 80% and 86%, clearly highlights this evidence.

Furthermore, the standard deviation of the dispersion azimuthal angular error distribution, σ_{err} , represents another relevant parameter affecting the global performances of the system. As expected, the lower σ_{err} , the higher the global transfer efficiency values are. The standard deviation error depends on the accuracy of the reflector manufacturing. The decrease of this parameter is generally associated to the increase of the reflector production costs. Fig. 6 correlates the reflector length to the global transfer efficiency for the two simulated values of σ_{err} , i.e. 0.005mm and 0.01mm.

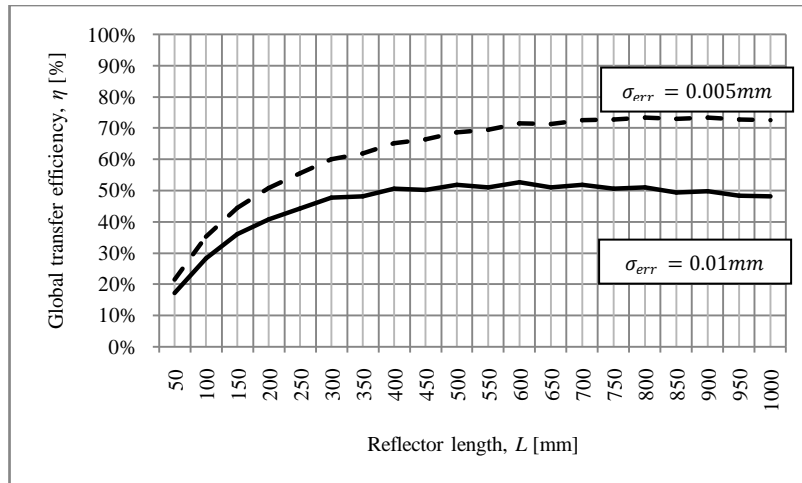


Figure 6: Correlation between the Reflector Length and the Global Transfer Efficiency for the Two Values of σ_{err} .

The results present similarities in the waveforms. Low values of the reflector length are associated to poor performances, i.e. $\eta < 30\%$. Optimal conditions are, respectively, for a reflector length of 800mm and $\sigma_{err} = 0.005\text{mm}$ and of 600mm for $\sigma_{err} = 0.01\text{mm}$. A significant performance increase occurs for values of L included in $[50,450]\text{mm}$ range, while for the higher values of the reflector length, i.e. $L > 500\text{mm}$, the global transfer efficiency presents comparable values. Finally, considering the gap between the performances in the trends identified by the two values of σ_{err} , an increase, from 4.241% to 24.466%, occurs. High values of σ_{err} have a crucial impact on the global transfer efficiency in presence of high values of L . In fact, long reflectors force the emitted rays to sweep out long trajectories from the source to the mirror and, then, from the mirror to the target. An anomaly in the trajectories generates an angular deviation of the ray path. Such a deviation is amplified by the distance between the mirror and the target. Consequently, if L increases the standard deviation of the dispersion azimuthal angular error distribution must have low values not to significantly reduce η .

Another relevant parameter affecting the mirror reflector design is the ellipsoid eccentricity, ϵ , defined in previous (8) and included in the $[0,1]$ range. It identifies the mutual position of the vertices and the foci. If ϵ is equal to 0 the ellipsoid is a sphere, i.e. $A = B$. Values of ϵ between 0 and 1 are for eccentric geometries in which $B < A$. If $\epsilon = 1$ the ellipsoid degenerates into a plane and the foci lay upon the vertices on the major axis. The developed multi-scenario analysis highlights a range of the optimal values for the ellipsoid eccentricity included between 0.75 and 0.9, as in Fig. 7, correlating the ellipsoidal mirror eccentricity to the values of η . Each dot represents one of the 3840 simulated scenarios.

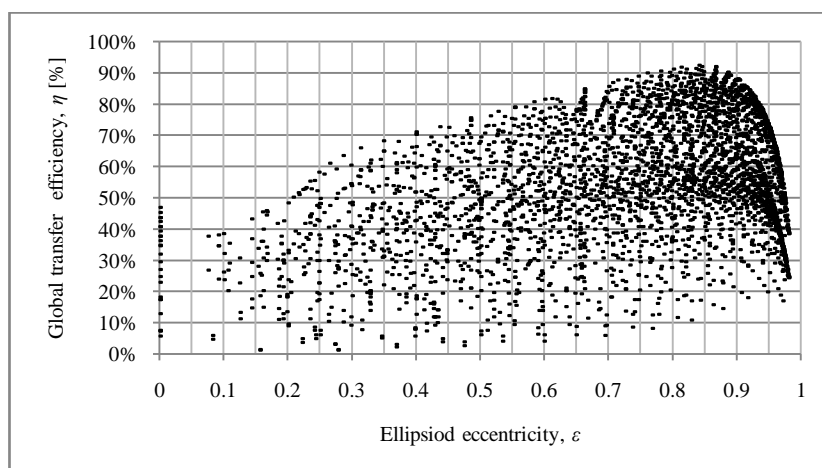


Figure 7: Correlation between the Ellipsoid Eccentricity and Global Transfer Efficiency.

This outcome may be in contrast to the major literature evidences suggesting low values of ε to maximize the reflector global transfer efficiency [16,18]. On the contrary, in the proposed analysis values of eccentricity close to zero generate the worst performances. A reasonable explanation for this evidence lies in the adopted reflector modeling approach. The literature ray-tracing models and related results approximate the reflector with an ellipsoid of revolution neglecting both the truncation section, i.e. the previously called TD parameter, and the hole necessary to install the light source. The proposed ray-tracing approach includes these two elements in the analytical model to provide a realistic and accurate description of the physical system. The presence of these elements significantly modifies the geometric and optic features of the solar simulator introducing the so-called losses at the reflector stage (see Fig. 3) that significantly contribute to the global transfer efficiency decrease, especially for the scenarios in which L and ε assume low values (see Table 3). In fact, if ε is low the foci are located far from the vertices and close to the ellipsoid geometric center, i.e. the point of intersection of the two axes. In this circumstance, the light source juts out from the reflector profile and a large number of the emitted rays does not hit the reflector surface. The lower the reflector length, the higher such losses are.

On the contrary, in eccentric reflectors the light source is close to the ellipsoid major axis vertex and a lower number of rays is lost. However, very high values of ε , i.e. $\varepsilon > 0.9$, cause a further increase of the losses at the reflector stage and a decrease of η . This is due to the presence of the hole for the light source installation. A focus point located close to the reflector vertex increases the value of N_H , i.e. the number of the rays lost due to the presence of the hole used to install the light source, so that, also in this case, the global transfer efficiency decreases. As introduced before, optimal values for the reflector eccentricity are in the [0.75,0.9] range.

V. CONCLUSIONS AND FURTHER RESEARCH

This paper presents an approach facing the effective design of solar simulators. The developed model reproduces the trajectories of the light rays considering the main physical and optic phenomena that occur from the source to the target area. The ellipsoidal reflector geometries are focused. In particular, the solar simulator reflector is a truncated ellipsoid of revolution with the light source located on one focus point and the target area on the other. The proposed ray-tracing model is integrated to a Monte Carlo simulation to study and compare the performances of several reflector geometries. A case study, based on a commercial xenon short arc lamp, is described simulating 3840 scenarios and varying four major parameters affecting the quality and reflectivity of the mirror surface, i.e. the ellipsoid major axis, the truncation diameter, the reflector length and the standard deviation of the azimuthal angular error distribution. For each simulated scenario, the data about the losses and the number of rays on target are collected and summarized in the three key performance indices proposed in (6) to (9) together with a statistic analysis of the distribution of rays on the target.

The main outcomes highlight the relevance of the proper design of the reflector shape to obtain high values of the global transfer efficiency. The gap between the best and worst scenarios is higher than 90%. Furthermore, correlations between the four considered parameters are highlighted. As example, high values of the reflector length, in presence of high values of the standard deviation of the azimuthal angular error distribution, amplify the global transfer efficiency decrease, while, low values of the ellipsoid eccentricity cause an increase of the lost rays.

The obtained parameter values, for the best scenario, are of 600mm for both the ellipsoid major semi-axis and reflector length, 325mm for the minor semi-axis and σ_{err} equals to 0.005mm. For this scenario, the global transfer efficiency is 92.407% while the distribution of rays on the target area presents a mean distance from the ellipsoid focus point of 8.284mm and a standard deviation of 6.387mm.

Both the model description and its application to the realistic case study convey to point out the interest of the proposed approach for scientists and practitioners. Its application before the system development and manufacture allows to simulate the system behavior and to assess the expected performances. Furthermore, the inclusion of the operative geometric constraints, e.g. the truncation diameter, the lamp installation hole, etc., to the ray-tracing model increases the approach applicability overcoming the assumptions of several of the models proposed by the recent literature.

Further research deals with a validation of the case study results through the development of the solar simulator and a further field-campaign. To this purpose, the authors already purchased the ellipsoidal reflector and they are now developing the overall structure of the solar simulator to collect the experimental data to be compared to the evidences coming from the proposed approach. At last the enlargement of the approach to multi source solar simulators and the inclusion of multiple reflection phenomena is encouraged.

REFERENCES

- [1] J. Petrash, P. Coray, M. Meier, M. Brack, P. Häberling, D. Wuillemin, and A. Steinfeld, A novel 50 kW 11,000 suns high-flux solar simulator based on an array of xenon arc lamps, *Journal of Solar Energy Engineering*, 129, 2007, 405-411M.
- [2] C. Domínguez, I. Antón, and G. Sala, Solar simulator for concentrator photovoltaic systems, *Optics express*, 16(19), 2008, 14894–14901.
- [3] C. Domínguez, S. Askins, I. Antón, and G. Sala, Characterization of five CPV module technologies with the Helios 3198 solar simulator, *IEEE*, 2009, 1004–1008.
- [4] M. Pravettoni, R. Galleano, E.D. Dunlop, and R.P. Kenny, Characterization of a pulsed solar simulator for concentrator photovoltaic cell calibration, *Measurement Science and Technology*, 21, 2010, 1-8.
- [5] H. Renh, and U. Hartwig, A solar simulator design for concentrating photovoltaics, *Proc. SPIE The International Society for Optical Engineering*, San Diego, CA, 2010, 1-4.
- [6] F. Hussain, M.Y.H. Othman, B. Yatim, H. Ruslan, and K. Sopian, Fabrication and irradiance mapping of low cost solar simulator for indoor testing of solar collector, *Journal of Solar Energy Engineering*, 133(4), 2011, 44502 1–4.

- [7] Q. Meng, Y. Wang, and L. Zhang, Irradiance characteristics and optimization design of a large-scale solar simulator, *Solar Energy*, 85, 2011, 1758-1767.
- [8] H. Amoh, Design for multi-solar simulator, Proc. SPIE The International Society for Optical Engineering, Denver, CO, 2004, 192-199.
- [9] Q. Meng, and Y. Wang, Testing and design of a low-cost large scale solar simulator, Proc. SPIE The International Society for Optical Engineering, San Diego CA, 2011, 8128.
- [10] K.R. Kruger, J.H. Davidson, and W. Lipiński, Design of a new 45 kWe high-flux solar simulator for high-temperature solar thermal and thermo-chemical research, *Journal of Solar Energy Engineering*, 133(4), 2011, 11013 1-8.
- [11] D.S. Codd, A. Carlson, J. Rees, and A.H. Slocum, A low cost high flux solar simulator, *Solar Energy*, 84, 2010, 2202-2212.
- [12] G. Johnston, On the analysis of surface error distributions on concentrated solar collectors, *Transactions of the ASME*, 117, 1995, 294-296.
- [13] C.F. Chen, C.H. Lin, and H.T. Jan, A solar concentrator with two reflection mirrors designed by using a ray tracing method, *Optik*, 121, 2010, 1042-1051.
- [14] Y. Ota, and K. Nishioka, 3-dimensional simulator for concentrator photovoltaic modules using ray-trace and circuit simulator, Proc. 35th IEEE Photovoltaic Specialists Conference, PVSC 2010, Honolulu, HI, 3065-3068.
- [15] T. Cooper, and A. Steinfeld, Derivation of the angular dispersion error distribution of mirror surfaces for Monte Carlo ray-tracing applications, *Journal of Solar Energy Engineering*, 133(4), 2011, 44501 1-4.
- [16] A. Steinfeld, Exchange factor between two spheres placed at the foci of a specularly reflecting ellipsoidal cavity, *International Communications in Heat and Mass Transfer*, 18, 1991, 19-26.
- [17] Osram, Technical information No. 5264, Available on-line: <http://www.osram.com> [accessed January 2013].
- [18] A. Steinfeld, and E.A. Fletcher, Solar energy absorption efficiency of an ellipsoidal receiver-reactor with specularly reflecting walls, *Energy*, 13(8), 1988, 609-614.

The Difference of Wall Elements State Including the FRF Function

Ph.D. Mariusz ZOLTOWSKI

University of Technology and Life Sciences in Bydgoszcz

Abstract: The recommendation of Polish PN - B-03002 norm shows a need of quality control of wall elements production, and classified them as elements of category I or II. This classification is decided in institution of quality control which should provide straight lines diagnostic tools.

Requirement of this norm establishing the partial coefficients of wall safety, of wall treatments to settlement the category of works realization on building site (A or B). They would support qualification " suitably qualified person controls " straight lines diagnostic methods indispensable the searches of new methods of opinion.

It recognizes the need of improvement the methods of investigation of wall building quality, and construction. In that article we considerate to test wall elements using the modal analysis and the delimitation of passage function FRF.

Key words: the modal analysis, function of passage the FRF, temporary course of trembling's.

I. Introduction

Existing constructions, such as: buildings, high poles, chimneys, foundations under machines, and roofs are subject to the environment and to trembling processes as well. The dynamics caused by wind, earthquakes, machines work, railway and road movement, explosions, and sea waves are important in the process of projecting constructions and influence safety and durability. Trembling in buildings decreases comfort of living, can have an influence on people working there, and can also threaten the safety level of the construction. The trembling can cause dynamic burden and even catastrophic destruction.

The previously mentioned recognizes the need of improving the methods for investigating the quality of wall building constructions, their diagnostic and the assessment of wall safety coefficients (PN - B-03002). The test used to determine the level of destruction of chosen materials was the experimental modal analysis and the concurrent procedure of this method - the trembling's estimators.

The new tools in this area of investigations concern the possibility of using modal analysis methods, and also modern logging and the processing of trembling to opinion the quality of wall elements. Practically it can be used for better understanding the behavior of constructions, which allows optimizing the projection and assessment of dangerous states.

Modal analysis has not been previously used for researches on buildings and constructions, but was adopted from the dynamics area of mechanical engineering. Its usefulness is greater for homogeneous structures of steel constructions, than for building materials such as wall elements, where every result of investigation is connected with the structure, the shape and the physical state of the sample. The fear is that the inhomogeneity and the coarse-grained structure of concrete and ceramics can be an obstacle for effectiveness of the measuring technique.

The task of this study is to check the usefulness of modal analysis in diagnosing homogeneous wall elements (bricks, notepads, and hollow blocks), as well as more heterogeneous walls fragments. The objective is to determine if the investigation parameters are useful in making a state diagnostic of the studied materials.

To do this the experimental modal analysis method and the signal function (FRF Function) of passage were used, with which it was able to see differences in the states of wall elements. The function is the relation between the input and output of strength signals

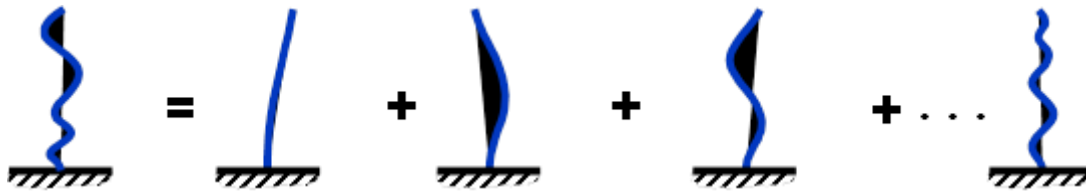
II. Environment of experimental modal analysis

The modal analysis is applied to the investigation of dynamic properties of varied constructions universally. In the diagnostics of construction state, the modal analysis can be applied to the modification of construction for aims of synthesizing the steering in arrangements of active reduction of trembling, as well as for aims of verifying and validating of numeric models

Modal analysis can be applied if the following conditions are fulfilled:

- arrangement is linear and its dynamics can be described as a linear arrangement of differential ordinary equations or partial;
- the coefficients of equations describing the dynamics of object are solid in the time of measurements;
- Existing possibility of performing measurements in all direction in order to identify the model;
- The studied arrangement fulfills the Maxwell's reciprocity principle;
- suppression in arrangement is small or proportional.

The possibility of using this method is determined by a limited number of liberty degrees because it is an important limitation for the application of the modal analysis.



Outline.1. Schedule of trembling straight lines [11]

Mathematically it can be defined as an unharnessed differential ordinary equations task, describing dynamics construction.

Theoretical modal analysis is defined as an own problem of matrix observation dependent from matrix of masses, stiffness and suppression. The theoretical modal analysis requires received a structural model study of the construction and the solution of own questions. Appointed here are the gatherings of own frequencies, suppression coefficients of own frequencies and figures of own trembling, which allow to make behavior simulations of the construction near any extortions. This was used in the projecting process, when there is no possibility of realizing investigations on objects.

Experimental modal analysis is one with technical identification of parameters in modal constructions. Experimental modal analysis is applied in practice as an investigation technique on property objects, both on stage constructing and exploitation. The identification of the object state in experimental modal analysis depends on extortion of the trembling, coming mostly from the phantom of acceleration. The modal model can be read from the stabilization diagram which presents accords that can be used to animate the trembling figure.

Exploitational modal analysis can be used to identify objects with large spatial sizes and masses. It is all about measurements the answer in extortion point being a result of working external strengths.

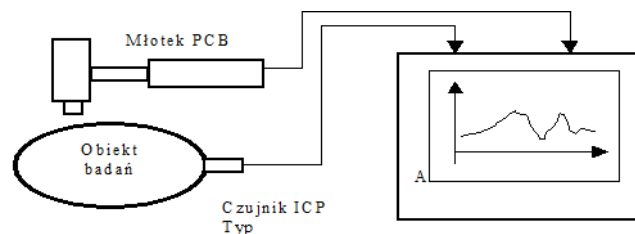
The diagnostic of destruction states of materials and building constructions is present more and more often in modal models. The objective of the method is to identify the changes of model parameters (on the case of modal model) It is sends with idea of this method that changes of model parameters (in this case of modal model), coming into being a result of waste, on basis of current observations of object. Modal model in method creates object without damage, as pattern, and modal model in time of exploitation was identified then and it studies from model his correlation for undamaged object.

Experimental modal analysis

The experimental analysis process of modal building construction and wall elements can be divided in five basic stages:

- The preparation of measurements;
- Acquisition of measurements (assembling) and processing signals;
- The estimation of parameters of the modal model;
- The verification and the validation of model; and
- The use of the model to simulate or the investigate the properties of construction elements.

The identification experiment in experimental modal analysis depends on extortion the trembling's near simultaneous measurement, of strength the object extorting and the answer of arrangement, the most often in figure of amplitude the accelerations of trembling's.



Outline.2. Investigation in experimental modal analysis [4]

III. Experiment in modal analysis

The experiment for identifying the destruction state of the studied wall elements is the basic source of information - and on its basis the value of measures and the structure of the model can be established. The quality of the received model depends on one side of the quality of the results of experimental investigations, and on the other side of the structure of the identified model. The modal analysis experiment can be divided in the following stages:

1. Planning:

- The choice of way of extorting trembling on the studied elements and the points of application,
- The choice of points of for measuring the trembling and the measuring apparatus,
- The choice of suitable measuring equipment,
- The choice of the modeling arrangement (the limitation of number of degrees liberty).

2. Calibration of the measuring track.
3. Acquisition and processing of the results.

The studied wall element shows the trembling force of signal extortion proportional to state of the destruction. The signal of extortion and the answer was used for further delimitation of the FRF function and the stabilization diagram.

The equipment necessary for the execution of the experiment of modal analysis consists of the following elements:

- the arrangement for measuring the extortion of movement and the answer,
- the arrangement of signals (the preliminary processing),
- the arrangement for processing and assembling the signals,
- the arrangement for generating the extorting signal, and
- the arrangement for arousing the trembling

The use of signals analyzer is the simplest machine with regard on service solution, however the most modern and gives the largest possibilities of specialized measuring interface on the working station. The basic operation that can be done by the signals analyzer is the regular analogue-digital processing, which makes possible applying digital technology in processing the modal analysis signals.

In modal investigations it is indifferent which of kinematic sizes of movement are being measured. In practice however the measurements of dislocation are shown in a low frequencies range, and acceleration in a high frequencies range. It is universally known that the measurements of speed are the most optimum in investigations for dynamics of construction with regard on the effective value of trembling speed, obtained by measuring the kinetic energy of trembling arrangements. However sensors that measure dislocations and speeds are comparatively heavy in relation to the studied materials and they can influence their behavior.

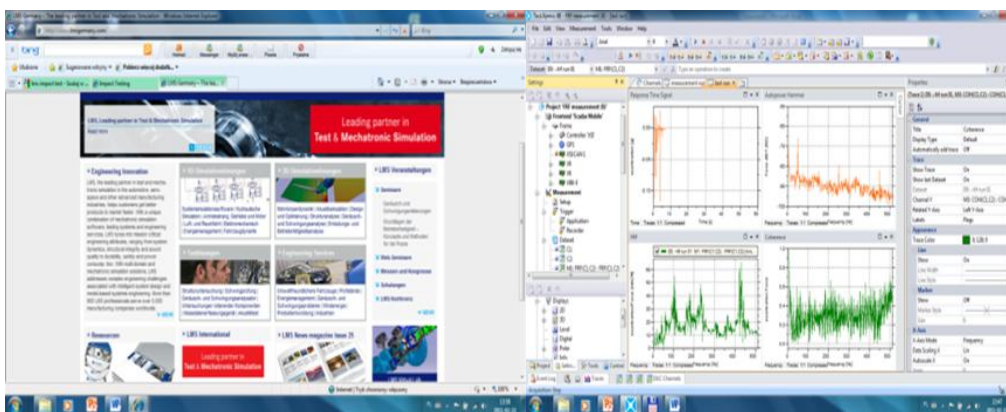
The sensors that measure accelerations have considerably smaller mass and therefore do not influence the movement of the arrangement. The additional advantage of sensor use is the fact that they receive integrated acceleration signals of speed and trembling dislocation. The backwards operation depends on differentiating trembling, which can lead to large mistakes particularly in range of higher frequencies. With this regard the sensors have their own resonance, which limits the frequency in which they can be applied.

The selection of the place for fastening the sensor is very important as it has influence on results of modal investigations. Sensors should be fixed in such way that they will not influence the trembling of arrangements; as well they should be fixed in characteristic places of the construction.

The experimental modal analysis requires precise laboratory conditions for the execution of investigations. Model must be subjected from mountain well-known and put extortions. Extortions can run away from these, which they act on object in time of normal exploitation. During experiment realization we can encounter the difficulty behavior peaceable with reality of shore conditions: fastening studied object. In the case of large models the realization of this experiment is very expensive.

IV. Measuring Software

To measurements of temporary courses of the extortion and the answer, also the qualification of FRF and COH function the most modern measuring apparatus, named LMS TEST.XPRESS, was used. This software makes possible in easy way to conduct the modal analysis of wall elements and many different building constructions.



Outline.4. Internet Shop window of manufacturer of software [www.ects.pl.]

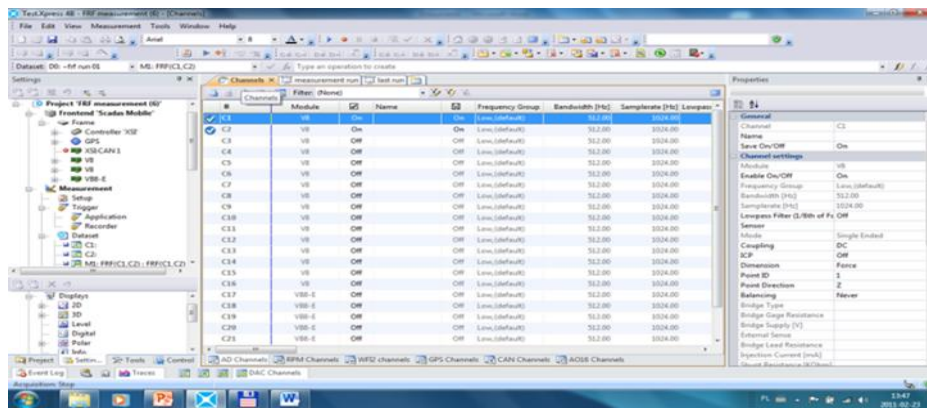
The program possesses an easy and friendly user interface. After the program is started a new project must be created by clicking on the new project icon. From this moment all measurements will be automatically recorded in the active project.

Defining all the necessary data for the calibration of the measuring track is the next step. Then, for the investigations to be conducted at this stage the quantity of active measuring channels must be defined. The number of channels depends on the measuring card and the number of slots it contains.



Outline.5. Example measuring segment[http://www.ects.pl]

For the measurement of temporary courses of strength two channels should be used. First calibrate the modal hammer (strength input), and second the output of trembling accelerations (signal passage through element). With measurements obtained from this channel calibration allows developing the FRF function.



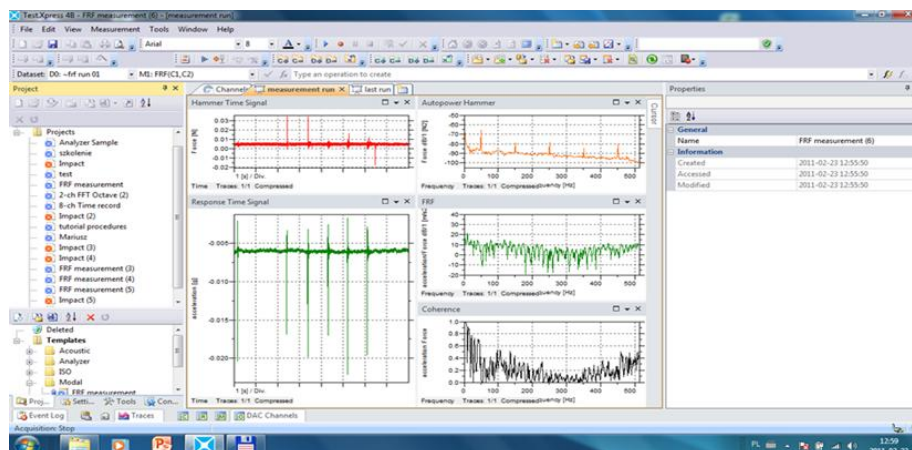
Outline. 6. Calibration of place of connecting the sensors - the own study

The calibration window that is shown in Outline 6 shows all the sensors that can be used to make the measurements, from which two have to be selected: C1 and C2. This Window opens after clicking on **channels**. On the right, the characteristic values are shown for each selected sensor. After the sensors have been calibrated and connected, then the investigation can proceed to performing the measurements by clicking on the record icon.

This article shows that using the LMS program it is possible to make measurements FRF function in wall elements and to obtain a graphic visualization of the FRF function. The measurements were made for different kind of materials in all directions.

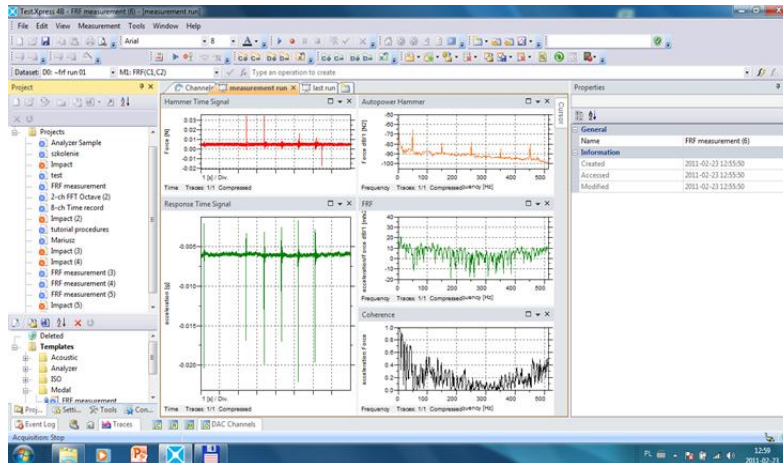
V. Results

The results are presented in real time in the center of screen for the time range of measurements. by all the time of leadership of investigation. The screen allows visualizing the temporary courses of extortions and the answer, as well as the function the FRF and the function of coherence.



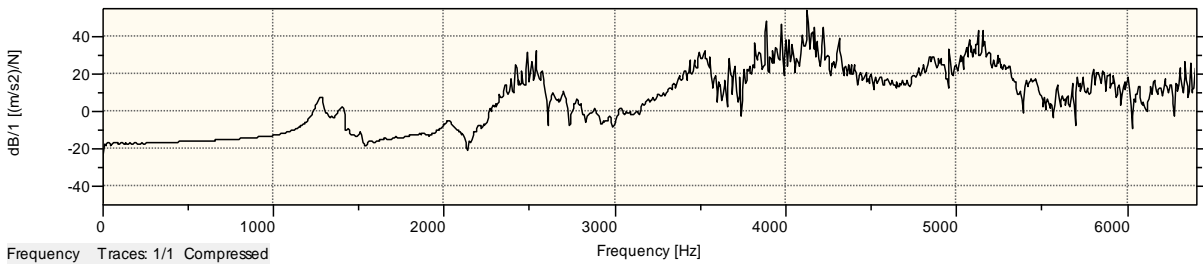
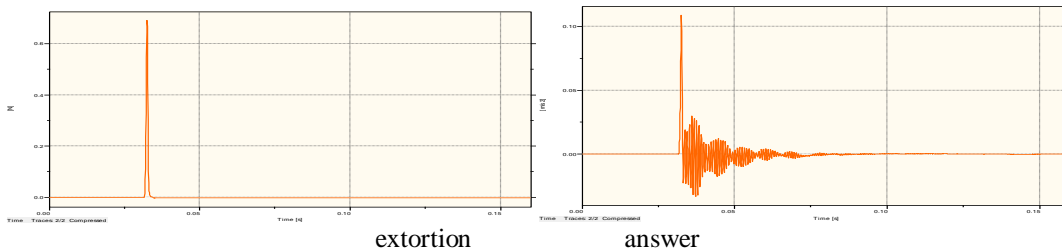
Outline.7. Example exposition of results of measurement - the own study

From a large group of materials, a fit and a damaged brick were selected to compare their fitness. Outline 8 shows the results obtained after performing measurements from three possible directions: X, Y, Z.



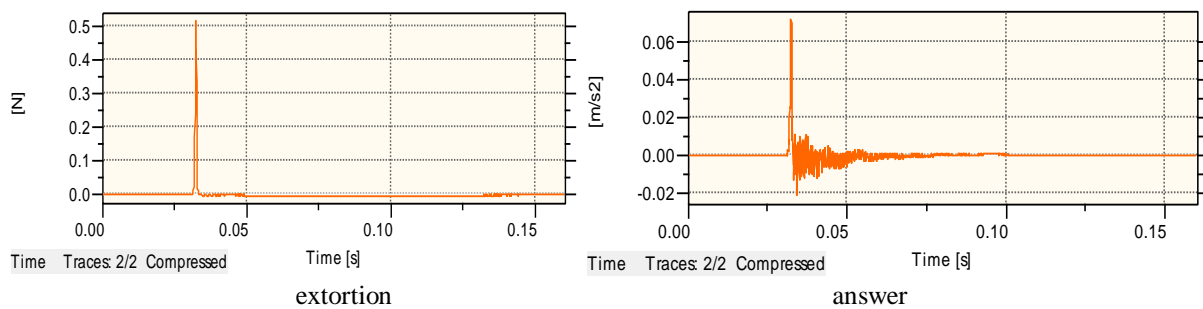
Outline.8. Example exposition of results of measurement - the own study

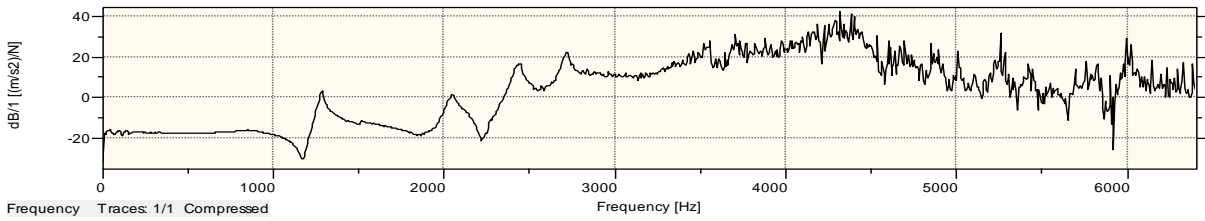
For a better visualization of the results of the investigation, the results are shown below separately for all axes. Every axle includes the graphic interpretation of input and output trembling signals and the FRF function that results from the extortion and answer frequencies.



FRF

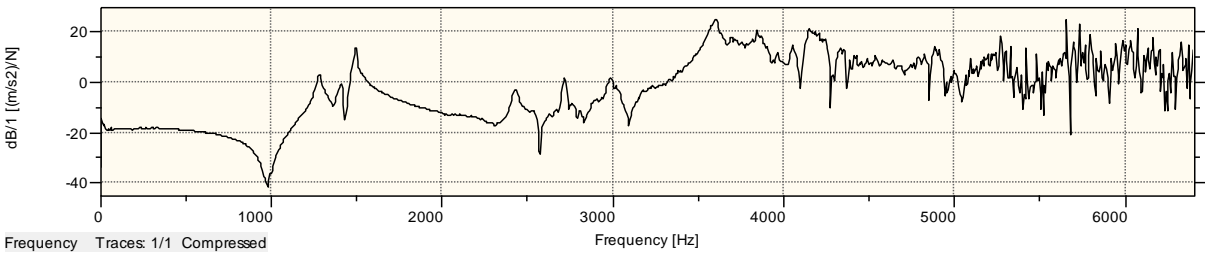
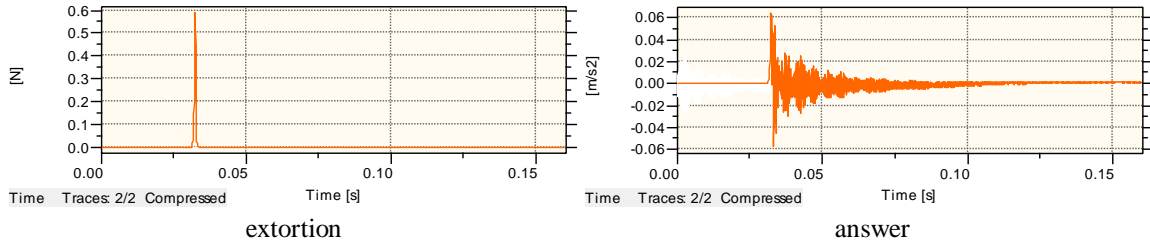
Outline.9. Composition of results of measurements (the temporary course of extortion, temporary course of answer, function the FRF) the full brick in axis X





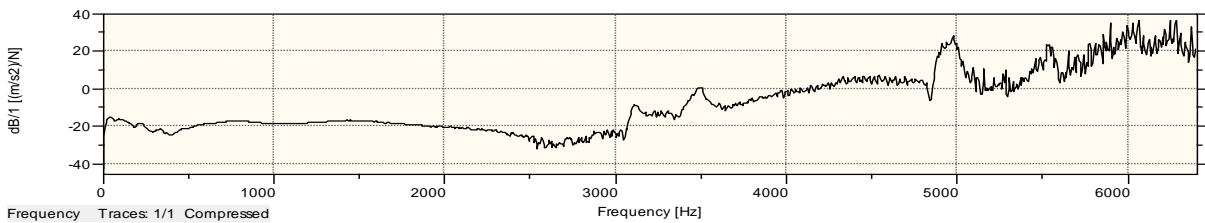
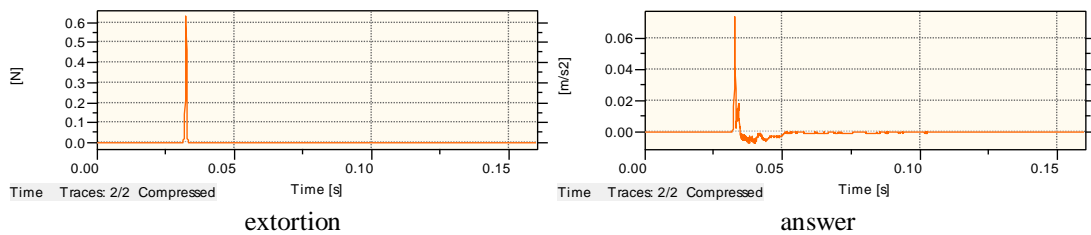
FRF

Outline.10. Composition of results of measurements (the temporary course of extortion, temporary course of answer, function the FRF) the damaged full brick in axis X



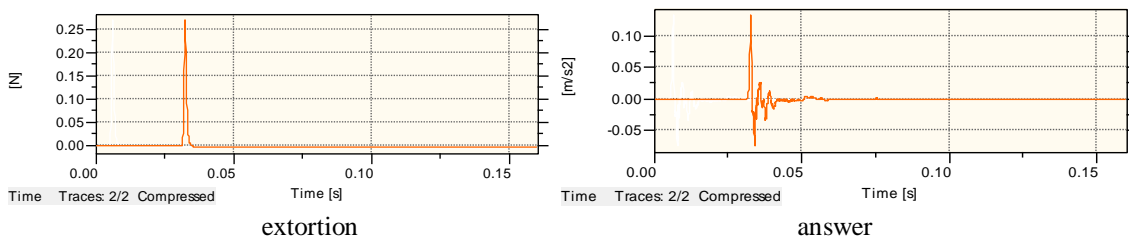
FRF

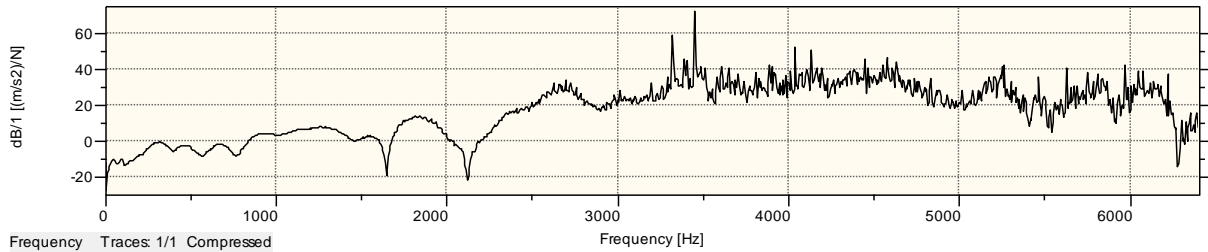
Outline.11. Composition of results of measurements (the temporary course of extortion, temporary course of answer, function the FRF) the full brick in axis Y



FRF

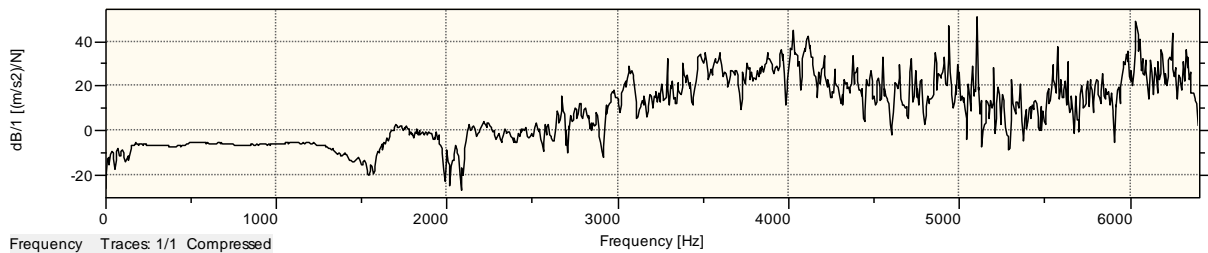
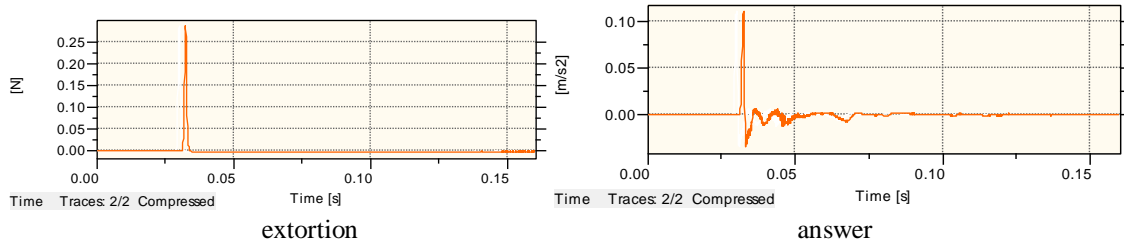
Outline.12. Composition of results of measurements (the temporary course of extortion, temporary course of answer, function the FRF) the damaged full brick in axis Y.





FRF

Outline.13. Composition of results of measurements (the temporary course of extortion, temporary course of answer, function the FRF) the full brick in axis Z.



FRF

Outline.13. Composition of results of measurements (the temporary course of extortion, temporary course of answer, function the FRF) the full brick in axis Z.

VI. Summary

The introduced results show the fact that the difference between good and bad materials can be observed from the quality of the FRF function generated through the passage of the signal from input to output. The change on the state of the studied construction materials can be reflected in the change of the value and the character of course of the FRF function. Therefore, the possibility exists of distinguishing the property of material constructions by using the experimental modal analysis. The performed identification investigations confirmed the usefulness of the LMS apparatus for investigations of constructional elements, what should be continued.

LITERATUR

- [1] Brunarski L.: Destructive methods of investigation of concrete. Arcade, Warsaw 1996.
- [2] Cempel C.: The basis the vibroacustik of diagnostics the machines. WNT, Warsaw 1982.
- [3] Cempel C., Tabaszewski M., Cracovian M.: The method of Extraction of Multidimensional Diagnostic Information, Materials XXX the Symposium Diagnostics of Machines, Hungarian Hill, 2003, s.109-118.
- [4] Cempel C.: Ekogospodarka - new challenges in education, investigations and technology. Meetings 2002.
- [5] Cempel C.: Innovative Developments in Systems Condition Monitoring, Keynote Lecture for DAMAS' 99, Damage Assessment of Structure Conference, Dublin 1999.
- [6] Cempel C.: Reduction of Redundancy of Symptom Observation Space in System Condition Monitoring. Bulletin of the Polish Academy of Sciences, Technical Sciences, Vol. 49, Just 2, 2001, pp267 - 284.
- [7] Carpenter's R.: Dynamic diagnostics in building. Building review, nr1 / 1993.
- [8] Carpenter's R.: The opinion of harmfulness of dynamic influences in building. Arcade, Warsaw 1973.
- [9] Carpenter's R.: The new possibilities of analysis and the diagnostics of antique buildings. Engineering and Building, No. 9/1998.
- [10] Carpenter's R.: The influence of dynamic burdens on murowe constructions. Workshop of the designer's work construction, Ustron 1999.
- [11] Der Kiureghian A.: And response spectrum method for random vibrations. Rep. Just. UCB / EERC -80-/ 15, Earth. Eng. Research Center, Univ. of California, Berkeley 1980.
- [12] Eykhoff P.: System identification, parameter and state estimation. N. Y. Pergamon Press 1981.

EXTREMALLY β -DISCONNECTEDNESS IN SMOOTH FUZZY β -CENTERED SYSTEM

T. Nithiya,¹ M.K. Uma,² E. Roja³

¹Department of Mathematics, Avs Engineering College, Salem-636003 Tamil Nadu, India

^{2,3}Department of Mathematics, Sri Sarada College for Women, Salem-636016 Tamil Nadu, India

Abstract: In this paper, we introduce maximal smooth fuzzy β -centered system, the smooth fuzzy space $\theta(R)$. Also extremally β -disconnectedness in smooth fuzzy β -centered system and its properties are studied.

Keywords: Maximal smooth fuzzy β -centered system, the smooth fuzzy space $\theta(R)$ and smooth fuzzy extremally β -disconnectedness.

2000 Mathematics Subject Classification: 54A40-03E72.

I. Introduction and Preliminaries

The concept of fuzzy set was introduced by Zadeh [8]. Since then the concept has invaded nearly all branches of mathematics. In 1985, a fuzzy topology on a set X was defined as a fuzzy subset T of the family I^X of fuzzy subsets of X satisfying three axioms, the basic properties of such a topology were represented by Sostak [6]. In 1992, Ramadan [4], studied the concepts of smooth topological spaces. The method of centered systems in the theory of topology was introduced in [3]. In 2007, the above concept was extended to fuzzy topological spaces by Uma, Roja and Balasubramanian [8]. In this paper, the method of β -centered system is studied in the theory of smooth fuzzy topology. The concept of extremally β -disconnectedness in maximal structure $\theta(R)$ of maximal smooth fuzzy β -centered system is introduced and its properties are studied.

Definition 1.1. [6]

A function $T: I^X \rightarrow I$ is called a smooth fuzzy topology on X if it satisfies the following conditions:

- a) $T(\bar{0}) = T(\bar{1}) = 1$
- b) $T(\mu_1 \wedge \mu_2) \geq T(\mu_1) \wedge T(\mu_2)$ for any $\mu_1, \mu_2 \in I^X$
- c) $T\left(\bigvee_{i \in \Gamma} \mu_i\right) \geq \bigwedge_{i \in \Gamma} T(\mu_i)$ For any $\{\mu_i\}_{i \in \Gamma} \in I^X$

The pair (X, T) is called a smooth fuzzy topological space.

Definition 1.2. [7]

Let R be a fuzzy Hausdroff space. A system $p = \{\lambda_\alpha\}$ of fuzzy open sets of R is called fuzzy centered system if any finite collection of fuzzy sets of the system has a non-zero intersection. The system p is called maximal fuzzy centered system or a fuzzy end if it cannot be included in any larger fuzzy centered system.

Definition 1.3. [7]

Let $\theta(R)$ denotes the collection of all fuzzy ends belonging to R . We introduce a fuzzy topology in $\theta(R)$ in the following way: Let P_λ be the set of all fuzzy ends that include λ as an element, where λ is a fuzzy open set of R . Now P_λ is a fuzzy neighbourhood of each fuzzy end contained in P_λ . Thus to each fuzzy open set of R , there corresponds a fuzzy neighbourhood P_λ in $\theta(R)$.

Definition 1.4. [7]

A fuzzy Hausdroff space R is extremally disconnected if the closure of an open set is open.

Definition 1.5. [1]

The fuzzy real line $R(L)$ is the set of all monotone decreasing elements $\lambda \in L^R$ satisfying $\bigvee \{\lambda(t) / t \in R\} = 1$ and $\bigwedge \{\lambda(t) / t \in R\} = 0$, after the identification of $\lambda, \mu \in L^R$ iff $\lambda(t-) = \mu(t-)$ and $\lambda(t+) = \mu(t+)$ for all $t \in R$, where $\lambda(t-) = \bigwedge \{\lambda(s) : s < t\}$ and $\lambda(t+) = \bigvee \{\lambda(s) : s > t\}$. The natural L -fuzzy topology on $R(L)$ is generated from the sub-basis $\{L_t, R_t\}$ where $L_t(\lambda) = \lambda(t-)$ and $R_t(\lambda) = \lambda(t+)$.

Definition 1.6. [2]

The L -fuzzy unit interval $I(L)$ is a subset of $R(L)$ such that $[\lambda] \in I(L)$ if $\lambda(t) = 1$ for $t < 0$ and $\lambda(t) = 0$ for $t > 1$.

Definition 1.7. [5]

A fuzzy set λ is quasi-coincident with a fuzzy set μ , denoted by $\lambda q \mu$, if there exists $x \in X$ such that $\lambda(x) + \mu(x) > 1$, otherwise $\lambda \not q \mu$.

II. The Spaces of maximal smooth fuzzy β -centered systems

In this section the maximal smooth fuzzy centered system is introduced and its properties are discussed.

Definition 2.1.

A smooth fuzzy topological space (X, T) is said to be smooth fuzzy β -Hausdorff iff for any two distinct fuzzy points x_{t_1}, x_{t_2} in X , there exists r -fuzzy β -open sets $\lambda, \mu \in I^X$ such that $x_{t_1} \in \lambda$ and $x_{t_2} \in \mu$ with $\lambda q \mu$.

Definition 2.2.

Let R be a smooth fuzzy β -Hausdorff space. A system $p_\beta = \{ \lambda_i \}$ of r -fuzzy β -open sets of R is called a smooth fuzzy β -centered system if any finite collection of $\{ \lambda_i \}$ is such that $\lambda_i \not q \lambda_j$ for $i \neq j$. The system p_β is called maximal smooth fuzzy β -centered system or a smooth fuzzy β -end if it cannot be included in any larger smooth fuzzy β -centered system.

Definition 2.3.

Let (X, T) be a smooth fuzzy topological space. Its $Q^*\beta$ -neighbourhood structure is a mapping $Q^* : X \times I^X \rightarrow I$ (X denotes the totality of all fuzzy points in X), defined by

$$Q^*(x_0^t, \lambda) = \sup \{ \mu : \mu \text{ is an } r\text{-fuzzy } \beta\text{-open set, } \mu \leq \lambda, x_0^t \in \mu \} \text{ and}$$

$$\lambda = \inf_{x_0^t q \lambda} Q^*(x_0^t, \lambda) \text{ is } r\text{-fuzzy } \beta\text{-open set.}$$

We note the following Properties of maximal smooth fuzzy β -centred system.

(1) If $\lambda_i \in p_\beta$ ($i = 1, 2, 3 \dots n$), then $\bigwedge_{i=1}^n \lambda_i \in p_\beta$.

Proof:

If $\lambda_i \in p_\beta$ ($i = 1, 2, 3 \dots n$), then $\lambda_i \not q \lambda_j$ for $i \neq j$. If $\bigwedge_{i=1}^n \lambda_i \notin p_\beta$, then $p_\beta \cup \{ \bigwedge_{i=1}^n \lambda_i \}$ will be a larger smooth fuzzy β -end than p_β .

This contradicts the maximality of p_β . Therefore, $\bigwedge_{i=1}^n \lambda_i \in p_\beta$.

(2) If $\bar{0} \neq \lambda < \mu$, $\lambda \in p_\beta$ and μ is an r -fuzzy β -open set, then $\mu \in p_\beta$.

Proof:

If $\mu \notin p_\beta$, then $p_\beta \cup \{ \mu \}$ will be a larger smooth fuzzy β -end than p_β . This contradicts the maximality of p_β . Therefore $\mu \in p_\beta$.

(3) If λ is r -fuzzy β -open set, then $\lambda \notin p_\beta$ iff there exists $\mu \in p_\beta$ such that $\lambda q \mu$.

Proof:

Let $\lambda \notin p_\beta$ be an r -fuzzy β -open set. If there exists no $\mu \in p_\beta$ such that $\lambda q \mu$, then $\lambda \not q \mu$ for all $\mu \in p_\beta$. That is, $p_\beta \cup \{ \lambda \}$ will be a larger smooth fuzzy β -end than p_β . This contradicts the maximality of p_β .

Conversely, suppose that there exists $\mu \in p_\beta$ such that $\lambda q \mu$. If $\lambda \in p_\beta$, then $\lambda \not q \mu$. Contradiction. Hence $\lambda \notin p_\beta$.

(3) If $\lambda_1 \vee \lambda_2 = \lambda_3 \in p_\beta$, λ_1 and λ_2 are r -fuzzy β -open sets in R with $\lambda_1 q \lambda_2$, then either $\lambda_1 \in p_\beta$ or $\lambda_2 \in p_\beta$.

Proof:

Let us suppose that both $\lambda_1 \in p_\beta$ and $\lambda_2 \in p_\beta$. Then $\lambda_1 \not q \lambda_2$. Contradiction. Hence either $\lambda_1 \in p_\beta$ or $\lambda_2 \in p_\beta$.

Note 2.1

Every smooth fuzzy β -centered system can be extended in atleast one way to a maximum one.

III. The Smooth Fuzzy maximal structure in $\theta(R)$.

In this section, smooth fuzzy maximal structure in the collection of all smooth fuzzy β -ends $\theta(R)$ is introduced and its properties are investigated.

Let $\theta(R)$ denotes the collection of all smooth fuzzy β -ends belonging to R . We introduce a smooth fuzzy maximal structure in $\theta(R)$ in the following way:

Let P_λ be the set of all smooth fuzzy β -ends that include λ as an element, where λ is a r -fuzzy β -open set of R . Now, P_λ is a smooth fuzzy Q^* β -neighbourhood structure of each smooth fuzzy β -end contained in P_λ . Thus to each r -fuzzy β -open set λ of R corresponds a smooth fuzzy Q^* β -neighbourhood structure P_λ in $\theta(R)$.

Proposition 3.1.

If λ and μ are r -fuzzy β -open sets, then

- (a) $P_{\lambda \vee \mu} = P_\lambda \cup P_\mu$.
- (b) $P_\lambda \cup P_{\bar{1}-C_{T(R)}(\lambda, r)} = \theta(R)$.

Proof:

(a) Let $p_\beta \in P_\lambda$. That is, $\lambda \in p_\beta$. Then by Property (2), $\lambda \vee \mu \in p_\beta$. That is, $p_\beta \in P_{\lambda \vee \mu}$. Hence $P_\lambda \cup P_\mu \subseteq P_{\lambda \vee \mu}$. Let $p_\beta \in P_{\lambda \vee \mu}$. That is, $\lambda \vee \mu \in p_\beta$. By the definition of P_λ , $\lambda \in p_\beta$ or $\mu \in p_\beta$. That is, $p_\beta \in P_\lambda$ or $p_\beta \in P_\mu$, therefore, $p_\beta \in P_\lambda \cup P_\mu$. This shows that $P_\lambda \cup P_\mu \supseteq P_{\lambda \vee \mu}$. Hence, $P_{\lambda \vee \mu} = P_\lambda \cup P_\mu$.

(b) If $p_\beta \notin P_{\bar{1}-C_{T(R)}(\lambda, r)}$, then $\bar{1} - C_{T(R)}(\lambda, r) \notin p_\beta$. That is, $\lambda \in p_\beta$ and $p_\beta \in P_\lambda$. Hence, $\theta(R) - P_{\bar{1}-C_{T(R)}(\lambda, r)} \subset P_\lambda$. If $p_\beta \in P_\lambda$, then $\lambda \in p_\beta$. That is, $\bar{1} - C_{T(R)}(\lambda, r) \notin p_\beta$, $p_\beta \notin P_{\bar{1}-C_{T(R)}(\lambda, r)}$. Therefore, $p_\beta \in \theta(R) - P_{\bar{1}-C_{T(R)}(\lambda, r)}$. That is, $P_\lambda \subset \theta(R) - P_{\bar{1}-C_{T(R)}(\lambda, r)}$. Hence, $P_\lambda \cup P_{\bar{1}-C_{T(R)}(\lambda, r)} = \theta(R)$.

Proposition 3.2.

$\theta(R)$ With the smooth fuzzy maximal structure described above is a smooth fuzzy β -compact space and has a base of smooth fuzzy Q^* β -neighbourhood structure $\{P_\lambda\}$ that are both r -fuzzy β -open and r -fuzzy β -closed.

Proof:

Each P_λ in $\theta(R)$ is a r -fuzzy β -open by definition and by (b) of Proposition 3.1, it follows that it is r -fuzzy β -closed. Thus $\theta(R)$ has a base of smooth fuzzy Q^* β -neighbourhood structure $\{P_\lambda\}$ that are both r -fuzzy β -open and r -fuzzy β -closed. We now show that $\theta(R)$ is smooth fuzzy β -compact. Let $\{P_{\lambda_\alpha}\}$ be a covering of $\theta(R)$ where each P_{λ_α} is r -fuzzy β -open. If it

is impossible to pick a finite sub covering from the covering, then no set of the form $\bar{1} - \bigvee_{i=1}^n \beta-C_{T(R)}(\lambda_{\alpha_i}, r)$ is $\bar{0}$, since otherwise the sets $P_{\lambda_{\alpha_i}}$ would form a finite covering of $\theta(R)$. Hence the sets $\bar{1} - \bigvee_{i=1}^n \beta-C_{T(R)}(\lambda_{\alpha_i}, r)$ form a smooth fuzzy β -centered system. It may be extended to a maximal smooth fuzzy β -centered system p_β . This maximal smooth fuzzy β -centered system is not contained in $\{P_{\lambda_\alpha}\}$ since it contains in particular, all the $\bar{1} - \beta-C_{T(R)}(\lambda_{\alpha_i}, r)$. This contradiction proves that $\theta(R)$ is smooth fuzzy β -compact.

IV. Smooth fuzzy Extremely β -Disconnectedness in the maximal structure $\theta(R)$.

Definition 4.1.

A smooth fuzzy β -Hausdorff space R is smooth fuzzy extremely β -disconnected if $\beta-C_{T(R)}(\lambda, r)$ is r -fuzzy β -open for any r -fuzzy β -open set λ , $r \in I_0$.

Proposition 4.1.

The maximal smooth fuzzy structure $\theta(R)$ of maximal smooth fuzzy β -centered system of R is smooth fuzzy extremely β -disconnected.

Proof:

The proof of this theorem follows from the following equation $P_{\bigvee_\alpha \lambda_\alpha} = \beta-C_{T(\theta(R))}(\bigcup_\alpha P_{\lambda_\alpha}, r)$, $r \in I_0$. If $\lambda < \mu$, it follows that $P_\lambda \subset P_\mu$ and therefore $\bigcup_\alpha P_{\lambda_\alpha} \subset \beta-C_{T(\theta(R))}(P_{\bigvee_\alpha \lambda_\alpha}, r)$. By Proposition 3.2, $P_{\bigvee_\alpha \lambda_\alpha}$ is r -fuzzy β -closed and therefore, $\beta-C_{T(\theta(R))}(\bigcup_\alpha P_{\lambda_\alpha}, r) \subset P_{\bigvee_\alpha \lambda_\alpha}$. Let p be an arbitrary element of $P_{\bigvee_\alpha \lambda_\alpha} = \bigcup_\alpha P_{\lambda_\alpha}$. Then by Pro.3.1 (a), $p_\beta \in \beta-C_{T(\theta(R))}(\bigcup_\alpha P_{\lambda_\alpha}, r)$. Therefore, $P_{\bigvee_\alpha \lambda_\alpha} \subset \beta-C_{T(\theta(R))}(\bigcup_\alpha P_{\lambda_\alpha}, r)$. Hence, $P_{\bigvee_\alpha \lambda_\alpha} = \beta-C_{T(\theta(R))}(\bigcup_\alpha P_{\lambda_\alpha}, r)$.

Note 4.1.

The maximal structure $\theta(R)$ of maximal smooth fuzzy β -centered system is smooth fuzzy extremally β -disconnected if $P_{\bigvee \lambda_\alpha} = \beta-C_{T(\theta(R))}(\bigcup_\alpha P_{\lambda_\alpha}, r)$ where λ_α 's r-fuzzy β -open sets. By Pro 3.1(a), it follows that $P_{\bigvee \lambda_\alpha} = \beta-C_{T(\theta(R))}(P_{\bigvee \lambda_\alpha}, r)$.

That is, $P_{\lambda_\Delta} = \beta-C_{T(\theta(R))}(P_{\lambda_\Delta}, r)$ where $\lambda_\Delta = \bigvee \lambda_\alpha$.

Proposition 4.2.

Let $\theta(R)$ be an maximal smooth fuzzy β -centered system of the smooth fuzzy β -Hausdorff space R . Then the following conditions are equivalent:

- (a) The space $\theta(R)$ is smooth fuzzy extremally β -disconnected.
- (b) For each r-fuzzy β -open P_{λ_Δ} , $\beta-I_{T(\theta(R))}(\theta(R) - P_{\lambda_\Delta}, r)$ is r-fuzzy β -closed, $r \in I_0$.
- (c) For each r-fuzzy β -open P_{λ_Δ} , $\beta-C_{T(\theta(R))}(P_{\lambda_\Delta}, r) + \beta-C_{T(\theta(R))}(\theta(R) - C_{T(\theta(R))}(P_{\lambda_\Delta}, r), r) = \theta(R)$, $r \in I_0$.
- (d) For every pair of collections of r-fuzzy β -open sets $\{P_{\lambda_\Delta}\}$ and $\{P_{\mu_\Delta}\}$ such that $\beta-C_{T(\theta(R))}(P_{\lambda_\Delta}, r) + P_{\mu_\Delta} = \theta(R)$, we have $\beta-C_{T(\theta(R))}(P_{\lambda_\Delta}, r) + \beta-C_{T(\theta(R))}(P_{\mu_\Delta}, r) = \theta(R)$, $r \in I_0$.

Proof:

(a) \Rightarrow (b).

Let $\theta(R)$ be an smooth fuzzy extremally β -disconnected space and suppose that P_{λ_Δ} be r-fuzzy β -open, $r \in I_0$. Now, $\beta-C_{T(\theta(R))}(P_{\lambda_\Delta}, r) = \theta(R) - \beta-I_{T(\theta(R))}(\theta(R) - P_{\lambda_\Delta}, r)$. Since $\theta(R)$ is smooth fuzzy extremally β -disconnected, $P_{\lambda_\Delta} = \beta-C_{T(\theta(R))}(P_{\lambda_\Delta}, r)$. Now, $P_{\lambda_\Delta} = \theta(R) - \beta-I_{T(\theta(R))}(\theta(R) - P_{\lambda_\Delta}, r)$. Since, P_{λ_Δ} is r-fuzzy β -open.

(b) \Rightarrow (c).

Suppose that P_{λ_Δ} be r-fuzzy β -open, $r \in I_0$. Then,

$$\begin{aligned} &\beta-C_{T(\theta(R))}(P_{\lambda_\Delta}, r) + \beta-C_{T(\theta(R))}(\theta(R) - \beta-C_{T(\theta(R))}(P_{\lambda_\Delta}, r), r) \\ &= \beta-C_{T(\theta(R))}(P_{\lambda_\Delta}, r) + \beta-C_{T(\theta(R))}(\beta-I_{T(\theta(R))}(\theta(R) - P_{\lambda_\Delta}, r), r) \\ &= \beta-C_{T(\theta(R))}(P_{\lambda_\Delta}, r) + \beta-I_{T(\theta(R))}(\theta(R) - P_{\lambda_\Delta}, r) \\ &= \beta-C_{T(\theta(R))}(P_{\lambda_\Delta}, r) + \theta(R) - \beta-C_{T(\theta(R))}(P_{\lambda_\Delta}, r) \\ &= \theta(R). \end{aligned}$$

(c) \Rightarrow (d).

Suppose that P_{λ_Δ} and P_{μ_Δ} are r-fuzzy β -open, $r \in I_0$, with

$$\beta-C_{T(\theta(R))}(P_{\lambda_\Delta}, r) + P_{\mu_\Delta} = \theta(R) \tag{4.3.1}$$

Now by (c), we have

$$\begin{aligned} \theta(R) &= \beta-C_{T(\theta(R))}(P_{\lambda_\Delta}, r) + \beta-C_{T(\theta(R))}(\theta(R) - \beta-C_{T(\theta(R))}(P_{\lambda_\Delta}, r), r) \\ &= \beta-C_{T(\theta(R))}(P_{\lambda_\Delta}, r) + \beta-C_{T(\theta(R))}(P_{\mu_\Delta}, r) \end{aligned} \tag{from (4.3.1)}$$

Hence, $\beta-C_{T(\theta(R))}(P_{\lambda_\Delta}, r) + \beta-C_{T(\theta(R))}(P_{\mu_\Delta}, r) = \theta(R)$.

(d) \Rightarrow (a).

Let us suppose that P_{μ_Δ} r-fuzzy β -open, $r \in I_0$ and let

$$P_{\lambda_\Delta} = \theta(R) - \beta-C_{T(\theta(R))}(P_{\mu_\Delta}, r) \tag{4.3.2}$$

This implies that P_{λ_Δ} is r-fuzzy β -open. By (d), we have

$$\beta-C_{T(\theta(R))}(P_{\lambda_\Delta}, r) + \beta-C_{T(\theta(R))}(P_{\mu_\Delta}, r) = \theta(R). \tag{4.3.3}$$

From (4.3.2) and (4.3.3) we have,

$P_{\lambda_\Delta} = \beta-C_{T(\theta(R))}(P_{\lambda_\Delta}, r)$. By Note 4.1, it follows that $\theta(R)$ is smooth fuzzy extremally β -disconnected.

Proposition 4.3.

Let $\theta(R)$ be the space of maximal smooth fuzzy β -centered system of the smooth fuzzy β -Hausdorff space R . Then, $\theta(R)$ is smooth fuzzy extremally β -disconnected iff for all r-fuzzy β -open P_{λ_Δ} and r-fuzzy β -closed P_{μ_Δ} with $P_{\lambda_\Delta} \subseteq P_{\mu_\Delta}$, $\beta-C_{T(\theta(R))}(P_{\lambda_\Delta}, r) \subseteq \beta-I_{T(\theta(R))}(P_{\mu_\Delta}, r)$, $r \in I_0$.

Proof:

Let P_{λ_Δ} be r-fuzzy β -open and P_{μ_Δ} be r-fuzzy β -closed, $r \in I_0$, with $P_{\lambda_\Delta} \subseteq P_{\mu_\Delta}$. Then $\beta-I_{T(\theta(R))}(P_{\lambda_\Delta}, r) \subseteq \beta-I_{T(\theta(R))}(P_{\mu_\Delta}, r)$. That is, $P_{\lambda_\Delta} \subseteq \beta-I_{T(\theta(R))}(P_{\mu_\Delta}, r)$. This implies that, $\beta-C_{T(\theta(R))}(P_{\lambda_\Delta}, r) \subseteq \beta-C_{T(\theta(R))}(\beta-I_{T(\theta(R))}(P_{\mu_\Delta}, r), r)$. By Proposition 4.2.(b), it follows that, $\beta-C_{T(\theta(R))}(P_{\lambda_\Delta}, r) \subseteq I_{T(\theta(R))}(P_{\lambda_\Delta}, r)$.

Conversely, suppose that $P_{\mu_{\Delta}}$ be r -fuzzy β -closed, $r \in I_0$. Then, $\beta-I_{T(\theta(R))}(P_{\mu_{\Delta}}, r) \subseteq P_{\mu_{\Delta}}$. By assumption, $\beta-C_{T(\theta(R))}(\beta-I_{T(\theta(R))}(P_{\mu_{\Delta}}, r), r) \subseteq \beta-I_{T(\theta(R))}(P_{\mu_{\Delta}}, r)$ (4.3.1)

But, $\beta-I_{T(\theta(R))}(P_{\mu_{\Delta}}, r) \subseteq \beta-C_{T(\theta(R))}(\beta-I_{T(\theta(R))}(P_{\mu_{\Delta}}, r), r)$ (4.3.2)

From (4.3.1) and (4.3.2), we get

$$\beta-I_{T(\theta(R))}(P_{\mu_{\Delta}}, r) = \beta-C_{T(\theta(R))}(\beta-I_{T(\theta(R))}(P_{\mu_{\Delta}}, r), r).$$

That is, $\beta-I_{T(\theta(R))}(P_{\mu_{\Delta}}, r)$ is r -fuzzy β -closed. By Proposition 4.2(b), it follows that $\theta(R)$ is smooth fuzzy extremally β -disconnected.

Remark 4.1.

Let $\theta(R)$ be an smooth fuzzy extremally β -disconnected space. Let $\{P_{\lambda_{\Delta_i}}, \theta(R) - P_{\mu_{\Delta_i}}, I \in N\}$ be a collection such that $P_{\lambda_{\Delta_i}}$ are r -fuzzy β -open and $P_{\mu_{\Delta_i}}$ are r -fuzzy β -closed, $r \in I_0$. Let $P_{\lambda_{\Delta}}, P_{\mu_{\Delta}}$ are both r -fuzzy β -open and r -fuzzy β -closed. If $P_{\lambda_{\Delta_i}} \subseteq P_{\lambda_{\Delta}} \subseteq P_{\mu_{\Delta_i}}$ and $P_{\lambda_{\Delta_i}} \subseteq P_{\mu_{\Delta_i}} \subseteq P_{\mu_{\Delta}}$, then there exists an $P_{\eta_{\Delta}}$ which is both r -fuzzy β -open and r -fuzzy β -closed such that $\beta-C_{T(\theta(R))}(P_{\lambda_{\Delta_i}}, r) \subseteq P_{\eta_{\Delta}} \subseteq \beta-I_{T(\theta(R))}(P_{\mu_{\Delta_i}}, r)$.

Proof:

By proposition 4.3, we have $\beta-C_{T(\theta(R))}(P_{\lambda_{\Delta_i}}, r) \subseteq \beta-C_{T(\theta(R))}(P_{\lambda_{\Delta}}, r) \cap \beta-I_{T(\theta(R))}(P_{\mu_{\Delta_i}}, r) \subseteq \beta-I_{T(\theta(R))}(P_{\mu_{\Delta_i}}, r)$. Therefore, $P_{\eta_{\Delta}} = \beta-C_{T(\theta(R))}(P_{\lambda_{\Delta}}, r) \cap \beta-I_{T(\theta(R))}(P_{\mu_{\Delta}}, r)$ is such that r -fuzzy β -open and r -fuzzy β -closed. Hence $\beta-C_{T(\theta(R))}(P_{\lambda_{\Delta_i}}, r) \subseteq P_{\eta_{\Delta}} \subseteq \beta-I_{T(\theta(R))}(P_{\mu_{\Delta_i}}, r)$.

Proposition 4.4.

Let $\theta(R)$ be an smooth fuzzy extremally β -disconnected space. Let $\{P_{\lambda_{\Delta_q}}\}_{q \in Q}$ and $\{P_{\mu_{\Delta_q}}\}_{q \in Q}$ be monotone increasing collections of r -fuzzy β -open and r -fuzzy β -closed sets and suppose that $P_{\lambda_{\Delta_{q_1}}} \subseteq P_{\mu_{\Delta_{q_2}}}$ whenever $q_1 < q_2$ (Q is the set of all rational numbers). Then there exists a monotone increasing collections $\{P_{\eta_{\Delta_q}}\}_{q \in Q}$ of r -fuzzy β -open and r -fuzzy β -closed sets such that $\beta-C_{T(\theta(R))}(P_{\lambda_{\Delta_{q_1}}}, r) \subseteq P_{\eta_{\Delta_{q_2}}}$ and $P_{\eta_{\Delta_{q_1}}} \subseteq \beta-I_{T(\theta(R))}(P_{\mu_{\Delta_{q_2}}}, r)$ whenever $q_1 < q_2$, for all r -fuzzy β -open sets $\lambda_{\Delta_q}, \mu_{\Delta_q}, \eta_{\Delta_q}, r \in I_0$.

Proof:

Let us arrange into a sequence $\{q_n\}$ of all rational numbers (without repetition). For every $n \geq 2$, we shall define inductively a collection $\{P_{\eta_{\Delta_{q_i}}} / 1 \leq i \leq n\}$ such that for all $i < n$

$$\left. \begin{aligned} \beta-C_{T(\theta(R))}(P_{\lambda_{\Delta_{q_i}}}, r) &\subseteq P_{\eta_{\Delta_{q_i}}} \text{ if } q < q_i \\ P_{\eta_{\Delta_{q_i}}} &\subseteq \beta-I_{T(\theta(R))}(P_{\mu_{\Delta_{q_i}}}, r) \text{ if } q_i < q \end{aligned} \right\} (S_n)$$

By Proposition 4.3.3, the countable collection $\{\beta-C_{T(\theta(R))}(P_{\lambda_{\Delta_{q_1}}}, r)\}$ and $\{\beta-I_{T(\theta(R))}(P_{\mu_{\Delta_{q_2}}}, r)\}$ satisfy $\beta-C_{T(\theta(R))}(P_{\lambda_{\Delta_{q_1}}}, r) \subseteq \beta-I_{T(\theta(R))}(P_{\mu_{\Delta_{q_2}}}, r)$ if $q_1 < q_2$. By Remark 4.3.1., there exists $P_{\delta_{\Delta_1}}$ which is both r -fuzzy β -open and r -fuzzy β -closed, with $\beta-C_{T(\theta(R))}(P_{\lambda_{\Delta_{q_1}}}, r) \subseteq P_{\delta_{\Delta_1}} \subseteq \beta-I_{T(\theta(R))}(P_{\mu_{\Delta_{q_2}}}, r)$. Setting $P_{\delta_{\Delta_1}} = P_{\eta_{\Delta_{q_1}}}$ we get (S_2) . Define $P_{\psi_{\Delta}} = \cup \{P_{\eta_{\Delta_{q_i}}} / i < n, q_i < q_n\} \cup P_{\lambda_{\Delta_{q_n}}}$ and $P_{\phi_{\Delta}} = \cap \{P_{\eta_{\Delta_{q_j}}} / j < n, q_j > q_n\} \cap P_{\mu_{\Delta_{q_n}}}$. Then, we have $\beta-C_{T(\theta(R))}(P_{\eta_{\Delta_{q_i}}}, r) \subseteq \beta-C_{T(\theta(R))}(P_{\psi_{\Delta}}, r) \subseteq \beta-I_{T(\theta(R))}(P_{\eta_{\Delta_{q_j}}}, r)$ and $\beta-C_{T(\theta(R))}(P_{\eta_{\Delta_{q_i}}}, r) \subseteq \beta-I_{T(\theta(R))}(P_{\phi_{\Delta}}, r) \subseteq \beta-I_{T(\theta(R))}(P_{\eta_{\Delta_{q_j}}}, r)$ whenever $q_i < q_n < q_j$ ($i < j < n$) and $P_{\lambda_{\Delta_{q_i}}} \subseteq \beta-C_{T(\theta(R))}(P_{\psi_{\Delta}}, r) \subseteq P_{\mu_{\Delta_{q_i}}}$ and $P_{\lambda_{\Delta_{q_i}}} \subseteq \beta-I_{T(\theta(R))}(P_{\phi_{\Delta}}, r) \subseteq P_{\mu_{\Delta_{q_i}}}$ whenever $q < q_n < q'$. This shows that the countable collections $\{P_{\eta_{\Delta_{q_i}}} / i < n, q_i < q_n\} \cup \{P_{\lambda_{\Delta_{q_i}}} / q < q_n\}$ and $\{P_{\eta_{\Delta_{q_j}}} / j < n, q_j > q_n\} \cup \{P_{\mu_{\Delta_{q_i}}} / q > q_n\}$ together with $P_{\psi_{\Delta}}$ and $P_{\phi_{\Delta}}$ fulfill all the conditions of Remark 4.1. Hence there exists a collection $P_{\delta_{\Delta_{q_n}}}$ which is r -fuzzy β -open and r -fuzzy β -closed such that

$$\begin{aligned} \beta-C_{T(\theta(R))}(P_{\delta_{\Delta_{q_n}}}, r) &\subseteq P_{\mu_{\Delta_{q_i}}} \text{ if } q > q_n. \\ P_{\lambda_{\Delta_{q_i}}} &\subseteq \beta-I_{T(\theta(R))}(P_{\delta_{\Delta_{q_n}}}, r) \text{ if } q < q_n \\ \beta-C_{T(\theta(R))}(P_{\eta_{\Delta_{q_i}}}, r) &\subseteq \beta-I_{T(\theta(R))}(P_{\delta_{\Delta_{q_n}}}, r) \text{ if } q_i < q_n \\ \beta-C_{T(\theta(R))}(P_{\delta_{\Delta_{q_n}}}, r) &\subseteq \beta-I_{T(\theta(R))}(P_{\eta_{\Delta_{q_j}}}, r) \text{ if } q_j > q_n \text{ where } 1 \leq i, j \leq n-1. \end{aligned}$$

Now setting $P_{\eta_{\Delta q_n}} = P_{\delta_{\Delta q_n}}$ we obtain the collections $P_{\eta_{\Delta q_1}}, P_{\eta_{\Delta q_2}}, \dots, P_{\eta_{\Delta q_n}}$, that satisfy (S_{n+1}) . Therefore the collection $\{ P_{\eta_{\Delta q_i}} / i = 1, 2, 3, \dots, n \}$ has the required property.

Definition 4.2.

Let $\theta(\mathbb{R})$ be an maximal smooth fuzzy β -centered system. The smooth fuzzy real line $\mathbb{R}^*(\mathbb{I})$ in smooth fuzzy β -centered system is the set of all monotone decreasing r -fuzzy β -sets $\{ P_{\lambda_{\Delta}} \}$ satisfying $\cup \{ P_{\lambda_{\Delta}(t)} / t \in \mathbb{R} \} = \theta(\mathbb{R})$ and $\cap \{ P_{\lambda_{\Delta}(t)} / t \in \mathbb{R} \} = \phi$, after the identification of $P_{\lambda_{\Delta}}$ and $P_{\mu_{\Delta}}$ iff $P_{\lambda_{\Delta}(t-)} = P_{\mu_{\Delta}(t-)}$ and $P_{\lambda_{\Delta}(t+)} = P_{\mu_{\Delta}(t+)}$ for all $t \in \mathbb{R}$, where $P_{\lambda_{\Delta}(t-)} = \cap \{ P_{\lambda_{\Delta}(s)} / s < t \}$ and $P_{\lambda_{\Delta}(t+)} = \cup \{ P_{\lambda_{\Delta}(s)} / s > t \}$. The natural smooth fuzzy topology on $\mathbb{R}^*(\mathbb{I})$ is generated from the sub-basis $\{ L_t^*, R_t^* \}$ where $L_t^*[P_{\lambda_{\Delta}}] = P_{\lambda_{\Delta}(t-)}$ and $R_t^*[P_{\lambda_{\Delta}}] = P_{\lambda_{\Delta}(t+)}$. A partial order on $\mathbb{R}^*(\mathbb{I})$ is defined by $[P_{\lambda_{\Delta}}] \leq [P_{\mu_{\Delta}}]$ iff $P_{\lambda_{\Delta}(t-)} \subseteq P_{\mu_{\Delta}(t-)}$ and $P_{\lambda_{\Delta}(t+)} \subseteq P_{\mu_{\Delta}(t+)}$ for all $t \in \mathbb{R}$.

Definition 4.3.

Let $\theta(\mathbb{R})$ be an maximal smooth fuzzy β -centered system. The smooth fuzzy unit interval $\mathbb{I}^*(\mathbb{I})$ in smooth fuzzy β -centered system is a subset of $\mathbb{R}^*(\mathbb{I})$ such that $[P_{\lambda_{\Delta}}] \in \mathbb{I}^*(\mathbb{I})$ if $P_{\lambda_{\Delta}(t)} = \theta(\mathbb{R})$ for $t < 0$ and $P_{\lambda_{\Delta}(t)} = \phi$ for $t > 1$ where λ_{Δ} 's are r -fuzzy β -open set and $t \in \mathbb{R}, r \in \mathbb{I}_0$.

Definition 4.4.

Let $\theta(\mathbb{R})$ be an maximal smooth fuzzy β -centered system. A mapping $f : \theta(\mathbb{R}) \rightarrow \mathbb{R}^*(\mathbb{I})$ is called lower (upper) smooth fuzzy β -continuous if $f^{-1}(R_t^*)$ (resp. $f^{-1}(L_t^*)$) is r -fuzzy β -open (resp. $f^{-1}(L_t^*)$ is r -fuzzy β -open and r -fuzzy β -closed set), for all $t \in \mathbb{R}, r \in \mathbb{I}_0$.

Proposition 4.5.

Let $\theta(\mathbb{R})$ be an maximal smooth fuzzy β -centered system. Let $f : \theta(\mathbb{R}) \rightarrow \mathbb{R}^*(\mathbb{I})$ be a mapping such that

$$f(P_{\lambda_{\Delta}(t)}) = \begin{cases} \theta(\mathbb{R}) & t < 0 \\ P_{\lambda_{\Delta}(t)} & 0 \leq t \leq 1 \\ \phi & t > 1 \end{cases}$$

Where λ_{Δ} is a r -fuzzy β -open set. Then f is lower (upper) smooth fuzzy β -continuous iff λ_{Δ} is a r -fuzzy β -open set (resp r -fuzzy β -closed).

Proof:

Now,

$$f^{-1}(R_t^*) = \begin{cases} \theta(\mathbb{R}) & t < 0 \\ 0 \leq t \leq 1 \\ \phi & t > 1 \end{cases}$$

implies that f is lower smooth fuzzy β -continuous iff $P_{\lambda_{\Delta}(t)}$ is r -fuzzy β -open.

Now,

$$f^{-1}(L_t^*) = \begin{cases} \theta(\mathbb{R}) & t < 0 \\ P_{\lambda_{\Delta}(t)} & 0 \leq t \leq 1 \\ \phi & t > 1 \end{cases}$$

implies that f is upper smooth fuzzy β -continuous iff $P_{\lambda_{\Delta}(t)}$ is r -fuzzy β -open and r -fuzzy β -closed.

Definition 4.5.

Let $\theta(\mathbb{R})$ be an maximal smooth fuzzy β -centered system. The characteristic function $\chi_{P_{\lambda_{\Delta}}}(P_{\lambda_{\Delta}})$ is a function $\chi_{P_{\lambda_{\Delta}}} : \theta(\mathbb{R}) \rightarrow \mathbb{I}^*(\mathbb{I})$ defined by $\chi_{P_{\lambda_{\Delta}}}(P_{\mu_{\Delta}}) = P_{\lambda_{\Delta}}$ if $P_{\mu_{\Delta}} \in \theta(\mathbb{R})$.

Definition 4.6.

Let $\theta(\mathbb{R})$ be an maximal smooth fuzzy β -centered system. Then $\chi_{P_{\lambda_{\Delta}}}$ is lower (resp. upper) smooth fuzzy β -continuous iff $P_{\lambda_{\Delta}}$ is r -fuzzy β -open (resp., $P_{\lambda_{\Delta}}$ is r -fuzzy β -open and r -fuzzy β -closed), $r \in \mathbb{I}_0$.

Definition 4.7.

Let $\theta(R)$ be an maximal smooth fuzzy β -centered system. Then $f : \theta(R) \rightarrow R^*(I)$ is said to be strongly smooth fuzzy β -continuous if $f^{-1}(R_t^*)$ is smooth fuzzy β -open and $f^{-1}(L_t^*)$ is both r-fuzzy β -open and r-fuzzy β -closed, for all $t \in R, r \in I_0$.

Proposition 4.7.

Let $\theta(R)$ be an maximal smooth fuzzy β -centered system. Then the following statements are equivalent :

- (a) $\theta(R)$ is an smooth fuzzy extremally β -disconnected space.
- (b) If $g, h : \theta(R) \rightarrow R^*(I)$, where g is lower smooth fuzzy β -continuous, h is upper smooth fuzzy β -continuous and $g \leq h$, then there exists a strong smooth fuzzy β -continuous function f such that $g \leq f \leq h$.
- (c) If $\theta(R) - P_{\lambda_\Delta}$ and P_{μ_Δ} are both r-fuzzy β -open and β -closed with $P_{\mu_\Delta} \subseteq P_{\lambda_\Delta}$, then there exist a strong smooth fuzzy β -continuous function $f : \theta(R) \rightarrow I$ such that $P_{\mu_\Delta} \subseteq (\theta(R) - L_1^*)f \subseteq R_0^*f \subseteq P_{\lambda_\Delta}$.

Proof:

(a) \Rightarrow (b)

Define $H_i = h^{-1}L_i^*$ and $G_i = g^{-1}(\theta(R) - R_i^*)$, $i \in Q$. Then we have two monotone increasing collections H_i which are r-fuzzy β -open sets and G_i r-fuzzy β -closed sets, $r \in I_0$. Moreover $H_i \subseteq G_j$ if $i < j$. By Proposition 4.3.4, there exists a monotone increasing collections of r-fuzzy β -open and r-fuzzy β -closed sets $\{ F_i \}_{i \in Q}$, such that $\beta-C_{T(\theta(R))}(H_i, r) \subseteq F_i$ and $F_i \subseteq \beta-I_{T(\theta(R))}(G_j, r)$ if $i < j$. Set $V_k = \bigcap_{i < k} (1 - F_i)$ such that V_k is a monotone decreasing collection of r-fuzzy β -open and r-fuzzy β -closed sets.

Moreover, $\beta-C_{T(\theta(R))}(V_k, r) \subseteq \beta-I_{T(\theta(R))}(V_j, r)$ whenever $k < j$.

$$\begin{aligned} \text{Therefore, } \bigcup_{k \in R} V_k &= \bigcup_{k \in R} \left(\bigcap_{i < k} (1 - F_i) \right) \\ &\supseteq \bigcup_{k \in R} \left(\bigcap_{i < k} (1 - G_i) \right) \\ &= \bigcup_{k \in R} \left(\bigcap_{i < k} g^{-1}(R_i^*) \right) \\ &= \bigcup_{k \in R} \left(g^{-1}(R_k^*) \right) \\ &= g^{-1} \left(\bigcup_{k \in R} R_k^* \right) \\ &= \theta(R). \end{aligned}$$

Similarly, $\bigcap_{k \in R} V_k = \phi$.

Define a function $f : \theta(R) \rightarrow R^*(I)$ satisfying the required properties. Let $f(P_{\lambda_\Delta_1}) = \eta_{\Delta_1}(t)$ where $P_{\eta_{\Delta_1}(t)}$ is a collection in V_k . To prove that f is strongly smooth fuzzy β -continuous. We observe that $\bigcup_{j > k} V_j = \bigcup_{j > k} \beta-I_{T(\theta(R))}(V_j, r)$ and $\bigcap_{j < k} V_j = \bigcap_{j < k} \beta-C_{T(\theta(R))}(V_j, r)$. Then $f^{-1}(R_k^*) = \bigcup_{j > k} V_j = \bigcup_{j > k} \beta-I_{T(\theta(R))}(V_j, r)$ is r-fuzzy β -open set and $f^{-1}(1 - L_k^*) = \bigcap_{j < k} V_j = \bigcap_{j < k} \beta-C_{T(\theta(R))}(V_j, r)$ is r-fuzzy β -closed and $f^{-1}(L_k^*)$ is r-fuzzy β -open set. Hence f is strongly smooth fuzzy β -continuous.

To show that $g \leq f \leq h$. That is, $g^{-1}(1 - L_t^*) \subseteq f^{-1}(1 - L_t^*) \subseteq h^{-1}(1 - L_t^*)$, $g^{-1}(R_t^*) \subseteq f^{-1}(R_t^*) \subseteq h^{-1}(R_t^*)$.

$$\begin{aligned} \text{Now, } g^{-1}(1 - L_t^*) &= \bigcap_{s < t} g^{-1}(1 - L_s^*) \\ &= \bigcap_{s < t} \bigcap_{p < s} g^{-1}(R_p^*) \\ &= \bigcap_{s < t} \bigcap_{p < s} (1 - G_p) \\ &\subseteq \bigcap_{s < t} \bigcap_{p < s} (1 - F_p) \\ &= \bigcap_{s < t} V_s \\ &= f^{-1}(1 - L_t^*) \\ f^{-1}(\theta(R) - L_t^*) &= \bigcap_{s < t} V_s \end{aligned}$$

$$\begin{aligned}
 &= \bigcap_{s < t} \bigcap_{p < s} (1 - F_p) \\
 &\subseteq \bigcap_{s < t} \bigcap_{p < s} (1 - H_p) \\
 &= \bigcap_{s < t} \bigcap_{p < s} h^{-1}(1 - L_p^*) \\
 &= \bigcap_{s < t} h^{-1}(1 - L_s^*) \\
 &= h^{-1}(1 - L_t^*)
 \end{aligned}$$

Similarly we obtain,

$$\begin{aligned}
 g^{-1}(R_t^*) &= \bigcup_{s > t} g^{-1}(R_s^*) \\
 &= \bigcup_{s > t} \bigcup_{p > s} g^{-1}(R_p^*) \\
 &= \bigcup_{s > t} \bigcup_{p > s} (1 - G_p) \\
 &\subseteq \bigcup_{s > t} \bigcap_{p < s} (1 - F_p) \\
 &= \bigcup_{s > t} V_s \\
 &= f^{-1}(R_t^*) \text{ and}
 \end{aligned}$$

$$\begin{aligned}
 f^{-1}(R_t^*) &= \bigcup_{s > t} V_s \\
 &= \bigcup_{s > t} \bigcap_{p < s} (1 - F_p) \\
 &\subseteq \bigcup_{s > t} \bigcap_{p < s} (1 - H_p) \\
 &= \bigcup_{s > t} \bigcap_{p < s} h^{-1}(1 - L_p^*) \\
 &= \bigcup_{s > t} h^{-1}(R_s^*) \\
 &= h^{-1}(R_t^*).
 \end{aligned}$$

Thus (b) is proved.

(b) \Rightarrow (c)

Suppose P_{λ_Δ} is r-fuzzy β -open set and r-fuzzy β -closed set and P_{μ_Δ} is r-fuzzy β -open set and r-fuzzy β -closed set with $P_{\mu_\Delta} \subseteq P_{\lambda_\Delta}$. Then $\chi_{P_{\mu_\Delta}} \subseteq \chi_{P_{\lambda_\Delta}}$, where $\chi_{P_{\mu_\Delta}}$, $\chi_{P_{\lambda_\Delta}}$ are lower and upper smooth fuzzy β -continuous function respectively. By (b), there exist a strongly smooth fuzzy β -continuous function $f : \theta(R) \rightarrow R(I)$ such that $\chi_{P_{\mu_\Delta}} \leq f \leq \chi_{P_{\lambda_\Delta}}$. Clearly $f(P_{\lambda_\Delta}) \in I^*(I)$ and $P_{\mu_\Delta} = (1 - L_1^*)\chi_{P_{\mu_\Delta}} \subseteq (1 - L_1^*)f \subseteq R_0^*f \subseteq R_0^* \chi_{P_{\lambda_\Delta}} \subseteq P_{\lambda_\Delta}$. Therefore, $P_{\mu_\Delta} \subseteq (1 - L_1^*)f \subseteq R_0^*f \subseteq P_{\lambda_\Delta}$.

(c) \Rightarrow (a)

By (c), it follows that $(1 - L_1^*)f$ and R_0^*f are r-fuzzy β -open and r-fuzzy β -closed. By Proposition 4.3, it follows that $\theta(R)$ is an smooth fuzzy extremally β -disconnected space.

V. Tietze Extension Theorem

In this section, Tietze Extension Theorem for smooth fuzzy extremally β -disconnected space is discussed.

Proposition 5.1.

Let $\theta(R)$ be a smooth fuzzy extremally β -disconnected space. Let $A \subseteq \theta(R)$ and the collection $\{ P_{\lambda_\Delta} \}$ in A such that $\chi_{P_{\lambda_\Delta}}$ is r-fuzzy β -open. Let $f : A \rightarrow I^*(I)$ be a strongly smooth fuzzy β -continuous function. Then, f has a strongly smooth fuzzy β -continuous extension over $\theta(R)$.

Proof:

Let $g, h : \theta(\mathbb{R}) \rightarrow I^*(I)$ be such that $g = f = h$ on A .

Now,

$$R_t^*g = \begin{cases} P_{\mu_{\Delta t}} \wedge \chi_{P_{\lambda_{\Delta}}} & \text{if } t \geq 0 \\ \theta(\mathbb{R}) & \text{if } t < 0 \end{cases} \text{ where } P_{\mu_{\Delta t}} \text{ is } r\text{-fuzzy } \beta\text{-open}$$

set and is such that $P_{\mu_{\Delta t}} = R_t^*g$ in A .

$$L_t^*h = \begin{cases} P_{\lambda_{\Delta t}} \wedge \chi_{P_{\lambda_{\Delta}}} & \text{if } t \leq 1 \\ \theta(\mathbb{R}) & \text{if } t > 1 \end{cases} \text{ where } P_{\lambda_{\Delta t}} \text{ is both } r\text{-fuzzy } \beta\text{-open and } \beta\text{-closed set is such that}$$

$P_{\lambda_{\Delta t}} = L_t^*h$ in A . Thus g is lower smooth fuzzy β -continuous, h is upper smooth fuzzy β -continuous and $g \leq h$. By

Proposition 4.7, there is a strong smooth fuzzy β -continuous function $F: \theta(\mathbb{R}) \rightarrow I^*(I)$ such that $g \leq F \leq h$. Hence $f \equiv F$ on A .

REFERENCES

- [1] GANTNER.T.E., STEINLAGE.R.C and WARREN.R.H: Compactness in fuzzy topological; spaces, J. Math. Anal. Appl., 62 (1978), 547-562.
- [2] HUTTON.B. : Normality in fuzzy topological spaces, J. Math. Anal. Appl., 43 (1973), 734-742.
- [3] ILLIADIS and FOMIN.S: The method of centred systems in the theory of topological spaces, N, 21(1966), 47 - 66.
- [4] RAMADAN A.A: A smooth topological spaces, Fuzzy Sets and Systems 48,371 (1992).
- [5] RAMADAN A.A, ABBAS. S.E. and ABD EL LATIF A.A.: On fuzzy bitopological spaces in Sostak's sense, Commun. Korean Math.Soc., 21 [2006] , 865 – 877.
- [6] SOSTAK A.P.: On a fuzzy topological structure. Rend. Circ. Matern Palermo (Ser II), 11 (1985), 89 – 103
- [7] UMA M.K., ROJA.E, BALASUBRAMANIAN.G: The method of centred systems in fuzzy topological spaces, The Journal of fuzzy mathematics, 15(4), 2007, 1 – 7.
- [8] ZADEH L.A.: Fuzzy sets. Information and Control, 8(1965), 338 – 353.

Efficient Image Retrieval Using Indexing Technique

Mr.T.Saravanan,¹ S.Dhivya,² C.Selvi³

Asst Professor/Dept of Computer Science Engineering, Selvam College Of Technology Namakkal

Abstract: Content Based Image Retrieval (CBIR) is an automatic process to search relevant images based on user input. The input could be parameters, sketches or example images. A typical CBIR process first extracts the image features and store them efficiently. Then it compares with images from the database and returns the results. Besides reading existing information, which already exists in digital photographs, and transformation of this information to MPEG-7, RF supports the creation of new metadata. Semantic information about the image is presented as directed graph, where the nodes reflect semantic objects, locations, agents, states, times or concepts and the edges define the relations between these semantic entities. To enhance retrieval efficiency content-based metadata is extracted and new instances of the image for faster visualization, like thumbnails, are created. The MPEG-7 description consists of the following parts: metadata description, creation information, media information, textual annotation, semantics, and visual descriptors.

Index Term: Text classification; Feature selection; K-Nearest Neighbor; Naïve Bayesian

I. INTRODUCTION

Content-Based image retrieval (CBIR) systems analyze the visual content description to organize and find images in databases. The retrieval process usually relies on presenting a visual query (natural or synthetic) to the systems, and extracting from a database the set of images that best fit the user request. Such mechanism, referred to as query-by-example, requires the definition of an image representation (a set of descriptive features) and of some similarity metrics to compare query and target images.

Several years of research in this field highlighted a number of problems related to this (apparently simple) process.

According to this, several additional mechanisms have been introduced to achieve better performance. Among them, relevance feedback (RF) proved to be a powerful tool to iteratively collect information from the user and transform it into a semantic bias in the retrieval process. RF increases the retrieval performance thanks to the fact that it enables the system to learn what is relevant or irrelevant to the user across successive retrieval-feedback cycles.

II. CONTENT BASED IMAGE RETRIEVAL

Content Based Image Retrieval (CBIR) is an automatic process to search relevant images based on user input. The input could be parameters, sketches or example images. A typical CBIR process first extracts the image features and store them efficiently. Then it compares with images from the database and returns the results. Besides reading existing information, which already exists in digital photographs, and transformation of this information to MPEG-7, RF supports the creation of new metadata. Semantic information about the image is presented as directed graph, where the nodes reflect semantic objects, locations, agents, states, times or concepts and the edges define the relations between these semantic entities.

The experimental metadata based image retrieval; Different types of retrieval mechanisms are supported:

- Content based image retrieval using the MPEG-7 descriptors Color Layout, Edge Histogram and Scalable Color.
- Graph based retrieval supporting wildcards for semantic relations and semantic objects.
- 2D data repository and result set visualization based on Fast Map & FDP algorithms.

Algorithms of feature extraction and similarity measure are very dependent on the features used. In each feature, there would be more than one representation. Among these representations, histogram is the most commonly used technique to describe features.

This introduces the techniques of CBIR, including a review on features used, feature representation and similarity measure.

1. Scalable Color Extraction Process
2. Color Layout Extraction Process
3. Edge Histogram Extraction Process
4. Scalable+ Color Extraction Process
5. Scalable+Color+EdgeExtraction Process.

2.1 RELEVANCE FEEDBACK

Here you can annotate the photos with free text and you can rate the quality. Pre existing metadata like EXIF or IPTC tags inside images is loaded and converted to MPEG-7. Here the second panel, the semantic description panel, is shown. It offers a tool for visual creation of MPEG-7 based semantic descriptions using a drawn directed graph. On the feature extraction panel the low-level descriptors that are automatically extracted are shown. Extracted MPEG-7 descriptors are Colour Layout, Scalable Colour and Edge Histogram.

The Characteristics of the Relevance Feedback

Since the general assumption is that every user.s need is different and time varying, the database cannot adopt a fixed clustering structure; and the total number of classes and the class membership are not available before-hand since these are assumed to be user-dependent and time varying as well. Of course, these rather extreme assumptions can be relaxed in a real-world application to the degree of choice.

A typical scenario for relevance feedback in content-based image retrieval is as follows:

- Step 1.** Machine provides initial retrieval results, through query-by-keyword, sketch, or example, etc.
- Step 2.** User provides judgment on the currently displayed images as to whether, and to what degree, they are relevant or irrelevant to her/his request.
- Step 3.** Machine learns and tries again. Go to step 2. If each image/region is represented by a point in a feature space, relevance feedback with only positive (i.e., relevant) examples can be cast as a density estimation or novelty detection .Scholkopf problem; while with both positive and negative training examples it becomes a classification problem, or an on-line learning problem in a batch mode, but with the following characteristics associated with this specific application scenario:

As MPEG-7 is a complex XML based standard, it would be no good idea to confront the user with a XML editor and an instruction manual as tools for expressing the semantics of a photo. As a result “Image RF”, was designed for supporting the user in the time consuming task of annotating photos.

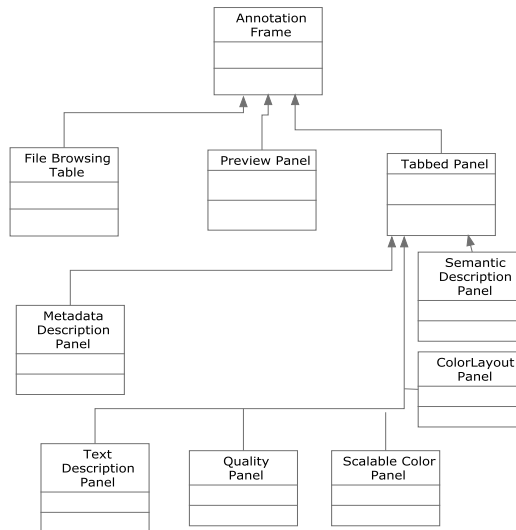


Fig1: Simplified RF UML diagram

Central part of RF is the so called “semantic description panel”. It allows the user to define semantic objects like agents, places, events and times which are saved on exit for reusing them the next time starting RF. These semantic objects can also be imported from an existing MPEG-7 file to allow exchange of objects between users and editing and creating those objects in a user preferred tool.

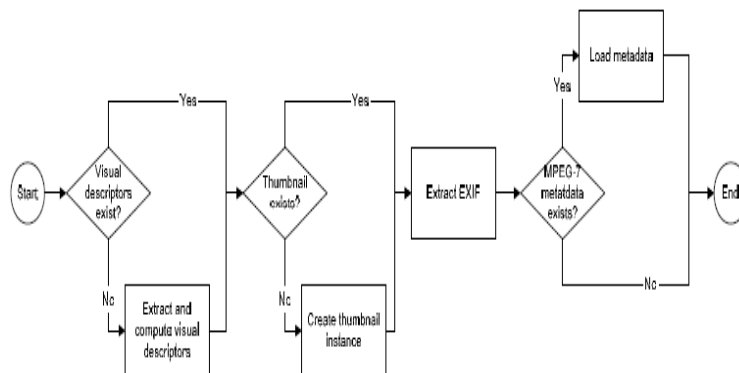


Fig 2. Loading an image for RF

Further a whole series can be pre-annotated for simplifying and speeding up the task of annotating multiple images. All images within the same context are placed in one file system folder and the user opens the first one using RF.

2.2 EDGE HISTOGRAM IMPLEMENTATION

MPEG-7 Visual Standard specifies a set of descriptors that can be used to measure similarity in images or video. Among them, the Edge Histogram Descriptor describes edge distribution with a histogram based on local edge distribution in an image. Since the Edge Histogram Descriptor recommended for the MPEG-7 standard represents only local edge distribution in the image, the matching performance for image retrieval may not be satisfactory. This paper proposes the use of global and semi-local edge histograms generated directly from the local histogram bins to increase the matching performance.

The image array is divided into DCT 4x4 sub images. Each sub image is further partitioned into non-overlapping square image blocks whose size depends on the resolution of the input image. The edges in each image-block are categorized into one of the following six types: vertical, horizontal, 45± diagonal, 135± diagonal, non directional Edge and no-edge. Now a 5-bin edge histogram of each sub image can be obtained. Each bin value is normalized by the total number of image-blocks in the sub image. The normalized bin values are nonlinearly quantized edge.

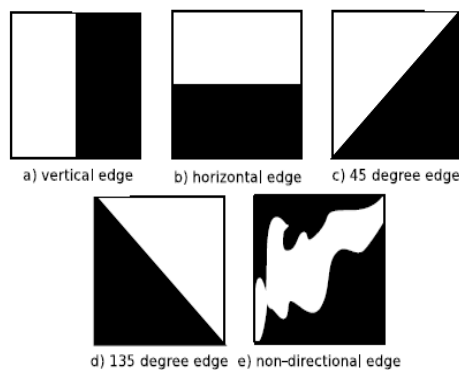


Fig3: Five different Edge Value

In this case, that particular image-block does not contribute to any of the 5 edge bins. Consequently, each image-block is classified into one of the 5 types of edge blocks or a nonedge block. Although the nonedge blocks do not contribute to any histogram bins, each histogram bin value is normalized by the total number of image-blocks including the nonedge blocks. This implies that the summation of all histogram bin values for each sub-image is less than or equal to 1.

2.3 COLOR LAYOUT IMPLEMENTATION

MPEG-7 Visual Standard specifies a set of descriptors that can be used to retrieve similar images from digital photo repository. Among them, the Color Layout Descriptor (CLD) represents the spatial distribution of colors in an image. The Edge Histogram Descriptor (EHD) describes edge distribution with a histogram based on local edge distribution in an image. These two features are very powerful features for CBIR systems, especially sketch-based image retrieval. Further, combining color and texture features in CBIR systems leads to more accurate results for image retrieval. In both the Color Layout Descriptor (CLD) and the Edge Histogram Descriptor (EHD), image features like color and edge distribution can be localized in separate 4 x 4 sub-images.

The image array is partitioned into 8x8 blocks. Representative colours are selected and expressed in YCbCr colour space. Each of the three components (Y, Cb and Cr) is transformed by 8x8 DCT (Discrete Cosine Transform). The resulting sets of DCT coefficients are zigzag-scanned and the first few coefficients are nonlinearly quantized to form the descriptor.

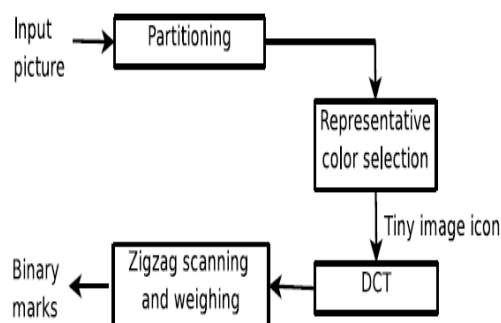


Fig4:the CLD extraction process

Step1: The image was loaded using *opencv* and the width and height of the image was obtained, from which the block width and block height of the *CLD* were calculated by dividing by 8. The division was done using truncation, so that if the image dimensions were not divisible by 8, the outermost pixels are not considered in the descriptor.

Step 2: Using the obtained information, the image data was parsed into three *4D* arrays, one for each color component, were a block can be accessed as a whole and pixels within each block could also be accessed by providing the index of the block and the index of the pixel inside the block.

Step3: A representative color was chosen for each block by averaging the values of all the pixels in each block. This results in three 8×8 arrays, one for each color component. This step is directly visualized in the first window of figure 2.

Step4 each 8×8 matrix was transformed to the *YCbCr* color space.

Step5: These will be again transformed by 8×8 *DCT* (Discrete Cosine Transform) to obtain three 8×8 *DCT* matrices of coefficients, one for each *YCbCr* component.

Step6: The *CLD* descriptor was formed by reading in zigzag order six coefficients from the *Y-DCT* matrix and three coefficients from each *DCT* matrix of the two chrominance components. The descriptor is saved as an array of 12 values.

2.4 DOMINANT COLOR DESCRIPTOR

This descriptor specifies a set of dominant colors in an image. It is good to represent color features where a small number of colors are enough to characterize the color information. The extraction algorithm quantizes the pixel color values into a set of dominant colors

2.5 SCALABLE COLOR DESCRIPTOR

This descriptor performs color histogram in HSV color space encoded by a Haar transform [MPEG, 2002]. The extraction is done by quantizing the image into a 256 bin HSV color space histogram and then using the Haar transform to reduce the number of bins. The output of the method is a vector with integer components, presented by a histogram with 64, 32 or 16 bins. The distance matching can be done either in the Haar coefficient domain or in the histogram domain. In the case where only the coefficient signs are retained, the matching can be done efficiently in the Haar coefficient domain by calculating the Hamming distance as the number of bit positions at which the binary bits are different using an XOR operation on the two descriptors to be compared.

III. IMAGE RETRIEVAL

3.1 QUERY REWEIGHTING

Some previous work keeps an eye on investigating what visual features are important for those images (positive examples) picked up by the users at each feedback (also called iteration in this paper). The notion behind QR is that, if the *i*th feature *f_i* exists in positive examples frequently, which convert image feature vectors to weighted-term vectors in early version of Multimedia Analysis and Retrieval another interactive approach that allows the user to submit a coarse initial query to refine her/his need via a set of relevance feedbacks.

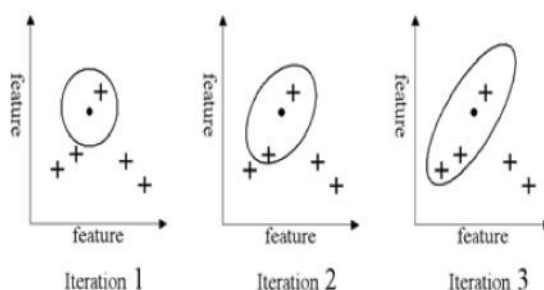


Fig5. Relevance feedback with generalized QR technique

3.2 QUERY POINT MOVEMENT

Another solution for enhancing the accuracy of image retrieval is moving the query point toward the contour of the user's preference in feature space. QPM regards multiple positive examples as a new query point at each feedback. After several forceful changes of location and contour, the query point should be close to a convex region of the user's interest. Further, combining color and texture features in CBIR systems leads to more accurate results for image retrieval.

3.3 QUERY EXPANSION

Because QR and QPM cannot elevate the quality of RF, QEX has been another hot technique in the solution space of RF recently. That is, straightforward search strategies, such as QR and QPM, cannot completely cover the user's interest spreading in the broad feature space.

Retrieval offers four different ways to search for a matching photo:

1. Searching through an XPath statement.
2. Defining search options through textboxes with various options.
3. Content based image retrieval using the visual descriptors ColorLayout and ScalableColor defined in the MPEG-7 standard.
4. Searching for a similar semantic description graph.

3.4 XPATH SEARCH

The first option is mainly used for developers and debugging of XPath statements, because all other retrieval mechanisms use XPath as query language. To search for matching documents using XPath requires detailed knowledge of the structure of the documents being searched, although basic statements like `//*[contains(.,'textToSearchFor')]` could be used querying documents without knowing the structure, but these statements only offer minimal retrieval features.

3.5 SEMANTIC SEARCH

The component of most interest is the panel offering a search mechanism for searching semantic descriptions.

This component allows the user to define a graph with minimum one to maximum three nodes and two possible relations. An asterisk is used as wildcard. A search graph which only contains one node with a word defining this node will return each MPEG-7 document wherein a semantic object containing the specified word is

IV. CONCLUSION AND FUTURE WORK

The process is about image search engine, not by text RF to the image by an end user, but also by the visual contents available into the image itself. The process reduces the number of required iterations and improves overall retrieval performance and Time will be consumed. That we can guarantee to get intended target.

The data stored and retrieved is accurate and gives enough information whenever the data is required in required format. All modules consist of necessary reports to help the user of the project to work easily and user-friendly. MPEG-7 matches many of the current requirements for a metadata standard for usage in a personal digital

Future work of this project is CBIR Systems prove that our approach is able to reach any given target image with fewer iterations in the worst and average cases. The application can be enhanced with the needs of the company. This project useful for image searching, in feature it is planned to connect semantic web-based image retrieval and facial recognition. This project increased efficiency and time consuming.

REFERENCES

- [1] D.H. Kim and C.W. Chung, "Qcluster: Relevance Feedback Using Adaptive Clustering for Content-Based Image Retrieval," Proc. ACM SIGMOD, pp. 599-610, 2003.
- [2] T. Qin, X.D. Zhang, T.Y. Liu, D.S. Wang, W.Y. Ma, and H.J. Zhang, "An Active Feedback Framework for Image Retrieval," Pattern Recognition Letters, vol. 29, pp. 637-646, Apr. 2008.
- [3] Sanjay N Talbar, Satishkumar L. Varma Color Spaces for Transform-based Image Retrieval" International Journal of Computer Applications (0975 – 8887) Volume 9– No.12, November 2010.
- [4] Mattia Broilo, Student Member, IEEE, and Francesco G. B. De Natale, Senior Member, IEEE, A Stochastic Approach to Image Retrieval Using Relevance Feedback and Particle Swarm Optimization IEEE TRANSACTIONS ON MULTIMEDIA, VOL. 12, NO. 4, JUNE 2010.
- [5] Wei Bian and Dacheng Tao, Member, IEEE Biased Discriminant Euclidean Embedding for Content-Based Image Retrieval, IEEE TRANSACTIONS ON IMAGE PROCESSING, VOL. 19, NO. 2, FEBRUARY 2010.
- [6] Danzhou Liu, Student Member, IEEE, Kien A. Hua, Senior Member, IEEE, Khanh Vu, and Ning Yu, Fast Query Point Movement Techniques for Large CBIR Systems, IEEE TRANSACTIONS ON KNOWLEDGE AND DATA ENGINEERING 2008.

Fuzzy Based Hysteresis Current Controlled Shunt Active Power Filter for Power Conditioning

P. V. Ram Kumar,¹ M. Surya Kalavathi²

¹Department of Electrical and Electronics Engineering, R.S.R Engineering College, Kavali, Nellore District, Andhra Pradesh, INDIA-524201

²Department of Electrical and Electronics Engineering, J.N.T.U. College of Engg, Hyderabad, INDIA – 500085

Abstract: Shunt Active power filters (SAPF) technology has emerged nowadays as a very suitable option for power quality improvement in electrical power systems control. This paper presents the simulation study of a fuzzy logic hysteresis band current controlled, three-phase SAPF to enhance power quality by harmonic elimination, power-factor correction, reactive power compensation and balancing of nonlinear loads. The advantage of fuzzy control is that it is based on a linguistic description and does not require a mathematical model of the system. Further, in this paper, the hysteresis based current control method is implemented for pulse width-modulation (PWM) switching signals. Results obtained by simulations with Matlab/Simulink show that dynamic behavior of the fuzzy controller is more effective than the conventional proportional-integral (PI) controller method on compensating reactive power and harmonic currents of the load. It is found to be more robust to changes in load and other system parameters compared to the conventional PI controller under steady state and transient conditions.

Keywords: Fuzzy logic controller, Hysteresis band current control, Power quality improvement, and Shunt active power filter

I. INTRODUCTION

Shunt active power filters (SAPF) represent a feasible solution to the problems caused by the non-linear loads. These loads draw non-sinusoidal currents from the 3-phase sinusoidal, balanced voltages which are classified as identified and unidentified loads. The SAPF can compensate for the harmonics, correct the power factor and work as a reactive power compensator, thus providing enhancement of power quality in the system [1, 2]. The control scheme of a SAPF must calculate the current reference waveform for each phase of the inverter, maintain the dc voltage constant, and generate inverter gating signals. The current reference circuit generates the reference currents required to compensate the load current harmonics and reactive power, and also try to maintain constant the dc voltage across the capacitor [3].

In literature [1- 14], most reference compensation current strategies of the SAPF are determined either with or without reference-frame transformations. For instance, the theory proposed in [1, 2] requires transformation of both source voltages and load currents from the a-b-c reference frame to α - β reference frame to determine the SAPF reference compensation currents in the three-phase three-wire system. For detecting the reference compensating current, the instantaneous active and reactive power theory (p-q theory) are widely used, which can provide an instantaneous and accurate reference compensating current [2, 3]. Grady *et al.* [4] have presented a survey of active power line conditioning methodologies with a list of the advantages and limitations of each one. Cavallini and Montanari [5] have proposed the unity power factor strategy known as classic strategy in which conditions the line currents to fit the voltage waveform, provides line current RMS values always lower than those obtained by keeping the instantaneous real power equal to its mean value. Chang and Shree [6] have proposed a simple and efficient compensation strategy that is suitable for three-phase shunt active power filters without reference-frame transformation requirement. Bhende *et al.* [7] have proposed Takagi-Sugeno (TS)-type fuzzy logic controller to a three-phase shunt active power filter and compared to conventional proportional-integral (PI) controller. Bhim Singh and Verma [8] have an indirect current control scheme of parallel hybrid power filter system consists of a shunt passive filter with an active filter in series with it connected at the point of common coupling (PCC) in parallel with nonlinear load. Bhuvanewari and Nair [9] have proposed an algorithm based on the real component of fundamental load current ($I \cos\Phi$). Suresh *et al.* [10] have presented the implementation of a hybrid adaptive fuzzy hysteresis current controller for shunt active power filter using i_d - i_q strategy. Tang *et al.* [11] have proposed a LCL-filter-based shunt active power filter which gives good switching harmonic suppression and minimizes the possibility of over-modulation.

Chandra *et al.* [12] have presented an improved control algorithm of the SAPF which used two closed loop PI controllers and carrier wave PWM signal generation. Akagi [13] has listed trends in active power line conditioners. Singh *et al.* [14] have presented a review on classification of active filters for power quality improvement based on converter type, topology and the number of phases.

In the generalized instantaneous reactive power theory [2], transformation of a-b-c axes to d - q synchronous reference frame is done for harmonic and reactive power compensation. However, the synchronous reference frame (SRF) strategy [3] only computes the sinusoidal fundamental components of the load currents; the reactive power compensation and a null neutral current thus cannot be achieved if the load imbalance at the fundamental frequency occurs. A phase-locked loop (PLL) per each phase must be used. In theory, the aforementioned approaches work very well on harmonic and/or reactive power compensation for nonlinear loads under ideal source voltages. However, if the source voltages are

imbalanced and/or distorted, the generated SAPF reference compensation currents are discrepant and the desired balanced/sinusoidal source currents cannot be maintained [6].

Among different PWM methods, hysteresis is one of the most popular PWM strategies [6- 10] and widely applied in SAPF for current quality compensation, owing to its advantages such as ease of implementation, fast dynamic response and current limiting capability.

Recently, fuzzy logic controllers have generated a great deal of interest in various applications and have been introduced in the power-electronics field. The advantages of fuzzy logic controllers over the conventional PI controller are that they do not need an accurate mathematical model; they can work with imprecise inputs, can handle nonlinearity, and may be more robust than the conventional PI controller. The Mamdani type of fuzzy controller used for the control of APF gives better results compared with the PI controller [7, 10, and 14].

To achieve full compensation of both reactive power and harmonic/neutral currents of the load, this paper presents a simple method to determine the SAPF reference compensation currents using dc voltage, PI and Fuzzy controller and source voltages. This method does not require any reference frame transformations. Hysteresis band current control PWM strategy is used to drive current controlled voltage source inverter (CC- VSI). The two schemes, conventional PI controller and Fuzzy controller are compared in this paper. A MATLAB based simulation is performed on proposed system and the results are presented to discuss in regard to the voltage regulation, harmonic elimination, power-factor correction and load balancing capabilities of the SAPF system.

II. CONTROL SCHEME OF SAPF

The control scheme of a shunt active power filter must calculate the current reference waveform for each phase of the inverter, maintain the dc voltage constant, and generate the inverter gating signals. The block diagram of the control scheme of a shunt active power filter is shown in Fig. 1. The current reference circuit generates the reference currents required to compensate the load current harmonics and reactive power, and also try to maintain constant the dc voltage across the electrolytic capacitors. Also, the compensation effectiveness of an active power filter depends on its ability to follow with a minimum error and time delay, the reference signal calculated to compensate the distorted load current. Finally, the dc voltage control unit must keep the total dc bus voltage constant and equal to a given reference value. The dc voltage control is achieved by adjusting the small amount of real power absorbed by the inverter. This small amount of real power is adjusted by changing the amplitude of the fundamental component of the reference current. Different control topologies of SAPF are well documented in recent years [1- 14].

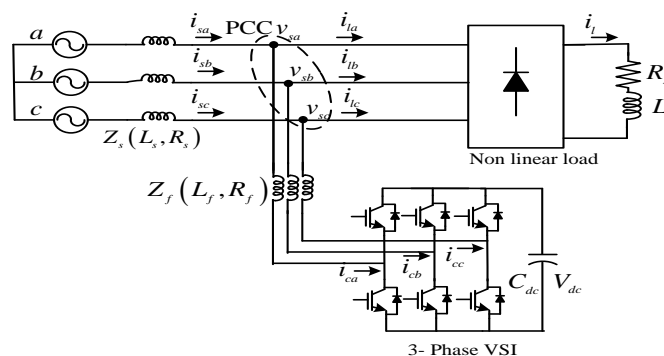


Figure 1: Basic Compensation Principle of Shunt Active Power Filter (SAPF)

2.1 Generation of Source Currents

SAPF is controlled to draw/supply a compensating current from/to the utility, so that it cancels current harmonics on the ac side and makes the source current in phase with the source voltage. From Fig. 1, the instantaneous currents can be written as:

$$i_s(t) = i_L(t) - i_c(t) \tag{1}$$

Source voltage is given by:

$$v_s(t) = V_m \sin \omega t \tag{2}$$

If the nonlinear load is applied, then the load current will have a fundamental component and harmonic components, which can be expressed as:

$$\begin{aligned} i_L(t) &= \sum_{n=1}^{\infty} I_n \sin(n\omega t + \phi_n) \\ &= I_1 \sin(n\omega t + \phi_1) + \sum_{n=2}^{\infty} I_n \sin(n\omega t + \phi_n) \end{aligned} \tag{3}$$

The instantaneous load power can be given as:

$$\begin{aligned}
 p_L(t) &= v_s(t) * i_L(t) \\
 &= V_m I_L \sin^2 \omega t * \cos \phi_1 + V_m I_L \sin \omega t * \cos \omega t * \sin \phi_1 \\
 &\quad + V_m \sin \omega t * \sum_{n=2}^{\infty} I_n \sin(n\omega t + \phi_n) \\
 &= p_f(t) + p_r(t) + p_h(t)
 \end{aligned} \tag{4}$$

From (4), the real power drawn by the load is:

$$p_f(t) = V_m I_L \sin^2 \omega t * \cos \phi_1 = v_s(t) * i_s(t) \tag{5}$$

From (5), the current supplied by the source, after compensation is:

$$i_s(t) = \frac{p_f(t)}{v_s(t)} = I_L * \cos \phi_1 * \sin \omega t = I_{sm} \sin \omega t$$

Where $I_{sm} = I_L * \cos \phi_1$

There are also some switching losses in the PWM converter and, hence, the utility must supply a small overhead for the capacitor leakage and converter switching losses in addition to the real power of the load. The total peak current supplied by the source (I_{sp}) is therefore:

$$I_{sp} = I_{sm} + I_{sl} \tag{6}$$

Where I_{sl} is the peak value of loss current.

If the active filter provides total reactive and harmonic power, then $i_s(t)$ will be in phase with the utility voltage and purely sinusoidal. At this time, the active filter must provide the following compensation current:

$$i_c(t) = i_L(t) - i_s(t) \tag{7}$$

2.2 Generation of Reference Source Currents

There are many possibilities to determine the reference current required to compensating the non-linear load. Normally, shunt active power filters are used to compensate the displacement power factor and low-frequency current harmonics generated by non-linear loads. One alternative to determine the current reference required by the VSI is the use of the instantaneous reactive power theory, proposed by Akagi [1], the other one is to obtain current components in $d-q$ or synchronous reference frame [2], and the third one to force the system line current to follow a perfectly sinusoidal template in phase with the respective phase-to-neutral voltage [3]. In this paper, a simple method is used to generate the source reference currents using DC voltage error and source voltage peak detection. The reason, why it is selected and functioning of the control method is explained below.

III. Proposed Method With Pi Controller

The aim of the method is to generate the current reference signal required to compensate reactive power and current harmonics. Basically, all the different schemes try to obtain the current reference signals that include the reactive components required to compensate the displacement power factor and the current harmonics generated by the non-linear load. Fig. 2 shows the PI controller based scheme used to generate the current reference signals required by a shunt active power filter. In this circuit, the distorted load current is filtered, extracting the fundamental component, I_L .

3.1 Design of DC Link Voltage PI Controller

The three phase reference currents (peak value) for the control of active filter are generated in accordance with the PI controller error between the average dc bus voltage $V_{dc}(n)$ and its reference value $V_{dcref}(n)$ of the active filter. The dc bus voltage error $V_e(n)$ at n^{th} sampling instant is:

$$V_e(n) = V_{dcref}(n) - V_{dc}(n) \tag{8}$$

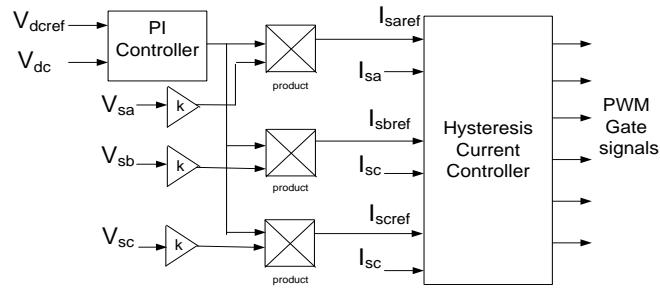


Figure 2: PI -hysteresis current controller based PWM generation using proposed method for SAPF.

This error signal $V_e(n)$ is processed in PI controller and output $K(n)$ at n^{th} sampling instant is expressed as:

$$K(n) = K(n-1) + K_p \{V_e(n) - V_e(n-1)\} + K_i \{V_e(n)\} \quad (9)$$

Where K_p and K_i are the gains of the PI controller.

The output of the PI controller has been considered as the amplitude of the desired source current, and the reference currents are estimated by multiplying this peak value with the unit sine vectors in phase with the source voltages. In order to provide the reactive power required by the load, the current signal obtained from the PI Controller I_{ll} is synchronized with the respective phase to- neutral source voltage so that the inverter ac output current is forced to lead the respective inverter output voltage, thereby generating the required reactive power and absorbing the real power necessary to supply the switching losses and also to maintain the dc voltage constant. The real power absorbed by the inverter is controlled by adjusting the amplitude of the fundamental current reference waveform, I_{ll} , obtained from the reference current generator.

Ideal compensation requires the mains current to be sinusoidal and in phase with the source voltage, irrespective of the load current nature. The source reference currents, after compensation, can be given as:

$$\begin{aligned} i_{sa}^* &= I_{sp} \sin \omega t \\ i_{sb}^* &= I_{sp} \sin(\omega t - 120^\circ) \\ i_{sc}^* &= I_{sp} \sin(\omega t + 120^\circ) \end{aligned} \quad (10)$$

Where I_{sp} is the amplitude of the desired source current, while the phase angle can be obtained from the source voltages. Hence, the waveform and phases of the source currents are known, and only the magnitudes of the source currents need to be determined.

The main characteristic of this method is the direct derivation of the compensating component by sensing dc voltage, source voltages and currents, without use of any reference frame transformation. Nevertheless, this PI controller presents a low frequency oscillation problem in the active power filter dc bus voltage. To improve this technique, fuzzy hysteresis band current controller has been implemented in this paper.

IV. PROPOSED FUZZY CONTROL ALGORITHM

Fig. 3 shows the schematic diagram of the fuzzy control scheme. In order to implement the control algorithm of a shunt active power filter in a closed loop, the dc capacitor voltage V_{dc} is sensed and then compared with the reference value V_{dcref} . In case of a fuzzy logic control scheme, the error $e = V_{dcref} - V_{dc}$ and integration of error signal $\int e$ are used as inputs for fuzzy processing. The output of the fuzzy controller after a limit is considered as the magnitude of peak reference current I_{max} . The switching signals for the PWM converter are obtained by comparing the actual source currents (i_{sa} , i_{sb} , i_{sc}) with the reference current templates (i_{sa}^* , i_{sb}^* , i_{sc}^*) in the hysteresis current controller. The output pulses are then given to the switching devices of the PWM converter.

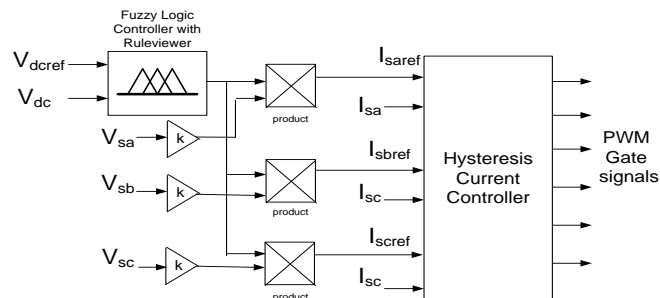


Figure 3: Fuzzy -hysteresis current controller based PWM generation using proposed method for SAPF.

4.1. Basic Fuzzy Algorithm

In a fuzzy logic controller, the control action is determined from the evaluation of ‘a’ set of simple linguistic rules. The development of the rules requires ‘a’ thorough understanding of the process to be controlled, but it does not require a mathematical model of the system. The design of a fuzzy logic controller requires the choice of membership functions. The membership functions should be chosen such that they cover the whole universe of discourse. It should be taken care that the membership functions overlap each other. This is done in order to avoid any kind of discontinuity with respect to the minor changes in the inputs. To achieve finer control, the membership functions near the zero region should be made narrow. Wider membership functions away from the zero region provides faster response to the system. Hence, the membership functions should be adjusted accordingly. After the appropriate membership functions are chosen, a rule base should be created. It consists of a number of Fuzzy If-Then rules that completely define the behaviour of the system. These rules very much resemble the human thought process, thereby providing artificial intelligence to the system [3].

The internal structure of the fuzzy controller is shown in Fig. 4. The error e and change of error ce are used numerical variables from the real system. To convert these numerical variables into linguistic variables, the following seven fuzzy levels or sets are chosen as: NB (negative big), NM (negative medium), NS (negative small), ZE (zero), PS (positive small), PM (positive medium), and PB (positive big) and presented in input and output normalized membership functions (Figs. 5 (a) and (b)).

The fuzzy controller is characterized as follows:

- (i) Seven fuzzy sets for each input and output.
- (ii) Triangular membership functions for simplicity.
- (iii) Fuzzification using continuous universe of discourse.
- (iv) Implication using Mamdani’s ‘min’ operator.
- (v) Defuzzification using the ‘centroid’ method.

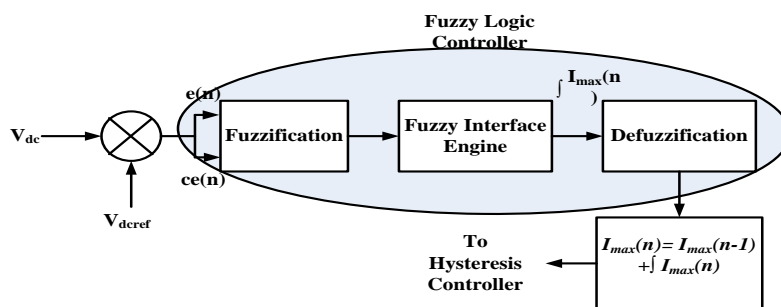


Figure 4: Internal Structure of Fuzzy controller.

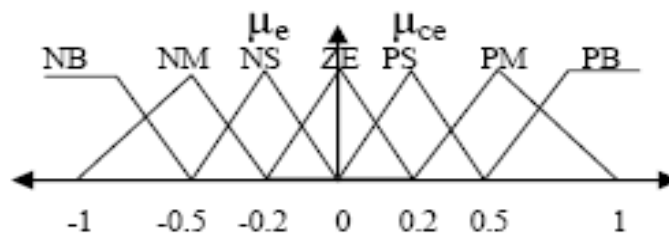


Figure 5(a): Input normalized membership function.

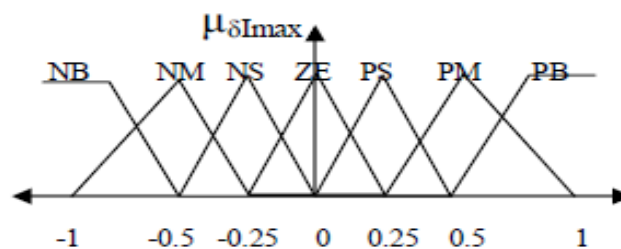


Figure 5(b): Output normalized membership function.

4.2. Rule Base

The elements of this rule base table are determined based on the theory that in the transient state, large errors need coarse control, which requires coarse input/output variables; in the steady state, small errors need fine control, which requires fine input/output variables. Based on this the elements of the rule table are obtained as shown in Table I, with ‘e’ and ‘ce’ as inputs.

Table.I Control Rule Base

	NB	N	NS	ZE	PS	PM	PB
ce		M					
e							
NB	NB	NB	NB	NB	NM	NS	ZE
N	NB	NB	NB	NM	NS	ZE	PS
NB	NB	NB	NM	NS	ZE	PS	PM
ZE	NB	NM	NS	ZE	PS	PM	PB
PS	NM	NS	ZE	PS	PM	PB	PB
P	NS	ZE	PS	PM	PB	PB	PB
PB	ZE	PS	PM	PB	PB	PB	PB

4.3 Hysteresis Current Controller for PWM Switching

The active filter is comprised of three-phase IGBT based current controlled VSI bridge. The upper device and the lower device in one phase leg of VSI are switched in complementary manner. The switching logic for “phase-a” is formulated as follows: if $i_{sa} < (i_{sa}^* - h_b)$, upper switch is OFF and lower switch is ON in the phase “a” leg then $S_a = 0$. If $i_{sa} > (i_{sa}^* + h_b)$ upper switch is ON and lower switch is OFF in the phase “a” leg then $S_a = 1$. Between the transitions the previous value of switches are maintained. Where, is switching function for switches of phase “a” and is the width of the hysteresis band around reference currents. Similarly, the switching logic of the other two phases (“b” and “c”) is formulated.

V. Simulation Results And Discussion

Following are the system parameters considered for the study of SAPF for both PI and Fuzzy controller. $V_s = 100$ V (Peak), $f = 50$ Hz, $R_s = 0.1 \Omega$, $L_s = 0.15$ mH, $R_f = 0.1 \Omega$, $L_f = 0.66$ mH, $R_l = 6.7, 15 \Omega$; $L_l = 20$ mH, $C_{DC} = 2000 \mu$ F, $V_{dcref} = 220$ V. In case of PI the gains chosen are $k_p = 0.2$ and $k_i = 9.32$. Initially, the load chosen is of $R_l = 6.7 \Omega$, $L_l = 20$ mH and later, the load has been changed to $R_l = 15 \Omega$, $L_l = 20$ mH. The performance results of shunt active power filter with PI controller are presented in Figures 7- 9. Fig.6 shows THD content of Load current, Source current with PI controller and with Fuzzy controller. In Fig.7 performance results of SAPF with PI controller are presented and results with fuzzy controller are presented in Fig. 8. Fig.9 shows results in support of power factor correction ability of SAPF. Comparisons of PI and fuzzy controllers are presented in Table II, III and IV based on % THD, settling time and overshoot. (Parameters notation is shown in Fig. 1.)

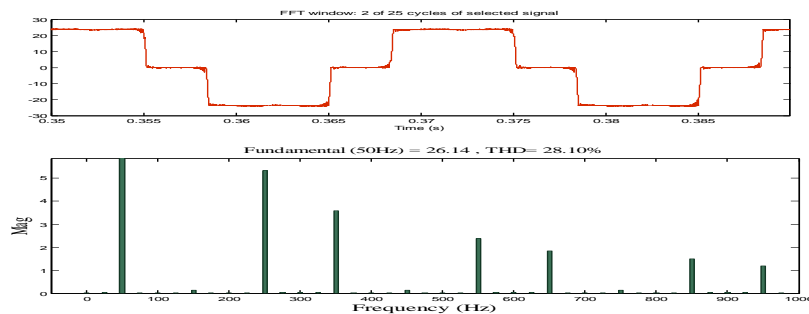


Figure 6 (a): THD % of load current

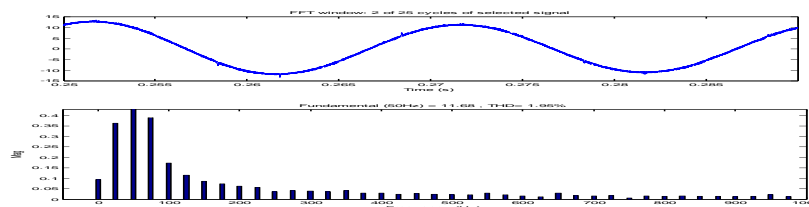


Figure.6 (b): THD % of Source current (PI)

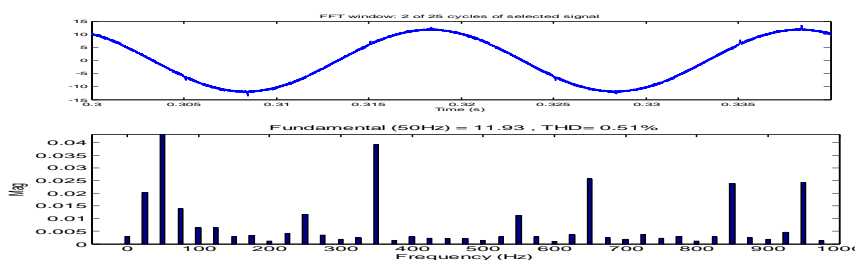


Figure.6(c) THD% of Source current (Fuzzy)

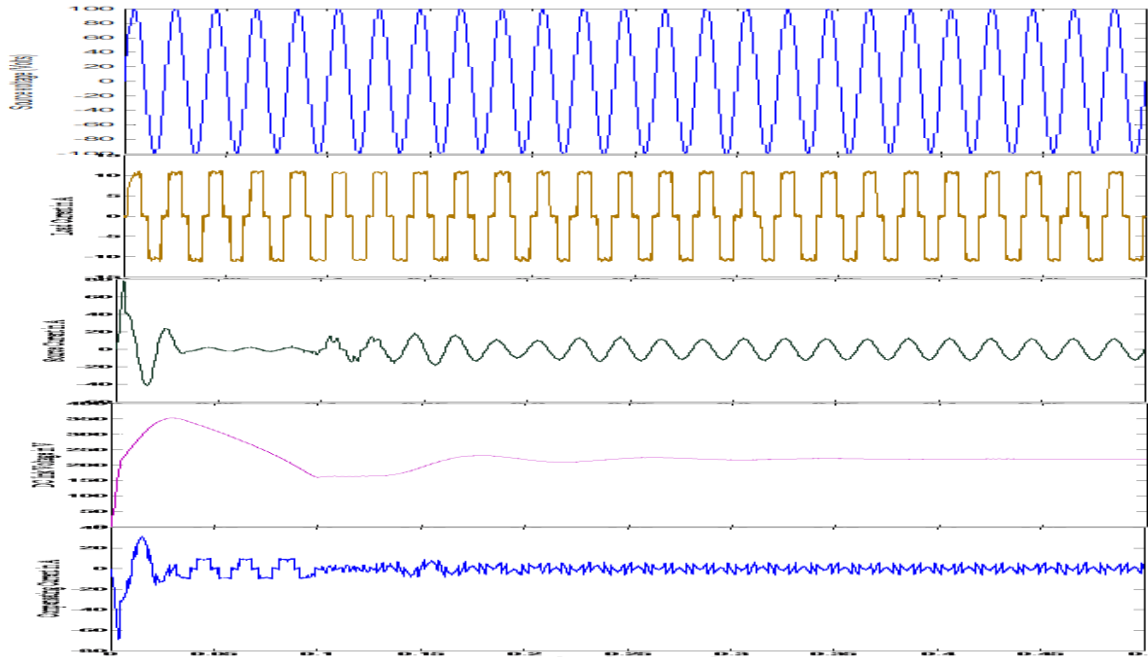


Figure.7: Performance results of shunt active power filter with PI controller for the load $R_l = 15 \Omega$, and $L_l = 20 \text{ mH}$.

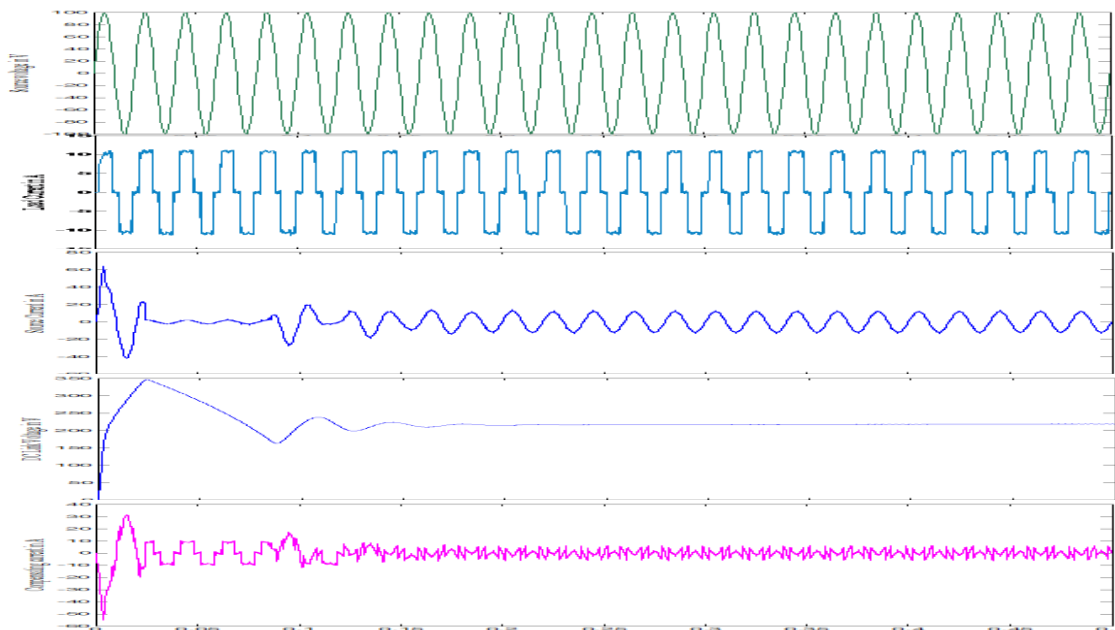


Figure.8: Performance results of shunt active power filter with fuzzy controller for the load $R_l = 15 \Omega$, and $L_l = 20 \text{ mH}$.

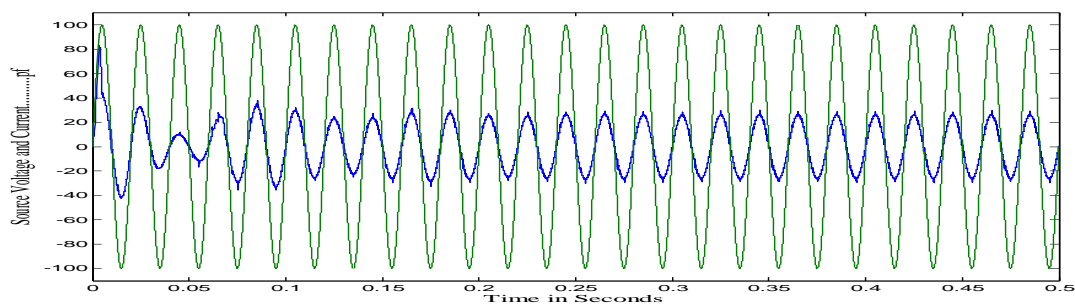


Figure 9(a): Source Voltage and current wave forms of Phase 'a' of PI controlled SAPF

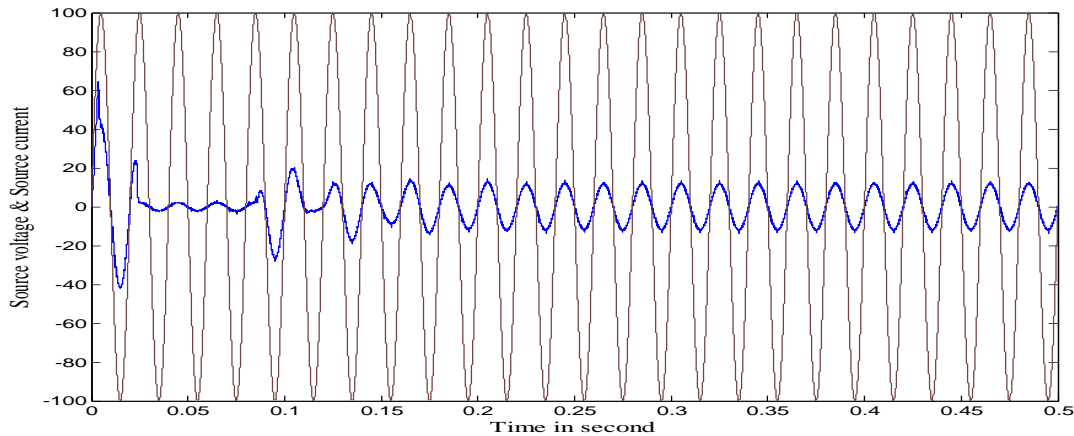


Figure 9(b): Source Voltage and current wave forms of Phase ‘a’ of Fuzzy controlled SAPF

TABLE.II: Thd % Comparison between Pi and Fuzzy Controllers

	% THD at two different loads	
	$R_1 = 6.7 \Omega$, $L_1 = 20\text{mH}$	$R_1 = 15\Omega$, $L_1 = 20\text{mH}$
Without controller	28.10	27.72
With PI controller	0.81	1.03
With Fuzzy controller	1.1	0.51

TABLE.III: Settling Time Comparison between Pi And Fuzzy Controllers

	Settling time for two different loadings (sec)	
	$R_1 = 6.7 \Omega$, $L_1 = 20\text{mH}$	$R_1 = 15\Omega$, $L_1 = 20\text{mH}$
With PI controller	0.26 s	0.33 s
With Fuzzy controller	0.18 s	0.24 s

TABLE.IV: Response of Pi and Fuzzy Controllers under Dynamic Load Conditions

	PI	Fuzzy
Switch on response (peak overshoot)	80 A	65 A
Settling time (after load change)	0.45 s	0.3 s
Load current overshoot (at load change)	45 A	35 A

VI. CONCLUSION

This paper has presented a simulation study of fuzzy based hysteresis current controlled shunt active power filter for harmonic and reactive power compensation of the non-linear load. A simple method is implemented to generate source reference currents without reference frame transformation using DC voltage regulator and source voltages. It gives less complexity in realizing the control circuit of the active power filter and still maintains good filter performance. The scheme has the advantage of simplicity and is able to provide self-supported dc bus of the active filter through power transfer from ac line at fundamental frequency. The performance of conventional PI controller and fuzzy controller has been studied and compared. Overall, the fuzzy controller gives the best SAPF performance in comparison with the PI controller in regards voltage regulation, % THD, settling time, current overshoot etc.

REFERENCES

- [1] H. Akagi, Y. Kanzawa, and A. Nabae "Instantaneous reactive power compensators comprising switching devices without energy Components" IEEE Transactions on Industrial Applications, Vol. 20, No. 3, pp. 625–630, 1984.
- [2] H. Akagi, E. Watanabe, M. Aredes "Instantaneous Power Theory and Applications to Power Conditioning: (Wiley-IEEE Press, 2007).
- [3] M.H. Rashid "Power Electronics Handbook: Devices, Circuits, and Application", (Elsevier Inc., Section Edition, 2007)
- [4] W. M. Grady, M. J. Samotyj and A. H. Noyola "Survey of Active Power Line Conditioning Methodologies" IEEETransaction on Power Delivery, Vol. 5, No. 3, pp. 1536- 1542, July 1990.
- [5] A. Cavallini and G. C. Montanari "Compensation Strategies for Shunt Active-Filter Control" IEEE Transactions on Power Electronics, Vol. 9, No. 6, pp. 587- 593, November 1994.
- [6] G. W. Chang, and T. C. Shee "A Novel Reference Compensation Current Strategy for Shunt Active Power Filter Control" IEEE Transactions on Power Delivery, Vol. 19, No. 4, pp. 1751 – 1758, October 2004.
- [7] C. N. Bhende, S. Mishra, and S. K. Jain "TS-Fuzzy-Controlled Active Power Filter for Load Compensation, IEEETransactions on Power Delivery, Vol. 21, No. 3, pp. 1459- 1465, July 2006.
- [8] Bhim Singh, and Vishal Verma "An Indirect Current Control of Hybrid Power Filter for Varying Loads" IEEETransactions on Power Delivery, Vol. 21, No. 1, pp. 178- 184, January 2006.
- [9] G. Bhubaneswar, and Manjula G. Nair "Design, Simulation, and Analog Circuit Implementation of a Three-Phase Shunt Active Filter Using the Icos Φ Algorithm" IEEE Transactions on Power Delivery, Vol. 23, No. 2, pp. 1222 – 1235, April 2008.
- [10] Y. Suresh A.K. Panda and M. Suresh "Real-time implementations of adaptive fuzzy hysteresis-band current control technique for shunt active power filter" Vol. 5, Iss. 7, pp. 1188–1195, IET Power Electronics, 2012.
- [11] Y. Tang, P. C. Loh, P. Wang, F. H. Choo, F. Gao, and F. Blaabjerg, "Generalized Design of High Performance Shunt Active Power Filter With Output LCL Filter" IEEE Transactions on Industrial Electronics, Vol. 59, No. 3, pp. 1443-1452, March 2012.
- [12] Ambrish Chandra, Bhim Singh, B. N. Singh, and Kamal Al-Haddad, "An Improved Control Algorithm of Shunt Active Filter for Voltage Regulation, Harmonic Elimination, Power-Factor Correction, and Balancing of Nonlinear Loads"IEEE Transactions on Power Electronics, Vol. 15, No. 3, pp. 495 -507, May 2000.
- [13] H. Akagi, New Trends in Active Filters for Power Conditioning" IEEE Transactions on Industry Applications, Vol32, No 6, pp. 1312- 1322, December 1996.
- [14] Bhim Singh, Kamal Al-Haddad, and Ambrish Chandra "A Review of Active Filters for Power Quality Improvement" IEEE Transactions on Industrial Electronics, Vol. 46, No. 5, pp. 60 – 71, October 1999.

Comparison between Hierarchical Based Routing Schemes for Wireless Sensor Network

Prashant Krishan,¹ Aysha Siddiqua²

¹M.Tech, Department of IT, Dehradun Institute of Technology, Uttarakhand, India

²Department of Information Technology, Dehradun Institute of Technology, India

Abstract: A Wireless Sensor Network is a collection of sensor nodes that have some properties like low cost, low power, limited network lifetime etc. These sensor nodes are deployed to the region of interest (Area monitoring, Air pollution monitoring, Forest fire detection, Water quality monitoring etc.) for gathering data. An important issue in wireless sensor networks is developing an energy-efficient routing protocol to increase the network lifetime of the network. Routing protocols can be divided on many basis either it is network structure or protocol operation. On the basis of network structure routing protocols can be further divided into three parts (Flat, Clustering-based, location-aware) In this paper, we simulate the static clustering based routing schemes EEPSC (Energy Efficient Protocol with Static Clustering) and EEEPSC (Extended Energy Efficient Protocol with Static Clustering). Our experimental results show that EEEPSC increases the network lifetime of a wireless sensor network.

Keywords: Clustering methods, energy efficiency, routing protocol, wireless sensor networks.

I. INTRODUCTION

A Wireless sensor Network is a collection of sensor nodes that are connected by wireless medium. Every sensor node equipped with data processing and communication capabilities. These networks can be used for home security, area monitoring, air pollution monitoring and earthquake warning. A wireless sensor networks have infinite scopes but they are limited to node battery lifetime. The network can be working while the battery power is adequate. In the related literature, there are many routing schemes in wireless sensor network. On the basis of network structure, the routing protocols can be divided into flat-based routing, hierarchical-based routing, location -based routing. In flat routing, every node has same work (sensing and sending the data to the sink). When every node has the same role, the network lifetime is less and this is the drawback of flat routing. In hierarchical routing, nodes have different role, less energy nodes sense the environment and high energy node send the data to the sink, so there is hierarchy maintained between high energy nodes and low energy nodes. In location-based routing, sensor nodes' positions are exploited to route data in the network.

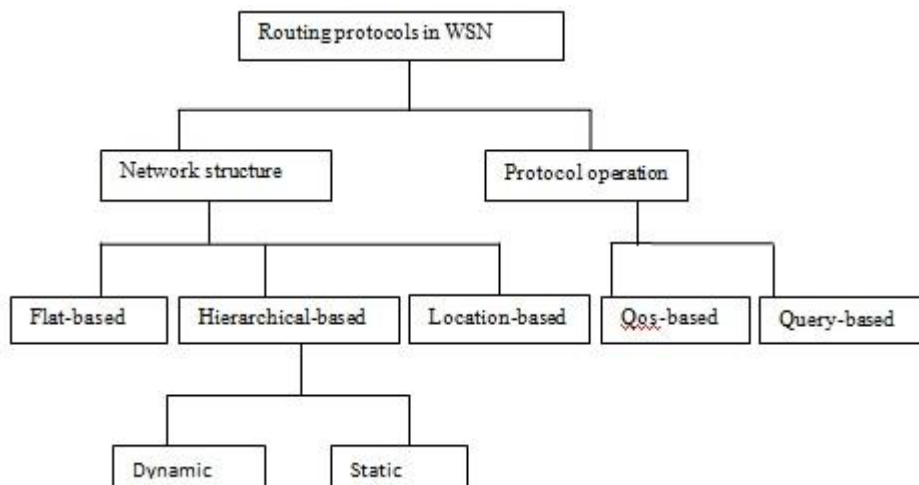


Figure 1: Classification of routing protocols

Hierarchical- based routing: In a hierarchical architecture, higher energy nodes can be used to process and send the information and lower energy nodes used to sense the environment. So there is a hierarchy of low and high energy nodes. The creation of clusters and assigning special tasks to cluster heads can affect the scalability, lifetime, and energy efficiency. Hierarchical routing is two-layer routing where one layer is used to select cluster heads and the other for routing. This can be further divided into two parts dynamic hierarchical based routing scheme and static hierarchical based routing scheme. In dynamic, clusters are formed dynamically whereas in static once the clusters are formed remains same throughout the network lifetime.

In this paper, we focus on the static hierarchical based routing protocols. EEPSC (Energy Efficient Protocol with Static Clustering) and EEEPSC (Extended Energy Efficient Protocol with Static Clustering) are the static hierarchical based routing protocols.

II. RELATED WORK

Energy Efficient Protocol with Static Clustering (EEPSC) is a static clustering based routing algorithm. EEPSC divided the network into static clusters, temporary-cluster-heads are used to distribute the energy load among high energy sensor nodes; thus extends the network lifetime and there is no overhead to select the clusters dynamically [2]. The operation of EEPSC is divided into rounds, where each round contains set-up phase, responsible node selection phase and steady state phase. Setup phase and responsible node selection phase are the cluster formation phase and steady state phase is responsible for sending the data to the base station.

2.1 Setup phase: In this phase, base station broadcasts $k-1$ different messages with different transmission powers, where k is the desired number of clusters. By broadcasting the $k=1$ message all the sensor nodes which are in the radio range of this message set their cluster id to k and inform the base station that they are member of the cluster k by transmitting a join-request.

2.2 Responsible node Selection phase: After the clusters are established, network starts its temporary-cluster head and cluster head selection phase begin. In every round, nodes send its energy level to the temporary cluster head in its time slot. Temporary-cluster head choose the sensor node with utmost energy level as cluster head.

2.3 Steady-state phase: The steady-state phase is broken into frames where nodes send their data to the CH during pre-allocated time slots. These data contain node ID and the measure of sensed parameter. The total energy expended in the system is greater using multi-hop routing than direct transmission to the base station; thus, we use direct transmission approach among CH and base station. The duration of each slot in which a node transmits data is constant, so the time to send a frame of data depends on the number of nodes in the cluster.

Extended Energy Efficient Protocol with Static Clustering is (EEEPSC) devised to reduce the inter cluster communication cost of EEPSC. it has also the same steps like EEPSC but there is a new term distance (between the cluster heads and the nodes) is calculated and the less distance node with high residual energy is choose as the cluster head.

2.4 Setup phase: In this phase, the base station broadcasts $(k-1)$ messages one-by-one with different transmission powers, where k is the desired number of clusters.

2.5 Responsible Node Selection Phase: In this phase, cluster-heads (CHs) for the current round and the temporary-cluster-heads (TCHs) for the next round are selected in each cluster. At the beginning of every round, nodes in each cluster send 2-tuple data (*Eresidual_j*, *dmean_{ij}*) to the *TCH_i*. Now *TCH_i* declares the node with the highest value of (*Eresidual/dmean*) as cluster head (*CH_i*) for the current round. Node with the second highest value of (*Eresidual/dmean*) is selected as *TCH_i* for next round. The newly declared *CH_i* broadcasts a round-start packet including responsible nodes' id (*CH_i* and *TCH_i*) towards the nodes of its cluster indicating the beginning of a round [3].

2.6 Steady state phase: In this phase, similar to EEPSC, nodes send their sensed data to corresponding CH during their pre-allocated fixed time slots indicating the fact that the time required for sending a frame depends upon the number of nodes in the cluster.

III. SIMULATION RESULTS

To validate the performance of EEPSC and EEPSC, we simulate EEPSC and EEPSC and utilize a network with 100 nodes randomly deployed between $(x=0, y=0)$ and $(x=100, y=100)$ and base station at $(50,175)$. The bandwidth of channel is set to 1 Mb/s, each data message is 500 bytes long, and the packet header for each type of packet is 25 bytes long. The initial power of all nodes is considered to be 2J and duration of each round is 20s. The number of clusters for above assumptions is optimized for $1 < k < 6$. So for the rest of the experiment, we set $k=4$.

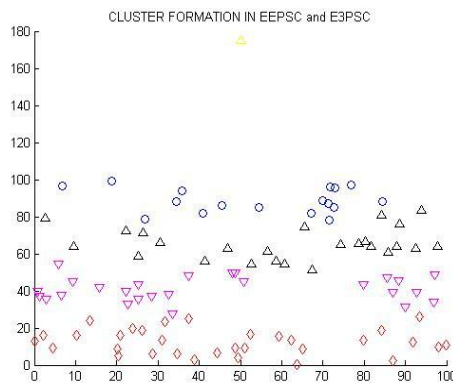


Figure 2: Cluster formation of eepsc and e3psc

This is the cluster formation (setup phase) in both eepsc and e3psc. The base stations send the messages of different transmission powers and the nodes corresponding power send the join request message to the base station.

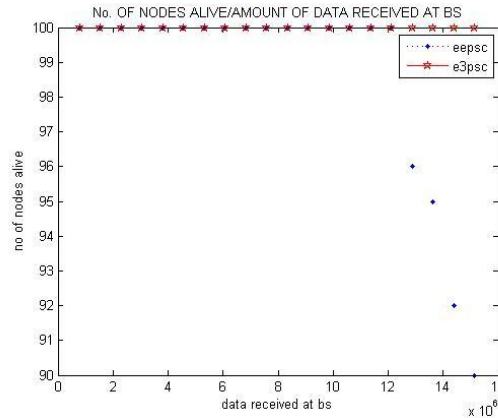


Figure 3: Number of nodes alive after sending the data to BS

The graph shows the number of nodes are alive after sending the data to base station.

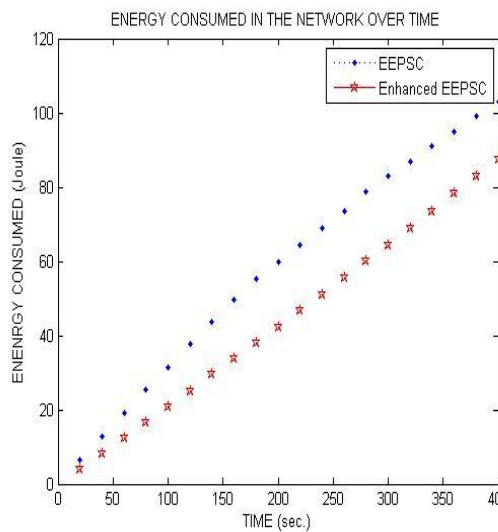


Figure 4: Energy consumption of algorithms (eepsc and e3psc)

The graph shows that the e3psc saves the significant amount of energy. So the e3psc is efficient routing scheme than eepsc.

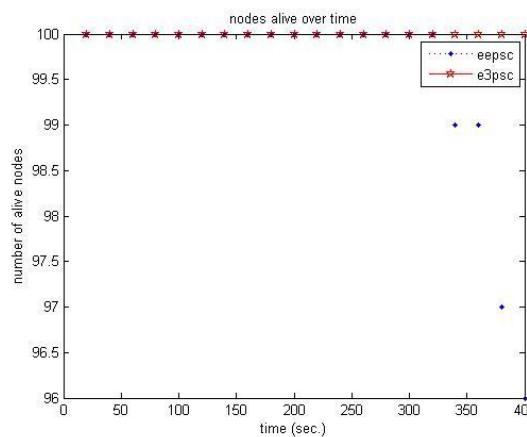


Figure 5: number of nodes alive over time.

The figure shows that the nodes alive are more in EEPSC than EEPSC.

IV. PARAMETERS AND ENVIRONMENT

To evaluate the performance of both schemes, MATLAB is used as a simulation tool. We consider the sensor nodes are deployed randomly across a plain area. Each node has the equal amount of energy at the beginning of the simulation. Following are the parameters and its values that are used in simulation environment.

TABLE 1: PARAMETERS AND VALUES

Parameter	EEPSC	EEEPSC
Network	100mx100m	100mx100 m
Base station position	50,175	50,175
Number of deployed nodes	100	100
Energy consumed by transceiver circuitry(Eelec)	50 nj/bit	50 nj/bit
Energy consumed by free space model (Efs)	10 pj/bit/m2	10 pj/bit/m2

The performance of the scheme is evaluated considering network lifetime as a parameter which is defined as the time until the last node dies in the network. Network lifetime is measured using two different yard-sticks: Number of nodes alive in the network— more number of nodes alive implies network lifetime lasts longer. Number of messages received at BS—More Number of messages received at BS implies more number of nodes is alive in the network leading to longer network lifetime.

V. CONCLUSION

In this paper the routing schemes (EEPSC, E3PSC) are simulated. The E3PSC is a modifying scheme over EEPSC. It has the advantage, increase the network lifetime and the number of nodes are more in EEEPSC than EEPSC. Our experiment is the comparative study of routing schemes.

REFERENCES

- [1] Jamal N. Al-karaki, Ahmed E.kamal, Routing Techniques In Wireless Sensor Networks: A survey
- [2] Amir Sepasi Zahmati, Bahman Abolhassani, Ali Ashgar Beheshti Shirazi, and Ali Shojee Bhaktiari, An energy-Efficient protocol With Static Clustering for Wireless Sensor network. Proceedings Of World Academy Of Science, Engineering And Technology VOLUME 22 JULY 2007 ISSN 1307-6884
- [3] Sandip Kumar Chaurasiya, Tumpa pal, Sipra Das Bit, An Enhanced Energy-Efficient Protocol With Static Clustering for WSN ICOIN 2011.
- [4] Wendi B. Heinemann, Anantha P. Chandrakasan, Hari Balakrishnan an Application-Specific Protocol Architecture for Wireless Micro sensor Network.IEEE Transactions On Wireless Communications, Vol 1, No.4, October 2002.
- [5] Ameer Ahmed Abbasi, Mohammad Younis A survey on clustering algorithms for Wireless Sensor Networks. Computer Communications 30(2007) 2826-2841.
- [6] Stephan Olariu, "Information assurance in wireless sensor networks", Sensor network research group, Old Dominion University.
- [7] C. Chong and S. P. Kumar, "Sensor Networks: Evolution, Opportunities, and Challenges", in Proceedings of the IEEE, vol. 91, no. 8, Aug. 2003.
- [8] Karp and H. T. Kung, "GPSR: greedy perimeter stateless routing for wireless networks", in Mobile Computing and Networking, 2000, pp. 243–254.
- [9] Holger Karl and Andreas Willig. "Protocols and architectures for Wireless Sensor Networks", Wiley, 2005, ISBN: 0470095105.
- [10] Akyildiz, W. Su, Y. Sankarasubramaniam, and E. Cayirci, "A survey on sensor networks", IEEE Communication Magazine, Aug. 2002.
- [11] [Wei Yen, Ching-Wei Chen and Cheng-hsiang Yang, "Single Gossiping with Directional Flooding Routing Protocol in Wireless Sensor Networks", in Proceedings IEEE, 2008.
- [12] K. Sohrabi et al., "Protocols for self-organization of a wireless sensor network", IEEE Personal Communications 7 (5) (2000) 16–27.
- [13] Chalermek Intanagonwiwat, Ramesh Govindan, Deborah Estrin, John Heinemann, and Fabio Silva, "Directed Diffusion for Wireless Sensor Networking", in Proceedings IEEE/ACM, Vol. 11, No. 1, Feb 2003.
- [14] A. Howard, M. J. Mataric, and G. S. Sukhatme. "Mobile Sensor Network Deployment using Potential Fields: A Distributed, Scalable Solution to the Area Coverage Problem. In DARS 02, Fukuoka, Japan, June 2002.
- [15] Brain P. Crow, Indra Widjaja, Jeon Geun Kim and Prescott T. Sakai, "IEEE 802.11 Wireless Local Area Networks", IEEE Communication Magazine, Vol. 35, Sep 1997
- [16] Shio kumar, singh, MP Singh, and DK singh. "A Survey of Energy-Efficient Hierarchical Cluster-Based Routing in Wireless Sensor Networks" Int. J. of Advanced Networking and Applications (2010), VOL: 02, Page: 570-580

“Design and Analysis of Composite Drive Shaft using ANSYS and Genetic Algorithm” A Critical Review

Sagar R Dharmadhikari,¹ Sachin G Mahakalkar,² Jayant P Giri,³
Nilesh D Khutafale⁴

¹PG Scholar Department of Mechanical Engineering YCCE (an autonomous institute), RTMNU Nagpur University (M.S) India 440011

²Associate Professor Department of Mechanical Engineering YCCE (an autonomous institute), RTMNU Nagpur University (M.S) India 440011

³Assistant Professor Department of Mechanical Engineering YCCE (an autonomous institute), RTMNU Nagpur University (M.S) India 440011

⁴Lecturer, Department of Mechanical Engineering Shri Datta meghe polytechnic, Nagpur (M.S) India 440011

Abstract: This study deals with the review of optimization of drive shaft using the Genetic Algorithm and ANSYS. Substitution of composite material over the conventional steel material for drive shaft has increasing the advantages of design due to its high specific stiffness and strength. Drive shaft is the main component of drive system of an automobile. Use of conventional steel for manufacturing of drive shaft has many disadvantages such as low specific stiffness and strength. Conventional drive shaft is made up into two parts to increase its fundamental natural bending frequency. Two piece drive shaft increases the weight of drive shaft which is not desirable in today's market. Many methods are available at present for the design optimization of structural systems and these methods based on mathematical programming techniques involving gradient search and direct search. These methods assume that the design variables are continuous. But in practical structural engineering optimization, almost all the design variables are discrete. This is due to the availability of components in standard sizes and constraints due to construction and manufacturing practices. This paper discusses the past work done on composite drive shafts using ANSYS and Genetic Algorithm.

Keywords: ANSYS, Composite Material, Drive Shaft, Genetic Algorithm, Optimization.

I. INTRODUCTION

Rapid technological advances in engineering design field result in finding the alternate solution for the conventional materials. The design engineers brought to a point to finding the materials which are more reliable than conventional materials. Researchers and designers are constantly looking for the solutions to provide stronger and durable materials which will answer the needs of fellow engineers. Drive shafts are used as power transmission tubing in many applications, including cooling towers, pumping sets, aerospace, trucks and automobiles. In the design of metallic shaft, knowing the torque and the allowable shear stress for the material, the size of the shaft's cross section can be determined. In the today's days there is a heavy requirement for light weight materials vehicle.

The conventional steel material is replaceable by advanced composite materials. Composite materials are favored by most of the scientist in the design of automobiles due to its higher specific strength and stiffness. Weeton et al. [1] stated the possibilities of replacing the conventional steel material by composites in the field of automobile. Weeton et al describe the possibilities of composites used to replace the steel leaf spring as well as steel drive shaft. The advanced composite materials such as graphite, carbon, Kevlar and glass with suitable resins are widely used because of their high specific strength (strength / density) and high specific modulus (modulus / density). The first application of composite drive shaft to automotive was the one developed by Spicer U-joint divisions of Dana Corporation for the Ford econoline van models in 1985. Drive shafts for power transmission are used in many applications, including cooling towers, pumping sets, aerospace, structures, and automobiles.

In metallic shaft design, knowing the torque and the allowable service shear stress for the material allows the size of the shaft's cross-section to be determined. Beard more et al. [2] is also states the potentials of composites in structural applications. Conventional steel drive shafts are manufacture in two pieces to increase its fundamental natural bending frequency. The conventional assembly of drive shaft is made up in two pieces and joined together by u-joints due to which the overall weight of the assembly is increased.

The composite drive shaft [3] has advantages like considerable weight reduction, symmetric composite assured the dynamic balance of increasing operating speed, electrically non conductive, custom end fitting considerations, vibrations and harshness (NVH), long fatigue life and also it reduce the bearing & journal wear. The materials usually have a lower modulus of elasticity which results in when torque peaks are occurred the drive shaft may works as a shock absorber. A drive shaft must operate through constantly changing angles between the transmission and rare axle. A GA proposed by the Goldberg [6] based on natural genetics will be studied in the second phase of study. Rajiv and Krishnamurthy [4] proposed a method for converting a constrained optimization problem into an unconstrained optimization problem. Kim et al. [9] minimizes the weight of composite laminates with play drop under a strength constraint using GA.

JH Park et al. [10] explains the various loading and boundary conditions for the optimal design of laminated composites. Vijayrangan et al. [7] had proposed the GA for the optimization of Composite Leaf spring. T Rangaswamy et

al. [8] defines the procedure to design and optimized the composite drive shaft using HM – Carbon / Epoxy by Genetic algorithm.

Now days all automobiles (which are having front engine rear wheel drive) have the transmission shaft as shown in fig.1 [3]. The reduction in weight of the drive system has the advantageous in overall weight reduction of automobiles which is a highly desirable goal of design engineer.

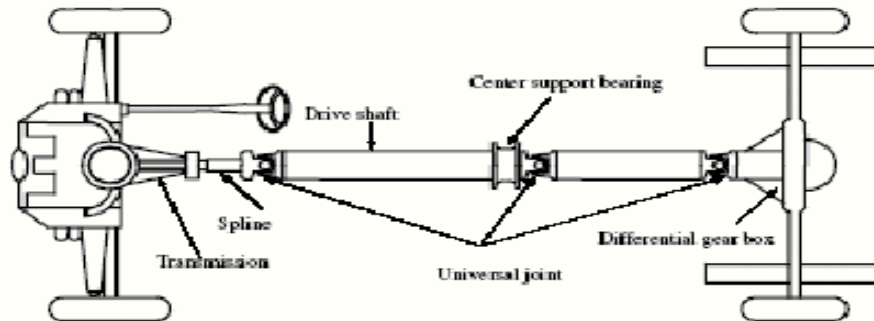


Fig. 1: Two Piece Drive Shaft Arrangement for Rear Wheel Vehicle Driving System

In the present work the focus is given on the replacement of the conventional steel drive shaft by the High Strength - Carbon / Epoxy material. A single piece composite drive shaft was designed and analyzed using the ANSYS 12.0.

II. COMPOSITE MATERIAL

Composite consist of two or more material phase that are combine to produce a material that has superior properties to these of its individual constituent. Technologically the most important composite are those in which the dispersed phase is in the form of fibre. The composite materials can be classified on the basis of micro structures, multi phases, reinforcements, manner of packing of fibers layered compositions, method of compositions, matrix system, processing methods, etc. [5] Composite materials can be classified as:

- 1) Polymer Matrix Composites.
- 2) Metal Matrix Composites.
- 3) Ceramic Composites.

The fibers are either long or short. Long and continuous fibers are easy to orient and process, where as short fibers cannot be controlled fully for proper orientation. The principal fibres in commercial use are various types of glass, carbon, graphite and Kevlar. All these fibers are incorporated in matrix form either in continuous length or in discontinuous length.

Table1: properties of HS – Carbon / Epoxy material.

Mechanical Properties	Symbol	Units	Steel	HS Carbon / Glass Epoxy
Young's Modulus	E	Gpa	207	210
Shear Modulus	G	Gpa	80	70
Poisson's ratio	N	-	0.3	0.3
Density	P	Kg/ M ³	7600	1600
Shear Strength	Ss	MPa	370	420

2.1 Advantages of composite materials over conventional materials

1. High strength to weight ratio.
2. High stiffness to weight ratio.
3. High impact resistance.
4. Better fatigue resistance.
5. Improved corrosion resistance.
6. Good thermal conductivity.
7. High damping capacity.
8. Low coefficient of thermal expansion.

III. SPECIFICATION OF THE PROBLEM

The passenger cars, small trucks and vans should have the torque transmission capacity more than 3500 Nm and fundamental natural bending frequency must be higher than 6500 rpm to avoid whirling vibrations. From the theory of whirling, it has been found that the critical speed of shaft is inversely proportional to the square of its length. So the vibration problem could be solve by increasing the length of shaft but it cannot be permitted due to space limitations. So that there is only an option to manufacturers to manufacture the shaft in two pieces.

IV. DESIGN REQUIREMENTS FOR STEEL DRIVE SHAFT

Table2: Design Parameters [8]

Parameter of Shaft	Symbol	Value	Unit
Outer Diameter	d_o	90	mm
Inner Diameter	d_i	83.36	mm
Length of the Shaft	L	1250	mm
Thickness of shaft	T	3.32	mm

4.1 Design of Steel Drive Shaft

Mass of the steel drive shaft,

$$m = \rho AL = \rho \times \frac{\pi}{4} \times (d_o^2 - d_i^2) \times L \dots (1)$$

$$= 7600 \times 3.14/4 \times (90^2 - 83.36^2) \times 1250$$

$$[m = 8.58 \text{ Kg}]$$

Torque transmission capacity of steel drive shaft,

$$T = S_s \times \frac{\pi}{16} \times [(d_o^4 - d_i^4) \times d_o] \dots (2)$$

$$[T = 55.93 \times 10^3 \text{ N-m}]$$

Fundamental Natural frequency,

The natural frequency can be found by using the two theories:

- 1) Timoshenko Beam theory
- 2) Bernoulli Euler Theory

Timoshenko Beam Theory-Ncrt

$$f_{nt} = K_s (30 \pi p^2) / L^2 \times \sqrt{(Er^2 / 2\rho)} \dots (3)$$

$$N_{crt} = 60 f_{nt} \dots (4)$$

f_{nt} = natural frequency base on Timoshenko beam theory, HZ

K_s = Shear coefficient of lateral natural frequency

$p = 1$, first natural frequency

r = mean radius of shaft

F_s = Shape factor, 2 for hollow circular cross section

n = no of ply thickness, 1 for steel shafts

$$1 / K_s^2 = 1 + (n^2 \pi^2 r^2) / 2L^2 \times [1 + f_s E / G] \dots (5)$$

$$1 / K_s^2 = 1 + (1^2 \pi^2 86.82^2) / 2 \times 1250^2 \times [1 + 2 \times 207 \times 10^3 / 80 \times 10^3]$$

$$[K_s = 0.982]$$

$$f_{nt} = 0.982 (30 \times \pi \times 1^2) / 1250 \times \sqrt{(207 \times 10^3 \times 86.68^2 / 2 \times 7600)}$$

$$[f_{nt} = 299.54 \text{ Hz}]$$

$$[N_{crt} = 17972.4 \text{ rpm}]$$

4.2 Design of Composite Drive Shaft

The specifications for the composite drive shaft are same as that of steel drive.

Mass of the Composite drive shaft

$$m = \rho AL = \rho \times \Pi / 4 \times (d_o^2 - d_i^2) \times L \dots (1)$$

$$= 1600 \times 3.14 / 4 \times (90^2 - 83.36^2) \times 1250$$

[m = 1.80 Kg]

4.3 Assumptions [9]

1. The shaft rotates at a constant speed about its longitudinal axis.
2. The shaft has a uniform, circular cross section.
3. The shaft is perfectly balanced, i.e., at every cross section, the mass center coincides with the geometric center.
4. All damping and nonlinear effects are excluded.
5. The stress-strain relationship for composite material is linear & elastic; hence, Hooke’s law is applicable for composite materials.
6. Acoustical fluid interactions are neglected, i.e., the shaft is assumed to be acting in a vacuum.
7. Since lamina is thin and no out-of-plane loads are applied, it is considered as under the plane stress.

4.4 Selection of Cross-Section

The drive shaft can be solid circular or hollow circular. Here hollow circular cross-section was chosen because:

- The hollow circular shafts are stronger in per kg weight than solid circular.
- The stress distribution in case of solid shaft is zero at the center and maximum at the outer surface while in hollow shaft stress variation is smaller. In solid shafts the material close to the center are not fully utilized.

Table3 - Material properties of composite material i.e. HS Carbon / Epoxy

Mechanical Properties	Units	HS – Carbon / Epoxy
E ₁₁	GPa	134
E ₂₂	GPa	70
G ₁₂	GPa	58
N	-	0.3
ρ	Kg / m ³	1600
St ₁ = Sc ₁	MPa	880
St ₂ = Sc ₂	MPa	60
S ₁₂	MPa	97

4.5 Torsional buckling capacity

The long thin hollow shafts are vulnerable to torsional buckling; so the possibility of the torsional buckling of the composite shaft was calculated by the expression for the torsional buckling load T_{cr} of a thin walled orthotropic tube :-

$$T_{cr} = (2\pi r^2 t) (0.272) (E_x E_y)^{0.25} (t/r)^{1.5} \dots \dots (6)$$

Where E_x and E_y are the Young’s modulus of the shaft in axial and hoop direction, r and t are the mean radius and thicknesses of composite shaft.

4.6 Lateral Vibrations

Natural frequency of composite shaft is based on Timoshenko’s beam theory,

$$f_{nt} = K_s \frac{30 \Pi p^2}{L^2} \sqrt{\frac{E_x r^2}{2\rho}} \dots \dots (7)$$

$$\frac{1}{K_s^2} = 1 + \frac{p^2 \Pi^2 r^2}{2L^2} \left[1 + \frac{f_s E_x}{G_{xy}} \right] \dots \dots (8)$$

Where f_{nt} and p are the natural and first natural frequency. K_s is the shear coefficient of the natural frequency (< 1), f_s is a shape factor (equals to 2) for hollow circular cross-sections.

Critical speed:

$$N_{crit} = 60 f_{nt}$$

V. DESIGN ANALYSIS

Finite element analysis is a computer based analysis technique for calculating the strength and behavior of structures. In the FEM the structure is represented as finite elements. These elements are joined at particular points which are called as nodes. The FEA is used to calculate the deflection, stresses, strains temperature, buckling behavior of the member.

In our project FEA is carried out by using the ANSYS 12.0. Initially we don’t know the displacement and other quantities like strains, stresses which are then calculated from nodal displacement.

5.1 Static analysis

A static analysis is used to determine the displacements, stresses, strains and forces in structures or components caused by loads that do not induce significant inertia and damping effects. A static analysis can however include steady inertia loads such as gravity, spinning and time varying loads. In static analysis loading and response conditions are assumed, that is the loads and the structure responses are assumed to vary slowly with respect to time. The kinds of loading that can be applied in static analysis includes, Externally applied forces, moments and pressures Steady state inertial forces such as gravity and spinning Imposed non-zero displacements. If the stress values obtained in this analysis crosses the allowable values it will result in the failure of the structure in the static condition itself. To avoid such a failure, this analysis is necessary.

5.2 Boundary conditions

The finite element model of HS Carbon / Epoxy shaft is shown in Figure .One end is fixed and torque is applied at other end.

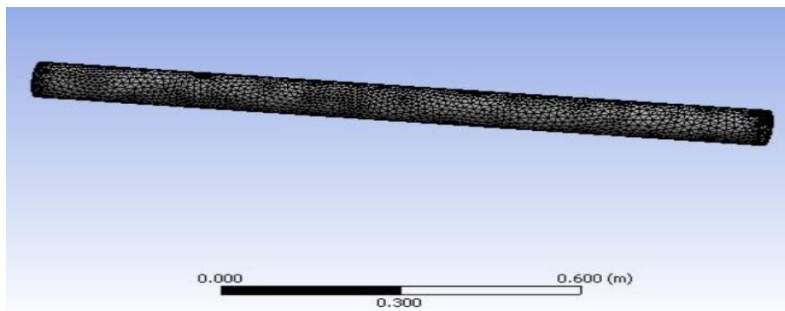


Fig: 2 - Finite element model of HS Carbon/Epoxy shaft.

5.3 Modal analysis

When an elastic system free from external forces can disturbed from its equilibrium position and vibrates under the influence of inherent forces and is said to be in the state of free vibration. It will vibrate at its natural frequency and its amplitude will gradually become smaller with time due to energy being dissipated by motion. The main parameters of interest in free vibration are natural frequency and the amplitude. The natural frequencies and the mode shapes are important parameters in the design of a structure for dynamic loading conditions.

Modal analysis is used to determine the vibration characteristics such as natural frequencies and mode shapes of a structure or a machine component while it is being designed. Modal analysis is used to determine the natural frequencies and mode shapes of a structure or a machine component. The rotational speed is limited by lateral stability considerations. Most designs are sub critical, i.e. rotational speed must be lower than the first natural bending frequency of the shaft. The natural frequency depends on the diameter of the shaft, thickness of the hollow shaft, specific stiffness and the length.

5.4 Buckling analysis

Buckling analysis is a technique used to determine buckling loads (critical loads) at which a structure becomes unstable, and buckled mode shapes. For thin walled shafts, the failure mode under an applied torque is torsional buckling rather than material failure. For a realistic driveshaft system, improved lateral stability characteristics must be achieved together with improved torque carrying capabilities.

VI. FINDINGS OF FINITE ELEMENT ANALYSIS

6.1 Steel Shaft

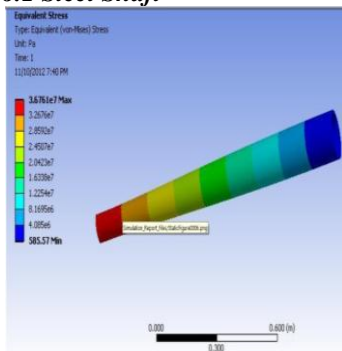


Fig. 3 Equivalent Stresses

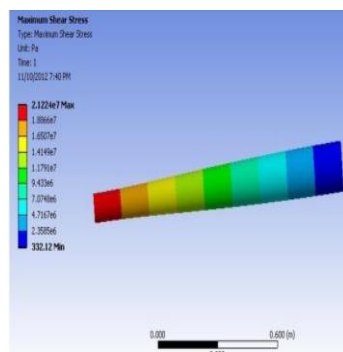


Fig. 4 Maximum Shear stresses

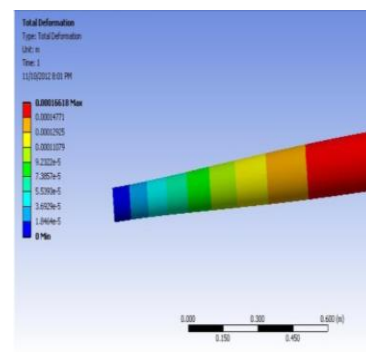


Fig. 5 Total Deformation

6.2 HS – Carbon / Epoxy

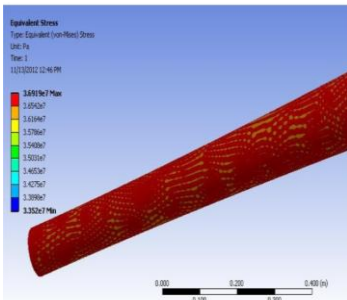


Fig. 6 Equivalent Stresses

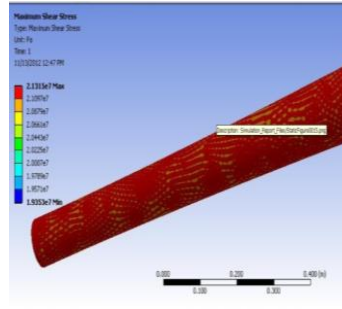


Fig. 7 Maximum Shear Stresses

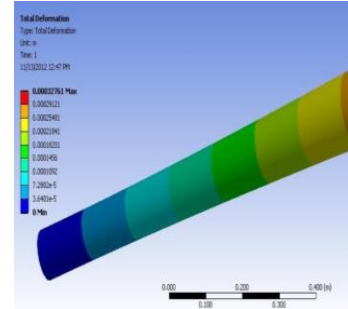


Fig. 8 Total Deformation

6.3 HM – Carbon / Epoxy

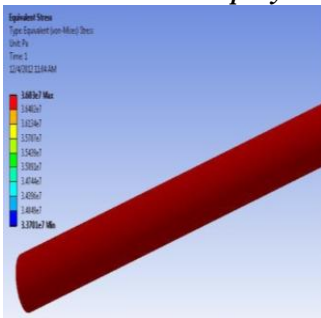


Fig. 9 Equivalent Stresses

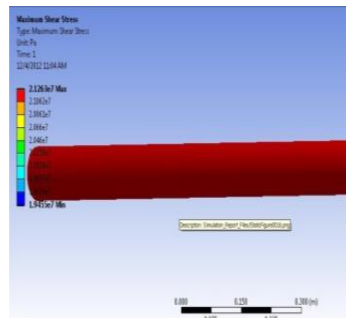


Fig. 10 Maximum Shear Stresses

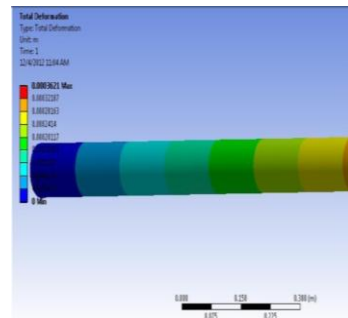


Fig. 11 Total Deformation

VII. DESIGN OPTIMIZATION – GENETIC ALGORITHM (GA)

Many methods are used for the design optimization that assumes all the design variables are continuous. But in actual structural optimization almost all the variables are discrete. The GA is a stochastic global search method that mimics the metaphor of natural biological evolution. GA operates on a population of potential solutions applying the principle of survival of the fittest to produce (hopefully) better and better approximations to a solution. At each generation, a new set of approximations is created by the process of selecting individuals according to their level of fitness in the problem domain and breeding them together using operators borrowed from natural genetics. This process leads to the evolution of populations of individuals that are better suited to their environment than the individuals that they were created from, just as in natural adaptation

7.1 Advantages of GA over other Optimization methods.

- GA does not require a problem specific knowledge to carry out a search. GA uses only the values of the objective function. For instance, calculus based search algorithms use derivative information to carry out a search.
- GA uses a population of points parallel at a time in contrast to the single point approach by the traditional optimization methods. That means at the same time GAs process a number of designs. In GA, the design variables are represented as strings of binary variables that correspond to the chromosomes in natural genetics. Thus the search method is naturally applicable for solving discrete and integer programming problems.
- GAs uses randomized operators in place of the usual deterministic ones. In every generation, a new set of strings is produced by using randomized parents selection and crossover from the old generation (old set of strings).
- GA does not require derivative information or other auxiliary knowledge only the objective function and corresponding fitness levels influence the directions of search.
- GAs use probabilistic transition rules, not deterministic ones.
- GAs work on an encoding of the parameter set rather than the parameter set itself (except in where real-valued individuals are used).

VIII. CONCLUSION

- The replacement of conventional drive shaft results in reduction in weight of automobile.
- The finite element analysis is used in this work to predict the deformation of shaft.
- The deflection of steel, HS Carbon / Epoxy and HM Carbon / Epoxy shafts was 0.00016618, 0.00032761 and 0.0003261 mm respectively.
- Natural frequency using Bernoulli – Euler and Timoshenko beam theories was compared. The frequency calculated by Bernoulli – Euler theory is high because it neglects the effect of rotary inertia & transverse shear.
- Hence the single piece High Strength Carbon / Epoxy composite drive shaft has been proposed to design to replace the two piece conventional steel drive shaft of an automobile.

The FEA analysis is done to validate the analytical calculations of the work.

The results of the work are encouraging and suggesting to replacement of conventional drive by composite has an added advantage.

The next phase of work consists of Optimization of shaft for the objective function as weight and fundamental natural frequency.

REFERENCES

- [1] John. W.et. al. Engineers Guide to Composite Materials, American Society for Metals, 1986.
- [2] Beardmore, P. et al. The Potential for Composites in Structural Automotive Applications J. of Composites Science and Technology 26 1986: pp. 251 – 281.
- [3] T. RANGASWAMY, et. al. “Optimal Sizing and stacking Sequence of Composite Drive shafts” ISSN 1392–1320 materials science (medžiagotyra). Vol.11, no.2. 2005
- [4] Rajeev S and Krishnamurthy, C.S, 1992 “Discrete Optimization of structure using Genetic Algorithm”, Journal of struct. Engg. ASCE Vol. 118 PP. 1233-1250
- [5] Pollard, A. Polymer Matrix Composites in Driveline Applications, GKN Tech., UK, 1989.
- [6] Goldberg, D. E. Genetic Algorithms in Search, Optimization and Machine Learning, Reading MA, Addison-Wesley, 1989
- [7] Vijayarangan, S., Rajendran, I. Optimal Design of a Composite Leaf Spring Using Genetic Algorithm Computers and Structures 79 2001: pp. 1121 – 1129.
- [8] T.Rangaswamy, et. al “Optimal Design and Analysis of Automotive Composite Drive Shaft”, International Symposium of Research Students on Materials Science and Engineering December 2002-04 Chennai India
- [9] Kim C D et. al. 1992, “Critical speed Analysis of Laminated Drive Shafts”, Composite Engg. Vol.3, pp. 633-643.
- [10] J. H. Park, J. H. Wang 2001, “Stacking sequence Design of Composite Laminates for maximum Strength Using Genetic Algorithm”, Journal of Composite Structures, Vol.52, pp. 217-231.

Experimental Evaluation of a Batch Hot Air Fluidized Bed Dryer

Oluwaleye. I.O.,¹ Adeyemi. M.B.²

Department of Mechanical Engineering Ekiti State University, Ado Ekiti

Abstract: The experimental evaluation of a batch hot air fluidized bed dryer for cassava particles is presented. The test rig of fluidized bed dryer consists of a vertical column 400mm diameter with a physical height of 2960mm, a regulated centrifugal blower powered by a 1.5 Hp electric motor, and an air heater with a thermostat for selection of drying temperature of the fluidizing medium. A bed of 1.555kg cassava particles were fluidized at three different air flow rates: 0.43 kg/s, 0.05 kg/s and 0.056 kg/s in succession. The drying temperatures considered are at an interval of 20 °C. The minimum drying temperature is 60 °C and the maximum temperature of 160 °C. The resident drying time for cassava particles in the dryer was found to decrease with increase in drying temperature. The heat source for drying came solely from the heated fluidizing air. It was also observed that the drying rate decreases with increase in air flow rate while it increases with drying temperature.

Keywords: fluidized; cassava, experimental, hot, air, drying

I. INTRODUCTION

Fluidization is the phenomenon of the solid-fluid contacting process in which a bed of solid particles is lifted and agitated by a rising stream of process fluid, thereby making the bed of solid particles behaves like fluid [1]. Drying is generally defined as the removals of volatile substances (a liquid) by means of heat from a material (mixture of substances) to yield a solid product. It is a fundamental unit operation in the chemical processing industries and it features prominently also in the food processing and mineral processing industries. Often, though not exclusively, the principal volatile substance is water. Principally, drying is essential to preserve the product from damage during storage i.e to prolong storage life. High moisture level and warm temperatures promote mould growth, insect growth and increase the respiration rate of the product. The products with high moisture percentage at the time of storage are liable to attack by fungal growth and toxic materials, which are harmful to human health [2].

The drying application of fluidization technique to a wide variety of particulate materials in industry dated as far back as 1940s according to Reay [3]. Currently, it is becoming popular for drying crushed minerals, sand, polymers, fertilizers, pharmaceuticals, crystalline materials and many other industrial and agricultural products. Fluidized drying among others has the advantage of high intensity of drying and high thermal efficiency with uniform and closely controllable temperature in the bed promoted by intensive solid mixing due to the presence of bubbles. It requires less drying time due to high rates of heat and mass transfer. The efficient gas-solid contact leads to compact unit and relatively low capital cost. Since there is no moving parts other than feeding and discharge mechanisms, except in the case of vibrating fluid bed, reliability is high and maintenance cost is low.

Cassava is known to contain cyanogenic glycosides (linamarin and lotaustralin) liable to produce hydrocyanic acid [4] which is poisonous. It was reported in literature that sun drying does eliminate a large proportion of the hydrocyanic acid [5]. This makes drying of cassava particles inevitable and significant. The report of Monroy-Rivera et al [6], shows that drying by heated air is more efficient at eliminating hydrocyanic acid. This makes the adoption of fluidization technique that is the direct contact of hot air with cassava particulate in a fluidized state a challenge that would solve perennial local problem associated with gari production. The technique enhances high intensity of heat and mass transfer. The good mixing of the particles in a fluid bed also enhances uniform frying within a short residence time.

A lot of experimental works had been done on the application of fluidized bed for various utilities including. Romankov [7] according to Hoebink and Rietema [8] proposed design procedures for fluidized bed dryer based on the total heat and mass balance of the whole apparatus. Prasad et.al [9] designed and fabricated a sample laboratory dryer capable of having stationary, semi-fluidized and fluidized drying conditions in a single unit. Drying experiments were conducted for parboiled rough rice with 10, 15, and 20 cm initial bed thickness at 40 to 80 degree Celsius of drying air for each three drying conditions. They observed that parboiled rough rice could be dried under semi-fluidized conditions without any significant milling loss and that drying time would also be largely reduced as compared to stationary- bed conditions. Grabowski et al. [10] developed a special drying method, using a laboratory scale fluidized bed dryer to reduce browning of grapes during drying. Fresh Thompson seedless grapes were initially dried by immersion in a fluidized bed of sugar. The flow rate of hot air at 45-60 degree Celsius was used to fluidized the sugar bed. Due to the simultaneous osmotic and convection drying effects, the drying time was reduced by factor of approximate 1.5 as compared to drying under a similar condition without added sugar. The major problem associated with the osmo-convective drying of grapes on a sugar bed was the stickiness, caused by sugar, on the fruit surface. This was reduced by partially substituting sugar with semolina to create fluidized bed.

Soponronnarit et al [11] conducted a feasibility study of paddy drying by fluidization technique. Operating parameters affecting product quality, drying capacity and energy consumption were investigated. Experimental results showed that drying rate of a paddy kernel was controlled by diffusion. However, drying capacity of dryer increased with

specific air flow rates and drying air temperatures. Energy consumption was reduced when specific air flow rate decreased or when fraction of recycled air increased. Maximum temperature should be limited to 115 degree Celsius and final moisture content of paddy at 24-25% dry basis if product qualities were maintained.

Soponronnarit et al [12] carried out a batch fluidized bed dryer design for corn drying. Drying characteristics of corn were investigated. The experimental results indicated that moisture transfer inside a corn kernel was controlled by internal diffusion by the following condition: inlet hot air temperatures of 120-200 degree C, superficial air velocities of 2.2-4 m/s, bed depths of 4-12 cm, fraction of air recycled of 0.5 – 0.9 and initial moisture content of corn of 43% dry-basis.

In this work, the performance evaluation of a batch hot air fluidized bed dryer for drying cassava particulates was carried out at various drying temperatures. The technique of fluidization was adopted following the work of Geldart [13] and Ogunleye [14] that classified cassava particles diameter within the range of 40 μ m and 500 μ m particles, which fluidized easily.

II. MATERIALS AND METHODS

The experimental test rig for the batch fluidized bed drying operation is shown in Figure 1. A drying temperature and flow rate were selected using the temperature and flow rate controllers. After a steady drying bed temperature was attained by monitoring with a chrome-aluminium thermocouple type K, a known mass of cassava particulates were introduced into the bed. The drying process started while the temperatures in the middle and along the height of the dryer column were monitored. Periodically, about 60g of the sample were withdrawn from the dryer and the percentage moisture content of the particles was tested with the aid of a moisture meter. The results obtained as the cassava particles made contact with the stream of hot air within a drying time of less than 60minutes are presented and discussed below.



Figure 1: Experimental set up of fluidized bed dryer model plant

III. RESULTS AND DISCUSSION

Particle and Air Temperature

As the cassava particles were introduced into the dryer, on contact with hot air from the inlet to the dryer, the temperature of the cassava particles gradually increased from room temperature to the drying temperature setting while at the same time their moisture content reduced gradually during the drying. Particle temperature versus drying time at 120°C drying temperature at various flow rates is shown in Figure 2. The particle temperature increases faster at a lower flow rate of the fluidizing air medium.

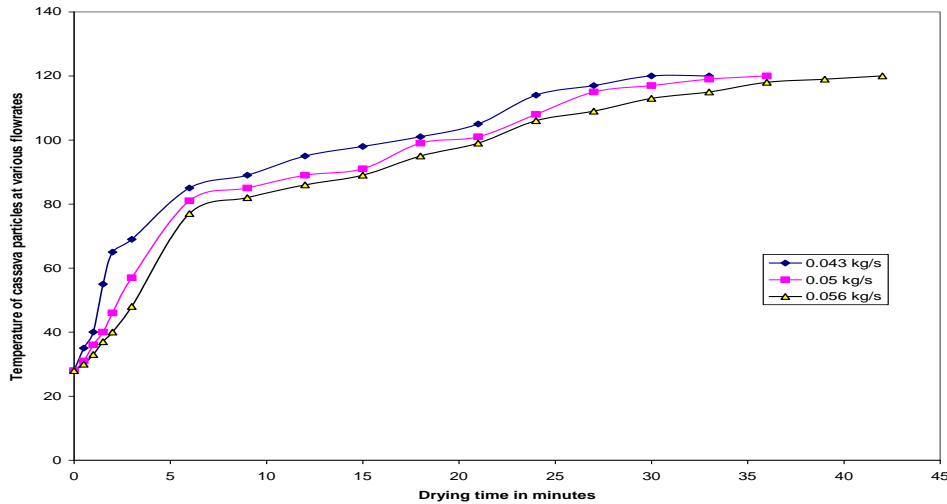


Figure 2: Cassava Particles' temperatures at various air flowrates for a given drying temperature of 120°C

As the hot air made contact with the wet cassava particles, the air temperature dropped sharply and then gradually increased towards the drying temperature setting as shown in Figure 3. It was observed that the air flow at the highest rate took shorter time to attain the temperature setting.

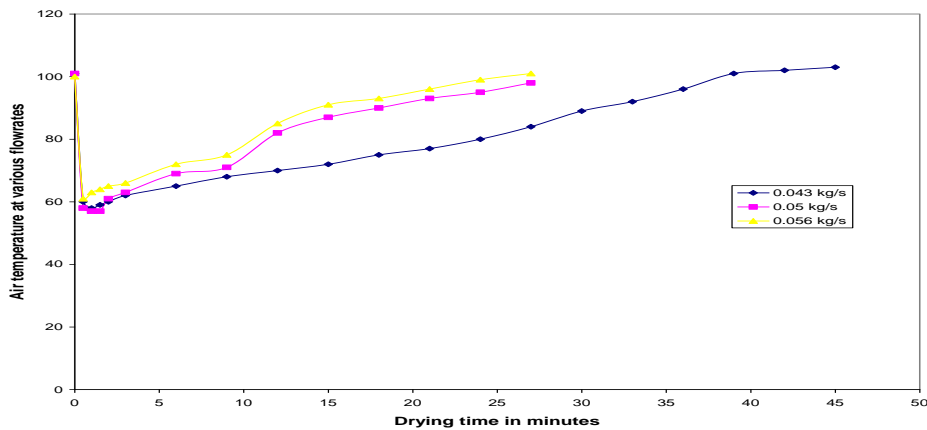


Figure 3: Typical temperature variation of the fluidizing medium after feeding at 120°C and at various flowrates

Moisture ratios versus time

The moisture ratio of the cassava particles versus drying time at various drying temperature is shown in Figure 4a. A typical moisture ratio and the cassava particle temperature at 120°C and at air flowrate of 0.043 kg/s is shown in Figure 4b. At drying temperatures of 60°C and 80°C, the moisture ratios versus times curves are straight lines, indicating that within the drying time considered at these temperatures, the falling rate of drying was not attained. There is not enough heat to remove bound moisture content of the cassava particles. But at temperatures of 100 °C to 160°C for the same drying time interval, the removal of bound moisture content of the cassava particles is appreciable and sufficient drying actually take place. Figure 4b shows a typical particle temperature rise and the moisture ratio versus drying time for an isothermal heating temperature of 120°C. The three distinct phases of drying processes are clearly seen on the typical heating temperature of 120°C shown and the corresponding moisture ratio with drying times. The diffusion model constant parameters at various drying temperatures are shown in Table I. A moisture ratio curve at a typical drying temperature of 120°C for various flow rates is shown in Figure 5. Table II shows their diffusion model constant parameters. The increase in flow rate of air produces less drying effect because in this experiment, the air flow is the only carrier of heat into the bed. The higher the flow rate of air the lesser the energy it carries into the bed for drying. In a situation where heat for drying is supplied through other means other than the air medium, increase in airflow rate will enhance the drying rate.

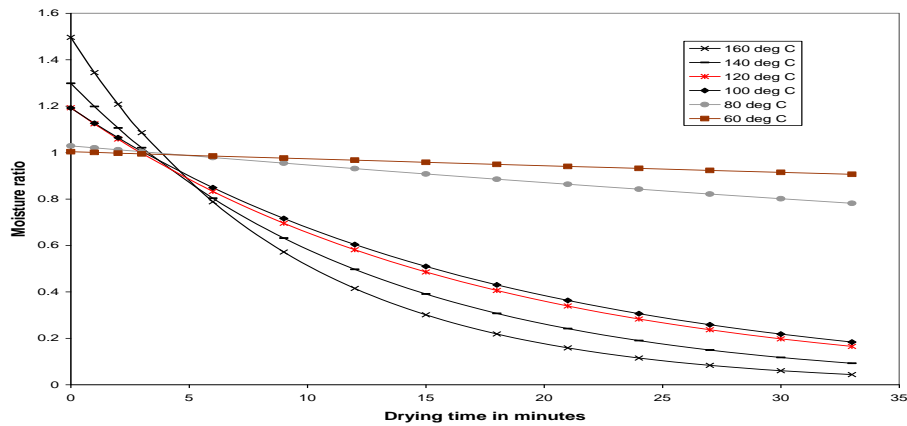


Figure 4a: Moisture ratios versus drying time at various drying temperatures indicated for air flowrate of 0.43 kg/s

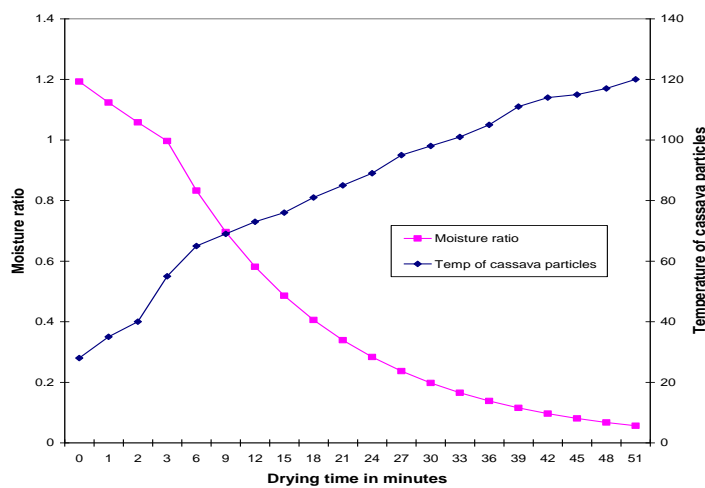


Figure 4b: Typical moisture ratio and particle temperature rise versus drying time at 120°C

Table I: Diffusion Model Constants for fluidized bed drying at different drying temperatures and at 0.043 kg/s obtained from regression analysis

Diffusion Constants	Drying Temperature °C					
	60	80	100	120	140	160
K_0	-0.00624	-0.0157	-0.05421	-0.0582	-0.07803	-0.10688
B_0	1.02798	1.08783	1.15769	1.17694	1.2778	1.496
Coefficient of R	-0.84177	-0.84742	-0.97752	-0.97351	-0.97506	-0.95888

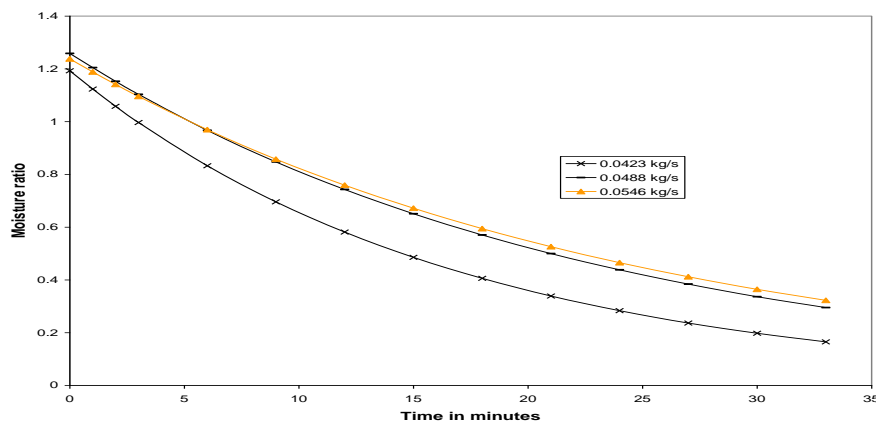


Figure 5: Moisture ratio versus time at various flow rate for a typical drying temperatures of 120°C

Table II: Diffusion Model Constants for fluidized bed drying at isothermal temperature of 120°C for various air flowrate obtained from regression analysis

Diffusion Constants	Drying Temperature 120°C		
	0.043 kg/s	0.05 kg/s	0.056 kg/s
K_0	-0.0599	-0.04397	-0.040763
B_0	1.192897	1.258697	1.23805
Coefficient of Correlationr	-0.96968	-0.92227	-0.919349

Drying rate versus free moisture content

The drying rate versus free moisture curve at 0.043kg/s flow rate of hot air, the fluidizing medium and at various drying temperatures is shown in Figure 6. At drying temperatures of 60°C and 80°C, the falling rate period is not reached within the drying period considered. Both constant drying rate and falling drying rate periods are present for drying temperatures 100°C to 160°C. The higher the drying temperatures, the greater the drying rates of the cassava particles. The critical free moisture content, critical drying rate and constant drying rate are found to increase with increase in drying temperatures as shown in Table III. At a typical drying temperature, the drying rates versus free moistures decreased with increase in flow rates of fluidizing medium as shown in Figure 7. In Table IV, the critical free moisture content, critical drying rate and constant drying rate at various flow rates are shown. The higher the air flow rate, lesser the heat is available for drying in the bed.

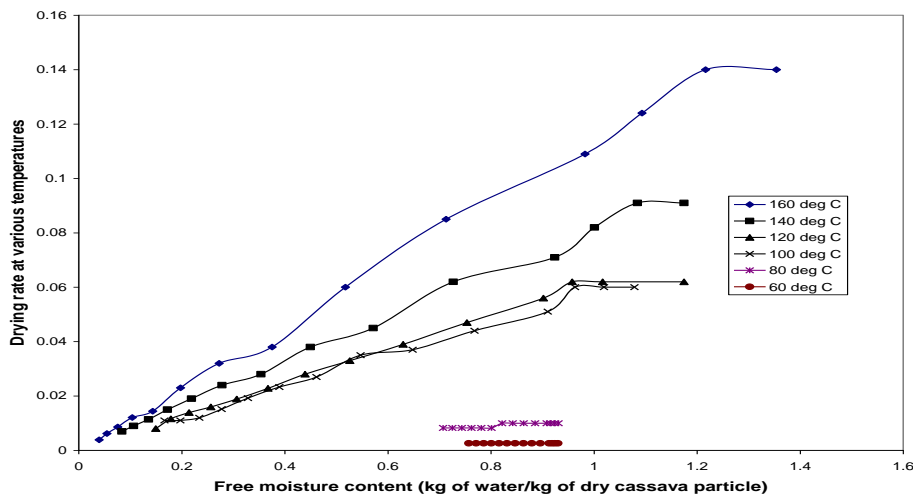


Figure 6: Drying rates of cassava particles with free moisture content at various drying temperatures at air flowrate of 0.043kg/s

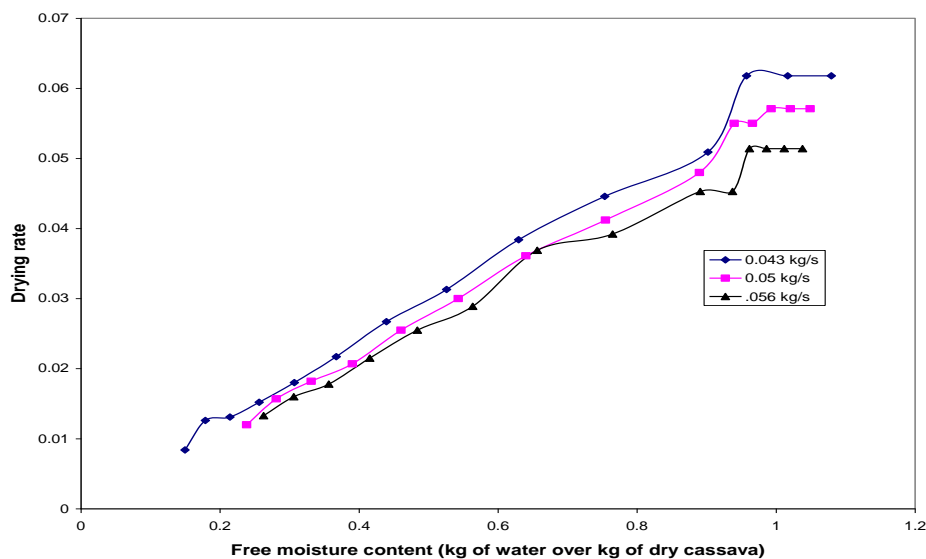


Figure 7: Drying rate of cassava particle at various flowrate for a typical drying temperature of 120°C

Table III: Critical free moisture content and drying rate at various fluidized bed drying temperatures

	Drying temperatures					
	60°C	80 °C	100 °C	120 °C	140 °C	160 °C
Critical free moisture Xc	.757021	0.801209	0.900346	0.901806	1.00091	1.09327
Critical drying rate Rc	0.0026	0.00824	0.051	0.056	0.082	0.124
Constant drying rate	.0026	0.01	.06	.062	.091	0.14

Table IV: Critical free moisture content and drying rate for fluidized bed drying at various air flowrate and at 120 °C

	Air flow rates		
	0.043kg/s	0.05kg/s	0.056kg/s
Critical free moisture Xc	0.957475	0.939879	0.890933
Critical drying rate Rc	0.056	0.055	0.0453

Comparison of oven and fluidized bed drying methods

The moisture ratio of cassava particulates at various drying time for a typical drying temperature of 120°C using oven and fluidized bed drying methods is shown in Figure 8. At a given time, the moisture ratio of the cassava particulate during fluidized drying is greater than that of oven drying sample. This is because the drying rate of cassava sample is greater in oven drying method than that of the fluidized method as shown in Figure 9. This is expected because 60 g of the cassava sample was used for oven drying analysis while 1.555kg of cassava sample was dried using a fluidized bed from which samples were taken at equal time interval for analysis.

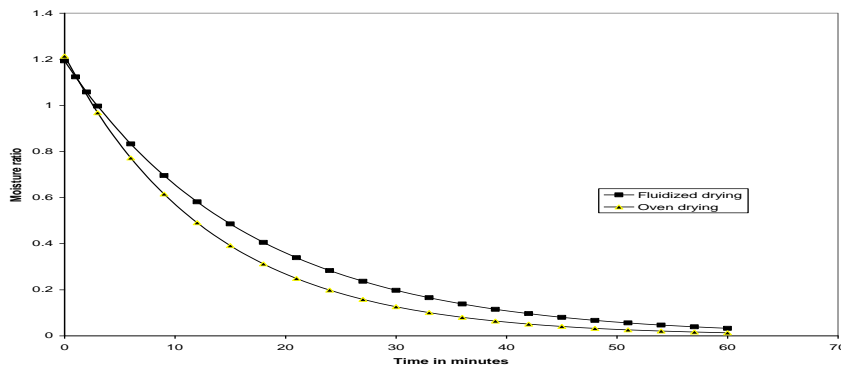


Figure 8: Moisture ratio of cassava particles versus drying time using fluidized bed and oven drying methods at 120°C typical drying temperature

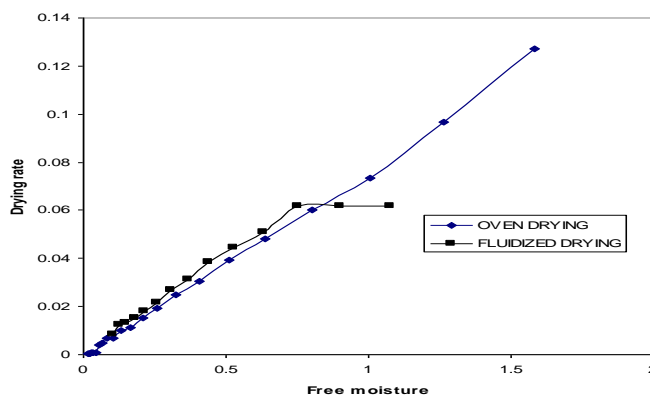


Figure 9: Drying rate of cassava particulates using fluidized bed and oven drying methods at typical drying temperature of 120°C

IV. CONCLUSION

The technique of fluidized bed drying for cassava particles is workable and viable. The product from the fluidized bed dryer is fine and uniformly dried. To ensure the product is hygienic for eating with reduced starch content, the dryer must be covered after the product is introduced for about 20 minutes depending on the drying temperature. A lower air flow rate is required at the initial stage when the product is undergoing a constant drying period. Beyond the constant drying period, the air flow rate must be increased to ensure particle mixing and to prevent localized heating of the cassava particles. This work so far has opened up an alternative technology for the production of gari from cassava particles. The design and the operation methods is simple and can be developed and mass produced to boost food production.

V. ACKNOWLEDGEMENT

The authors are grateful to the Ekiti State University for the support and sponsorship of this research work.

REFERENCES

- [1] Daizo Kunii and Octave Levenspiel (1991), Fluidization Engineering, Butterworth-Heinemann, USA, pp 1-13, 15-58
- [2] Sharma, V.K., Sanjay S. and Garg, H.P.(1991), Mathematical Modelling and Experimental Evaluation of a natural Convection Type Solar Cabinet Dryer, Energy Conversion and management, Vol. 31, No 1, pp 65-74
- [3] Reay, D. (1986), Fluid Bed Drying, In Gas Fluidization Technology, Ed. By D.Geldart, John Wiley and Sons, pp. 259-284,
- [4] Nartey, F., (1981),Cyanogenesis in Tropical Peeds and Foodstuff, In Cyanide in Biology, Ed. by Wennesland, B., Coon, E.E., Knowles, C.J.,Westley J and Wissing, F., Academic press, London, page 115-132.
- [5] Cooke, R.D. and Maduagwu, E.N.,(1978), The Effect of Simple Processing on the Cyanide Content of Cassava Chips, Journal of Food Technology, vol 13, page 299-306
- [6] Monroy-Rivera, J.A., Lebert, A., Marty, C., Muchnic, J., and Bimbenet, J.J.,(1991) Simulation of Cyanoglucosidic Compounds Elimination in Cassava During Drying In Drying '91 Ed. by Mujumdar A.S. and Filkova', I. Elsevier Science Publishers, Amsterdam, Page 463-470
- [7] Romankov, P.G.(1971), Drying, In Fluidization , Ed. By Davidson J. F. and Harrison D., Academic Press, London
- [8] Hoebink, J.H.B.J and Rietema, K. (1980), Drying Granular Solids in Fluidized Bed I and II, Chemical Engineering Science, Vol 35, pp 2135-2140 and pp 2257-2265
- [9] Prasad, B.S.V.; Chandra, P.K.; Bal, S.(1994), Drying paraboiled rough rice in stationary, semi-fluidized, and fluidized bed, Transactions of the ASAE v 37 n 2 Mar-Apr 1994 , IIT Kharagpur, India. pp 589-594
- [10] Grabowski, S.; Mujumdar, A.S.; Ramaswamy, H.S.; Strumillo, C. (1994), Drying Technology v 12 n5 July, Macdonald Campus of McGill Univ, Ste Anne de Bellevue, Que, Canada. pp 1211-1219
- [11] Soponronnarit, Somchart and Prachayawarakorn, Somkiat (1994), Optimum strategy for fluidized bed paddy drying , Drying Technology v 12 n7 October , King Mongkut's Inst of Technology Thonburi, Bangkok, Thailand pp. 1667-1686
- [12] Soponronnarit, Somchart; Pongtornkulpanich, Anan; Prachayawarakorn, Somkiat (1997), Drying characteristics of corn in fluidized be dryer, Drying Technology v 15 n 5 May King Mongkut's Inst of Technology Thonburi, Bangkok, Thailand pp. 1603-1615
- [13] Geldart, D. (1986), Characterization of fluidized powders, In Gas Fluidization Technology, Ed. By D.Geldart, John Wiley and Sons, pp. 33-51,
- [14] Ogunleye, I.O. (2003), "Feasibility study of Fluidization Technique for Cassava Particulate Drying", Proceedings of Nigerian Drying Symposium on Drying Technology as a Tool for Sustainable Development on 20-23 October, 2003, University of Port Harcourt, Nigerian, pp 65-75

A PSO Optimized Layered Approach for Parametric Clustering on Weather Dataset

Shikha Verma,¹ Kiran Jyoti²

¹Student, Guru Nanak Dev Engineering College Ludhiana, Punjab

²Asstt. Prof, Guru Nanak Dev Engineering College Ludhiana, Punjab

Abstract: Clustering is the process to present the data in an effective and organized way. There are number of existing clustering approaches but most of them suffer with problem of data distribution. If the distribution is non linear it gives impurities in clustering process. The propose work is about to improve the accuracy of such clustering algorithm. Here we are presenting the work on time series oriented database to present the work. Here we are presenting the three layer architecture, where first layer perform the partitioning based on time series and second layer will perform the basic clustering. The PSO is finally implemented to remove the impurities from the dataset.

Keywords: Clustering, CMeans, KMeans, Dataset, Feature

I. INTRODUCTION

Clustering is a fundamental problem in machine learning and has been approached in many ways. Clustering can be considered the most important unsupervised learning technique; so, as every other problem of this kind, it deals with finding a *structure* in a collection of unlabeled data. There are different clustering algorithms. The k-centers clustering algorithm is one of the popular algorithm. Clustering is used because following some reasons:

- Simplifications
- Pattern detection
- Useful in data concept construction
- Unsupervised learning process

A new clustering approach called Affinity Propagation was introduced by Brenden J. Frey and Delbert Dueck in 2007. Affinity Propagation has many advantages over other clustering algorithms like simplicity, general applicability, lower errors and good performance. Affinity Propagation takes as input a collection of real valued similarities between data points. It is distance based clustering algorithm and similarity measure are calculated in the form of Euclidean distance. Real valued messages are exchanged between data points until a high quality set of exemplars and corresponding clusters gradually emerges.

Each data point i sends a responsibility $r(i, k)$ to candidate exemplar indicating how much it favors the candidate exemplar over other candidates. Availability $a(i, k)$ is sent from candidate exemplar to data points indicating how well the candidate exemplar can act as a cluster center for the data points. At the end of each iteration, availability and responsibility are combined to identify the exemplar.

$$r(i, k) = s(i, k) - \max \{ \sum a(i, k') + s(i, k') \}$$

where $s(i, k)$ is the similarity between data point i and candidate exemplar k , $a(i, k')$ is availability of other candidate exemplar k' to data point i , $s(i, k')$ is the similarity between data point i and other candidate exemplar k .

$$a(i, k) = \min \{ 0, r(k, k) + \sum \max \{ 0, r(i', k) \} \}$$

where $a(i, k)$ is the availability of candidate exemplar k to data point i , $r(k, k)$ is self responsibility of candidate exemplar k , $r(i', k)$ is the responsibility from other data point i' to the same candidate exemplar k . and other candidate exemplar k

$$a(k, k) = \sum \max \{ 0, r(i', k) \}$$

Where $a(k, k)$ is self availability of candidate exemplar k and $r(i', k)$ is the responsibility from other data point i' to the same candidate exemplar k .

Clustering is "the process of organizing objects into groups whose members are similar in some way". A *cluster* is therefore a collection of objects which are "similar" between them and are "dissimilar" to the objects belonging to other clusters

A. Clustering as unsupervised classification

As for Classification, we have a multivariate dataset; a set of cases, each of which has multiple attributes/variables. Each case is represented as a record, (or row), and to each attribute variable there is an associated column. The whole comprises the caseset. The attributes may be of any type; nominal, ordinal, continuous, etc..., but the in Cluster Analysis none of these attributes is taken to be a classification variable. The objective is to obtain a rule which puts all the cases into groups, or clusters. it may then define a nominal classification variable which assigns a distinct label to each cluster. We do not know the final classification variable before we do the clustering; the objective is to define such a variable.

Hence, clustering is said to be an unsupervised classification method; unsupervised, because we do not know the classes of any of the cases before we do the clustering. We do not have class values to guide (or "supervise") the training of our algorithm to obtain classification rules.

We should note that one or more of the attributes in our case set may in fact be nominal classification variables. However, as far as our Clustering of the case set is concerned they are just nominal variables and are not treated as classification variables for the clustering analysis.

B. Distance Matrices

If we have two cases, C1 and C2 say, which have continuous variables x and y, taking values (x₁, y₁) and (x₂, y₂) respectively, then we can plot the two cases in x-y space as in Figure 1.

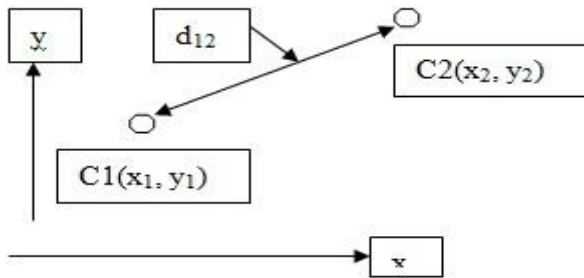


Figure 1: Euclidean distance

Using Pythagorus's Theorem, we may write

$$d_{12} = \sqrt{(x_2 - x_1)^2 + (y_2 - y_1)^2}$$

This is the Euclidean distance between the two cases, "in the x-y state-space". We often say that we have defined a "distance metric" when we have defined the formula for the distance between two cases.

If the two cases are characterized by p continuous variables (x₁, x₂, ...x_i, ...x_p say) rather than two (i.e. x, y), [Note: x → x₁ so x(case 2) → x₁(case 2) ≡ x₁(2); similarly y₂ → x₂(2)], then we may generalize the Euclidean distance to:

$$d_{12} = \sqrt{\sum_{i=1}^p (x_i(2) - x_i(1))^2}$$

This can be generalized further to the Minkowski metric:

$$d_{12} = \sqrt[m]{\sum_{i=1}^p |x_i(2) - x_i(1)|^m}$$

where |x| denotes the absolute value of x, (i.e. the size, without the sign).

C. Standardization

If the values of the variables are in different units then it is likely that some of the variables will take vary large values, and hence the "distance" between two cases, on this variable, can be a big number. Other variables may be small in value, or not vary much between cases, in which case the difference in this variable between the two cases will be small. Hence in the distance metrics considered above, are dependent on the choice of units for the variables involved. The variables with high variability will dominate the metric. We can overcome this by standardizing the variables.

D. Similarity Measure

A measure of the similarity (or closeness) between two cases must take its highest value when the two cases have identical values of all variables, (i.e. when the two

cases are coincident in multivariable space). The similarity measure must decrease monotonically as the case variable values increase, i.e. as the distance between the cases increases. Hence, any monotonically decreasing function of distance will be a possible similarity measure. If we want the similarity measure to take value 1 when the cases are coincident, then we might consider:

D. Particle Swarm Optimization

PSO was first proposed by Kennedy and Eberhart [9]. The main principle behind this optimisation method is communication. In PSO there is a group of particles that look for the best solution within the search area. If a particle finds a better value for the objective function, the particle will communicate this result to the rest of the particles. All the particles in the PSO have "memory" and they modify these memorized values as the optimisation routine advances. The recorded values are: velocity (V), position (p), best previous performance (pbest) and best group performance (gbest). The velocity describes how fast a particle should move from its current position which contains the coordinates of the particle. The last two parameters are the recorded best values that have been found during the iterations. A simple PSO algorithm is expressed as [9]:

II. LITERATURE SURVEY

Lei Jiang defined a work on "Hybrid Adaptive Niche to Improve Particle Swarm Optimization Clustering Algorithm". This paper use adaptive niche particle swarm algorithm to improve clustering And it is also studied the impact of different fitness optimization function to clustering data [1]. Shuai Li, Xin-Jun Wang, Ying Zhang defined a work on "X-SPA: Spatial Characteristic PSO Clustering Algorithm with Efficient Estimation of the Number of Cluster". In this paper author unifies Particle Swarm optimization (PSO) algorithm and Bayesian Information Criterion (BIC), proposes a numeric clustering algorithm. Chaos and space characteristic ideas are involved in the algorithm to avoid local optimal problem. Furthermore, BIC is also involved to provide an efficient estimation of the number of cluster [2].

Rehab F. Abdel-Kader presented a work on "Genetically Improved PSO Algorithm for Efficient Data Clustering. The proposed algorithm combines the ability of the globalized searching of the evolutionary algorithms and the fast convergence of the k-means algorithm and can avoid the drawback of both. The performance of the proposed algorithm is evaluated through several benchmark datasets. The experimental results show that the proposed algorithm is highly forceful and outperforms the previous approaches such as SA, ACO, PSO and k-means for the partitioned clustering problem [3]. Surat Srinoy presented a work on "Combination Artificial Ant Clustering and K-PSO Clustering Approach to Network Security Model", His paper presents natural based data mining algorithm approach to data clustering. Artificial ant clustering algorithm is used to initially create raw clusters and then these clusters are refined using k-mean particle swarm optimization (KPSO). KPSO that has been developed as evolutionary-based clustering technique [4].

Shafiq Alam has defined a work on “Particle Swarm Optimization Based Hierarchical Agglomerative Clustering The proposed algorithm exploits the swarm intelligence of cooperating agents in a decentralized environment. The experimental results were compared with benchmark clustering techniques, which include K-means, PSO clustering, Hierarchical Agglomerative clustering (HAC) and Density-Based Spatial

Clustering of Applications with Noise (DBSCAN). The results are evidence of the effectiveness of Swarm based clustering and the capability to perform clustering in a hierarchical agglomerative manner [5]. Alireza Ahmadyard presented a novel work on “Combining PSO and k-means to Enhance Data Clustering”. In this paper we propose a clustering method based on combination of the particle swarm optimization (PSO) and the k-mean algorithm. PSO algorithm was showed to successfully converge during the initial stages of a global search, but around global optimum, the search process will become very slow. On the contrary, k-means algorithm can achieve faster convergence to optimum solution [6].

III. PROPOSED APPROACH

The proposed work is improvement of the data clustering algorithm with effect of Particle Swarm Optimization. Here the improvement is expected in terms of accuracy and the efficiency. The proposed work will be affected with 3 dimensions of improvement in data clustering. As the first dimension the data will be segmented according to the time series. Such as in case of temperature the time series will be according to the seasonal parameters. Once the data is segmented, The clustering algorithm will be implemented on it.

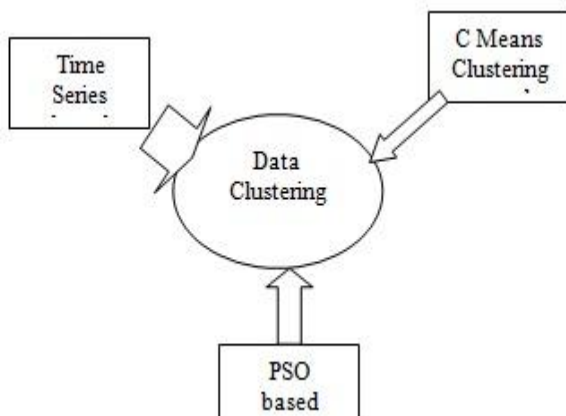


Figure 2: Three Dimensional Clustering

The clustering algorithm will perform the actual data categorization according to the data values. Here either C-Means or the K-Means algorithm will be implemented based on the dataset. This work will be done only once. The clustering algorithm is the seed of the proposed algorithm. Once the clustering done the refinement over the dataset is performed by the PSO. The PSO will use the output of the clustering algorithm and generate a Hybrid algorithm. The work of PSO is first to find the best fitness function and then pass this clustered dataset on this fitness function. The fitness function will be generated respective to the cluster as well as the whole dataset. The fitness function will accept a

particular data item and verify that whether it should belong to the cluster or not after examine the cluster data. To implement the PSO some parameters are required. These parameters will be decided according to the dataset and the deficiencies in the clustered dataset.

The basic algorithm for the PSO that will be implemented is given as under

- 1: Initialize a population array of particles with random positions and velocities on D - dimensions in the search space.
- 2: For each particle, evaluate the desired optimization fitness function in D variables.
- 3: Compare particle's fitness evaluation with its $pbest_i$. If current value is better than $pbest_i$, then set $pbest_i$ equal to the current value, and p_i equal to the current location x_i in D - dimensional space.
- 4: Identify the particle in the neighborhood with the best success so far, and assign its index to the variable g .
- 5: Change the velocity and position of the particle according to the equation (3)
- 6: If a criterion is met (usually a sufficiently good fitness or a maximum number of iterations), exit.
- 7: If criteria are not met, go to step 2

The presented work is implemented for the weather dataset under the different attributes. These attributes includes the temperature, rainfall, humidity etc. The process on this dataset is performed under a three layered approach. The algorithmic process is given as under

Table 1: Proposed Algorithm

Step 1:	Accept Whole Dataset As Input
Step 2:	Arrange the Dataset According to Years
Step 3:	Find the Instance Count for Each Year
Step 4:	Find the ThresholdCount Value for whole Dataset
Step 5:	Remove the Year Dataset Having Count(Year)<ThresholdCount
Step 6:	Represent the Remaing as Training Dataset
Step 7:	Select N-points as initial centroids
Step 8:	Repeat
a.	Form N-clusters by assigning each point to its closest centroid
b.	Recompute the centroid of each cluster
Step 9:	Until centroid does not change
Step10:	Run PSO on initial clusters generated by Clustering Algorithms
a.	Initialize the Particles (Clusters)
b.	Initialize Population size and maximum iterations
c.	Initialize clusters to input data
d.	Evaluate fitness value and accordingly find personal best and global best position
Step 11:	Start with an initial set of particles, typically randomly distributed throughout the design space.
Step 12:	Calculate a velocity vector for each particle in the swarm.
Step 13:	Update the position of each particle, using its previous position and the updated velocity vector.
Step 14:	Repeat From Step 10 and Exit on reaching stopping criteria (maximum number of iterations).

IV. RESULTS

The presented clustering approach is implemented on weather dataset in mat lab 7.8 environment. The initial dataset contains about 10000 instances and having 7 attributes. The dataset is containing the data between years 1970 and 2010. As the first layer the time series segmentation is performed and the data values of specific years are pruned as these are found less effective. The dataset remained after the pruning process is shown in table 2 with description of specific years.

Table 2: Pruned Dataset

1971, 1972, 1974, 1976, 1977, 1978,	1979,
1981, 1984, 1986, 1987, 1988,	1991, 1993,
1994, 1996, 1998, 2000,	2001, 2003, 2005,
2009	

Initial data contains 10000 instances and after the pruning process about 6700 records left. To perform the pruning, the time series segmentation is been implemented in this work. After the pruning process, the C-Menas clustering is performed over the dataset. In this work, we have divided the complete dataset in 4 clusters under the different attributes. Figure 3, 4, 5 are showing the outcome of 1st cluster under three attributes respectively i.e. temperature, rain and humidity.

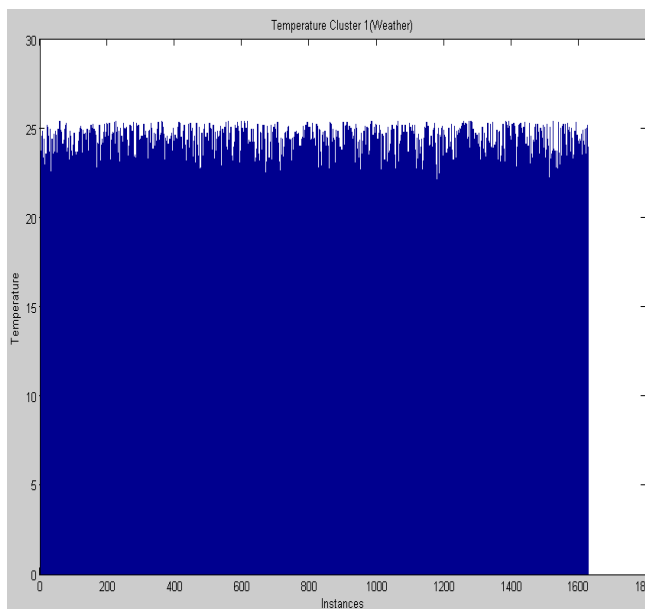


Figure 3: Cluster 1(Temperature)

As we can see figure 3 is showing the outcome of clustering on temperature dataset. As we can see in this figure, the data obtained in cluster 1 is shown. This particular cluster is having about 1600 instances and contains the temperature values between 22 to 25.

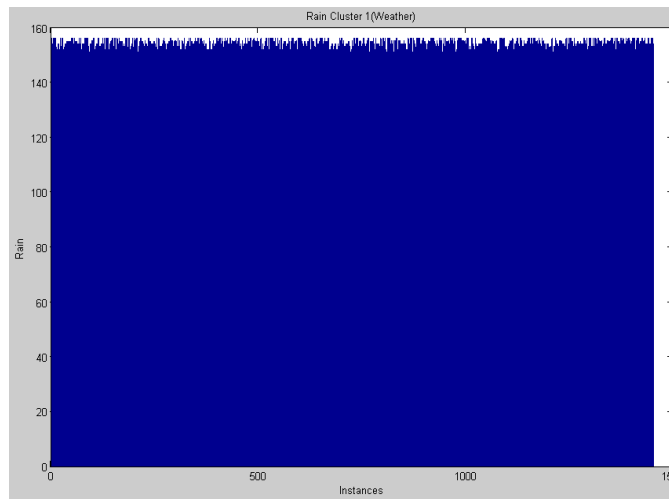


Figure 4: Cluster 1(Rain)

Figure 4 is showing the outcome of clustering on Rain dataset. As we can see in this figure, the data obtained in cluster 1 is shown. This particular cluster is having about 1400 instances and contains the temperature values between 150 to 160. Out of 6700 instances, only 1400 instances are having that much of rainfall.

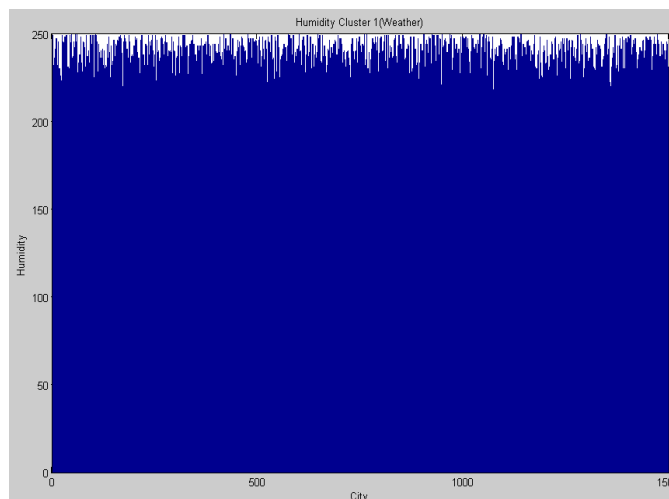


Figure 5: Cluster 1(Humidity)

As we can see figure 5 is showing the outcome of clustering on Humidity dataset. As we can see in this figure, the data obtained in cluster 1 is shown. This particular cluster is having about 1500 instances and contains the temperature values between 220 to 250.

V. CONCLUSION

The presented work is about to improve the clustering process by implementing a three layered approach. The first layer is the filtration layer to identify the most appropriate dataset on which clustering will be performed. On the second layer, the actual clustering process is performed. Finally, the PSO is used to adjust the boundary values and to optimize the outcome of clustering process.

REFERENCES

- [1] Jiang Lixin Ding, "Hybrid Adaptive Niche to Improve Particle Swarm Optimization Clustering Algorithm", 978-1-4244-9953-3/11 ©2011 IEEE
- [2] Shuai Li, Xin-Jun Wang, "X-SPA: Spatial Characteristic PSO Clustering Algorithm with Efficient Estimation of the Number of Cluster", Fifth International Conference on Fuzzy Systems and Knowledge Discovery, 978-0-7695-3305-6/08 © 2008 IEEE
- [3] Rehab F. Abdel-Kader, "Genetically Improved PSO Algorithm for Efficient Data Clustering", 2010 Second International Conference on Machine Learning and Computing, 978-0-7695-3977-5/10 © 2010 IEEE
- [4] Surat Srinoy, "Combination Artificial Ant Clustering and K-PSO Clustering Approach to Network Security Model", IEEE 2006
- [5] Shafiq Alam, Gillian Dobbie, Patricia Riddle, M. Asif Naeem, "Particle Swarm Optimization Based Hierarchical Agglomerative Clustering", 2010 IEEE/WIC/ACM International Conference on Web Intelligence and Intelligent Agent Technology
- [6] Alireza Ahmadyfard, Hamidreza Modares, "Combining PSO and k-means to Enhance Data Clustering", 2008 International Symposium on Telecommunications, 978-1-4244-2751-2/08 ©2008 IEEE
- [7] [7] Dongyun Wang, "Clustering Research of fabric deformation comfort using bi-swarm PSO algorithm", World Congress on Intelligent Control and Automation July 6-9 2010, Jinan, China
- [8] [8] Junyan Chen, "Research on Application of Clustering Algorithm Based on PSO for the Web Usage Pattern", 1-4244-1312-5/07© 2007 IEEE
- [9] [9] Jinxin Dong, Minyong Qi, "A New Clustering Algorithm Based on PSO with the Jumping Mechanism of SA", 2009 Third International Symposium on Intelligent Information Technology Application
- [10] Brendan J. Frey and Delbert Dueck, "Clustering by Passing messages Between Data Points" University of Toronto *Science*, Vol **315**, 972–976, February 2007.
- [11] Bryan Conroy and Yongxin Taylor Xi. "Semi Supervised Clustering Using Affinity Propagation". August 24, 2009.
- [12] Supporting Material available at <http://www.psi.toronto.edu/affinitypropagation>
- [13] Delbert Dueck and Brendan J. Frey. "Non-metric affinity propagation for unsupervised image categorization". In IEEE Int. Conf. Computer Vision (ICCV), 2007

Experimental Investigation of Performance Parameters of Four Stroke Single Cylinder Direct Injection Diesel Engine Operating On Rice Bran Oil & Rice Bran Oil Methyl Ester

Indu Prakash Sahu,¹ Nitin Shrivastava,² Vipin Shrivastava,³ Akhand Pratap Singh⁴

^{1,2,3}Department of Mechanical Engineering, University Institute of Technology - RGPV, Bhopal

⁴Department of Mechanical Engineering, Shree Institute of Science & Technology, Bhopal

Abstract: The conventional fuel crisis arising and ecological concerns have directed to look for alternative fuels of bio-origin sources like edible and non-edible oils. That can be produced from forests, vegetable oil crops, and oil bearing biomass materials. The increasing oil prices rapidly in our life day by day. In environmental aspects, it is require to increase energy independence and produce employment are inspiring the countries around the whole world in support of biofuels research, invention and production. Biodiesel production is an important method which requires a sustained study and optimization process because of its advantageous ecological aspects and its renewable nature. Biodiesel fuel is clean burning diesel alternative and has several attractive characteristics including biodegradability, renewability, low emission and non toxic.

The main objectives of this study to produce biodiesel from Rice Bran Oil (RBO) by transesterification (alcoholysis) process and investigated the performance parameters of single cylinder four stroke diesel engines operating on Rice Bran Oil (RBO) & Rice Bran Oil Methyl Ester (RBOME) blends. Biodiesel is an alternative fuel to the broadly used petroleum-diesel fuel. Biodiesel can be produced by domestic and non-domestic sources such as Rice Bran Oil, Soybeans, Karanja, Cotton seeds, Coconuts, Jatropa, Rubber seed, Ratanjot Oil, Rapeseeds oil etc. and thus these reduces dependence on retreating petroleum fuel from distant sources. The main reason of the transesterification process is to decrease the viscosity of oil.

The brake specific energy consumption (BSEC) was increased as the blends were increased for constant engine speed and same engine brake load than that of petroleum-diesel. As the loads were increased the BSFC of diesel engine increased in comparison to diesel fuel. The BSFC of diesel engine were increased 9.1% and 5.69 % respectively for RBO 30 & RBOME 30 blends. The brake thermal efficiency (BTE) of diesel engine at constant speed of 1500 rpm and 12 kg brake load was decreased by 4.7% and 3.0% respectively when the engine fuelled with RBO 30 & RBOME 30 blends.

The performance parameters of diesel engine fuelled with RBO 10 & RBOME 10 were more closely to diesel fuel when the engine runs at 1500 rpm and for same brake load. The engine produce almost same brake power and brake specific fuel consumption (BSFC) is almost same for 10% blends of RBO and RBOME. The Engine tests demonstrated that rice bran oil methyl esters (RBOME) produced slightly higher brake thermal efficiency (BTE) than rice bran oil (RBO). The rice bran oil consumed slightly more fuel than methyl ester.

Keyword: Diesel engine, RBO, RBOME, Performance

I. Introduction

The lack of known petroleum fuels will create more attractive renewable energy sources [1, 2]. The biodiesels are derived from plant oils; they produce negligible net green house gas emissions [3]. Biodiesel can be directly used as a fuel in diesel engines without any modification of the existing design. Biodiesel can be considered as a promising alternative fuel for the diesel engines since its fuel characteristics are almost same as the petroleum diesel fuel [4]. Due to higher viscosity and lower heat content of biodiesel direct to the lower brake thermal efficiency of diesel engine. Higher viscosity causes poor fuel atomization during the injection of biodiesel fuel, resulted increasing the engine deposits and also fuel pump consumes more energy to pump the fuel which wears out the elements of fuel pump and injectors [5]. The use of raw vegetable oils in diesel engines without any engine modification results in poor engine performance and leads to wear out the engine components [6]. The investigations showed that esters of vegetable oils provide improved engine performance and minimize the emissions in compared to raw vegetable oils. It was investigated that the use of esterified vegetable oils as biofuel for diesel engine. The esterified sunflower oil 15% blend by volume with diesel fuel showed best combustion and performance in terms of total fuel consumption (FC), specific fuel consumption (SFC), brake thermal efficiency (BTE) and cylinder peak pressure etc. [7].

As a substitute fuel Mahua oil is the most suitable fuel for diesel engine. It was investigated that the Mahua oil could be easily substituted up to 20% blend in diesel without any major difference in power output, brake thermal efficiency (BTE) and brake specific fuel consumption (BSFC). The performance of diesel engine increased with Mahua oil blends by the increase in compression ratio from 16:1 to 20:1 [8]. The brake thermal efficiency (BTE), HC, CO, and soot concentration of diesel engine decreased and NOx emissions were slightly increased by addition of the rice bran oil methyl ester (RBOME) in diesel [9]. It is investigated that the BSFC of CI engine for karanja biodiesel and its blends with diesel are extremely closed to diesel fuel. At full engine load BSFC for neat biodiesel (B100) is increased by about 9% as compared to diesel [10, 11]. It is investigated that the brake specific energy consumption (BSEC) of waste frying methyl ester (WFOME) was increased by 8.0% and brake thermal efficiency (BTE) was decreased by 7.6% while the BSEC of WFOEE was increased by 10.3% and Brake thermal efficiency was decreased by 9.3% in comparison to diesel fuel at 50% engine brake load [12]. It

was investigated that the brake thermal efficiency (BTE) of diesel engine decreased with the increase in blend percent in diesel. The values of BTE for diesel and karanja biodiesel are most closed to each other. When the neat biodiesel (B100) used in diesel engine at full engine load the brake thermal efficiency (BTE) is decreased by 2.92% as compared to diesel. The values of BTE for full engine load and at 18 Compression Ratio are recorded 28.65%, 28.75%, 29.32%, 30.05%, 30.5%, and 31.25% for B100, B80, B60, B40, B20, and diesel fuel respectively [13].

It was investigated that the brake specific energy consumption (BSEC) of diesel engine fuelled with 50 and 100% blends increased by 12.44 and 8.91% as compared to neat diesel fuel, whereas the average increase of the BSFC was observed to be 27.73% and 15.31%, respectively. The diesel fuel, B50 and B100 KOME showed an average increase of 0.85, 0.8 and 1.1% increased BSEC with the 10% EGR in comparison with the same fuel without EGR [14]. The thermal efficiencies recorded with COB, POB, and ROB was 28.04, 33.05, and 30.05%, respectively, at 100% load. Maximum brake thermal efficiency of 23.1% was observed with biodiesel (WCO-ME), which is 6% lower than that of diesel at 100% load condition [15]. COB showed less brake thermal efficiency (BTE) as compared to POB and ROB due to its higher viscosity and low volatility [16]. The maximum brake thermal efficiency (BTE) diesel engine is obtained 21.18% with KJB 20 while the lowest BTE is obtained 19.26% with KJB80 blends. KJB20 blends give the better results as compared to other biodiesel combinations [17]. It provides lubricating properties that can reduce engine wear and extend engine life [18].

II. Experimental Setup

The detail of technical specification of diesel engine is mention on table 1.

Table 1: Technical Specification CI Engine

Engine Parameters	Details
Make	Kirloskar Oil Engine, Pune
Model	SV1
Type	Vertical, Totally Enclosed, CI, Four Stroke Engine, Water Cooled
No. Of Cylinder:	ONE
Bore Size	87.5 mm
Stroke Length	110 mm
Cubic Capacity	662 CC
Compression Ratio	16.5:1
Engine RPM	1500
Rate of Output	5.88kW / 8 HP

Figure 1: Single Cylinder Four Stroke Diesel (CI) Engine Experimental Setup



III. Results & Discussion

3.1 Properties of Fuels

The detail of various fuel properties of RBO, RBOME, and diesel have taken out by the help of Indian Oil Corporation Limited, Bhopal, and the department of chemistry in University Institute of Technology, Bhopal. The various fuel properties are compared in detail in table 2.

Table 2: Compared the Physical properties of RBO, RBOME & Diesel

Property	RBO	RBOME	Diesel
Density at 50 °C (kg/m ³)	0.900	0.867	0.830
Specific Gravity	0.909	0.8825	0.836
Kinematic Viscosity at 40°C (cst)	41.7	4.72	2.636
Cloud Point (°C)	3.8	2.1	6.2
Pour Point (°C)	-12.0	3.0	2
Flash Point (°C) at 40°C	251	156	71
Fire Point (°C) at 40°C	173	164	78
Heat Content (kJ/kg)	36200	38830	41860

3.2 Performance of Diesel (CI) Engine

All experiments are performed at constant engine speed of 1500 RPM and variable engine brake load. The data recorded from the various experiments for evaluating the performance of single cylinder direct injection diesel engine.

The performance test of diesel engine fuelled with RBO & RBOME was resulted the increased brake specific fuel consumption (BSFC) as the engine brake loads were increased in comparison to diesel engine. The brake thermal efficiency (BTE) of diesel engine fuelled with RBO & RBOME decreased in comparison to diesel fuel when the percentage of blends increases. As the percentage of blends was increased the fuel consumptions (FC) of diesel engine slightly increased as the engine brake load and blends percentage were increased in comparison to diesel fuel. When diesel engine fuelled with RBO 30 and RBOME 30 blends engine consumed around 9.0% and 5.6% respectively more fuel at constant engine speed of 1500 rpm and 12 kg engine brake load as compared to conventional diesel. When the RBO 30 was used in diesel engine the fuel consumption has increased around 3-4% more than that of RBOME 30 blends for same load. For the same brake power the brake specific fuel consumption of diesel engine is slightly increased than that of petroleum-diesel. When rice bran oil blends are used in diesel engine, engine consumed slightly more energy in comparison to RBOME and conventional diesel for each blends and same engine brake load.

(1) Fuel Consumption

Figure 2 shows the variation in fuel consumption for diesel, RBO & RBOME when various blends are used in diesel engine. As the loads are increased the diesel engine consumed more fuel in comparison to diesel fuel. The fuel consumption (FC) of RBO 10 and RBOME 10 was increased around 3.4% and 1.5% than that of diesel while the fuel consumption (FC) of RBO 30 and RBOME 30 is increased by approximately 8.4% and 5.4% than that of diesel fuel when the engine runs at constant speed of 1500 rpm and 12 kg brake load. It is observed that at the same brake load engine consumed more fuel (RBO & RBOME) in comparison to conventional diesel fuel. During testing of diesel engine fuelled with rice bran oil engine consumed approximately 3.11% more fuel than that of the RBOME for same engine speed and 12 kg brake load. The fuel consumption of diesel engine for RBO 10 and RBOME 10 blends were slightly closed to diesel fuel.

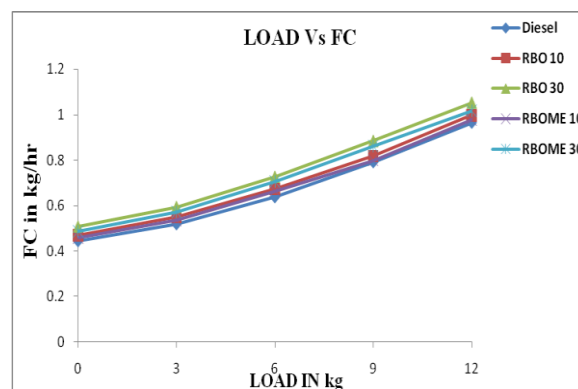


Figure 2: Variation in Fuel Consumption with Varying Load for Diesel, RBO & RBOME blends

(2) Brake Specific Fuel Consumption

Figure 3 shows the variation in brake specific fuel consumption (BSFC) with varying load for diesel, RBO & RBOME blends. It was resulted that the brake specific fuel consumption (BSFC) is higher than that of diesel when the RBO and RBOME blends were used in diesel engine. The BSFC of diesel engine was slightly decreased as the engine brake load

increased. The BSFC of diesel engine fuelled with RBO 10 and RBOME 10 blends were 3.4% and 1.5% while the RBO 30 and RBOME 30 were around 8.4% & 5.4% respectively more brake specific fuel consumption than that of diesel fuel at 1500 rpm engine speed and 12 kg brake load. During testing of diesel engine RBO consumed 3.11% more brake specific fuel consumption than that of the RBOME when engine runs at constant speed of 1500 rpm and 12 kg brake load. The brake specific fuel consumption is an essential parameter by which compare the engines and determine the fuel efficiency of engines.

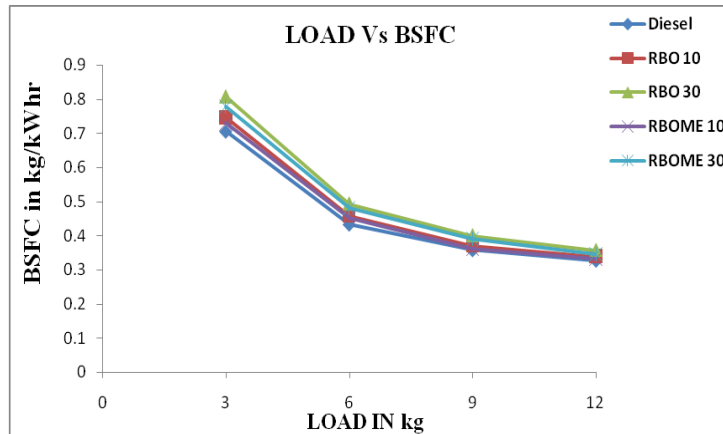


Figure 3: Variation in Brake Specific Fuel Consumption with Varying Load for Diesel, RBO & RBOME blends

(3) Brake Specific Energy Consumption

Figure 4 shows variation in brake specific energy consumption (BSEC) with varying load for diesel, RBO & RBOME blends. It was resulted that the BSEC of diesel engine has higher energy consumption than that of diesel when the blends were used 10% and 30%. The brake energy consumption of diesel engine was more closely to RBO 10 and RBOME 10 blends. The BSEC of diesel engine was slightly decreased as the engine brake loads were increased. The BSEC of RBO 10 and RBOME 10 blends were increased approximately 2.11% and 0.70% while BSEC of diesel engine was increased approximately 4.7% and 3.1% when the blends were used RBO 30 & RBOME 30 respectively consumed more energy as compared to diesel fuel. During testing of diesel engine rice bran oil consumed about 1.54% more energy than that of the RBOME when engine runs at constant speed of 1500 rpm and 12 kg engine load.

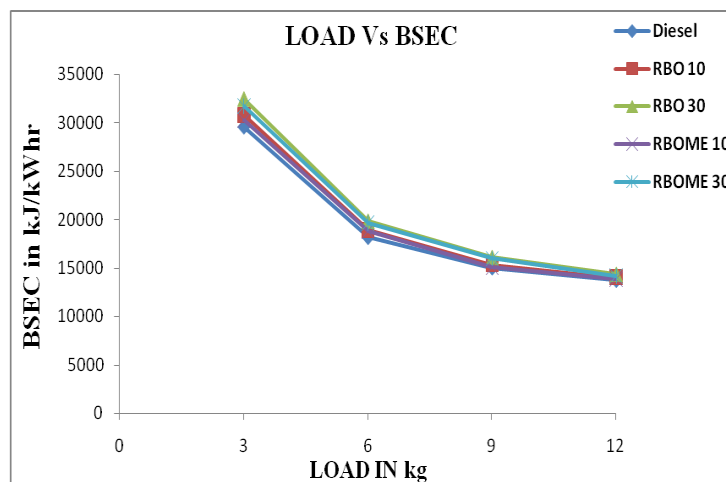


Figure 4: Variation in Brake Specific Energy Consumption with Varying Load for Diesel, RBO & RBOME blends

(4) Brake Thermal Efficiency

Figure 11 shows the variation in the brake thermal efficiency (BTE) of diesel engine fuelled with diesel, RBO and RBOME blends at various load. The brake thermal efficiency (BTE) of RBO and RBOME is decreased as the blends were increased. The brake thermal efficiency (BTE) of diesel engine used with RBO 10 & RBOME 10 blends were slightly closed to petroleum-diesel. The brake thermal efficiency of RBO 10 and RBOME 10 is less around 2.0% and 0.7% respectively than that of petroleum-diesel while the brake thermal efficiency of RBO 30 and RBOME 30 were less around 4.5% and 3.0% respectively in comparison to diesel fuel at 1500 rpm constant engine speed and 12 kg brake load. It is observed that the brake thermal efficiency of RBO 10 was decreased by 1.4% in comparison to RBOME 10 and in similar way the brake thermal efficiency of RBO 30 blends were decreased by 1.5% as compared to RBOME 30 blends.

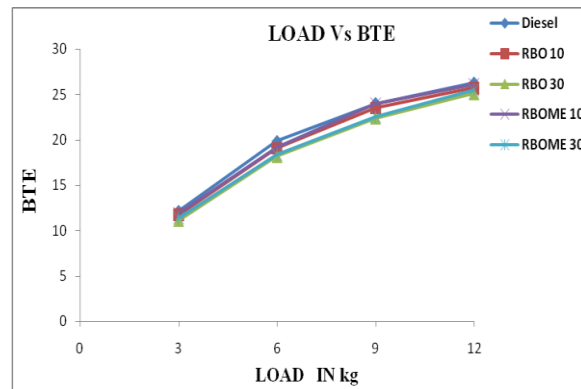


Figure 5: Variation in Brake Thermal Efficiency with Varying Load for Diesel, RBO & RBOME blends

IV. Conclusion

The specific gravity and flash point of RBO & RBOME are higher as compared to diesel fuel. It is concluded that the use of RBO & RBOME blends slightly increases the brake specific fuel consumption (BSFC) as compared to diesel fuel for constant engine speed and same brake load. It was concluded that the brake thermal efficiency of diesel engine fuelled with RBO 10 & RBOME 10 blends were more closely to conventional diesel fuel. The maximum brake thermal efficiency of diesel engine was observed approximately 25.72% and 26.08% for RBO 10 and RBOME 10 blends. The BSFC of the RBO and RBOME blends were higher than that of the diesel fuel. When 30% RBO and RBOME are used in diesel engine RBO consumed 3.11% more fuel in comparison to RBOME. It is concluded that the performance test of diesel engine more closed to RBO 10 and RBOME 10 blends.

It is concluded that both fuels (RBO & RBOME) are suitable alternatives for diesel engine. Biodiesel obtained from rice bran oil can be used as a substitute fuel for conventional diesel fuel in future.

References

- [1] Refaat A.A., et al., Production optimization and quality assessment of biodiesel from waste vegetable oil. *International Journal of Environment Science and Technology*, 5 (1), 2008, pp. 75–82
- [2] Demirbas A., Progress and recent trends in biodiesel fuels, *Energy Conversion and Management*, 50 (1), 2009, pp. 14–34
- [3] Peterson C. L., Hustrulid T., Carbon cycle for rapeseed oil biodiesel fuels, *Biomass and Bioenergy* 14 (2), 1998, pp. 91–101
- [4] Canakci M. and Van Gerpen J. H., Comparison of engine performance and emission for petroleum diesel, yellow grease biodiesel & soybean oil biodiesel. *Transaction of ASAE*, 46 (4), 2003, pp. 937–943
- [5] Kinast J. A., Production of biodiesels from multiple feedstocks and properties of biodiesels and biodiesel/diesel blends, Des Plaines, National Renewable Energy Laboratory Report, Department of Energy, U.S., 2001
- [6] Bari S., Yu C.W., Lim T.H., Performance deterioration and durability issues while running a diesel engine with crude palm oil, *Proc Instn Mech Engrs. Part (D), J Automobile Engineering* 216, 2002, pp. 785–792
- [7] K. Anbumani and A. P. Singh, Experimental investigation the use of vegetable oils as biofuel for compression ignition engine, *Journal of ARISER*, 5(2), 2009, pp. 87-97
- [8] Bhatt Y. C., N. S. Murthy and R. K. Datta, Use of mahua oil as a diesel fuel extender, *Journal of Institute of Engineers (India)* 85, 2004, pp. 10–14
- [9] Lakshmi Narayana Rao, G. S. Subramani, S. Santhanam, et al., Combustion and emission characteristics of a diesel engine fuelled with rice bran oil methyl ester and its diesel blends, *Thermal Science* 12, 2008, pp. 139–150
- [10] Puhan S., N. Vedaraman, B. V. B. Ram, et al. Mahua oil (*Madhuca Indica* seed oil) methyl ester as biodiesel-preparation and emission characteristics, *Biomass and Bioenergy* 28, 2005, pp. 87–93
- [11] Ramadhas A. S., S. Jayaraj, C. Muraleedharan, Characterization and effect of using rubber seed oil as fuel in the compression ignition engines, *Renewable Energy* 30, 2005, pp. 795–803
- [12] Akhand Pratap Singh, Nitin Shrivastava, A comparative study of performance parameters of single cylinder diesel engine operating on waste frying oil methyl ester and waste frying oil methyl ester, *IJCRR*, vol. 04 (21), Nov. 2012, pp. 156-162
- [13] H. K. Amarnath, P. Prabhakaran, A Study on the Thermal Performance and Emissions of a Variable Compression Ratio Diesel Engine Fuelled with Karanja Biodiesel and the Optimization of Parameters Based on Experimental Data, *International Journal of Green Energy* 9 (8), 2012, pp. 841-863
- [14] Nitin Shrivastava, S. N. Varma & Mukesh Pandey, Experimental investigation of diesel engine using EGR and fuelled with Karanja oil methyl ester, *International Journal of Sustainable Engineering*, 2012, DOI:10.1080/19397038.2012.749310
- [15] G. R. Kannan, K. R. Balasubramanian, S.P. Sivapirakasam et al., Studies on biodiesel production and its effect on DI diesel engine performance, emission and combustion characteristics, *International Journal of Ambient Energy*, 32 (4), 2011, pp. 179-193
- [16] M. Satyanarayana, C. Muraleedharan, Investigations on Performance and Emission Characteristics of Vegetable Oil Biodiesels as Fuels in a Single Cylinder Direct Injection Diesel Engine, *Energy Sources, Part A: Recovery, Utilization, and Environmental Effects*, 34 (2), 2011, pp. 177-186
- [17] Ganesh Shirasath, M. S. Tandale, S. V. Khandal, et al., Blends of karanja and jatropha biodiesels for diesel engine applications, *International Journal of Sustainable Engineering*, 5(3), 2012, pp. 252-264
- [18] Von Wedel R., Technical handbook for marine biodiesel in recreational boats, prepared for National Renewable Energy Laboratory, US Department of Energy, Subcontract No.: ACG-7-16688-01 under Prime Cont. No.: DE-AC36-83CH10093, 1999, pp.32

Background Subtraction Techniques: Systematic Evaluation and Comparative Analysis

Mrs. Clara Shanthi.G,¹ Mr.Saravanan.E²

¹ Final Year Student, M.Tech CSE Department, Dr.M.G.R.Educational and Research Institute University Tamil Nadu, India

² Asst.Professor CSE Department, Dr.M.G.R.Educational And Research Institute University, Tamil Nadu, India

Abstract: This paper presents a technique for motion detection that incorporates several innovative mechanisms. our proposed technique stores, a set of values taken in the past at the same location or in the neighborhood of each pixel. It then compares this set to the current pixel value in order to determine whether that pixel belongs to the background, and adapts the model by choosing randomly which values to substitute from the background model. This approach differs from those based upon the classical belief that the oldest values should be replaced first. In this future enhancement of paper is remotely we are checking and providing the security to our system. So whenever user getting sms from server system, the user can possible to get the images also by using the server system ip address.

Index Terms: Remote based technique, Background subtraction, computer vision, image motion analysis, image segmentation, learning (artificial intelli-gence), pixel classification, real-time systems, surveillance, vision and scene understanding, video signal processing.

I. INTRODUCTION

This work describes a new 3D cone-shape illumination model (CSIM) and a robust background subtraction scheme involving shadow and highlight removal for indoor-environmental surveillance. Foreground objects can be precisely extracted for various post-processing procedures such as recognition. Gaussian mixture model (GMM) is applied to construct a color-based probabilistic background model (CBM) that contains the short-term color-based background model (STCBM) and the long-term color-based background model (LTCBM). STCBM and LTCBM are then proposed to build the gradient-based version of the probabilistic background model (GBM) and the CSIM. In the CSIM, a new dynamic cone-shape boundary in the RGB color space is proposed to distinguish pixels among shadow, highlight and foreground. Furthermore, CBM can be used to determine the threshold values of CSIM. A novel scheme combining the CBM, GBM and CSIM is proposed to determine the background. The effectiveness of the proposed method is demonstrated via experiments in a complex indoor environment The capability of extracting moving objects from a video sequence is a fundamental and crucial problem of many vision systems that include video surveillance [1, 2], traffic a monitoring [3], human detection and tracking for video teleconferencing or human-machine interface [4, 5, 6], video editing, among other applications. Typically, the common approach for discriminating moving object from the background scene is background subtraction. The idea is to subtract the current image from a reference image, which is acquired from a static background during a period of time.

The subtraction leaves only non-stationary or new objects, which include the objects' entire silhouette region. The technique has been used for years in many vision systems as a preprocessing step for object detection and tracking [for examples, [1, 4, 5, 7, 8]. The results of the existing algorithms are fairly good; in addition, many of them run in real-time. However, many of these algorithms are susceptible to both global and local illumination changes such as shadows and highlights. These cause the consequent processes, e.g. tracking, recognition, etc., to fail. The accuracy and efficiency of the detection are very crucial to those tasks. This problem is the underlying motivation of this work. We want to develop a robust and efficiently computed background subtraction algorithm that is able to cope with the local illumination change problems, such as shadows and highlights, as well as the global illumination changes. Being able to detect shadows is also very useful to many applications especially in "Shape from Shadow" problems. Our method must also address requirements of sensitivity, reliability, robustness, and speed of detection.

In this paper, we present a novel algorithm for detecting moving objects from a static background scene that contains shading and shadows using color images. In next section, we propose a new computational color model (brightness distortion and chromaticity distortion) that helps us to distinguish shading background from the ordinary background or moving foreground objects. Next, we propose an algorithm for pixel classification and threshold selection. Experimental results and sample applications are shown in Section 4 and 5 respectively.

II. COLOR MODEL

One of the fundamental abilities of human vision is color constancy. Humans tend to be able to assign a constant color to an object even under changing of illumination over time or space. The perceived color of a point in a scene depends on many factors including physical properties of the point on the surface of the object. Important physical properties of the surface in color vision are surface spectral re-reflectance properties, which are invariant to changes of illumination, scene composition or geometry. On Lambertian, or perfect matte surfaces, the perceived color is the product of illumination and surface spectral reflectance. This led to our idea of designing a color model that Separates these two terms; in other words, that separates the brightness from the chromaticity component. illustrates the proposed color model in three-dimensional

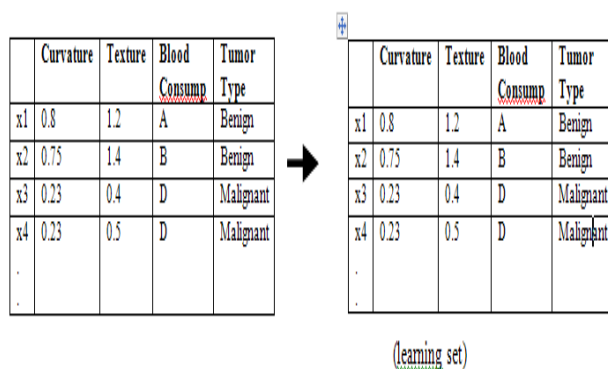
RGB space. Consider a pixel, in the image; let $E_i = [ER(i); EG(i); EB(i)]$ represent the pixel's expected RGB color in the reference or background image. The line OE_i passing through the origin and the point E_i is called expected chromaticity line.

III. MOVING OBJECT DETECTION

The first step in tracking objects is separating the objects from the background. Two common methods are motion segmentation and background subtraction. Motion segmentation is basically a threshold of the difference between the current image and sequence images by assuming that the background does not change over successive frames. This method is easy and fast in many applications, but some problems appear when tracking multiple objects or when an object stops. Hence, we turn to the other method, background subtraction, at the expense of updating the background.

IV. BACKGROUND SUBTRACTION

The basic scheme of background subtraction is to subtract the image from a reference image that models the background scene. Typically, the basic steps of the algorithm are as follows: Background modeling constructs a reference image representing the background. Threshold selection determines appropriate threshold values used in the subtraction operation to obtain a desired detection rate. We are performing background subtraction by using k-means algorithm. We recall from the previous clustering allows for *unsupervised learning*. That is, the machine / software will learn on its own, using the data (learning set), and will classify the objects into a particular class – for example, if our class (decision) attribute is tumor *Type* and its values.



V. K-MEANS ALGORITHM

In statistics and data mining, **k-means clustering** is a method of cluster analysis which aims to partition n observations into k clusters in which each observation belongs to the cluster with the nearest mean. This results into a partitioning of the data space into Voronoi cells.

The problem is computationally difficult (NP-hard), however there are efficient heuristic algorithms that are commonly employed that converge fast to a local optimum. These are usually similar to the expectation-maximization algorithm for mixtures of Gaussian distributions via an iterative refinement approach employed by both algorithms. Additionally, they both use cluster centers to model the data, however k -means clustering tends to find clusters of comparable spatial extend, while the Expectation-maximization mechanism allows clusters to have different shapes.

- A clustering algorithm
- An approximation to an NP-hard combinatorial optimization problem
- It is unsupervised
- “ K ” stands for number of clusters, it is a user input to the algorithm
- From a set of data points or observations (all numerical), K -means attempts to classify them into K clusters
- The algorithm is iterative in nature

We describe our approach to segmenting moving objects from the color video data supplied by a nominally stationary camera. There are two main contributions in our work. The first contribution augments Zivkovic and Heijden's recursively updated Gaussian mixture model approach, with a multidimensional Gaussian kernel spatio-temporal smoothing transform. We show that this improves the segmentation performance of the original approach, particularly in adverse imaging conditions, such as when there is camera vibration.

Our second contribution is to present a comprehensive comparative evaluation of shadow and highlight detection approaches, which is an essential component of background subtraction in unconstrained outdoor scenes. A comparative evaluation of these approaches over different color-spaces is currently lacking in the literature. We show that both segmentation and shadow removal performs best when we use RGB color spaces.

We consider the case of a nominally static camera observing a scene, such as is the case in many visual surveillance applications, and we aim to generate a background/foreground segmentation, with automatic removal of any shadows cast by

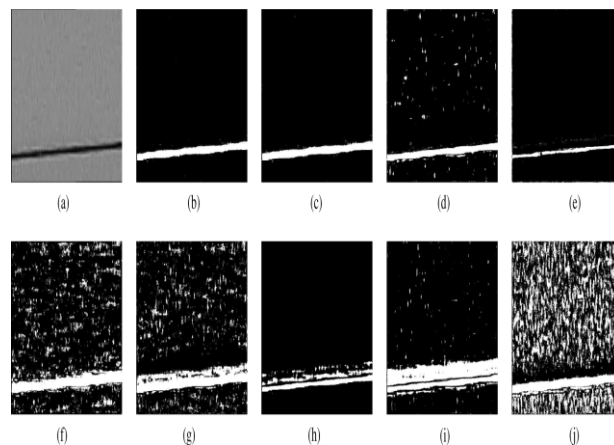
the Fore ground object onto the background. In real applications, cameras are often mounted metal poles, which can oscillate in the wind, thus making the problem more difficult. This problem is also addressed in this paper.

To segment moving objects, a background model is built from the data and objects are segmented if they appear significantly different from this modeled background. Significant problems to be addressed include (i) how to correctly and efficiently model and update the background model, (ii) how to deal with camera vibration and (iii) how to deal with shadows. In this paper our contributions are a spatio-temporal filtering improvement to Zivkovic's recursively updated Gaussian mixture model approach and a comprehensive evaluation of shadow/highlight detection across different color spaces, which is currently lacking in the literature. We also present quantitative results of our complete foreground/background segmentation system with shadow removal in several real-world scenarios. This is valuable to those developing pragmatic visual surveillance solutions that demand high quality foreground segmentation.

A robust visual segmentation system should not depend on careful placement of the camera; rather it should be robust to whatever is in its visual field, whatever lighting effects occur or whatever the weather conditions. It should be capable of dealing with movement through cluttered areas, objects overlapping in the visual field, shadows, lighting changes, effects of moving elements of the scene (e.g. camera vibration, swaying trees) and slow-moving objects. The simplest form of the background model is a time-averaged background image. However, this method suffers from many problems, for example it requires a large memory and a training period absent of foreground objects. Static foreground objects during the training period would be considered as a part of background. This limits their utility in real time applications.

A Gaussian mixture model (GMM) was proposed by Friedman and Russell [2] and it was refined for real-time tracking by Stauffer and Grimson [3]. The algorithm relies on the assumptions that the background is visible more frequently than any foreground regions and that it has models with relatively narrow variances. The system can deal with real-time outdoor scenes with lighting changes, repetitive motions from clutter, and long-term scene changes. Many adaptive GMM model have been proposed to improve the background subtraction method since that original work. Power and Schoonees [4] presented a GMM model employed with a hysteresis threshold.

They introduced a faster and more logical application of the fundamental approximation than that used in the paper [5]. The standard GMM update equations have been extended to improve the speed and adaptation of the model [6][7]. All these GMMs use a fixed number of components. Zivkovic et al. [1] presented an improved GMM model adaptively chooses the number of Gaussian mixture components for each pixel on-line, according to a Bayesian perspective. We call this method the Zivkovic-Heijden Gaussian mixture model (ZHGM) in the remainder of this paper.



Another main challenge in the application of background subtraction is identifying shadows that objects cast which also move along with them in the scene. Shadows cause serious problems while segmenting and extracting moving objects due to the misclassification of shadow points as foreground. Prati et al. [8] presented a survey of moving shadow detection approaches. Cucchiardi et al. proposed the detection of moving objects, ghosts and shadows in HSV colour space and gave a comparison of different background subtraction methods.

Fig1.Create the Database

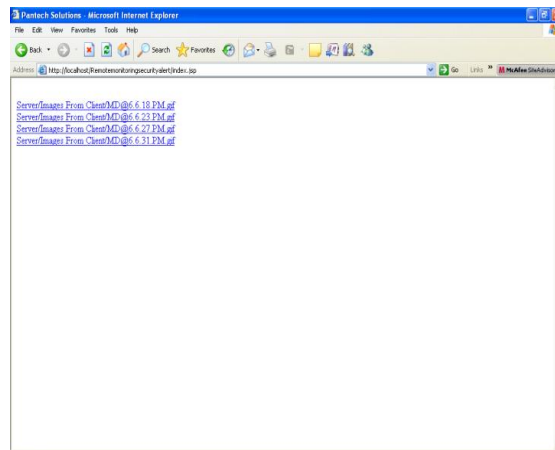


Fig 2.Show the Result in web logic server

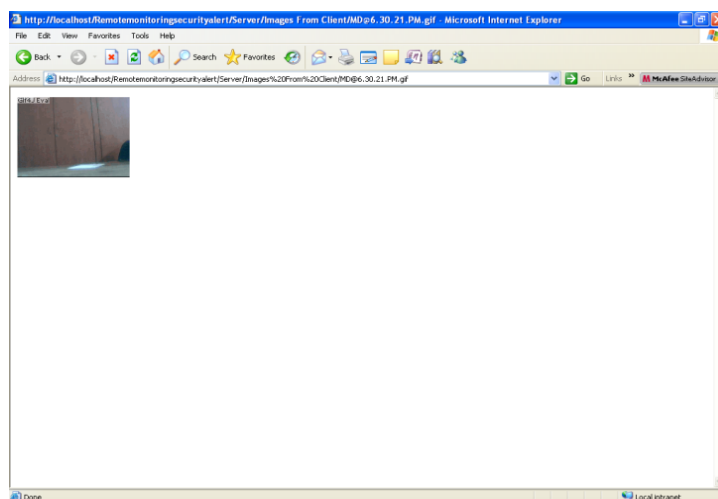


Fig7.Final Result

VI.CONCLUSION

A technology of background subtraction for real time monitoring system was proposed in this paper. The obvious keystone of my work is studying the principle of the background subtraction, discussing the problem of the background, and exploring the base resolve method of the problem. Experiment shows that the method has good performance and efficiency. Future enhancements alert the user sending multimedia sms by using GSM (global system for mobile communication) Modem, and then it is very efficiently find out unauthorized person.

REFERENCES

- [1] F. De la Torre, E. Martinez, M. E. Santamaria and .A. Moran, "Moving Object Detection and Tracking System: a Real-time implementation", Proceedings of the Symposium on Signal and Image Processing GRETSI 97Grenoble, 1997.
- [2] I. Haritaoglu, D. Harwood and L.S. Davis, "W4: Real- Time Surveillance of People and Their Activities", IEEE Trans. Pattern Analysis and Machine Intelligence, 22(8),2000, pp. 809-822.
- [3] L. Li, W. Huang, I. Y. H. Gu, and Q. Tian."Foregroundobject detection from videos containing complex background". In MULTIMEDIA '03: Proceedings of the eleventh ACM international conference on Multimedia, pages 2–10, New York, NY, USA, 2003. ACM.
- [4] Zhou, Q.; Aggarwal, J. K.; "Tracking and classifying moving objects from video", Proc of 2nd IEEE Intl Workshop on performance Evaluation of Tracking and Surveillance (PETS'2001), Kauai, Hawaii, USA (December 2001).
- [5] C. Stauffer and W. E. L. Grimson, "Adaptive backgroundmixture models for real-time tracking," in Proc. IEEE Conf. Computer Vision and Pattern Recognition, 1999, pp. 246–252.
- [6] R. T. Collins, A. J. Lipton, T. Kanade, H. Fujiyoshi, D.Duggins, Y. Tsin, D. Tolliver, N. Enomoto, O. Hasegawa, P.Burt, and L. Wixson, "A system for video surveillance and monitoring," Tech.Rep. CMU-RI-TR-00- 12, The Robotics Inst., Carnegie Mellon Univ.,
- [7] L. Maddalena and A. Petrosino, "A self-organizing approach to detection of moving patterns for real-time applications," in Proc. 2nd Int. Symp. Brain, Vision, and Artificial Intelligence, 2007, pp. 181–190, Lecture Notes Comput. Sci. 4729.
- [8] M. Piccardi, "Background subtraction techniques: a review," in Proc. IEEE Int. Conf. Systems, Man, Cybernetics, 2004, pp. 3099–3104.

A Review on Study of Jaw Plates of Jaw Crusher

Ramkrushna S. More,¹ Sunil J.Rajpal²

¹Pursuing M.E. Mechanical Engineering, Department, Babasaheb Naik college of Engineering, pusad, India

²Assistant Professor, Mechanical Engineering, Department, Babasaheb Naik college of Engineering, pusad, India

Abstract: Crushers are major size reduction equipment used in mechanical, metallurgical and allied industries which crushes different types of soft and hard materials. swing jaw plates are takes direct part into this oprations.hence the design and analysis are very important. This paper focuses on review of a work carried out by researchers on analysis of swing jaw plate i.e. kinematic & dynamic analysis of the jaw crusher.due to which the design quality of jaw crusher are improved, though their were so many researcher work done on analysis, but still there is so many area of scope to develop the analysis of swing jaw plate.

I. Introduction

A Jaws crusher consist of two plates one job being fixed and other being mount by pitman mechanism due which the crushing can be done in one stroke due small moment of jaw plates. these two plates form a taper chute so that material can be crushed, as the load acts on the plates its wearing rate is high hence high wear resistant material is used generally magnese still are used a heavy flywheel is use to crushed the tough materials which provides the required inertia. Double Toggle jaw crushers may feature hydraulic toggle adjusting mechanisms. It is shown below Figure

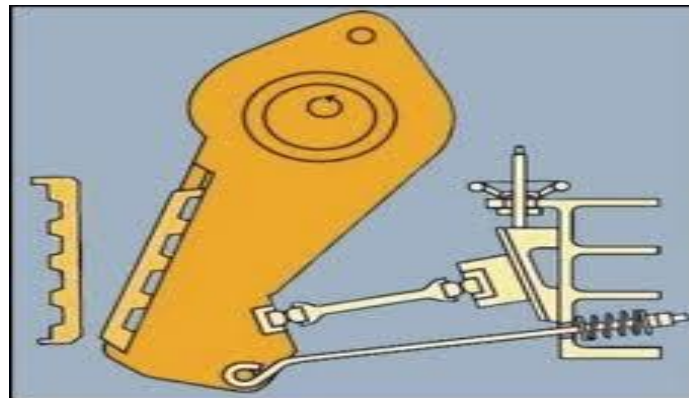


Fig.1 Elevation View of Jaw Crusher

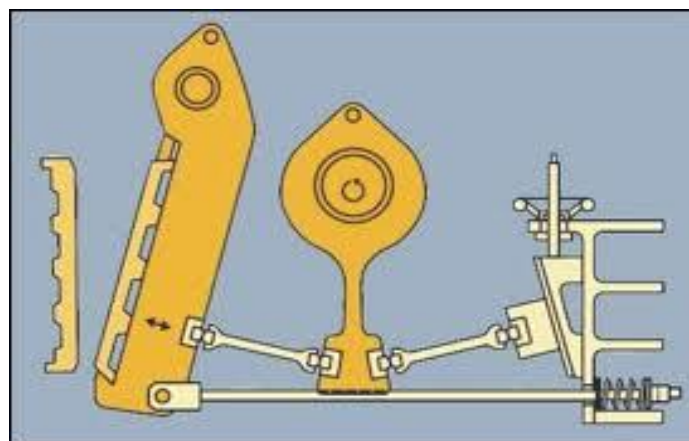


Fig.2 Elevation View of Jaw Crusher

II. Dynamic Analysis & Kinematic Analysis

CHARLES H. DOWDING, in 1981, Department of Civil Engineering, Northwestern University. Evanston. IL (U.S.A.)[1].works on reduction of weight of swing jaw plate by reduction of energy consumed in crushing by using "Point Load- Deformation Relationships along with interactive failure of rock particles and Design of Jaw Crusher Plates" point loading various sizes of materials

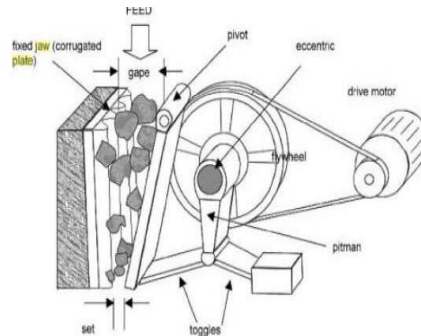


Fig.3 Elevation View of Jaw Crusher

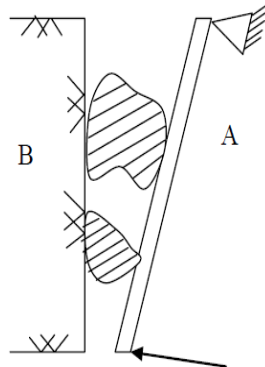


Fig.4 Idealized view

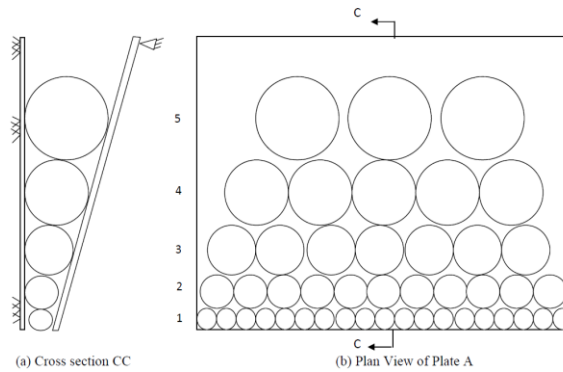


Fig.5 Cross section & plan view

In this study point-loading of cylinders (or discs) was undertaken to model behavior of irregular rock particles. Modeling irregular particle behavior with that of cylinders can be appropriate by consideration of work presented by Hamamatsu and Oka. From photo elastic studies of plate-loaded spheres and point-loaded cubes, prisms and ellipsoids, they determined that the stresses produced in plate- and point-loaded spheres of identical diameter were equal. Thus, the plate idealization may be replaced by the point load shown in Figure 4. They also showed that point-load failure of a sphere was equal to that of a point-loaded ellipsoid. Therefore ultimate point loads on spheres will be approximately equal to ultimate point loads on cylinders (or discs).

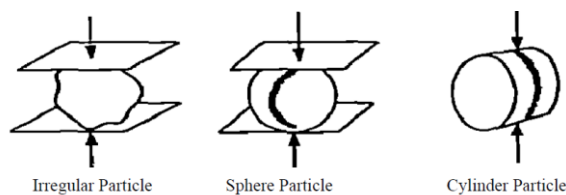


Figure 6: Comparison of plate point loaded particles

The interactive model of rock and swing-plate deformation shows a calculated reduction in both swing plate mass and maximum toggle force, compared to the no interactive assumption of simultaneous failure. These theoretical reductions indicate that design of new energy-efficient systems should include deformation properties of the crushed material. Design of

crushers for specific rock types must consider the variability of point load strength and deformability implicit in any rock type name and quarry sized sampling region.

As the rock particles comes between the fixed and moving plate it get crushed hence the design of plates must be improved .on this domain Gupta Ashok and Yan D.S. [2] worked in design of jaw crushers which impart an impact on a rock particle placed between a fixed and a moving plate. this faces of plate made up of hardened steel it may be flat or corrugated. He puts some equations for designing of plate of crusher

$$\begin{aligned} \text{Height of jaw plate} &= 4.0 \times \text{Gape} \\ \text{Width of jaw plat (W)} &> 1.3 \times \text{Gape} \\ &< 3.0 \times \text{Gape} \\ \text{Throw (T)} &= 0.0502(\text{Gape})^{0.85} \end{aligned}$$

Where the crusher gape is in meters

As the reciprocating action removes the moving jaw away from the fixed jaw the broken rock particles slip down, but are again caught at the next movement of the swinging jaw and crushed. This process is repeated until the particle sizes are smaller than the smallest opening between the crusher plates at the bottom of the crusher (the closed set). For a smooth reciprocating action of the moving jaws, heavy flywheels are used in both types of crushers.

Guangjun FAN, Fusheng MU [3] worked on the certain domain, called the liner domain, of the coupler plane is chosen to discuss the kinetic characteristic of a liner or a crushing interface in the domain. Based on the computation and the analysis of the practical kinetic characteristic of the points along a liner paralleling to the direction of coupler line, some kinematics arguments are determined in order to build some kinetic characteristic arguments for the computing, analyzing and designing

Bharule Ajay Suresh in 2009[4] Department of Mechanical Engineering National Institute of Technology, Rourkela works on the swing jaw plate for Design of lighter weight jaw plate by using and varying no of stiffeners for different thickness. as the energy required for the crushing the material decrease due to which the weight of swing jaw plate is decrease. This paper use point-load deformation failure (PDF) relationships along with interactive failure of rock particles as a model for such a weight reduction for the design and analysis of the swing plate.

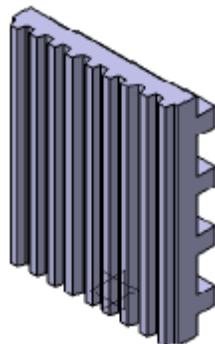


Fig.7: Jaw plate with stiffeners

The present jaw plate models accurately predict the various stresses for plates. As the as the number of stiffener increases the strength/weight ratio of the jaw plate increases making it stronger than that of without stiffener. And hence the stiffened plate models which leads to 25% saving in energy, of course this 25% is an estimate.

Gabor M. Voros [5] presents the development of a new plate stiffener element and the subsequent application in determine impact loads of different stiffened plates. In structural modeling, the plate and the stiffener are treated as separate finite elements where the displacement compatibility transformation takes into account the torsion – flexural coupling in the stiffener and the eccentricity of internal forces between the beam – plate parts. The model becomes considerably more flexible due to this coupling technique. The development of the stiffener is based on a general beam theory, which includes the constraint torsional warping effect and the second order terms of finite rotations. Numerical tests are presented to demonstrate the importance of torsion warping constraints. As part of the validation of the results, complete shell finite element analyses were made for stiffened plates

Kadid Abdel rim [6] carried out investigation to examine the behavior of stiffened plates subjected to impact loading. He worked to determine the response of the plates with different stiffener configurations and consider the effect of mesh dependency, loading duration, and strain-rate sensitivity. Numerical solutions are obtained by using the finite element method and the central difference method for the time integration of the non-linear equations of motion. Special emphasis is focused on the evolution of mid-point displacements, and plastic strain energy. The results obtained allow an insight into the effect of stiffener configurations and of the above parameters on the response of the plates under uniform blast loading and indicate that stiffener configurations and time duration can affect their overall behavior

CAO Jinxi, RONG Xingfu, YANG Shichun, in 2006[7] have developed Jaw Plate Kinematical Analysis For Single toggle Jaw Crusher Design, College of Mechanical Engineering, Taiyuan University of Technology, Taiyuan, China .Jaw crusher is a kind of size reduction machine which is widely used in the mining and aggregates industry. The interaction

between jaw plates and material particles brings the inevitable and serious wear to the jaw plates during the jaw crusher operation, which not only decreases the efficiency, but also increases the cost and the energy consumption of the jaw crusher. The movement of the moving jaw is described in detail. The breakage force is tested in the experiment and some information on the particles flow is gained by analyzing the force distribution. Based on the movement analysis of the moving jaw and the crushing force distribution analysis, the jaw plates wear is analyzed on a macroscopic level. The result of the wear analysis can explain some of the phenomenon in practice. With the rock material breakage character taken into consideration, the blindness brought by the traditional empirical designing can be greatly decreased. It is helpful to design the crusher for improved performance. Jaw crusher structure diagram shown in figure

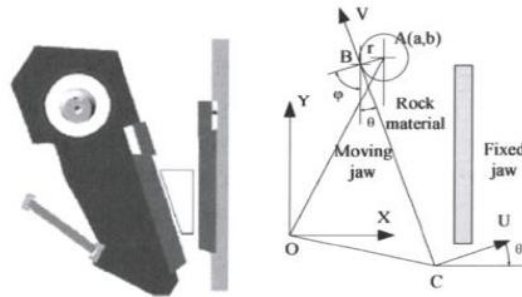


Figure.8: Single toggle jaw crusher & jaw crusher structure

The performance of jaw crusher is mainly determined by the kinetic characteristic of the liner during the crushing process. The practical kinetic characteristic of the liners which are located in certain domain of the coupler plane are computed and discussed in the paper titled “Investigation on Kinetic Features of Multi-Liners in Coupler Plane of Single Toggle Jaw Crusher” by Cao Jinxi, Qin Zhiyu, Wang Guopeng, Rong Xingfu, Yang Shichun 2007[8], IEEE, College of Mechanical Engineering, Taiyuan University of Technology, Taiyuan. Based on those computing results and analysis for the points chosen from the liners paralleling coupler plane, unique Swing features and kinematics arguments are determined in order to build the kinetic characteristic arguments. The job is helpful for a design of new prototype of this kind of machine on optimizing the frame, designing the chamber and recognizing the Crushing character. Kinetic characteristic of the crushing interface or the liner. Based on the computation and the analysis of the practical kinetic characteristic of the points in the liner domain, some traditional motion parameters and some kinetic arguments are calculated. According to the requirement for the squeezing motion of different zone in the crushing chamber, the chamber geometry can be improved

So many 3-D parametric software are use for modeling function To reduce the development cycle and improve the design quality of jaw crusher, by using this point Yuming Guan, Zhitao Zhang, Qianwei Zhang, Hebei University Of Technology Hebut Tianjin, China 2011[9] IEEE ,”Modeling simulation and Kinematic analysis base on Pro/Engineer for Jaw Crusher mechanism” takes full advantage of the Function module of the Pro/Engineer platform to make model simulation and dynamic analysis on the actual jaw crusher mechanism, and provided the updated path for the design and manufacture of Jaw Crusher. Interference detection module is one important module of the Pro/E simulation platform, and is also one key technology of the computer graphics, and has been widely applied in the fields of virtual simulation. The appropriate level of interference detection is selected according to the need of motion simulation and collision detection of the system is carried according to the settings. The model will be shown in figure

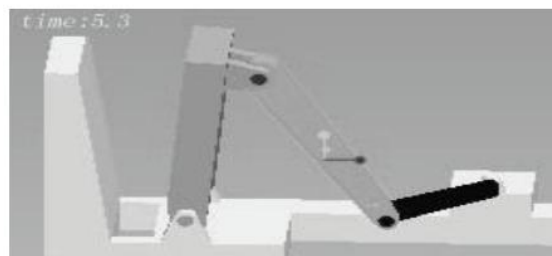


Figure.9: The complete virtual assembly chart of jaw crusher

In this module, many types, such as the reaction force, impulse, and static load of different positions can also be defined to carry out static analysis, kinematics analysis and dynamic analysis. It has very important significance for the life of the specific parts. Specific process will be no longer introduced. The dynamic analysis diagram shown in figure

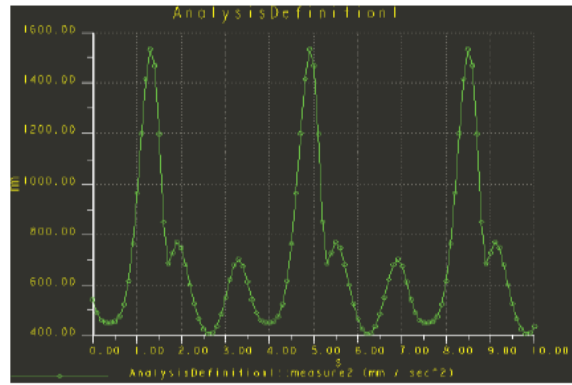


Figure.10: The output image of the acceleration

III. Conclusion

As the jaws plate of jaw crusher are very important part hence study its Kinematics and dynamic analysis are very important for improved design and also improving the operating performance of the plate This concept of kinematics is followed by number of researches for their application. This paper provides the background of swing jaw plate of jaw crusher Kinematics to carried out further research work in future.

References

- [1] CHARLES H. DOWDING, 1981, "Point Load Deformation Relationships and Design of Jaw Crusher Plates" Department of Civil Engineering. Northwestern University. Evanston. IL (U.S.A.)
- [2] Gupta Ashok, Yan D.S. "Mineral Processing Design and Operation-An introduction", Published by Elsevier, 2006, Pages 99-127.
- [3] Guangjun FAN, Fusheng MU, "The Study of Breaking Force of Jaw Crusher", Hunan Metallurgy, Volume 14, Issue 6 July, 2001, Pages 115-123
- [4] Bharule Ajay Suresh, Computer aided design and Analysis of Swing Jaw Plate of Jaw Crusher, NIT Rourkela, 1-11, 2009
- [5] Gabor M. Voros "Finite element analysis of stiffened plates" Mechanical Engineering Volume51Issue2, 2007, Pages 105-112
- [6] Kadid Abdelkrim "Stiffened Plates Subjected to Uniform Blast Loading" Journal of Civil Engineering and Management, Volume14, Issue3, July 2008, Pages155-161.
- [7] CAO Jinxi, RONG Xingfu, YANG Shichun, in 2006, Jaw Plate Kinematical Analysis For Single toggle Jaw Crusher Design, College of Mechanical Engineering, Taiyuan University of Technology, Taiyuan, 030024, China
- [8] Cao Jinxi, Qin Zhiyu, Wang Guopeng, Rong Xingfu, Yang Shichun (2007) "Investigation on Kinetic Features of Multi-Liners in Coupler Plane of Single Toggle Jaw Crusher" IEEE, College of Mechanical Engineering, Taiyuan University of Technology, Taiyuan, Page 1639-1641
- [9] Yuming Guan, Zhitao Zhang, Qianwei Zhang, (2011) IEEE, "Modeling Simulation and Kinematic Analysis Base On Pro/Engineer For Jaw Crusher Mechanism" Hebei University Of Technology Hebut Tianjin, China, Page 1407-1409.

A research work on Employee Satisfaction measurement with special reference to KRIBHCO, Surat

Ekta Sinha

Asst. Professor, Uka Tarsadia University, Gujarat

Abstract: This research work has been done to measure the satisfaction level of employees with special reference to KRIBHCO, Surat. Today to sustain in such a competitive market its very important to retain good employees, that contribute towards the attainment of Organizational goal and customer satisfaction as well. Many researchers have worked in this area with different organizations but this kind of research work has not been done before in KRIBHCO, Surat. We went ahead in this research with sample size of 150 employees based on systematic sampling. Data was collected based on structured questionnaire method on Likert five point scale for 23 major variables which were reduced to five factors namely Empowerment & Work Environment, Working Relation, Salary & Future prospects, Training & work Involvement and Job Rotation. We found the employees to be satisfied on the basis of above said five factors. For the purpose of data analysis we used IBM SPSS 20. We performed factor analysis to reduce the data and non parametric tests as Kruskal-Wallis and Mann Whitney Rank test. Chi-Square tests were performed to view the satisfaction level of the employees against each major variables found after dimension reduction. We also found that a few important factors that normally contribute to the employee satisfaction, didn't have much influence on employee satisfaction in KRIBHCO, Surat, such as : welfare measures, role clarity, freedom of decision making and recognition at work. The innovativeness and creativeness of employees also took a back seat as far as satisfaction level was concerned.

Keywords: Job Satisfaction, role clarity, empowerment and job rotation.

I. Introduction of the Research Topic and Literature Review

Staff well-being and their level of satisfaction and engagement has been found to directly impact on organizational performance and ultimately organizational success. It is an obvious statement but high employee satisfaction levels can reduce employee turnover. Dissatisfied employees tend to perform below their capabilities, result in high turnover of staff and leave their jobs relatively quickly, and are not very likely to recommend your company as an employer. Satisfied employees tend to contribute more in terms of Organizational productivity and maintaining a commitment to customer satisfaction. Staff satisfaction surveys give employees 'a voice' and also allows the pinpointing of problematic areas, leading to the raising of staff satisfaction levels, developing and reviewing of staff management, and optimizing corporate communications. This is a Research work done in the similar field with special reference to KRIBHCO, Surat. Many researchers have done such surveys with different organizations before also.

Dr. R. Anitha (sep. 2011) studied the Job Satisfaction of Paper Mill Employees with Special Reference to Udumalpet and Palani Taluk. Satisfaction level of the employees was measured on the basis of employees working conditions, rewards, welfare measures & job security. The 100 employees were selected after considering time and cost. The method of simple random sampling was undertaken for the research purpose. The Convenience method of sampling is used to collect the data from the respondents. The collected data had been analyzed by using Percentage analysis & Chi square test.

Halil Zaim, Selim Zaim, measured Employee Satisfaction in Small and Medium Sized Enterprises, by using factors such as pay and benefits, peers, management, working environment and superiors. The survey instrument was composed of questions relating to employee satisfaction and loyalty. A multi-item scale was developed to operationalise the employee satisfaction construct in a manufacturing context. In the second part of the survey instrument, a single question regarding employee's overall evaluation of organization loyalty was asked. Each item related to employee satisfaction context and employee loyalty was rated on a five-point scale, ranging from "very low" to "very high". The sample of the study was selected randomly from the database of Turkish Small Business Administration (KOSGEB). The study focused on the textile industry including textile mill products and apparel. The findings showed that there is a positive linear relationship between all these five factors of employee satisfaction and employee loyalty. However, among these factors, pay and benefits was found to be the most important criterion followed by management and working environment.

Brikend Aziri, (2011) studied Job Satisfaction and found that Job satisfaction is under the influence of a series of factors such as: The nature of work, Salary, Advancement opportunities, Management, Work groups and Work conditions. It is one of the major challenges for today's organization. Job satisfaction represents a combination of positive or negative feelings that workers have towards their work. Meanwhile, when a worker employed in a business organization, brings with it the needs, desires and experiences which determinates expectations that he has dismissed. Job satisfaction represents the extent to which expectations are and match the real awards. Job satisfaction is closely linked to that individual's behavior in the work place (Davis et al., 1985).

Job satisfaction is a worker's sense of achievement and success on the job. It is generally perceived to be directly linked to productivity as well as to personal well-being. Job satisfaction implies doing a job one enjoys, doing it well and being rewarded for one's efforts. Job satisfaction further implies enthusiasm and happiness with one's work. Job satisfaction

is the key ingredient that leads to recognition, income, promotion, and the achievement of other goals that lead to a feeling of fulfillment (Kaliski, 2007).

A study was made on Employee Satisfaction in Banking Sector by M. L. Meena and G. S. Dangayach, (2012). The objective of this study was to analyze employee satisfaction of Private Sector Banks and Public Sector Banks, and the Banks in Rajasthan were chosen as the population for the study. Five banks were considered in this study, in which, three were public sector banks (State Bank of India, Bank of Baroda, and Punjab National Bank) and remaining two were private sector banks (ICICI Bank and HDFC Bank). Total three hundred fifteen (63 from each bank) employees were considered as the samples in this study. It was found that satisfied employees made positive contributions to the organizational effectiveness and performance.

A study was conducted on Employee satisfaction in cement industry of Chhattisgarh by Daljeet Singh Wadhwa, Manoj Verghese & Dalvinder Singh Wadhwa (September 2011). This study focused on three factors namely Behavioral, organizational and environmental factors. The report focused on all of these factors and attempted to find the relation between these factors and employee job satisfaction and it was found that all the three factors have a positive impact on job satisfaction. The study concluded that organizational factors are the most important aspect for job satisfaction of the employees in a company i.e. if the employees are treated equally and fairly and they are properly supervised, their level of satisfaction can be increased towards their job. The research design used in the research was descriptive. This research was used because it is a good structured instrument for collection of data. The research method used was survey method. The research technique used was Questionnaire. The data was collected using primary data with a sample size of 150.

In all the above research, Researchers have found that for the growth of any organization employee satisfaction is very important. A few factors that were prominent to the employee satisfaction in the researches before were income, promotion, feeling of fulfillment, work environment, relations with superior ect. We have also included these variables in our study but two factors that were not included by the above researchers in their study but had been included by us were Job Rotation and Employee Empowerment. Our research is comprehensive with 23 variables to measure the satisfaction level of employees.

II. Research Methodology

Objective:

H₀₁: Employees are satisfied in the Organization

H₀₂: Employee satisfaction does not differ regarding salary with respect to Experience

H₀₃: Employee satisfaction does not differ regarding training opportunities with respect to different age Groups

H₀₄: there is no difference of satisfaction between the gender groups regarding job rotation

Research Design:

Descriptive research has been applied, which is also known as statistical research, describes data and characteristics about the population or phenomenon being studied.

Sources of Data:

To cater the need of the research we have used primary (self constructed structured Questionnaire) as well as secondary sources of data (web sites, journals etc.)

Data Collection Tool:

Structured questionnaire was prepared to interview the employees of the organization on distinct 23 parameters like: salary, job rotation, work environment welfare measures at the organization etc. measured on Likert five point scale, which was later reduced to 5 factors with help of factor analysis.

Sampling Method:

Under the probabilistic sampling techniques, systematic sampling was done.

Sample Size:

Sample sizes of 150 employees from various departments were taken for the research purpose.

Statistical Tools:

We have used IBM SPSS 20 (Statistical Package for the Social Sciences), for data analysis.

III. Data Analysis & Interpretation

Factor Analysis

To find out major factors that contribute towards the employee satisfaction, data reduction technique was used.

KMO and Bartlett's Test

Table 1

Kaiser-Meyer-Olkin Measure of Sampling Adequacy.		0.904
Bartlett's Test of Sphericity	Approx. Chi-Square	1632.894
	Df	253
	Sig.	0

From table 1, we found that the value for Kaiser-Meyer-Olkin Measure of Sampling Adequacy was more than 0.6, and it is 0.904 also Bartlett's Test of Sphericity has sig value less than 0.05 at 5 % level of significance. So factor analysis was conducted successfully for data reduction.

Rotated Component Matrix

Table 2

	1	2	3	4	5
authority for duties	0.755				
respect from superiors	0.657				
working hours of the job	0.649				
treated fairly	0.524				
supportive manager	0.513				
freedom for decision making					
recognition at work					
teamwork atmosphere		0.732			
mistakes treated in a positive manner		0.677			
listens to your suggestions		0.634			
comfortably discuss personal issues		0.633			
receive guidance from manager		0.626			
very well informed about role					
satisfactory salary			0.845		
good career prospects			0.645		
opportunities for further study			0.548		
Appreciation of creativity & innovative Ideas					
satisfactory welfare facilities					
involvement in management decisions				0.698	
training opportunities				0.534	
Potential Utilized				0.512	
correct work division					
job rotation					0.823

On the basis of Table 2 we found five components, for our 23 variables. Based on the item loadings, these factors were respectively labeled as

1. The factor "Empowerment & work Environment" explains the 1st component.
2. The factor "working relationship" explains the 2nd component.
3. The factor "Salary & Future Prospects" explains the 3rd component
4. The factor "Training & work Involvement" explains the 4th component
5. The factor "Job Rotation explains" the 5th component.

Here we found that a few important factors that normally contribute to the employee satisfaction, does not have much influence in employee satisfaction in KRIBHCO, Surat, such as: welfare measures, role clarity, freedom of decision making and recognition at work. The innovativeness and creativeness also takes a back seat.

All the above factors together were capable of explaining 61.099% of variance according to Table 3.

Total Variance Explained

Table 3

Component	Rotation Sums of Squared Loadings	% of Variance	Cumulative %
	Total		
1	3.654	15.889	15.889
2	3.524	15.323	31.212
3	2.794	12.148	43.359
4	2.497	10.856	54.215
5	1.583	6.884	61.099

Tests of Normality

H₀: distribution of sample data is normal

H₁: distribution of sample data is normal

Table 4

Variables	Kolmogorov-Smirnov			Shapiro-Wilk		
	Statistic	Df	Sig.	Statistic	Df	Sig.
supportive manager	0.323	150	0	0.742	150	0
authority for duties	0.301	150	0	0.844	150	0
training opportunities	0.275	150	0	0.87	150	0
treated fairly	0.324	150	0	0.818	150	0
respect from superiors	0.295	150	0	0.749	150	0
Potential Utilized	0.316	150	0	0.816	150	0
Appreciation of creativity	0.271	150	0	0.869	150	0
job rotation	0.274	150	0	0.845	150	0
recognition at work	0.332	150	0	0.794	150	0
satisfactory salary	0.258	150	0	0.782	150	0
freedom for decision making	0.249	150	0	0.879	150	0
good career prospects	0.288	150	0	0.85	150	0
comfortably discuss personal issues	0.318	150	0	0.822	150	0
mistakes treated in a positive manner	0.324	150	0	0.807	150	0
satisfactory welfare facilities	0.289	150	0	0.802	150	0
correct work division	0.244	150	0	0.888	150	0
listens to your suggestions	0.353	150	0	0.757	150	0
receive guidance from manager	0.336	150	0	0.775	150	0
involvement in management decisions	0.215	150	0	0.899	150	0
opportunities for futher study	0.248	150	0	0.877	150	0
teamwork atmosphere	0.307	150	0	0.822	150	0
working hours of the job	0.304	150	0	0.805	150	0
very well informed about role	0.353	150	0	0.737	150	0

From table 4 we found that Kolmogorov-Smirnov test of normality had the sig. value for all the variables under consideration less than 0.05 at 5% level of significance. Thus we failed to accept the null hypothesis. So we went ahead for non parametric tests.

Measurement of Satisfaction level of Employees based on Chi-Square Test Statistics against Major Variables found after Factor Analysis

H₀: Employees are satisfied in the Organization

H₁: Employees are not satisfied in the Organization

The 1st factor EMPOWERMENT & WORK ENVIRONMENT includes authority for duties, respect from superiors, working hours of the job, treated fairly & supportive managers.

Chi-Square test statistics for Factor 1

Table 5

	supportive manager	authority for duties	treated fairly	respect from superiors	working hours of the job
Chi-Square	147.133a	115.133a	138.067a	179.133a	122.667a
Df	4	4	4	4	4
Asymp. Sig.	0	0	0	0	0

From Table 5 we found that for all the variables under factor 1 had a significance value less than 0.05 at 5% level of significance, thus we fail to accept the null hypothesis. Thus we could say that employees are satisfied within the organization.

Chi-Square test statistics for Factor 2

Table 6

	comfortably discuss personal issues	mistakes treated in a positive manner	listens to your suggestions	receive guidance from manager	teamwork atmosphere
Chi-Square	122.800a	148.867a	190.067a	163.200a	135.267a
Df	4	4	4	4	4
Asymp. Sig.	0	0	0	0	0

From Table 6 we found that for all the variables under factor 2 had a significance value less than 0.05 at 5% level of significance, thus we fail to accept the null hypothesis. Thus we could say that employees are satisfied within the organization.

Chi-Square test statistics for Factor 3

Table 7

	satisfactory salary	good career prospects	opportunities for further study
Chi-Square	119.467a	113.133a	62.333a
Df	4	4	4
Asymp. Sig.	0	0	0

From Table 7 we found that for all the variables under factor 3 had a significance value less than 0.05 at 5% level of significance, thus we fail to accept the null hypothesis. Thus we could say that employees are satisfied within the organization.

Chi-Square test statistics for Factor 4

Table 8

	training opportunities	Potential Utilized	involvement in management decisions
Chi-Square	63.000a	114.667a	50.467a
Df	4	4	4
Asymp. Sig.	0	0	0

From Table 8 we found that for all the variables under factor 4 had a significance value less than 0.05 at 5% level of significance, thus we fail to accept the null hypothesis. Thus we could say that employees are satisfied within the organization.

Chi-Square test statistics for Factor 5

Table 9

	job rotation
Chi-Square	95.667a
Df	4
Asymp. Sig.	0

From Table 9 we found that for all the variables under factor 5 had a significance value less than 0.05 at 5% level of significance, thus we fail to accept the null hypothesis. Thus we could say that employees are satisfied within the organization.

Furthermore we were interested to know employee satisfaction level on the basis of following test objectives:-

- Employee Experience and employee satisfaction regarding salary.
- Employee Age and employee satisfaction regarding training opportunities
- Employee Gender and employee satisfaction regarding job rotation

Kruskal-Wallis Test - 1

H₀: Employee satisfaction does not differ regarding salary with respect to experience.

H₁: Employee satisfaction does differ regarding salary with respect to experience.

Test Statistics

Table 10

Test Statistics ^{a,b}	
	satisfactory salary
Chi-Square	17.65
Df	3
Asymp. Sig.	0.001
a. Kruskal Wallis Test	
b. Grouping Variable: experience	

Here we found table 10 show that the asymptotic sig value is 0.001 which is < 0.05 , at 5% level of significance. Hence we fail to accept the null hypothesis. This shows that the satisfaction level of employees regarding their salary differ with respect to their experience. So we needed to know that how much employee differ on their satisfaction level regarding their salary on the basis of their experience. For this we preferred rank table and from table 11 we concluded that employees having experience between 21 to 35 had the highest mean rank of 84.53, hence we could say that they were the ones who strongly agreed to the salary they received. And employees having experience less than 5 years were not satisfied with the salary they withdrew, because their mean rank was lowest at 49.37.

Rank

Table 11

	experience	N	Mean Rank
satisfactory salary	Less than 5 years	31	49.37
	5 to 20 years	28	78.29
	21 to 35 years	85	84.53
	More than 35 years	6	69.58
	Total	150	

Kruskal-Wallis Test – 2

H₀: Employee satisfaction does not differ regarding training opportunities with respect to different age Groups.

H₁: Employee satisfaction does differ regarding training opportunities with respect to different age Groups.

Test Statistics^{a, b}

Table 12

	training opportunities
Chi-Square	8.177
Df	4
Asymp. Sig.	0.085
a. Kruskal Wallis Test	
b. Grouping Variable: age	

On the basis of table 7 we found that the asymptotic sig value was 0.085 which was greater than 0.05 at 5% level of significance. So we failed to reject the null hypothesis. Hence we concluded that irrespective of their age groups, employees were satisfied with the training opportunities they got in the organization.

Mann-Whitney Test

H₀: There is no difference of satisfaction between the gender groups regarding job rotation.

H₁: There is difference of satisfaction between the gender groups regarding job rotation.

Test Statistics^a

Table 13

	job rotation
Mann-Whitney U	338.5
Wilcoxon on W	366.5
Z	-1.545
Asymp. Sig. (2-tailed)	0.122
a. Grouping Variable: gender	

On the basis of table 13 we found that no matter to whichever gender group employees belonged, they were satisfied regarding the job rotation policy of the organization, which according to them enhances their skills and competencies.

IV. Conclusion

- We found that the overall employees with special reference to KRIBHCO, Surat were satisfied with their organization.
- We also found that with respect to experience the satisfaction level of the employees differ significantly regarding salary.
- It could also be concluded that there was no difference of satisfaction level regarding training opportunities between different age groups.
- Conclusion could also be made that between gender groups there exists no significant difference in satisfaction level of employees regarding job rotation policy of the company.

References

Websites:

- [1] <http://mrp.ase.ro/no34/f7.pdf>
- [2] <http://jms.nonolympictimes.org/Articles/Article6.pdf>

Journals

- [1] Meena M. L. and Dangayach G.S.,(2012), “Analysis of Employee Satisfaction in Banking Sector”, International Journal of Humanities and Applied Sciences (IJHAS) Vol. 1, No. 2, ISSN 2277 – 4386
- [2] Dr. Anitha R., Sep (2011), “A Study on Job Satisfaction of Paper Mill Employees with Special Reference to Udumalpet and Palani Taluk”, Journal of Management and Science, Vol. 1, No.1, pp. 36-47.
- [3] Zaim Halil, Zaim Selim, “Measuring Employee Satisfaction in Small and Medium Sized Enterprises” , Faith University, Turkey
- [4] Aziri Brikend (2011), “Job Satisfaction”, Management Research and Practice vol. 3 issue 4, pp: 77-86
- [5] Wadhwa Singh Daljeet, Verghese Manoj & Wadhwa Singh Dalvinder, September (2011), “A Study on Factors Influencing Employee Job Satisfaction-A Study in Cement Industry of Chhattisgarh”, International Journal of Management & Business studies (IJMBS) Vol. 1, Issue 3

Modelling and Simulation of High Step up Dc-Dc Converter for Micro Grid Application

B.D.S Prasad,¹ Dr. M Siva Kumar²

¹EEE, Gudlavalleru Engineering College/ JNTUK, INDIA

²PROFESSOR & HOD Department of Electrical & Electronics Engineering, JNTUK, INDIA

Abstract: The distributed generation (DG) systems based on the renewable energy sources have rapidly developed in recent years. These DG systems are powered by micro sources such as fuel cells, photovoltaic (PV) systems, and batteries. The micro grid concept consists of two stages, in the first stage the low level voltage from the pv cell is converted to high level voltage by using DC-DC converter. In the second stage the high level DC voltage is converted into AC voltage by using an inverter and is supplied to load. This paper proposes a novel High Step-up DC-DC converter for micro grid application. The proposed converter is modelled and simulated along with pv cell and inverter through MATLAB/SIMULINK for AC load. The proposed converter has high voltage gain and efficiency. The results are successfully verified.

Keyword: Coupled inductor, distributed generation (DG) system, high step-up, Multilevel Inverter, Cascaded H Bridge multilevel inverter.

I. Introduction

Distributed generation (DG) systems based on renewable energy sources (RES) have experienced a fast development in recent years. With more DG units being integrated into the power system, a recent concept, called microgrid, is developed by grouping a cluster of loads and parallel DG units in a local area. The microgrid can operate in grid-connected mode or autonomous islanding mode and benefits both the utility and customers in terms of efficiency, reliability and power quality.

Each DG system has an energy source and a storage system, a grid-interfacing voltage source inverter (VSI) and output LC filters. In the grid-connected operation, the microgrid is connected to the grid at the point of common coupling (PCC) through a static transfer switch (STS), and each DG unit generates proper real and reactive power (according to the dispatched references or from the maximum power point tracking). In islanding operation, the DG units continue to supply power to the microgrid loads and they should be able to share the total load demand according to their respective ratings.

Numerous industrial applications have begun to require higher power apparatus in recent years. Some medium voltage motor drives and utility applications require medium voltage and megawatt power level. For a medium voltage grid, it is troublesome to connect only one power semiconductor switch directly. As a result, a multilevel power converter structure has been introduced as an alternative in high power and medium voltage situations. A multilevel converter not only achieves high power ratings, but also enables the use of renewable energy sources and drive applications.

With the advancement of power electronics and emergence of new multilevel converter topologies, it is possible to work at voltage levels beyond the classic semiconductor limits. The multilevel converters achieve high-voltage switching by means of a series of voltage steps, each of which lies within the ratings of the individual power devices. Among the multilevel Converters, the cascaded H-bridge topology (CHB) is particularly attractive in high-voltage applications, because it requires the least number of components to synthesize the same number of voltage levels.

These converter topologies can generate high-quality voltage waveforms with power semiconductor switches operating at a frequency near the fundamental [5]. Although, in low-power applications, the switching frequency of the power switches is not restricted, a low switching frequency can increase the efficiency of the converter. Additionally, multilevel converters feature several dc links, making possible the independent voltage controls.

In this paper, a load-connected PV power system with high voltage gain is proposed. The steady-state model analysis and the control strategy of the system are presented. The load connected PV system includes two power-processing stages: a high step-up ZVT-interleaved boost converter for boosting a low voltage of PV array up to the high dc-bus voltage, which is not less than load side voltage level; and a multilevel inverter for inverting the dc current into a sinusoidal waveform synchronized with the utility system.

The distributed generation (DG) systems based on the renewable energy sources have rapidly developed in recent years [1], [2]. These DG systems are powered by micro sources such as fuel cells, photovoltaic (PV) systems, and batteries [3]–[7]. Fig. 1 shows a PV distributed system in which the solar source is low dc input voltage. PV sources can also connect in series to obtain sufficient dc voltage for generating actuality voltage; however, it is difficult to realize a series connection of the PV source without incurring a shadow effect [8], [9]. High step-up DC-DC converters are generally used as the front end converters to step from low voltage (12–40 v) up to high voltage (380–400 v) [10]. High step-up DC-DC converters are required to have a large conversion ratio, high efficiency, and small volume.

This paper proposes a high efficiency, high step-up voltage gain, and clamp-mode converter and applied to load with the help of multilevel inverter. The proposed converter adds two pairs of additional capacitors and diodes to achieve high step-up voltage gain. The coupled inductor is used as both a forward and fly back type; thus, the two capacitors can be charged in parallel and discharged in series via the coupled inductor. The transit current does not flow through the main switch compared with earlier studies. Thus, the proposed converter has low conduction loss. Additionally, this converter

allows significant weight and volume reduction compared with other converters. Another benefit is that the voltage stresses on the main switch and output diode are reduced. However, the leakage inductor of the coupled inductor may cause high power loss and voltage spike. Thus, a passive clamping circuit is needed to recycle the leakage-inductor energy of the coupled inductor and to clamp the voltage across the main switch. The reverse-recovery problems in the diodes are alleviated, and thus, high efficiency can be achieved.

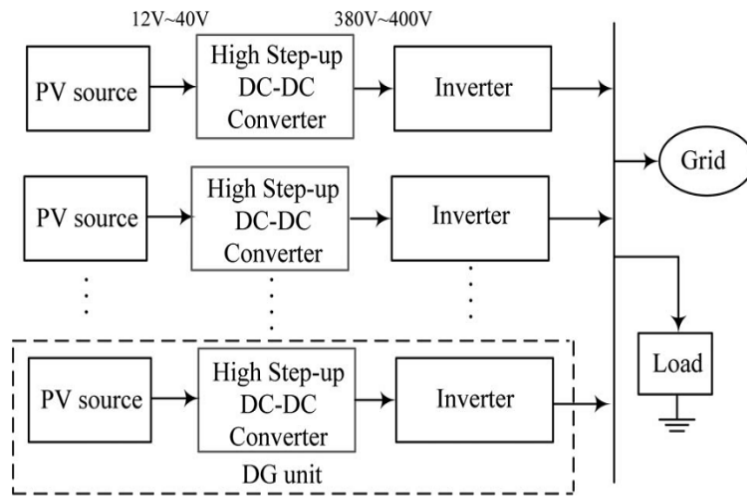


Fig. 1. PV distributed system

II. Proposed Converter

Fig. 2 shows the circuit topology of the proposed converter. This converter consists of dc input voltage V_{in} , power switch S , coupled inductors N_p and N_s , one clamp diode D_1 , clamp capacitor C_1 , two blocking capacitors C_2 and C_3 , two blocking diodes D_2 and D_3 , output diode D_o , and output capacitor C_o . The coupled inductor is modeled as the magnetizing inductor L_m and leakage inductor L_k . To simplify the circuit analysis, the following conditions are assumed.

- 1) Capacitors C_2 , C_3 , and C_o are large enough that V_{c2} , V_{c3} , and V_o are considered to be constant in one switching period.
- 2) The power MOSFET and diodes are treated as ideal, but the parasitic capacitor of the power switch is considered.
- 3) The coupling coefficient of coupled inductor k is equal to $L_m / (L_m + L_k)$ and the turns ratio of coupled inductor n is equal to N_s / N_p .

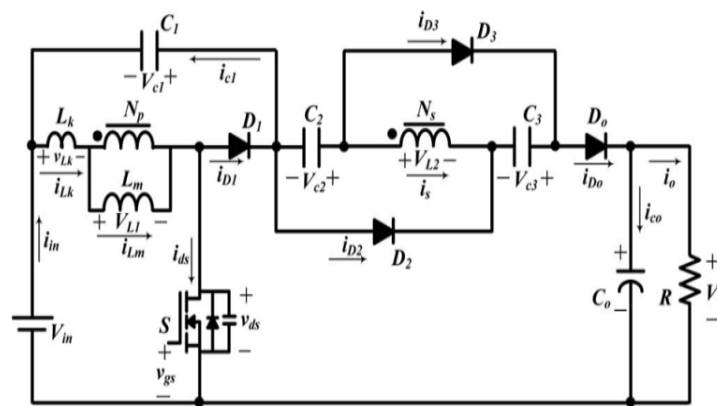


Fig. 2. Circuit configure of the proposed converter.

A. Continuous-Conduction Mode (CCM) Operation

- 1) Mode I [t_0, t_1]: During this time interval, S is turned on. Diodes D_1 , D_2 , and D_3 are turned off, and D_o is turned on. The current-flow path is shown in Fig.3. The primary-side current of the coupled inductor i_{Lk} is increased linearly. The magnetizing inductor L_m stores its energy from dc source V_{in} . Due to the leakage inductor L_k , the secondary-side current of the coupled inductor i is decreased linearly. The voltage across the secondary side winding of the coupled inductor V_{L2} , and blocking voltages V_{c2} and V_{c3} are connected in series to charge the output capacitor C_o and to provide the energy to the load R . When the current is becomes zero, dc source V_{in} begins to charge capacitors C_2 and C_3 via the coupled inductor. When i_{Lk} is equal to i_{Lm} at $t = t_1$, this operating mode ends.

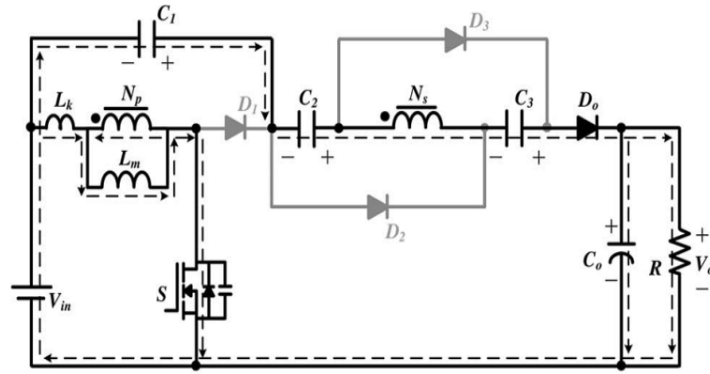


Fig.3. Current flowing path of Mode-I during one switching period at CCM operation.

- 2) Mode II [t_1, t_2]: During this time interval, S is still turned on. Diodes D_1 and D_0 are turned off, and D_2 and D_3 are turned on. The current-flow path is shown in Fig. 4. The magnetizing inductor L_m is stored energy from dc source V_{in} . Some of the energy from DC source V_{in} transfers to the secondary side of the coupled inductor to charge the capacitors C_2 and C_3 . Voltages V_{c2} and V_{c3} are approximately equal to nV_{in} . Output capacitor C_0 provides the energy to load R. This operating mode ends when switch S is turned off at $t = t_2$.

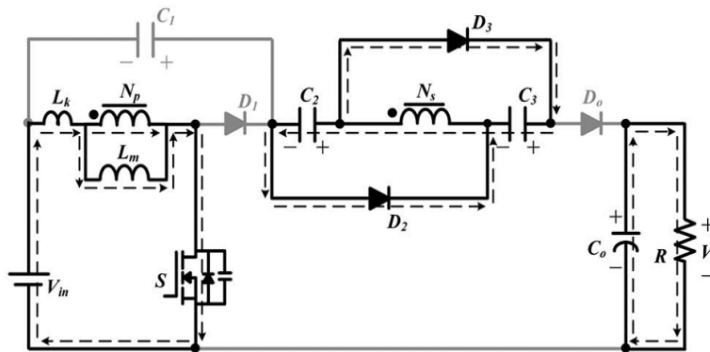


Fig.4. Current flowing path of Mode-II during one switching period at CCM operation.

- 3) Mode III [t_2, t_3]: During this time interval, S is turned off. Diodes D_1 and D_0 are turned off, and D_2 and D_3 are turned on. The current-flow path is shown in Fig. 5. The energies of leakage inductor L_k and magnetizing inductor L_m are released to the parasitic capacitor C_{ds} of switch S. The capacitors C_2 and C_3 are still charged by the DC source V_{in} via the coupled inductor. The output capacitor C_0 provides energy to load R. When the capacitor voltage $V_{in} + V_{ds}$ is equal to V_{c1} at $t = t_3$, diode D_1 conducts and this operating mode ends.

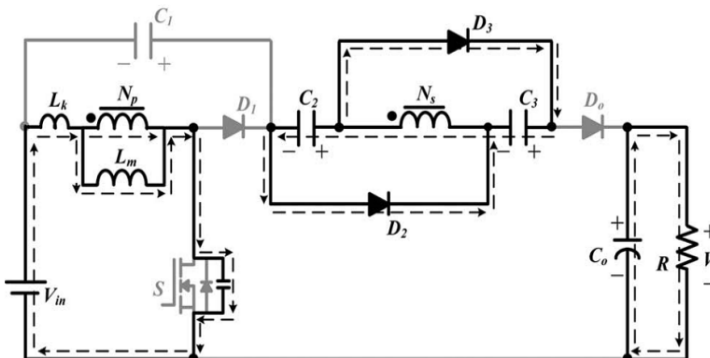


Fig.5. Current flowing path of Mode-III during one switching period at CCM operation.

- 4) Mode IV [t_3, t_4]: During this time interval, S is turned off. Diodes D_1 , D_2 , and D_3 are turned on and D_0 is turned off. The current-flow path is shown in Fig.6. The energies of leakage inductor L_k and magnetizing inductor L_m are released to the clamp capacitor C_1 . Some of the energy stored in L_m starts to release to capacitors C_2 and C_3 in parallel via the coupled inductor until secondary current is equals to zero. Meanwhile, current i_{Lk} is decreased quickly. Thus, diodes D_2 and D_3 are cut off at $t = t_4$, and this operating mode ends.

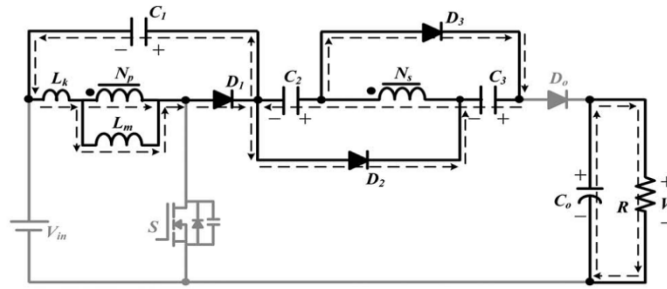


Fig.6. Current flowing path of Mode-IV during one switching period at CCM operation.

- 5) Mode V [t_4, t_5]: During this time interval, \$S\$ is turned off. Diodes \$D_1\$ and \$D_0\$ are turned on, and \$D_2\$ and \$D_3\$ are turned off. The current-flow path is shown in Fig.7. The energies of leakage inductor \$L_k\$ and magnetizing inductor \$L_m\$ are released to the clamp capacitor \$C_1\$. The primary and secondary windings of the coupled inductor, DC sources \$V_{in}\$, and capacitors \$C_2\$ and \$C_3\$ are in series to transfer their energies to the output capacitor \$C_0\$ and load \$R\$. This operating mode ends when capacitor \$C_1\$ starts to discharge at \$t = t_5\$.

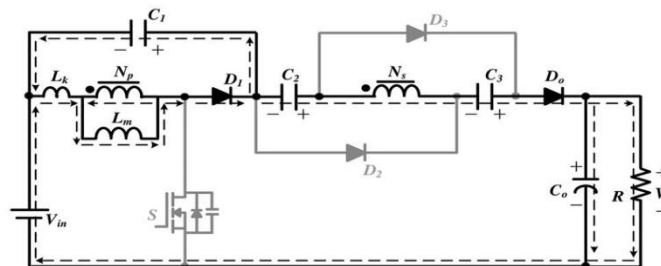


Fig.7. Current flowing path of Mode-V during one switching period at CCM operation.

- 6) Mode VI [t_5, t_6]: During this time interval, \$S\$ is still turned off. Diodes \$D_1\$ and \$D_0\$ are turned on, and \$D_2\$ and \$D_3\$ are turned off. The current-flow path is shown in Fig.8. The primary-side and secondary-side windings of the coupled inductor, DC sources \$V_{in}\$, and capacitors \$C_1, C_2\$, and \$C_3\$ transfer their energies to the output capacitor \$C_0\$ and load \$R\$. This mode ends at \$t = t_6\$ when \$S\$ is turned on at the beginning of the next switching period.

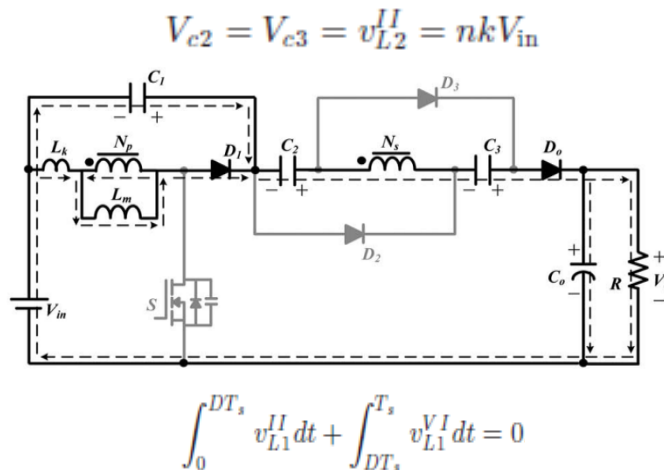


Fig.8. Current flowing path of Mode-VI during one switching period at CCM operation.

III. STEADY-STATE ANALYSIS OF THE PROPOSED CONVERTER

A. CCM Operation

At modes IV and V, the energy of the leakage inductor \$L_k\$ is released to the clamped capacitor \$C_1\$. According to previous work [15], the duty cycle of the released energy can be expressed as

$$D_{C1} = \frac{t_{C1}}{T_s} = \frac{2(1-D)}{n+1} \dots \dots \dots (1)$$

Where \$T_s\$ is the switching period, \$D_{c1}\$ is the duty ratio of the switch, and \$t_{c1}\$ is the time of modes IV and V. By applying the voltage-second balance principle on \$L_m\$, the voltage across the capacitor \$C_1\$ can be represented by

$$V_{C1} = \frac{D}{1-D} V_{in} \frac{(1+K)+(1-K)n}{2} \dots\dots\dots (2)$$

Since the time durations of modes I, III, and IV are significantly short, only modes II, V, and VI are considered in CCM operation for the steady-state analysis. In the time period of mode II, the following equations can be written based on Fig.:

$$v_{L1}^{II} = \frac{L_m}{L_m + L_{k1}} V_{in} = kV_{in} \dots\dots\dots (3)$$

$$v_{L2}^{II} = nv_{L1}^{II} = nkV_{in}. \dots\dots\dots (4)$$

Thus, the voltage across capacitors C2 and C3 can be written as

$$V_{c2} = V_{c3} = v_{L2}^{II} = nkV_{in}. \dots\dots\dots (5)$$

During the time duration of modes V and VI, the following equation can be formulated based on Fig.:

$$v_{L2}^V = v_{L2}^{VI} = V_{in} + V_{c1} + V_{c2} + V_{c3} - V_o \dots\dots\dots (6)$$

Thus, the voltage across the magnetizing inductor Lm can be derived as

$$v_{L1}^V = v_{L1}^{VI} = \frac{v_{L2}^{VI}}{n} = \frac{V_{in} + V_{c1} + V_{c2} + V_{c3} - V_o}{n} \dots\dots\dots (7)$$

Using the volt-second balance principle on Lm, the following equation is given

$$\int_0^{DT_s} v_{L1}^{II} dt + \int_{DT_s}^{T_s} v_{L1}^{VI} dt = 0. \dots\dots\dots (8)$$

Substituting (2), (3), (5), and (7) into (8), the voltage gain is obtained as

$$M_{CCM} = \frac{1+nk}{1-D} + nk + \frac{D}{1-D} \cdot \frac{(1-k)(n-1)}{2} \dots\dots\dots (9)$$

The schematic of the voltage gain versus the duty ratio under various coupling coefficients of the coupled inductor is shown in Fig... It is seen that the voltage gain is not very sensitive to the coupling coefficient. When k is equal to 1, the ideal voltage gain is written as

$$M_{CCM} = \frac{1+n}{1-D} + n \dots\dots\dots (10)$$

If the proposed converter is operated in boundary condition mode, the voltage gain of CCM operation is equal to the voltage gain of DCM operation. From (10), the boundary normalized magnetizing inductor time constant τ_{LmB} can be derived as

$$\tau_{LmB} = \frac{D(1-D)^2}{2(1+n)(1+2n-nD)} \dots\dots\dots (11)$$

IV. Matlab/Simulink Modelling And Simulation Results

The Converter Proposed in Section II is Modelled and Simulated as shown in figure 9.

Here the simulation is carried out in two cases

1. Proposed high step-up DC/DC converter.
2. Proposed high step-up DC/DC converter applied to AC load.

Case 1: Proposed high step-up DC/DC converter:

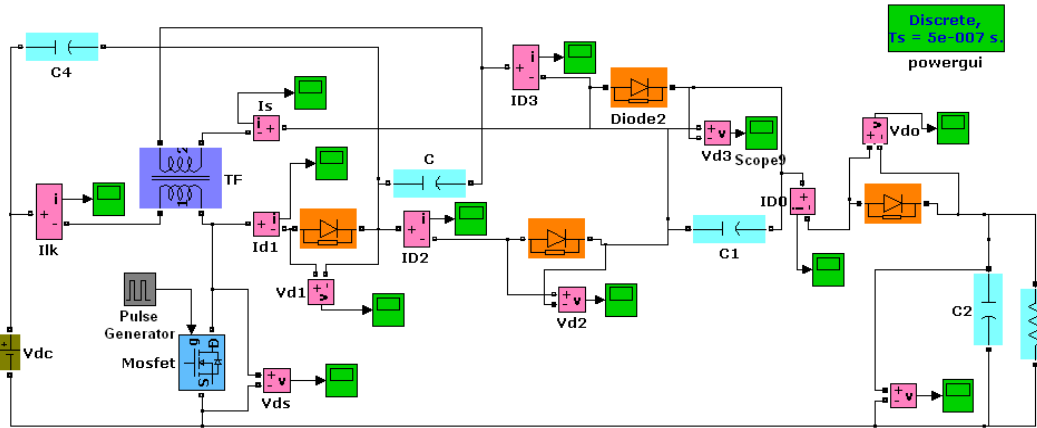


Fig.9. MATLAB/SIMULINK circuit of the converter

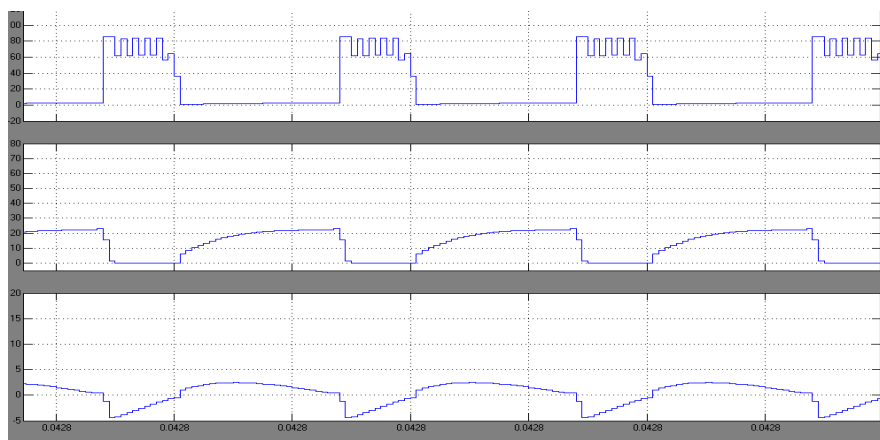


Fig.10. Shows the proposed converter Output waveforms of proposed converter V_{DS} , I_{LK} , I_s

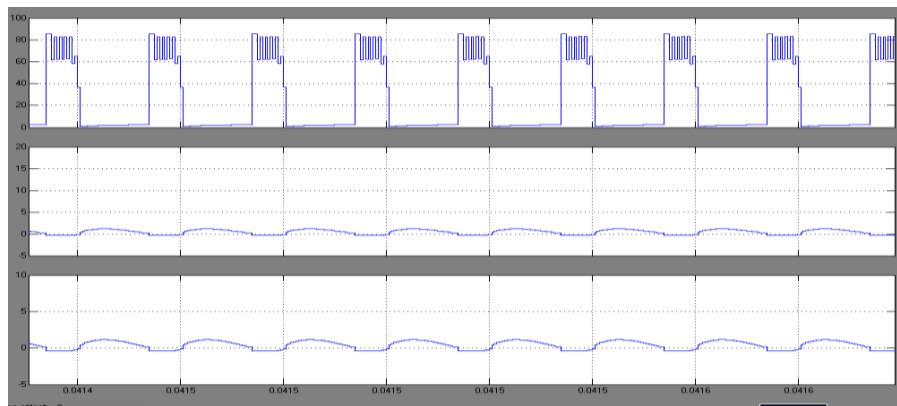


Fig 11: waveforms of V_{DS} , I_{D2} , I_{D3}

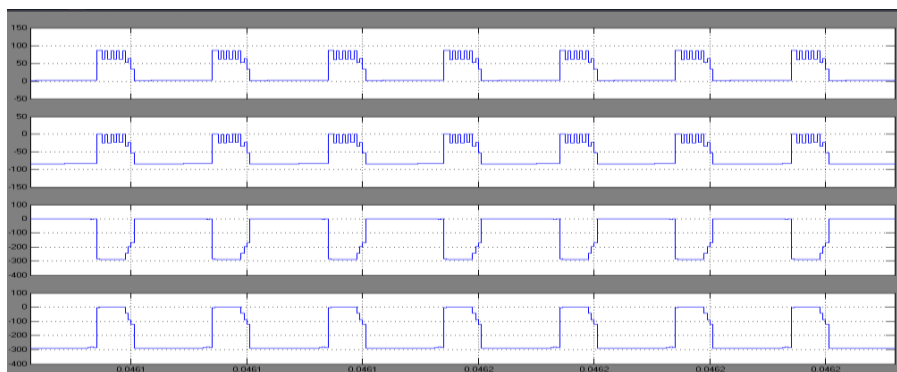


Fig.12: Waveforms of V_{DS} , V_{D1} , V_{D2} , V_{D0}

Case 2: Proposed high step-up DC/DC converter applied to AC load.

The above Fig 10, Fig 11, Fig12 shows the waveforms of current through leakage inductor I_{LK} , current Through secondary I_s , current through diode D_2 I_{D2} , current through diode D_3 I_{D3} , voltage across diode D_1 V_{D1} , Voltage across diode D_2 V_{D2} , voltage across output diode D_0 V_{D0}

Fig.13 shows the MATLAB/SIMULINK circuit of the proposed high step-up DC/DC converter applied to AC load with photo voltaic cell as the input.

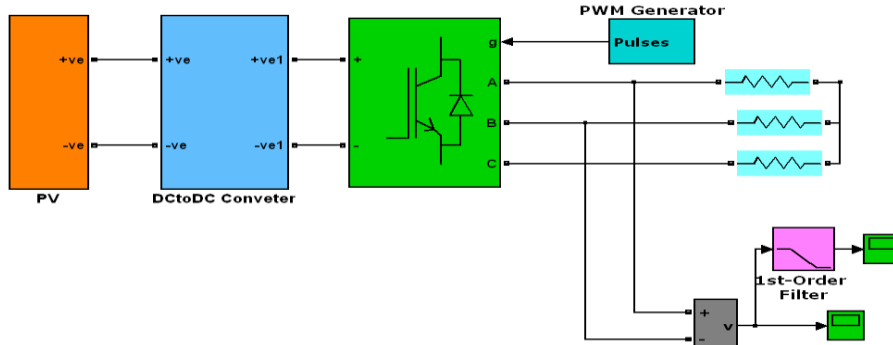


Fig.13 SIMULINK model of the micro grid with pv cell,DC-DC converter, inverter

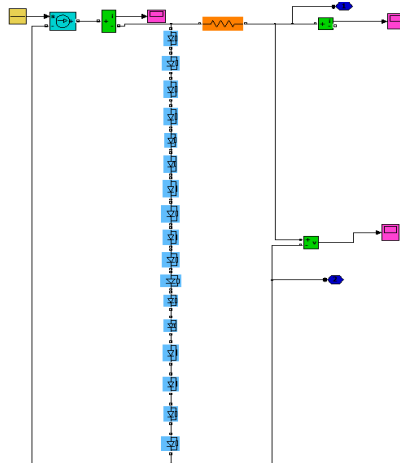


Fig.14 Photovoltaic cell model

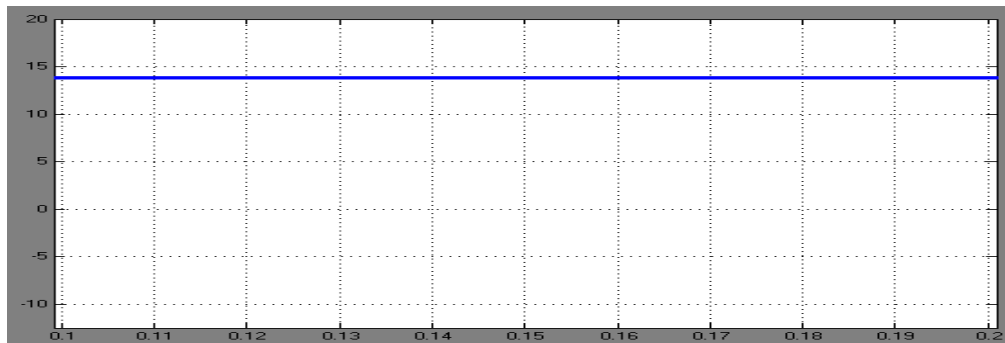


Fig.15 PV model voltage waveform

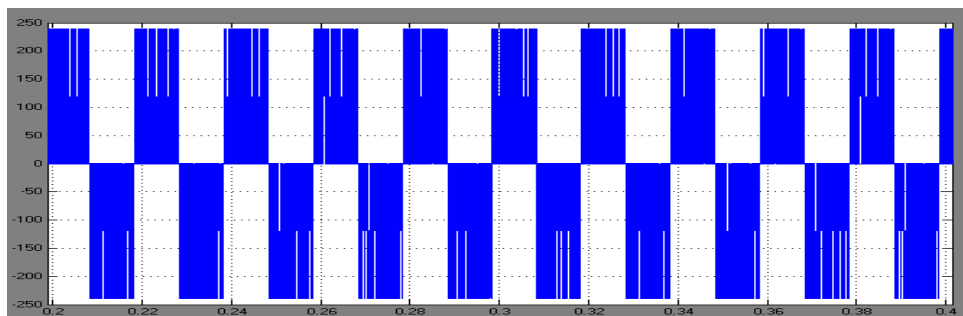


Fig.16 Inverter output voltage without filter

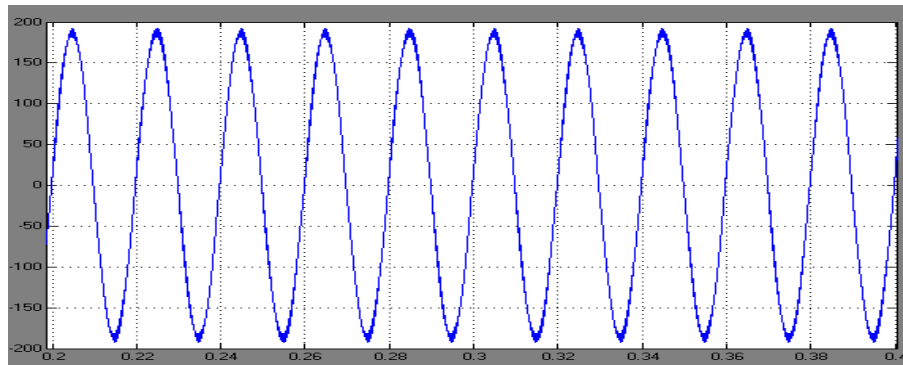


Fig.17 Inverter output voltage with filter

V. Conclusion

This paper proposed a novel, high efficiency, and high step-up DC–DC converter applied to AC load with the help of inverter. By using the capacitor charged in parallel and discharged in a series by the coupled inductor, high step-up voltage gain and high efficiency are achieved. The steady-state analyses of voltage gain and boundary operating condition are discussed in detail. A prototype circuit of the proposed converter is built in the MATLAB/SIMULINK environment. The voltage stress on the main switches is 90V; thus, low voltage ratings and low on-state resistance levels R_{DS} (ON) switch can be selected. Moreover, the proposed converter has simple structure.

References

- [1] Yi-Ping Hsieh, Jiann-Fuh Chen, Tsorng-Juu Liang and Lung-Sheng Yang. "A Novel High Step-Up DC–DC Converter for a Microgrid System". IEEE TRANSACTIONS ON POWER ELECTRONICS, VOL. 26, NO. 4, APRIL 2011
- [2] Yi. Li, D. M. Vilathgamuwa, and P. H. Loh, "Design, analysis, and realtime testing of a controller for multibus microgrid system," IEEE Trans. Power Electron., vol. 19, no. 5, pp. 1195–1204, Jul. 2004.
- [3] C. L. Chen, Y. W. J. S. Lai, Y. S. Lee, and D. Martin, "Design of parallel inverters for smooth mode transfer microgrid applications," IEEE Trans. Power Electron., vol. 25, no. 1, pp. 6–15, Jan. 2010.
- [4] A. Timbus, M. Liserre, R. Teodorescu, P. Rodriguez, and F. Blaabjerg, "Evaluation of current controllers for distributed power generation systems," IEEE Trans. Power Electron., vol. 24, no. 3, pp. 654–664, Mar. 2009.
- [5] Y. A.-R. I. Mohamed and E. F. El Saadany, "Hybrid variable-structure control with evolutionary optimum-tuning algorithm for fast grid-voltage regulation using inverter-based distributed generation," IEEE Trans. Power Electron., vol. 23, no. 3, pp. 1334–1341, May 2008.
- [6] Y. A.-R. I. Mohamed and E. F. El Saadany, "Adaptive decentralized droop controller to preserve power sharing stability of paralleled inverters in distributed generation microgrids," IEEE Trans. Power Electron., vol. 23, no. 6, pp. 2806–2816, Nov. 2008.
- [7] Y. W. Li and C. -N. Kao, "An accurate power control strategy for power electronics interfaced distributed generation units operating in a low voltage multibus microgrid," IEEE Trans. Power Electron., vol. 24, no. 12, pp. 2977–2988, Dec. 2009.
- [8] H. Karimi, A. Yazdani, and R. Iravani, "Negative-sequence current injection for fast islanding detection of a distributed resource unit," IEEE Trans. Power Electron., vol. 23, no. 1, pp. 298–307, Jan. 2008.
- [9] T. Shimizu, K. Wada, and N. Nakamura, "Flyback-type single-phase utility interactive inverter with power pulsation decoupling on the dc input for an ac photovoltaic module system," IEEE Trans. Power Electron., vol. 21, no. 5, pp. 1264–1272, Sep. 2006.
- [10] L. Palma, M. H. Todorovic, and P. Enjeti, "A high gain transformer less DC–DC converter for fuel-cell applications," in Proc. IEEE Power Electron. Spec. Conf. (PESC), 2005, pp. 2514–2520.
- [11] P. Biczek, "Power electronic converters in dc microgrid," in Proc. IEEE Compact. Power Electron. Conf. (CPE), 2007, pp. 1–6.
- [12] A. M. Salamah, S. J. Finney, and B. W. Williams, "Single-phase voltage source inverter with a bidirectional buck–boost stage for harmonic injection and distributed generation," IEEE Trans. Power Electron., vol. 24, no. 2, pp. 376–387, Feb. 2009.

A Novel Data Leakage Detection

Priyanka Barge,¹ Pratibha Dhawale,² Namrata Kolashetti³
Ass. Prof., Department of Computer Engineering, NIRMALA CHOUHAN

Abstract: This paper contains concept of data leakage, its causes of leakage and different techniques to detect the data leakage. The value of the data is incredible, so it should not be leaked or altered. In the field of IT, huge database is being used. This database is shared with multiple people at a time. But during this sharing of the data, there are huge chances of data vulnerability, leakage or alteration. So, to prevent these problems, a data leakage detection system has been proposed. This paper includes brief idea about data leakage detection and a methodology to detect the data leakage persons.

Keywords: Guilty agent, data distributor, watermarking, fake object, data leakage.

I. Introduction

Data leakage is defined as the accidental or unintentional distribution of private or sensitive data to unauthorized entity. Sensitive data of companies and organizations includes intellectual property (IP), financial information, patient information, personal credit-card data, and other information depending on the business and the industry.

Furthermore, in many cases, sensitive data is shared among various stakeholders such as employees working from outside the organizational premises (e.g., on laptops), business partners and customers. This increases the risk of confidential information falling into unauthorized hands. Whether caused by malicious intent, or an inadvertent mistake, by an insider or outsider, exposed sensitive information can seriously hurt an organization.

The potential damage and adverse consequences of a data leak incident can be classified into the following two categories: direct and indirect loss[3]. Direct loss refers to tangible damage that is easy to measure and estimate quantitatively. Indirect loss, on the other hand, is much harder to quantify and has a much broader impact in terms of cost, place and time. Direct loss includes violating regulations (such as those protecting customer privacy) resulting in fine/settlement/customer compensation fees; litigation of lawsuits; loss of future sales; costs of investigation and remedial/restoration fees. Indirect loss includes reduced share-price as a result of the negative publicity; damage to company's goodwill and reputation; customer abandonment; and exposure of Intellectual Property (business plans, code, financial reports, and meeting agendas) to competitors.

II. Existing System

Traditionally, leakage detection is handled by watermarking, e.g., a unique code is embedded in each distributed copy. If that copy is later discovered in the hands of an unauthorized party, the leaker can be identified. Watermarks can be very useful in some cases, but again, involve some modification of the original data. Furthermore, watermarks can sometimes be destroyed if the data recipient is malicious. E.g. A hospital may give patient records to researchers who will devise new treatments. Similarly, a company may have partnerships with other companies that require sharing customer data. Another enterprise may outsource its data processing, so data must be given to various other companies. We call the owner of the data the distributor and the supposedly trusted third parties the agents.

III. Proposed System

Our goal is to detect, when the distributor's sensitive data has been leaked by agents, and if possible to identify the agent that leaked the data. Perturbation is a very useful technique where the data is modified and made "less sensitive" before being handed to agents. We propose to develop unobtrusive techniques for detecting leakage of a set of objects or records.

In this section, we propose to develop a model for assessing the "guilt" of agents. We also present algorithms for distributing objects to agents, in a way that improves our chances of identifying a leaker. Finally, we also consider the option of adding "fake" objects to the distributed set. Such objects do not correspond to real entities but appear realistic to the agents. In a sense, the fake objects acts as a type of watermark for the entire set, without modifying any individual members [2]. If it turns out an agent was given one or more fake objects that were leaked, then the distributor can be more confident that agent was guilty.

IV. Methodology

4.1 Entities And Agents

Distributor owns set of data objects $T = \{t_1, t_2, \dots, t_n\}$. Distributor has to share some of the objects with set of agents $U_1, U_2 \dots U_n$, but does not wish the object be leaked to other third parties. The objects in T could be of any type and size, e.g., they could be tuples in a relation or relations in a database.

An agent U_i receives a subset R_i of objects T , determined either by a sample request or an explicit request.

- **Evaluation of Explicit Data Request Algorithms**

In this request the agent will send the request with appropriate condition. Agent gives the input as request with input as well as the condition for the request. After processing on the data he will get the new data by adding fake object using watermarking technique.

Explicit request $R_i = \text{EXPLICIT}(T, \text{cond}_i)$: Agent U_i receives all T objects that satisfy cond_i .

- **Evaluation of Sample Data Request Algorithms**

In this request agent request does not have condition. The agent sends the request without condition as per his query he will get the data by adding fake object using watermarking technique.

Sample request = $\text{SAMPLE}(T, m_i)$: Any subset of m_i records from T can be given to U_i .

4.2 Guilty Agents

Suppose that after giving objects to agents, the distributor discovers that a set S belongs to T has leaked. This means that the third party, called the target, has been caught in possession of S .

We say an agent U_i is guilty and if it contributes one or more object to target. We denote the event that agent U_i is guilty as G_i and the event that agent U_i is guilty for a given leaked set S as $G_i|S$. Our next step is to estimate $\Pr\{G_i|S\}$, i.e. the probability that agent U_i is guilty given evidence S .

4.3 Related Work

Here we proposed a watermarking algorithm that embeds the watermark bits in the least significant bits (LSB) of selected attributes of a selected subset of tuples. This technique does not provide mechanism for multibit watermarks, instead only secret key is used. For each tuple, a secure message authenticated code (MAC) is computed using the secret key and tuple's primary key. The computed MAC is used to select candidate tuples, attributes and LSB position in the selected attributes. However, the watermark can be easily compromised by very trivial attacks. For example a simple manipulation of the data by shifting the LSB is one position easily leads to watermark loss without much damage to the data. Therefore LSB based data hiding technique is not resilient. Moreover, it assumes that the LSB bits in any tuple can be altered without checking data constraints. Simple unconstrained LSB manipulations can easily generate undesirable results. Thus such technique is not resilient to deletion and insertion attacks.

V. User Model

To compute this $\Pr\{G_i|S\}$, we need an estimate for the probability that values in S can be "guessed" by the target. We call this estimate p_t , the probability that object t can be guessed by the target.

Probability p_t is analogous to the probabilities used in designing fault-tolerant systems. That is, to estimate how likely it is that a system will be operational throughout a given period, we need the probabilities that individual components will or will not fail. A component failure in our case is the event that the target guesses an object of S . The component failure is used to compute the overall system reliability, while we use the probability of guessing to identify agents that have leaked information. The component failure probabilities are estimated based on experiments, just as we propose to estimate the p_t 's. Similarly, the component probabilities are usually conservative estimates, rather than exact numbers. For example, say we use a component failure probability that is higher than the actual probability, and we design our system to provide a desired high level of reliability. Then we will know that the actual system will have at least that level of reliability, but possibly higher. In the same way, if we use p_t 's that are higher than the true values, we will know that the agents will be guilty with at least the computed probabilities.

VI. Data Allocation Problem

The main focus of our paper is the data allocation problem: how can the distributor "intelligently" give data to agents in order to improve the chances of detecting a guilty agent?

6.1 Fake Objects

The idea of perturbing data to detect leakage is not new. In our case, we are perturbing the set of distributor objects by adding fake elements. In some applications, fake objects may cause fewer problems than perturbing real objects. For example, say the distributed data objects are medical records and the agents are hospitals. In this case, even small modifications to the records of actual patients may be undesirable. However, the addition of some fake medical records may be acceptable, since no patient matches these records, and hence no one will ever be treated based on fake records.

Our use of fake objects is inspired by the use of "trace" records in mailing lists. In this case, company A sells to company B a mailing list to be used once (e.g., to send advertisements). Company A adds trace records that contain addresses owned by company A. Thus, each time company B uses the purchased mailing list, A receives copies of the mailing. These records are a type of fake objects that help identify improper use of data.

The distributor creates and adds fake objects to the data that he distributes to agents. We let $F_i \subseteq R_i$ be the subset of fake objects that agent U_i receives. Fake objects must be created carefully so that agents cannot distinguish them from real objects.

6.2 Optimization Problem

The Optimization Module is the distributor's data allocation to agents has one constraint and one objective. The distributor's constraint is to satisfy agents' requests, by providing them with the number of objects they request or with all available objects that satisfy their conditions. His objective is to be able to detect an agent who leaks any portion of his data.

VII. Conclusion

In a perfect world there would be no need to hand over sensitive data to agents that may unknowingly or maliciously leak it. And even if we had to hand over sensitive data, in a perfect world we could watermark each object so that we could trace its origins with absolute certainty. However, in many cases we must indeed work with agents that may not be 100% trusted, and we may not be certain if a leaked object came from an agent or from some other source, since certain data cannot admit watermarks.

In spite of these difficulties, we have shown it is possible to assess the likelihood that an agent is responsible for a leak, based on the overlap of his data with the leaked data and the data of other agents, and based on the probability that objects can be "guessed" by other means. Our model is relatively simple, but we believe it captures the essential trade-offs. The algorithms we have presented implement a variety of data distribution strategies that can improve the distributor's chances of identifying a leaker. We have shown that distributing objects judiciously can make a significant difference in identifying guilty agents, especially in cases where there is large overlap in the data that agents must receive.

7.1 Advantages

- It is possible to assess the likelihood that an agent is responsible for a leak, based on the overlap of his data with the leaked data and the data of other agents and based on the probability that objects can be guessed by other means [1].

Disadvantages

- In given watermarking algorithm, watermark can be easily compromised by very trivial attacks. For example a simple manipulation of the data by shifting the LSB is one position easily leads to watermark loss without much damage to the data. Therefore LSB based data hiding technique is not resilient.

VIII. Acknowledge

For all the efforts behind this paper work, we first would like to express our sincere thanks to the staff of Dept. of computer Engg., for their extended help and suggestions at every stage. It is with a great sense of gratitude that I acknowledge the support, time to time suggestions to my guide prof. Nirmala Chouhan, Prof. G. M. Bhandari(HOD) and prof. Jayant Jadhav (Project Co-ordinator).

References

- [1] P. Papadimitriou and H. Garcia-Molina, "Data leakage detection," IEEE Transactions on Knowledge and Data Engineering, pages 51-63, volume 23, 2011.
- [2] R. Agrawal and J. Kiernan, "Watermarking Relational Databases," Proc. 28th Int'l Conf. Very Large Data Bases (VLDB '02), VLDB Endowment, pp. 155-166, 2002.
- [3] Sandip A. Kale, Prof. S.V. Kulkarni/ IOSR Journal of Computer Engineering (IOSRJCE) ISSN:2278-0661 Volume 1, Issue 6 (July-Aug 2012), PP 32-35 www.iosrjournals.org/ page Data Leakage Detection : A Survey

Finite Element Analysis on Temperature Distribution of Turning Process

Mr. Yash R. Bhoyar¹, Prof. P. D. Kamble²

¹M.Tech (CAD/CAM) 2nd yr., Dept. of Mechanical, Yeshwantrao Chavan College of Engineering, Hingna Road Nagpur and 441110, India

²Asst. Professor, Dept. of Mechanical, Yeshwantrao Chavan College of Engineering, Hingna Road Nagpur And 441110, India

ABSTRACT: The aim of this study is to create a finite element analysis simulation model in order to obtain solutions of the cutting forces, specific cutting energy and adequate temperatures occurring at different points through the chip/tool contact region and the coating/substrate boundary for a range of cutting tool materials and defined cutting conditions. Interfacial temperature in machining plays a major role in tool wear and can also result in modifications to the properties of the work piece and tool materials. As there is a general move towards dry machining, for environmental reasons, it is increasingly important to understand how machining temperature are affected by the process variables involved (cutting speed, feed rate, tool geometry, etc.) and by other factors such as tool wear.

Keywords: turning process; FEA; data measurements

I. INTRODUCTION

The turning process is used widely in industry and has countless applications. Traditionally, the process has been used to reduce the diameter of cylindrical work piece, or to change a work piece of non-circular cross-section. This is done by rotating the work piece about this of the machine's spindle and removing the work piece material with the cutting tool which is fed in the perpendicular direction. For the past fifty years metal cutting researchers have developed many modeling techniques including analytical techniques, slip-line solutions, empirical approaches and finite element techniques. In recent years, the finite element analysis has particularly become the main tool for simulating metal cutting processes. Finite element analysis are widely used for calculating the stress, strain, strain-rate and temperature distributions in the primary, secondary and tertiary sub-cutting zones. In consequence, temperatures in the tool, chip and workpiece, as well as cutting forces, plastic deformation (shear angles and chip thickness), chip formation and possibly its breaking can be determined faster than using costly and time consuming experiments. In this work, mechanically based models are developed that are able to predict the effect of various process variables on the performance measures of interests such as cutting forces, tool breakages, and surface accuracy.

1.1 The Turning Process

Turning is a very important machining process in which a single-point cutting tool removes material from the surface of a rotating cylindrical work piece. The cutting tool is feed linearly in a direction parallel to the axis of rotation. Turning is carried out on a lathe that provides the power to turn the work piece at a given rotational speed and to feed the cutting tool at a specified rate and depth of cut. Therefore, three cutting parameters, i.e. cutting speed, feed rate, and depth of cut, need to be determined in a turning operation [14].

Two basic models are in focus: orthogonal (two force) models, and oblique (three-force) models. Most machining processes are oblique but the orthogonal model studies are easier to simulate and they can be useful: adequate for understanding the basic mechanics of machining processes [13].

1.2 Finite Element Analysis of Turning Process

Finite element analysis is a most useful and accurate approach for the determination of field variables that is made possible by advancements in computational and processing power of computers and thus it is almost used for all the computer aided design methodologies in recent years. Applications range from deformation and stress analysis to field analysis of heat flux, fluid flow, magnetic flux, seepage and other flow problem. In this method of analysis, a complex region defining a continuum is discretized into simple geometric shapes called finite elements. The Present work is also based on the application of finite element for thermal analysis of single point cutting tool for turning operation. Once the model developed for determination of temperature field for single point cutting tool, it can also be implemented for other multipoint processes like drilling, milling or grinding also.

In this paper, a finite element code DEFORM-3D and ANSYS (13.0) was also applied to construct a coupled thermo-mechanical finite element model of plane-strain orthogonal metal cutting with continuous chip formation produced by plane-faced uncoated and differently coated carbide tools. The entire cutting process is simulated, i.e. from the initial to the steady state phase. The work piece material of choice, AISI 1040 carbon steel (mild steel), is modeled as thermo elastic-plastic, while the flow stress is considered to be a function of strain, strain-rate and temperature to represent better the real behavior in cutting. Friction between the tool and chip is of Coulomb type with the μ value of 0.5 [1].

1.2.1 Heat generation in machining

Heat generation while machining has significant influence on machining. It can increase tool wear and thereby reduce tool life [12]. It gives rise to thermal softening of cutting tool. It is commonly accepted that both the wear and failure mechanisms which develop in cutting tools are predominantly influenced by temperature and it also results in modification to the properties of work piece and tool material such as hardness. In order to predict the wear and failure characteristics of a tool, it is necessary to quantify the temperatures which develop during the cutting operation.

In machining operations, mechanical work is converted to heat through the plastic deformation involved in chip formation and through friction between the tool and work piece. Figure 1 shows three regions of heat generation in turning; which are, the shear zone, the chip-tool interface and the tool-work piece interface zone [12]:

The shear zone: The shear zone, where the main plastic deformation takes place due to shear energy. This heat raises the temperature of the chip. Part of this heat is carried away by the chip when it moves upward along the tool. Considering a continuous type chip, as the cutting speed increases for a given rate of feed, the chip thickness decreases and less shear energy is required for chip deformation so the chip is heated less from this deformation. About 80-85% of the heat generated in shear zone.

The chip-tool interface zone: The chip-tool interface zone, where secondary plastic deformation due to friction between the heated chip and tool takes place. This causes a further rise in the temperature of the chip. This chip-tool interface contributes 15-20% of heat generated.

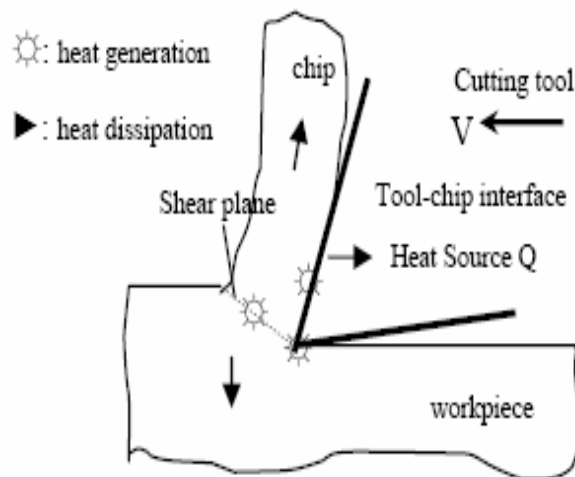


Fig 1: Zones of heat generation & dissipation during the metal cutting process.

The tool-work piece interface zone: The work-tool interface zone 3, at flanks where frictional rubbing occurs. This area contributes 1-3% of heat generated. As the portion of heat that flows into the tool cause very high temperature in vicinity of tool tip which in turn decrease the hardness of the tool material and in extreme case may even cause melting. The wear rate of tool therefore increases, resulting in a decrease in useful life of the tool. It is increasingly important to understand how Machining temperature is affected by the process variable involved which is cutting speed, feed rate, and tool geometry.

1.3. Data Measurement

1.3.1 Temperature Measurement

There are number of methods for measuring the chip tool interface temperature: Tool work thermocouple, Radiation pyrometers, embedded thermocouples, temperature sensitive paints and indirect calorimetric technique [4]. Of all these methods, the tool work thermocouple technique is the most widely used technique for the measurement of the average chip tool interface temperature. The other methods suffer from various disadvantages such as slow response, indirectness, and complications in measurement [4].

The cutting speeds used in experimentation made response times of the temperature measurement devices an important criterion. The temperature measurement devices also had to be robust and have a wide measurement range. K-type thermocouples were thus chosen as one of the temperature measurement devices. Thermocouples (contact temperature measurement device) are the most frequently used temperature transducers. A thermocouple is created when two dissimilar materials touch and the contact point produce a small open-circuit voltage as a function of temperature. Welded tip insulated K-type (chro-mel-alumel) thermocouples were used in these experiments. They have minimum continuous temperature of -200°C , a maximum continuous temperature of $+1100^{\circ}\text{C}$ [3].

The Pyrometers is technical advances have made it possible today to measure not only high temperatures but also temperatures far below freezing point from a distance and without making contact with the object to be measured.

Pyrometer Types:

- Spectral band pyrometers
- Total band pyrometers
- Ratio Pyrometers (2 color pyrometers)
- Disappearing filament optical pyrometer (portable)
- Infrared pyrometer
- Laser pyrometer

We use AME Optical Pyrometers, which work on very sophisticated mechanism. This thermal device detect temperature of an object by reckoning the emitted, reflected and transmitted energy by means of optical sensors & detectors and show temperature reading on display panel. The temperature Range is 300⁰ to 1100° C.

II. LITERATURE REVIEW

A Review of literature describes to study of the Temperature distribution of turning process with the help of finite element analysis.

Typical approaches for numerical modeling of metal cutting processes are Lagrangian and Eulerian techniques, as well as a combination of both called an arbitrary Lagrangian–Eulerian formulation [2,10]. It should be noticed that all these methods are mathematically equivalent. The major feature of Lagrangian formulation used in this study is that the mesh is attached to the work piece.

Also, the finite element analysis were performed by Johnson-Cook's constitutive equation with three different sets of material constants (found by the application of several methods) is implemented in the FE model to study the behavior of Ti6Al4V alloy during the machining process in conventional and high speed regimes [8]. Demand for higher productivity and good quality for machining parts has encourage many researchers to study the effects of machining parameters using FEM simulation using either two or three dimensions version [9].

The effect of tool thermal property on cutting forces has not been addressed systemically and analytically. To model the effect of tool thermal property on cutting forces, this study modifies Oxley's predictive machining theory by analytically modeling the thermal behaviors of the primary and the secondary heat sources. Furthermore, to generalize the modeling approach, a modified Johnson–Cook equation is applied in the modified Oxley's approach to represent the work piece material property as a function of strain, strain rate, and temperature [11].

Several experiments have been conducted to determine the amount of heat generated and cutting temperature during machining. Analytical as well as Numerical methods were applied with an objective of calculating the peak and average temperature at shear zone where first, second and tertiary deformation takes place. The method involved analysis of heat conduction for both moving and stationary heat sources. The heat conduction effect too was analyzed where the unknown boundary values of heat flux were obtained from interior heat distribution [7].

D. O'Sullivan, M. Cotterell [3], presented the results the tool chip interface temperature measurement by the tool work thermocouple technique. Tool chip interface temperature is analyzed under a wide range of cutting condition during turning of aluminum alloys grade: 6082-T6 with tungsten carbide tools. The total work done by a cutting tool in removing metal can be determined from the force component on cutting tool. Approximately, all of this work or energy is converted into heat which is dissipated into the chip, tool and workpiece material. And experiment focus on the use of the infrared camera to monitor the process.

L. B. Abhang, M. Hameedullah [4], In this study, the temperature generated on the cutting tool and experimental methods for the measurement of temperatures are reviewed. Special attention has been paid to tool- work thermocouple method and an experimental setup fabricated to measure the temperature on the cutting tool and work piece junction during metal cutting is described. With this method, the average temperature at the tool-chip interface is measured. The output of the thermocouple is in the mill volt range and measured by a digital milli-voltmeter.

S.R. Carvalho, S.M.M. Lima e Silva, A.R. Machado, G. Guimaraes [15], The thermal model is obtained by a numerical solution of the transient three-dimensional heat diffusion equation that considers both the tool and the tool holder assembly. To determine the solution equation the finite volume method is used. Changing in the thermal properties with the temperature and heat losses by convection are also considered. Several cutting tests using cemented carbide tools were performed in order to check the model and to verify the influence of the cutting parameters on the temperature field.

Asmaa A. kawi [16], Finite element method is a successful technique to perform analysis to estimate cutting temperatures, a possibility of developing temperature forms adequately representing metal cutting temperature as a Polynomial models of third, fourth and fifth degree with time that give steady state temperature and for the four alloys steel used and different operation conditions. All alloys have a sever increasing temperature with increasing feed rate, while it looks less sharp with increasing cutting speed .Also the ratio of the number of nodes have maximum temperature for any operating conditions and any alloy used with respect to the total number of nodes is less than 1%.

Mofid Mahdi, Liangchi Zhang [17], This study considered the chip breaking and developed a 2D cutting force model with the finite element method. The variation of the cutting force was investigated carefully against both the cutting condition and the anisotropy of the material with the following development: (a) a constitutive model of a homogeneous anisotropic elastic material under plane deformation; (b) a failure model of the work material based on the Tsai Hill criterion; (c) a contact model of the mechanisms of the cutting process. A comparison with experimental measurements showed that the constitutive model leads to a reasonable prediction.

Adeel H. Suhail, N. Ismail, S. V. Wong and N.A. Abdul Jalil [6], the focus of present experimental study is to optimize the cutting parameters using two performance measures, workpiece surface temperature and surface roughness. Optimal cutting parameters for each performance measure were obtained employing Taguchi techniques. The orthogonal array, signal to noise ratio and analysis of variance were employed to study the performance characteristics in turning operation.

H.S. Qi, B. Mills [18], New flow zone model is developed during turning process, based on the concept of the cutting interface, which occurs where the shear strain rate of chip deformation reaches a maximum and not where the speed of the chip is zero. The model is a dynamic model and it explains the dynamic contact behavior between chip and the tool. The model enables changes and accumulation of changes in micro-machining to be related to tool wear and workpiece surface integrity. It will be able to produce information on changes in micro cutting conditions and the effect of change and the accumulation of such change on the tool wear and the surface integrity of the workpiece machined. The new flow zone model is used to interpret the tool wear processes occurring when machining three grades of austenitic stainless steel.

Tugrul Ozel, Taylan Altan [19], It shows a methodology to determine simultaneously (a) the flow stress at high deformation rates and temperatures that are encountered in the cutting zone, and (b) the friction at the chip-tool interface. This information is necessary to simulate high-speed machining using FEA based programs. A flow stress model based on process dependent parameters such as strain, strain-rate and temperature was used together with a friction model based on shear flow stress of the workpiece at the chip-tool interface. High-speed cutting experiments and process simulations were utilized to determine the unknown parameters in flow stress and friction models.

Xiaoping Yang, C. Richard Liu [20], Friction modeling in metal cutting has been recognized as one of the most important and challenging tasks facing researchers engaged in modeling of machining operations. To address this issue from the perspective of predicting machining induced residual stresses, a new stress-based polynomial model of friction behavior in machining is proposed. The feasibility of this methodology is demonstrated by performing finite element analyses. A sensitivity study is performed by comparing the cutting force and residual stress predicted based on this new model with those based on a model using an average coefficient of friction deduced from cutting forces and a model using an average coefficient of friction deduced from stresses.

Finite element Simulations has been successfully applied for modeling plain strain orthogonal metal cutting simulations based on Lagrangian techniques and thermo, mechanically coupled modeling software with adaptive remeshing. Large number of input parameters such as large deformation, high strain rate, temperature effects, tool – chip contact and friction models [7].

Taguchi can conveniently optimize the cutting parameters with several experimental runs well designed. Taguchi parameter design can optimize the performance characteristics through the settings of design parameters and reduce the sensitivity of the system performance to source of variation. On the other hand, it used to identify the most significant variables and interaction effects [6].

A series of experiments was conducted to obtain the surface temperature of the work piece by the aid of the infrared thermometer and surface roughness by the aid of stylus type tester. Taguchi method is being applied in to select the control factors levels (Cutting speed, Feed rate and depth of cut) that minimize the effect of noise factors on the response (surface roughness) and get the relationship between the signal factor (work piece surface temperature) and the response, to come up with the optimal surface roughness value using the rate of change for the response relative to the signal factor [6].

Following are the assumptions made to define how the problem is going to be solved as well as how and where to apply the boundary conditions:-

1. The cutting speed was kept not constant.
2. The width of cut taken was larger than the feed.
3. The cutting velocity vector was perpendicular to cutting edge.
4. Constant friction at tool-chip interaction and tool-work piece interaction.
5. The initial coolant temperature is selected as the room temperature.

Several attempts have been made to develop methods for accurately predicting the effects of machining operations over the past several decades. A common approach for assessing machining performance is tool wear/tool-life. Tool-wear/tool-life is one of the most significant and necessary parameters required for process planning and total machining economics. A review of numerous theoretical and experimental techniques for predictive assessment of tool-wear and tool-life reveals that eight different types of tool-wear/tool-life relationships are commonly being used for dry machining as shown in table,

Table 1: Tool life and Tool wear rate models

Empirical Tool Life Models	Tool Wear Rate Models
<p>Taylor's basic equation: $VL^n = C_1 \quad (n, C_1 = \text{Constants})$</p>	<p>Takeyama & Murata's wear model (considering abrasive wear and diffusive wear): $\frac{dW}{dt} = G(v, f) + D \exp\left(\frac{-E}{RT}\right)$ (G,D = constants)</p>
<p>Taylor's extended equation: $L = \frac{C_2}{V^p f^q d^r} \quad (p, q, r, C_2 = \text{constants})$</p>	
<p>Taylor's extended equation: $V = \frac{C_3}{L^m f^p d^q (BHN/200)^r}$ (m,p,q,r,C₃ = constants)</p>	<p>Usui's wear model (considering adhesive wear): $\frac{dW}{dt} = A \sigma_n V_s \exp\left(\frac{-B}{T}\right)$ (A,B = Constants)</p>
<p>Temperature-based equation (known as Hasting's tool life equation): $TL^B = A$ (A,B = constants)</p>	

III. CONCLUSION

Based on the review, the following conclusions have been observed:

1. In consequence, the maximum interface temperature exists in the vicinity of the cutting edge i.e. in the first part of the tool-chip contact.
2. Increased cutting speeds (VC) resulted in decreased cutting tool forces and machined surface temperatures.
3. Tool wear resulted in increased cutting tool forces and machined surface temperature.
4. Force has been found to be an important variable in the generation of surface temperature.
5. Thus, it is possible to increase machine utilization and decrease production cost in an automated Manufacturing environment.
6. Increasing the rake angle in positive section caused the decrease of the cutting force. On the other hand, increasing the rake angle in negative section increases the cutting force.
7. The formation of built-up layers in metal cutting processes is very common with a variety of layers formed having different compositions and effectiveness in reducing cutting tool wear.

IV. FUTURE SCOPE

Turning Process is a important machining process in which a single-point cutting tool and cutting inserts removes material from the surface of a rotating cylindrical work piece, so by the finite element analysis on temperature distribution of turning process helps to determine problems were occur in tool and workpiece like plastic deformation, mechanical breakage, cutting edge blunting, brittle fracture and tool wear can reduce and by the considering optimized parameter we can find minimum surface roughness and high surface finish. Also we can increases tool life.

ACKNOWLEDGEMENTS

I express my sincere gratitude to my guide, Prof. P. D. Kamble, Asst. Professor, Mechanical Department, Yeshwantrao Chavan College of Engineering for his valuable guidance, proper advice, and careful reviews of my work at all stages, and their highly appreciated instruction and constant encouragement during the course of my work on this paper.

I am highly thankful to Dr. S. P. Untawale, Professor and H.O.D., Mechanical Department, Yeshwantrao Chavan College of Engineering for his expert advice, technical suggestions and moral support during in this work.

REFERENCES

- [1] W. Grzesik, M. Bartoszek and P. Niesłony. Finite element modeling of temperature distribution in the cutting zone in turning processes with differently coated tools., 13th international scientific conference. 2005.pp 1-4
- [2] M. H. El-Axir . A methode of modeling residual stress distribution in turning for different material., International journal of Machine tool & Manufacture 42 (2002) 1055-1063
- [3] D. O'Sullivan, M. Cotterell. Temperature measurement in single point turning., D. O'Sullivan, M. Cotterell . Journal of Materials Processing Technology 118 (2001)
- [4] L. B. Abhang, M. Hameedullah . The Measurement of chip-tool interface Temperature in the Turning of steel., International Journal of Computer Communication and Information System, 2010
- [5] S. R. Carvalho, S. M. M. Lima e Silva, A. R. Machado, G. Guimaraes. Temperature determination at the chip-tool interface using an inverse thermal model considering the tooland tool holder., Journal of Material Processing Technology 179 (2006)

- [6] Adeel H. Suhail, N. Ismail, S. V. Wong and N.A. Abdul Jalil. Optimization of cutting Parameter Based on Surface Roughness and Assistance of Workpiece Surface Temperature in Turning Process., *America J. of Engineering and Applied Science* 105, 2010
- [7] Ram Chandra Kisku. Modelling of Temperature profile in turning with uncoated and coated cemented carbide insert., *National Institute of Technology*, 2011 pp 1-37
- [8] Domenico Umbrello. Finite element simulation of conventional and high speed machining of Ti6Al4V alloy., *journal of materials processing technology* 196 (2008) 79-87
- [9] Hendri Yandra¹, Jaharah A. Ghani² & Che Hassan Haron. Effect of Rake angle on Stress, Strain and Temperature on the Edge of carbide cutting tool in Orthogonal Cutting using FEM Simulation., *ITB J. Eng. Sci.*, vol. 42, No.2, 2010
- [10] O. Pantal_e, J.-L. Bacaria, O. Dalverny, R. Rakotomalala, S. Caperaa. 2D and 3D numerical models of metal cutting with damage effects., *Comput. Methods Appl. Mech. Engrg.* 193 (2004)
- [11] Albert J. Shih. Finite Element Analysis of Rake angle Effect in Orthogonal Metal Cutting., Elsevier Science (1996) Vol. 38, pp, 1-17
- [12] Jaroslav Mackerle. Finite-element analysis and simulation of machining: a bibliography., *Journal of Materials Processing Technology* 86 (1999) 17-44
- [13] W. H. Yang, Y. S. Tarn. Design optimization of cutting parameters for turning operations based on Taguchi Method. *Journal of Processing Technology* 84 (1998) 122-129
- [14] Dr. S.S. Chaudhari, S.S. Khedkar, N.B. Borkar. Optimization of process parameters using Taguchi approach with minimum quantity lubrication for turning. *International Journal of Engineering Research and Applications (IJERA)*. Vol. 1, Issue 4, pp. 1268-1273
- [15] S. R. Carvalho, S. M. M. Lima e Silva, A. R. Machado, G. Guimaraes. Temperature determination at the chip-tool interface using an inverse thermal model considering the tool and tool holder., *Journal of Material Processing Technology* 179 (2006)
- [16] Asmaa A. Kawi. Temperature behaviour of some alloy steels in Turning Process under different operating conditions., *Al-Qadisiya Journal for Engineering Sciences*, 2011 Vol. 4 No. 3
- [17] Mohid Mahdi, Liangchi Zhang. A Finite element model for the orthogonal cutting of fiber-reinforced composite materials., *Journal of Material Processing Technology* 113 (2001) 373-377
- [18] H.S. Qi, B. Mills. Formation of a transfer layer at the tool-chip interface during machining., *Wear* 245 (2000) 136-147
- [19] Tugrul Ozel, Taylan Altan. Determination of workpiece flow stress and friction at the chip-tool contact for high-speed cutting., *International Journal of Machine Tools & Manufacture* 40 (2000) 133-152
- [20] Xiaoping Yang, C. Richard Liu. A new stress-based model of friction behavior in machining and its significant impact on residual stresses computed by finite element method., *International Journal of Mechanical Sciences* 44 (2002) 703-723

A DATA MINING ANALYSIS & APPROACH WITH INTRUSION DETECTION / PREVENTION FROM REAL

Meenakshi.RM,¹ Mr.E.Saravanan²

¹Final Year Student, M.Tech CSE Department, Dr.M.G.R.Educational and Research Institute University, Tamil Nadu, India

²Assistant Professor, Dr.M.G.R.Educational and Research Institute University, Tamil Nadu, India

Abstract: We propose a mechanism for false positive/negative assessment with multiple IDSs/IPs to collect FP and FN cases from real-world traffic and statistically analyze these cases. False positives and false negatives happen to every intrusion detection and intrusion prevention system. IDSs/IPs can identify a normal activity as malicious one, causing a false positive (FP) or malicious traffic as normal, causing a false negative (FN). To create a pool of traffic traces causing possible FPs and FNs to IDSs using Attack Session Extraction (ASE). Statistically analyze the packet by preprocessing based on protocol for each layer. Based on that Binary classifiers are generated for each class of event using relevant features for the class using classification algorithm. Binary classifiers are derived from the training sample by considering all classes other than the current class. Analyzing the KDD data set for pattern matching and the effect of combining different classifiers can be explained with the theory of bias-variance decomposition using multi boosting.

Index Terms: False Positive, False Negative, Intrusion Detection/Prevention, Packet Trace, Network Measurement, Peer to Peer Traffic Analysis.

I. Introduction

Intrusion detection and prevention systems (IDPS) are primarily focused on identifying possible incidents, logging information about them, and reporting attempts. In addition, organizations use IDPS for other purposes, such as identifying problems with security policies, documenting existing threats, and deterring individuals from violating security policies. Data mining based intrusion detection algorithms aim to solve the problems of analyzing the huge volumes of audit data and realizing performance optimization of detection rules. An IDS/IPs monitors the activities of a given environment and decides whether these activities are malicious or normal based on system integrity, confidentiality and the availability of information resources. As soon as a malicious or an intrusive event is detected, the IDS produces a relative alert and passes it to the network administrator promptly while the IPS not only executes what the IDS does but also blocks network traffic from the suspected malicious source. FPs and FNs cause several problems. For example, FNs generate unauthorized or abnormal activities on the Internet or in computer systems. On the other hand, a lot of FPs may easily conceal real attacks and thus overwhelm the security operator. When real attacks occur true positives (real alerts) are deeply buried within FPs, so it is easy for the security operator to miss them.

The existing work monitor and analyze system calls, application logs, file-system modifications using communication protocol between a connected device. Drawback is the hackers recover the embedding data in original image because the data placed in particular bit position.

II. Overview of the Approach

The aim of the proposed system is to monitor and analyze real network traffic in a computer network like a network sniffer and collects network logs. Then the collected network logs are analyzed for rule violations by using data mining algorithms. When any rule violation is detected, the overall approach of the proposed system is clearly portrait in the flow chart diagram "Fig 1". The steps involved in this system are

1. Receive the network packet and extract the attributes by protocols HTTP,FTP,SMTP etc;
2. Transmit raw packet to the network and gather statistical information on the real network.
3. Binary classifiers are generated for each class of event using relevant features for the class and classification Algorithm.
4. Binary classifiers are derived from the training sample by considering all classes other than the current class.
5. The main purpose is to select different features for different classes by applying the information gain or gain ratio in order to identify relevant features for each binary classifier.
6. The effect of combining different classifiers can be explained with the theory of bias-variance decomposition.

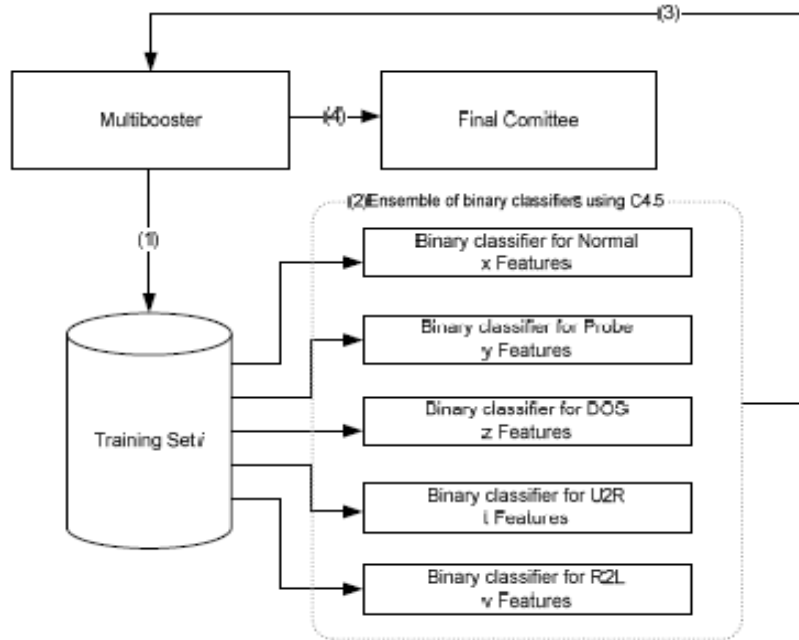


Fig 1 flow chart of proposed system

III. False Positive /Negative Assessment

FP and FN rates are two important metrics in measuring the accuracy of a network security system, such as an IDS or IPS. It has been demonstrated that even a small rate (1 in 10,000) of FPs could generate an unacceptable number of FPs in practical detections. The assessment is important to IDS/IPS developers trying to optimize the accuracy of detection by reducing both FPs and FNs, because the FP/FN rate limits the performance of network security systems due to the base-rate fallacy phenomenon. The statistical analyses in this work can elucidate the causes and rankings of FPs and FNs, thus allowing developers to avoid similar pitfalls during their product development.

Second, after detecting the potential FPs/FNs/TPs/TNs, this work replays the extracted packet trace according to the log of the DUTs (Device Under test) again. This step is called trace verification because it verifies whether this case is reproducible to the original DUTs. This case is a reproducible FP/FN/TP/TN when it meets the following two conditions.

- I. For any DUT, it must produce an alert if it did last time.
- II. The two alerts must be the same when one came from some DUT last time and the other is produced by the same DUT this time.

IV. C 4.5 Classification Algorithm

In general, steps in C4.5 algorithm to build Binary tree are:

1. Choose attribute for root node
2. Create branch for each value of that attribute
3. Split cases according to branches
4. Repeat process for each branch until all cases in the branch have the same class

Choosing which attribute to be a root is based on highest gain of each attribute. To count the gain, we use formula 1, below:

$$Gain(S, A) = Entropy(S) - \sum_{i=1}^n \frac{|S_i|}{|S|} * Entropy(S_i) \quad (1)$$

With:

- {S1, ..., Si, ..., Sn} = partition
- s of S according to values of attribute A
- n = number of attributes A
- |Si| = number of cases in the partition Si
- |S| = total number of cases in S

$$Entropy(S) = \sum_{i=1}^n - p_i * \log_2 p_i \dots\dots\dots(2)$$

With:

S: Case Set

N: number of cases in the partition S

Pi: Proportion of Si to S

V. Experimental Setup

Our proposed model is implemented by LAN and tested. An example the entire incoming packet processed in LAN. With necessary details about the packets in the fig(1) respectively.

No.	Captured	Source IP	Destinati...	Captured	Hardware	Code	Method	Header	Redirect	Source M.	Frame Ty.	Destinati...	SYN Flag	ACK Flag	Transmis...
0	Mon Mar ...	Not Avail...	Not Avail...	153	Not Avail...	00:90:1a...	-30620	00:16:ec...	Not Avail...	Not Avail...	Not Avail...				
1	Mon Mar ...	Not Avail...	Not Avail...	327	Not Avail...	00:16:ec...	-30620	00:90:1a...	Not Avail...	Not Avail...	Not Avail...				
2	Mon Mar ...	Not Avail...	Not Avail...	153	Not Avail...	00:90:1a...	-30620	00:16:ec...	Not Avail...	Not Avail...	Not Avail...				
3	Mon Mar ...	Not Avail...	Not Avail...	327	Not Avail...	00:16:ec...	-30620	00:90:1a...	Not Avail...	Not Avail...	Not Avail...				
4	Mon Mar ...	Not Avail...	Not Avail...	151	Not Avail...	00:90:1a...	-30620	00:16:ec...	Not Avail...	Not Avail...	Not Avail...				
5	Mon Mar ...	Not Avail...	Not Avail...	361	Not Avail...	00:16:ec...	-30620	00:90:1a...	Not Avail...	Not Avail...	Not Avail...				
6	Mon Mar ...	Not Avail...	Not Avail...	153	Not Avail...	00:90:1a...	-30620	00:16:ec...	Not Avail...	Not Avail...	Not Avail...				
7	Mon Mar ...	Not Avail...	Not Avail...	327	Not Avail...	00:16:ec...	-30620	00:90:1a...	Not Avail...	Not Avail...	Not Avail...				
8	Mon Mar ...	Not Avail...	Not Avail...	153	Not Avail...	00:90:1a...	-30620	00:16:ec...	Not Avail...	Not Avail...	Not Avail...				
9	Mon Mar ...	Not Avail...	Not Avail...	327	Not Avail...	00:16:ec...	-30620	00:90:1a...	Not Avail...	Not Avail...	Not Avail...				
10	Mon Mar ...	Not Avail...	Not Avail...	204	Not Avail...	00:90:1a...	-30620	00:16:ec...	Not Avail...	Not Avail...	Not Avail...				
11	Mon Mar ...	Not Avail...	Not Avail...	108	Not Avail...	00:16:ec...	-30620	00:90:1a...	Not Avail...	Not Avail...	Not Avail...				
12	Mon Mar ...	Not Avail...	Not Avail...	74	Not Avail...	00:90:1a...	-30620	00:16:ec...	Not Avail...	Not Avail...	Not Avail...				
13	Mon Mar ...	Not Avail...	Not Avail...	148	Not Avail...	00:90:1a...	-30620	00:16:ec...	Not Avail...	Not Avail...	Not Avail...				
14	Mon Mar ...	Not Avail...	Not Avail...	331	Not Avail...	00:16:ec...	-30620	00:90:1a...	Not Avail...	Not Avail...	Not Avail...				
15	Mon Mar ...	Not Avail...	Not Avail...	89	Not Avail...	00:90:1a...	-30620	00:16:ec...	Not Avail...	Not Avail...	Not Avail...				
16	Mon Mar ...	Not Avail...	Not Avail...	62	Not Avail...	00:16:ec...	-30620	00:90:1a...	Not Avail...	Not Avail...	Not Avail...				
17	Mon Mar ...	Not Avail...	Not Avail...	204	Not Avail...	00:90:1a...	-30620	00:16:ec...	Not Avail...	Not Avail...	Not Avail...				
18	Mon Mar ...	Not Avail...	Not Avail...	108	Not Avail...	00:16:ec...	-30620	00:90:1a...	Not Avail...	Not Avail...	Not Avail...				
19	Mon Mar ...	Not Avail...	Not Avail...	74	Not Avail...	00:90:1a...	-30620	00:16:ec...	Not Avail...	Not Avail...	Not Avail...				
20	Mon Mar ...	Not Avail...	Not Avail...	148	Not Avail...	00:90:1a...	-30620	00:16:ec...	Not Avail...	Not Avail...	Not Avail...				
21	Mon Mar ...	Not Avail...	Not Avail...	331	Not Avail...	00:16:ec...	-30620	00:90:1a...	Not Avail...	Not Avail...	Not Avail...				
22	Mon Mar ...	Not Avail...	Not Avail...	153	Not Avail...	00:90:1a...	-30620	00:16:ec...	Not Avail...	Not Avail...	Not Avail...				
23	Mon Mar ...	Not Avail...	Not Avail...	327	Not Avail...	00:16:ec...	-30620	00:90:1a...	Not Avail...	Not Avail...	Not Avail...				
24	Mon Mar ...	Not Avail...	Not Avail...	153	Not Avail...	00:90:1a...	-30620	00:16:ec...	Not Avail...	Not Avail...	Not Avail...				
25	Mon Mar ...	Not Avail...	Not Avail...	327	Not Avail...	00:16:ec...	-30620	00:90:1a...	Not Avail...	Not Avail...	Not Avail...				
26	Mon Mar ...	Not Avail...	Not Avail...	151	Not Avail...	00:90:1a...	-30620	00:16:ec...	Not Avail...	Not Avail...	Not Avail...				
27	Mon Mar ...	Not Avail...	Not Avail...	361	Not Avail...	00:16:ec...	-30620	00:90:1a...	Not Avail...	Not Avail...	Not Avail...				
28	Mon Mar ...	Not Avail...	Not Avail...	153	Not Avail...	00:90:1a...	-30620	00:16:ec...	Not Avail...	Not Avail...	Not Avail...				
29	Mon Mar ...	Not Avail...	Not Avail...	327	Not Avail...	00:16:ec...	-30620	00:90:1a...	Not Avail...	Not Avail...	Not Avail...				

Fig 1: Processing of incoming packet in the LAN

During preprocessing cumulative pie graph for network layer protocol ratio measurements is shown in the fig(2) respectively. Each and every variation in the packet will reflect in the graph automatically.

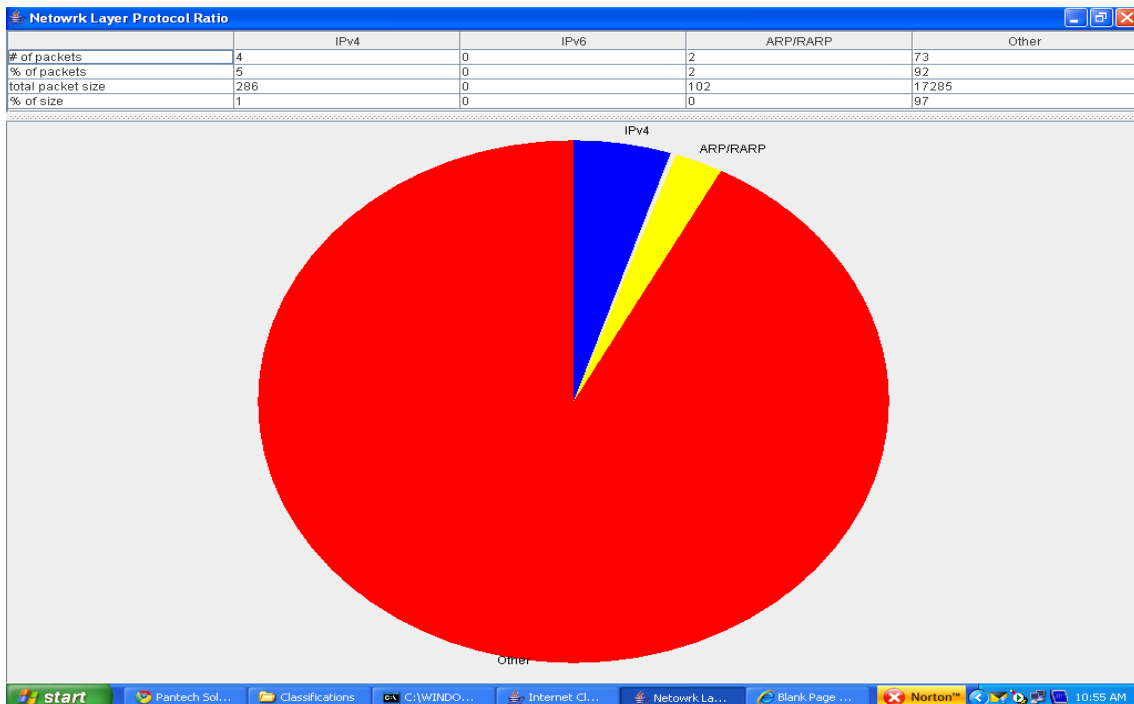


Fig 2: Network layer protocol ratio during preprocessing

During preprocessing continuous graph for network layer protocol ratio is shown in the fig (3) respectively

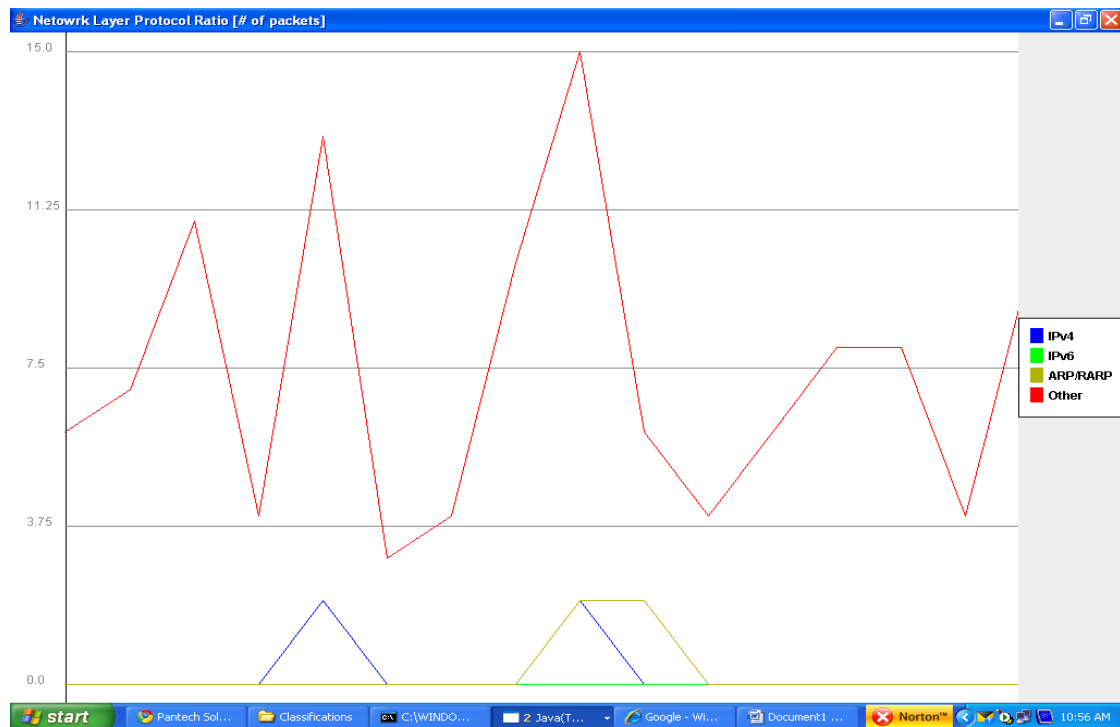


Fig 3: Continuous graph network layer protocol ratio

VI. Conclusion

In this paper, we first propose a false positive/false negative assessment with C 4.5 classification algorithm based on binary tree. Packet has been preprocessed in the LAN. C4.5 binary classification done by pattern matching with KDD dataset. Multi boosting technique is used to check the features of the data. The advantages of our proposed system is

1. Implementation of C 4.5 classification algorithm is more efficient when compared to decision tree.
2. If some problem or attack occurs we can easily find out the location where the attack occurs exactly.
3. If frequent message or DOS attack occur we can logoff the remote machine.
4. Alert message in case of problem.
5. Multi boosting is data mining technique for checking the algorithm
6. For each operating system different applications have to be used, regardless they are doing exactly the same.

Finally, although our model focuses on FP/FN assessment based on preprocessing, binary classifiers, Analysing the data set and multi boosting. The model is designed for dataset for all the features of data attribute relative file format. Our result based on client operating system. Server operating system will be studied in our future enhancements.

References

- [1] H. G. Kayacik and A. N. Zincir-Heywood, "Using Intrusion Detection Systems with a Firewall: Evaluation on DARPA 99 Dataset", Project in Dalhousie University, [Online]. Available: <http://projects.cs.dal.ca/projectx/files/NIMS06-2003.pdf>.
- [2] DARPA 99 Intrusion Detection Data Set Attack Documentation. [Online]. Available: <http://www.ll.mit.edu/IST/ideval/docs/1999/attackDB.html>.
- [3] V. Corey, C. Peterman, S. Shearin, M. S. Greenberg, J. V. Bokkelen, "Network Forensics Analysis," IEEE Internet Computing, vol.6, no.6, pp. 60-66, 2002.
- [4] W. D. Yu, D. Aravind, P. Supthaweesuk, "Software Vulnerability Analysis for Web Services Software Systems," iscc, pp. 740-748, 11th IEEE Symposium on Computers and Communications (ISCC'06), 2006.
- [5] M. Bailey, E. Cooke, F. Jahanian, D. Watson, Jose Nazario, "The Blaster Worm: Then and Now," IEEE Security and Privacy, vol. 03, no. 4, pp. 26-31, 2005.
- [6] C. L. Schuba, I. V. Krsul, M. G. Kuhn, E. H. Spafford, A. Sundaram, D. Zamboni, "Analysis of a Denial of Service Attack on TCP," sp, p. 0208, 1997 IEEE Symposium on Security and Privacy, 1997.
- [7] V. Paxson, "An analysis of using reflectors for distributed denial-of-service attacks" ACM SIGCOMM Computer Communication Review, 2001.
- [8] M. Roesch, "Network Security: Snort - Lightweight Intrusion Detection for Networks", Proceedings of the 13th USENIX conference on System administration, November. 1999.

Comparative Analysis of Transformer and Transformer Less-Based Variable DC Power Supply

B.O.Omijeh,¹ N.Onyekachukwu,² P.O. Nwachukwu³

^{1, 2, 3}Electrical and Electronics Engineering Department, university of Port Harcourt, River State

Abstract: Electronics circuitry needs DC power source of a specific value to work effectively. This paper considers the design and evaluation of transformer-based and transformer less-based variable regulated DC power supply with the aim of presenting a comparative analysis between them; and their respective areas of applications. The quality, cost, size, weight, performance and efficient production of DC power supply thus pose a great deal of concern and attention in the DC power production of any electronic device. The design methodology used in this work involves Software design for component selection, improved hardware design, computer simulation and evaluation of transformation, rectification, filtration and regulation stages for both transformer-based and transformer less -based adjustable DC power supply with graphical outputs. The results obtained after following the design specification was very satisfactory. The transformer-based has a robust output current and well isolated from the supply voltage, which makes it more suitable for high current application, highly reliable for powering electronics devices while the transformer less based DC source has smaller size, weight and cheaper so as to miniaturize electronics devices but limited to low current devices . It also generates far less noise, heat, input harmonic distortion levels, and higher transient response but lack of proper isolation unlike its counterpart thus result in lower Mean Time To Failure (MTTF).Transformer less variable DC power supply should be considered a viable option for lower power, small and low current applications where achieving the highest availability is not the top concern and cost, size and weight restrictions inhibit the use of traditional transformer-based DC power supply.

Keywords: transformer, transformer-less, voltage regulator, simulation, variable DC power supply.

I. Introduction

In electrical and telecommunication engineering field, systems and equipments like amplifiers, satellites, microwave link systems to name but a few depend upon the availability of a stable and quality well regulated Direct Current (DC) power supplies for their correct operations. No electronics laboratory or technology is complete without a well regulated (or variable) DC power supply. It is the first essential element required in any electronics device. The construction, design and evaluation of this piece of electronic equipment- will find use both now and in future. The main and basic requirements of a well regulated DC power supply unit are Isolation between source and load, Low ripple, Low output impedance, Power factor, High transient response, Low levels of input harmonic distortion , Reduced power losses ,Good regulations, Strict output short-circuits protection, Workable size and weight.

II. Related Works

In the work published by Mike Papadimitriou (----), LM317 was used for varying DC power supply. It is an adjustable 3-terminal positive voltage regulator capable of supplying in excess of 1.5A over an output voltage range of 1.2 V to 37 V. This voltage regulator is exceptionally easy to use and requires only two external resistors and capacitor to set the output voltage.

In a similar work by National Microchip co-operation (-----) on Transformer-less Power Supplies, resistor was used as the transformation device and a reliable circuit diagram was given that works fine in computer simulation but the circuit offered no protection against over-current and over voltage issue.

Williams, O.A. (1995) on Design and Construction of a Regulated Power Supply Unit used LM 78 XX device like the later. The voltage regulator is exceptionally easy to use and employs internal current limiting but capable of supplying in excess of 1.0A over an output voltage range of 1.2 V to 21 V and lacks internal thermal shutdown capability.

Ron J (2002) in his work, dealt with transformer-less power supply using X-rated capacitor for low current applications of 100mA current ratings and a voltage of 12V. It was effective but the main disadvantage was that, it offered no isolation from the supply voltage and presents more of a safety issue.

In the work published by Kiran Shrestha (Nov 2004) on Transformer less 12V Dual Power Supply. In this work two voltage output was achieved +12V and -12V using zener diode. This was proved and tested but still lacks protection against over-current and over voltage.

In a similar work, Garage (2006) designed a variable DC power supply using LM 78XX. All the stages were effectively considered except the protection stage.

In work published by Mohamkumar (2006) on Transformer less power supply, x-rated capacitor was used as transformation device instead of the transformer; and proved the effectiveness and efficiency of the x-rated capacitor and gave a well detailed circuit diagram of a fixed DC power supply using zener diode

In the work published by Shamsul and Bin (Nov 2010) on Development of DC Power supply using power electronics applications, a fixed DC power supply was developed, simulated and proved to have worked effectively but the

input supply voltage lacks protection circuit, the output of the transformer lacked noise suppression capacitor and the LM 317 T was not protected.

Emerson Network Power (2012) contained vital information on comparing transformer based and transformer less uninterruptible power supplies. In this work emphasis were made on the uniqueness, differences and similarities between transformer and transformer-less based devices.

III. Design Methodology

The design methodology of both the transformer and transformer less based system involves five stages as shown in Fig.1 and Fig.2.

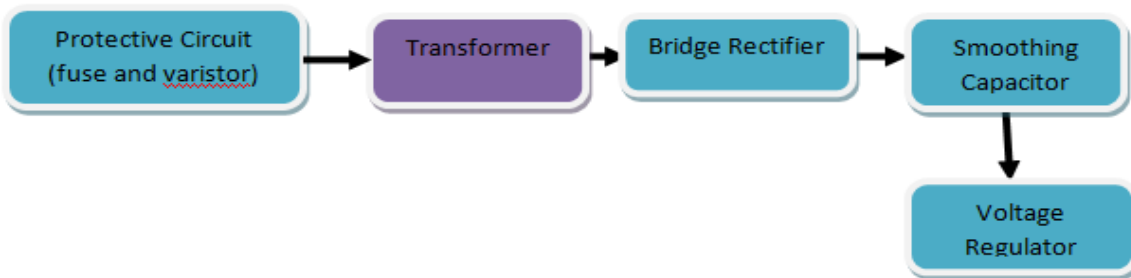


Fig.1: flow diagram of transformer-based DC power supply

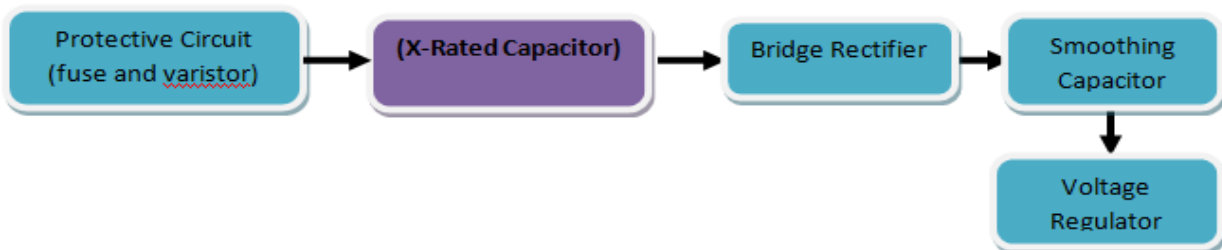


Fig.2: flow diagram of transformer less DC power supply

A. The protection stage provides reliable and economical protection against high voltage transients, surges and over-current which may be produced. It comprises of fuse and varistor.

In this work, the maximum current is 4A for the transformer-based and 1A for the transformer less type thus stating the rating of the fuse to be used in each of them. Since the main supply voltage is approximately $230V_{ac}$, the voltage rating of the varistor used $250V_{ac}$; the protection circuit is as shown below:

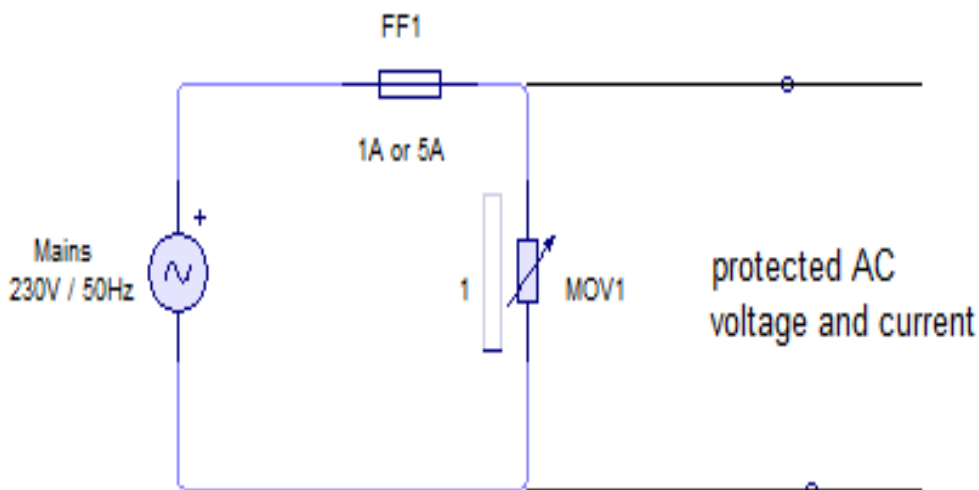


Fig.3: Protection circuit from the mains

3.1 Transformation stage is used to transform the incoming line voltage of $230V_{ac}$ down to a required voltage value for the power supply unit. For the two types of power supply that is the transformer less and the transformer based power supply, **x-rated capacitor** and **step-down transformer** are used respectively.

- **Step-down transformer:** The simulation waveform circuit analysis shown below involves both the protection and the transformation stage using transformer as the transformation device.

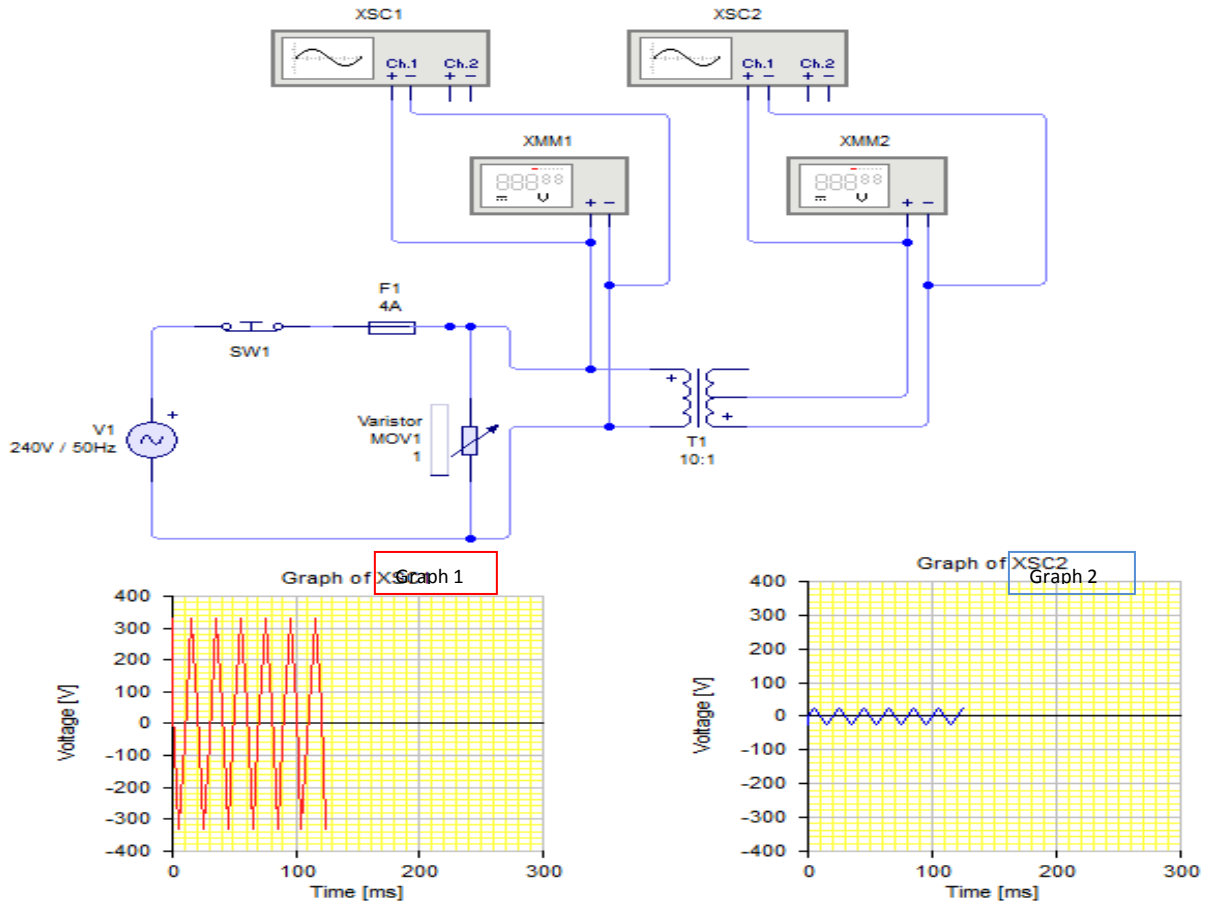


Fig. 4: waveform analysis of both protection and transformation stage for transformer based DC power supply
 Using this formula

$$\text{turns ratio} = \frac{V_p}{V_s} = \frac{N_p}{N_s}$$

Where: V_p =primary (input) voltage, N_p =number of turns on the primary coil, V_s =secondary (output) voltage
 N_s = number of turns on the secondary coil.

To produce a desired output voltage of 24 Vdc, a turn ratio of 10:1 transformer was chosen, thus.

$$\frac{240_p}{V_s} = \frac{10_p}{1_s}$$

$$V_s = 24 \text{ volts}$$

- **X-rated AC capacitor:** The simulation waveform circuit analysis shown below involves both the protection and the transformation stage using transformer as the transformation device.

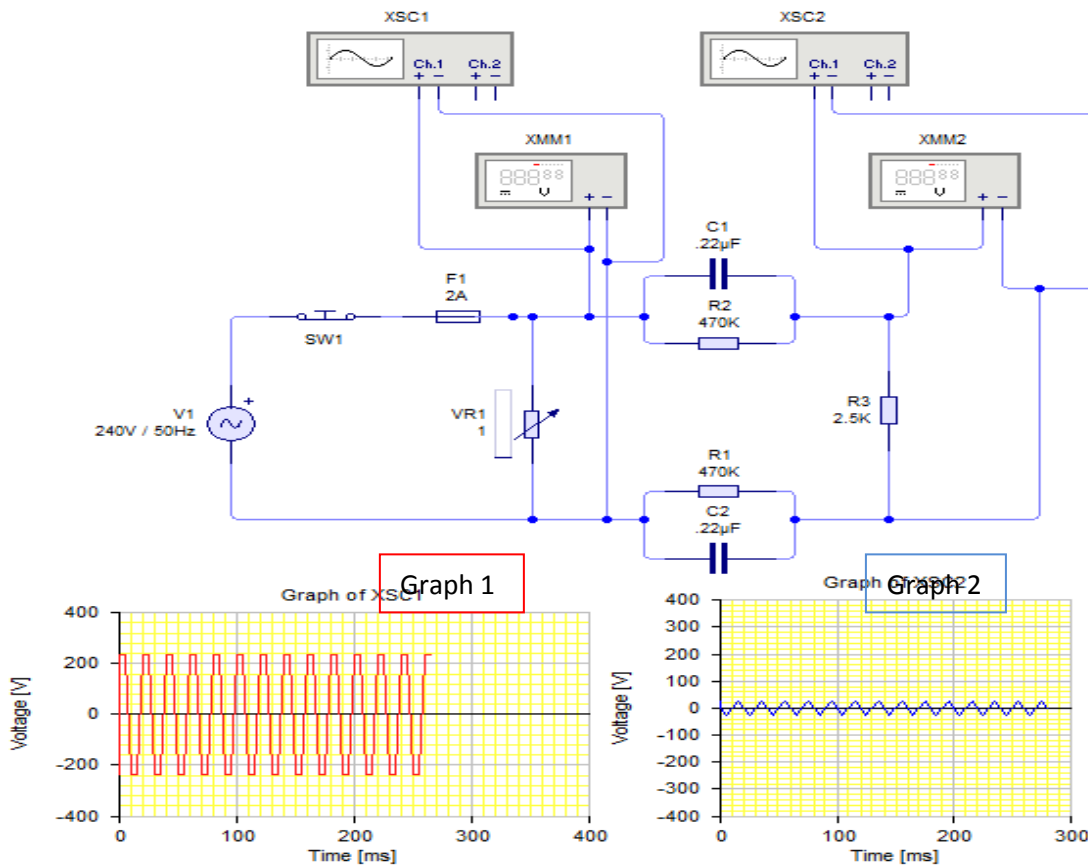


Figure 5: waveform analysis of both protection and transformation stage for transformer less based DC power supply
 The reactance (X_c) of the capacitor (C) in the mains frequency (f) can be calculated using the formula:

$$X_c = \frac{1}{2\pi fC}$$

From the formula above, if an X-rated capacitor of $2.2\mu f$ is used as shown in figure 15, the reactance (X_c) will be as shown:

$$X_c = \frac{1}{2\pi * 50HZ * 2.2e - 6F}$$

$$X_c = \frac{1}{6.9115e - 4} \Omega$$

$$X_c = 1.44686k \Omega$$

The current that would be produced from a $2.2\mu f / 400V$ X-rated capacitor with an ac source of $230 V_{ac}$ can be gotten using the ohmic equation:

$$V = IR \text{ or } V = IX_c$$

$$I = 165.88 \text{ mA}$$

This value $I = 165.88 \text{ mA}$ is the ideal current value, but the actual current from a $2.2\mu f - 225k / 400V$ X-rated capacitor with an ac source of $230 V_{ac}$ is 100 mA cited from Table 2 . Practically a single $2.2\mu f$ X-rated capacitor could give a current (I) of 100 mA , therefore, three of the $2.2\mu f$ X-rated capacitor connected in parallel with each other would give a current of 300 mA (i.e. three times 100 mA), this current rating is well over sufficient for all low current devices.

3.2 Rectification stage is the stage after transformation stage that aids in the conversion of AC to DC signal. In this work a full wave rectification is used, because of its fundamental advantages over the half wave rectifier counterpart. Bridge rectifier is used rather its counterpart because it does not require a special centre tapped transformer, thereby reducing its size and cost. The bridge rectifier consists of 4 IN4001 silicon diodes.

Livewire simulation of both the transformation and rectification stage for the transformer based and transformer less based Dc power supply are as shown below.

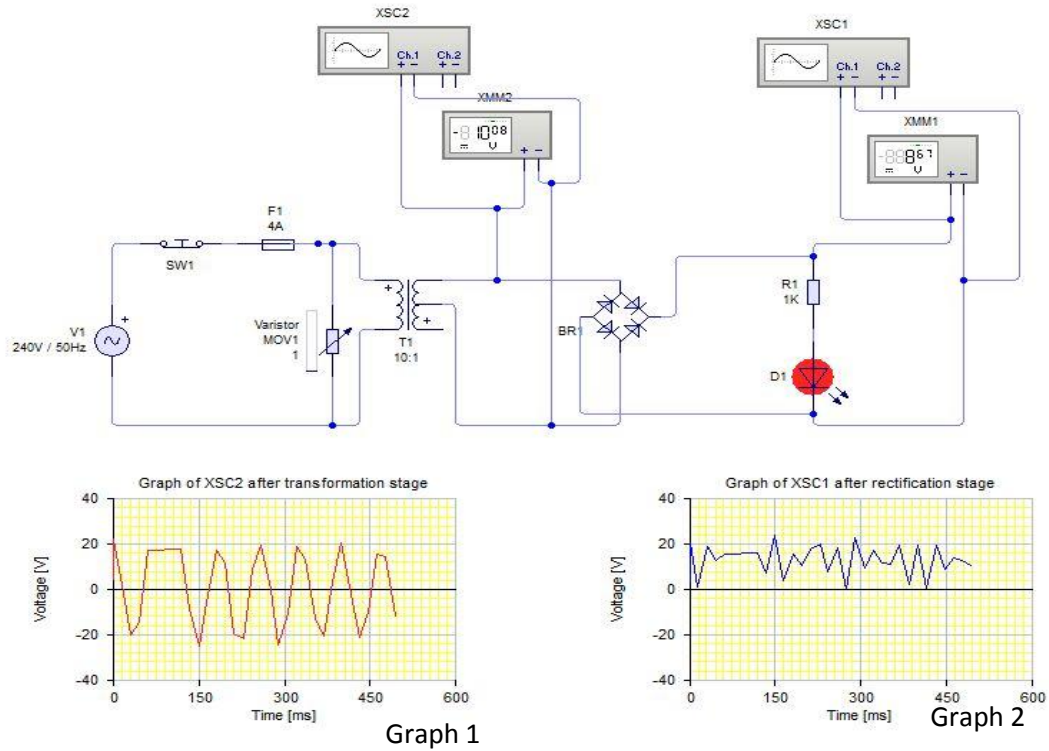


Fig. 6: waveform analysis of transformation and rectification stage for the transformer based circuit

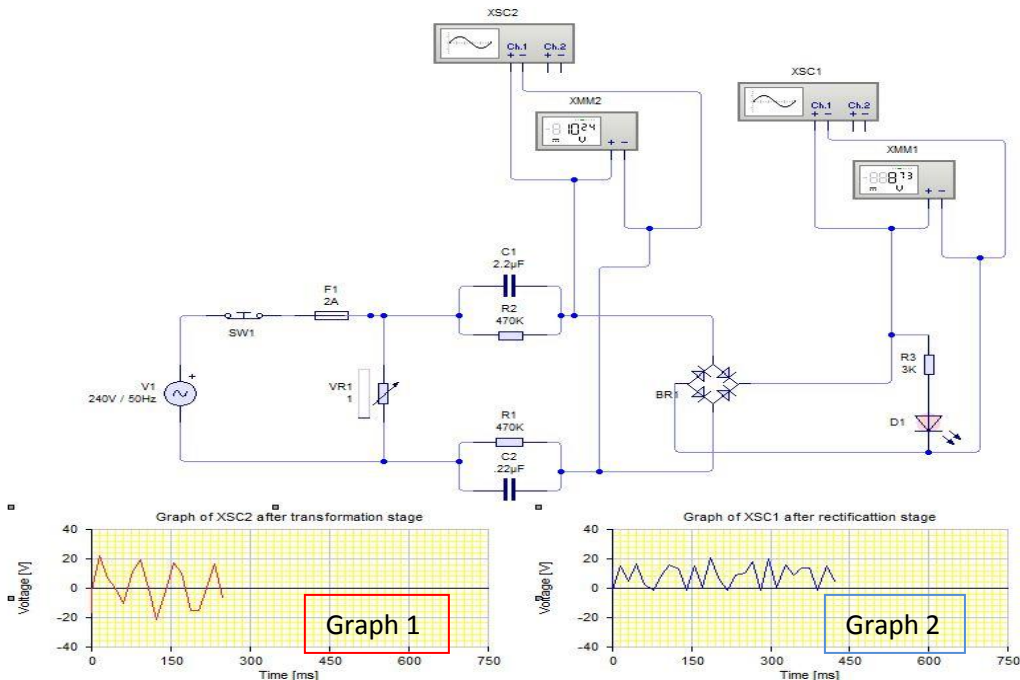


Figure 7: waveform analysis of transformation and rectification stage for the transformer less based circuit
From the figures 6 and 7 above the following mathematical expressions can be deduced.

V_s =Output AC signal from transformation stage

$V_{s,rms} = V_s \sqrt{2}$ =Peak to Peak AC signal from transformation stage

When passed through a bridge rectifier, the DC output signal is given by:

$$V_p = V_s - 2V_d = \text{DC output signal}$$

$$V_{p,rms} = V_p \sqrt{2} = \text{DC output signal (peak to peak)}$$

Note that in a full wave bridge rectifier only 2 of the 4 diodes works simultaneously at any given time. Each of the diodes has a voltage drop ranging from 0.4 to 0.7 V.

Reduction after rectification stage in the DC output voltage is as a result of the voltages drop across the two diodes ($2V_d$) of the bridge rectifier.

The output DC voltage of the rectification stage has so many ripples in it that it cannot be used to power any useful device. It require a filter to improve on the output signal.

3.3 Filtration stage: Smoothing Capacitor is used to generate ripple free DC. Its function is to convert half wave / full wave output signal of the rectifier into smooth DC signal. Livewire simulation of both the rectification and filtration stage for the transformer based and transformer less based Dc power supply are as shown below.

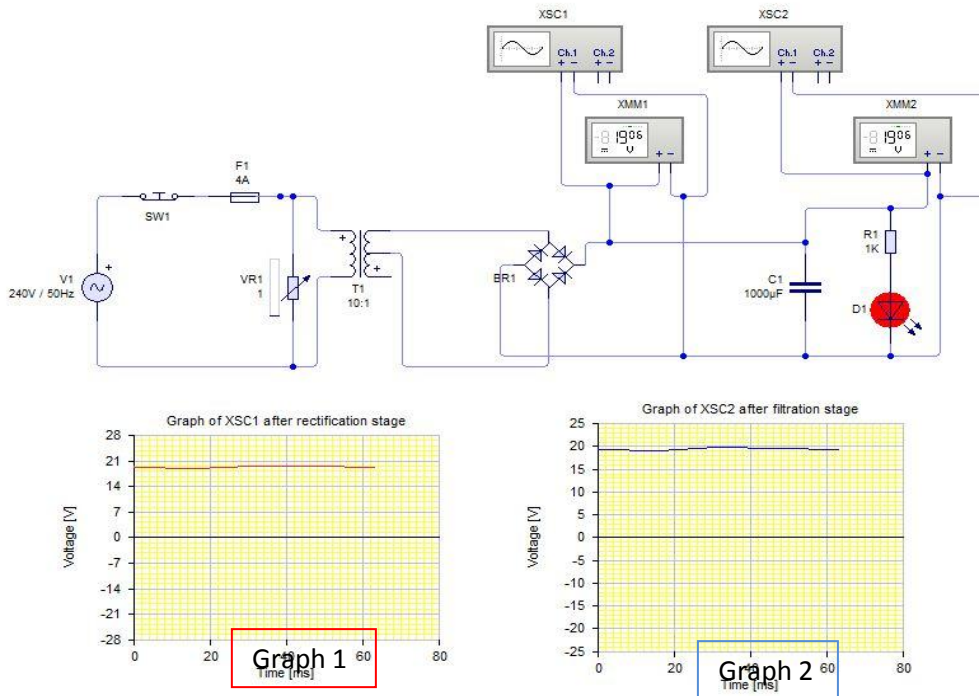


Figure 8: waveform circuit analysis of rectification and filtration stage for the transformer based circuit

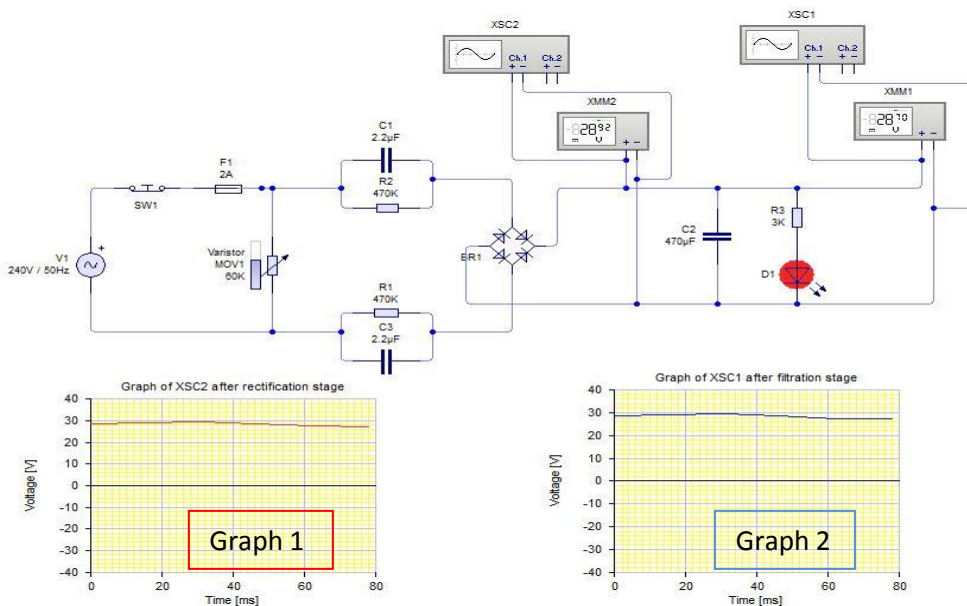


Figure 9: waveform circuit analysis of rectification and filtration stage for the transformer based circuit

The power rating and the capacitance of the capacitor are two most important aspects to be considered while selecting the smoothing capacitor. The power rating must be greater than the off load output voltage of the power supply. The capacitance value determines the amount of ripples that appear in the DC output when the load takes current (The larger the capacitor -for a given load, the smaller the ripple voltage).

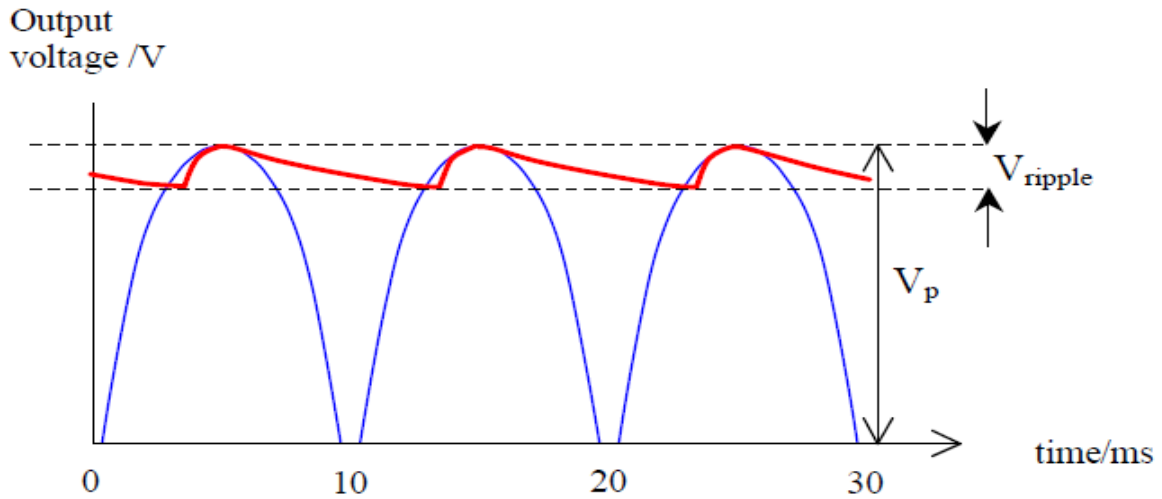


Figure 10: Output waveform of bridge rectifier with RC filter

As the output voltage from the bridge drops the capacitor discharges through the load and so a ripple voltage, V_r , appears on the output from the supply. The size of this voltage depends on the load resistance, R_L , the size of the smoothing capacitor, C , and the peak value of the output voltage, V_p , and is given by:

$$V_r = \left(\frac{V_p}{R_L C} \right) \Delta t$$

$$V_{DC,max} = 1.4 * V_p$$

$$V_{DC,min} = V_{DC,max} - V_p$$

$$V_{DC,average} = \frac{V_{DC,max} - V_{DC,min}}{2}$$

Where:

V_r = ripple voltage

V_p = Peak voltage

R_L = load impedance

V_{DC} = DC voltage

Δt = time between successive peaks of the output waveform from the rectifier circuit.

This will be 10ms if the ac frequency is 50Hz and a full wave bridge rectifier circuit is used. (But 20ms if a half wave rectifier circuit is used; the question could specify a different supply frequency, e.g. 60Hz, which would also affect Δt . This formula is an approximation and assumes that the ripple voltage is small. If the ripple voltage exceeds ~10% this formula becomes increasingly inaccurate.

3.4 Regulation stage: voltage regulation stage steps down and keeps voltage on a certain value and also suppresses unregulated voltage ripples that might have occurred or exist even after the filtration stage thereby producing a perfectly parallel output voltage, which can be used to power any device within the design ratings. The project evaluated two voltage regulators namely; LM317 and zener diode in the production of variable DC power supply.

- **LM317** is an adjustable 3-terminal positive voltage regulator capable of supplying in excess of 1.5A over an output voltage range of 1.2 V to 37 V. This voltage regulator is exceptionally easy to use and requires only two external resistors and capacitor to set the output voltage. (cited in National (2012), LM317 Regulator Datasheet Data Sheet)Further, it employs internal current limiting, thermal shutdown and safe area compensation, making it essentially blow-out proof. This device can also be used to make a programmable output regulator or as a precision current regulator. Livewire simulation of both the filtration and regulation stage for the transformer based Variable Dc power supply is as shown below.

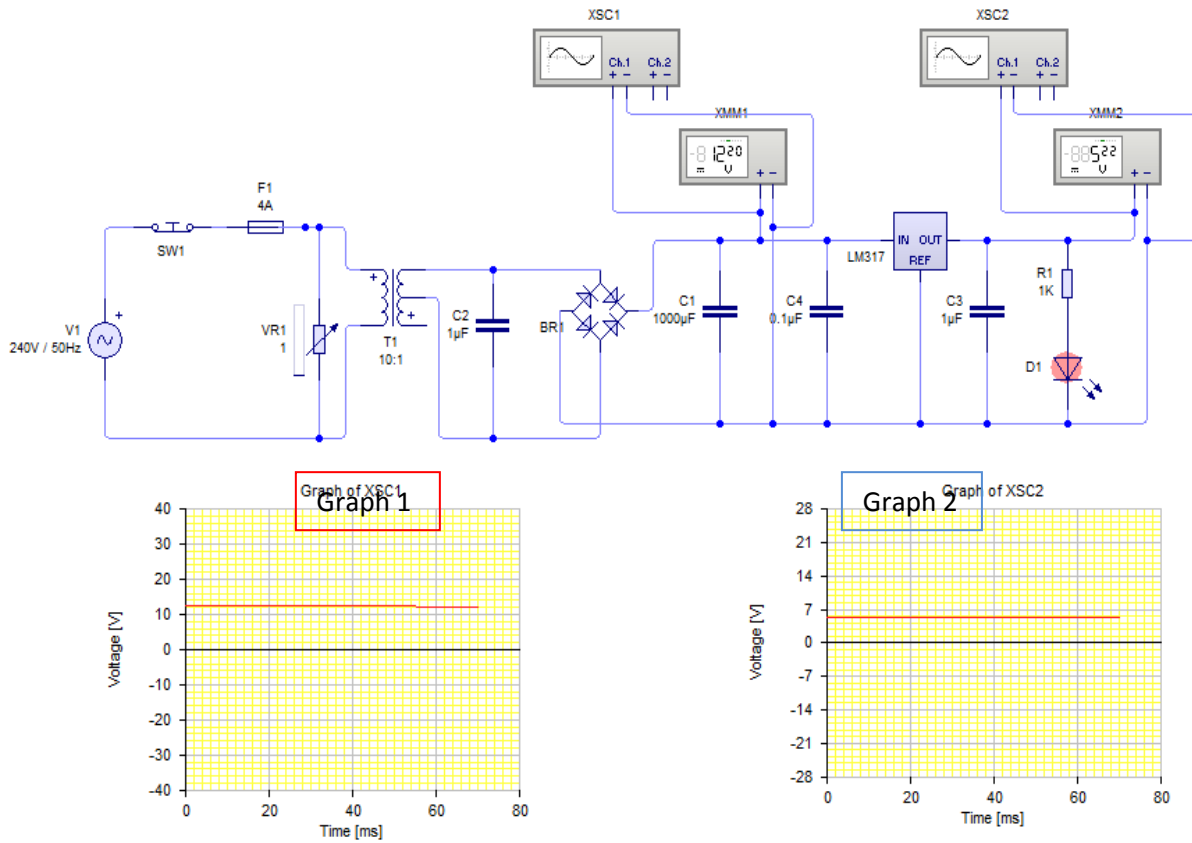


Figure 11: Waveform circuit analysis of filtration and regulation stage for the transformer based circuit using LM 317
From the figure 11 above, C3 is added to the output of the voltage regulator to improve the transient response. The voltage output of the equation is given as

$$V_{out} = 1.25 \times \left(1 + \frac{R2}{R1}\right) + I_{adj} \times R2$$

Where:

R2 = adjustable resistor

R1 = LM317 resistor

I_{adj} = adjustment pin current

From the LM 317 data sheet, the adjustment pin current is very small, its $50\mu A$ typical and $100\mu A$ maximum, thus the equation can be re-expressed as since the adjustment current is very small and negligible:

$$V_{out} = 1.25 \times \left(1 + \frac{R2}{R1}\right)$$

R1 should be very small preferably within the ranges of 200Ω to 500Ω because of the minimum load current requirement for the LM 317.

$$R1 = R2 \times \frac{1.25}{V_{out} - 1.25} \Omega$$

$$R2 = R1 \times \frac{V_{out} - 1.25}{1.25} \Omega$$

- Zener diode is preferably used in transformer less DC power supply instead of LM 317 regulator because experiment shows that X-Rated Capacitor with LM317 is highly unstable when the its being adjusted from one voltage value to the next. The livewire simulation of X-rated capacitor with LM series devices is as shown below:

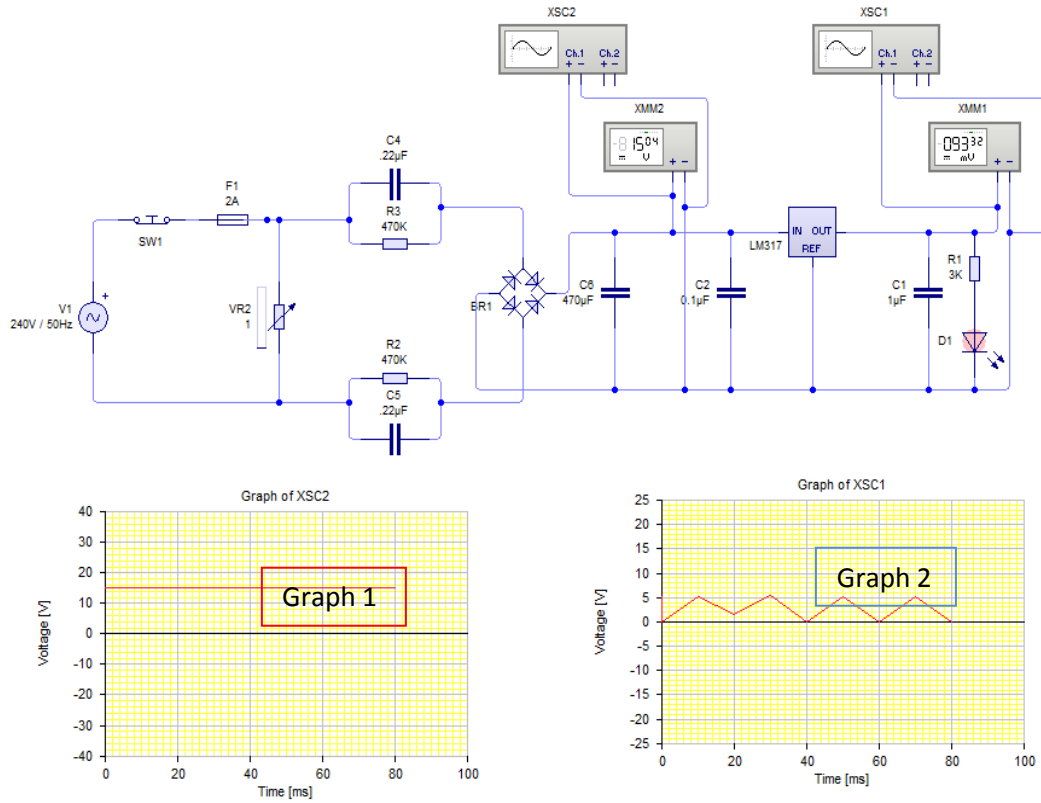


Figure 12: Waveform circuit analysis of filtration and regulation stage for the transformer less based circuit using LM 317. The ripple produced is too much, thus making it ineffective in powering any electronics device; instead zener diode regulation method is employed. The livewire simulation of zener diode regulation is as shown below.

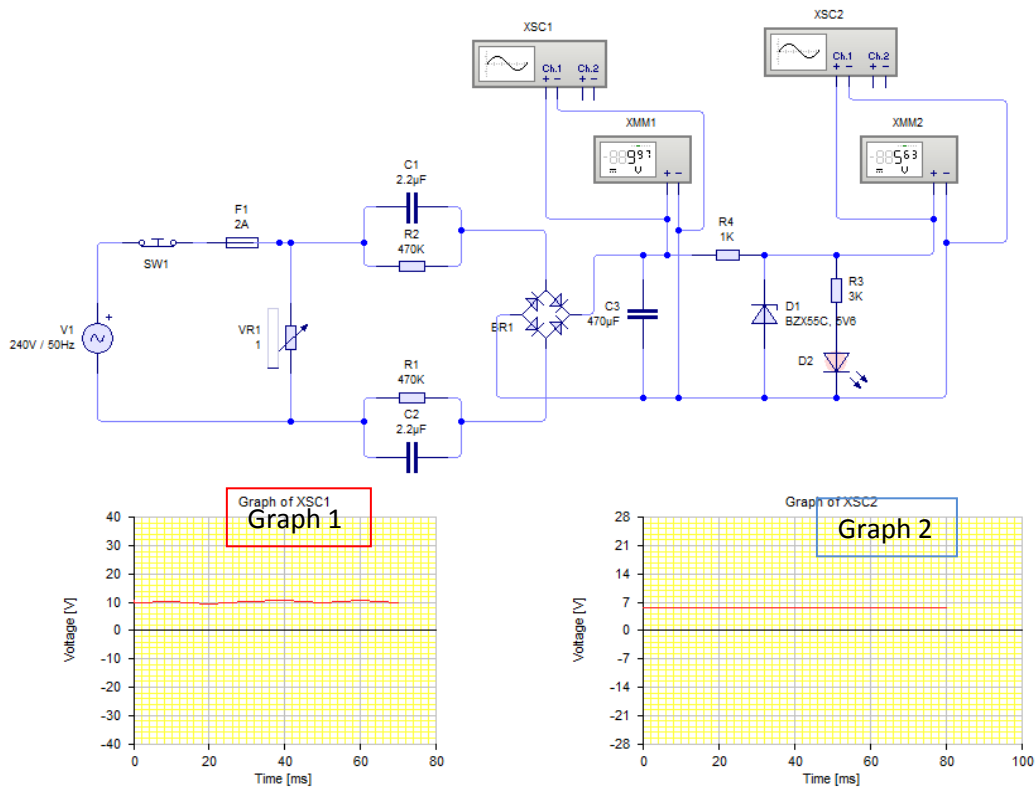


Figure 13: Waveform circuit analysis of filtration and regulation stage for the transformer less based circuit using LM 317.

3.5 Working principle of Capacitive Variable DC Power Supply

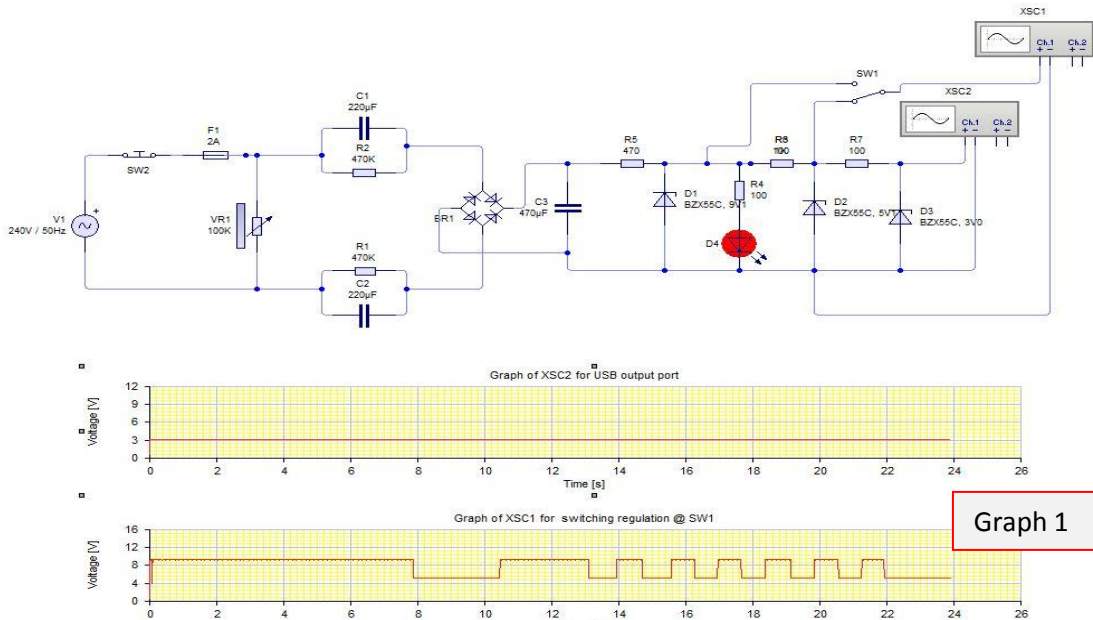


Figure 14: Detailed Circuit diagram of a Switching Regulation Method using Zener Diode for Transformer less Variable DC Power Supply

The figure 14 shown above is a transformer less or capacitive power supply. This capacitor power supply can deliver 12 volt DC and 100mA current to power low current devices. It is provided with surge protection and is totally isolated from mains supply using two X-rated capacitors in the phase and neutral lines. So the connected device is safe even if the phase and neutral lines changes.

The main supply is also connected to the protection circuit comprising of safety fuse in the phase line and an MOV across the phase and neutral lines as safety measure if there is voltage spike or short circuit in the mains.

The safety circuit is in turn connected across the two 225k J (2.2µF) 400 volts X rated capacitor that is in parallel with R1 and R2 known as the bleeder resistor. These resistors help remove the stored current from the capacitor when the circuit is unplugged.

A full wave rectifier is used to rectify the low voltage AC from the X-rated capacitors and C3 removes ripples from the DC. With this design, around 24 volts at 100mA current will be available in the output. This 24 volt DC can be regulated to required output voltage using a suitable 1 watt Zener.

Three zener diodes: ZD1=12V and ZD=5V are alternated by switch SW2 while ZD3 is outputted through the USB ports.

3.6 Working principle of Transformer Based Variable DC Power Supply

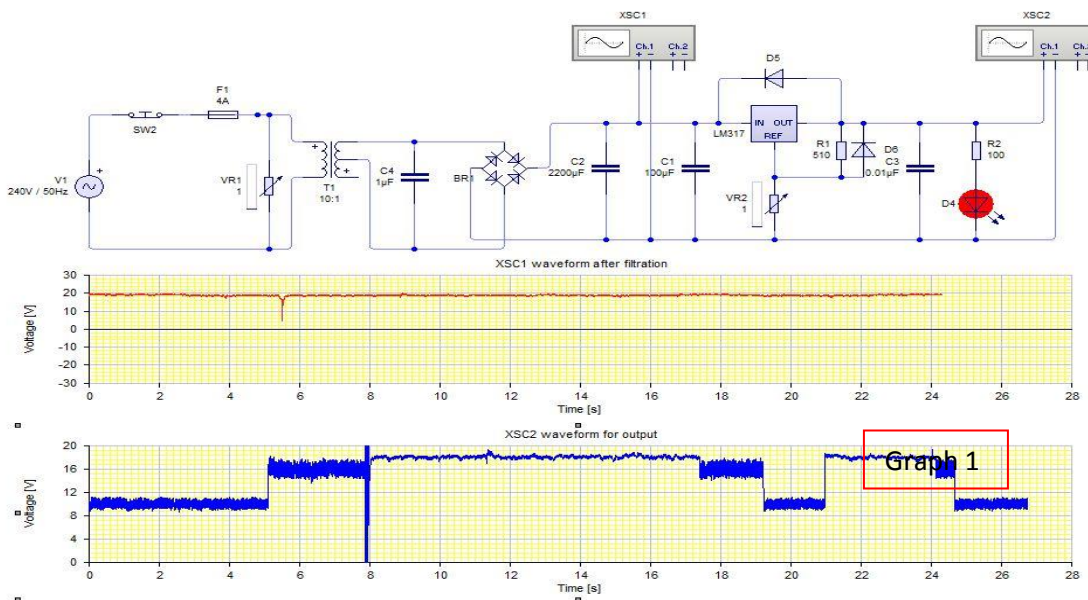


Figure 15: Detailed Circuit diagram of a Transformer Based Regulation using LM 317 for Transformer Variable DC Power Supply

From the figure 15 above, the transformer based variable regulated DC power supply utilizes a supply voltage of 230 Vac and an AC frequency of 60 Hz which is then connected to the protection circuit comprising of a fuse of 1.5 A and varistor of 250 Vac. The protection circuit is connected to the transformer of ratio 10:1 that transforms the AC voltage to the required low voltage of 23V ac.

The stepped down voltage of the transformer is then connected to the bridge rectifier that rectifies the AC voltage to the DC voltage, which is then filtered by a smoothing capacitor C2 and regulated by a voltage regulator (LM 317 T) resulting in an output of 19 V dc and 1.5 A under the right configuration of resistors (R1 and VR2) , capacitors (C1, C3, C4, C5) and diodes about the regulator.

- The resistors aids in the variation of the regulator outputs
 - The capacitors-
 - a. C1 and C4: help reduce high frequency noise from the mains
 - b. C3: helps increasing the transient response
 - c. C5:helps increase the ripple rejection capability of the regulator
 - The diode provides additional protection for the LM 317 voltage regulator against blow back current.
- The circuit diagram from the figure above was implemented on a Vero board.

IV. Results and Discussion

Table 1 gives the exact detailed amount of each of the electronics components used in the hardware implementation of both the transformer less based and transformer based Variable DC Power Supply

Table 1: Transformer less based Variable DC Power Supply Cost Evaluation

Name	Number	Amount (in Naira)
Switch (SW1 and SW2)	2	100
Fuse (2A)	1	20
Varistor (250 Vac)	1	150
X-rated Capacitor (C1 and C2-225K/400V)	2	300
Bleeder Resistor (R1 and R2- 470K,1W))	2	50
Bridge Diode (4-diodes-IN4007)	1	200
Filter Capacitor (470uF/50V)	1	50
Resistor (R3,R5,R6- 100 ohms, 1W)	3	150
Zener Diode (12V/1W)	1	20
LED Resistor (R4-1K, 1/4W)	1	20
LED (red)	1	30
Zener Diode (5V/1W)	1	20
Zener Diode (3.7V/1W)	1	20
USB Female port	1	50
Package (box, lead and Vero Board)	3	500
Total	21	1680

Table 2: Transformer based Variable DC Power Supply Cost Evaluation

Transformer based Variable DC Power Supply Cost Evaluation		
Name	Number	Amount (#)
Switch (SW1)	1	50
Fuse (4A)	1	30
Varistor (250 Vac)	1	150
Transformer (24V/1.5A)	1	600
Noise Suppressor Capacitor (C2 and C4)	2	100
Filter Capacitor (C1-1000uF/50V)	1	70
Ripple Rejection Capacitor (C5-1uF/16V)	1	50
Transients Capacitor (C3-1uF/25V)	1	50
LM 317 Resistor (R1-240 ohms,1W)	1	50
LM 317 Variable Resistor (VR1-5K)	1	150
LM317 Protective Diodes (IN4007)	2	40
VR1 knob	1	100
Packaging	1	1180
Total	15	2620

The results and key difference between transformer less and transformer based variable DC power supply based on the key requirements of DC power supply are as shown in table 3

Table 3: The results of transformer less and transformer variable DC power supply

Factors		Transformer less DC power supply (capacitive power supply)	Transformer DC power supply
1: Protection Stage	Result:	From figure 4- the device was effectively protected from fatal shock, over current and voltage but still caution is required when handling without its package.	Still figure 3- same but it has an added advantage in that it completely isolates the supply voltage from the remaining stages via transformer.
	Status:	Satisfactory	Excellent
2: Transformation stage	Result:	From figure 5- the device was very effective in that the supply voltage of 240Vac was reduced to 24 Vac as stated in the datasheet of 225K x-rated capacitor (<i>calculation cited in section 3.2.2</i>)	From figure 4-excelent transformation of supply voltage to the 24Vac based on the rating of the transformer (<i>turn ratio- calculation is cited in section 3.2.1</i>)
	Status:	Excellent	Excellent
3: Rectification Stage	Result:	From figure 7- the waveform on this stage was well rectified via bridge rectifier	From figure 6- same result as figure 17
	Status:	Excellent	Excellent
4: Filtration stage	Result:	From figure 8-the waveform and the hardware showed well filtered DC signals with a smoothing capacitor of 470Uf	From figure 7-the waveform and the hardware showed well filtered DC signals with a smoothing capacitor of 1000uF (<i>calculation is cited in section 3.4</i>)
	Status:	Excellent	Excellent
4: Regulation stage	Fixed	Result:	From figure 12, graph 2- using LM series electronics component regulator the resulting waveform had a lot of ripples as though the DC power was unfiltered while using zener diode as the regulator the resulting waveform showed an excellently filtered DC signal as shown in figure 13, graph 2
		Status:	Satisfactory (<i>limitation to use LM series devices</i>)
	Variable	Result:	From figure 14-using a switching regulation method the resulting waveform showed three voltage levels variation using zener diodes; graph 1 showed a constant voltage of 3.7 volts while graph 2 showed voltage switched between 5 and 10 volts.
		Status:	Excellent
6: Robust	Output Current	Result:	The current of the X-rated capacitor is limited to low current devices as stated in its datasheet.
		Status:	Satisfactory
	Output Voltage	Result:	From table 2: any voltage value can be obtained but at low current.
		Status:	Excellent
7: Power Loss	Result:	The power loss in this device is negligible because of low current flow through the device.	
	Status:	Excellent	
8: Noise Production	Result:	No Noise produced	
	Status:	Excellent	
9: Input Harmonics Distortion	Result:	Lower harmonics distortion than its counterpart	
	Status:	Excellent	
10: Cost, Size and Weight	Result:	From table 1: it is cheap. Smaller size and lighter weight than its counterpart	
	Status:	Excellent	

Both technologies have their place in today's power efficiency and safety scenarios but the key differences (as shown in table 3) can be deduced from the following key requirement of a proper DC source are: Isolation between source and load, Noise yield, High transient response, Levels of input harmonic distortion, Power losses and , efficiency, Workable size and weight

The transformer-based has a robust output current and well isolated from the supply voltage, which makes it more suitable for high current application, highly reliable for powering electronics devices; the results were excellent for all the five stages involved in the production of DC power supply.

The main purpose behind the introduction of transformer less units was because of cost effectiveness and to sell out the total bodily size and weight so as to miniaturise electronics devices. It also generates far less noise, heat, lower input harmonic distortion levels, high transient response than transformer-based circuitry but it is limited to low current application devices and lack of proper isolation unlike its counterpart thus results in lower Mean Time To Failure (MTTF).

V. Conclusion

In this paper, a comparative analysis of Transformer-based and Transformer less-based variable DC Power supply systems have been achieved with their design analysis successfully presented too.

The software design and design simulation of the both transformer less and transformer based variable DC power supply with their performance analysis using livewire simulation software was satisfactory.

Hardware production of transformer less of variable voltage between 3-10 Volts, 100mA and transformer based of variable voltage between 1.25 -25 Volts, 1.5A DC power supply was tested and results were satisfactory.

The transformer-based has a robust output current and well isolated from the supply voltage, which makes it more suitable for high current application, highly reliable for powering electronics devices while the transformer less based DC source has smaller size, weight and cheaper so as to miniaturize electronics devices but limited to low current devices . It also generates far less noise, heat, input harmonic distortion levels, and higher transient response but lack of proper isolation unlike its counterpart thus result in lower Mean Time To Failure (MTTF).

Transformer less variable DC power supply should be considered a viable option for lower power, small and low current applications where achieving the highest availability is not the top concern and cost, size and weight restrictions inhibit the use of traditional transformer-based DC power supply.

Reference

- [1] AN954, Transformer less Power Supplies- ww1.microchip.com/downloads/en/appnotes/00954A.pdf (Accessed on 02/09/12)
- [2] Emerson Network Power (2012): Comparing transformer based and transformer less uninterruptible power supplies – www.hebrt.com (accessed on 02/09/12)
- [3] Garage (2012), Variable power supply - www.engineersgarage.com (Accessed on 02/09/12).
- [4] Horowitz, P. and Hill, W. (1980): Art of Electronics. Cambridge Press: Cambridge, UK.
- [5] Kiran Shrestha (Nov 2004): Transformer less 12V Dual Power Supply- <http://www.docstoc.com/docs/17245578/Power-supply> (Accessed on 12/10/12)
- [6] Mohamkumar (2006): Transformer less power supply- www.engineersgarage.com (Accessed on 02/09/12)
- [7] Mike Papadimitriou (-----) ,LM317 VARIABLE POWER SUPPLY- <http://www.diy-electronic-projects.com> (Accessed on 12/10/12)
- [8] National (2012), LM317 Regulator Datasheet Data Sheet- <http://www.national.com/pf/LM/LM317.html> (Accessed on 02/09/12)
- [9] Ron J (2002): Transformer less Power Supplies- www.zen22142.zen.co.uk/Circuits/Power/tps.htm (Accessed on 24/11/12)
- [10] Ron Roscoe (2012): course materials for 6.01 Introductory Analog Electronics Laboratory, spring 2007. MIT Open Course Ware- <http://ocw.mit.edu/>, Massachusetts Institute of Technology (Accessed on 02/09/12)
- [11] Shamsul Arifin Bin Zial, (Nov 2010): Development of DC Power supply using power electronics applications
- [12] Stan D'Souza (1999), Transformer less Power Supply- [www.garcia-cuervo.net/.../transformerless power supply tb0](http://www.garcia-cuervo.net/.../transformerless_power_supply_tb0) (Accessed on 12/10/12)
- [13] Theraja, B.L. and Theraja, A.K. (2002): A Textbook of Electrical Technology. 23rd ed. S. Chand: New Delhi, India.
- [14] Williams, O.A. (1995): Design and Construction of a Regulated Power Supply Unit. Cambridge Press: Cambridge, UK.
- [15] Wikipedia (2012), Power Supplies- http://en.wikipedia.org/wiki/power_supply (Accessed on 02/09/12)

Content Extraction with text mining using natural language processing for anatomy based topic summarization

K.FouziaSulthana,¹ N.Kanya²

¹Final Year Student, M.Tech CSE Department, Dr.M.G.R.Educational and Research Institute University, Tamil Nadu, India
²Associate Professor of CSE and IT Department, Dr.M.G.R.Educational And Research Institute University, Tamil Nadu, India

Abstract: Inorder to get exact content for the web browsers when searching for some information we have combined two methods together.The first method is text mining using natural language processing and parse tree query language, the second method is TSCAN (Topic summarization and Content Anatomy).

In the first method, when a sentence is given for searching, the sentence is converted into a automatic query formation using natural language processing tools and information is retrieved using text mining methods.

In the second method a temporal similarity (TS) function is implemented to generate the event dependencies and context similarity to form an evolution graph of the topic search.

Both methods are integrated together to make the quality of the extraction of required content efficient and easier.

Keywords:TSCAN, Natural Language Processing, TextMining, Information Extraction,PTQL

I. Introduction

Information Extraction is a process which develops methods for fetching structured information from natural language text. The extraction of entities and relationships between entities is the best example of structured information.

INFORMATION EXTRACTION is typically seen as a one-time process for the extraction of a particular kind of relationships of interest from a document collection .The purpose of information extraction (IE) is to find desired pieces of information in natural language texts and stores them in a form that is suitable for automatic processing. IE is usually deployed as a pipeline of special-purpose programs, which include sentence splitters, tokenizes, named entity recognizers, shallow or deep syntactic parsers, and extraction based on a collection of patterns.

It provides automated query generation components so that casual users do not have to learn the query language in order to perform extraction.

We performed experiments to highlight two important aspects of an information extraction system: efficiency and quality of extraction. By applying our methods to a number of records in databases, the benefit of this method is efficient for real-time applications. The Text Processor in this responsible for corpus processing and storage of the processed information in the Parse Tree Database (PTDB). The extraction patterns over parse trees can be expressed in our proposed parse tree query language. The Parse Tree Query Language(PTQL)query evaluator takes a PTQL query and transforms it into keyword-based queries and SQL queries, which are evaluated by the underlying RDBMS and information retrieval (IR) engine. To speed up query evaluation, the index builder creates an inverted index for the indexing of sentences according to words and the corresponding entity typesThe architectural diagram is shown in fig.1, clearly describes our approach.

ARCHITECTURAL DIAGRAM:

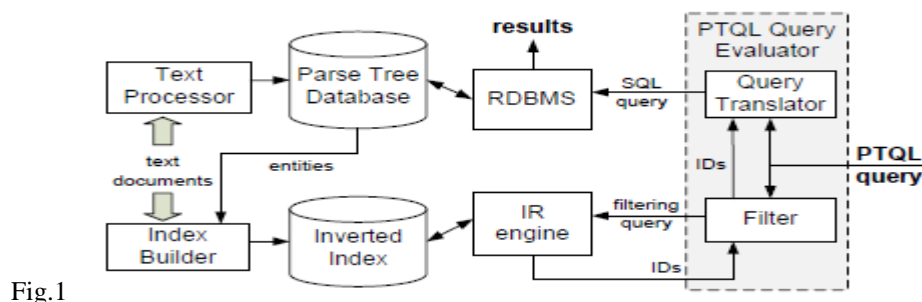


Fig.1

A typical IE setting involves a pipeline of text processing modules in order to perform relationship extraction.

These include:

Sentence splitting: identifies sentences from a paragraph of text

Tokenization: identifies word tokens from sentences

Named entity recognition: identifies mentions of entity types of interest

Syntactic parsing: identifies grammatical structures of sentences

Pattern matching: obtains relationships based on a set of extraction patterns that utilize lexical,syntactic and semantic features

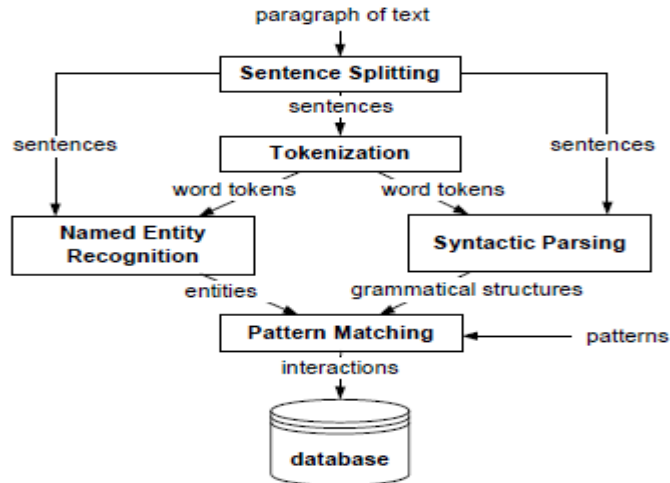


Fig. 2. A workflow of text processing modules that takes a paragraph of text as input to perform relationship extraction.

II. Tscan System

In this section, we present our model and the methods used in the proposed topic anatomy system.

2.1 Topic Model:

A topic is a real world incident that comprises one or more themes, which are related to a finer incident, a description, or a dialogue about a certain issue. During the lifespan of a topic, one theme may attract more attention than the others, and is thus reported by more documents. We define an event as a significant theme development that continues for a period of time. Naturally, all the events taken together form the storyline(s) of the topic. Although the events of a theme are temporally disjoint, they are considered semantically dependent in order to express the development of the theme. Moreover, events in different themes may be associated because of their temporal proximity and context similarity. The proposed method identifies themes and events from the topic's documents, and connects associated events to form the topic's evolution graph. In addition, the identified events are summarized to help readers better comprehend the storyline(s) of the topic. Fig. 3 illustrates the relationships between the themes, events, and event dependencies of a topic in the proposed model.

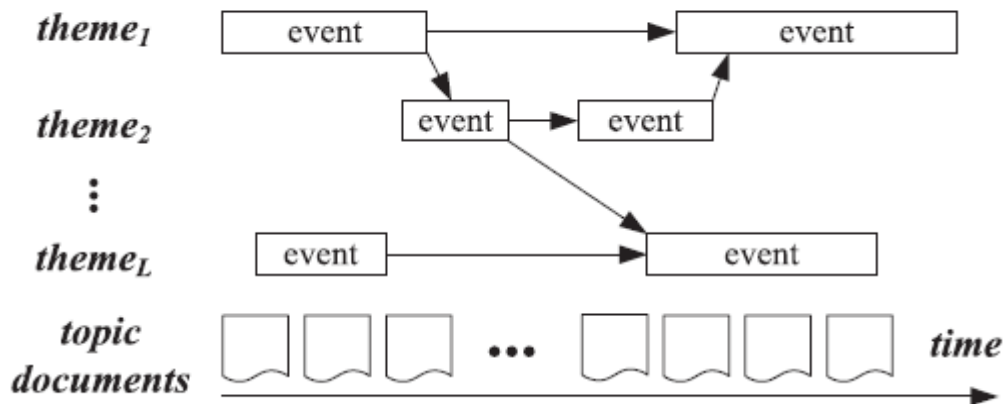


Fig. 3. The relationships between themes, events, and event dependencies.

2.2 Theme Generation:

A matrix $A=B^T B$ is called a block association matrix, is asymmetric matrix in which the (i,j) -entry is the inner product of columns i and j in matrix B . As a column of B is the term vector of a block, A represents the interblock association. Hence, entries with a large value imply a high correlation between the corresponding pair of blocks. A theme of

a topic is regarded as an aggregated semantic profile of a collection of blocks, and can be represented as a vector v of dimension n , where each entry denotes the degree of correlation of a block to the theme.

2.3 Event Segmentation and Summarization:

A theme v_j in is a normalized eigenvector of dimension n , where the (i,j) entry indicates the correlation between a block i and a theme j . As topic blocks are indexed chronologically, a sequence of entries in v_j with high values can be taken as a noteworthy event embedded in the theme, and valleys (i.e., a sequence of small values) in v_j may be event boundaries. However, according to the definition of eigenvectors, the signs of entries in an eigenvector are invertible. Both the positive and negative entries of an eigenvector contain meaningful semantics for describing a certain concept embedded in a document corpus and the amplitude of an entry determines the degree of its correlation to the concept. The tasks of event segmentation and speech endpoint detection are similar in that they both try to identify important segments of sequential data. In addition, it is the amplitude of sequential data that determines the data's importance.

2.3 Evolution Graph Construction:

Automatic induction of event dependencies is often difficult due to the lack of sufficient domain knowledge and effective knowledge induction mechanisms. However, as event dependencies usually involve similar contextual information, such as the same locations and person names, they can be identified through word usage analysis. Our approach, which is based on this rationale, involves two procedures. First, we link events segmented from the same theme sequentially to reflect the theme's development. Then, we use a temporal similarity function to capture the dependencies of events in different themes. For two events, e_i and e_j , belonging to different themes, we calculate their temporal similarity between these two events and providing the graph description from the result.

III. Integrating NLP and PTQL with Text Mining and Anatomy Based Topic Summarization

Natural Language Processing(NLP) is a field of computer science,artificial intelligence,and linguistics concerned with the interactions between computers and natural languages. It is used to transfer normal sentence to structured query text.

Since we are integrating both these methods,it will be easy for searching and retrieving documents.We can see the parse trees developed for the queries for the givensentences. Integrated architecture is as shown in the fig 4.

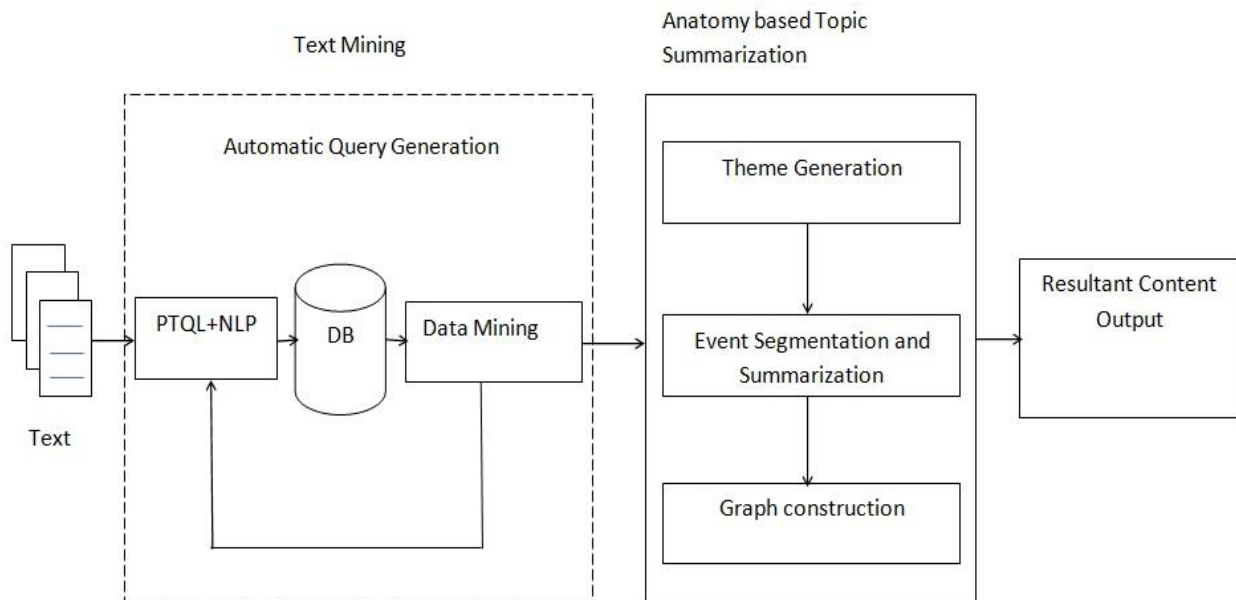


Fig 4 Integrated architectural diagram for content extraction

IV. Discussion and Conclusion

PTQL has the ability to perform a variety of information extraction tasks by taking advantage of parse trees unlike other query languages. Currently PTQL lacks the support of common features such as regular expression as frequently used by entity extraction task. PTQL also does not provide the ability to compute statistics across multiple extraction such as taking redundancy into account for boosting the confidence of an extracted fact.

Publishing activities on the Internet are now so prevalent that when a fresh news topic occurs, autonomous users may publish their opinions during the topic's life span. To help Internet users grasp the gist of a topic covered by a large number of topic documents, text mining and topic summarization methods have been proposed to highlight the core information in the documents and also for the automatic query generation.

References

- [1] J. Allan, J. Carbonell, G. Doddington, J. Yamron, and Y. Yang, "Topic Detection and Tracking Pilot Study: Final Report," Proc. USDefense Advanced Research Projects Agency (DARPA) Broadcast News Transcription and Understanding Workshop, pp. 194-218, 1998.
- [2] V. Hatzivassiloglou, L. Gravano, and A. Maganti, "An Investigation of Linguistic Features and Clustering Algorithms for Topical Document Clustering," Proc. 23rd Ann. Int'l ACM SIGIR Conf. Research and Development in Information Retrieval, pp. 224-231, 2000.
- [3] C.D. Manning, P. Raghavan, and H. Schutze, Introduction to Information Retrieval. Cambridge Univ. Press, 2008.
- [4] Y. Yang, T. Pierce, and J. Carbonell, "A Study on Retrospective and Online Event Detection," Proc. 21st Ann. Int'l ACM SIGIR Conf. Research and Development in Information Retrieval, pp. 28-36, 1998.
- [5] C.C. Chen, M.C. Chen, and M.S. Chen, "An Adaptive Threshold Framework for Event Detection Using HMM-Based Life Profiles," ACM Trans. Information Systems, vol. 27, no. 2, pp. 1-35, 2009.
- [6] D. D. Sleator and D. Temperley, "Parsing English with a Link Grammar," in Third Intl. Workshop on Parsing Technologies, 1993.
- [7] R. Leaman and G. Gonzalez, "Banner: An executable survey of advances in biomedical named entity recognition," in Pacific Symposium on Bio computing 13, 2008, pp. 652-663.
- [8] A. R. Aronson, "Effective mapping of biomedical text to the umls met thesaurus: the metamap program." in Proceedings of the AMIA Symposium. American Medical Informatics Association, 2001, p. 17.
- [9] M. J. Cafarella and O. Etzioni, "A search engine for natural language applications," in WWW'05, 2005.
- [10] T. Cheng and K. C.-C. Chang, "Entity search engine: Towards agile best-effort information integration over the web," in CIDR, 2007.
- [11] H. Bast and I. Weber, "The Complete Search Engine: Interactive, efficient, and towards IR & DB integration," in CIDR, 2007, pp. 88-95.
- [12] S. Bird, Y. Chen, S. B. Davidson, H. Lee, and Y. Zheng, "Extending XPath to support linguistic queries," in Workshop on Programming Language Technologies for XML (PLAN-X), 2005.
- [13] S. Geetha, G. S. Ananda Mala, N. Kanya, "A survey on information extraction using entity relation based methods," SEISCON 2011.
- [14] N. Kanya, S. Geetha, "Information Extraction - A Text mining approach" ICTES 2007.

Meshfree Simulation of the Penetration of Thick Metal Structure by Rigid Penetrator

Kalilou Sidibé,¹ Guangyao Li²

¹Ecole Nationale d'Ingénieurs Abderrahmane Baba Touré, 410, Avenue Van Vollenhoven, BP 242 Bamako, République du Mali,

²College of Mechanical and Automotive Engineering, Hunan University, 410082 Changsha, P.R. China,

Abstract: The Reproducing Kernel Particle Method (RKPM) has been used for the simulation of the penetration of thick metal blocks by rigid penetrator. The particle to segment contact algorithm has been used for the contact detection as well the contact constraints implementation. In the study it is found that the finite element method without remeshing fails in earlier stage of the penetration process while the RKPM goes beyond very large deformation. The effectiveness of the RKPM for the simulation of the large deformation of mechanical structure is confirmed.

Keywords: large deformation, mechanical contact, penetration, RKPM.

I. Introduction

Nowadays, the meshless or meshfree methods are widely used in mechanical science and engineering applications because of their advantages over the finite element methods (FEM); especially in the simulation of problems involving large deformations and distortions of the structure. Among the meshfree methods are: Smoothed Particle Hydrodynamics (SPH) [1, 2]; Diffuse Element Method (DEM) [3]; Element-Free Galerkin (EFG) [2, 4, 5, 6]; Reproducing Kernel Particle Method (RKPM) [7-17]; Partition of Unity Method (PUM) [18] and so forth.

The simulation of the penetration requires the development of contact algorithms which can be classified into two categories, contact searching algorithm and contact constraints algorithm. The contact searching consists of finding the contacting boundaries (contacting particles/nodes). The contact constraints algorithm is concerned with the implementation of the so-called impenetrability condition which does not allow overlapping between bodies, in other words two bodies cannot occupy the same space at the same time.

In the framework of FEM, several contact searching algorithm have been developed. These contact searching algorithms include the master-slave contact algorithm [19, 20]; the single surface contact algorithm [19, 20], the hierarchy territory contact algorithm [21], and the pinball contact algorithm [22, 23]. In the framework of meshless method, the particle to particle contact algorithm [24, 25], the meshfree contact-detection algorithm [11, 12], the particle to segment contact algorithm [13, 15-17],... were developed. In the particle to segment contact algorithm the boundaries of the bodies are represented by particles located on the boundary, and these particles are interconnected to form polygons fitting the boundary without overlapping. The algorithm is developed for the simulation of the contact between a flexible body and several rigid bodies as encountered in metal forming where the work piece is deformable and the tools are usually assumed to be rigid. This algorithm was found to very effective as it has the advantage to allow the correct evaluation of the interpenetration used for the determination of the contact constraints [13, 15, 16]. Therefore in this work, it will be used for the simulation of the penetration process.

II. RKPM discretization

The reproducing kernel particle method (RKPM) is systematically formulated in [7-11]. The RKPM uses the finite integral representation of a function $u(\mathbf{x})$ in a domain Ω_x .

$$u^a(\mathbf{x}) = \int_{\Omega_x} \Phi_a(\mathbf{x} - \mathbf{y})u(\mathbf{y})d\Omega_x \quad (1)$$

Where $u^a(\mathbf{x})$ is the approximation of function $u(\mathbf{x})$ and $\Phi_a(\mathbf{x} - \mathbf{y})$ is the kernel function with compact support a .

Discrediting the domain Ω_x by a set of particles $\{\mathbf{x}_1, \mathbf{x}_2, \dots, \mathbf{x}_{NP}\}$, where \mathbf{x}_I is the position vector of particle I , and NP is the total number of particles; the integral is approximated by the following summation:

$$u^h(\mathbf{x}) = \sum_{I=1}^{NP} \mathbf{N}_I(\mathbf{x})u(\mathbf{x}_I) \quad (2)$$

Where $\mathbf{N}_I(\mathbf{x})$ is the RKPM shape function defined to be?

$$\mathbf{N}_I(\mathbf{x}) = \mathbf{C}(\mathbf{x}; \mathbf{x} - \mathbf{x}_I)\Phi_a(\mathbf{x} - \mathbf{x}_I)\Delta\mathbf{V}_I \quad (3)$$

$\mathbf{C}(\mathbf{x}; \mathbf{x} - \mathbf{x}_I)$ is the correction function introduced to improve the accuracy of the approximation near the boundaries and ΔV_I is the volume of particle I and the subscript h is associated with a discretized domain.

The application of the principle of virtual work and the particles approximation to the equation of the conservation of the linear momentum lead to the equation of motion for contact problems [13]:

$$\mathbf{f}_I^{ext} - \mathbf{f}_I^{int} + \mathbf{f}_I^{cont} = \mathbf{M}_{IJ} \ddot{\mathbf{d}}_J \quad (4)$$

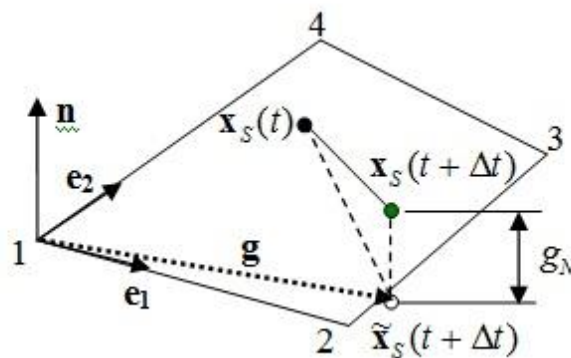
Where:

- \mathbf{f}_I^{ext} : the external force of particle I
- \mathbf{f}_I^{int} : the internal force of particle I
- $\ddot{\mathbf{d}}_J$: the generalized acceleration of particle J
- \mathbf{f}_I^{cont} : the contact force of particle I (see **part III**)
- $M_{IJ} = \int_{\Omega_0} \rho_0 N_I N_J d\Omega$ is the consistent mass matrix which can be approximated by row sum technique.

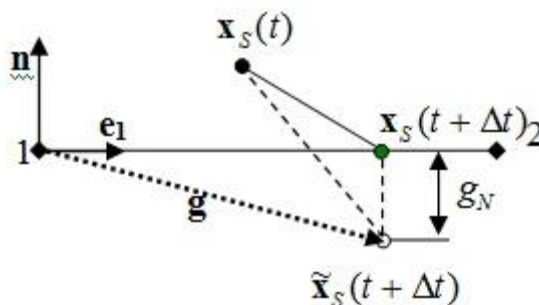
III. Particle To Segment Contact Algorithm

In this work, the particle to segment contact algorithm is used for the contact simulation. The particle to segment contact algorithm was developed by G. Li et al [13] for 3D problems and by K. Sidibe et al. [15] for 2D problems. Applications of the contact algorithm to sheet metal forming are done by K. Sidibe et al. [16, 17]. An updated version of this algorithm for flexible bodies called ‘reversible particle to segment contact algorithm’ was developed by K. Sidibe et al. [16] to handle the mechanical contact between deformable bodies. Designated for the simulation of the metal forming analysis, the particle to segment contact algorithm modelled the tools as rigid bodies and the work piece as flexible (deformable) body. In 2D, the boundaries of the rigid tools are discretized by piecewise linear segments while in 3D the boundaries of tools assumed to be rigid are modelled by flat segments.

Every time step, prior to the calling to the contact-subroutine, the trial accelerations, velocities and displacements are computed from the explicit time routine. The trial positions of the particles, obtained from the trial displacements, are then used to check whether there is overlapping between the bodies. Whenever any overlapping is found the contact forces are evaluated and applied to cancel the interpenetration of the bodies as shown in Figure 1.



(a) 3D



(b) 2D

Figure 1. Correction of trial position of the penetrating slave particle S

In **Figure 1**: $\mathbf{x}_S(t)$ is the position of S at time t (before penetration), $\tilde{\mathbf{x}}_S(t + \Delta t)$ trial position of S at time $t + \Delta t$ and $\mathbf{x}_S(t + \Delta t)$ corrected position of S at time $t + \Delta t$ (after application of contact forces); \mathbf{n} is the normal unit vector of the contact segment pointing out from the segment toward the flexible body, \mathbf{e}_1 and \mathbf{e}_2 are the tangential unit vectors on the edges of the segment and g_N is the normal gap.

As shown in **Figure 1**, the normal gap is given by:

$$g_N = \mathbf{g} \cdot \mathbf{n} = (\tilde{\mathbf{x}}_S(t + \Delta t) - \mathbf{x}_1(t + \Delta t)) \cdot \mathbf{n} \quad (5)$$

For each penetrating slave particle, the penalty force necessary to cancel the penetration is evaluated by:

$$\mathbf{f}_N(s) = -\frac{m_s g_N}{\Delta t^2} \mathbf{n} = f_n \cdot \mathbf{n} \quad (6)$$

The Coulomb friction model is adopted to evaluate the friction between the contacting bodies. Frictional force applied to oppose the relative tangential displacement at the contact interface is given by:

$$\mathbf{f}_T(s) = -\min\left(\mu f_n, \left\| \frac{m_s}{\Delta t} \mathbf{v}_r \right\| \right) \frac{\mathbf{v}_r}{\|\mathbf{v}_r\|} \quad (7)$$

Where μ the friction coefficient on the contact is interface and \mathbf{v}_r is the tangential component of the relative velocity of the slave particle S with respect to the contact segment.

The resultant of the contact forces, on a given slave particle J is calculated by

$$\mathbf{f}_J = \mathbf{f}_N(J) + \mathbf{f}_T(J) \quad (8)$$

The force vectors calculated above are the exact nodal force vectors for each penetrating particle, to satisfy the impenetrability and friction conditions at the interface. Therefore the exact nodal force is re-distributed to a non-local 'fictitious force'. The fictitious force vector for a particle I is calculated as follows.

$$\mathbf{f}_I^{cont} = \sum_J \mathbf{f}_J N_I(\mathbf{X}_J) \quad (9)$$

IV. Numerical Applications

Our current RKPM computer codes were tested and validated through standard test by G. Li et al. [13] for 3D formulation and K. Sidibe et al. [14] for the 2D formulation. Also the 3D implementation of the particle to segment contact algorithm was validated by G. Li et al. [13] and the 2D implemented by K. Sidibe et al. [15] for bulk metal forming. This work deals with the extension of these codes to the penetration simulation, the basic formulation staying the same. Details about the implementation in the computer code can be found in K. Sidibe et al. [16].

To further investigate on the effectiveness of the RKPM for large deformation analysis, the problem of penetration is considered in this section. Both two and three-dimensional penetration simulations are treated. The material of the work pieces is assumed to be an elastoplastic with isotropic non-linear strain hardening law defined as

$$\sigma = \mathbf{K}(\varepsilon_0 + \varepsilon_p)^n \quad (10)$$

Where σ is the stress and ε_p the plastic strain, the parameters defining the material used for the simulation are given in Table 1.

4.1 Two-dimensional penetration simulation

A rigid penetrator of width 4mm with round nose is moved downward with a constant velocity of 10m/s, and penetrates a work piece of $100 \times 25 \text{mm}^2$. The statement of the problem is shown in **Figure 2**. A plane strain formulation is used. The contact between the penetrator and the target is assumed to be frictionless. The work piece is discretized by a set of 4992 particles distributed with various particles densities as shown in **Figure 3-a**. The damaged shape of the workpiece is shown in **Figure 3-b**. Using the finite element method (FEM) commercial code LS-DYNA3D without remeshing, mesh overlapping is observed in earlier stage of the deformation as shown in **Figure 4**.

4.2 Three-dimensional penetration simulation

A cylindrical rigid penetrator (radius 5.11mm) with round nose penetrates a thick steel plate ($71.12 \times 15.24 \times 25.4 \text{mm}^3$). The penetrator is initially inclined at 45° and attacks the target with constant velocity of (50m/s, 0,

-50m/s). The target is discretized by a set of 5330 particles distributed with various particles densities as shown in **Figure 5-a**. The damage shape of the plate is shown in **Figure 5-b**.

4.3 Discussion

Analysing the results obtained, we can see that successful simulation of the penetration has been done. For a block of metal such large deformations might lead to mechanical fracture or rupture. Our current RKPM code does not take into account the mechanical fracture. The implementation of the mechanical fracture in our RKPM code is under investigation and might be a subject of future papers.

Table 1 Material parameters of the work pieces for the simulation

Parameter	value
Young's modulus (E)	71Gpa
Poisson's ration (ν)	0.33
ϵ_0	0.0166
K	576.79Mpa
n	0.3593
Mass density	1700kg/m ³

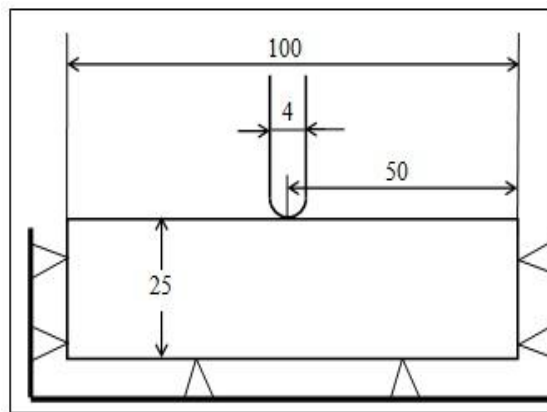


Figure 2 Statement of the two-dimensional penetration problem

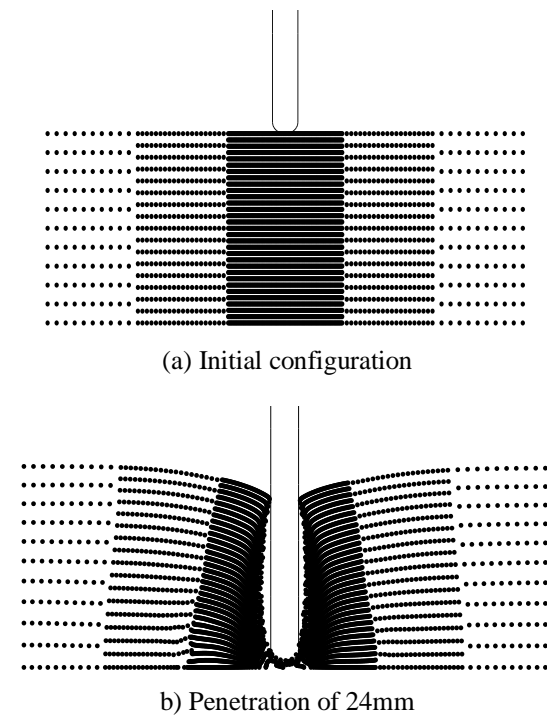


Figure 3 Simulation of two-dimensional penetration

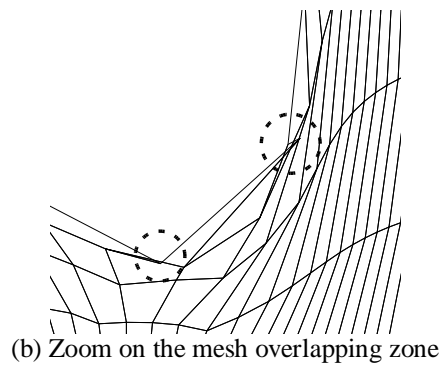
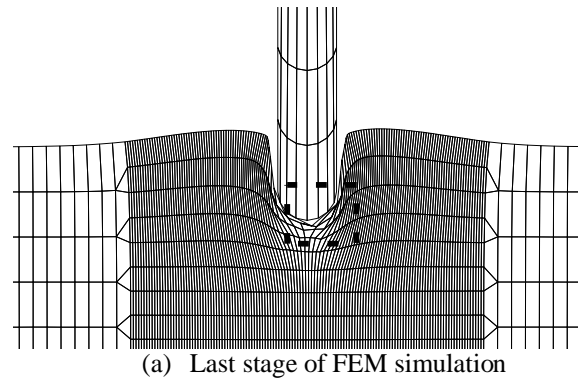


Figure 4 Mesh overlapping when using FEM without adaptivity for the simulation of two-dimensional penetration

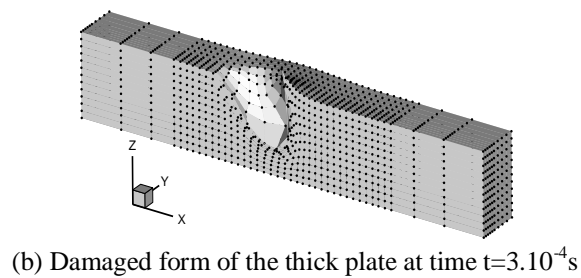
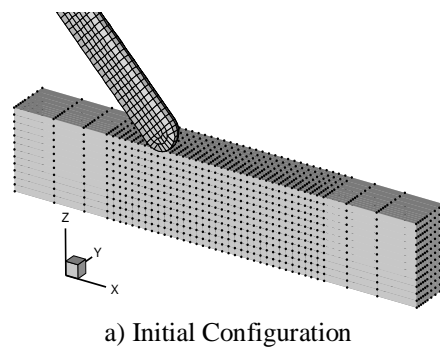


Figure 5 Simulation of the 3D-penetration

V. Conclusion

The particle to segment contact algorithm, correctly implemented in the Reproducing kernel Particle Method, has been successfully used for the simulation of the damage-penetration of thick metal. Both 2D and 3D problems are treated. As seen through this work, earlier failure of the computation is observed when using the FEM. The effectiveness of RKPM for large deformation is confirmed and to make more realistic simulation mechanical rupture model must be implemented in our current RKPM code.

VI. Acknowledgement

This work was partially supported by TWAS under Research Grant N° 09-143 RG and ENI-ABT under Research Grant N°001/ENI-ABT/2010.

References

- [1] R.A Gingold, J.J. Monaghan. Smoothed particle hydrodynamics theory and application to non-spherical stars, Monthly Notices of the Royal Astronomical Society, Vol. 181, pp. 375-389, 1977.
- [2] T. Belytschko, Y. Krongauz, D. Organ, M. Fleming, P. Krysl. Meshless Methods: An Overview and Recent Developments. Comput Methods Appl.Mech. Engrg, special issue on Meshless Methods, Vol. 139, pp. 3-47, 1996.
- [3] B. Nayroles, G. Touzot, P. Villon. Generalizing the finite element method: diffuse approximation and diffuse elements. Computational Mechanics, Vol. 10, pp. 307-318, 1992.
- [4] T. Belytschko, Y.Y. Lu, L. Gu. Element Free Galerkin Method, Int. J. Numer. Meth. Engrn., Vol. 37, pp. 229-256, 1994.
- [5] J. Dolbow, T. Belytschko. An Introduction to Programming the Meshless Element Free Galerkin Method, Archives in Computational Mechanics, Vol. 5 (3), pp. 207-241, 1998.
- [6] X.L. Chen, G.R. Liu, S.P. Lim. An element free Galerkin method for the free vibration analysis of composite laminates of complicated shape. COMPOS STRUCT, Vol. 59 (2), pp. 279-289, 2003.
- [7] W. K. Liu, S. Jun, Y. F. Zhang. Reproducing Kernel Particle Methods, Int j. Numer. Meth. Fluids, Vol. 20, pp. 1081-1106, 1995.
- [8] W.K. Liu, S. Jun, S. Li, J. Adee, T. Belytschko. Reproducing Kernel Particle Methods for structural dynamics, Int. J. Numer. Meth. Engrg, Vol. 38, pp. 1655-1679, 1995.
- [9] J.S. Chen, C. Pan, C.T. Wu. Large deformation analysis of rubber based on a reproducing kernel particle method, Computational Mechanics, Vol. 19, pp. 211-227, 1997.
- [10] J.S. Chen, C. Pan, C.T. Wu, W. K. Liu. Reproducing kernel particle methods for large deformation analysis of non-linear structures, Comput Methods Appl.Mech. Engrg, Vol. 139, pp. 195-227, 1996.
- [11] S. Li, W. Hao, W. K. Liu. Numerical simulations of large deformation of thin shell structures using meshfree methods, Computational Mechanics, Vol. 25, pp. 102-116, 2000.
- [12] S. Li, D. Qian, W. K. Liu, T. Belytschko. A Meshfree Contact-detection Algorithm, Comput. Methods Appl. Mech. Engrg., Vol. 190, pp. 3271-3292, 2000.
- [13] G. Li, K. Sidibe, G.R. Liu. Meshfree method for 3D bulk forming analysis with lower order integration scheme, Engineering Analysis with Boundary Elements, Vol. 28, pp. 1283-1292, 2004.
- [14] K. Sidibe, T. Sanogo, A. Ouane, G. Li. Lower Integration Rule and Benchmark Test Procedure for 2D Meshfree Methods, Journal Africain de Communication Scientifique, Vol. 7, pp. 799-805, 2009.
- [15] K. Sidibe, G. Li, A. Ouane, H. Bokar. Numerical simulation of mechanical contact problems using the RKPM with lower integration scheme, Rev. Ivoir. Sci. technol., Vol 14, PP 147-158, 2009.
- [16] K. Sidibe, G. Li. Numerical simulation of the mechanical contact between flexible bodies by using a reversible particle to segment contact algorithm in meshfree methods, Journal des Sciences Pour l'Ingénieur, Vol 13, PP 79-87, 2011.
- [17] K. Sidibe, G. Li. A Meshfree Simulation of the Draw Bending of Sheet Metal, International Journal of Scientific & Engineering Research, Volume 3, Issue 10, PP 1-5, 2012.
- [18] J.M. Melenk, I. Babuska. The partition of unity finite element method: Basic theory and application, Comput. Methods Appl. Mech. Engrg, Vol. 139, pp. 289-314, 1996.
- [19] J.O. Hallquist, G.L. Goudreau, D.J. Benson. Sliding interfaces with contact-impact in large-scale lagrangian computation, Comput. Methods Appl. Mech. Engrg., Vol. 51, pp. 107-137, 1985.
- [20] J.O. Hallquist, LS-DYNA3D Theoretical Manual, Livermore Software Technology Corporation, Livermore, 1998.
- [21] Z.H. Zhong. Finite Element Procedures for Contact-Impact, Oxford University Press, 1993.
- [22] T. Belytschko, M.O. Neal. Contact-Lmpact by the Pinball Algorithm with Penalty and Lagrangian Methods, Int. J. Numer. Meth. Engrg., Vol. 31, pp. 547-572, 1991.
- [23] T. Belytschko, I.S. Yeh. The splitting pinball method for contact-impact problems, Comput. Methods Appl. Mech. Engrg., Vol. 105, 375-393, 1993.
- [24] R. Vignjevic, J. Campbell. A penalty approach for contact in smoothed particle hydrodynamics, International Journal of Impact Engineering, Vol. 23, pp. 945-956, 1999.
- [25] J. Cambell, R. Vignjevic, L. Libersky. A contact algorithm for smoothed particle hydrodynamics, Comput Methods Appl.Mech. Engrg, Vol. 184, pp. 49-65, 2000.

A Novel Soft Switching Lcl-T Buck Dc–Dc Converter System

A Mallikarjuna Prasad,¹ D Subbarayudu,² S Sivanagaraju³ U Chaithanya⁴

¹Research Scholar, JNTUK, Kakinada, A.P., India, 533003

²Director, Sreenivasa College of Engineering & Technology, Kurnool, India, 518004

³Associate Professor and HOD, JNTU Kakinada, Kakinada, India, 533003

⁴Assistant professor, ST.Johns College of Engineering & Technology, Kurnool, India, 518360

Abstract: The DC-DC Converter topologies have received increasing attention in recent years for Low power and high performance applications. The advantages DC-DC buck converters includes increased efficiency, reduced size, reduced EMI, faster transient response and improved reliability. The front end LCL-T in a buck converter is connected in sequence manner to improve the electrical performances and to reduce the switching losses. It futures several merits such as multi output capability and also will associate with one or two capacitors so has to improve resonant operations. This paper deals with simulation and implementation of LCL-T buck converter. Open loop and closed loop models are developed and they are simulated. The digital simulation is done by using MATLAB/SimPowerSystems tool and the simulation results are presented here.

Index Terms: Digital simulation, LCL-T buck converter, High input voltage.

I. Introduction

Generally a LC parameters buck converter topology and its variations exhibit satisfactory performance in majority of applications where output voltage is lesser than input voltage. The performance of buck converter can be improved by implementing a buck converter with multiple switches and/or extra inductor parameters.

With conventional method the four switches must withstand the input voltage during the ‘off’ period. In certain applications such as railway traction the input voltages values will be high. Then each transistor would sustain only half of input voltage. This approach beyond the safe operating point of power transistors. It has leded the designer with narrow applications. The best way to meet the requirements is to increase the breakdown voltage of a transistor. It leads to the disadvantages of higher on resistance and increases the cost then it would be better if the device is operated at half of the value of the voltage. In conventional method single transistor is assumed as two transistors connected in series. The two switches share the voltage equally, with voltage balancing components.

Then definitely the two transistors have to with stand only half of its input voltages. The conventional method approaches satisfy well with disadvantages of increase in cost of eight power switches for the circuit and the voltages balancing device. In this paper the two legs of a full bridge are connected in series. The node joining these two legs is held at half of the input voltage, using the bypass/filter capacitors which are connected two inputs of rails.

The proposed circuit can be operated with

- 1) Capacitive turn –off neglecting to reduce switching power losses during turn-off (snubbing).
- 2) Resonant changes over which leads to zero voltage turn-on so as to eliminate turn-on switching losses

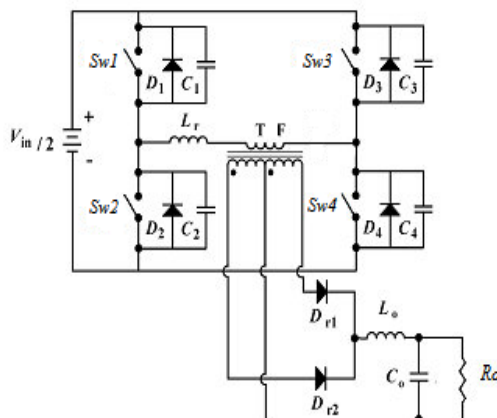


Fig 1. Conventional full-bridge converter

The coevals of new converter can be implemented by modifications in the connections of the components. First of all a capacitor is connected in series with a transformer as shown in fig 2.

The proposed converter circuit is designed by substituting input voltage source by two input capacitors as shown in fig 3. In this proposed circuit the upper leg consists of two switches Sw1 & Sw2 the lower leg consists of two switches Sw3 & Sw4.

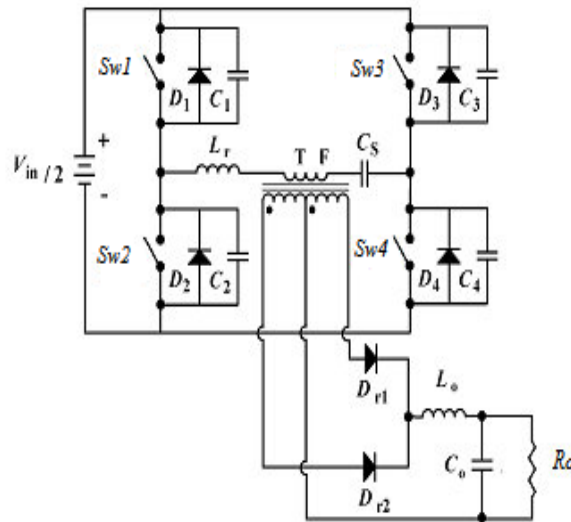


Fig. 2. Full-bridge converter with capacitor in series with transformer primary

II. LCL-T Buck Converter

The proposed converter is derived from the conventional full bridge topology presented in fig 1 and fig 2 respectively. Therefore, several operation characteristics of the full-bridge converter are also presented by the proposed structure. Fig 3 shows the power-stage circuit. The upper leg comprises The switches used in this circuit is metal oxide semiconductor field effect transistor (MOSFET). The internal substrate diode of a MOSFET switch conducts inverse polarity current and it also clamps the switching reverse voltage at about 1V, the capacitive turn-off snubbing is achieved by the MOSFET internal Con capacitances, which is used as C₁-C₄.

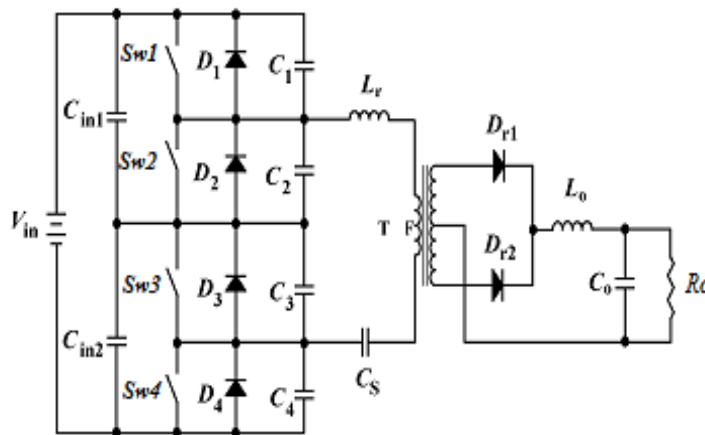


Fig.3. the proposed LCL-T Buck converter.

The capacitors Cin1 & Cin2 generate a bypassed dc midpoint voltage $V_{in}/2$ and by pass the input voltage.

When the switch is in "OFF" state each switch has a voltage of $V_{in}/2$ across its terminals. The dc voltage is blocked from being applied to L_r and TRF using the capacitance C_s the C_s capacitance value should be large enough to act as dc voltage source and to prevent the dc current being applied through L_r & TRF. The inductances L_r makes the capacitors C_1 - C_4 charges & discharges with its stored energy during the conduction period i.e provided between turning off one pair of switches & turning on the other pair. This makes the switch voltage to be zero before it is turned on. The isolation between the load and source is provided by the transformer. The diodes D_{r1} & D_{r2} rectify the rectangular wave output of a transformer. The inductances L_0 and capacitance C_0 filter the ripples from the rectified output.

From the output wave forms of proposed LCL-T type buck converter of fig 4, the voltage $V_{in}/2$ across the switches during off period is due to the join point of C_{in1} & C_{in2} which is at voltage $V_{in}/2$. The voltage across Sw1 or Sw2 is same as voltage at C_{in1} similarly the voltage of Sw3 or Sw4 are same as C_{in2} but both of those capacitor voltages are $V_{in}/2$.

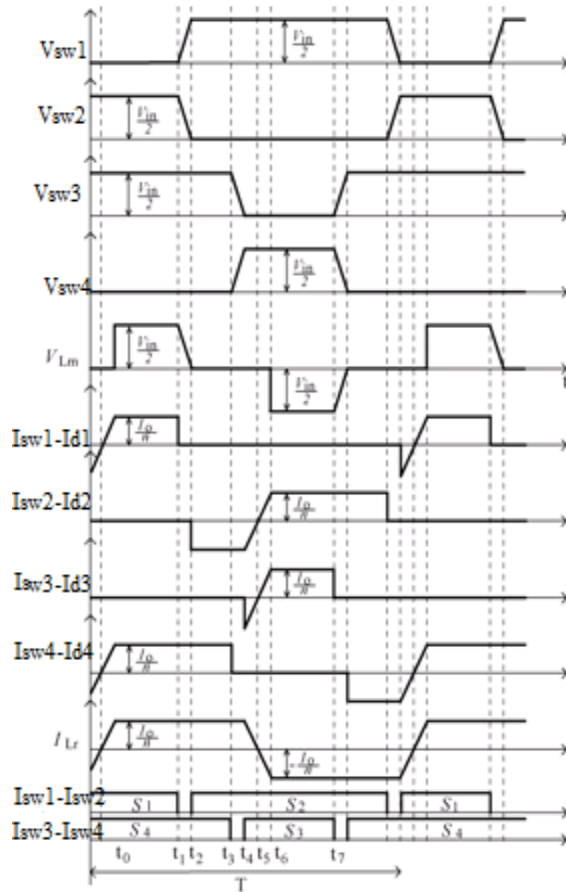


Fig.4. Waveforms of LCL-T type Buck Converter

The principle of operation is analyzed adopting ideal conditions, but some considerations must be done in a During the freewheeling period the capacitor's Cin1 & Cin2 will get charged & discharged, which occurs at the stage3 and at second half period of its operation .If the switch timing sequence of the switcher are a symmetry then the voltages across the capacitors can be other than the Vin/2. A very large asymmetry is needed to deviate from the ideal voltage value of Vin/2.

In first mode of operation the input capacitor's receiver energy from the source and in the sixth mode the stored energy is transferred to the load. The voltage source capacitor's are designed to have low ripple voltage 5% to 10%, these capacitor at converter start up discharged to Vcs=0. As server capacitance valve is very low. The voltage (Vcs) changes rapidly and in some switching cycle reaches a ideal valve. A current protection circuit is used to protect from excessive switch peak current during the transition.

B. Turn-On and Turn-Off Switching

Turn off:- In proposed converter the commutation process is similar to that of the classical Z Vs PWM full bridge converter. The loss that occurred during turned off are reduced by the snubber capacitors which are in parallel with the switches. The switch current flows through the commutation capacitor, changing the capacitor when it is turned off. Thus the capacitor voltage reaches the voltage Vc in. Due to this the voltage and current during crossing in the switch is minimized and the turn-off losses are minimized.

Turn on:- The proposed converter uses the zero-voltage turn-on to reduce the turn-on switching losses. The converter operating at high DC voltage the zero-voltage turn-on is very important, because the power dissipated in switching at non-zero discharged. Switches Sw2 and Sw4 turn-off in the power-transfer stage (stage 1 in Section III), and the output current referred to the primary accomplishes the charge and discharge of the snubber capacitors (linearly with time). The large stored energy of the ripple-filter inductor Lo is available for this purpose, so, as a practical matter, Sw2 and Sw4 and will always are turned-on at zero voltage.

But switches Sw3 and Sw4 turn-off in the free-wheeling stage during which the transformer is short circuited by the output rectifier. Thus, only the energy stored in the circuit inductance Lx (that includes the transformer primary- side leakage inductance) is available to charge and discharge the snubber capacitors, in a resonant way.

The minimum current that maintains zero-voltage turn-on for Sw1 or Sw3 is expressed in equation 1.

$$I_{min} = \frac{V_{in}}{2} \cdot \sqrt{\frac{2.C}{L_r}} \quad (1)$$

C is a snubber capacitor. The primary side current required to achieve zero-voltage turn on decreases as the value of (L_r) is large, but the inductance is limited by reduction of duty ratio.

III. SIMULATION RESULTS

Four switched Simulink model for LCL-T buck dc-dc converter is shown in fig 5, the input dc voltage is rectified into high switching AC frequencies using four switches LCL-T buck inverter.

Switching pulses are given to Sw1&Sw4, Sw2&Sw3 are shown in figures 6&7 and also their input voltages, output voltage & output current are shown in figures 8&9. The dc output voltage is variation at 600V.

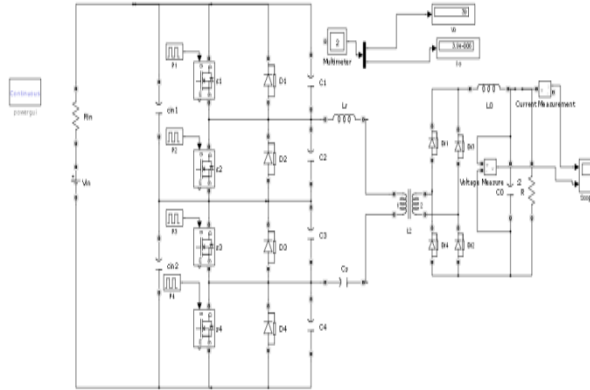


Fig 5. Simulation of the proposed LCL-T Buck converter.

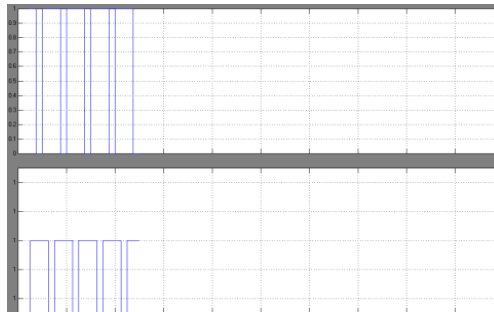


Fig 6. Driving pulses of S_1 & S_2

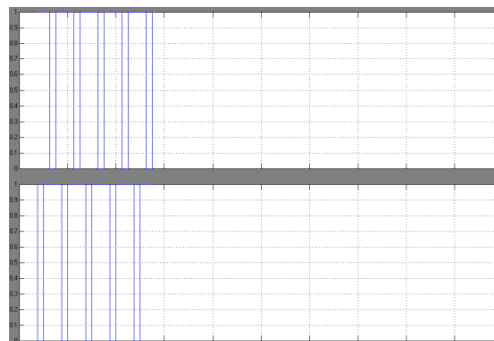


Fig 7. Driving pulses of S_3 & S_4

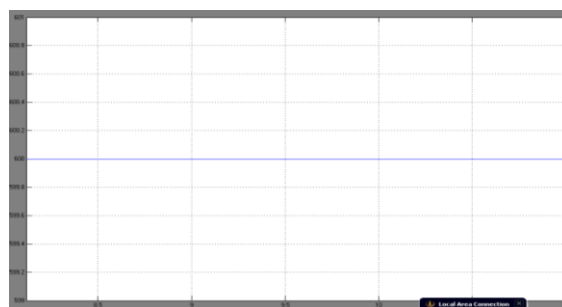


Fig.8 Input voltage

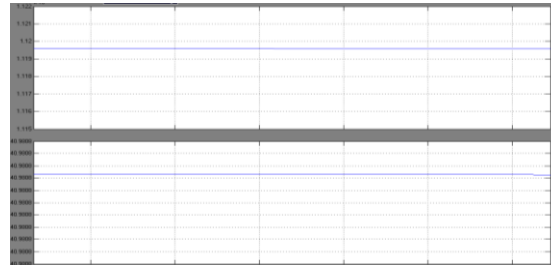


Fig.9 output voltage & output current

The closed loop system circuit model is shown in Fig 10. the closed loop system its output response is feedback and it is sensed, compared with an input reference voltage. The error can be through a PI controller. The output of PI controller refers with pulse width to maintain the output constant and their responses shown in Figures 11&12. it can be observe that the output voltage remains constant due to closed loop action of the system.

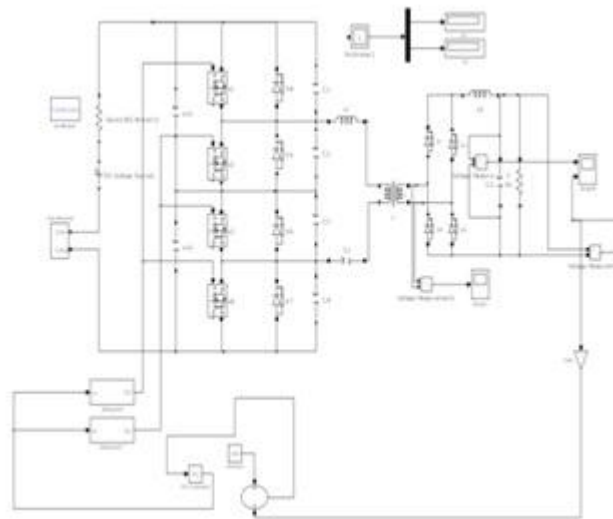


Fig.10. Closed loop model of two inductor boost Converter circuit

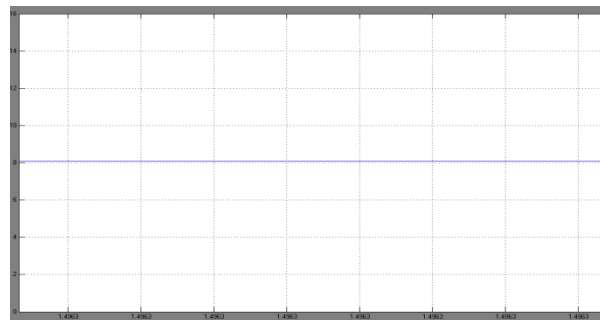


Fig.11 Input Voltage



Fig.12. Output voltage with disturbance

IV. Conclusion

The proposed four switch LCL-T buck dc-dc converter system is simulated using MATLAB/Simulink and the results are presented. And it is observed the switching losses have been reduced and the converter output efficiency is more than that of conventional full bridge buck converter.

And the open loop & closed loop controlled four switched LCL-T buck dc-dc converter system is simulated using MATLAB/Simulink and the results are presented. The closed loop system acquires constant voltage. This four switch LCL-T power circuit topology is well suited to its economical-realization.

References

- [1] E. S. Kim, Y. B. Byun, T. G. Koo, K. Y. Joe, and Y. H. Kim, "An improved three level ZVZCS Dc/Dc converter using a tapped inductor and a snubber capacitor," in Proc. Power Conversion Conf. (PCC'02), Osaka, Japan, 2002, pp. 115–121.
- [2] E. S. Kim, Y. B. Byun, Y. H. Kim, and Y. G. Hong, "A three level ZVZCS phase-shifted Dc/Dc converter using a tapped inductor and a snubber capacitor," in Proc. IEEE Applied Power Electronics Conf. (APEC), 2001.
- [3] F. Canales, P. M. Barbosa, and F. Lee, "A zero voltage and zero current switching three-level dc/dc converter," in Proc. IEEE Applied Power Electronics Conf. (APEC), 2000, pp. 314–320.
- [4] T. F. Wu and J. C. Hung, "A PDM controlled series resonant multi-level converter applied for x-ray generators," in Proc. IEEE Power Electronics Specialists Conf. (PESC), 1999.
- [5] I. Barbi, R. Gules, R. Redl, and N. O. Sokal, "Dc/Dc converter for high input voltage: four switches with peak voltage of $V_{in}/2$, capacitive turn-off snubbing and zero-voltage turn-on," in Proc. IEEE Power Electronics Specialists Conf. (PESC), 1998, pp. 1–7.
- [6] R. Redl and L. Balogh, "Soft-switching full-bridge dc/dc converting," U.S. Patent 5 198 969, Mar. 30, 1993.
- [7] J. R. Pinheiro and I. Barbi, "The three-level ZVS-PWM DC-to-DC converter," IEEE Trans. Power Electron., vol. 8, pp. 486–492, Oct. 1993.
- [8] L. Balogh, R. Redl, and N. O. Sokal, "A novel soft-switching full-bridge DC-DC converter: analysis, design considerations, and experimental resultant 1.5 kW, 100 kHz," IEEE Trans. Power Electron., vol. 6, pp.408–418, July 1991.



A Mallikarjuna Prasad has graduated from MADRAS university in the year 2001 and obtained his M.E from Sathyabama University in the year 2004, his nine years of teaching experience, exposed himself to be an authors for '3' titles currently he is working in the area of high power density dc-dc converters and also a research scholar in JNTU KAKINADA.



Dr D SubbaRayudu received B.E degree in Electrical Engineering from S.V. University, Tirupati, India in 1960; He has obtained his M.Sc (Engg) degree from Madras University in 1962 and Ph.D degree from Indian Institute of Technology, Madras, India in 1977. At present, he is working as Director in Sreenivasa College of engineering and Technology, Kurnool, India. Apart from his curriculum his interests is in Power Electronic Converters.



Dr S Sivanagaraju gained his Masters Degree in 2000 from IIT, Kharagpur and did his PhD from J.N.T. University in 2004. He is currently working as Associate professor and HOD in the Department of Electrical Engineering J.N.T.U. College of Engg, Kakinada, and Andhra Pradesh, India. For incredible performance he was awarded two national awards (*Pandit Madan Mohan Malaviya memorial prize award and Best paper prize award*) from the institution of engineers (India) for the year 2003-04. He is referee for IEE Proceedings-Generation Transmission and Distribution and also International journal of Emerging Electrical Power System. To his credit he has 50 publications in National and International journals and conference, His areas of interests Include, Distribution Automation, Genetic Algorithm application to distribution systems and Power Electronics.



U. CHAITHANYA has obtained his B.Tech from JNTU Ananthapur in the year 2008. He has obtained his M.Tech from JNTU University Ananthapur in the year 2010. He has 3 years of teaching experience.. He is working in the area of high power electronics and control applications.

Investigation on Behaviour of Fly Ash Based Geopolymer Concrete in Acidic Environment

Mr. K. Madhan Gopal,¹ Mr. B. Naga Kiran²

Assistant Professor, Department of civil Engg. RGM CET, Nandyal, India-518 501.

Abstract: Geopolymer concrete results from the reaction of a source material that is rich in silica and alumina with alkaline liquid. The term geopolymer was introduced by Davidovits; geopolymers are members of the family of inorganic polymers. Geopolymer binders have been reported as being acid resistant and thus are promising and alternative binders for sewer pipe manufacture. This paper presents experimental data on the Behavior of fly ash based geopolymer concrete exposed to 5% acid solutions for up to 4 weeks. A class F fly ash based geopolymer concrete was initially cured for 24 hours at 60°C. And also the obtained results were compared with the conventional concrete exposed to 5% acid solutions for up to 4 weeks. The compressive strength of geopolymer concrete and conventional concrete of 150-mm cubes at an age of 28 days were 32MPa and 48.5MPa, respectively. Initially concrete cubes were cured for a period of 28 days and later cubes were immersed in acid solutions, After immersion in a 5 % acid solutions, samples were tested at 7, 14 and 28 days. The mass loss, compressive strength reductions were determined. In this experimental work 3 type of acid solutions are used, i.e., HCl, H₂SO₄ and MgSO₄.

The results confirmed that Geopolymer concrete is highly resistant to acid in terms of a very low mass loss and compressive strength loss when compared to conventional concrete.

Key Words: Geopolymer; Fly ash; Alkaline Liquid; Acid Resistance; Acidic Environment

I. Introduction

In spite of a long-term recognition of the problem of sulphuric acid corrosion in concrete sewer pipes, this issue has not been satisfactorily resolved. A research looked at ways of enhancing the acid resistance of Portland Cement (PC) based concretes, using the partial replacement of Portland cement by supplementary materials, the use of epoxy modified binders, and the use of limestone as a sacrificial aggregate [Song et al 2003]. The acid attack in terms of mass loss was reduced; however, even the improved concretes lost significant mass with immersion time.

Sulphuric acid resistant binders are still required to enhance the long-term performance of concrete in sulphuric acid corrosion environments. Geopolymer binders might be a promising alternative in the development of acid resistant concrete. Since Geopolymers are a novel binder that relies on alumina-silicate rather than calcium silicate hydrate bonds for structural integrity, they have been reported as being acid resistant.

This paper reports experimental data on the response of Alkaline Activated Fly ash based Geopolymer (AAFG) concrete against 5% acid solutions for up to 4 weeks, in terms of visual inspection, mass change, and residual compressive strength. In this experimental work 3 type of acid solutions are used, i.e., HCl, H₂SO₄ and MgSO₄. And also the obtained results were compared with the conventional concrete exposed to 5% acid solutions for up to 4 weeks.

II. Mix Design Of Geopolymer And Conventional Concrete

2.1 CONVENTIONAL CONCRETE

Grade of concrete is M30

Mix proportion (1m³ of concrete):

Water : Cement : FA : CA : 191.6 : 430.00 : 538.70 : 1214.91
 0.45 : 1 : 1.25 : 2.82

2.2 GEOPOLYMER CONCRETE

Materials	Mass (kg/m ³)	
Coarse aggregates:	20 mm	277
	14 mm	370
	7 mm	647
Fine sand		554
Fly ash (low-calcium ASTM Class F)		394
Sodium silicate solution(SiO ₂ / Na ₂ O =2)		113
Sodium hydroxide solution		45 (8 Molar)

Table 1: Geopolymer Concrete Mixture Proportions

III. Materials

Fly ash: Fly ash belonging to class-F obtained from Vijayawada thermal Power Station in Andhra Pradesh was used in the present investigation. The specific gravity of the fly ash was 1.975.

Alkaline Liquid: A combination of sodium silicate solution and sodium hydroxide solution was chosen as the alkaline liquid.

Fine aggregate: The fine aggregate used is natural sand obtained from the river Godavari conforming to grading zone-II of table 4 of IS: 383-1970. The specific gravity of the fine aggregate was 2.61.

Cement: The type of cement used all throughout the experiment was Ordinary Portland Cement of grade 53. The specific gravity of the fly ash was 3.10.

Coarse aggregate: The crushed coarse aggregate of maximum size 16 mm, 60% of it passing through 16 mm IS sieve and retaining on 12.5mm IS sieve and 40% of this passing through 12.5 mm IS sieve and retaining on 4.75 mm IS sieve size obtained from the local crushing plant, Rajahmundry, East Godavari, is used in the present study. The specific gravity of the coarse aggregate was 2.77.

Water: Potable fresh water available from local sources was used for both mixing and curing.

Acids: The various acids used in the investigation are HCl, H₂SO₄ and MgSO₄ each of 5% concentration.

IV. Experimental Programme

In this experimental work, properties of materials used in the experimental work were determined. Then Fly ash based geopolymer concrete cubes and conventional concrete (M30 Grade) cubes of size 150mm×150mm×150mm were cast.

Now, geopolymer concrete cubes and conventional concrete cubes were cured for a period of 28 days. Generally, heat curing is recommended for geopolymer concrete and heat curing was done at a temperature of 60⁰c for a period of 24 hours. After completion of curing process, weight of both conventional and geopolymer concrete cubes were taken. Later, concrete specimens were immersed in 5% of acidic solutions (HCl, H₂SO₄, MgSO₄) for a period of 7, 14, 28 days.

After completion of immersion period, concrete specimens were taken out and allowed for drying for a period of 1 day and weight of concrete cubes were determined. And also, the compressive strength of concrete cubes after acid immersion was determined by using U.T.M. and the obtained results are compared. Residual compressive strength and percentage weight loss of geopolymer and conventional concrete cubes after acid immersion have been studied and compared.

Compressive strength of reference mixes:

Compressive strength of geopolymer concrete after 28 days of curing was 32MPa

Compressive strength of conventional concrete after 28 days of curing was 49.53 MPa.

V. Results And Discussion

The compressive strength test on hardened concrete was performed on U.T.M. Three 150x150x150 mm concrete cubes were tested for every compressive strength test. The results given in various Figures and Tables are the mean of these values. The curing media was replaced with fresh solution at the end of every week to maintain the same concentration (5%) throughout the exposure period.

Residual compressive strength on acid immersion:

S.No	Type of concrete	Compressive strength at 28days (Before acid immersion) (N/mm ²)	Compressive strength After 7 days of acid immersion (N/mm ²)		
			Type of Acid		
			HCl	H ₂ SO ₄	MgSO ₄
1	C. C(M30)	49.53	44.34	35	45
2	G.C	32	29.44	27.36	28.8

Table 2: Residual compressive strength after 7 days of acid immersion.

S.No	Type of concrete	Compressive strength at 28days (Before acid immersion) (N/mm ²)	Compressive strength After 14 days of acid immersion (N/mm ²)		
			Type of Acid		
			HCl	H ₂ SO ₄	MgSO ₄
1	C. C(M30)	49.53	42.35	29	44
2	G.C	32	28.6	25.69	27.52

Table 3: Residual compressive strength after 14 days of acid immersion.

S.No	Type of concrete	Compressive strength at 28days (Before acid immersion) (N/mm ²)	Compressive strength After 28 days of acid immersion (N/mm ²)		
			Type of Acid		
			HCl	H ₂ SO ₄	MgSO ₄
1	C. C(M30)	49.53	40.86	21	42
2	G.C	32	27.5	23.2	26.4

Table 4: Residual compressive strength after 28 days of acid immersion.

Percentage loss of compressive strength after acid immersion:

S.No	Type of concrete	% loss of Compressive strength After 7 days of acid immersion(N/mm ²)		
		Type of Acid		
		HCl	H ₂ SO ₄	MgSO ₄
1	C. C(M30)	11	29.76	9.61
2	G.C	8	14.5	10

Table 5: Percentage loss of compressive strength after 7 days of acid immersion.

S.No	Type of concrete	% loss of Compressive strength After 14 days of acid immersion (N/mm ²)		
		Type of Acid		
		HCl	H ₂ SO ₄	MgSO ₄
1	C. C(M30)	15	41.80	11.69
2	G.C	9.9	19.7	14

Table 6: Percentage loss of compressive strength after 14 days of acid immersion.

S.No	Type of concrete	% loss of Compressive strength After 28 days of acid immersion (N/mm ²)		
		Type of Acid		
		HCl	H ₂ SO ₄	MgSO ₄
1	C. C(M30)	18	57.85	15.65
2	G.C	14.06	27.5	17.5

Table 7: Percentage loss of compressive strength after 28 days of acid immersion.

Durability Studies

S.No	Type of Acid	Weight of concrete cubes after 28 days of casting and before acid immersion in days for (Kg)			Weight of concrete cubes after acid immersion in days (Kg)		
		7	14	28	7	14	28
		1	HCl	8.78	8.80	8.76	8.58
2	H ₂ SO ₄	8.79	8.78	8.7	8.30	8.20	8.0
3	MgSO ₄	8.78	8.79	8.8	8.60	8.60	8.56

Table 8: Conventional concrete

S.No	Type of Acid	Weight of concrete cubes after 28 days of casting and before acid immersion in days for (Kg)			Weight of concrete cubes after acid immersion in days (Kg)		
		7	14	28	7	14	28
		1	HCl	7.84	7.85	7.83	7.8
2	H ₂ SO ₄	7.95	7.78	7.82	7.87	7.64	7.65
3	MgSO ₄	7.88	7.9	7.8	7.85	7.86	7.74

Table 9: Geopolymer concrete

Percentage weight loss on acid immersion.

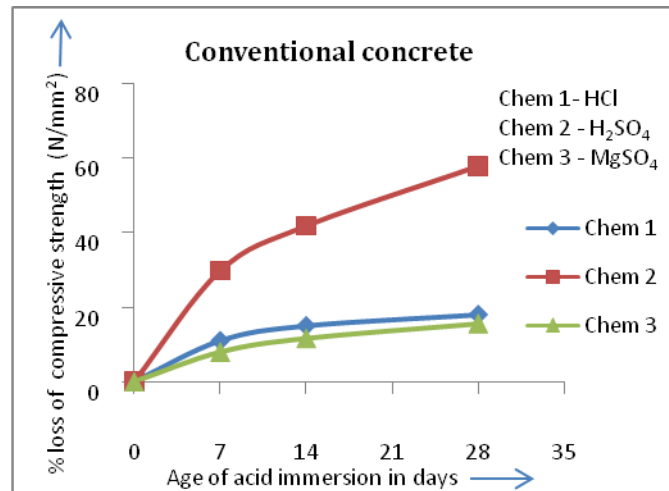
S.No	Type of Acid	% Weight loss of concrete cubes after acid immersion		
		Age of acid immersion in days		
		7	14	28
1	HCl	2.2%	3.06%	3.76%
2	H ₂ SO ₄	5.5%	6.6%	8%
3	MgSO ₄	2.0%	2.16%	2.72%

Table 10: Conventional concrete

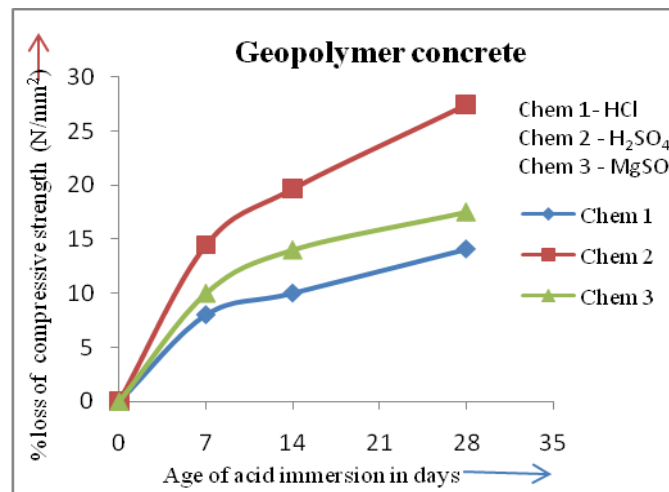
S.No	Type of Acid	% Weight loss of concrete cubes after acid immersion		
		Age of acid immersion in days		
		7	14	28
1	HCl	0.4%	0.7%	0.9%
2	H ₂ SO ₄	1.0%	1.7%	2.2%
3	MgSO ₄	0.3%	0.5%	0.7%

Table 11: Geopolymer concrete

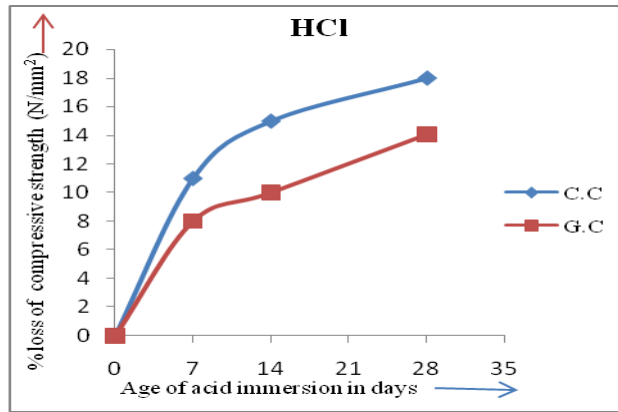
GRAPHS



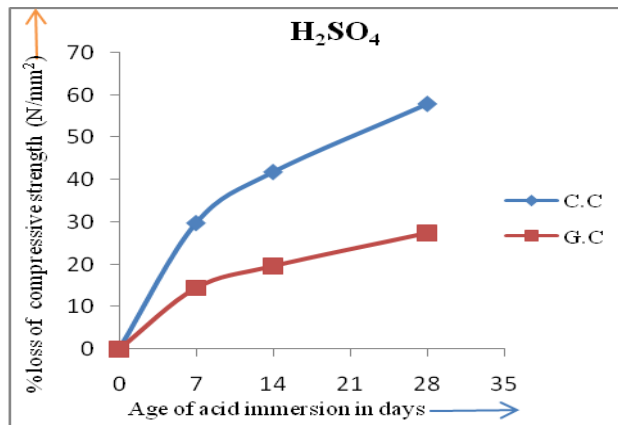
Graph 1: % loss of compressive strength in Conventional concrete



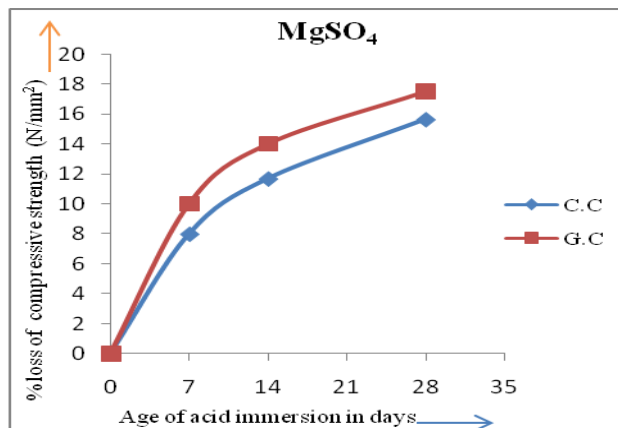
Graph 2: % loss of compressive strength in Geopolymer concrete



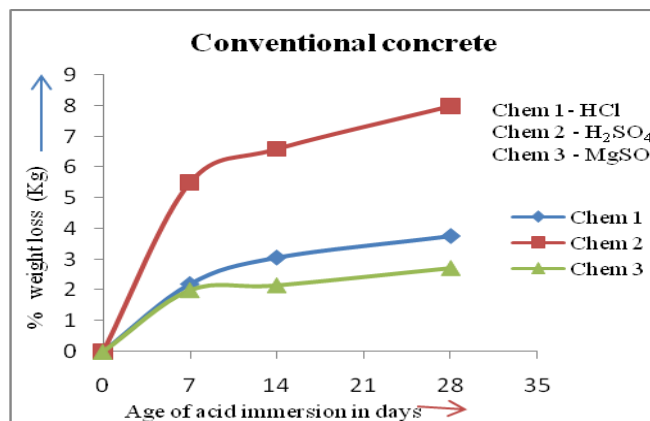
Graph 3: % loss of compressive strength in HCl acid



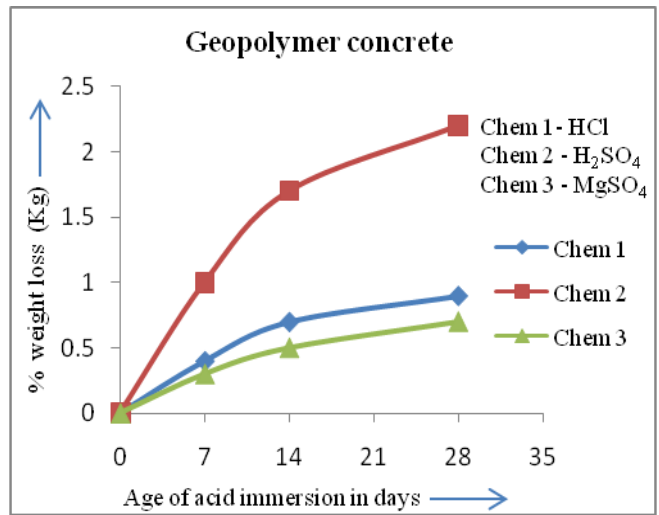
Graph 4: % loss of compressive strength in H₂SO₄



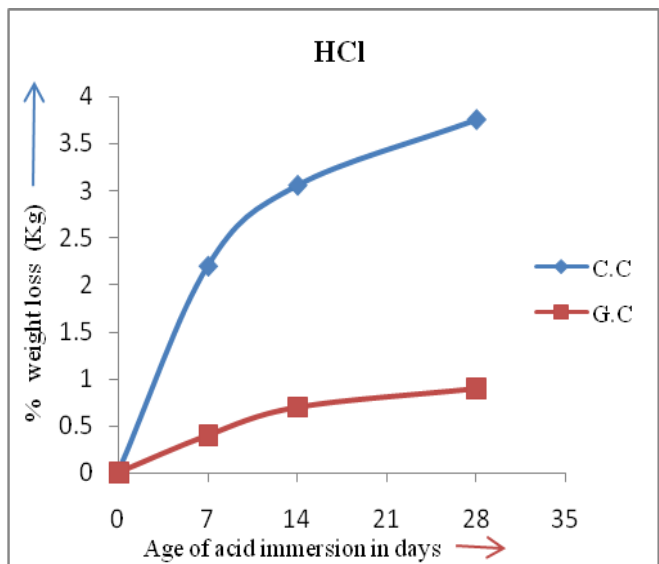
Graph 5: % loss of compressive strength in MgSO₄



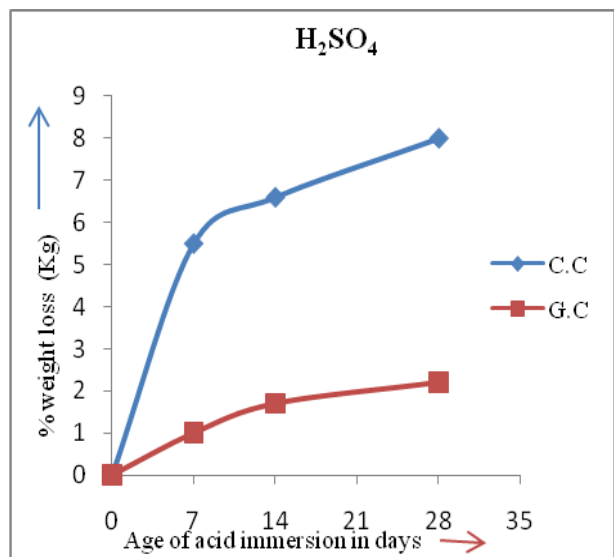
Graph 6: % weight loss in Conventional concrete



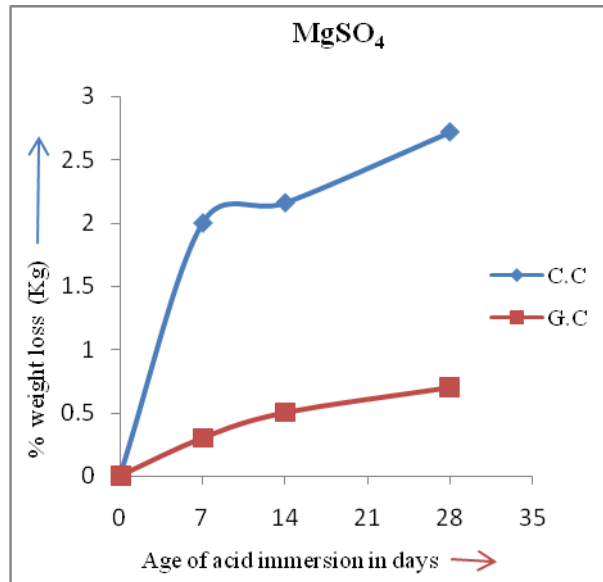
Graph 7: % weight loss in Geopolymer concrete



Graph 8: % weight loss in HCl acid



Graph 9: % weight loss in H₂SO₄ acid



Graph 10: % weight loss in MgSO₄ acid

VI. Conclusions

The following conclusions are made based on the laboratory experiments carried out in this investigation.

1. Geopolymer concrete mixes resisted acid attack in a better way as compared to conventional concrete at all ages of exposure to HCl, H₂SO₄.
2. It is observed that the percentage loss of Compressive strength of all Geopolymer Concrete mixes are considerably lower than that of Conventional concrete mixes at all ages of acid exposure.
3. It is also observed that the maximum loss of compressive strength and weight occurs in case of H₂SO₄ acid immersion as compared to HCl and MgSO₄.
4. The loss of compressive strength of conventional concrete is almost double the loss of compressive strength of geopolymer concrete in H₂SO₄ acid immersion at all ages.
5. The percentage weight loss of Conventional concrete is more when compared to Geopolymer concrete. This is true for all the acids tried in this investigation.
6. It is observed that the loss of compressive strength of Geopolymer concrete is more when compared to conventional concrete in MgSO₄ immersion. So Geopolymer concrete is sensitive to MgSO₄.
7. The weight loss of Geopolymer concrete is very low when Geopolymer concrete mixes are exposed to 5% acid attack.

References

- [1] Bakharev, T. (2005a). Durability of geopolymer materials in sodium and magnesium sulfate solutions. Cement And Concrete Research
- [2] Davidovits, J. (1988b). Geopolymer Chemistry and Properties.
- [3] Davidovits, J. (1991). Geopolymers: Inorganic Polymeric New Materials. Journal of Thermal Analysis.
- [4] Davidovits, J. (1994b). Properties of Geopolymer Cements.
- [5] Hardjito, D., Wallah, S. E., & Rangan, B. V. (2002b). Study on Engineering Properties of Fly Ash-Based Geopolymer Concrete.
- [6] Hardjito, D., & Rangan, B. V. (2005). Development and Properties of Low-Calcium Fly Ash-Based Geopolymer Concrete. Research Report GC1, Perth, Australia: Faculty of Engineering, Curtin University of Technology.

A Microstrip Patch Antenna with Aperture Coupler Technique At 5.8 GHz & 2 GHz

Manpreet Kaur,¹ Mrs. Amanpreet Kaur,² Dr. Rajesh Khanna³

¹Student, ECED Thapar University, Patiala
²Astt.Professor, ECED Thapar University, Patiala
³Professor, ECED Thapar University

Abstract: This paper presents the basic design of a microstrip patch antenna with aperture coupling. This design is simulated using CST Microwave Studio 2009 software based on given operating frequency. The gain and Directivity of an antenna are 6.169dB and 5.580dBi at 5.8GHz & 7.699dB and 8.480dBi at 2GHz. The results are analyzed and discussed in terms of return loss, gain, directivity. E and H-fields and radiation pattern using CST Microwave Studio.

Keywords: Aperture coupled microstrip patch antenna (ACMPA), return loss, bandwidth, gain, Single feed Single frequency, CST2009 Microwave Studio.

I. Introduction

Modern wireless communication systems are developing rapidly, and bandwidth requirement for many applications increases day by day, so an antennas which, is required to have a wideband, good radiation performances and gain. This requirement can be fulfilled by a new aperture coupled micro strip antenna for low & high frequencies. "A review of aperture coupled micro strip antennas". This paper gives history, operation, development and application of microstrip antenna [5]. Single layer microstrip line feed elements are typically limited to bandwidths of 2 to 5%. But aperture coupled antenna provides up to 10 to 15 % bandwidth with single layer [6-8]. The simple designing and easy manufacturability of the microstrip patch antenna make it preferred choice for many wireless applications. [1]

Figure1 shows an overview of a micro strip patch antenna design with aperture coupled technique. In this figure two substrates; one for feed line and another for patch are formed. A slot is formed at centre of ground and feed line is below the second substrate as shown in figure 1.

These types of antennas are more popular, because of the patches and slots can be any shape and this gives the improvement in the performance of micro strip patch antennas.

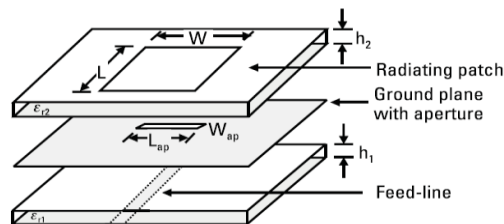


Figure1: Basic micro strip patch antenna with aperture coupler technique

II. Design-I: Microstrip patch Antenna at 5.8GHz

To design a single micro strip patch antenna which consists of a rectangular patch, a rectangular slot and a feed line are attached to different substrate or same substrate and these are interfaced to each other through slot in ground. The selection of antenna dielectric substrate is very important for better performance with required thickness and loss tangent. Substrate used is an important factor in designing a micro strip antenna .The dielectric constants are usually in the range of $2.2 \leq \epsilon_r \leq 12$ depending on the substrate used.

Basic design steps for designing are given below: [2].

1. For given value of dielectric constant 4.7 and operating frequency 5.8Ghz, & the height of substrate the remaining parameters for patch and feed line are calculated using the following equations and the final values are given in table (i):

The length and width of patch can be calculated after calculating the values of effective length(ΔL) and effective dielectric constant (ϵ_{eff}) by selecting any substrate (any value of ϵ_r) [9-10]. After calculation of LP and WP, next step is to calculate:

Now we calculate L and W of ground (Substrate Dimension):

- a) We calculate W of ground using the equation given below:

$$W_g = 6h + W \dots \dots \dots (i)$$

b) We calculate L of ground using the equation given below:

$$L_g = 6h + L \dots \dots \dots (ii)$$

TableI:-Dimension of the designed antenna with aperture feed:

Operating frequency	5.8GHz
Return Loss	<-10dB
Substrate Material	FR4
Substrate Height	1.6mm
Copper Thickness	0.035mm
Dielectric Constant	4.7
Patch	4.3×8.5mm
Feed	3.8×1.3mm
Slot	3×1.4mm

III. CST Simulation Results and patterns: Return Loss & Smith Chart

The return loss should be maximum for better performance and wideband requirement. Thus we measure required band at return loss -10dB. The return loss plot for the designed antenna with aperture feed is shown in figure 2 as below. The bandwidth is about 566.8MHz (6.216-5.6491GHz), from figure 3 it is clear that the antenna is matched at 50Ω impedance which shows the impedance bandwidth of the antenna is 567MHz [3].

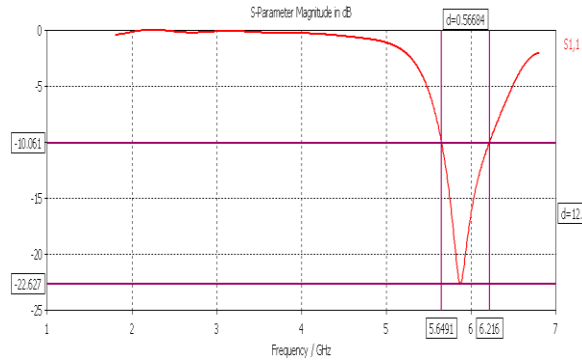


Figure 2: Return loss

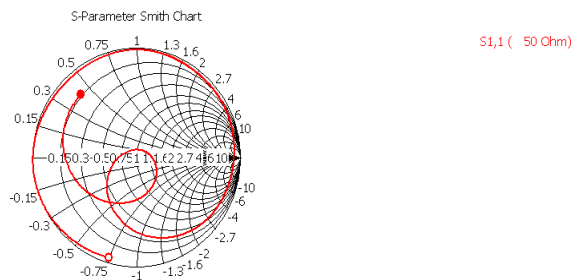


Figure3: Smith chart [S11]

Radiation Pattern:

An antenna radiation pattern is defined as “a mathematical function or a graphical representation of the radiation properties of the antenna as a function of space co-ordinates. Figure 4 shows the 3Dradiation pattern plot for the proposed antenna with 6.169dB gain at 5.8GHz frequency.

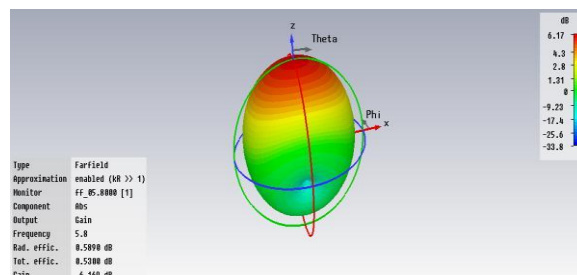


Figure4: 3D-Radiation pattern plot

E-field:

Figure 5 shows the E-field 3D-plot for the proposed antenna with $E_{max} = 20.53\text{dBV/m}$ at 5.8GHz frequency.

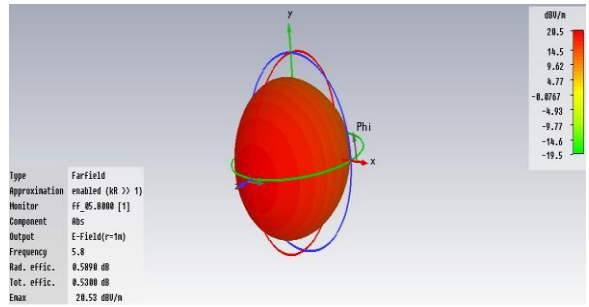


Figure5: 3D-field-plot

Gain:

Gain of an antenna in Figure 6 shows the gain is 6.169dB with main lobe 6.2dB for polar- plot of the proposed antenna.

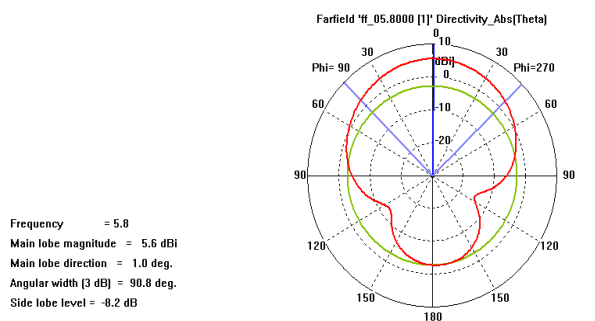


Figure6: Gain polar- plot

Directivity:

The directivity of an antenna is the ratio of the radiation intensity in a given direction from the antenna to the radiation intensity averaged over all directions. Figure7 shows directivity 5.580dBi at 58GHz for far-field and polar-plot in Figure8

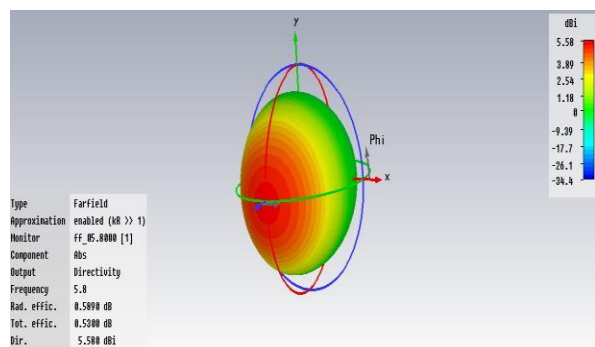


Figure7-3D directivity plot

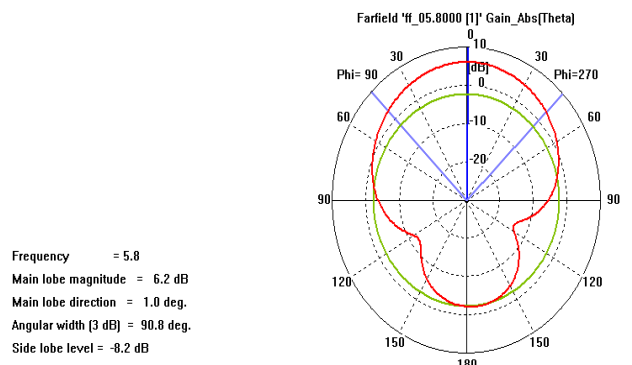


Figure8: polar- plot of directivity

VSWR:

The VSWR is shown in figure9 below. As it is known that for an antenna to have a considerable performance with best matching the VSWR should be <2, this antenna having a VSWR of 1.159 shows desired performance characteristics.

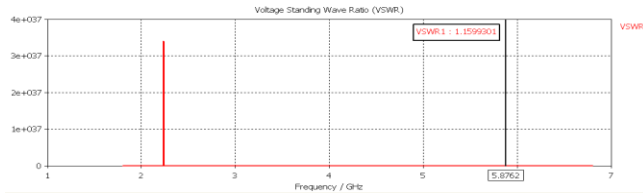


Figure9: VSWR

Design-II: Antenna at 2.2GHz (WLAN): This is another proposed antenna with aperture fed for WLAN covering the 2.4 GHz band. The radiating patch and the microstrip feed line are separated by the ground plane. Coupling between the patch and the feed line is made through a slot or an aperture cut in the ground plane. Also there is a third substrate used between patch and ground. The dimensions which are considered from for increasing BW of the antenna with aperture feed are given in table below and these are calculated using the procedure discussed above in the eq: [4]

Table II:-Dimension of the designed antenna with aperture feed:

Operating frequency	2GHz
Return Loss	-10dB
Substrate Material	FR4,Foam
Substrate Height (mm)	1.58,17
Patch	24×33mm
Dielectric Constant	4.4, 1.07

In the design air/foam (permittivity=1/1.07) has been used as antenna substrate with a thickness of 17mm.

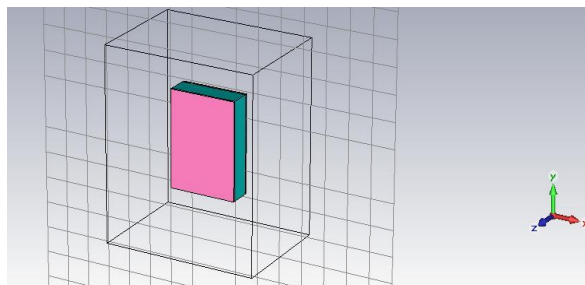


Figure10: Geometry dimension of antenna

This is diagram using CST2009 for aperture coupled antenna. In this case we use FR4, Foam material as a substrate and the basic dimensions are given in table above.

IV. Return Loss & Smith Chart

The return loss should be maximum for better wideband requirement. Thus we measure return loss at -10dB. The return loss plot for the designed antenna is shown in figure11 as below. The 10dB BW is about 431.36MHz (2.3372-1.9059GHz). Figure 12 shows the smith chart results at 52.88Ω impedance.

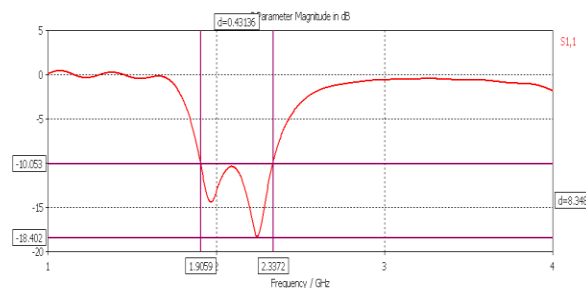


Figure11: Simulated return loss [S11]

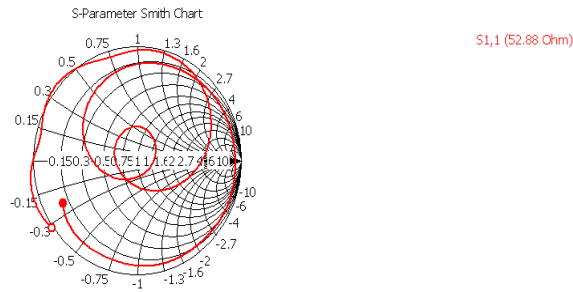


Figure12: Smith chart [S11]

Radiation Pattern:

Figure13 shows the radiation pattern plot for the proposed antenna with gain 8.480dB at

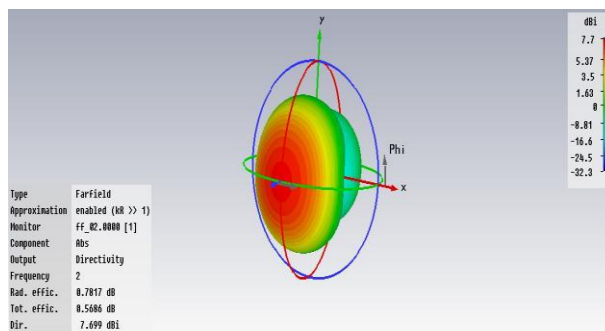


Figure13: 3D Radiation pattern plot

2GHz frequency for far-field

H-field:

Figure14 & Figure15 shows the H-field 3D-plot & H-field polar-plot for the proposed antenna with $H_{max} = -28.49\text{dBA/m}$ at 2GHz frequency.

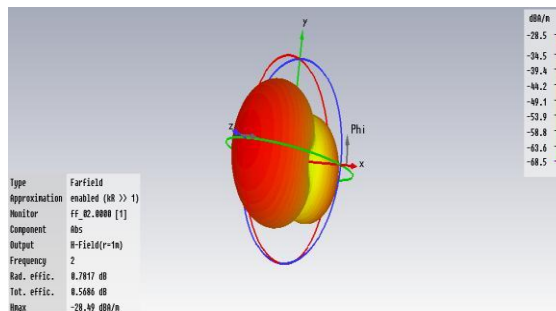


Figure14: 3D-plot H-field

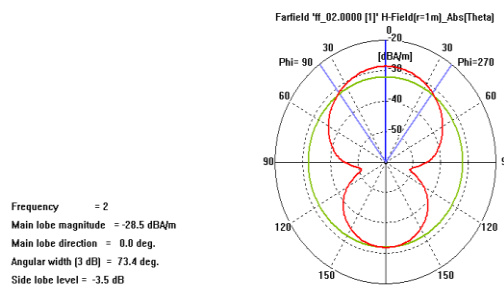


Figure15: polar-plot of H-field

Gain:

Figure16 shows the (gain) 3D-plot for the proposed antenna.

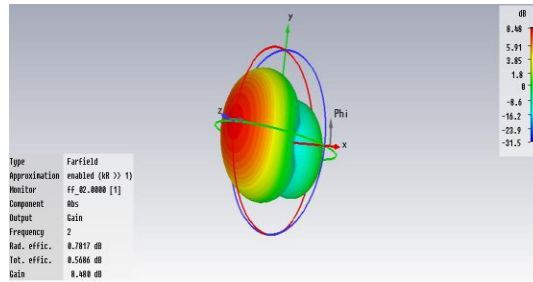


Figure-16

Directivity:

Figure17 show directivity 7.699dBi at 2GHz for far-field. Directivity polar-plot is shown below in Figure 23.

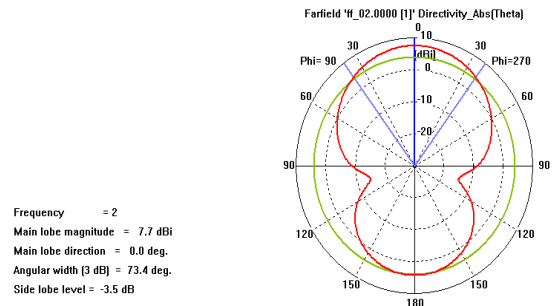


Figure17: polar- plot of directivity

V. Effects of varying different parameters of the antenna

Patch L and W:

As the patch length is increased the Resonating frequency decreases. And as patch width increased the resonant resistance decreases and it also affects the resonant frequency. Figure 18 shows the graph for width of patch. At $w = 33$ we are getting an optimized performance.

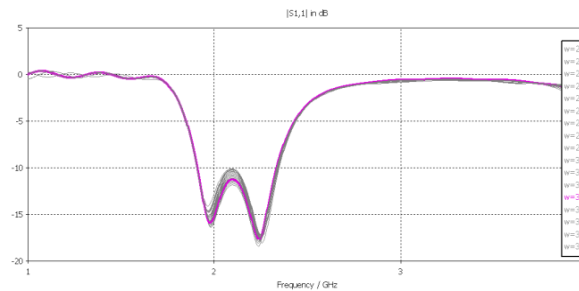


Figure18: width of patch

Slot L and W

The coupling level is primarily determined by the length of the coupling aperture, as well as back radiation level. The aperture should therefore be made no larger than is required for impedance matching. When the aperture length is increased then the return loss increased. If the ratio for L and W of slot is 1/10, there is decrease in the coupling level. Figure19 and figure20 shows the graph for sweep on width and selected width of slot, here „i” is slot width and „f” is the length, at figure21 and figure22 shows the length of slot. The $i=2.8$ and $f=5.88$ is selected.

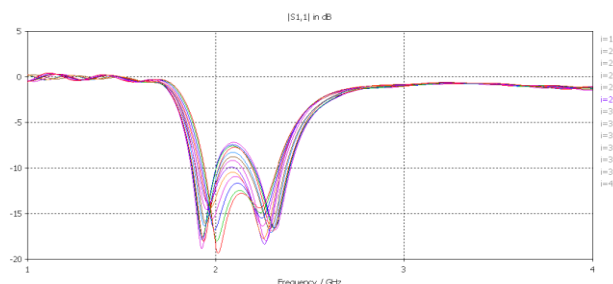


Figure19: Widthofslot

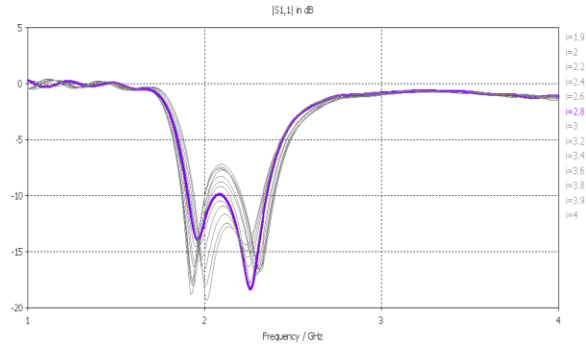


Figure20: Selected slot width

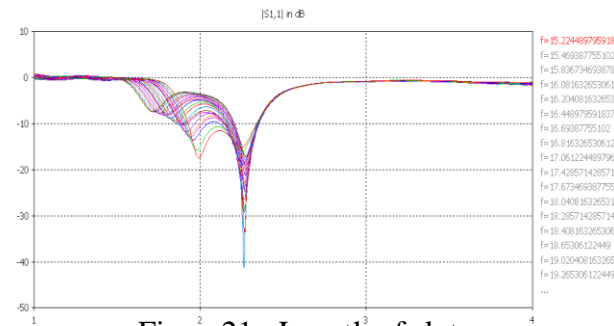


Figure21: Length of slot

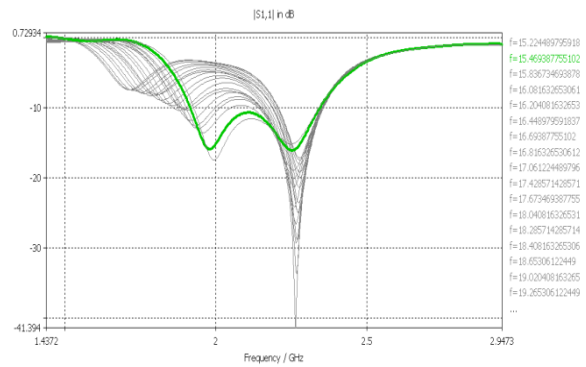


Figure22: Selected length of slot

Feed L and W:

The length of feed also affects the coupling level. When length of feed increased, there is decrease in coupling level. The width of feed controls the line impedance of the feed. The feed line width is represented by „p” as shown in Figure23 below and p=2 is selected.

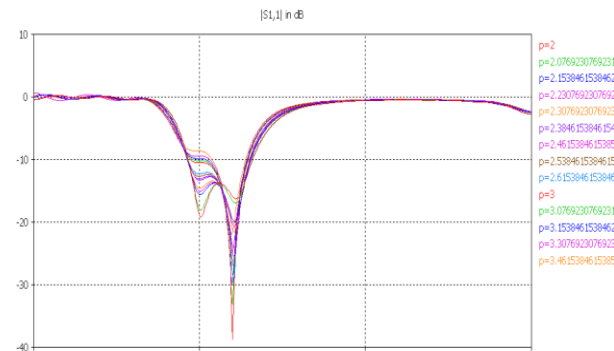


Figure23: Width of feed

VI. Results and discussion

The single band antennas, in first design, it resonates in (6.216-5.6491GHz) with BW of about 566.8MHz, which covers the WiMAX range. In second design, it resonates in (2.3372-1.9059GHz) with 10dB bandwidth is about 431.36MHz for WLAN. The minimum return loss is obtained at the resonating frequency 5.8GHz is -22.627dB. The line impedance of the antenna is 50Ω and at 2GHz return loss is -18.422dB with line impedance 52.88Ω. The parameters that are studied at different frequencies of antennas are listed in the TableIII.

TableIII: Comparision

Parameters	Single Band	Single Band
Frequency	5.8GHz	2GHz
Directivity (dBi)	5.580	7.699
Gain (dB)	6.169	8.480
E-field(dB V/m)	20.53	23.04
H-field(dB A/m)	-30.99	-28.49

VII. Conclusion and Scope

It is concluded that the antennas designed for resonant frequencies of 5.8GHz and at 2GHz give very good results with the optimized selected dimensions. The directivity and gain of the antenna are good enough to be used for the personal communication system and WiMAX/WLAN applications. The antennas has simulated for the desired results. Further the antennas can be fabricated using the selected substrates following IC fabrication techniques and then these can be tested for the desired performance in an anechoic chamber using a VNA.

References

- [1] D. M. Pozar, "Microstrip antenna aperture-coupled to a microstripline", Lett, vol. 21, no. 2, pp. 49-50, Jan. 1985.
- [2] C. A. Balanis, Antenna Theory, 3rd ed. John Wiley & Sons, Hoboken, NJ, 2005.
- [3] M. T. Ali, S.Muhamud @ Kayat, N.R.Abd Rahman, and Norsuzila Ya'acob,"A Microstrip Patch Antenna with Aperture Coupler Technique at 5.8 GHz" IEEE International Conference on System Engineering and Technology (ICSET), 2011. [4] Srivatsa Bhargava J "Aperture coupled Wide-Band Micro Strip Antenna Design"
- [5] David M. Pozar, "A Review of Aperture coupled Microstrip Antennas" History, Operation, Development, and applications.
- [6] J. -F. Zurcher, "The SSFIP: A global concept for high performance broadband planar antennas", Electronics Letters, vol.24, pp.1433-1435, November 1988.
- [7] Stephen D. Targonski and David M. Pozar, Fellow, "Design of Wideband Circularly Polarized Aperture-Coupled Micro strip Antennas" IEEE Transaction on Antennas and Propagation, Vol. 41, NO. 2, pp.214-220, Feb 1993.
- [8] F. Croq and A. Papiernik, "Large Bandwidth aperture-coupled microstrip antenna", Electronics Letters, Vol. 26, pp.1293-1294, 2nd August 1990.
- [9] Rajesh Kumar Vishwakarma, Sanjay Tiwari, "Aperture Coupled Microstrip Antenna for Dual-Band" Wireless Engineering and Technology, 2011, 2.93-101.
- [10] Manoj Singh, Ananjun Basu and S.K.Koul "Design of Aperture Coupled Fed Microstrip Antenna for Wireless Communication", IEEE, Indian Conference, Pg No: 1-5, 2006

Generation and Transmission of Electrical Power through Solar Power Satellite (SPS)

Mr. Gaurav Tanwar,

Asstt. Prof. Mohd. Ilyas, Mr. Raj Kumar Singh

Abstract: In this paper a new technique is discussed to generate and transmit electrical power using solar power. The solar energy can be converted into electrical energy by using solar cells. Solar energy is available in large amount continuously in free space which can be utilized by solar power satellite (SPS) to convert it into electrical form. This electrical power can be transmitted to the earth using microwave technology which can be received by using rectifying antenna placed on the ground. Rectenna must have a diameter of about 2-3 Km range.

Index Terms: Solar power satellite (SPS), Rectenna, Transmitted, Microwave technology.

I. INTRODUCTION

Solar power satellite (SPS) attracts attention as clean energy which does not take out CO₂ and can solve an environmental problem and the energy problem of drain of a fossil fuel. In outer space there is an uninterrupted availability of huge amount of solar energy in the form of light and heat. So the use of satellites primarily aimed at collecting the solar energy and beam it back to the earth is being considered. Efficiency is much higher than the solar power placed on the ground as a base power supply which can be supplied for 24 hours. As a consequence of an ever-increasing world-wide energy demand and of a need for a clean energy source, the solar power satellite (SPS) concept has been explored by scientists and engineers. In a typical SPS system, solar energy is collected in space by a satellite in a geostationary orbit. The solar energy is converted to direct current by solar cells, and the direct current is in turn used to power microwave generators in the gigahertz frequency (microwave) range. The generators feed a highly directive satellite-borne antenna, which beams the energy to the Earth. On the ground, a rectifying antenna (rectenna) converts the microwave energy from the satellite into direct current, which, after suitable processing, is fed to the terrestrial power grid. Two critical aspects that have motivated research into SPS systems are the lack of attenuation of the solar flux by the Earth's atmosphere, and the twenty-four-hour availability of the energy, except around midnight during the equinox periods.

II. DESIGNING PARAMETERS

A solar power satellite is a very large-area satellite in an appropriate orbit, which would function as an electric power plant in space. The satellite would consist of three main parts: a solar-energy collector to convert solar energy into dc electric power, a dc-to-microwave converter and a large antenna array to beam the microwave power to the ground. For the production of 1 GW of dc power, the solar collector would need to have an area of 10 km², and would consist of either photovoltaic cells or solar thermal turbines. The dc-to-microwave converter could be realized using either a microwave-tube system or a semiconductor system, or a combination of both. For transmitting the power to the ground, frequency bands around 5.8 GHz or 2.45 GHz have been proposed, which are within the microwave radio windows of the atmosphere. Concerning the power transmission efficiency of the WPT, there are some good optical approaches in Russia [2] [3].

In addition to the SPS orbiter, a ground-based power-receiving site has to be constructed, consisting of a device to receive and rectify the microwave power beam, i.e. to convert it back to dc electric power. This device is called a rectenna (rectifying antenna). The dimensions of the rectenna site on the ground depend on the microwave frequency and the size of the transmitting antenna. A model system, operating at 2.45 GHz, would use a rectenna site with a diameter of 4 km and a satellite-based transmitting antenna with a diameter of 2 km. The peak microwave power-flux density at the rectenna site would then be 300 W/m²; if a Gaussian power profile of the transmitted beam is assumed. The beam-intensity pattern would be nonuniform, with a higher intensity in the centre of the rectenna and a lower intensity at its periphery. For human safety requirements, the maximum-allowable microwave power level has been set to 10 W/m² in most countries, and the SPS power-flux density would be constructed to satisfy this requirement at the periphery of the rectenna. After suitable power conditioning, the electric output of the rectenna would be delivered to the power network. More details about the SPS concept can be found in [1].

Typical parameters of the transmitting antenna of the SPS [4]

JAXA: Japan Aerospace Exploration Agency, NASA: National Aeronautics and Space Administration, DOE: U.S. Department Of Energy

Model	Old JAXA Model	JAXA1 Model	JAXA2 Model	NASA /DOE Model
Frequency (GHz)	5.80	5.80	5.80	2.45
Diameter of transmitting antenna	2.60 km ϕ	1.00 km ϕ	1.93 km ϕ	1.00 km ϕ
Amplitude taper	10 dB Gaussian	10 dB Gaussian	10 Db Gaussian	10 dB Gaussian
Output power	1.3 GW	1.3 GW	1.3 GW	1.3 GW
Max. power density at center	63 mW/cm ²	420 mW/cm ²	114 mW/cm ²	2.2 W/cm ²
Min. power density	6.3 mW/cm ²	42 mW/cm ²	11.4 mW/cm ²	0.22 W/cm ²
Antenna spacing	0.75 λ	0.75 λ	0.75 λ	0.75 λ
Power/ antenna (No. of elements)	0.95 W (3.54 billion)	6.1W (540 million)	1.7 W (1,950 million)	185 W (97 million)
Rectenna Diameter	2.0 km ϕ	3.4 Km ϕ	2.45 km ϕ	1 km ϕ
Max. Power Density	180 mW/c m ²	26 mW/cm ²	100 mW/cm ²	23 mW/c m ²
Collection Efficiency	96.5 %	86 %	87 %	89 %

III. HISTORICAL VIEW

The first concept of an SPS system was proposed by P. Glaser in 1968 [5], after a series of experiments on microwave power transmission [6, 7]. Following this article, the United States conducted an extensive feasibility study in 1978-1980. The feasibility study was a joint effort of NASA (National Aeronautics and Space Administration) and the Department of Energy. A reference model was proposed in 1979, known as the NASA/DoE reference model [8]. An SPS system using mirrors for sunlight concentration on the solar cells, the Integrated Symmetrical Concentrator, was also proposed. It uses 24 or 36 plane mirrors of 500 m diameter for a concentration factor of two or four [9].

Japanese scientists and engineers started their SPS research in the early 1980s. They conducted a series of microwave power-transmission experiments, such as the world's first rocket experiment with powerful microwave transmission in the ionosphere [10], experiments on the ground, computer simulations, theoretical investigations, and system studies for a demonstration experiment. After a conceptual study phase, two Japanese organizations have recently proposed their own models. JAXA (Japan Aerospace Exploration Agency) proposed an SPS 5.8 GHz/1 GW model, which is different from the NASA/DoE model.

Coherent Set of Numerical Values

Assuming that an SPS unit will generate 1 GW effective power on the ground, the characteristic efficiencies are summarized in Table 1. The figures are given for a 2.45- GHz unit; corresponding values for a 5.8-GHz unit are not fundamentally different. Therefore, in order to generate 1 GW at the ground, one needs to collect about 14 GW in space. Since the solar radiation power flux is equal to 1.37 kW/m², one needs a solar-panel area of approximately 10 km². The transmitted RF power is $14 \times 0.13 \times 0.78 \approx 1.44$ GW. Taking into account the RF collection efficiency of 87%, the RF power received at the ground level is $P = 1.25$ GW. The efficiency of the microwave power transmission (dc-microwave-dc) is the product of the efficiencies given in lines 2-4 of Table 1, i.e. 54%. (Actually, 54.18% was demonstrated and certified in a NASA laboratory test).

Quantity	Efficiency
Solar-power-to-dc-power efficiency	13%
dc-power-to-RF-power efficiency	78%
RF collection efficiency	87%
RF-power-to-dc-power (rectenna)	80%
Total efficiency	7%

Economic Issues

There are four main factors that determine the power- production costs of an SPS system: photovoltaic module efficiency and costs, mass-specific power production (W/ kg) of the solar modules and the transmission system, microwave power-transmission efficiency, and ~~launch cost~~. The target is an efficiency of about 50% for the total microwave power transmission dc-microwave-dc conversion, and a specific power output of 1 kW/kg for the whole microwave power-transmission system. The published SPS cost estimates are based on a launch cost of USD150/kg [1]. All these assumptions lead to an estimated energy-generation cost of approximately USD0.1-0.2 per kWh for an SPS system.

A direct comparison of the output power from a space-based solar power unit with that from a terrestrial photovoltaic array with equal area is not straightforward. On one hand, a simple estimate of the energy output yields an advantage of about a factor 2.5 for the SPS.

For the SPS system, 1.37 kW/m^2 solar power flux in space \times 0.07 overall SPS efficiency (Table 1) \times 24 h = 2.3 kWh/m²/day.

For a terrestrial solar-cell array, 5 kWh/m^2 /day average solar power flux at a sunny place (Arizona) \times 0.17 solar cell efficiency = 0.85 kWh/ m²/day.

IV. SPS RADIO TECHNOLOGIES

1. **Microwave Power Transmission:** In the microwave power- transmission system, radio waves would be used as carriers of energy. The main parameters of the microwave power- transmission system for the SPS system are the frequency, the diameter of the transmitting antenna, the output power (beamed to the Earth), and the maximum power-flux density. Efficiency is very important for the microwave power- transmission system. Assuming the SPS transmitting- antenna-to-rectenna propagation path is optimum, the following efficiencies will be important: dc-to-radio- frequency (RF) conversion, RF-to-dc conversion, and beam- collecting efficiencies. Conversion efficiencies higher than 80% for both RF-dc and dc-RF conversions are necessary to make the cost of the SPS system reasonable. A phased antenna array is planned for the SPS system, in order to obtain high- efficiency beam collection under the condition of fluctuating SPS attitudes. Depending on the frequency of the microwave power transmission, e.g. 2.45 GHz or 5.8 GHz, the number of antenna elements per square meter would need to be of the order of 100 or 400, where the power delivered by a single element would be 10 W or 2.5 W, respectively [1].
2. **Microwave Power Devices:** Many possibilities have been proposed for the microwave generators, such as microwave vacuum tubes (klystrons, magnetrons, travelling-wave tube amplifiers), semiconductor transmitters, and combinations of both technologies. These types of generators have been compared with respect to their efficiency, output power, weight, and emitted harmonics [1]. Compared to semiconductor technologies, a microwave tube has higher efficiency, lower cost, and a smaller power-to-weight ratio (kW/kg). From a manufacturing point of view, recent semiconductor technologies could be useful for SPS systems.
3. **Rectennas:** The rectenna (located on the Earth) receives the microwave power from the SPS and converts it to dc electricity. The rectenna is composed of an RF antenna, a low-pass filter, and a rectifier. Various rectenna schemes have been proposed, and the maximum conversion efficiencies anticipated so far are 91.4% at 2.45 GHz and 82% at 5.8 GHz.
4. **Control and Calibration:** Another important issue concerning the space-based microwave antenna is the necessarily high precision of the control of the beam direction. This is important for two reasons: to maximize the energy transferred to the Earth and to limit radiation in undesired directions, in order to avoid adverse effects on existing telecommunications, passive radio-detection systems, and biological systems. This goal may be achieved with the concept of a retro directive array, in which the rectenna sends a pilot signal to the SPS in order to indicate its position before the power beam is transmitted. This pilot beam is then used to direct the power beam back along exactly the same path as the pilot beam: in the retro directive direction. Emergency procedures should be defined and have to be applied when the beam direction is not contained within the predefined angle of 0.0005°. Technologies to achieve these goals are presently under study.

V. MICROWAVE POWER TRANSMISSION EFFECTS ON HUMAN HEALTH

Above the centre of the rectenna, the SPS power-flux density will be considerably higher than the currently permissible safety levels for human beings. The ICNIRP (International Commission on Non-Ionizing Radiation Protection) and Japan both apply limits of 50 W/m² and 10 W/m² for 2.45 GHz and 5.8 GHz, respectively. Established safety limits for

microwave exposure are exceeded in an area around and above the rectenna during normal operation of the SPS access would need to be carefully controlled to ensure that environmental safety and health standards are maintained. It should be noted that there are currently insufficient data on specific microwave power-transmission effects on human health, and that standards for this particular application are not sufficiently developed. Taking into consideration the importance of this field, more studies are urgently needed regarding human health and its bioeffects

VI. CONCLUSION

The increasing global energy demand is likely to continue for many decades. New power plants of all sizes will be built. Fossil fuels will run out in another 3-4 decades. However energy independence is something only Space based solar power can deliver. Space based solar power (SBSP) concept is attractive because it is much more advantageous than ground based solar power. It has been predicted that by 2030, the world needs 30TW power from renewable energy sources and solar energy alone has the capability of producing around 600TW. The levels of CO₂ gas emission can be minimized and brought under control. Thus the problem of global warming will be solved to a great extent. Based on current research space based solar power should no longer be envisioned as requiring unimaginably large initial investments. Moreover, space solar power systems appear to possess many significant environmental advantages when compared to alternative approaches to meeting increasing terrestrial demands for energy including necessity of considerably less land area than terrestrial based solar power systems. Though the success of space solar power depends on successful development of key technology, it is certain the result will be worth the effort. Space solar power can completely solve our energy problems long term. The sooner we start and the harder we work, the shorter "long term" will be.

References

- [1] H. Matsumoto and K. Hashimoto (eds.), Report of the URSI inter Commission Working Group on SPS, URSI, 2006.
- [2] Vaganov, R. B., "Maximum Power Transmission between Two Apertures with the Help of a Wave Beam", Journal of Communications Technology and Electronics, vol.42, no.4, 1997, pp.430-435.
- [3] Garmash, V.N., Katsenelenbaum B.Z., S.S.Shaposhnikov, S.S., V. N. Tioulpakov, and R. B.Vaganov, "Some Possible Methods of the Diffraction Expansion Decrease", Proc.of SPS'97, 1997. Pp.87-92.
- [4] Supporting Document for the URSI White Paper on Solar Power Satellite Systems, 2006
- [5] P. Glaser, "Power from the Sun: It's Future," Science, 162, 22 November 1968.
- [6] W. C. Brown, "Satellite Power Stations: A New Source of Energy," IEEE Spectrum, 10, 3, 1973, pp. 38-47.
- [7] W. C. Brown, "The History of Power Transmission by Radio Waves," IEEE Transactions on Microwave Theory and Techniques, MTT-32, 1984, pp. 1230-1242.
- [8] US Department of Energy and NASA, "Satellite Power System, Concept Development and Evaluation Program, Reference System Report," October 1978 (published January 1979).
- [9] H. Feingold, et al., "Evaluation of Comparison of Space Solar Power Concepts," IAC-02-R.1.08, IAF, 2002 H. Matsumoto, N. Kaya, I. Kimura, S. Miyatake, M. Nagatomo, and T. Obayashi, "MINIX Project Toward the Solar Power Satellite - Rocket Experiment of Microwave Energy Transmission and Associated Nonlinear Plasma Physics in the Ionosphere," ISAS Space Energy Symposium, 1982, pp. 69-76.

Automated Data Validation Testing Tool for Data Migration Quality Assurance

Priyanka Paygude¹, P. R. Devale²

¹Research Scholar, ²Professor

Department of Information Technology, Bharati Vidyapeeth University College of Engineering, Pune, India

Abstract: Data migration has become one of the most demanding proposals for IT company managers. Even though these projects earn high business benefits, such as reduced costs, improved productivity, and data manageability, they likely to involve a high level of risk due to the huge volume and criticalness of moved data. In order to reduce risk and guarantee that the data has been migrated and transformed successfully, it is essential to employ a thorough Quality Assurance (QA) strategy in migration projects. Testing is a key phase of migration project for delivering a successful migrated data and addressing any issues prior and after the migration process.

Manual testing for data validation process is time consuming and inaccurate; so automated data validation assure data quality with highly reduced time, cost and maintaining good data quality. The paper proposed automation of data migration validation testing process for quality assurance and risk control across industries.

Keywords: Automation Testing, Data Migration, Data Quality, Data Validation, ETL

I. INTRODUCTION

Data is a precious asset for any company. So, any unplanned transfer of data can be very risky for company. In reality, planning is the top most success factor for any data migration project, independent of underline complexity. Appropriate thorough planning reduces the business impact such as application downtime, overall performance degradation, and technical incompatibilities, risk for example, completeness risk, semantic risk, data corruption/loss.

Each reason for migrating data is motivated by the need to find new efficiencies, better manage risk and stay competitive, as follows:

- Systems Consolidations: Firms are looking for reducing structural costs by standardizing on modern, cost-effective platforms and technologies; and by retiring inflexible and hard to continue legacy applications.
- M&A Activity: merger and acquisition (M&A) activities has created large organizations with a wide range of technologies that require complex IT integration programs to support merged business entities [3].
- System Upgrades: Implementation of novel business-models and processes brings along new functional and non-functional requirements no longer supported by the existing application [4].
- Ever changing legal regulations, technological progress and upgrades.

Many companies are using Business Intelligence (BI) for making managerial strategic decisions in the expectation of gaining a competitive lead in today's hard business platforms. Mostly firms uses sampling technique to test data which covers far less than 10% of data under test. Therefore, remaining at least 90% of data is untested. Thus decisions typically fail due to incorrect, untested data, which will cost their firms millions of dollars. [6]

The objective of paper is to propose an automated approach for data migration validation testing and data quality assurance.

II. DATA MIGRATION OVERVIEW

Data transfer can be of two types: first, a simple data movement that is moving data from source database to target database without restructuring and second, data migration. Data migration is the process of transferring data between computer storages, types, formats, or computer system. It is the process of moving data from the old database(s) to a new database. We called old database as a legacy or source database and this database is migrated to the new database, called as target or destination database. The data migration process becomes a difficult challenge when source and target databases are different in their internal structures. So, simple import/export procedures will not work. Thus data migration process is better to perform using automated ETL (Extract – Transform - Load) tools than doing manually.

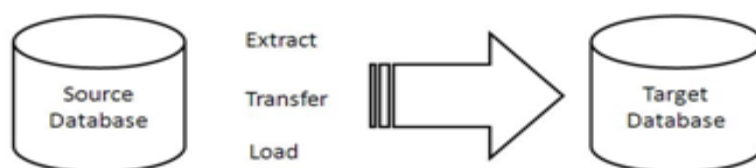


Fig. 1 Data Migration Overview

Data migration is a one-time process. It involves the re-structuring of data such as fields being merged, or formats being changed, or transforming data in various other ways. If no-restructuring takes place then we would call this data movement [2].

III. LITERATURE SURVEY

This segment sheds light on work published in the area of testing, quality assurance and data quality issues in data migration projects.

Authors has undergone literature review stage and evolved with the problem statement with the help of work, has published till today in the area of data quality and data validations in data migration projects.

Florian Matthes, Christopher Schulz, Klaus Haller, “Testing and Quality Assurance in data migration projects,” 2011 - discusses practice-based testing and quality assurance techniques to reduce or even eliminate data migration risks.

Bloor Research (2007) - Data Migration Projects Are Risky: 84% of data migration projects fail to meet expectations, 37% experience budget overruns, and 67% are not delivered on time.

Lixian Xing, Yanhong Li, “Design and Application of Data Migration System in Heterogeneous Database”, 2010 - paper is based on database migration project and methodically introduces technique issues of data migration involving manual work which may contribute to organizations that have data migration demands.

Robert M. Bruckner, Josef Schiefer Institute of Software Technology (1999) - describes the portfolio theory for automatically processing information about data quality in data warehouse environments.

Manjunath T N, Ravindra S Hegadi and Archana R A, “A Study On Sampling Techniques For Data Testing”(2012) - This paper emphasis on proposing model to do quality checks for huge database migrations using random sampling techniques.

Manjunath T.N, Ravindra S Hegadi Ravi kumar G.K (2011) - Discussed and analyzed possible set of causes of data quality issues from exhaustive survey and discussions with SMEs.

This paper is proposing the method of automating the data validation testing for data migrations for quality assurance and risk management in migration process, resulting in effort and cost reduction with improved data quality parameters.

IV. ONGOING METHODOLOGIES

Designing and implementing the successful migration of high volume data, unstructured content is always challenging. And testing, validating, or otherwise quality assuring results adds greatly to its complexity, cost, risks, and the time required for completion. After the migration process completes, the process of data validation testing starts for assuring user about the integrity of the migrated data.

Various methods are used for data migration validation testing:

1. Sampling Technique:

Sampling technique assumes that error is uniformly distributed, which is not true in real scenario. A sample is a group of units selected from a larger dataset of population. Valid conclusions can be drawn, by studying the samples. Random sampling is mostly used sampling method. Sampling is the process of selecting a small number of elements from a larger defined target dataset such that the information gathered from the small dataset will allow judgments to be made about the larger datasets [7].

Cons:

- Highly inefficient, error-prone process
- Requiring major manual involvement
- Time consuming comparisons of source and target systems.
- Ad-hoc procedures with limited coverage
- Final results are not 100% reliable

2. Writing ‘MINUS’ queries:

In this, an individual ‘SELECT’ query executed on both the databases/tables and then, ‘MINUS’ operation is used between the source and target select query result. Then the output contains records of source which are not contained in the target.

But result only shows the extra rows that are in the Source but the target lacks and not the extra rows that are in target but the Source lacks. Thus ‘MINUS’ queries needs to be executed twice (Source-to-Target and Target-to-Source). This double query execution, consumes more time and resources utilization [9].

```
SELECT emp_id  
FROM emp_table;  
MINUS  
SELECT cust_id  
FROM cust_table;
```

Cons:

- Double query execution, consumes more time and resources utilization.

- Only provides n of rows not present in target database/ table, no other validation like data type mismatch, null values, data corruption etc.

Traditional data validation testing techniques are highly time and resource consuming, with limited data coverage leading errors that may go undetected. These limitations can be address using an automation testing approach.

Using an automated approach for data validation testing, will make the testing process deterministic rather than procedural and can validate 100% of the migrated data along with taking care of business constraints used during transformation.

V. PROPOSED SYSTEM

The proposed tool will automate the entire testing process, from scheduling to execution to comparison to reporting across multiple database platforms that helps companies eliminate risks associated with migrations process.

A. Automated Proposed Testing Model

Mapping data is the key document for any migration project, which contains a mapping relation between source and target database. This document is a logical data map between source and target database along with transformation constraints. User will map source database with target database along with the input of mapping document that is created in migration process.

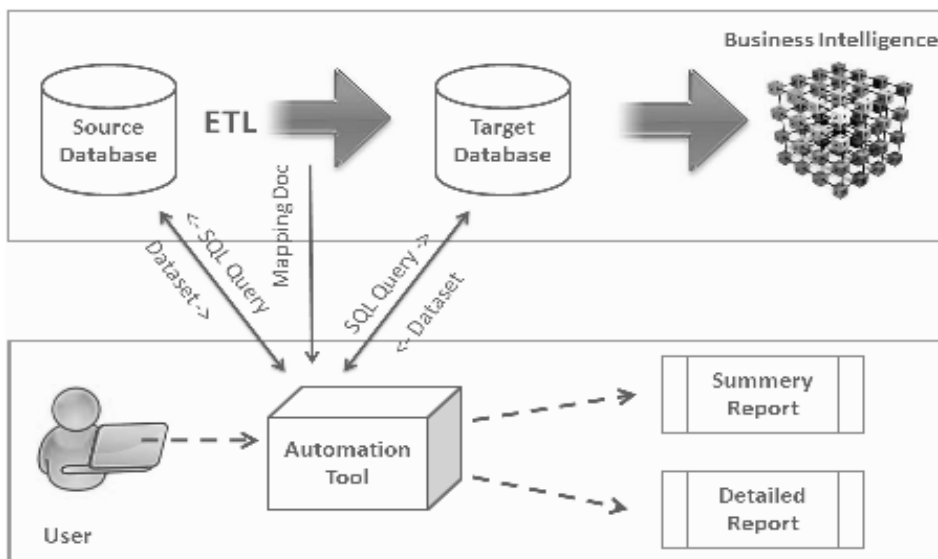


Fig. 3: Architecture for Automating Data Validation

Query to be fire on databases, will be different based on the underline database platforms. User will write either own query or chose a query from snippets. This query will automatically map to source and target database by considering underline database platforms. These queries will be fire on individual database, which in turn return a dataset. Datasets, return from source and target database will be compared by automation tool. Based on comparison result, data mismatches will be logged into summery and detail report.

B. Modules of Proposed System

The proposed methodology consisting of four modules, which are explained with the associated features in the following sub-sections. The modules are divided as

1) Test Design Library

It takes total control of test design. Test design is the foundation of any powerful testing.

- Reusable Query Snippets – Brings flexibility and reduce time in the process of query design. Snippet libraries consist of various basic query fragments that one can use to modularize queries, helping to speed up the process.
- Allow to paste queries created using yours favorite editor, to execute on respective databases.

2) Test Scheduling

Allow user to Schedule testing by time for maximum productivity

- Simplify the process by scheduling tests for the specific times when the underline architecture is available, or for a window of time when other activities will have least impact.
- Build Scenarios for scheduling your execution runs at specific dates and times

3) Live Dashboard

GUI showing live status of test execution process

- Drill-down into data as processes it to examine results as they become available during execution
- Real-time statistics for each executed Queries and for the Scenario execution as a whole
- Export detailed results in Excel, CSV or XML formats to share, store

4) Reporting

Use reports to share both high-level and detailed views of testing. Two Types of Reports will be generated:

- High-Level report gives view of testing success from high end, like total records affected, time taken, total no of defects etc.
- Detail-level report gives record level detailing.
- Export reports as PDF, XML, HTML files to share within organization or for future audit needs

C. Process of Automated Data Validation Testing

Once the process of migrating data from source to target database is done with the help of ETL tool, data validation testing can be started.

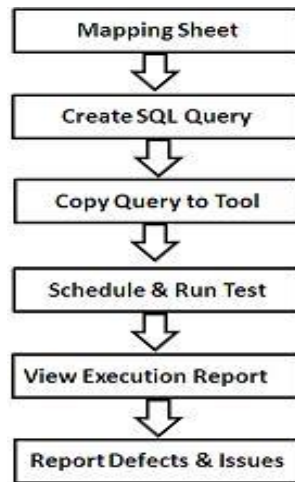


Fig. 4: Stages of automated data validation testing

Prerequisites to start automated data validation testing are:

- A. Read only access to source and target schemas/tables along with database connectivity.
- B. Data mapping document, created for ETL process of data migration.

Steps discuss below for data validation testing:

1. Review mapping sheet: This sheet is a logical data map that describes the mapping between target and source database, along with information of transformation rules.
2. Create SQL query: User can create SQL queries for both source and target database using any SQL editor.
3. Copy Queries to tool: User will copy created SQL queries for source and target database to tool.
4. Schedule & Run Test: Automation testing tool will allow user to schedule test for particular date, time and then run test on scheduled time.
5. View Execution Report: Automation data migration testing tool will generate two reports of run test: summery and detail report, showing result of test run.
6. Reports Defects & Issues: Detected defects in run test are logged to defect repository.

VI. ASSURING DATA QUALITY

Below table describe some common defects that proposed automated testing tool will find in data migration projects, to avoid the adverse effect that any of these anomalies can cause data migration project fail, and ultimately Business Intelligence [5].

Following table shows various test cases that tool will test:

Table 1. Data inconsistencies

Data inconsistency	Description	Example
Data Truncation	Loss of data due to truncation of data field	Source data field value “Mumbai City” is being truncated to “Mumbai C” It happens because target data field is having less or incorrect length to capture the entire source data field.
Data Type Mismatch	Dissimilarity in source and target data types.	Source data field for Interest Rate was float; however, Target data field is set to int.
Missing Data	Values of some data fields missing in either source or target databases.	Missing data values while transferring data from source to target database or data value is not completely transfer to target database.
Duplicate Records	Records which are similar to two or more records, called as duplicate records.	Record of employee with unique employee id is repeated more than one.
Transformation Logic Errors	Transformation logic is not followed causing errors in data values	Default integer data value of source database is to be transfer into target database in percentage format, which is not done properly in migration process causing bad data.
Null Translation	Incorrect transformation of source NULL values to target database.	NULL values of source data field are supposed to transform by default value in target data field. However, due to incorrect logic of implementation, it results in the target data field containing NULL values.

VII. CONCLUSION

Data migration is a tough project with high level of risks like time overruns, budget etc. Use of quality ETL tool will minimize the risk of defects in data of target database. Even though, testing of data for its validation is important and can't be overlooked. Testing validity of data using manual or just writing 'MINUS' querise, are not the effective way causing risk with data quality. Here, the proposed system assure data quality using standardize way of data testing in migration projects across the enterprise, multiple platforms, and applications. Using proposed solution, one can save time, cost, and manual efforts; along with data quality assurance.

References

- [1] Florian Matthes, Christopher Schulz, Klaus Haller, “Testing and Quality Assurance in data migration projects,” 2011 27th IEEE International Conference on Software Maintenance(ICSM)
- [2] P. Howard and C. Potter, “Data migration in the global 2000 - research, forecasts and survey results,” London, United Kingdom, p. 29, 2007
- [3] Sagar Khandelwal, Kannan Subramanian and Rohit Garg, “Next Generation Cross Technology Test Data Solution for M&A”, 2011 27th IEEE International Conference on Software Maintenance (ICSM)
- [4] Endava, “Data Migration - The Endava Approach,” London, United Kingdom, p. 11, 2007
- [5] John Hess, “Dealing With Missing Values in The Data Warehouse” *A Report of Stonebridge Technologies, Inc-1998*
- [6] C. Burry and D. Mancusi, “How to plan for data migration,” 2004
- [7] Manjunath T N, Ravindra S Hegadi and Archana R A, “A study on sampling techniques for data testing”, International Journal of Computer Science and Communication, Vol. 3, No. 1, January-June 2012, pp. 13-16
- [8] IBM, “Best practices for data migration - Methodologies for assessing, planning, moving and validating data migration,” Somers, NY, USA, p. 16, 2009
- [9] Manjunath T N, Ravindra S Hegadi, Mohan H S, ”Automated Data Validation for Data Migration Security”, *IJCA Online*, 30/number 6/3642-5088: ISBN: 978-93-80864-89-0.